Scientific Programming

Scientific Programming and Artificial Intelligence for Sensor Data Stream Analysis

Lead Guest Editor: Le Sun
Guest Editors: Hai Dong, Xiao-Xia Yin, and Siuly Siuly

Scientific Programming and Artificial Intelligence for Sensor Data Stream Analysis

Scientific Programming and Artificial Intelligence for Sensor Data Stream Analysis

Lead Guest Editor: Le Sun
Guest Editors: Hai Dong, Xiao-Xia Yin, and Siuly Siuly

Contents

Contents

Contents

Contents

Hindawi
Scientific Programming
Volume 2023, Article ID 9878754, 1 page
https://doi.org/10.1155/2023/9878754

Retraction

Retracted: Application of Intelligent Sensor Algorithm in Student Management Information Fusion

Scientific Programming

Received 1 August 2023; Accepted 1 August 2023; Published 2 August 2023

This article has been retracted by Hindawi following an investigation undertaken by the publisher [1]. This investigation has uncovered evidence of one or more of the following indicators of systematic manipulation of the publication process:

(1) Discrepancies in scope
(2) Discrepancies in the description of the research reported
(3) Discrepancies between the availability of data and the research described
(4) Inappropriate citations
(5) Incoherent, meaningless and/or irrelevant content included in the article
(6) Peer-review manipulation

The presence of these indicators undermines our confidence in the integrity of the article's content and we cannot, therefore, vouch for its reliability. Please note that this notice is intended solely to alert readers that the content of this article is unreliable. We have not investigated whether authors were aware of or involved in the systematic manipulation of the publication process.

Wiley and Hindawi regrets that the usual quality checks did not identify these issues before publication and have since put additional measures in place to safeguard research integrity.

We wish to credit our own Research Integrity and Research Publishing teams and anonymous and named external researchers and research integrity experts for contributing to this investigation.

The corresponding author, as the representative of all authors, has been given the opportunity to register their agreement or disagreement to this retraction. We have kept a record of any response received.

References

[1] Y. Li, "Application of Intelligent Sensor Algorithm in Student Management Information Fusion," *Scientific Programming*, vol. 2021, Article ID 3053538, 12 pages, 2021.

Hindawi
Scientific Programming
Volume 2023, Article ID 9861963, 1 page
https://doi.org/10.1155/2023/9861963

Retraction

Retracted: Construction of Innovation and Entrepreneurship Platform Based on Deep Learning Algorithm

Scientific Programming

Received 1 August 2023; Accepted 1 August 2023; Published 2 August 2023

This article has been retracted by Hindawi following an investigation undertaken by the publisher [1]. This investigation has uncovered evidence of one or more of the following indicators of systematic manipulation of the publication process:

(1) Discrepancies in scope
(2) Discrepancies in the description of the research reported
(3) Discrepancies between the availability of data and the research described
(4) Inappropriate citations
(5) Incoherent, meaningless and/or irrelevant content included in the article
(6) Peer-review manipulation

The presence of these indicators undermines our confidence in the integrity of the article's content and we cannot, therefore, vouch for its reliability. Please note that this notice is intended solely to alert readers that the content of this article is unreliable. We have not investigated whether authors were aware of or involved in the systematic manipulation of the publication process.

Wiley and Hindawi regrets that the usual quality checks did not identify these issues before publication and have since put additional measures in place to safeguard research integrity.

We wish to credit our own Research Integrity and Research Publishing teams and anonymous and named external researchers and research integrity experts for contributing to this investigation.

The corresponding author, as the representative of all authors, has been given the opportunity to register their agreement or disagreement to this retraction. We have kept a record of any response received.

References

[1] J. Li and Y. Zhao, "Construction of Innovation and Entrepreneurship Platform Based on Deep Learning Algorithm," *Scientific Programming*, vol. 2021, Article ID 1833979, 7 pages, 2021.

Hindawi
Scientific Programming
Volume 2023, Article ID 9841980, 1 page
https://doi.org/10.1155/2023/9841980

Retraction

Retracted: Research on Chord-Constrained Two-Track Music Generation Based on Improved GAN Networks

Scientific Programming

Received 1 August 2023; Accepted 1 August 2023; Published 2 August 2023

This article has been retracted by Hindawi following an investigation undertaken by the publisher [1]. This investigation has uncovered evidence of one or more of the following indicators of systematic manipulation of the publication process:

(1) Discrepancies in scope
(2) Discrepancies in the description of the research reported
(3) Discrepancies between the availability of data and the research described
(4) Inappropriate citations
(5) Incoherent, meaningless and/or irrelevant content included in the article
(6) Peer-review manipulation

The presence of these indicators undermines our confidence in the integrity of the article's content and we cannot, therefore, vouch for its reliability. Please note that this notice is intended solely to alert readers that the content of this article is unreliable. We have not investigated whether authors were aware of or involved in the systematic manipulation of the publication process.

Wiley and Hindawi regrets that the usual quality checks did not identify these issues before publication and have since put additional measures in place to safeguard research integrity.

We wish to credit our own Research Integrity and Research Publishing teams and anonymous and named external researchers and research integrity experts for contributing to this investigation.

The corresponding author, as the representative of all authors, has been given the opportunity to register their agreement or disagreement to this retraction. We have kept a record of any response received.

References

[1] X. Li and Y. Niu, "Research on Chord-Constrained Two-Track Music Generation Based on Improved GAN Networks," *Scientific Programming*, vol. 2022, Article ID 5882468, 7 pages, 2022.

Hindawi
Scientific Programming
Volume 2023, Article ID 9828320, 1 page
https://doi.org/10.1155/2023/9828320

Retraction

Retracted: Intelligent Prediction Algorithm of Cross-Border E-Commerce Logistics Cost Based on Cloud Computing

Scientific Programming

Received 1 August 2023; Accepted 1 August 2023; Published 2 August 2023

This article has been retracted by Hindawi following an investigation undertaken by the publisher [1]. This investigation has uncovered evidence of one or more of the following indicators of systematic manipulation of the publication process:

(1) Discrepancies in scope
(2) Discrepancies in the description of the research reported
(3) Discrepancies between the availability of data and the research described
(4) Inappropriate citations
(5) Incoherent, meaningless and/or irrelevant content included in the article
(6) Peer-review manipulation

The presence of these indicators undermines our confidence in the integrity of the article's content and we cannot, therefore, vouch for its reliability. Please note that this notice is intended solely to alert readers that the content of this article is unreliable. We have not investigated whether authors were aware of or involved in the systematic manipulation of the publication process.

Wiley and Hindawi regrets that the usual quality checks did not identify these issues before publication and have since put additional measures in place to safeguard research integrity.

We wish to credit our own Research Integrity and Research Publishing teams and anonymous and named external researchers and research integrity experts for contributing to this investigation.

The corresponding author, as the representative of all authors, has been given the opportunity to register their agreement or disagreement to this retraction. We have kept a record of any response received.

References

[1] W. Gao, "Intelligent Prediction Algorithm of Cross-Border E-Commerce Logistics Cost Based on Cloud Computing," *Scientific Programming*, vol. 2021, Article ID 7038294, 10 pages, 2021.

Hindawi
Scientific Programming
Volume 2023, Article ID 9795181, 1 page
https://doi.org/10.1155/2023/9795181

Retraction

Retracted: Economic Market Fluctuation Model Based on Internet of Things Technology

Scientific Programming

Received 1 August 2023; Accepted 1 August 2023; Published 2 August 2023

This article has been retracted by Hindawi following an investigation undertaken by the publisher [1]. This investigation has uncovered evidence of one or more of the following indicators of systematic manipulation of the publication process:

(1) Discrepancies in scope
(2) Discrepancies in the description of the research reported
(3) Discrepancies between the availability of data and the research described
(4) Inappropriate citations
(5) Incoherent, meaningless and/or irrelevant content included in the article
(6) Peer-review manipulation

The presence of these indicators undermines our confidence in the integrity of the article's content and we cannot, therefore, vouch for its reliability. Please note that this notice is intended solely to alert readers that the content of this article is unreliable. We have not investigated whether authors were aware of or involved in the systematic manipulation of the publication process.

Wiley and Hindawi regrets that the usual quality checks did not identify these issues before publication and have since put additional measures in place to safeguard research integrity.

We wish to credit our own Research Integrity and Research Publishing teams and anonymous and named external researchers and research integrity experts for contributing to this investigation.

The corresponding author, as the representative of all authors, has been given the opportunity to register their agreement or disagreement to this retraction. We have kept a record of any response received.

References

[1] L. Zhai, "Economic Market Fluctuation Model Based on Internet of Things Technology," *Scientific Programming*, vol. 2022, Article ID 2296823, 11 pages, 2022.

Hindawi
Scientific Programming
Volume 2023, Article ID 9790230, 1 page
https://doi.org/10.1155/2023/9790230

Retraction

Retracted: Research on Students' Adaptive Learning System Based on Deep Learning Model

Scientific Programming

Received 1 August 2023; Accepted 1 August 2023; Published 2 August 2023

This article has been retracted by Hindawi following an investigation undertaken by the publisher [1]. This investigation has uncovered evidence of one or more of the following indicators of systematic manipulation of the publication process:

(1) Discrepancies in scope
(2) Discrepancies in the description of the research reported
(3) Discrepancies between the availability of data and the research described
(4) Inappropriate citations
(5) Incoherent, meaningless and/or irrelevant content included in the article
(6) Peer-review manipulation

The presence of these indicators undermines our confidence in the integrity of the article's content and we cannot, therefore, vouch for its reliability. Please note that this notice is intended solely to alert readers that the content of this article is unreliable. We have not investigated whether authors were aware of or involved in the systematic manipulation of the publication process.

Wiley and Hindawi regrets that the usual quality checks did not identify these issues before publication and have since put additional measures in place to safeguard research integrity.

We wish to credit our own Research Integrity and Research Publishing teams and anonymous and named external researchers and research integrity experts for contributing to this investigation.

The corresponding author, as the representative of all authors, has been given the opportunity to register their agreement or disagreement to this retraction. We have kept a record of any response received.

References

[1] X. Yang, Z. Zhou, and Y. Xiao, "Research on Students' Adaptive Learning System Based on Deep Learning Model," *Scientific Programming*, vol. 2021, Article ID 6593438, 13 pages, 2021.

Hindawi
Scientific Programming
Volume 2023, Article ID 9763951, 1 page
https://doi.org/10.1155/2023/9763951

Retraction

Retracted: Design of a Panoramic Virtual Dynamic Display System for Digital Museums Based on Visual Interaction Technology

Scientific Programming

Received 1 August 2023; Accepted 1 August 2023; Published 2 August 2023

This article has been retracted by Hindawi following an investigation undertaken by the publisher [1]. This investigation has uncovered evidence of one or more of the following indicators of systematic manipulation of the publication process:

(1) Discrepancies in scope
(2) Discrepancies in the description of the research reported
(3) Discrepancies between the availability of data and the research described
(4) Inappropriate citations
(5) Incoherent, meaningless and/or irrelevant content included in the article
(6) Peer-review manipulation

The presence of these indicators undermines our confidence in the integrity of the article's content and we cannot, therefore, vouch for its reliability. Please note that this notice is intended solely to alert readers that the content of this article is unreliable. We have not investigated whether authors were aware of or involved in the systematic manipulation of the publication process.

Wiley and Hindawi regrets that the usual quality checks did not identify these issues before publication and have since put additional measures in place to safeguard research integrity.

We wish to credit our own Research Integrity and Research Publishing teams and anonymous and named external researchers and research integrity experts for contributing to this investigation.

The corresponding author, as the representative of all authors, has been given the opportunity to register their agreement or disagreement to this retraction. We have kept a record of any response received.

References

[1] J. Wang, "Design of a Panoramic Virtual Dynamic Display System for Digital Museums Based on Visual Interaction Technology," *Scientific Programming*, vol. 2022, Article ID 1626448, 7 pages, 2022.

Hindawi
Scientific Programming
Volume 2023, Article ID 9763290, 1 page
https://doi.org/10.1155/2023/9763290

Retraction

Retracted: Collocation Features in Translated Texts Based on English Analogy Corpus

Scientific Programming

Received 1 August 2023; Accepted 1 August 2023; Published 2 August 2023

This article has been retracted by Hindawi following an investigation undertaken by the publisher [1]. This investigation has uncovered evidence of one or more of the following indicators of systematic manipulation of the publication process:

(1) Discrepancies in scope
(2) Discrepancies in the description of the research reported
(3) Discrepancies between the availability of data and the research described
(4) Inappropriate citations
(5) Incoherent, meaningless and/or irrelevant content included in the article
(6) Peer-review manipulation

The presence of these indicators undermines our confidence in the integrity of the article's content and we cannot, therefore, vouch for its reliability. Please note that this notice is intended solely to alert readers that the content of this article is unreliable. We have not investigated whether authors were aware of or involved in the systematic manipulation of the publication process.

Wiley and Hindawi regrets that the usual quality checks did not identify these issues before publication and have since put additional measures in place to safeguard research integrity.

We wish to credit our own Research Integrity and Research Publishing teams and anonymous and named external researchers and research integrity experts for contributing to this investigation.

The corresponding author, as the representative of all authors, has been given the opportunity to register their agreement or disagreement to this retraction. We have kept a record of any response received.

References

[1] B. Liu and J. Wang, "Collocation Features in Translated Texts Based on English Analogy Corpus," *Scientific Programming*, vol. 2022, Article ID 8294254, 7 pages, 2022.

Hindawi
Scientific Programming
Volume 2022, Article ID 4671381, 7 pages
https://doi.org/10.1155/2022/4671381

Research Article

Detecting Anomaly Data for IoT Sensor Networks

Zhe Wei [1] and Fang Wang [2]

[1]School of Computer Science, Civil Aviation Flight University of China, Guanghan 618307, China
[2]School of Science, Civil Aviation Flight University of China, Guanghan 618307, China

Correspondence should be addressed to Zhe Wei; findwei@foxmail.com

Received 21 January 2022; Revised 5 April 2022; Accepted 4 May 2022; Published 21 May 2022

Academic Editor: Le Sun

The Internet of Things, or IoT, has been widely recognized as a new perception paradigm for interacting between the digital world and the physical one. Acting as the interface and integral part of the Internet of Things, sensors embedded within the network are the principal components that collect the unprocessed data, and these sensors are usually deployed in unattended, hostile, or harsh areas, which inevitably makes the sensor readings prone to faults and even anomalies. Therefore, the quality of sensor readings will ultimately affect the quality of various data-oriented IoT services, and the sensor data are of vital importance affecting the performance of the system. However, the data anomaly detection is a nontrivial task for IoT because sensors are usually resource-constrained devices with limited computing, communication, and capacity. Therefore, an efficient and lightweight detecting method is needed to meet the requirements. In this study, we deal with the anomaly data by detecting the source sensor nodes through combination methods of the local outlier factor and time series. Simulations show that the proposed method can effectively detect the anomaly data and presents a better normal data rate.

1. Introduction

The Internet of Things, or IoT, has received extensive attention in the past few years by the research community owning to the progress of computing and real-time connections between data and devices and has been used in many application fields such as smart home/office, automobile, and medical assistance to solve practical problems [1–3]. The IoT depicts a future computing scenario where everyday physical objects will be connected to the Internet and identify themselves [4]. Nowadays, the Internet of Things is becoming a more and more important infrastructure component, and due to the heterogeneity of IoT devices, the data exchange between IoT sensors and various applications achieves rapid growth.

However, with the wide spread applications of the IoT, security threats are also becoming increasingly prominent [5–8]. The IoT is vulnerable to attacks from communication channels, which has become a common security problem [9]. IoT sensor failure may interrupt the system control [10], thus interrupting the services provided by the IoT system. The distributed deployment of IoT sensors makes networking more convenient, but it also brings more difficult risks [11]. In addition, many IoT applications are of heterogeneous components such as different sensors, services, protocols, and communication technologies like Zigbee, WiFi, and Bluetooth, which generate the complexity of the network management [12]. Therefore, anomaly data come into existence accompanied by the threats, attacks, risks, integration of heterogeneous technologies, and various IoT applications.

In the field of data mining and statistics, anomalies are usually referred to as either deviants or outliers [13]. The definition of anomaly data given in [14] is that anomaly data are data points that behave very differently from others or conform to some predefined abnormal behaviors. The definition of anomaly given in [15] is that it is an observation deviating so much from others to generate uncertainties. According to [16], the main causes of anomaly data are of two aspects: (1) internal malfunction, i.e., noise and fault caused by sensor hardware and software failure; (2) external influence, i.e., specific events occur in the places where nodes are deployed. Essentially, anomaly-based detection is an intrusion detection mechanism, it can be used to perceive important network mode attacks [17], and anomaly detection refers to identifying suspicious data items, events, or observations that are significantly different from most other data [18]. The application of anomaly detection can make certain contributions to the IoT data protection [19], and it is resource friendly and provides more extensive detection, which is very suitable for IoT sensor network applications [20].

Nevertheless, the anomaly data detection is a nontrivial task for IoT. The IoT nodes are usually resource-constrained sensors with low-cost embedded systems [21], and traditional anomaly detection solutions cannot be directly applied into IoT [22]. For this reason, it is important that a trade-off solution be found to the problem with decent accuracy while bringing minimum overhead.

This research aims to detect the anomaly sensor data under the IoT environment. Different from other works that focus on analyzing the sensor data and evaluating the analyzed results by certain rules, according to the dynamic features of IoT networks, our proposed method tries to trace and identify the source nodes that generate or cause the anomaly data, and by identifying and confirming the suspected nodes, the anomaly data can be eventually deleted from the network. This study uses combination methods of local outlier factor and time series. The local outlier factor is applied to check the abnormal data so as to label the related sensor node as suspected one. Due to the dynamic changing environment of the IoT network, nodes might be influenced by the temporary error or communication interference resulting in being labeled as suspected nodes. Thus time series method is used to evaluate and further confirm these potential suspected nodes from the perspective of time windows.

The main contribution of this work is to provide a lightweight yet effective method for anomaly data detection in IoT sensor networks, due to the fact that sensors in IoT are usually resource-constrained devices in terms of computing, communication, and capacity. To this end, both the methods used in this study are of ease computing. Specifically, the local outlier factor is a density-based detecting algorithm which is simpler and not particularly picky about the distribution of datasets. By contrast, most of the other anomaly detection algorithms are based on statistical methods or borrow some clustering algorithms for anomaly identification; besides, the datasets obeying a specific probability distribution are usually assumed. Further, in the time series, instead of directly using traditional methods, Chebyshev polynomials are applied for the approximation of time series especially in comparing the similarity of two time series, which is also lightweight in computing and can be done through the related polynomial coefficients.

The remainder of this study is organized as follows. Section 2 presents the related works about the anomaly detection for sensor data and related definitions and classifications. Section 3 introduces the local outlier factor and time series methods in detail, on which our proposed method is based. Simulations are presented in Section 4, and Section 5 concludes this work.

2. Related Works

Anomaly detection comes from the data mining and statistics field, and it establishes a standard model to judge whether the relevant data match the model. According to [23], the anomaly detection algorithm for sensor data is classified as three aspects, i.e. (1) statistical method, which classifies the anomalies by measuring the probability of the measured data relative to the model; (2) proximity-based method, which relies on the distance between measured data to distinguish abnormal data from correct data; (3) prediction-based method, in which the past measurement data are used to train the model and it can predict the next measured value in the sensor data.

Machine learning-based anomaly detection methods have received much attention in the research community. The machine learning algorithms are used on the interested data and train the related models through the pattern extraction [24], based on which the anomaly detection uses machine learning technology to detect abnormal activities in network traffic packets [25]. Pathak et al. [4] applied supervised and unsupervised machine learning to solve the tampering problem of sensors in the Internet of Things. In [4], the real-time view of traffic pattern is considered to train the unsupervised machine learning method based on isolated forest for anomaly detection; it creates labels according to the traffic pattern, uses the decision tree supervision method to monitor all Internet of Things traffic on the gateway, and sends an alarm to the administrator when an anomaly is detected.

Kim et al. [13] provided a method for real-time detection and notification of abnormal conditions through machine learning by generating synthetic datasets for learning real-time data anomaly detection algorithms and by testing models based on gated recursive units and long-term and short-term memory for predicting time series data anomalies. Kim et al. [13] detected and notified abnormal conditions in the worker environment through sensor data. The method is based on the prediction-based anomaly detection method and neural network and is evaluated using synthetic data generated from time series with trend, season, and noise components. Kim et al. [13] further explained how to use neural networks to detect anomalies and how to evaluate the proposed model. Based on the combination of machine learning and visual data analysis, Vasily et al. [26] proposed an anomaly detection method in wireless sensor networks. Taking a water management system as an example, the method is tested, and the necessary datasets are generated by using the software model for testing anomaly detection.

Different from other works that mainly focus on the network layer and application layer, an adaptive context-aware anomaly detection method is proposed in [10] which centers on the physical properties of the IoT sensor system and identifies anomalous incidents in the environment properties of the system. This method uses a sensor association algorithm which can generate sensor fingerprints, cluster these fingerprints, and extract the context of the system. Then, according to the contextual information and through long short-term memory neural network and Gaussian estimator, the anomalies in the system together with the source could be detected.

Through distinguishing hostile events about the traffic pattern in the distributed smart space orchestration system, Reddy et al. [9] presented an anomaly detection system with characteristic examination. Reddy et al. [9] used a method based on supervised meta algorithm called bagging (which is one of the ensemble meta estimator learning technologies [27] and considers multiple predictors to calculate the aggregation predictor) to classify and process malicious operations and train the classifier-based anomaly detection to build a clarification model according to the intrusion data and predict the system by identifying when the system is in an abnormal state.

The authors in [16] studied the sensor fault and external event detection scheme in wireless sensor networks. Based on spatiotemporal fusion, Chen et al. [16] proposed a distributed anomaly detection method for wireless sensor networks based on one-class quarter-spherical support vector machine (QSSVM). In this method, the QSSVM model is trained to obtain relevant parameters, then the trained model is used to classify the streaming data in the network, and then the abnormal data types are determined and divided into noise, faults, and events. By converting unsupervised time series data into supervised form, Das et al. [28] proposed a segmentation-based anomaly detection method of IoT sensor data. In order to ensure that the data are not affected by inherent noise, the method performs Holt–Winters exponential smoothing [29] on the dataset and then trains a long-term memory neural network for the anomaly detection. Blockchain is a distributed network with some unique functions such as decentralization, transparency, and system autonomy [30], which can enhance network security and cooperation in the Internet of Things.

3. Preliminaries

In this research, our proposed method is mainly composed of two components, i.e., local outlier factor and Chebyshev polynomials-based time series, and as mentioned previously, both the components or methods are lightweight in computing and are applicable to resource-constrained IoT sensor nodes when dealing with anomaly data. They are introduced as follows.

Local outlier factor, or LOF, is a nearest neighbor algorithm. It attributes a fault or outlier score to each sensor reading based on the number of measurements around its K-nearest neighbors and the number of measurements around the sensor reading. Sensor readings with high scores are flagged as abnormal [31]. Anomalous data or outliers are treated as sensor data streams that are significantly different from normal behavioral data, and outlier detection can detect a high probability of false reads or data corruption, thereby ensuring the quality of data collected by sensors [32].

LOF is density-based outlier detection which has a fundamental assumption that the density around a nonoutlier object should be similar to the density around its neighborhood, while the density around an outlier object should be significantly different from that around its neighborhood. By assigning each data point an outlier factor that depends on the neighborhood density, it then evaluates whether the data point is an outlier. The larger the anomaly factor of the data is, the more likely the data are anomalous. The advantage of LOF is that it gives the degree to which a data point is an outlier [33].

The LOF algorithm is constructed on two main components, namely, the reachable distance and the local reachable density [34–36]. Based on the distance between the object p and each point in its k neighbors, the reachable distance is defined as

$$reach-dist_k(p,o) = \max\{k-dist(o), d(p,o)\}. \tag{1}$$

According to the mean distance of each data object in the neighborhood, a density parameter can be obtained, called the local reachable density, which is defined as

$$Lrd_k(p) = \frac{1}{\sum_{o\in N_k(p)} reach-di\ st_k(p,o)/|N_k(p)|}. \tag{2}$$

Through the mean value of the ratio of the local reachable density of p to the local reachable density of its nearest k neighbors, the local outlier factor of p is defined as

$$LOF_k(p) = \frac{\sum_{o\in N_k(p)} Lrd_k(o)/Lrd_k(p)}{|N_k(p)|}. \tag{3}$$

The idea behind LOF algorithm is to calculate outliers by drawing a circle centered on any but specific data point p, so that at least k data points are in the circle, and see how dense the neighborhood around p is [33].

A feature of the data generated by the IoT sensors is that due to the observed changes in the nature of the phenomenon, the data distribution may change in the network life cycle, and the anomaly detection technology must be able to adapt to the nonstationary data distribution to achieve the best performance [37]. To this end, the time series approach is applied in our proposed method.

As mentioned earlier, instead of directly using traditional time series methods, Chebyshev polynomials are applied here as a lightweight method for approximating the time series especially in comparing the similarity of two time series, in which it is not necessary to calculate all polynomials, and the similarity can be observed by comparing the related Chebyshev coefficients [38]. In [39], let $P_m(t)$ be a polynomial of t with degree m and $P_m(t) = cos(mcos^{-1}(t))$, where $t \in [-1, 1]$. Because of $cosm\theta + cos(m-2)\theta = 2cos\theta cos(m-1)\theta$, $P_m(t) = cos(mcos^{-1}(t))$ can be rewritten into a recurrence relation, i.e., $P_m(t) = 2tP_{m-1}(t) - P_{m-2}(t)$, where $m \geq 2$. Due to the characteristics of Chebyshev polynomials, for an arbitrary function $f(t)$, it can be approximated as $f(t) \approx c_0P_0 + c_1P_1 + \ldots + c_mP_m$, where $c_0, \ldots c_m$ denote the coefficients of Chebyshev polynomials. Further, according to the Gauss–Chebyshev formula [40], the coefficients are defined as

$$\begin{cases} c_0 = \frac{1}{m}\sum_{j=1}^{m} f(t_j)P_0(t_j) = \frac{1}{m}\sum_{j=1}^{m} f(t_j) & i = 0 \\ c_i = \frac{2}{m}\sum_{j=1}^{m} f(t_j)P_i(t_j) & 1 \le i \le m \end{cases}. \quad (4)$$

Equation (4) is only applicable to interval functions and cannot be directly applied to the time series of coefficient calculation. Discrete sequences need to be extended to interval functions. Assume $T = \{(t_1, v_1), \ldots, (t_N, v_N)\}$ is a time series where $-1 \le t_1 < \ldots < t_N \le 1$ and time t is normalized in $[-1, 1]$ resulting in the division of interval $[-1, 1]$ into N disjoint subintervals as follows [39].

$$I_i = \begin{cases} \left[-1, \frac{t_1 + t_2}{2}\right] & if\ i = 1 \\ \left[\frac{t_{i-1} + t_i}{2}, \frac{t_i + t_{i+1}}{2}\right] & if\ 2 \le i \le N-1 \\ \left[\frac{t_{N-1} + t_N}{2}, 1\right] & if\ i = N \end{cases}. \quad (5)$$

Map v_i into an interval function denoted by $g(t) = v_i$ where $t \in I_i$ $1 \le i \le N$. Being extended into an interval function, the time series is defined by

$$f'(t) = \frac{g(t)}{\sqrt{w(t)|I_i|}}, \quad (6)$$

where $t \in I_i$, $1 \le i \le N$, $|I_i|$ is the length of subinterval I_i, and $w(t)$ is the weight function defined as $w(t) = 1/\sqrt{1-t^2}$[39]. The Chebyshev coefficients of time series are now calculated as follows, and the details of the above calculation steps can be referred to [39].

$$\begin{cases} c_0 = \frac{1}{N}\sum_{j=1}^{N} f'(t_j)P_0(t_j) = \frac{1}{N}\sum_{j=1}^{N} f(t_j) & i = 0 \\ c_i = \frac{2}{N}\sum_{j=1}^{N} f'(t_j)P_i(t_j) & 1 \le i \le N \end{cases}. \quad (7)$$

4. Simulations

An IoT sensor cluster is formed to sense the oxygen content of a certain workshop. The oxygen content in an ordinary workshop environment shall be 18%~21%, or else ventilation measures shall be taken if it is not within this range. Each sensor forwards related data to a base station (BS). The cluster consists of 80 nodes, of which 20 are malicious nodes and 60 are normal nodes. Assume that normal sensor nodes correctly sense and forward the data, while malicious nodes selectively falsify or modify the normal oxygen content data into the range rather than 18% ~ 21% so as to damage the system. Besides, several other assumptions are also made: (1) all nodes form a star topology and are evenly distributed in a circular area centered on a base station; (2) each node has a unique ID, and the header of each packet includes source node ID, packet group length, and packet sequence number; (3) sensor nodes have 1% communication error and the direct communication between each sensor node and the base station is also assumed.

The base station regularly sends oxygen content requests to the sensor nodes in the network. When a request ends, the BS node firstly uses the LOF algorithm to analyze the data received from the network, checks the abnormal data, and labels its corresponding sender nodes as suspected ones. Secondly, the time series method is used to track and analyze the suspected nodes with regard to their subsequent data in the following requests. When the analysis result is greater than the given threshold, these nodes are confirmed to be malicious. Then, the BS will not accept the data from these malicious nodes any more.

Suppose d_i and d_j are two data time series, and let c_{d_i} and c_{d_j} be the corresponding vectors of Chebyshev coefficients with $c_{d_i} = [x_0, \ldots, x_m]$ and $c_{d_j} = [y_0, \ldots, y_m]$. By comparing the corresponding Chebyshev coefficients, the similarity of the two time series can be obtained. In consideration of computing simplicity and node energy saving, the Euclidean distance is applied here and it is defined as

$$Dist\left(c_{d_i}, c_{d_j}\right) = \sqrt{\frac{\pi}{2}\sum_{k=0}^{m}(x_k - y_k)^2}. \quad (8)$$

A threshold μ is set in this method for measuring the distance, e.g., if $Di\ st(c_{d_i}, c_{d_j}) \ge \mu$ is established, it indicates that the result of time series comparison is abnormal, and the related sensor node is considered malicious and should be isolated from the network.

In Figures 1–3, we test the normal data rate, or NDR. NDR is the ratio of the amount of normal data received to the amount of normal data the base station should receive. m is the number of Chebyshev coefficients and μ is the threshold for similarity calculation. len represents the length of the time series, making it equal to a certain number of queries initiated by the BS in the different tests. We divide the simulations into three groups to test the influence of these three parameters on NDR, respectively.

In Figure 1, as the number of base station queries increases, the NDR values of the three sets of comparison parameters continue to increase, among which ($m = 4$, $\mu = 0.9$, len = 10) is the fastest followed by both ($m = 3$, $\mu = 0.9$, len = 10) and ($m = 2$, $\mu = 0.9$, len = 10), which are relatively the slowest. For example, for the 100th query, the NDR values of the three groups are about 0.85, 0.84, and 0.82, respectively. This is because the time series and related similarity computations help to expand the anomalous patterns of anomaly nodes and identify them efficiently. It can also be noticed in Figure 1 that different coefficients have different effects on NDR. For example, the NDR at $m = 4$ is significantly higher than that at $m = 2$. But the increase of m means that more coefficients are needed which will definitely make the calculation more complicated. It can be seen that

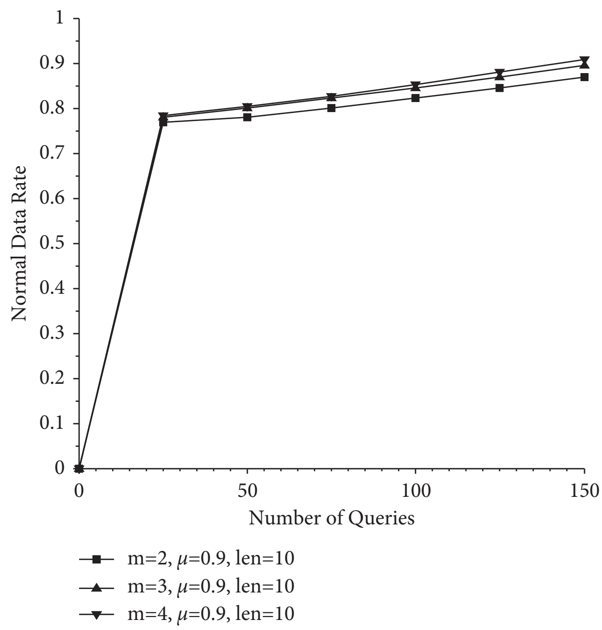

Figure 1: Normal data rate ($m = 2/3/4$, $\mu = 0.9$, len = 10).

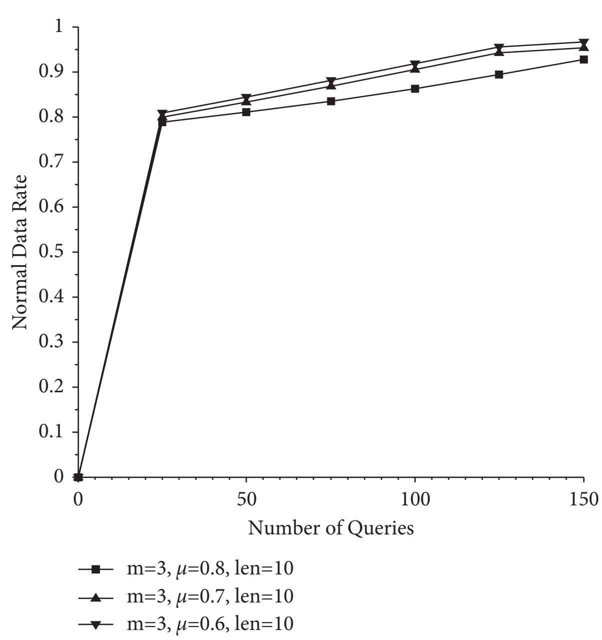

Figure 2: Normal data rate ($m = 3$, $\mu = 0.8/0.7/0.6$, len = 10).

the NDR at $m = 4$ is similar to the NDR at $m = 3$. Therefore, this study recommends $m = 3$.

To make the similarity calculation more strict, different thresholds μ are set in Figure 2. As is shown in the test, more anomaly nodes are being identified, resulting in higher NDR. For instance, for the 100th query, the NDR values of the three groups are about 0.91, 0.90, and 0.86, respectively. Note that μ should be appropriately reduced; otherwise, normal nodes will be misjudged as anomaly nodes. This is because normal nodes cannot guarantee 100% trouble-free operation in the event of a communication error or even a dead battery. As can be seen from Figure 2, the difference between

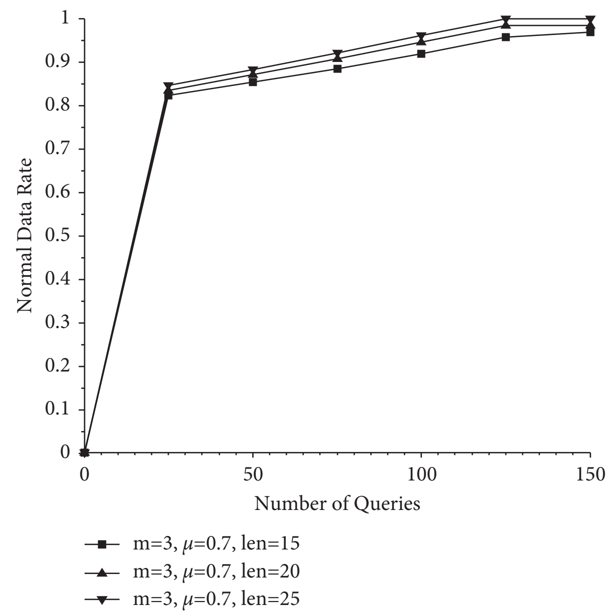

Figure 3: Normal data rate ($m = 3$, $\mu = 0.7$, len = 15/20/25).

the NDR at $\mu = 0.7$ and NDR at $\mu = 0.6$ is small, so $\mu = 0.7$ is recommended. Similar test result trends can also be seen in Figure 3, where different len values are set. For example, still for the 100th query, the NDR with len = 25 is around 0.96 and is much higher than the others. Higher len values indicate larger time windows and the higher the len value is, the better the NDR effect becomes. However, the increase of len will also increase the complexity of calculation, so it should be chosen wisely.

5. Conclusions

The data quality collected by sensor nodes is affected by anomalies like abnormal events and malicious attacks, and when the anomaly datasets enter the system, the overall system performance would be affected making the system unreliable. Therefore, anomaly detection is a necessary process to ensure the quality of sensor data before it is used for analysis and decision making. In the field of Internet of Things, anomaly detection is an ongoing research field aiming to provide protection against abnormal sensor readings. In addition, due to its low price and commercial attraction, security has not been given much priority. Therefore, it is necessary to protect Internet of Things devices and smart homes from potentially destructive abnormal data and related source sensor nodes.

Data Availability

The data used to support the findings of this study are available from the corresponding author upon request.

Conflicts of Interest

The authors declare that there are no conflicts of interest regarding the publication of this paper.

Acknowledgments

The authors would like to express their gratitude to the Civil Aviation Information Technology Research Center of CAFUC for the support and help. This study was partially supported by the Scientific Project of CAFUC under grant nos. JG2022-06 and J2022-042, the Central University Teaching Reform Project under grant nos. E2020044 and E2021038, Civil Aviation Professional Project under grant nos. 0252109 and MHJY2022038, and the Sichuan Science and Technology Program under grant nos. 2022YFG0190 and 2022JDR0116.

References

[1] Y. Wang, L. Sun, and S. Subramani, "CAB: classifying arrhythmias based on imbalanced sensor data," *KSII Transactions on Internet & Information Systems*, vol. 15, no. 7, pp. 2304–2320, 2021.
[2] L. Sun, Q. Yu, D. Peng, S. Subramani, and X. Wang, "Fogmed: a fog-based framework for disease prognosis based medical sensor data streams," *Computers, Materials & Continua*, vol. 66, no. 1, pp. 603–619, 2020.
[3] L. Sun, Y. Wang, Z. Qu, and N. N. Xiong, "BeatClass: A Sustainable ECG Classification System in IoT-Based eHealth," *IEEE Internet of Things Journal*, vol. 9, 2021.
[4] A. K. Pathak, S. Saguna, K. Mitra, and C. Åhlund, "Anomaly Detection Using Machine Learning to Discover Sensor Tampering in IoT Systems," in *Proceedings of the ICC 2021 - IEEE International Conference on Communications*, pp. 1–6, Montreal, QC, USA, June 2021.
[5] E. Borgia, "The Internet of things vision: key features, applications and open issues," *Computer Communications*, vol. 54, pp. 1–31, 2014.
[6] I. Alrashdi, A. Alqazzaz, E. Aloufi, R. Alharthi, M. Zohdy, and H. Ming, "AD-IoT: anomaly detection of IoT cyberattacks in smart city using machine learning," ", in *Proceedings of the IEEE 9th Annual Computing and Communication Workshop and Conference*, pp. 305–310, Las Vegas, NV, USA, January 2019.
[7] M. Wu, L. Tan, and N. Xiong, "A structure fidelity approach for big data collection in wireless sensor networks," *Sensors*, vol. 15, no. 1, pp. 248–273, 2014.
[8] S. Huang, A. Liu, S. Zhang, T. Wang, and N. N. Xiong, "BD-VTE: a novel baseline data based verifiable trust evaluation scheme for smart network systems," *IEEE Transactions on Network Science and Engineering*, vol. 8, 2020.
[9] D. K. K. Reddy, H. S. Behera, G. M. S. Pratyusha, and R. Karri, "Ensemble bagging approach for IoT sensor based anomaly detection," *Lecture Notes in Electrical Engineering*, vol. 702, pp. 647–665, 2021.
[10] R. Yasaei, F. Hernandez, and M. A. A. Faruque, "IoT-CAD," *Proceedings of the 39th International Conference on Computer-Aided Design*, vol. 9, pp. 1–9, 2020.
[11] X. Yang, Y. Chen, X. Qian, T. Li, and X. Lv, "BCEAD: a blockchain-empowered ensemble anomaly detection for wireless sensor network via isolation forest," *Security and Communication Networks*, vol. 2021, pp. 1–10, Article ID 9430132, 2021.
[12] F. Restuccia and S. T. D'Oro, "Securing the Internet of things in the age of machine learning and software-defined networking," *IEEE Internet of Things Journal*, vol. 5, no. 6, pp. 4829–4842, 2018.
[13] J. Kim, Y. W. Cho, and D. Kim, "Anomaly detection of environmental sensor data using recurrent neural network at the edge device," in *Proceedings of the International Conference on Information and Communication Technology Convergence*, pp. 1624–1628, ICTC), Jeju, Korea (South), October 2020.
[14] S. Sadik and L. Gruenwald, "Online outlier detection for data streams," in *Proceedings of the IDEAS 2011 Proceedings of the 15th Symposium on International Database Engineering & Applications*, pp. 88–96, Barcelona, Spain, December 2011.
[15] K. Haseeb and N. M. Q. O. E. K. N. W. T. Abbas, "RCER: reliable cluster-based energy-aware routing protocol for heterogeneous wireless sensor networks," *PLoS One*, vol. 14, no. 9, pp. e0222009–24, 2019.
[16] Z. Chen, H. Wu, H. Zhu, and Y. Miao, "Distributed anomaly detection method in wireless sensor networks based on temporal-spatial QSSVM," *Advances in Intelligent Systems and Computing*, vol. 905, pp. 934–943, 2020.
[17] E. Hodo and X. A. P.-L. E. C. R. Bellekens, "Threat analysis of IoT networks using artificial neural network intrusion detection system," *2016 International Symposium on Networks, Computers and Communications (ISNCC)*, in *Proceedings of the 2016 2016 International Symposium on Networks, Computers and Communications (ISNCC)*, pp. 1–6, Yasmine Hammamet, Tunisia, May 2016.
[18] T. Fernando and H. S. S. C. Gammulle, "Deep learning for medical anomaly detection - a survey," *ACM Computing Surveys*, vol. 54, no. 7, pp. 1–37, 2022.
[19] M. H. Bhuyan, D. K. Bhattacharyya, and J. K. Kalita, "Network anomaly detection: methods, systems and tools," *IEEE Communications Surveys & Tutorials*, vol. 16, no. 1, pp. 303–336, 2014.
[20] D. Ramotsoela, A. Abu-Mahfouz, and G. Hancke, "A survey of anomaly detection in industrial wireless sensor networks with critical water system infrastructure as a case study," *Sensors*, vol. 18, no. 8, pp. 2491–2524, 2018.
[21] D. Widhalm, K. M. Goeschka, W. Kastner, and SoK, "A taxonomy for anomaly detection in wireless sensor networks focused on node-level techniques," *Proceedings of the 15th International Conference on Availability, Reliability and Security*, vol. 17, pp. 1–10, 2020.
[22] M. Rassam, A. Zainal, and M. Maarof, "Advancements of data anomaly detection research in wireless sensor networks: a survey and open issues," *Sensors*, vol. 13, no. 8, pp. 10087–10122, 2013.
[23] V. Chandola, A. Banerjee, and V. Kumar, "Anomaly detection," *ACM Computing Surveys*, vol. 41, no. 3, pp. 1–58, 2009.
[24] A. A. Elngar and S. Bhatt, "IoT-based efficient tamper detection mechanism for healthcare application," *IJ Network Security*, vol. 20, no. 3, pp. 489–495, 2018.
[25] R. K. Shrivastava, S. Mishra, V. E. Archana, and C. Hota, "Preventing data tampering in IoT networks," in *Proceedings of the IEEE International Conference on Advanced Networks and Telecommunications Systems*, pp. 1–6, Goa, India, December 2019.
[26] A. A. Vasily, V. Desnitsky, I. Kotenko, E. Novikova, and A. Shulepov, "Combined approach to anomaly detection inWireless sensor networks on example of water management system," in *Proceedings of the 10th Mediterranean Conference on Embedded Computing*, pp. 7–10, Budva, Montenegro, June 2021.
[27] L. Breiman, "Bagging predictors," *Machine Learning*, vol. 24, no. 2, pp. 123–140, 1996.
[28] T. Das, R. M. ShuklaT, and S. Sengupta, "Imposters among us: a supervised learning approach to anomaly detection in IoT

sensor data," in *Proceedings of the IEEE 7th World Forum on Internet of Things*, pp. 818–823, New Orleans, LA, USA, July 2021.

[29] P. R. Winters, "Forecasting sales by exponentially weighted moving averages," *Management Science*, vol. 6, no. 3, pp. 324–342, 1960.

[30] K. Christidis and M. Devetsikiotis, "Blockchains and smart contracts for the Internet of things," *IEEE Access*, vol. 4, pp. 2292–2303, 2016.

[31] M. Ahmed, A. Naser Mahmood, and J. Hu, "A survey of network anomaly detection techniques," *Journal of Network and Computer Applications*, vol. 60, pp. 19–31, 2016.

[32] A. Gaddam, T. Wilkin, and M. Angelova, "Anomaly detection models for detecting sensor faults and outliers in the IoT - a survey," *2019 13th International Conference on Sensing Technology (ICST)*, in *Proceedings of the 2019 13th International Conference on Sensing Technology (ICST)*, pp. 1–6, Sydney, NSW, Australia, December 2019.

[33] D. McDonald and S. S. F. Sanchez, "A survey of methods for finding outliers in wireless sensor networks," *Journal of Network and Systems Management*, vol. 23, no. 1, pp. 163–182, 2015.

[34] Z. Gan and X. Zhou, "Abnormal network traffic detection based on improved LOF algorithm," *2018 10th International Conference on Intelligent Human-Machine Systems and Cybernetics (IHMSC)*, vol. 1, pp. 142–145, 2018.

[35] M. M. Breunig and H.-P. R. T. J. Kriegel, "Lof," *ACM SIGMOD Record*, vol. 29, no. 2, pp. 93–104, 2000.

[36] F. Wang, Z. Wei, and X. Zuo, "Anomaly IoT node detection based on local outlier factor and time series," *Computers, Materials & Continua*, vol. 64, no. 2, pp. 1063–1073, 2020.

[37] C. OReilly, A. Gluhak, M. A. Imran, and S. Rajasegarar, "Anomaly detection in wireless sensor networks in a non-stationary environment," *IEEE Communications Surveys & Tutorials*, vol. 16, no. 3, pp. 1413–1432, 2014.

[38] F. Wang and Z. Wei, "A statistical trust for detecting malicious nodes in IoT sensor networks," *IEICE - Transactions on Fundamentals of Electronics, Communications and Computer Sciences*, vol. E104.A, no. 8, pp. 1084–1087, 2021.

[39] Y. Cai and R. Ng, "Indexing spatio-temporal trajectories with Chebyshev polynomials," *Proceedings of the 2004 ACM SIGMOD international conference on Management of data - SIGMOD '04"*, in *Proceedings of the 2004 ACM SIGMOD international conference on Management of data - SIGMOD '04*, pp. 599–610, Paris, France, June 2004.

[40] J. C. Mason and D. Handscomb, *Chebyshev Polynomials"*, Chapman & Hall, 2003.

Hindawi
Scientific Programming
Volume 2023, Article ID 9763951, 1 page
https://doi.org/10.1155/2023/9763951

Retraction

Retracted: Design of a Panoramic Virtual Dynamic Display System for Digital Museums Based on Visual Interaction Technology

Scientific Programming

Received 1 August 2023; Accepted 1 August 2023; Published 2 August 2023

This article has been retracted by Hindawi following an investigation undertaken by the publisher [1]. This investigation has uncovered evidence of one or more of the following indicators of systematic manipulation of the publication process:

(1) Discrepancies in scope
(2) Discrepancies in the description of the research reported
(3) Discrepancies between the availability of data and the research described
(4) Inappropriate citations
(5) Incoherent, meaningless and/or irrelevant content included in the article
(6) Peer-review manipulation

The presence of these indicators undermines our confidence in the integrity of the article's content and we cannot, therefore, vouch for its reliability. Please note that this notice is intended solely to alert readers that the content of this article is unreliable. We have not investigated whether authors were aware of or involved in the systematic manipulation of the publication process.

Wiley and Hindawi regrets that the usual quality checks did not identify these issues before publication and have since put additional measures in place to safeguard research integrity.

We wish to credit our own Research Integrity and Research Publishing teams and anonymous and named external researchers and research integrity experts for contributing to this investigation.

The corresponding author, as the representative of all authors, has been given the opportunity to register their agreement or disagreement to this retraction. We have kept a record of any response received.

References

[1] J. Wang, "Design of a Panoramic Virtual Dynamic Display System for Digital Museums Based on Visual Interaction Technology," *Scientific Programming*, vol. 2022, Article ID 1626448, 7 pages, 2022.

Hindawi
Scientific Programming
Volume 2022, Article ID 1626448, 7 pages
https://doi.org/10.1155/2022/1626448

Research Article

Design of a Panoramic Virtual Dynamic Display System for Digital Museums Based on Visual Interaction Technology

Jing Wang

Shanxi Vocational University of Engineering Science and Technology, College of Art and Design, Shanxi 030012, China

Correspondence should be addressed to Jing Wang; wangjing@sxgkd.edu.cn

Received 6 January 2022; Accepted 2 March 2022; Published 21 April 2022

Academic Editor: Le Sun

To address the spatial and temporal limitations of historical museums, a panoramic virtual dynamic display system for digital museums is designed using visual interactive technology. The VM file is generated by using the Digital Museum Design module to obtain a list of available objects, and the VM file is analysed by the Digital Museum View module to stretch and change the two-dimensional flat map into a three-dimensional spatial map for viewers to browse. The system software designs the technical construction process of the digital museum, uses a linearisation algorithm to calculate the number of clicks, visualises the font according to the number of clicks reflecting the weights, and builds a tag cloud component to provide interactive services to facilitate efficient understanding of the museum information by the viewer.

1. Introduction

When browsing through museums, people are constrained by the conditions and time available to view ancient artefacts up close and for long periods of time. To address the spatial and temporal limitations of historical museums[1], digital museums have emerged. The definition of a digital museum is narrowly defined as the reproduction of museum exhibits through digital technology, and broadly defined as a virtual representation of the real world that exists only within the network [2]. As an integrated result of technological applications combined with artistic displays, the digital museum has one of the most important characteristics—interactivity [3]—which determines whether the visitor can have a high-quality visual interactive experience during the visit [4].

The rapid development of technology has led to the maturation of multimedia and VR technologies, and interaction technologies have now evolved from static two-dimensional interfaces to multidimensional information spaces [5], with the basis for this leap forward being research and design for multilevel, dynamic user behaviour in virtual environments. Therefore, the design of a panoramic virtual dynamic display system for digital museums based on visual interaction technology will facilitate visitors to access and understand museum information more efficiently [6–10].

Virtual reality combined with architectural sketch models allows the imagination to be realised and the spatial experience to be experienced from a human perspective, changing the building form and the relationship with the site at any time according to the actual spatial experience [11]. The change in spatial perception brought about by the change of form can be experienced at any time, and the ambiguity and coherence of the design will not be interrupted, while the digital graphic representation is at the same time precise and easy to adjust later [12].

2. The Advantages of Combining Virtual Reality with Architecture

2.1. Moving Away from the Traditional Linear Design Process. Most designers today still prefer sketching in the early stages of architectural design [13, 14]. Sketching is an interactive process of visual design thinking, where the architect's design concept and imagination are clues to the meaning of the sketch, while this abstract graphic medium triggers the architect's imagination. However, the vagueness of the sketch design often makes the building shape limited by the site a large gap from the imagination, and the pre-construction design is often we always want a "so big" building, rather than a building with precise volume. The current predesign process is often a combination of sketching and sketching of moulds to find the most suitable solution [15].

It is a process of discussing the relationship between space and space, between building and site. This process is often a compromise between imagination and actual scale, between sensibility and rationality [16]. In this case, sketches or sketches are often inappropriate in terms of their actual size, or in other words, they are only good for looking at, but not for using [17].

2.2. Immersive Experience Architecture. In conducting architectural design often through the designer's perspective of a bird's eye view or master plan, few designers are able to tour the space from the user's or visitor's perspective, which is largely limited by the designer's imagination and spatial perception [18]. Through virtual reality labs, designers can refine their architectural proposals through 3D visualisation, interactive controls and group discussions. This method of learning provides a vivid learning journey that allows designers to understand their knowledge better than if they were instructed or lectured individually by a teacher, who can ask designers to tour their own spaces as users and experience the differences between different design perspectives [16]. It is often easy for junior designers to design a building in such a way that the connection between the plan and the façade is severed or only one of the two is emphasised, often resulting in windows that are well designed on the façade but do not work well from an internal user perspective, or even dark room for the sake of the façade. Often the window arrangement on the façade is completely different from what was thought of in the earlier plan design. Students often prefer to follow the OMA (Figure 1) approach of a spatial structure + curtain wall, using floor-to-ceiling windows or simply not opening them on the façade, but rarely do they consider the impact of windows on the perception of space and changes in light and shade in the interior, because the existing teaching and architectural presentation is not sufficient to express the changes in light and shade that windows bring to the interior [19]. Virtual reality combined with architectural education brings more new design ideas than traditional teaching, such as design from the perspective of window openings and interior light and shade or comfort of use.

2.3. Assisting Designers with a Sense of Scale. By combining virtual reality software with modeling software such as Sketch up and Rhino to create virtual reality scenes, designers can experience the spatial layout, flow and building materials of an architectural design in an 'immersion' way, changing the traditional situation of using only photographic materials and drawings to describe the interior and exterior of a building. It facilitates the designer's understanding of the architectural space [20]. The difficulty of translating the physical dimensions of a building space into a physical perception is

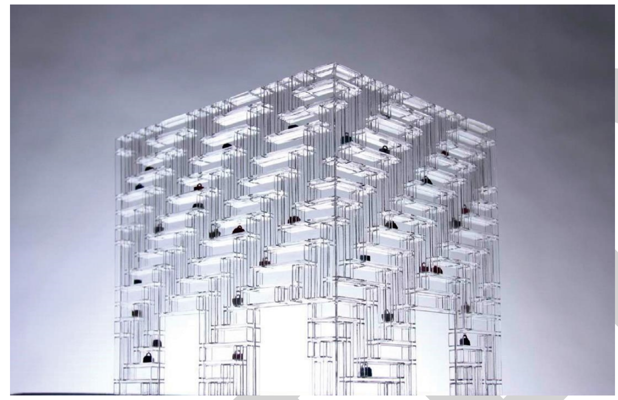

Figure 1: Spatialised structure of the OMA Shenzhen Stock Exchange Building headquarters + curtain wall design approach.

addressed. Virtual reality can be an alternative when site visits are costly and difficult to arrange due to health and safety issues. The combination of virtual reality experience of different architectural space and lectures by teachers can better assist designers in understanding space and scale. Building setbacks, safe evacuation distances and other codes are no longer cold numbers for designers, and virtual reality can be used to simulate space that does not meet the code requirements in order to experience their shortcomings and reinforce designers' knowledge of the code requirements [20].

2.4. Emphasis on Building Structure and Construction Techniques. Currently many designers do not consider their designs from a construction point of view, nor from a practical use point of view, and the building design is often just an empty box, with sections only looking for the simplest and best drawn sections, symbolically expressing the position of beams, slabs and columns [21]. The traditional teaching system allows designers to understand the construction of buildings only through classroom lectures and pictures. The combination of virtual reality software and BIM models allows for a realistic teaching model, showing designers the animation of the building assembly process and combining theory with practice. Most designers only consider which materials or colours to use in general, but few consider the size or modulus of the specific materials to be used. Virtual reality allows designers to experience the texture and effect of the material from a human point of view, improving the details of the building [22].

3. Digital Museum Dynamic Panoramic Virtual Display System

3.1. Overall Structural Design. The Digital Museum Dynamic Panorama virtual display system consists of a viewer and object database management module, a digital museum design module and a digital museum viewing module, see Figure 2.

In Figure 2, the main function of the viewer and the object database management module is to correct, add and delete objects in the MySQL database and FTP server; the main function of the digital museum design module is to

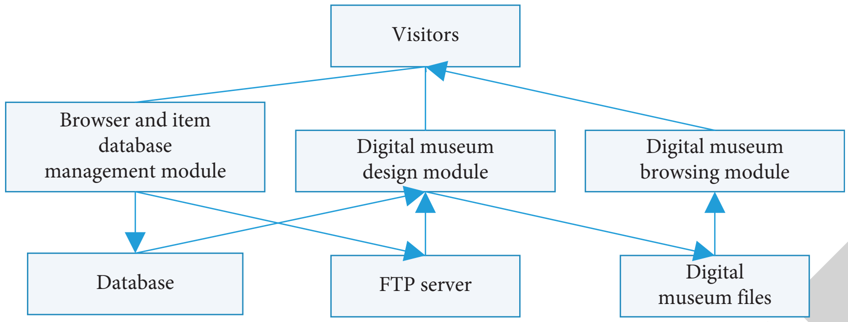

Figure 2: Architectural framework of the digital museum dynamic panoramic virtual display system.

access the information of the objects for viewing, download the information from the MySQL database and FTP server to the local area, and the viewer sets up the two-dimensional floor plan of the digital museum according to their needs. The viewer sets up a 2D floor plan of the digital museum according to their needs and then builds a VM model file [23]; the digital museum viewer module analyses the VM model file and displays a dynamic panorama of the digital museum that has been built.

3.2. Digital Museum Design Module. The digital museum design module ensures that the viewer is provided with a list of objects available in the database according to the viewer level after successfully logging into system. A 2D plan of the digital museum is generated in the drawing board and images are selected from the local plan as textures for the different areas of the digital museum. The objects listed in the object information list are placed in the 2D plane of the digital museum display system and a VM file is generated, as shown in Figure 3.

The information stored in the VM file includes: the number of vertices and the location of the different vertices in the 2D plan of the digitised museum; the number of objects, their IDs and their locations in the digitised museum; and the initial position of the viewer set in this module.

3.3. Digital Museum Navigation Module. The main function of the digital museum viewer module is to analyse the VM file in the digital museum design module, stretch and change the 2D plan view in the digital museum design module into a 3D spatial view [24], and provide the viewer with the viewer, as shown in Figure 4.

The VM file containing information about the digital museum is accessed through the Digital Museum Design module, and the VM file is opened through the Digital Museum Browser module to access the information contained in the digital museum. Within the digital museum display system, the viewer is able to roam through the VM file using the keyboard [25].

3.4. Software Design

3.4.1. Digital Museum Technology Building Process Design. The need of the viewer is fundamental to a digital museum display system. In order to meet the needs of the viewer, the

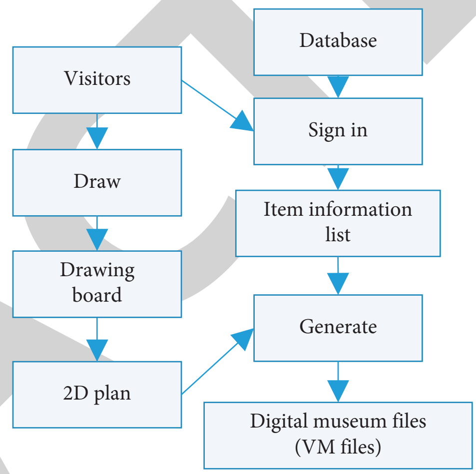

Figure 3: Digital museum design module.

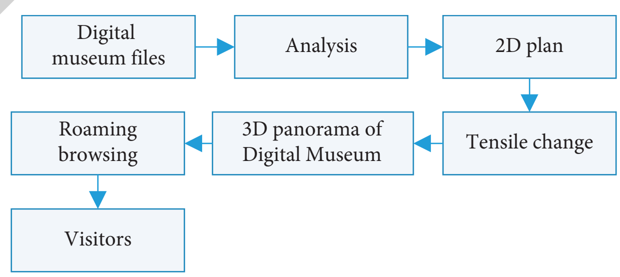

Figure 4: Design of the digital museum browsing module.

technical construction process of the digital museum is based on display design, human interaction theory and visualisation techniques, as shown in Figure 5.

Theme identification and requirements analysis phase focuses on a comprehensive analysis of the theme of the digital museum display system. The need and feasibility of the theme is studied, and the system structure is comprehensively planned based on the theme, while the ultimate functions and objectives of the digital museum are defined. The overall architecture design phase is based on the results of the previous analysis and defines the overall framework for the scenarios, presentation methods and functional objectives of the digital museum. The 3D modeling software is used to construct the planned museum scene and the required models, set the lighting and materials and other performance effects, and obtain a realistic browsing experience. The

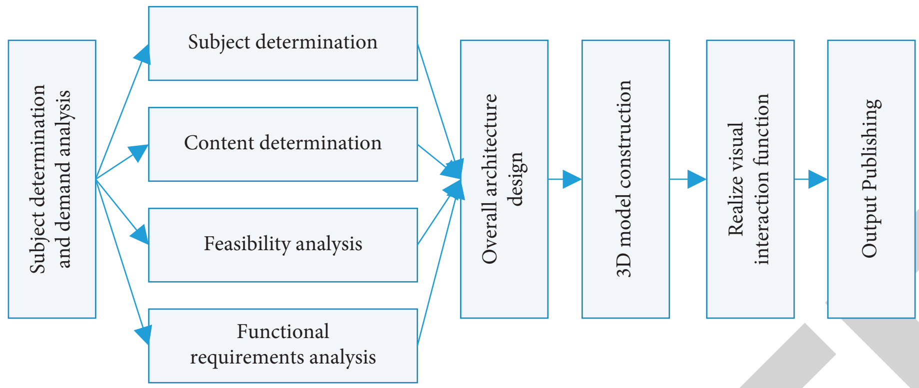

FIGURE 5: Digital museum technology building process.

interactive visualisation phase imports the completed museum scene and model into the interactive visualisation software and optimises it for high-quality interactive visualisation. Once the visualisation has been implemented, the museum visualisation is exported as a web page or an executable file and published on the corresponding website [1].

3.4.2. Tag Cloud Component Design. A collection of weighted tags, known as a tag cloud, reflects the differences in tag weight based on differential fonts and other visualisation, and viewers use tags to connect to relevant information. The tag cloud component is used in the display system, where tags are constructed by viewers and experts, and the topics and categories of information are presented through tags, which are used by viewers to obtain information related to the topic. The font size in the tag cloud component is based on tag weight. The number of tag visits describes the tag weight and the difference in font size reflects the information that is more frequently viewed.

The Tag Bean Java class, which stores information such as tag name, builds time and tag link, stores the tag topics and their corresponding Tag Bean objects in a HashMap, data type included in Java. The core of the Tag Cloud component is how to scientifically map the number of tag clicks to the differences in tag fonts. The number of clicks on all tags in the database is unevenly distributed, similar to a normal distribution. The system uses a linearisation algorithm to calculate the number of clicks in order to distribute the number of user clicks evenly across the foot variance interval, as follows :

$$E = \sqrt{\sum_{i=1,2,\ldots,m} \frac{\left(\mathrm{hitNum}_i - \mathrm{meanNum}\right)^2}{m}}, \tag{1}$$

$$W = \frac{\mathrm{maxSize} - \mathrm{minSize}}{4E}, \tag{2}$$

$$\mathrm{FontSize}_i = W\left(\mathrm{hitNum}_i - \mathrm{meanNum}\right) + \mathrm{midSize}, \tag{3}$$

where: E, W and $\mathrm{FontSize}_i$ are the average difference in label clicks, linear slope and label i font variance, respectively;, and meanNum are the number of clicks on label i, the total number of labels in the database and the average of all label clicks, respectively; maxSize, minSize and midSize are the maximum value of the label font variance interval, the minimum value of the label font variance interval and the middle value of the font variance, respectively and the middle value of the font difference.

The first step in the calculation process is to determine the E of the total number of tag clicks; the deviation error of the total number of tag clicks is obtained by aggregation from -2E to 2E, and W is determined by equation (3); on this basis, the font difference value of tag i is determined using the values of meanNum and midSize, etc.

4. Experimental Analysis

4.1. Virtual Display Effects. The results of the virtual display of the digital museum in Figure 6 show that the system is able to effectively display the digital museum exhibition hall and the exterior of the digital museum.

4.2. Practicality. The results of the questionnaire survey were analysed in Figures 7 and 8 to verify the practicality of the system. The results of the questionnaire survey are shown in Figures 7 and 8. Based on these advantages, designers and science, education, culture and health stakeholders are more likely to use the digital museum display system to browse and learn about museums, while institutions and enterprises are less likely to prefer digital museums to physical museums due to the constraints. The above findings suggest that the digital museum virtual display system designed in this paper has a high degree of practicality [26, 27].

4.3. VR Technology Combined with Architectural Design. The virtual reality facility is designed to be used by groups of 30 participants and allows teachers and designers to view designs from multiple perspectives in a three-dimensional format and to navigate through the virtual space in real time. The semi-immersive virtual reality lab includes several workstations for designers and teachers dedicated to 3D modeling and visualisation. 2–3 sets of virtual roaming headsets, screen for display and projection equipment. The designers work in groups to experience the virtual roaming

Figure 6: Results of the dynamic panoramic virtual presentation of the digital museum.

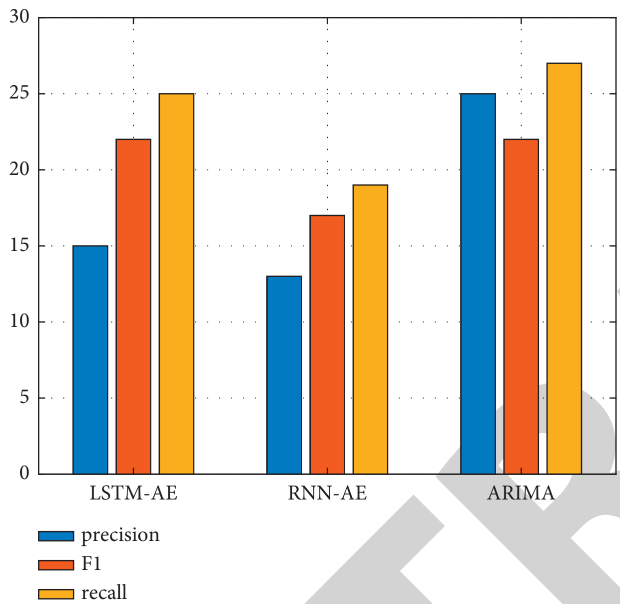

Figure 7: Points of interest for visiting the virtual display system of the digital museum in this paper.

experience with each other, discussing the advantages and disadvantages of each other's solutions, and the teachers provide guidance in relation to the virtual roaming experience, as showed in Figure 9.

The design drawings should be carefully drawn, accurately expressing the design intention, and drawn in AutoCAD or Tianzheng, with the depth of drawing meeting the requirements of the national architectural scheme design depth, minimising errors and expressing the scheme correctly and vividly according to the requirements of the assignment. The colour and composition of the drawings and the methods of expression should be finalised. Stage 5: Finishing stage: Production of results, modeling of the results, submission of all results, an evaluation of drawings, selection of outstanding design works through software to create virtual reality scenes, evaluation of architectural design from a three-dimensional perspective. Designers team up to roam around each other to experience the architectural scheme, and the teacher gives comments or modifications in conjunction with the roaming experience, the effect of which is shown in Figure 10.

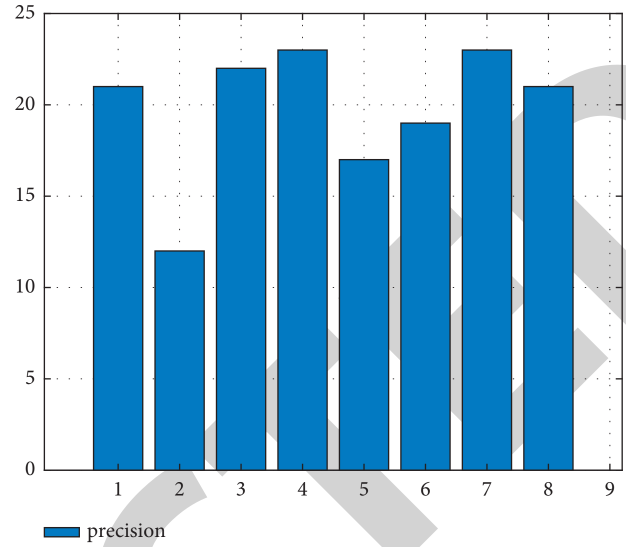

Figure 8: Changes in museum staff turnover.

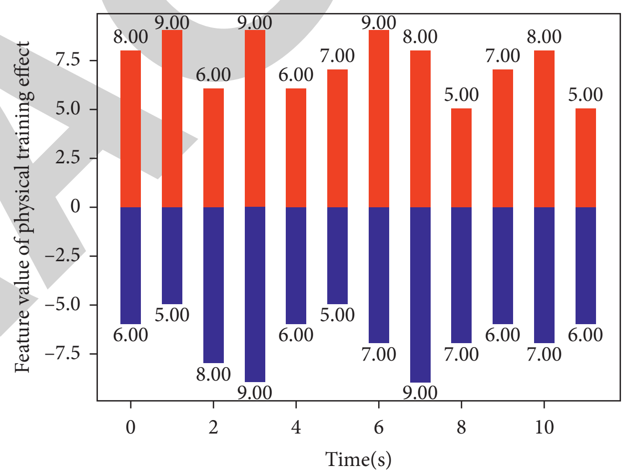

Figure 9: Different experience effects.

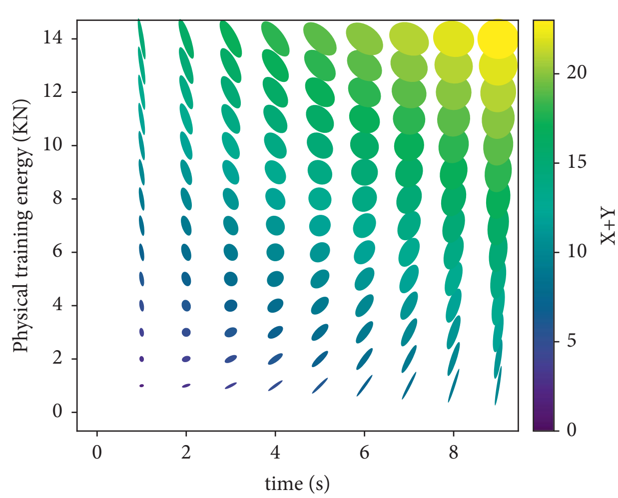

Figure 10: Effect of different roaming designs.

5. Conclusions

This paper builds a panoramic virtual dynamic display system for digital museums based on visual interaction technology, which is implemented through the viewer and object database management module, the digital museum design module and the digital museum browsing module.The results show that the system can not only effectively display the museum panorama, but also has the advantages of comprehensive object information, technological innovation, autonomous operation, time saving and animation display compared to the physical museum, and can achieve a full-scale, efficient and high-precision virtual display.

Data Availability

The experimental data used to support the findings of this study are available from the corresponding author upon request.

Conflicts of Interest

The authors declared that they have no conflicts of interest regarding this work.

Acknowledgments

This project was supported by the Key project of Shanxi Provincial Federation of Social Sciences: Based on the ecological forest park platform to promote the collaborative development and management of urban and rural culture and art in Shanxi Province (SSKLZDKT2021126).

References

[1] R. G. Wang, H. L. Dong, and M. W. Wu, "Research and design of digital museum based on virtual reality," *Advanced Materials Research*, vol. 926-930, pp. 2516–2520, 2014.
[2] S. C. Kim and D. S. Kwon, "Haptic interaction with objects in a picture based on pose estimation," *Multimedia Tools and Applications*, vol. 72, no. 2, pp. 2041–2062, 2014.
[3] G. J. Kintz, "Autostereoscopic properties of spherical panoramic virtual displays," *Sid Symposium Digest of Technical Papers*, vol. 30, no. 1, pp. 1000–1003, 2012.
[4] S. Tsekeridou and I. Pitas, "Content-based video parsing and indexing based on audio-visual interaction," *IEEE Transactions on Circuits and Systems for Video Technology*, vol. 11, no. 4, p. 522, 2001.
[5] E. Kilinci, "AN analysis OF virtual museum WHICH provides 360 degree panoramic image IN terms OF graphich design," *The Turkish Online Journal of Design Art and Communication*, vol. 5, no. 4, pp. 57–65, 2015.
[6] Y. Xu, C. Yang, and J. Zhong, "Robot Teaching by Teleoperation Based on Visual Interaction and Extreme Learning Machine," *NEUROCOMPUTING*, 2017.
[7] C. K. Chui, J. Teo, Z. Wang et al., "Integrative haptic and visual interaction for simulation of PMMA injection during vertebroplasty," *Studies in Health Technology & Informatics*, vol. 119, pp. 96–98, 2006.
[8] P. W. Kwan, K. Kameyama, J. Gao, and T. Kazuo, "CONTENT-BASED image retrieval OF cultural heritage symbols BY interaction OF visual perspectives," *International Journal of Pattern Recognition and Artificial Intelligence*, vol. 25, no. 5, pp. 643–673, 2011.
[9] D. H. Jonathan, W. Reed, and K. Katsuko, "The effect of interactivity with a music video game on second language vocabulary recall," *Language, Learning and Technology*, vol. 14, no. 2, pp. 74–94, 2010.
[10] A. Jalalian, S. Chalup, and M. Ostwald, "Agent-agent interaction as a component of agent-environment interaction in the modelling and analysis of pedestrian visual behaviour[J]," *Technology and Health Care*, vol. 19, no. 6, pp. 391–400, 2011.
[11] J. M. Harp, P. A. Demkowicz, P. L. Winston, and S. James, "An analysis of nuclear fuel burnup in the AGR-1 TRISO fuel experiment using gamma spectrometry, mass spectrometry, and computational simulation techniques," *Nuclear Engineering and Design*, vol. 278, pp. 395–405, 2014.
[12] M. D. Tsai and M. S. Hsieh, "Accurate visual and haptic burring surgery simulation based on a volumetric model," *Journal of X-Ray Science and Technology*, vol. 18, no. 1, p. 69, 2010.
[13] H. Li, D. Zeng, L. Chen, Q. Chen, M. Wang, and C. Zhang, "Immune multipath reliable transmission with fault tolerance in wireless sensor networks," in *Proceedings of the International Conference on Bio-Inspired Computing: Theories and Applications*, pp. 513–517, Springer, Singapore, 2016.
[14] D. Zachary and R. Stan, "Online issue mapping of international news and information design," *Human It Tidskrift För Studier Av It Ur Ett Humanvetenskapligt Perspektiv*, vol. 8, no. 3, 2006.
[15] Y. Fangming, "Real-time construction of 3D welding torch in virtual space for welding training simulator," *International Journal of Engineering and Manufacturing*, vol. 9, no. 5, pp. 34–45, 2019.
[16] S. A. Xia, "Design and implementation of campus 3D virtual walkthrough system - take hunan science and technology university as an example," *Applied Mechanics and Materials*, vol. 268-270, pp. 1926–1929, 2013.
[17] L. Du, Z. Wang, L. Wang et al., "Adaptive visual interaction based multi-target future state prediction for autonomous driving vehicles," *IEEE Transactions on Vehicular Technology*, vol. 68, no. 5, pp. 4249–4261, 2019.
[18] H. Joo, "A study on the interaction types of interactive advertising based on the digital signage," *KOREA SCIENCE & ART FORUM*, vol. 14, pp. 271–284, 2013.
[19] N. Wang, J. Z. Zhao, and Y. Xue, "Design and implementation of electronic guide system for museums based on PDA," *Application Research of Computers*, vol. 24, no. 12, p. 291, 2007.
[20] C. H. Cao, Y. N. Tang, D. Y. Huang, G. WeiMin, and Z. Chunjiong, "IIBE: An improved identity-based encryption algorithm for wsn security," *Security and Communication Networks*, vol. 2021, Article ID 8527068, 8 pages, 2021.
[21] Y. Jiang, J. Hong, W. Wang, and Q. Jue, "Least squares method-based quantitative modeling on visual comfort for VDT display interface," *International Journal of Advanced Manufacturing Technology*, vol. 84, no. 1-4, pp. 381–391, 2016.
[22] L. H. M. D. Arruda, C. De, C. Silva, R. Attux, H. H. Hornung, and D. S. Arantes, "Analysis of user interaction with a brain-computer interface based on steady-state visually evoked potentials: case study of a game," *Computational Intelligence and Neuroscience*, vol. 2018, Article ID 4920132, 10 pages, 2018.
[23] D. C. Frezzo, J. T. Behrens, and R. J. Mislevy, "Design patterns for learning and assessment: facilitating the introduction of a complex simulation-based learning environment into a

Hindawi
Scientific Programming
Volume 2022, Article ID 9662374, 8 pages
https://doi.org/10.1155/2022/9662374

Research Article

Study on Temperature Sensor Data Anomaly Diagnosis Method Based on Deep Neural Network

Wei Jing, Peng Wang, and Ningchao Zhang

Department of Electronic Information Engineering, Xi'an Technological University, Xi'an 710021, China

Correspondence should be addressed to Ningchao Zhang; ningch@mls.sinanet.com

Received 13 January 2022; Accepted 22 March 2022; Published 12 April 2022

Academic Editor: Le Sun

In order to solve the problems of low accuracy and low efficiency of traditional sensor data anomaly diagnosis methods, a new temperature sensor data anomaly diagnosis method based on deep neural network is proposed in this paper. Firstly, the temperature sensor data in a running cycle is collected, and the characteristics of the temperature sensor data are extracted by the sliding window technology. Secondly, based on the feature extraction results, a deep neural network model for anomaly diagnosis of temperature sensor data is constructed. The feature data are input into the model, and the result obtained is the diagnosis result. Finally, the simulation comparison experiment is carried out. The experimental results show that the error rate of feature extraction of temperature sensor data in this method changes between −2.1% and 5.9%, the diagnosis accuracy remains above 95%, the average diagnosis time is only 59 ms, and the diagnosis efficiency is high.

1. Introduction

At present, the development speed of intelligent sensors is getting faster and faster. Therefore, temperature sensors have been transformed from traditional analog to digital and intelligent [1]. Temperature sensors mainly ensure the accuracy of temperature data collection through the cooperation of hardware and software, saving a lot of design and manufacturing costs, so they have been widely used in various social fields [2]. And temperature sensor with the support of hardware and software will be linked with various microprocessor temperature sensors, and the wireless network is used to transmit data to upload, or to the specified device, but once the sensor fails, it may result in abnormal temperature sensor data [3], so you need to diagnose abnormal temperature sensor data. Therefore, it is very important to design a temperature sensor data anomaly diagnosis method to judge the running state of intelligent sensors.

For the anomaly diagnosis of temperature sensor data, relatively good research results have emerged in related fields. For example, reference [4] proposed an anomaly diagnosis method of temperature sensor data based on a dual prediction model. This method mainly collected the operation data of multiple temperature sensors. The data were cleaned and deduplicated. Based on this, a support vector machine (SVM) and least squares support vector machine (LS-SVM) prediction model was built. The model is used to predict the operating state of the temperature sensor data, and the abnormality diagnosis of the temperature sensor data is realized by combining the prediction results. However, in practical application, it is found that this method takes a long time to diagnose abnormal temperature sensor data. Reference [5] proposed a temperature sensor data anomaly diagnosis method based on multiple lag regression model. This method mainly takes the building wood structure as the research object. The temperature sensor data are arranged in the building to collect the building temperature change data. Combined with the collected data, a multiple lag regression model to analyze the autocorrelation is built, periodicity and heteroscedasticity of the data. According to these characteristics, the abnormal data of the temperature sensor are diagnosed. However, this method has the problem of low diagnostic accuracy, and the practical application effect is not good. Ding et al. [6] proposed a method for abnormal temperature sensor data diagnosis based on serial correlation analysis. The temperature sensor data are collected, and the multi-dimensional time series of the sensor data are segmented and normalized, so as to obtain the judgment matrix of data correlation and obtain the correlation judgment result of the data. According to the results, a time series correlation graph model is established, and the model is used to distinguish normal temperature sensor data and abnormal temperature sensor data. The abnormal data of the temperature sensor is diagnosed. The temperature sensor data are abnormal. However, this method has the problem of high error rate of temperature sensor data feature extraction, which is far from ideal application effect.

In the process of using traditional methods to diagnose the abnormal data of temperature sensor, the performance of the abnormal diagnosis model of building temperature sensor data is poor because the characteristics and extraction of temperature sensor are not analyzed. This paper aims to solve the problem of low diagnosis accuracy and efficiency of traditional sensor data abnormal diagnosis methods, and a temperature sensor data anomaly diagnosis method based on a deep neural network is proposed. Therefore, this method has the characteristics of high temperature sensor data anomaly diagnosis accuracy and diagnosis efficiency. The overall design scheme of the method is as follows:

(1) Collect the temperature sensor data within a running cycle, and use the sliding window technology to extract the temperature sensor data characteristics

(2) Based on the result of feature extraction, a deep neural network model for anomaly diagnosis of temperature sensor data is constructed. The characteristic data are input into the model, and the result obtained is the diagnosis result.

(3) Compare the error rate of feature extraction of temperature sensor data, anomaly diagnosis accuracy, and efficiency of temperature sensor data of different methods through experiments.

2. Design of Temperature Sensor Data Anomaly Diagnosis Method

2.1. Temperature Sensor Data Collection. In order to achieve the comprehensive goal of data acquisition accuracy and efficiency of temperature sensor, this paper introduces a K-means algorithm to design the data acquisition process of temperature sensor. The operation cycle of temperature sensor is set to 6 months, and the sampling time interval is set to 1 s so as to collect more complete and reliable data to the greatest extent.

Suppose there is a periodic temperature sensor dataset represented by $\{x_1, x_2, \ldots, x_N\}$, which mainly includes N observation series of random variable x [7, 8]. The goal of k-means clustering is to divide dataset N into k categories, at which a vector-value u_k is introduced, where $k = 1, \ldots, K$ and u_k are the central values of the first cluster. The goal of clustering is to find each data point category and vector u_k so that the sum of squares of the distance between each data point and u_k can reach the minimum [9].

Suppose x_n is used to represent the node vector, and a set of corresponding binary indicator variable r_{nk} is introduced, where $k = 1, \ldots, K$ means that the node vector x_n belongs to class K, and x_n is assigned to class k; then, $r_{nk} = 1$ exists, and the objective function is defined in the following form:

$$J = \sum_{n=1}^{N} \sum_{k=1}^{K} r_{nk} x_n - u_k^2. \tag{1}$$

In the above formula, J represents the sum of the square of the distance between each data point and the center vector of the cluster to which it is assigned. Now, the key is to find the value of $\{r_{nk}\}$ and $\{u_k\}$ to achieve the minimum value.

First, we determine the value of r_{nk}. J given by equation (1) is a linear function of r_{nk}, so it is easy to obtain an analytical solution for r_{nk}. Each data is independent, so we can choose to optimize each n separately, as long as we ensure that the value of $x_n - u_k^2$ is small. Here, let $r_{nk} = 1$. In language description, we simply set the clustering of data nodes as the nearest clustering center. The function expression is as follows:

$$r_{nk} = \begin{cases} 1, & k = \operatorname{argmin}_j x_n - u_k^2, \\ 0, & \text{other}. \end{cases} \tag{2}$$

Here, if we take the derivative of the objective function and make it equal to 0, then the minimum value can be obtained, which can be expressed as

$$2 \sum_{n=1}^{N} r_{nk} \left(x_n - u_k \right) = 0, \tag{3}$$

Through solution, we obtain

$$u_k = \frac{\sum_n r_{nk} x_n}{\sum_n r_{nk}}. \tag{4}$$

For the data type in this paper, the dataset objects in the network are cooperative sensor node sets, and each temperature sensor set is a data vector [10]. Among them, n such dataset vectors form a set G, and the data of these n datasets are initialized into K categories, as shown in Figure 1:

The temperature sensor data acquisition process based on the K-means algorithm is shown as follows:

(1) K objects are randomly selected from set G of node group data set as the initial class center

(2) According to the class center value, the dataset value in the G sets is compared with the class center value, and the remaining n objects are divided into each class by comparing the minimum distance value.

(3) Update the class center value and recalculate the center value of each class through all the data values of the classes that have been classified.

(4) Calculate the criterion function and redistribute

(5) If it meets the threshold, output the data collection result of a periodic temperature sensor; otherwise, return to Step 2

2.2. Feature Extraction Based on Sliding Window. Suppose that the data of a periodic temperature sensor is expressed as $X \in \mathbb{R}^{N \times J}$ in the form of a two-dimensional matrix, where N

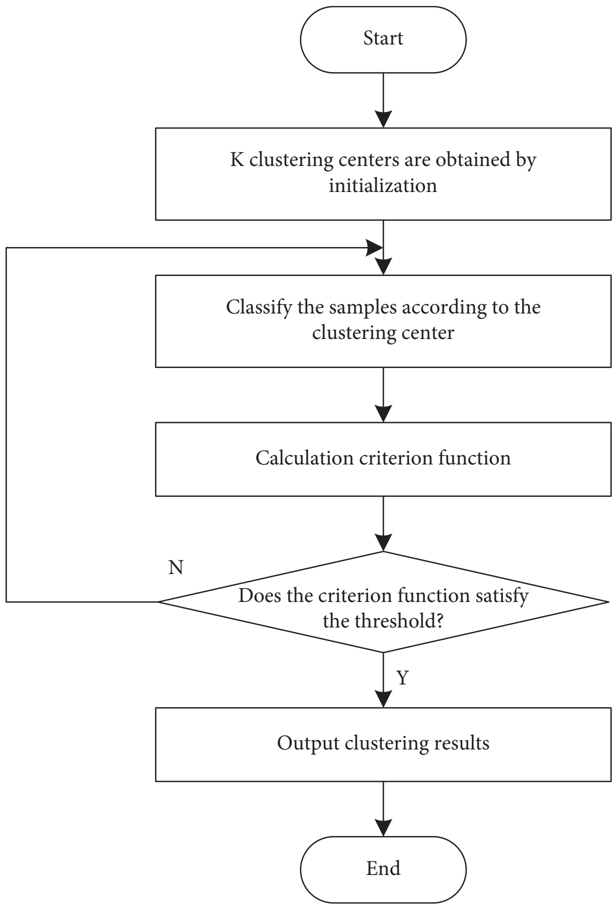

Figure 1: Temperature sensor data acquisition process based on K-means algorithm.

and J represent the number of process samples and the number of process variables, respectively. This two-dimensional data matrix is segmented along the sampling direction by a sliding window H [11]; that is, matrix X is segmented along the horizontal axis after transposing. Assuming that the sliding step of the window is H and the data of each window is $X_k^T \in \mathbb{R}^{N\times J}$, the principal component analysis method is applied to these two-dimensional matrices [12], from which the temperature sensor data features in each window can be extracted.

The projection of the original set of sample points on the a-th principal axis constitutes the synthesis variable $t_a(H\times 1)$, where $a = 1, 2, \ldots, A$. Assuming that the variation information carried by the fifth principal component 6 is represented by $\mathrm{Var}(t_a)$, the following relationship exists:

$$\mathrm{Var}(t_1) \geq \mathrm{Var}(t_2) \geq \cdots \geq \mathrm{Var}(t_A) > 0. \tag{5}$$

Original sample space $X = (x_{nj})_{N\times J} = [x(1), \ldots, x(J)]$, and a comprehensive variable t_1 is a linear combination of $x(1), \ldots, x(J)$, namely:

$$t_1 = Xp_1, \quad p_1 = 1. \tag{6}$$

In order to make t_1 carry the most original variation information, the variance of t_1 is required to reach the maximum value, and the variance of t_1 is

$$\mathrm{Var}(t_1) = \frac{1}{H}t_1^2 = \frac{1}{H}p_1^T X^T X p_1 = p_1^T R p_1. \tag{7}$$

In the above formula, $R = X^T X$ is the covariance matrix of X.

The above problems are translated into the solution of the following optimization problems:

$$\max_{p_1=1} p_1^T R p_1. \tag{8}$$

We write λ_1 as Lagrange operator, and let

$$\lambda_1 = p_1^T R p_1 - \lambda_1\left(p_1^T p_1 - 1\right). \tag{9}$$

We take the partial derivatives of p_1 and λ_1 of L, respectively:

$$\begin{aligned} \frac{\partial L}{\partial p_1} &= 2Rp_1 - 2\lambda_1 p_1 = 0, \\ \frac{\partial L}{\partial p_1} &= -\left(p_1^T p_1 - 1\right) = 0. \end{aligned} \tag{10}$$

We obtain

$$\begin{aligned} Rp_1 &= \lambda_1 p_1, \\ \mathrm{Var}(t_1) &= p_1^T R p_1 = p_1^T(\lambda_1 p_1) = \lambda_1 p_1^T p_1 = \lambda_1. \end{aligned} \tag{11}$$

We assume that p_1 is the first principal axis, and $t_1 = Xp_1$ is called the first principal component [13], so the second principal axis p_2 is obtained by analogy, where p_2 is orthonormal p_1, $p_2^T p_1 = 0, p_2^2$, and the second principal component $t_2 = Xp_2$ is the second largest component carrying variation information, and $\mathrm{Var}(t_2)$ is second only to $\mathrm{Var}(t_1)$. So, we have $\mathrm{Var}(t_1) \geq \mathrm{Var}(t_2) \geq \cdots \geq \mathrm{Var}(t_A) > 0$. Therefore, if the data variation is used to reflect the information in the data, the first principal component t_1 carries the most information, followed by t_2 times. A total of J principal components were extracted. Matrix X is decomposed into the sum of the cross product of A subspaces, namely, principal component decomposition, and the extraction results of temperature sensor data features are obtained. The specific calculation formula is as follows:

$$TP^T = \sum_{a=1}^{A} t_a p_a^T = t_1 p_1^T + t_2 p_2^T + \cdots + t_A p_A^T. \tag{12}$$

In the above formula, T and P are principal component score matrix and load matrix, respectively, t_a is $H\times 1$-dimensional principal component vector, and p_a is $J\times 1$-dimensional load vector, which is also the projection direction of principal components [14].

2.3. Data Anomaly Diagnosis Based on Deep Neural Network Model. Deep neural networks (DNNs) can be understood as a neural network with many hidden layers, also known as deep feedforward network (DFN) and multilayer perceptron (MLP). The deep neural network has many advantages such as high speed and low error, and has been widely used in various fields. Therefore, this paper uses the deep neural network model to diagnose the data anomaly of temperature sensor. The topology of deep neural network is shown in Figure 2.

The measures to improve the generalization performance of the deep neural network are as follows:

(1) Use more data: on the premise of conditions, obtaining as much training data as possible is the most ideal method. More data can fully learn the model and easily improve the generalization ability.

(2) Use larger batches: under the condition of the same number of iterations and learning rate, using more data in each batch will help the model better learn the correct mode, and the output result of the model will be more stable.

(3) Adjust data distribution: the data distribution in most scenarios is uneven. If the model learns too much about a certain type of data, its output results will tend to this type of data. At this time, the generalization ability can be improved to a certain extent by adjusting the input data distribution.

In the deep neural network, the input information is tagged, so the deep neural network can be simplified into a simple modeling unit, as shown in Figure 3.

In order to ensure the integrity of data, a decoder was added [15]. Therefore, the autoencoder modeling unit is shown in Figure 4.

In order to minimize the network reconstruction error [16], this paper constructed a new multilayer autoencoder, whose structure is shown in Figure 5.

In order to minimize errors, this paper mainly uses the attention mechanism to train the deep neural network model, and the process is as follows:

The usual convolution operation in the deep neural network can be formulated as follows:

$$Y = X \odot W. \tag{13}$$

In the above formula, W is the 4-dimensional tensor, and $W_{(i,j,k,l)}$ is the weight parameter of the position of the y-th channel input in the i-th convolution kernel.

The attention mechanism can further constrain and adjust each factor by observing globally and learning the relationship between each parameter and its influence on the result. After this restriction is introduced in the training process of convolution, the parameters of the convolution layer supervised by the attention mechanism can be expressed in the following form:

$$W^a_{(i,j,k,l)} = W_{(i,j,k,l)} \cdot \mathrm{att}_{(i,j,k,l)}. \tag{14}$$

In the above formula, att is the attention weight obtained after global observation, and $W_{(i,j,k,l)}{}'$ obtained will be used for the final convolutional feature extraction. It can be divided into two parts: channel attention and shape attention.

$$W^a_{(i,j,k,l)} = W_{(i,j,k,l)} \cdot \mathrm{att}^c_{(i,j)} \cdot \mathrm{att}^s_{(i,k,l)}. \tag{15}$$

The information of different channels can be considered as the image description information extracted from different angles or using different features, and the filter will combine these feature information with different weights. Some features are focused on, while others tend to be ignored. Channel attention applies this idea.

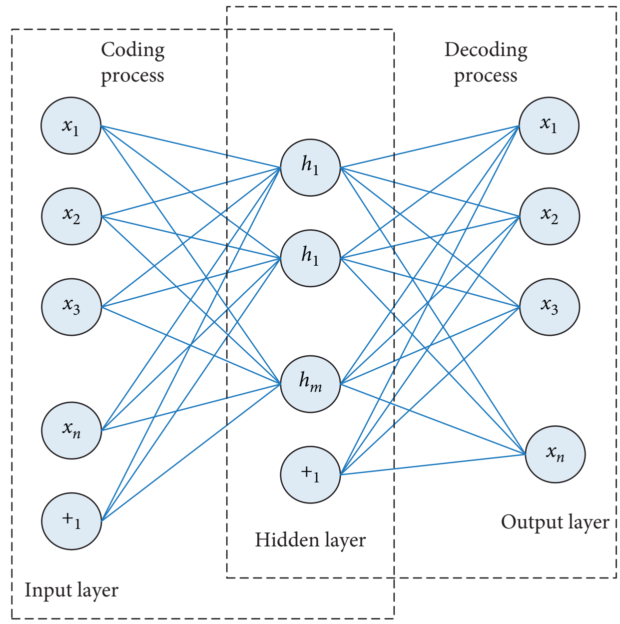

Figure 2: Topology of deep neural network.

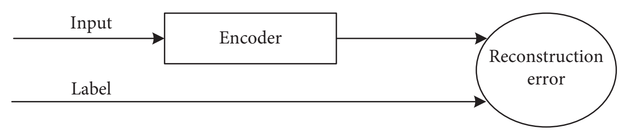

Figure 3: Simple modeling unit.

The average response of the convolution kernel i to the input channel y can be represented by the average value of the filter weights of the corresponding channel, namely:

$$\mathrm{avg}^c_{(i,j)} = \mathrm{mean}\left(W_{(i,j,k,l)}\right) = \frac{1}{WH}\sum_{k=0}^{H-1}\sum_{l=0}^{WS-1} W_{(i,j,k,l)}. \tag{16}$$

The average response of these channels is then input into the full connection layer used to analyze their relationships, and the Sigmoid activation function is used as the threshold.

$$\mathrm{att}^c = \mathrm{sigmoid}\left(fc^c\left(\mathrm{avg}^c\right)\right). \tag{17}$$

In this representation, the attention weight of each channel can be related to the filter parameters of other channels, introducing the interaction between channels. Similarly, the shape of the convolution kernel is usually used to describe the importance of features extracted from different positions of the filter, and the response weight of each position can be obtained by averaging the weights of all channels at that position.

$$\mathrm{avg}^s_{(i,k,l)} = \mathrm{mean}\left(W_{(i,j,k,l)}\right) = \frac{1}{C}\sum_{j=0}^{C-1} W_{(i,j,k,l)}. \tag{18}$$

A similar attention model can then be used to obtain shape weights.

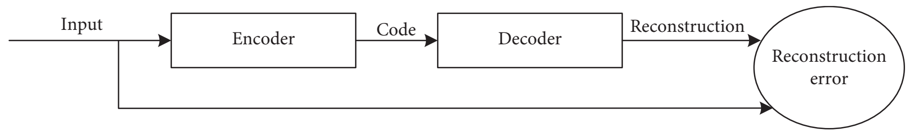

Figure 4: Modeling unit of autoencoder.

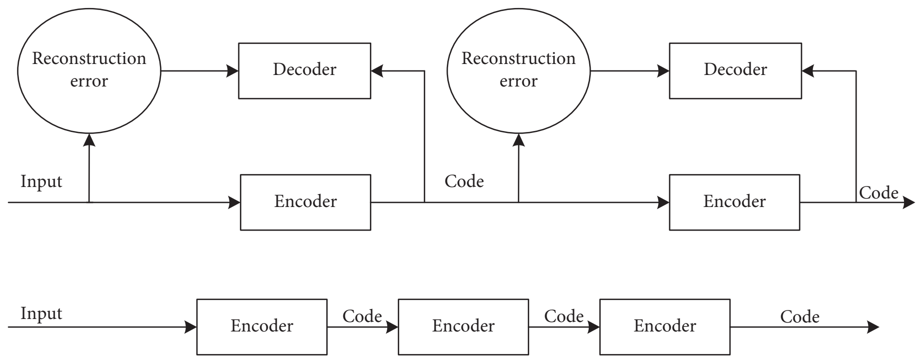

Figure 5: Structure of multilayer autoencoder.

$$att^s = \text{sigmoid}\left(fc^s\left(avg^s\right)\right). \tag{19}$$

At this point, for each parameter of the convolution layer, the parameter ultimately affected by the global parameter can be obtained through formula (15). After the training of the network is completed, the weights obtained by the attention mechanism can be directly solidified on the original parameters of the convolutional layer without recalculation during the network operation.

The characteristic data are input into the trained deep neural network model, and the result is the anomaly diagnosis result of temperature sensor data.

3. Simulation Experiment Design

3.1. Experimental Scheme. To verify the validity of the temperature sensor data anomaly diagnosis method based on the deep neural network designed in this paper as the research objective, a simulation experiment scheme is designed. The specific experimental scheme is as follows:

(1) Experimental environment: in order to ensure the authenticity of experimental results, experimental environmental parameters need to be designed in detail in this experiment. The specific parameter settings are shown in Table 1.

(2) Experimental data: multiple types of temperature sensors are taken as research objects to keep them running, and the operating data of temperature sensors are taken as experimental sample data, and the collected data are denoised to improve the authenticity of the simulation results. Because the setting of experimental parameters will affect the simulation results, in order to maximize the accuracy of the simulation experiment, the simulation experimental parameters are adjusted many times in this experiment, and the parameters in the optimal running state of the simulation software are taken as the initial simulation parameters.

(3) Experimental methods and evaluation indicators.

Table 1: Experimental parameter settings.

Project	Parameter
CPU	Intel Xeon
CPU hard disk capacity	1.5 T
CPU frequency	1.2 GHz
Random access memory	128 GB
Operating system	Windows 10
Monitor resolution	1280 * 1024
Interface type	USB
Network band	2.4–2.5 GHz
Transmission rate	28 Mb/s
Simulation software	MATLAB 7.0

In this paper, reference [4] method and reference [5] method are selected as experimental comparison methods, and the practical application effects of the two methods and the proposed method are verified by comparing the error rate of feature extraction, diagnostic accuracy, and diagnostic efficiency of temperature sensor data.

Among them, the lower the error rate of temperature sensor data feature extraction, the higher the accuracy of data feature extraction, and the more accurate the result of feature extraction. The diagnostic accuracy is an important index to verify the anomaly diagnosis method of temperature sensor data. The higher the anomaly diagnosis accuracy of temperature sensor data, the more accurate the diagnosis result is. The diagnostic efficiency of temperature sensor data refers to the time it takes to diagnose temperature sensor data anomalies. The shorter the diagnostic time, the higher the diagnostic efficiency.

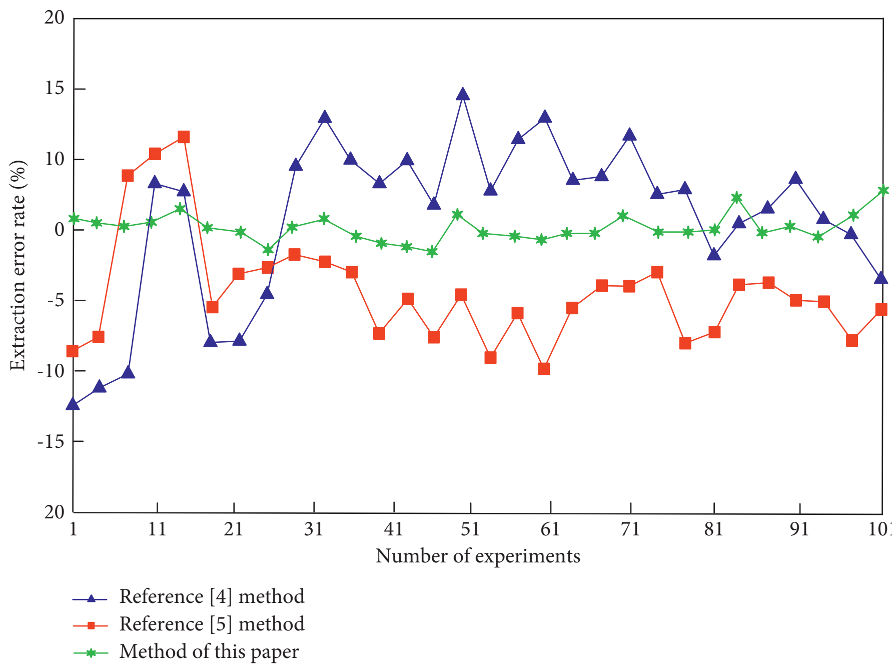

Figure 6: Error rate of feature extraction from temperature sensor data.

3.2. Analysis of Experimental Results

3.2.1. Data Feature Extraction Error. The error rate of feature extraction of temperature sensor data by reference [4] method, reference [5] method, and this method is compared, and the results are shown in Figure 6.

According to the data in Figure 6, the error rate of feature extraction of temperature sensor data in reference [4] is between −12.5% and 14.65%, and that of temperature sensor data in reference [5] is between −9.6% and 12.15%. Compared with these two comparison methods, the error rate of temperature sensor data feature extraction in this method varies from −2.1% to 5.9%, which is the lowest among the three methods. The reason is that this method uses the K-means algorithm to collect the temperature sensor data in an operation cycle and uses the sliding window technology to extract the temperature sensor data features, which improves the accuracy of temperature sensor data feature extraction, and can lay a solid data foundation for subsequent diagnosis and analysis.

3.2.2. Diagnostic Accuracy. The diagnostic accuracy of abnormal temperature sensor data of reference [4] method, reference [5] method, and this method is compared, and the results are shown in Figure 7.

According to the data in Figure 7, the minimum and maximum diagnostic accuracy of abnormal temperature sensor data in reference [4] are 73% and 93%, respectively, and the minimum and maximum diagnostic accuracy of abnormal temperature sensor data in reference [5] are 76% and 91%, respectively. Compared with these two methods, the anomaly diagnosis accuracy of temperature sensor data obtained by the proposed method is always above 95%, which is much higher than the two experimental comparison methods, indicating that the anomaly diagnosis results of temperature sensor data obtained by the proposed method are more accurate. The reason is that this method constructs a deep neural network model for abnormal diagnosis of temperature sensor data, inputs the characteristic data into the model, and the obtained result is the diagnosis result.

3.2.3. Diagnostic Efficiency. The anomaly diagnosis time of temperature sensor data of reference [4] method, reference [5] method, and this method is compared to test the diagnosis efficiency of different methods. The results are shown in Table 2.

According to the average value of anomaly diagnosis time of temperature sensor data of different methods after multiple experiments, the diagnosis efficiency of different methods can be obtained. The average value of anomaly diagnosis time of temperature sensor data of reference [4] method is 263 ms, and the average value of anomaly diagnosis time of temperature sensor data of reference [5] method is 140 ms. Compared with these two methods, the average value of anomaly diagnosis time of temperature sensor data in this method is the lowest, only 59 ms, which proves that this method has the highest efficiency and the best practical application effect. The reason is that this method uses the K-means algorithm to collect the temperature sensor data in a running cycle, constructs a deep neural network model for abnormal diagnosis of temperature sensor data, and inputs the characteristic data into the model to realize abnormal diagnosis.

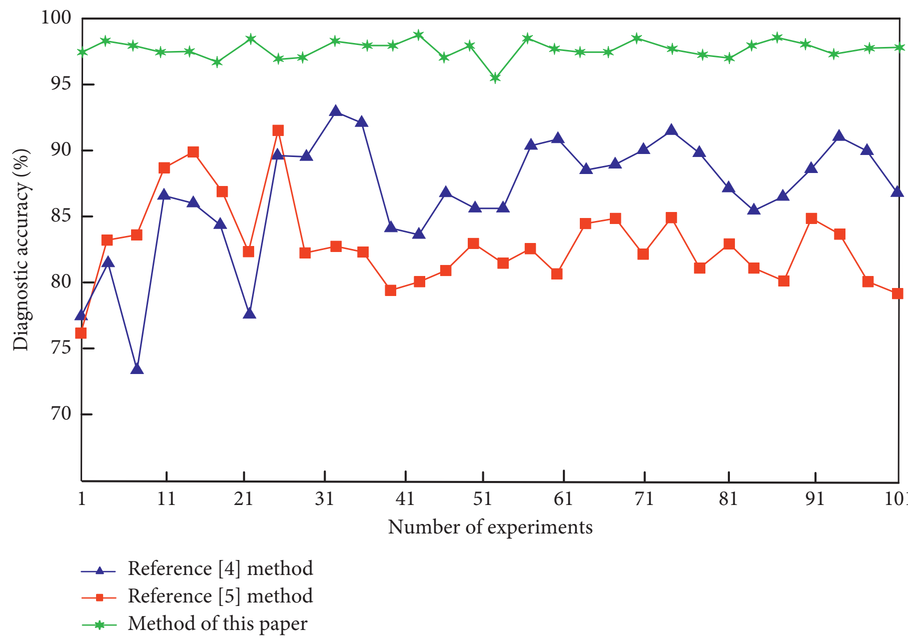

Figure 7: Temperature sensor data anomaly diagnosis accuracy.

Table 2: Anomaly diagnosis time of temperature sensor data (unit: ms).

Number of experiments	Reference [4] method	Reference [5] method	Method of this method
1	256	160	59
11	352	151	57
21	247	134	55
31	269	178	63
41	284	163	57
51	267	175	58
61	243	121	63
71	217	106	64
81	285	137	52
91	244	113	69
101	231	107	57
Average value	263	140	59

4. Conclusion

As people production and living standards continue to improve, various sensors has been widely applied in all fields, especially the temperature sensor because of its high precision and convenient advantages, such as the application on a large scale in the areas of agricultural production, scientific research and life, but also easy to appear abnormal temperature sensor data. Therefore, it is necessary to diagnose abnormal temperature sensor data. Aiming at the problems of high error rate of current temperature sensor data feature extraction, abnormal diagnosis accuracy, and low efficiency of temperature sensor data, this paper proposes a temperature sensor data anomaly diagnosis method based on the deep neural network. Finally, a comparative simulation experiment is conducted to verify the performance of the proposed method in data anomaly diagnosis. The experimental results show that the error rate of feature extraction of temperature sensor data in this method varies from −2.1% ~ 5.9%, the diagnosis accuracy remains above 95%, and the average diagnosis time is only 59 ms, indicating that this method has low error rate of feature extraction of temperature sensor data, high accuracy, and efficiency of abnormal diagnosis of temperature sensor data. It can fully solve the problems of traditional methods and can be widely used in the field of temperature sensor data anomaly diagnosis.

Data Availability

The temperature sensor data used to support the findings of this study are available from the corresponding author upon request.

Conflicts of Interest

The authors declare that they have no conflicts of interest.

Acknowledgments

This work was supported by Key Program for International Science and Technology Cooperation Projects of Shaanxi Province: 2021KWZ-20, The Key Research Project of Shaanxi Science and Technology: 2021JY-324, and Department Scientific Research Plan Projects of Shannxi Provincial Education Department: 20JK0688.

References

[1] A. Malakzadeh, M. Didar, and M. Mansoursamaei, "SNR enhancement of a Raman distributed temperature sensor using partial window-based non local means method," *Optical and Quantum Electronics*, vol. 53, no. 3, pp. 147–158, 2021.

[2] S. Wang, P. Niu, S. Liu et al., "Curvature and temperature sensor based on anti-resonant effect combined with multimode interference," *IEEE Photonics Technology Letters*, vol. 33, no. 3, pp. 127–130, 2021.

[3] C. Xu, Z. Xu, H. Chen, C. Liu, and C. Ma, "Tunable and highly sensitive temperature sensor based on graphene photonic crystal fiber," *Chinese Physics*, vol. 30, no. 11, Article ID 118103, 2021.

[4] Y. J. Li, H. X. Chen, and J. Y. Liu, "Anomaly diagnosis strategy of multi online energy consumption data based on double prediction model," *Refrigeration Technology*, vol. 39, no. 3, pp. 36–41, 2019.

[5] N. Yang, D. Y. Dai, and S. J. Qin, "Anomaly diagnosis of monitoring data of ancient wooden structures," *Journal of Vibration Engineering*, vol. 32, no. 1, pp. 64–71, 2019.

[6] X. O. Ding, S. J. Yu, and M. X. Wang, "Anomaly detection of industrial time series data based on correlation analysis," *Journal of Software*, vol. 31, no. 3, pp. 726–747, 2020.

[7] B. Xu, M. Jang, D. Fyfe, and A. R. Hasan, "Clean-up period flow rate estimation from Multi Discrete Temperature Sensor data," *Journal of Petroleum Science and Engineering*, vol. 194, no. 1, Article ID 107452, 2020.

[8] Y. Zhang, R. Wang, S. Li, and S. Qi, "Temperature sensor denoising algorithm based on curve fitting and compound kalman filtering," *Sensors*, vol. 20, no. 7, pp. 1959–1968, 2020.

[9] B. Marchiori, S. Regal, Y. Arango, R. Delattre, S. Blayac, and M. Ramuz, "PVDF-TrFE-Based stretchable contact and noncontact temperature sensor for E-skin application," *Sensors*, vol. 20, no. 3, pp. 623–631, 2020.

[10] M. Pullinger, J. Kilgour, N. Goddard et al., "The IDEAL household energy dataset, electricity, gas, contextual sensor data and survey data for 255 UK homes," *Scientific Data*, vol. 8, no. 1, p. 146, 2021.

[11] H. A. Saeed, H. Wang, M. Peng, A. Hussain, and A. Nawaz, "Online fault monitoring based on deep neural network & sliding window technique," *Progress in Nuclear Energy*, vol. 121, no. 1, pp. 103236–103245, 2020.

[12] X.-G. Guo, P.-Y. Hong, and T.-M. Laleg-Kirati, "Calibration and validation for a real-time membrane bioreactor: a sliding window approach," *Journal of Process Control*, vol. 98, no. 6, pp. 92–105, 2021.

[13] E. Al-Wajih and R. Ghazali, "Improving the accuracy for offline Arabic digit recognition using sliding window approach," *Iranian Journal of Science and Technology, Transactions of Electrical Engineering*, vol. 44, no. 4, pp. 1633–1644, 2020.

[14] A. K. Singh and V. K. Srivastava, "A tri-nucleotide mapping scheme based on residual volume of amino acids for short length exon prediction using sliding window DFT method," *Network Modeling Analysis in Health Informatics and Bioinformatics*, vol. 9, no. 1, pp. 1–13, 2020.

[15] H. Chen, Y. H. Zeng, and J. E. Fang, "Research on anomaly diagnosis of time series data on special equipment," *Information & Systems Engineering*, vol. 12, no. 6, pp. 113–116, 2021.

[16] Y. Y. Chen and X. H. Lu, "Big data anomaly extraction algorithm based on uncorrelation test," *Computer Simulation*, vol. 38, no. 3, pp. 245–248, 2021.

Hindawi
Scientific Programming
Volume 2023, Article ID 9763290, 1 page
https://doi.org/10.1155/2023/9763290

Retraction

Retracted: Collocation Features in Translated Texts Based on English Analogy Corpus

Scientific Programming

Received 1 August 2023; Accepted 1 August 2023; Published 2 August 2023

This article has been retracted by Hindawi following an investigation undertaken by the publisher [1]. This investigation has uncovered evidence of one or more of the following indicators of systematic manipulation of the publication process:

(1) Discrepancies in scope
(2) Discrepancies in the description of the research reported
(3) Discrepancies between the availability of data and the research described
(4) Inappropriate citations
(5) Incoherent, meaningless and/or irrelevant content included in the article
(6) Peer-review manipulation

The presence of these indicators undermines our confidence in the integrity of the article's content and we cannot, therefore, vouch for its reliability. Please note that this notice is intended solely to alert readers that the content of this article is unreliable. We have not investigated whether authors were aware of or involved in the systematic manipulation of the publication process.

Wiley and Hindawi regrets that the usual quality checks did not identify these issues before publication and have since put additional measures in place to safeguard research integrity.

We wish to credit our own Research Integrity and Research Publishing teams and anonymous and named external researchers and research integrity experts for contributing to this investigation.

The corresponding author, as the representative of all authors, has been given the opportunity to register their agreement or disagreement to this retraction. We have kept a record of any response received.

References

[1] B. Liu and J. Wang, "Collocation Features in Translated Texts Based on English Analogy Corpus," *Scientific Programming*, vol. 2022, Article ID 8294254, 7 pages, 2022.

Hindawi
Scientific Programming
Volume 2022, Article ID 8294254, 7 pages
https://doi.org/10.1155/2022/8294254

Research Article

Collocation Features in Translated Texts Based on English Analogy Corpus

Bin Liu and Jing Wang

School of Foreign Studies, Suqain University, Suqian 223800, Jiangsu, China

Correspondence should be addressed to Bin Liu; binliuandy@squ.edu.cn

Received 8 December 2021; Accepted 9 March 2022; Published 30 March 2022

Academic Editor: Le Sun

The aim of this paper is to explore the characteristics of the use of verbal collocations in English, to compare the use of verbal collocations in the English translation and the original English text, and then to compare and analyse the characteristics of the choice of verbal collocations in the English text. In this paper, we take bilateral marked causative complex sentences as the object of study and use deep learning methods to automatically explore the implied features of complex sentences while incorporating the significant knowledge of relational words in linguistic research. The experimental results achieved an F1 value of 92.13%, which is better than that of the existing comparison models, demonstrating the effectiveness of the method.

1. Introduction

A corpus is a large collection of natural language materials, both written and spoken, collected systematically and scientifically for research purpose. A corpus is a large collection of authentic and reliable linguistic materials that provides a comprehensive and accurate representation of a language or an aspect of language, providing a wide range of verbal material for language research and revolutionising the way language research is conducted [1]. Since the 1980s, corpus-based translation research has become a new research paradigm in the field of translation research at home and abroad. Corpus translation studies take translated texts as the object of study and adopt the mode of combining intra-linguistic and inter-linguistic comparisons to describe and explain translation phenomena from a large-scale translated text or translated language as a whole, so as to explore the essence of translation [2, 3]. The corpus provides a new tool for translation studies, opening up new ideas and expanding the scope of translation research. Baker classifies translation corpora designed for different research purposes into three categories: parallel corpora, multilingual corpora, and analogical corpora, of which Baker considers the analogical corpus to be the most significant for translation research [4].

Through the comparative analysis of two texts in the analogical corpus, the researcher can explore the norms of translation in a particular historical and cultural context and discover some specific patterns of translated texts, i.e., the universality of translation. The salient features of the translated language are in the area of vocabulary, mainly in the conventionalisation of words used in the translated texts and the emergence of new word combinations [5, 6]. This new combination of words is a reflection of the lexical collocation characteristic of translated texts [7]. The linguistic features of the translated text are therefore highlighted in the lexical aspect, especially in the collocation of words, where the differences in collocation patterns reflect the differences between the original text and the translated text. The lexical collocation features reflect the specific meaning of the linguistic forms realised in the context and truly reflect the frequently used, habitual collocation forms of words in linguistic communication [8].

In recent years, with the continuous development of corpus translation science, studies on the lexical collocation characteristics of translated texts based on corpus have emerged at home and abroad, but empirical studies on lexical collocations in English translations of Chinese medicine texts using corpus are not common [9, 10].

Therefore, in this paper, the authors use the corpus to conduct a statistical study on the use of verb-name collocations in the English translation of TCM texts and the original medical English texts and then compare and analyse the patterns of verb-name collocations in medical texts, with the aim of providing some reference for the English translation of TCM texts, i.e., how to select suitable words for collocation in the English translation of TCM texts, and discovering lexical collocations.

2. Related Studies

Complex sentences are classified as marked or unmarked according to whether they contain relational words or not. At present, automatic recognition of marked compound sentence categories is mainly based on rule-based methods and machine learning methods. Wang et al. [11] combined the syntactic theory of Chinese compound sentences and the theory of relational tagging collocation to automatically identify the relational category of biological non-full-state marked compound sentences; the calculation method of semantic relatedness was used to calculate the relatedness of two words, so as to identify the relational category of compound sentences [12]. Igaab and Abdulhasan [13] used decision tree algorithms to extract features such as lexical properties to identify causal and juxtaposition relations between Chinese sentences.

For the recognition of relationship categories of unlabeled compound sentences, deep learning methods are mostly used for the recognition of relationship categories of unlabeled compound sentences due to the lack of relationship words and the absence of obvious manual recognition features [14]. Li et al. [15] used an attention-based mechanism of convolutional neural network on a Chinese chapter book library [16] for the recognition of unlabeled compound sentence relations. Algburi and Igaab [17] combined word vectors with lexical features as the input of the model and used CNN to classify unlabeled complex sentence relations. The study of unlabeled complex sentences still faces some difficulties, namely, the difficulty of data annotation, the relatively small amount of training data, and the uneven distribution of data among categories, which easily leads to overfitting of the model and makes the model's generalisation ability insufficient. Among the many deep learning models, the transformer model [18] has a simple network architecture with an attention mechanism as its main structure [19]. In this paper, we explore the fusion of relational word features in deep learning models to enable automatic recognition of biological marked causal complex sentence relations.

3. Data Statistics and Analysis

3.1. Word Frequency Statistics. Word frequency is the total number of occurrences of a word item or a class of words in the corpus, and counting word frequency can provide certain reference information about the stylistic or linguistic features of a discourse. The study of word collocation should centre on the behaviour of real words, and collocation studies should be conducted mainly by selecting real words as nodal words; the behaviour of functional or grammatical words has mostly been described in detail by grammarians [20, 21]. Therefore, the first criterion for choosing nodal words in this paper is real words. Moreover, of the four main categories of real words (nouns, verbs, adjectives, and adverbs), nouns and verbs have the highest collocation power, thus further defining the nodal words studied in this paper as verbs. The following statistics are commonly used in English text bases: the number of tokens, number of the types, type/token ratio, word length, average word length, and so on [22]. In this paper, WordSmith 5.0 was used to obtain statistics on the common parameters of the self-built TCM English corpus and then rank the verb morphology of the corpus in descending order of frequency [23].

3.2. Extraction of Collocations for Verbal Structures. The collocation of these three verbs (influences, caused, and treating) in the self-built TCM English corpus was searched using AntConc software [24], which requires that the collocation must be in the lexical noun form and that they serve as an object of the sentence. Therefore, collocation that did not meet the requirements of the study was eliminated, leaving 200 significant collocations for each of the three verbs. Since the BNC has its own search data analysis function, which allows the selection of collocations in different genres of texts from different generations, the three verbs (influences, caused, and treating) were directly entered into the BNC and the collocations that met the requirements of the study were selected and then analysed quantitatively and qualitatively with the previous data [25, 26].

3.3. Analysis of Data. In Figure 1, the verb influence is most often found in the native English corpus with sphere, followed by decisions, and in the translated English corpus with factors, followed by range; in Figure 2, the verb cause is most often found in the native English corpus with trouble, followed by harm, and in the translated English corpus with damage, followed by problems; in Figure 3, the verb treat is most often found in the passive form with damage, followed by problems. The verb cause tends to occur in the passive form with damage, followed by problems in the translated English corpus; from Figure 3, the verb treat tends to occur most often with patients in the native English corpus, followed by symptoms, while treating tends to occur in the progressive tense in the translated English corpus. It is often found in the progressive tense, most often with disease, followed by pain [27].

The number of collocations of nodal words selected in the native English corpus is significantly higher than that in the translated English corpus, which indicates that the medical English native texts are more varied in terms of word usage and use a larger vocabulary than the translated texts, which is not beyond expectation since, after all, English translations of Chinese medical texts are mostly done by translators and are not as rich in terms of word usage as the native English texts. Once widely accepted, some high-frequency word combinations in translated texts may enter the target language and become the translation counterparts of several near-sense expressions, thus partially confirming the tendency of translated languages towards lexical simplification.

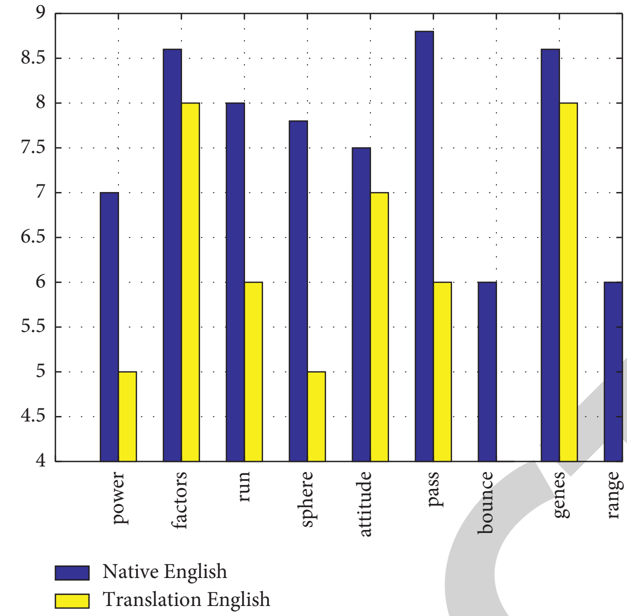

Figure 1: Comparison of the number of verb-noun collocations of nodal words.

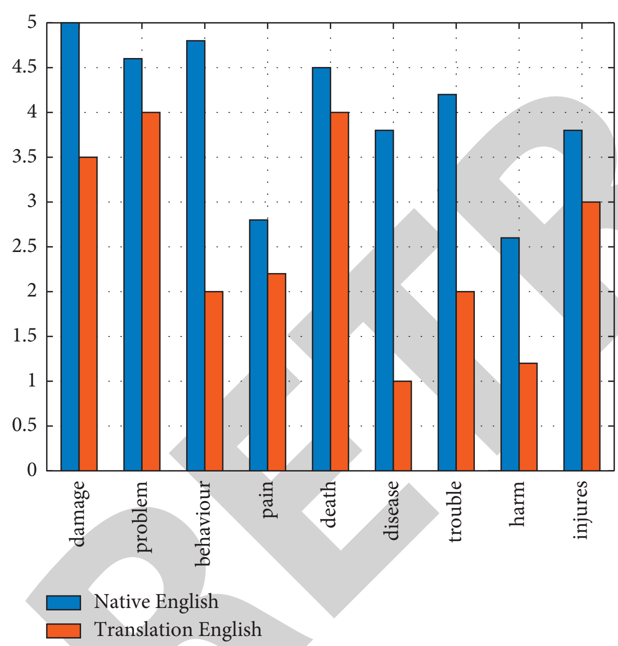

Figure 2: A comparative figure of the number of verb-noun collocations of the nodal word caused.

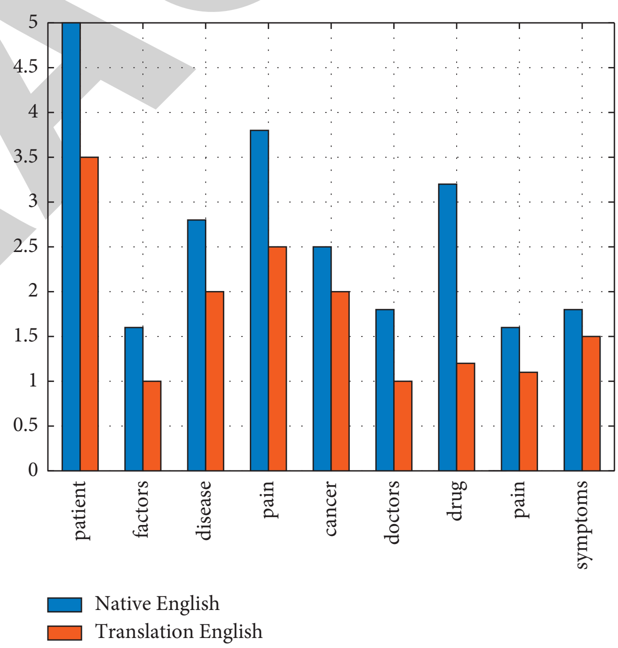

Figure 3: Number pairs of verb names of node word "treating."

4. The Transformer Model

4.1. Model Structure. Transformer is essentially an encoder decoder structure, which is composed of multiattention mechanism and feedforward neural network [28]. The multiheaded attention mechanism combines the context with the distant words and processes all words in parallel, thus achieving parallel computation and capturing the global semantic information. The structure of the RM-transformer model used in this paper is shown in Figure 4.

4.2. Model Input. In this paper, a pretrained word2vec word vector [29] is stitched with relational word features as model input. The 6-dimensional one-hot encoding is used for the relational word features, and all words in the word list are represented by the 6-dimensional relational word features. The first dimension uses 1 and 0 to indicate the presence or absence of a relation, and the next 5 dimensions correspond to the 5 relations of cause and effect, hypothesis, condition, inference, and purpose. Gensim's word2vec model is used to train a 122 dimensional word vector, which is then stitched with the 6-dimensional relational word feature vector to

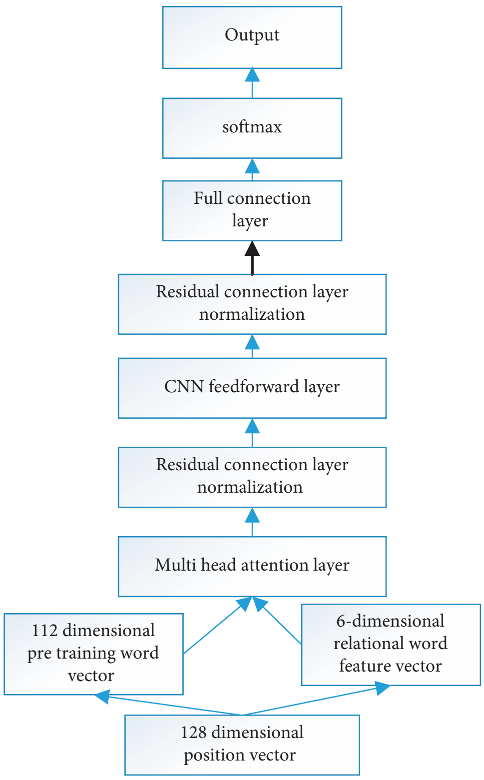

Figure 4: Structure of the RM-transformer.

obtain a 128-dimensional vector. If an input sentence is of length n, W_j $(j=1, \ldots, n)$ denotes the pretrained word vector for the jth word and R_j $(j=1, \ldots, n)$ denotes the relational word vector for the jth word. Then, the vector WR for each word is represented as follows:

$$WR_j = W_j \oplus R_j, \tag{1}$$

where $\oplus$ indicates a splicing operation.

The multiheaded attention mechanism can obtain the information of long-distance features and can also perform parallel calculation, but it cannot represent the position information of the input sentence. Here, using Position Embedding proposed by Google [30], each position is encoded so that the multiheaded attention mechanism can obtain the position information of each word. The equation for the position vector is shown in equations (2) and (3).

$$P_{(j,2i)} = \sin\left(\frac{\text{pos}}{10000^{(2i/d_{\text{model}})}}\right), \tag{2}$$

$$P_{(j,2i+1)} = \cos\left(\frac{\text{pos}}{10000^{(2i/d_{\text{model}})}}\right), \tag{3}$$

where j $(j=1, \ldots, n)$ is used to represent the position information of the word, P_j (odd and even positions) represents the position vector at the jth position, and i is the index of each value in the vector. $d_{\text{model}} = 128$ is consistent with the dimensionality of the word vector after adding features. At even positions, sine coding is used; at odd positions, cosine coding is used. The vector representation of the input model is as follows:

$$\text{Vector}_j = WR_j + P_j, \tag{4}$$

where + indicates direct summation of word vectors.

4.3. Transformer Feature Extraction. Self-attention is the calculation of the weight of each word vector on the input, which randomly initializes a set of weight matrices Q, K, V. Q, K, V refer to the result of multiplying the word vectors of the input model with a random initialization matrix, and d_k is the dimension of the Q, K vectors [31] and is calculated as follows:

$$\text{attention}(Q, K, V) = \text{softmax}\left(\frac{QK^{\mathrm{T}}}{\sqrt{d_k}}\right)V. \tag{5}$$

The self-attention layer is used to obtain the global semantic information of the input sentence, and after the self-attention layer, a feedforward layer is connected. NN uses a one-dimensional convolution operation and first performs an inner layer convolution operation, with the number of inner layer filters using the parameters set by oneself, using the relu activation function. The inner convolution operation is then performed, with the number of outer filtrators being the same as the dimensionality of the word vector, ensuring that the dimensionality of the input CNN is consistent with the dimensionality of the output. After the above process of transformer feature extraction, the output is fed into the next transformer encoder. Once the feature extraction is complete, a fully connected lawyer and a software layer are used to output the probability distribution for each category [32].

5. Experimentation and Analysis

5.1. Experimental Data. In this paper, we identify the relational categories of biological marked causal compound sentences, and the datasets are the Corpus of Chinese Compound Sentences (CCCS), an annotated corpus from Huazhong Normal University, and THUCNews, Tsinghua News Classification Corpus [33]. The CCCS is a special corpus of 658 Chinese compound sentences (447 items) from the People's Daily and the Yangtze River Daily [15]. The Tsinghua News Corpus THUCNews is a filtered corpus of 14 types of short-text news items, based on historical data from the Sina News RSS feed from 2005 to 2011 [19]. A total of 91,646 two-sentence marked causal compound sentences were annotated, forming a corpus abbreviated as CTCCCS (the Corpus of Two-Sentence Causal Chinese Compound Sentences), and the data distribution of each relationship category in the dataset is listed in Table 1. In the experiment, 75% of the data were selected as the training set and 25% of the data were selected as the test set, and the data were divided as listed in Table 2.

5.2. Experimental Comparison and Analysis. The experiment compares each of the same hyperparameter settings of the model and the values of different weights in CNN [3, 4, 5]. It can be known that convolution kernels of different sizes can

Table 1: Data distribution of the CTCCCS corpus by relationship category.

Relationship category	Number of complex sentence instances	Scale (%)
Causal class	30180	32.93
Hypothetical class	31444	34.31
Condition class	11576	12.63
Target class	12438	13.57
Inference class	6008	6.56

Table 2: CTCCCS dataset division.

Relationship category	Number of training sets	Number of test sets
Causal class	22635	7545
Hypothetical class	31444	7861
Condition class	8682	2894
Target class	93287	3110
Inference class	4506	1502

capture features of different sizes, which are more effective than data fitting using a single convolution kernel.

The number of layers in the LSTM and BiLSTM is set to 1, and the hidden layer is set to 128. The experimental results are listed in Table 3. The accuracy of the model was improved by 3.27%, 0.98%, and 0.3%, respectively. Compared to the transformer model without the addition of relational features, accuracy improved by 13.74%. Using a fixed sequence length of 100 in the model, the RM-transformer improved the precision, recall, and F1 values more significantly compared to the CNN, by 3.38%, 2.83%, and 3%, respectively. The learning of long-range features may be difficult, although multiple convolutional kernels of different sizes are used to capture features of different sizes.

The RM-transformer performs parallel computation through a multiheaded attention mechanism while learning global feature information and then learning sequential local features through the CNN feedforward layer, thus achieving better results than CNN.

The RM-transformer has an improvement of 1.26% and 0.18% in F1 values compared to the LSTM and BiLSTM, respectively, which is not particularly significant compared to the CNN. The recall of RM-transformer is 0.12% lower than that of LSTM. LSTM and BiLSTM are relatively mature in dealing with input text sequences and can learn the long-range features of the sequences, but LSTM relies on the above information and BiLSTM relies on the contextual information. The self-attention mechanism in the RM-transformer enables the direct correlation of long-range features to obtain global features, and the RM-transformer can achieve similar effects as the LSTM and BiLSTM. This paper has limited manually annotated data, and the parallel computational power of the transformer may be able to have better results when experimenting on a more data-rich complex sentence dataset. When comparing the RM-transformer with the transformer model without adding relational features, the F1 value increased by 11.63%, which is a significant improvement, indicating that relational words play a very important role in determining the relationship of causal complex sentences. Although the deep learning model can automatically mine the text for some semantic and other feature information, it can be made more effective by adding some obvious manually identified features. The results of the classification experiments for each category of cause-effect complex sentences are listed in Table 4.

Table 3: Comparison of experimental results for each model.

Algorithm	Accuracy	Precision	Recall	F1
Transformer	81.35	82.33	79.05	80.50
CNN	89.79	88.84	89.44	89.13
LSTM	92.08	89.61	92.39	90.87
BiLSTM	92.76	91.99	91.96	91.95
RM-transformer	93.06	92.22	92.27	92.13

Table 4: Correct classification rates for each category of causal complex sentences.

Relationship category	Accuracy (%)
Causal class	93.25
Hypothetical class	92.41
Condition class	95.20
Target class	96.85
Inference class	83.69

From Table 4, it can be seen that the recognition rate of inferred compound sentences is significantly lower than that of other categories. The possible reasons for the classification errors in the experiment are as follows. (1) The corpus of the experiment is mostly from the news corpus, and inferred compound sentences are used infrequently, so the collected corpus is on the low side, and overfitting occurs during the training process. (2) There are multiple quasi-relatives (words that can act as relatives) in the sentences, corresponding to different categories. In this sentence, "since" indicates an inferred relationship, but "that" can indicate both a hypothetical and an inferred relationship, which should have been judged as a hypothetical relationship [34, 35].

Next, the dependent syntactic tree [18] can be used as input to incorporate richer syntactic information, and the graphical CNN model [19] can be used for the recognition of relational categories of marked compound sentences to further improve the accuracy of compound sentence category recognition.

6. Conclusions

In summary, an analogous study of collocation characteristics of verbal names in English translations based on the corpus found the following.

(1) Compared with other texts, verbal-name collocations in the English language are more concise, passive forms are used more frequently, verbal-name

collocation patterns are relatively fixed, and the choice of English vocabulary reflects the professional and concise nature of the medical language, with a simple and logical collocation structure.

(2) The choice of words in the English translation is somewhat narrower than that in the original English text, and the nodal words have far less influence on the collocations than the target language, reflecting the fact that the translator is influenced by the source language when translating and has certain limitations in word choice, which differs from the target language in the use of verbs.

A corpus can provide a large amount of authentic and natural linguistic data for text translation and provide a more objective and comprehensive picture of the characteristics and intrinsic patterns of Chinese medical English. The use of English corpus to study lexical collocation features can help explore the universal laws of Chinese medical English translation, grasp the characteristics of the translated text itself, and provide a basis for the standardisation of English terminology. At the same time, by searching the corpus of native speakers, exploring the constitutive rules of medical English vocabulary as well as customary collocation, and digging deeper into the meanings of English words, new translation ideas and translation methods can be provided for English translations.

Data Availability

The raw data supporting the conclusions of this article will be made available by the authors, without undue reservation.

Conflicts of Interest

The authors declare that they have no conflicts of interest.

References

[1] S.-Ho Han, "A review of research on restaurant brand personality: a focus on the hospitality and tourism journals listed at korea research foundation," *Journal of Tourism Sciences*, vol. 35, no. 2, pp. 337–353, 2011.

[2] K. Ahrens, H. Zeng, and S. H. R. Wong, "Using a corpus of English and Chinese political speeches for metaphor analysis," in *Proceedings of the Eleventh International Conference on Language Resources and Evaluation (LREC 2018)*, Miyazaki, Japan, May 2018.

[3] F. Mohamad and N. Abdul Malik, "Metaphor, religion, and gender: a case study of metaphor analysis in islamic motivational speech corpus/Norasyikin Abdul Malik and Faizah Mohamad," *International Journal of Modern Languages and Applied Linguistics (IJMAL)*, vol. 5, no. 3, pp. 95–121, 2021.

[4] T. Wang and S. Ge, "Corpus-based semantic prosody study of English-Chinese translation: taking trump's popular saying "it is what it is" as an example," in *Learning Technologies and Systems*, pp. 420–429, Springer, New York, NY, USA, 2020.

[5] P. Boontam, "A corpus-based study of food-related metaphors in English and Thai," *The Academic Journal: Faculty of Humanities and Social Sciences Nakhonsawan Rajabhat University*, vol. 6, no. 1, pp. 1–43, 2019.

[6] M.-L. Chen, "A corpus-based study on imagery and symbolism in Goldblatt's translation of Red Sorghum," *Babel. Revue internationale de la traduction/International Journal of Translation*, vol. 65, no. 3, pp. 399–423, 2019.

[7] G. Liu and X. Zhang, "The meaning-shift unit of Chinese intensifiers: a corpus-based study," *Journal of Language Teaching and Research*, vol. 12, no. 1, pp. 111–119, 2021.

[8] Y. Wang, "Book review: understanding metaphor through corpora: a case study of metaphors in nineteenth century writing," *International Journal of Translation, Interpretation, and Applied Linguistics (IJTIAL)*, vol. 3, no. 2, pp. 50–55, 2021.

[9] H. Feng, I. Crezee, and L. Grant, "Form and meaning in collocations: a corpus-driven study on translation universals in Chinese-to-English business translation," *Perspectives*, vol. 26, no. 5, pp. 677–690, 2018.

[10] E. F. Nurhidayat, E. Apriani, and S. Edy, "The analysis of cohesive devices used by tertiary English students in writing English paragraphs," *International Journal of Multicultural and Multireligious Understanding*, vol. 8, no. 4, pp. 70–81, 2021.

[11] L. Wang, C. Zhang, Q. Chen et al., "A communication strategy of proactive nodes based on loop theorem in wireless sensor networks," in *Proceedings of the 2018 Ninth International Conference on Intelligent Control and Information Processing (ICICIP)*, pp. 160–167, IEEE, Wanzhou, China, November 2018.

[12] S. Perdana, S. Fajaruddin, G. E. Kiswaga, A. Ariyanto, and A. Fujiastuti, "Experiential meaning breadth variations of the English-bahasa Indonesia alice in wonderland movie texts," *Script Journal: Journal of Linguistics and English Teaching*, vol. 6, no. 1, pp. 44–55, 2021.

[13] Z. K. Igaab and H. Abdulhasan, "Collocation in English and Arabic: a contrastive study," *English Language and Literature Studies*, vol. 8, no. 4, pp. 89–103, 2018.

[14] Z. K. Igaab, "The pragmatics of blackmail in English and Iraqi-Arabic," *International Linguistics Research*, vol. 4, no. 3, 72 pages, 2021.

[15] B. Li, Y. Li, C. Xu et al., "The niutrans machine translation systems for wmt19," in *Proceedings of the Fourth Conference on Machine Translation*, vol. 2, pp. 257–266, Florence, Italy, August 2019.

[16] D. Suparno, M. Farkhan, and M. A. Wahab, "Word formation in modern standard Arabic Palestinian and Tunisian," *AIUA Journal of Islamic Education*, vol. 1, no. 1, pp. 65–88, 2019.

[17] B. Y. J. Algburi and Z. K. Igaab, "Defamation in English and Arabic: a pragmatic contrastive study," *International Linguistics Research*, vol. 4, no. 2, 31 pages, 2021.

[18] H. Feng, *Form, Meaning and Function in Collocation: A Corpus Study on Commercial Chinese-to-English Translation*, Routledge, England, UK, 2020.

[19] K. Saito, "Multi- or single-word units? The role of collocation use in comprehensible and contextually appropriate second language speech," *Language Learning*, vol. 70, no. 2, pp. 548–588, 2020.

[20] R. Raksangob Wijitsopon, "Collocations and local textual functions of quantifiers in learner English essays," *Linguistic Research*, vol. 34, no. 1, pp. 1–49, 2017.

[21] H. Li, D. Zeng, L. Chen, Q. Chen, M. Wang, and C. Zhang, "Immune multipath reliable transmission with fault tolerance in wireless sensor networks," in *Proceedings of the International Conference on Bio-Inspired Computing: Theories and Applications*, pp. 513–517, Springer, Singapore, October 2016.

[22] M. Jafar Jabbari and N. Kavoosi, "An investigation into the collocations used in the translation of official documents from

Hindawi
Scientific Programming
Volume 2023, Article ID 9841980, 1 page
https://doi.org/10.1155/2023/9841980

Retraction

Retracted: Research on Chord-Constrained Two-Track Music Generation Based on Improved GAN Networks

Scientific Programming

Received 1 August 2023; Accepted 1 August 2023; Published 2 August 2023

This article has been retracted by Hindawi following an investigation undertaken by the publisher [1]. This investigation has uncovered evidence of one or more of the following indicators of systematic manipulation of the publication process:

(1) Discrepancies in scope
(2) Discrepancies in the description of the research reported
(3) Discrepancies between the availability of data and the research described
(4) Inappropriate citations
(5) Incoherent, meaningless and/or irrelevant content included in the article
(6) Peer-review manipulation

The presence of these indicators undermines our confidence in the integrity of the article's content and we cannot, therefore, vouch for its reliability. Please note that this notice is intended solely to alert readers that the content of this article is unreliable. We have not investigated whether authors were aware of or involved in the systematic manipulation of the publication process.

Wiley and Hindawi regrets that the usual quality checks did not identify these issues before publication and have since put additional measures in place to safeguard research integrity.

We wish to credit our own Research Integrity and Research Publishing teams and anonymous and named external researchers and research integrity experts for contributing to this investigation.

The corresponding author, as the representative of all authors, has been given the opportunity to register their agreement or disagreement to this retraction. We have kept a record of any response received.

References

[1] X. Li and Y. Niu, "Research on Chord-Constrained Two-Track Music Generation Based on Improved GAN Networks," *Scientific Programming*, vol. 2022, Article ID 5882468, 7 pages, 2022.

Hindawi
Scientific Programming
Volume 2022, Article ID 5882468, 7 pages
https://doi.org/10.1155/2022/5882468

Research Article

Research on Chord-Constrained Two-Track Music Generation Based on Improved GAN Networks

Xinru Li and Yizhen Niu

Xinyang Vocational and Technical College, Xinyang 464000, Henan, China

Correspondence should be addressed to Yizhen Niu; nyz@xyvtc.edu.cn

Received 6 December 2021; Revised 19 February 2022; Accepted 22 February 2022; Published 16 March 2022

Academic Editor: Le Sun

Chords have a role in music for emotional expression, and the generated melodies have more richness through the constraining effect of chords. In this paper, based on a GAN network music generation model based on chord features, a GRU network is used in chord feature extraction in order to autonomously learn chords at $1:t-1$ moments and generate chords at t moments, by saving the hidden layer state of each batch and constructing a layer of GRU combined with a generator, thus achieving the effect of automatically learning the overall style of chords. The performance of the four models is gradually optimized by weighted averaging, and the melodic pleasantness generated by all four models has a significant positive correlation with musical coherence and creativity.

1. Introduction

Music is an important form of artistic expression in our lives, closely related to us and an integral part of our lives. It can be used to soothe the mood and express emotions, and different tunes and melodies can express different emotions, resulting in countless classics. This is why there are a wide variety of styles and genres of music, which can be divided into pop, classical and pop music (Bach, Beethoven, Mozart), jazz, R&B, rock and roll, and vocal and instrumental music [1]. In recent decades, with the rise of the Internet industry and the significant improvement in the performance of computer hardware, the cost of generating a series of digital audio files regarding audio production, audio editing, audio recording, etc. has significantly reduced the threshold for nonprofessionals to enter the field of music, causing the number of music creations to grow exponentially, and the music industry has become an important area of the cultural market, with the series of Jitterbug, Racer, etc. With the emergence of streaming media and the maturation of the Internet, the competition for music platforms has gradually changed from competition for copyright and content to competition for audio diversity and multimodal content combined with graphics and video. Users' demand for this has also become more urgent [2, 3].

Artificial intelligence (AI) composition is a technique for generating digital music using algorithms, neural networks, and other executions [4]. AI is a technology that enables computers to learn and simulate human thought processes and behavioral capabilities through training. Stochastic algorithms, such as Gaussian noise, are often used as input in AI compositions, which undergo a finite number of state transitions and conditional constraints to generate the final sequence of notes [5]. Composition is the process by which a music creator creates music through a series of theoretical systems such as polyphony, harmonics, orchestration, etc. It is a process of expressing creative ideas [6]. Composing logarithmically is a new way of composing music. Compared with the traditional mode of music composition, it can combine human creativity, emotional expression, aesthetics, and other intelligent operations with the computing power of computers, human-computer interaction systems, automation control, and other technologies to break through the professional technical constraints of human composition and create more novel musical effects, while saving human costs and improving the efficiency of music composition.

This makes it easier for nonprofessional musicians to enter the hall of music creation and enjoy the joy of creation, while professional musicians are assisted by computer-generated musical works in different forms and styles to develop new innovative ideas and muses for composers.

Most current music generation neural network models use recurrent neural networks (RNNs) and their variants. Neural networks used for music generation usually use all the music information from previous events as a condition for generating the current music, and the generated music information will also be too repetitive, which greatly reduces the interest of the music [7]. When using only GAN to generate music, they are prone to unstable training, gradient disappearance, and pattern running, and do not take into account the time dependence, which can reduce the authenticity of the generated music. The chord feature-based GAN network music generation model (DCC_GAN) and the overall style-based GAN network music generation model (DCG_GAN) generate music in which the generator CNN and the moderator CNN are trained together and generate music melodies under the constraints of the chord CNN module, and the generated results are fed to the discriminator CNN, which submits the feedback to the generator [8, 9].

Music as a kind of auditory art, brings not only auditory feelings, but also can directly hit people's hearts and express their emotions, among which pop music is a style form that can fully express human emotions through popular melodies and words that can be combined with different cultural backgrounds in different countries and regions around the world to form a very different style of pop music, and with development of deep learning, China has made some achievements in natural language processing, speech recognition, image processing, etc., but the research in the field of music generation is still at an elementary level, and there is a lot of room for development [10]. In the traditional composition field, composers need to have solid musical skills and musicianship, and it takes a long time to create excellent works, which is relatively difficult for people who love music but are not strong in music. Using deep neural networks to generate music can provide a vast creative platform for people who love music and bring a vast market and economic benefits, and the future is immeasurable [11, 12].

2. Convolutional Adversarial Generative Network-Based Model

A convolutional GAN for symbolic-domain music generation was proposed in 2017 by Richard Yang, which is based on the principle of applying a convolutional GAN model to the music generation domain to form a convolutional GAN for symbolic-domain music generation (MidiNet). adversarial network for symbolic-domain music generation [13]. The model is fed with a preprocessed music melody dataset, trained by a generator CNN and a moderator CNN, and the generated results are fed to a discriminator CNN, which feeds the output of the discriminator CNN to the generator CNN so that the whole model forms a game process and finally outputs a better music melody.

2.1. Datasets. The input to the music generation model based on convolutional adversarial generative networks is a collection of popular music melodies in nope format reprocessed to a melody bar count of 50,496 (789 MB), a chord bar count of 50,496 (5.01 MB), a memory size of 5.01 MB, a dimension of 13, and a piano roll format with 16 note units, a pitch range of C4-B5, and random noise of Gaussian white noise of length 100 [14].

2.2. Model Structure. The model used in this paper is based on GAN for optimization, which has opened up a new era of neural networks since Ian Goodfellow proposed GAN in 2014 [15].

An artificial neural network (ANN), referred to as a neural network (NN), is a mathematical model that mimics the behavioral characteristics of biological neural networks and processes data to achieve human artificial intelligence [16]. Machine learning techniques for human artificial intelligence [17]. A neural network is shown in Figure 1 as a typical three-layer neural network framework, including an input layer, a hidden layer, an activation layer, an output layer, and a normalization process for the output.

The neural network graph has three neurons in the input layer and four neurons in the hidden layer. An activation function is added after the hidden layer to add a nonlinear factor to the results of the matrix operations, mapping the features to a high-dimensional nonlinear interval for interpretation. The output layer has two neurons, and the output of the output layer is normalized so that the data are restricted to a certain range, thus eliminating the undesirable effects caused by odd sample data [18].

The internal structure of the neural network: this structure is shown in Figure 2 as a processing unit of the neural network, x_i is the input from the i-th neuron; w is the connection weight of the i-th neuron, equivalent to the eigenvalue. The absolute value of the weight represents the size of the influence of the input signal on the neuron, θ_j is the bias, also known as the threshold, after the activation function to obtain the output results, the output results are shown in equation (1), [19].

$$y = f\left(\sum_{i=1}^{n} w_i x_i - \theta\right). \quad (1)$$

2.3. Generative Adversarial Networks. The GAN is primarily trained as a generator and a discriminator neural network, where the two networks are played to obtain the better result of the two networks. A high-performance discriminator is used for identification [20]. The input music, which may be generated by the generator, is identified by the discriminator, and if it is real music, the identification result is true, and if it is generated music, the identification result is false. The result of the identification by the discriminator gives

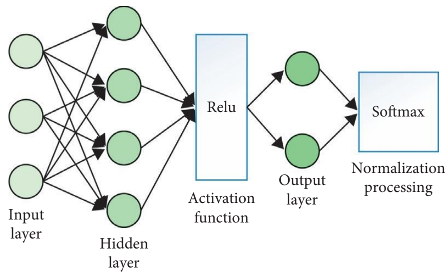

FIGURE 1: Neural network diagram.

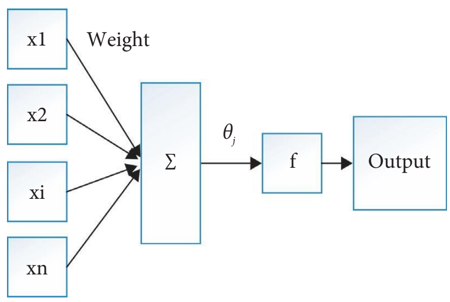

FIGURE 2: Diagram of the internal structure of the neural network.

feedback to the generator to improve its performance in generating music, and the generator also gives feedback to the discriminator to improve its performance in generating music [21]. The initial stage of the GAN network (as shown in Figure 3) is mainly used in image generation, in which the two networks play a game, each trying to beat the other to achieve its own performance improvement. The ultimate goal is to use the generator network to generate music melodies that can be faked.

2.4. Music Generation Models Based on Convolutional GAN. The GAN is a game between a generator neural network and a discriminator neural network in which the two networks are trained to give the best result of the two networks, and the identification of real and generated music is described [22]. The two networks are eventually better; the generator network is trained so that the generated music is highly similar to the real music and the discriminator network is highly discriminative. The initial stage of the GAN network was mainly used for image generation, where the generator and discriminator networks were used to generate the real music. Each network tries to beat the other to improve the performance of its own network. The ultimate goal is to use the generator network to generate music melodies that can be falsely described as real [23].

In the MidiNet model, it consists of a moderator CNN, a generator CNN, and a discriminator CNN. In the moderator CNN, the input is a two-dimensional starter bar, which is convoluted into four layers, with each layer outputting a corresponding starter bar to be combined with the generator CNN; in the generator CNN, the input is a one-dimensional chord and random noise, which is also conserved in four

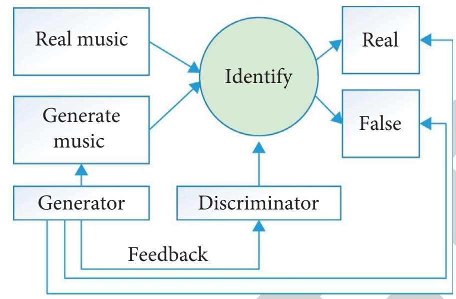

FIGURE 3: GAN network structure.

layers, with each layer combining with the starter bar generated by the moderator to generate a new melody [24]; in the discriminator CNN, the input is either a real melody or a generated In the discriminator CNN, the input is either the real melody or the generated melody, and the start bars and chords are added through two layers of convolution and one layer of full concatenation, resulting in a discriminated output.

2.5. Model Objectives. The total objective formula is as in equation (2). The discriminator CNN is equation (3), and the generator CNN is equation (4). Where x~data(x) denotes sampling from real data, z~pc (z) denotes sampling from a random distribution, D denotes the discriminator network, and G denotes the generator network. In the discriminator network equation (3), the goal is to identify whether the input is a real melody or a generated melody, and the generation process is shown in Figure 4. If the data comes from real data, the discriminator probability is the maximum, and the purpose of doing log conversion is similar to log-likelihood, which does not affect the monotonicity of the function, but makes the operation more simple [25]; if the data comes from a Gaussian noise distribution, the input of the discriminator is the result generated by the generator, then the probability of the discriminator network will fall and $1 - D(G(z))$ will rise, and then take the log conversion so that the probability of equation (3) takes the maximum value. For the generator network equation (4), the goal is to generate melodies that can fool over the discriminator network, the generation process is illustrated in Figure 5, the data x comes from the generated data i.e., the result generated by the Gaussian noise z, then the probability of $D(G(z))$ goes up and the probability of $\log(1 - D(G(z))$ goes down, and finally the minimum value of the generator network is obtained.

$$\begin{aligned}\operatorname{minmax}_G V(D, G) = {} & \mathbb{E}_{\mathrm{X}\sim p_{\mathrm{data}}(\mathrm{X})}[\log(D(\mathrm{X}))] \\ & + \mathbb{E}_{\mathbf{z}\sim p_z(\mathrm{z})}[\log(1 - D(G(\mathrm{z})))],\end{aligned} \tag{2}$$

$$\max_D E_{X_{\alpha Pdta}}[\log D(\mathrm{x})] + E_{Z\sim\beta_{iz}}[\log(1 - D(G(z))], \tag{3}$$

$$\min_G E_{X_N P(x)}[\log(1 - D(G(z))]. \tag{4}$$

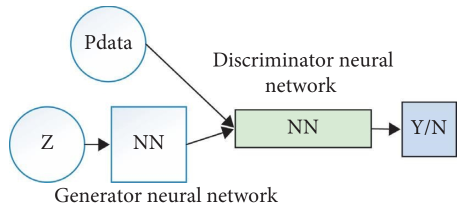

FIGURE 4: Discriminator network diagram.

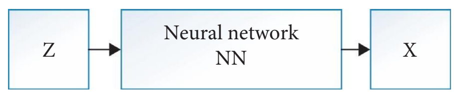

FIGURE 5: Generator network diagram.

3. Experimental Results and Analysis

3.1. Experimental Results. This paper uses the music theory rule-based music generation model, the DCC_GAN model, and the DCG_GAN model to generate a large number of musical melodies after training with chord constraints and time dependence. The model with chord constraints and time-dependent training to generate a large number of musical melodies. The melodies generated are more coherent, pleasant, and innovative than those generated by the baseline model. Here, the DCG_GAN model, for example, generates melodies in the nyc format as shown in Figure 6, and performs different rounds (1 epoch, 100 epoch, and 200 epoch). (100 epoch, 200 epoch) iterations, all selecting the first two bars of the first phrase of each round for observation, and as the number of training rounds increased, the notes became more varied and the resulting melodies more diverse [26].

The generated music in midi format is displayed as a piano roll in the MidiEditor software by selecting the first four bars of each melody as shown in Figure 7.

The experimental results of the baseline model are shown in Figure 7, which shows that the generation process tends to level off in both the chord and melody sections.

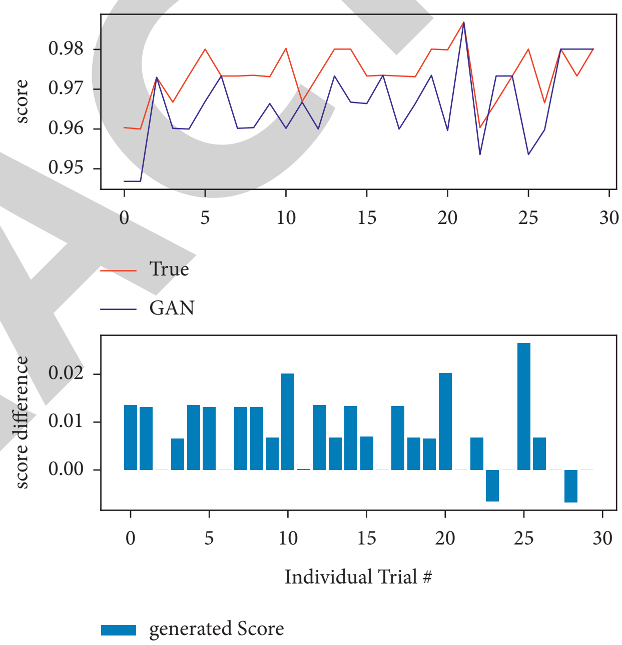

FIGURE 6: DCG_GAN model generation results (1 epoch, 100 epoch, and 200 epoch).

3.2. Assessment and Analysis. There are currently no scientifically rigorous and objective evaluation criteria for music melody generation, and the main evaluation method is based on the subjective evaluation of the user. The evaluation perspective is based on the coherence, ear-friendliness, and interest of the generated music melodies, with the baseline model's generated music melodies as a control group, and the music theory rule-based music generation model, the chord feature-based GAN network music generation model, and the overall style-based GAN music generation model. The GAN network music generation models are based on chord features and the GAN network music generation models are based on overall style. The four groups of models were trained for 200 rounds, and the generated music files were processed through a python library. The generated music files were converted from the nyc format to midi format by the Python library piano roll, and then the melodies in midi format were converted to MP3 format by MIDI 3 Pro software, and finally, the generated music melodies were evaluated and analyzed [27].

A total of 50 people was evaluated, 40 of whom were general listeners and 10 of whom were music professionals (music-related learners or instrumentalists), and the three groups of results were evaluated in terms of their melodic coherence, fearfulness, and creativity. The results were evaluated on a five-point scale, with 1 being the least effective, 5 being the most effective, and so on, and a weighted average of 50 scores produced the following results are shown in Table 1, [28].

The evaluation results were analyzed using a weighted average method in the two-track music generation based on chord-constrained GAN networks. For the four groups of models, the results were calculated as 40% for 40 general listeners and 60% for 10 music professionals, as in equation

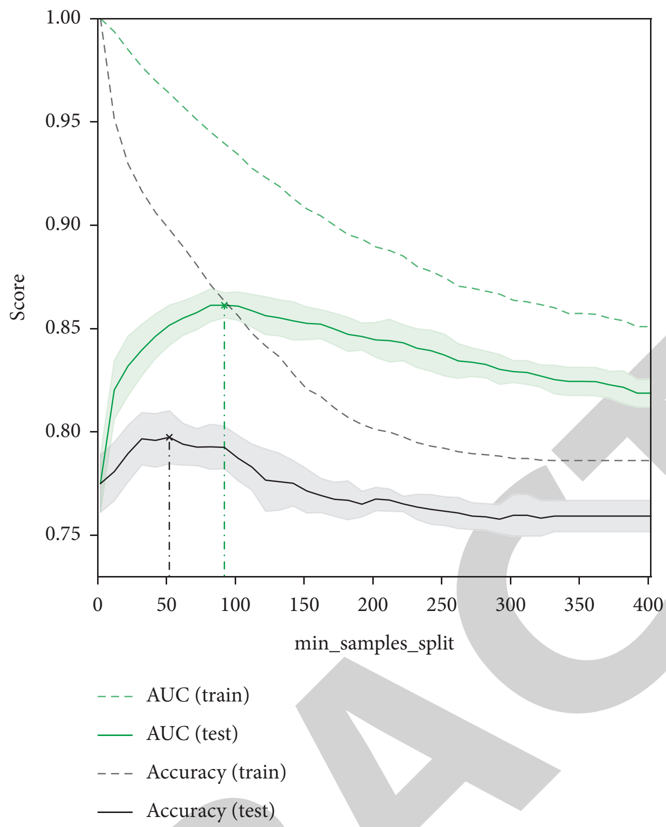

FIGURE 7: Baseline model experimental results.

TABLE 1: Subjective evaluation of experimental results of MidiNet, Rakuhari-based, DCC_GAN, and DCG_GAN models.

Model/Performance	Ordinary audience			Music professionals		
	Continuity	Pleasant ear	Innovation	Continuity	Pleasant ear	Innovation
MidiNet	3.0	3.1	3.2	2.2	2.5	2.1
Based on music theory	3.1	3.1	3.1	2.6	2.6	3.2
DCC_GAN	3.3	3.5	3.5	3.0	3.0	2.6
DCG_GAN	3.8	3.8	3.6	3.6	3.8	3.2

TABLE 2: Weighted average results of musical melodies generated by the four groups of models.

Model	Average audience score	Professional musician score	Total score
MidiNet	3.07	2.27	2.59
Based on music theory	3.10	2.72	2.87
DCC_GAN	3.40	2.92	3.11
DCG_GAN	3.76	3.58	3.65

(5). The weighting of the three performance evaluation metrics of coherence, earliness, and innovation was analyzed as 5 : 3:2, resulting in the performance analysis of the four groups of models in Table 2. The performance of the models gradually improves, and the melodies generated are more realistic and pleasing to the ear [29, 30].

$$\overline{x} = \frac{x_1 f_1 + x_2 f_2 + x_3 f_3 + \cdots + x_k f_k}{\sum_1^k f_i}. \quad (5)$$

In music, the core of the generated results is the fearfulness of the generated music. Therefore, the fearfulness of the melodies generated by the four groups of models was

Table 3: Analysis of the correlation between melodic pleasantness and coherence and creativity of the music generated by the four groups of models (Pearson correlation).

Model	Correlation coefficient between agreeableness and coherence	Correlation coefficient between pleasant ear and innovation
MidiNet	0.674	0.432
Based on music theory	0.698	0.385
DCC_GAN	0.571	0.475
DCG_GAN	0.788	0.514

correlated with the coherence and creativity, respectively, according to the Pearson correlation coefficient as in equation (6). The results of the analysis are shown in Table 3 [31].

$$r = \frac{N\sum x_i y_i - \sum x_i \sum y_i}{\sqrt{N\sum x_i^2 - \left(\sum x_i\right)^2}\sqrt{N\sum y_i^2 - \left(\sum y_i\right)^2}}. \tag{6}$$

4. Conclusions

This paper introduces the baseline model in this experiment, the music generation model based on convolutional adversarial generative network, which is divided into two subsections: the first subsection introduces the dataset used in the model training process, including the data et format, data type, total amount of data, and data units; the second subsection introduces the model structure of the baseline model, including GAN. By introducing the baseline model, the baseline model can be better optimized for subsequent work.

Data Availability

The raw data supporting the conclusions of this article will be made available by the authors without undue reservation.

Conflicts of Interest

The authors declare that they have no conflicts of interest regarding this work.

References

[1] C. H. Cao, Y. N. Tang, and D. Y. Huang, "IIBE: An improved identity-based encryption algorithm for WSN security," *Security and Communication Networks*, vol. 2021, 2021.

[2] D. Wu, C. Zhang, L. Ji, R. Ran, H. Wu, and Y. Xu, "Forest fire recognition based on feature extraction from multi-view images," *Traitement du Signal*, vol. 38, no. 3, pp. 775–783, 2021.

[3] L. Wang, C. Zhang, Q. Chen et al., "A communication strategy of proactive nodes based on loop theorem in wireless sensor networks," in *Proceedings of the 2018 Ninth International Conference on Intelligent Control and Information Processing (ICICIP)*, pp. 160–167, IEEE, Wanzhou, China, 2018.

[4] H. Li, D. Zeng, and L. Chen, "Immune multipath reliable transmission with fault tolerance in wireless sensor networks," in *Proceedings of the International Conference on Bio-Inspired Computing: Theories and Applications*, pp. 513–517, Springer, Singapore, 2016.

[5] H. Purwins, B. Li, T. Virtanen, J. Schluter, S.-Y. Chang, and T. Sainath, "Deep learning for audio signal processing," *IEEE Journal of Selected Topics in Signal Processing*, vol. 13, no. 2, pp. 206–219, 2019.

[6] S. Oore, I. Simon, S. Dieleman, D. Eck, and K. Simonyan, "This time with feeling: Learning expressive musical performance," *Neural Computing & Applications*, vol. 32, no. 4, pp. 955–967, 2020.

[7] V. S. Parekh and M. A. Jacobs, "Deep learning and radiomics in precision medicine," *Expert review of precision medicine and drug development*, vol. 4, no. 2, pp. 59–72, 2019.

[8] G. Brunner, Y. Wang, R. Wattenhofer, and S. Zhao, "Symbolic music genre transfer with cyclegan," in *Proceedings of the 2018 IEEE 30th International Conference on Tools with Artificial Intelligence (ICTAI)*, pp. 786–793, IEEE, Volos, Greece, Nov. 2018.

[9] B. L. Sturm, O. Ben-Tal, Ú. Monaghan et al., "Machine learning research that matters for music creation: A case study," *Journal of New Music Research*, vol. 48, no. 1, pp. 36–55, 2019.

[10] L.-C. Yang and A. Lerch, "On the evaluation of generative models in music," *Neural Computing & Applications*, vol. 32, no. 9, pp. 4773–4784, 2020.

[11] X. Zhao, S. Wang, and L. Sun, "Single and sequential sampling plans for multi-attribute products and multi-class lot in reliability test," *IEEE Access*, vol. 7, pp. 81145–81155, 2019.

[12] J. Wu, X. Liu, X. Hu, and J. Zhu, "PopMNet: Generating structured pop music melodies using neural networks," *Artificial Intelligence*, vol. 286, p. 103303, 2020.

[13] K. Tatar and P. Pasquier, "Musical agents: A typology and state of the art towards musical metacreation," *Journal of New Music Research*, vol. 48, no. 1, pp. 56–105, 2019.

[14] C. Gan, D. Huang, P. Chen, J. B. Tenenbaum, and A. Torralba, "Foley music: Learning to generate music from videos, Computer Vision - ECCV 2020," in *Proceedings of the Computer Vision–ECCV 2020: 16th European Conference*, pp. 758–775, Springer International Publishing, Glasgow, UK, August 2020.

[15] J. Zhang and D. Tao, "Empowering things with intelligence: A survey of the progress, challenges, and opportunities in artificial intelligence of things," *IEEE Internet of Things Journal*, vol. 8, no. 10, pp. 7789–7817, 2020.

[16] I. P. Yamshchikov and A. Tikhonov, "Music generation with variational recurrent autoencoder supported by history," *SN Applied Sciences*, vol. 2, no. 12, pp. 1–7, 2020.

[17] W. T. Lu and L. Su, *Transferring the Style of Homophonic Music Using Recurrent Neural Networks and Autoregressive Model*, pp. 740–746, ISMIR, 2018.

[18] D. Makris, M. Kaliakatsos-Papakostas, I. Karydis, and K. L. Kermanidis, "Conditional neural sequence learners for

Hindawi
Scientific Programming
Volume 2022, Article ID 5095966, 14 pages
https://doi.org/10.1155/2022/5095966

Research Article

Research on Bridge Structural Damage Identification

Yi Sun,[1,2] Kun Ma,[1] Dongfa Sheng,[2] Dewen Liu,[2] and Bihui Dai[1,2]

[1]*Faculty of Civil Engineering and Mechanics, Kunming University of Science and Technology, Kunming 650500, China*
[2]*Institute of Civil Engineering, Southwest Forestry University, Kunming 650224, China*

Correspondence should be addressed to Kun Ma; 11305063@kust.edu.cn

Received 2 December 2021; Revised 17 January 2022; Accepted 22 January 2022; Published 16 March 2022

Academic Editor: Le Sun

The traditional identification methods have limited ability to identify damage location of bridge structures. Therefore, a bridge structural damage location identification method based on deep learning is proposed. In addition, the sigmoid function is the activation function, and the cross entropy is the cost function. Meanwhile, take the Gaussian noise as the addition method and take the softmax as the classifier. So the constructed SDAE deep learning model can realize damage location identification of the simply supported the continuous beam bridges. Compared with the traditional identification methods of bridge structures, namely BP network and SVM, the proposed method shows higher identification accuracy and antinoise performance. Here, the average identification accuracy of the method for continuous beam bridge is 99.8%. As can be seen that the proposed method is more suitable for practical bridge structure damage location identification.

1. Intoduction

The development of social economy is inseparable from transportation. Bridge, as an important part of transportation, plays an important role in connecting the north and south. The safety of its structure is related to the safety of transportation, and it affects people's life. Once the bridge structure is seriously damaged, it will inevitably cause traffic accidents. In order to ensure the safe operation of bridges, it is of great significance to identify the damage of bridge structures. With the development of data transmission and processing technology, the nondestructive detection of bridge structures has been widely used. At present, the nondestructive detection and identification methods of bridge structures are mainly based on vibration identification methods, including the method based on modal domain data, the method based on time domain data, the method based on time-frequency domain data, and the method based on intelligent algorithm. For example, Xijun Ye and Boscato et al. proposed an adaptive signal denoising method based on genetic algorithm and singular value decomposition. By selecting SNR as fitness function, the genetic algorithm is introduced to automatically optimize p and r parameters. Then the inverse singular value decomposition is performed to obtain the denoised signal[1, 2]. This method is helpful to improve the identification accuracy of bridge structural damage location. Considering that the long-term effect of vehicle load is an important cause of fatigue, local damage, aging, reliability reduction, and so on, Jihwan Kim and Lili Li et al. proposed a bridge vehicle load model and carrying capacity evaluation method based on dynamic weighing system [3, 4]. Xiao-qin Li and Shiqiang Qin et al. discussed the strategy and scheme of multiscale finite element simulation of long-span bridge structures with the goal of structural damage diagnosis and safety assessment[5, 6]. Based on the analysis of the error sources of the finite element model, an error hierarchical correction method for the long-span bridges structure model is proposed. In addition, based on the finite element modeling and model modification process of cable-stayed bridge of the Runyang Yangtze River Bridge, a multiscale finite element simulation method for damage diagnosis and safety assessment of long-span cable-stayed bridge is proposed. Xianzheng Yu and Marco Furinghetti et al. established and modified the finite element model of the bridge structure to accurately simulate the behavior and working state of the bridge structure [7, 8]. On this basis, combining the finite element forward analysis with the signal inverse identification to evaluate the daily work of the bridge and the impact of various disasters on the structure. To a certain extent, the above research methods have realized the location of damage parts to different bridge structures, but the positioning accuracy and antinoise performance need to be improved. Therefore, in order to improve the identification accuracy and antinoise performance of the algorithm for bridge structure damage location, and based on deep learning model, this paper proposes a bridge structure damage location identification method based on stacked denoising autoencoder.

1.1. Introduction to SDAE Model. SDAE is a common model in deep learning, it is formed by stacking several denoising autoencoders. However, on the basis of autoencoder, the denoising autoencoder is a network. First, it can add noise to the training data and randomly mask part of training data. Subsequently, it forces the model to learn denoising and restore the input data. Therefore, to understand the principle of SDAE, the first is to understand the structure and training mode of autoencoder and denoising autoencoder.

1.2. Introduction to Autoencoder. Autoencoder consists of encoder and decoder, including input layer, hidden layer, and output layer, as shown in Figure 1. Wherein, the encoder is responsible for mapping the input vector to the hidden layer through the activation function, so as to obtain the feature expression of a higher level, as shown in formula (1) [9]. The decoder is responsible for mapping the hidden layer feature representation to the original input, and its function expression is shown in formula (2) [10].

$$z = f(x) = s\left(W^{(1)}x + b^{(1)}\right), \tag{1}$$

$$x' = g(z) = s\left(W^{(2)}x + b^{(2)}\right). \tag{2}$$

Formula (1) shows that x represents the input vector, z represents the encoder output vector, $W^{(1)}$ represents the input weight of the hidden layer, $b^{(1)}$ represents the input bias of the hidden layer, and s represents the activation function.

Formula (2) shows that x' represents the output matrix, $W^{(2)}$ represents the input weight of the output layer, and $b^{(2)}$ represents the input bias of the output layer.

The training method of the autoencoder is unsupervised learning, and the network parameter $\theta = \{W^{(1)}, W^{(2)}$ $b^{(1)}, b^{(2)}\}$ is adjusted to make the final output X^* as close as possible to the original input X. Its error function is defined as square error, as shown in

$$L = \|x - g(f(x))\|^2. \tag{3}$$

The weight and bias can be updated according to the error back propagation and gradient descent algorithm, and the optimal parameter θ can be obtained.

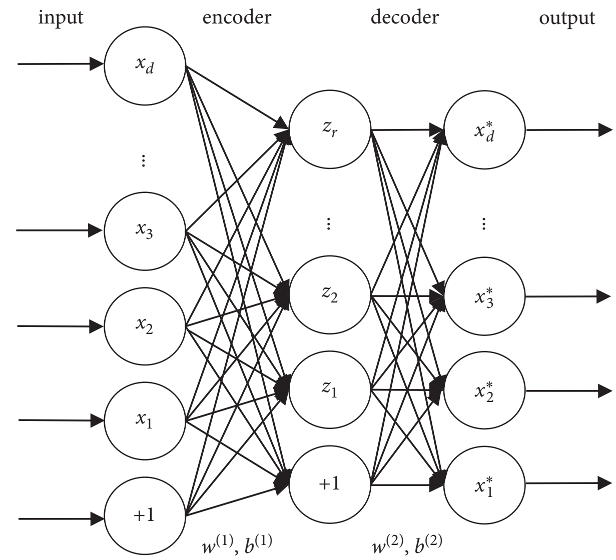

Figure 1: Schematic diagram of autoencoder structure.

1.3. Denoising Autoencoder. Denoising autoencoder takes the data with added noise as input and outputs the predicted original data without noise through training. Its denoising principle is shown in Figure 2. In the figure, x represents the original data, x_1 represents the data with noise, and y represents the feature obtained by encoding x_I in the hidden layer of the denoising autoencoder, Z represents the original data restored by decoding y, and L_D (x,z) represents the error function.

The training of denoising autoencoder makes the error function L_D minimum. Since random noise is added to the denoising autoencoder, formula (3) can be rewritten as

$$L_D = \|X - g(f(XI))\|^2. \tag{4}$$

The weight and bias can also be updated by using error back propagation and gradient descent algorithm, and the optimal parameter θ can be obtained.

For SDAE, the training method is that initially determine the parameters of a single denoising autoencoder through unsupervised learning, then use the BP algorithm to conduct supervised learning for all denoising autoencoders, and fine-tune the global parameters.

1.4. BP Algorithm Parameter Tuning. BP algorithm includes two stages, namely information forward calculation and error back propagation, and its common activation function is shown in the following formula[11].

$$f(u) = \frac{1}{1 + e^{-\lambda u}}. \tag{5}$$

In the information forward calculation stage, the input and output of neuron j in network k layer can be expressed as formula (6). The weight of update method in the error back propagation stage is shown in formula (7).

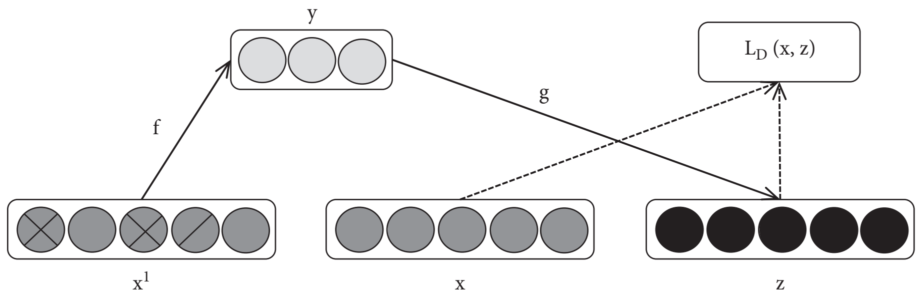

Figure 2: Denoising autoencoder training principle.

$$y_j^{(k)} = f_j^{(k)}\left(\sum_{i=1}^{N_{t-1}} \omega_{ij}^{(k-1)} y_i^{(k-1)} - \theta_j^{(k)}\right), \quad k = 1, 2, \ldots, M;\ j = 1, 2, \ldots N_k, \tag{6}$$

$$\omega_{ij}^{(k-1)}(t+1) = \omega_{ij}^{k-1}(t) + \eta \sum_{h=1}^{I} \delta_{hj}^{(k)} y_{hk}^{(k-1)}. \tag{7}$$

Formula (6) shows that M represents the total number of layers; N_k represents the total number of neurons in k layer; $\omega_{ij}^{(k-1)}$ represents the connection weight between neuron i of k-1 layer and this neuron; $\theta_j^{(k)}$ represents the neuron offset value; and $y_j^{(k)}$ represents the output of neuron i of k-1 layer.

Formula (7) shows that $0 < \eta < 1$ represents the learning step and δ represents the error transmission term. For the output layer, it can be calculated by formula (8), and the other layers can be calculated by formula (9).

$$\delta_{hj}^{(M)} = \left(\hat{y}_{hj}^{(M)} - y_{hj}^{(M)}\right) f_j\left(y_{hj}^{(M)}\right), \tag{8}$$

$$\delta_{hj}^{(k)} = f_j\left(y_{hj}^{(k)}\right) \sum_{i=1}^{N_{k+1}} \delta_{hj}^{(k+1)} \omega_{ij}^{(k)}(t). \tag{9}$$

where $\hat{y}_{hj}^{(M)}$ and $y_{hj}^{(M)}$ are the actual output and expected output values of BP algorithm, respectively.

Finally, the output error of BP algorithm can be expressed as [12]

$$\varepsilon = \sum_{h=1}^{I} \sum_{j=1}^{N_M} \left(\hat{y}_{hj}^{(M)} - y_{hj}^{(M)}\right)^2. \tag{10}$$

It can be seen from the above analysis that SDAE can obtain the most representative features of the original samples from the input samples with noise through multiple stacked denoising autoencoders, which is conducive to enhancing the robustness of the model. Considering the possibility of distortion in the data collection of the bridge structure, which is similar to adding noise data to the real data, SDAE can be used to analyze the data of the bridge structure. Therefore, this paper proposes an identification method of bridge structural damage location based on SDAE.

2. Bridge Structural Damage Location Identification Based on SDAE

2.1. SDAE Model Construction

2.1.1. Activation Function Selection. The activation function can satisfy the nonlinear arbitrary function mapping between input and output information, and it can make the model have the ability of learning complex data. Therefore, the selection of activation function is particularly important. At present, the common activation functions in deep learning models mainly include Tanh, ReLu, and Sigmoid functions. The Tanh function expression is shown in formula (11) [13], and the derivative function expression is shown in formula (12) [14]. There is advantage of improving model training efficiency, but it is prone to zigzag phenomenon. Therefore, the optimal value is difficult to be obtained in the training [15]. The ReLu function expression is shown in formula (13) [16], and the derivative function expression is shown in formula (14) [17]. Here, the problem of gradient disappearance can be effectively solved. However, the point will never be activated when the input value is negative, which results that the training data lack diversity [18]. Sigmoid function can fit the function well, but there is the problem of gradient disappearance, which can be solved by pretraining and BP algorithm fine-tuning [19]. So this paper selects Sigmoid function as the activation function.

$$\begin{aligned} f(x) &= 2sigmoid(2x), \\ -1 &= \frac{2}{1+e^{-2x}}, \\ -1 &= \frac{e^x - e^{-x}}{e^x + e^{-x}}. \end{aligned} \tag{11}$$

$$f'(x) = 1 - (f(x))^2, \tag{12}$$

$$f(x) = \max(0, x), \tag{13}$$

$$f\prime(x) = \begin{cases} 0 & x < 0, \\ 1 & x \geq 0, \end{cases} \tag{14}$$

Sigmoid function is a nonlinear transformation function, whose mathematical description is shown in formula (15). Its output range is between (0, 1). Since the function is continuously derivable, its derivative function can be expressed as formula (16).

$$f(x) = \frac{1}{1+e^{-x}}, \tag{15}$$

$$f\prime(x) = f(x)(1 - f(x)). \tag{16}$$

2.1.2. Cost Function Selection. The cost function is a function that measures the error between the predicted value and the real value of the model. The cost function is used to calculate the partial derivative for the weight and applied to the gradient descent algorithm to update the weight of each layer. And the deep learning model with learning ability can be obtained. Therefore, the cost function of SDAE needs to be determined. At present, cost functions used in deep learning models are mainly cross entropy cost functions, as shown in formula (17) [20]. In addition, the mean square cost function is shown in formula (18) [21]. Compared with the mean cost function, the cross entropy cost function is more suitable for classification tasks [22]. Because the bridge structural damage location identification is actually a classification task, the cross entropy cost function is selected as the SDAE cost function in this paper.

$$C = -\frac{1}{n}\sum_{i=1}^{n}\left[x_i In\left(x_i^*\right) + \left(1 - x_i\right)In\left(1 - x_i^*\right)\right], \tag{17}$$

$$C = \frac{1}{2n}\sum_{i=1}^{n}\left\|x_i^* - x_i\right\|^2. \tag{18}$$

Among them, x_i^* and x_i represent the predicted value and the true value, respectively. N represents the total number of training samples.

2.1.3. Selection of Noise Adding Method. The data of bridge structure usually include the damage data, so the data of bridge structure can be simulated by adding noise. The methods of adding noise mainly include salt and pepper noise and Gaussian noise. Among them, salt-and-pepper noise is usually used in image processing [23]. Since the identification of bridge structural damage location does not involve image processing, the Gaussian noise is selected as the method to add noise. Gaussian noise means that the probability density function of noise obeys normal distribution, as shown in formula (19).

$$P(x) = \sqrt{\frac{1}{2\pi\sigma^2}\exp\left(-\frac{1}{2\sigma^2}(x-\mu)^2\right)}. \tag{19}$$

where μ and σ^2 represent the mean and variance of the Gaussian distribution, respectively.

Add Gaussian noise to the input vector and obtain

$$x_i^* = x_i \cdot \eta \cdot normmd(0, 1). \tag{20}$$

Here, x_i and x_i^* represent the input data before and after processing noise i, respectively, η represents noise level; and *normrnd* (0, 1) represents Gaussian noise with mean value 0 and variance 1.

2.1.4. Classifier Selection. Classifiers are used to classify the test samples. And classifiers are an essential part of deep learning models. At present, the common classifiers for deep learning models mainly include SVM, BP network, and Softmax. Among them, the SVM is mainly used to deal with linear separable classification problems. The classification form of BP network is regression value. And the Softmax conducts classification through probability expression, which is closer to the identification of bridge structural damage location in this paper [24]. Therefore, softmax classifier is selected as SDAE classifier. For softmax classifier, if the input is x, the output is k-dimensional vector, and k represents the total number of categories, and its mathematical expression is [25]:

$$h_\omega(x) = \begin{bmatrix} p\left(y^{(i)} = 1|x^{(i)};\omega\right) \\ p\left(y^{(i)} = 2|x^{(i)};\omega\right) \\ \vdots \\ p\left(y^{(i)} = k|x^{(i)};\omega\right) \end{bmatrix} = \frac{1}{\sum_{j=1}^{k} e^{\omega_j^T x^{(i)}}} \begin{bmatrix} e^{\omega_1^T x^{(i)}} \\ e^{\omega_2^T x^{(i)}} \\ \vdots \\ e^{\omega_k^T x^{(i)}} \end{bmatrix}. \tag{21}$$

where ω represents the weight parameter.

On the basis of the above analysis, the SDAE model constructed in this paper is shown in Table 1.

2.2. Identification Process. According to the constructed SDAE model, the identification method of bridge structural damage position is designed as Figure 3. First of all, the bridge structure sample data are divided into unlabeled sample and labeled sample data set. Then, the denoising autoencoder is used to conduct unsupervised learning and pretraining for unlabeled data, and the samples meeting the error requirements are input into SDAE for training. Meanwhile, the labeled samples are trained by SDAE for supervised learning and pretraining. When the training results meet the error, the SDAE model is constructed. At last, the constructed SDAE model is adopted to identify the damage locations of test samples and output the results. It can be seen that the bridge structural damage location identification based on SDAE is realized.

Table 1: SDAE model settings.

Deep learning model	Activation function	Cost function	Noise adding mode	Classifier
SDAE	Sigomid	Cross entropy cost function	Gaussian noise	Saftmaxclassifier

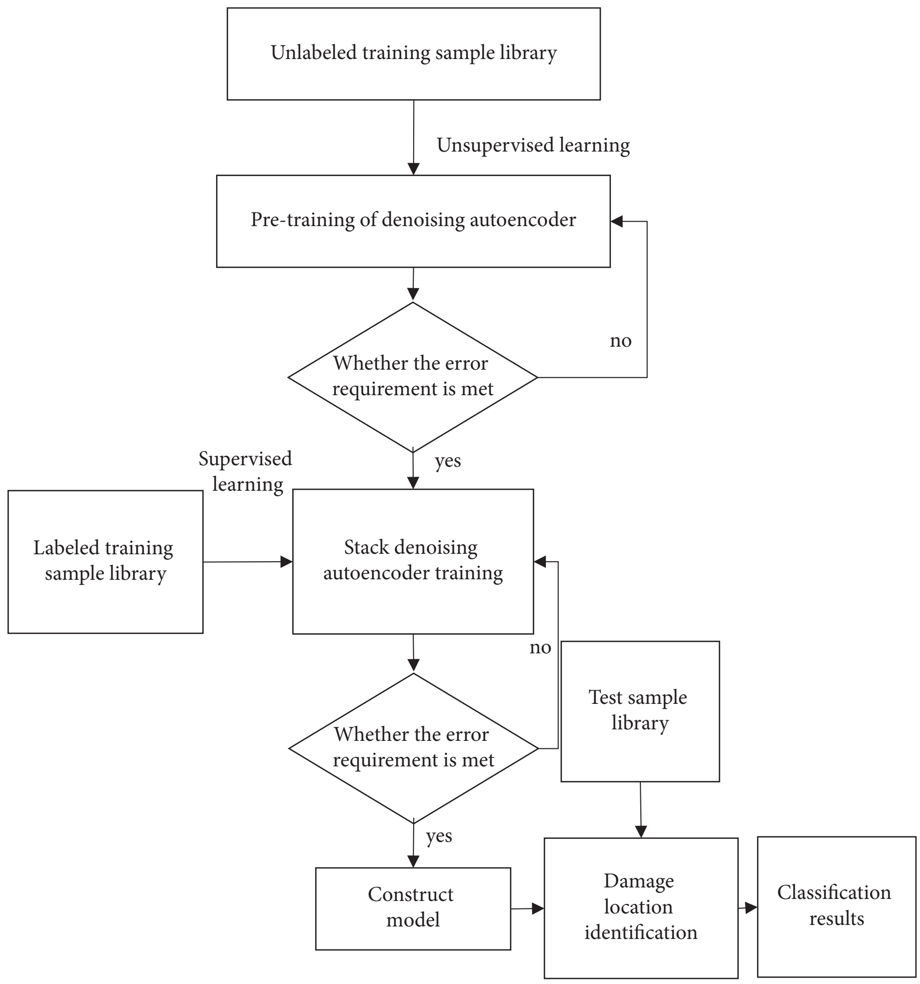

Figure 3: Bridge structural damage location identification process based on SDAE.

3. Simulation Experiment

3.1. Experimental Environment. This experiment is simulated on ANSYS finite element analysis software and MATLAB platform. The net span of the simply supported beam bridge model is 10 m, the concrete grade is C50, the beam cross-sectional area is $0.2\,m^2$, the inertia moment of unit section is $0.0042\,m^4$, the beam height is 0.5 m, the density is $\rho = 2500\,kg/m^3$, and the elastic modulus is 3.5×104 MPa[26–29]. Its unit division and plate-beam interface are shown in Figure 4. As can be seen from the figure, the simply supported beam bridge model is divided into 20 units and 21 nodes. Node 1 and node 21 are end nodes of the bridge, which are fixed hinge supports and sliding supports, respectively. Among them, the main beam is simulated by Bean3 unit, the horizontal and vertical displacements are used for node 1 constraint, and the vertical displacements are used for node 21 constraint.

The continuous beam bridge model is a two-span continuous beam bridge. The net span is $(24 + 24)$ m, the concrete grade is C50, the beam sectional area is $0.18\,m^2$, the inertia moment of unit section is $0.0054\,m^4$, the beam height is 0.6 m, the density is $\rho = 2500\,kg/m^3$, and the elastic modulus is 3.5×104 MPa. The unit division and plate-beam interface are shown in Figure 5. As can be seen from the figure, the continuous beam bridge model was divided into 24 units and 25 nodes. The length of each unit is 2m. Node 1, node 13, and node 25 are end nodes of the bridge, which are interactive supports, fixed hinge supports, and sliding supports, respectively. Among them, the main beam is simulated by Bean3 unit. The node 1 and node 25 are constrained by displacement cross the bridge, vertical angle along the bridge, and vertical displacement. The node 13 is constrained by displacement cross the bridge, displacement along the bridge, vertical displacement, and vertical angle along the bridge.

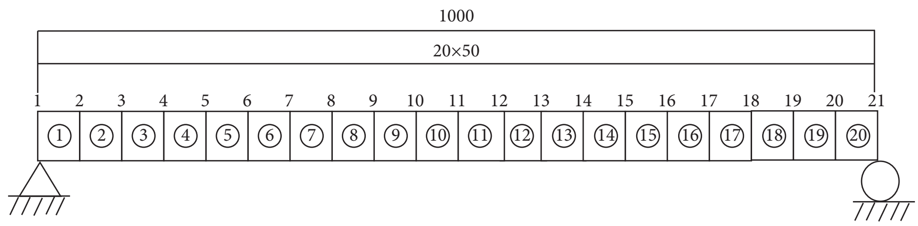

Figure 4: Schematic diagram of simply-supported beam bridge.

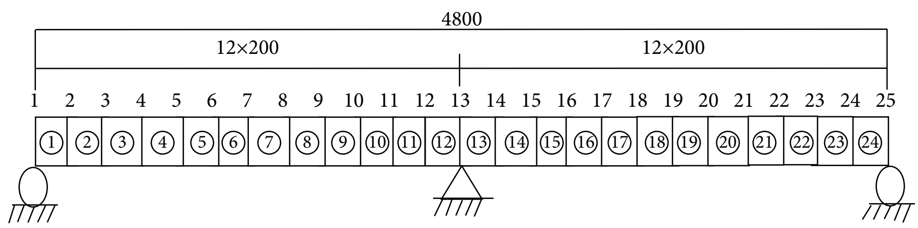

Figure 5: Schematic diagram of continuous beam bridge.

3.2. Damage Samples of Bridge Structures

3.2.1. Damage Index and Training Sample Database Determination. Combining the various literature, the acceleration response value of the measuring point is selected as the damage index of the bridge structure position identification. Totally, 270 groups of measuring point accelerations are used as a training sample database for damage location identification of simply supported beam bridges. In total, 12600 groups of measuring point accelerations are selected as a training sample database for damage location identification of continuous beam bridges.

3.2.2. Simply Supported Beam Bridge

Damage Condition. A moving load with a directional speed of 18 km/h is placed on the bridge, and the reduction of elastic modulus of material is defined as the damage degree. If the elastic modulus is reduced by 10%, the damage degree is 10% and substituted by the concentrated force $F = 100\,\mathrm{kN}$. Finally, there are seven damage conditions in this experiment, including no damage state and certain damage degree of a damage unit. The corresponding damage labels are shown in Table 2.

Sample Preprocessing. Under the action of moving load, the vertical acceleration values of nodes 5, 9, 13, and 17 in the 3 s of the simple beam bridge are randomly selected as the damage index [30]. Among them, the corresponding acceleration-time curve to each node in nondamage state is shown in Figure 6.

Z-score is used to conduct standardized preprocessing for the training samples and test samples, and sample I for SDAE training and test can be obtained, as shown in Figure 7.

3.2.3. Continuous Beam Bridge

Damage Condition. A moving load with a directional speed of 18 km/h is placed on the bridge, and the reduction of elastic modulus of material is defined as the damage degree. If the elastic modulus is reduced by 10%, the damage degree is 10%, and substituted by the concentrated force $F = 100\,\mathrm{kN}$. In order to be different from simply supported beam bridge, multiple unit damage is added in the experiment. Finally, the damage label database of the set test samples is shown in Table 3.

Sample Preprocessing. Under the action of moving load, all the vertical acceleration response values of nodes 4, 7, 10, 11, 19, and 22 within 5.8 s of continuous girder bridge are randomly selected as the training sample database. Among them, the damage degree is 40%, and the damage unite is No. 3. The corresponding acceleration-time curve of each node at this unit state is shown in Figure 8.

Z-score is adopted to perform standardized preprocessing for training samples and test samples, and sample II for SDAE training and test can be obtained, as shown in Figure 9.

3.3. Results and Analysis

3.3.1. Damage Location Identification of Simply Supported Beam Bridges

Analysis of Recognition Results. The test sample of preprocessed sample I is used as the input data of SDAE, and the recognition results of deep learning model are shown in Table 4. In the table, the first category represents nondamaged unit, the second category represents the No. 3 damaged unit, the third category represents the No. 7 damaged unit, and the fourth category represents the No. 11 damaged unit. As can be seen from the table, the identification accuracy of the proposed method for all damage categories has been reached 93.3%. Among them, the recognition accuracy of undamaged unit and No. 7 damaged unit is 100%, the recognition accuracy of No. 3 damaged unit is 90%, and the recognition accuracy of No. 11 damaged unit

Table 2: Damage labels of simply supported bridge samples.

Damage condition number	Boundary conditions	Loading condition: Concentration force size (kN)	Movement speed	Start	End	Damage unit	Damage degree	Label
JZLQ1	Boundary conditions of simply supported beam	100	18 km/h	Node 1	Node 21	No	No	1st category
JZLQ2	Boundary conditions of simply supported beam	100	18 km/h	Node 1	Node 21	No. 3	45%	2nd category
JZLQ3	Boundary conditions of simply supported beam	100	18 km/h	Node 1	Node 21	No. 3	55%	2nd category
JZLQ4	Boundary conditions of simply supported beam	100	18 km/h	Node 1	Node 21	No. 7	5%	3rd category
JZLQ5	Boundary conditions of simply supported beam	100	18 km/h	Node 1	Node 21	No. 7	95%	3rd category
JZLQ6	Boundary conditions of simply supported beam	100	18 km/h	Node 1	Node 21	No. 11	25%	4th category
JZLQ7	Boundary conditions of simply supported beam	100	18 km/h	Node 1	Node 21	No. 11	55%	4th category

is 88.9%. Therefore, the proposed method for the each damage unit location identification of simply supported beam bridge has certain effectiveness.

In order to verify the effectiveness of the proposed method for damage location identification of simply supported beam bridges with noise data, 5%, 10%, and 15% Gaussian noise are added to the input data of training data and test data in sample I, respectively. Meanwhile, the proposed method is adopted to identify, and the results are obtained as shown in Table 5. As can be seen from the table, under different noise conditions, the proposed method has a high recognition accuracy, which reaches 93.3%. Therefore, the SDAE proposed in this paper can effectively identify the location of each damage unit of a simply supported beam bridge.

Performance Comparison. In order to verify the identification performance of the proposed method, the proposed method and the traditional damage location identification methods of simply supported beam bridges, such as BP network and SVM, are used to identify sample I under the condition of no noise. The results are shown in Table 6. As can be seen from the table, compared with BP network and SVM comparative identification methods, the proposed identification method based on SDAE has the highest identification accuracy and a certain advantages.

Under different Gaussian noise conditions, the recognition results of BP network, SVM, and the proposed method are shown in Figure 10. As can be seen from the figure, compared with the traditional identification methods BP network and SVM, the proposed method has obvious advantages in recognition accuracy. With the increase of noise level, the recognition accuracy of both BP network and SVM shows a decreasing trend, and the recognition accuracy of the proposed method remains stable. Therefore, the identification performance of the proposed method is better than that of traditional identification methods for simply supported beam bridges, and it has certain practical application value.

3.3.2. Damage Location Identification of Continuous Beam Bridges. Analysis of Recognition Results. The test samples of preprocessed sample II are used as the input data of SDAE, and the recognition results of deep learning model are obtained as shown in Table 7. As can be seen from the table, the average identification accuracy of the method proposed for multiple damage units of continuous beam bridges is higher, which reaches 99.8%. Among them, when the damage unit is No. 3, the recognition accuracy of the first damage category is 98.2%. When the damage unit is No. 10, the recognition accuracy of the second damage category is 98.2%. The recognition accuracy of other damage categories containing multiple damage units is 100%. Therefore, compared with a single damage unit, the method proposed in this paper has a higher identification accuracy for the damage position of continuous girder bridges with multiple damage units simultaneously. The reason is that the more the damage units are, the greater the impact on the carrying capacity of the bridge structure is, and the more obvious the topological relationship between the damage category and the acceleration response value of the monitoring point is. It can be seen that it is conducive to SDAE classification, so as to improve the identification accuracy of the algorithm.

In order to verify the effectiveness of the proposed method in identifying the damage position of continuous beam bridges with noise data, the 5%, 10%, and 15% Gaussian noise are added to the input data of training data and test data in sample II. And the proposed method is used to identify the damage position, and the results are obtained as shown in Table 8. It can be seen from the table that under different noise conditions, the method proposed in this paper has high recognition accuracy, with an average recognition accuracy of 99.8%. Therefore, the proposed SDAE can effectively identify the location of each damage unit of continuous beam bridges, and it has certain practical application value.

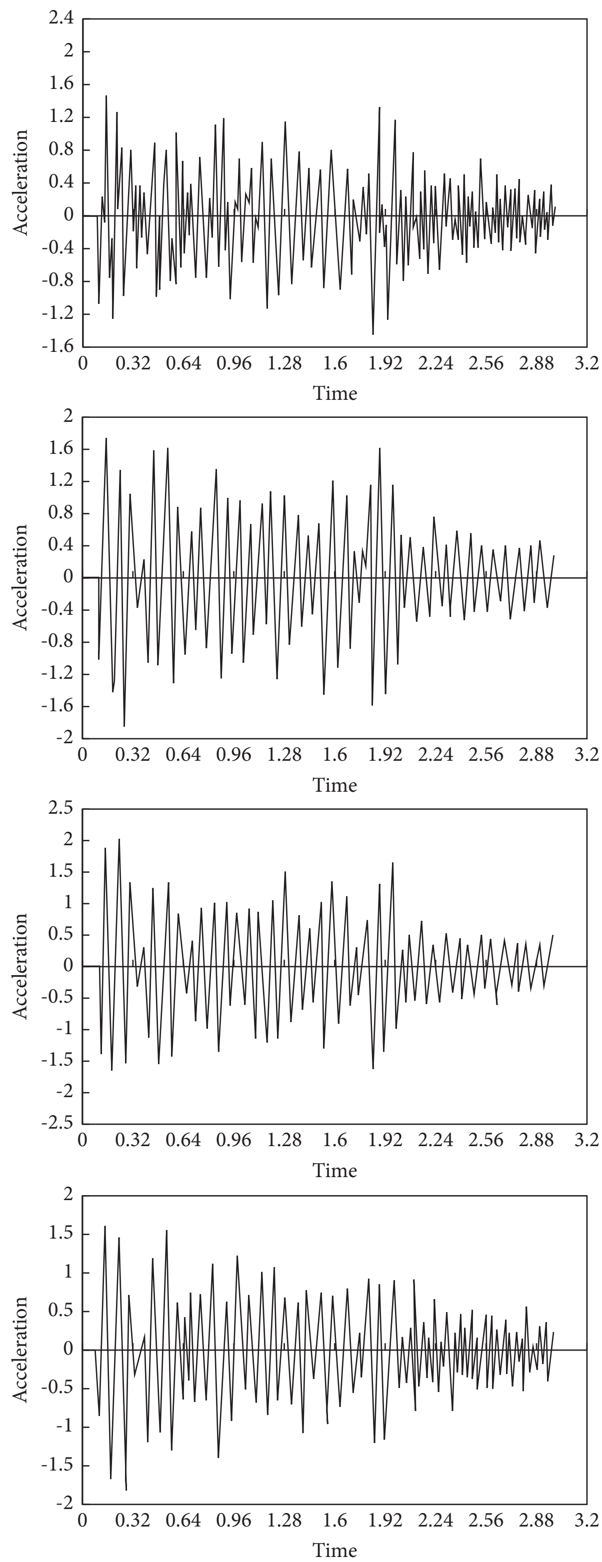

Figure 6: Acceleration-time curves of nodes.

Performance Comparison. In order to verify the identification performance of the proposed method, the proposed method and the traditional damage location identification methods of continuous beam bridges, such as BP network and SVM, are used to identify sample I under the condition of no noise. The results are shown in Table 9. As can be seen from the table, compared with BP network and SVM comparative identification methods,

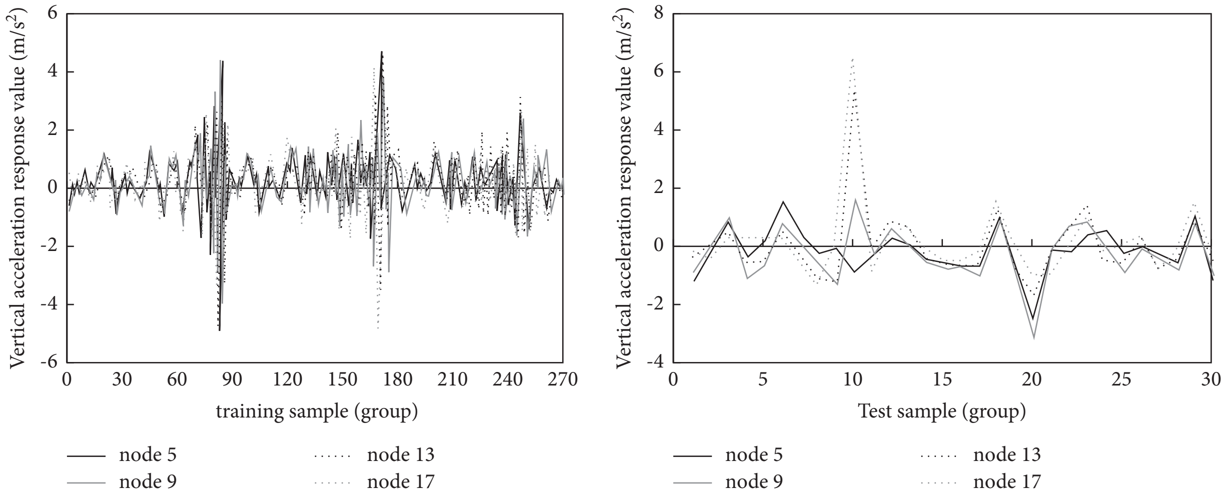

(a) (b)

Figure 7: Training set and test set after preprocessing sample I. (a) Preprocessed training samples. (b) Preprocessed test samples.

Table 3: Damage labels of continuous beam bridge samples.

Damage condition number	Boundary conditions	Loading condition				Damage unit	Damage degree	Label
		Concentration force size (kN)	Movement speed	Start	End			
LXLQ1	Continuous beam bridge boundary conditions	100	18 km/h	Node 1	Node 25	3	40%	1st category
LXLQ2	Continuous beam bridge boundary conditions	100	18 km/h	Node 1	Node 25	10	15%	2nd category
LXLQ3	Continuous beam bridge boundary conditions	100	18 km/h	Node 1	Node 25	21	55%	3rd category
LXLQ4	Continuous beam bridge boundary conditions	100	18 km/h	Node 1	Node 25	6.9	30%, 30%	4th category
LXLQ5	Continuous beam bridge boundary conditions	100	18 km/h	Node 1	Node 25	11, 19	15%, 15%	5th category
LXLQ6	Continuous beam bridge boundary conditions	100	18 km/h	Node 1	Node 25	5, 22	30%, 60%	6th category
LXLQ7	Continuous beam bridge boundary conditions	100	18 km/h	Node 1	Node 25	4, 8, 11	10%, 10%, 10%	7th category
LXLQ8	Continuous beam bridge boundary conditions	100	18 km/h	Node 1	Node 25	9, 15, 20	45%, 45%, 45%	8th category
LXLQ9	Continuous beam bridge boundary conditions	100	18 km/h	Node 1	Node 25	5, 15, 20	60%, 60%, 60%	9th category

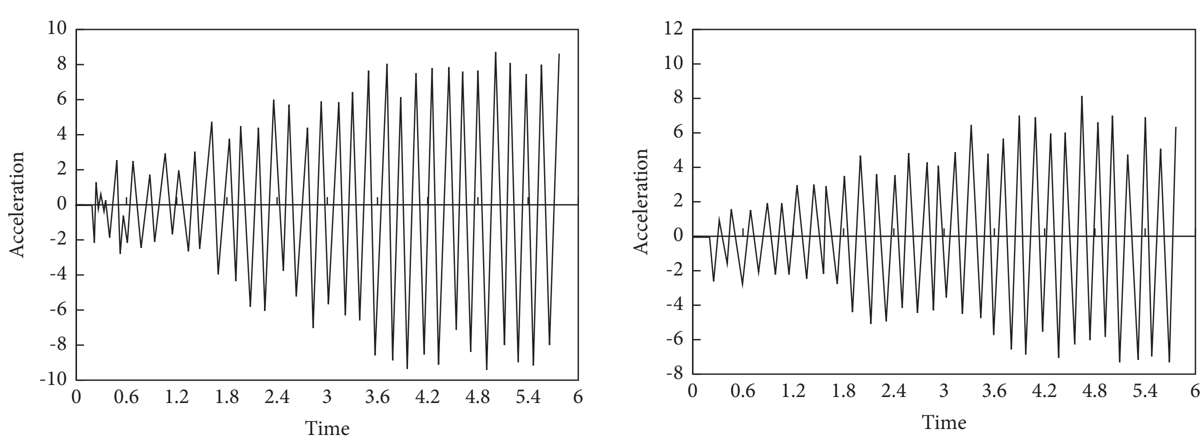

(a) (b)

Figure 8: Continued.

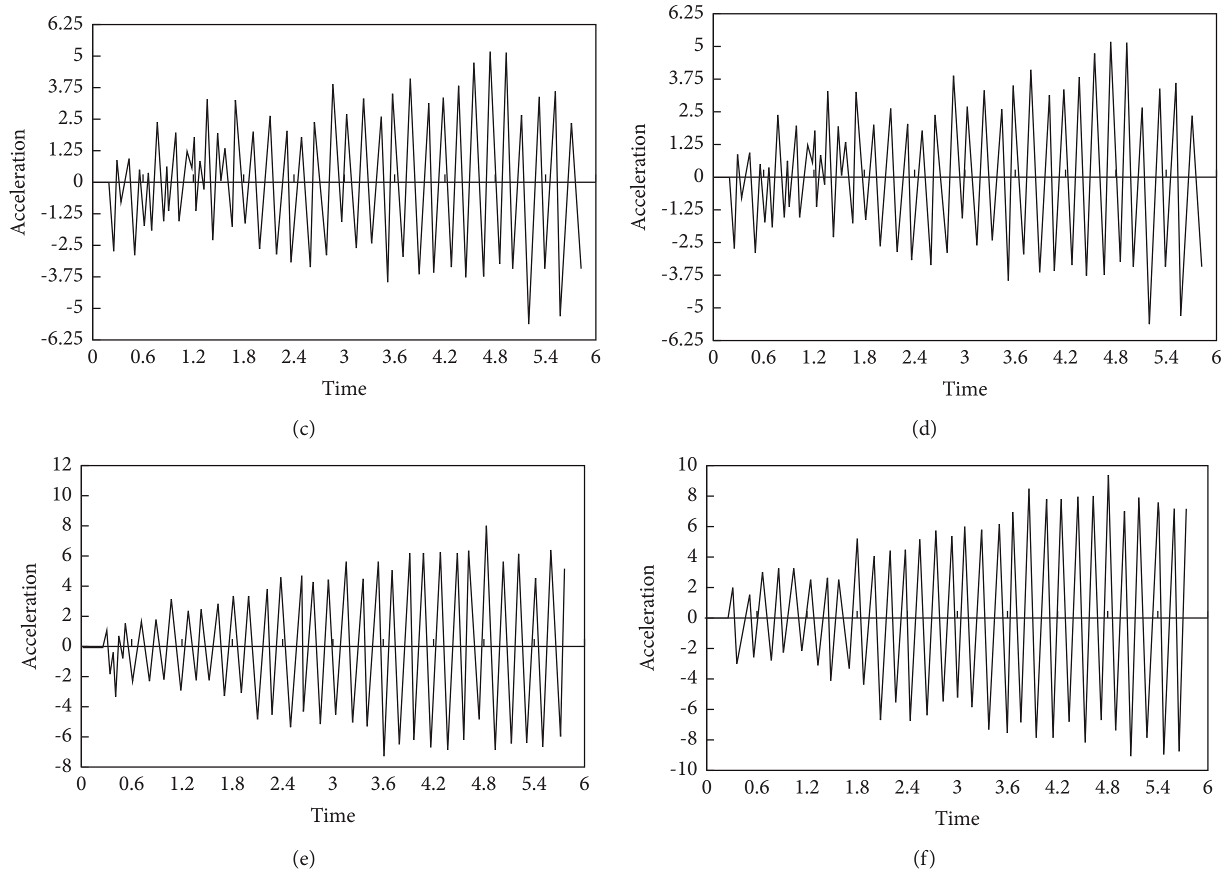

Figure 8: Acceleration-time curves of nodes. (a) Node 4. (b) Node 5. (c) Node 6. (d) Node 7. (e) Node 8. (f) Node 9.

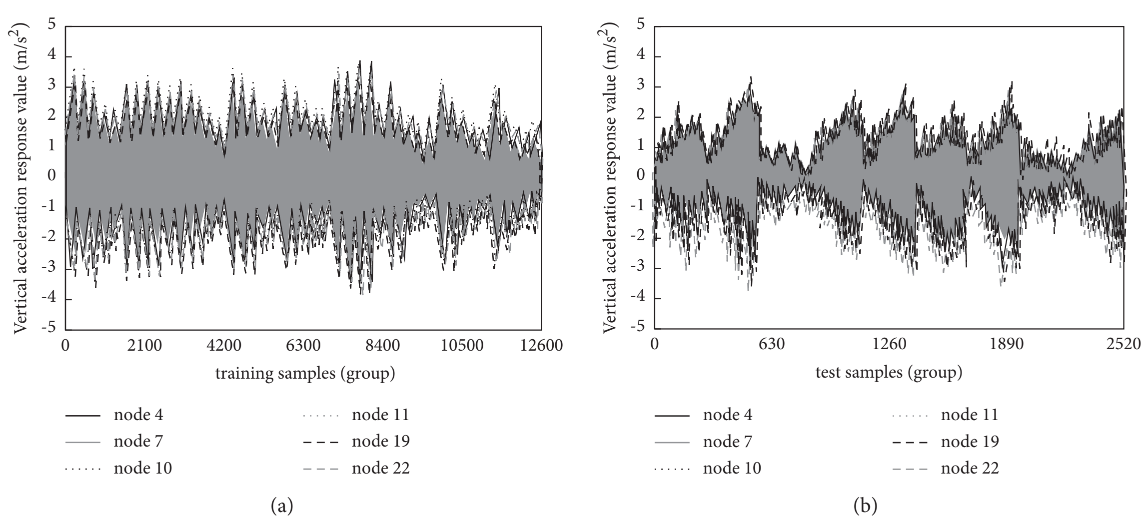

Figure 9: Training set and test set after preprocessing sample II. (a) Preprocessed training samples. (b) Preprocessed test samples.

Table 4: Damage location identification results of simply supported beam bridges.

Damage category	Total number of actual categories	The number of accurate classifications	Accuracy (%)
1st category	1	1	93.33
2nd category	10	9	
3rd category	10	10	
4th category	9	8	

Table 5: Damage location identification results of simply supported beam bridges under different noise conditions.

Project	The number of actual categories	Correct classification at 0% noise	Correct classification at 5% noise	Correct classification at 10% noise	Correct classification at 15% noise
1st category	1	1	1	1	1
2nd category	10	9	9	9	9
3rd category	10	10	10	10	10
4th category	9	8	8	S	8
Accuracy	——	93.33%	93.33%	93.33%	93.33%

Table 6: Recognition results comparison of different recognition methods without noise.

Project	The number of actual categories	The SDAE algorithm is correct	The BP neural network algorithm is correct	The SVM algorithm is correct
1st category	1	1	0	0
2nd category	10	9	1	6
3rd category	10	10	7	3
4th category	9	8	3	3
Accuracy	——	93.33%	36.67%	40.00%

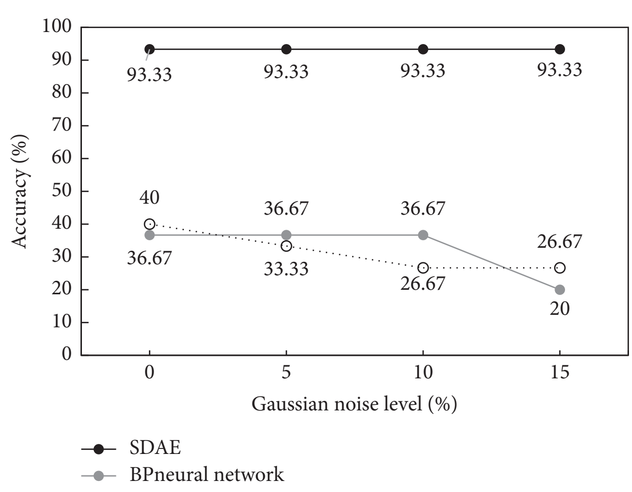

Figure 10: Recognition results comparison of different recognition methods under different noise conditions.

the proposed identification method based on SDAE has the highest identification accuracy, which has certain advantages.

Under different Gaussian noise conditions, the recognition results of BP network, SVM, and the proposed method are shown in Figure 11. As can be seen from the

Table 7: Damage location identification results of continuous beam bridges.

Damage category	Total number of actual categories	The number of accurate classifications	Accuracy (%)
1st category	280	275	
2nd category	280	279	
3rd category	280	280	
4th category	280	280	
5th category	280	280	99.76
6th category	280	280	
7th category	280	280	
8th category	280	280	
9th category	280	280	

Table 8: Damage location identification results of continuous beam bridges under different noise conditions.

Project	The number of actual categories	Correct classification at 0% noise	Correct classification at 5% noise	Correct classification at 10% noise	Correct classification at 15% noise
1st category	280	275	275	275	275
2nd category	280	279	279	279	279
3rd category	280	280	280	2S0	280
4th category	280	280	280	280	280
5th category	280	280	280	280	280
6th category	280	280	280	280	280
7th category	280	280	280	280	280
8th category	280	280	280	280	280
9th category	280	280	280	280	2S0
Accuracy	—	99.76%	99.76%	99.76%	99.76%

Table 9: Recognition results comparison of different recognition methods without noise.

Project	The number of actual categories	The SDAE algorithm is correct	The BP neural network algorithm is correct	The SVM algorithm is correct
1st category	2S0	275	0	0
2nd category	280	279	50	34
3rd category	280	280	0	0
4th category	280	280	19	2
5th category	280	280	17	1
6th category	2S0	280	24	0
7th category	2S0	280	48	6
8th category	280	280	63	0
9th category	280	280	43	223
Accuracy	—	99.76%	10.48%	10.56%

figure, compared with the traditional identification methods BP network and SVM, the proposed method has obvious advantages in recognition accuracy. With the increase of noise level, the recognition accuracy of both BP network and SVM method shows small fluctuation, while the recognition accuracy of the proposed method always maintains a high recognition accuracy, which is up to 99.8%. Therefore, the identification performance of the proposed method is better

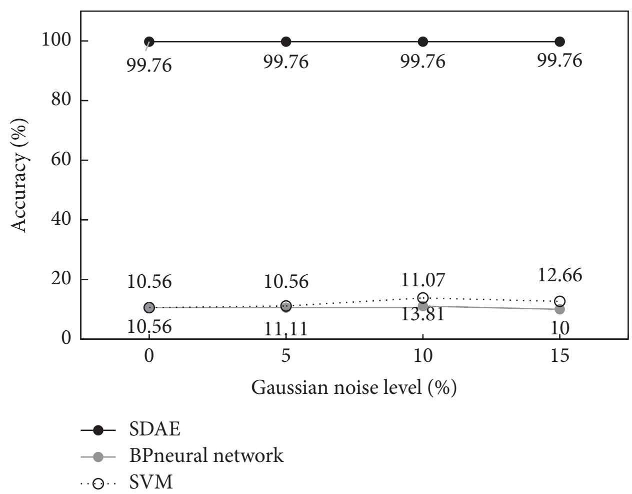

Figure 11: Recognition accuracy comparison of different algorithms under different noise conditions.

than that of traditional identification methods for continuous beam bridges, and it has a certain practical application value.

4. Conclusion

To sum up, the damage location identification method of bridge structure based on deep learning proposed in this paper can effectively identify the damage location of simply supported and continuous beam bridges by using SDAE. Compared with the traditional bridge structure recognition method BP network and the SVM method, the proposed method shows a higher recognition accuracy and antinoise performance. And the average identification accuracy for continuous beam bridge of multiple damage unit reaches 99.8%. It can be seen that the proposed method has obvious advantage on the damage location identification of actual bridge structures. Although there are some achievements, all the conclusions are based on software simulation, namely theory. Obviously, it lack of practical test support, so the proposed method has certain limitations. What is more, the constructed damage index is relatively single. In the practical application, the damage index of bridge structure is complex and diverse, so the selection of damage index needs to be further strengthened. Meanwhile, the practicality and persuasiveness of the proposed method also need to be improved.

Data Availability

The experimental are available from the corresponding author upon request.

Conflicts of Interest

The authors declare that they have no conflicts of interest regarding this work.

References

[1] X. Ye, Z. Sun, and B. Chen, "Research on modal parameters identification of bridge structure based on adaptive signal denoising method," *Cluster Computing*, vol. 22, no. 6, Article ID 14377, 2019.

[2] F. Marco, A. Pavese, F. Lunghi, and D. Silvestri, "Strategies of structural health monitoring for bridges based on cloud computing," *Journal of Civil Structural Health Monitoring*, vol. 9, no. 5, pp. 607–616, 2019.

[3] J. Kim and J. Song, "A comprehensive probabilistic model of traffic loads based on weigh-in-motion data for applications to bridge structures," *KSCE Journal of Civil Engineering*, vol. 23, no. 8, pp. 3628–3643, 2019.

[4] L. Li, L. Zhang, G. Liu, Q. Li, and X. An, "Sensor fault localization with accumulated residual contribution rate for bridge SHM," *Cluster Computing*, vol. 22, no. S4, pp. 7821–7829, 2019.

[5] X.-Q. Li, Q.-J. Chen, and Z.-D. Ding, "Structural damage diagnosis and fine scale finite element intelligence simulation of long span cable stayed bridges," *Cluster Computing*, vol. 22, no. 2, pp. 4101–4107, 2019.

[6] S. Qin, Y. Zhou, H. Cao, and M. A. Wahab, "Model updating in complex bridge structures using kriging model ensemble with genetic algorithm," *KSCE Journal of Civil Engineering*, vol. 22, no. 9, pp. 3567–3578, 2018.

[7] X. Yu, J. Chen, Q. Xu, and Z. Zhou, "Research on the influence factors of thermal cracking in mass concrete by model experiments," *KSCE Journal of Civil Engineering*, vol. 22, no. 8, pp. 2906–2915, 2018.

[8] G. Boscato and A. Dal Cin, "Experimental and numerical evaluation of structural dynamic behavior of Rialto Bridge in Venice," *Journal of Civil Structural Health Monitoring*, vol. 7, no. 4, pp. 557–572, 2017.

[9] W. Meng, W. Zelin, W. Xiaoyu, P. Jialuo, and S. Yu, "Prediction of TBM penetration rate based on Monte Carlo-BP neural network," *Neural Computing & Applications*, vol. 33, pp. 1–9, 2020.

[10] J. Li, C. Men, J. Qi, B. Yang, and R. Liu, "Impact factor analysis, prediction, and mapping of soil corrosion of carbon steel across China based on MIV-BP artificial neural network and GIS," *Journal of Soils and Sediments*, vol. 20, pp. 1–13, 2020.

[11] Y. Feifei, J. Mou, K. Sun, and R. Chu, "Lossless image compression-encryption algorithm based on BP neural network and chaotic system," *Multimedia Tools and Applications*, vol. 79, pp. 1–30, 2020.

[12] C. Xiwen, L. Xiaoqian, and L. Ruiqing, "Ultrasonic power load forecasting based on BP neural network," *Journal of the Institution of Engineers: Series C: Mechanical, Production, Aerospace and Marine Engineering*, vol. 101, no. 23, pp. 383–390, 2020.

[13] K. Linying, Z. Wenyao, and Y. Gab-Geun, "VR design of public facilities in historical blocks based on BP neural network," *Neural Processing Letters*, vol. 53, pp. 1–10, 2020.

[14] Q. Ge, H. Jiang, M. He, and Y. Zhu, "Power load forecast based on fuzzy BP neural networks with dynamical estimation of weights," *International Journal of Fuzzy Systems*, vol. 22, pp. 956–969, 2020.

[15] S. Wang, "Multisensor data fusion of motion monitoring system based on BP neural network," *The Journal of Supercomputing: An International Journal of High-Performance Computer Design, Analysis, and Use*, vol. 76, no. 2, pp. 1642–1656, 2020.

[16] H. You, L. Yu, S. Tian et al., "MC-Net: multiple max-pooling integration module and cross multi-scale deconvolution network," *Knowledge-Based Systems*, vol. 231, 2021.

[17] W. Jin, A. Marco, and J. Gwanggil, "Reconstruction of missing color-channel data using a three-step back propagation neural network," *International Journal of Machine Learning and Cybernetics*, vol. 10, no. 10, pp. 2631–2642, 2019.

[18] J. Wang and L. Xia, "Abnormal behavior detection in videos using deep learning," *Cluster Computing: The Journal of Networks, Software Tools and Applications*, vol. 22, no. 11, pp. 9229–9239, 2019.

[19] Ś. Krzysztof, K. Paweł, and K. Jacek, "Autoencoder-based image processing framework for object appearance modifications," *Neural Computing & Applications*, vol. 22, pp. 1–12, 2020.

[20] J. Choi and H. Chae, "methCancer-gen: a DNA methylome dataset generator for user-specified cancer type based on conditional variational autoencoder," *BMC Bioinformatics*, vol. 21, no. 4, pp. 766–304, 2020.

[21] F. Rong, J. Sha, Q. Xu, and B. Hu, "A new deep sparse autoencoder for community detection in complex networks," *EURASIP Journal on Wireless Communications and Networking*, vol. 2020, no. 8, pp. 75–174, 2020.

[22] B. Gourav, A. Himanshu, and R. Rinkle, "AutoTrustRec: recommender system with social trust and deep learning using AutoEncoder," *Multimedia Tools and Applications*, vol. 79, pp. 1–16, 2020.

[23] A. Shotaro, R. Asaoka, T. Yamashita et al., "Visualizing the dynamic change of Ocular Response Analyzer waveform using Variational Autoencoder in association with the peripapillary retinal arteries angle," *Scientific Reports*, vol. 10, no. 1, pp. 1739–1748, 2020.

[24] L. Amina, O. Salima, and F. Holger, "PathME: pathway based multi-modal sparse autoencoders for clustering of patient-level multi-omics data," *BMC Bioinformatics*, vol. 21, no. 8, pp. 747–752, 2020.

[25] H. Hong-Gui, Z. Hui-Juan, and Q. Jun-Fei, "Robust deep neural network using fuzzy denoising autoencoder," *International Journal of Fuzzy Systems*, vol. 22, pp. 1–20, 2020.

[26] M. Zerkouk and B. Chikhaoui, "Spatio-temporal abnormal behavior prediction in elderly persons using deep learning models," *Sensors*, vol. 20, no. 8, 2020.

[27] H. Fu, F. Liang, B. Lei et al., "Improved hybrid layered image compression using deep learning and traditional codecs," *Signal Processing: Image Communication*, vol. 82, Article ID 115774, 2020.

[28] K. I. M. Yoonhee, D. Yun, and H. Lee, "A non-intrusive speech intelligibility estimation method based on deep learning using autoencoder features," *IEICE - Transactions on Info and Systems*, vol. E103.D, pp. 714-715, 2020.

[29] J. Gracewell and M. John, "Dynamic background modeling using deep learning autoencoder network," *Multimedia Tools and Applications: International Journal*, vol. 79, no. 9, pp. 4639–4659, 2020.

[30] H. Faming, J. Zhang, C. Zhou, Y. Wang, J. Huang, and L. Zhu, "A deep learning algorithm using a fully connected sparse autoencoder neural network for landslide susceptibility prediction," *Landslides: Journal of the International Consortium on Landslides*, vol. 17, no. 5, pp. 217–229, 2020.

Hindawi
Scientific Programming
Volume 2022, Article ID 1921378, 9 pages
https://doi.org/10.1155/2022/1921378

Research Article

Research on the Settlement Prediction Model of Foundation Pit Based on the Improved PSO-SVM Model

Zhibin Song,[1] Shurong Liu,[2] Mingyue Jiang,[1] and Suling Yao[1]

[1] *College of Urban Construction, Hebei Normal University of Science & Technology, Qin Huangdao 066000, China*
[2] *School of Mathematics and Information Science & Technology, Hebei Normal University of Science & Technology, Qin Huangdao 066000, China*

Correspondence should be addressed to Zhibin Song; szb0987@hevttc.edu.cn

Received 16 December 2021; Revised 11 January 2022; Accepted 22 January 2022; Published 10 March 2022

Academic Editor: Le Sun

This paper presents a settlement prediction method based on PSO optimized SVM for improving the accuracy of foundation pit settlement prediction. Firstly, the method uses the SA algorithm to improve the traditional PSO algorithm, and thus, the overall optimization-seeking ability of the PSO algorithm is improved. Secondly, the improved PSO algorithm is used to train the SVM algorithm. Finally, the optimal SVM model is obtained, and the trained model is used in foundation pit settlement prediction. The results suggest that the settling results obtained from the optimized model are closer to the actual values and also more advantageous in indicators such as RMSE. The fitting value $R^2 = 0.9641$, which is greater, indicates a better fitting effect. Thus, it is indicated that the improvement method is feasible.

1. Introduction

In recent years, with the continuous improvement of China's economic level, technology, and urbanization, a variety of high-rise buildings have been erected. During construction, foundation pit construction is an essential part, which directly affects the quality of the whole architecture. If the foundation pit settlement is not predicted and monitored in time, architecture is at very high risk of tilting and collapsing, thus causing serious safety accidents and endangering people's personal and property safety. Therefore, the use of current information technology for the prediction and real-time monitoring of foundation settlement changes is an inevitable choice in the field of building construction, which greatly improves the service life and stability of buildings. At present, the method of predicting foundation settlement has changed from traditional artificial prediction to prediction by various neural network algorithms of machine learning, such as BP neural network, CNN, and Gray theory, which are more applied. The above algorithms have achieved better application results in the fields of image classification recognition and fault diagnosis prediction. With the wide application and popularization of machine learning, more and more intelligent algorithms are proposed and applied to subsidence deformation monitoring, such as particle swarm optimization (PSO) algorithm, and support vector machine (SVM) is also utilized. In terms of specific research, Yan Lv et al. proposed and constructed a settlement prediction model by combining Gray theory and BP neural network. The experimental results indicate that the accuracy rate of prediction of the model stands at 75%, and it can be applied in the prediction of foundation pit settlement engineering, which has a certain reference value [1]; Zhang et al. collected a large amount of foundation settlement data from several projects and summarized 17 main factors affecting ground settlement, which provided a strong database for settlement prediction [2]; for genetic optimization of extreme-value learning machine, Yang proposed three different activation functions for the extreme learning machine (ELM) model based on a genetic algorithm. The test results show that the constructed Ga-ELMsin model has high prediction accuracy. The computational accuracy of the ELM model can be effectively improved with the addition of a genetic algorithm [3]. Wei Jiameng et al. proposed to apply the Newton–Cotes quadrature formula to the nonisometric GM(1, 1) modeling and applied it to the prediction and real-time monitoring of building settlement and deformation. The analysis reveals that the proposed prediction method can be monitored and analyzed in the building settlement changes. The fit is improved by about 30%, and the prediction accuracy of the new model is significantly better than that of the traditional model [4]. Shi-fan et al. proposed a GWO-ELM model to enable training and prediction of ground subsidence. The optimized GWO-ELM model has significantly improved prediction ability and better prediction effect [5]. Zhan et al. proposed an Elman network-based surface settlement prediction method to predict the surface settlement of deep foundation pits in oceanic lots and then correct the predicted values by the Markov chain model, thus further improving the accurate prediction of deep foundation pits in deep marine areas. They also found that this method has a good denoising effect and is practical through practice [6]. Liu et al. constructed a tunnel settlement prediction model represented by Zhengzhou based on the currently available monitoring data. By using this model, the Zhengzhou tunnel can be monitored and predicted in real time, and the specific location and orientation of settlement can be discovered in time so that timely maintenance can be carried out to ensure the normal operation of the subway [7].

The above study shows that combining machine learning and neural networks for settlement prediction has become the mainstream of current thinking. In this study, two typical algorithms, PSO and SVM, are combined to make predictions regarding the settlement of foundation pits.

2. Basic Methods

2.1. Support Vector Machine Model. Support vector machine (SVM), a new machine learning method, is often industrially used as a classifier and contributes to the development and application of deep learning algorithms as well. It was invented by Vapnik's team on the basis of statistical learning theory [8–11]. Currently, SVM is gaining momentum in a number of research fields, including image recognition and classification, face recognition and classification, and time series prediction [12–15]. As a typical binary classification model, SVM, by separating positive and negative planes through the hyperplane and introducing a linear classification criterion with a maximum interval, empowers the linearizer with nonlinear capability with the help of kernel tricks (nonlinear mapping). Compared with traditional machine learning algorithms, SVM features with adaptability, generalization, a short period needed for training, and a minor chance of being trapped in local search, etc. Therefore, SVM is applied in many fields as a way of solving complex real-life problems [16, 17].

2.1.1. The Basic Idea of the SVM Algorithm. As an effective supervised learning method, SVM includes interval, dyadic, and kernel tricks. From a mathematical point of view, SVM provides the optimal algorithm for convex quadratic programming [18–20]. The classification algorithms of SVM are shown in Figure 1.

In Figure 1, the black and white dots denote two types of samples, and the sample dots distributed on the separating plane are the support vectors. Then, "2" denotes the optimal separating hyperplane found by SVM, and "1" and "3" denote the separating hyperplane nearest to the optimal separating hyperplane. The distance between "1" and "3" is the margin, and when the margin reaches the maximum, it is the optimal hyperplane. With the help of the discriminant function of $f(x) = \omega\varphi(x) + b$, which is also called the separating hyperplane, SVM finds the optimal separating plane.

(1) Linearly Separable SVM. It is assumed that the training sample set $\{(x_i, y_i), i = 1, 2, \ldots n\}$ includes 2 classes, where the first class is labeled as $y_i = 1$ and the second class is labeled as $y_i = -1$. When the samples are sorted out by using the separating hyperplane $\omega x + b = 0$, the constraint condition is as follows [21]:

$$y_i(\omega \cdot x_i + b) - 1 \geq 0 i = 1, 2, \ldots n. \tag{1}$$

The distance between point x and separating hyperplane is given by

$$d(\omega, b, x) = \frac{|\omega \cdot x_i + b|}{\|\omega\|}. \tag{2}$$

The distance between the two separating hyperplanes is given by

$$\min \frac{|\omega \cdot x_i + b|}{\|\omega\|} - \max \frac{|\omega \cdot x_i + b|}{\|\omega\|} = \frac{2}{\|\omega\|}. \tag{3}$$

According to the above analysis, SVM is optimized to find optimal hyperplane, i.e., the optimal hyperplane is obtained by solving min $1/2\|\omega\|^2$ which can be expressed by the following equation:

$$\begin{cases} \min \dfrac{1}{2}, & \|\omega\|^2, \\ \text{s.t } y_i(\omega \cdot x_i + b) \geq 1, & i = 1, 2, \ldots n. \end{cases} \tag{4}$$

As convex quadratic programming can only be solved by a global optimal solution, which makes the process of solution simple, the global optimal solution can be derived by calculating the extrema. In solving convex quadratic programming, a combination of structural and empirical risk needs to be considered, and we can get the following equation after the Lagrangian function is introduced into equations (3)–(4) based on the Lagrangian duality [22]:

$$L(\omega, b, a) = \frac{1}{2}\|\omega\|^2 - \sum_{i=1}^{n} a_i[y_i(\omega \cdot x_i + b) - 1], \tag{5}$$

where $a_i > 0 (i = 1, 2, \ldots, n)$ denotes the Lagrangian coefficients.

Find the partial derivatives of ω and b, respectively, and make them equal to zero as follows:

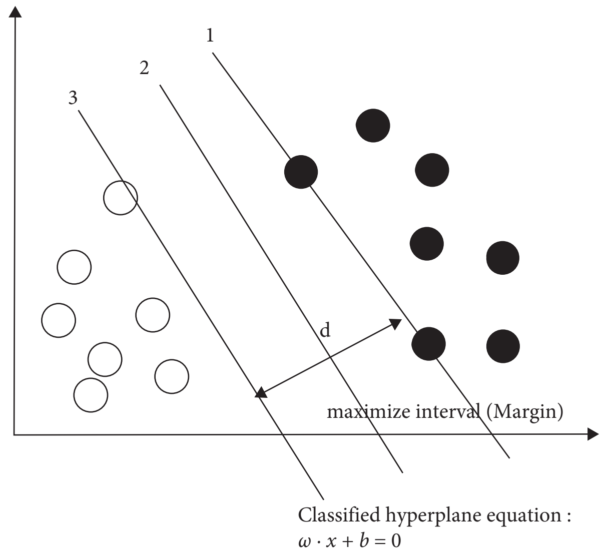

Figure 1: Classification diagram.

$$\begin{aligned}\frac{\partial L}{\partial \omega} &= \omega - \sum_{i=1}^{n} a_i \left(y_i x_i\right) \\ &= 0, \\ \frac{\partial L}{\partial b} &= \sum_{i=1}^{n} a_i y_i \\ &= 0.\end{aligned} \tag{6}$$

After collation, we can get

$$\begin{aligned}\omega &= \sum_{i=1}^{n} a_i \left(y_i x_i\right), \\ \sum_{l=1}^{n} a_i y_i &= o.\end{aligned} \tag{7}$$

Substituting the above results into equations (3)–(5), we can get

$$L(\omega, b, a) = -\frac{1}{2}\sum_{i=1}^{n}\sum_{j=1}^{n} a_i a_j y_i y_j \left(x_i \cdot x_j\right) + \sum_{i=1}^{n} a_i. \tag{8}$$

Therefore, the original problem of optimization can be transformed into the Lagrangian dual problem as the following equation:

$$\begin{cases} \max\text{: } L(a) = \sum_{i=1}^{n} a_i - \frac{1}{2}\sum_{i=1}^{n}\sum_{j=1}^{n} a_i a_j y_i y_j x_i x_j, \\ s.t \sum_{i=1}^{n} a_i y_i = 0 a_i \geq 0. \end{cases} \tag{9}$$

As $a^{\bullet} = \left(a_1^{\bullet}, a_2^{\bullet}, \ldots a_n^{\bullet}\right)^T$ denotes the optimal solution of the Lagrangian dual problem, the solution of the original optimization problem can be expressed as follows:

$$\begin{cases} \omega^{\bullet} = \sum_{i=1}^{n} a_i^{\bullet} y_i x_i, \\ b^{\bullet} = y_i - \sum_{i=1}^{n} a_i^{\bullet} y_i \left(x_i \cdot x_j\right), \end{cases} \tag{10}$$

where x_i and x_j denote any pair of support vectors in the two categories. With the above derivation process, the classification function identifying the final optimal hyperplane is expressed as follows:

$$f(x) = \operatorname{sgn}\left[\sum_{i=1}^{n} a_i^{\bullet} y_i \left(x \cdot x_i\right) + b\right]. \tag{11}$$

(2) Nonlinear SVM. On the basis of nonlinear mapping functions, achieving the mapping of sample data from low-dimensional space to feature space (high-dimensional space), nonlinear problems are converted into linear ones. The training efficiency of SVM can be significantly improved by choosing appropriate kernel functions to perform inner product operations in the initial space or the high-dimensional space, provided that the Mercer condition is met.

2.2. The Principle of Particle Swarm Optimization. Particle swarm optimization (PSO) is an iteration-based evolutionary algorithm, which was developed by Eberhart et al. The foraging behavior in birds is observed, and the algorithm has been widely applied in artificial intelligence.

The foraging behavior in birds is analyzed by describing each bird in the flock as a particle. Each particle represents a potential solution to an optimization problem. However, the particle is a two-dimensional optimization vector in a two-dimensional optimization problem. In addition, the particle is a multibit optimization vector in a multidimensional optimization problem. Therefore, the bird flock is a swarm of particles. Assuming that there are m particles in the D-dimensional target search space, if the optimization objective function value is used to characterize the particle merit where the position of any particle is $X_i = \left(x_i^1, x_i^2, \ldots x_i^D\right)$ and velocity is $V_i = \left(v_i^1, v_i^2, \ldots v_i^D\right)$, the smaller the objective function value, the nearer the particle tends to the extreme position and the better the particle quality is. After a limited search of optimization, the optimal position of a single particle is $P_i = \left(p_i^1, p_i^2, \ldots p_i^D\right)$ and the optimal position in the swarm of particles is $P_g = \left(p_g^1, p_g^2, \ldots p_g^D\right)$.

After a round of particle position iteration, the fitness values should be updated simultaneously. Comparing the fitness values of new particles with those of personal best values and group best values, we shall update the Pbest position of the personal best values and Gbest position of the group best values with the following equation:

$$\begin{aligned} V_{i\,d}^{k+1} &= \omega V_{i\,d}^{k} + c_1 r_1 \left(P_{i\,d}^{k} - X_{i\,d}^{k}\right) + c_2 r_2 \left(P_{g\,d}^{k} - X_{i\,d}^{k}\right), \\ X_{i\,d}^{k+1} &= X_{i\,d}^{k} + V_{i\,d}^{k+1}, \end{aligned} \tag{12}$$

where c_1 and c_2 are the learning factors and ω represents the weight. Then, r_1 and r_2 denote the random number in the interval [0, 1]. $V_{i\,d}^{k+1}$ together with $V_{i\,d}^{k}$ and $X_{i\,d}^{k+1}$ together with $X_{i\,d}^{k}$ are the particle velocity and particle displacement at the next moment and the current moment, respectively.

2.2.1. The Flow of PSO. PSO is used to update particle positions and velocities in the solution space and continues to find the best particles in the process, which can be illustrated in Figure 2.

(1) Initialize the particle swarm: randomly select the initial particles in the solution space and set the velocity and motion direction of the initial particles as well as the learning factors, inertia weights, and other parameters.
(2) Calculate the fitness value: the fitness value of the current particle is solved to determine the personal best value. Then the group best value is determined by comparison.
(3) Update the velocity and position of particles: regulate particle velocity by comprehensively considering personal best value and group best value, and guide the particles to move at this velocity.
(4) Output the optimal solution: after a round of iterations, if meeting termination condition, the optimal solution can be obtained; if not meeting termination condition, skip to step 2 until the termination condition is met or the number of iterations is reached.

3. The Construction of a Settlement Prediction Model of Foundation Pit Based on the Improved PSO-SVM Model

3.1. SA Algorithm. Simulated annealing (SA) algorithm, proposed by Metropolis as a heuristic algorithm through simulating the annealing process, is often used to solve some solutions that are difficult to denote in theoretical and mathematical derivations. While the molecular motion within a solid at high temperature is fast and the molecule energy is high, as the temperature decreases, the molecular motion tends to slow down and transits from the disordered state to the ordered state. During the annealing process, the solid matter can reach thermal equilibrium at any temperature, and the thermal equilibrium at this time is equivalent to the local optimal solution. Then, as the thermal energy of the solid matter is the lowest and a new thermal equilibrium appears when cooling down to the lowest temperature, the thermal equilibrium at this time is equivalent to the global optimal solution. Compared with the PSO algorithm, the SA algorithm features with a remarkable advantage in global search and therefore is suitable for solving large-scale combinatorial optimization problems [23].

3.2. The Principle and Flow of the SA-PSO Algorithm

3.2.1. The Principle of the SA-PSO Algorithm. The SA-PSO algorithm improves the overall application by using the SA algorithm to compensate for its shortcomings on the basis of the PSO algorithm. As the receive state is determined based on a probability formula in the SA algorithm, if $f(x(k+1)) < f(x(k))$, receive state is $x(k+1)$; otherwise, $x(k+1)$ will be received based on the probability $p = \exp(f(x(k+1)) - f(x(k))/T)$. Since the setting situation of the initial value has little effect on the probability value of the SA algorithm, the optimal solution can be calculated according to the probability formula. The SA algorithm changes the annealing temperature through the adjustment function, which means the difference in the particle fitness values is apparent if the temperature at the initial stage is high. As the particle search range expands simultaneously in the process of cooling down, the fitness of the particles is close to the optimal solution when the annealing temperature tends to zero. In addition to the more optimal solutions in the current state, the SA algorithm, when receiving new solutions with a certain probability to receive solutions that do not fully satisfy the conditions, strengthens its global search capability consequently. Apparently, the combination of the two algorithms enables better application performance as the SA algorithm compensates for the shortcomings of the PSO algorithm [24, 25].

3.2.2. Flow of the SA-PSO Algorithm. Combined with the previous discussion, the SA-PSO algorithm features with the advantages of fast convergence and strong global search capability, etc. The implementation procedures are shown as follows [26]:

(1) Perform initialization of particle position and velocity based on the PSO algorithm.
(2) Select an appropriate fitness function to obtain the personal best fitness value P_i as well as the group best fitness value P_g.
(3) Set the initial temperature $t_o = \text{fitness}(p_g)/\log 5$. $\text{fitness}(p_g)$ denotes the fitness value of the optimal particle.
(4) Introduce the SA algorithm to obtain the fitness value of each particle at the initial temperature.

$$TF(p_i) = \frac{e^{-(f(p_i)-f(p_g))/t}}{\sum_{i=1}^{N} e^{-(f(p_i)-f(p_g))/t}}. \tag{13}$$

(5) Update particle position and particle velocity based on the PSO algorithm.
(6) Solve for the updated particle fitness values.
(7) Perform annealing treatment.
(8) If the termination condition is met, stop iteration and output the result. Otherwise, skip to step 4, and repeat the steps above until the termination condition is met.

3.3. The Construction of the Settlement Prediction Model of Foundation Pit of Improved SVM on the Basis of SA-PSO. To improve the accuracy of foundation pit settlement prediction, firstly this paper uses the PSO algorithm to optimize

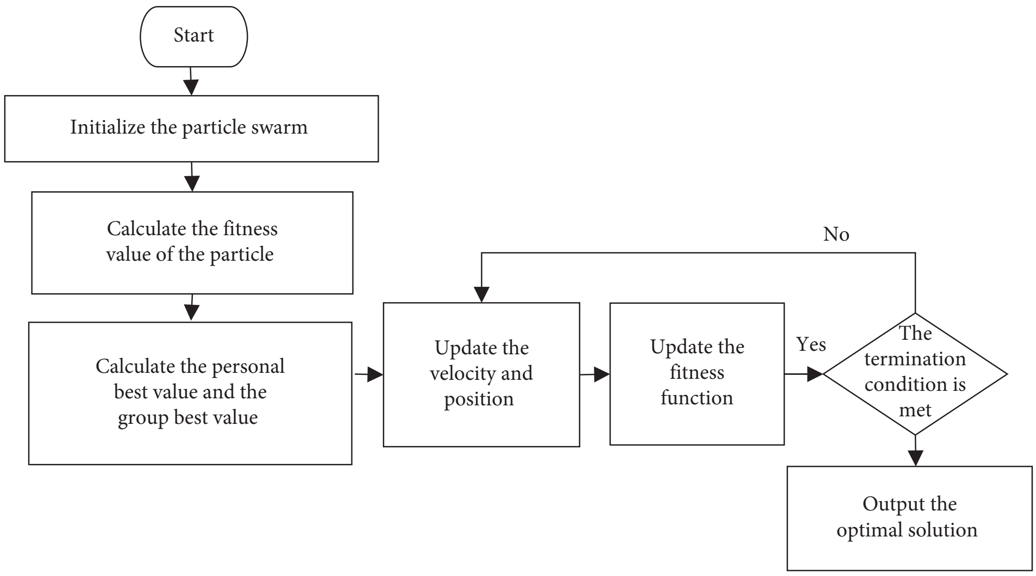

Figure 2: Flowchart of particle swarm optimization parameter optimization.

the covariates (g, C) in the SVM model. Optimization search, however, may be trapped in the circle of local optimization search. In this regard, by invoking the SA algorithm to improve the PSO algorithm, this paper developed a better-performing SA-PSO algorithm, which can determine the optimal solution of parameters in a more efficient and accurate manner. Therefore, the SVM model based on the SA-PSO algorithm can strongly back the settlement prediction of the foundation pit.

The flowchart of the SA-PSO algorithm for SVM model parameter optimization is shown in Figure 3.

(1) Data acquisition and collation: the raw data of settlement are preprocessed, and then phase space is reconstructed to establish a time series of phase space. Next, put the collated data into the prediction set and training set, respectively, and thus, by comprehensively applying the Cao method and mutual information, the optimal embedding dimension m and time delay r are determined.

(2) Processing by normalization method: the data in the prediction set and training set need to be normalized by the following equation for the purpose of avoiding data redundancy:

$$y = \frac{2x - x_{\max} - x_{\min}}{x_{\max} - x_{\min}}, \tag{14}$$

where $x_{\min}$ and $x_{\max}$ denote the minimum and maximum values in the original data, respectively. Here, x denotes the observed data and y denotes the normalized data.

(3) Set the velocity of the initial particle and apply the fitness function $f(x) = 1/n\sum_{j=1}^{n}(y_i - \hat{y}_i)^2$, so as to solve the personal best fitness value p_i and the group best fitness value p_g.

(4) Simulate annealing initialization on the basis of the SA algorithm. By setting the initial temperature $t_o = \text{fitness}(p_g)/\log 5$, solve for the initial solution S and the current fitness values, and then update p_i and p_g.

(5) Calculate the updated solution S1, and update the particle position and velocity through the PSO algorithm. In the meantime, solve for the new fitness value.

(6) Follow the rules in the simulated annealing. If $f(S1) < f(S)$, so $S1 = S$ at this point, i.e., receive state S1; if $f(S1) < f(S)$, then S remains unchanged at this point.

(7) Update p_i and p_g based on the new fitness values.

(8) If the termination condition is met, you can stop the iteration and output the result; otherwise, skip to step 1, and repeat steps above until the termination condition is met.

4. The Engineering Application of the Improved PSO-SVM Model

4.1. SA-PSO-SVM Model Training Results. Data from a monitoring point, which represents the maximum settlement, were selected as the base data, and the data were normalized where the slack variable is 0.02 and other parameters are set. Then, the predictions of data from the test set were simulated on the MATLAB, a software platform, by optimizing the model, and quantitative analysis was conducted by combining the application of four indicators, which are goodness of fit $R^2 = [\sum_{i=1}^{n}(\hat{y}(i) - \overline{f})(y(i) - \overline{y}_t)]^2 / \sum_{i=1}^{n}(\hat{y}(i) - \overline{f})^2 \sum_{i=1}^{n}(y(i) - \overline{y}_t)^2$, root mean square relative error $\text{RMSE} = \sqrt{1/n\sum_{i=1}^{n}(y_i - \hat{y}_t)^2}$, mean absolute error $\text{MAE} = (1/n)\sum_{i=1}^{n}|y_i - \hat{y}|$, and residual sum of squares $SSE = \sum_{i=1}^{n}(y_i - \hat{y}_i)^2$. In this case, goodness of fit R^2 characterizes the degree of influence of the independent variables in the model on the joint process of the dependent

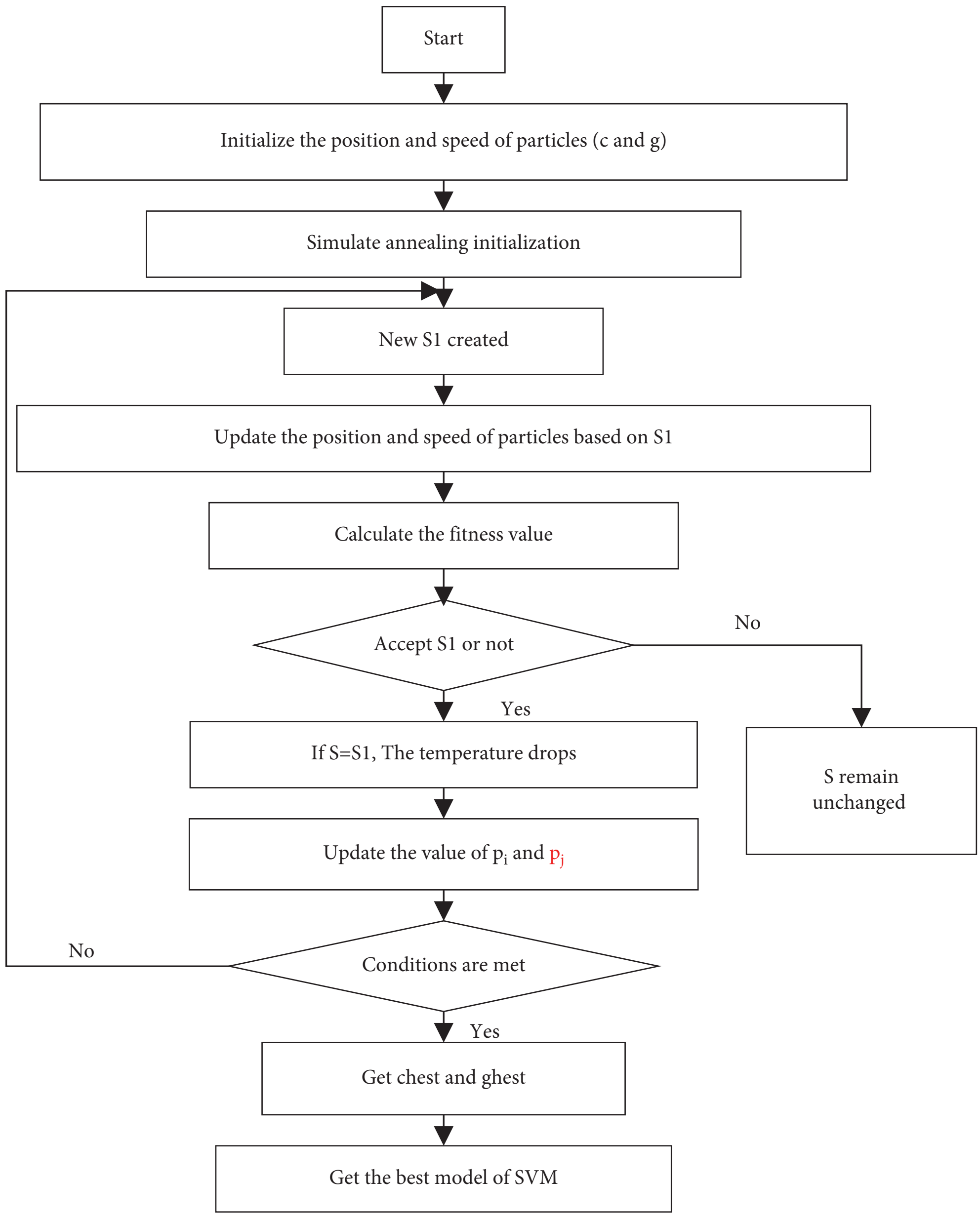

FIGURE 3: Flowchart of the SA-PSO algorithm for SVM model parameter optimization.

variable, where tending to 1 implies that the model has a good fitness degree. Then the root mean square relative error *RMSE* means the dispersion of the prediction results, and the mean absolute error *MAE* represents the prediction accuracy of the model.

The prediction results are displayed in Figure 4.

According to the analysis in Figure 4, the SA-PSO-SVM model to train and predict has a good fitting degree. The change curve of settlement predicted by the model basically fits the change curve of the settlement obtained from actual observation. Relevant data and ratings are shown in Table 1.

When analyzed in conjunction with Table 1, the prediction accuracy of the SA-PSO-SVM model is better than that of the PSO-SVM model. The relative error of the root mean square is 0.2134. In addition, the prediction curve of the SA-PSO-SVM model has a good fitting degree with the actual curve, and its goodness of fit is 0.9962, which is higher than that of the PSO-SVM model. Moreover, when the SA-PSO-SVM model has lower requirements for data, it has better robust performance; besides, the SA-PSO-SVM model can produce prediction results that are closer to the actual values since it is less likely to fall into the defect of local extremes; furthermore, the SA-PSO-SVM model can effectively handle nonlinear data and maintain a high convergence rate in the search process.

The SA-PSO-SVM model was used to predict the settlement at the JC15 monitoring point for Period 32 with the input values (−18.04, −18.36, and −18.72). Then, the output values from Period 32 were reinput into the model and used

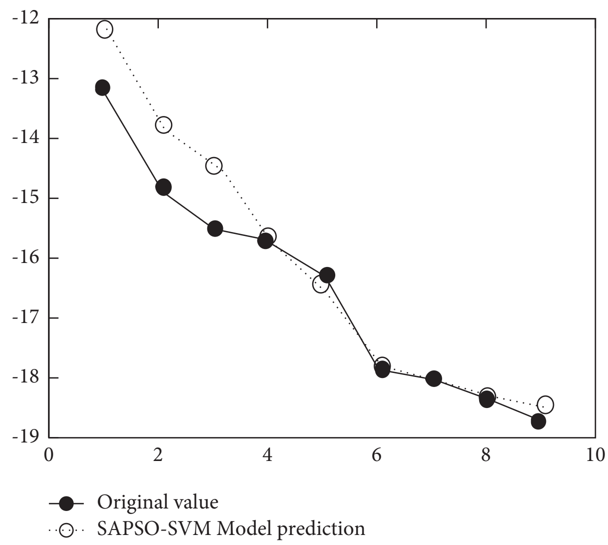

Figure 4: SA-PSO-SVM model training and prediction result graph.

Table 1: Comparison of results of model processing.

Model index	PSO-SVM	SA-PSO-SVM
RMSE	0.3135	0.2134
SSE	3.0477	1.4121
MAE	0.2719	0.1706
R^2(goodness of fit)	0.9685	0.9962

to predict the settlement for Period 33, and the results obtained are listed in Table 2.

According to the predicted results, the settlement of monitoring points for Periods 32 and 33 is −18.83 mm and −18.91 mm, respectively, both of which are below the warning value ($H_{\text{prediction}} \leq 25\text{mm}$), and therefore, the current foundation pit works are judged to be safe in terms of construction.

4.2. Comparison and Analysis of the Three Models. To test the prediction accuracy of the SVM regression prediction model, the PSO-SVM prediction model and the SA-PSO-SVM prediction model are used in this section. Under the three models, data are predicted from the training set and test set at JC15 monitoring points, and we obtained the results presented in Table 3 and Figure 5.

The best fitness of the SA-PSO-SVM model outperforms that of the PSO-SVM model and consistently outperforms the fitness value of the SVM regression prediction model throughout the iterations. As the best fitness value of the SA-PSO-SVM model converges to 2.31×10^{-4}, the corresponding optimal covariate is the kernel function $g = 0.0572$ and the optimal penalty parameter is $C = 65.0981$, which is shown in Table 4.

As the curves of fitting predictions of the three prediction models have a good fitness degree to the curves from actual observation, all three prediction models can provide assistance to the settlement prediction.

Table 2: Simulation results of support vector machine optimization.

Cycle	Input value			SA-PSO-SVM
32	−18.04	−18.36	−18.72	−18.83
33	−18.36	−18.72	−18.83	−18.91

Table 3: Comparison of the accuracy of the three model treatments (unit: mm).

	SVM	PSO-SVM	SA-PSO-SVM
RMSE	0.6038	03135	0.2134
SSE	11.3001	3.0477	1.4121
MAE	0.4583	0.2719	0.1706
R^2	0.9241	0.9685	0.9962

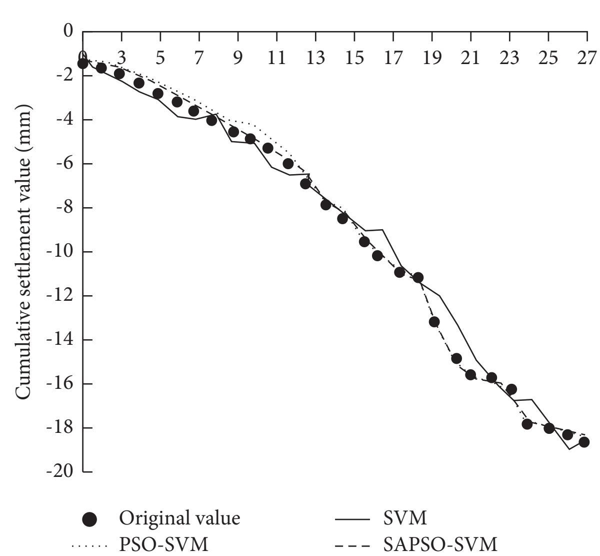

Figure 5: Comparison of the predicted and actual values of the three models.

Table 4: Optimization results of SVM parameters.

Model	C	G
SVM	87.6513	0.0633
PSO-SVM	86.6892	0.0617
SA-PSO-SVM	65.0981	0.0572

In addition, the root mean square relative errors are 0.6038 mm, 0.3135 mm, and 0.2134 mm, respectively. Besides, the MAE and SSE values of the SA-PSO-SVM model are the smallest among the three models, which are 0.1706 and 1.41221, respectively. Then, the goodness of fit of the SA-PSO-SVM model, which is equal to 0.996172, is higher than those of the other two models.

4.3. Validation and Analysis of Prediction Models. According to the engineering application results of the three models, the SA-PSO-SVM model is superior to the remaining two models in terms of overall performance. To further verify the reliability of the above conclusion, in this section, we combined the data from the JC30 monitoring point, the submaximum settlement, for analysis and verification.

For the cumulative settlement data at the JC30 monitoring point, settlement predictions were made by applying the SVM regression prediction model, PSO-SVM prediction model, and SA-PSO-SVM prediction model. The results are presented in Figure 6.

It can be seen that the maximum residual values corresponding to the SVM regression model, the PSO-SVM model, and the SA-PSO-SVM model are −1.97 mm, −0.63 mm, and 0.35 mm, respectively, and it therefore indicates that the settlement prediction curves of all three models basically match the original data curves. Furthermore, the SA-PSO-SVM model presents better fitting results than the other two models, with a goodness of fit of 0.9641.

The accuracy of data processing of the three models is listed in Table 5.

It can be seen that the root mean square relative error of the SA-PSO-SVM model, which is only 0.1889, is significantly smaller than those of the SVM regression model and the PSO-SVM model. Then, the SSE value and MAE value of the SA-PSO-SVM model, which are 1.1067 and 0.1693, respectively, are also the smallest among the three models. Therefore, it confirms that the proposed SA-PSO-SVM model has better robust performance in data processing and can search for global optimal solution efficiently. Furthermore, the PSO-SVM model also shows good adaptability to nonlinear time-series settlement data and can finally achieve the expected prediction accuracy.

The three models were used to predict the settlement at the JC30 monitoring point for Periods 32 and 33, respectively, and the results obtained are listed in Table 6.

According to Table 6, based on the SVM regression model, PSO-SVM model, and SA-PSO-SVM model, the cumulative settlement at the JC30 monitoring point for Period 32 and 33 is all below the warning value ($H_{\text{prediction}} \leq 25$mm). Therefore, the current foundation pit project can be judged as safe in terms of construction.

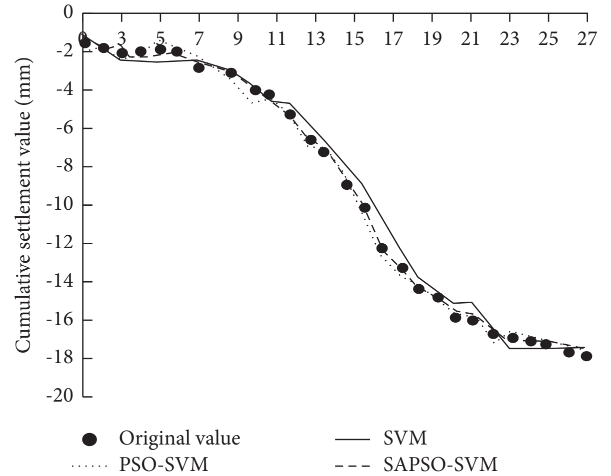

Figure 6: Prediction results of JC30 monitoring points.

Table 5: Processing accuracy of the three models (unit: mm).

	SVM	PSO-SVM	SAPSO-SVM
RMSE	0.6791	0.3208	0.1889
SSE	14.2956	3.1912	1.1067
MAE	0.4426	0.2909	0.1693
R^2(goodness of fit)	0.8924	0.9285	0.9641

Table 6: Numerical prediction results of three models for JC30 monitoring points.

Cycle	SVM	PSO-SVM	SA-PSO-SVM
32	−18.02	−17.73	−17.86
33	−18.21	−17.84	−17.75

5. Conclusion

Based on the analysis and validation above, the SA algorithm is used to improve the PSO algorithm, so as to optimize the parameters of the SVM model. Thus, the needs of settlement prediction of the foundation pit are met.

Data Availability

The experimental data used to support the findings of this study are available from the corresponding author upon request.

Conflicts of Interest

The authors declare that they have no conflicts of interest regarding this work.

References

[1] Y. Lv, T Liu, J Ma, and S Wei, "Study on settlement prediction model of deep foundation pit in sand and pebble strata based on grey theory and BP neural network," *Arabian Journal of Geosciences*, vol. 13, no. 23, pp. 1–13, 2020.

[2] K. Zhang, H.-M. Lyu, S.-L. Shen, A. Zhou, and Z.-Y. Yin, "Data on evolutionary hybrid neural network approach to predict shield tunneling-induced ground settlements," *Data in Brief*, vol. 33, Article ID 106432, 2020.

[3] R. Yang, "Research on settlement prediction of small water conservancy project based on ELM model optimized by genetic algorithm," *E3S Web of Conferences*, vol. 248, Article ID 03065, 2021.

[4] W. Jiameng, H. Jiang, and J. Diao, "Application of non-equidistant gray model based on optimization of background value in settlement prediction," *IOP Conference Series: Earth and Environmental Science*, vol. 636, no. 1, Article ID 012004, 2021.

[5] Q Shi-fan, T Jun-kun, Z Yong-gang et al., "Settlement prediction of foundation pit excavation based on the GWO-ELM model considering different states of influence," *Advances in Civil Engineering*, vol. 2021, Article ID 8896210, 11 pages, 2021.

[6] Y. Zhan, J Zhang, Q Liu, and P Zheng, "A new prediction method for surface settlement of deep foundation pit in pelagic division based on Elman-Markov model," *Arabian Journal of Geosciences*, vol. 14, no. 14, 2021.

[7] J. Liu, Y. Yang, and C. Yang, "Analysis and prediction of long-term settlement of metro shield tunnel in saturated sand[J]," *Geotechnical & Geological Engineering*, vol. 39, no. 7, pp. 1–12, 2021.

[8] C. Vishakha, S. Pandey, and S. Kumar, "Optimizing the performance of vehicular delay tolerant networks using multi-objective PSO and artificial intelligence," *Computer Communications*, vol. 177, pp. 10–23, 2021.

[9] Z. Rahnama and G. R. Ansarifar, "Predicting and optimizing the thermal-hydraulic, natural circulation, and neutronics parameters in the NuScale nuclear reactor using nanofluid as a coolant via machine learning methods through GA, PSO and HPSOGA algorithms," *Annals of Nuclear Energy*, vol. 161, 2021.

[10] W. Zhu, N. Rad Hima, and H. Mahdi, "A chaos recurrent ANFIS optimized by PSO to predict ground vibration generated in rock blasting," *Applied Soft Computing Journal*, vol. 108, 2021.

[11] A. Malik, Y Tikhamarine, S. S Sammen, S. I Abba, and S Shahid, "Prediction of Meteorological Drought by Using Hybrid Support Vector Regression Optimized with HHO versus PSO algorithms," *Environmental Science and Pollution Research*, pp. 1–20, 2021.

[12] A. Abdolhossein, M Kazemi, M. S Sanie, and S. S Heydari, "Synchronization of SA and AV node oscillators using PSO optimized RBF-based controllers and comparison with SMC," *International Journal of Bio-Science and Bio-Technology*, vol. 8, no. 2, pp. 45–62, 2016.

[13] C. Peng, S. Lei, C Jia-Hao, and H Zhiqiang, "Simulation annealing diagnosis algorithm method for optimized forecast of the dynamic response of floating offshore wind turbines," *Journal of Hydrodynamics*, vol. 33, no. 2, pp. 216–225, 2021.

[14] H. Tian, Y. Chang, and Li Kun, "Robust Optimization of the Continuous Annealing Process Based on a Novel Multi-Objective Dragonfly Algorithm," *Engineering Applications of Artificial Intelligence*, vol. 106, 2021.

[15] W. Chen, J Chen, H. J Sun, and Z Chen, "Simulation and analysis of irregular multicoil B 0 shimming in C-type permanent magnets using genetic algorithm and simulated annealing," *Applied Magnetic Resonance*, vol. 50, no. 1-3, pp. 227–242, 2019.

[16] Z. Zhou, S. Liu, and K. Huang, "Research on airport trailer emergency scheduling model based on genetic simulation annealing algorithm," *IOP Conference Series: Materials Science and Engineering*, vol. 383, no. 1, 2018.

[17] M. Liu, Y. Shi, J. Yan, and Y. Yan, "Lattice Boltzmann simulation of flow and heat transfer in random porous media constructed by simulated annealing algorithm," *Applied Thermal Engineering*, vol. 115, pp. 1348–1356, 2017.

[18] J. Lee, S Hong, H Cho, B Lyu, M Kim, and J Kim, "Machine Learning-Based Energy Optimization for On-Site SMR Hydrogen production," *Energy Conversion and Management*, vol. 244, 2021.

[19] X. Xiong, Y Xiao, Y Zhang, J Qiu, J Zhang, and T Yildirim, "A fusion data preprocessing method and its application in complex industrial power consumption prediction," *Mechatronics*, vol. 77, 2021.

[20] Y. Wang, J Wang, Z Li, and H Yang, "Design of a combined system based on two-stage data preprocessing and multi-objective optimization for wind speed prediction," *Energy*, vol. 231, 2021.

[21] X.-an Bi, Y Xie, H Wu, and L Xu, "Identification of differential brain regions in MCI progression via clustering-evolutionary weighted SVM ensemble algorithm," *Frontiers of Computer Science*, vol. 15, no. 6, pp. 1–9, 2021.

[22] İ. Sümeyya, T Hakan, G Fidan et al., "hybSVM: bacterial colony optimization algorithm based SVM for malignant melanoma detection," *Engineering Science and Technology, an International Journal*, vol. 24, no. 5, pp. 1059–1071, 2021.

[23] X. Zhang, "The Co-pilot position of vehicle noise quality prediction based on SVM," *IOP Conference Series: Materials Science and Engineering*, vol. 735, no. 1, Article ID 012064, 2020.

[24] H. Zhang, J Wang, Z Chen, Y Pan, Z Lu, and Z Liu, "An SVM-based NAND flash endurance prediction method," *Micromachines*, vol. 12, no. 7, 2021.

[25] W. Huang, H Liu, Y Zhang et al., "Railway dangerous goods transportation system risk identification: comparisons among SVM, PSO-SVM, GA-SVM and GS-SVM," *Applied Soft Computing Journal*, vol. 109, 2021.

[26] J. Wang, H. Jiang, and Q. Chen, "High-precision recognition of wheat mildew degree based on colorimetric sensor technique combined with multivariate analysis[J]," *Microchemical Journal*, vol. 168, 2021.

Hindawi
Scientific Programming
Volume 2022, Article ID 7349548, 11 pages
https://doi.org/10.1155/2022/7349548

Research Article

Motion Action Analysis at Basketball Sports Scene Based on Image Processing

Jun Liu

School of Physical Education, University of South China, Hengyang 421001, China

Correspondence should be addressed to Jun Liu; 2001001439@usc.edu.cn

Received 9 December 2021; Revised 17 January 2022; Accepted 11 February 2022; Published 7 March 2022

Academic Editor: Le Sun

To solve the problems of low accuracy and high time cost in manual recording and statistics of basketball data, an automatic analysis method of motion action under the basketball sports scene based on the spatial temporal graph convolutional neural network is proposed. By using the graph structure in the data structure to model the joints and limbs of the human body, and using the spatial temporal graph structure to model the posture action, the extraction and estimation of human body posture in basketball sports scenes are realized. Then, training combined with transfer learning, the recognition of motion fuzzy posture is realized through the classification and application of a label subset. Finally, using the self-made OpenCV to collect and calibrate NBA basketball videos, the effectiveness of the proposed method is verified by analyzing the motion action. The results show that the proposed method based on the spatial temporal graph convolutional neural network can recognize all kinds of movements in different basketball scenes. The average recognition accuracy is more than 75%. It can be seen that the method has certain practical application value. Compared with the common motion analysis method feature descriptors, the motion action analysis method based on the spatial temporal graph convolution neural network has higher identification accuracy and can be used for motion action analysis in the actual basketball sports scenes.

1. Related Work

Basketball is one of the most popular sports competitions. The analysis of motion action in the basketball sports scene is helpful to improve basketball players' skills. In addition, it can make basketball coaches and athletes quickly master their own sports characteristics. At present, the analysis mainly relies on manual, and the posture estimation is processed by manual marking basketball video. This method usually has problems of low efficiency, low accuracy, high cost, and so on. To solve the above problems, Yu et al. proposed to use MeanShift to process and track the features of motion videos. The tracking and recognition accuracy of this method is 96.04% and 97.10%, respectively, which has ideal effects [1]. Liu et al. proposed an improved ghosting suppression and adaptive visual background extraction algorithm to effectively remove the ghosting problem in motion videos [2]. Li et al. detected and tracked moving targets by combining FPGA and image processing, which realize the functions such as image acquisition, image gray scale, image filtering, and interframe difference [3]. Bin et al. recognized students' standing behavior in a class based on the region of interest (ROI) and face tracking [4]. Huang detected 3d image targets and introduced a deep learning algorithm, thus greatly improving the accuracy of detection [5]. In addition to the above studies, Sun and Manikandaprabu et al. also proposed target detection and tracking methods [6–12]. The above research provides a lot of useful methods for the tracking of motion targets. Therefore, this paper combines basketball movement to detect and recognize basketball motions so as to provide a new method for the processing of sports video images.

The motion action analysis at the basketball sports scene has made great progress, but its overall performance still needs to be improved. On the one hand, the prediction effect of human posture joint points in the basketball sports scene is not satisfactory. On the other hand, the boundary of estimating motion in basketball is relatively fuzzy, which increases the difficulty of research [13–15]. Therefore, in order to solve the above problems, on the basis of the existing research, utilizing the powerful learning ability of the spatial temporal graph convolutional network (ST-GCN), this study proposes a method of analysis of motion action in basketball sports scene based on image processing and spatial temporal convolutional neural network. What is more, by using the graph structure in the data structure to model the human joint points and limbs, and using the spatial temporal graph structure to model the posture action, the human posture in the basketball sports scene is extracted and estimated. Then, by dividing and applying the label subset, and combining it with migration learning training, the recognition of motion fuzzy posture is realized.

2. Introduction of Spatial Temporal Graph Convolutional Neural Networks

The spatial temporal graph convolution neural network redefines convolution according to the graph structure, and it enables the graph structure to perform convolution operations. In 2D image convolution, the feature maps of the whole process are two-dimensional pixels. The convolution step is set as 1, and 0 is added at the appropriate position of boundary to obtain the output feature graph with the same size as the input feature graph. For the input f in c channels, convolution kernel with size $a * b$ is adopted for convolution; then, the output feature map of position (x, y) is as follows [16]:

$$\begin{aligned} g(x, y) &= f(x, y) * W(x, y) \\ &= \sum_{s=-a}^{a} \sum_{t=-b}^{b} f(s, t) W(s-x, t-y). \end{aligned} \tag{1}$$

In the convolutional neural network, the convolution of the convolution kernel W is the weighted overlay of the corresponding position of the image and the convolution kernel, so the above equation can be rewritten as

$$g(x, y) = \sum_{h=-a}^{a} \sum_{w=-b}^{b} f(p(x, y, h, w)) \cdot W(h, w), \tag{2}$$

where p represents the sampling function, which is responsible for extracting the field of (x, y) and (x, y) itself, which can be expressed as:

$$p(x, y, h, w) = (x, y) + p'(p, w). \tag{3}$$

Here, W is the matrix of c channels, the weighted result obtained from the input sampling inner product of c channels, which represents the weight function.

Formula (2) is extended and graph convolution is defined as follows:

(1) Feature mapping of all nodes (including c-dimensional feature vector) is

$$f_{\text{in}}^{t}: V^{t} \longrightarrow R^{c}. \tag{4}$$

(2) In the image field, the sampling function $p(h, w)$ extracts the points around the center of gravity. In the image structure, for node v_{ti}, the sampling function extracts its adjacent point set $B(v_{ti})\{v_{tj} | d(v_{tj}, v_{ti}) \leq D\}$, where $d(v_{tj}, v_{ti})$ represents the minimum distance between the nodes v_{tj} and v_{ti}. Therefore, the sampling function p: $B(v_{ti}) \longrightarrow V$ can be expressed as

$$p(v_{ti}, v_{tj}) = v_{tj}. \tag{5}$$

Considering that the connection between human body joints is sparse, this study takes the joint whose adjacent distance is 1, so $D = 1$ is set.

(3) Two-dimensional image pixels are arranged in squares. Any location field is arranged from top to bottom and from left to right. However, for a general graph structure, adjacent nodes have no fixed order. So instead of labeling and building a weight function node by node, this paper divides the set of the adjacent node $B(v_{ti})$ of the node v_{ti} into a fixed number of K subsets. Meanwhile, it codes the (c, K) dimensional tensor to map adjacent nodes to corresponding label subsets:

$$l_{ti}: B(v_{ti}) \longrightarrow \{0, \ldots, K-1\}. \tag{6}$$

The weight function can be expressed as

$$W(v_{ti}, v_{tj}) = W'(l_{ti}(v_{tj})). \tag{7}$$

Using the newly defined sampling function and weight function to rewrite formula (2), then we get

$$f_{\text{out}}(v_{ti}) = \sum_{v_{tj} \in B(v_{ti})} \frac{1}{z_{ti}(v_{tj})} f_{\text{in}}(p(v_{ti}, v_{tj})) \cdot W(v_{ti}, v_{tj}), \tag{8}$$

where $Z_{ti}(v_{tj})$ is the normalized term, which is equal to the number of subsets. And it is used to measure the influence of different subsets on the output result, which can be calculated by the formula as follows:

$$Z_{ti}(v_{tj}) = \left| \{ v_{tk} | l_{ti}(v_{tk}) = l_{ti}(v_{tj}) \} \right|. \tag{9}$$

Substituting formulas (5) and (7) into formula (9),we obtain

$$f_{\text{out}}(v_{ti}) = \sum_{v_{tj} \in B(v_{ti})} \frac{1}{z_{ti}(v_{tj})} f_{\text{in}}(v_{tj}) \cdot W'(l_{ti}(v_{tj})). \tag{10}$$

(4) Formula (10) is used to establish the spatial temporal graph convolution model of human posture sequence. First of all, the two adjacent frames with the same node are connected according to the graph structure to form the edge set E_F. Then, multiple spatial graphs are connected into the spatial temporal structure, which realizes the spatial temporal graph convolution. Finally, the spatial adjacent point set is extended to adjacent frame nodes as follows [17, 18]:

$$B\left(v_{ti}\right)=\left\{v_{qj} \mid d\left(v_{qi}, v_{ti}\right) \leq K,|q-t| \leq\left|\frac{\Gamma}{2}\right|\right\}. \tag{11}$$

Here, Γ is the parameter, representing the time length of the spatial temporal convolution kernel. And it is responsible for setting the distance threshold of adjacent nodes added into the subset to less than $\Gamma/2$ from v_{ti} in the time axle distance.

The spatial temporal convolution sampling function is the same as the convolution sampling function of each frame graph in formula (5). The weight function is for the root node v_{ti}, and the label mapping $l_{\mathrm{ST}}\left(v_{qj}\right)$ of adjacent node set of the spatial temporal graph structure can be expressed as

$$l_{\mathrm{ST}}\left(v_{qi}\right)=l_{ti}\left(v_{tj}\right)+\left(q-t+\left[\frac{\Gamma}{2}\right]\right) \times K. \tag{12}$$

Here, $l_{ti}\left(v_{tj}\right)$ represents the label mapping of the adjacent node set of node v_{ti} in each frame.

3. Basketball Motion Analysis Method Based on Spatial Temporal Graph Convolutional Network

3.1. Overall Process. According to the characteristics of the above spatial temporal graph convolution network, the specific process of the basketball motion analysis method is designed, as shown in Figure 1. First of all, according to the node sequence formed by each human body joint of input multiple frames, the label subset is divided by the label division strategy. Then, the input tensor is constructed by transforming the spatial temporal graph convolution network into spatial temporal graph convolution. Finally, using the spatial temporal graph convolutional neural network to train and classify output, the analysis of basketball movement is realized. Each key part is explained as follows.

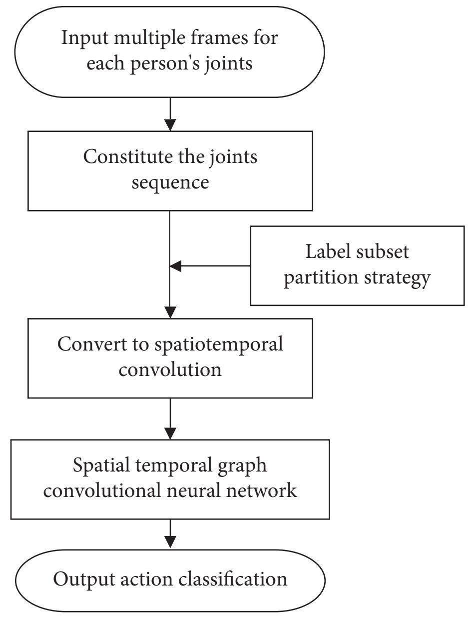

Figure 1: Basketball movement analysis flow based on spatio-temporal graph convolution network.

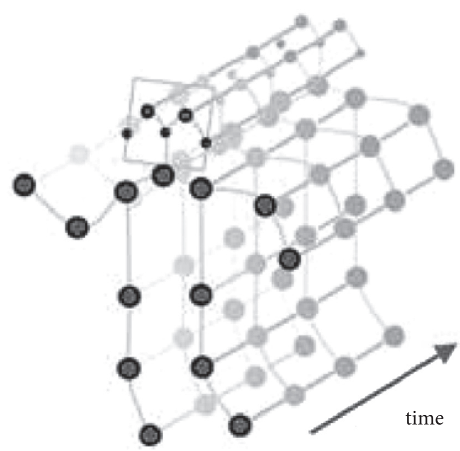

Figure 2: Temporal and spatial diagram of human joint sequence.

3.2. Construction of the Structural Input of Human Body Joint Sequence Diagram. According to the multiple joint matching algorithm, the graph structure in the data structure is adopted to model the human body joints and limbs, and the spatial temporal graph structure is adopted to model the posture action, as shown in Figure 2 [19–22].

For a T frame, the basketball movement video with N joint posture sequences of each frame can be defined as an undirected temporal and spatial diagram $G=(V, E)$, where V is the input of the convolutional neural network, and it represents the total number of joints in posture sequence [23]. Calculating by formula (13), we obtain the corresponding coordinate confidence of each coordinate point and posture estimation output heat map. In addition, the edge of the spatial temporal graph structure can be decomposed into the edge set of each frame and the edge set between two adjacent frames, which are expressed as formulas (14) and (15), respectively, where H represents the joint of the human limb, and all edges of E_F represent the locus of the joint [24].

$$V=\left\{v_{ti} \mid t=1, \ldots, T, i=1, \ldots, N\right\}. \tag{13}$$

$$E_s=\left\{v_{ti} v_{tj} \mid t=\tau,(i, j) \in H\right\}, \tag{14}$$

$$E_F=\left\{v_{ti} v_{(t+1) i}\right\}. \tag{15}$$

3.3. Label Subset Partition Strategy. The subset of labels in this study is divided by reference to the ST-GCN partition strategy. ST-GCN partition strategy includes unified partition, partition by distance, and partition by spatial structure, as shown in Figure 3. In the figure, Figure 3(b) is a unified partition strategy, which is the most direct and simple partition strategy. By dividing the whole set of adjacent point, the corresponding graph convolution is calculated as the inner product of feature vectors and weight vectors of

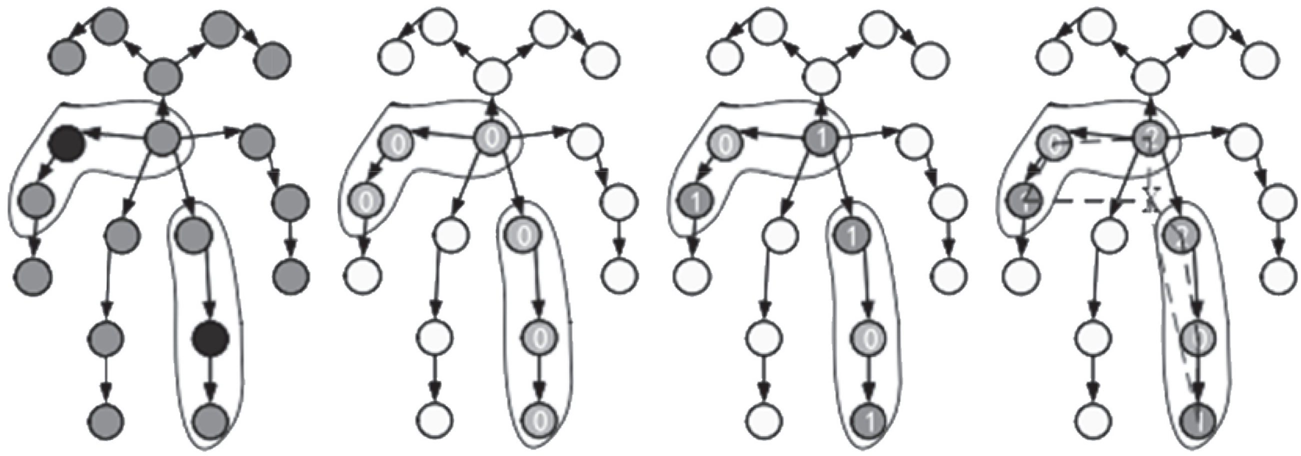

(a) (b) (c) (d)

Figure 3: Label subset partition strategy.

each adjacent node to v_{ij}. Therefore, it can be seen that the unified partition strategy is to calculate the inner product of all adjacent nodes' average feature vector and weight vector, which is easy to lead to the loss of local features. So, this method is not the best posture sequence classification method [25].

Figure 3(c) is the partition strategy by distance, which is based on the distance $d(\cdot, v_{ti})$ from the root node v_{ti}. In this study, D is set to 1, so the root node itself can be regarded as a subset, that is, $D = 0$. The adjacent nodes with distance $D = 1$ can form a subset. Therefore, the partition strategy can include two vectors with different weights to model the local differential characteristics. Label quantity divided by distance is $K = 2$, and the label is

$$l_{ti}(v_{ti}) = d\left(v_{tj} \cdot v_{ti}\right). \tag{16}$$

Figure 3(d) shows the subset partition of adjacent point labels based on the spatial distribution of human body joints, where X is the center of the human body, and the adjacent point labels include three label subsets, such as the root node itself, centrifugal group, and centripetal group. In this paper, the center of gravity of the human body is obtained by averaging the coordinates of all the nodes. According to the spatial distribution, the number of labels is $K = 3$, and the labels are

$$l_{ti}\left(v_{tj}\right) = \begin{cases} 0, & \text{if } r_j = r_i, \\ 1, & \text{if } r_j = r_i, \\ 2, & \text{if } r_j = r_i. \end{cases} \tag{17}$$

Here, r_i represents the average distance from the gravity of each frame to the joint i in the training set.

3.4. Implementation of ST-GCN Based on Label Subset. The method of ST-GCN in the case of single frame is shown in the formula as follows:

$$f_{\text{out}} = \wedge^{-1/2}(A + I)\wedge^{-1/2} f_{\text{in}} W, \tag{18}$$

$$\wedge^{ii} = \sum_j \left(A^{ij} + I^{ij}\right), \tag{19}$$

where $\wedge^{ii}$ represents the normalized term; A represents the adjacency matrix of the human joint connection; I stands for the self-connected identity matrix; W represents the weight matrix formed by stacking the weight vectors of the output channel.

Considering that there are multiple subsets of labels in practice, the spatiotemporal graph convolution cannot form $\wedge^{-1/2}(A + I)\wedge^{-1/2}$. Therefore, it is necessary that the input performs tensor multiplication with the normalized adjacency matrix, and the result performs the time dimension convolution with the standard convolution of length $1 \times \Gamma$. The input feature graph can be expressed as a (C, T, V) dimensional tensor, where C is (x, y) score, V represents the joint number, and T represents the sequence length. The adjacency matrix can be expressed by multiple matrices Aj, namely $(A + I) = \sum_j A_j$. So, formula (20) can be expressed by formula (21), which is shown as follows:

$$f_{\text{out}} = \sum_j \wedge_j^{-1/2} A_j \wedge_j^{-1/2} f_{\text{in}} W_j, \tag{20}$$

$$\wedge_j^{ii} = \sum_k \left(A_j^{ik}\right) + a. \tag{21}$$

To avoid that the denominator is 0, this article sets $a = 0.001$.

4. Results and Analysis

4.1. Experimental Environment and Basketball Movement Classification. In Python, the results were counted and displayed by using pyqt5 and openCV, and the posture estimation is processed by using OpenPose. Basketball movement classification is the premise of action analysis. This study is based according to the current commonly used basketball Kinetics dataset to classify the basketball movements. Four types of basketball-related actions are obtained, namely running with the ball, layup, pitching, and playing basketball. Among them, playing basketball includes a series of basketball actions, which belongs to multiple basketball action categories. So this experiment only selected three kinds of actions, such as running with the ball, layup, and throwing the ball, as the basketball movement category. In addition, considering the possible state of movement of basketball players on the court, this experiment complements four types of actions: running without the ball, passing the ball, catching the ball, standing, or defending. Finally, the basketball action category in this experiment contains a total of seven kinds of actions, as shown in Table 1.

4.2. Data Sources and Preprocessing. In this experiment, video clips of NBA standard games collected by the self-developed basketball action capture gadget are used as the experimental data. Tools include play, stop, fast forward, fast back, and jump to the specified frame function. In addition, there is a tracking algorithm consisting of two parallel forward networks added into the tool, where one network is used to calculate the representation of template features, and the other network is a tracking network. The center point feature and the template feature are used to find the most similar location as the boundary frame.

Considering that the center of the calibration frame of the tracking algorithm is usually target center, and the size of the calibration frame varies with the size of the target. It has a great influence on the target posture extraction. Therefore, this study sets the clipping frame center to the standard frame center and sets its size to 368×368 consistent with the network input size. In addition, in order to enlarge the dataset, the captured video is flipped horizontally in this study. At the same time, considering that the calibration tool may have untraceable situations of targets in complex scenes, this paper uses the manual calibration method to track. Finally, the number of videos obtained in this lab is shown in Table 2.

4.3. Network Structure and Parameter Settings. The method of basketball motion action analysis based on the spatial temporal graph convolution is constructed in this study. The spatial temporal graph convolution network structure of ST-GCN is designed in Figure 4. In the figure, the left figure is a spatial temporal graph convolution network formed by stacking seven-layer ST-GCN modules. The fourth layer network is used to compress the feature information of the time dimension, and it doubles the number of feature channels. The spatiotemporal dimension convolution step for the convolution kernel of this layer network is 2. The middle figure is a specific form of the ST-GCN module, whose input dimension is (B, C, T, V, N), where B represents the batch size, C represents (x, y) score obtained from the posture estimation model, T represents the sequence length with an initial value of 300, $V = 18$ represents the joint number, and N represents the maximum output number of posture estimation. Since this study only focuses on the central target action, N is set to 1. By multiplying the tensor with its corresponding normalized transformation matrix, it can perform convolution with the general two-dimensional convolution W_j.

Furthermore, to achieve basketball movement classification, it is necessary to map the output characteristic information of the ST-GCN module. Here, average pooling is used to compress the output features, and full convolution is used to map the features to seven types of basketball action channels. Finally, the dimensions are changed into (1, 7) for classification.

At last, the experiment sets the temporal dimension graph convolution kernel size of the spatial temporal convolution network to 9. And following the label subset division strategy, the spatial dimension graph convolution kernel size is set as 1, 2, or 3. The initial parameters of the spatial temporal graph convolution network are Kinetics pretraining network parameters of transfer ST-GCN training, and the final classification layer parameters are initialized by the Gaussian distribution. An Adam optimizer is used to update the training process, and the basic learning rate is 0.001. When the 960 epoch is trained, the gradient is decreased by 90% at 320, 480, 640, and 800 epochs.

4.4. Experimental Results. To analyze the influence of different frame lengths as input on the recognition effect of the proposed method, and under the premise of other parameters remaining unchanged, the model training is processed with frame lengths of 130, 150, 170, 190, 210, and 230 as input. The results are shown in Figure 5. As can be seen from the table, the recognition effects of most models on motion actions improve with the increase of the frame length, while the recognition effects of some motion actions jump and decline with the increase of the frame length. Overall, the accuracy of Top1 is improved with the increase of the frame length. When the frame length exceeds 190, the recognition effect is not improved because the excessive frame length leads to redundancy. It can be seen that the space is wasted and the effective frame loss is increased. Therefore, this study sets the frame length to 190.

To analyze the influence of label subset division strategy on the motion recognition effect, this paper divided the label subset according to unified division, distance division, and spatial structure division strategy. And the proposed method is adopted for identification. The results are shown in Figure 6. As can be seen from the table, label subsets divided by distance and spatial structure have better effects compared with unified division. The reason is that the subset obtained by unified division is a single subset, which contains less information and has weak information expression ability. However, the subset obtained by distance division and spatial structure division has more information than the subset obtained by unified division, so its effect is better. Compared with the spatial structure division method, the representation by distance division is less, and the action recognition accuracy of the two methods is close.

Table 1: Classification of basketball movement.

Basketball action category						
Pass the ball	Catch a ball	Layup	Pitching	Run without the ball	Run with the ball	Standing or defending

Table 2: Collection quantity statistics.

	Pass the ball	Catch a ball	Layup	Pitching	Run without the ball	Run with the ball	Standing or defending
Training set	105	91	74	61	145	68	89
Testing set	47	68	18	21	61	19	23

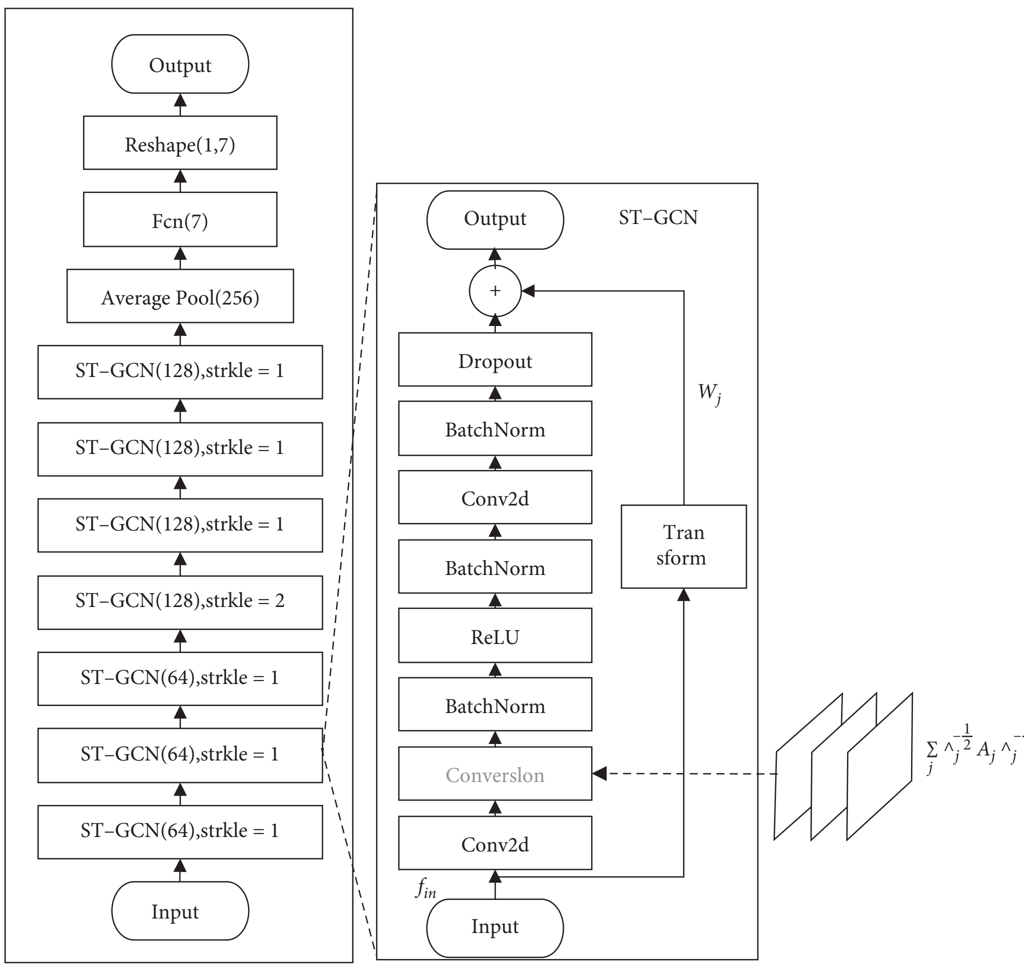

Figure 4: Convolution network structure of migration ST-GCN spatiotemporal diagram.

Therefore, this study chooses the spatial structure division strategy to divide label subsets.

To analyze the influence of different network structures on the model recognition results, different network structures are adopted after the input frame length and label subset division strategy are determined, as shown in Figure 7. Testing the recognition effect of the model on the motion actions, the results are shown in Figure 8. As can be seen from the table, changes in network layers and network structure have a limited effect on improving the accuracy of model recognition results. Compared with the model using the transfer learning method, the accuracy of Top1 is lower. The reason is that the amount of data in the dataset is limited, and more information is not obtained through transfer learning, so its adaptability cannot be effectively improved.

To verify the effectiveness of the proposed method, the proposed method is used to verify it on the experimental dataset. Compared with different motion action recognition methods, the results are shown in Table 3. It can be seen from the table that the method proposed in this study has the best action identification effect in most basketball sports scenes. Although the identification effect of running with the ball is lower than that of the feature descriptor method, the overall

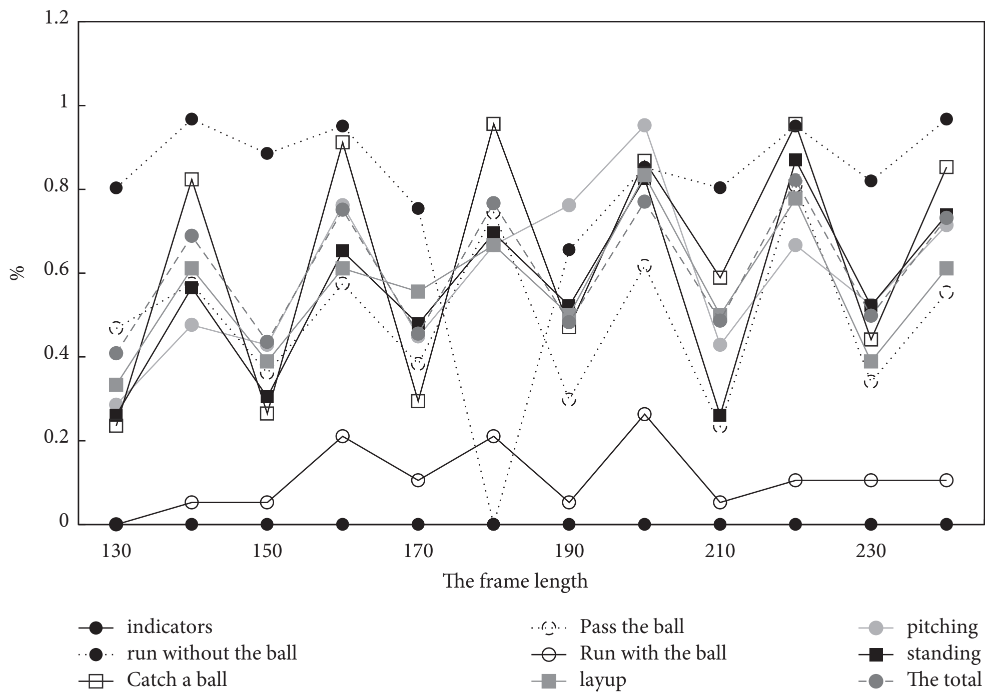

Figure 5: Effects of different frame lengths on recognition results.

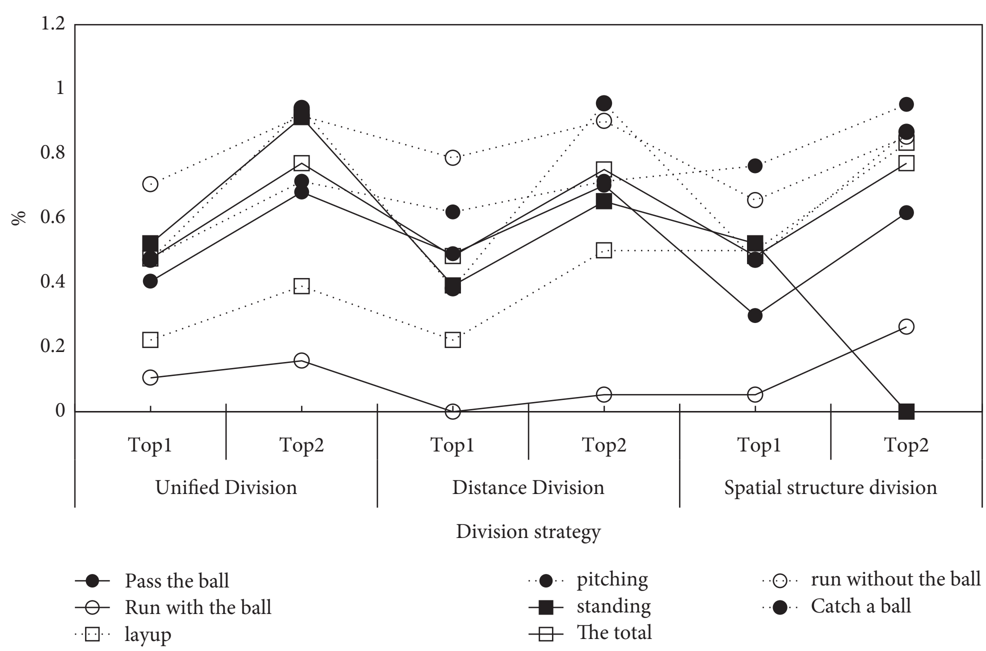

Figure 6: Effects of different partition strategies on action recognition.

action identification effect is better. Therefore, the method proposed in this study is effective to some extent.

Significantly, it can be seen from the test results that the recognition accuracy of two similar movements, running without the ball and running with the ball, is quite different. The recognition accuracy of the proposed method for running without the ball is more than 75%, while that for running with the ball is only about 21%. In order to analyze the causes, this study selects the typical movements of running with and without the ball in the experimental dataset to analyze, as shown in Figure 9. Here, running with the ball and running without the ball are both movements of swinging hands and running with both legs, and the posture joints of the actions are highly similar. Running with the ball has more arm swing than running without the ball. After the images are input into the network and the results of

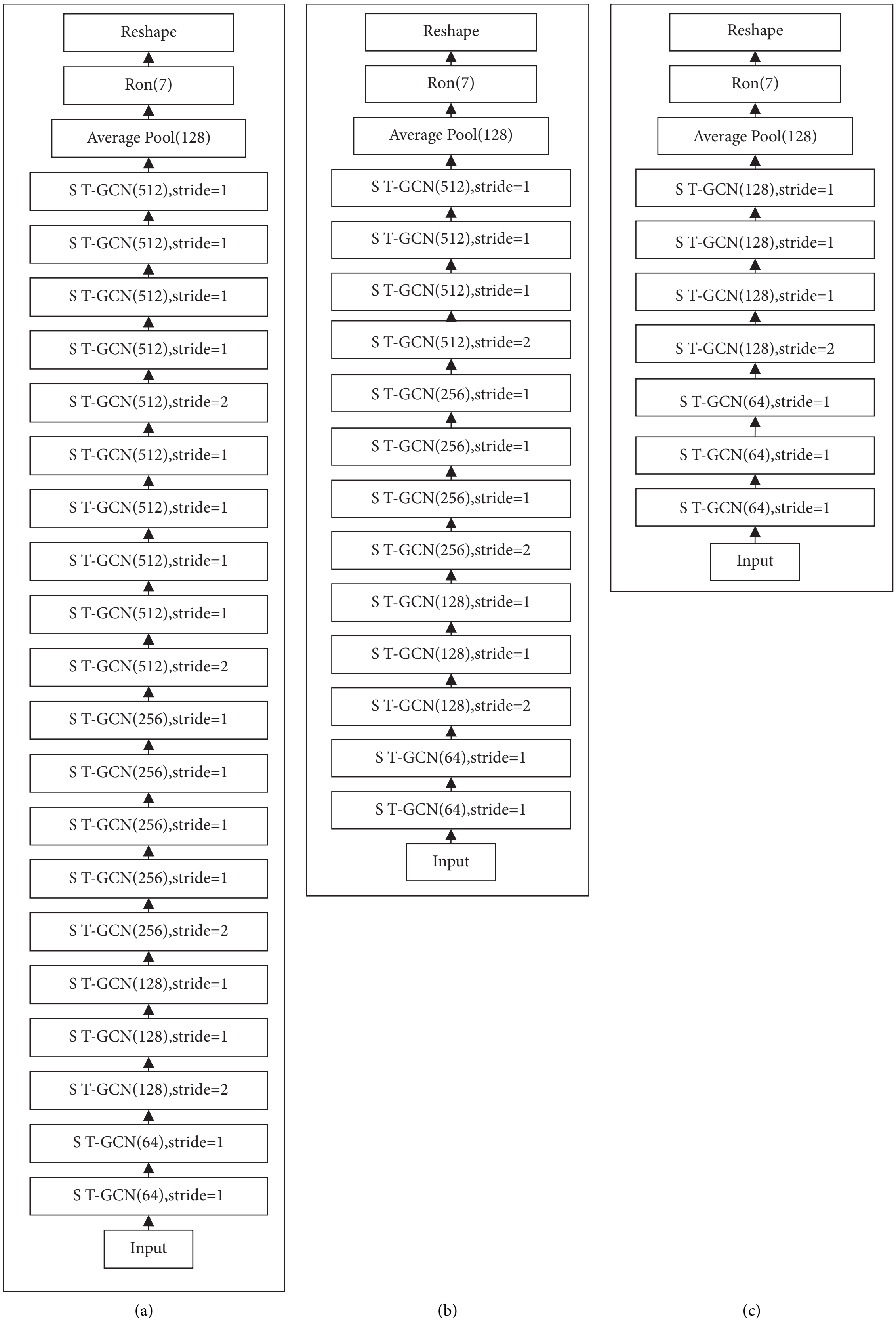

Figure 7: Network structure test. (a) ClassVGG19, (b) 15 storey structure, and (c) 7 storey structure.

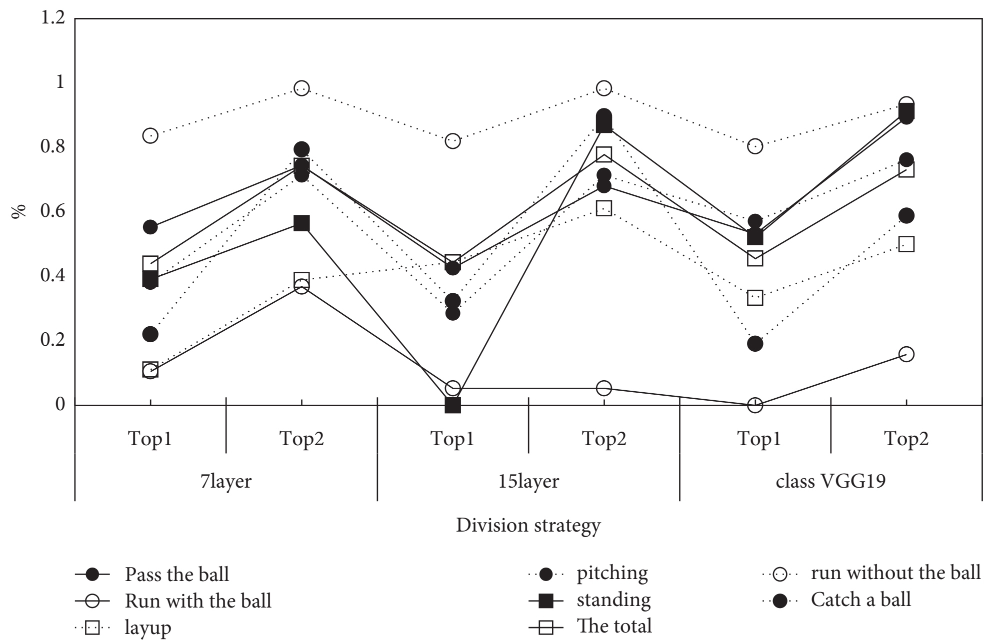

FIGURE 8: Comparison of test results of network models with different structures.

TABLE 3: Comparison of identification results of different methods.

Frame length	Indicators	Pass the ball (%)	Pitching (%)	Run without the ball (%)	Run with the ball (%)	Standing (%)	Catch a ball (%)	Layup (%)	Total (%)
LSTM	Top1	21.28	23.81	47.54	5.26	17.39	14.71	22.22	24.51
	Top2	31.91	42.86	50.82	10.53	30.43	48.53	33.33	40.08
Res-CNN	Top1	25.53	28.57	49.18	10.53	30 43	19.12	38.89	29.96
	Top2	51.06	47.62	555	15.79	47.83	63.24	44.44	51.75
Paper method	Top1	38.30	42.86	75.41	10.53	47.83	29.41	55.56	45.53
	Top2	74.47	66.67	83.61	21.05	69.57	95.59	66.67	76 67

(a) (b)

FIGURE 9: Basketball movement. (a) Running with the ball and (b) running without the ball.

misjudgment are checked, it can be found that the reason for the low recognition failure rate of running without the ball may be that the training data occupy a large proportion in the training set, and the reason for the low recognition failure rate of running with the ball is that it is easy to misjudge it as running without the ball. In addition, the sphere is considered to be added into the posture estimation as a joint. However, for the small amount of calibration data, the recognition effect has not reached the expected standard, so the study has not obtained a satisfactory solution to this problem.

5. Conclusion

To sum up, the motion action analysis method at basketball sports scene based on the spatial temporal graph convolutional neural network is proposed. And the human joints and limbs are modeled by using the graph structure in the data structure, and the posture movement is modeled by the spatial temporal graph structure, which realizes the body posture extraction and estimation at the basketball scenarios. The motion fuzzy posture recognition is realized by dividing and applying the tag subset and training with transfer learning. When the spatial temporal graph convolution network has 11 layers, the input length is 190 frames. And when the label subsets are divided by the spatial structure, the network has the highest recognition effect and recognition accuracy in the basketball sports scene, reaching more than 75%.

Compared with other identification methods such as feature descriptors, this method has higher identification accuracy, and it can be used for the motion action identification and analysis in actual basketball sports scenes. Although some achievements have been made in this study, there are still some shortcomings to be improved. Especially, for the low recognition accuracy of running with the ball and easily misjudged as running without the ball, the new identification methods of the ball should be combined to distinguish in the future study so as to improve its recognition accuracy.

Data Availability

The experimental data used to support the findings of the study are available from the corresponding author upon request.

Conflicts of Interest

The author declares no conflicts of interest.

References

[1] H. Yu, A. Sharma, and P. Sharma, "Adaptive strategy for sports video moving target detection and tracking technology based on mean shift algorithm," *International Journal of System Assurance Engineering and Management*, pp. 1–11, 2021.

[2] L. Liu, G.-h. Chai, and Z. Qu, "Moving target detection based on improved ghost suppression and adaptive visual background extraction," *Journal of Central South University*, vol. 28, no. 3, pp. 747–759, 2021.

[3] W. Li et al., "Moving target detection method based on FPGA," *Scientific Journal of Intelligent Systems Research*, vol. 3, no. 3, 2021.

[4] B. Wu, C. Wang, W. Huang, D. Huang, and H. Peng, "Recognition of student classroom behaviors based on moving target detection," *Traitement du Signal*, vol. 38, no. 1, pp. 215–220, 2021.

[5] L. Huang, "Moving target detection method of three-dimensional image of whip leg technique in s," *Journal of Physics: Conference Series*, vol. 1744, no. 4, Article ID 042216, 2021.

[6] W. Sun, D. Yan, J. Huang, and C. Sun, "Small-scale moving target detection in aerial image by deep inverse reinforcement learning," *Soft Computing*, vol. 24, no. 8, pp. 5897–5908, 2020.

[7] M. Bharat Kumar and P. Rajesh Kumar, "Bayesian fusion strategy for moving target detection in multichannel SAR framework[J]," *Evolutionary Intelligence*, pp. 1–14, 2020.

[8] W. Zhang and W. Sun, "Research on small moving target detection algorithm based on complex scene," *Journal of Physics: Conference Series*, vol. 1738, no. 1, Article ID 012093, 2021.

[9] L. Yaofeng and Y. Ma, "Internet of moving target detection method based on nonparametric background model," *International Journal of Computers and Applications*, vol. 43, no. 2, pp. 193–198, 2021.

[10] Z. Zhao and G. Lu, "Target motion detection algorithm based on dynamic threshold[J]," *Journal of Physics: Conference Series*, vol. 1738, no. 1, Article ID 012085, 2021.

[11] N. A. L. L. A. S. I. V. A. M. Manikandaprabu and S. E. N. N. I. A. P. P. A. N. Vijayachitra, "Moving human target detection and tracking in video frames[J]," *Studies in Informatics and Control*, vol. 30, no. 1, pp. 119–129, 2021.

[12] Q. Yang, W. Shi, J. Chen, and Y. Tang, "Localization of hard joints in human pose estimation based on residual down-sampling and attention mechanism[J]," *The Visual Computer*, pp. 1–13, 2021.

[13] W. Chen, Y. Fan, and Ye Zhang, "Dynamic gesture recognition based on iCPM and RNN[J]," *Journal of Physics: Conference Series*, vol. 1684, no. 1, Article ID 012066, 2020.

[14] H. Zhang, H. Dou, and B. Li, "Research on human action recognition algorithm based on sine feature," *Journal of Physics: Conference Series*, vol. 1518, no. 1, Article ID 012024, 2020.

[15] Li-Q. Hu, Z.-Q. Cai, Li-N. Xing, and Xu Tan, "Human action recognition via learning joint points information toward big AI system[J]," *Journal of Visual Communication and Image Representation*, 2019.

[16] M. Khan, Mustaqeem, U. Amin et al., "Human action recognition using attention based LSTM network with dilated CNN features[J]," *Future Generation Computer Systems*, vol. 125, 2021.

[17] J. Chen, R. Samuel, D. Jackson, and P. Parthasarathy, "LSTM with bio inspired algorithm for action recognition in sports videos," *J]. Image and Vision Computing*, Article ID 104214, 2021.

[18] Ye Lei and S. Ye, "Deep learning for skeleton-based action recognition[J]," *Journal of Physics: Conference Series*, no. 1, p. 1883, 2021.

[19] K.-H. Wu and C.-T. Chiu, "Action recognition using multi-scale temporal shift module and temporal feature difference extraction based on 2D CNN," *Journal of Software Engineering and Applications*, vol. 14, no. 05, pp. 172–188, 2021.

[20] A. Vijay Anant, K. Deepak, and C. G. Suresh, "Human action recognition using CNN-svm model[J]," *Advances in Science and Technology*, vol. 105, pp. 282–290, 2021.

[21] J. Yang, F. Wang, and J. Yang, "A review of action recognition based on Convolutional Neural Network[J]," *Journal of Physics: Conference Series*, vol. 1827, no. 1, Article ID 012138, 2021.

[22] A. Kumar, S. Kushwaha, and R. Khurana, "Fusing dynamic images and depth motion maps for action recognition in

surveillance systems[J]," *International Journal of Sensors, Wireless Communications & Control*, vol. 11, no. 1, pp. 107–113, 2021.

[23] D. zheng, H. Li, H. Li, and S. Yin, "Action recognition based on the modified t," *International Journal of Mathematics and Soft Computing*, vol. 6, no. 6, pp. 15–23, 2020.

[24] J. Lee and H. Jung, "TUHAD: taekwondo unit technique human action dataset with key frame-based CNN action recognition[J]," *Sensors*, vol. 20, no. 17, 2020.

[25] S. Hoshino, K. Niimura, and K. Niimura, "Robot vision system for human detection and action recognition," *Journal of Advanced Computational Intelligence and Intelligent Informatics*, vol. 24, no. 3, pp. 346–356, 2020.

Hindawi
Scientific Programming
Volume 2022, Article ID 4667677, 8 pages
https://doi.org/10.1155/2022/4667677

Research Article

Application of Convolutional Neural Network in Emotion Recognition of Ideological and Political Teachers in Colleges and Universities

Bo Gao

Xingjian College, Xijing University, Xi'an, Shaanxi 710123, China

Correspondence should be addressed to Bo Gao; 20120057@xijing.edu.cn

Received 23 November 2021; Revised 6 December 2021; Accepted 11 December 2021; Published 28 February 2022

Academic Editor: Le Sun

With the update of Internet technology and the development of we-media, ideological and political education in colleges and universities has been greatly impacted. Higher requirements are put forward for ideological and political teachers in colleges and universities, whose emotions seriously affect the quality and effect of teaching. Aiming at the problems of poor network generalization ability and large computation amount caused by many network parameters in the existing emotion recognition methods, a face emotion recognition method based on convolutional neural network is proposed. The network structure of nested Maxout multilayer perceptron layer is constructed by optimizing the convolutional neural model. Maxout can enhance the feature extraction capability of the convolutional layer of convolutional neural network. Meanwhile, Maxout performs linear combination of target features to select the most effective feature information. Then, the pretraining model is used for emotion recognition training. The strong perception ability of the model for facial features is retained by changing the important parameters. Simulation results demonstrate that this method has a higher recognition rate of face emotion and can effectively achieve accurate face emotion classification.

1. Introduction

China's education, especially higher education, has highlighted abundant problems with the rapid development in a new historical period [1]. In the new era, it is highly required to adhere to moral cultivation and put ideological and political work through the whole process of higher education teaching. At the highest level of the education system, university education is related to the future development of the country and the great rejuvenation of the Chinese nation. Therefore, more attention should be paid to the importance of ideological and political education [2]. Teachers, as engineers of human soul, shoulder the sacred mission of teaching and educating people. As a preacher, we should first understand the way and channel; that is, every word and action of teachers is the benchmark for students to learn [3]. Ideological and political teachers in colleges and universities are practitioners of ideological and political education, and their emotions are the key factors affecting teaching quality and efficiency.

Emotion is an individual's subjective feeling and psychological behavior response to stimuli, and, also, has a strong dominant effect on individual psychological and physiological activities [4]. Both positive and negative emotional responses have a Sino-Arab influence on the normal functioning of the organism. With the further development of curriculum reform, the work intensity of teachers increases, and the teaching process becomes more complicated. Teachers are prone to emotional problems due to work pressure and complexity of irritable communication [5]. Improving teachers' emotional management ability is helpful to alleviate and solve teachers' emotional problems. Good emotional management ability can correctly guide positive emotions and maintain teachers' physical and mental health. At the same time, teachers' emotional reaction state has a direct impact on teaching quality and efficiency. Teachers have excellent emotional management ability and can fully mobilize positive emotions to activate the classroom atmosphere, so as to ensure good results in education and teaching [6].

In the process of interpersonal communication, people usually judge the emotion of the other party according to the change of facial expression [7], so as to better communicate. Facial emotion is an extremely important way of language communication, and also an important mean of communication between people. Literature [8] divides emotions into six basic forms, including sadness, happiness, fear, disgust, surprise, and anger. Facial emotion recognition technology is a combination of physiology, psychology, image processing, machine vision, pattern recognition, and other research fields [9]. Moreover, it is a further development of face recognition, which mainly includes three steps of face image pretreatment, facial feature extraction and emotion recognition [10], as shown in Figure 1. This paper focuses on the direction of facial feature extraction for further research.

Convolution neural network (CNN) [11] is a branch of deep feedforward neural network, which has been widely applied in the field of image recognition. CNN is composed of one-dimensional, two-dimensional, and three-dimensional convolutional neural networks, which are applied to sequential data processing, image text recognition, and medical image and video data recognition, respectively. Literature [12] constructed a new 3D CNN convolution motion recognition method to obtain feature information from spatial and temporal dimensions. Literature [13] proposed a new postural convolutional neural network descriptor (P-CNN) for emotion recognition. Literature [14] proposed a method for driver emotion recognition based on convolutional neural network.

All the above studies on human emotion recognition are based on the extended convolutional neural network model require manual feature labelling. Its network generalization ability is poor, while the calculation amount is increased due to the network parameters. Besides, the ability of feature acquisition needs to be further improved. To solve these problems, this paper proposes a convolutional neural network based facial emotion recognition method. The innovations and contributions of this paper are listed below.

(1) Firstly, the convolutional neural network model is optimized, and then the nested Maxout multilayer perceptron network is constructed for improving the fitting ability of the algorithm and improving the recognition accuracy of the model.

(2) The target features are linearly combined by nested Maxout to select the most effective feature information. The experimental results show that the proposed method achieves good effect on the accuracy of teachers' emotion recognition, and can accurately classify faces' emotions.

The chapter structure of this paper is as follows. The recommendation algorithm proposed in this paper is

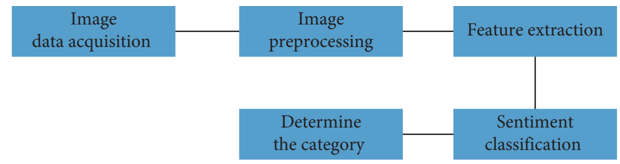

Figure 1: Main steps of facial expression recognition.

described in the next s. The convolutional neural network structure is constructed in section three. Section four focuses on the neural network training. Section five is experiment and analysis. Section six is the conclusion.

2. The Recommendation Algorithm Proposed in This Paper

2.1. Structural Characteristics of Convolutional Neural Network. Network structures such as multilayer perceptron, convolution kernel, pooling layer, local connection, and full-time sharing are widely used in convolutional neural network structures. These applications greatly reduce the time and space complexity of neural network. In addition, it greatly reduces the weight parameters of network structure, which is also beneficial to the training of neural network.

2.1.1. Local Connection. Local connections are also called sparse connections. Inspired by the visual neural structure in biology, neurons in the visual cortex receive local information (that is, these neurons only respond to stimuli in certain areas). The spatial relation of image pixels is strongly correlated with the close pixels; otherwise, the correlation is weak. As a result, the neuron receives only the local receptive field it is responsible for, and does not need to perceive all pixels. The local information of perception is then integrated into global perception by local information fusion of the next layer. Local connection can greatly reduce the number of weights between layers of convolutional neural network and carry out feature dimension reduction. Then, effective features are screened for neural network learning and training to improve the learning efficiency of the model.

2.1.2. Weight Sharing. Weight sharing means that the same convolution kernel is used to process the whole input image. Features extracted locally are the same as those extracted in other parts, and the same learning features can be used in other locations. The weight sharing of convolutional neural network reduces feature dimension and parameter number. Also, the time and space complexity of neural network are reduced.

2.1.3. Multilayer Convolution Kernel. After the first convolutional layer of the convolutional neural network carries out the convolution operation, the feature graph obtained by the convolutional layer is some shallow features of the image, such as edge information and line outline, in addition to other information. For image recognition, deep features are needed, and shallow features cannot fully express the semantic information of the image. One convolution kernel can only obtain the same feature graph. To obtain deeper features, multilayer convolution kernel is required to extract feature information and form feature maps of various information.

In the field of image recognition, the feature hierarchy of input image is born. As shown in Figure 2, you start with the original input pixels and go up to simple lines and textures made up of pixels. Then, the lines and textures form patterns, and finally the individual patterns form objects in the image. In the whole process, the shallow features are found through the original input, and then the shallow features are further mined to find the middle features, and the last step is to obtain the deep features. It is impossible to find deep features directly from raw inputs. In short, single-layer convolution usually acquires shallow features, and it is possible to acquire deeper features by increasing the number of convolution layers.

2.1.4. Principle of Convolution Process. The convolutional layer carries out the convolution operation on the image, and the obtained feature map contains the structural features of the original image, and the deep-seated features can better express the essential meaning information of the image. The convolution of the function is defined as follows. For two continuous integrable functions $h(i)$ and $a(i)$ on R, their convolution $b(i)$ is as follows:.

$$b(i) = \int_{-\infty}^{\infty} h(\tau)a(i-\tau)\mathrm{d}\tau, \tag{1}$$

where the convolution of $h(i)$ on $a(i)$ is denoted as $h(i) * a(i)$, representing the integral of the product of and $a(\alpha - i)$ in the domain of definition. α is the independent variable of the convolution function $b(i)$, which is the position of the convolution.

The convolution calculation process is to transform the picture into a data matrix, and the wandering window is a convolution kernel matrix. After the convolution processing of $M * M$ convolution kernel for an $N * N$ image, the feature graph of $(N - M + 1) * (N - M + 1)$ will be obtained.

2.2. Softmax Classifier. The promotion and application of Logistic regression model [15] formed Softmax classifier to solve the problem of multiple classification. The optimized convolutional neural network model in this paper uses Softmax to classify behaviors. Assume that abnormal behaviors are divided into z and classified. There are w video sequences of sample data. Suppose the convolutional neural network training dataset is N.

$$N = \left\{\left(i^{(1)}, j^{(1)}\right), \left(i^{(2)}, j^{(2)}\right), \ldots, \left(i^{(w)}, j^{(w)}\right)\right\}, \tag{2}$$

where $i^{(x)}$ is the x input sample. $j^{(x)}$ is the behavior label of sample x, $j^{(x)} \in \{1, 2, \ldots, z\}$.

For each input $i^{(x)}$, Softmax classifier calculates the probability for each class. The calculation equation is as follows:

$$U(j = yi)j = 1, 2, \ldots, z. \tag{3}$$

From the vector point of view, the equation for calculating the function is as follows:

$$h\left(i^{(x)}|\theta\right) = \begin{bmatrix} u\left(j^{(x)} = 1|i^{(x)}, \theta\right) \\ u\left(j^{(x)} = 2|i^{(x)}, \theta\right) \\ \vdots \\ u\left(j^{(x)} = z|i^{(x)}, \theta\right) \end{bmatrix} = \frac{1}{\sum_{y=1}^{z} g_y^{\theta_y^T i^{(x)}}} \begin{bmatrix} e^{\theta_1^T i^{(x)}} \\ e^{\theta_2^T i^{(x)}} \\ \vdots \\ e^{\theta_z^T i^{(x)}} \end{bmatrix}. \tag{4}$$

In the equation, θ represents neural network parameters. So, there are z behaviors, and each behavior has a probability value. The value of probability ranges as follows [0,1], and the probability sum of z abnormal behaviors is 1. The output of the neural network corresponds to the probability of the behavior and that probability corresponds to the label of the behavior.

During neural network training, Softmax is used for behavior classification, and the loss function is calculated as follows:

$$L(\theta) = -\frac{1}{w}\sum_{x=1}^{w}\sum_{y=1}^{z} 1\left\{y^{(x)} = j\right\}\log\frac{e_j^{\theta} x^{(i)}}{\sum_{l=1}^{k} e^{\theta_l^T x^{(i)}}}, \tag{5}$$

where $1\{y^{(x)} = j\}$ represents an exponential function. When $y^{(x)}$ is equal to j, the output is 1. Otherwise, the output is 0, and its output is the label matrix of abnormal behavior.

In general, gradient descent algorithm is used to calculate the loss function in the process of backpropagation, and the calculation equation is as follows:

$$\frac{\partial L(\theta)}{\partial \theta} = -\frac{1}{w} i^{(x)}\left[1\left\{j^{(x)} = y\right\} - u\left(j^{(x)} = y \mid i^{(x)}; \theta\right)\right]. \tag{6}$$

Equation (6) is used to obtain the gradient of the loss function to the weight function, and the gradient is used to guide the adjustment of neural network model parameters until the end of neural network training and the optimal weight parameters are obtained.

3. Construct Convolutional Neural Network Structure

Traditional CNN uses single-layer linear convolution in the convolution layer, which does not perform well in the extraction of nonlinear features and abstract features hidden in complex images. The activation function has strong fitting ability and can fit all characteristic patterns when the number of neurons is sufficient. Therefore, the nested

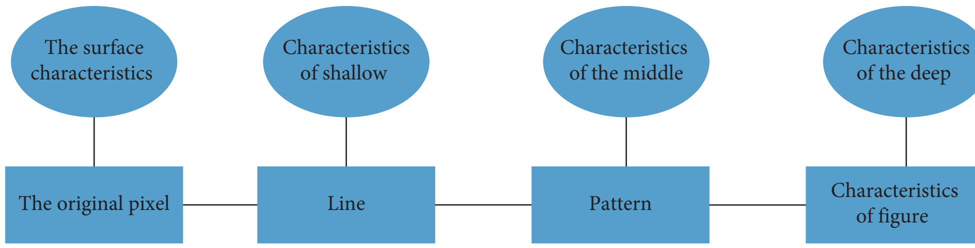

FIGURE 2: Schematic diagram of feature extraction process.

Maxout MLP (Multilayer Perception) layer [16] is combined with the activation function to improve the fitting ability of the algorithm and the recognition accuracy of the model.

3.1. Determination of Nesting Layers. The number of linear regions in neural networks with nested Maxout layers increases as the number of Maxout layers increases. In addition, the number of linear regions in ReLU and Maxout networks increases exponentially with the number of layers. Maxout networks tend to overfit training datasets in the absence of model regularization. It is attributed to the fact that Maxout network can recognize the most valuable input information in the training process and is easy to carry out feature coadaptation.

The method in this paper was tested on a dataset using a different number of Maxout layer fragments, as shown in Figure 3. The test results of combining Maxout fragments with Maxout layer and Batch Normalization (BN) [17] layer fragments show that the nested model has reached saturation state when Maxout fragment is 5. As shown in Figure 3, the number of layers 5 is the best choice.

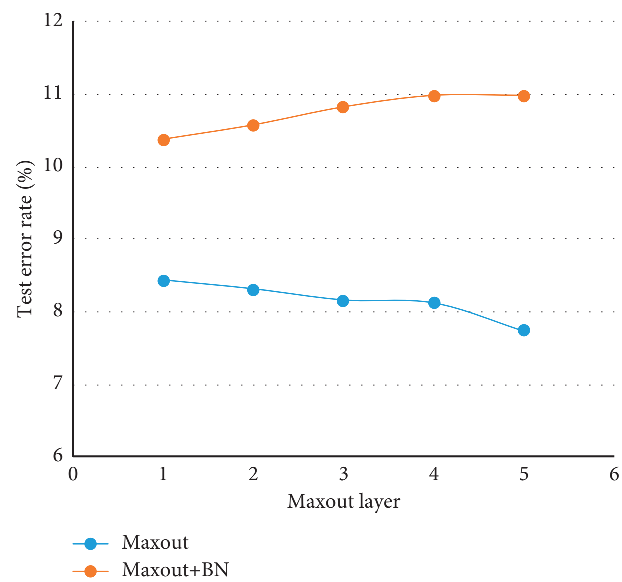

FIGURE 3: Different number of Maxout layer test results.

3.2. Selection of Pooling Layer. In general, researchers will select the largest pooling layer for sampling, which is more representative in extracting features by using average pooling pools effective features across all pooling layers. The irrelevant feature information in the input image can be suppressed by average pooling and discarded by maximum merging. The average pool is an extension of the global average pool, where the model tries to extract information from each local patch to facilitate abstraction into feature maps. The nested structure can extract abstract representative information from each part, making more distinguishable information embedded in the feature map. Spatial average pooling is used in each pooling layer to aggregate local spatial information. In the CIFAR-10 dataset without data expansion, the comparison results of test error rates of the maximum and average pooling layer are shown in Table 1.

TABLE 1: Comparison of maximum and average pooling layer test error rates.

The adopted pooling layer	Test error rate/%
Max pooling	8.75
Avg pooling	7.81

3.3. Building a Nesting Layer. Convolution layer of nested multilayer Maxout network is constructed. That is, Maxout MLP is used to extract features based on nested network structure, and the constructed convolutional neural network model uses batch standardization to reduce saturation and pressure difference to prevent overfitting. In addition, the basic features obtained by mean pool aggregation Maxout MLP are applied across all pool layer to increase the robustness of object space transformation as follows:

$$h_{x,y,z} = \max_{w\in[1,t]}\left(m_{z_w}^{T} i_{x,y} + d_{z_w}\right), \tag{7}$$

where (x, y) is the position of pixels in the feature graph. $i_{x,y}$ is an input block centered on pixel (x, y). z_w is the channel $h_{x,y,z}$ for indexed feature mapping. T is the number of MLP layers. From another perspective, the Maxout unit is equivalent to the cross-channel maximum pooling layer on the convolution layer. Cross-channel maximum pooling layer selects the maximum output to be entered for the next layer. Maxout cells help solve the problem of fading gradients because gradients flow through each maximum cell.

The feature mapping in the nested Maxout MLP layer module is calculated as follows:

$$h^1_{x,y,t_1} = BN\left(\left(m^1_{t_1}\right)^T i_{x,y} + d^1_{t_y}\right),$$
$$h^2_{x,y,t_2} = \max_{w\in[1,z]}\left(BN\left(\left(m^2_{t_w}\right)^T h^1_{x,y} + d^2_{t_w}\right)\right), \tag{8}$$
$$h^3_{x,y,t_3} = \max_{w\in[1,z]}\left(BN\left(\left(m^3_{t_w}\right)^T h^2_{x,y} + d^3_{t_w}\right)\right),$$

where $BN(\cdot)$ represents the batch normalization layer. (x, y) is the position of pixels in the feature graph. $i_{x,y}$ is an input block centered on pixel (x, y). z_t is the serial number of each channel in the feature graph. t is the number of layers of nested Maxout MLP. The batch standardization layer can be applied before activating the function. In this case, nonlinear elements tend to produce activation with a stable distribution, reducing saturation. As shown in Figure 4, the convolutional layer structure diagram of nested Maxout layer is constructed.

3.4. Building a Nested Maxout Layer Convolutional Neural Network Model. By superposing the convolutional layer model of four nested Maxout layers, the whole structure of convolutional neural network with nested Maxout MLP layers is formed.

The network structure of the nested Maxout MLP layer is equivalent to a cascading cross-channel parameter pool and a cross-channel maximum pool on the convolutional layer. Nested structures can combine feature maps linearly and select the combination of the most effective information to output to the next layer. The nested structure reduces saturation by applying batch normalization and can encode the information in the activation patterns of paths or Maxout fragments, thus enhancing the discrimination ability of the deep architecture of the convolutional neural network.

4. Train the Neural Network

The training process of neural network model adopts error backpropagation algorithm and is divided into forward propagation stage and backpropagation stage. In the forward propagation stage, each hidden layer of the neural network receives the output of the previous layer, and the output of this layer is calculated by activating the activation function. In the backpropagation stage, the loss function is used to calculate the output error of the neural network, meanwhile, the error of each hidden layer of the neural network is calculated layer by layer. The error of each hidden layer is used as the updating basis of the weight parameters of the previous hidden layer. The training steps of neural network algorithm are shown in Figure 5.

Step 1. Randomly initialize the ownership value and threshold of the network. The value range is (−1, 1).

Step 2. For the training samples $(i_x, j_{x,})$, the actual network output is calculated as follows:

$$\hat{j}^x_y = h\left(\beta_y - \theta_y\right). \tag{9}$$

In the equation, $f(\cdot)$represents the activation function Sigmoid function. θ_y represents the threshold of the y neuron in the output layer of the neural network. β_y represents the input of the y neuron in the output layer of the neural network:

$$\beta_j = \sum_{x=1}^{t} m_{x,y} i_x, \tag{10}$$

where $m_{x,y}$ represents the weight between the $x$neuron in the hidden layer of the neural network, and the $y$neuron in the output layer of the neural network.

Step 3. Calculate the mean square error of convolutional neural network on(i_x, j_x). The calculation equation is as follows:

$$G = \frac{1}{2}\sum_{x=1}^{w}\left(\hat{j}^x_y - j^x_y\right)^2, \tag{11}$$

where $\hat{j}^x_y$ represents the actual output of the convolutional neural network. j^x_y represents the expected output of the convolutional neural network.

Step 4. Check whether the conditions are met, that is, whether the error is less than the minimum value allowed by the learning error or the learning time reaches the set minimum number. If the conditions are not met, the weights of the convolutional neural network are updated, and the weights and thresholds of the neural network are adjusted according to the gradient direction of the target. Assume that the learning rate of neural network training process is η, and the weight update calculation equation of neural network is as follows:

$$\begin{aligned}\Delta m_{xy} &= -\eta\frac{\partial G}{\partial m_{xy}}\\ &= \eta\hat{j}^x_y\left(1-\hat{j}^x_j\right)\left(j^x_y-\hat{j}^x_j\right)i_x.\end{aligned} \tag{12}$$

Step 5. Repeat Step 2 to Step 4 until the end condition is met. That is, the neural network training is complete, and the weights and thresholds of the neural network are fixed.

5. Experimental Results and Data Analysis

In this paper, the GPU version of PyTorch framework is adopted, and the hardware platform is Ubuntu 20.04.2 with dual-core Intel 4.4ghz CPU, Tesla K80 GPU, 2 TB hard disk memory, and 12 GB running memory. Because there is no public dataset related to ideological and political teachers' emotions, the two widely used datasets are used to verify the validity of the algorithm, such as CK + dataset and Oulu-CASIA dataset. The input images of the two tasks were normalized to 112 ∗ 112 pixels after face detection and matching using multi-task convolutional neural network. The stochastic gradient descent of the driving quantity was used as the

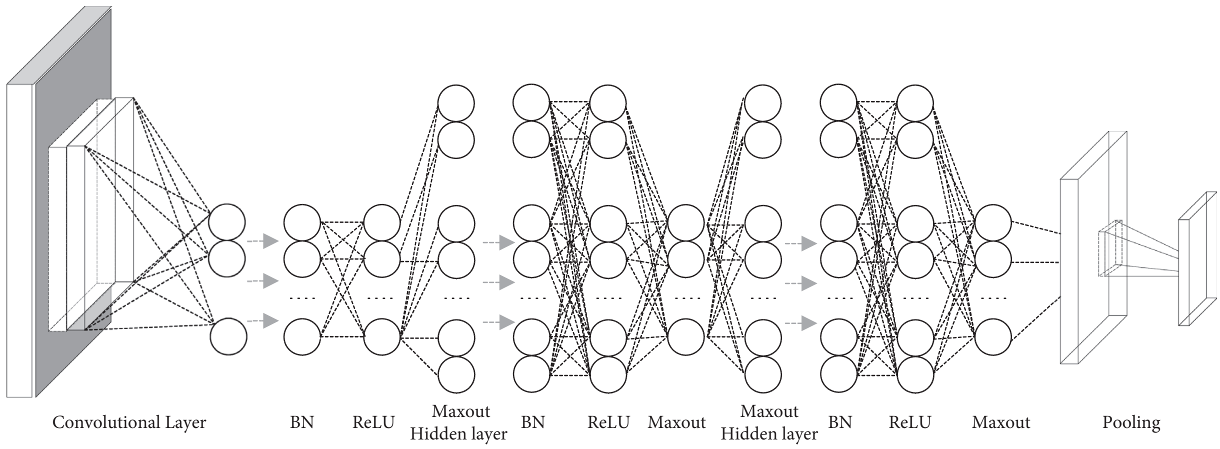

FIGURE 4: The CNN layer structure diagram of nested Maxout layer.

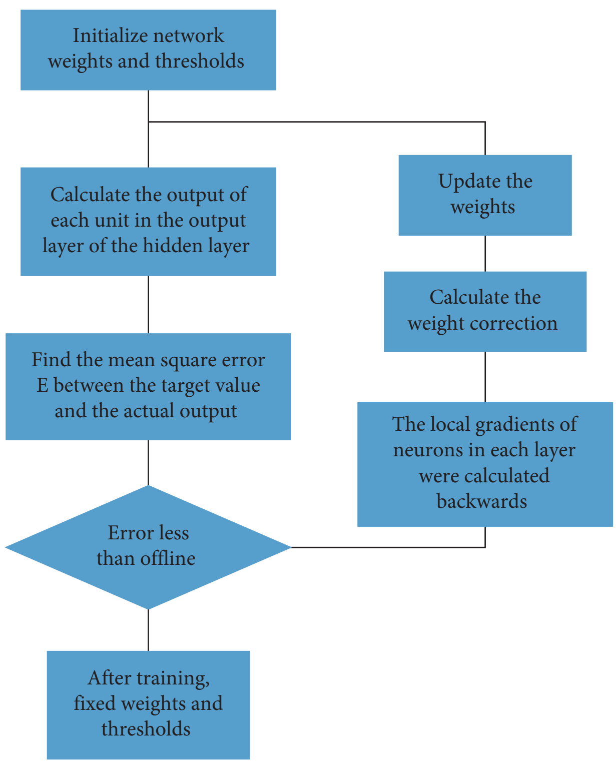

FIGURE 5: The training steps of proposed algorithm.

optimizer in both training stages, and the momentum was set as 0.9, and the weight attenuation term was set as 0.0005. Random horizontal flip was used for data enhancement. In the first stage, CASIA-WebFace is used to train the face recognition model. ArcFace was selected as the loss function, and the batch size was set to 256. A total of 70 epochs were trained in the network, and the initial learning rate was 0.1. Since the 40th epoch, the learning rate of every 10 epochs has decreased to 1/10 of that of the previous epoch. After the face recognition model training, the part before the full connection layer was used for the second stage emotion recognition training. At this time, the batch size was set as 32, the initial learning rate was set as 0.01, and the learning rate was reduced by 1/10 of the current value for every 5 epochs, and a total of 25 epochs were trained.

5.1. CK+ Dataset. CK+ is a dataset collected in a laboratory setting, containing 593 video sequences from 123 subjects. Six basic emotions were classified in the experiment, and only 309 sequences were selected from 106 subjects. Then, 927 images were extracted from the last 3 frames of each sequence where the emotional intensity peaked. Finally, the selected images are divided into 10 subsets according to the ascending order of person ID, and the identity-independent tenfold cross verification is carried out. The average accuracy of cross-validation is shown in Table 2. As can be indicated from Table 1, the proposed method achieves 98.75% recognition rate. Figure 6 shows the confusion matrix on CK+. It can be seen that the algorithm has the best recognition effect on disgust, happiness, and sadness, while anger and fear have fewer samples and are relatively difficult to identify.

5.2. Oulu-CASIA Dataset. Oulu-CASIA is a dataset collected in a laboratory setting. It includes sequences of 2880 images from 80 subjects and is labeled with six categories of basic emotion labels. 480 image sequences taken under normal lighting conditions were selected. Similar to CK+ database, the last 3 peak frames in each sequence are selected to form a total of 1440 images, and each emotion has the same number of images. Then, identity-independent is done tenfold cross authentication. Table 3 shows the recognition rates of the six basic emotions on Oulu-CASIA.

It can be seen that the proposed method achieves comparable results with advanced algorithms. The accuracy of the algorithm is slightly lower than fine tuning because the pretrained face recognition network is trained by using Internet images. Oulu-CASIA's images include a variety of light conditions in a laboratory setting. This difference in image distribution makes the pretrained face model have weak perception ability for such images, thus resulting in poor performance. Figure 7 is the confusion matrix on Oulu-CASIA. It is indicated that the algorithm has the best performance in recognizing happiness and surprise, while its performance in recognizing fear and disgust is relatively weak.

Table 2: The overall accuracy on CK + database.

Methods	Precision (%)
Literature [18]	97.14
Literature [19]	97.29
Literature [20]	98.41
Literature [21]	98.32
Literature [22]	98.62
The proposed method	**98.75**

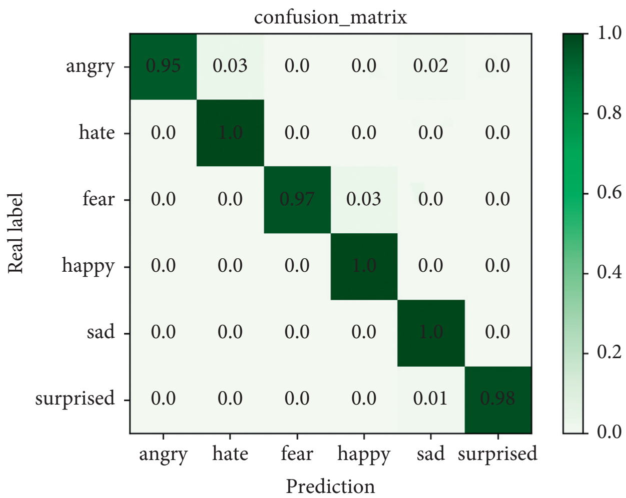

Figure 6: The confusion matrix on the CK+ dataset.

Table 3: The overall accuracy on Oulu-CASIA database.

Methods	Precision/%
Literature [18]	81.35
Literature [19]	84.48
Literature [20]	87.64
Literature [23]	88.12
Literature [24]	88.24
Literature [25]	86.47
The proposed method	**88.31**

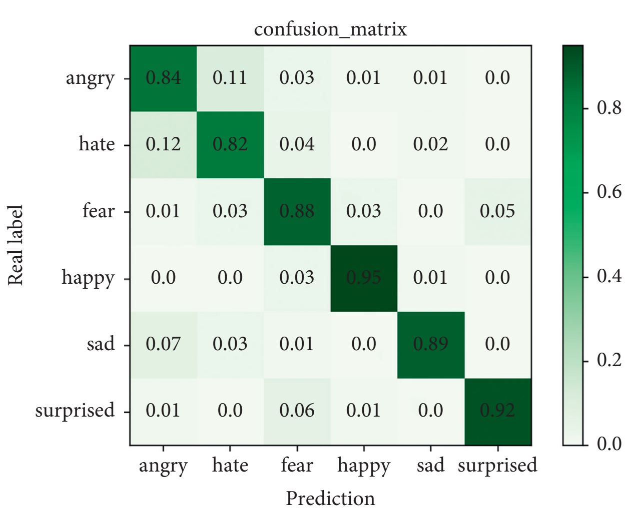

Figure 7: The confusion matrix on the Oulu-CASIA dataset.

6. Conclusion

In the new era, strengthening ideological and political education in colleges and universities has far-reaching practical significance. Ideological and political education not only can promote the comprehensive and harmonious development of college students, but also can be the inevitable requirement of building a harmonious society. With the development of curriculum reform, colleges and universities put forward higher requirements for ideological and political teachers. Since ideological and political teachers serve as the executor of ideological and political education, personal emotions of those people directly affect the effect and quality of teaching. Therefore, ideological and political teachers should pay attention to the change of their own emotions, trying to improve their own emotional management ability. This paper proposes the application of convolutional neural network in emotion recognition of ideological and political teachers in universities. Through the network structure of nested Maxout MLP layer, the ability of neural network to extract nonlinear features and abstract features hidden in complex images is improved. Using the activation function, ReLU in the nested layer can improve the performance of neural networks and feature patterns. Nested structures use batch normalization to desaturate. Simultaneously, the information in activation mode of path or Maxout fragment is encoded to enhance the discrimination ability of deep architecture of convolutional neural network. As the ability of extracting facial features is basically retained, the model's processing ability for the diversity of facial expression images in real world environment is enhanced, the performance is improved more obviously, and the recognition rate is higher. In the future, the author will analyze the performance of the algorithm in this paper and establish a public facial expression recognition database of ideological and political teachers in universities.

Abbreviations

CNN: Convolution neural network
P-CNN: Postural convolutional neural network
MLP: Multilayer Perception.

Data Availability

The labeled datasets used to support the findings of this study are available from the corresponding author upon request.

Conflicts of Interest

The author declares no competing interests.

References

[1] J. Huang, "Successes and challenges: online teaching and learning of chemistry in higher education in China in the time of COVID-19," *Journal of Chemical Education*, vol. 97, no. 9, pp. 2810–2814, 2020.

[2] J. Zhang, X. Hu, Z. Ning et al., "Energy-latency tradeoff for energy-aware offloading in mobile edge computing networks," *IEEE Internet of Things Journal*, Date of Publication, vol. 5, no. 4, pp. 2633–2645, 2018.

[3] L. A. Shepard, K. L. Davidson, and R. Bowman, "How Middle-School Mathematics Teachers Use Interim and Benchmark Assessment Data. CRESST Report 807," *National Center for Research on Evaluation, Standards, and Student Testing (CRESST)*, Oxford University, Oxford, UK, 2011.

[4] H. D. Critchley and S. N. Garfinkel, "Interoception and emotion," *Current opinion in psychology*, vol. 17, pp. 7–14, 2017.

[5] K. Y. Wong, T. Sulaiman, A. Ibrahim, A. G. K Mohd, O Hassan, and W. M. W Jaafar, "Secondary School Teachers Psychological Status and Competencies in E-Teaching during Covid-19," *Heliyon*, vol. 7, Article ID e08238, 2021.

[6] P. A. Jennings, *Mindfulness for Teachers: Simple Skills for Peace and Productivity in the Classroom (The Norton Series on the Social Neuroscience of education)*, WW Norton & Company, NY, USA, 2015.

[7] M. G. Calvo and L. Nummenmaa, "Perceptual and affective mechanisms in facial expression recognition: an integrative review," *Cognition & Emotion*, vol. 30, no. 6, pp. 1081–1106, 2016.

[8] Y. Susanto, A. G. Livingstone, B. C. Ng, E. Cambria, and E. Cambria, "The hourglass model revisited," *IEEE Intelligent Systems*, vol. 35, no. 5, pp. 96–102, 2020.

[9] Z. Ning, X. Hu, Z. Chen et al., "A cooperative quality-aware service access system for social Internet of vehicles," *IEEE Internet of Things Journal*, Date of Publication, vol. 5, no. 4, pp. 2506–2517, 2018.

[10] K. Dharavath, F. A. Talukdar, and R. H. Laskar, "Improving face recognition rate with image preprocessing," *Indian Journal of Science and Technology*, vol. 7, no. 8, pp. 1170–1175, 2014.

[11] S. Albawi, T. A. Mohammed, and S. Al-Zawi, "Understanding of a convolutional neural network[C]//2017 international conference on engineering and technology (ICET)," *IEEE*, pp. 1–6, 2017.

[12] H. Peng, B. Hu, Q. Shi et al., "Removal of ocular artifacts in EEG-an improved approach combining DWT and ANC for portable Applications," *IEEE journal of biomedical and health informatics*, Date of Publication, vol. 17, no. 3, pp. 600–607, 2013.

[13] M. Khokhlova, C. Migniot, and A. Dipanda, "3D Point Cloud Descriptor for Posture Recognition," in *Proceedings of the International Conference on Computer Vision Theory and Applications*, pp. 161–168, Dalian, China, January 2018.

[14] S. Yan, Y. Teng, J. S. Smith, and B Zhang, "Driver Behavior Recognition Based on Deep Convolutional Neural networks," in *Proceedings of the 2016 12th International Conference on Natural Computation, Fuzzy Systems and Knowledge Discovery (ICNC-FSKD)*, pp. 636–641, IEEE, Changsha, China, August 2016.

[15] D. W. Hosmer Jr, S. Lemeshow, and R. X. Sturdivant, *Applied Logistic regression*, John Wiley & Sons, NJ, USA, 2013.

[16] J. M. Pérez-Rúa, V. Vielzeuf, S. Pateux, M Baccouche, and F Jurie, "Mfas: Multimodal Fusion Architecture search," in *Proceedings of the IEEE/CVF Conference on Computer Vision and Pattern Recognition*, pp. 6966–6975, Long Beach, CA, USA, June 2019.

[17] X. Hu, J. Cheng, M. Zhou et al., "Emotion-Aware cognitive system in multi-channel cognitive radio ad hoc networks," *IEEE Communications Magazine*, vol. 56, no. 4, pp. 180–187, 2018.

[18] H. Jung, S. Lee, S. Park, I Lee, C Ahn, and J Kim, "Deep temporal appearance-geometry network for facial expression recognition," 2015, https://arxiv.org/abs/1503.01532.

[19] Z. Yu, Q. Liu, and G. Liu, "Deeper cascaded peak-piloted network for weak expression recognition," *The Visual Computer*, vol. 34, no. 12, pp. 1691–1699, 2018.

[20] W. Wei and K. Qiao, "Jakub nowak, marcinkorytkowski rafa? Scherer, marcin Wo?niak, accurate and fast url phishing detector: a convolutional neural network approach," *Computer Networks*, vol. 178, Article ID 107275, 2020.

[21] Y. Li, J. Liu, Z. Tang, and B. Lei, "Deep spatial-temporal feature fusion from adaptive dynamic functional connectivity for MCI identification," *IEEE Transactions on Medical Imaging*, vol. 39, no. 9, pp. 2818–2830, 2020.

[22] W. Wei, H. Song, W. Li, P. Shen, and A. Vasilakos, "Gradient-driven parking navigation using a continuous information potential field based on wireless sensor network," *Information Sciences*, vol. 408, no. 2, pp. 100–114, 2017.

[23] H. Yang, U. Ciftci, and L. Yin, "Facial Expression Recognition by De-expression Residue learning," in *Proceedings of the IEEE Conference on Computer Vision and Pattern Recognition*, pp. 2168–2177, Salt Lake City, UT, USA, June 2018.

[24] X. Liu, B. V. K. Vijaya Kumar, P. Jia, and J. You, "Hard negative generation for identity-disentangled facial expression recognition," *Pattern Recognition*, vol. 88, pp. 1–12, 2019.

[25] D. Gera and S. Balasubramanian, "Landmark guidance independent spatio-channel attention and complementary context information based facial expression recognition," *Pattern Recognition Letters*, vol. 145, pp. 58–66, 2021.

Hindawi
Scientific Programming
Volume 2022, Article ID 7390098, 12 pages
https://doi.org/10.1155/2022/7390098

Research Article

Classification and Regression Tree Models for Remote Recognition of Black and Odorous Water Bodies Based on Sensor Networks

Qichao Zhao[1,2] **Xuxin Dong**[2,3] **Guohong Li**[1,2] **Yongtao Jin**[1,2] **Xiufeng Yang**[1,2] **and Yandan Qu**[1,2]

[1]*School of Remote Sensing and Information Engineering, North China Institute of Aerospace Engineering, Langfang, Hebei 06500, China*
[2]*Hebei Collaborative Innovation Center for Aerospace Remote Sensing Information Processing and Application, Langfang, Hebei 06500, China*
[3]*School of Electronic Information Engineering, Hebei University of Technology, Tianjin 100101, China*

Correspondence should be addressed to Qichao Zhao; theoddone1987@163.com

Received 7 December 2021; Revised 5 January 2022; Accepted 22 January 2022; Published 25 February 2022

Academic Editor: Le Sun

Black and odorous water bodies represent a topic of significant interest in the field of water pollution prevention and control. Remote sensing technology is increasingly exploited for the monitoring of black and odorous water bodies because of its high efficiency and large-scale monitoring potential. In the present study, the Sentinel-2A imagery data were combined with data obtained by measuring spectral properties of black and odorous water bodies to produce a classification and regression tree (CART) model-based improved remote sensing recognition method for such water bodies. This method transforms the traditional single-feature empirical threshold segmentation algorithm to a multi-feature fuzzy decision-tree classification algorithm. The results reveal overall accuracy values of 84.78%, 92.85%, and 72.23% for the CART decision-tree algorithm, the confidence zone classification, and the fuzzy zone node classification, respectively. The method proposed in the present study enables the highly precise extraction of features representing black and odorous water bodies from satellite imagery. The characterization of confidence and fuzzy zones minimizes the need for field inspections, and it enhances the efficiency of diverse applications including engineering.

1. Introduction

Black and odorous characteristics, that is, a dark color associated with an unpleasant odor, reflect extreme organic pollution of a water body [1]. Owing to the discharge of tremendous exogenous organic matter into water bodies from anthropogenic activities, oxygen in such an environment is consumed by the biochemical activities of aerobic microorganisms, thereby creating anoxic or anaerobic conditions. These conditions promote the death and decomposition of algae and other aquatic organisms. The associated processes produce gases with obvious odors, such as H_2S and NH_3, while metals, such as Fe and Mn, are reduced to dark-colored sulfides. In recent years, because of the rapid economic and societal development, severe black and odorous water problems have been experienced in many cities in China, and these seriously threaten the urban ecological environment and the health and safety of residents [2, 3]. In 2015, the State Council of the PRC issued the *Action Plan for Prevention and Control of Water Pollution*, in which the monitoring and treatment of black and odorous water bodies were included as important measures of water pollution prevention and control. In fact, based on this document, black and odorous water bodies in built-up areas in cities across the country must be eliminated before the end of 2030. To implement the *Action Plan for Prevention* *and Control of Water Pollution*, the Ministry of Housing and Urban-Rural Development and the Ministry of Environmental Protection jointly issued the *Guidelines for the Remediation of Urban Black and Odorous Water* (herein after referred to as *the Guide*), in which several technical issues associated with the monitoring and treatment of black and odorous water bodies were clarified [1].

Conventional black and odorous water monitoring relies on manual sampling and verification, and the results obtained are usually based on the experience of the on-site staff and the chemical data for the water samples. This method, however, is time-consuming and labor-intensive, and thus, it is challenging for regional monitoring. Concurrently, because black and odorous water bodies are usually small and dispersed, their identification using artificial methods, which are often characterized by blind areas and dead ends, is difficult. However, satellite remote sensing technology involves continuous and large-scale monitoring characteristics. The spectral differences between black and odorous and regular water bodies can facilitate the extraction of features representing the former from satellite imagery, thereby providing a rapid and reliable method for the identification and monitoring of black and odorous water bodies in urban areas [4]. In 2016, the Institute of Remote Sensing and Digital Earth of the Chinese Academy of Sciences in collaboration with the Satellite Environment Application Center of the Ministry of Environmental Protection conducted a remote sensing screening and verification study of black and odorous water bodies in Beijing, Shenyang, Taiyuan, and other cities. A related study was considered one of the ten major investigations in the field of remote sensing in China.

At present, shallow learning models that are commonly employed in China for the recognition of black and odorous water bodies through remote sensing mainly involve the following: (1) threshold segmentation based on a single feature and (2) empirical decision tree based on multiple features. The former approach relies on indexes generated from the spectral differences between black and odorous and regular water bodies. These indexes are obtained through statistical analysis of data from field samples. For example, Wen et al. proposed a band ratio method for the extraction of black and odorous water features from remote sensing imagery [5]. Li et al. also advanced a WCI and combined several remote sensing imagery signals to distinguish the two types of water [6]. In fact, Li et al. utilized the Nemerow comprehensive pollution index (NCPI) to characterize the extent of pollution of urban water bodies and compared the results retrieved using six regression models. A regression model suitable for calculating the NCPI of a scene to detect black and odorous water bodies was then obtained [7]. Yao et al. employed verification data from Shenyang to improve the band ratio method and then introduced the BOI algorithm [8]. Furthermore, Yao et al. proposed an HI threshold segmentation method based on PlanetScope images [9], while Zhang et al. enhanced the HI by suggesting the HCI [10]. Nevertheless, most of these methods utilize a single feature to perform the threshold segmentation based on a spectral analysis or a comprehensive comparison. In contrast, Li et al. proposed a classification based on an empirical decision tree involving multiple features and then proposed the DBWI, GR-NIR AWI, NDBWI, and green band features [11]. Reasonable thresholds to facilitate the identification and classification of black and odorous water bodies were also set.

Although high extraction accuracy values were achieved in some areas according to previous investigations, empirical methods were employed in most of these studies for the selection of features and determination of thresholds, and thus, these involve uncertainties. In addition, because black and odorous water bodies originate from multiple causes, mildly black and odorous water bodies can be difficult to distinguish from regular water bodies, which creates a so-called "fuzzy area" in classifications. Therefore, existing methods, especially the single feature threshold segmentation, exhibit shortcomings. To eliminate these limitations, in the present study, the CART decision-tree was employed on remote sensing and field data for Langfang in Hebei Province to propose a superior remote sensing method for recognizing black and odorous water bodies. The Gini coefficient minimization criterion and the binary recursive segmentation were used to determine the characteristics and thresholds, and then a decision-tree model was constructed for classification. The category attributes of leaf nodes were defined by calculating the degree of membership, and this created fuzzy and confidence zones. The proposed method is characterized by high classification accuracy, and the fuzzy and confidence zones generated can facilitate field inspections and improve the efficiency of different applications including engineering.

2. Materials and Methods

In the present study, pits and ponds in Langfang were utilized to evaluate the suitability of remote sensing for the identification and monitoring black and odorous water bodies in areas of high pollution, scattered water bodies, and manual verification challenges. A total of 94 samples were collected from these water bodies in 2021 [12]. The transparency (SD), dissolved oxygen (DO), and redox potential (ORP) of the waters were measured on-site, while the ammonia nitrogen (NH_3–N) was determined in the laboratory using the samples collected [13–16]. The samples were divided into black and odorous and regular water bodies based on the four physicochemical parameters measured (see Table 1). According to the criteria in Table 1, 47 of the water bodies were regular, while the other 47 were black and odorous (Figure 1). Among the 94 samples, 47 were randomly selected as the training set for data analysis and model training, while the remaining 47 served as the validation set for accuracy assessment. Concurrently, the Sentinel-2 imagery was employed for monitoring of the water bodies using remote sensing technology. Owing to the high spatiotemporal resolution, the Sentinel-2 imagery is widely utilized in monitoring the land surface, such as the vegetation, soil cover, and water bodies. The Sentinel-2 image contains 13 bands, and the blue (B), green (G), red (R), and near-infrared (NIR) bands involve an identical resolution of

Table 1: Summary of indexes and ranges used for the characterizing of black and odorous water bodies in urban areas.

Classification index	Range
SD	0–25 cm
DO	0–2 mg/L
ORP	0–50 MV
NH3–N	≤8 mg/L

Figure 1: Map displaying the location of sampling points in the present study.

10 m [17, 18]. Considering that most pits and ponds in Langfang cover >3,000 m^2, the 10 m band resolution of the Sentinel-2 imagery data was suitable for the present study. To enhance the relationship to the field sampling time, Sentinel-2A data in synchronous transit were utilized to generate spectral data for the field sampling points, to create sample sets and images, and to perform analysis.

The spectral curves of the two types of water bodies based on preprocessing of data for the visible (VIS) and NIR bands are displayed in Figures 2 and 3. As shown in Figure 2, compared with the regular water bodies, the black and odorous water bodies exhibit low reflectivity values, and the associated spectral curves for the Rrs (G) – Rrs (B) and Rrs (G) – Rrs (R) display relatively gentle changes. Generally, the optical characteristics of water are determined by algal pigment contents, suspended solids, and colored dissolved organic matters. Because of extreme organic pollution, black and odorous water bodies are often enriched in organic pollutants and nutrients. Consequently, black and odorous water bodies usually have higher contents of organic matters and suspended solids than regular water bodies. In addition, nutrients would promote the growth of algae, thereby increasing the algal pigment contents. These pollutants and pigments account for changes in the optical properties of water bodies. For example, the high absorption and low backscattering of the colored dissolved organic matter and algal pigments significantly reduce the reflectivity of water in the VIS bands, so that the black and odorous water bodies usually have lower reflectance in blue, green, and red bands, thus the Rrs (B) + Rrs (G) + Rrs (R) was also utilized as the feature of black and odorous water bodies.

These observations are consistent with those reported in previous studies. Owing to spectral differences between the two types of water bodies in the VIS and NIR bands, multiple indexes for the extraction of features representing black and odorous water bodies were derived from sampling data by setting empirical thresholds (see Table 2). However, because black and odorous water bodies originate from diverse causes and the optical properties of some are comparable to those of regular water bodies, fuzzy areas are missed if just one spectral index is used for the extraction of features, and this negatively affects the classification accuracy. Based on data generated in the present study, four typical indexes including the band ratio (BD), BOI, HI, and WCI (Table 2) were tested, and the results are shown in Figure 4. In the spectral index range between N1 and N2, several black and odorous water samples overlap with regular water samples, and this area is termed the fuzzy area. This fuzzy area causes misclassification of black and odorous waters and elevates the uncertainty in the selection of the threshold. The threshold selection is often then subjective, and this affects the classification accuracy.

Obviously, the effective identification of black and odorous water bodies using a single feature is difficult. Therefore, in the present study, multiple features are exploited to establish a remote sensing recognition model for black and odorous water bodies. In previous studies, the Rrs (NIR) was utilized as the analysis feature, but because algal bloom and duckweed can cause regular water bodies to exhibit optical properties comparable to those of black and odorous water bodies, in the present study, it was not considered in the selection of features to prevent the introduction of additional errors [19–22]. Therefore, based on the analysis of spectral features, the Rrs (G) – Rrs (B), Rrs (G) – Rrs (R), and Rrs (B) + Rrs (G) + Rrs (R) were used to extract features for the recognition of black and odorous water bodies through remote sensing. These combinations reflect spectral differences between the two types of water bodies better because of the following: the Rrs (B) + Rrs (G) + Rrs (R) is the sum of reflectance in the visible light band, in which a black and odorous water body is characterized by a low reflectivity; the Rrs (G) – Rrs (B) and Rrs (G) – Rrs (R) are the reflectance differences between the G and B and the G and R bands, respectively, which reflect the smoothness of curves in the band ranges.

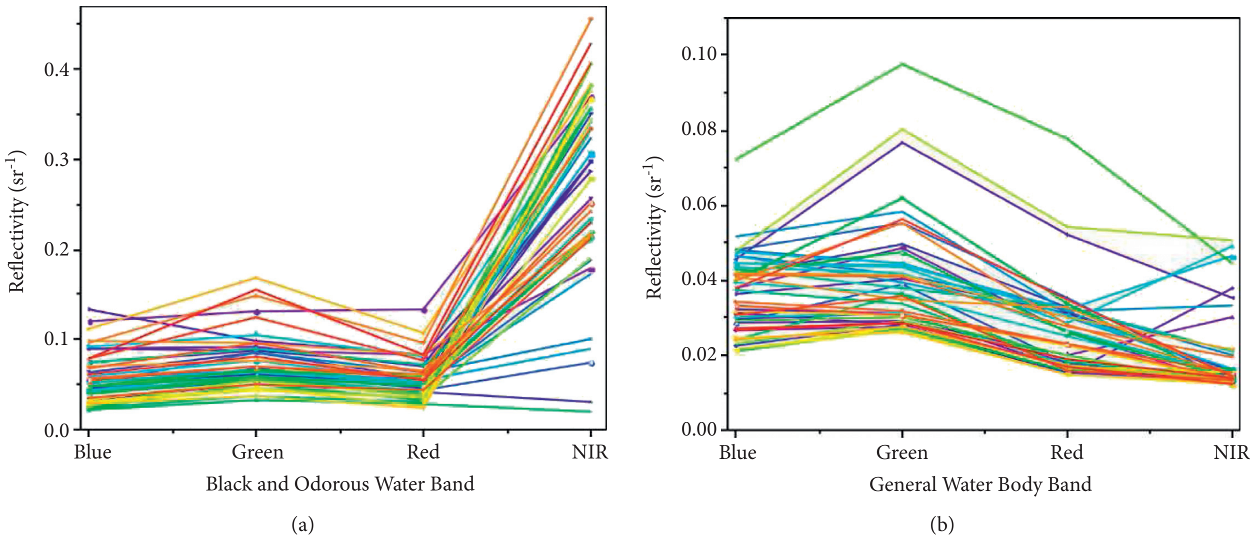

Figure 2: Plots showing remote sensing reflectance data for (a) black and odorous water bodies and (b) regular water bodies.

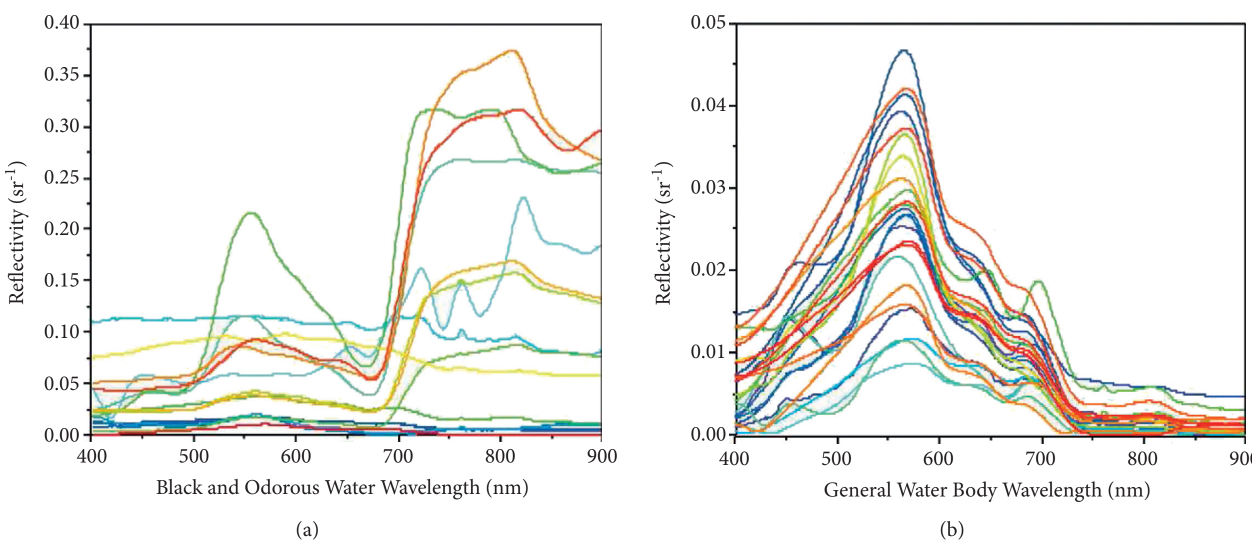

Figure 3: Plots showing measured reflectance data for (a) black and odorous water bodies and (b) regular water bodies.

Table 2: Summary of typical indexes associated with the threshold segmentation method.

Method	Expression	Extraction range	Threshold	Reference
BD	$BD = \frac{Rrs(G) - Rrs(R)}{Rrs(G) + Rrs(R)}$	$N_1 \leq BD \leq N_2$	$N_1 = 0.006$ $N_2 = 0.115$	[5]
WCI	$WC = \frac{(Rrs(G) - Rrs(B)/\Delta\lambda_{GB})}{(Rrs(R) - Rrs(G)/\Delta\lambda_{RG})}$	$N_1 \leq WCI \leq N_2$	$N_1 = 0$ $N_2 = 1$	[6]
BOI	$BOI = \frac{Rrs(G) - Rrs(R)}{Rrs(B) + Rrs(G) + Rrs(R)}$	$BOI \leq N$	$N = 0.065$	[8]
HI	$HI = Rrs(NIR) + Rrs(R) - Rrs(B)$	$HI > N$	$N = 0.085$	[9]

In the present study, calculations for all features were expressed in identical units (sr^{-1}), while the training and test data sets were generated by random sampling. The 47 samples in the training set included 23 black and odorous water and 24 regular water samples, while those in the test set comprised 24 black and odorous water and 23 regular

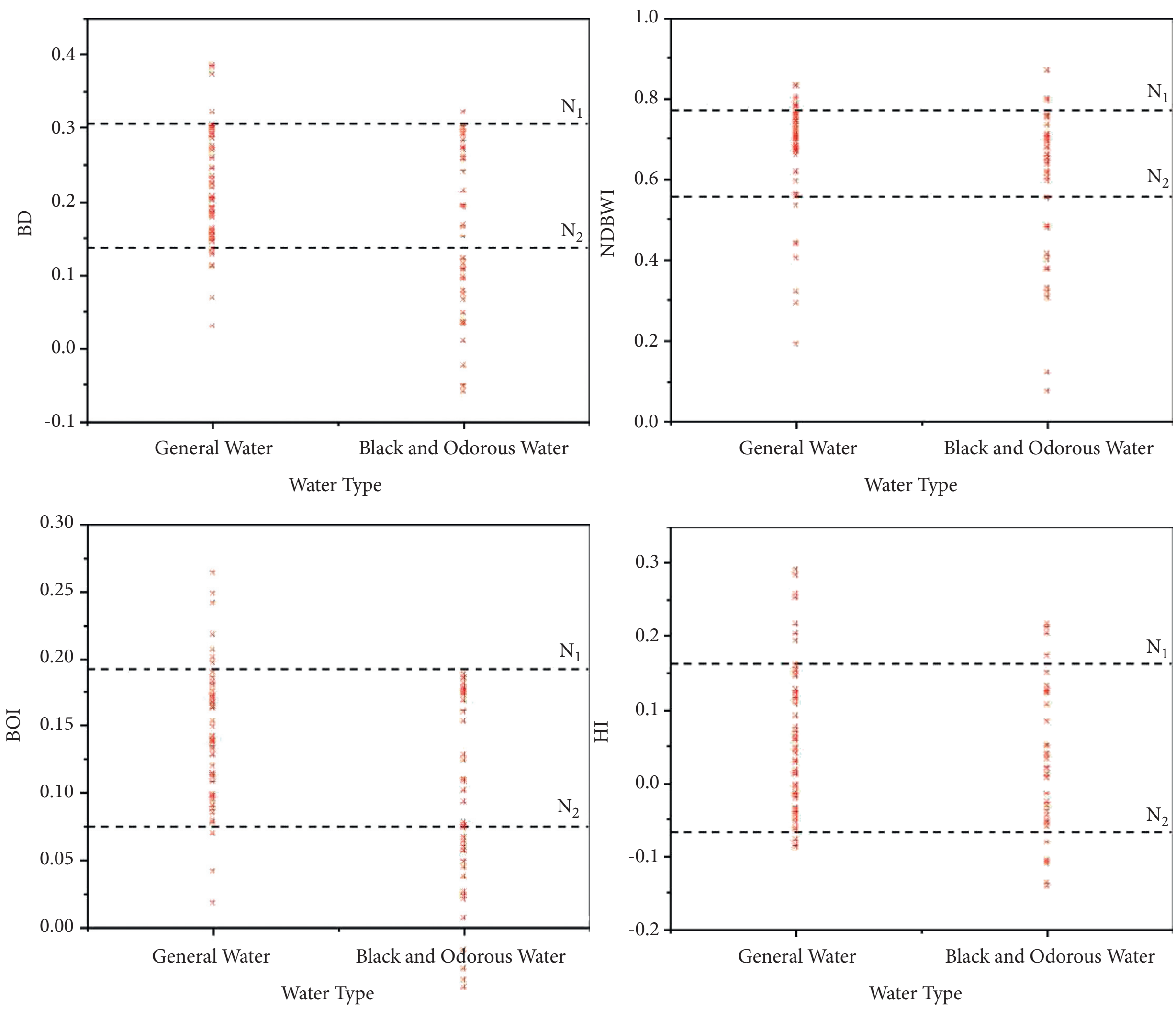

Figure 4: Plots displaying the confidence and fuzzy zones based on four models.

water samples. The CART model was constructed hierarchically and progressively according to the training set. Starting from the root node of the first layer, internal or leaf nodes were generated layer by layer and point by point according to the principle of the minimum Gini index. Then, pruning was performed, and the CART model construction was completed. A flowchart showing components of the algorithm is displayed in Figure 5 [23–25].

3. Results

The CART model decision tree obtained in the present study is shown in Figure 6. According to the Rrs (G) – Rrs (B), Rrs(R) – Rrs (G), and Rrs (B) + Rrs (G) + Rrs (R) features, a classification involving categories A–D was produced. This classification from the CART model is based on the degree of membership, which represents the probability of a set belonging to a black and odorous water body (Table 3) and the location of its size in the [0,1] interval. Initially, each set was divided into a confidence and a fuzzy area according to the degree of membership [26, 27]. A set with a degree of membership of 0 or 1 was assigned to the confidence area, and the category attributes of the associated set were then determined. The number 1 was then assigned to a black and odorous water body, while 0 was attributed to a regular water body [28]. The set with degrees of membership in the [0, 1] interval was assigned to the fuzzy area, and the category attributes of this set were uncertain. Considering the principle of the maximum likelihood classification, the set with degrees of membership in the [0.5, 1] interval was defined as black and odorous water bodies in the fuzzy area, while those in the [0, 0.5] are regular water bodies in the fuzzy area. Data for the attributes of category A–D, which are based on the principles examined, are presented in Table 3.

3.1. Model Accuracy Evaluation and Analysis.

The test set was used to verify the accuracy of the model, and this was calculated using the following expression:

$$\text{Accuarcy} = \frac{M}{N} \times 100\%, \tag{1}$$

where n represents the total number of sample points and M is the number of correct sample points. Among the 47

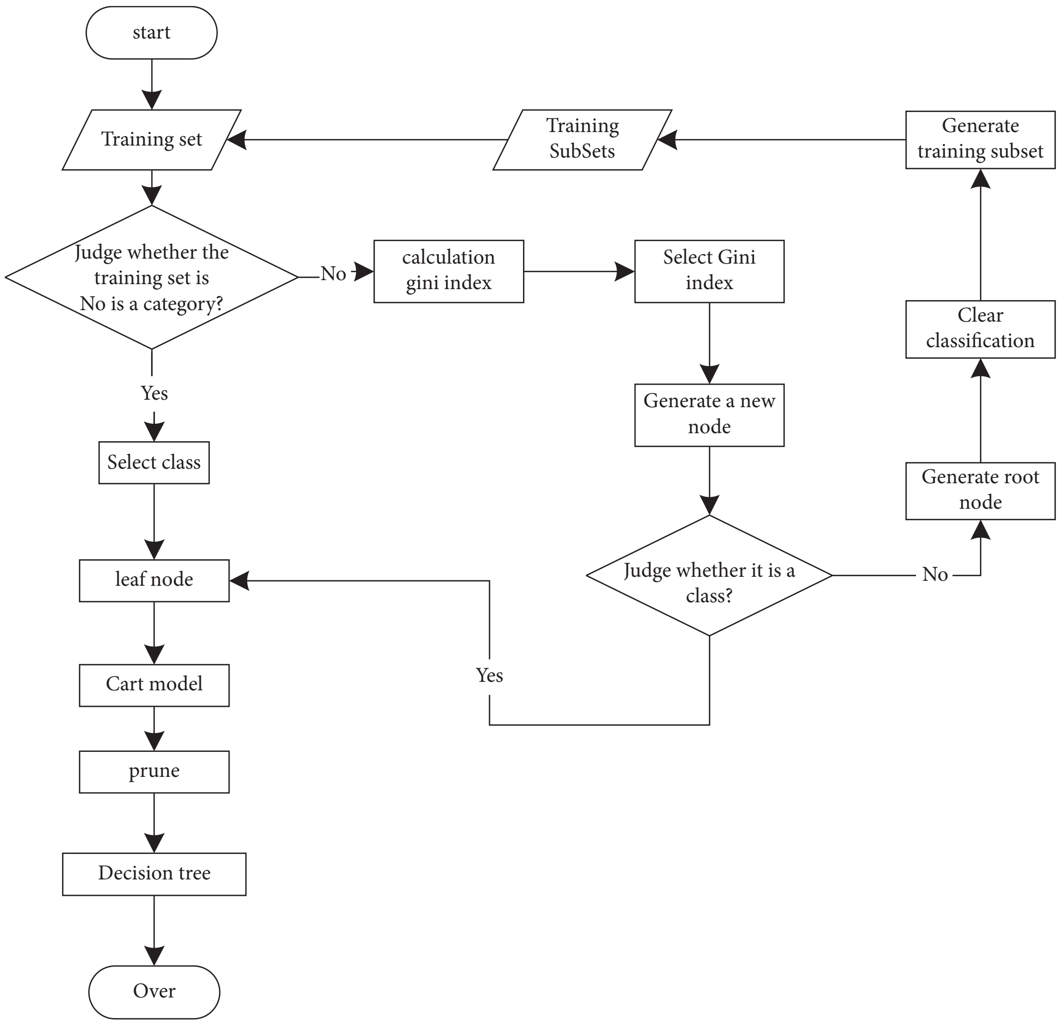

Figure 5: Flowchart showing the components of the CART algorithm.

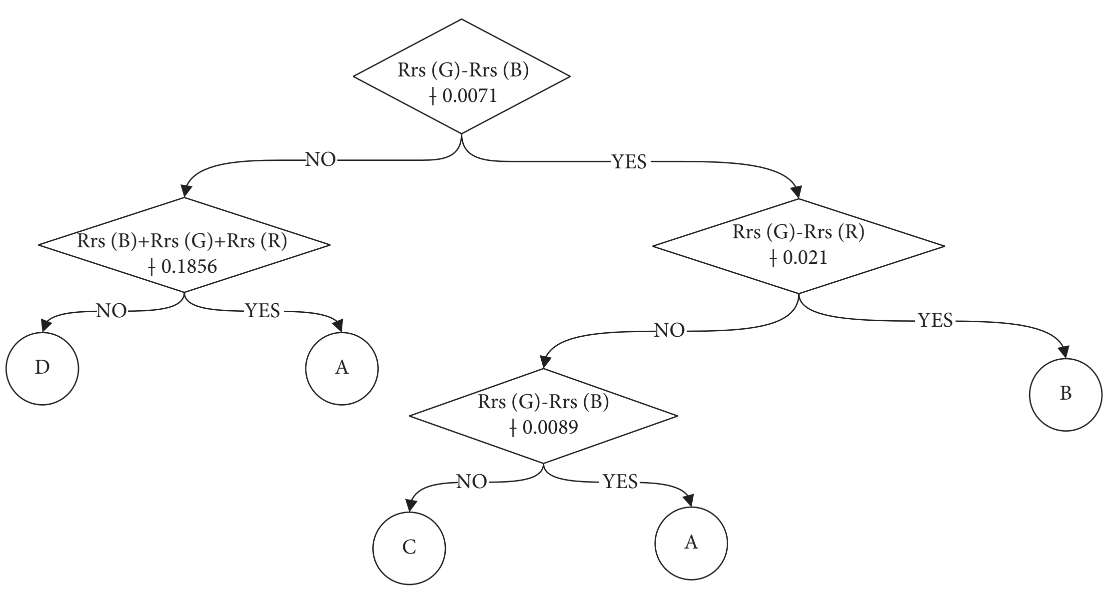

Figure 6: Illustration of the CART model decision tree obtained in the present study.

Table 3: Summary of the classification and membership categories obtained from the CART model.

Category	Membership	Region	Type
A	1	Confidence area	Black and odorous water
B	0.60	Fuzzy area	Black and odorous water
C	0.49	Fuzzy area	Regular water
D	0	Confidence area	Regular water

sample points in the test set, the results reveal that 39 were correctly classified, which produced an overall accuracy of 82.97%. The associated kappa coefficient of 0.7571 highlights the consistency of the data and the accuracy of the model. The results from the CART model were then compared with those obtained from other approaches commonly used to extract features representing black and odorous water bodies. According to the existing methods, the training set serves for recalibration of the threshold and the extraction of features associated with black and odorous water bodies, whereas the test set is utilized to evaluate the accuracy. According to the results, the CART model proposed in the present study produced the highest accuracy (82.97%), followed by the multi-feature decision tree model of Li (74.19%), and then the single-feature threshold segmentation models (BOI = 73.12%, WCI = 72.04%, and BD = 63.44%).

In the present study, the extraction accuracy of the confidence and fuzzy zones were also evaluated. For the test set, among the 32 samples extracted into the confidence zone, 29 were correctly classified, and this represents an accuracy of 90.63%. Relatedly, out of the 15 samples extracted into the fuzzy area, 10 were correctly classified, yielding an accuracy of 66.67%. Evidently, the error involved in the CART model originates largely from the fuzzy zone. This is mainly because black and odorous water bodies are linked to multiple causes, and thus, some are mistaken for regular water bodies in the feature space.

3.2. Temporal and Spatial Characteristics of a Black and Odorous Water Body. Based on the decision-tree model established, remote sensing monitoring was performed from July to September 2021 (Figures 7–9), and 30 points were randomly selected for field verification each month. The accuracy values from the monitoring and verification study are presented in Table 4. Obviously, the accuracy of this model for applications is good, and thus, it is suitable for engineering endeavors requiring the identification of black and odorous water bodies. In addition to the classification of water bodies, overall, the distribution of black and odorous water bodies decreases each month from July to September 2021. At the end of September, no black and odorous water body is present in built-up areas in all counties (cities and districts), and thus, this problem was effectively controlled. This effectiveness is attributed to the intensive measures introduced in all localities in recent years. However, an imbalance in the treatment of black and odorous water bodies in Langfang still exists. Several black and odorous water bodies are present in rural areas and at boundaries between urban and rural areas, which highlight characteristics of the overall distribution and local aggregation. Hotspots are concentrated in the north, central, east, and south areas of Langfang. The terrain in the central, east, and south areas are relatively low, and pits and ponds are common. In the north, the animal husbandry and food processing industries are relatively developed in Sanhe and Dachang County, while the central, east, and south areas are characterized by concentrated enterprises and high population densities. Therefore, activities associated with production and life, which involve the discharge of sewage, are higher in these three regions referred to above, and these elevate the probability of creating black and odorous water bodies.

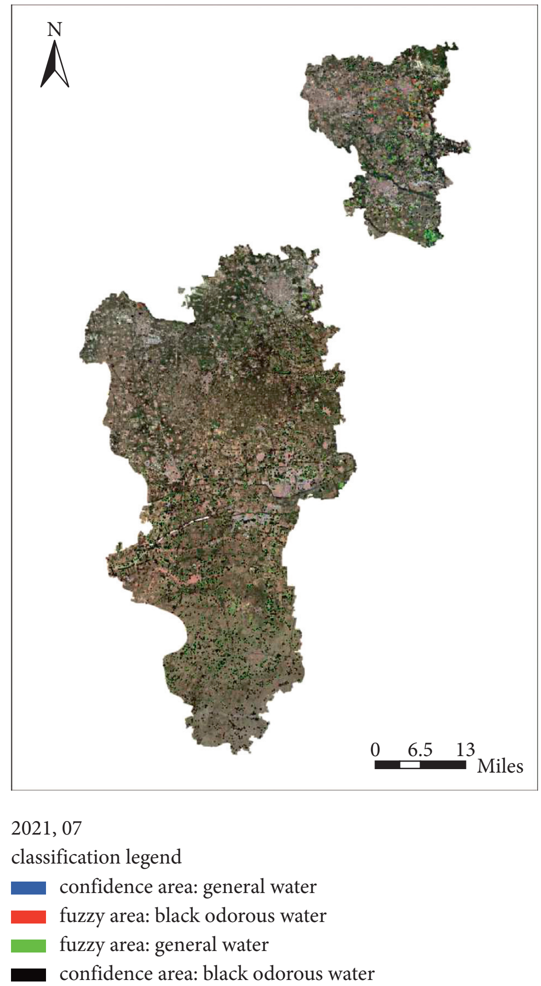

Figure 7: Map displaying the black and odorous water bodies identification results for July 2021.

3.3. Analysis of the Cause of a Black and Odorous Water Body. Evidently, from July to September 2021, black and odorous water bodies decreased significantly in Langfang. In fact, black and odorous water bodies were eliminated in built-up areas (cities and districts), and thus, major bodies

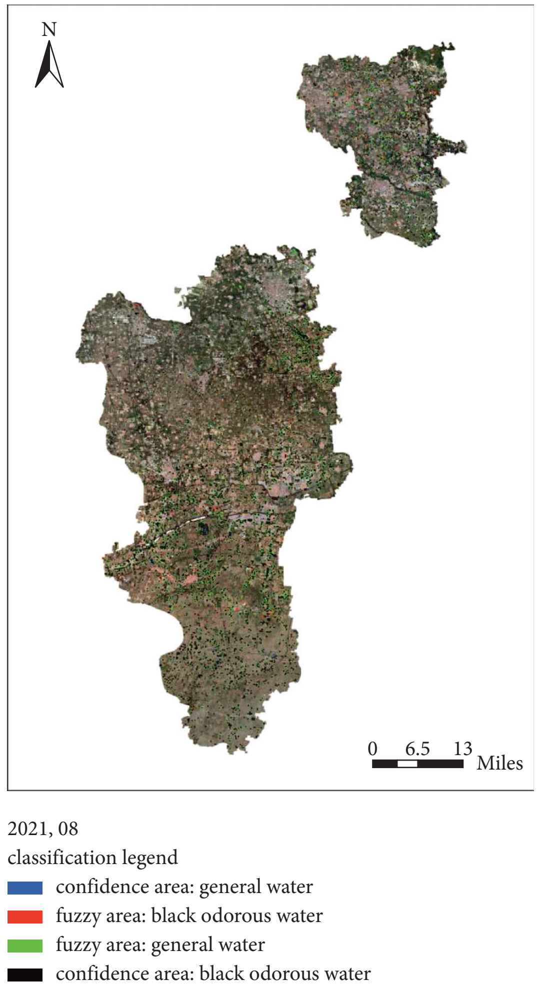

Figure 8: Map showing the black and odorous water bodies identification results for August 2021.

disappeared, while small local bodies remained in rural and urban-rural areas, because of the regulations implemented in Langfang in recent years. Regarding counties (cities and districts) and other built-up areas, because of the adequate treatment of black and odorous water bodies, the remediation effect is obvious. At present, almost no black and odorous water body is present in counties (cities and districts) and other built-up areas; however, in rural and urban-rural areas, black and odorous water bodies are more difficult to control because of the high traffic and poor underground pipe network [29–34]. Therefore, although black and odorous water bodies have been significantly reduced in these areas, their elimination still requires time. Considering the field verification results (Figure 10), the formation of black and odorous water bodies in rural areas of Langfang is attributed mainly to the following:

(1) Garbage removal and management problems: owing to the untimely removal and transportation of garbage in rural areas, pits and ponds are the main stacking places, and thus, leachates from domestic garbage invade water bodies through processes at the surface.

(2) Domestic sewage discharge problem: in rural areas, because of the poor underground pipe network, domestic sewage is commonly discharged into pits and ponds, and this promotes the accumulation of organic matter.

(3) Agricultural activities and livestock and poultry breeding: the main economic activities in rural areas are agriculture and aquaculture. Applied chemical fertilizers and livestock and poultry manure are transported into surrounding pits and ponds through the surface runoff.

(4) Poor fluidity and insufficient self-purification capacity of the pit and ponds: pits and ponds are abundant in rural areas of Langfang, and in low-lying areas, the waters in these originate mostly from surface runoff.

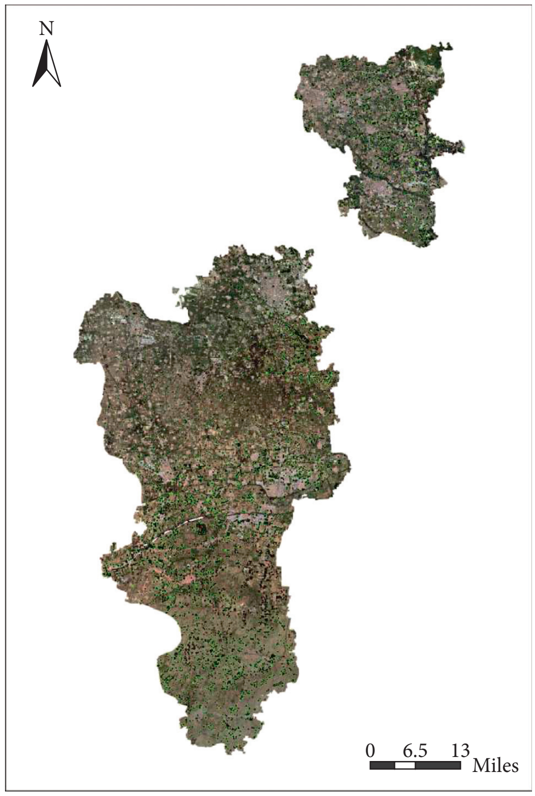

2021, 09
classification legend
confidence area: general water
fuzzy area: black odorous water
fuzzy area: general water
confidence area: black odorous water

Figure 9: Map displaying the black and odorous water bodies identification results for September 2021.

Table 4: Summary of the field verification accuracy data.

Time	Overall accuracy (%)	Fuzzy area accuracy (%)	Confidence area accuracy (%)
July 2021	75.86	66.67	85.71
August 2021	75	68.75	81.25
September 2021	73.34	64.29	75

(a) (b) (c)

Figure 10: Continued.

(d) (e) (f)

(g) (h) (i)

Figure 10: Photos showing field verification results associated with remote sensing monitoring of black and odorous water bodies in Langfang.

These bodies generally occupy small areas, which are characterized by poor fluidity and inadequate self-purification capacities, and these limitations are favorable for the production of black and odorous water bodies.

4. Discussion

In the engineering application of remote sensing monitoring of black and odorous water bodies, after the extraction of the associated features, field verification or remote sensing interpretation marks are also required for discrimination and to improve the accuracy. The CART model utilized in the present study adequately differentiates the extracted features associated with black and odorous water bodies and, thus, optimizes the classification accuracy. According to the results, the accuracy of extracting features representing black and odorous water bodies in the confidence zone is ideal. In engineering applications, such features can henceforth be extracted without field verification or visual interpretation. Results for the fuzzy area reveal samples that can easily be confused with regular water samples, and this area is characterized by a relatively low accuracy. Field verification or visual interpretation, however, can be performed as needed to improve the accuracy. The CART model and the confidence and fuzzy zones proposed in the present study can lessen the field verification burden for diverse applications. The proposed approach can improve the efficiency of engineering applications because of its high accuracy for the extraction of features representing black and odorous waters.

5. Conclusions

In the present study, water samples collected from 94 pits and ponds in Langfang, Hebei Province, in 2021 were characterized. These data were combined with data from the Sentinel-2a imagery for the same period to highlight spectral differences between black and odorous water and regular water bodies. Based on the CART model algorithm, an improved method for identifying black and odorous water bodies through remote sensing was proposed. Three features extraction parameters including the RRs (R) − RRs (G), RRs (B) + RRs (G) + RRs (R), and RRs (NIR), were used to create a decision-tree model. The results produced a classification, which facilitated the extraction of information associated with black and odorous water bodies. The main findings of the present study are summarized as follows:

(1) Spectral differences in the visible bands distinguished black and odorous water bodies from others. Overall, black and odorous water bodies produced weak reflectance values in the visible bands, and the spectral curve variation was relatively gentle. The Rrs (R) − Rrs (B), Rrs (R) − Rrs(G), and Rrs (B) + Rrs (G) + Rrs (R) exhibited potential for adequate characterization of these features, and thus, these can be exploited for the extraction of black and odorous water bodies information from remote sensing data.

(2) The CART model was constructed based on the Gini index minimization criterion, and the classification reflected the degree of membership of leaf nodes. Features associated with a degree of membership value ≥0.5 were considered as black and odorous water bodies, while regular water bodies showed values <0.5. According to the test set data, the overall accuracy of the CART model was 84.78%, while the kappa coefficient was 0.783, which highlights a superior potential for the extraction of black and odorous water features from satellite imagery.

(3) In the present study, the confidence and fuzzy regions were defined according to the degree of membership. The classification accuracy associated with the confidence region was 90.63%, while that of the fuzzy area was 66.67%. The classification method proposed in the present study alleviates the field verification and satellite data interpretation to identify black and odorous water bodies, which enhances the efficiency of diverse applications, especially engineering.

Data Availability

The experimental data used to support the findings of this study are available from the corresponding author upon request.

Conflicts of Interest

The authors declare that there are no conflicts of interest.

Authors' Contributions

Q.Z. and X.D. conceived and designed the study; Q.Z., X.D., and Y.Q. collected and analyzed the data; Q.Z. and X.D. wrote the manuscript; and G.L. and Y.J. reviewed and edited the manuscript. All authors have read and agreed to the published version of the manuscript.

Acknowledgments

This research was funded by the National Key R&D Program of China (2019YFE0127300), Science and Technology Project of Hebei Education Department (ZD2019138), Defense Industrial Technology Development Program (JCKY201907D004), S&T Program of Hebei (D2020409005), and full-time introduced Top Talents Scientific Research Projects in Hebei Province (2020HBQZYC002). The authors thank their group members for their help in the fieldwork.

References

[1] Ministry of Housing and Urban-Rural Development of the People's Republic of China, Ministry of Environmental Protection of the people's Republic of China, and Ministry of Environmental Protection of the Ministry of Housing and Urban-Rural Development, *Notice of Guidelines for the Remediation of Urban Black and Odorous Waters*, https://www.mohurdgov.cn/wjfb/201509/t20150911_224828, 2015.

[2] H. Angel, Y. Y. Zhi, and W. Amy, "Emerging digital environmental governance in China: the case of black and smelly waters in China," *Journal of Environmental Planning and Management*, vol. 63, no. 1, 2020.

[3] H. C. Zhou, "Action plan for water pollution prevention and control," *Journalof Green China*, no. 8, pp. 50–53, 2017.

[4] Z. Qian, L. S. Han, Y. Li et al., "Research on spatiotemporal evolution law of black and odorous water body in Guangzhou city," *Journal of Geoinformatics in Sustainable Ecosystem and Society*, vol. 1228, pp. 273–289, 2019.

[5] S. Wen, Q. Wang, and Y.-M. Li, "Remote sensing recognition of urban black and odorous water bodies based on high-resolution images: taking Nanjing as an example," *Journal of Environmental Sciences*, vol. 39, no. 1, pp. 57–67, 2018.

[6] J. Q. Li, J. G. Li, and L. Zhu, "Remote sensing recognition and ground verification of black and smelly water bodies in Taiyuan City," *J . Journal of Remote Sensing*, vol. 23, no. 4, pp. 773–784, 2019.

[7] F. W. Li, X. W. Zheng, W. Zhou, X. C. Zhou, and L. Q. Cao, "Monitoring of urban black-odor water based on Nemerow index and gradient boosting decision tree regression using UAV-borne hyperspectral imagery," *Journal of Remote Sensing*, vol. 11, no. 20, 2019.

[8] Y. Yao, Q. Shen, and L. Zhu, "Remote sensing recognition of black and odorous water bodies in Shenyang based on Gaofen No. 2," *Journal of Remote Sensing*, vol. 23, no. 2, pp. 230–242, 2019.

[9] H. M. Yao, Y. N. Lu, and Z. Q. Gong, "Research on black and stinky water recognition method in Qinzhou city, guangxi based on PlanetScope image," *Journal of Environmental Engineering*, vol. 37, no. 10, pp. 35–43, 2019.

[10] X. Zhang, J. B. Lai, and J. G. Li, "Remote sensing recognition of black and smelly water bodies in Shenzhen based on Gaofen-1 image," *Journal of Science Technology and Engineering*, vol. 19, no. 4, pp. 268–274, 2019.

[11] L. L. Li, Y. M. Li, and H. Lu, "Remote sensing classification of urban black and odorous water bodies based on decision tree," *Journal of Environmental Sciences*, vol. 41, no. 11, pp. 5060–5072, 2020.

[12] Q. An, Q. Fu, and J. Qiao, "Discussion on the current situation and protection measures of water resources in Langfang City," *Journal of Groundwater*, vol. 42, no. 1, pp. 155–157, 2020.

[13] B. Ma and X. M. Yang, "Measurement of oxidation-reduction potential (ORP) in black and odorous water and its influencing factors," *Journal of Instrument User*, vol. 28, no. 9, pp. 110–112, 2021.

[14] J. Q. Zhang, F. Yin, H. W. Wang, and S. X. Wang, "Comparative study on the methods of measuring water transparency," *Journal of Agricultural Technology and Equipment*, vol. 11, pp. 76-77, 2018.

[15] C. B. Zhang, "NIRS-ANN non-destructive quantitative analysis of total nitrogen in water quality monitoring," *Journal of Science and Technology Information*, no. 26, pp. 379-380, 2009.

[16] W. Y. Dai and L. Sun, "Detection method of dissolved oxygen in water," *Journal of Anhui Agricultural Science Bulletin*, vol. 19, pp. 77–79, 2007.

[17] C. Xu and Z. H. Hao, "Data characteristics and application potential analysis of the sentinel satellite Sentinel-2A," *Journal of Science and Technology Horizons*, no. 16, pp. 48–50, 2018.

[18] L. X. OuYang, Q. Li Xin, and F. M. Hui, "Data characteristics and application potential analysis of the sentinel satellite Sentinel-1A," *Journal of Polar Research*, vol. 29, no. 2, pp. 286–295, 2017.

[19] P. Xu, N. Na, S. Gao, and C. Geng, "Determination of sodium alginate in algae by near-infrared spectroscopy," *Desalination and Water Treatment*, vol. 168, pp. 117–122, 2019.

[20] H. Y. Cao, *Optical Characteristics Analysis of Black and Odorous Water Bodies in Typical Cities in China and Remote Sensing Recognition Model Research*, Southwest Jiaotong University, 2017.

[21] H. T. Duan, R. H. Ma, L. S. Arthur, Q. Shen, H. Yin, and Y. Zhang, "Optical characterization of black water blooms in

eutrophic waters," *Journal of The Science of the total environment*, vol. 482-483, pp. 174–183, 2014.

[22] L. Zhang, "Determination of water pollutants based on convolutional neural network near infrared spectroscopy," *Journal of Chemical Analysis And Meterage*, vol. 30, no. 8, pp. 24–27, 2021.

[23] V. U. Lev, S. K. Maxim, and F. P. A. Coolen, "Imprecise weighted extensions of random forests for classification and regression," *Journal of Applied Soft Computing Journal*, vol. 92, 2020.

[24] O. Cristina and W. . Louis, "A complete fuzzy decision tree technique," *Journal of Fuzzy Sets and Systems*, vol. 138, no. 2, 2003.

[25] R. A. Ganjoei, H. Akbarifard, M. Mashinchi, and S. A Majid Jalaee Esfandabadi, "Estimation of upper and lower bounds of Gini coefficient by fuzzy data," *Data in Brief*, vol. 29, Article ID 105288, 2020.

[26] X. C. Wang, X. D. Liu, and P. Witold, "Fuzzy rule based decision trees," *Journal of Pattern Recognition*, vol. 48, no. 1, 2015.

[27] R. Smita, M. Samrat, and E. Asif, "Dispersion ratio based decision tree model for classification," *Journal of Expert Systems With Applications*, vol. 116, 2018.

[28] X. L. Zhou and D. Yan, "Model tree pruning," *International Journal of Machine Learning and Cybernetics*, vol. 10, no. 12, 2019.

[29] Z. J. Jin, "Research on difficulties in urban river governance and environmental rehabilitation strategies," *Journal of Water Conservancy Technical Supervision*, no. 9, pp. 112–114, 2021.

[30] Y. Geng and X. Li, "Discussion on the treatment of black and odorous water bodies in rural areas and the extent of rural sewage treatment," *Journal of Science and Technology Innovation and Application*, vol. 11, no. 24, pp. 144–146, 2021.

[31] L. Sun, W. Ma, and J. H. Wu, "Research on progress of urban black and odorous water treatment and water conservancy measures," *Journal of China Rural Water and Hydropower*, no. 8, pp. 23–28, 2021.

[32] H. Wang, C. Mei, J. H. Liu, and J. Wang, "Current status and prospects of urban water problem governance in my country," *Journal of China Water Resources*, no. 14, pp. 4–7, 2021.

[33] C. Z. Li and N. Liu, "Pollution analysis of urban black and odorous water bodies and research on treatment technology," *Journal of Energy Conservation and Environmental Protection*, no. 7, pp. 72-73, 2021.

[34] E. L. Liu, J. Y. Ma, and C. C. Wang, "Discussion on the progress and suggestions of the treatment of black and odorous water bodies in rural areas," *Journal of Guangdong Chemical Industry*, vol. 48, no. 12, Article ID 136, 2021.

Hindawi
Scientific Programming
Volume 2022, Article ID 9327131, 7 pages
https://doi.org/10.1155/2022/9327131

Research Article

Design and Research of Physical Education Platform Based on Artificial Intelligence

Yufeng Ba [1] and Zhenfeng Liu [2]

[1] Institute of Physical Education, Henan Agriculture University, Zhengzhou 450046, Henan, China
[2] School of Physical Education, Henan University, Kaifeng 475001, Henan, China

Correspondence should be addressed to Zhenfeng Liu; lzfgkx@163.com

Received 25 November 2021; Revised 25 December 2021; Accepted 12 January 2022; Published 22 February 2022

Academic Editor: Le Sun

With the continuous development of information technology, conventional physical education teaching methods are no longer applicable. In order to ensure the objectivity of college physical education evaluation, this paper designs a set of college physical education management information system based on artificial intelligence technology. The weighting algorithm in the student performance evaluation module and teacher performance evaluation module in the system adopts the intelligent algorithm based on FNN neural network. Experimental verification shows that the intelligent algorithm based on the FNN neural network can effectively predict the students' score in the national college physical education examination, which can provide a more objective basis for teacher performance evaluation.

1. Introduction

Wang Yuqing said in the study that physical education in colleges and universities in China is divided into physical education major, physical education major, and nonphysical education major [1]. Wang Ming said in the study which professional terms such as sports management and competition management are nonphysical education majors [2]. Li Feifei said that, according to the requirements of the Ministry of Education, nonsports majors need to receive at least 2 hours of formal physical education every week [3]. Wen Jiao said in a study on college physical education that the premise for students to obtain graduation qualification is that their physical performance passes the national unified physical education examination [4]. Li Zhang has proposed the university sports test content in the study. The test contents include middle and long distance running (1500m for boys and 800m for girls), standing long jump or high jump, throwing (shot put, rubber ball, and long handle grenade throw are optional), physical flexibility (generally sitting forward flexion), and learning a competition [5]. LiuYanRu also further explained to the college sports test that, in addition to competition events, running, jumping, throwing, flexibility, and other tests all pass the score line strictly [6]. Zhang Jianye explains the other events in the college sports tests: competition events can generally be selected from badminton, tennis, table tennis, basketball, volleyball and other ball games, or martial arts [7].

Li Zihao carried out research on the effectiveness of physical education teaching in universities. In the early research, students' physical education achievements were only constrained by the unified examination of national college physical education curriculum, so too many examination oriented elements were integrated into physical education [8]. The study believes that the core goal of college physical education should be to improve students' comprehensive physical quality and ensure students' physical and mental health during their study in school. Li Xianshu considers that students' physical and mental health is difficult to be effectively controlled by the traditional index factor method [9], so artificial intelligence algorithm is introduced to construct fuzzy evaluation factors for students' physical and mental health, so as to evaluate the achievements of physical education in colleges and universities.

Fuzzy factor method uses fuzzy neural network (FNN) to analyze multiple controllable indexes of students. Gaobin illustrates the FNN, indicating that FNN is a double variable that presses the data into a [0,1] interval [10] and uses this variable to control the teaching results of physical education teachers.

2. Comprehensive Evaluation Model of College Students' Physical Education Achievements

Yang Dapeng in his study proposed that, in the actual management of college students, students' physical fitness test and physical education examination can directly reflect students' physical education curriculum level [11]. YongBai (2016) stated in the study that, in addition, students' vital capacity, body fat rate, and other indicators were investigated by general surgical examination in students' regular physical examination and students' SAS and SDS level in general psychiatric examination can reflect students' physical and mental health from a certain angle [12]. The logical relationship between the above four categories of data and related subcategories is shown in Figure 1.

In Figure 1, the general surgical examination data and physical examination data in physical examination belong to dimensional data, which can be recognized by FNN only after dimensionless normalization. Other data belong to dimensionless data and can be directly input into FNN. The fuzzy convolution result of FNN can be directly used as the fuzzy evaluation result of students' physical education achievement. The results of the above dimensionless normalization algorithm is shown (1) as

$$y_i = \frac{x_i - \min(x)}{\max(x) - \min(x)}, \tag{1}$$

where x_i is the i input value in x sequence, y_i is the dimensionless output value corresponding to the i input value in sequence x, $\min(x)$ is the minimum value of sequence x, and $\max(x)$ is the maximum value of sequence x.

The data sorted by the above minmax module are all data in the [0,1] interval, while mental health data such as SDS and SAS and physical examination result data are dimensionless data. If there are no special requirements, SDS and SAS will count in the [0,10] interval according to the 10 point system, and the physical examination results will count in the [0100] interval according to the 100 point system. In order to reduce the complexity of the statistical process of this module, when it is required to issue SDS and SAS evaluation, directly input the 1-point system results; that is, the original results are formed in the [0,1] interval, and the physical examination results are also directly issued in the 1-point system results; that is, the original results are formed in the [0,1] interval.

The statistical significance of FNN neural network is to summarize all the above input data into a double precision data as the actual evaluation result data of students. If there is no subsequent data processing, FNN neural network will be trained to converge to a double precision variable in the [0,1] interval. This variable is multiplied by 100 to form a 100 point evaluation result as the final physical education achievement of students. The node function of the neural network selects polynomial depth iterative regression function (2):

$$y = \sum_{i=1}^{n} \sum_{j=0}^{5} A_j x_i^j, \tag{2}$$

where n is the number of nodes of the previous neural network, j is the polynomial order, and A_j is the coefficient to be regressed of the j order polynomial. Other mathematical symbols have the same meaning as (1).

3. Construction of Artificial Intelligence System for College Physical Education

Based on the comprehensive analysis of the above neural network model, it is found that, in addition to the system administrator, the system needs four roles, namely, the assessed students, physical education teachers, surgeons, and psychologists. Surgeons fill in the results of general surgical examinations, psychologists fill in the results of SAS and SDS scales, and physical education teachers fill in the results of the national unified physical education examination and physical fitness test in colleges and universities. In addition to cooperating with the above four inspections, students have the authority to query the transcripts. The transcripts will also be submitted to the Academic Affairs Office for teaching quality evaluation and to the student work office for student performance summary management. The system architecture is shown in Figure 2:

In Figure 2, FNN neural network and predata processing process have been deeply analyzed in the previous text. Here, we focus on the postprocessing of students' transcripts. The system provides the general query function of students' transcripts; that is, entering the student number can query the transcripts of the specified students, and entering the class name can access the summary table of the transcripts of the whole class, including the descending sorting of scores, and the classified statistics of excellent (80–100 points), pass (60–80 points), and fail (0–60 points). At the same time, teachers' postperformance is evaluated according to the change and distribution of students' performance. Because other statistical work algorithms are relatively simple and limited by space, they are not discussed here. Only the teacher postperformance evaluation algorithm is expanded as Figure 3.

In Figure 3, another group of FNN neural networks is used to evaluate teacher performance. The node function of the neural network is consistent with that of the FNN network in Figure 2. Refer to (2), and the data preprocessing algorithm before the neural network refers to (1). If the traditional teacher performance evaluation scheme based on the weighted factor method is adopted, because the weighted factor itself has a systematic error and the systematic error may be aimed at different students' basic physical conditions, differences in colleges and departments, differences in students' gender and age, etc., the evaluation reliability cannot be effectively

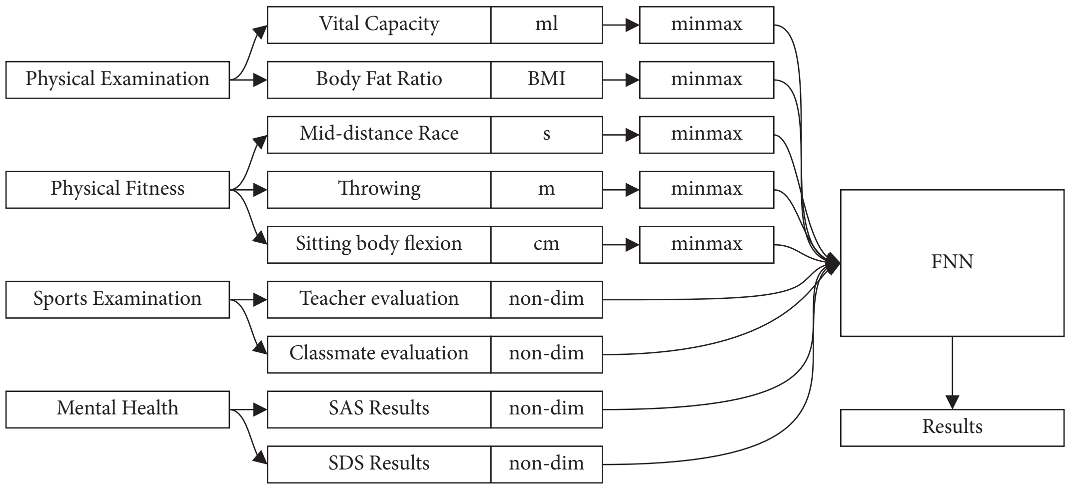

Figure 1: Evaluation index of physical education in colleges and universities and its machine learning analysis.

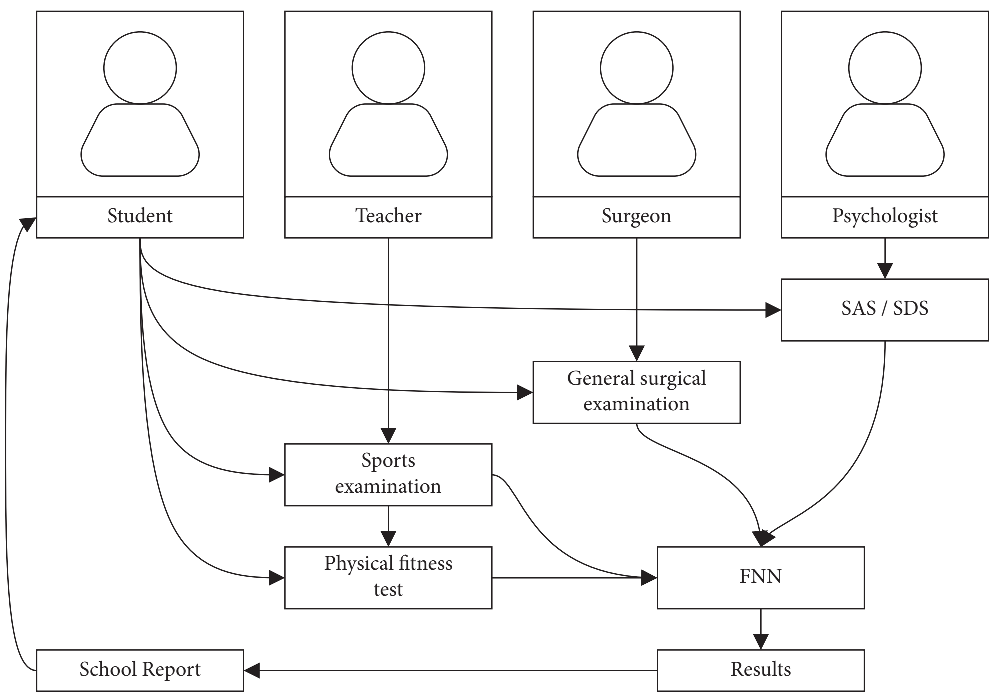

Figure 2: Architecture diagram of the artificial intelligence system (FNN) for physical education teaching evaluation in colleges and universities.

guaranteed. In this study, FNN neural network is selected for the comprehensive evaluation of students' physical education performance, and it also realizes the comprehensive evaluation of teachers' performance.

4. Overall Simulation Verification of System Effectiveness

Taking the real original files of 21 nonsports majors in 2018 and 2019 in 2020–2021 academic year as the data source, the analysis environment is constructed in MATLAB, the traditional method is used to analyze student performance and teacher performance as the reference group, and the artificial intelligence method designed in this study is used to analyze student performance and teacher performance as the observation group. The following three validation studies were carried out.

4.1. Correlation between Artificial Intelligence Evaluation and National Physical Education Examination Results. In order to verify the role of the artificial intelligence method designed in this study in student achievement and teacher achievement, the R2 value was obtained by the linear regression method under SPSS, and t value and P value were obtained by bivariate t calibration.

The R2 values were counted as the ratio of the regression residue to the mean residue (3):

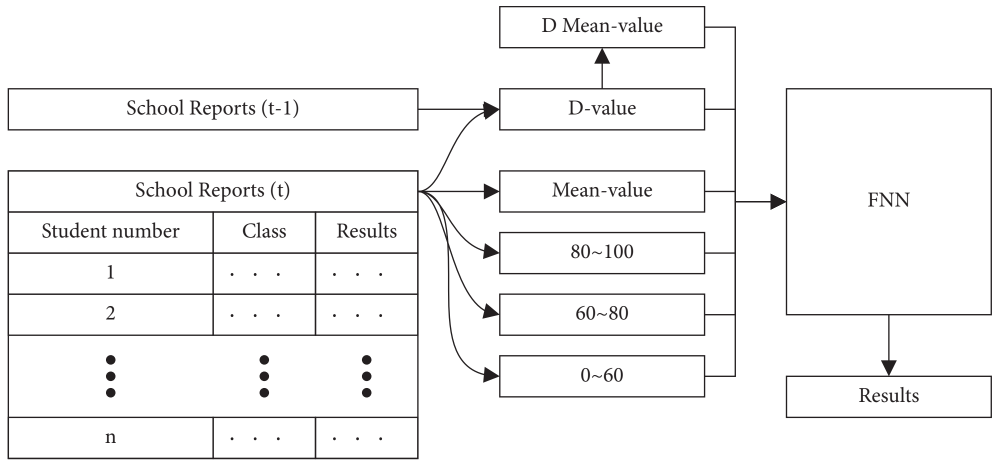

Figure 3: Schematic diagram of the teacher performance evaluation system.

$$R^2 = \frac{\sum_i (x_i - \overline{x})}{\sum_i (x_i - \tilde{x}_i)},$$
$$\overline{x} = \frac{1}{n}\sum_{i=1}^{n} x_i, \tag{3}$$

where $\overline{x}$ is the mean value of the test sample sequence, x_i is the regression value in the sequence, i is the input value in the sequence, and n is the number of test samples.

The T value and P value of bivariate t-check come from the bivariate t-check process, where t value is the value value of the output result. When $t > 10.000$, it is considered that there is a statistical difference between the two columns of data, and the greater the T value, the greater the statistical difference; the P value is the log value of the output result. When $p < 0.05$, it is considered that the result data are within the confidence space. When $p < 0.01$, it is considered that the result data have a significant statistical significance. The smaller the p value, the higher the degree of confidence. Subject to the length, only the calculation algorithm of T value (value) is explained here (4):

$$t_{\text{Value}} = \frac{\overline{x} - \mu}{\left(\sigma_x / \sqrt{n-1}\right)}, \overline{x},$$
$$\mu = \frac{1}{n, m}\sum_{i=1}^{n,m} x_i, \tag{4}$$
$$\sigma_x = \frac{1}{n-1}\sqrt{\sum_{i=1}^{n} (x_i - \overline{x})^2},$$

where x means the average value of the investigation sample sequence and μ means the average value of the reference sequence. n is the number of nodes of the investigation sample sequence, m is the number of nodes of the reference sample sequence, and σ means the standard deviation rate of the investigation sample sequence. Firstly, the linear regression method is used to calculate the correlation between the national unified examination results and the comprehensive evaluation results of the system, and Figure 4 is obtained.

In Figure 4, there is a significant linear relationship between the results of the National Physical Education unified examination and the comprehensive evaluation value of the system, $R^2 = 0.9509$ and $P = 0.003$, because the comprehensive evaluation process of the system does not introduce the results of the National Physical Education unified examination, but according to the results of the physical education classroom teaching test, it can be considered that the system has a certain predictive value for the results of the National Physical Education unified examination. The R^2 value calculation scheme is the ratio of regression variance to linear variance, which can calculate the difference between the regression result and the original result.

In the actual correlation analysis, in addition to the results of the National Physical Education unified examination, it also investigates the results of SDS and SAS evaluation, comprehensive physical examination evaluation, and surgical examination evaluation of students in the evaluation of students' mental health and introduces the bivariate t-test analysis results of the above evaluation results and the comprehensive evaluation results of artificial intelligence given by the system. The above analysis results are shown in Table 1.

In Table 1, there are significant statistical consistency ($T > 10.000$, $p < 0.01$) and linear correlation ($R2 > 0.75$, $p < 0.01$) between the five data and the comprehensive evaluation results of artificial intelligence given in this study. However, there are some statistical differences between the relevant data. For example, the comprehensive evaluation results of artificial intelligence given by the system are highly correlated with the results of the national physical examination, physical fitness test, and general surgical examination (both T value and R2 value are large), but slightly less correlated with the results of mental health examination (SAS and SDS) (both T value and R2 value are small).

In Figure 5, the correlation between the national unified assessment results and the comprehensive evaluation of the artificial intelligence system is calculated by the linear

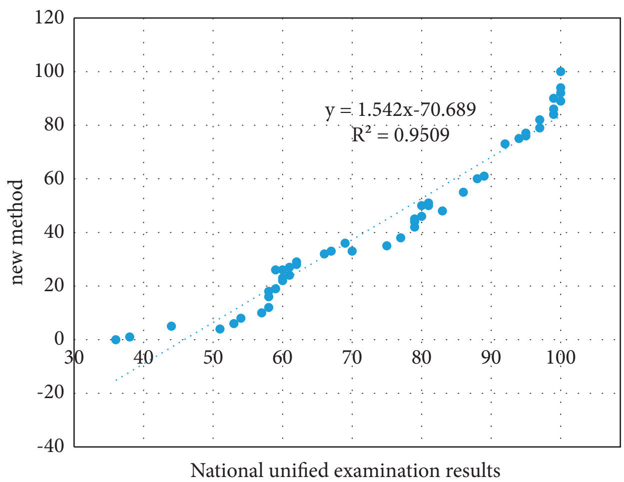

Figure 4: Linear regression results of national unified examination results and comprehensive evaluation results of the system.

regression method to compare the differences between the original assessment items and artificial intelligence system.

4.2. After Using the Artificial Intelligence Comprehensive Evaluation System, the Statistical Results of Teachers' Performance Change. There are 24 PE teachers in our school. The evaluation results of the original teaching evaluation teachers' performance are counted, and then, the artificial intelligence teacher performance evaluation method given by the system is used to evaluate the teachers' performance. The comparison results are shown in Table 2.

In Table 2, on the premise that the evaluation scheme remains unchanged, the probability of teachers in the physical education teaching group obtaining advanced teachers decreases from 25% to 17%. Among the four teachers who obtain advanced teachers in the new scheme, three teachers are different from the previous evaluation result list, accounting for 75%, while the probability of backward teachers increases from 21% to 33%, and one teacher is different from the previous evaluation result list, accounting for 18%. That is, the new scheme has more stringent requirements for teachers and puts forward higher requirements for college physical education teachers.

In Figure 6, through the analysis of the correlation between the old and new schemes on teachers' performance evaluation results and using the artificial intelligence teachers' performance evaluation method given by the system to evaluate teachers' performance, it is found that the probability of obtaining senior teachers has decreased by 8%, the performance evaluation of teachers is more strict, and the probability of teachers with poor evaluation is higher, and it is concluded that the new scheme has higher requirements for PE teachers and the judgment results are more rigorous.

4.3. Investigation and Statistics of Teachers' and Students' Subjective Feelings about the Evaluation Results of the System. Because the above simulation process is aimed at the student performance and teacher performance in the academic year 2020–2021, 500 students are selected as the survey object, and all 24 teachers are selected as the survey object. They are required to "support," "no objection," and "oppose" the change of the evaluation system by displaying the previous evaluation results and the evaluation results given by the new system; the statistics of three evaluation results are shown in Table 3:

In Table 3, although the evaluation of teachers in the new system is more harsh, the support rate of teachers for the new system has increased from 25.0% to 37.5% and the opposition rate has decreased from 62.5% to 41.7% compared with the previous system. The fundamental reason is that the evaluation criteria for teachers in the new system are more comprehensive and objective, and teachers can perform more actively in their work, the ratio of labor pay to labor return is more significant. Students' evaluation results of the new system are much higher than those of the previous system, in which the support rate has increased from 29.8% to 79.2%, and the opposition rate has decreased from 58.2% to 11.8%.

In Figure 7, through the analysis of the correlation between the new scheme and the support rate of teachers, the evaluation standard of the new scheme is more objective, which improves the enthusiasm of teachers in all aspects and increases the interaction between teachers and students so

Table 1: Correlation analysis between relevant data and comprehensive evaluation results of the system.

Comparison items	Regression analysis		Bivariate t-check	
	R^2	P	t	P
Unified examination results	0.9509	0.003	86.273	0.004
SDS	0.8364	0.007	65.126	0.007
SAS	0.7913	0.006	71.235	0.007
Physical fitness test results	0.9758	0.002	92.715	0.004
Surgical examination results	0.8674	0.003	88.594	0.003

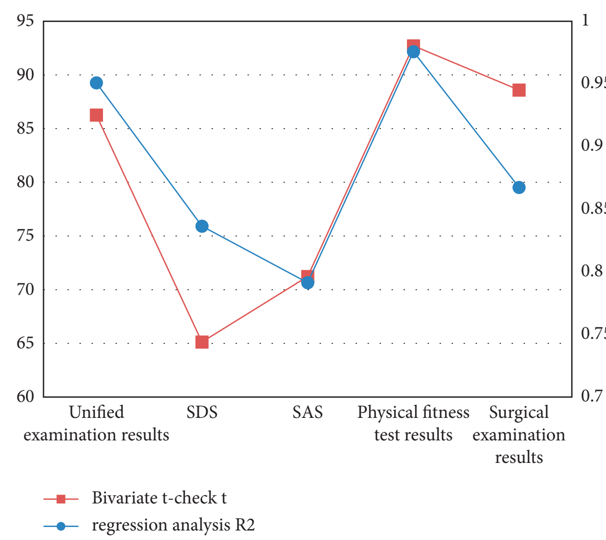

Figure 5: Correlation between student assessment items and comprehensive evaluation of artificial intelligence.

Table 2: Impact of new and old systems on teachers' performance evaluation results.

Comparison items	Advanced teacher			Backward teachers		
	Total	Difference	Overlap	Total	Difference	Overlap
Previous method	6 (25)	—	—	5 (21)	—	—
New method	4 (17)	3 (75)	2 (50)	8 (33)	1 (18)	4 (50)

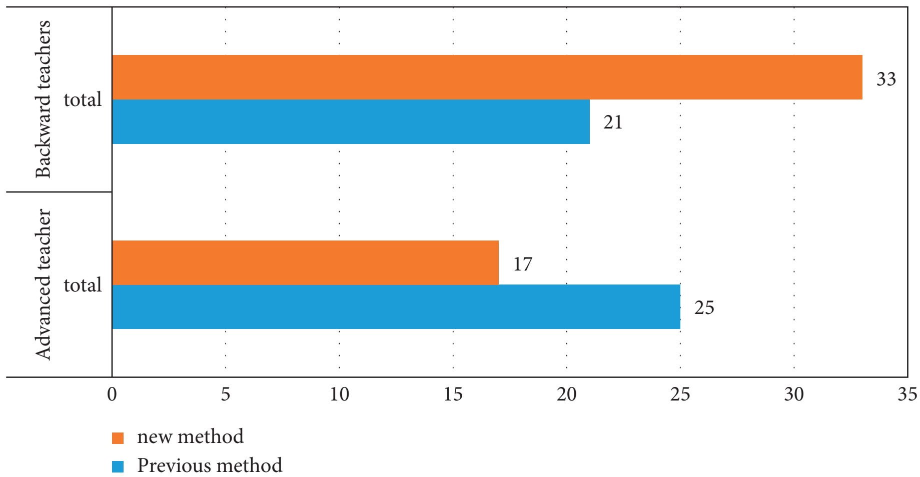

Figure 6: Correlation between old and new schemes and teachers' performance evaluation results.

Table 3: Statistics of support rate for the new system among students and teachers.

Comparison items	Student $n = 500$			Teacher $n = 24$		
	Support	No obj	Oppose	Support	No obj	Oppose
Previous method	149 (29.8)	60 (12)	291 (58.2)	6 (25)	3 (12.5)	15 (62.5)
New method	396 (79.2)	45 (9)	59 (11.8)	9 (37.5)	5 (20.8)	10 (41.7)

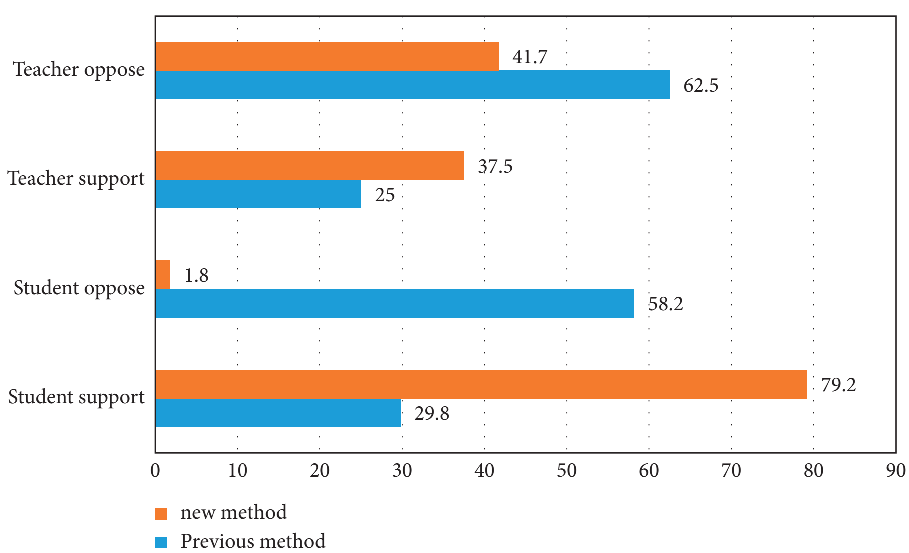

Figure 7: Correlation between the new scheme and the support rate of teachers.

that the evaluation results of students are much higher than those of the old scheme and the new scheme obtains higher support rate among teachers.

5. Summary

In the college physical education management information system, the artificial intelligence evaluation method is used to replace the previous weighted index evaluation method so that the data displayed in the conventional teaching link can intuitively predict the National Physical Education unified examination results, and the evaluation of students' performance and teachers' performance are more objective and comprehensive. However, compared with the comprehensive artificial intelligence system, subject to the historical problems of the current technical system and the college physical education teaching information management system, as well as the linkage restriction of the evaluation mechanism of the surrounding teaching groups, the system cannot realize the comprehensive intervention of the artificial intelligence system in the college physical education teaching process. The follow-up research will further sort out the process, deepen the teaching reform, and further the application of artificial intelligence system.

Data Availability

No data were used to support this study.

Disclosure

The authors confirm that the content of the manuscript has not been published or submitted for publication elsewhere.

Conflicts of Interest

The authors declare that they have no potential conflicts of interest in this study.

Authors' Contributions

All authors have seen the manuscript and approved to submit to the journal.

References

[1] Y. Wang and S.-B. Tsai, "Physical education teaching in colleges and universities assisted by virtual reality technology based on artificial intelligence," *Mathematical Problems in Engineering*, vol. 2021, Article ID 5582716, 11 pages, 2021.

[2] M. Wang, "Design of college physical education teaching system based on artificial intelligence technology," *Journal of Physics: Conference Series*, vol. 1852, no. 4, 2021.

[3] F. Li, "Information teaching platform of college physical education based on artificial intelligence technology," *Journal of Physics: Conference Series*, vol. 1852, no. 2, 2021.

[4] J. Wen, "Innovative application of artificial intelligence technology in college physical education," *Journal of Physics: Conference Series*, vol. 1881, no. 4, 2021.

[5] Z. Li, "Application of artificial intelligence technology in college physical education," *Journal of Physics: Conference Series*, vol. 1651, no. 1, 2020.

[6] Y. R. Liu, "An artificial intelligence and machine vision based evaluation of physical education teaching," *Journal of Intelligent and Fuzzy Systems*, vol. 40, no. 2, 2021.

[7] J. Zhang, "Reform and innovation of artificial intelligence technology for information service in university physical education," *Journal of Intelligent and Fuzzy Systems*, vol. 40, no. 2, 2021.

[8] Z. Li and H. Wang, "The effectiveness of physical education teaching in college based on Artificial intelligence methods," *Journal of Intelligent and Fuzzy Systems*, vol. 40, no. 2, 2021.

[9] X. Li and R. Li, "Applying artificial intelligence in physical education and future perspectives," *Sustainability*, vol. 13, no. 1, 2021.

[10] Gaobin, H. N. Cao and Z. Z. Liu, An artificial intelligence fuzzy system for improvement of physical education teaching method," *Journal of Intelligent and Fuzzy Systems*, vol. 40, no. 2, 2021.

[11] D. Yang, E. S. Oh, and Y. Wang, "Hybrid physical education teaching and curriculum design based on a voice interactive artificial intelligence educational robot," *Sustainability*, vol. 12, no. 19, 2020.

[12] B. Yong, "Design and research of intelligent evaluation system of physical education teaching based on artificial intelligence expert decision system," *Journal of Residuals Science & Technology*, vol. 13, no. 5, 2016.

Hindawi
Scientific Programming
Volume 2022, Article ID 2809222, 12 pages
https://doi.org/10.1155/2022/2809222

Research Article

Discriminative Similarity-Balanced Online Hashing for Supervised Image Retrieval

Chen Chen,[1] **Xiaoqin Wang**,[1] **Xiao Chen**,[2] **Rushi Lan**,[1] **Zhenbing Liu**,[1] **and Xiaonan Luo**[1]

[1]*Guangxi Key Laboratory of Image and Graphic Intelligent Processing, Guilin University of Electronic Technology, Guilin 541004, China*
[2]*Ministry of Education Key Laboratory of Cognitive Radio and Information Processing, Guilin University of Electronic Technology, Guilin 541004, China*

Correspondence should be addressed to Rushi Lan; rslan2016@163.com

Received 26 October 2021; Revised 26 November 2021; Accepted 2 December 2021; Published 12 February 2022

Academic Editor: Le Sun

When virtualizing large-scale images of the real world, online hashing provides an efficient scheme for fast retrieval and compact storage. It converts high-dimensional streaming data into compact binary hash codes while saving the structural characteristics between samples into the Hamming space. Existing works usually update the hashing function based on the similarity between input data, or design a codebook to assign code words for each single input sample. However, assigning code words to multiple samples while retaining the balanced similarity of the image instances is still challenging. To address this issue, we propose a novel discriminative similarity-balanced online hashing (DSBOH) framework in this work. In particular, we first obtain the Hadamard codebook that guides the generation of discriminative binary codes according to label information. Then, we maintain the correlation between the new data and the previously arrived data by the balanced similarity matrix, which is also generated by semantic information. Finally, we joined the Hadamard codebook and the balanced similarity matrix into a unified hashing function to simultaneously maintain discrimination and balanced similarity. The proposed method is optimized by an alternating optimization technique. Extensive experiments on the CIFAR-10, MNIST, and Places205 datasets demonstrate that our proposed DSBOH performs better than several state-of-the-art online hashing methods in terms of effectiveness and efficiency.

1. Introduction

With the widespread use of digital monitoring facilities and the Internet, the generated streaming data have also increased correspondingly [1–4]. The processing of streaming data needs to be performed in approximately real time, which is very difficult for high-dimensional multimedia data such as images and videos [5, 6]. Online hashing can encode high-dimensional streaming data that arrive online into compact binary codes with low storage and efficient computation [7, 8]. In particular, it preserves the relationship among the samples into the Hamming space and updates the hashing function in the light of the newly arrived data to adapt to the new data instance [9, 10]. In view of the advantages of low storage and efficient computation, online hashing is widely applied in education, finance, military, among other industries [11–14].

Most existing online hashing methods have been devoted to the trade-off between accuracy and efficiency [15–17]. According to the learning strategy, people divide these techniques into unsupervised online hashing and supervised online hashing [18–20]. The well-known unsupervised methods mainly include online sketch hashing (SketchHash) [21], FasteR online sketch hash (FROSH) [22], and zero-mean sketch [23]. SketchHash designs the hashing function with the sketch scheme [21]. FROSH uses the independent subsampling random Hadamard transform on various small data blocks to get a compact and accurate sketch while speeding up the sketching procedure [22]. The zero-mean sketch method solves the uncertainty problem of the offset value and improves the data processing efficiency by zero-mean sketch [23]. Supervised methods obtain better performance than unsupervised methods in most instances because of the utilization of label information. Some representative works include online hashing (OKH) [24, 25], adaptive hashing (AdaptHash) [26], online supervised hashing (OSH) [27, 28], online hashing with mutual information (MIHash) [29], balanced similarity for online discrete hashing (BSODH) [30], and Hadamard codebook-based online hashing (HCOH) [31]. These methods have achieved satisfactory performance.

However, some existing supervised online hashing methods still achieve unsatisfactory accuracy in real applications as they ignore any discriminative and balanced similarity. More specifically, HCOH generates discriminative binary codes with maximum information entropy by the Hadamard codebook, but ignores the local neighbor relationship among samples and only processes a single input. On the other hand, BSODH only considers balanced similarity based on the pairwise relationship and neglects the global data distribution, which results in a decrease in accuracy [32, 33]. Hence, both HCOH and BSODH have problems when applied to real applications.

In this work, we put forward a novel discriminative similarity-balanced online hashing (DSBOH) framework, which can simultaneously preserve the global distribution information of data and pairwise relationships between samples to generate discriminate hash codes with maximum information entropy. In particular, first, we maintain the maximum information entropy of hash codes via a Hadamard codebook. Then, the pairwise similarity matrix is adjusted to ensure that the updated scheme of balanced hash codes is used to preserve the correlation between the new and existing data. Finally, we combine the above attributes into a unified hashing function. An alternating iterative algorithm is used to solve the proposed DSBOH method. Compared with several state-of-the-art online hashing techniques, remarkable results have been achieved by our proposed DSBOH method.

In summary, the main contributions of this work include the following:

(i) The Hadamard matrix is used to ensure that the hash codes with maximum information entropy are separable and can deal with situations with unknown number of categories.

(ii) We preserve the balanced similarity between newly arrived data and previously arrived data into the generated Hamming space using the inner product to deal with uneven data distribution.

(iii) We combine the Hadamard codebook and the balanced similarity matrix into a unified hashing function to simultaneously maintain the discrimination and balanced similarity of the hashing modal.

(iv) The alternating iterative algorithm is used to optimize the proposed method, and experimental results verify that our method performs much better than several state-of-the-art online hashing techniques.

The remainder of this study is organized as follows. Section 2 gives a brief overview of the related works. In Section 3, we elaborate on the framework and optimization of the proposed method. Section 4 details the experimental results and analyses. Finally, we conclude the paper in Section 5.

2. Related Work

In this section, we present supervised methods, such as OKH [24, 25], OSH [27, 28], AdaptHash [26], MIHash [29], and BSODH [30].

Huang et al. first proposed a prototype based on online hashing termed OKH [24]. In each current iteration, a new pair of data samples is used, a pair of sample similarity loss functions is designed according to the Hamming distance, and the prediction loss referring to Ref. [34] is used. The function evaluates whether the operating hashing projection vector suits the new data and expects the model to save as much of the historical information of the previous round of projection vectors as possible during the update process. To make the original online hashing algorithm more perfect in loss function theory, an improved weakly supervised online hashing learning model [25], which does not require the label information of the data, is proposed for the loss threshold of the hashing modal. The new objective function is designed to calculate the disparity between the Hamming distances of pairwise data, and the upper limit loss of the online hash theory is rigorously analyzed. Second, because the hashing function learned in the algorithm update relies on new data, it easily falls into local deviations according to the characteristics of online hash algorithms to adapt to the new data; a multimodal strategy is produced to reduce such deviations.

Cakir et al. proposed the OSH method [27], which adapts to data changes, and the label types of datasets are unknown. A random method is used to generate the codebook, so that the code generated by the hashing function and the category matching error in the corresponding codebook are minimized [35]. To ensure the last round of information, the previous hashing functions are linearly combined and superimposed; however, the codebook structure directly determines the coding efficiency. Therefore, in the follow-up literature, an improved online supervised hashing [28] is proposed for this problem. The ECOC codebook is applied according to online supervised hashing, which improves the space efficiency and solves the original Hamming loss formula. Complexity proposes an efficient solution method based on the upper boundary, which improves the time efficiency of the algorithm.

AdaptHash [26] uses the relationship between data sample similarity and Hamming distance to solve the problem of how online models adapt to current data. First, the objective function is constructed using the similarity of current sample pairs and the Hamming distance relationship combined with the minimum loss variance function [36], and the gradient descent algorithm is used to solve the hash projection vector; the objective function is further generalized to make similar or unsimilar sample data pairs. The Hamming distance is minimized (maximized) to reduce the update redundancy caused by the update mechanism; finally, the hinge loss function [37] is used to filter the hash map with the largest error, and the iterative calculation is reentered until the number of iterations reaches the set value.

MIHash [29] adopts the theory of quantitative information coding to obtain high-quality hash code that eliminates unnecessary hash table updates. The mutual information between the dataset samples is well correlated with standard evaluation indicators and is used to calculate the information entropy. When optimizing the mutual information target, differentiable histogram merging technology is used to derive stochastic gradient descent-based optimization rules, and finally, the differentiated rules are utilized to merge the derived histograms and apply them to the learning objective function. This work is dedicated to the synchronization of the hash code and the hashing function updates and effectively reduces the reconstruction of the hash table.

BSODH [30] studies the relationship between new data and previously arrived data. This work considers that the problem of online hashing is attributed to two issues: updating imbalance and optimization inefficiency. The above authors recommend asymmetric graph regularization techniques to keep the relevance of online streaming data and previously accumulated datasets. To deal with data imbalance in the learning stage of online hashing, BSODH designs a new balanced similarity matrix between new data and previously arrived data, which tackles the challenge of quantization error brought by relaxation learning in the discrete optimization method in online learning and reveals advanced results compared with the quantization-based schemes.

In addition, some existing offline deep hashing methods [38–42] use deep learning techniques to train the hashing function and map the image data into low-dimensional binary codes to complete the mission of image retrieval, but as the amount of data increases, the retraining model consumes more time whenever new data arrive. For example, deep transfer hashing (DTH) [42] trains a CNN model and inputs the online generated image pairs and their labels into the network. The loss function of the model makes the outputs of similar instances close, while the outputs of dissimilar instances are pushed farther, thus obtaining the binary codes representing the semantic structure of the original image pairs. However, this method requires a complex relaxation process and a relatively large number of bits to obtain satisfactory retrieval results.

3. The Proposed Framework

Figure 1 shows the overall framework of our proposed discriminative similarity-balanced online hashing (DSBOH), which contains two main modules, namely discriminative codebook and balanced similarity. The details of the proposed DSBOH are presented as follows.

3.1. Notations. Assume that N d-dimensional data denoted as $X^t = [x_1^t, x_2^t, \ldots, x_{n_t}^t] \in R^{d\times n_t}$ are fed into the system at the t stage, whose corresponding label L is expressed as $L^t = [l_1^t, l_2^t, \ldots, l_{n_t}^t] \in N^{n_t}$. Our goal is to generate k-dimensional binary codes $B^t = [b_1^t, b_2^t, \ldots, b_{n_t}^t] \in \{1, -1\}^{k\times n_t}$, $k \ll d$. The mapping matrix to be learned for reducing the d-dimensional real-valued data X^t to k-dimensional binary data B^t is represented as $W^t \in R^{d\times k}$. The expression of B^t is defined as follows:

$$B^t = F\left(X^t\right) = \operatorname{sgn}\left(W^{tT} X^t\right), \tag{1}$$

where $F(\cdot)$ represents the hashing function, W^{tT} represents the transposition of W^t, and $\operatorname{sgn}(\cdot)$ is the symbolic function defined as follows:

$$\operatorname{sgn}(x) = \begin{cases} 1, & 0 \le x, \\ -1, & 0 > x. \end{cases} \tag{2}$$

To retain the similarity or dissimilarity relationship between the newly arrived streaming data and the previously arrived data, we consider constructing the hashing function with a similarity matrix. At the t stage, the currently arriving data are defined as $X_c^t = [x_{c1}^t, x_{c2}^t, \ldots, x_{cn_t}^t]$ whose corresponding labels are represented as L_c^t, and the generated hash codes are represented as B_c^t. The data arriving before the t stage are $X_a^t = [X_c^1, X_c^2, \ldots, X_c^{t-1}]$ whose corresponding labels are represented as L_a^t, and the generated hash codes are represented as B_a^t. All symbol notations utilized in this study are presented in Table 1.

3.2. Hadamard Codebook. To maintain the maximum information entropy of hash codes, we construct a Hadamard codebook in three steps. First, we generate an orthogonal Hadamard matrix that is 2^q-dimensional (q is a positive integer) according to the definition $C_{ij} = (-1)^{(i-1)(j-1)}$, where C_{ij} is the jth element of the ith row in matrix C. The Hadamard matrix can generate independent hash codes that satisfy two principles of the error-correcting output code: the Hamming distance between columns is maximized to ensure a significant difference between classifiers, and the Hamming distance between rows is maximized to have a strong error correction ability. Attention should be paid to guarantee that the dimension of the Hadamard matrix is a bit larger than the number of labels. Second, we assign data from the same class to the same column vector of the Hadamard matrix C to be the target vector in the Hadamard codebook $\widetilde{C}$. In particular, when a batch of new data is received, we randomly and nonrepeatedly select certain columns in the Hadamard matrix to construct virtual multilabel vectors in the Hadamard codebook. When the label of the new data is the same as the data that arrived before, it is assigned to the same column vector. These vectors are aggregated to form a codebook $\widetilde{C}$. Finally, we use locality-sensitive hashing (LSH) [43] to align the code length of the Hadamard codebook with that of the hash codes.

To maintain the independence of the hash code and retain the global distribution information, we define the loss function L_1 based on the Hadamard codebook as follows:

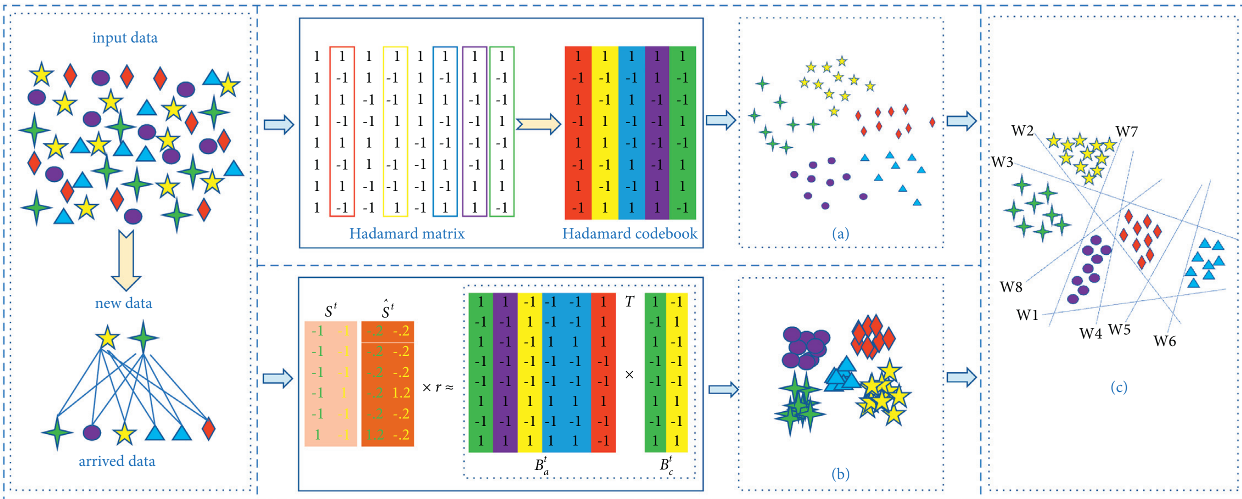

FIGURE 1: The overall framework of the proposed discriminative similarity-balanced online hashing (DSBOH). (a) The hash codes generated by the constructed Hadamard codebook for the input data are independent of each other, but the similar relationship between the data is ignored. (b) The similarity matrix constructed from the new data and the arrived data guides the generated hash codes to have a stronger classification ability but ignores the global data distribution. (c) The proposed algorithm can generate more discriminative hash codes for satisfactory retrieval results.

TABLE 1: Notations utilized in this study.

Symbol	Notations
X^t	Input data at t stage
L^t	Label of X^t
B^t	Binary codes generated for X^t
W^t	Hashing mapping matrix at t stage
X_c^t	Data arriving currently at t stage
L_c^t	Label of X_c^t
B_c^t	Binary codes generated for X_c^t
X_a^t	Data all arriving before t stage
L_a^t	Label of X_a^t
B_a^t	Binary codes generated for X_a^t
d	Dimension of input data
k	Dimension of binary code
N	Number of input data
n_t	Number of input data at t stage

$$L_1 = \min_{W^t} \left\| F\left(X^t\right) - \widetilde{C}_{J_{(x^t)}} \right\|_F^2, \tag{3}$$

where $\widetilde{C}_i$ represents the ith column of codebook $\widetilde{C}$, $J_{(x_i^t)}$ denotes the label category of x_i^t, and $\|\cdot\|_F$ is the Frobenius norm of a matrix.

3.3. Balanced Similarity. Suppose that there are two input data x_i and x_j, the corresponding labels are l_i and l_j and the hash codes are expressed as $B_i = [b_{i1}, b_{i2}, \ldots, b_{ik}]^T \in \{1, -1\}^{k\times 1}$ and $B_j = [b_{j1}, b_{j2}, \ldots, b_{jk}]^T \in \{1, -1\}^{k\times 1}$, respectively. S_{ij} represents the similarity matrix of x_i and x_j. If x_i and x_j belong to one category, that is, $l_i = l_j$, then $S_{ij} = 1$. We expect that the hash codes within the same category are the same; that is, $B_i = [b_{i1}, b_{i2}, \ldots, b_{ik}]^T = [b_{j1}, b_{j2}, \ldots, b_{jk}]^T = B_j$. Because the product of the same binary codes is 1, $B_j^T B_j = k = kS_{ij}$. Conversely, if x_i and x_j are within different categories, that is, $l_i \neq l_j$, then $S_{ij} = -1$. We also expect that the hash codes from different categories are different; that is, $B_i = [b_{i1}, b_{i2}, \ldots, b_{ik}]^T = [-b_{j1}, -b_{j2}, \ldots, -b_{jk}]^T = -B_j$. Because the product result of the different binary codes is -1, $B_i^T B_j = -k = kS_{ij}$. In sum, the product of B_i^T and B_j has a common value with kS_{ij}, which means that we can retain the similarity relationship of input data into the Hamming space through the above method as follows:

$$\min_{B_i^t, B_j^t} \left\| B_i^{tT} B_j^t - kS_{ij}^t \right\|_F^2. \tag{4}$$

To keep the similarity relationship constructed from the newly arrived data X_c^t at the t stage and the data X_a^t before the t stage in the Hamming space, the relationship between the inner product of the binary codes B_c^t and B_a^t and similarity S^t is used. In addition, with the increase in the new instances, the similarity matrix S^t becomes more and more sparse because most image pairs are dissimilar [30]. To prevent the model from overly relying on dissimilar information and ignoring the information of similar pairs, we adjust the similarity matrix according to the similarity and dissimilarity and convert the similarity matrix S^t to the balanced similarity matrix $\widetilde{S}^t$ by multiplying by different balance factors. The balanced similarity matrix $\widetilde{S}^t$ is defined as follows:

$$\widetilde{S}_{ij}^t = \begin{cases} \mu_s S_{ij}^t, & S_{ij}^t = 1, \\ \mu_d S_{ij}^t, & S_{ij}^t = -1, \end{cases} \tag{5}$$

where $\widetilde{S}_{ij}^t$ and S_{ij}^t represent the element in the ith row and jth column of matrices $\widetilde{S}^t$ and S^t, respectively. μ_s denotes the impact factor of the similarity pairs, while μ_d denotes the impact factor of the dissimilarity pairs. When μ_s is greater than μ_d, the Hamming distance between similar pairs will decrease, while that between dissimilar pairs will increase. By adjusting the two balance factors, the problem of data imbalance can be solved. Thus, the loss function of balanced similarity can be defined as follows:

$$L_2 = \min_{B_a^t, B_c^t} \left\| B_c^{tT} B_a^t - k\widetilde{S}^t \right\|_F^2, \\ s.t.\ B_c^t \in \{1,-1\}^{k\times n_t}, \quad B_a^t \in \{1,-1\}^{k\times m_t}, \tag{6}$$

where $m_t = \sum_{i=1}^{t-1} n_i$ denotes the total number of instances that arrived before t stage.

3.4. Overall Formulation. Different from HCOH and BSODH, which find the global data distribution or balanced similarity via a local neighbor relationship, DSBOH aims to generate discriminative binary codes for single or multiple inputs by preserving global distribution information with the help of Hadamard codebook and local pairwise relationship between the newly arrived data and the previously arrived data in a seamless framework. When the data explode, the modal still has a strong generalization ability because we consider retaining the semantic relationship between the data at different stages. Furthermore, hash codes are independent and discriminative due to the use of codebook. Therefore, we combine loss function L_1 of the Hadamard codebook hashing function in equation (3) and loss function L_2 of balanced similarity preservation in equation (6) into the same objective function, which is expressed as follows:

$$\min_{B_a^t, B_c^t, W^t} \left\| B_c^{tT} B_a^t - k\widetilde{S}^t \right\|_F^2 + \lambda^t \left\| F\left(X^t\right) - \widetilde{C}_{J\left(X^t\right)} \right\|_F^2, \\ \text{s.t. } B_c^t \in \{1,-1\}^{k\times n_t}, \quad B_a^t \in \{1,-1\}^{k\times m_t}, \tag{7}$$

where λ^t is the parameter to control the importance.

To minimize the quantization error between learned hashing function $F(X^t)$ and the target hash code B^t, the quantized loss function is defined as follows:

$$\min_{W^t} \left\| F\left(X^t\right) - B^t \right\|_F^2. \tag{8}$$

Finally, adding equation (8) into (7), and adding the Frobenius norm of W^t as a regular term, the overall formulation is expressed as follows:

$$L = \min_{B_a^t, B_c^t, W^t} \left\| B_c^{tT} B_a^t - k\widetilde{S}^t \right\|_F^2 + \lambda^t \left\| F\left(X^t\right) - \widetilde{C}_{J\left(X^t\right)} \right\|_F^2 + \sigma^t \left\| F\left(X^t\right) - B^t \right\|_F^2 + \varepsilon^t \left\| W^t \right\|_F^2, \\ \text{s.t.} \begin{cases} B_c^t \in \{1,-1\}^{k\times n_t}, \\ B_a^t \in \{1,-1\}^{k\times m_t}, \end{cases} \tag{9}$$

where σ^t and ϵ^t are parameters to control the importance of each module.

3.5. Alternating Optimization. Owing to the discrete restrictions of the binary codes, the optimization problem of the variables in equation (9) is nonconvex [44, 45]. In this regard, an alternating optimization technique is adopted to deal with our proposed loss function L. That is, when a variable is updated, others are fixed as constants. The specific details of the implementation are introduced as follows.

(1) Solving W^t: fix B_a^t and B_c^t, so that the first term in equation (9) can be eliminated. The objective function becomes:

$$\min_{W^t} \lambda^t \left\| F\left(X^t\right) - \widetilde{C}_{J\left(X^t\right)} \right\|_F^2 + \sigma^t \left\| F\left(X^t\right) - B_c^t \right\|_F^2 + \varepsilon^t \left\| W^t \right\|_F^2. \tag{10}$$

Replacing the formula $F(X^t) = \operatorname{sgn}(W^{tT} X^t)$ in equation (1) with $F(X^t) = \tanh(W^{tT} X^t)$ for optimization convenience, we obtain the following:

$$\min_{W^t} \left\| \tan h\left(W^{tT} X_c^t\right) - \widetilde{C}_{J\left(X_c^t\right)} \right\|_F^2 + \sigma^t \left\| \tanh\left(W^{tT} X_c^t\right) - B_c^t \right\|_F^2 + \varepsilon^t \left\| W^t \right\|_F^2. \tag{11}$$

Using the formula of matrix A:

$$\|A\|_F = \sqrt{tr\left(A^T A\right)} = \sqrt{tr\left(AA^T\right)}. \tag{12}$$

We convert equation (11) into the form of the trace of the matrix as follows:

$$\min_{W^t} tr\left(\left(W^{tT} X_c^t - \widetilde{C}_{J\left(X_c^t\right)}\right)\left(X_c^{tT} W^t - \widetilde{C}_{J\left(X_c^t\right)}^T\right)\right) \\ + \sigma^t tr\left(\left(W^{tT} X_c^t - B_c^t\right)\left(X_c^{tT} W^t - B_c^{tT}\right)\right) \\ + \varepsilon^t tr\left(W^t W^{tT}\right). \tag{13}$$

After simplification, we obtain the following:

$$\min_{W^t}\left[\left(1+\sigma^t\right)X_c^t X_c^{tT}+\int^t I\right]tr\left(W^t W^{tT}\right) - 2tr\left(W^{tT}X_c^t\left(\widetilde{C}_{J_{\left(X_c^t\right)}}+\sigma^t B_c^t\right)\right), \tag{14}$$

where I stands for the d-dimensional identity matrix. Equation (14) takes the partial derivative of W^t and makes the result zero. That is:

$$\left[\left(1+\sigma^t\right)X_c^t X_c^{tT}+\varepsilon^t I\right]W^t - X_c^t\left(\widetilde{C}_{J_{\left(X_c^t\right)}}+\sigma^t B_c^t\right)=0. \tag{15}$$

Therefore, we update W^t with the following equation:

$$W^t=\left[\left(1+\sigma^t\right)X_c^t X_c^{tT}+\varepsilon^t I\right]^{-1}X_c^t\left(\widetilde{C}^T_{J_{\left(X^t\right)}}+\sigma^t B_c^{tT}\right). \tag{16}$$

(2) Solving B_a^t: fix W^t and B_c^t; therefore, only the first term remains in equation (9). The objective function now becomes:

$$\min_{B_a^t, B_c^t, W^t}\left\|B_c^{tT}B_a^t-k\widetilde{S}^t\right\|_F^2. \tag{17}$$

According to Ref. [46], the F norm is changed to the $L1$ norm; the result is as follows:

$$B_a^t=\operatorname{sgn}\left(B_c^t\widetilde{S}^t\right). \tag{18}$$

(3) Solving B_c^t: fix W^t and B_a^t. Equation (9) becomes:

$$\min_{B_c^t}\left\|B_c^{tT}B_a^t-k\widetilde{S}^t\right\|_F^2+\sigma^t\left\|F\left(X^t\right)-B_s^t\right\|_F^2. \tag{19}$$

For further optimization, we remove irrelevant items and obtain the following:

$$\min_{B_c^t}\left\|B_c^{tT}B_a^t\right\|_F^2-2tr\left(P^T B_s^T\right), \tag{20}$$

where $P=k\lambda^t B_a^t\widetilde{S}^{t^T}+\sigma^t W^{tT}X_c^t$. According to supervised discrete hashing (SDH) [6] and BSODH [30], the optimization in equation (20) is NP hard, so we turn the matrix into a combination of row vectors, transferring the problem into row by row updating. That is to say, equation (20) becomes:

$$\min_{\vec{b}_{cr}}\left\|\widetilde{b}_{ar}^{tT}\widetilde{b}_{cr}^t+\widetilde{B}_a^{t^T}\widetilde{B}_c^t\right\|_F^2-2tr\left(\widetilde{p_{ar}^t}^T\widetilde{b}_{cr}^t+\widetilde{P}^{t^T}\widetilde{B}_c^t\right), \tag{21}$$

where $\widetilde{b}_{cr}^t$, $\widetilde{b}_{ar}^t$, and $\widetilde{p}_r$ are the rth row of B_c^t, B_a^t, and P; $\widetilde{B}_c^t$, $\widetilde{B}_a^t$, and $\widetilde{P}^t$ are the remaining parts of B_c^t, B_a^t, and P except for the rth row, respectively. The above formula is expanded to obtain the following:

$$\min_{\vec{b}_{cr}}\left\|\widetilde{b_{ar}^t}^T\widetilde{b}_{cr}^t\right\|_F^2+\left\|\widetilde{B}_a^{t^T}\widetilde{B}_c^t\right\|_F^2+2tr\left(\widetilde{B}_c^{t^T}\widetilde{B}_a^t\widetilde{b_{ar}^t}^T\right) - 2tr\left(\widetilde{p_{ar}^t}^T\widetilde{b}_{cr}^t\right)-2tr\left(\widetilde{P}^{t^T}\widetilde{B}_c^t\right), \tag{22}$$

The equation (22) is simplified to obtain the following:

$$\min_{\vec{b}_{cr}} tr\left(\left(\widetilde{B}_c^{t^T}\widetilde{B}_a^t\widetilde{b_{ar}^t}^T-\widetilde{p}_r^{t^T}\right)\widetilde{b}_{cr}^t\right). \tag{23}$$

Therefore, we update row by row according to the following rules:

$$\widetilde{b}_{cr}^t=\operatorname{sgn}\left(\widetilde{p}_r-\widetilde{b}_{ar}^t\widetilde{B}_a^{t^T}\widetilde{B}_c^t\right). \tag{24}$$

The proposed DSBOH is summarized in Algorithm 1.

Input: training instances X; labels L; the number of data batches T; code length k; parameters $\lambda^t, \sigma^t, \epsilon^t$.
Output: binary codes B and hash map matrix W.
Initialize W and W_{LSH} with the normal Gaussian distribution
Generate Hadamard matrix of r-dimension
if $r \neq k$ **then**
Adopt LSH for Hadamard to get codebook C
else
Make Hadamard as codebook C
end if
while $T \leftarrow 1$ **do**
Denote the data coming currently as X_c^t
Set $X_a^t = [X_a^t; X_c^t]$, $B_a^t = [B_a^t; B_c^t]$
Compute S according to labels
Update W^t via equation (16) and B_a^t via equation (18)
while r becomes $k \leftarrow 1$ **do**
Update b_{cr}^t via equation (24)
end while
end while
Set $W = W^t$ and calculate $B^t = \operatorname{sgn}(W^{tT}X^t)$
Return W, B

4. Experiments

To prove the effectiveness of DSBOH, extensive experiments on three widely used image datasets are conducted in this section and compared them with several advanced online hashing techniques.

4.1. Datasets. CIFAR-10 [47] is an inclusively applied dataset for image retrieval and classification. It is composed of 60,000 samples selected from ten classes, and each sample is represented by 4096-dimensional CNN features. The ten classes are airplane, automobile, bird, cat, deer, dog, frog, horse, ship, and truck. Each category includes 6,000 samples. We randomly select 5,900 samples from each category as the training set; the remaining images are set as the testing set. From the training set, 20,000 instances are utilized for learning hashing functions [31]. Twenty example images from each category of CIFAR-10 are shown in Figure 2.

MNIST consists of 70,000 hand-written digital images with 10 categories, which include numbers 0 to 9; each image is represented by a 784-dimensional vector. We randomly sample 100 instances from each class to construct the testing set and make use of the remaining part to compose the training set. 20,000 images randomly selected from the training set are used to learn the hash model [18]. We randomly select 27 example instances from each class to show in Figure 3.

Places205 [48] is a large-scale scene-centric dataset that contains 205 common scene categories and 2.5 million images with labels. First, the fc-7 layer of AlexNet [49] calculates the features of each image, and then, PCA is exploited to simplify these features into 128-dimensional vectors. We stochastically choose 20 images from each category to form the test set, and the others automatically consist of the training set. 100,000 images in the training set are randomly selected to learn the hashing functions. Two hundred randomly picked images of Places205 are shown in Figure 4.

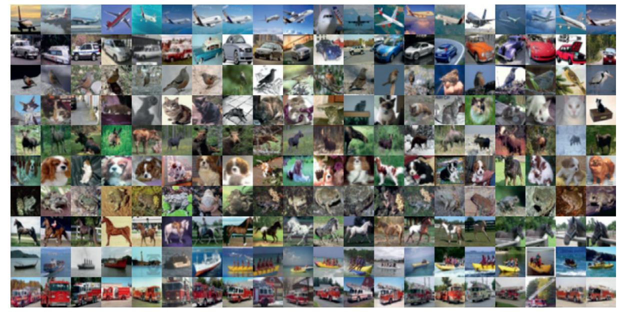

Figure 2: Example images of CIFAR-10 dataset.

Figure 3: Example images of MNIST dataset.

Figure 4: Example images of Places205 dataset.

4.2. Experimental Settings

4.2.1. Parameter Settings. According to experience, the ranges of λ^t, σ^t, and ϵ^t for the proposed DSBOH are set in {0: 0.05: 5}. For the CIFAR-10 dataset, the best combination for $(\lambda^t, \sigma^t, \epsilon^t)$ is empirically adopted to $(0.7, 0.3, 0.8)$. For the MNIST dataset, we set $(0.1, 0.3, 1.2)$ as the configuration of $(\lambda^t, \sigma^t, \epsilon^t)$. For the Places205 dataset, $(0.1, 0.8, 0.2)$ corresponds to $(\lambda^t, \sigma^t, \epsilon^t)$. Table 2 shows the detailed parameters of DSBOH on the CIFAR-10, MNIST, and Places205 datasets. In addition, we conducted experiments with hash codes of different lengths from the set [8, 16, 32, 48, 64, 128]. It is worth mentioning that SketchHash requires the size of a batch greater than that of hash codes [21]. Thence, we only show the results of SketchHash under 64 bits.

Table 2: Parameter settings to CIFAR-10, MNIST, and Places205 on DSBOH.

Parameter	CIFAR-10	MNIST	Places205
λ^t	0.7	0.1	0.1
σ^t	0.3	0.3	0.8
ϵ^t	0.8	1.2	1.2
μ_s	1.5	1.5	1.5
μ_d	0.5	0.5	0.5
n_t	2000	20 000	20 000

4.2.2. Evaluation Protocols. To evaluate the proposed method, we apply a set of widely adopted protocols, which includes the mean average precision (mAP), the average accuracy of the first 1000 retrieved samples (mAP@1000), which is used for the large dataset Places205 to reduce the calculation time, precision within a Hamming sphere with a radius of 2 centered on every query point (Precision@H2), and the average precision of top-R retrieving neighbors (Precision@R). We also compare the running time on CIFAR-10 and MNIST with other methods. Additionally, the precision-recall curves on CIFAR-10 and MNIST are adopted to evaluate our proposed method.

4.2.3. Compared Methods. We contrast the proposed DSBOH with several advanced online hashing methods, including OKH [25], OSH [28], AdaptHash [26], SketchHash [21], and BSODH [30]. All the results of the above methods are implemented via the publicly available source codes. We implement all the methods using MATLAB on a single computer equipped with a 3.0 GHz Intel Core i5-8500 CPU and 16 GB RAM; all results shown in this work are the average of the three runs.

Table 3: mAP and Precision@H2 results on CIFAR-10 for 8, 16, 32, 48, 64, and 128 bits.

Methods	mAP						PrecisionH2					
	8 bits	16 bits	32 bits	48 bits	64 bits	128 bits	8 bits	16 bits	32 bits	48 bits	64 bits	128 bits
OKH [25]	0.100	0.134	0.223	0.252	0.268	0.350	0.100	0.175	0.100	0.452	0.175	0.372
OSH [28]	0.123	0.126	0.129	0.131	0.127	0.125	0.120	0.123	0.137	0.117	0.083	0.038
AdaptHash [26]	0.116	0.138	0.216	0.297	0.305	0.293	0.114	0.254	0.185	0.093	0.166	0.164
SketchHash [21]	0.248	0.301	0.302	0.327	——	——	0.256	0.431	0.385	0.059	——	——
BSODH [30]	**0.564**	0.604	0.689	0.656	0.709	0.711	0.305	0.582	0.691	**0.697**	**0.690**	**0.602**
DSBOH	0.556	**0.669**	**0.703**	**0.696**	**0.720**	**0.727**	**0.411**	**0.730**	**0.737**	0.655	0.552	0.371

The first-ranked results are given in bold.

Table 4: mAP and Precision@H2 results on MNIST for 8, 16, 32, 48, 64, and 128 bits.

Methods	mAP						Precision@H2					
	8 bits	16 bits	32 bits	48 bits	64 bits	128 bits	8 bits	16 bits	32 bits	48 bits	64 bits	128 bits
OKH [25]	0.100	0.155	0.224	0.273	0.301	0.404	0.100	0.220	0.457	0.724	0.522	0.124
OSH [28]	0.130	0.144	0.130	0.148	0.146	0.143	0.131	0.146	0.192	0.134	0.109	0.019
AdaptHash [26]	0.138	0.207	0.319	0.318	0.292	0.208	0.153	0.442	0.535	0.335	0.163	0.168
SketchHash [21]	0.257	0.312	0.348	0.369	——	——	0.261	0.596	0.691	0.251	——	——
BSODH [30]	0.593	0.700	0.747	0.743	0.766	0.760	0.308	0.709	0.826	**0.804**	**0.814**	**0.643**
DSBOH	**0.596**	**0.721**	**0.759**	**0.751**	**0.781**	**0.781**	**0.403**	**0.803**	**0.849**	0.788	0.651	0.415

The first-ranked results are given in bold.

Table 5: mAP@1000 and Precision@H2 results on Places205 for 8, 16, 32, 48, 64, and 128 bits.

Methods	mAP@1000						Precision@H2					
	8 bits	16 bits	32 bits	48 bits	64 bits	128 bits	8 bits	16 bits	32 bits	48 bits	64 bits	128 bits
OKH [25]	0.018	0.033	0.122	0.048	0.114	0.258	0.007	0.010	0.026	0.017	**0.217**	0.075
OSH [28]	0.018	0.021	0.022	0.032	0.043	0.164	0.007	0.009	0.012	0.023	0.030	0.059
AdaptHash [26]	0.028	0.097	0.195	0.223	0.222	0.229	0.009	0.051	0.012	0.185	0.021	0.022
SketchHash [21]	**0.052**	0.120	0.202	0.242	——	——	**0.017**	0.066	0.220	0.176	——	——
BSODH [30]	0.035	**0.174**	**0.250**	0.273	0.308	0.337	0.009	**0.101**	0.241	**0.246**	0.212	**0.101**
DSBOH	0.046	0.154	0.249	**0.286**	**0.313**	**0.347**	0.011	0.089	**0.264**	0.175	0.119	0.037

The first-ranked results are given in bold.

4.3. Results and Discussion. First, we can observe the experimental results of mAP and Precision@H2 on CIFAR-10 in Table 3. From this table, we can find that (1) mAP: in the case of 16 bits, 32 bits, 48 bits, 64 bits, and 128 bits hash codes, our proposed method has improved the second-best BSODH method by 6.5%, 1.4%, 4.0%, 1.1%, and 1.6%, respectively, and the mAP of DSBOH is slightly lower than that of BSODH. (2) Precision@H2: in the case of 8 bits, 16 bits, and 32 bits, our proposed method is 10.6%, 14.8%, and 4.6% better than the second-best BSODH, respectively. Although the mAP at 48 bits, 64 bits, and 128 bits of our proposed DSBOH slightly decreases compared with BSODH, our DSBOH performs better than other online hashing methods.

Table 4 shows the mAP and Precision@H2 results of our raised DSBOH and compared techniques on the MNIST dataset. The consequences indicate that (1) mAP: the proposed DSBOH accomplishes an increase of 0.3%, 2.1%, 1.2%, 0.8%, 1.5%, and 2.1% for mAP compared with the second-best BSODH in 8 bits, 16 bits, 32 bits, 48 bits, 64 bits, and 128 bits. Hence, the superiorities of DSBOH are demonstrated. (2) Precision@H2: the Precision@H2 of our DSBOH is much better than BSODH by 9.5%, 9.4%, and 2.3% for the 8 bits, 16 bits, and 32 bits, respectively. The performance of our DSBOH is slightly lower than that of BSODH in terms of 48 bits, 64 bits, and 128 bits.

The experimental consequences of mAP@1000 and Precision@H2 on the Places205 database are expressed in Table 5. From this table, we can learn that (1) mAP@1000: our proposed DSBOH is 1.3%, 0.5%, and 1.0% better than the second-best BSODH in terms of 48 bits, 64 bits, and 128 bits, respectively, and ranks second in terms of 8 bits, 16 bits, and 32 bits. (2) Precision@H2: the outcome of Precision@H2 for our DSBOH is the highest at 32 bits and 2.3% higher than the second-best method. For other hash bit lengths, DSBOH slightly decreases compared with the best.

For further verification of the performance of our DSBOH, we execute comparative experiments on Precision@R under 16 bits, 32 bits, and 64 bits hash codes on the CIFAR-10 and MNIST datasets. As shown in Figure 5, the proposed approach continuously reveals the best Precision@R, which demonstrates the superiority of DSBOH. In addition, the precision-recall curves on the CIFAR-10 and MNIST datasets are shown in Figures 6(a) and 6(b), respectively. Both curves wrap more curves, which proves the effectiveness of our algorithm. To clearly show the performance, we calculate the blue area under the curve (AUC) of the PR curves on CIFAR-10 and MNIST and obtain 95.70%

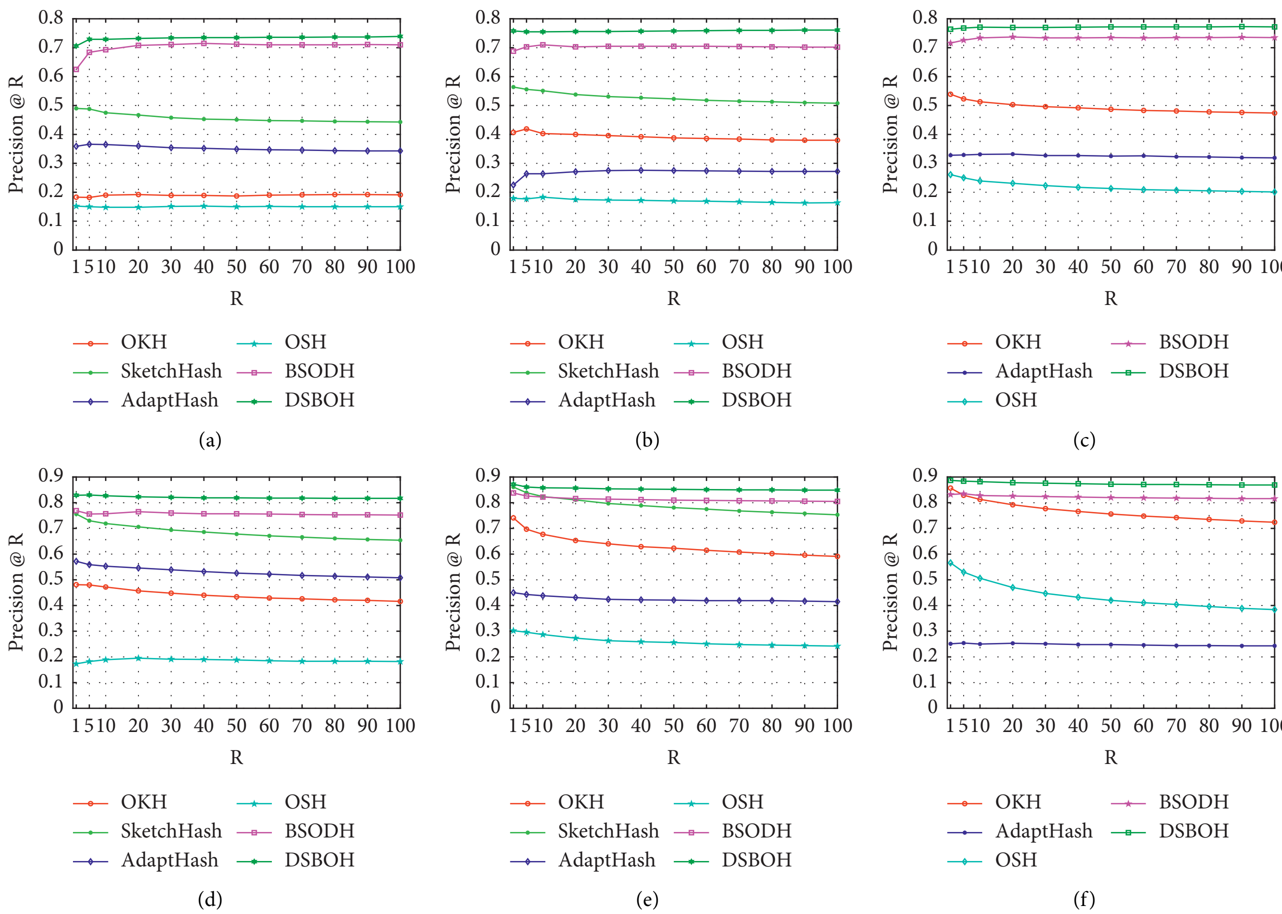

Figure 5: Precision@R curves of compared algorithms on CIFAR-10 and MNIST. (a) 16 hash bits on CIFAR-10, (b) 32 hash bits on CIFAR-10, (c) 64 hash bits on CIFAR-10, (d) 16 hash bits on MNIST, (e) 32 hash bits on MNIST, and (f) 64 hash bits on MNIST.

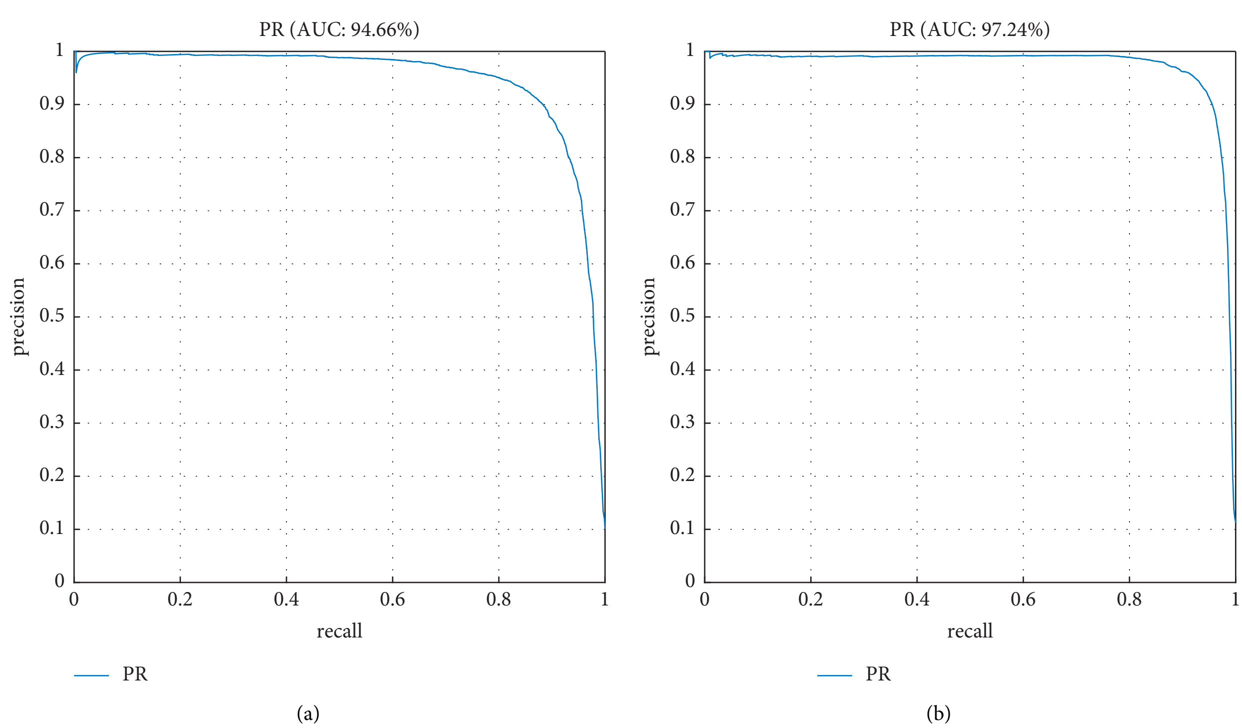

Figure 6: Precision-recall curve on CIFAR-10 and MNIST under 32 bit hashing codes. (a) PR curve on CIFAR-10 and (b) PR curve on MNIST.

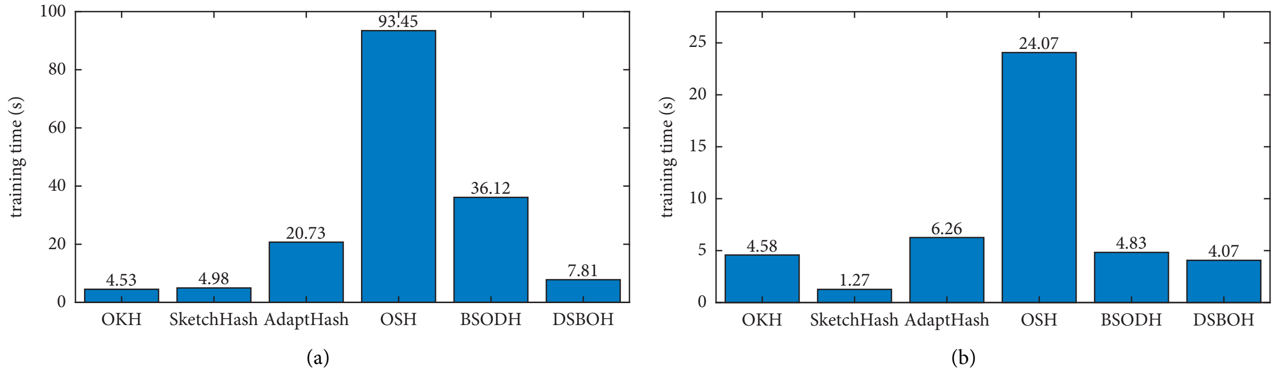

FIGURE 7: Training time of compared methods on CIFAR-10 and MNIST under 32 bit hashing codes. (a) Training time of compared methods on CIFAR-10 and (b) training time of compared methods on MNIST.

and 97.28% AUCs, respectively, which verifies that our learning model has a double high ratio of precision and recall.

4.4. Training Efficiency. Figure 7 presents the training time of our proposed method and compared approaches in terms of 32 bits on the CIFAR-10 dataset and MNIST dataset. As for Figure 7(a), we notice that our proposed DSBOH runs faster than AdaptHash, OSH, and BSODH but is very similar to OKH and SketchHash. We find that in CIFAR-10, although OKH and SketchHash have the shortest training time, their model accuracy is very poor. The training time spent by DSBOH is the shortest among the remaining algorithms, and the training efficiency is the highest. According to Figure 7(b), the training time of every method for comparison exceeds our proposed DSBOH except for SketchHash. Therefore, our algorithm is efficient for online image retrieval.

5. Conclusion

In this study, we bring forward DSBOH as a novel scheme that combines global distribution and balanced similarity to generate discriminative hash codes for image retrieval. To this end, we utilize the Hadamard codebook to assist the construction of the hashing function and keep the similarity between the newly arrived samples and the previously arrived samples from the original real value space into the Hamming space. Vast experiments on three benchmark datasets demonstrated that DSBOH shows significant advantages in effectiveness and efficiency compared with several innovatory online hashing methods. Since we use the codebook to assign code words to single-label images, the problem of code word assignment applied to multilabel image retrieval is worthy of further study. It is also possible to study a codebook that can better store the structure information of the image data in the future.

Data Availability

The data used to support the findings of this study are available from the corresponding author upon request.

Conflicts of Interest

The authors declare that they have no conflicts of interest.

Acknowledgments

This work was partially supported by the National Natural Science Foundation of China (nos. 62 172 120, 61762028, and 61 962 014), Guangxi Science and Technology Project (nos. AD18281079, 2019GXNSFFA245014, 2019AC20014, and AB19110038), Ministry of Education Key Laboratory of Cognitive Radio and Information Processing (no. CRKL190109), and Guangxi Key Laboratory of Intelligent Processing Computer Image and Graphics (no. GIIP2001).

References

[1] H. Lu, R. Yang, Z. Deng, Y. Zhang, G. Gao, and R. Lan, "Chinese image captioning via fuzzy attention-based densenet-bilstm," *ACM Transactions on Multimedia Computing, Communications, and Applications*, vol. 17, no. 1, 2021.

[2] H. Liu, R. Ji, J. Wang, and C. Shen, "Ordinal constraint binary coding for approximate nearest neighbor search," *IEEE Transactions on Pattern Analysis and Machine Intelligence*, vol. 41, no. 4, pp. 941–955, 2019.

[3] H. Wang, X. Liu, and X. Nie, "Supervised discrete hashing through similarity learning," *Multimedia Tools and Applications*, vol. 80, no. 11, Article ID 16215, 2021.

[4] S. Ge, C. Li, S. Zhao, and D. Zeng, "Occluded face recognition in the wild by identity-diversity inpainting," *IEEE Transactions on Circuits and Systems for Video Technology*, vol. 30, no. 10, pp. 3387–3397, 2020.

[5] X. Wang, R. Lan, H. Wang, Z. Liu, and X. Luo, "Fine-grained correlation analysis for medical image retrieval," *Computers & Electrical Engineering*, vol. 90, Article ID 106992, 2021.

[6] F. Shen, C. Shen, W. Liu, and H. T. Shen, "Supervised discrete hashing," in *Proceedings of the 2015 IEEE Conference on Computer Vision and Pattern Recognition (CVPR)*, pp. 37–45, Boston, MA, USA, June 2015.

[7] J.-P. Heo, Y. Lee, J. He, S.-F. Chang, and S.-E. Yoon, "Spherical hashing: binary code embedding with hyperspheres," *IEEE Transactions on Pattern Analysis and Machine Intelligence*, vol. 37, no. 11, pp. 2304–2316, 2015.

[8] M. Hashemi and M. Hall, "Detecting and classifying online dark visual propaganda," *Image and Vision Computing*, vol. 89, pp. 95–105, 2019.
[9] J. Wang, T. Zhang, J. Song, N. Sebe, and H. T. Shen, "A survey on learning to hash," *IEEE Transactions on Pattern Analysis and Machine Intelligence*, vol. 40, no. 99, p. 1, 2016.
[10] Z. Chen, H. Lu, S. Tian et al., "Construction of a hierarchical feature enhancement network and its application in fault recognition," *IEEE Transactions on Industrial Informatics*, vol. 17, no. 7, pp. 4827–4836, 2021.
[11] P. Wang, D. Wang, X. Zhang et al., "Numerical and experimental study on the maneuverability of an active propeller control based wave glider," *Applied Ocean Research*, vol. 104, 2020.
[12] X. Zhang, X. Li, Y. Liu, and F. Feng, "A survey on freehand sketch recognition and retrieval," *Image and Vision Computing*, vol. 89, pp. 67–87, 2019.
[13] R. Lan, Y. Zhou, Z. Liu, and X. Luo, "Prior knowledge-based probabilistic collaborative representation for visual recognition," *IEEE Transactions on Cybernetics*, vol. 50, no. 4, pp. 1498–1508, 2020.
[14] S. Ge, Z. Luo, C. Zhang, Y. Hua, and D. Tao, "Distilling channels for efficient deep tracking," *IEEE Transactions on Image Processing*, vol. 29, pp. 2610–2621, 2020.
[15] Z. Liu, F. Chen, and S. Duan, "Distributed fast supervised discrete hashing," *IEEE Access*, vol. 7, 2019.
[16] P. K. Agarwal and R. Sharathkumar, "Streaming algorithms for extent problems in high dimensions," *Algorithmica*, vol. 72, no. 1, pp. 83–98, 2015.
[17] S. Hong, H. Park, J.-S. No, T. Helleseth, and Y.-S. Kim, "Near-optimal partial Hadamard codebook construction using binary sequences obtained from quadratic residue mapping," *IEEE Transactions on Information Theory*, vol. 60, no. 6, pp. 3698–3705, 2014.
[18] W. Liu, J. Wang, R. Ji, Y. Jiang, and S. Chang, "Supervised hashing with kernels," in *Proceedings of the 2012 IEEE Conference on Computer Vision and Pattern Recognition*, pp. 2074–2081, Providence, RI, USA, June 2012.
[19] U. Chaudhuri, B. Banerjee, A. Bhattacharya, and M. Datcu, "Crossatnet–a novel cross-attention based framework for sketch-based image retrieval," *Image and Vision Computing*, vol. 104, 2020.
[20] J. Tan, T. Zhang, L. Zhao, X. Luo, and Y. Y. Tang, "A robust image representation method against illumination and occlusion variations," *Image and Vision Computing*, vol. 112, 2021.
[21] C. Leng, J. Wu, J. Cheng, X. Bai, and H. Lu, "Online sketching hashing," in *Proceedings of the IEEE Conference on Computer Vision Pattern Recognition*, pp. 2503–2511, Boston, MA, USA, June 2015.
[22] X. Chen, I. King, and M. R. Lyu, "Frosh: faster online sketching hashing," in *Proceedings of the Thirty-Third Conference on Uncertainty in Artificial Intelligence, UAI 2017*, E. Gal, K. Kersting, and A. T. Ihler, Eds., pp. 1790–2022pp. 1790–, Sydney, Australia, August 2017.
[23] Y. Long, L. Liu, S. Fumin, L. Shao, and L. Xuelong, "Zero-shot learning using synthesised unseen visual data with diffusion regularisation," *IEEE Transactions on Pattern Analysis and Machine Intelligence*, vol. 40, p. 99, 2017.
[24] L.-K. Huang, Q. Yang, and W.-S. Zheng, "Online hashing," in *Proceedings of the IJCAI International Joint Conference on Artificial Intelligence*, pp. 1422–1428, Beijing, China, August 2013.
[25] L.-K. Huang, Q. Yang, and W.-S. Zheng, "Online hashing," *IEEE Transactions on Neural Networks and Learning Systems*, vol. 29, no. 6, pp. 2309–2322, 2018.
[26] F. Cakir and S. Sclaroff, "Adaptive hashing for fast similarity search," in *Proceedings of the 2015 IEEE International Conference on Computer Vision (ICCV)*, pp. 1044–1052, Santiago, Chile, December 2015.
[27] F. Cakir and S. Sclaroff, "Online supervised hashing," in *Proceedings of the International Conference on Image Processing, ICIP*, pp. 2606–2610, Quebec City, Canada, September 2015.
[28] F. Cakir, S. A. Bargal, and S. Sclaroff, "Online supervised hashing," *Computer Vision and Image Understanding*, vol. 156, pp. 162–173, 2017.
[29] F. Cakir, K. He, S. A. Bargal, and S. S. Mihash, "Online hashing with mutual information," in *Proceedings of the 2017 IEEE International Conference on Computer Vision (ICCV)*, pp. 437–445, Venice, Italy, March 2017.
[30] M. Lin, R. Ji, H. Liu, X. Sun, Y. Wu, and Y. Wu, "Towards optimal discrete online hashing with balanced similarity," in *Proceedings of the 33rd AAAI Conference on Artificial Intelligence, AAAI*, pp. 8722–8729, Honolulu, Hawai, February 2019.
[31] M. Lin, R. Ji, H. Liu, and Y. Wu, "Supervised online hashing via Hadamard codebook learning," in *Proceedings of the 2018 ACM Multimedia Conference*, pp. 1635–1643, Seoul, Korea, October 2018.
[32] D. Wang, Q. Wang, Y. An, X. Gao, and Y. Tian, "Online collective matrix factorization hashing for large-scale cross-media retrieval," in *Proceedings of the 43rd International ACM SIGIR Conference on Research and Development in Information Retrieval*, pp. 1409–1418, Virtual Event, China, July 2020.
[33] Z. Qian, J. Xu, K. Zheng, P. Zhao, and X. Zhou, "Semantic-aware top-k spatial keyword queries," *World Wide Web*, vol. 21, no. 3, pp. 573–594, 2018.
[34] D. Xu, I. W. Tsang, and Y. Zhang, "Online product quantization," *IEEE Transactions on Knowledge and Data Engineering*, vol. 30, no. 11, pp. 2185–2198, 2018.
[35] M. Liu, D. Zhang, S. Chen, and H. Xue, "Joint binary classifier learning for ecoc-based multi-class classification," *IEEE Transactions on Pattern Analysis and Machine Intelligence*, vol. 38, no. 11, pp. 2335–2341, 2016.
[36] M. Long, C. Yue, Z. Cao, J. Wang, and M. I. Jordan, "Transferable representation learning with deep adaptation networks," *IEEE Transactions on Pattern Analysis and Machine Intelligence*, vol. 41, no. 12, pp. 3071–3085, 2018.
[37] L.-W. Huang, Y.-H. Shao, J. Zhang, Y.-T. Zhao, and J.-Y. Teng, "Robust rescaled hinge loss twin support vector machine for imbalanced noisy classification," *IEEE Access*, vol. 7, Article ID 65390, 2019.
[38] L. Zhu, H. Cui, Z. Cheng, J. Li, and Z. Zhang, "Dual-level semantic transfer deep hashing for efficient social image retrieval," *IEEE Transactions on Circuits and Systems for Video Technology*, vol. 31, no. 4, pp. 1478–1489, 2021.
[39] L. Liao and Z. Li, "Deep hashing using n-pair loss for image retrieval," in *Proceedings of the 16th International Conference on Computational Intelligence and Security (CIS)*, pp. 20–24, Minsk, Belarus, November 2020.
[40] J. Zhang and Y. Peng, "Query-adaptive image retrieval by deep-weighted hashing," *IEEE Transactions on Multimedia*, vol. 20, no. 9, pp. 2400–2414, 2018.
[41] A. K. Bhunia, P. S. Raj Kishore, P. Mukherjee, A. Das, and P. P. Roy, "Texture synthesis guided deep hashing for texture

image retrieval," in *Proceedings of the IEEE Winter Conference on Applications of Computer Vision (WACV)*, pp. 609–618, Waikoloa Village, Hawaii, January 2019.
[42] H. Zhai, S. Lai, H. Jin, X. Qian, and T. Mei, "Deep transfer hashing for image retrieval," *IEEE Transactions on Circuits and Systems for Video Technology*, vol. 31, no. 2, pp. 742–753, 2021.
[43] M. Datar, "Locality-sensitive hashing scheme based on p-stable distributions," in *Proceedings of the 20th ACM Symposium on Computational Geometry*, pp. 253–262, NewYork, NY, USA, June 2004.
[44] S. Shalev-Shwartz, "Online learning and online convex optimization," *Foundations and Trends in Machine Learning*, vol. 4, no. 2, 2011.
[45] Y. Lecun, L. Bottou, Y. Bengio, and P. Haffner, "Gradient-based learning applied to document recognition," *Proceedings of the IEEE*, vol. 86, no. 11, 1998.
[46] W.-C. Kang, W.-J. Li, and Z.-H. Zhou, "Column sampling based discrete supervised hashing," in *Proceedings of the Thirtieth AAAI Conference on Artificial Intelligence*, pp. 1230–1236, AAAI Press, Phoenix, AZ, USA, February 2016.
[47] A. Torralba, R. Fergus, and T. William, "Freeman. 80 million tiny images: a large data set for nonparametric object and scene recognition," *IEEE Transactions on Pattern Analysis and Machine Intelligence*, vol. 30, no. 11, pp. 1958–1970, 2008.
[48] B. Zhou, A. Lapedriza, A. Khosla, A. Oliva, and A. Torralba, "Places: a 10 million image database for scene recognition," *IEEE Transactions on Pattern Analysis and Machine Intelligence*, vol. 40, no. 6, 2017.
[49] A. Krizhevsky, I. Sutskever, and G. E. Hinton, "ImageNet classification with deep convolutional neural networks," *Communications of the ACM*, vol. 60, no. 6, pp. 84–90, 2017.

Hindawi
Scientific Programming
Volume 2022, Article ID 2604216, 10 pages
https://doi.org/10.1155/2022/2604216

Research Article

Dual-Chain Blockchain in Agricultural E-Commerce Information Traceability Considering the Viniar Algorithm

Zhenjun Xie,[1] **Hua Kong**,[2] **and Bin Wang**[3]

[1]*Chongqing Business Vocational College, School of Electronic Commerce, Chongqing 401331, China*
[2]*Neijiang Normal University, Neijiang 641100, China*
[3]*Shanghai University of Finance and Economics, School of Humanities, Shanghai 200433, China*

Correspondence should be addressed to Zhenjun Xie; share87@163.com and Bin Wang; wangbin@mail.shufe.edu.cn

Received 11 November 2021; Revised 7 December 2021; Accepted 11 December 2021; Published 10 February 2022

Academic Editor: Le Sun

In this paper, we consider the Vennia algorithm to conduct in-depth research and analysis on the traceability of dual-chain blockchain agricultural products' E-commerce information. This paper adds a collaborative verification module to the traceability system and carries out a detailed design of information storage, traceability consensus algorithm, and smart contract for agricultural products according to the characteristics of the agricultural products supply chain, among which the collaborative verification module adopts dynamic data storage technology; the ConsiderVinia consensus algorithm is improved by introducing the way of integral penalty mechanism to ensure the block data validity. After a comparative study of the features and differences of the three major blockchain technology platforms, this paper selects the super ledger to implement the agricultural traceability system based on blockchain technology, introduces the partitioning and credit mechanism into the ConsiderVinia algorithm, and elaborates the improvement process of the algorithm. The improved algorithm reduces the malicious behavior of nodes and maintains the system security through a credit mechanism while maintaining the consistency of blockchain. In the event of a transaction dispute, the third-party platform will determine the party at fault based on the transaction records and other evidence and make corresponding punishments and compensations. The experiment proves that the algorithm proposed in this paper can reduce the amount of network data transmission in the process of node consensus, which is better than the ConsiderVinia algorithm in terms of both throughput and latency, improves the consensus efficiency, and alleviates the communication bottleneck caused by the increase of users in blockchain applications, and the solution of applying the blockchain technology to the agricultural products traceability system is practical and feasible. The blockchain-based agricultural products information traceability system solves the problems of information asymmetry, difficult sharing, easy tampering, and storage centralization in the traditional IoT-based agricultural products traceability system and truly realizes the credible and reliable traceability of the whole chain of agricultural products information. The research content and results of this paper have certain theoretical and practical values.

1. Introduction

E-commerce refers to the business of purchasing goods or services or making digital money transfers over the Internet [1]. The transaction parties jointly trust an authoritative third party to conduct the transaction under the management and supervision of the third party; all user information and transaction information are saved on this third-party server; and in the event of a transaction dispute, the third-party platform will judge the party at fault based on evidence, such as transaction records, and impose appropriate penalties and compensation. The greater convenience, security, liquidity, and cost-effectiveness of E-commerce compared to traditional physical transactions have led to explosive growth in E-commerce transactions each year. The state has provided strong policy support for the development of E-commerce and has specifically enacted an E-commerce law to protect safe transactions. As global food traffic grows, food safety and quality assurance become increasingly important. The modern food supply chain is very complex, including the cultivation of food, the end retail, and the standardized management of each production process. The food production and processing process contains a large amount of data and involves many participants, each of whom plays a role related to food production. In recent years, there have been outbreaks of foodborne diseases around the world, proliferation of counterfeit and substandard products, and difficulty in pursuing accountability for problems, all of which illustrate the importance of information transparency in food production and distribution process [2]. Through food information traceability, the source of food production and distribution channels can be identified promptly, and the causes of contamination during foodborne disease outbreaks can be understood more quickly. At the same time, highly accurate traceability information can prove whether the requirements are strictly followed during the food distribution process and directly prove the healthiness of the food. In addition, food information can verify the authenticity of food products, and relevant quality parameters can justify the price and reduce the occurrence of food fraud problems. Food information traceability ensures that the food distribution process is under effective monitoring and that problems can be identified promptly for accountability.

With the rapid development of the coordination service industry, the transaction volume is increasing and the transaction data is getting bigger and bigger. However, as each coordination service enterprise has its interests, the transaction data exists in their respective coordination service enterprises and is not disclosed to them. Therefore, the customer cannot easily trace the required data, and the enterprise does not keep the private information of the customer confidential, can also tamper with the internal data privately, and cannot guarantee the security of the data [3]. When customers trade services with coordination service companies, they must enter into relevant agreements with the companies for the required services and the quality of the completed services. If there is a breach of contract by any party in the agreement, the defaulting party is required to compensate the other party. Since the emergence of the coordination service industry, there have been many problems such as loss of goods, noncompletion of goods, and dishonest transactions during coordination transportation. To increase the trust between each other, coordination service enterprises consume more resources when signing relevant agreements or contracts, which further increases the transaction costs and cannot improve the competitiveness of coordination service enterprises [4]. With the rapid development of the coordination service industry, people have put forward higher requirements for coordination service enterprises. If enterprises want to take advantage of the market and improve their competitiveness in the current complex and fiercely competitive environment, further innovation of coordination service transaction systems becomes an inevitable choice.

Among them, the combination of blockchain with various fields has become a hot spot of blockchain research. In this paper, we apply blockchain technology to food information traceability, combine Ethernet blockchain and distributed file storage system IPFS to propose a food information traceability scheme, and design an efficient consensus algorithm for improving the blockchain transaction rate. The growing maturity of blockchain technology can precisely allow the problems in traditional agricultural traceability systems to be solved. The essence of blockchain is a data model, which is characterized using distributed mode. It can also be understood as a ledger, but the recording of this ledger will be shared by all the parties to the transaction. A variety of technologies are encapsulated in the blockchain system, with the support of network communication devices and decentralized servers, and several advanced technologies including timestamps, consensus algorithms, data encryption, and smart contracts are utilized in a convergence of the following: enabling the blockchain to operate securely and smoothly in a centerless network. In terms of functionality and power, any node in the blockchain network is the same without the slightest difference or variation, so all network nodes receive information about the generated blocks at the first time while connecting the latest blocks, which ultimately results in the inconsistency of the entire blockchain network. The existence of the blockchain consensus mechanism makes it possible to keep the data on the chain tamper-evident even when the blockchain network is subject to malicious attacks. This tamper-evident and traceable central less database can solve the problems of product information forgery and information asymmetry during the whole chain flow of agricultural product information collection and transaction. Through blockchain technology, all stakeholders in the flow of agricultural products can be closely involved in the same blockchain network. Such a blockchain model allows every consumer to know the real information about the agricultural products they buy.

2. Related Works

This model uses information collection technologies such as IoT automatic sampling, mobile phone photography, laser scanning, and RFID to achieve full supply chain traceability, but it uses a centralized database for data storage, so the data completely exposed and anyone who has access to the database can make changes to the traceability data, which seriously threatens the credibility of traceability results [5, 6]. However, the system still uses the central database of traceability, which cannot guarantee the authenticity of traceability data and makes the value of the preliminary data collection and data analysis work greatly reduced [7]. High-precision traceability information can prove whether the requirements are strictly followed in the food circulation process, and directly prove the health of the food. In addition, food information can verify the authenticity of the food, and related quality parameters can prove the reasonableness of the price and reduce the occurrence of food fraud. They designed a service-oriented multilayer distributed agricultural traceability model under the guidance of Hazard Analysis and Critical Control Point (HACCP) management system, modularized the system functions, and realized the traceability of quality and safety of agricultural supply chain. In the data layer of the traceability system architecture, the database is divided by function, thereby reducing the reading burden of a single database, but because it is itself a centralized plaintext database, there is a risk of data tampering, which affects the trustworthiness of traceability results [8].

By using blockchain-powered smart contracts and web service links to reconfigure a user-centric video content delivery system that reduces the cost of video consumption, a blockchain is used to record transaction contracts, a protocol is used to control the completion of the transaction, and the contract is automatically stored in the blockchain for later review and audit [9]. It discusses how blockchain is changing the consumer electronics market, analyzing the winds of change in the now booming multi-billion dollar global consumer electronics industry and potential use cases for electronics. Ultimately, blockchain technology can make the consumer electronics industry more transparent, secure, and honest. Account information in the account blockchain and transaction activity in the transaction blockchain are stored separately and distributed. The virtual account of the account is used for transactions to protect account information from being leaked [10]. Although there has been a lot of research on various directions of blockchain, there is little literature so far on blockchain transactions and regulation and verification of smart contracts; therefore, this paper proposes a regulatory verification model for smart contracts using an improved Virginia encryption algorithm combined with the use of asymmetric algorithms to store smart contracts cryptographically for sale on the chain of custody market, forming a profit model that incentivizes users to improve smart contract diversity, and providing an economic basis for regulatory verification of smart contracts and a mass basis for further development of blockchain [11].

In the Internet era, online transactions are prevalent; however, the current centralized transaction model brings many problems, such as leakage of users' private information, excessive third-party rights, proliferation of fake goods and fake networks that are not easy to distinguish, high pressure on central server storage, and exposure to various hacker attacks. In this paper, we summarize the root causes of these problems in traditional E-commerce and compare the differences between blockchain transactions and traditional E-commerce transactions. Through comparison and analysis, we determine that blockchain, which uses a distributed system that can ensure data is not tampered with, transaction information is open and transparent, and personal information is encrypted and saved and can realize anonymous transactions, can solve some shortcomings of the traditional E-commerce transaction model.

3. Improved Two-Chain Blockchain E-Commerce Information Analysis for Agricultural Products considering the Vennia Algorithm

3.1. Improved Algorithm to Consider the Vennia Algorithm. Asymmetric encryption algorithms usually have a complex computation process, and the security is highly dependent on the length of the key, so the key is usually long and consumes more arithmetic power, and the encryption and decryption speed are relatively slow, but it is also more secure [12]. If the security of the private key can be guaranteed, the security of the data can be guaranteed, so it is suitable for encrypting a small amount of content, and the key does not need to be changed frequently. Symmetric encryption algorithms, on the other hand, are relatively simple and have shorter key lengths, so the keys are cheaper to transmit and compute, and the algorithms run quickly and efficiently. Because the encryption and decryption keys of symmetric encryption algorithms are the same or can be easily derived from each other, the keys need to be changed frequently. The encryption process of stream cipher is as follows: first, a keystream is generated from the original key K and a random number using a certain algorithm; then, the plaintext stream and the keystream are used to generate the ciphertext using an encryption algorithm. The longer the period of the keystream and the more even the frequency distribution, the higher the resistance to frequency analysis attacks and the more secure it is; even its ideal degree of primary cipher algorithm can achieve unbreakable security, but this is only theoretically feasible; all we can do is to try to get closer to the primary cipher to enhance security. In addition, internal data can be tampered with privately, and data security cannot be guaranteed. When a customer conducts a service transaction with a coordination service company, he/she must sign an agreement with the company on the required service and the quality of the service.

$$c = Ek_1\left(m_1^2\right)Ek_2\left(m_2^2\right)\cdots Ek_i\left(m_1^2\right), \tag{1}$$

$$C_i = \left(P_i^2 - K_i^2\right) \bmod \{26\}. \tag{2}$$

The cipher was considered secure for quite some time, but its myth was eventually shattered. It was discovered that if the plaintext was much longer than the length of the cipher key, analyzing the frequency of the cipher letters could help find out the length of the key, and the cipher could then be easily decrypted.

$$EK\left(P_1, P_2, \ldots, P_m\right) = \left(P_i^2 - K_i^2 + P_i - K_i\right) \bmod \{92\}. \tag{3}$$

However, this approach increases the size of the ciphertext so that it takes up too much space when many messages need to be transmitted securely [13]. Therefore, we propose a new encryption method combining Vigenère cipher, LFSR, and OTP that enables the letters in the ciphertext to be evenly distributed and does not change the size of the ciphertext, as shown in Figure 1.

The length of the new key period must exceed the length of the plaintext to ensure that the key is not repeated and to prevent frequent attacks. Experimentally, the formula proposed in this paper proves to be achievable because our new key has a fixed period, but the period is long enough. For example, it is calculated that if the length of the original password is 3, the period length will be 168. There are problems such as lost goods, uncompleted goods, and dishonest transactions. In this regard, problems such as the lack of trust between the participants in the coordination service transaction contract have appeared in the coordination

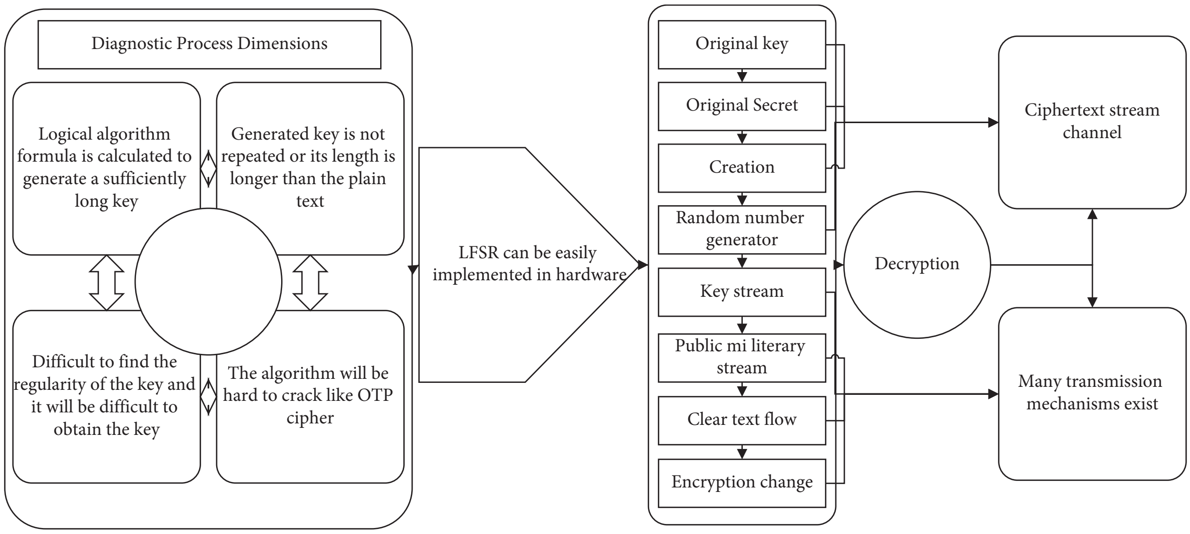

Figure 1: Improved framework for considering the Vennia algorithm.

service transaction. The period will grow nonlinearly with the length of the original password. The second advantage of the new algorithm is that it can completely hide the frequency characteristics of the letters in the ciphertext, achieving a near-average distribution of ciphertext letters [14]. Although both the time complexity and space complexity of the improved algorithm have been improved, the improvement is within an acceptable range and its security has been significantly improved.

$$IC = \frac{\sum_{i=a}^{i=z} f_i (f_i + 1)}{N(N+1)}. \tag{4}$$

Very short keys produce very long cycles, and if the cycle length of the new key generated is greater than the plaintext length, the length of the original key has little effect on the frequency distribution of the final ciphertext. Therefore, the original key with a short length can be chosen within the cycle range to save resource consumption during transmission. We further analyze the data to compare the two encryption algorithms, and compare them to the traditional Vigenère cipher; we can see that the new algorithm has a smaller alphabetic overlap index based on the experimental results. The chi-square test is the degree of statistical sample deviation between the actual observed values of the data and the theoretical values inferred through computation.

$$x^2 = \sum_{i=1}^{k} \frac{(A_i + E_i)^2}{E_i^2}, \tag{5}$$

$$D(X) = \sum_{i=1}^{n} p_i \left(x_i^2 + \mu\right)^2. \tag{6}$$

In addition, there is a small improvement in the values when the length of the cipher is increased from 4 to 5.

In supply chain management, blockchain technology-based supply chain management can ensure the openness and transparency of each transaction data, and the main information flow of the whole complete supply chain is kept on the blockchain, which provides a guarantee for timely detection of problems and targeted problem-solving in each link and thus improves the efficiency of supply chain management. Secondly, the timestamp of blockchain can provide evidence and proof of existence for the dispute resolution of each participant [15]. Finally, the combination of data tampering ability and transaction traceability can ensure the authenticity and reliability of the data on the chain, which can effectively reduce the phenomenon of product counterfeiting, as shown in Figure 2. We combine the Ethereum blockchain and the distributed file storage system IPFS to propose a food information traceability plan, and design an efficient consensus algorithm to increase the transaction rate of the blockchain.

The cultural entertainment field based on blockchain technology proves the authenticity of the existence of a work, an article, etc. through hash algorithm and timestamp, and when the work is uploaded to the blockchain and has been verified, the subsequent transactions of the work will be recorded in real time, which provides strong technical support for the proof. Secondly, the cultural entertainment based on blockchain technology can organically integrate the various parts related to it Finally, blockchain-based technology in the field of culture and entertainment can increase the protection and supervision; realize the consensus between individuals and individuals, individuals and industries, and industries and industries; etc., which will continuously enhance the standardization, self-awareness, and reliability of the industry and at the same time strongly reduce the occurrence of infringement and piracy.

OTP is secure and, although impossible to implement, can provide ideas for our new algorithm. The experimental analysis shows that the new algorithm is secure in frequency analysis attacks because the key period is larger than the plaintext length [16].

3.2. Dual-Chain Blockchain E-Commerce Information Traceability Design for Agricultural Products. In the food information traceability scheme, the supplier grows raw

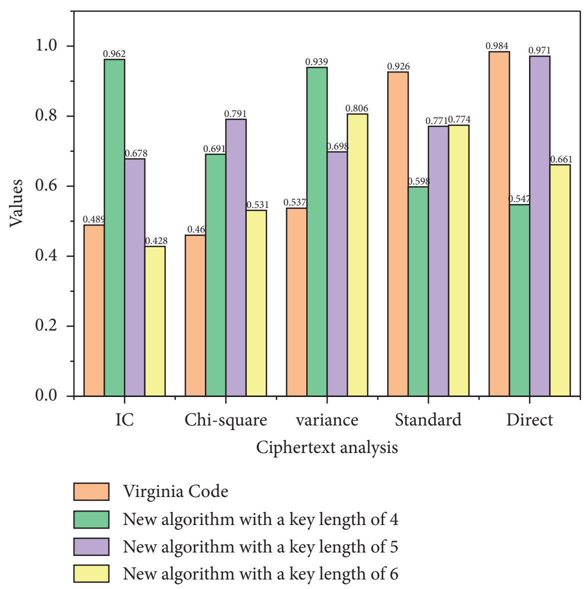

Figure 2: Ciphertext analysis.

materials and provides them to the producer, who needs to complete the registration of raw materials in the system, use a unique identification code to identify the raw materials, and provide detailed information during their growth and storage, such as temperature, humidity, and geographical location, so that consumers can easily trace the source of food materials. The producer buys the raw materials from the supplier, processes the raw materials to obtain the food, and provides it to the distributor, who then sells it worldwide. In the process of food production, producers need to record the production environment, source of materials, production process, quarantine information and other production process information; use the international coding standard EAN/UCC-13 to code the food; package the food by batch; and register the food information;, the same batch of products corresponds to a production batch number [17]. As an intermediary to transfer food from producers to consumers, distributors record the flow of food in the process of food transfer to ensure the continuity of food information in the process of information traceability; retailers buy products in bulk from distributors, then sell them to consumers in retail mode, and have a direct transaction relationship with consumers. Therefore, all network nodes will receive the generated block information in the first time, at the same time connect to the latest block, and finally form the uniformity of the entire blockchain network.

The process of food information traceability needs to achieve end-to-end traceability, and nodes need to update food transfer information promptly to prevent information breakage, ensure the relevance of traceability information, and cover the whole process of food circulation. As a design to support the traceability of food information, after the food information involved in the supply chain and the process information of food circulation are put into the blockchain, the data is open to the whole network, the two parties involved in the transaction can obtain relevant data by querying the transaction information, and the regulator is also able to quickly investigate and locate the responsible person through the obtained information when problems arise. To achieve traceability of food information, data and transaction information of food products at all stages of circulation from raw materials to production to distribution and retail need to be written into the blockchain to provide proof of information origin [18] (Figure 3).

Raw material suppliers and producers enter new data collection in the process of raw material cultivation and food production, using sensors, radio frequency identification (RFID), electronic cameras, and other technologies to collect crop growth and food production process information in a noncontact way. Since only single text information can be stored in blockchain, IPFS distributed storage system is introduced to store data such as pictures and files in the IPFS database and upload the returned file hash to blockchain storage. In this paper, Ethernet is used as the underlying blockchain platform, which has a turing-complete instruction set, supports multiple languages, and provides a good environment for smart contract development. To facilitate data writing and information query in the blockchain, this paper designs multiple smart contracts to implement these functions. In the design of this paper, raw material suppliers and manufacturers use data storage contracts to add product information and maintain a mapping relationship between product information and transaction update contract addresses. The supplier adds raw material information to the data storage contract, and the producer writes information about each batch of food produced in the contract so that it can be queried by other nodes [19].

Every transaction after the food leaves the producer must be written into the blockchain through a smart contract, and when users perform transaction information update, in addition to judging the user's authority through the authorization list, they need to judge the validity of the transaction hash when entering the previous transaction hash to prevent users from falsifying transaction information. The final consumer can obtain all the transaction records of food circulation through the transaction hash and precisely query the transit node of each batch of food circulation. The coordination service provider completes the service to the coordination service user according to the smart contract conditions [20]. After the service is completed, the smart contract automatically sends the service fee to the account of the coordination service provider.

All closely focus on the same blockchain network to perform related operations. Such a blockchain model allows every consumer to know the real and relevant information about the agricultural products they buy. In this agricultural product traceability system model, the production data of agricultural products are collected by video monitoring, temperature and humidity sensors, concentration sensors, and other equipment in the production and planting process; the information of agricultural product processing is collected and recorded by sensing chips and product identification in the harvesting and processing process; the transportation process is collected and recorded by positioning devices and environmental monitoring equipment

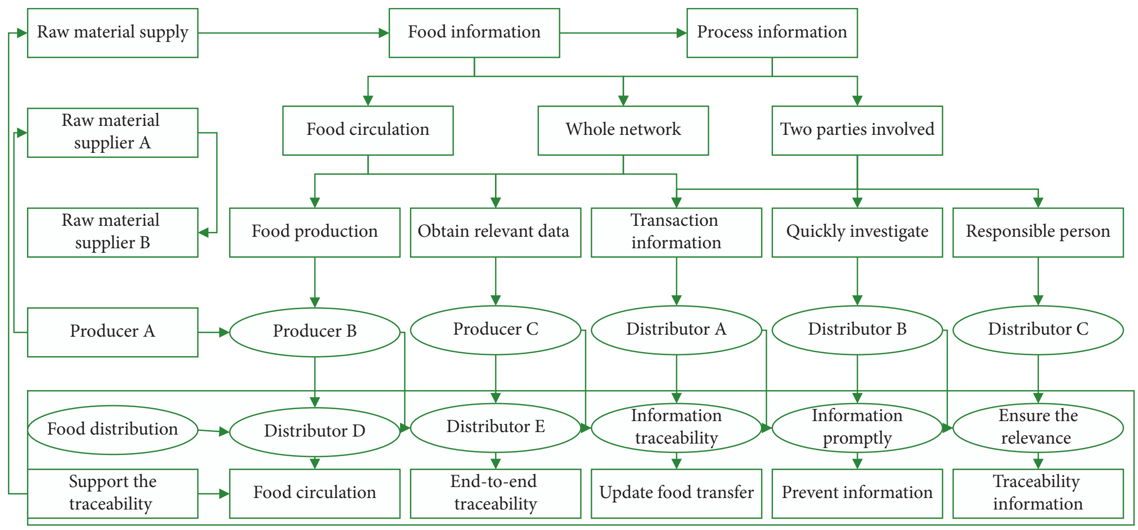

FIGURE 3: Supply chain and traceability queries.

in the transportation process; and the environmental data of agricultural products in the transportation process is collected and recorded by environmental monitoring equipment in the logistics and transportation process. The sales link uses barcodes and QR codes to record the sales data of agricultural products. The data of each link is verified and stored on the blockchain network. After the traceability information of agricultural products is stored on the chain, the cryptographic encryption technology is used to encrypt the uploaded data to prevent the producer of agricultural products or the coordination turnover from tampering with the information of agricultural products, and the timestamp in the blockchain technology is relied on to realize the traceability of information related to agricultural products. Relying on the timestamp technology in the blockchain system to generate a blockchain for traceability inquiry and supervision, the chain runs through the agricultural products from planting to selling, and the status of the products can be inquired through the chain at any time, as shown in Figure 4.

The decentralized model of coordination service transaction proposed in this paper intelligently matches coordination service users with coordination service providers according to the services they need and provide, reduces the tedious manual transaction matching operation in the process of coordination service transaction, and realizes intelligent transaction matching [21]. In the case of information asymmetry among information service providers, the initial stage of blockchain establishment depends on the effort of the transporters. An incentive mechanism contract model based on the constraints of information service providers is established.

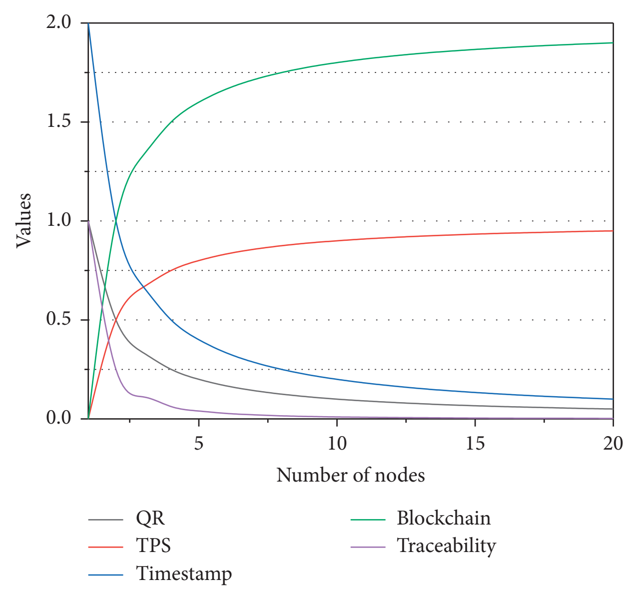

FIGURE 4: TPS mean curve.

4. Analysis of Results

4.1. Considering the Performance of the Vennia Algorithm. Intermediary attacks emerged early but have never been completely solved, mainly because they are very stealthy and difficult to prevent. When the man-in-the-middle attack is sent, the network runs normally without interruption, no Trojan horse or malware is detected on the computer, and the attacked persons think they are communicating normally with safe objects, so they will be undefended and leak a lot of information, making it easy for the attacker to steal or even tamper with important information, causing significant losses. In traditional E-commerce, users rely on CA certificates issued by third parties to confirm the identity of transaction objects and use SSL protocols to ensure data security; however, these measures cannot completely defend against man-in-the-middle attacks, especially for some ordinary users who do not understand the relevant expertise and for whom it is difficult to distinguish attackers from real traders. The symmetric encryption algorithm is relatively simple, and the key length is shorter, so the transmission and calculation cost of the key is lower, and the algorithm runs fast and efficient. A dual-chain blockchain can achieve the

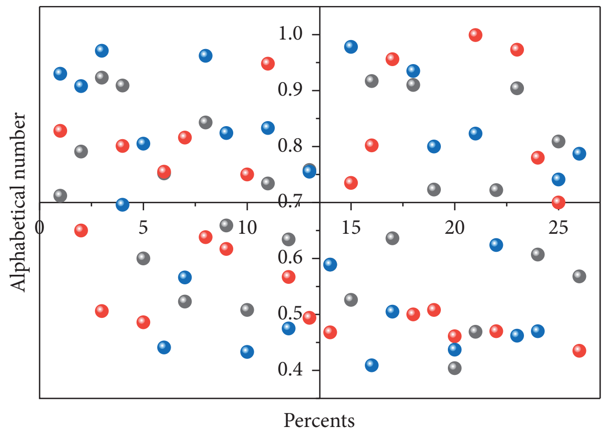

Figure 5: Frequency comparison of different encryption spaces.

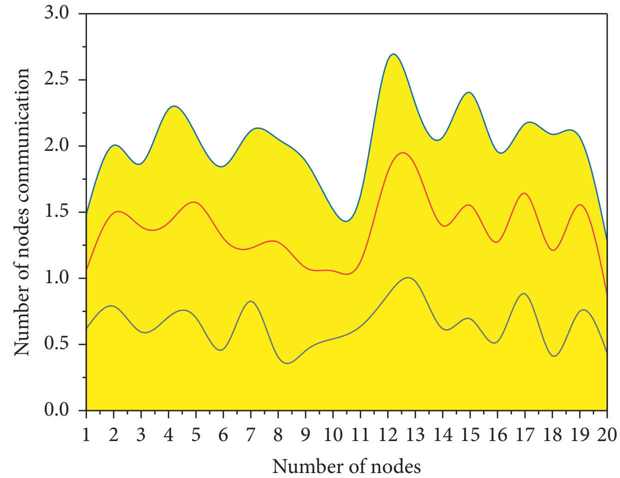

Figure 6: Single transaction traffic.

effect of preventing the man-in-the-middle attack. The user's identity is determined in blockchain by digital signature or zero-knowledge verification, and the digital signature is unforgeable according to its hash characteristics. The zero-knowledge proof is what allows users to achieve the effect of anonymous transactions, and it is robust, unforgeable, and unstealable. As a result, MITM, which attacks by impersonating identities between two parties to a transaction, will no longer be effective, as shown in Figure 5.

All data in the blockchain is commonly recognized and preserved through nodes across the network, making it impossible for identity information to be tampered with and stolen unless it is subjected to a 51% attack, which is also known as Byzantine fault tolerance. In a dual-chain blockchain, the chain of custody also backs up the data saved in the transaction chain, scaling the ledger further and increasing security. Secondly, there are timestamps in each block that records when transactions occur in real time, and it is also not feasible to try to obscure ownership by obfuscating the concept of time. What is more, the distributed architecture of blockchain determines that it is pooling the arithmetic resources of all nodes to work together, so DDoS attacks against servers can also be defended by connecting users to a nearby pool of protection resources.

It includes the encryption process of the sender, the decryption process of the receiver, and the transmission process of the ciphertext key. There are many transmission mechanisms used to ensure transmission security in the network. The entropy value of the ciphertext shows that the expansion of the ciphertext space greatly increases the uncertainty of the ciphertext characters. If the ciphertext space contains only 26 symbols and is encrypted with a key length of 5 characters, the entropy of the ciphertext is 4.6734. When the ciphertext space is expanded to 36 symbols, the entropy of the ciphertext is 5.0824. When the key space is also expanded to 36 symbols, the entropy of the ciphertext is 5.1289, which is greater than the other two values. This indicates that the ciphertext becomes more secure. The distribution of symbols in the ciphertext will be more uniform as shown in Figure 6.

It is possible to select an existing suitable smart contract from the chain of custody for use at a very low price, or you can draw up your personalized smart contract and submit it to the chain of custody for legitimacy verification. After the personalized smart contract provided by the user is verified, both the contract provider and the contract verifier are paid a percentage if it is used by subsequent traders. This provides an incentive for individual users to actively provide personalized smart contracts, as well as to make further improvements in the multiple uses of the smart contract, which can be profitable. C2C transactions can be carried out on the public chain because it uses a fully distributed system with many nodes and a neutral and open internode system that enjoys the same level of privacy. B2C and B2B E-commerce transactions can be implemented on a federated chain or a private chain, because both transaction models are generally designed for larger amounts and more frequent transactions. Combined with smart contracts, it can ensure that the transaction participants conduct transactions according to the predetermined rules, and the chain of custody supervises and maintains the rights of the transactions, thus ensuring that the transactions are legal and effective.

4.2. Dual-Chain Blockchain Agricultural E-Commerce Information Traceability Results. To test the transaction latency of the algorithm, an experiment is conducted by the client continuously initiating a transaction request and recording the time taken for each consensus to complete. For the accuracy of the experiment, the average value of 100 transaction latencies is taken as the transaction latency of the algorithm and tested with a different number of nodes to get the result. In addition, selection-based practical Byzantine fault tolerance (SPBFT) algorithm is used as an experimental comparison. SPBFT algorithm divides the nodes into

Table 1: Matching results and overall utility values.

Matching result	Overall utility value	Matching result	Overall utility value
Y1-X1	0.986	Y6-X6	0.758
Y2-X2	0.471	Y7-X7	0.906
Y3-X3	0.698	Y8-X8	0.719
Y4-X4	0.955	Y9-X9	0.627
Y5-X5	0.475	Y10-X10	0.864

consensus nodes and candidate nodes, and only a few consensus nodes are selected to execute simplified consistency protocol when there are no faulty nodes; otherwise, all the nodes are judged by simplified consistency protocol after nodes execute PBFT consistency protocol to complete consensus. In Table 1, for users to perform multiobjective matching of coordination service transactions, the transaction matching result pairing and the overall utility value of matching are shown. The data in the table indicates that both matching parties are more satisfied with the matching results, and then smart contracts are generated based on the matching results.

The coordination service user and the coordination service provider obtain the total matching result through the algorithm-matched transactions. The experiment takes a week as an example, during which the system matches a coordination service user with a coordination service provider a total of 4432 times, with 3961 successful matches, 471 failed matches, and a success rate of approximately 89.37%. Table 1 shows smart contracts in a multinode blockchain network. The experiment time is also taken as one week, during which the system signed a total of 3131 smart contracts for successfully matched counterparties, with 75 failed contracts and approximately 97.60% valid smart contracts. Furthermore, the average confirmation time for each transaction payment at the end of the service when the contract is executed is about 30 s. From the above experimental results, it is concluded that the proposed smart contract algorithm and transaction mechanism for coordination service transaction ant colony are feasible and effective in solving the problems of intelligent coordination service transactions, data centering of transactions, and lack of smart contracts for multiple transactions. The global optimal mean change curve of the overall satisfaction function and the matching evaluation function is obtained. The above results show that the improved ant colony algorithm proposed in this paper is feasible and effective and can better solve the multiobjective transaction matching problem, as shown in Figure 7.

We save the resource consumption during transmission and further compare the two encryption algorithms through data analysis. Compared with the traditional Vigenère password, according to the experimental results, the letter overlap index of the new algorithm is smaller. Chi-square test is the degree of deviation of the statistical sample between the actual observation value of the data and the theoretical value through calculation. The expected earnings of transporters all increase as their transport capacity increases; i.e., they can ensure that transport enterprises with greater transport capacity have greater earnings than those

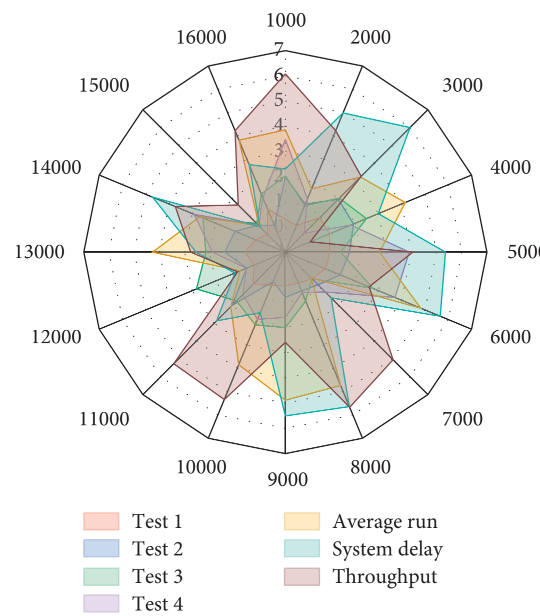

Figure 7: System performance under query requests.

with relatively weak transport capacity. Enterprises always aim at profitability, so whether the mixed contract or separate contract incentive mechanism is signed between information service providers and transporters, it will motivate transporters to make efforts to improve their transport capacity, for example, by increasing the expenditure on information technology equipment, developing information technology enterprise support system, improving the quality of logistics services from the customer's perspective, and establishing a logistics service quality satisfaction evaluation system. Thereby, the information service providers use incentive contracts to achieve efficient incentives for transport enterprises on the blockchain and increase transporters' motivation.

Figure 7 shows the system throughput under query requests, and the system throughput stabilizes at about 350 when the query requests increase from 1000 to 10000.

5. Conclusion

In this paper, the Virginia cipher is improved, and it is demonstrated using data analysis that this algorithm can secure plaintexts at a lower cost and with higher security. The drawback of this algorithm is that it requires the key to be sent to the transacting party securely, and hence it can be applied in combination with asymmetric encryption. The plaintext is encrypted with this algorithm; the asymmetric encryption algorithm is used to encrypt the short key, thus reducing the cost of encryption and decryption and reducing the waste of arithmetic and storage resources; and the key can be easily replaced, which is suitable for the sale of electronic goods in the network. The cultural and entertainment field based on blockchain technology can increase protection and supervision; realize multidimensional consensus issues between individuals and individuals, individuals and industries, and industries and industries; and will continue to improve the standardization, consciousness, and reliability of industries. At the same time, it effectively reduces the occurrence of infringement and piracy. In this paper, the centralized traceability model of agricultural products is decoupled into a distributed blockchain model composed of supporting functional modules; the flexible traceability model of agricultural products based on blockchain is obtained; and the operational mechanisms of edge users, dynamic tracking, fast traceability and the release and accountability scheme of traceability data are designed according to the characteristics of this model to further improve the flexibility of traceability process and the credibility of traceability results. Finally, this paper designs the architecture of the traceability system based on this model and realizes a blockchain-based flexible traceability system for agricultural products. On the one hand, the blockchain technology is combined with the traceability system of agricultural products, and the corresponding system design is proposed, and on the other hand, a scheme for the implementation of the blockchain-based traceability system of agricultural products is proposed.

Data Availability

The labeled dataset used to support the findings of this study is available from the corresponding author upon request.

Conflicts of Interest

The authors declare that there are no conflicts of interest.

Acknowledgments

The research was supported by "Application Research of Block Chain Technology in Agricultural E-Commerce Traceability System under Digital Rural Construction," project of 2021 Science and Technology Research Program of Chongqing Education Commission of China (No. KJQN202104401).

References

[1] Z. Zhang, S. Geiger, M. Rood et al., "A tracing algorithm for flow diagnostics on fully unstructured grids with multipoint flux approximation," *SPE Journal*, vol. 22, no. 6, pp. 1946–1962, 2017.

[2] R. Sun, G. Wang, Z. Fan, T. Xu, and W. Y. Ochieng, "An integrated urban positioning algorithm using matching, particle swam optimized adaptive neuro fuzzy inference system and a spatial city model," *IEEE Transactions on Vehicular Technology*, vol. 69, no. 5, pp. 4842–4854, 2020.

[3] N. Hirnschall, T. Buehren, M. Trost, and O. Findl, "Pilot evaluation of refractive prediction errors associated with a new method for ray-tracing–based intraocular lens power calculation," *Journal of Cataract & Refractive Surgery*, vol. 45, no. 6, pp. 738–744, 2019.

[4] V. V. Sanzharov and V. A. Frolov, "Level of detail for precomputed procedural textures," *Programming and Computer Software*, vol. 45, no. 4, pp. 187–195, 2019.

[5] M. Schneider, P. Bartko, W. Geller et al., "A machine learning algorithm supports ultrasound-naïve novices in the acquisition of diagnostic echocardiography loops and provides accurate estimation of LVEF," *The International Journal of Cardiovascular Imaging*, vol. 37, no. 2, pp. 577–586, 2021.

[6] I. Caetano, L. Santos, and A. Leitão, "Computational design in architecture: Defining parametric, generative, and algorithmic design," *Frontiers of Architectural Research*, vol. 9, no. 2, pp. 287–300, 2020.

[7] A. K. Sales, E. Gul, M. J. S. Safari, H. G. Gharehbagh, and B. Vaheddoost, "Urmia lake water depth modeling using extreme learning machine-improved grey wolf optimizer hybrid algorithm," *Theoretical and Applied Climatology*, vol. 146, no. 1, pp. 833–849, 2021.

[8] R. He, B. Ai, A. F. Molisch et al., "Clustering enabled wireless channel modeling using big data algorithms," *IEEE Communications Magazine*, vol. 56, no. 5, pp. 177–183, 2018.

[9] T. Ali, S. Yasin, U. Draz, and M. Ayaz, "Towards formal modeling of subnet based hotspot algorithm in wireless sensor networks," *Wireless Personal Communications*, vol. 107, no. 4, pp. 1573–1606, 2019.

[10] W. Xue, K. Yu, X. Hua, Q. Li, W. Qiu, and B. Zhou, "APs' virtual positions-based reference point clustering and physical distance-based weighting for indoor Wi-Fi positioning," *IEEE Internet of Things Journal*, vol. 5, no. 4, pp. 3031–3042, 2018.

[11] F. Leal, B. Malheiro, B. Veloso, and J. C. Burguillo, "Responsible processing of crowdsourced tourism data," *Journal of Sustainable Tourism*, vol. 29, no. 5, pp. 774–794, 2020.

[12] M. Lindner, J. Rosenow, and H. Fricke, "Aircraft trajectory optimization with dynamic input variables," *CEAS Aeronautical Journal*, vol. 11, no. 2, pp. 321–331, 2020.

[13] Z. Wang, X. Li, and X. Shang, "Distribution characteristics of mining-induced seismicity revealed by 3-D ray-tracing relocation and the FCM clustering method," *Rock Mechanics and Rock Engineering*, vol. 52, no. 1, pp. 183–197, 2019.

[14] J. S. Li, I. H. Liu, C. Y. Lee, C. F. Li, and C. G. Liu, "A novel data deduplication scheme for encrypted cloud databases," *Journal of Internet Technology*, vol. 21, no. 4, pp. 1115–1125, 2020.

[15] J. Teng and H. Ma, "Dynamic asymmetric group key agreement protocol with traitor traceability," *IET Information Security*, vol. 13, no. 6, pp. 703–710, 2019.

[16] F. Belkadi, J. Le Duigou, L. Dall'Olio, G. Besombes, and A. Bernard, "Knowledge-based platform for traceability and simulation monitoring applied to design of experiments process: an open source architecture," *Journal of Engineering Design*, vol. 30, no. 8-9, pp. 311–335, 2019.

[17] F. Li, H. Li, B. Niu, and J. Chen, "Privacy computing: concept, computing framework, and future development trends," *Engineering*, vol. 5, no. 6, pp. 1179–1192, 2019.

[18] T. Sato, Y. Iwamoto, S. Hashimoto et al., "Features of particle and heavy ion transport code system (PHITS) version 3.02," *Journal of Nuclear Science and Technology*, vol. 55, no. 6, pp. 684–690, 2018.

[19] G. Wu, K. Wang, J. Zhang, and J. He, "A lightweight and efficient encryption scheme based on LFSR," *International Journal of Embedded Systems*, vol. 10, no. 3, pp. 225–232, 2018.

[20] S. Dong, "Improved label propagation algorithm for overlapping community detection," *Computing*, vol. 102, no. 10, pp. 2185–2198, 2020.
[21] R. He, Q. Li, B. Ai et al., "A kernel-power-density-based algorithm for channel multipath components clustering," *IEEE Transactions on Wireless Communications*, vol. 16, no. 11, pp. 7138–7151, 2017.

Hindawi
Scientific Programming
Volume 2022, Article ID 5891909, 9 pages
https://doi.org/10.1155/2022/5891909

Research Article

Coordinated Development of Logistics Development and Low-Carbon Environmental Economy Base on AHP-DEA Model

Jinlan Wang, Huiwen Li, and Huifang Guo

Management School, Hainan University, Haikou 570208, China

Correspondence should be addressed to Huiwen Li; 20125300210017@hainanu.edu.cn

Received 3 December 2021; Revised 26 December 2021; Accepted 6 January 2022; Published 2 February 2022

Academic Editor: Le Sun

With the intensification of global environmental pollution and the overexploitation of resources and energy, low-carbon environmental economy (LCEE) has become the important means for countries in the world to achieve sustainable economic, resource, and environmental development. Therefore, the research on the coordinated development of logistics development and LCEE is very necessary in the development of our country's LCEE. Firstly, this paper discusses the development level of logistics industry in Hainan Province from five aspects: energy consumption, carbon emission, carbon productivity, economic benefit index, and carbon emission efficiency. Secondly, choose carbon emission intensity to represent the development level of low-carbon economy. Based on the efficiency coefficient method, coefficient of variation method, linear weighting method, spatial description method, and system evolution equation method, the coordination measurement method is adopted. Finally, the coordinated development of logistics development and low-carbon environmental economy in Hainan Province is analyzed. On this basis, this paper puts forward the related promotion strategies for the coordinated development of logistics development and logistics industry in Hainan. The research results show that the system coupling degree in Hainan Province is about 0.9, indicating that the logistics industry and the low-carbon economic subsystem have a relatively high degree of coupling development. Compared with other provinces, Hainan's level of coupled and coordinated development is at the upstream level.

1. Introduction

The LCEE is my country's face of global warming, high resource and energy consumption, high pollutant emissions, and increasingly severe atmospheric environment, so as to promote my country to seize the future economic and industrial development and raise the commanding heights. At present, countries all over the world are fiercely competing in new energy and new technologies, which also poses a very serious challenge to the development of my country's LCEE, but at the same time it is also a huge opportunity for the development of LCEE.

Literature [1] found that there is an interactive relationship by studying the relationship between the logistics industry and the regional economy. Logistics industry is more important in the development of regional economy, which affects the speed and efficiency of regional economy [2]. LCEE is the main line of controlling greenhouse gases such as carbon dioxide and changing energy [3], production, and lifestyles. The low-carbon environmental economic model [4] is a win-win model for the coordinated development of ecological environment and economic environment. The manufacturing industry and the logistics industry [5–9] are interdependent, but the linkage between the two will cause a lot of pollution, and we can promote the low carbonization of the two to reduce pollution. The logistics industry has been greatly developed after the emergence of e-commerce [10], and the logistics industry has become an important pillar industry for regional economic development. Nowadays, the logistics industry not only plays an important pillar role in the regional economy but also becomes a restrictive element of the speed and efficiency of the regional economy. There are still some problems in my country's logistics management [12], which lead to unreasonable resource allocation and serious waste. Concentrated, efficient, and economical [13–15] use of resources is an important way to achieve a low-carbon environment and economic development. The development of modern logistics has a certain positive effect on the intensive use of resources. To achieve low-carbon environmental economic development, it is necessary to further integrate and utilize existing logistics resources and strengthen the construction and connection of logistics infrastructure. It is of great significance to learn from foreign experience [16], explore my country's logistics development in a low-carbon environment economy, strengthen international strategic low-carbon logistics planning, formulate specific low-carbon logistics policies and regulations, and standardize low-carbon logistics goals. Green logistics has become one of the important directions for the development of modern logistics industry [17]. In order to promote the healthy development of green logistics, relevant departments must seize new opportunities and strive to build a trading support system consisting of an emission standard system, a trading rule system, and a supporting platform system.

2. The Coordinated Development of Logistics and LCEE

Coordination is the interaction and mutual influence between two or more systems. Coordination is in the nature of the development process overall effect of the interaction between the various elements of the system or generated, emphasizing the mutual cooperation between elements to achieve a stable and orderly development process.

Measurement methods play a great role in all fields of society; in the social and economic field, the main utilization aspects are the compound system such as the coupling of economy and ecological environment, the coupling of industry and urban development, and the coupling of economy and human settlement environment. The main research direction is the role of the relationship between subsystems in promoting the benign interactive development of the compound system. Coordination measurement methods mainly include the following: based on efficiency coefficient, coefficient of variation method, linear weighted sum method, spatial description method, system evolution equation method, etc., as shown in Table 1.

Comparing and analyzing the advantages and disadvantages of the above coordination measurement methods based on the efficiency coefficient method can better reflect the coordinated development of logistics economy, so this paper chooses the efficiency coefficient method to analyze the coordinated development of logistics economy.

3. DEA Model

3.1. Carbon Emission Estimation Method. At present, there is no special statistical data or calculation standard of carbon emissions in China, so we can only estimate carbon emissions. In this paper, the IPCC inventory method is chosen, which uses the carbon emission coefficient and energy consumption in the National Greenhouse Gas Inventory Guide. Its advantages are easy to obtain data and wide application range. Therefore, referring to other literature studies, this paper selects the IPCC inventory preparation method to estimate carbon emissions, and the specific calculation formula is defined.

$$C^t = \sum_{i=1}^{n} E_i^t \theta_i \delta_i. \tag{1}$$

Here, C^t is the carbon emission of regional logistics in the t period, E_i^t is the energy consumption in the t period i, including raw coal, coke, crude oil, gasoline, kerosene, diesel, fuel oil, natural gas, and liquefied petroleum gas (nine types of energy), θ_i is the reference coefficient of the i-th energy converted into standard coal, and δ_i is the carbon emission coefficient of the i-th energy.

3.2. Carbon Productivity. Carbon productivity is the GDP output efficiency per unit of carbon dioxide, and its role is to reflect the economic benefits produced by the unit of carbon dioxide emissions. Carbon productivity is also defined as the reciprocal relationship between "carbon average" and "unit carbon emission intensity". The process of reducing carbon emissions is the process of increasing carbon productivity, and the decline of carbon intensity indicates the improvement of carbon productivity. The specific calculation formula is as follows:

$$\text{carbon productivity} = \frac{\text{output}}{CO_2 \text{ emission}}. \tag{2}$$

3.3. Carbon Emissions Per Capita. Social and economic development should not only consider the carrying capacity of ecological environment, more consideration should be given to the rational distribution, but also been unanimously recognized internationally. Per capita carbon emissions can exclude the influence of regional population size, so per capita carbon emissions can better reflect the characteristics of total carbon emissions. The calculation formula is as follows:

$$\text{carbon emissions per capita} = \frac{CO_2 \text{ emissions}}{\text{number of people}}. \tag{3}$$

3.4. Economic Efficiency Index (EEI). The rapid growth of social economy is closely related to regional carbon emissions. Therefore, this paper draws lessons from other literature studies. The EEI is used to measure the relationship between GDP and carbon emissions in various provinces of China. That is, the EEI is equal to the proportion of the contribution rate of logistics industry to GDP and the contribution rate of logistics industry carbon emissions to overall carbon emissions. If the proportion of carbon emissions of logistics industry in a province is greater than the contribution rate of GDP, it indicates that the economic efficiency is relatively low. The logistics industry in the province and other banks interact in carbon emissions, whereas the regional economic efficiency is relatively high.

Table 1: System evolution equation method.

Method	Formula	Advantages and disadvantages
Multivariable synthesis method	$C=\sum_{i=1}^{n} w_i U_A(u_i)$ where A is the stable region of the system; effect of $U_A(u_i)$ as variable u_i on system order	The calculation is simple and easy to operate, and the reference index determination is inconsistent and the comparability is poor
Efficiency coefficient method	$C=\left\{f(X)g(Y)/[f(X)+g(Y)/2]^2\right\}^k D=C,T; T=\alpha f(x)+\beta g(y)$ where $f(x)$ and $g(y)$ are evaluation functions; $C\in[0,1]$; D is coordination degree, T is comprehensive evaluation index, and α and β are weights	It is simple and easy to introduce order parameters, and it is difficult to select reasonable indexes
Coefficient of variation method	$C=\alpha c_m+\beta c_n+\gamma c_u$ where $\alpha,\beta,$ and γ are coefficients; $c_m, c_n,$ *an d* c_u are subsystems	The model is simple, the principle is clear, and the selection of the two system indexes should be accurate and representative
Spatial description method	$I_{XY}(C(t))=1-\sqrt{\alpha_1[I_x(t)-I_{XY}(t)]^2-\alpha_2[I_Y(t)-I_{XY}(t)]^2}$. Among them, X and Y are two subsystems; $I_x(t)$ and $I_Y(t)$ are the degrees of development of two subsystems; $I_{XY}(t)$ is the average level of the development of two subsystems; α_1 and α_2 are the weights	Analyze the coordination degree from static and dynamic; to calculate the coordination degree of multisystem, the model is complex and the amount of calculation is large
System evolution equation	$\mathrm{d}x(t)/\mathrm{d}t=f(x_1,x_2\ldots x_n)V_A=\mathrm{d}A/\mathrm{d}t\, V_B=\mathrm{d}B/\mathrm{d}t \tan\theta=V_A/V_B$. Among them, A and B are two subsystems; V_A and V_B are the evolution rates of the two subsystems; θ is the coupling degree of the coupled system	Considering the dynamic changes of the system with time, the coordination degree of the system is divided into absolute coordination degree and relative coordination degree, which is complicated in operation and requires high continuity of indicators and data

$$\mathrm{EEI}=\frac{GL_i/G_I}{CL_i/C_i}, \tag{4}$$

where GL_i and G_I are the output value of logistics industry and GDP of each province and the carbon emissions of logistics industry in CL_i and C_i and the total carbon emissions of each province.

3.5. Calculation Method of Carbon Emission Efficiency. Carbon emission efficiency refers to the maximum output capacity under constant input, or the minimum input required for a certain output. The DEA model has been used to study carbon emission efficiency in many literature studies. DEA models include CCR, BCC, etc. The CCR model takes decision-making efficiency as the final goal and constructs the DEA model with constant return to scale. Adding constraints to the CCR model becomes the BCC model. The traditional DEA and BCC models are constructed to measure the technical efficiency of carbon dioxide emissions. The BCC model can be expressed as follows:

$$\mathrm{Min}\left[\theta_{i_0}-\varepsilon\left(e^T s^+ + e^T s^-\right)\right], \tag{5}$$

$$\text{s.t.}\left\{\sum_{i=1}^{N} x_i\lambda_i + s^- = \theta_{i_0}x_{i_0}\sum_{i=1}^{N} y_i\lambda_i - s^+ = y_{i_0}\sum_{i=1}^{N}\lambda_i = 1,\quad \lambda_i\ge 0,\ i=1,2,\ldots,ns^+\ge 0, s^-\ge 0.\right. \tag{6}$$

Here, s^+ and s^- are slack variables, e^T is the unit row vector, θ_{i_0} is the relative efficiency value of the decision-making unit, and λ is the weight vector.

4. Analysis of the Characteristics of the Logistics Industry

4.1. Carbon Emissions of the Logistics Industry in Provinces. According to formula (1), the carbon emissions of logistics industry in China's provinces from 2016 to 2019 are calculated, as shown in Table 2.

The carbon emissions of logistics industry in China's provinces maintained a rapid growth trend from 2016 to 2019, and there were great differences and imbalances in carbon emissions among provinces. At present, the development of China's logistics industry depends on energy consumption, mainly traditional coal and oil. Although the logistics industry has grown rapidly, it has led to more carbon dioxide emissions. Therefore, the development of China's logistics industry needs to change to the development mode of low emission, high efficiency, and high energy efficiency and get rid of the traditional extensive

Table 2: Carbon emissions of the logistics industry in China's provinces from 2016 to 2019 (unit: 10,000 tons).

Province	2016	2017	2018	2019
Beijing	443.9	558.4	648.1	684.8
Tianjin	179.6	236.2	284.1	335.7
Hebei	486.6	537.2	569.8	701.1
Shanxi	333.5	473.1	524	553.8
Inner Mongolia	654.2	776.9	934.1	1083.2
Liaoning	844.5	982.7	1123.2	1289.7
Jilin Province	200.3	254.8	290.4	351.1
Heilongjiang	267.4	281.9	505.8	571.7
Shanghai	951	1034.1	1092.5	1103.2
Jiangsu	561.5	681.9	853.5	1004.6
Zhejiang	578.1	730	819.5	915.6
Anhui Province	242.7	379	467.4	577.9
Fujian	337.4	440.2	504.7	598.3
Jiangxi	213.2	269.3	327.2	383.9
Shandong	1089.3	1451.3	1676.5	2126.1
Henan	497.5	599.3	709.8	757.1
Hubei	590.2	684.6	842.5	999.4
Hunan	355	455.1	548.5	613.3
Guangdong	1062.3	1379.5	1582.1	1826.7
Guangxi	309.4	378.5	448.3	581.7
Hainan	80.7	152.7	176.6	178.9
Chongqing	267.1	342.4	400.1	451.6
Sichuan	470.4	622.5	699.5	782.1
Guizhou	206.7	257.4	330.6	427.7
Yunnan	352.3	387.9	519.3	595.1
Shaanxi	332.3	476.7	561.3	604
Gansu Province	200.7	226	241.2	245.2
Qinghai	38.1	59.9	75.7	76.2
Ningxia	34.7	62.8	86.9	96.6
Xinjiang	316.8	347.9	374.4	484.9

development mode, high energy consumption, and high pollution development mode.

The growth of coal and oil consumption in Hainan Province is not high from 2016 to 2019 in Table 3. Combined with Table 2, logistics industry level is lower than that of a province with large carbon emissions, but it provides a good environment for promoting the coordinated development of logistics development and LCEE.

4.2. Carbon Productivity Analysis. Carbon productivity, that is, the carbon emissions generated by unit GDP growth, is a relative indicator to measure the efficiency of carbon emissions and can also reflect the dependence of economic growth on high energy consuming industries. Therefore, this paper selects carbon productivity to measure the carbon emission level of regional logistics industry, and calculates the carbon productivity of logistics industry according to formula (2). The results are shown in Table 4.

As can be seen from Table 4, from 2013 to 2019, the carbon productivity of logistics industry in 30 provinces showed great differences. It can be seen that the carbon productivity of logistics industry in Hainan Province is on the rise and the growth rate is relatively large. The carbon productivity is as high as 20,000 yuan/ton of coal. The carbon productivity of logistics industry is much higher than that of other provinces. It means that Hainan Province pays more attention to the quality of economic growth while the logistics industry is growing rapidly, and can effectively use the input of science and technology, resources, and environment, so that the logistics industry has been effectively developed under the LCEE, and the good effect of coordinated development between logistics development and LCEE has been achieved.

4.3. Economic Efficiency Index Analysis. According to formula (4), the EEI of logistics industry in China's provinces from 2013 to 2019 is calculated, as shown in Table 5.

As can be seen from Table 5, on the whole, the EEI of Hainan Province from 2013 to 2019 was less than 0.5. It shows that the development of logistics industry in Hainan Province depends on the development mode of high energy input and high carbon emission output to a great extent, and the low level of energy utilization efficiency in the development of logistics industry means that the utilization of energy efficiency in the development of logistics industry in Hainan Province needs to be improved urgently. However, in 2018–2019, the EEI of Hainan Province has greatly increased to 0.93. Combined with Table 4, it shows that Hainan Province is actively developing LCEE, changing the development mode of logistics industry, and striving to achieve coordinated development of logistics development and LCEE.

4.4. Calculation of Carbon Emission Efficiency of the Logistics Industry. In this paper, DEAP2.1 software is used to solve formulas (5) and (6), and the carbon emission efficiency of logistics industry in 30 provinces of China from 2013 to 2019 is calculated. The results are shown in Table 6.

The carbon emission efficiency of logistics industry in Hainan Province is about 0.8 in Table 6, and the carbon emission efficiency is relatively high, indicating that Hainan Province pays more attention to the effective utilization of labor, capital, energy, and environment. Improving the utilization rate of all elements of logistics development is also conducive to the transformation of logistics development mode to low carbon and promotes the coordinated development of logistics development, low-carbon environment, and economy.

5. Analysis of Coordinated Development between Logistics Development and LCEE

5.1. Construction of the Evaluation Index System. Low energy consumption, low emission, and high efficiency are the advantages of LCEE. LCEE requires China to transform to low carbon. The evaluation idea of coordinated development of logistics industry and low-carbon economy is shown in Figure 1. Firstly, after a large number of literature retrieval, the index system is sorted out; second, scientific treatment of indicators; thirdly, obtain the original data of indicators by inquiring the statistical yearbook; and fourthly, this paper analyzes the coordination degree and coupling degree between logistics industry and low-carbon economy by using

Table 3: Total energy consumption structure between Hainan Province and the whole country.

Year	Coal		Oil	
	Hainan	Whole country	Hainan	Whole country
2016	30.72	71.1	39.22	18.8
2017	30.02	70.3	40.68	18.3
2018	32.12	70.4	41.68	17.9
2019	31.63	68	40.34	19

Table 4: Carbon productivity of the logistics industry in China's provinces from 2013 to 2019.

Province	2013	2014	2015	2016	2017	2018	2019
Hainan	1.83	1.87	2.12	2.21	2.53	2.58	2.51
Beijing	1.13	0.92	1.04	1.17	1.26	1.25	1.29
Tianjin	1.57	1.49	2.05	2.25	2.31	2.33	2.15
Hebei	2.34	2.49	2.83	3.25	3.66	3.69	3.37
Shandong	1.29	1.12	1.15	1.3	1.49	1.58	1.61
Shanghai	0.79	0.91	1.03	1.01	1.14	1.19	1.2
Jiangsu	0.77	0.75	0.84	0.85	1.05	1.17	1.07
Zhejiang	1.32	1.4	1.4	1.36	1.49	1.44	1.38
Guangdong	1.33	1.57	1.58	1.68	1.11	1.17	1.08
Fujian	0.77	0.74	0.65	0.73	0.82	0.84	0.85
Shaanxi	1.27	1.26	1.24	1.33	1.5	1.5	1.44
Shanxi	1.92	1.76	1.27	1.15	1.29	1.29	1.21
Inner Mongolia	1.88	1.77	1.75	1.78	1.95	2.08	1.95
Henan	1.52	1.55	1.51	1.54	1.6	1.8	1.75
Hubei	1.28	1.5	1.22	1.2	1.41	1.39	1.28
Hunan	1.72	1.81	1.41	1.28	1.38	1.57	1.72
Jiangxi	0.81	0.83	0.97	1.02	1.05	1.14	1.07
Anhui	1.32	1.3	1.59	1.58	1.77	1.84	1.9
Gansu Province	1.18	1.16	1.18	1.18	1.34	1.71	1.41
Qinghai	0.98	0.99	1.03	1.14	1.35	1.33	1.15
Ningxia	0.96	0.73	0.62	0.61	0.72	0.8	0.77
Xinjiang	0.97	0.96	1.05	1.01	1.17	1.23	1.27
Guangxi	1.07	1.05	0.86	0.85	0.93	0.97	0.95
Chongqing	0.77	0.73	1.6	1.62	1.84	1.82	1.8
Sichuan	0.55	0.59	0.49	0.38	0.43	0.47	0.45
Guizhou	0.92	0.88	0.92	0.9	1.01	1.09	1.08
Yunnan	0.87	0.97	0.99	0.99	1.21	1.36	1.4
Liaoning	0.86	0.82	0.92	0.98	1.01	1	0.95
Jilin Province	1.25	1.3	2.01	1.95	2.22	2.28	2.06
Heilongjiang	0.55	0.57	0.63	0.61	0.71	0.8	0.86

index standardization data and weight, so as to provide theoretical basis for the coordinated development of logistics development and LCEE in China.

The construction principles of evaluation index system are as follows: 1. Scientific principle; 2. the principle of low carbonization; and 3. dynamic principle. China's logistics industry has high GDP, low energy utilization rate, and high carbon emissions. Under the constraint of resources and environment, it depends on resource elements and has a great impact on ecological environment. The proposal of low-carbon economy can promote the transformation of China's logistics industry to low-carbon development mode, so as to consume less resources, improve energy utilization rate, reduce carbon emissions and obtain higher output, and realize the sustainable development of resources and environment. Referring to the relevant literature research results, this paper selects the evaluation index from three aspects: economic aggregate, economic scale, and economic benefit for regional economy, and selects the logistics subsystem from three aspects: logistics industry scale, logistics industry structure, and logistics benefit, and constructs the index system of coordinated development between logistics industry and low-carbon economy, as shown in Table 7.

Table 5: Economic benefit index of the logistics industry in each province from 2013 to 2019.

Province	2013	2014	2015	2016	2017	2018	2019
Hainan	0.35	0.28	0.35	0.33	0.36	0.31	0.93
Beijing	0.22	0.15	0.19	0.17	0.17	0.12	0.28
Tianjin	0.54	0.38	0.55	0.6	0.57	0.47	0.84
Hebei	1.03	1.06	1.16	1.29	1.4	1.28	3.13
Shandong	0.53	0.39	0.43	0.4	0.38	0.39	0.77
Shanghai	0.23	0.22	0.27	0.2	0.22	0.16	1.58
Jiangsu	0.55	0.47	0.48	0.45	0.5	0.49	0.83
Zhejiang	0.44	0.35	0.33	0.28	0.31	0.22	0.85
Guangdong	0.49	0.44	0.53	0.47	0.29	0.25	0.81
Fujian	0.23	0.2	0.18	0.17	0.19	0.16	0.3
Shaanxi	0.25	0.21	0.23	0.21	0.23	0.18	0.48
Shanxi	0.37	0.28	0.21	0.15	0.17	0.13	0.64
Inner Mongolia	0.29	0.21	0.29	0.29	0.29	0.25	0.64
Henan	0.31	0.25	0.28	0.24	0.24	0.23	0.67
Hubei	0.38	0.38	0.33	0.31	0.36	0.32	0.8
Hunan	0.29	0.25	0.2	0.16	0.19	0.19	0.94
Jiangxi	0.23	0.19	0.23	0.18	0.18	0.14	0.51
Anhui	0.28	0.21	0.26	0.21	0.21	0.2	0.71
Gansu	0.23	0.18	0.22	0.18	0.2	0.21	0.39
Qinghai	0.19	0.15	0.18	0.18	0.27	0.25	0.54
Ningxia	0.68	0.44	0.37	0.3	0.33	0.29	0.4
Xinjiang	0.13	0.1	0.12	0.08	0.12	0.1	0.47
Guangxi	0.21	0.17	0.16	0.13	0.15	0.11	0.35
Chongqing	0.19	0.13	0.28	0.24	0.26	0.19	1.79
Sichuan	0.2	0.16	0.14	0.09	0.11	0.08	0.29
Guizhou	0.36	0.29	0.33	0.27	0.28	0.25	0.81
Yunnan	0.6	0.56	0.56	0.45	0.53	0.5	1.27
Liaoning	0.27	0.25	0.3	0.26	0.26	0.21	0.66
Jilin	0.4	0.5	0.72	0.57	0.58	0.79	1.15
Heilongjiang	0.37	0.34	0.39	0.34	0.39	0.37	1.05

5.2. Coordinated Development Model. The efficiency coefficient of logistics industry and low-carbon economy subsystem to system order can be expressed as follows:

$$u_{ij} = \begin{cases} \dfrac{x_{ij} - \beta_{ij}}{\alpha_{ij} - \beta_{ij}}, \\ \\ \dfrac{\alpha_{ij} - x_{ij}}{\alpha_{ij} - \beta_{ij}}. \end{cases} \tag{7}$$

In formula (7), u_{ij} is the contribution degree of the variable x_{ij} to the efficiency function of the coupled system, and α_{ij} and $\beta_{ij,}$ respectively, represent the upper and lower limit values of the sequence parameter of the stability critical point of the coupled system.

Because the logistics industry subsystem and the low-carbon economy subsystem are interactive but different, the

Table 6: Carbon emission efficiency of the logistics industry in each province from 2013 to 2019.

Province	2013	2014	2015	2016	2017	2018	2019
Hainan	0.82	0.87	0.83	0.78	0.72	0.69	0.88
Beijing	0.85	0.88	1.02	0.83	0.78	0.68	0.98
Tianjin	0.77	0.73	1.02	0.68	0.73	0.74	0.98
Hebei	0.57	0.56	0.76	0.73	0.78	0.71	0.85
Shandong	0.68	0.63	0.61	0.52	0.6	0.55	0.88
Shanghai	0.69	0.6	1.02	0.85	0.81	0.82	0.98
Jiangsu	0.72	0.69	1.02	0.77	0.84	0.83	0.8
Zhejiang	0.73	0.82	0.82	0.81	0.79	0.72	0.97
Guangdong	0.66	0.63	1.02	0.8	0.88	0.84	0.82
Fujian	0.77	0.72	0.81	0.67	0.66	0.68	0.98
Shaanxi	0.81	0.79	0.74	0.72	0.78	0.75	0.83
Shanxi	0.57	0.65	0.78	0.77	0.84	0.8	0.74
Inner Mongolia	0.64	0.68	0.79	0.7	0.77	0.74	0.75
Henan	0.68	0.67	0.85	0.85	0.85	0.8	0.76
Hubei	0.66	0.75	0.94	0.89	0.92	0.89	0.89
Hunan	0.72	0.65	0.72	0.7	0.73	0.71	0.66
Jiangxi	0.75	0.67	0.78	0.81	0.85	0.83	0.78
Anhui	0.8	0.82	0.88	0.88	0.94	0.91	0.89
Gansu	0.89	0.78	1.02	0.92	1.01	0.99	0.85
Qinghai	0.6	0.58	0.7	0.68	0.76	0.72	0.74
Ningxia	0.68	0.56	0.81	0.8	0.83	0.75	0.98
Xinjiang	0.63	0.72	0.84	0.8	0.82	0.83	0.98
Guangxi	0.66	0.66	0.76	0.75	0.61	0.6	0.98
Chongqing	0.53	0.51	0.55	0.45	0.52	0.51	0.74
Sichuan	0.51	0.47	0.54	0.52	0.57	0.56	0.89
Guizhou	0.61	0.69	0.75	0.76	0.69	0.69	0.93
Yunnan	0.49	0.46	0.49	0.45	0.53	0.49	0.98
Liaoning	0.68	0.71	0.54	0.53	0.54	0.51	0.98
Jilin	0.58	0.53	0.57	0.55	0.64	0.57	0.69
Heilongjiang	0.42	0.49	0.58	0.57	0.57	0.51	0.73

total contribution to the order degree of each parameter in the subsystem is expressed by the integration method, using geometric average method and linear weighted sum method:

$$u_i = \sum_{i=1}^{m} \lambda_{ij} u_{ij},$$
$$\sum_{j=1}^{m} \lambda_{ij} = 1. \tag{8}$$

Here, u_{ij} is the order parameter of the system and λ_{ij} is the weight of each order parameter.

5.3. System Coupling Degree Model. The concept and model of capacitive coupling in physics are introduced in this paper, which is applied to the interaction between multiple subsystems. The coupling model can be expressed as follows:

$$C_n = \left\{ \frac{u_1, u_2 \cdots u_m}{\left[\prod\left(u_i + u_j\right)\right]} \right\}^{1/n}, \quad C \in [0,1], \tag{9}$$

where $n = 2$; the formula evolves as shown in formula (10), which represents the coupling model of the composite system:

$$C = \sqrt{\frac{(u_1 \times u_2)}{(u_1 + u_2)^2}}. \tag{10}$$

Here, the coupling degree index of logistics industry and low-carbon economy complex system is C, which means that the comprehensive evaluation indexes of logistics industry and low-carbon economy development are u_1 and u_2, respectively.

This paper constructs the coupling coordination function between logistics system and low-carbon economy system to reflect the coupling of the system. The coordination model of the composite system is as follows:

$$T = \alpha u_1 + \beta u_2,$$
$$D(u_1, u_2) = \sqrt{C \times T}. \tag{11}$$

Here, T is the low-carbon comprehensive development index; D is the coordinated development index; C, u_1, u_2 are the same as above; α, β are undetermined coefficients; and the value is 0.5 in this paper.

5.4. Criteria for the Division of Coordinated Development. According to the coupling theory, this paper divides the coordination types of logistics industry and low-carbon economy into six types: $C = 1$ is benign resonance coupling; $0.8 < C < 1$ is high level coupling; $0.5 < C < 0.8$ is the running-in period; $0.3 < C \leq 0.5$ is the antiseptic period; $0 < C \leq 0.3$ is low level coupling; and $C = 0$ is the irrelevant state. The coordination degree of the coupling system between logistics industry and regional economy is divided into twelve types and seven comparative relationship types in Table 8.

5.5. Correlation Analysis between Logistics Development and Low-Carbon Economy. Using formula (11), the coordinated development degree of composite system in Hainan Province from 2010 to 2020 is obtained, and the calculation results are shown in Table 9.

The coupling degree of Hainan's logistics industry and low-carbon economic development is in the range of 0.9–1.0, and the coupling degree is at a relatively high level of development, indicating that Hainan's logistics development and LCEE have a relatively high level of coordinated development.

Figure 2 shows that in the process of economic development, the influence of the three industries changes. Because Hainan's economy is a province of tourism economy, the tertiary industry, as a pillar industry, shows a strong economic growth rate and proportion. The development of primary industry and secondary industry is relatively slow and the proportion is small.

In Figure 3, we can see that under the low-carbon economic environment of Hainan Province, the GDP of each region is on the rise. Combining Table 10 and Figure 2, we can see that the tertiary industry where the logistics

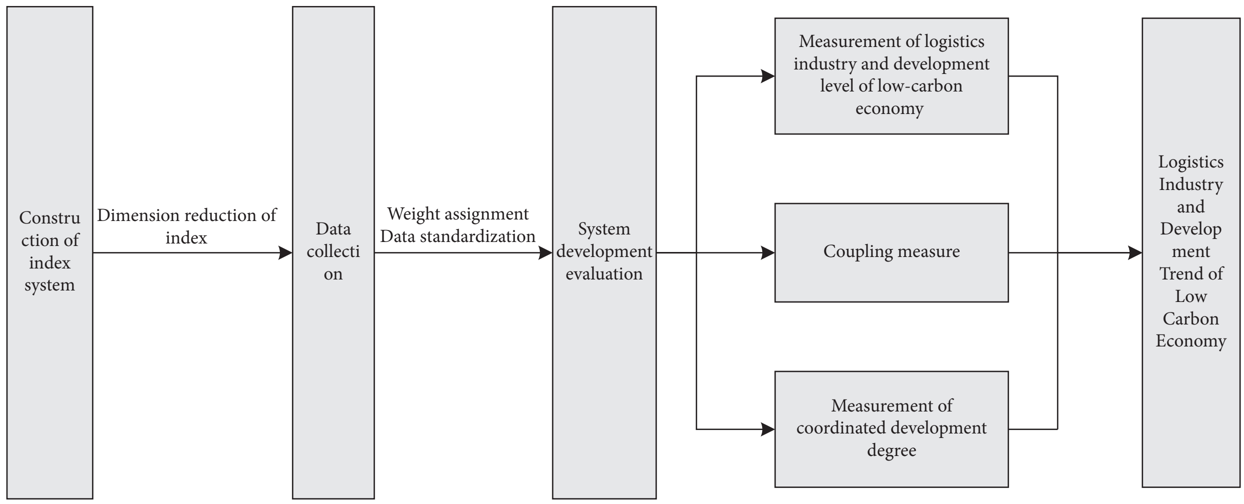

Figure 1: The evaluation idea of coordinated development of logistics industry and low-carbon economy.

Table 7: Evaluation index system of the logistics industry and low-carbon economy system.

System	First-class index	Secondary index	Indicator interpretation
Economic system	Economic aggregate	Per capita GDP	Reflect the level of regional economic development (100 million yuan)
		Investment in fixed assets of the whole society	Including the construction and purchase of fixed assets (100 million yuan)

Table 8: Classification and standards of coordinated development of logistics industry and low-carbon economy.

Degree of coordination	Coupling coordination type	Value range	Types of contrast relation between u_1 and u_2
Extreme coordination	Extreme coupling coordination	$0.90 < D \leq 1.0$	$u_1 < u_2$: logistics industry lagging
	High-quality coupling coordination	$0.80 < D \leq 0.90$	$0.8 < u_1/u_2 \leq 1$: the logistics industry is relatively lagging
Highly coordinated	Good coupling and coordination	$0.70 < D \leq 0.80$	$0.6 < u_1/u_2 \leq 0.8$: the logistics industry is seriously lagging behind
	Intermediate coupling coordination	$0.60 < D \leq 0.70$	$0 < u_1/u_2 \leq 0.6$: the logistics industry is extremely lagging
Moderate coordination	Primary coupling coordination	$0.50 < D \leq 0.60$	$u_1 > u_2$: low-carbon economy lagging
	Harmony and coordination	$0.40 < D \leq 0.50$	$0.8 < u_1/u_2 \leq 1$: low-carbon economy is relatively lagging
	Reluctantly reconcile and coordinate	$0.30 < D \leq 0.40$	$0.6 < u_1/u_2 \leq 0.8$: low-carbon economy severely lagging behind
Low coordination	Mild incongruity	$0.20 < D \leq 0.30$	$0 < u_1/u_2 \leq 0.6$: low-carbon economy extremely lagging
	Serious incongruity	$0.10 < D \leq 0.20$	$u_1 = u_2$: the logistics industry and the low-carbon economy are synchronized
	Extremely incongruous	$0 \leq D \leq 0.10$	

Table 9: Coupling degree between the logistics industry and low-carbon economy in Hainan.

Province	2010	2011	2012	2013	2014	2015	2016	2017	2018	2019	2020
Hainan	0.95	0.92	0.93	0.9	0.91	0.89	0.93	0.97	0.92	0.93	0.98

industry of Hainan Province is located accounts for the total production of Hainan Province. About 45% of the value and the tertiary industry GDP value added by Hainan Province's logistics industry far exceeds that of other industries. With a relatively high level of coordinated development of logistics development and LCEE, the logistics industry in Hainan

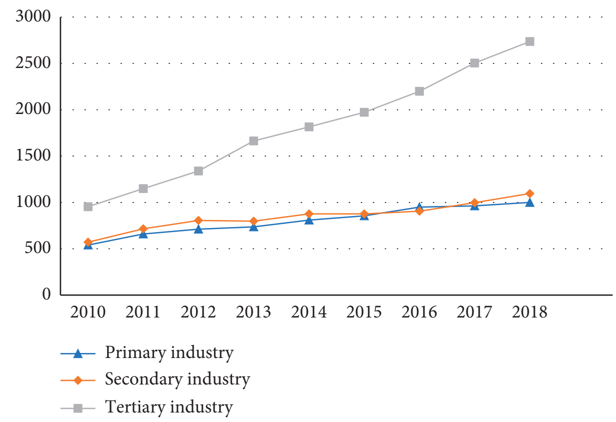

FIGURE 2: Trend chart of added value of three major industries in Hainan Province from 2010 to 2018.

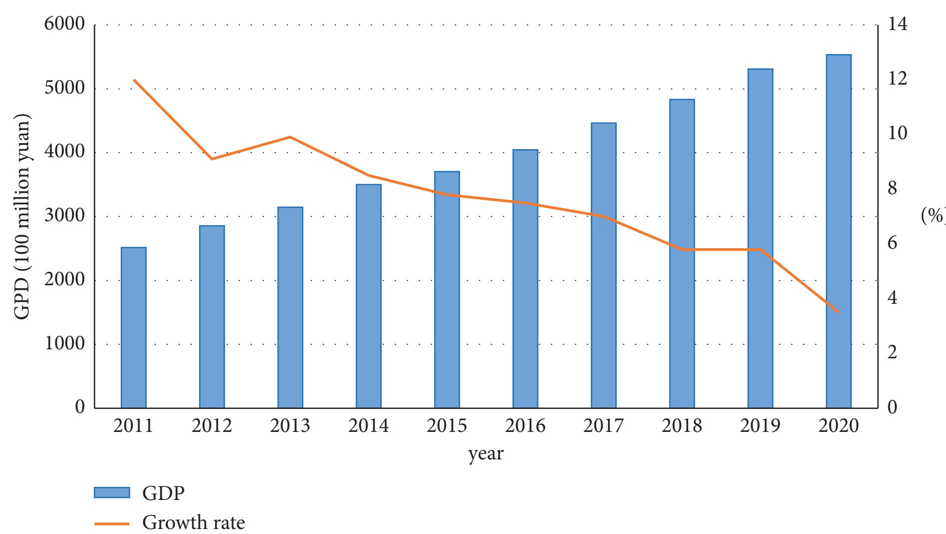

FIGURE 3: The province's GDP in a low-carbon environment from 2011 to 2020.

TABLE 10: GDP structure of Hainan Province from 2010 to 2020.

Industry	2010	2011	2012	2013	2014	2015	2016	2017	2018	2019	2020
Primary industry	26.1	26.1	24.9	24.6	24.4	24.1	24	22.3	21	20.35	20.5
Secondary industry	27.7	28.3	28.2	26	24.8	23.6	22.3	22	23	20.07	19.1
Tertiary industry	46.2	45.6	46.9	49.4	50.8	52.3	53.7	55.7	57	58.95	60.4

Province has been developing rapidly. It has done a very good job in the coordinated development of low-carbon environment and economy.

6. Conclusion

The logistics industry is the main driving force of my country's current economic growth and social progress. However, the proposal of an LCEE has brought severe challenges to the subsequent development of my country's logistics industry. The coordinated development of low-carbon environment and economy is also a huge development opportunity. Under the serious threat of the shortage of resources and energy in our country and the destruction of the ecological environment, the coordinated development of logistics and LCEE is imperative. In order to realize the sustainable development of resources, environment, and social economy, it is necessary to study the coordinated development of logistics development and LCEE. Taking Hainan Province as an example, this paper constructs an evaluation index system for the coordinated development of Hainan's logistics development and low-carbon economy and uses a coupling coordination model to measure the coordinated development of China's Hainan Province's logistics industry and low-carbon economy.

Data Availability

The experimental data used to support the findings of this study are available from the corresponding author upon request.

Conflicts of Interest

The authors declare that they have no conflicts of interest regarding this work.

References

[1] L. Zhang, Q. L. Dong, and S. Liang, "A study on the coordinated development of node cities logistics industry and regional economy——based on the panel data of national logistics node cities," *East China Economic Management*, vol. 29, no. 2, pp. 67–73, 2015.

[2] H. Zheng, "Research on the coordinated development of logistics industry and economy in Hebei Province," in *Proceedings of the International Conference on Future Information Technology & Management Engineering*, pp. 321–324, IEEE, Changzhou, China, October 2010.

[3] C. Jianhua, "Study on the coordinated development of circular economy and low carbon economy," in *Proceedings of the 2016 International Conference on Tourism and Development (ICTD2016)*, pp. 233–238, Hainan, China, October 2016.

[4] Z. Q. Wang, W. Q. Tian, and J. Wang, "A research on the development of low-carbon economy based on the view of the logistics industry," *Advanced Materials Research*, vol. 573-574, pp. 955–959, 2012.

[5] M. Lei, H. Yang, X. Xiao, L. Ye, and J. Zhou, "Industry linkage and low-carbon development——based on logistics industry & manufacturing industry," *Meteorological and Environmental Research*, vol. 5, no. 8, pp. 10–22, 2017.

[6] C. Feng, L. Yisheng, and H. Guowei, "Analysis of the development of low-carbon logistics based on a low-carbon economy," in *Proceedings of the International Conference on Low-Carbon Transportation and Logistics, and Green Buildings(LTLGB 2012)*, pp. 673–679, Springer, Beijing, China, May 2013.

[7] M. Qingguo, "Study on the coordinated development of energy resources based on low-carbon economy," *Ecology and Environmental Sciences*, vol. 20, no. 12, pp. 192–195, 2011.

[8] M. Shi, "Environmental pollution and measurement of low-carbon logistics efficiency in China's logistics industry," *Nature Environment and Pollution Technology*, vol. 17, no. 4, pp. 1339–1346, 2018.

[9] J. Bao and H. Li, "Study on the harmonious development of carbon emission and eco-environment in logistics industry --taking beijing-tianjin a- hebei as an example," *IOP Conference Series: Earth and Environmental Science*, vol. 450, no. 1, Article ID 012069, 2020.

[10] W. Qian, Q. Jian, S. O. Business, and J. University, "Research on the coordinated development of logistics industry efficiency and economic growth based on node city," *Journal of Industrial Technological Economics*, vol. 295, no. 5, pp. 21–30, 2018.

[11] H.-l. Zheng, "The research about coordinated development of logistics industry and economy in Hebei province," in *Proceedings of the 2010 International Conference on Future Information Technology and Management Engineering (FITME 2010)IEEE*, pp. 321–324, Jiangsu, China, October 2010.

[12] D. F. Wang and L. Resourcesamp, "Implementation of green logistics management strategy under low carbon economy environment," *Logistics Engineering and Management*, vol. 39, no. 1, pp. 55-56, 2017.

[13] M. Q. Zhang, Y. Zhou, and C. L. Zhou, "A study on coordinated development of logistics industry and regional economy based on symbiotic theory," *Journal of Beijing Jiaotong University*, vol. 11, no. 1, pp. 33–40, 2012.

[14] Z. Tang and L. Zhou, "Empirical research on influence to low carbon economy of logistics industry development," *Ecological Economy*, vol. 32, no. 11, pp. 84–87, 2016.

[15] F. Xie, X. J. Huang, and R. Q. Jiang, "An evaluation on coordinate development of China's modern logistics and low carbon economy," *Journal of Jiangxi University of Finance and Economics*, vol. 93, no. 3, pp. 11–19, 2014.

[16] Q. Ren, "Influence of low carbon logistics industry in foreign countries on development of China's low carbon logistics industry," *Environmental Science and Management*, vol. 43, no. 9, pp. 41–44, 2018.

[17] B. Dong, "Low carbon economy and the development of China's green logistics," *China Circulation Economy Editorial Department*, vol. 25, no. 5, pp. 33–37, 2011.

Hindawi
Scientific Programming
Volume 2022, Article ID 7479361, 8 pages
https://doi.org/10.1155/2022/7479361

Research Article

Study on Low-Cost, Low-Voltage Multiprogrammable Nonvolatile Memory Cells for UHF Tag Chips

Na Bai, Chao Li, Yao Hua Xu, and Yi Wang

Key Laboratory of Computational Intelligence and Signal Processing, Ministry of Education (Anhui University), School of Integrated Circuit, School of Electronic Information Engineering, Anhui University, Hefei 230601, China

Correspondence should be addressed to Yao Hua Xu; xyh@ahu.edu.cn

Received 30 September 2021; Accepted 9 December 2021; Published 31 January 2022

Academic Editor: Hai Dong

This paper proposes a low-voltage, low-cost multiple-time-programmable nonvolatile memory (MTP NVM) based on a standard CMOS 0.13 μm process for UHF RFID chip applications. The design of the differential structure cell using the tunneling effect reduces the read and write voltage. The read and write simulation test results show that the read and write operating voltage is 10 V, which is 30% lower than that of conventional EEPROMs. Because the UHF RFID tag chip requires higher voltage reduction, the structured memory cell is well suited for UHF RFID applications.

1. Introduction

In Ultra High Frequency (UHF) Radio Frequency Identification RFID tag chips, nonvolatile memory (NVM) occupies an important position in the entire UHF RFID tag as the carrier for storing information. Since NVM consumes most energy in a UHF tag chip, the voltage of NVM will have the most direct impact on the overall tag cost. To reduce the cost of the UHF tag chip, the NVM part must be designed for low voltage. Electrically erasable memory (EEPROM) is used as the memory for RFID tags by traditional RFID manufacturers due to its mature technology. In a conventional UHF tag chip, the NVM is the main power consumption module of the tag chip when it performs write operations. Because NVM needs charge pump to generate high voltage to provide voltage signal to the corresponding location of the storage unit when writing, reducing voltage becomes extremely important for NVM of UHF tags. Reducing the read/write voltage and cost of the NVM will be of great importance to the development of UHF RFID tag chips.

In this paper, we propose an MTP NVM cell based on the standard CMOS process to address the high operating voltage of EEPROM. The cell is a differential structure, which reduces the read and writes voltage. It has lower cost and lower voltage than the conventional EEPROM memory cell.

2. System Architecture and Storage Units

The basic composition of the tag chip is shown in Figure 1, which includes the Radio Frequency (RF) analog front-end, digital baseband, and memory three parts [1]; the main role of each part in the entire tag chip is as follows.

The RF analog front-end is the rectification of the modulated RF signal received from the antenna into a DC voltage that powers the entire chip and demodulates the modulated signal, thus enabling backscatter modulation, etc. The function of the digital baseband module is to complete the processing of data. The digital baseband parses the commands transmitted by the analog front-end, responds to the commands according to the corresponding protocol, decodes the baseband signals and stores the information data in the memory. Alternatively, the data are obtained from the memory according to the command and are encoded and then transmitted to the analog front-end. The memory is to complete the storage of data.

The NVM system architecture consists of the components shown in Figure 2. Many storage units are arranged according to certain rules to form a storage array [2], and all data are stored in the storage array. Under the command and coordination of the built-in controller, the row decoder and row driver work together to allow the system to select a row

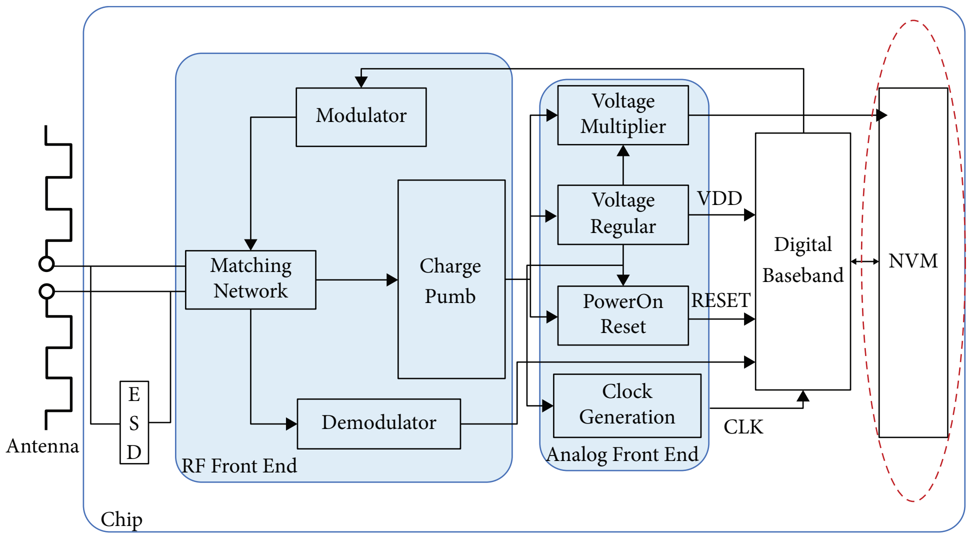

Figure 1: The basic components of a label chip.

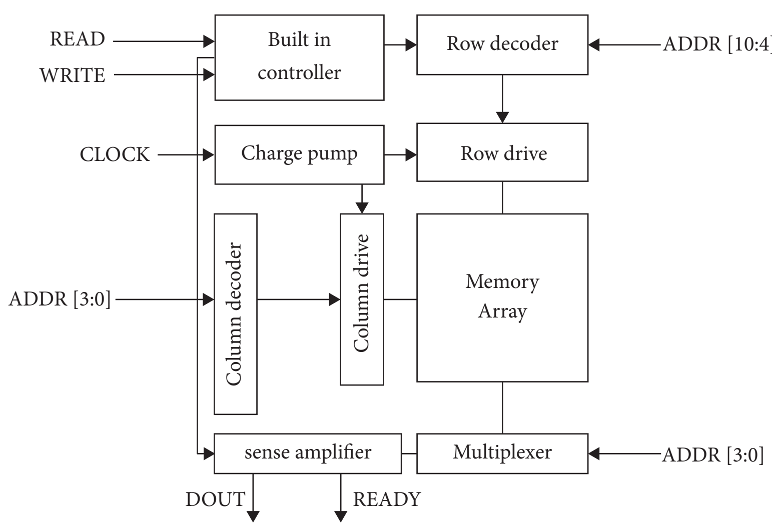

Figure 2: NVM system architecture.

(logically a word) in the array, while the column decoder, column driver, and multiplexer selector work together to select a column (logically a bit) within the selected word. The charge pump generates the high voltage required for programming during write operations. The sense amplifier converts the current analog given by the memory cell to digital logic levels during read operations.

The part of conventional RFID memory generally uses EEPROM memory cell, whose reference structure is shown in Figure 3. The structure has two transistors, M1 tube is used as a selector tube and its gate is connected to voltage VSG. M2 tube is used as a control tube to store data and its gate is connected to voltage VCG. When VCG and VSG are added with high voltage and VS and VD are grounded, a positive electric field is formed between the floating gate and the drain. Due to the F-N tunneling effect, electrons enter the floating gate from the drain side, causing the floating gate to accumulate a negative charge and the threshold voltage to rise. The above process is defined as an “erase” operation, when the data “1” is stored. When VCG is grounded, VSG and VD are connected to high voltage and VS is suspended, a negative electric field is formed between the floating gate and the drain, electrons return from the floating gate to the drain, the floating gate discharges, and the threshold voltage returns to normal. The above process is defined as a “programming” operation, at which time the data “0” is stored.

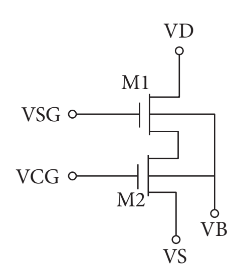

Figure 3: EEPROM memory cell structure.

EEPROM can perform memory read and write operations. Still, because it requires a special process and a multilayer mask, a differential structure MTP memory cell compatible with the standard CMOS process is designed for these deficiencies in this paper concerning the structure in literature [3]. The memory cell is programmed with the high-efficiency tunneling effect-Fowler–Nordheim (the tunneling effect is expanded in detail in Section 3), which enables fast writing and reduces the burden on the high-voltage generation circuit. As shown in Figure 4, M3 is defined as the reading tube, M1C, M1T, M2, M0C, M0T, M3; these six PMOS tubes together form a nonvolatile memory cell of the differential structure. There are two floating gates in this memory cell: M1C and M1T are connected to form the left floating gate FG1, and M0C and M0T are connected to form the right floating gate FG0. These two floating gates store unequal charges, respectively. The two floating gates store unequal charges, which then form different voltages on the two floating gates. When the corresponding bias voltage is added to the memory cell, the output ports RBL1 and RBL0 will generate differential currents I_{RBL1} and I_{RBL0}, which in practice need to be compared by a sense amplifier to distinguish the value stored in the memory cell (logic "0" or logic "1"). This enhances the output, and it is possible to define the output logic "0" for $I_{\mathrm{RBL0}} > I_{\mathrm{RBL1}}$ and "1" for $I_{\mathrm{RBL1}} > I_{\mathrm{RBL0}}$. The memory cell stores data mainly by the charge movement (injection or removal of electrons) on the floating gate of the PMOS transistor, i.e., the change of charge.

MTP memory cells require no additional process steps and masks, are compatible with standard CMOS processes, and offer a significant cost advantage over EEPROMs, which require additional processes and multiple masks at a fraction of the cost of standard CMOS processes.

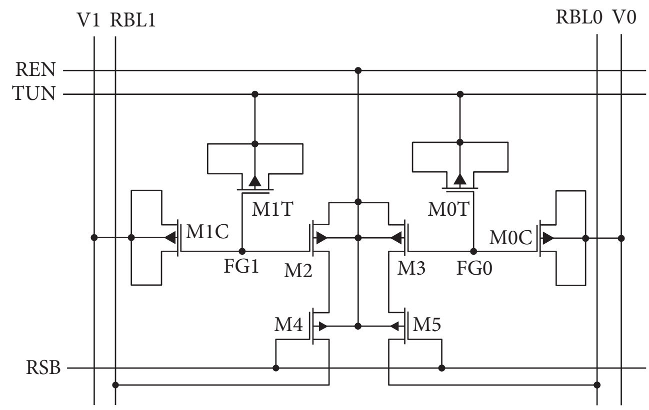

Figure 4: Storage cell structure.

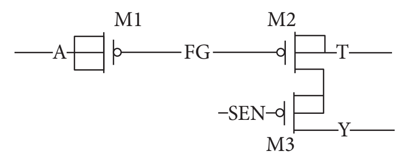

Figure 5: Schematic diagram of the circuit structure.

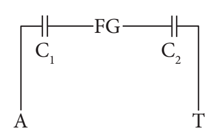

Figure 6: Schematic diagram of a capacitor voltage divider.

3. Fowler–Nordheim Tunneling Effect

The MTP memory cell achieves the capture and removal of electrons by the attempted penetration effect, according to the principle of capacitive voltage division, as shown in Figures 5 and 6 [4].

It can be simply assumed that V_A is the voltage on the port A connected to the source-drain-substrate of M1 tube; C_1 is the capacitance from the floating gate to the source-drain-substrate of M1 tube; V_T is the voltage on the port T connected to the source-substrate of M2 tube [2]; C_2 is the capacitance from the floating gate to the source-drain-substrate of M2 tube; the charge on the floating gate FG is Q_{FG} [5]; V_{FG} is the voltage on the floating gate FG; Q_0 is the initial charge when the control tube is M1; and Q_0 is the initial charge when the voltage on the floating grid is also at "0" potential when the "0" potential is biased on the control tube M1 and the tunneling tube M2 at the same time. Then the floating grid charge Q_{FG} and the floating grid voltage V_{FG} are

$$Q_{FG} = (V_{FG} - V_A)C_1 + (V_{FG} - V_T)C_2 + Q_0, \tag{1}$$

$$V_{FG} = \frac{C_1}{C_1 + C_2}V_A + \frac{C_2}{C_1 + C_2}V_T + \frac{Q_{FG} + Q_0}{C_1 + C_2}. \tag{2}$$

Define the coupling coefficient of the control tube as $\alpha_1 = C_1/(C_1 + C_2)$. The coupling coefficient of the tunnel penetration tube is $\alpha_2 = C_2/(C_1 + C_2) = 1 - \alpha_1$. The coupling coefficient of the general control tube can reach 0.9 or more, while the coupling coefficient of the tunneling tube is very low. This can effectively reduce the operating voltage, and equation (2) can also be written as

$$V_{FG} = \alpha_1 V_A + \alpha_2 V_T + \frac{Q_{FG} + Q_0}{C_1 + C_2}. \tag{3}$$

Here, it can be seen that the voltage V_{FG} on the floating gate is mainly influenced by the voltage on the control tube M1 port A [6]. When a high voltage V_A is applied on the control tube M1 port A and a 0 potential is applied on the port T of the tunneling tube M2, the voltage on the floating gate will be close to the high voltage V_A; when the electric field that can be formed on the gate oxide layer of the tunneling tube is as high as 1 e^9 V/m, using the F-N tunneling effect in the channel, the charge across the gate oxide layer reaches the polycrystal in the floating gate. The charge on the floating gate changes, and thus the voltage on the floating gate change to

$$\Delta V_{FG} = \frac{\Delta Q_{FG}}{C_1 + C_2}. \tag{4}$$

If the read voltage VS is applied from the source terminal T of the tunneling tube M2 during the read operation, the read current output from the drain terminal flows out from the Y port through the selector tube M3 so that the memory cell can be treated as a single MOS tube during the read operation, and the A terminal of the control tube is equivalent to its gate terminal; however, when the voltage on the floating gate changes due to the change of charge, it can be derived from (2), which is equivalent to the voltage change ΔV_A on the "gate" A, i.e,$\Delta V_{FG} = \Delta Q_{FG}/C_1 + C_2$.

$$\Delta V_A = \frac{\Delta Q_{FG}}{C_1}. \tag{5}$$

Then, during the read operation, the memory cell storing data "1" has a threshold voltage with a different state than the memory cell storing data "0" due to the different charge changes on the floating gate.

$$\Delta V_{th} = \frac{\Delta Q_{FG}}{C_1}. \tag{6}$$

The data change of the memory cell is achieved by a programming operation and an erase operation where a high voltage is applied to the control tube of the memory cell during the programming operation [7]. Due to the principle of capacitive voltage division, the voltage on the floating gate is much higher than the voltage on the tunneling tube, which results in a tunneling effect on the gate of the tunneling tube [8]. This allows the floating gate to trap or remove the charge. The state of the floating gate then reflects the change in charge.

4. Floating Grid State Analysis

Because of the existence of the tunneling effect, the charge can be shuttled between the tunneling tube and the floating gate, and the read/write operation of the memory cell is done by the change of the state of the floating gate (that is, the change of the number of charges). Since there is no bias voltage at both ends of the transistor at the moment $T = 0$ (i.e., the initial state), the state of the floating gate is also without voltage change. There is no charge in the floating gate in this state, which is equivalent to two capacitors in series, and its state is shown in Figure 7.

A bias voltage of 10 V is added to the *VA* and *VT* terminals from the moment $T = 1$. Changing the amount of floating gate charge is to add the corresponding bias voltage to the transistor [8]. At the time of data writing, i.e., the floating gate captures charge. At the time of data erasure, the floating gate erases the charge. The process is shown in Figures 8 and 9, starting from the initial state ($T = 0$), i.e., $VA = VT = 0$ V, when the floating gate voltage is also 0 V. The subsequent states ($T = 1$, 2, 3) add bias voltages to *VA* and *VT*, i.e., $VA = 10$ V, $VT = 0$ V, which causes the gate oxide layer of one of the MOS transistors to form a corresponding electric field to change the total amount of charge on the floating gate. After adding the corresponding bias voltage, the cross capacitive coupling between the two transistors forms a strong electric field in the gate oxide layer of the MT of the attempted transistor, and the charge can pass through the gate oxide layer of the MOS tube by the F-N attempted penetration effect. After capturing the charge from the floating gate ($T = 2$) and continuously adding bias voltage at both ends for some time, the voltage change of the floating gate can make the electric field of the gate oxide layer decrease, thus slowing down the process of attempted penetration. At this point, the bias voltage at both ends of the transistor ($T = 3$) is removed, and the charge of the floating gate has been changed [9].

The relationship between the floating gate voltage and the MC side [9], and the MT side is shown in Figure 10. The simulation result is shown as the solid line in the above figure by setting the voltage at the MC terminal to 0–3.5 V and setting the voltage at the MT terminal to zero. The other process is reversed, setting the voltage at the MT terminal to 0–3.5 V and setting the bias voltage at the MC terminal to zero [3]. The simulation result is shown as the dashed line in the above figure. When the voltage at the MC side of the control terminal changes from 0 to 3.5 V without adding the bias voltage at the MT side, it can be seen that the voltage of the floating gate also increases, and the other process is similar. It can be seen that the MC terminal has a greater effect on the floating gate than the MT terminal does on the floating gate, from which it can be seen that the voltage of the floating gate is mainly controlled by the voltage at the MC terminal [6].

On the other hand, the device modeling and simulation of the memory cell using Synopsys, Sentaurus TCAD (Technology Computer-Aided Design) software in reference [5], are shown in Figure 11 with three different initial charges states after an erase programming operation. All three simulation results can achieve the same erase stable state and stable program state. After each erase operation, the charge on the floating gate changes to $Q_{FG} = 6.931\ e^{-15}$; after the erase operation, the charge on the floating gate is $Q_{FG} = -1.666\ e^{-14}$, thus proving that the charge can be shuttled between the tunneling-pass tube [10] and the floating gate to store and erase information.

5. Simulation Analysis

The MTP memory array is arranged according to the cell structure given above, the memory cells are in symmetric form, and the 16 memory cells are arranged in parallel by bit expansion, with all REN, TUN, and RSB connected, as a basis for word expansion to a 512-bit memory array. In addition, the array of memory consists of a row control circuit, column control circuit, and read circuit. Its structure is shown in Figure 12, and then the read and write function is verified.

5.1. Main Function Timing Diagram.

The most important operations of memory are read and write command operations. Before the read and write signals are powered on, the corresponding data lines and address lines are ready and waiting to be undone after the operation is completed. And its same moment can only execute one of the read and write commands.

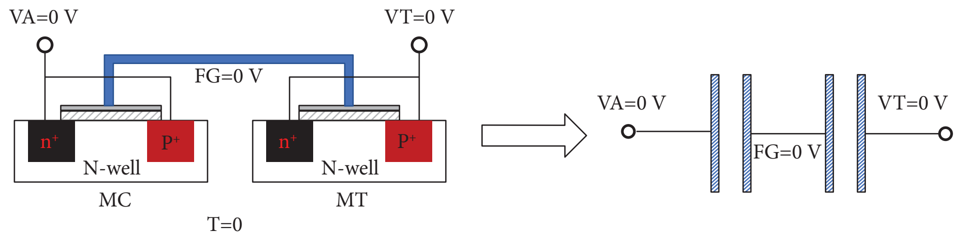

FIGURE 7: Floating gate state without bias voltage.

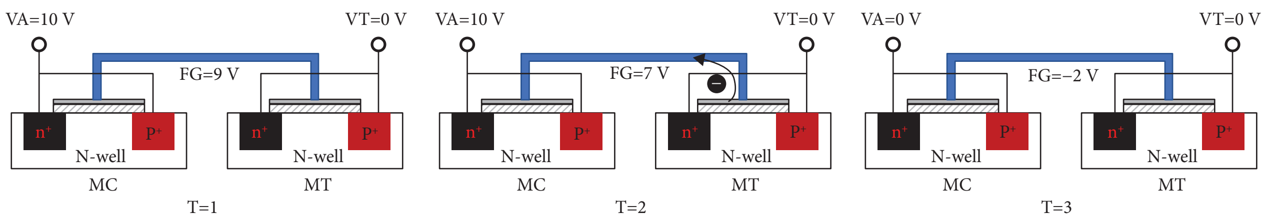

FIGURE 8: Schematic diagram of charge capture by FG.

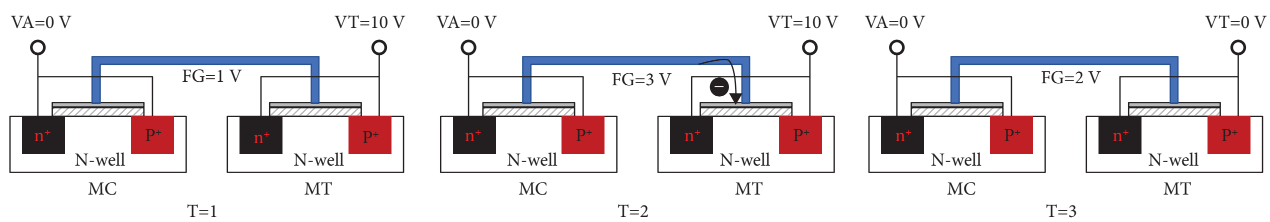

FIGURE 9: Schematic diagram of FG erasure charge.

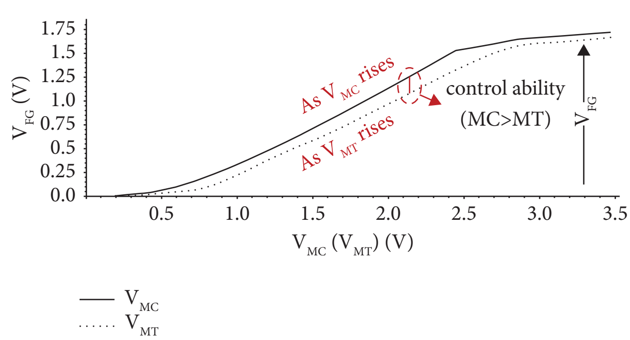

FIGURE 10: Relationship between floating gate voltage and MC and MT bias voltage.

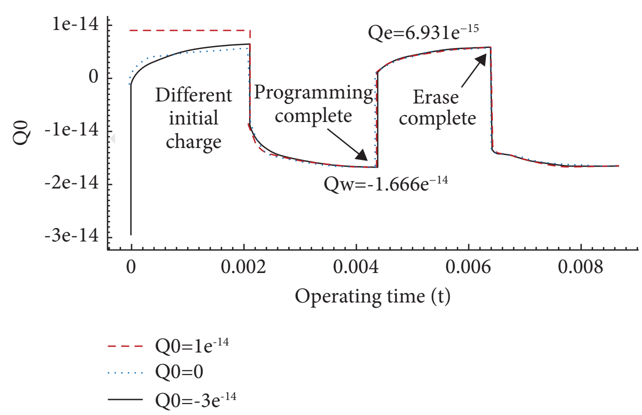

FIGURE 11: Floating gate charge state.

5.1.1. Read Operation Timing. Its state is shown in Figure 13(a). When the memory IP_EN = "1" is idle, it receives the read command READ sent by the digital baseband, and the READY signal becomes "0." The internal decoding circuit of the memory decodes the long-prepared address data and enables to read the corresponding address data. The READY signal returns to "1" after DOUT reads the result from the idle state.

5.1.2. Write Operation Timing. Its state is shown in Figure 13(b). When the memory IP_EN = "1" is idle, the read command WRITE is received from the digital baseband, and the READY signal becomes "0." The internal decoding circuit of the memory decodes the long-prepared address data, enables the corresponding address data, and is written to the memory. The READY signal returns to "1" when the write operation continues for some time and is completed.

5.2. Read and Write Command Simulation. The simulation result of the write operation is shown in Figure 14: when the external Write signal is input, the control circuit first sends the Erase signal to perform the erase operation for 2 ms, and when the erase operation is completed, the control circuit continues to send the Program programming signal. The

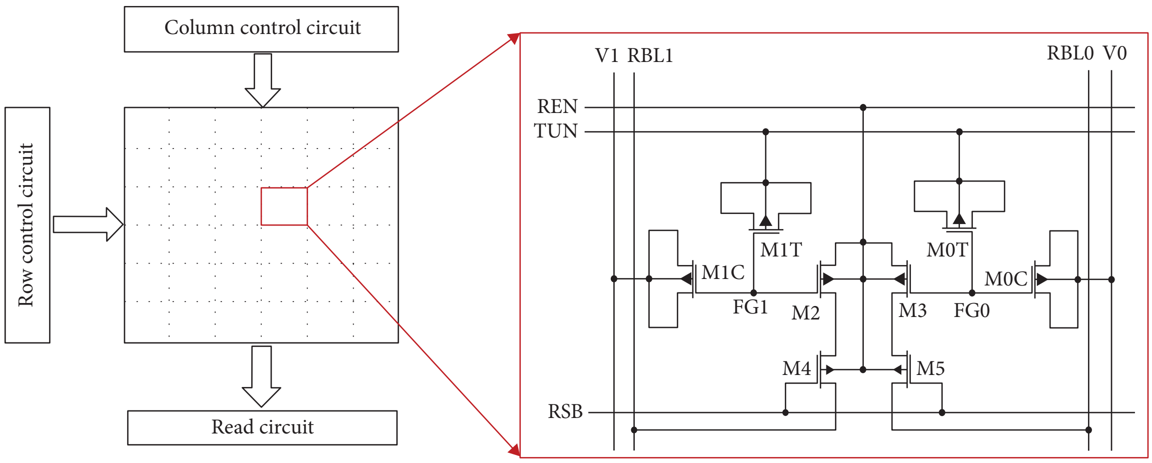

Figure 12: Storage array schematic.

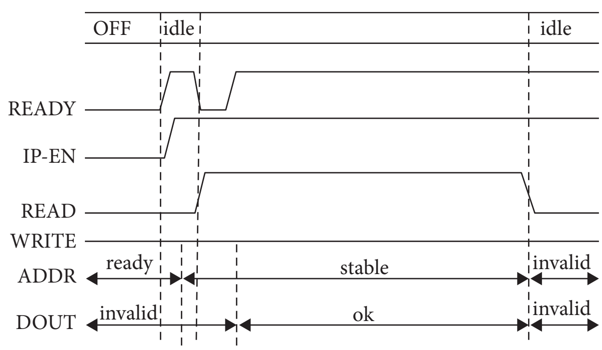

Figure 13: (a) Timing diagram of a read operation. (b) Timing diagram of a write operation.

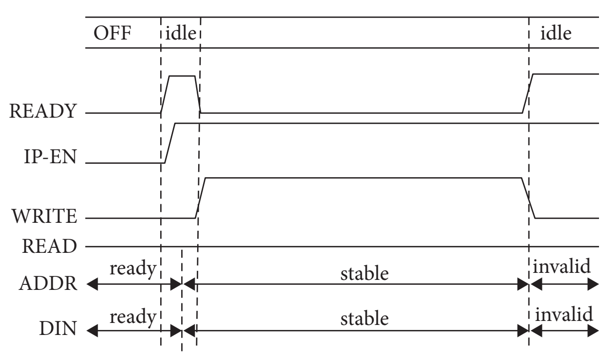

Figure 14: Simulation results of a write command.

charge pump turns on with the Erase or Program start. The output high voltage V_h and V_m have about 0.2 ms jump when the two signals alternate, which is about 2.6 ms in the figure, and the simulation result shows that the charge pump needs 60 us to rise to the required high voltage, and the output result is $V_h = 10.1$ V or so, and $V_m = 4.8$ V. The output of the charge pump turns on with the Erase or Program off, the output high voltage V_h drops from 10.1 V to 500 mV in 100 ns time, and V_h drops from 4.8 V to 31 mV in 100 ns time. Output signal is “1” when V_h reaches 10 V, and below 10 V, the output signal. The Ready signal changes from “1” to “0” after the Write signal comes, and when the write operation is completed, it changes from “0” to “1” when the write operation is completed. The dashed line in the figure shows the drop at 4.6 ms for the execution of the Read command.

The simulation result of the Read command is shown in Figure 15. When the Read command is applied outside the memory, the memory control circuit sends out the Control-Read signal, which lasts for 0.1 ms, and Ready drops to “0” signal at 4.6 ms. Then DOUT rises to “1” signal, and at 4.7 ms Read turns off, the Control-Read signal also follows to turn off; then, DOUT drops to “0” signal at 4.7 ms.

From the above read/write simulation and functional timing diagram, it can be seen that the memory cell designed in this paper can achieve the basic read/write function of the memory, and the high voltage required during the read/write operation is 10 V, which is about 30% lower than the 16 V required for conventional EEPROM.

While the simulation of the read and write commands of the memory is given above to verify the read and write functions of the memory, the voltage distribution of each port inside the memory cell is given below, as shown in Figure 16, which lists the block diagram of the MTP array and the detailed voltage distribution for the write and read operations of the MTP cell in the selected and unselected rows of the MTP array. During the programming operation, a high voltage difference of 10 V is added in the two electrodes of FG1 (FG0) and REN. Electrons will be injected into FG1 (FG0) from the M2 (M3) channel to reduce the FG1 potential until the voltage difference between FG1 (FG0) and REN is less than the tunneling threshold. For unselected MTP cells during erase and program operations, the voltage distribution ensures that the voltage difference across all devices is less than the tunneling channel threshold, thus avoiding a tunneling effect to maintain the original state. For read operations, the MUX block is responsible for the row and column where the selected cell is located. A sensing amplifier based on a positive feedback scheme is used to improve the read sensitivity of the current difference signal on RBL0 and RBL1.

From the voltage distribution of MTP above and the signal diagram of EEPROM ports given in the literature [6], Table 1 compares the voltage of MTP and EEPROM ports, it

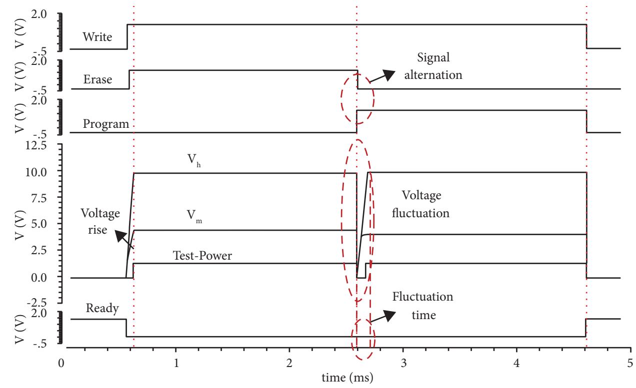

FIGURE 15: Read command simulation results.

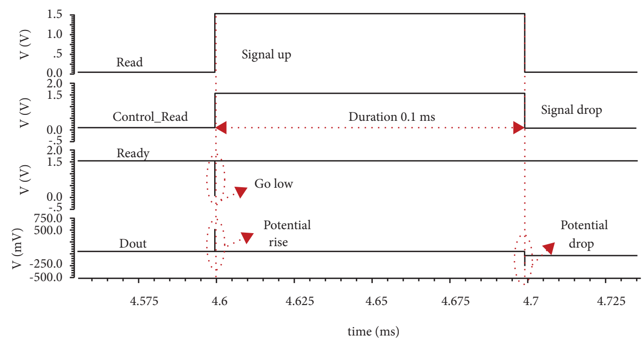

FIGURE 16: Voltage distribution for write and read operation of MTP.

TABLE 1: Voltage of each port of MTP and EEPROM.

MTP storage unit offset					
Operation	V0	V1	TUN	REN	RSB
Writing '1'	0	10 V	10 V	0	5 V
Writing '0'	10 V	0	10 V	0	5 V
Writing protection	5 V	5 V	5 V	5 V	5 V
Reading protection	0	0	0	1 V	0
EEPROM storage unit signal offset					
Operation	VSG	VCG	VD	VS	VB
Program	16 V	0	13.5 V	Floating	0
Erase	16 V	15 V	0	0	0
Read	1.8 V	1.8 V	1.5 V	0	0

can be seen that, for the write operation, MTP requires 10 V (V1 = TUN = 10 V) and EEPROM requires 16 V (VSG = 16 V) for programming. The dashed lines in the table show that the voltage required for the MTP is much lower than the EEPROM voltage of 16 V or more, so the low voltage characteristic of the MTP makes it ideal for UHF RFID applications.

6. Conclusions

UHF electronic tag chip as a key component in the Internet of Things has been widely used worldwide and is the focus of current research. One of the cores of UHF electronic tag chip is memory; traditional RFID manufacturers use EEPROM as the memory of RFID tags, but in the UHF tag chip needs to reduce the voltage and cost, EEPROM has a high cost (need special coprocess support and multilayer mask) and high voltage deficiencies, and for these deficiencies this paper uses standard CMOS process to design the MTP. On the other hand, the high voltage required for the read/write process is about 10 V, which is 30% lower than that of conventional EEPROM.

Data Availability

All data included in this study are available upon request to the corresponding author.

Conflicts of Interest

The authors declare no conflicts of interest regarding the publication of this paper.

Authors' Contributions

YHX and CL designed the method and wrote the paper; NB and YW performed the experiments and analyzed the data; all authors have read and agreed to the published version of the manuscript.

Acknowledgments

This research was funded by the National Natural Science Foundation of China (no. 61204039) and the Key Laboratory of Computational Intelligence and Signal Processing, Ministry of Education (no. 2020A012).

References

[1] N. Bai, L. Wang, Y. Xu, and Y. Wang, "Design of a digital baseband processor for UHF tags," *Electronics*, vol. 10, no. 17, p. 2060, 2021.

[2] K. Ming, X. Zhang, S. Ren, and J. Sun, "Spatial Pyramid Pooling in Deep Convolutional Networks for Visual Recognition," *IEEE Transactions on Pattern Analysis & Machine Intelligence*, no. 9, pp. 1904–1916, 2015.

[3] S. Li, L. Cai, Y. Xiao et al., "A 20 dBm passive UHF RFID tag IC with MTP NVM in 0.13-μm standard CMOS process. Circuits and systems I: regular papers," *IEEE Transactions on*, vol. 99, pp. 1–14, 2020.

[4] M. Takahashi, S. Wang, T. Horiuchi, Q. Li, K. Y. Yun, and S. Sakai, "Novel Ferroelectric CMOS Circuits as a Nonvolatile Logic," *American Physical Society*, vol. 44, no. 7, pp. 467-468, 2008.

[5] B. Wang, L. Man-Kay, J. Yi, T. Chi-ying, and A Bermak, "A -12.3 dBm UHF passive RFID sense tag for grid thermal monitoring," *A IEEE Transactions on Industrial Electronics*, vol. 66, no. 11, pp. 8811–8820, 2019.

[6] Li De, *An Optimized 512bit EEPROM Design for RFID Tag Chips. Diss*, Tianjin University, Tianjin, China, 2012.

[7] L. Ma, K. Hu, Y. Zhu, and H. Chen, "Cooperative artificial bee colony algorithm for multi-objective RFID network planning," *Journal of Network and Computer Applications*, vol. 42, pp. 143–162, 2014.

[8] X. Wang, J. Zhang, Z. Yu, S. Mao, S. C. G. Periaswamy, and J. Patton, "On remote temperature sensing using commercial UHF RFID tags," *IEEE Internet of Things Journal*, vol. 6, pp. 10715–10727, 2019.

[9] J. Shen, X. Wang, B. Wang et al., "Fully Integrated Passive UHF RFID Transponder IC with a Sensitivity of −12 dBm," in *Proceedings of the IEEE International Symposium on Circuits & Systems IEEE*, Beijing, China, May 2013.

[10] Z. Jin, *Research on Key Technologies in the Design of Passive UHF Radio Frequency Identification Tags*, Xi Dian University, Xi'an, China, 2011.

Hindawi
Scientific Programming
Volume 2022, Article ID 8529229, 10 pages
https://doi.org/10.1155/2022/8529229

Research Article

Application of 3D Printing Reconstruction Algorithm in Ancient Ceramic Restoration

Hongchang Wu [1] and Yamin Ma [2]

[1] School of Ceramics, Pingdingshan University, Pingdingshan, Henan 467000, China
[2] School of Art and Design, Pingdingshan University, Pingdingshan, Henan 467000, China

Correspondence should be addressed to Hongchang Wu; 3119@pdsu.edu.cn

Received 1 December 2021; Revised 22 December 2021; Accepted 28 December 2021; Published 29 January 2022

Academic Editor: Le Sun

The study of the ancient ceramic is of great significance to the identification of authenticity, value recognition, cultural types, and dissemination channels of the ceramic. In this study, a series of technical problems such as ceramic contour extraction, image distortion correction, and nonlinear contour modeling for 3D printing of rotating body under complex background were solved and a restoration algorithm for the shape of ancient ceramics was proposed. Then, an accurate contour model is established by using the two-dimensional images of the rotating ancient ceramics to reconstruct the three-dimensional model of the ceramic shape. The experimental results show that the modeling algorithm for three-dimensional printed ceramics can accurately obtain the three-dimensional model of rotating ancient ceramics, which is of certain significance to explore a new direction of the research and development of three-dimensional printed ancient ceramics.

1. Introduction

Archaeological Ceramics in China have a long history and are rich in cultural relics. With the continuous improvement of material life in Chinese society, more and more people are interested in ceramic cultural relics, and the identification, protection, and inheritance of ancient ceramics are increasingly important. In the identification process of ancient ceramics, the origin and age of products are the most important, and its technical difficulty is also the highest [1]. Since ancient times, the main method of source and date identification is the use of human eye recognition, that is, relying on the long-term accumulated experience of appraisers to judge, inevitably into the influence of subjective factors, more importantly, the lack of multi-information data management and big data analysis, resulting in a lot of useful information hidden in it being ignored or misread [2]. With the appearance of 3D printing technology, this technology provides a better technical means for the finishing of ceramic materials. It is flexible in design, can print highly complex structure, with precise three-dimensional size, and can simultaneously build multiple print objects at one time, significantly improving production efficiency. This research status of ancient ceramics seriously affects the inheritance and development of ancient ceramic technology [3].

In the multiple ceramic product information, the product type has the distinct characteristics of times and regions, so the ancient ceramic type plays an incomparable role in the identification and numerical simulations [4]. In the information age, the extraction and analysis of the morphological characteristics of ancient porcelain in different historical periods and different structural characteristics can provide reference for the traceability of ancient porcelain and the identification of authenticity. This work is of great significance to further study the relationship between the artistic characteristics of ceramics and culture and aesthetics. Traditional potteries are typically made from a mixture of powder and binder or other additives, processed using conventional techniques such as injection molding, molding, casting, and gel casting, and sintered green at higher temperatures for densification [5, 6]. However, these ceramic molding techniques are limited by long processing time and high cost. Furthermore, those algorithms used for studying archaeological ceramic, mainly concerning the axially symmetric geometry recognition, which is a geometry property of the greater region of a vessel [7]. For ancient ceramic, the elements not regarded as this category of axially symmetric geometry can be discerned in general [8].

With the appearance of 3D printing technology, this technology provides a better technical means for the finishing of ceramic materials [9, 10]. It is flexible in design, can print highly complex structure, with precise three-dimensional size, and can simultaneously build multiple print objects, significantly improving the restoration efficiency of ancient ceramics. The earliest 3D printing technology for potteries was developed and realized in the 1990s. With the continuous development of 3D printing technology and the increasing demand for ancient ceramic restoration, personalized design and processing can also be realized through 3D printing technology [11]. However, for complex potteries, especially ancient ceramics used for structural restoration, such as restored bowls, vases, and other handicrafts, their complex geometric shape and interconnection between the internal apertures lead to their difficult processing, which presents a great challenge for the processing of materials. 3D printing technology has developed from the initial melting deposition manufacturing, inkjet printing technology to prepare ceramic green, and then sintering, to the present integration of laser sintering and light curing molding new technology [12]. As presented in Figure 1, 3D printing technology has been widely used in ceramic industry, such as multifunctional ceramics, high temperature resistant materials, aerospace industry, medical engineering, and cultural relic restoration [13].

The study on the dimensions of the properties is significant for identifying the tools applied in the creation of the decoration. However, it is difficult and inefficient to accurately extract ceramic types and to obtain the real parameters of ceramic types by conventional measurement methods due to the diversity and complexity of ancient ceramic products [14]. Furthermore, most ancient ceramics are genuinely stored in the museum and with private collectors; for reasons of security or privacy, the owner of these ceramic products or unit is generally not willing to put their expensive ancient ceramics for equipment scanning and data acquisition, even if reluctantly agreed to also pass through the complex procedures, making ancient ceramics 3D scanning data [15]. All these have caused the serious shortage of digital data of ancient ceramic ware in the era of big data with information expansion, which has seriously restricted the progress of research on big data of ceramic wares. In recent years, using machine vision technology to accurately restore two-dimensional image information to three-dimensional model has become a new direction of ancient ceramics research [16–18]. Some scholars have done some work in the curve fitting of a skimming bottle. Besides, the edge characteristics of skimming bowl have been studied [17, 19]. Although many researchers have tried to obtain the ancient ceramic shape by using various image processing methods, due to the problems of two-dimensional image distortion, complex image background, and large difference in image quality, the extracted model error is large, and the restored 3D model deformation is serious [20]. These problems have long been difficult to break through and become the shackles of the development of 3D printing technology of ancient ceramics [21–25].

In view of this background, this paper under the background of solving complex contour extraction and image distortion correction, under the premise of technical bottlenecks, developed a set of technologies based on machine vision of the ancient porcelain ware three-dimensional reduction algorithm; this algorithm can go through nonlinear image enhancement, the distortion compensation, and curve fitting such as machine vision and pattern recognition technology to build accurate model of the ancient porcelain ware. The complete information of ancient ceramic ware type can be obtained by a few parameters.

2. Structure of 3D Printing Construction Method

2.1. 3D Restoration Algorithm. This study used three-dimensional virtual models to reconstruct the ancient ceramic. Hence, the term samples are the ancient ceramic bottles from Chinese museum. In this study, three different ancient Chinese ceramic vases were used for three-dimensional morphological analysis. The 3D restoration algorithm mainly includes image enhancement, image distortion correction, modeling, and 3D reproduction of ancient ceramic. The working principle diagram of 3D reduction algorithm for ancient ceramic vessel type is shown in Figure 2, which is core studying object of this paper. A special recognition process of real ancient potteries based on three-dimensional calculations by computer is used for analyzing the discrete model generated by real scans. Besides, the original surface is approximated by triangular surface of the three-dimensional models. Through the complex processing of 3D data, the 3D geometric model is obtained, which contains low-level geometric information, such as the coordinates of points and the normals of triangles, and advanced information, such as measurement of ceramic bottle radius. For ancient ceramic bottles, the above evaluation is complex due to the limited grid sampling range, manufacturing errors, and other factors [26].

2.2. Three-Dimensional Reconstruction Technique. Accurate extraction of ancient ceramic wares from 2D image contour is the first step to shape three-dimensional reduction, but because of the variety of forms, the image with low pixel restored by the 3D model is far from the real ancient porcelain, and, precision is very low; you cannot even get a three-dimensional model. Accordingly, this algorithm first uses the edge of images, which is enhanced by wavelet transform to improve the discernibility of the edge of ancient potteries, and the edge contour of ancient potteries is clearly extracted and accurately located. The specific process is as follows.

Equations (1) and (2) are used to perform two-dimensional discrete wavelet transform on the image $F(x, y)$ with the original image size of $M \times N$ and decompose the original image

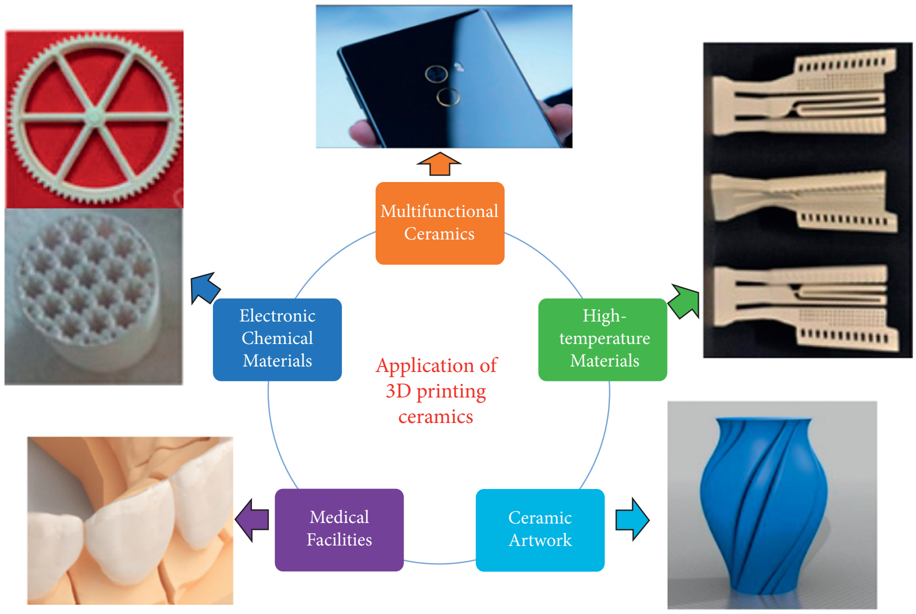

FIGURE 1: Application field of 3D printing technology.

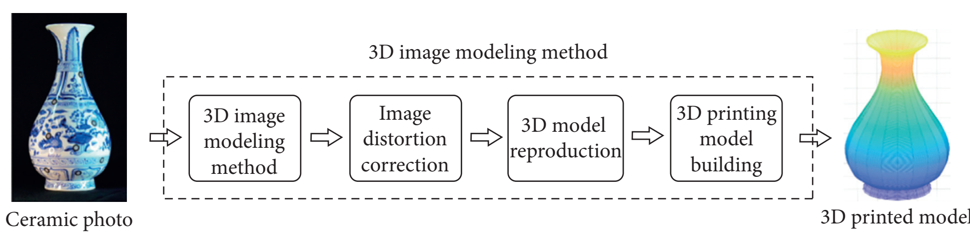

FIGURE 2: Working principle diagram of 3D reduction algorithm for ancient ceramic vessel type.

into a low frequency subimage band containing image contour information and a high-frequency subimage band dominated by background noise. By adjusting the weight of the approximate coefficient Wφ and the detail coefficient Wiψ of the high and low frequency subbands in equations (1) and (2) after wavelet transform, the sharpness of the image contour can be improved and the image noise can be further reduced. Finally, the inverse wavelet transform formula is used to synthesize the image after edge enhancement, which can realize the image edge enhancement and achieve the purpose of highlighting the edge contour of ceramic ware images.

$$W_{\phi}(j_0, M, N) = \frac{1}{\sqrt{MN}} \sum_{x=0}^{M-1} \sum_{y=0}^{N-1} f(x, y)\phi_{j_0,M,N}(x, y), \quad (1)$$

$$W_{\psi}^{i}(j, M, N) = \frac{1}{\sqrt{MN}} \sum_{x=0}^{M-1} \sum_{y=0}^{N-1} f(x, y)\psi_{j,M,N}^{i}(x, y), i = \{H, V, D\}, \quad (2)$$

where W_{φ} is the approximate coefficient of image contour information. W^{i}_{ψ} is the detail coefficient of identification image. $\varphi_{\mathrm{j0,M,N}}$ are scale basis functions. $\psi_{\mathrm{ij,\ M,\ N}}$ are translation basis functions. $\{H, V, D\}$ respectively represent different orientation image details.

By adjusting the weight of the approximate coefficient W_{φ} and the detail coefficient $W_{i\psi}$ of the high and low frequency subbands in equations (1) and (2) after wavelet transform, the sharpness of the contour can be improved.

$$f(x, y) = \frac{1}{\sqrt{MN}} \sum_{M} \sum_{N} W_{\phi}(j_0, M, N)\phi_{j_0,M,N}(x, y) + \frac{1}{\sqrt{MN}} \sum_{i=H,V,D} \sum_{j=j_0}^{\alpha} \sum_{M} \sum_{N} W_{\psi}^{i}(j, M, N)\psi_{j,M,N}^{i}(x, y). \quad (3)$$

2.3. Adaptive Perspective Correction of 2D Images. Based on the 2D images, the image distortion caused by the shooting angle, distance, and lens difference will greatly affect the 3D restoration accuracy of the device. Therefore, this paper proposes a method to estimate the shooting angle of an image using elliptic Hough transform, which can accurately estimate the shooting angle of the camera relative to each region of the image. On this basis, the perspective transform method is used to realize the distortion compensation of two-dimensional image partition [27].

(1) According to the contour image of ancient ceramics, extract the contour curves of its top and bottom.
(2) Elliptic contour detection algorithm based on Hough transform is used to fit the elliptic models of the top and bottom of contour image.
(3) Calculate the shooting angle of the image according to the ellipse. The angle calculation process is shown in Figure 3. Under ideal conditions, assuming that the camera is a parallel incident ray, when the camera shoots a ceramic shape with a radius of M at angle θ, the PQVW surface on the top of the ceramic shape forms an ellipse in the ABCD plane, and the shooting angle can be calculated by the algorithm. Similarly, the shooting angle of the lower edge of the ancient ceramics can be obtained by extracting contour lines of the lower edge according to the contour line. The values l and l ' are the longitudinal dimensions before and after correction [28].

$$\frac{l' = l}{\cos\left(\arcsin\,\theta_i\right)}. \tag{4}$$

(4) According to the upper and lower angles θu and θd, the imaging angle $\theta\, I$ of each horizontal section of the two-dimensional plane of ancient ceramics can be estimated. The image shooting angle and distance calculated in steps (1) ~ (3) can be used as relevant parameters of perspective transformation to realize adaptive adjustment of perspective correction algorithm and complete automatic image calibration. For intermediate condition, the empirical function is applied as the follows.

where, C_1 and C_2 are empirical parameters, and γ_j is maximum tangent value of the dihedral angle.

$$w_j = c_1 e^{-\gamma_j^{c_2}} \tag{5}$$

The membership function satisfies the normality condition because of the generic node:

$$\mu_e + \mu_{r1=Ri} + \mu_{-r1=Ri} = 1. \tag{6}$$

A comparison between the node p_j on the boundary region F_j and the node p_k is used as the following dissimilarity parameter D (p_j, F_j):

$$D\left(p_k, F_j\right) = \frac{\left|\mu_e^k - \mu_e^{F_j}\right| + \left|\mu_{r1=\overline{R}i}^k - \mu_{r1=\overline{R}_i}^{F_j}\right|}{\left|\mu_e^k + \mu_e^{F_j}\right| + \left|\mu_{r1=\overline{R}i}^k + \mu_{r1=\overline{R}_i}^{F_j}\right|}, \tag{7}$$

where μ_{ek} is the evaluated membership functions at the node p_k.

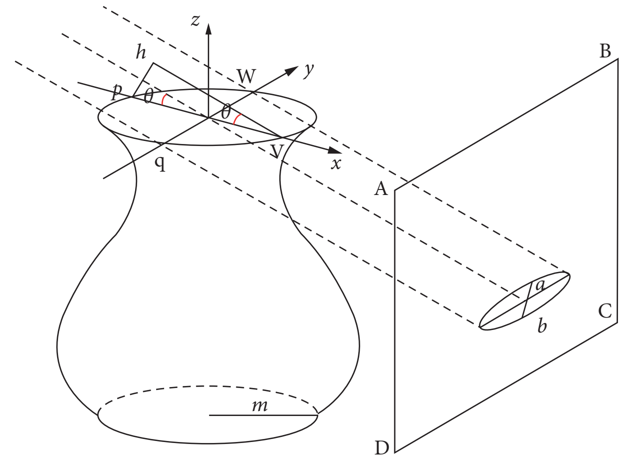

Figure 3: Geometric properties of shooting angle in the simulation model.

$$\mu_e^{F_j} = \sum_{p_j \in F_j} \frac{\mu_e^j}{n_t},$$
$$\mu_{r1=\overline{R}i}^{F_j} = \sum_{p_j \in F_j} \frac{\mu_{r1=\overline{R}i}^j}{n_t}. \tag{8}$$

In this study, the value μ_{rk1} is assigned as shown in equation (9).

$$\mu_{rk1} = R_i. \tag{9}$$

2.4. Modeling of Shape and Edge of Ancient Ceramic Ware Based on Neural Network Technology. The lateral edge contour baseline was extracted from the ancient ceramic edge contour image after distortion correction, and the mathematical model of the baseline was constructed. The accuracy of the edge contour model directly affects the effect of 3D modeling. In principle, neural network can approximate any nonlinear curve, so this paper uses back-propagation (BP) neural network to accurately model the baseline of ancient ceramic side edge contour [29].

A specific BP neural network with three layers is used in the study. They are input layer, hidden layer, and output layer [17]. Both the input layer and the output layer of the network have one node; that is, the input layer receives the horizontal coordinate data of 1×1 side edge curve, and the output layer generates the vertical coordinate data of 1×1 side edge curve prediction. The hidden layer activation function uses nonlinear Sigmoid function to map input and output data nonlinearly. In building a network of hidden layer nodes, in order to guarantee the network error converges to the premise as small as possible, to reduce the training time of network and at the same time avoid network overfitting phenomenon of samples, the experiment is done many times to adjust the network parameters, and finally selected use of 30 nodes of neurons in hidden layer neural network structure is set up. In this paper, MSE means the mean square error. In order to ensure the training accuracy, the number of network iterations is set as 500, and the MSE converges to 0 during the training. The samples and labels are continuously sent into the constructed BP network. Through the forward propagation of signals and the parameter feedback modification based on error, the network continuously descends to the gradient direction according to the deviation and iteratively adjusts the weights and thresholds of each neuron node until the error drops to the target range. The neural network transfer model adopted in this paper is shown in equations (10) and (11).

$$y_l' = f\left(\omega_{1l}x_i\right), l = 1, 2, \ \ldots\ldots, L, \tag{10}$$

$$y_i = f\left(\sum_{l=0}^{L} \omega_{2l} y_l'\right), l = 1, 2, \ldots\ldots, L. \tag{11}$$

The key of network model is used for the acquisition of training samples and tags. The samples and labels used in this paper are the horizontal and vertical coordinates corresponding to the side edge contour. After contour extraction and distortion correction of the original ancient ceramic image, the upper left, upper right, lower left, and lower right endpoints of the corrected ancient ceramic contour image were extracted as the starting and ending endpoints of the two side edge contour lines according to the change of contour edge curvature, so as to obtain the accurate side edge curves. After that, the symmetrical central axis was obtained through the four endpoints and used as the X-ray to extract every pixel on any side edge contour and map its horizontal and vertical coordinates of the corresponding X axis, which were used as training samples of neural network and tag training in this paper.

2.5. 3D Reconstruction Algorithm Flow of Ancient Ceramics. The curve model of ancient ceramic side edge contour established by BP neural network contains complete information about the shape of the rotating body ancient ceramic, which can be saved as the original data of the shape. Therefore, the 3D model of the shape can be obtained by rotating around the central axis of the shape through the curve model, which is the final 3D reproduction model of the ancient ceramic shape.

The complete flowchart of the algorithm in this paper is shown in Figure 4. In the process, K is used to represent the times of image enhancement algorithm, while the interactive extraction module is an auxiliary means when automatic curve extraction is not accurate enough. The specific steps are as follows:

(1) Use wavelet transform to read the original image, sharpen and enhance the contour while reducing the image noise, and then use edge detection algorithm to extract the image edge contour; image enhancement algorithm can be used repeatedly to achieve the best effect; here set a maximum of three times; after exceeding the upper limit, use interactive extraction algorithm to assist extraction. Based on wavelet transform, a new method for detecting transient signals of three-dimensional model has been applied.

(2) Perform angle distortion correction algorithm on the extracted contour image to obtain the corrected ancient ceramic contour image.

(3) Extract the baseline of the side edge contour of the corrected image, and enhance it with the interactive operation-assisted extraction algorithm in the program.

(4) The extracted side edge contour is modeled by using neural network. Then, it is rotated around the central axis to obtain the 3D model of the ancient ceramic image of the rotating body.

3. Computer Experiment and Analysis

The ancient ceramic wares were scanned by 3D printing model with cultural relics type contactless digital scanning and measuring equipment and the point cloud data obtained from the standard ancient ceramic objects were used as the standard size to verify the accuracy of the proposed method.

3.1. Working Process of 3D Reduction Algorithm. The method has been used in the study of refactoring shapes on an ancient vase, which is a very critical test case. In this experiment, two-dimensional images of common jade pot spring vase were used as objects to show the complete restoration process of ancient ceramics from two-dimensional images to 3D models in detail. Through the steps of contour enhancement, angle distortion correction, side edge contour curve modeling, and 3D reconstruction of ceramic shape, the 3D restoration of ceramic shape is completed. The restore steps are shown in Figure 5.

Through simulation experiments, the adaptive perspective correction algorithm and the traditional distortion correction algorithm are, respectively, used to extract the side edge contour of ancient ceramics, and then the accuracy of the two algorithms is compared. The experimental results are shown in Figure 6. The left and right red curves in the figure are standard edge contour curves of jade spring bottles, which are fitted by interpolation function according to the physical standard point cloud data obtained by 3D scanner. The blue curve on the left is the edge contour curve of the jade pot spring bottle after processing the two-dimensional image with the traditional perspective correction method. The blue curve on the right is the edge contour curve of the jade pot spring bottle after processing the 2D image with the perspective correction algorithm in this paper. By comparison, it is found that the algorithm in this paper plays a significant role in improving the fitting accuracy of the area with large curve fitting error (the part circled in Figure 6), which makes the fitting error decrease from 2.65% to 0.81%.

In order to verify the accuracy of the neural network fitting curve, the neural network algorithm in this paper is compared with the traditional polynomial interpolation function through experiments, and the accuracy difference

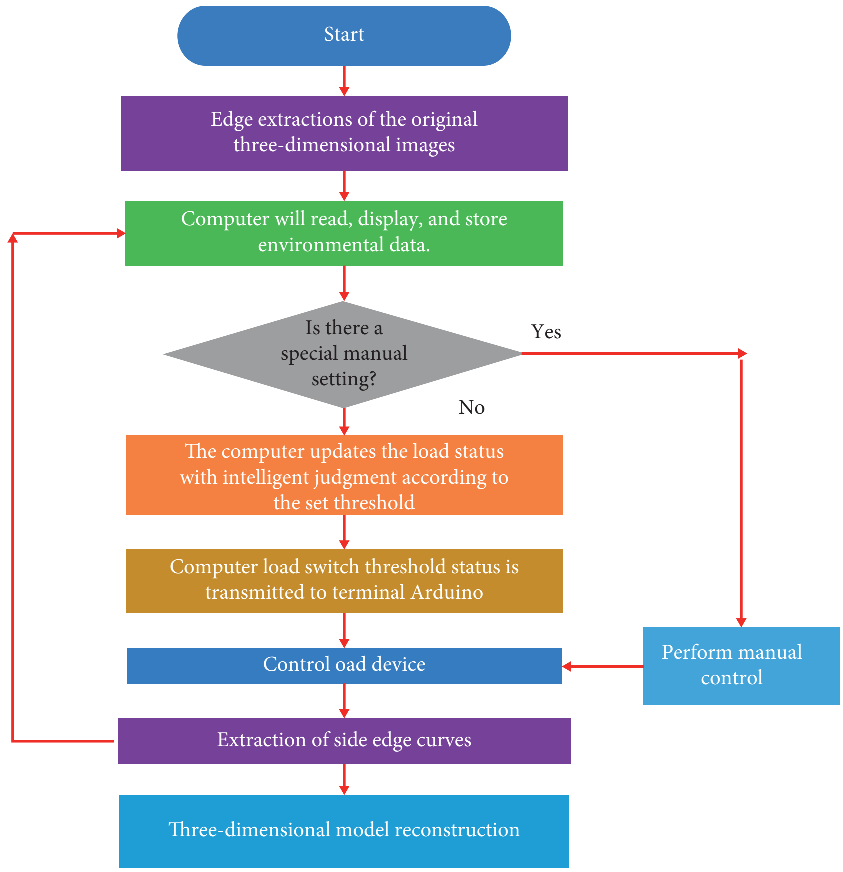

Figure 4: Flow diagram of the calculating algorithm.

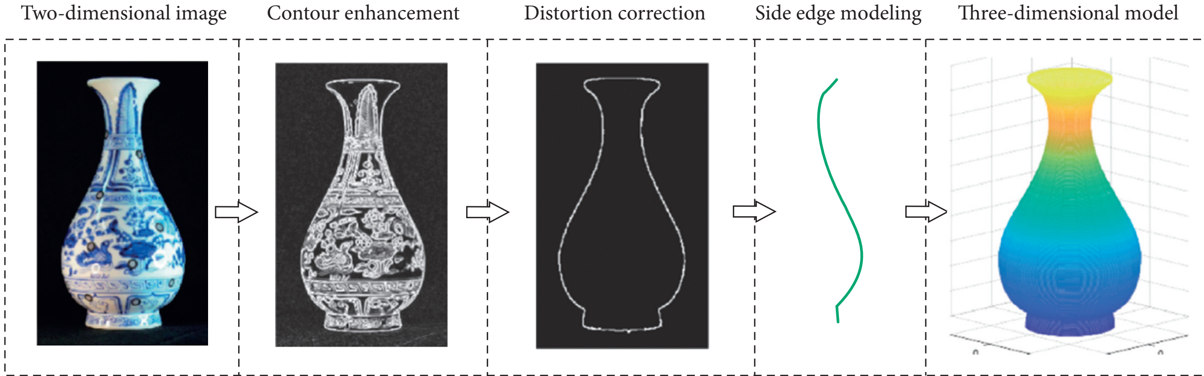

Figure 5: Steps of 3D restoration of the sample.

between the two methods in constructing the side edge model of ancient ceramics is compared. Figure 6 shows the convergence curve of MSE error with iterative training when BP network is trained using sample data of ancient ceramic side edge curve. It shows the effect diagram of modeling the contour curve of the side edge of the mulberry grape tank constructed by using the above-mentioned methods. After 500 iterations, the MSE error of the curve is only 5, about 12×10^{-3}. As can be seen from Figure 6, the overall effect of the two methods on modeling the side edge of ancient ceramic bottles is relatively good. However, it can be seen from the effect diagram of the local contour detail model of the edge of ancient ceramic bottles constructed by the proposed method that the curve model constructed in this paper is more approximate to the contour details of the strange parts such as neck, tail, and base of the ceramic bottle.

It can be seen that the MSE error of the curve is only about 0.052% and the overall effect of the two methods on modeling the side edge of mulberry grape pot is relatively good. However, it can be seen from the local contour detail model of side edge of mulberry grape pot constructed in Figure 6 that the curve model constructed by the method in this paper is more approximate to the contour details of the

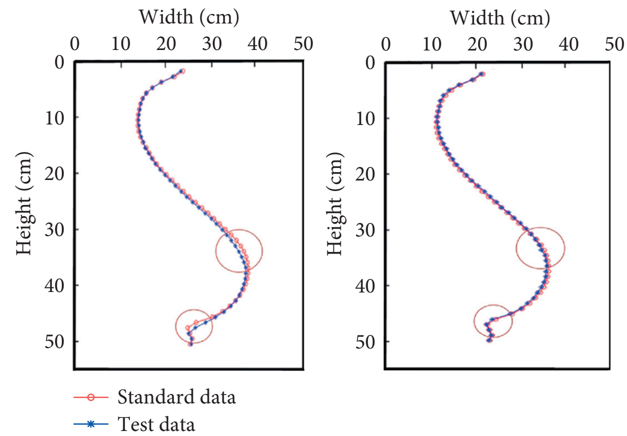

Figure 6: Comparison of distortion correction effect of side edge contour curve of the 2D image.

strange parts such as neck, tail, and base. The data show that the mean square error (MSE) of the precision of mold fitting is only 5.12×10^{-3}, much smaller than the traditional method of mean square error (MSE) 1.2×10^{-2}; for the realization of three-dimensional accurate reduction of ancient ceramics lay a solid foundation.

3.2. Accuracy Experiment of 3D Reduction Algorithm. The results of reconstruction of 3D restored ancient ceramics are shown in Figure 7. In order to verify the restoration accuracy of the algorithm, 50 points were extracted from the point cloud coordinate data obtained from the physical object scanned by the 3D scanner as standard data to test the accuracy of the algorithm builder model. The calculating data of the sample analysis is listed in Table 1. The 2D images of ancient ceramics were obtained by changing the shooting angle and distance to verify the accuracy and robustness of the algorithm in 3D restoration. Besides, the test distance is the distance between the camera lens and the center of ancient ceramics, and the test angle is the included angle between the lens and the horizontal ground when the lens center is aligned with the center of ancient ceramics. The image quality of pictures under different conditions is expressed by using the degree of desirable, H_NRMSD is the percentage of longitudinal normalized root mean square error, and W_NRMSD is the percentage of normalized root mean square error in horizontal direction.

Comparing the data of the 3D model, the standard model is obtained by the algorithm flow in this paper. The H_NRMSD and W_NRMSD both mean the error of model size. H represents height and W represents width. It is found that the errors of the algorithm under H_NRMSD and W_NRMSD indexes are all less than 1.00. Then, it can be seen that the algorithm can restore 3D objects using 2D images. With a high restoration accuracy and strong robustness, the reconstruction process adapts to changes in shooting conditions and overcomes the technical problems such as the image distortion and nonlinear contour model that cannot be completely solved in traditional 3D restoration results.

3.3. Precision Experiment of 3D Reconstruction. In order to further test the restoration accuracy of 3D printing model algorithm, two 3D scanners, the noncontact digital scanning and measuring equipment of cultural relics and the advanced 3D scanner Einscan-SP on the market, were used to scan the ancient ceramic samples, respectively. They are denoted as scanner I and scanner II below. The height data and side edge contour data extracted from the two sets of point cloud data were integrated and compared with the data extracted by the algorithm in this paper. The experimental test data are shown in Table 2. The data obtained from scanner I was used as the standard value to verify and compare the accuracy of the proposed method and the scanner II. H1 and W1 in Table 2 represent the vertical and horizontal precision of the ceramic contour model constructed by the algorithm in this paper. Meanwhile, H and W represent the vertical and horizontal precision of the data acquired by the scanner II. According to the testing data in Table 2, the modeling accuracy of the algorithm in this paper is closer to the standard data of the scanner. Besides, this conclusion can be seen more intuitively.

Through simulation experiments, the adaptive perspective correction algorithm and the traditional distortion correction algorithm are, respectively, used to extract the side edge contour of ancient ceramics, and then the accuracy of the two algorithms is compared. The experimental results are shown in Figure 8. The left and right red curves are standard edge contour curves of jade spring bottles, which are fitted by interpolation function according to the physical standard point cloud data obtained by 3D scanner. The blue curve on the left is the contour curve of the bottle side after processing the 2D image with the traditional perspective correction method. The blue curve on the right is the edge contour curve of the jade pot spring bottle after processing the 2D image with the perspective correction algorithm in this paper.

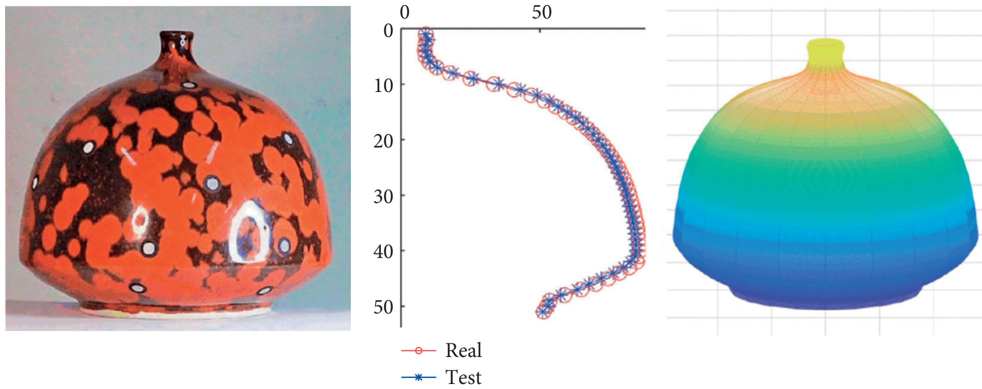

Figure 7: 3D reconstruction control diagram of this model.

Table 1: The calculating data of the sample analysis.

Distance (cm)	Angle/°	H_NRMSD (%)	W_NRMSD (%)
100	−15	1.19	1.24
100	−10	0.93	1.44
100	−5	0.63	1.27
100	0	0.21	1.32
100	5	0.62	1.27
100	10	0.88	1.25
100	15	1.14	1.35
150	−15	0.83	1.11
150	−10	0.64	1.43
150	15	0.47	1.36
150	0	0.26	1.14
150	5	0.40	1.18
150	10	0.76	1.18
150	15	1.08	1.2
200	−15	0.83	1.11
200	−10	0.64	1.43
200	−5	0.47	1.36
200	0	0.26	1.14
200	5	0.40	1.18
200	10	0.76	1.18
200	15	1.08	1.2

Table 2: The calculating data of the sample analysis.

Distance (cm)	Angle/°	H_NRMSD (%)	W_NRMSD (%)
100	−10	1.13	1.14
100	−5	1.03	0.97
100	0	0.61	0.62
100	5	0.82	0.57
100	10	1.08	1.15
150	−10	0.74	1.23
150	−5	0.67	1.06
150	0	0.29	0.74
150	5	0.71	1.08
150	10	1.06	1.38
200	−10	1.14	1.35
200	−5	0.87	1.16
200	0	0.39	0.75
200	5	0.90	1.08
200	10	1.06	1.28

Figure 8: Comparison data of the side edges of the model.

4. Conclusion

In this study, a series of technical problems such as ceramic contour extraction, image distortion correction, and nonlinear contour modeling for 3D printing of rotating body under complex background were solved and a restoration algorithm for the shape of ancient ceramics was proposed. The following conclusions are drawn.

(1) An accurate contour model is established by using the two-dimensional images of the rotating ancient ceramics to reconstruct the three-dimensional model of the ceramic shape. By studying a series of algorithms such as image enhancement, image distortion correction, modeling, and 3D reproduction of ancient ceramics, a complete 3D restoration algorithm of ancient ceramics was obtained.

(2) Experimental results show that when the shooting angle is from −10° to 10° and the resolution is above 40,000 pixels, the algorithm can be used to reduce the

shooting angle to less than 1. Accurate reduction of 3D model of ceramic ware has error less than 6%.

(3) The modeling algorithm for three-dimensional printed ceramics can accurately obtain the three-dimensional model of rotating ancient ceramics, which is of certain significance to explore a new direction of the research and development of three-dimensional printed ancient ceramics. Therefore, the algorithm proposed in this study greatly facilitates the analysis, research, restoration, and display of ancient ceramics and provides a new method for the study of ancient ceramics.

(4) With the continuous development and progress of 3D printing equipment, combined with the integration and intersection of multidisciplinary knowledge such as digitization, biomedical engineering, and medical imaging, 3D printing technology can not only customize personalized bioceramics products, but also realize the restoration of ancient ceramic crafts through 3D reconstruction technology. There is reason to believe that 3D printing technology will certainly become one of the key technologies in the development of the restoration of cultural relics.

Data Availability

The data used to support the findings of this study are available from the corresponding author upon request.

Conflicts of Interest

The authors declare that they have no conflicts of interest.

Acknowledgments

This work was supported by Pingdingshan University.

References

[1] J. Deckers, J. Vleugels, and J. P. Kruthl, “Additive manufacturing of ceramics: a review,” *Journal of Ceramic Science and Technology*, vol. 5, no. 4, pp. 245–260, 2014.

[2] M. Alksne, M. Kalvaityte, E. Simoliunas et al., “In vitro comparison of 3D printed polylactic acid/hydroxyapatite and polylactic acid/bioglass composite scaffolds: insights into materials for bone regeneration,” *Journal of the Mechanical Behavior of Biomedical Materials*, vol. 104, no. 4, 13 pages, Article ID 103641, 2020.

[3] Z. C. Eckel, C. Zhou, J. H. Martin, A. J. Jacobsen, W. B. Carter, and T. A. Schaedler, “Additive manufacturing of polymer-derived ceramics,” *Science*, vol. 351, no. 6268, pp. 58–62, 2016.

[4] Z. Dong, Y. Ni, X. Yang et al., “Characterization and analysis of fluoride calcium silicate composite interface in remineralization of dental enamel,” *Composites Part B: Engineering*, vol. 153, no. 2, pp. 393–397, 2018.

[5] B. Francesco, N. Giorgia, and V. B. Chiara, “Bioceramics and scaffolds: a winning combination for tissue engineering,” *Frontiers in Bioengineering and Biotechnology*, vol. 3, no. 1, pp. 202–219, 2015.

[6] I. Denry and J. Kelly, “State of the art of zirconia for dental applications,” *Dental Materials*, vol. 24, no. 3, pp. 299–307, 2008.

[7] L. Di Angelo, P. Di Stefano, and C. Pane, “Automatic dimensional characterisation of pottery,” *Journal of Cultural Heritage*, vol. 26, pp. 118–128, 2017.

[8] G. T. Oruzbaeva, “Scanning electron microscopy study of the microstructure of ancient issyk-kul ceramic[J],” *Glass and Ceramics*, vol. 77, no. 7-8, pp. 284–287, 2020.

[9] H. Shao, Y. He, J. Fu et al., “3D printing magnesium-doped wollastonite/β-TCP bioceramics scaffolds with high strength and adjustable degradation,” *Journal of the European Ceramic Society*, vol. 36, no. 6, pp. 1495–1503, 2016.

[10] H. Wu, Y. Cheng, W. Liu et al., “Effect of the particle size and the debinding process on the density of alumina ceramics fabricated by 3D printing based on stereolithography,” *Ceramics International*, vol. 42, no. 15, Article ID 17290, 2016.

[11] G. Liu, Y. Zhao, G. Wu, and J. Lu, “Origami and 4D printing of elastomer-derived ceramic structures,” *Science Advances*, vol. 4, pp. 1–10, 2018.

[12] S.-S. Liu, M. Li, J.-M. Wu, A.-N. Chen, Y.-S. Shi, and C.-H. Li, “Preparation of high-porosity Al2O3 ceramic foams via selective laser sintering of Al2O3 poly-hollow microspheres,” *Ceramics International*, vol. 46, no. 4, pp. 4240–4247, 2020.

[13] L. Chen, Q. Zhang, J. Yao et al., “formation of Mn-Co-Ni-O nanoceramic microspheres using in situ ink-jet printing: sintering process effect on the microstructure and electrical properties,” *Small*, vol. 12, no. 36, pp. 5027–5033, 2016.

[14] Y. de Hazan and D. Penner, “SiC and SiOC ceramic articles produced by stereolithography of acrylate modified polycarbosilane systems,” *Journal of the European Ceramic Society*, vol. 37, no. 16, pp. 5205–5212, 2017.

[15] Z. Pan, Y. Wang, H. Huang, Z. Ling, Y. Dai, and S. Ke, “Recent development on preparation of ceramic inks in ink-jet printing,” *Ceramics International*, vol. 41, no. 10, Article ID 12515, 2015.

[16] B. Han and D. L. Yang, “Research on normalization of printed image based on transmission transform [J],” *Computer Engineering and Applications*, vol. 55, no. 23, pp. 188–193, 2019.

[17] H. Gu, Q. Fu, B. Sheng, E. Cai, and G. Tang, “Effect of pore-forming agent quantity on pore structure, phase composition, micro-hardness of gradient bioceramic coatings under optimal laser process parameters et al Effect of pore-forming agent quantity on pore structure phase composition micro-hardness of gradient bioceramic coatings under optimal laser processparameters,” *Ceramics International Ceram. Int.*vol. 46, no. 8, Article ID 11275, 2020.

[18] A.-N. Chen, M. Li, J.-M. Wu et al., “Enhancement mechanism of mechanical performance of highly porous mullite ceramics with bimodal pore structures prepared by selective laser sintering,” *Journal of Alloys and Compounds*, vol. 776, pp. 486–494, 2019.

[19] Y. Fu, G. Xu, Z. Chen, C. liu, D. Wang, and C. Lao, “Multiple metals doped polymer-derived SiOC ceramics for 3D printing,” *Ceramics International*, vol. 44, no. 10, Article ID 11030, 2018.

[20] X. Li, S. Li, W. Bai et al., “Method for rectifying image deviation based on perspective transformation,” *IOP Conference Series: Materials Science and Engineering*, vol. 231, Article ID 012029, 2017.

[21] J. McKenzie-Clark, “Distinguishing between rouletting and chattering on ancient mediterranean pottery,” *American Journal of Archaeology*, vol. 119, no. 1, pp. 137–143, 2015.

[22] X. P. Wu, Y. P. Guan, W. D. Li, J. Wu, J. M. Wu, and Z. X. Zhao, “Classification and recognition of ancient

ceramics by visible-near-infrared spectroscopy," *Spectroscopy and Spectral Analysis*, vol. 39, no. 3, pp. 756–764, 2019.

[23] Z. Wu, W. Liu, H. Wu et al., "Research into the mechanical properties, sintering mechanism and microstructure evolution of Al2O3-ZrO2 composites fabricated by a stereolithography-based 3D printing method," *Materials Chemistry and Physics*, vol. 207, pp. 1–10, 2018.

[24] A.-N. Chen, J.-M. Wu, Y.-X. Liu et al., "Fabrication of porous fibrous alumina ceramics by direct coagulation casting combined with 3D printing," *Ceramics International*, vol. 44, no. 5, pp. 4845–4852, 2018.

[25] A. Rabani, J. Madariaga, C. Bouvier, and D. Axinte, "An approach for using iterative learning for controlling the jet penetration depth in abrasive waterjet milling," *Journal of Manufacturing Processes*, vol. 22, no. 4, pp. 99–107, 2016.

[26] J. Emil, L. Oscar, J. Jan, O. Lyckfeldt, and E. Adolfsson, "Influence of resin composition on the defect formation in alumina manufactured by stereolithography," *Materials*, vol. 10, no. 2, p. 138, 2017.

[27] T. Mu, F. Wang, X. Wang, and H. Luo, "Research on ancient ceramic identification by artificial intelligence," *Ceramics International*, vol. 45, no. 14, Article ID 18140, 2019.

[28] H. Li, Y. Liu, Y. Liu, Q. Zeng, and J. Liang, "Silica strengthened alumina ceramic cores prepared by 3D printing," *Journal of the European Ceramic Society*, vol. 41, no. 4, pp. 2938–2947, 2021.

[29] H. Shao, J. He, T. Lin, Z. Zhang, Y. Zhang, and S. Liu, "3D gel-printing of hydroxyapatite scaffold for bone tissue engineering," *Ceramics International*, vol. 45, no. 1, pp. 1163–1170, 2019.

Hindawi
Scientific Programming
Volume 2022, Article ID 9212856, 10 pages
https://doi.org/10.1155/2022/9212856

Research Article

A Gaussian Process Classification and Target Recognition Algorithm for SAR Images

Na Yang and Yongtao Zhang

Department of Information and Electronic Engineering, Shangqiu Institute of Technology, Shangqiu 476000, China

Correspondence should be addressed to Yongtao Zhang; ytzjw@sqgxy.edu.cn

Received 22 November 2021; Revised 20 December 2021; Accepted 4 January 2022; Published 20 January 2022

Academic Editor: Le Sun

Synthetic aperture Radar (SAR) uses the relative movement of the Radar and the target to pick up echoes of the detected area and image it. In contrast to optical imaging, SAR imaging systems are not affected by weather and time and can detect targets in harsh conditions. Therefore, the SAR image has important application value in military and civilian purposes. This paper introduces the classification of Gaussian process. Gaussian process classification is a probabilistic classification algorithm based on Bass frame. This is a complete probability expression. Based on Gaussian process and SAR data, Gaussian process classification algorithm for SAR images is studied in this paper. In this paper, we introduce the basic principle of Gaussian process, briefly analyze the basic theory of classification and the characteristics of SAR images, provide the evaluation index system of image classification, and give the SAR classification model of Gaussian process. Taking Laplace approximation as an example, several classification algorithms are introduced directly. Based on the two classifications, we propose an indirect multipurpose classification method and a multifunction classification method for two-pair two-Gaussian processes. The SAR image algorithm based on the two categories is relatively simple and achieves certain results.

1. Introduction

Synthetic aperture Radar (SAR) is an active modern high-resolution microwave imaging Radar [1]. SAR is an active Earth observation system, which can be installed on aircraft, satellites, spacecraft, and other flight platforms to observe the Earth all day and in all weather conditions and has a certain ability to penetrate the surface. SAR improves azimuth and range resolution by using synthetic aperture and pulse compression techniques. It breaks the boundary of Radar camera mode in the past and improves the camera ability of the observation area. Compared with other remote sensing imaging systems, the number of synthetic apertures has increased [2]. The Radar imaging system cannot be affected by light and bad weather and can take necessary ground scenes in one day and in all weather conditions. Because of the above advantages, SAR imaging technology is widely used in resource exploration, land exploration, wartime hostile target inspection, etc. and also has great application to people's livelihood [3]. It has great application potential. When the 5.12 Wenchuan earthquake occurred, it was difficult to obtain rescue information and monitor disasters due to the harsh local climatic conditions. Synthetic aperture Radar can overcome these problems well [4].

With the continuous exploration and development of SAR imaging technology, the demand for SAR image data is getting higher and higher. However, on the other hand, SAR images are quite different from optical images and have the characteristics of correlated noise [5, 6]. This makes the readability of SAR images much stronger than that of optical images, which makes it difficult for scientific researchers to interpret them manually. Therefore, it is difficult to automatically recognize SAR images at present. Automatic Target Recognition (ATR) technology for SAR images is becoming more and more important and becomes an important research direction [7].

In military warfare, with the development of electronic information countermeasure technology, the outcome of electronic warfare has become one of the decisive factors. Especially in the complex electromagnetic environment, it is very important to identify and detect the enemy's intentional camouflage.

Automatic recognition of conventional SAR images requires complex steps such as filter noise reduction, image optimization, and image classification [8]. For automatic recognition of conventional SAR images, complex steps such as image preprocessing, feature extraction, image classification, and recognition are required. The specific process is shown in Figure 1.

There are too many processing steps, and the speed and accuracy cannot meet the actual military needs. Because of the excellent performance of Gaussian process in image processing, SAR image ATR based on Gaussian process has become the focus of research [9]. Gaussian process is a kind of stochastic process in probability theory and mathematical statistics, which makes it easier to classify and segment images. A large number of studies show that Gaussian process technology can be used to effectively process SAR images [10].

2. SAR Image Classification Algorithm Based on Gaussian Process

2.1. Research Status of Gaussian Process. Machine learning has been studied for more than a century, and many theories have been formed, but the research on Gaussian process is relatively late. Since 1970s and 1980s, Gaussian process has been applied to geostatistics in the name of Gaussian process regression, such as mineral exploration and remote sensing monitoring [11]. The main problem to be solved is the low-dimensional problem of geoscience statistics, and there is a lack of research on the probability of models and the independence of kernel functions.

Hagan first proposed the use of Gaussian process in the regression model in 1978. Later, Devid J. C. Mackey proposed to establish empirical models by nonlinear parameterization of models, such as radial basis function and layer perceptron. Subsequently, bar Shalom and Fortmann used the Kalman filter to explain the stationary one-dimensional Gaussian process [12].

In 1990s, people made a deeper exploration of kernel function in machine learning. A famous example is support vector machine. At this stage, the application of Gaussian process in machine science has attracted some attention [13]. For example, in 1992, Mackey proposed a framework using Gaussian processes by using approximation methods. However, until 1996, Neal found that its nodes obey Gaussian distribution in the research of Bayesian neural network and Gaussian process began to attract wide attention [14].

In recent years, Gaussian process has been applied to predictive control and soft sensor modeling because of its good model reliability and can meet the requirements of industrial field application. At the same time, it has been further studied in the field of machine learning [15, 16].

2.2. Fundamentals of Gaussian Process

2.2.1. Machine Learning Theory. Machine learning breeds strong vitality [17]. This is to find out the rules between data by analyzing the characteristics and association of data and to mine all kinds of information needed by human beings at a deeper level. Several common learning methods are briefly introduced as follows:

(1) *Description-Based Learning* [18]. In a data area, we describe a concrete example, find the main factors associated with the concrete example, and finally perform the process of forming a generalized concept.

(2) *Analogical Learning* [19]. We compare two data regions, find the similarities between them, and explain the unsolved problems of other data regions from the related theories of one data region [20, 21].

(3) *Concentrate on Your Studies.* We reason about the existing instances and summarize the specific hypothesis process. From the special to the ordinary, from the simple to the complex, using the local to the whole method, we summarize the learning.

As can be seen from Figure 2, the machine learning system is always on optimized learning mode. By providing back the results from the executive part to the learning part and optimizing the knowledge base all the time, the whole model is optimized. The most important thing in machine learning is to derive learning patterns through training sample data. Therefore, machine learning needs to first determine the learning objects (X, Y) and training samples, learn the sample data with corresponding learning methods, and derive the learning model. Finally, according to the model, a value Y is obtained for any input X, which is a vector and contains the hidden information in the data, that is, the necessary information. The mathematical representation of machine learning, which selects the function that best represents the training result from the given $f(x, a)$. The selection is trained only based on the sample data and does not depend on prior knowledge of the sample data that is known in advance. Whether the learning model is suitable to be evaluated by the difference $L\ (Y, F\ (X, A))$ between the sample Y value and the value $F\ (X, A)$ obtained under the machine learning condition is established by

$$R(a) = \int L(y, f(x,a))dF(x,y). \tag{1}$$

The training sample consists of a probability distribution $F(x,y) = F(x)F(y\,|\,x)$ composed of n pairs of observed data $(x_1, y_1), \ldots, (x_n, y_n)$ under independent and identical distribution conditions. In most practical cases, $F(x, y)$ in training is unknown.

The powerful feature extraction ability of CNN depends on the convolution operation of the target image expansion by the convolution kernel. The new value obtained by dot product and sum operation on the image is the eigenvalue of each point pixel [22]. At the level of data structure, both image and convolution kernel are essentially a numerical

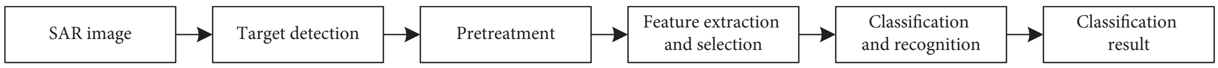

Figure 1: SAR automatic recognition flow.

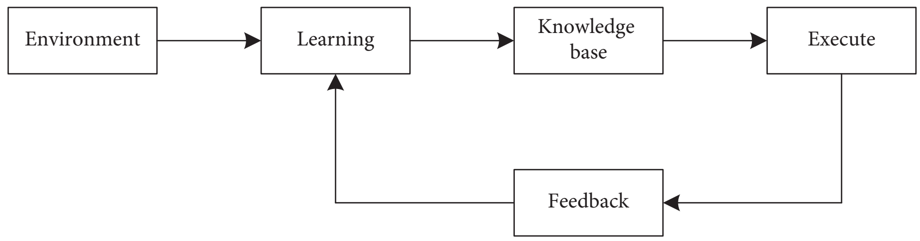

Figure 2: Machine learning system model.

matrix, in which the size of image matrix is $W \times W \times D$ and the size of convolution kernel square matrix is $F \times F \times D$. D above represents the depth of the image channel, W represents the side length of the image, and F represents the side length of the convolution kernel. A single channel image with depth 1 and width and height 5 and a convolution kernel with side length 3 are used for convolution operation display. The convolution kernel firstly covers the left vertex area of the feature map and carries out dot product and sum operation on the pixel values in the covered area to obtain the pixel values in the red virtual box in the output feature map, which is the first calculation step of convolution. The green virtual box is the coverage area where the convolution kernel shifts to the right by one unit length and then repeats the dot product and summation operation in the first step to obtain the value of pixels in the green virtual box in the output feature map. Here, the unit length of the convolution kernel shifts to the right is called the moving step size, which is represented by S, and this process is the second step of the convolution operation process. When the convolution kernel repeats the above steps and traverses the image matrix from left to right and from top to bottom, it completes a convolution operation process and finally obtains a 3×3 output feature map.

By substituting the corresponding numerical value, the value of N is 3, that is, the size of the output characteristic map is 3×3. It can be seen from the whole convolution operation process that the convolution kernel in each operation process has not changed, and this operation ensures the invariance of the internal parameters of the kernel, that is, weight sharing, which avoids the problem of excessive increase of parameters. In addition, the above convolution operation still brings some problems, such as the reduction of feature image size and insufficient utilization of image edge information. Facing the above problems, we can use filling strategy at the edge of the image to solve them. The edge of the image is filled with pixels with a length of 1 and a value of 0, and the feature image with a size of 5×5 can be obtained by recalculating with a convolution kernel with a size of 3×3, which makes the output image keep the same size as the input image and makes full use of the edge pixels of the original image.

2.2.2. Bayesian Theory. Bayesian theory takes the form of

$$p(\theta \mid x) = \frac{p(\theta) p(\theta \mid x)}{p(x)} = \frac{p(\theta) p(\theta \mid x)}{\int p(\theta) p(\theta \mid x)} \mathrm{d}\theta. \tag{2}$$

2.3. Classification Decision Theory. The output of the regression model is converted into class probability by response function, and the following model is adopted:

$$p(C_1 \mid x) = \lambda\left(x^T w\right), \lambda(z) = \frac{1}{1 + \exp(-z)}. \tag{3}$$

Up to now, there is no correct answer as to which method to choose. Compared with the direct generation method, the indirect reference method has the advantage that when the modeling of $p(y \mid z)$ is direct, the x dimension is high and the prior density of the class distribution of data is relatively easy to obtain and the practical problem may be more complicated if the direct generation method is adopted, so the indirect reference method is adopted in this paper.

Common optical images are easier to recognize, while SAR images have poor recognition ability because of their features. The synthetic aperture Radar (SAR) imaging system firstly collects the electromagnetic wave reflected from the measured object from the sensor and uses SAR imaging algorithm to reproduce the SAR image in reverse. According to the transmitting and receiving mode of the electromagnetic wave of the sensor, the imaging mode of SAR image can be divided into vertical polarization (V) and horizontal polarization (H). After the two combinations, there are four camera modes: HH, HV, VH, and VV. The color optical image has three channels: R, G, and B. SAR images have different channel numbers according to different shooting methods. SAR images are divided into three types according to the number of image channels: unipolarized, dual-polarized, and multipolarized. As the number of channels in a SAR image increases, it contains more information.

The Radar image can be obtained by processing the reflected electromagnetic wave signal of the detected object. However, SAR images have fatal shortcomings. Coherent point noise produces interference phenomenon when the target rotates, which leads to anomaly. The gray value of the image shakes violently in a certain range, which is bright and dark, and has a sense of wear. The recognition ability of SAR images is reduced, which makes it difficult to recognize SAR images.

When the surface of the photographing area is uneven, electromagnetic signals reflected from a plurality of different objects are superimposed and returned. Because the surface of each object is uneven, the distance between the SAR imaging system and receiver is random and the signal received by the receiver is related to frequency, but the phase and random change are strong. It is going to return one degree.

Assuming that the imaging area is K scatterers and has an echo reflected on each object, phase P, and amplitude A, the echo signal received by the receiver after superposition of all scatterer echoes is as follows:

$$z = Ae^{j\varphi} = \sum_{i=1}^{k} A_i e^{j\varphi_i}, \tag{4}$$

where A and φ represent the amplitude and phase of the echo received by the receiver. From the above formula, it is found that when the Radar imaging system moves, the echo path changes and the corresponding phase changes, which affects the whole echo signal. Because of the shortcomings in photography principle, random correlated speckle noise will be produced during photography. In this way, SAR images also produce randomness. On the other hand, SAR images are particularly sensitive to each other's position angle. If the same detected object is shot at different angles, it will cause dramatic changes in SAR images.

There is a very complex correlation between coherent point noise and SAR image information, such as gray value and reflection intensity. K distribution, Weibull distribution, and lognormal distribution, which are often used now, explain the statistical characteristics of SAR images.

2.3.1. K Distribution. For high-resolution SAR images, we will use K distribution to describe its probability density:

$$p(x) = \frac{2}{b\Gamma(v)}\left(\frac{x}{b}\right)^{v/2} K_{v-1}\left(2\sqrt{\frac{x}{b}}\right)(x>0, v>0, b>0), \tag{5}$$

where b is the scale parameter, v is the shape parameter, and K_v is the modified Bassel function of the second kind.

The expectation and variance of the probability density function are as follows:

$$E(x) = \frac{b\Gamma(v+(1/2))\Gamma((3/2))}{\Gamma(v)}, \tag{6}$$

$$\operatorname{var}(x) = b^2\left[v - \frac{\Gamma^2(v+(1/2))\Gamma^2((3/2))}{\Gamma^2(v)}\right]. \tag{7}$$

2.3.2. Weibull Distribution. Weibull distribution is more suitable for describing SAR images, and its probability density function can be expressed as

$$p(x) = \frac{c}{b}\left(\frac{x}{b}\right)^{c-1}\exp\left[-\left(\frac{x}{b}\right)^{c}\right]. \tag{8}$$

Expectations and variances are as follows:

$$E(x) = b\Gamma\left(1+c^{-1}\right), \tag{9}$$

$$\operatorname{var}(x) = b^2\left[\Gamma\left(1+2c^{-1}\right) - \Gamma^2\left(1+c^{-1}\right)\right]. \tag{10}$$

2.3.3. Lognormal Distribution. When SAR imaging, there is a main target to be detected, which is suitable to be described by lognormal distribution. The probability density function is as follows:

$$p(x) = \frac{1}{x\sigma\sqrt{2\pi}}\exp\left(\frac{-(\ln(x)-\mu)^2}{2\sigma^2}\right), \tag{11}$$

where μ denotes scale parameter and s denotes shape parameter. Expectations and variances can be expressed as

$$E(x) = e^{(\mu+(\sigma^2/2))}, \tag{12}$$

$$\operatorname{var}(x) = e^{2(\mu+\sigma^2)} - e^{(2\mu+\sigma^2)}. \tag{13}$$

We should use different distribution models to fit the distribution according to the actual situation.

2.4. Classification Accuracy Evaluation System. The classification accuracy of SAR images is mainly based on the measured images on the ground. With the development of SAR remote sensing technology and the complexity of various applications, the accuracy evaluation of SAR image classification becomes more and more important.

2.4.1. Confusion Matrix. The real classification of land surface is expressed by confusion matrix. The values of each column are the same as the true aberration of the surface. The number of categories corresponds to the category image.

2.4.2. Accuracy of Users and Producers. The accuracy of a particular category classification can be determined by calculating the accuracy of a user (UserAcery, UA) and a producer (Producer Accuracy, PA). The specific formula is as follows:

$$\begin{aligned} \mathrm{UA}_i &= M_{ii} \mid \sum_{j=1}^{T} M_{ij}, \\ \mathrm{PA}_i &= M_{ii} \mid \sum_{i=1}^{T} M_{ij}. \end{aligned} \tag{14}$$

2.4.3. Kappa Coefficient. The Kappa coefficient can be calculated by the following formula:

$$Kp = \left(n\left(\sum_{i=1}^{T} M_{ii}\right) - \sum_{i=1}^{T}\left(\sum_{j=1}^{T} M_{ij}\sum_{j=1}^{T} M_{ji}\right)\right) \mid \left(n^2 - \sum_{i=1}^{T}\left(\sum_{j=1}^{T} M_{ij}\sum_{j=1}^{T} M_{ji}\right)\right). \quad (15)$$

2.5. SAR Image Classification Algorithm Based on Gaussian Process. Taking the second classification as an example, this section briefly introduces the SAR classification algorithm of Gaussian process. The training data $D = (x_i, y_i)$, $i = \{1, 2, \ldots, n\}$ is given, the predicted output y_* takes into account the target value x_* of the sample, and the Gaussian noise usually including zero mean variance σ_n^2 is specifically $y = f(x) + \varepsilon$, where $\varepsilon \sim N(0, \sigma_n^2)$, that is,

$$p(y \mid f) = N\left(y \mid f, \sigma_n^2\right). \quad (16)$$

Gaussian process extends multi-Gaussian distribution to an infinite number of random variables. Its kernel function is k:

$$p(f) = N(0, k). \quad (17)$$

Find the edge distribution of $p(y)$:

$$p(y) = \int p(y \mid f)p(f)\mathrm{d}f = N(y \mid 0, C). \quad (18)$$

When a similar function is configured as a Probit function and the Gaussian result is converted to a probability value, the target variable y follows the Bernoulli distribution:

$$p(y \mid f) = \sigma(f)^y (1 - \sigma(f))^{1-y}. \quad (19)$$

Let $f(x_1), f(x_2) \ldots\ldots f(x_N), f(x_*)$ be denoted as vector f_{N+1}. For f_{N+1}, the form is

$$p(f_{N+1}) = N(f_{N+1} \mid 0, C_{N+1}), \quad (20)$$

where

$$C_{N+1} = \begin{bmatrix} C_N & K \\ K^T & C \end{bmatrix}. \quad (21)$$

For the classification problem, the distribution form is

$$p(y_* = 1 \mid y) = \int p(y_* = 1 \mid f_*)p(f_* \mid y)\mathrm{d}f_*. \quad (22)$$

According to the two classifications, multipurpose classification is carried out. Most of them adopt a pair of multifunctional classifications.

The logarithmic likelihood function of Gaussian process is as follows:

$$\ln p(y \mid \theta) = -\frac{1}{2}\ln\left|C_N\right| - \frac{1}{2}y^T C_N^{-1} y - \frac{N}{2}\ln(2\pi). \quad (23)$$

The partial derivative of logarithmic likelihood function for hyperparameters is

$$\frac{\partial}{\partial\theta_i}\ln p(y \mid \theta) = -\frac{1}{2}\mathrm{tr}\left(C_N^{-1}\frac{\partial C_N}{\partial\theta_i}\right) + \frac{1}{2}y^T C_N^{-1}\frac{\partial C_N}{\partial\theta_i}C_N^{-1}y. \quad (24)$$

3. SAR Image Classification Model Based on Multitarget Strategy Gaussian Process

Most of Gaussian process classification algorithms take two classifications as examples, and SAR images include many target categories. Firstly, this paper introduces the direct multipurpose classification and puts forward the indirect multipurpose classification according to the two classifications.

3.1. Multipurpose Classification Algorithm for Direct Gaussian Processes. Suppose there is a data set (x, y) consisting of n training samples, x is the observation data, and the corresponding category label is y, and $f = (f_1^1 \ldots f_n^1, f_1^2 \ldots f_n^2, \ldots, f_1^C \ldots f_n^C)^T$ is a potential function that divides the whole sample n into vector C. In the covariance of C, the classification is sometimes denoted by C below. The probability distribution of F is $F \sim \mathrm{N}(0, K)$. It is assumed that the computation between F is independent, K belongs to block diagonal structure, Y is a vector with the same dimension as F, and for $I = 1, \ldots, N$, its corresponding value is 1 and otherwise, it is 0.

The output of the Softmax function at training point i is π_i^c:

$$p(y_i^c \mid f_i) = \pi_i^c = \frac{\exp(f_i^c)}{\sum_c \exp(f_i^c)}. \quad (25)$$

At this time, a record c with the same length as f is included. The vector of i represents n. The multifunctional learning formula is a nonstandard delayed classification label.

$$\Psi(f) = -\frac{1}{2}f^T K^{-1} f + y^T f - \sum_{i=1}^{n}\log\left(\sum_{c=1}^{C}\exp(f_i^c)\right) - \frac{1}{2}\log|K| - \frac{C_n}{2}\log 2\pi. \quad (26)$$

Derivation of f on both sides of equation (26) results in

$$\nabla\Psi = -K^{-1} + y - \pi. \tag{27}$$

It can be seen from the extreme value formula that when formula (27) is zero, $\widehat{f} = K(y - \widehat{\pi})$ is the maximum value. Derivation is performed again, and it satisfies

$$-\frac{\partial^2}{\partial f_i^c \partial f_i^c} \log \sum_j \exp\left(f_i^j\right) = \pi_i^c \delta_{cc} + \pi_i^c \pi_i^c. \tag{28}$$

We have

$$\nabla\nabla\Psi = -K^{-1} - W. \tag{29}$$

The Newton method is used to search ψ, which satisfies the following conditions:

$$f^{new} = \left(K^{-1} + W\right)^{-1} (Wf + y - \pi). \tag{30}$$

If you need to predict the test point x_*, you can get a posterior distribution $q(f_* \mid X, y, x_*)(f(x_*) = f_* = (f_*^1, \ldots, f_*^c)^T)$. In general, use

$$q(f_* \mid X, y, x_*) = \int p(f_* \mid X, x_*, f) q(f_* \mid X, y) \mathrm{d}f. \tag{31}$$

Since $p(f_* \mid X, x_*, f)$ and $q(f_* \mid X, y)$ follow Gaussian distribution, $p(f_* \mid X, x_*, f)$ follows Gaussian distribution according to the properties of Gaussian distribution. The projected average values for category C are as follows:

$$E_q[f^c \mid X, y, x_*] = k_c(x_*)^T K_c^{-1} f = k_c(x_*)^T (y^c - \pi). \tag{32}$$

The final equation is obtained from equation (31). By defining the matrix of $Cn \times C$,

$$Q_* = \begin{pmatrix} k_1(x_*) & \cdots & 0 \\ \vdots & \ddots & \vdots \\ 0 & \cdots & k_C(x_*) \end{pmatrix}. \tag{33}$$

Equation (32) is transformed into equation (33).

$$E_q[f_* \mid y] = Q_*^T (y - \pi). \tag{34}$$

Or, we can get the following:

$$\mathrm{cov}_q(f_* \mid X, y, x_*) = \mathrm{diag}(k(x_*, x_*)) - Q_*^T \left(K + W^{-1}\right)^{-1} Q. \tag{35}$$

For both classifications, it is necessary to transform the average value of Gaussian distribution. Edge likelihood can be obtained as follows:

$$\log p(y \mid X, \theta) - \log q(y \mid X, \theta) = -\frac{1}{2} f^T K^{-1} f + y^T f - \sum_{c=1}^{C} \log\left(\sum_{c=1}^{c} \exp\left(f_i^c\right)\right) - \frac{1}{2} \log\left|I_{C_n} + W^{1/2} K W^{1/2}\right|. \tag{36}$$

Suppose W is not a diagonal matrix and K is a block diagonal matrix of $C_n \times C_n$ size. By analyzing the inherent structure of the matrix, it can be modified before using $K^{-1} + W$:

$$\left(K^{-1} + W\right)^{-1} = K - K\left(K^{-1} + W\right)^{-1} K. \tag{37}$$

The matrix inversion lemma used in this case is

$$\left(A^{-1} + B^{-1}\right)^{-1} = A - (A + B)A = B - B(A + B)^{-1} B. \tag{38}$$

$K^{-1} + W + W$ is inverted. First, the inverse transformation of the W matrix is applied to the matrix of equation (34).

$$W^{-1} = \left(D - \pi\pi^T\right)^{-1} = D^{-1} - R\left(I - R^{-1} K R\right)^{-1} R^T = D^{-1}, \tag{39}$$

where $D = \mathrm{diag}(\pi)$; the matrix of $C_{n \times n}$ size composed of the identity matrix of I_n is $R = D^{-1}\pi$.

Bring W^{-1} in

$$\left(K^{-1} + W\right)^{-1} = E - ER\left(\sum_c E_c\right)^{-1} R^T E. \tag{40}$$

3.2. Multipurpose Classification Algorithm for Indirect Gaussian Processes. The one-to-multipurpose classification described in the above section is one of the multipurpose classifications of indirect Gaussian processes. Support vector machine (SVM) can only deal with two classification problems at first, but it cannot deal with many classification problems directly. This section refers to SVM promotion mode and is based on two classification algorithms. The two-to-two Gaussian model of class C classification is shown. This method allows application from two classifications to multiple classifications.

For a given training set $D(X, Y)$ and test data x_*, $x = [x_1, x_2, \ldots, x_n]^T$ and $y = [y_1, y_2, \ldots, y_n]^T$. In order to train a classifier between two classes, for M class problems, two classifiers need to be constructed in the training stage. Each classifier collects any two types of data for training. The type of test data x_* is determined by the maximum counting method. The method introduced above is fast and has high classification accuracy. The algorithm of this method is as follows:

(1) Initialize the input values for each class
(2) In the training stage, select any two data for training and construct two classifiers
(3) In the training stage, train two classifiers finally between two classes
(4) In the test phase, when the test data x_* are classified and discriminated in the training between class i and class j, if the output result of these two classifiers is 1, it belongs to class i of test data x_*

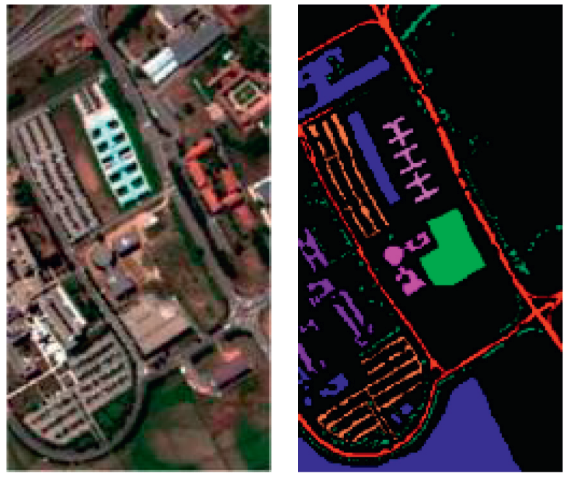

(a) (b)

Figure 3: Pavia University basic information. (a) Original image. (b) Sample distribution.

Table 1: Category and feature information of labeled samples at Pavia University and corresponding categories.

Category	Ground object information	Number of samples	Proportion of each sample (%)
1	Asphalt	161631	15.50
2	Meadow	18649	43.60
3	Gravel	2099	4.91
4	Trees	3064	7.16
5	Painted metal sheet	1345	3.14
6	Bare soil	5029	11.76
7	Asphalt waterproofing	1330	3.11
8	Brick from necklace	3682	8.61
9	Shadow	947	2.21
Total		42779	100

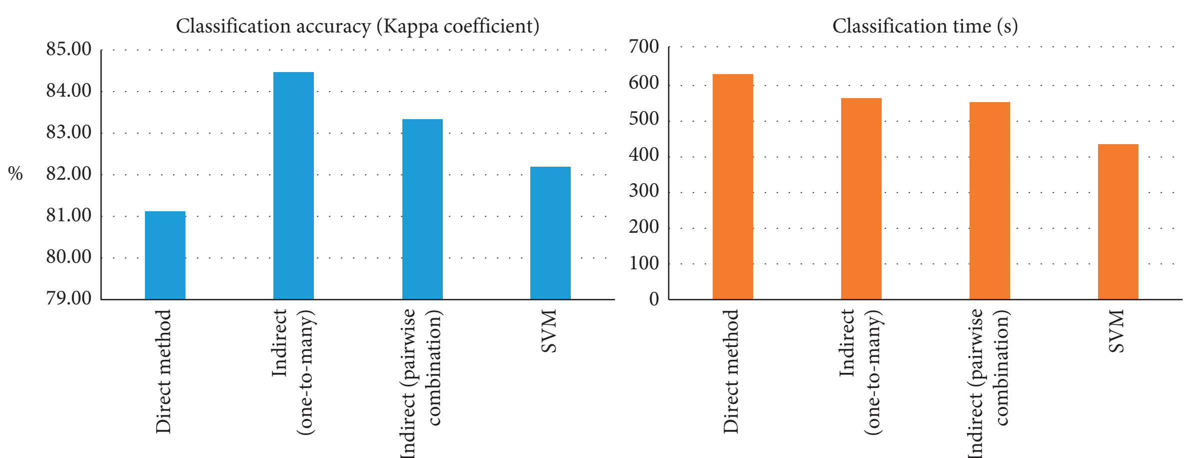

Figure 4: Classification accuracy and time of Pavia University in different ways. In order to analyze and compare more intuitively, compare this figure with classified Figure 5.

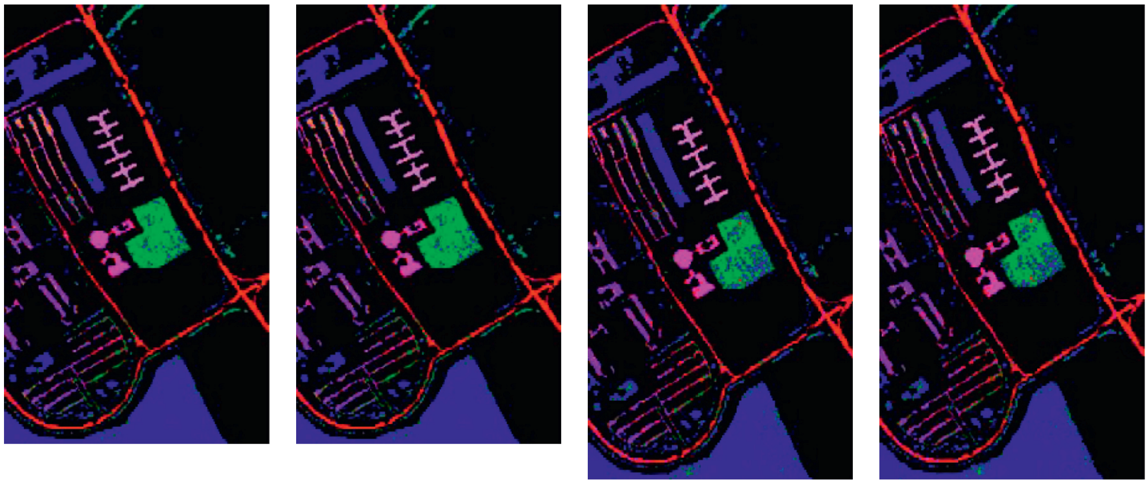

(a) (b) (c) (d)

Figure 5: Pavia University classification renderings. (a) Direct method. (b) Indirect method (one-to-many). (c) Indirect method (two-on-two). (d) SVM.

Table 2: Classification results of different methods.

Algorithm	20	40	80	110	165	220
LNP	—	—	—	94.11	95.97	96.05
Triple-GAN	—	—	—	95.97	96.13	96.11
Improved-GAN	—	—	—	95.02	97.26	98.07
SVM	76.43	87.95	92.48	—	—	—
Adaboost	75.68	86.45	91.95	—	—	—
GAN	84.39	90.13	94.29	—	—	—
MGAN	85.23	90.82	94.91	—	—	—
Classification algorithm of indirect Gaussian process	95.20	98.8	99.88	—	—	—

During the test phase, the test data x_* are calculated. Among the various other numerical values, the largest class of numerical values is the class of x_*.

4. Experiment

The data used in this experiment are from the website of the National University of Bus, Spain. The actual classification samples of the experimental image include 9 kinds of samples, but it can be seen that the data when the samples are discarded are external black stripes.

Figure 3(a) is an original image of Pavia University showing the distribution of the samples shown in Figure 3(b), with irregular land distribution and high degree of crushing. Specifically, the ratio of training samples to prediction samples is about 1 : 8.

Table 1 shows the specific category information and corresponding quantity of samples.

In this experiment, the comparison between indirect multipurpose classification algorithm and support vector machine verifies the direct multipurpose classification algorithm. The experimental results are shown in Figure 4. The approximation algorithms used in experiments are all Laplace approximation methods.

As can be seen from Figures 4 and 5, even if the direct or indirect Gaussian process is applied to SAR classification, the classification accuracy is better than SVM. It is better to classify more kinds of SAR than to classify SAR directly according to the indirect strategy of two classifications. The classification accuracy of SAR images is preferably one-to-many.

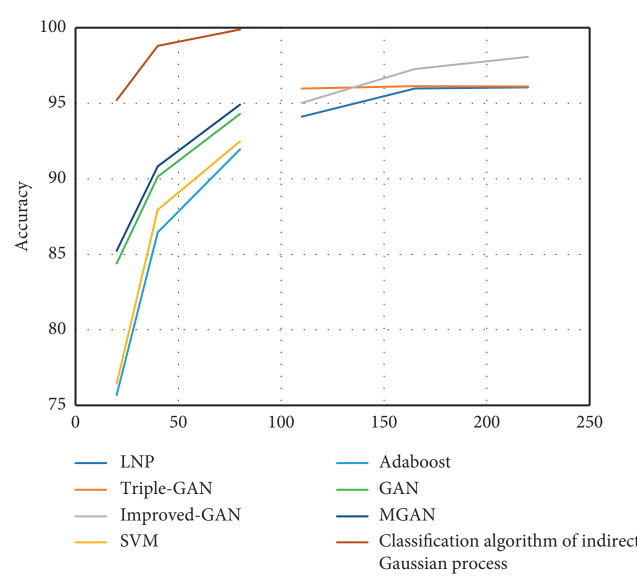

Figure 6: Classification results of various methods.

This paper compares the classification methods for evaluating performance in other MSTAR datasets including LNP, imported-GAN, MGAN, and triple-GAN. LNP assumes that each data point can obtain information from adjacent data and reconstruct it linearly. Triple-GAN uses three network modules, discriminator, generator, and classifier, to achieve the best results of the deep countermeasure model. Indirect Gaussian process classification algorithm achieves the best results in classification and can use the latest training model. MGAN improves images generated using dynamically tuned multirecognizer architecture and improves classification accuracy. The results of typical machine learning methods, for example, SVM and Adaboost, are compared. In the comparative experiment, the same number of labeled samples were used to randomly select samples, and the experimental results were compared with the quantitative results of the paper. The method we use is indirect Gaussian process classification algorithm. The comparison results are shown in Table 2. Figure 6 shows the classification accuracy of methods with different amounts of tag training data.

5. Conclusion

This paper describes the characteristics of SAR images and the difficulty of processing and extracts the advantages of Gaussian process classification in SAR images. Finally, the evaluation index of image classification is given, and a certain standard of Gaussian SAR classification algorithm is given to evaluate the classified image and its basic program is introduced.

Based on the analysis and introduction of machine learning theory and Bessel principle, this paper expounds the basic principle of Gaussian process. This paper introduces the basic theory of classification, then leads to the fact that classification usually needs to be solved, and discusses it in detail. This paper describes the characteristics of SAR image and the difficulty of processing and extracts the advantages of Gaussian process classification in SAR image processing. Finally, we give the evaluation index of image classification, give a certain standard of Gaussian process SAR classification algorithm to evaluate the classified image, and introduce its basic program.

Data Availability

The experimental data used to support the findings of this study are available from the corresponding author upon request.

Conflicts of Interest

The authors declare that they have no conflicts of interest regarding this work.

Acknowledgments

This work was sponsored in part by Henan Province Higher Education Training Program for Young Core Teachers, under Grant no. 2021GGJS192.

References

[1] M. Stasolla, J. J. Mallorquí, G. Margarit, C. Santamaria, and N. Walker, "A comparative study of operational vessel detectors for maritime surveillance using satellite-borne synthetic aperture radar," *IEEE Journal of Selected Topics in Applied Earth Observations and Remote Sensing*, vol. 9, no. 6, pp. 2687–2701, 2019.

[2] G. Shu, N. Wang, W. Wang et al., "A novel vortex synthetic aperture radar imaging system: decreasing the pulse repetition frequency without increasing the antenna aperture," *IEEE Transactions on Geoscience and Remote Sensing*, vol. 60, pp. 1–14, 2022.

[3] Y. Xiang, "Exploration of the application of artificial intelligence technology in mechatronics technology based on," *Journal of Physics: Conference Series*, vol. 1915, no. 2, Article ID 22059, 2021.

[4] S. K. Ahmad, F. Hossain, H. Eldardiry, and T. M. Pavelsky, "A fusion approach for water area classification using visible, near infrared and synthetic aperture radar for south asian conditions," *IEEE Transactions on Geoscience and Remote Sensing*, vol. 58, no. 4, pp. 2471–2480, 2020.

[5] E. Shah, P. Jayaprasad, and M. E. James, "Image fusion of SAR and optical images for identifying antarctic ice features," *Journal of the Indian Society of Remote Sensing*, vol. 47, no. 12, pp. 2113–2127, 2019.

[6] L. Wan, Y. Xiang, and H. You, "An object-based hierarchical compound classification method for change detection in heterogeneous optical and SAR images," *IEEE Transactions on Geoscience and Remote Sensing*, vol. 57, no. 12, pp. 9941–9959, 2019.

[7] L. Wang, X. Bai, C. Gong, and F. Zhou, "Hybrid inference network for few-shot SAR automatic target recognition," *IEEE Transactions on Geoscience and Remote Sensing*, vol. 59, no. 11, pp. 9257–9269, 2021.

[8] G. Chen, L. Wang, and M. M. Kamruzzaman, "Spectral classification of ecological spatial polarization SAR image based on target decomposition algorithm and machine learning," *Neural Computing & Applications*, vol. 32, no. 10, pp. 5449–5460, 2020.

[9] M. Touafria and Q. Yang, "SAR-ATR method based on dual convolution capsule network," *IET Radar, Sonar & Navigation*, vol. 14, no. 12, pp. 1870–1878, 2020.

[10] Y. Endo, M. Halabisky, L. M. Moskal, and S. Koshimura, "Wetland surface water detection from multipath SAR images using Gaussian process-based temporal interpolation," *Remote Sensing*, vol. 12, no. 11, 1756 pages, 2020.

[11] A. Maran Beena and A. K. Pani, "Fault detection of complex processes using nonlinear mean function based Gaussian process regression: application to the Tennessee eastman process," *Arabian Journal for Science and Engineering*, vol. 46, no. 7, pp. 6369–6390, 2020.

[12] M. Khorrami and A. Aghamohammadi, "Thermal conduction in a quasi-stationary one-dimensional lattice system," *International Journal of Modern Physics B*, vol. 33, no. 17, Article ID 1950178, 2019.

[13] Y.-H. Chen, Y.-Z. Xie, X.-Y. Ge et al., "Vulnerability assessment of equipment excited by disturbances based on support vector machine and Gaussian process regression," *IEEE Transactions on Electromagnetic Compatibility*, vol. 63, no. 1, pp. 103–110, 2021.

[14] G. B. Chen, Z. Sun, and L. Zhang, "Road identification algorithm for remote sensing images based on wavelet

transform and recursive operator," *IEEE Access*, vol. 8, pp. 141824–141837, 2020.
[15] X. Chen, Y. Tian, T. Zhang, and J. Gao, "Differential evolution based manifold Gaussian process machine learning for microwave filter's parameter extraction," *IEEE Access*, vol. 8, pp. 146450–146462, 2020.
[16] R. Anandaroop and M. David, "Bayesian geophysical inversion with trans-dimensional Gaussian process machine learning," *Geophysical Journal International*, vol. 217, no. 3, pp. 1706–1726, 2019.
[17] R. Xu, N. Chen, Y. Chen, and Z. Chen, "Downscaling and projection of multi-CMIP5 precipitation using machine learning methods in the upper han river basin," *Advances in Meteorology*, vol. 217, no. 4, pp. 1706–1726, 2020.
[18] T. Tanti, D. A. Kurniawan, W. Sukarni, E. Erika, and R. Hoyi, "Description of student responses toward the implementation of problem-based learning model in physics learning," *JIPF (Jurnal Ilmu Pendidikan Fisika)*, vol. 6, no. 1, 30 pages, 2021.
[19] M. Klenk and K. Forbus, "Exploiting persistent mappings in cross-domain analogical learning of physical domains," *Artificial Intelligence*, vol. 195, pp. 398–417, 2013.
[20] X. Ning, K. Gong, W. Li, L. Zhang, X. Bai, and S. Tian, "Feature refinement and filter network for person re-identification," *IEEE Transactions on Circuits and Systems for Video Technology*, vol. 31, no. 9, pp. 3391–3402, 2021.
[21] X. Ning, W. Li, B. Tang, and H. He, "BULDP: biomimetic uncorrelated locality discriminant projection for feature extraction in face recognition," *IEEE Transactions on Image Processing*, vol. 27, no. 5, pp. 2575–2586, 2018.
[22] X. Peng, X. Zhang, Y. Li, and B. Liu, "Research on image feature extraction and retrieval algorithms based on convolutional neural network," *Journal of Visual Communication and Image Representation*, vol. 69, no. 6, Article ID 102705, 2019.

Hindawi
Scientific Programming
Volume 2022, Article ID 5031639, 9 pages
https://doi.org/10.1155/2022/5031639

Research Article

Dialectical Analysis of Comparative Pedagogy Based on Multiple Intelligences Evaluation

Ningning Liu,[1] **Ruige Jiang**,[2] **and Xiaoxia Tai**[1]

[1]*School of Primary Education, Xingtai University, Xingtai, Hebei 054000, China*
[2]*Department of Educational Sciences, XingTai University, Xingtai, Hebei 054000, China*

Correspondence should be addressed to Ruige Jiang; 201920479@xttc.edu.cn

Received 18 October 2021; Revised 11 November 2021; Accepted 25 November 2021; Published 20 January 2022

Academic Editor: Le Sun

As a common and mature algorithm, the neural network algorithm has been widely used in many industries throughout the country. The traditional dialectical analysis method for multiple intelligences evaluation in comparative education cannot meet the dialectical needs with different characteristics, the information big data model of multiple intelligences evaluation based on neural network algorithm has been gradually applied to several evaluation systems of comparative education. This paper studies the application of neural network algorithms in the dialectical analysis of comparative education in China and puts forward multiple intelligences evaluation model based on neural network algorithm, which can realize the intelligent evaluation of comparative education according to the characteristics of teaching behavior. At the same time, the idea of random big data acquisition is combined with digital feature analysis based on neural network algorithm and particle swarm optimization algorithm. Finally, the experimental results show that the dialectical analysis model of comparative education based on multiple intelligences evaluation of neural network algorithm can efficiently process the education data with tracking intelligence, which achieves a new breakthrough in the multiple intelligences evaluation of comparative education in China and saves a lot of time for the dialectical analysis process.

1. Introduction

It is a new branch in the field of educational science. There are different opinions on what is comparative education. Most comparative education scholars believe that we should study the major international education problems in the development of world education from the reality of various countries, rather than conceive a formal theoretical system of little practical significance from the abstract definition. From the viewpoint and method of Marxism, the comparative pedagogy uses the viewpoint and method of dialectical materialism and historical materialism to make comprehensive use of relevant new science and technology to study the current education in different countries, nationalities, and regions in the world. On the basis of discussing their respective economic, political, philosophical, and national traditional characteristics, this paper studies some common characteristics, development laws, and general trends of education and makes a scientific prediction, so as to learn from each other's strong points and make up for their weaknesses according to their national characteristics and other specific conditions, give full play to the best role of education, and serve to improve the quality of education and the people's cultural and scientific level. The basic characteristics of comparative pedagogy are international, which require comparative education. At least comparative research should be carried out on the education of more than two countries. It is cross-national, international, and comparable. In international education, only by comparison can we identify and only by identification can we explore scientific conclusions in line with the objective law as a reference for our country. Comprehensive or interdisciplinary, the task of comparative pedagogy research is to concentrate the achievements of several social disciplines on the research of education in various countries. It spans the scope of several disciplines.

The research on multiple intelligences evaluation in the dialectic analysis of comparative pedagogy in China has gradually become a hot topic in the field of comparative education. With the development of the mobile internet industry in China, the dialectic analysis methods of comparative pedagogy are increasing, which makes the intelligent evaluation scheme also put forward new challenges in terms of rapidity and universality [1]. Therefore, how to solve the dialectical analysis model of comparative education of multiple intelligences assessment has become an important challenge in comparative education industry research in China. As of May 2021, many scholars have studied different aspects of the dialectical analysis of comparative pedagogy and have made many achievements. Scholars found that in the process of dialectical analysis of comparative education, most scholars still adopt the traditional questionnaire analysis method but ignore the authenticity of the intelligent algorithm for data acquisition and processing. Therefore, an intelligent data evaluation model based on the genetic algorithm is proposed [2].

2. Related Work

The scholars have proposed that the development of the three-dimensional comparative pedagogy dialectical analysis method should be emphasized [3]. Through the intelligent multielement evaluation system based on micro-nano flexible sensor, the evaluation and construction based on intelligent algorithm and evaluation method should be strengthened, the multi-design and attention of intelligent evaluation scheme should be improved, and the evaluation quality of comparative education should also be paid attention [4]. According to the multi-factor relationship theory in comparative education, researchers propose a new intelligent evaluation solution and analyze the relationship between the traditional dialectic analysis field and the integrated solution of intelligent evaluation [5]. The scholars improved the evaluation method by combining the principal component analysis and other relevant theories, constructing the intelligent evaluation system based on the traditional particle swarm optimization, and explaining the practical significance of the dialectical evaluation system with the theory of modern analytical science [6]. Scholars found that most of the existing researches have not involved the dialectical analysis mode of comparative pedagogy based on multiple intelligences evaluation and also did not carry out modular processing of comparative pedagogy. Research hotspot has not built relevant models for this aspect [7]. The scholars analyze from the convenience of comparative education. Because of the strong specific problems, they do not have the rapidity, unity, and universality of the dialectic analysis scheme in comparative education; therefore, it is difficult to achieve the modular processing of dialectical intelligence based on the characteristics of comparative education data and comparative education [8]. Scholars found that the mainstream dialectic analysis system of comparative education has not developed to a very mature stage of technology, and more is based on specific problems or specific views of solution design [9]. Researchers found that there are still many shortcomings in the error rate of the comparative education model and the stability of relevant algorithms in the market. Therefore, the comparative education model based on a neural network algorithm is adopted. The results show that the model is in line with the development trend of mobile internet [10]. In view of the above research status, this study establishes a comparative pedagogical dialectic analysis model of multi-agent evaluation from the aspect of neural network algorithm.

This research is divided into three parts. The first part introduces the basic idea and the application of neural network algorithm and analyzes the application of neural network algorithm in the establishment of a dialectical analysis model of comparative education based on multi-agent evaluation [11]. The second part realizes the automatic analysis of the dialectic analysis and quantitative evaluation of comparative pedagogy and the intelligent processing of the data of the automatic two-way comparative pedagogy dialectic analysis. Then, the multiple intelligences evaluation is realized through the data processing in the process of the dialectical analysis of the relevant comparative education [12]. The third part studies the feasibility and practical application effect of the dialectical analysis model of comparative pedagogy based on multiple agent intelligences evaluation through design experiments.

3. Establishment of Multiple Intelligences Evaluation Model Based on Neural Network Algorithm

In order to study the factors that affect the establishment of a multi-agent evaluation model, this paper proposes a multi-agent evaluation model based on a neural network algorithm. In the process of scientific research, it is necessary to compare the complex factors and interference factors in the dialectical analysis of pedagogy. The neural network algorithm (one of the local optimal algorithms) refers to the best choice to solve the problem. The typical neural network structure is a forward network with three or more layers without feedback and no interconnection structure in the layer [13]. That is, it does not consider the overall optimal, what it does is the local optimal solution to some extent [14]. In the process of solving, the neural network algorithm cannot get the overall optimal solution for all problems but depends on the selection of neurons and neural nodes. The selected optimization strategy must have no effect; that is, the process before a state will not affect the later state, only related to the current state [15]. The common types and frameworks of the system in cloud computing and data analysis are shown in Figure 1.

At present, the mainstream local intelligence analysis algorithm is based on the basic principle of local optimization. After the dialectical analysis of quantitative evaluation and comparative education, it selects the two-way neural regulation and group processing of the local optimal approach to form a locally optimal solution method with the “best two-way interaction characteristics” [16]. Based on the above analysis of the neural network algorithm, in the study

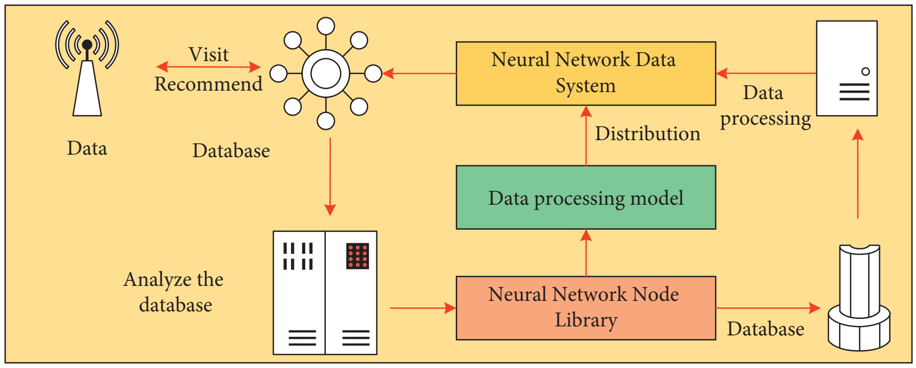

Figure 1: Common types and frameworks of the algorithm.

of the coupling relationship between the comparative education and other factors, this model uses the neural network algorithm based on the optimal ganglion point structure and selects three characteristic parameters related to the dialectical analysis and influence the index of comparative education. In this paper, a model of dialectic analysis coupling relationship and analytic recognition of comparative education based on neural network algorithm is proposed [17]. Through the research on the educational value, educational level, integrity of teaching mode, and teaching effect of comparative pedagogy, this paper clearly defines the whole coupling relationship and the hierarchical framework and index relationship of the analytical system. This paper evaluates the scientificity and objectivity of the model from multiple perspectives, explores the establishment of an intelligent multiple evaluation model from multiple perspectives, and then classifies and analyzes the characteristics of the analysis results after coupling analysis combined with local neural network algorithm, to realize intelligent evaluation.

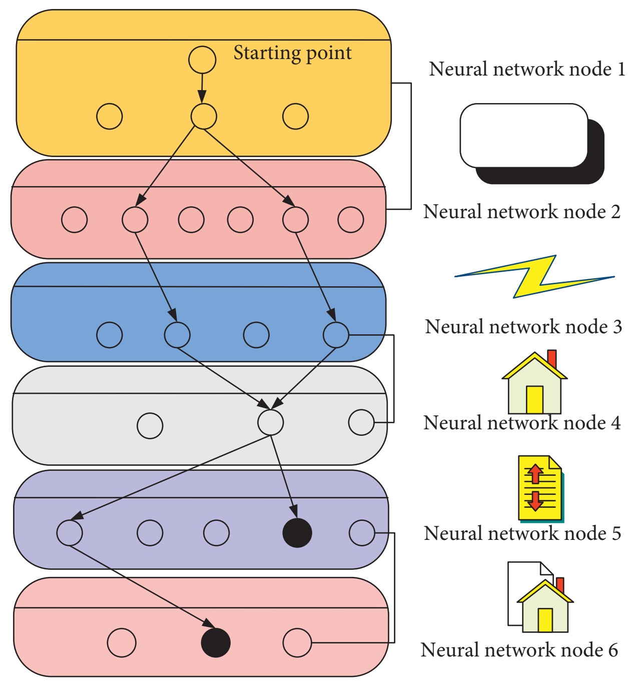

Figure 2: Self-learning process based on neural network nodes.

4. Dialectical Analysis Model of Comparative Pedagogy Based on Multiple Intelligences Assessment

4.1. The Construction Process of Dialectical Analysis Model of Comparative Education Based on Neural Network Algorithm. In the process of studying the dialectical analysis model of comparative pedagogy, the neural network algorithm will be modified with the error reverse propagation, thus improving the accuracy of target input pattern recognition. In this mode, the algorithm can be used to improve the accuracy of target input pattern recognition, and the comparative pedagogy model of multi-agent evaluation based on neural network algorithm is to self-study and realize the construction of multi-agent evaluation on the basis of constantly revised methods. Therefore, the neural network learning method used in this neural network algorithm is called the error reverse propagation algorithm, which is a learning method of error function falling according to the gradient. The self-learning process based on neural network nodes is shown in Figure 2.

The process characteristics of the construction and implementation of the multi-agent evaluation are based on the random selection of the integrated comparative pedagogy in one aspect. The neural network model we know is not to distinguish the whole software to be evaluated but to identify and judge the local evaluation module of the overall comparative education needs, and the optimal comparative pedagogy module is obtained, which meets the minimum value of multiple intelligences evaluation of demand. Therefore, for the comparative pedagogy model of multi-agent evaluation, first, the specific numerical range of the general requirements of comparative education required by the neural network algorithm will be obtained by using the big data information and intelligent processing of the historical-comparative pedagogy process. Then, the neural network algorithm is used to search for the optimal solution, then, the multi-agent evaluation model with universal data analysis is selected [18].

The model of comparative pedagogy dialectic analysis based on multi-agent evaluation based on neural network algorithm mentioned in this paper can combine the traditional comparative pedagogy dialectic analysis with the existing artificial intelligence comparative pedagogy dialectic analysis link and carry out weight analysis and treatment to different degrees. In this way, the relevant bugs in the dialectical analysis process will be greatly reduced. This also shows that the higher the practical adaptability of the dialectical analysis mode of this comparative pedagogy is, that is, the process of data analysis can be evaluated quickly and modularized through the multi-agent evaluation process, then the evaluation degree will become better with the multiple self-learning of neural network algorithm. In the process of dialectical analysis of comparative pedagogy, the discriminant process of multiple intelligences assessment can be used (the principle of discrimination is shown in Figure 3).

Other neural network algorithms continue to gradually enlarge the search range that meets the minimum demand value of modular processing in the target group of the collective process to be evaluated, so as to achieve accurate search in a certain type of data processing, and then realize the batch processing and modular rapid evaluation of this type of data analysis process [19]. In addition, data multiple discrimination is to randomly select two data from all the data to be evaluated and then judge the information characteristics of the evaluation demand degree [20]. The process of “forward calculation output-backpropagation error” is repeated many times according to a certain probability until the error is reduced to an acceptable range, and the learning, training, and judgment process of the multiple intelligences evaluation models of neural network ends with it; finally, we can achieve the accurate dialectical analysis and quantitative processing of comparative education.

The comparative education demand model of multiple intelligences assessment based on neural network algorithm uses neural network algorithm for self-learning. The threshold value θ_j of each processing unit is set to simulate the action potential of biological neurons, and the first derivative $f'(x)$ of its related function is as follows:

$$\begin{aligned} f'(x) &= \frac{-1}{\left(1+e^{-x}\right)^2} e^{-x}(-1) = \frac{-1}{1+e^{-x}} \frac{e^{-x}}{1+e^{-x}} \\ &= f(x)[1-f(x)] \end{aligned} \tag{1}$$

where x is the data to be measured and $f(x)$ is the correlation function.

The first batch of target data to be evaluated is normalized, and the normalization equation $y_{n+k}(x)$ is as follows:

$$y_{n+k}(x) = \sum_{i=0}^{k-1} \alpha_i y_{n+i}(x) + h \sum_{i=0}^{k} \beta_i f_{n+i}(x), \tag{2}$$

where α_i is the value before processing, α_i is the value after processing, and $y_{n+k}(x)$ is the sample function. The input layer data is imported into the first neural node of the hidden layer for operation as follows:

$$\begin{cases} y' = \lambda y, \\ y(x) = y_0 \end{cases}, \tag{3}$$

where λ is a complex number, which is also called the verification equation of the model, and its true solution is as follows：

$$y(x) = y_0 e^{\lambda(x-a)} \tag{4}$$

The random probability model and neural network algorithm are used to solve the problem; for different practical problems, the results can be expressed as follows:

$$\left(1 - h\lambda\beta_k\right) y_{n+k} = \sum_{i=0}^{k-1} \left(\alpha_i + h\lambda\beta_i\right) y_{n+i}, \tag{5}$$

where α_i is the value before processing, β_k is the value after processing, and y_{n+i} is the extremum function. The input layer data λ is imported into the first neural node of the hidden layer h for operation:

$$y_n = r^n. \tag{6}$$

There are

$$\left(1 - h\lambda\beta_k\right) r^{n+k} = \sum_{i=0}^{k-1} \left(\alpha_i + h\lambda\beta_i\right) r^{n+i}. \tag{7}$$

Its equivalent form is

$$\left(1 - h\lambda\beta_k\right) r^{k} = \sum_{i=0}^{k-1} \left(\alpha_i + h\lambda\beta_i\right) r^{i}. \tag{8}$$

We call the above formula the characteristic confidence solving formula based on probabilistic random variables and their numerical characteristics. Remember

$$\pi(r; h\lambda) = \left(1 - h\lambda\beta_k\right) r^{k} - \sum_{i=0}^{k-1} \left(\alpha_i + h\lambda\beta_i\right) r^{i}. \tag{9}$$

The above formula is regarded as the limit characteristic error degree in solving the probability distribution model.

Definition 1. Note $\overline{h} = h\lambda$, for a given $\overline{h}$, the root of a stable polynomial needs to satisfy

$$\left|r_s\right| < 1, \quad s = 1, 2, \ldots k. \tag{10}$$

In the process of dialectical analysis of related data in different arrays, the different differentiation analysis process is shown in Figure 4.

4.2. The Multi Intelligences Evaluation Process of Comparative Pedagogy Data Based on Neural Network Algorithm. The process of error backpropagation is the process of error transfer from the output layer to the hidden layer [21]. Moreover, the correction error of each hidden layer processing unit is generated by the combined effect of the correction errors transmitted by different output layer processing units [22]. Based on this, we need to carry on the

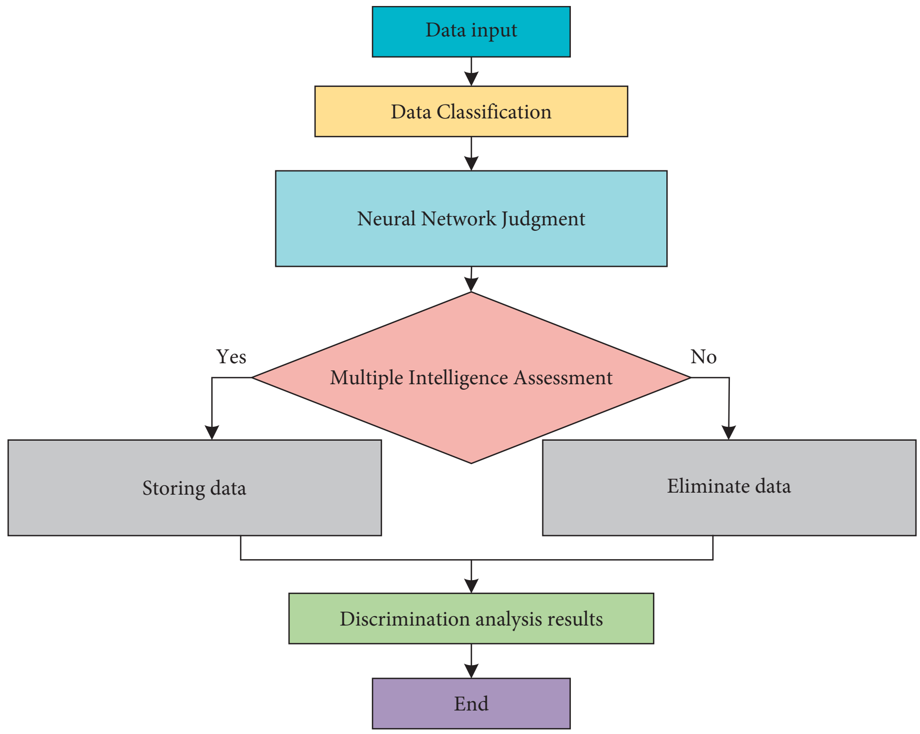

FIGURE 3: Discrimination process of multiple intelligences evaluation of data.

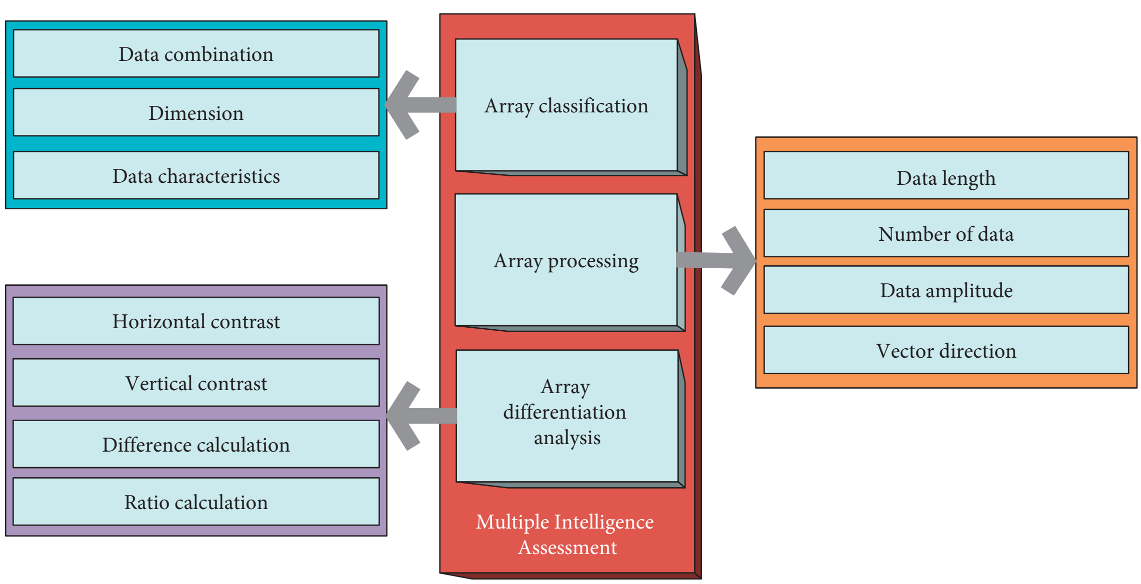

FIGURE 4: Differential analysis process of data.

initial processing to the computer program under the neural network algorithm.

First, we need to consider the initial value problem in comparative education, which can be solved by the following formula:

$$\begin{cases} \dfrac{dy}{dx} = f(x, y), \\ \\ y(x_o) = y_o. \end{cases} \tag{11}$$

In order to obtain its numerical solution on an equidistant scattered point $x_1 < x_2 < \cdots < x_n < \cdots$, it is first discretized. Let $h = x_i - x_{i-1}\,(i = 1, 2\cdots)$ simplify the above formula and solve it by distribution, and the following formula can be obtained:

$$y(x_{n+1}) = y(x_n) + hy'(x_n) + \frac{h^2}{2!}y''(\xi_n), \xi_n \in (x_n, x_{n+1}). \tag{12}$$

Then, when h is sufficiently small, the error term $h^2/2y''(\xi_n)$ is omitted, the approximation of y_n is used to replace $y(x_n)$, the approximation of y_{n+1} is used to replace $y(x_{n+1})$, and $y'(x_n) = f(x_n, y(x_n))$ is noticed:

$$\begin{cases} y_0 = y(x_o), \\ y_{n+1} = y_n + hf(x_n, y_n), \quad n = 0, 1, \ldots, \end{cases} \tag{13}$$

Among them, $x_n = x_0 + nh, h = b - a/N$. The method of using (13) to solve the formula is called the multiple intelligences evaluation method based on neural network. And in the neural network algorithm, the simulation results of three groups of data are shown in Figure 5.

This study combines the idea of big data random collection and digital feature analysis based on neural network algorithm and particle swarm optimization algorithm and constructs the multiple intelligences evaluation bases in random data collection and digital feature analysis rules by simulating the "multiple neural node calculation rules" in the process of "neural network" modeling and rendering. The effectiveness of the method is tested by random simulation of three groups of data, and the simulation results are shown in Figure 6.

The simulation results show that the formulation of the strategy can effectively improve the collaborative work efficiency of probabilistic random variables in the process of collecting and storing massive random data and can effectively solve the problem of the computational complexity of probabilistic random variables and their digital characteristics in the process of dialectical analysis of comparative education [23]. Therefore, if we use difference instead of differentiation, we can get

$$\frac{y(x_{n+1}) - y(x_n)}{h} \approx y'(x_n) = f((x_n), y(x_n)). \tag{14}$$

If we integrate $y' = f(x, y(x))$ over $[x_n, x_{n+1}]$, we get

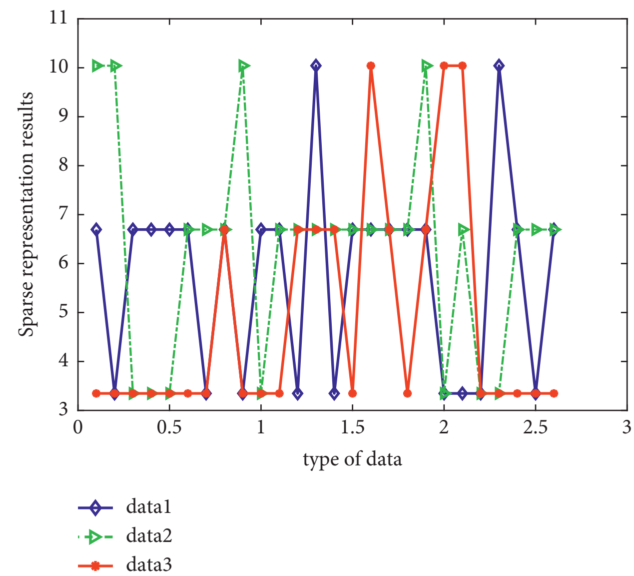

Figure 5: Simulation results in the process of multiple cycles of three sets of data.

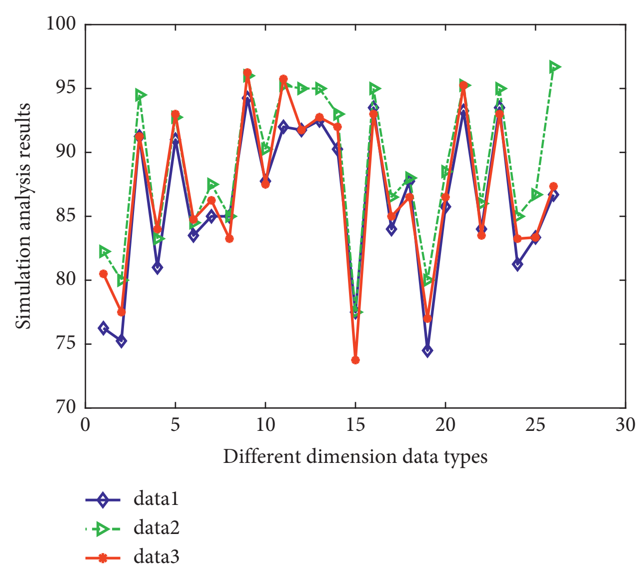

Figure 6: Random test simulation on three sets of data.

$$y(x_{n+1}) - y(x_n) = \int f(x, y(x))dx, \tag{15}$$

where h is the disturbance factor and $f(x_n, y(x_n))$ is the assignment function, the approximation of y_n is used to replace $y(x_n)$, and the approximation of y_{n+1} is used to replace $y(x_{n+1})$. The tangent equation is $y = y_0 + f(x_0, y_0)(x - x_0)$. When $x = x_1$, the approximate value of $y(x_1)$ is $y_0 + f(x_0, y_0)(x_1 - x_0)$, and it is recorded as y_1. This is the approximate common solution of calculating $y(x_1)$ when $x = x_1$ is obtained.

In this process, different data types of comparative education are dialectically analyzed, and the data of three groups are simulated. The results are shown in Figure 7.

5. Result Analysis and Discussion

5.1. Experimental Verification Process of Dialectical Analysis in Comparative Education Based on Multiple Intelligences Assessment. The neural network trains it through the training set, in which the training set data includes input value and output value. Each time a datum is entered, the weight of hidden layer nodes will be adjusted to make the output value as close as possible to the expected value. After a large amount of data training, the weights in the neural network are continuously adjusted to achieve the best weight. The weight obtains sample knowledge in the form of data and reflects the characteristics and the correlation of sample data.

According to the neural network algorithm and the intelligent analysis model of big data information based on a variety of dialectical analysis needs of comparative pedagogy, the experimental data are analyzed by pairwise comparison. Through the data processing of the optimized neural network algorithm based on multiple comparisons, the evaluation sample data of different modules required by comparative pedagogy are obtained. Unified orthogonal processing is implemented for the unique vector data of each comparative education process to realize the matching of initialization weight and a minimum threshold of evaluation demand required by the relevant neural network. Three groups of experimental data are tested, and the results are shown in Figure 8.

The experimental results are shown in Table 1. The data results in Table 1 show that the characteristic of this multiple intelligences evaluation scheme based on big data analysis and neural network algorithm is that it does not need to track and judge the individual characteristics that need to be dialectically analyzed in advance, but realizes the modular processing of multiple intelligences evaluation in the process of dialectical analysis of comparative education based on neural network algorithm, it is a new attempt in the process of dialectical analysis of comparative education.

6. Analysis of Experimental Results

In this paper, the data to be evaluated and the evaluated data are taken as the test objects, and the output image of the relevant experimental results is shown in Figure 9.

Through the analysis of the big data system of education information, we can know that the necessity of the two groups of data analysis is very different, and the experimental data results of the dialectical analysis are shown in Table 2.

The data in Table 2 are optimized and updated based on the neural network algorithm, and the results are shown in Table 3.

The experimental results show that the proposed dialectical analysis model of comparative education based on neural network algorithm and multiple intelligences evaluation can achieve quantitative analysis with high accuracy, and its analysis results have good reliability.

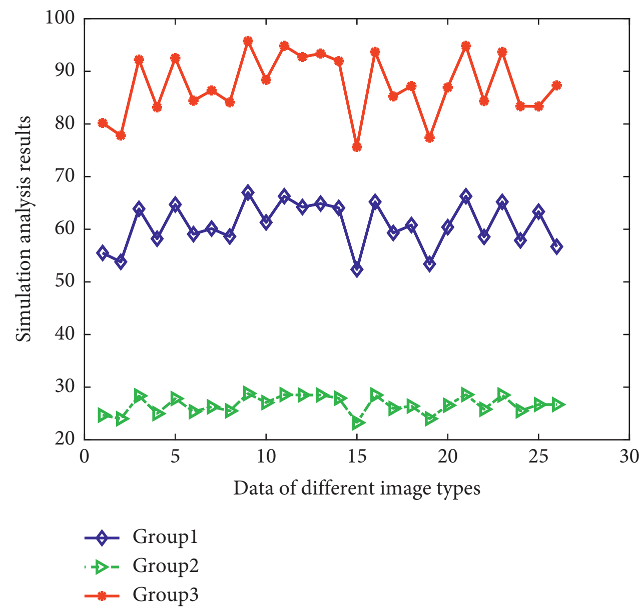

FIGURE 7: Dialectical analysis of the three groups of data simulation results.

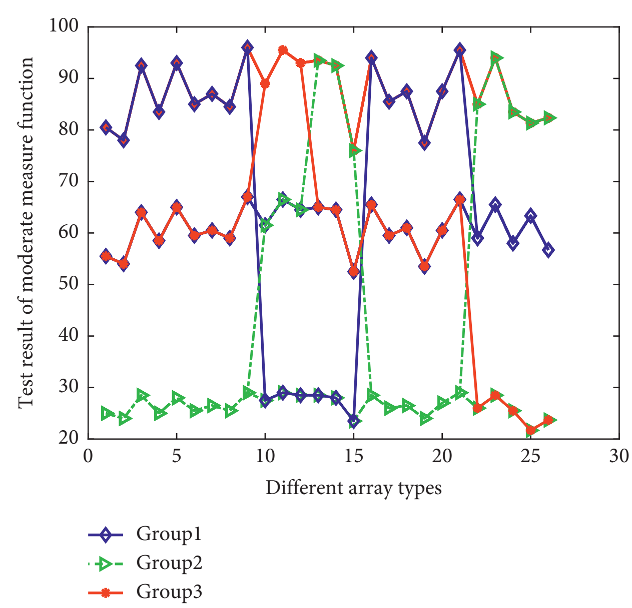

FIGURE 8: Experimental test results on three sets of experimental data.

TABLE 1: The numerical results of example 1.

Method	h	Results	Absolute error	Relative error
3rd order	1/50	$2.5671E-033$	$2.6526E-034$	$9.8230E-002$
3rd order	1/100	$2.7236E-033$	$2.9954E-035$	$1.8750E-002$
4th order	1/50	$2.6868E-033$	$8.1123E-036$	$3.2130E-003$
4th order	1/100	$2.6791E-033$	$5.0526E-037$	$1.9541E-004$
5th order	1/50	$2.6456E-033$	$1.3350E-036$	$4.8759E-004$
5th order	1/100	$2.6754E-033$	$3.8683E-038$	$1.4352E-005$
6th order	1/50	$1.4096E-047$	$2.6776E-033$	$1.4730E-000$
6th order	1/100	$1.4754E-047$	$2.7896E-033$	$1.0457E-000$
7th order	1/50	$6.7542E-030$	$6.4435E-030$	$2.9236E+003$

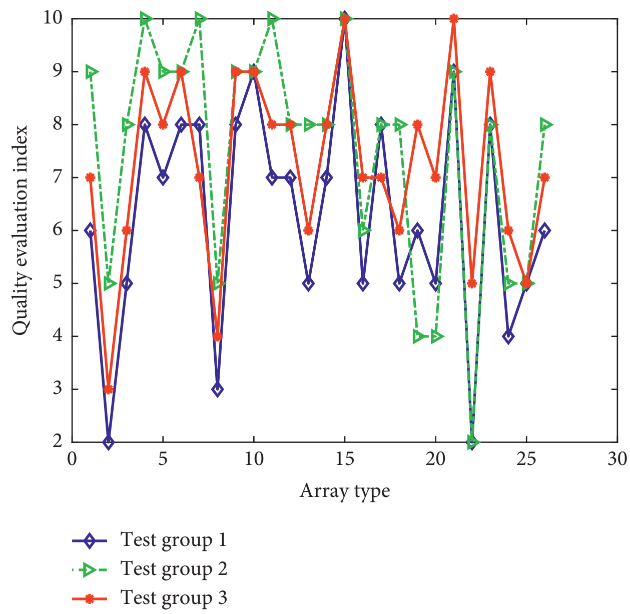

Figure 9: Analysis image of experimental results.

Table 2: Unoptimized experimental error analysis.

h	Err
0.1	$5.5E-008$
0.01	$4.8877E-004$
0.001	$4.7875E-004$

Table 3: Analysis of experimental error after optimization.

h	Err
0.1	$5.3E-004$
0.01	$4.6896E-004$
0.001	$4.3470E-006$

7. Conclusion

This paper first reviews the current research status and existing problems of the comparative education model of multiple intelligences evaluation in the dialectical analysis of comparative education in China, then puts forward the dialectical analysis model of comparative education model based on multiple intelligences evaluation, and finally tests the effect of this model in the process of comparative education through experiments. The experimental results show that in the comparative education model based on neural network algorithm, the model can quickly judge the dialectical analysis needs of the data to be evaluated. The results show that the dialectical analysis model has a great improvement in the reliability of multiple intelligences evaluation, and the error between the modular processing degree of comparative education and the normal known comparative education degree is within the stable standard reference range, the accuracy of the error has met the requirements of the current process of comparative education. It can be applied to the multiple intelligences assessment of comparative education and can realize the modular processing in the process of comparative education. However, the dialectical analysis model does not consider other factors of different types, so it can be further studied from the aspect of accuracy error.

Data Availability

The data used to support the findings of this study are available from the corresponding author upon request.

Conflicts of Interest

The authors declare that there are no conflicts of interest.

References

[1] J. Zhang, X. Hu, Z. Ning et al., "Energy-latency tradeoff for energy-aware offloading in mobile edge computing networks," *IEEE Internet of Things Journal*, vol. 5, no. 4, pp. 2633–2645, 2018.

[2] K. Li, S. Qi, H. Yang, L. Zhou, and D. Song, "Extensible image object co-segmentation with sparse cooperative relations - sciencedirect," *Information Sciences*, vol. 521, no. 14, pp. 422–434, 2020.

[3] D. Baldwin, J. Gustafson, L. Pickup et al., "Development and external validation of a new convolutional neural networks algorithm derived artificial intelligence tool to predict malignancy in pulmonary nodules," *Lung Cancer*, vol. 139, no. 1, pp. S7–S8, 2020.

[4] L. Bramslw, G. Naithani, and A. Hafez, "Improving competing voices segregation for hearing impaired listeners using a low-latency deep neural network algorithm," *Journal of the Acoustical Society of America*, vol. 144, no. 1, pp. 172–185, 2018.

[5] G. Chen, F. Wang, and S. Qu, "Pseudo-image and sparse points: vehicle detection with 2D LIDAR revisited by deep learning-based methods," *IEEE Transactions on Intelligent Transportation Systems*, vol. 21, no. 12, pp. 1–13, 2020.

[6] I. Y. Ha, M. Wilms, and H. Handels, "Model-based sparse-to-dense image registration for realtime respiratory motion estimation in image-guided interventions," *IEEE Transactions on Biomedical Engineering*, vol. 66, no. 2, pp. 302–310, 2019.

[7] J. Hrisko, P. Ramamurthy, and Y. Yu, "Urban air temperature model using GOES-16 LST and a diurnal regressive neural network algorithm," *Remote Sensing of Environment*, vol. 237, no. 6, Article ID 111495, 2019.

[8] J. Ishioka, Y. Matsuoka, S. Uehara et al., "Computer-aided diagnosis of prostate cancer on magnetic resonance imaging using a convolutional neural network algorithm," *BJU International*, vol. 122, no. 3, pp. 411–417, 2018.

[9] J. Ji, F. Ren, H. F. Ji, Y. F. Yao, and G. F. Hou, "Generalised non-locally centralised image de-noising using sparse dictionary," *IET Image Processing*, vol. 12, no. 7, pp. 1072–1078, 2018.

[10] T. Kim, *Affect Theory and Comparative Education Discourse. Essays on Fear and Loathing in Response to Global Educational Policy and Practice : By Irving Epstein*, 90 pages, Bloomsbury Academic, London and New York, 2019.

[11] E. L. Kolsbjerg, A. A. Peterson, and B. Hammer, "Neural-network-enhanced evolutionary algorithm applied to supported metal nanoparticles," *Physical Review B*, vol. 97, no. 19, Article ID 195424, 2018.

[12] J. H. Lee and S. N. Jeong, "Efficacy of deep convolutional neural network algorithm for the identification and classification of dental implant systems, using panoramic and periapical radiographs," *A pilot study. Medicine*, vol. 99, 2020.
[13] Y. Li, W. Dong, X. Xie, G. Shi, J. Wu, and X. Li, "Image super-resolution with parametric sparse model learning," *IEEE Transactions on Image Processing*, vol. 27, no. 9, pp. 4638–4650, 2018.
[14] Z. Ning, X. Hu, Z. Chen et al., "A cooperative quality-aware service access system for social internet of vehicles," *IEEE Internet of Things Journal*, vol. 5, no. 4, pp. 2506–2517, 2018.
[15] M. Luo, S. Zhong, L. Yao, W Tu, W Nsengiyumva, and W Chen, "Thin thermally grown oxide thickness detection in thermal barrier coatings based on SWT-BP neural network algorithm and terahertz technology," *Applied Optics*, vol. 59, no. 13, pp. 4097–4104, 2020.
[16] F. Menashy, "Reimagining comparative education through the lens of science fiction: an introduction to the special section of book and media essay reviews," *Comparative Education Review*, vol. 64, no. 1, pp. 137-138, 2020.
[17] A. Naveed and M. Arnot, "Exploring Educational and Social Inequality through the Polyphonic Voices of the Poor: A Habitus Listening Guide for the Analysis of Family-Schooling Relations," *Comparative Education*, vol. 55, no. 2, pp. 1–22, 2018.
[18] L. Sheng, F. Yuan, S. Zhang, H. Song, and S. Chen, "L_0 sparse regularization-based image blind deblurring approach for solid waste image restoration," *IEEE Transactions on Industrial Electronics*, vol. 66, no. 12, pp. 9837–9845, 2019.
[19] V. Khezri, E. Yasari, M. Panahi, and A. Khosravi, "Hybrid artificial neural network-genetic algorithm-based technique to optimize a steady-state gas-to-liquids plant," *Industrial & Engineering Chemistry Research*, vol. 59, no. 18, pp. 8674–8687, 2020.
[20] S. Xiang, Z. Ren, and Y. Zhang, "Training a multi-layer photonic spiking neural network with modified supervised learning algorithm based on photonic STDP," *IEEE Journal of Selected Topics in Quantum Electronics*, vol. 99, p. 1, 2020.
[21] Y. Li, J. Chen, and Z. Li, "A case study of debris flow risk assessment and hazard range prediction based on a neural network algorithm and finite volume shallow water flow model," *Environmental Earth Sciences*, vol. 80, no. 7, 2021.
[22] Z. Zhang, H. Liu, J. Shu, H. Nie, and N. Xiong, "On automatic recommender algorithm with regularized convolutional neural network and IR technology in the self-regulated learning process," *Infrared Physics & Technology*, vol. 105, Article ID 103211, 2020.
[23] X. Hu, J. Cheng, M. Zhou et al., "Emotion-Aware cognitive system in multi-channel cognitive radio ad hoc networks," *IEEE Communications Magazine*, vol. 56, no. 4, pp. 180–187, 2018.

Hindawi
Scientific Programming
Volume 2022, Article ID 1544767, 10 pages
https://doi.org/10.1155/2022/1544767

Research Article

A Recommendation Method of National Fitness Items Based on Neural Network Algorithm

Liangming Li[1] and Aihua Yang[2]

[1]*School of Physical Education, Hunan University of Science and Technology, Xiangtan, 411201, China*
[2]*School of Physical Education, Changsha University of Science and Technology, Changsha, 410076, China*

Correspondence should be addressed to Aihua Yang; 001962@csust.edu.cn

Received 12 November 2021; Revised 28 November 2021; Accepted 3 December 2021; Published 18 January 2022

Academic Editor: Le Sun

In order to improve the effectiveness of national fitness programs, this article analyzes the method of national fitness items recommendation based on a neural network algorithm. By using the time and space characteristics of fitness users' sign-in, a novel POI recommendation model is proposed, and a novel fusion method is proposed to combine similarity and spatial similarity to achieve the final similarity calculation based on fitness users' temporal and spatial preferences. In addition, in order to model the spatial similarity of fitness users, the Voronoi diagram is constructed by using the geographic locations of all POIs. Finally, this paper constructs a recommendation system for national fitness items based on a neural network algorithm. The experimental research results show that the national fitness program recommendation system proposed in this article basically meets the expected demand.

1. Introduction

The implementation of the national fitness program and the development of mass sports have improved the overall quantity and quality of China's sports population. However, only participating in physical exercises cannot meet people's fitness needs. The development of sports events, especially mass sports events, should be enriched. The relationship between mass physical exercises and mass sports events complements and promotes each other. Mass sports events are the display of the results of mass sports exercises, the best test of fitness activities, can better motivate and drive the masses to participate in sports exercises, and play a "leveraging" role in setting off a mass sports climax. Mass sports are the basis for conducting mass sports events, and they support and guarantee the development of mass sports events [1]. Mass sports events set off a fitness craze among the masses, allowing them to show their strong physiques and fighting spirit, while also forming a carnival that focuses on participation, national fitness, and happy sports. Moreover, they promote the improvement of the masses' awareness of physical exercise and the development of lifelong physical exercise habits, so that fitness can be integrated into the daily life of the masses [2].

National fitness is an important foundation for building a healthy China and an inevitable requirement for the people to yearn for a better life. The improvement of the national fitness system can enhance the country's overall national strength and reflect the level of social civilization. This study conducted research on the construction of the nationwide fitness system, deeply explores the relevant laws, regulations, policy documents, etc. promulgated by China for the development of nationwide fitness programs and finds the problems and shortcomings in the development of nationwide fitness programs. This has important practical significance for improving the construction of the nationwide fitness system, fully implementing the nationwide fitness strategy, and accelerating the construction of a sports power [3].

With the continuous development and progress of the times, the domestic economic development continues to accelerate, people's income is further increased, the quality of life is improved, and people's needs for quality of life and sports activities are increasing. However, from the current basic situation, there are still many problems in public sports services, and the quality level cannot meet actual needs. With the holding of the Olympic Games, the whole people's love for sports has set off a frenzy on the land of China. The manifestation of this contradiction is very prominent.

With the continuous development and progress of the times, people have more and more demands for quality of life and sports activities. However, judging from the current domestic basic situation, there are serious deficiencies in the supply and construction of related infrastructure. Everyone has a relatively limited number of fitness venues. The common problem is that the existing fitness venues are not used efficiently at this stage. The popularity of fitness education among people is generally low. There are no unified system standard, legal conditions, and scientific and reasonable fitness requirements for the development of fitness among the whole people. It is necessary to continuously rationalize the operation mode and operation mechanism of the national fitness program and improve and innovatively deepen reforms.

According to the actual needs of the national fitness program, this paper combines the neural network algorithm to construct the national fitness program recommendation system to improve the recommendation efficiency of the national fitness program.

2. Related Works

For the understanding of the national fitness program's mechanism, Ferguson et al.'s [4] point of view is that it can provide all the people with basic conditions for physical exercise activities and the creation of the environment to meet public's basic requirements for physical fitness. The physical quality has been significantly improved, and the related services and guarantee systems are produced by it. Kimasi et al.'s [5] view is that the national fitness system should be a system that has a direct impact on and restricts the participation of all people in fitness activities, comprehensively improves the overall physique of the people, and serves, adapts, and guarantees a comprehensive physique. The basic structural framework of the mechanism is the organization, activity, and material guarantee related to fitness activities. There are many support systems that can meet diversified and different requirements at the same time. Service and management are as important as the integrity structure, openness, and effectiveness. Literature [6] conducts research and analysis on the relevant systems of social sports instructors. The system mechanism of sports instructors has two parts: "Social Sports Instructor Technical Grade System" and "Social Sports Instructor National Professional Standards." The research direction of the literature [7] is to focus on the basic status of fitness for all the people in China. Through investigation and analysis, it is concluded that the problems in the process of fitness for the whole people are as follows: the source of funds is relatively single, there is no professional social nature, sports instructors, there is no conscious structure of participating in physical exercises in the subconsciousness of farmers [8], and the sports management mechanism in rural areas is very backward [9]. The research direction of the literature [10] is the characteristics of the population participating in sports. In terms of gender, men are generally higher than women. In terms of geographic composition, cities are generally higher than rural areas and the east is higher than the west. In terms of age, the two ends are taller, and the middle is shorter like a pommel horse-shaped structure. At the same time, it also clearly pointed out that the entry point for the improvement of the demographic structure in sports is the country's policy solution to social problems.

When the researcher Dong Li analyzed, according to the relevance of content and level, the formation of the national fitness system was divided into categories [11]. Divided according to the level, the national fitness mechanism can be divided into national and provincial levels in different regions, and a more detailed national fitness system should be built in the city to form the entire national fitness-related mechanism in the city [12]. To distinguish from the level, the content structure of the national fitness system is composed of basic services and basic guarantees, and a comprehensive analysis on the existing relationship level should be conducted. Comprehensive research on various elements should be conducted, and a reasonable combination should be carried out. Continuous improvement of the operation form and operation system of the fitness business and coordination of all the elements should be carried out, so as to give full play to the basic role of the national fitness operation mechanism [13]. According to the analysis carried out by Mountjoy et al. [14], the factors that influence the national fitness service mechanism include different types. The basic content can be summarized as the formulation and implementation of policies and systems, the arrangement and organization of fitness activities, the investment of funds, and so on.. Regarding the supply and construction of related infrastructure, the collection and analysis of information and materials, etc., through the research and analysis of these levels, we can more scientifically and reasonably grasp the operating mechanism related to national fitness. Pulido et al. [15] points out that the establishment of a national fitness service mechanism needs to focus on research and development from the following five aspects: publicity, construction of facilities and equipment, scientific guidance, dynamic monitoring, and organizational management.

3. A Recommendation Method of National Fitness Items Based on a Neural Network Algorithm

This paper proposes a novel POI recommendation model by using the time and space characteristics of fitness users' sign-in. The POI recommendation problem is defined as follows: when the sign-in record of the target fitness user is given, the main task of POI recommendation is to recommend the top-k positions that may be of interest to the fitness user. Table 1 lists some symbols that need to be used.

The model implements the POI personalized recommendation problem. The general idea is as follows: after the target fitness user u_i is given, the system first searches for a collection of fitness users with similar temporal and spatial characteristics to the target fitness user u_i. In addition, the personalized recommendation system should not set a fixed K-nearest neighbor value for all fitness users. Therefore, our system has proposed a set of adaptive K-nearest neighbor algorithm, which can select different K-nearest neighbors for different fitness users, so as to provide personalized location recommendation services for fitness users. Finally, based on the idea of collaborative filtering, suitable points of interest are selected and recommended to target fitness users.

Our model is designed with two modules: a fitness user similarity module that integrates temporal and spatial characteristics and a point-of-interest recommendation module. The details of these two modules will be introduced below.

In order to find fitness user groups with temporal and spatial similarity to the target fitness user, this research will model the temporal and spatial characteristics of fitness users, respectively, and then, design a personalized calculation method of fitness user similarity.

Generally, fitness users display different preferences at different time intervals. Each time interval is represented by a time ID, and the timestamp of each check-in record belongs to an interval. In order to model the time characteristics of fitness users, we construct a third-order tensor $X \in R^{U\times T\times C}$, where U, T, and C represent the number of fitness users, the number of time intervals, and the number of categories, respectively.

The tensor decomposition can be used to alleviate missing or sparse data and explore the potential associations of fitness users, time, and POI categories. To avoid those negative values which have no meaning for the preference measure during the restoration process, we add non-negative constraints in the decomposition process. The decomposition formula is as follows:

$$X = G\times_1 A\times_2 B\times_3 C. \tag{1}$$

After non-negative tensor decomposition, we obtain a time-related preference matrix for each fitness user, as shown in Figure 1. In order to more accurately infer the time preference characteristics of fitness users, we normalize the sum of each row of the matrix. Therefore, the matrix shows a certain fitness user's preference for POI categories at different time intervals.

We use PT_i to represent the time category preference matrix of the fitness user u_i. $PT_i(1,1)$ represents the access probability of the fitness user u_i accessing the POI of the category c_1 at a time interval t_1. Therefore, the similarity of preferences of different fitness users based on time is expressed as follows [16]:

Table 1: Symbol description.

Symbol	Illustrate
U	Collection of all fitness users
u_i	The i-th fitness user in U
P	Collection of all POIs
p_i	The i-th sign-in point in P
S_i	Collection of check-in points visited by the fitness user u_i
PT	Time category preference matrix of fitness users
K	Number of similar fitness users

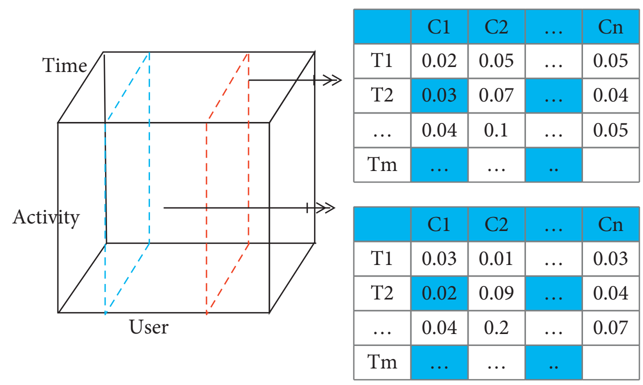

Figure 1: Time influence modeling.

$$\varphi_{u_i,u_j} = \frac{\sum\left(PT_i \odot PT_j\right)}{\sqrt{\sum_{s_{i,k}\in PT_i} s_{i,k}^2}\sqrt{\sum_{s_{j,k}\in PT_j} s_{j,k}^2}}. \tag{2}$$

In order to model the spatial activity preferences of fitness users, we use the geographic locations of all POIs to construct a Voronoi diagram. Specifically, as shown in Figure 2, the entire city is divided into multiple Voronoi grids. Therefore, a fitness user's spatial activity preference can be reflected by including a set of POIs that he has visited.

We use the Voronoi diagram to check the geographic check-in locations of fitness users because the Voronoi diagram can define whether two POIs are adjacent or not more reasonably than the Euclidean distance. In different areas of the city, the distribution of interest points of fitness users when signing in may be sparse or dense. Obviously, in sparse areas, the area of Voronoi grid cells is relatively large, while in dense areas, where check-in points are distributed, the area of Voronoi grid cells is relatively small. Therefore, it can provide an adaptive estimate of the distance between POIs.

After the Voronoi diagram is constructed, we can measure the similarity of the spatial activities of the two fitness users by exploring whether there are overlaps or adjacent Voronoi grid units in the check-in records of the two fitness users. For two fitness users u_i and u_j, our steps to calculate the spatial similarity are as follows:

(1) For each check-in point p_r in the fitness user check-in set, we use formula (3) to calculate the similarity of each check-in point p [17]:

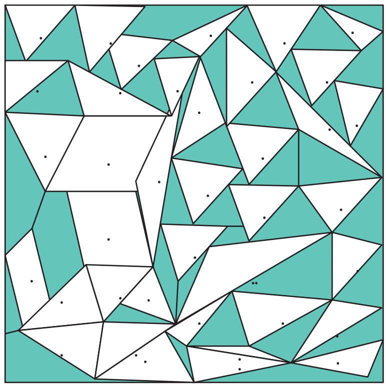

Figure 2: Example of a Voronoi diagram.

$$y_r = \log\left(\frac{|U|}{n_r}\right). \quad (3)$$

Among them, U represents the total number of fitness users in the check-in set, and n_r is the number of fitness users who have visited p_r.

(2) The algorithm constructs an array Y to store the similarity of each POI and uses the minimum and maximum normalization method to realize the normalization of Y.

(3) The algorithm constructs set S_i and S_j to store fitness users u_i- and u_j-visited check-in points, respectively. The algorithm constructs set A and B such that $A = S_i \cap S_j$ and $B = S_i \cup S_j$.

(4) The algorithm constructs a set C such that C=B-A. The D set is a subset of the C set. The D set stores each pair of adjacent POIs visited by fitness users u_i and u_j in the Voronoi diagram. Therefore, we use formula (4) to count the spatial similarity between u_i and u_j [18]:

$$\omega_{u_i,u_j} = \frac{\sum_{p_r \in A} y_r + 1/2 \sum_{\{p_m,p_n\} \in D} \left(y_m + y_n/2\right)}{|B|}. \quad (4)$$

After two fitness users u_i and u_j are given, we first calculate the time similarity and spatial similarity, respectively. A novel fusion method is proposed to combine them together to realize the final similarity calculation based on the temporal and spatial preferences of fitness users. Our model uses two weights to reflect the influence of time preference and spatial preference characteristics, respectively. The specific calculation is as

$$sim_{\left(u_i,u_j\right)} = \alpha\varphi_{u_i,u_j} + \beta\omega_{u_i,u_j}. \quad (5)$$

By using our fusion similarity calculation method, the similarity between each pair of fitness users can be obtained. We set the number of neighbors $K = \{1,2,3,4, \ldots, 20\}$ and set the fitness user u_i. According to the top K most similar fitness users, the recommended score for each POI can be calculated as follows:

$$score(i, j, k) = \sum_{u_q \in K} sim\left(u_i, u_q\right) \times r_{q,j}, \quad (6)$$

$$r_{q,j} = Min_i + \frac{Max_i - Min_i}{Max_q - Min_q} \times \left(f_{q,j} - Min_q\right). \quad (7)$$

In formula (7), $f_{q,j}$ represents the access probability of the fitness user u_q at the check-in point p_j. In formula (6), $r_{q,j}$ is the result of the normalization of $f_{q,j}$. $r_{q,j}$ represents the pseudoscoring of the fitness user u_q on the p_j at the check-in point. The range of the check-in probability of the fitness user n at each POI is between Max_i and Min_i.

In order to improve the accuracy of the recommendation, we use an adaptive K-nearest neighbor algorithm to determine the value of K. That is, for different fitness users, we select a different number of similar fitness users to generate the corresponding recommendation list. The specific steps of our algorithm are as follows:

(1) For different K value selections, we use formula (8) to calculate the corresponding recommendation error:

$$error_i = \sum_{j \in S_i} \frac{\left|r_{i,j} - score(i, j, k)\right|}{\left|S_i\right|}. \quad (8)$$

In formula (8), $r_{i,j}$ represents the pseudorating of the fitness user u_i on the check-in point p_j. Score(i,j,k) represents the recommendation score of the fitness user u_i on the check-in point p_j based on the top K most similar fitness users. S_i represents the records of POIs actually visited by fitness users in the training set.

(2) The algorithm selects the K value that causes the least error as the number of the most similar fitness user groups to recommend points of interest.

Then, we propose the next POI recommendation system. We will describe the overall framework of the model. As shown in Figure 3, our next POI recommendation system consists of two main parts: a context-aware similarity calculation module and a point-of-interest recommendation module.

For each fitness user, we connect all check-in records to construct a virtual trajectory of the fitness user. Therefore, each fitness user has six virtual trajectories corresponding to 6 time intervals.

Figure 4 shows the construction of a virtual trajectory for fitness users. The Voronoi diagram is constructed by using three kinds of information: time, latitude, and longitude. Moreover, the constructed trajectory is not the real exercise trajectory of the fitness user but a virtual trajectory constructed by Voronoi, and the virtual trajectory is only used for the calculation of the similarity of the fitness user.

We set a target fitness user u_i. t_k is the geographic location of the check-in point p_k, and c_k represents a specific category of the check-in point p_k [19].

We first set a virtual trajectory for the target fitness user u_i.

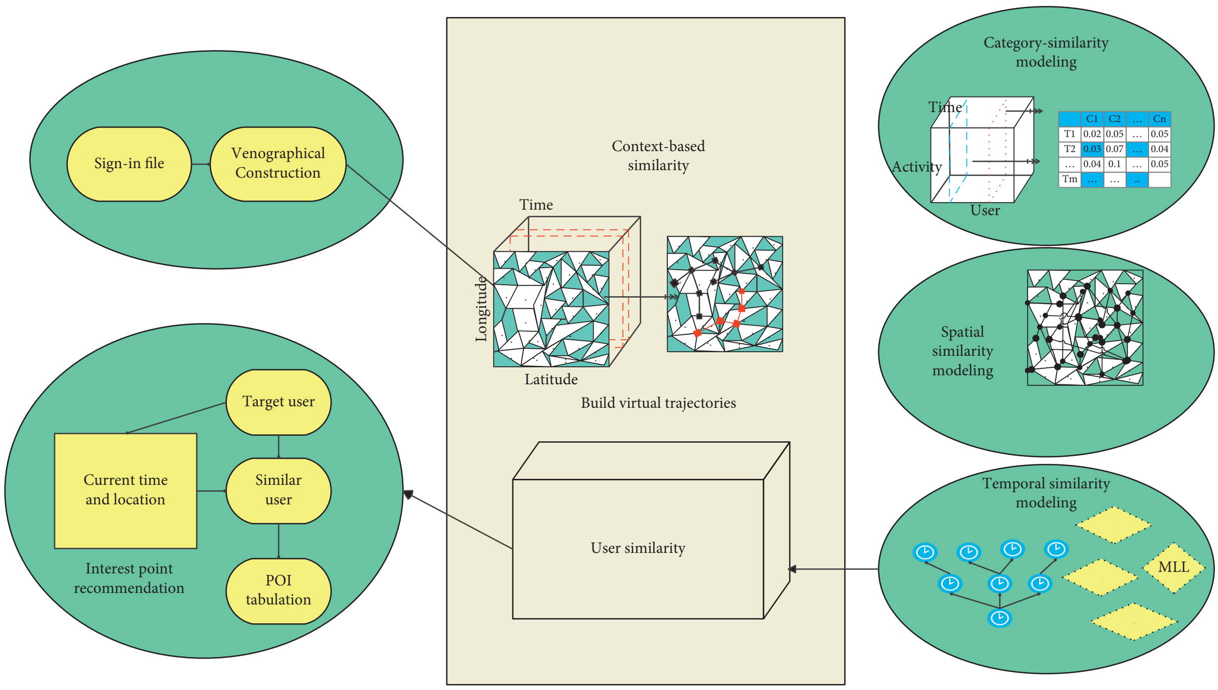

Figure 3: Schematic diagram of the system model.

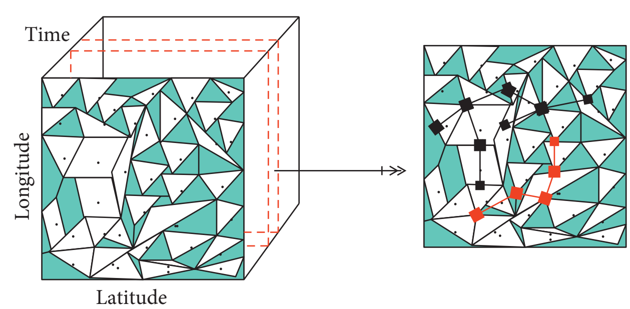

Figure 4: Example of construction of the virtual trajectory for fitness users.

We divide the virtual trajectory of the fitness user u_i into n groups. The detailed steps are as follows:

(1) The algorithm constructs an empty set $\mathrm{group_k}$ for each sign-in point $p_k\,(p_k \in L_q^i)$ of the fitness user u_i.

(2) The algorithm constructs a virtual trajectory for the fitness user u_j, denoted by L_q^j.

For each check-in point $p_k\,(p_k \in L_q^i)$, the algorithm calculates $|t_m - t_k|$.

The algorithm compares each time distance and finds the check-in point p_{mn} closest to p_m in the check-in time, where $p_{\min} \in L_q^i$.

Figure 5 shows an example diagram of the trajectory division, and there may be empty sets in these groups.

By considering the time characteristics, our method successfully converts the trajectory similarity calculation into the similarity calculation between each check-in point p_x and the check-in point in the corresponding group. The specific similarity calculation formula is as follows:

$$simuser\left(u_i, u_j\right) = \frac{\sum_{k=1}^{n} sim\left(p_k, group_k\right)}{n}, \tag{9}$$

$$sim\left(p_k, group_k\right) = \frac{\sum_{p_m \in \mathrm{group}} simpoint\left(p_k, p_m\right)}{\left|group_k\right|}. \tag{10}$$

Specifically, in formula (9), $\mathrm{simuser}(p_k, \mathrm{sroup}_k)$ represents the fitness track between fitness users U_i and U_j in a given time interval. n represents the virtual fitness track length of the fitness user u_i. $\mathrm{sim}\,(p_k, \mathrm{sroup}_k)$ represents the similarity between the fitness location $p_k\,(p_k \in L_q^i)$ and its corresponding set. In formula (10), $\mathrm{sim}\,(p_k, \mathrm{sroup}_k)$ represents the similarity between the fitness location $p_k\,(p_k \in L_q^i)$ as well as $p_m\,(p_k \in \mathrm{group}_k)$ of the fitness user u [20].

To model the spatial similarity of fitness users, we construct the Voronoi diagram. Each unit contains one and only one POI. Therefore, the spatial-related preferences of fitness users can be reflected by including the POIs they have visited. The Voronoi diagram defines whether there is a spatial proximity relationship between two POIs more

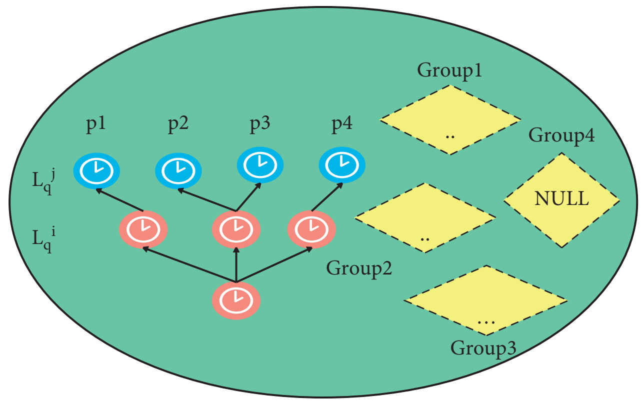

FIGURE 5: Schematic diagram of fitness user trajectory grouping.

reasonably than the Euclidean distance, and it can provide an adaptive estimate of the distance between POIs.

The calculation method of the geographic similarity based on the Voronoi diagram is described. When the time interval T_x is given:

(1) The algorithm determines the set of adjacent points. They are defined as adjacent points.

(2) The algorithm adds an undirected edge.

We use equation (11) to calculate the spatial similarity:

$$\omega(p_k, p_m) = \begin{cases} 1, & s = 0, \\ \dfrac{2^{-d}}{2^{s-1}}, & s \geq 1. \end{cases} \tag{11}$$

Figure 6 shows a constructed undirected graph. In Figure 6, the shortest path length from p_k to p_m is 4, so $s = 4$.

First, the algorithm constructs a fitness user category sign-in matrix and then uses the matrix factorization technology to recover the lost data.

After obtaining a fitness user category sign-in matrix, C represents the total number of categories. Therefore, each column of Q represents the check-in frequency of fitness users in a certain category, which can be regarded as the feature vector of the category.

For each sign-in point $p_k\,(p_k \in L_q^i)$,

$$\psi_{(p_k, p_m)} = \frac{\overrightarrow{c_{p_k}} \cdot \overrightarrow{c_{p_m}}}{\sqrt{\left|\overrightarrow{c_{p_k}}\right|^2} \times \sqrt{\left|\overrightarrow{c_{p_m}}\right|^2}}. \tag{12}$$

In formula (12), $\overrightarrow{c_{p_k}}$ and $\overrightarrow{c_{p_m}}$ represent the category feature vectors corresponding to their check-in points, respectively.

After a given target fitness user u_i, we calculate contextual perception similarity between the fitness user u_i and other fitness user u_j. The detailed steps are as follows:

(1) The algorithm constructs group_k as shown in the previous section. Each sign-in point $p_m\,(p_m \in \text{group}_k)$ and p_k share similar time characteristics. Repeat the following operations until all check-in points in group_k are traversed:

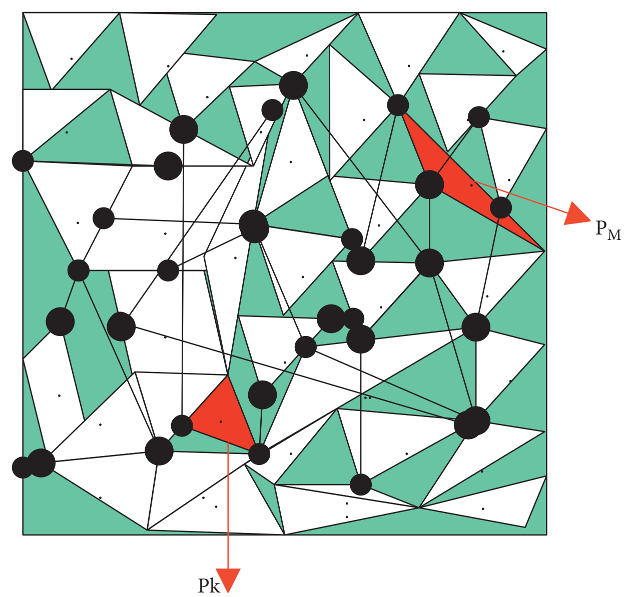

FIGURE 6: Spatial distance modeling for fitness users.

(i) The algorithm uses formula (11) to calculate the spatial similarity $\omega_{(p_k, p_m)}$ between sign-in points p_k and p_m and uses formula (12) to calculate the category similarity $\psi_{(p_k, p_m)}$ between sign-in points p_k and p_m.

(ii) The algorithm uses formula (13) to calculate the overall similarity between sign-in points p_k and p_m.

$$simpoint(p_k, p_m) = \psi_{(p_k, p_m)} \psi_{(p_k, p_m)}. \tag{13}$$

(2) The algorithm calculates the similarity between the sign-in point p_k and its corresponding set group_k by using formula (11).

The algorithm calculates the context-aware similarity between the fitness user u_i and fitness user u_j by using formula (9).

After calculating the similarity between the target fitness user U_i and other fitness user U_j, we construct a Sui set to

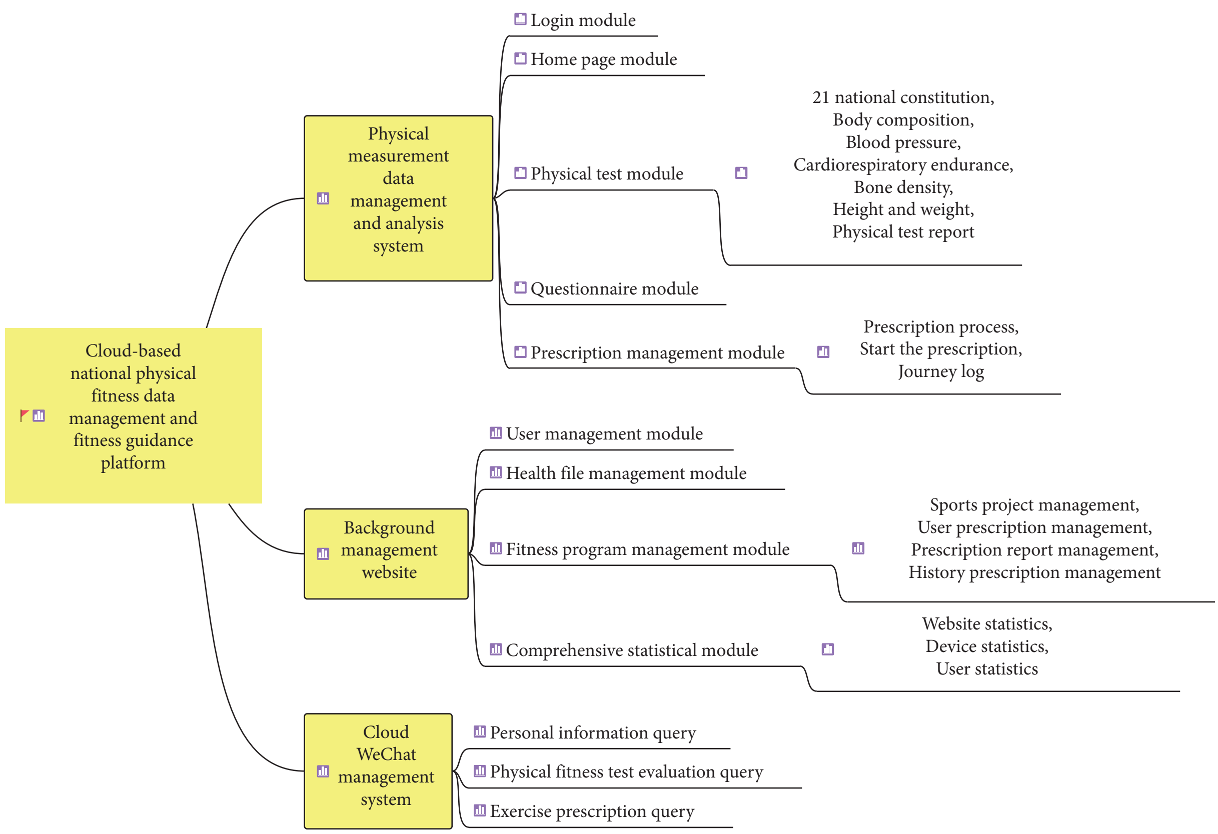

Figure 7: National fitness item recommendation system based on a neural network algorithm.

store the top k most similar fitness users of the target fitness user U_i. Therefore, $|S_{u_i}| = k$, a recommended list of target fitness user u_i. The detailed steps are as follows:

(1) The algorithm constructs a set CP_{u_i}, which contains all the POIs visited by fitness users in S_{u_i}.

(2) The algorithm sets the distance threshold λ to determine the recommended area. The recommended area is a circle with the current position of the target fitness user u_i as the center and λ as the radius.

(3) For each sign-in point $p_m\,(p_m \in CP_{u_i})$, we set the formula:

$$\Phi(l, p_m) = \begin{cases} \lambda^{-1}, & d_{(l,p_m)} \le \lambda, \\ d^{-1}_{(l,p_m)}, & d_{(l,p_m)} > \lambda. \end{cases} \tag{14}$$

Specifically, l is the current position of the fitness user u_i. $d_{(l,p_m)}$ represents the Euclidean distance between l and p_m.

(4) The algorithm uses formula (15) to calculate the pseudoscoring:

$$score(u_i, p_m) = \sum_{k=1}^{S_{u_i}} \left(simuser(u_i, u_k) f(u_k, p_m) \Phi(l, p_m)\right). \tag{15}$$

Among them, $f(u_k, p_m)$ represents the pseudoscore of the fitness user $u_k\,(u_k \in S_{u_i})$ to the check-in point p_m, which is counted by

$$f(u_k, p_m) = \frac{N(u_k, p_m)}{|L_k^q|}. \tag{16}$$

Among them, $f(u_k, p_m)$ represents the number of visits by the fitness user u_k to check-in point p_m, and $f(u_k, p_m)$ represents the total number of check-in points visited by the fitness user u_k in a time interval T_q.

(5) After obtaining the pseudoscoring of each POI in CP_{u_i}, the algorithm arranges in descending order and recommends the first k POIs.

4. National Fitness Item Recommendation System Based on a Neural Network Algorithm

Based on the above neural network recommendation algorithm, the nationwide fitness item recommendation system based on the neural network algorithm constructed in this article is shown in Figure 7.

The design of the overall service process of the platform is shown in Figure 8:

After the above model is constructed, the effect of the model is evaluated. First, the effect of neural network algorithm fitness data processing is evaluated, and the result is shown in Figure 9.

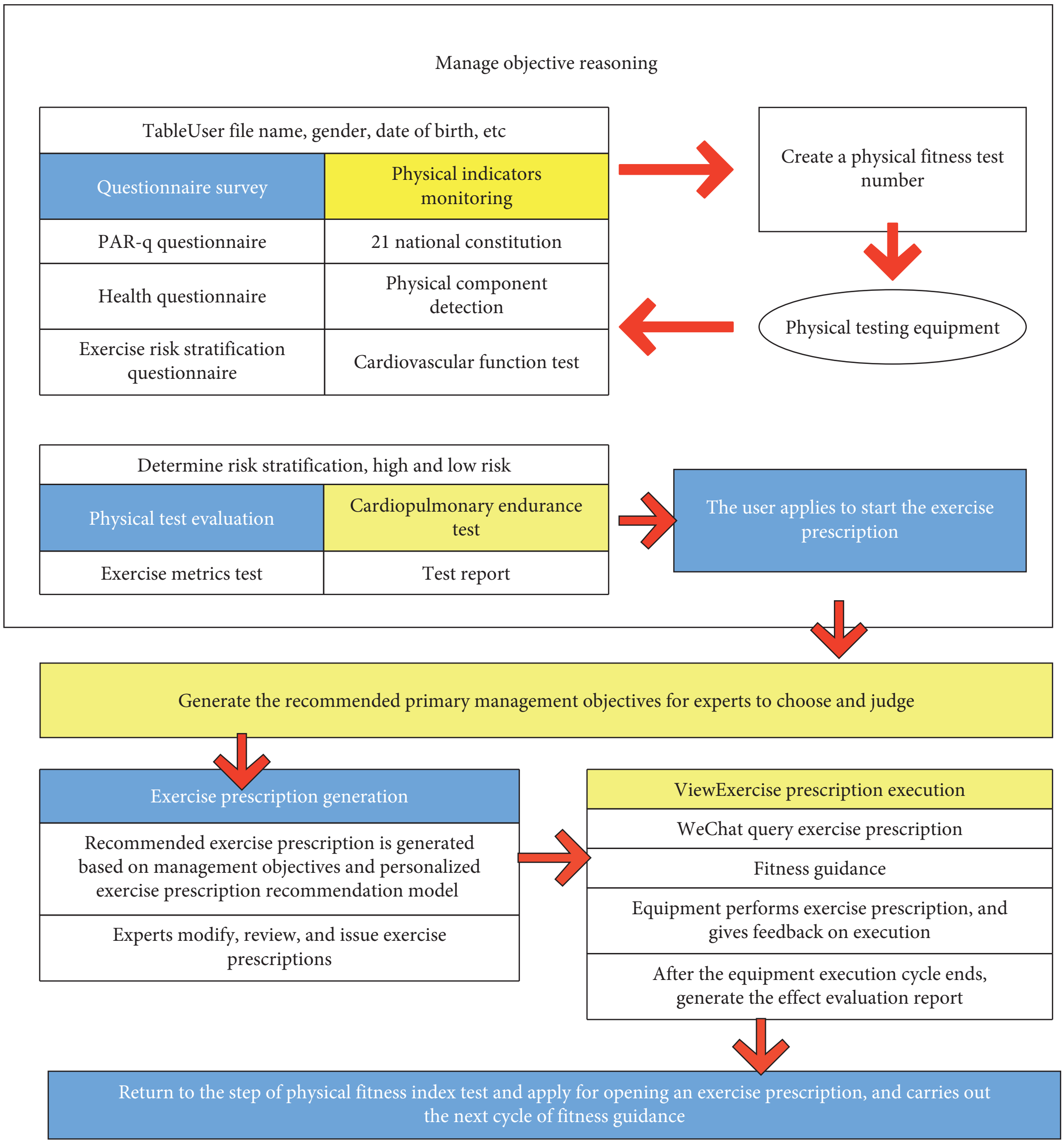

Figure 8: The overall service process of the platform.

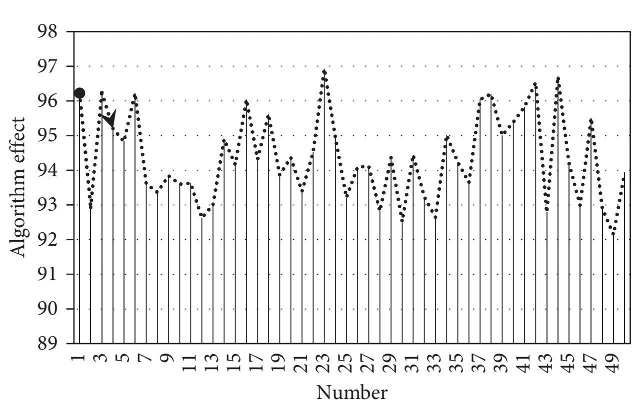

Figure 9: Neural network algorithm data processing.

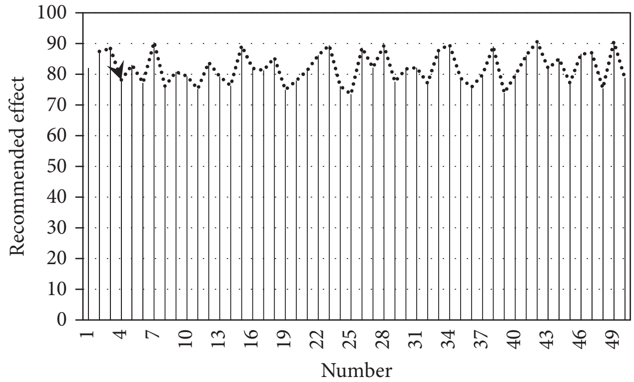

Figure 10: Recommendation effect of national fitness items based on the neural network algorithm.

It can be seen from the above research that the neural network algorithm proposed in this paper has a good data processing effect on the fitness data. On this basis, the effect of the national fitness item recommendation of the system in this paper is verified, and the result is shown in Figure 10.

From the above research, it can be known that the recommendation method of national fitness items based on the neural network algorithm has a certain effect.

5. Conclusion

National fitness activities have developed rapidly, and related achievements in the field of sports have entered a new level. At this stage, the problem that China faces in national fitness is the uneven development of public services. The main task at this stage is to use the construction of public service facilities to solve the problems and contradictions in China's fitness industry. Secondly, China's social public undertakings in the fields of education, culture, health, etc. have initially established competitive sports activities to win glory for the national Olympics. However, the public service system in the field of national fitness is relatively backward and to a certain extent cannot meet the national demand for physical fitness. According to the actual needs of the national fitness program, this paper combines the neural network algorithm to construct the national fitness program recommendation system to improve the recommendation efficiency of the national fitness program. The experimental research results verify that the method proposed in this article has a good performance in the recommendation efficiency of national fitness programs.

Data Availability

The labeled dataset used to support the findings of this study is available from the corresponding author upon request.

Conflicts of Interest

The authors declare that there are no conflicts of interest.

Acknowledgments

The research was supported by a project supported by Hunan Social Science Achievements Evaluation Committee in 2021 (No. XSP21YBZ061).

References

[1] A. H. Riley and C. Callahan, "Shoulder rehabilitation protocol and equipment fit recommendations for the wheelchair sport athlete with shoulder pain," *Sports Medicine and Arthroscopy Review*, vol. 27, no. 2, pp. 67–72, 2019.

[2] C. A. Emery and K. Pasanen, "Current trends in sport injury prevention," *Best Practice & Research Clinical Rheumatology*, vol. 33, no. 1, pp. 3–15, 2019.

[3] V. M. Shulyatyev and M. A. Bulavina, "Sport interview: strategy, design and content," *Theory and Practice of Physical Culture*, vol. 7, no. 9, p. 18, 2019.

[4] L. J. Ferguson, K. T. Carlson, and D. Rogers, "Moving towards reconciliation through sport: sharing our process of exploring team saskatchewan experiences at the North American indigenous games," *Journal of Exercise, Movement, and Sport (SCAPPS refereed abstracts repository)*, vol. 51, no. 1, p. 99, 2019.

[5] K. Kimasi, V. Shojaei, and M. R. Boroumand, "Investigation of safety conditions at gymnasia in different organizations," *Journal of Humanities Insights*, vol. 3, no. 2, pp. 70–74, 2019.

[6] K. Reinhart and B. Wichmann, "The TuS Fortschritt Magdeburg-Neustadt (soccer section) in the GDR - an example of amateur socialist sport," *Soccer and Society*, vol. 21, no. 4, pp. 408–420, 2020.

[7] C. Abanazir, "E-sport and the EU: the view from the English bridge union," *The International Sports Law Journal*, vol. 18, no. 3, pp. 102–113, 2019.

[8] A. Gerke, K. Babiak, G. Dickson, and M. Desbordes, "Developmental processes and motivations for linkages in cross-sectoral sport clusters," *Sport Management Review*, vol. 21, no. 2, pp. 133–146, 2018.

[9] A. I. Pogrebnoy and I. O. Komlev, "Sport institutions reporting to Ministry of Sport of Russian Federation: intellectual property, invention activity, patenting and legal consulting service analysis," *Theory and Practice of Physical Culture*, vol. 23, no. 2, pp. 6–8, 2018.

[10] D. C. Ilies, R. Buhas, and M. Ilies, "Sport activities and leisure in Nature 2000 protected area-Red Valley, Romania," *Journal*

of Environmental Protection and Ecology, vol. 19, no. 1, pp. 367–372, 2018.

[11] A. I. Kondrukh, “Practical shooting sport in Russian sport system: essential specifications and features,” *Theory and Practice of Physical Culture*, vol. 21, no. 5, pp. 75–77, 2017.

[12] R. Giulianotti and D. Numerato, “Global sport and consumer culture: an introduction,” *Journal of Consumer Culture*, vol. 18, no. 2, pp. 229–240, 2018.

[13] A. G. Gurinovich and G. V. Petrova, “Key priorities of physical education and sport sector budgeting laws and regulations in the Russian Federation,” *Theory and Practice of Physical Culture*, vol. 6, no. 4, p. 34, 2019.

[14] M. Mountjoy, A. Costa, R. Budgett et al., “Health promotion through sport: international sport federations’ priorities, actions and opportunities,” *British Journal of Sports Medicine*, vol. 52, no. 1, pp. 54–60, 2018.

[15] J. J. Pulido, D. Sánchez-Oliva, P. A. Sánchez-Miguel, D. Amado, and T. García-Calvo, “Sport commitment in young soccer players: a self-determination perspective,” *International Journal of Sports Science & Coaching*, vol. 13, no. 2, pp. 243–252, 2018.

[16] J. Cristiani, J. C. Martins-Bressan, B. Longarela, L. Galatti, and R. Reverdito, “Clubs SOCIO-deportivos en UN municipio brasileño: ESPACIO, EQUIPOS Y CONTENIDOS [Sport clubs in Brazil: facilities, equipment and content in][Clubes socio-esportivos em município brasileiro: espaço, equipamentos e conteúdos]. E-balonmano. com,” *Revista de Ciencias del Deporte*, vol. 13, no. 2, pp. 105–112, 2017.

[17] E. Happ, M. Schnitzer, and M. Peters, “Sport-specific factors affecting location decisions in business to business sport manufacturing companies: a qualitative study in the Alps,” *International Journal of Sport Management and Marketing*, vol. 21, no. 1-2, pp. 21–48, 2021.

[18] M. Castro-Sánchez, F. Zurita-Ortega, and R. Chacón-Cuberos, “Motivation towards sport based on sociodemographic variables in university students from Granada,” *Journal of Sport and Health Research*, vol. 11, no. 1, pp. 55–68, 2019.

[19] S. M. Hadlow, D. Panchuk, D. L. Mann, M. R. Portus, and B. Abernethy, “Modified perceptual training in sport: a new classification framework,” *Journal of Science and Medicine in Sport*, vol. 21, no. 9, pp. 950–958, 2018.

[20] J. H. Du Plessis and M. Berteanu, “The importance of prosthetic devices in sport activities for Romanian amputees who compete in Paralympic competitions,” *Medicina Sportiva: Journal of Romanian Sports Medicine Society*, vol. 16, no. 1, pp. 3197–3204, 2020.

Hindawi
Scientific Programming
Volume 2022, Article ID 1880811, 12 pages
https://doi.org/10.1155/2022/1880811

Research Article

Discussion on Application of Embedded Operating System in Dual-Core Smart Electric Meter

Xuesong Zhao,[1] Bensong Zhang,[2] Shihong Yin,[1] Qianxian Xie,[1] Leping Zhang,[2] and Haowen Wu[3]

[1]*Metrology Management Institute, Shenzhen Power Supply Bureau Co., Ltd., Shenzhen, Guangdong 518001, China*
[2]*Metrology Center, CSG Digital Grid Research Institute Co., Ltd., Guangzhou, Guangdong 510700, China*
[3]*Communication and Internet of Things Division, Digital Grid Branch of CSG Digital Grid Research Institute Co., Ltd., Guangzhou, Guangdong 510700, China*

Correspondence should be addressed to Xuesong Zhao; xuesongzhao2021@163.com

Received 17 November 2021; Revised 1 December 2021; Accepted 7 December 2021; Published 18 January 2022

Academic Editor: Le Sun

The new generation of smart meters need to realize the requirements of flexible expansion of advanced applications and transplantation of application software across hardware platforms. The software platform composed of operating system and middle layer service components is conducive to reducing the cost of software and hardware development and management. This paper first introduces the research and development background of the new generation smart meter, then introduces its overall software and hardware architecture and management unit hardware development platform, then introduces the construction of development environment and development tools and the basic functions based on the software platform, and finally introduces the development practice of application software. The large-scale promotion of the new generation of smart meters has become a development trend. This paper has a good reference for the application software development based on the new generation of smart meter software platform and is conducive to promoting the large-scale application of the new generation of smart meters.

1. Introduction

With the development of social economy, the demand for electric power in various fields is increasing rapidly. Meanwhile, the demand for power supply reliability, security, power quality, and power service is becoming higher and higher. For power supply enterprises, to give full play to the potential of power equipment, to provide low-cost, high-quality, safe, reliable electricity and high-quality comprehensive services, is an effective means to improve the competitiveness of enterprises and promote economic benefits. In order to achieve a win-win situation between power users and power supply enterprises, it is necessary to mobilize the subjective initiative of tens of millions of power users to use electricity reasonably and save electricity. At the same time, it is also necessary for power enterprises to continuously optimize the structure and realize the rational allocation of electric energy. In order to achieve a win-win situation, many countries and organizations have proposed the construction of flexible and standardized, clean and friendly, safe and economic smart power grid, and regard the construction of smart power grid as the primary direction of future power grid construction. As the terminal of smart grid extending to users, smart electricity meter is the key link between users and power enterprises. In order to build a sound and mature smart grid, the current management mode of electric energy distribution and use is changing from extensive to intensive, just as the current implementation of stepped electricity price, peak-valley electricity price, distributed generation, and other measures are the embodiment of this change. Intelligent electric energy is an important carrier of technological innovation, so every change of electricity management mode is promoting the renewal of electricity meters. In order to adapt to this trend and achieve long-term utilization of resources, it is urgent to launch a universal smart electricity meter that can realize power management mode transformation without replacing hardware but only updating software.

With the rapid implementation of China's smart power grid and digital power grid construction, as an important part of electricity consumption, the number of smart meters keeps growing rapidly. By the end of 2019, the number of smart meters in China has exceeded 600 million.

Under the situation of increasing pressure on global resources and environment, how to allocate energy resources scientifically and rationally, achieve maximum utilization of energy resources, and at the same time ensure the healthy development of energy resources is a difficult problem faced by all countries. In order to promote the implementation of IR46 standard in China [1], China's JJF1245 series technical specifications will be officially released and implemented. This series of technical specifications clearly divide the legal and nonlegal measurement functions of the new generation smart meters and also define the basic technical framework for the software and hardware design of the new generation smart meters, as shown in Table 1 [2].

The concept of smart electricity meter was put forward as early as the end of the twentieth century, but the characteristics of the early smart electricity meter are mainly reflected in the basic functions such as remote centralized meter reading and digitalization. At present, the proposal of smart power grid and AMI model has promoted the function and characteristics of smart electricity meter to an unprecedented height. At present, smart electricity meter has developed from a simple electric energy metering and billing device to an intelligent device integrating measurement, execution, communication, fault protection, and response. As the core component in the process of smart grid construction, it will have broad application prospects. Therefore, relevant enterprises and research institutions at home and abroad have attached great importance to the research and development of multifunctional smart meters. Many smart chip suppliers have also launched a variety of smart meter solutions, and a large number of smart-meter-related literature has also emerged. Some power supply and production enterprises also jointly issued a lot of smart-meter-related standards, and a variety of smart meter products appear in the market. At present, smart electricity meters at home and abroad can be divided into multifunction meters, compound rate meters, prepaid meters, carrier meters, network meters, etc., and can also be combined according to user requirements.

2. New Generation Smart Meter

The new generation smart meter needs to meet the requirements of IR46 international standard and JJF1245 technical specification. Therefore, this paper puts forward the software and hardware architecture design scheme of the new generation smart meter as shown in Figure 1.

It is mainly to meet the needs of two aspects: one is to achieve the separation of legal measurement function (measurement core software) and nonlegal function (management core software) [3] and, second, to support independent apps to flexibly meet differentiated functional needs such as load identification, orderly charging, and contract power purchase, and support the construction of smart electricity meter application market ecology. The embedded operating system is introduced into the management unit, which forms the software platform of the new generation smart meter together with the middle-tier components. The application software is completely decoupled from the hardware platform, thus achieving the purpose of simplifying application development and adapting to iterative upgrade of applications [4].

3. Hardware Design of New Generation Smart Meter Management Unit

The hardware architecture of the new generation intelligent watt-hour meter as shown in Figure 2 is mainly divided into three parts: communication unit, management unit, and metering unit [3, 5]. The following figure shows the hardware schematic diagram and prototype of the management unit, and the main key components are the management MCU chip. The MCU chip of the management unit is a STMicroelectronics product with Cortex-M4 core, with the highest frequency of 100 MHz. On-chip RAM capacity is 320K, and on-chip FLASH capacity is 1M. Five UART ports, two SPI ports, and one 7816 port can support up to 24 GPIO, and the chip package is LQFP64.

The management unit nonvolatile memory is divided into EEPROM, on-chip flash memory, and off-chip flash memory. EEPROM is accessed through the device file, and the application reads and writes data according to the address in the device. The on-chip flash memory is managed by the read-only file system flashfs. Off-chip flash memory is divided into two parts: one is directly read and written by applications using bare sector devices, and the other is managed by power-off secure file system littlefs [6–8].

To meet the needs of users and power supply enterprises, in addition to the original metering and data display functions, the new generation of smart meters also needs to have two-way communication, remote intelligent indoor tripping protection, and good human-computer interaction functions. Higher design requirements for the smart meter management unit are proposed for scalability, intelligence, and adaptability [9–12]. On-chip FLASH storage files include bootloader boot program; the starting address is the running address after power-on; Rtos image, started by bootloader; Start parameter, rtos starts service components and basic applications according to this file, and allocates resources and permissions for them; Service component and APPlication app in middle layer [13–15]. Off-chip LFLASH storage files include application backup, application to be upgraded, power freeze, and event data. Off-chip EEPROM mainly stores application data. And it also supports a number of LCD module interfaces that have these peripheral hardware resources to meet the design requirements of the terminal [12, 14].

Table 1: Function division of legal software and nonlegal software of new generation smart meter.

Functional item	Legal software part	Nonlegal software part
1	Measurement of electrical parameters (such as voltage, current, active power, reactive power, and frequency)	Calculation, storage, and freezing of electric energy rate (including setting of rate and time period)
2	Measurement of electrical energy (e.g., active energy and reactive energy)	Calculation and storage of maximum demand (including the maximum demand of each rate)
3	Or clock maintenance	Display mode and display of nonlegal related content
4	Protection of proprietary parameters of equipment	In addition to the legal system related functions of the event record
5	Freezing of electrical parameters and energy data	Implementation of external data communication interface (such as infrared, RS485, carrier, wireless, etc.)
6	Event records of clearing, upgrading, timing, and modifying equipment-specific parameters	Control function (such as control of load switch)
7	Software interface between legal related software and non-legal related software	Alarm function
8	Methods to ensure the safety of functions related to legal system	Cost control function
9	Identification of legal-related software	Other functions not mentioned
10	Display of legal related contents	—

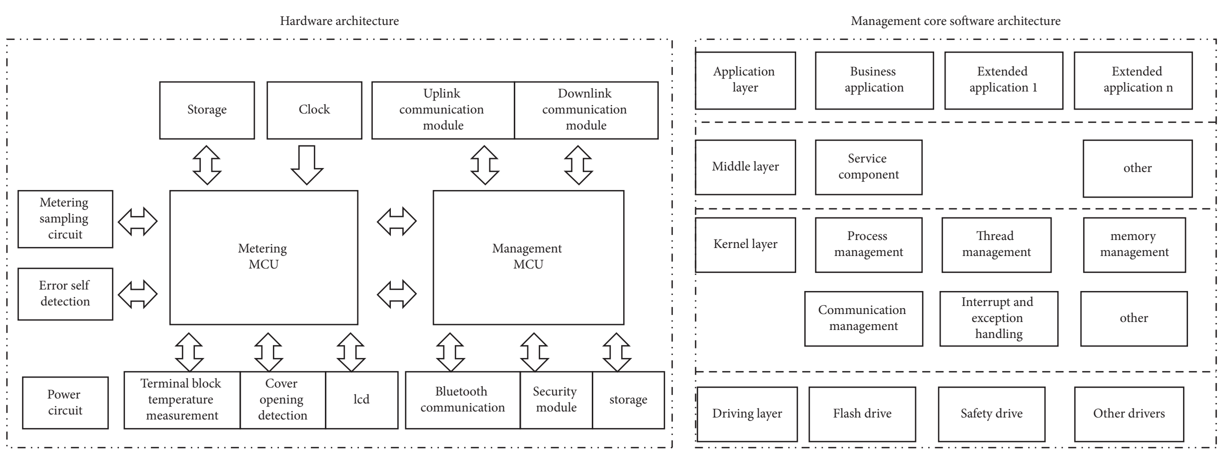

Figure 1: Typical application scheme of new generation smart meter.

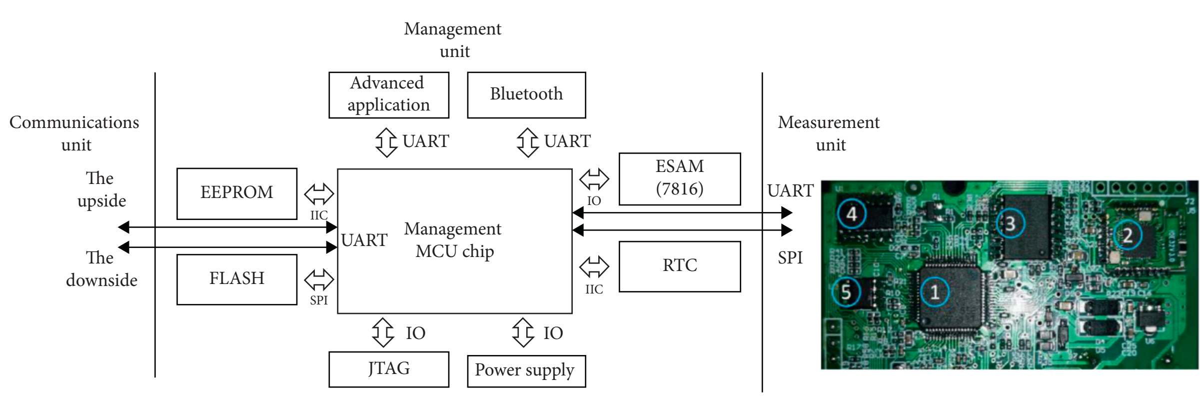

Figure 2: Hardware schematic diagram and prototype of management unit.

4. New Generation Smart Meter Management Unit Software Platform

The software of the new generation smart meter management unit is hierarchically designed as kernel layer, middle layer, and application layer, as shown in Figure 3. The application layer is based on the software platform built by the core layer and the middle layer to realize the specific business functions of the smart meter, including a basic application and multiple extended applications.

The kernel layer mainly includes the operating system kernel, device drivers, and many specific functions built by

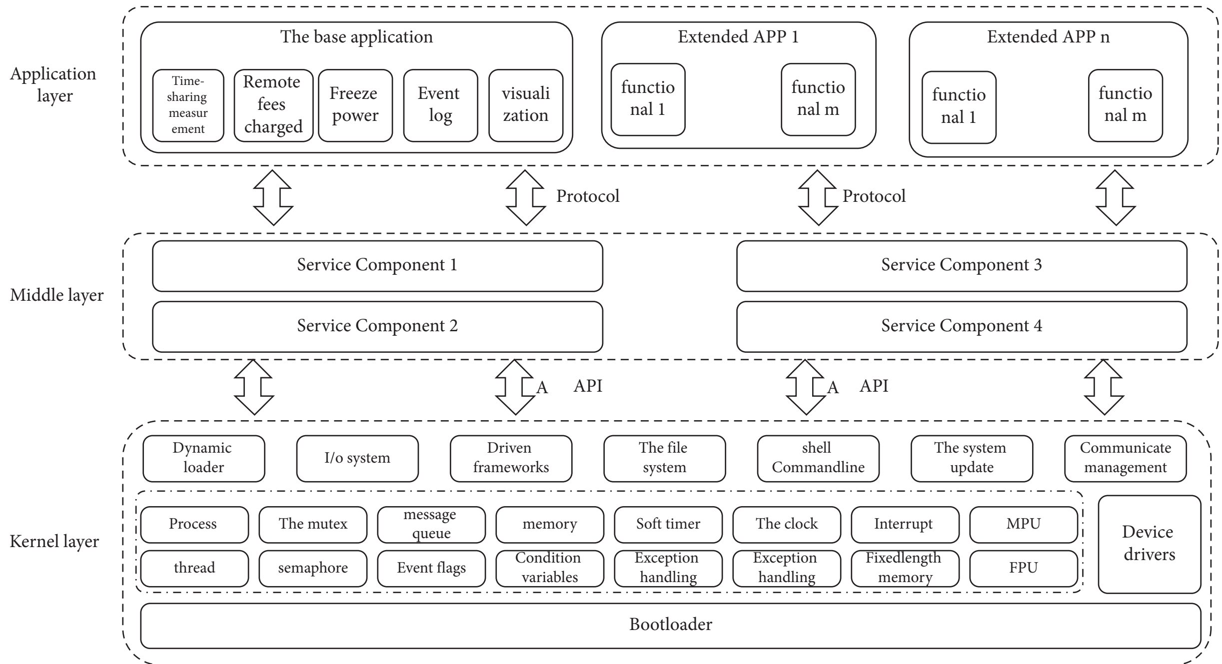

Figure 3: Snap-in software platform.

the operating system. These specific functions are customized according to the requirements of smart meters to realize task scheduling and resource allocation and have the characteristics of standardized programming interfaces, extensible function modules, and portable operating system kernel [8–10, 16]. The middle layer realizes the decoupling between the operating system and the electricity meter service and improves the stability and universality of the operating system. The middle layer runs on the system kernel and provides common services and component support for the application layer. This scheme mainly includes virtual bus service component, communication management service component, measurement management service component, and platform management service component as shown in Figure 3.

5. Development Environment Building and Development Tools

Software is the soul of a system; if a system is without software, then its hardware circuit will lose the value of existence. Only by combining the two can the system function be realized. In the actual system, if a software system with perfect functions and excellent performance is configured for the hardware circuit, it can not only make up for some defects of the hardware circuit, but also greatly reduce the design cost [17]. More importantly, only in this way can the hardware give full play to its functions [18].

This system design chooses the embedded system with the operating system because the embedded system with the operating system is better than the embedded system without the operating system in real time, tailoring open and scalability, and strong stability. At the same time, compared with the embedded system without operating system, the embedded system with operating system is also portable and deterministic.

To develop application software based on the new generation smart meter software platform, the development environment should be set up first, which mainly includes integrated development environment software, new generation smart meter prototype (including management unit), Jlink simulator, and upper computer debugging software as shown in Figure 4, realizing the adaptation of operating system to hardware platform, complete the development of hardware interface and peripheral driver, and realizing the transplantation and testing of software system. Finally, the application software is developed based on the API interface provided by the operating system and the intermediate layer protocol data structure.

The integrated development environment software (IDE) used in this paper is IoT Studio, and its main functions are RTOS project management and program debugging as shown in Figure 5. IoT Studio can create RTOS Base project, RTOS Bsp project, RTOS App project, RTOS App Static Lib project, RTOS Kernel Static Lib project, and RTOS Unit Test project. Support downloading and debugging BSP project and App project with one click of J-Link. IoT Studio mainly integrates the following development tools as shown in Figure 5.

(1) Compiler tool chain optimized for platform

(2) Intelligent code editor

(3) Code coverage analysis tool

(4) Code static analysis tool

(5) Support debugging tools through emulators such as J-Link

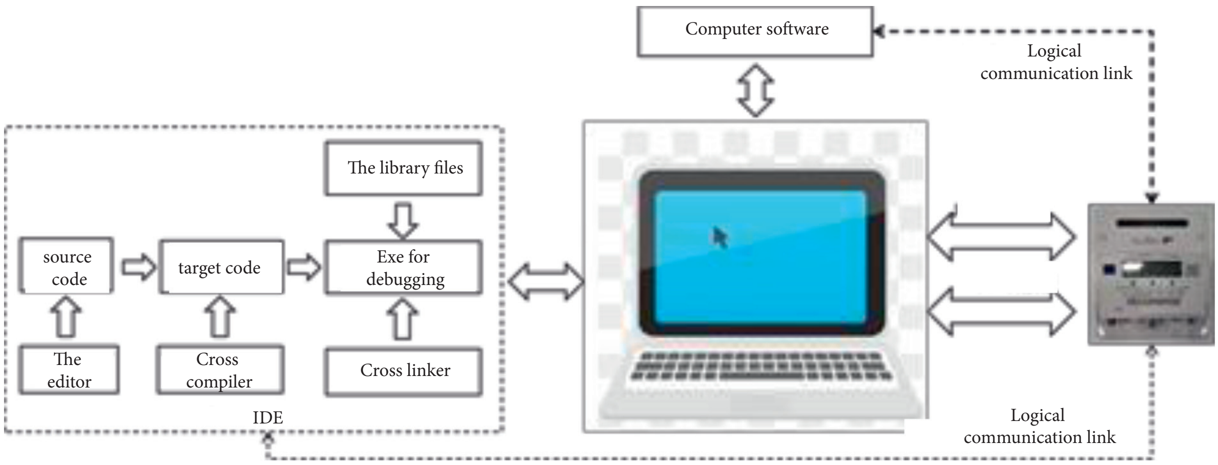

Figure 4: Embedded application software cross development.

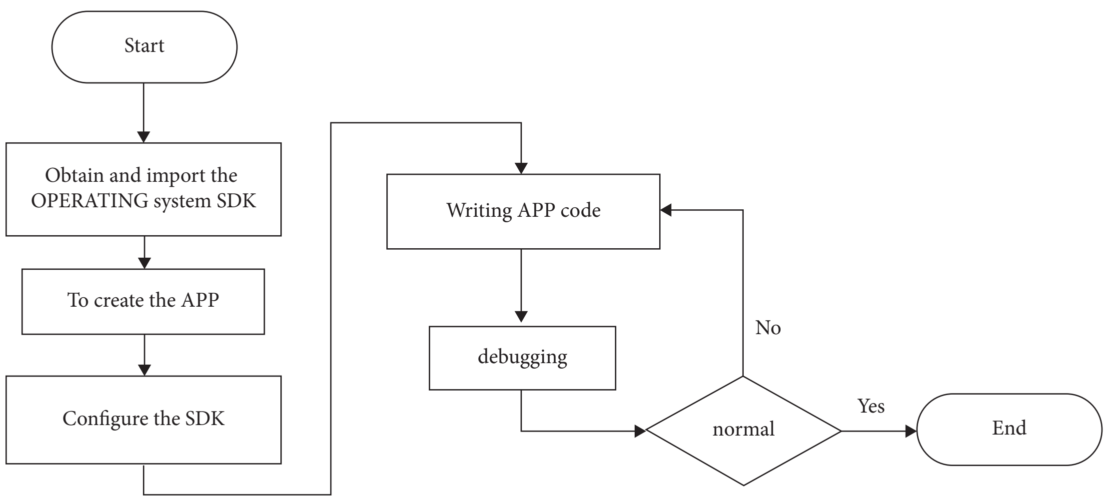

Figure 5: IDE usage flow.

RTOS Image Packager is an image of RTOS operating system and an application packaging tool. The tool specially provides the factory firmware generation function, which can package the BootLoader image, operating system image, startup parameters, and application image into a factory firmware. In the mass production stage, the packaged factory firmware only needs to be burned into Flash as shown in Figure 6.

RTOS AutoTester is an automatic testing tool for RTOS operating system. The tool integrates the functions of firmware writing, Shell terminal, and modem protocol file sending and has the function of C language automatic test script execution as shown in Figure 7.

6. Basic Functions of Software Platform

The platform provides rich functions for application software development. The core functions are process management, thread management, interprocess communication, thread synchronization and communication, clock and soft timer management, interrupt/exception management, multiprocess security isolation, dynamic loading, and low-power consumption management [19]. The extended functions are mainly memory management, system update, file system, IO system and drive framework, etc., and can be extended according to actual requirements. Among them, kernel layer and kernel component layer work in CPU privilege mode, while middle layer components and application layer work in CPU user mode. The following mainly introduces the common functions and API interfaces of application software development.

6.1. Process Management. It is the smallest unit for operating system to allocate resources. Common API interfaces are ms_process_self () to get the current process ID, ms_process_kill () to kill the specified process, ms_process_exit () to voluntarily exit, and ms_process_find () to find the process.

Process management mainly has the following functions:

(1) The number of processes is configurable

(2) Process memory resources can be configured (minimum 4K, 2 to the nth power kb)

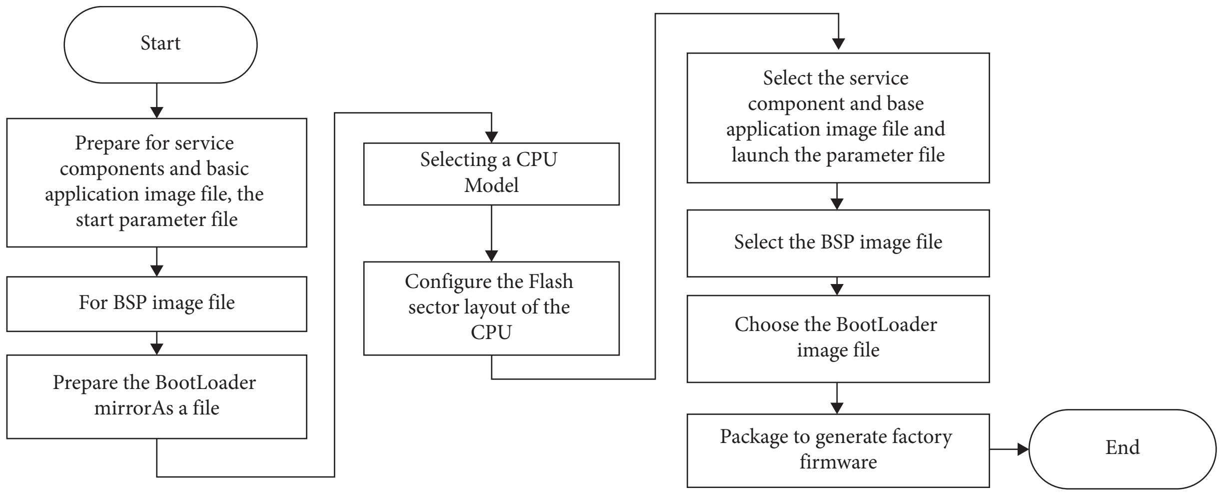

Figure 6: Use process of software packaging tools.

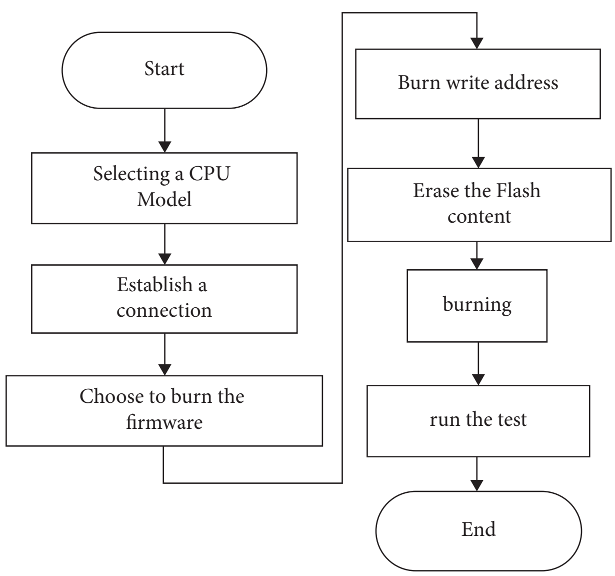

Figure 7: Use process of test tools.

(3) Process kernel resources can be configured (maximum number of threads, number of kernel objects, and number of open files)

(4) Process permissions can be configured (EEPROM access space, privileged system call)

(5) Process address spaces are isolated from each other

6.2. Thread Management. Thread is the basic unit of task scheduling in operating system. Commonly used API interfaces are as follows: ms_thread_create () creates a ready thread, ms_thread_init () creates a suspended thread, ms_thread_self () gets the ID of the current thread, ms_thread_kill () kills a thread, ms_thread_exit () the current thread voluntarily exits, the ms_thread_suspend () suspends a thread, the ms_thread_resume () resumes a thread, and the ms_thread_yield () current thread gives up the CPU usage right. Thread management mainly has the following functions:

(1) Support 64 priorities

(2) Support high priority preemption and time slice rotation scheduling with the same priority

(3) Decompose tasks and simplify execution logic

6.3. IO System. IO system as shown in Figure 8, also known as I/O system, isolates the direct access of applications to hardware devices and unifies various hardware access interfaces. The replacement of hardware devices no longer needs to modify the application code, but only needs to add the corresponding hardware drivers in the operating system. Commonly used API interfaces are ms_io_creat () file, ms_io_open () file, ms_io_close () file, ms_io_read () file, ms_io_write () file, ms_io_ioctl() IO control, ms. IO system mainly has the following functions:

(1) All devices can be accessed as files

(2) File operation interface supports POSIX flag

(3) C library file interface is supported

(4) Provide a more resource-efficient system interface

6.4. IPC. The interprocess communication mechanism as shown in Figure 9 involved in this paper mainly includes named pipe and shared memory. Common API interfaces are as follows: ms_pipe_dev_create () creates a pipeline device, ms_shm_dev_create () creates a shared memory device (kernel space), ms_io_open () opens a pipeline or shared memory device, ms_io_read () reads pipeline data, and ms_io_write () writes.

6.5. Service Data Routing Distribution. The virtual bus service component is the data flow center, and each service and APP need to distribute data through the virtual bus, so as to realize the communication and data interaction between each service and app. The main functions are as follows: safe and efficient well-known read/write pipeline is adopted for interprocess communication, data routing and forwarding of interprocess protocol, support for

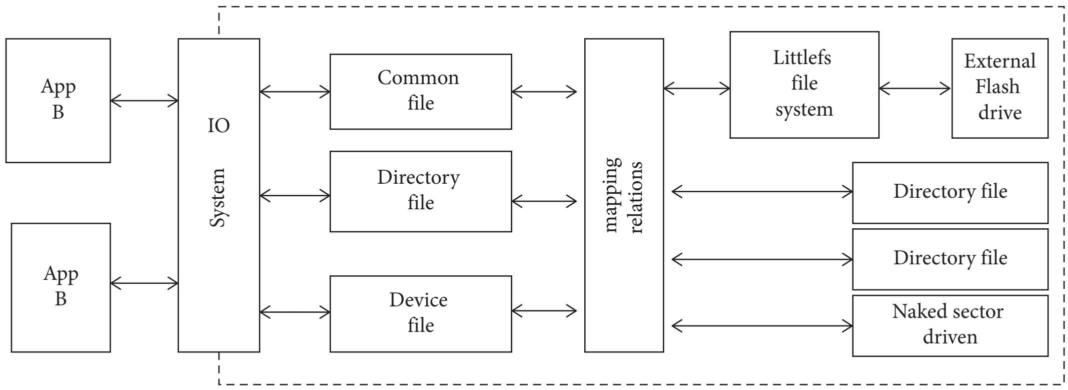

FIGURE 8: IO system.

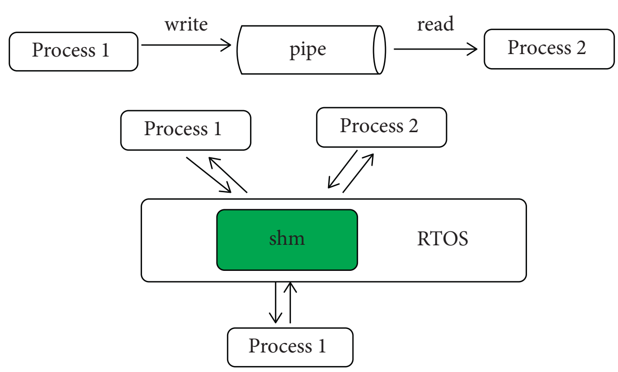

FIGURE 9: Pipeline and shared memory communication.

registration of DL/T645 extended protocol data identifier, support for pipeline registration of extended APP, and support for combination data reading. The format of protocol data frame is shown in Table 2.

The source address and destination address coding rules are shown in Table 3.

Description of interface between virtual bus component and each service component and application is shown in Table 4.

7. Application Software Development Practice

This paper only introduces the basic application APP in detail as a concrete practice, which needs to meet the Technical Requirements of the New Generation Single-phase Smart Energy Meter in South Power Grid, including basic functions, extended functions, dual-core interactive functions, and data security functions.

The architecture of the basic application app as shown in Figure 10 is divided into six modules, which are the basic application app virtual bus module, time-sharing measurement module, display module, meter reading freezing module, event recording module, and control module. The APPlication APP virtual bus module realizes the internal data interaction of each functional module of the basic application app and realizes the interaction between the basic application app and external data; the time-sharing metering module realizes time-sharing rate electricity metering, ladder electricity metering, and rate electricity synchronization after the management core is plugged and unplugged. The meter reading freezing module realizes five types of electricity data freezing, completes multiple backups, and realizes supplementary freezing. The display module realizes display functions such as tracking display and organizes display data for use by the metering core. The event recording module records various events according to the configuration and stores them in EEPROM. The control module realizes the functions of remote charge control, opening and closing, self-protection, and so on. The following mainly introduces the main workflow of the basic application APP virtual bus module, freezing module, and display module.

7.1. Virtual Bus Module. As shown in Figure 11, the data from outside is distributed to the other five modules through the basic application app virtual bus module.

(1) Create a thread to monitor, and receive and analyze the data distributed by virtual bus. In order to ensure the real-time reception, select function is used to monitor and avoid polling and sleep waiting.

(2) The received data is judged and distributed to specific modules through control words and data identification, and the API interface of

Table 2: Protocol data frame format.

name	Meaning	Member
agrform_t	Communication frame header structure between 4 services and basic application app	FristSepa: identifier, fixed as 0×68 CAID: source address, address of initiator Said: destination address, response module address encryption: encryption method MetersAddr: type of protocol communication address AgreType: protocol type ComType: command type overRbye1: and verify that all save fields are reserved to use the length of DataLen: uplink/downlink 645 protocol frame
AgrDataBuf	Frame content data	Complete 645 frames of data of uplink/downlink 645 protocol (from the starter 68 to the terminator 16)
pipe_t	Pipe type	The trend of data, such as V_BUS_TO_COM_SRV, indicates the pipeline from virtual bus to communication management service, virtual bus receiving pipeline, and communication management service sending pipeline

Table 3: Source address and destination address coding rules of protocol data frames.

bit7	bit6	bit5	bit4	bit3	bit2	bit1	bit0
Process number					Every thread number in APP, 0–7		
0: initial value					0: main thread		
1: basic APP					Basic APP		
2: communication service					0: general basic application app		
3: metering management service					1: time-sharing measurement		
4: platform management service					2: demand measurement		
5: extended app1					3: freezing		
6: extended app2					4: display		
7: extended app3				Reserve	5: cost control		
8: expand app4					6: event		
9: expand app5					Communication APP		
10: expand app6					1: uplink carrier		
11: extend app7					2: downlink Bluetooth		
12: extend app8					3: load identification		
13: extend app9					4: other communications (continuous coding)		
14: extend app10							
15: virtual bus service					Other processes		

corresponding modules is called. There are three API interfaces: get, set, and action.

(3) When each module actively requests data or actively operates a task, it judges whether it is internal module data. If it is internal module data, it directly calls the get, set, and action functions of the basic application app, calls the API interface of the corresponding module, and replies to the data.

(4) If each module actively requests external data, it needs to call the get, set, and action functions encapsulated by the basic application app, write the external pipeline of the basic application app, and obtain data through the virtual bus. After the virtual bus obtains the data, it returns the data to the basic application app through the pipeline, and the basic application app sends it back to each module through the message queue. Set, get, and action functions encapsulated by the basic application app package the message queue internally, which is used for the interaction between the basic application app general thread and each module thread as shown in Figure 11.

7.2. Freeze Module. According to the interaction with other modules of basic application APP, the freezing module can be divided into two parts: the other module reads the data of freezing module and the freezing module obtains the data of other modules. The running process of frozen thread is shown in Figure 12.

Table 4: Interface description between virtual bus components and various service components and applications.

Interface function	Description	Input	Operate	Output
Pipeline function	The virtual bus automatically creates a pipeline with other apps and services.	Pipeline no.	Judging whether the pipeline exists or not	Do all communication channels exist?
		Pipeline communication frame (CA and SA are consistent, single frame, multiframe, small data frame, and large data frame)	Send the pipeline communication frame to the virtual bus service through the corresponding pipeline	The virtual bus is distributed through the corresponding pipeline data
Virtual bus data distribution function	The virtual bus performs correct distribution processing according to the data identification and control code in the data frame	The data identification of metering service management constitutes the pipeline communication frame	Send the pipeline communication frame to the virtual bus through the corresponding pipeline	Whether the virtual bus distributed data is distributed through the pipeline of metering management service, comparing the integrity and legitimacy of distributed data
		The data identifier managed by the platform management service constitutes a pipeline communication frame		Whether the virtual bus distributed data is distributed through the pipeline of platform management service, comparing the integrity and legitimacy of distributed data
		The data identifier of the management service management constitutes a communication frame		Whether the virtual bus distributed data is distributed through the pipeline of communication management service, comparing the integrity and legitimacy of distributed data
		The data identifier managed by the basic app is used to form a pipeline communication frame		Whether the virtual bus distributed data is distributed through the pipeline of basic application app, comparing the integrity and legitimacy of distributed data
		Compose pipeline communication frame through transparent transmission control code		Whether the virtual bus is forwarded to the corresponding extended app pipeline according to the object code SA of the extended app, and the integrity and legitimacy of the distributed data are compared
The virtual bus supports the extended app registration function	According to the extended app registration information, the virtual bus creates a corresponding pipeline and stores the extended app registration information	The extended app registration information constitutes a pipeline frame, and the extended app registration information is read to constitute a pipeline frame	Send the pipeline frame to the virtual bus through the extended app reservation registration pipeline	The virtual bus establishes the corresponding extended app communication pipeline according to the registration information and returns the stored extended app registration information

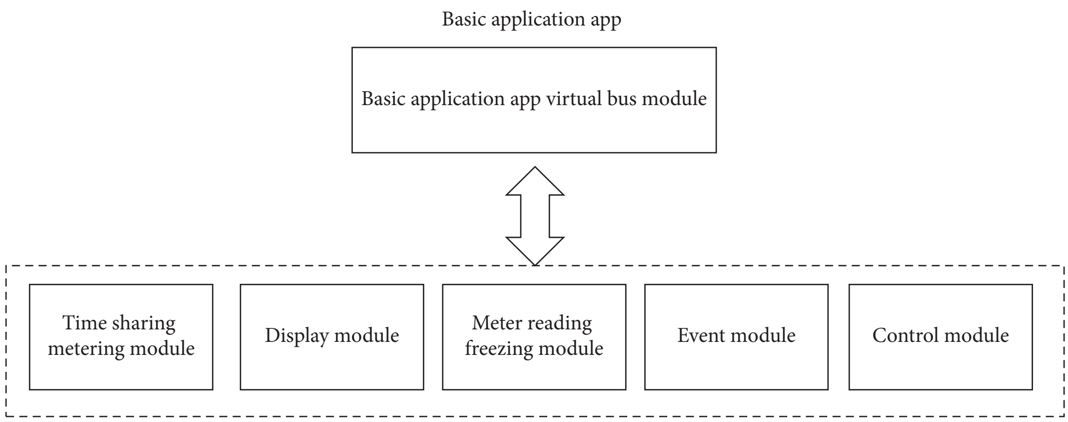

Figure 10: Software architecture of metering basic application APP.

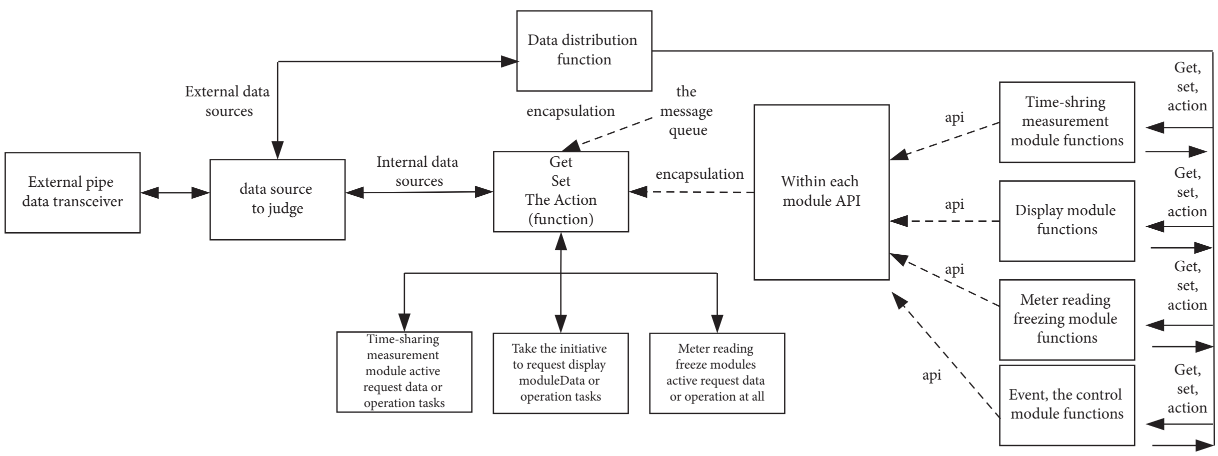

Figure 11: Virtual bus module data distribution process.

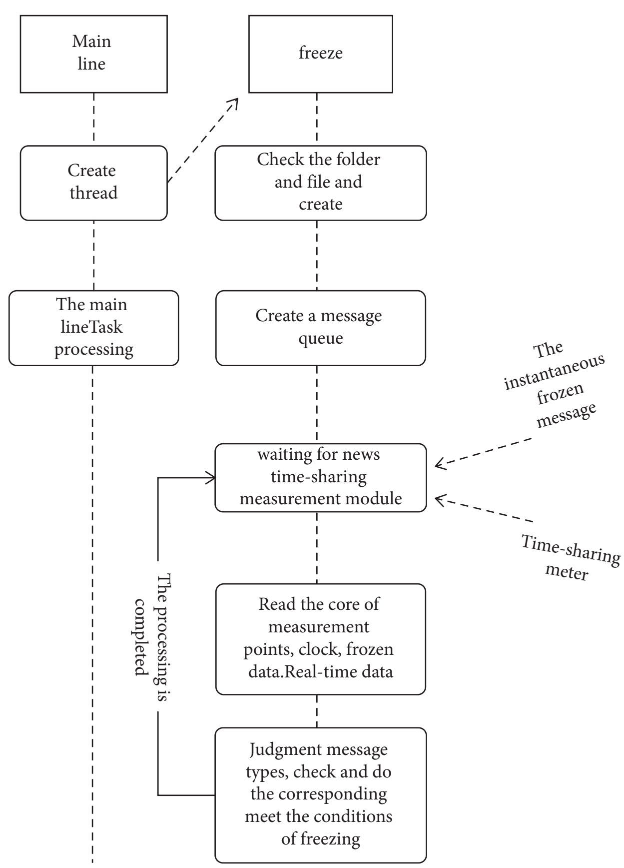

Figure 12: Freezing thread running process.

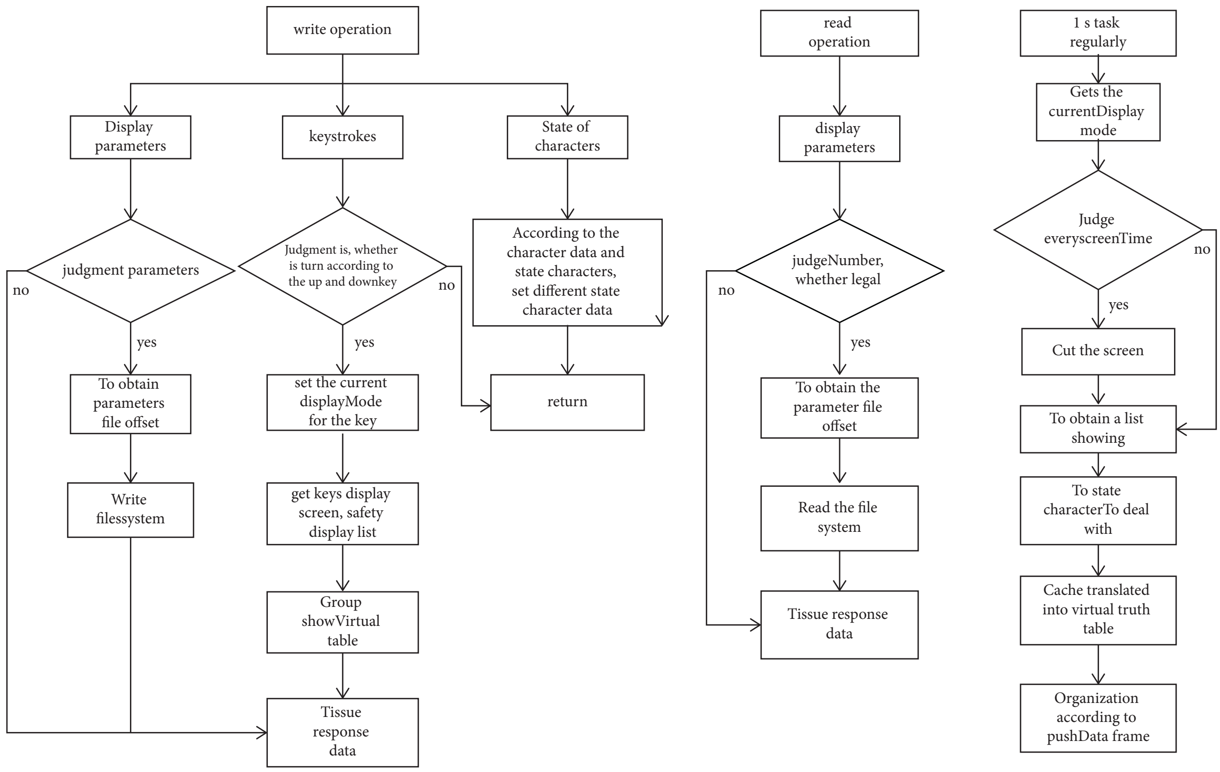

Figure 13: Display thread write operation, read operation, and display processing flow.

7.3. Display Module. The display module mainly includes three parts: writing operation of the display module, reading operation of display parameters, and 1s timing display data processing. The running process of the display thread is shown in Figure 13.

8. Conclusion

Based on the new generation smart meter software and hardware platform, this paper builds an application software development environment by using IDE and related tools and puts forward the concrete practice of business application software development, which has good reference significance for other application software development based on the new generation smart meter software and hardware platform. The simple development and quick iteration of the application software are conducive to promoting the large-scale application of the new generation of smart meters and have laid a solid technical foundation for meeting the differentiated business needs of the new generation of smart meters within their 15-year service life and building a grand application ecological market in the future [11–19].

Data Availability

The labeled dataset used to support the findings of this study is available from the corresponding author upon request.

Conflicts of Interest

The authors declare no conflicts of interest.

Acknowledgments

This study was supported by the Research Project of China Southern Power Grid Co., Ltd. (JY-O-JL-20-002)

References

[1] M. Liu, L. Zhou, C. Miao, W. Wu, and J. Xiang, “Discussion on the development of a new generation of intelligent electric energy meters,” *Electrical Measurement and Instrument*, vol. 54, no. 18, pp. 94–100, 2017.

[2] Jjf1245-2019, *Type Evaluation Outline of Mounted AC Electric Energy Meter*, State Administration of Market Supervision, Beijing, China, 2020.

[3] Z. Zhou, D. Zhao, H. Zhang, J. Du, and W. Wang, “Research on key technologies of dual-core watt-hour meter master control based on IR46 standard,” *Application of Electronic Technology*, vol. 43, no. 10, pp. 7–11+19, 2017.

[4] J. Li, S. Bai, and Z. Wang, “Smart meter based on MQX operating system,” *China Science and Technology Information*, vol. 01, pp. 50-51, 2016.

[5] X. Ou, Y. Zeng, X. Ran, X. Wang, and X. Ou, “Research on software reliability design and test of IR46 intelligent electric energy meter,” *Electrical Measurement and Instrument*, vol. 56, no. 19, pp. 147–152, 2019.

[6] J. P. Sun, *Research and Implementation of Embedded File System Based on Flash Memory*, xidian university, Xi ’an, China, 2008.

[7] T. Ling, Y. Xu, S. Shen, and R. L. Zhang, “A design method of embedded file system with power-off security,” *Application of Single Chip Microcomputer and Embedded System*, vol. 5, pp. 33–36, 2019.

[8] Gj/b7718-2012, *Technical Requirements of Military Embedded Operating System*, General Armament Department of Chinese People’s Liberation Army, Beijing, China, 2013.

[9] J. Cheng, J. Lou, Y. Cao, and M. Xu, "A general test software architecture design for avionics products," *Measurement and Control Technology*, vol. 39, no. 4, pp. 33–37, 2020.

[10] X. Zhang, *Research and Implementation of Key Technologies of Embedded System of Internet of Things Based on Mbed*, Shenyang Institute of Computing Technology, Chinese Academy of Sciences, Shenyang, China, 2018.

[11] L. Gao, Z. Wang, J. Zhou, and C. Zhang, "Design of smart home system based on ZigBee technology and R&D for application," *Energy and Power Engineering*, vol. 08, no. 1, pp. 13–22, 2016.

[12] F. L. Huang and S. Y. Tseng, "Predictable smart home system integrated with heterogeneous network and cloud computing," in *Proceedings of the 2016 International Conference on Machine Learning and Cybernetics (ICMLC)*, July 2016.

[13] Y. H. Lin, "A cloud analytics-based electrical energy management architecture empowered by edge analytics AIduino with push notifications for demand-side management," in *Proceedings of the 2019 IEEE 2nd International Conference on Power and Energy Applications (ICPEA)*, Singapore, April 2019.

[14] A. Muti and L. Fatzinger, "System And method for scheduling posts on a web site," 2013.

[15] M. H. Yaghmaee Moghaddam and A. Leon-Garcia, "A fog-based internet of energy architecture for transactive energy management systems," *IEEE Internet of Things Journal*, vol. 5, no. 2, pp. 1055–1069, 2018.

[16] H. H. Chang, C. L. Lin, and L. S. Weng, "Application of artificial intelligence and non-intrusive energy-managing system to economic dispatch strategy for cogeneration system and utility," in *Proceedings of the International Conference on Computer Supported Cooperative Work in Design*, May 2009.

[17] L. Yu-Hsiu and H. Yu-Chen, "Residential consumer-centric demand-side management based on energy disaggregation-piloting constrained swarm intelligence: towards edge computing," *Sensors*, vol. 18, no. 5, p. 1365, 2018.

[18] H. Hafiz, J. Nadeem, I. Sohail, U. H. Qadeer, A. Khursheed, and A. Musaed, "An efficient demand side management system with a new optimized home energy management controller in smart grid," *Energies*, vol. 11, no. 1, p. 190, 2018.

[19] T. Ming, J. Zuo, Z. Liu, A. Castiglione, and F. Palmieri, "Multi-layer cloud architectural model and ontology-based security service framework for IoT-based smart homes," *Future Generation Computer Systems*, vol. 78, pp. 1040–1051, 2016.

Hindawi
Scientific Programming
Volume 2022, Article ID 2227049, 12 pages
https://doi.org/10.1155/2022/2227049

Research Article

Monitoring, Prediction, and Evaluation of Mountain Geological Hazards Based on InSAR Technology

Fan Yang,[1,2] Zhongrong Jiang,[1] Junqian Ren,[2,3] and Jian Lv[1,2,4]

[1]*SiChuan HuaDi Building Engineering Co. Ltd, Chengdu 610081, China*
[2]*Chengdu University of Technology, Chengdu 610059, China*
[3]*Sichuan Highway Planning, Survey, Design and Research Institute Ltd, Chengdu 610041, China*
[4]*School of Geographic Science and Remote Sensing, Guangzhou University, Guangzhou 510006, China*

Correspondence should be addressed to Jian Lv; 1819500009@e.gzhu.edu.cn

Received 23 November 2021; Accepted 18 December 2021; Published 17 January 2022

Academic Editor: Le Sun

When traditional geological hazard survey methods are used for deformation monitoring in mountainous areas, it often shows the disadvantages of low applicability of monitoring methods and limited accuracy of detection results. In recent years, synthetic aperture radar interferometry (InSAR) technology has incomparable advantages in surface deformation monitoring, such as all-weather detection, wide detection range, high detection accuracy, and low detection cost. At the same time, InSAR technology can also provide data and technical support for the subsequent task of potential geological disaster point identification and geological disaster risk zoning in the study area. Alos-2 radar is selected; in this paper the satellite image is the research data, and the InSAR technology is used to complete the surface deformation detection. Then, based on the previous surface deformation monitoring results, the potential geological disaster points in the study area are extracted, and the distribution law and incubation conditions of the disaster points are analyzed and described. According to the field conditions of a certain area, the surface distribution, development causes, and inducing mechanism of the potential geological disaster points are explored; the results show that the development of geological disasters in the study area is affected by many factors such as landform, geological environment, climate, hydrology, and human activities. Based on this, 11 factors such as formation lithology, slope, and river are used as evaluation factors for mountain geological disaster monitoring, prediction, and evaluation analysis. Finally, the improved analytic hierarchy process information model is used to complete the monitoring, prediction, evaluation, and analysis of regional geological hazards in the study area. In this paper, the improved AHP-information method is used to classify the risk of mountain geological disasters in the study area. Finally, the evaluation results are verified, which proves that the improved AHP-information method is reliable, and its mountain geological disaster monitoring and prediction evaluation effect is better than the traditional AHP-information method.

1. Introduction

Under the influence of basic geographical environment factors such as fragile geological environment, huge topographic relief, and complex stratum lithology, the regional surface deformation of mountains in some areas is active [1]. In addition, under the trigger of strong geological tectonic movement, rainfall, and other factors, all kinds of geological disasters in the county show a trend of frequent occurrence, easy occurrence, and high incidence for a long time [2]. Due to the special topographic and geological conditions and abundant vegetation coverage in the study area, geological disasters are concealed, which makes it difficult to realize early prediction in the process of disaster prevention and control and easily causes large-scale social, economic, and personnel losses [3]. When the traditional geological hazard survey method is used to monitor the deformation in mountainous areas, it often shows the shortcomings of low applicability of the monitoring method and limited accuracy of the detection results [4]. Therefore, through the InSAR technology, to effectively identify the potential geological disasters and to prevent and control become the focus of this paper [5, 6].

2. InSAR Technology

Usually, InSAR technology is applied to DEM construction and surface deformation monitoring [6]. In the early stage of the development of InSAR technology, due to the defects of some characteristics of radar images, the surveying and mapping accuracy is limited. In recent years, with the improvement of interferometry technology and the establishment of many SAR satellite systems, InSAR technology has been more mature applied to topographic survey and deformation monitoring [7].

2.1. InSAR Fundamentals. InSAR technology can be used to complete the task of acquiring DEM data. The key principle of this technology is to realize two or more observation processes in the same research area, and different observation processes are required to have proper viewing angle difference during imaging, so as to achieve the purpose of acquiring single-view complex images with high coherence [8]. Then, the image interference processing flow is completed in turn, and the Earth surface elevation data is extracted according to its interference phase information. Complete the above series of operations, that is, to realize the construction of DEM in the research area [9].

Figure 1 shows the geometric relationship diagram when InSAR system observes the surface and obtains the surface elevation information. In Figure 1, S_1 and S_2 represent the position of radar antenna during two imaging processes, which can be obtained from the orbital parameters of the satellite itself, and B is the spatial distance between them, which is called baseline. R_1 and R_2 are the oblique distances from the two antennas to the ground observation points, respectively. α represents the angle between the baseline and the horizontal direction, θ is the incident angle, H is the height of the antenna track, and h is the elevation of the measured ground point target relative to the reference ellipsoid.

The phase information contained in radar echo signal can be divided into two parts: one is the phase information reflecting the characteristics of the target point itself, and the other is the phase value representing the distance between the ground point and the antenna. This kind of information is the part that can be used to retrieve the position of the ground target point. In the course of two radar observations, the ground target point can be regarded as unchanged, so the characteristic phase of the target point itself is consistent in each radar echo signal. Therefore, from the phase information of the distance between the target and the antenna, we can know that the echo signal of the antenna S_1 is

$$\phi_1 = 2\pi \frac{2R_1}{\lambda}. \quad (1)$$

The echo signal phase of antenna S_2 is

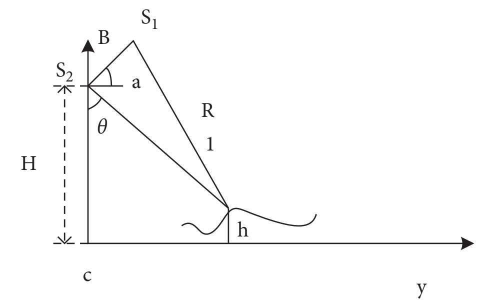

Figure 1: Geometric diagram of InSAR system.

$$\phi_2 = 2\pi \frac{2R_2}{\lambda}, \quad (2)$$

where λ is the wavelength of radar signal. In this way, the interference phase difference between two images can be expressed:

$$\Delta\phi = \phi_1 - \phi_2 = -\frac{4\pi}{\lambda}\left(R_1 - R_2\right) = -\frac{4\pi}{\lambda}\delta. \quad (3)$$

In the process of generating interferogram, due to the difference of incident angle and azimuth, the objects with the same name in two SAR images cannot be completely aligned, so it is necessary to register them. After the registration operation is completed, the interference phase difference in equation (3) can be obtained from the generated interferogram by using the processed image to complete the multiplex multiplication [10]. It can be seen from equation (3) that, for the same ground target point, the echo phase difference is proportional to the oblique distance difference. After two echo signals from the same target unit are multiplied together, the phase difference obtained is only determined by the oblique distance difference, which is related to the elevation of the ground unit. From the geometric relationship information shown in Figure 1, equation (4) can be obtained:

$$R_2^2 = R_1^2 + B^2 - 2R_1 B\cos\left(\alpha + \frac{\pi}{2} - \theta\right). \quad (4)$$

Make a transformation to get

$$\sin(\theta - \alpha) = \frac{R_1^2 - R_2^2 + B^2}{2R_1 B} = \frac{\left(R_1 + R_2\right)}{2R_1 B} + \frac{B}{2R_1}. \quad (5)$$

According to the actual situation of SAR system observation, baseline B can be ignored compared with R_1 and R_2 alone, and at the same time, $(R_1 - R_2)$ is far less than R_1. By transforming equation (5), we can get

$$\sin(\theta - \alpha) \approx \frac{R_1 - R_2}{B} = -\frac{\lambda\Delta\varphi}{4\pi B}. \quad (6)$$

Thus, α, B, and H are obtained from the orbital attitude data, and from the geometric relationship shown in Figure 1:

$$h = H - R_1 \cos\theta. \quad (7)$$

In the actual operation process, after the data undergoes triangulation operation, the interference solution result obtained is the main value of its phase information, which is always between $[-\pi, \pi]$, and its true value can be obtained only after subsequent phase unwrapping.

2.2. D-InSAR Technology. The key of D-InSAR technology is to make two or more SAR images in the same area complete the process of differential interference, from which the surface deformation data of the study area can be obtained [11]. The deformation information can be expressed by the observation and imaging results of radar antennas for the same target objects. That is, when there is surface deformation, the phase reflecting the spatial position change between the ground target and the observation antenna can be extracted from the image pair interference processing results, so as to realize the regional deformation monitoring. After two previous observation and imaging processes are completed, the interference phase can be obtained from the interference measurement results at this time. The key components of the interference phase can be divided into: morphological phase (φ_{def}), reference ellipsoid phase (φ_{o}), terrain phase (φ_{topo}), atmospheric phase (φ_{atm}), random noise phase (φ_{noise}), etc., which are expressed by formula (8) as follows:

$$\varphi = \varphi_{\text{def}} + \varphi_o + \varphi_{\text{topo}} + \varphi_{\text{atm}} + \varphi_{\text{noise}}. \tag{8}$$

In the process of regional surface deformation monitoring noise phases such as reference ellipsoid atmosphere and terrain will have great interference on deformation detection. These error phases should be removed as much as possible to obtain more accurate regional surface deformation monitoring results. According to the difference of the methods of obtaining the terrain phase φ_{topo} process, the synthetic aperture radar differential interferometry is divided into two-pass, three-pass, and four-pass methods, which is still the main method to realize D-InSAR.

2.2.1. Fundamentals. In the actual process of D-InSAR, the terrain phase is obtained by converting the digital elevation data from outside to the radar system. The process of removing the terrain phase information from the original interference results is another core content besides the interference to the differential interference when using D-InSAR to detect the regional surface deformation. Figure 2 shows a geometric schematic diagram of obtaining surface deformation by two-orbit D-InSAR [12, 13].

Similar to the principle of InSAR altimetry, point P in the figure is the ground point observed by satellites twice, S_1 and S_2 are antenna positions, f represents the distance difference between the two antennas S_1 and S_2 and the ground observation point P, α is the angle between the baseline and the horizontal direction, and θ is the incident angle. At this time, the observation point P itself has a displacement of Δd in the line of sight. The surface deformation information of the study area can be solved by calculating the phase change phase, and the calculation formula is as

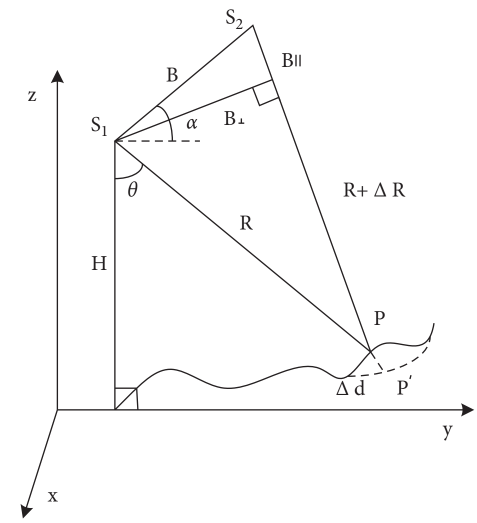

Figure 2: Geometric schematic diagram of two-orbit D-InSAR.

$$\varphi_{\text{def}} = \varphi - \varphi_o - \varphi_{\text{topo}}. \tag{9}$$

$$\Delta \text{d} = \frac{4\pi}{\lambda}\varphi_{\text{def}}, \tag{10}$$

where λ is the wavelength of the band; Δd is the deformation along the radar line of sight. It can be seen from the formula that, assuming that the phase value obtained from the differential interferometry results has a periodic change of 2π, the specific value of the relative regional surface deformation Δd is half wavelength length $\lambda/2$, which indicates that D-InSAR is highly sensitive to surface deformation. The expression process of equation (9) belongs to the case where the error phases such as atmosphere and reference ellipsoid are ignored for convenience of understanding. D-InSAR technology can monitor centimeter-level or even sub-centimeter-level microdeformation, which greatly improves the monitoring ability of surface deformation monitoring means.

2.2.2. Data Processing Flow. When D-InSAR is used to obtain surface deformation information by differential processing of interference phase, its data processing flow is shown in Figure 3.

The core of D-InSAR technique for ground deformation calculation is the differential processing of interference phase. The data processing flow is roughly divided into three parts: data preprocessing, differential interference calculation, and deformation calculation.

2.3. SBAS-InSAR Technology. Short baseline subset method is proposed by Berardino et al. on the basis of previous research results. When using this technology to generate interferogram, it requires short spatiotemporal baseline interference pairs, which can effectively reduce temporal decoherence and spatial decoherence [14].

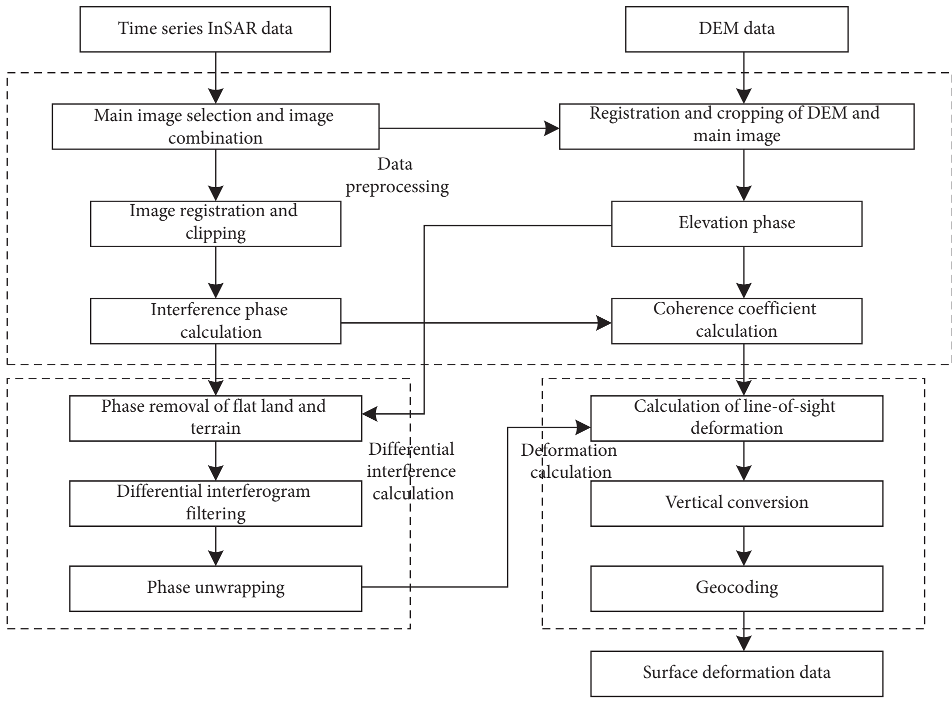

Figure 3: Flowchart of D-InSAR processing.

2.3.1. Fundamentals. An important step in the realization of SBAS-InSAR technology is to complete the subset division of all SAR images. This process is to divide the image set into different short baseline subsets according to the influence of spatial and temporal baselines on the coherence of images and complete the calculation of interference phase of each image pair in the subset. At this time, the number of interference pairs is obviously increased, and the coherence of each interferogram is also enhanced compared with the previous case where only a single main image is used. The differential interferograms are linked by singular value decomposition (SVD), which can restrain the effect of DEM error and atmospheric phase delay on the phase variation and finally obtain the least square solution.

The specific process is as follows:

(1) Assuming there are $N+1$ SAR images in $[t_o, t_1, t_2, t_3, \ldots, t_n]$ time period, the interference pairs with M pairs of spatiotemporal baselines within the threshold condition can be obtained by any combination, and M should meet the requirements of equation.

$$\frac{N}{2} \le M \le \frac{N(N-1)}{2}. \tag{11}$$

Assuming that the i-th interferogram is obtained by removing terrain phase, filtering interferogram, and unwrapping phase, the time of acquisition of main image and slave image is t_B and t_A, respectively, and the interference phase at (a, r) in radar coordinate system can be expressed as

$$\Delta\varphi_i(a,r) \approx \frac{4\pi}{\lambda}\left[d_{t_A}(a,r) - d_{t_B}(a,r)\right]. \tag{12}$$

$d_{t_A}(a,r)$ and $d_{t_B}(a,r)$ are the phases of the pixels (a, r) at time t_A and time t_B relative to the initial time t_0, respectively, and λ is the wavelength of the band.

(2) At time $= t_0$, $d_0 = 0$, the vector corresponding to the phase of the sequential SAR image is expressed as

$$\varphi^t = [\varphi_1, \cdots, \varphi_n]. \tag{13}$$

At the pixel (a, r), let IE be the master image and IS be the slave image, corresponding to all M interference pairs:

$$\begin{cases} \mathrm{IE} = [\mathrm{IE}_1, \cdots, \mathrm{IE}_M] \\ \mathrm{IS} = [\mathrm{IS}_1, \cdots, \mathrm{IS}_M] \end{cases}. \tag{14}$$

Then the phase of all differential interferograms is

$$\Delta\varphi_i(a,r) = \varphi\left(t_{IE_i}\right) - \varphi\left(t_{IS_i}\right), \tag{15}$$

where $t_{IE_i} > t_{IS_i}$, $i = 1, 2, \ldots, M$, can be expressed as

$$\Delta\varphi = G\varphi. \tag{16}$$

In formulas (3)–(16), G is a matrix of order $M \times N$, which represents a system of equations composed of N unknowns and M equations. It can be seen that, in the matrix, each row corresponds to a differential interference pair, and each column represents the corresponding SAR images from t_0 to t_N in turn.

When the interference pairs are located in the same small baseline set, the least square method is used to estimate the deformation value of the time series in the subset. When there are multiple subsets and the matrix is not rank matrix, the SVD method should be used to realize the joint solution of the subsets, so as to extract the cumulative deformation results on the time series.

2.3.2. Data Processing Flow. In the processing flow of SBAS-InSAR technology, the key to the realization of this technology is to construct a number of interference pair subsets reasonably. This process requires that the combined spatiotemporal baseline of each subset of internal interference pairs should be in the threshold range needed to form a high-quality interferogram. This technique can be simply understood as the interferometric measurement method of the surface deformation change process in the study area during the study period by solving the differential interference phase in the time series.

The flow of surface deformation detection using SBAS-InSAR method is shown in Figure 4. Its data processing flow includes data preprocessing, differential interference calculation, time and space deformation estimation, and so on.

3. Monitoring, Prediction, and Evaluation of Mountain Geological Disasters Based on Improved AHP-Information Quantity Method

In recent years, the frequent geological disasters in China not only cause serious economic losses to the society, but also seriously threaten people's lives and disturb the normal life of residents, which has aroused widespread concern from people from all walks of life [15]. Therefore, the identification of potential geological hazards and the study of their spatial and temporal distribution are of great significance in disaster prevention and control, and at the same time, it is also the premise of further quantitative analysis of geological hazards.

The information of mountain surface deformation detected by InSAR technology has high reliability and accuracy, which is the basis of early identification of potential geological disasters. Combined with GIS spatial analysis and visual interpretation, the hidden danger points of potential geological disasters can be extracted, and the deformation characteristics of mountain surface in time and space can be further analyzed [16].

At present, there are many statistical analysis models for geological disaster risk analysis. When the information quantity method of information theory is applied to the risk assessment of geological disasters, it has the characteristics of combining qualitative and quantitative analysis. According to the influence degree of different influencing factors on geological disasters, the risk of geological disasters can be effectively assessed. Analytic Hierarchy Process (AHP) is a fast method to determine weights, which can be used to assign weights to different evaluation factors in geological hazard risk assessment [17, 18]. In this paper, the weighted information model based on AHP is adopted, which not only considers the advantages of AHP that fully considers the subjective experience of experts, but also combines with the objective information in the information model [19, 20].

3.1. Information Quantity Method

3.1. Information Quantity Method. The information quantity method originated in the United States, and in China, it was first quoted by Professor Yan Tongzhen to predict the surface landslide and then gradually widely used in the geological disaster risk assessment in the geological disaster-prone areas in China. As far as the information quantity method itself is concerned, its central idea is to use the information quantity value to reflect the difficulty of geological disasters in the study area based on the information quantity contributed by various influencing factors to geological disasters [21]. This method is practical and simple and can be used to predict the development law of geological disasters. In general, the information quantity value is used as a quantitative index to quantitatively describe the risk of geological disasters with probability situation. The greater the information quantity value obtained, the more likely the geological disasters to occur, and vice versa.

3.1.1. Basic Theoretical Model. When applying the method of information quantity to realize the risk assessment of geological hazards, the information quantity provided by the actual geological disasters is used to express the action degree of each influencing factor with information quantity, which can reflect the contribution degree of these influencing factors to the development of surface geological disasters. For geological disaster event B, X_{ij} is the factor affecting its occurrence (where $i = 1, 2, \ldots, n$, I is the selected disaster influencing factor; $J = 1, 2, \ldots, M$, and J is the subinterval divided by each influencing factor); then the $I_{X_{ij}\longrightarrow B}$ expression of geological disaster information provided by a single influencing factor is as follows:

$$I_{X_{ij}\longrightarrow B} = \ln\frac{P\left(B/X_{ij}\right)}{P(B)}\ (j = 1, 2, \cdots, n). \tag{17}$$

Among them, $P(B/X_{ij})$ corresponds to the development probability of geological disaster class B in the J section within the disaster impact factor X_i; $P(B)$ represents the regional background value, that is, the probability of occurrence of ground disaster B under the regional background conditions; N represents the number of selected types of disaster impact factors; M represents the number of secondary impact factor segments divided by each disaster impact factor.

In the process of actual data processing, it is often impossible to directly obtain the data needed to calculate the information amount of geological disasters. Under normal circumstances, in order to facilitate subsequent calculation, the probability value represented by $P(B/X_{ij})$ is selected to be

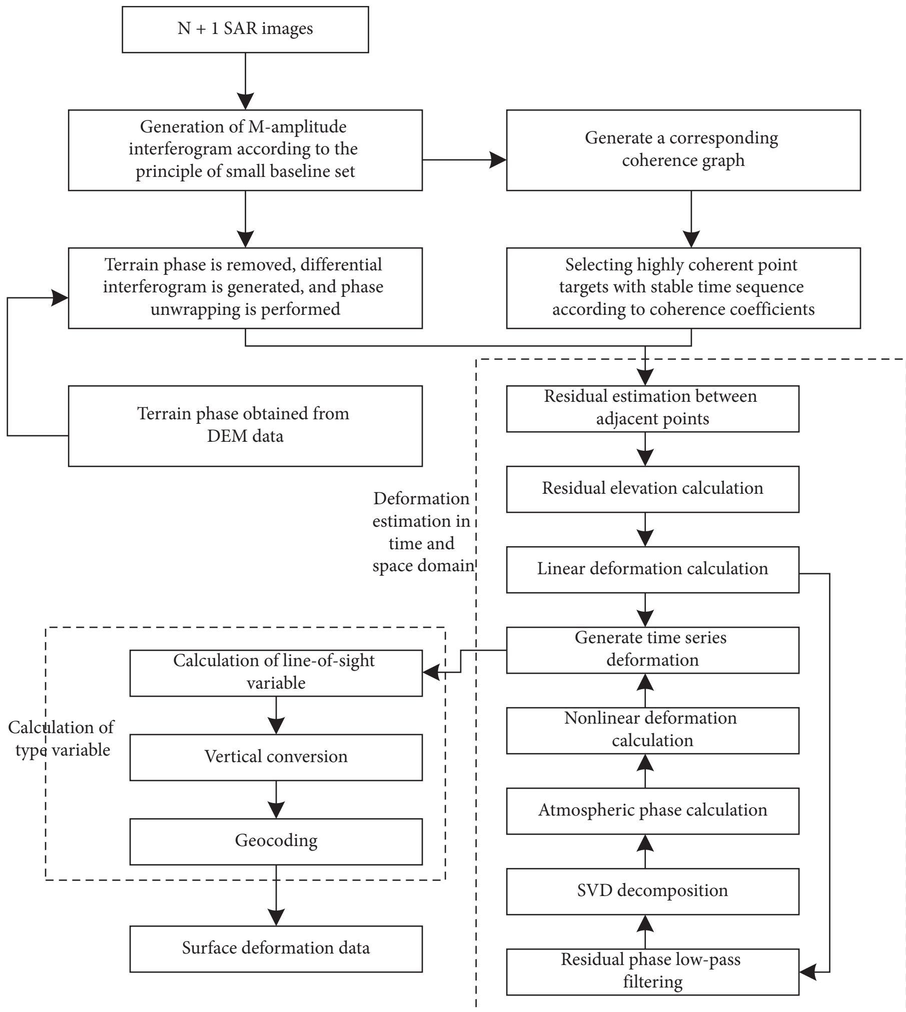

Figure 4: SBAS-InSAR data processing flow.

converted into the sample frequency value. The specific calculation formula is as follows:

$$I_{X_{ij}\longrightarrow B} = \ln \frac{N_{ij}/S_{ij}}{N/S}\ (j = 1, 2, \cdots, n). \tag{18}$$

Among them, the value $I_{X_{ij}\longrightarrow B}$ can represent the amount of information provided by the J section for the development of geological disaster class B within the disaster impact factor X_i; N_{ij} represents the area value or the number of development points of disaster B in the J section within the disaster impact factor X_i; N_{ij} represents the distribution area value of the J section in the study area in the disaster impact factor X_i; N represents the area value covered by all geological disasters or the number of all developed geological disasters in the whole study area; S represents the total area of the whole study area.

The actual process of geological hazard risk assessment in the study area is to divide the study area into several assessment units and finally need to calculate and obtain the comprehensive information value of each assessment unit. To sum up, the information value is affected by the combination of various influencing factors, and the comprehensive information value I of all evaluation units can be calculated by using the following formula:

$$I = \sum_{i=1}^{n} I_{X_{ij}\longrightarrow B}. \tag{19}$$

Using information quantity model to complete the study of regional disaster risk assessment in a specific study area can be understood as taking each evaluation unit as an independent research unit and taking each evaluation factor as the premise of risk assessment, calculating the total information quantity of each independent research unit, and comparing the calculated information quantity values. The specific information value obtained from the above operations can be used to indicate that when the independent evaluation unit to which the information belongs is affected by various geological disaster influencing factors, the probability of geological disasters is greater, indicating that the geographical area where the evaluation unit is located is more likely to break out geological disasters, and it is necessary to focus on monitoring and take timely prevention and control measures.

3.1.2. Weighted Information Volume Model. In order to enhance the accuracy of the evaluation results, this study takes the conventional information as the premise, supplemented by the corresponding weight value of each evaluation factor to complete the whole evaluation process. Generally speaking, the conventional process of information calculation is based on the effect degree of various influencing factors on the development of geological disasters in the evaluation unit layer. Conventional information quantity model can be understood as the idea that, in the process of calculating information quantity, the weight of all factors is given to 1, while weighted information quantity method can apply subjective experience of experts to the evaluation process according to objective facts, which has higher rationality and reliability.

The weight W_i of evaluation factors at all levels is obtained by the weight acquisition method, and the total value of weighted information I_w is

$$I_{\mathrm{w}} = \sum_{i=1}^{n} W_i I_{X_{ij} \longrightarrow B}, \tag{20}$$

where $I_{X_{ij} \longrightarrow B}$ is the information value of a single influencing factor.

When the weighted information model is used to evaluate the hazard of land disasters in the study area, the evaluation index is the total information value I_{w}.. When evaluating the risk of geological disasters in each geographical unit, the probability of occurrence increases with the increase of total information I_w.

Through the previous research on the methods of determining the weight I_w, we can see that the current mainstream methods include analytic hierarchy process, principal component analysis, and so on. In this study, the analytic hierarchy process (AHP) is used to obtain the weight of impact factors, and different weights are given according to the difference of the impact degree of each disaster factor, and the total information weight is obtained by weighting. Weighted information method will complement the advantages of analytic hierarchy process and information method and make the evaluation results more accurate.

3.2. Selection of Evaluation Factors in the Study Area. Through the analysis of the factors affecting the distribution of potential geological disasters and the research results of scholars at home and abroad, it can be seen that the development of geological disasters is affected by many factors. The selection of influencing factors needed in the study should fully consider the availability of data, the scope and environment of the study area, and the requirements of research accuracy. Therefore, in the process of geological hazard risk assessment in different study areas, the selected evaluation factors are usually different.

Combined with the actual geographical conditions of a certain area selected in this paper, the influencing factors of this study area are divided into natural environment factors, social environment factors, and disaster-inducing factors. Among them, the basic natural environment factors are divided into topographic factors (including slope, elevation, aspect, and topographic relief), geological factors (geological structure, stratum lithology), basic features (rivers), ecological factors referring to vegetation coverage, social and environmental factors referring to roads, and inducing factors including earthquakes and rainfall.

In this study, ASTER GDEM elevation data with resolution of 30 m is selected as reference DEM, and on the basis of this data, the slope, aspect, and fluctuation data of the study area are obtained.

Some impact factor data cannot be obtained directly and need to be obtained after certain data processing operations. The specific process of obtaining rainfall in the study area is as follows: the annual average rainfall data of the national meteorological stations in the area and its surrounding counties in recent 15 years are obtained by Kriging spatial interpolation method. In order to facilitate the calculation of the follow-up evaluation process, the operation of properly merging and adjusting rainfall level areas is made. Earthquake intensity data are obtained according to China Seismological Network.

The average annual rainfall in the study area is subdivided into 11 rainfall levels, and the lowest and highest rainfall levels are less than 550 mm and more than 640 mm, respectively. Earthquake intensity is divided into four grades, and the intensity grade decreases around the focal point.

Based on the detailed analysis of the basic data of the experimental area, the pixel dichotomy model is adopted as the acquisition method of vegetation coverage data in this study. That is, the Landsat 8 digital products are processed by using the pixel dichotomy model based on the normalized vegetation index (NDVI), and the formula is as follows:

$$\begin{aligned} \mathrm{NDVI} &= fc \times \mathrm{NDVI}_{\mathrm{veg}} + (1 - fc)\mathrm{NDVI}_{\mathrm{soil}}, \\ fc &= \frac{\left(\mathrm{NDVI} - \mathrm{NDVI}_{\mathrm{soil}}\right)}{\left(\mathrm{NDVI}_{\mathrm{veg}} - \mathrm{NDVI}_{\mathrm{soil}}\right)}, \end{aligned} \tag{21}$$

where *fc* is vegetation coverage; $\mathrm{NDVI}_{\mathrm{soil}}$ is the normalized vegetation index value of bare soil without vegetation coverage area; $\mathrm{NDVI}_{\mathrm{veg}}$ is the normalized vegetation index value of the area completely covered by vegetation.

In the course of actual hazard assessment, the criteria of assessment factors are as follows: elevation is divided into six grades: <1500 m, 1500 m~2000 m, 2000 m~2500 m, 2500 m~3000 m, 3000 m~3500 m, and > 3500 m; the slope is divided into six grades: 0~10, 10~20, 20~30, 30~40, 40~50, and >50. The slope direction is divided into four directions: north and northeast, east and southeast, south and southwest, west and northwest. The buffer distance of fault zone is defined as 3 km, 6 km and 9 km, and the study is divided into

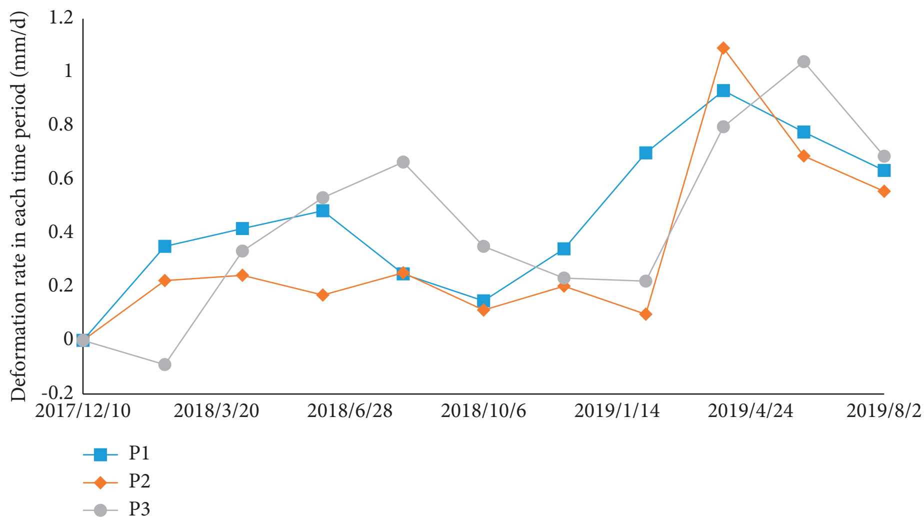

Figure 5: Deformation rate in each period.

five grades of fault zone influence areas. According to the earthquake intensity, the research is divided into four grades: V, VII, Vl, and IX. According to stratigraphic lithology, the study is divided into three areas. According to the average annual rainfall, the study area is divided into five grades: <560 mm, 560 mm~590 mm, 590 mm~620 mm, 620 mm–650 mm, and >650 mm. According to the buffer distance of 0.5 km, 1 km, and 1.5 km, the study area is divided into four grades. The study area is divided into six grades according to the buffer distance of 200 m, 600 m, 1000 m, 1400 m, and 1800m. The topographic relief degree is divided into six grades: ≤100 m, 100 m~200 m, 200 m–300 m, 300 m–400 m, 400 m~500 m, and >500 m. Vegetation coverage is divided into five grades according to <50%, 50%–60%, 60%–70%, 70%–80%, and >80%.

3.3. Determination of Weight of Evaluation Factor. In general, the weight calculation methods include geometric average method, arithmetic average method, and eigenvector method. In order to improve the reliability of the results, this paper abandons the single calculation method used in the conventional thinking and chooses three weight calculation methods instead and takes the average value of each method as the final weight.

The formula of geometric average method is

$$W_i = \frac{\left(\prod_{j=1}^{n} a_{ij}\right)^{1/n}}{\sum_{i=1}^{n}\left(\prod_{j=1}^{n} a_{ij}\right)^{1/n}}, i = 1, 2, \ldots, n. \tag{22}$$

The arithmetic average formula is

$$W_i = \frac{1}{n}\sum_{j=1}^{n}\frac{a_{ij}}{\sum_{k=1}^{n} a_{kj}}, j = 1, 2, \ldots, n. \tag{23}$$

The eigenvector method formula is

$$UW = \lambda_{\max} W, \tag{24}$$

where a_{ij} is the element of the judgment matrix, n is the number of columns of the judgment matrix, and u is the judgment matrix. Average the three calculation results, and get the final weight value of each evaluation factor.

4. Experiment

4.1. Evaluation Process

4.1.1. Analysis of Spatial and Temporal Pattern Distribution Characteristics of Potential Mountain Geological Disaster Points. The deformation information of the three feature points in the time series is counted, and the deformation rate in each period is as shown in Figure 5, and the accumulated deformation is as shown in Figure 6.

4.1.2. Information Quantity Method. In this study, the potential geological hazard points extracted by SBAS-InSAR technology are used as the basic research data for monitoring, forecasting, evaluation, and analysis of mountain geological hazards, and then the information amount is calculated. In this process, the grid unit of 30 m × 30 m is used as the evaluation unit. The information value reflected by the types of secondary influencing factors divided from each evaluation index can be obtained. In practical application, the amount of information is the reference index of the effect degree of each secondary influencing factor on the development of geological disasters in the study area.

See Table 1 for the distribution of each evaluation index and its specific information value in the study area.

According to the meaning of information model, the greater the information value, the easier it is to have geological disasters. When the information value of the secondary influencing factors in the table is greater than 0, it shows that the probability of developing geological disasters under the influence of this factor is above the overall development level of mountain disasters affected by this factor in the study area. By the same token, when the information

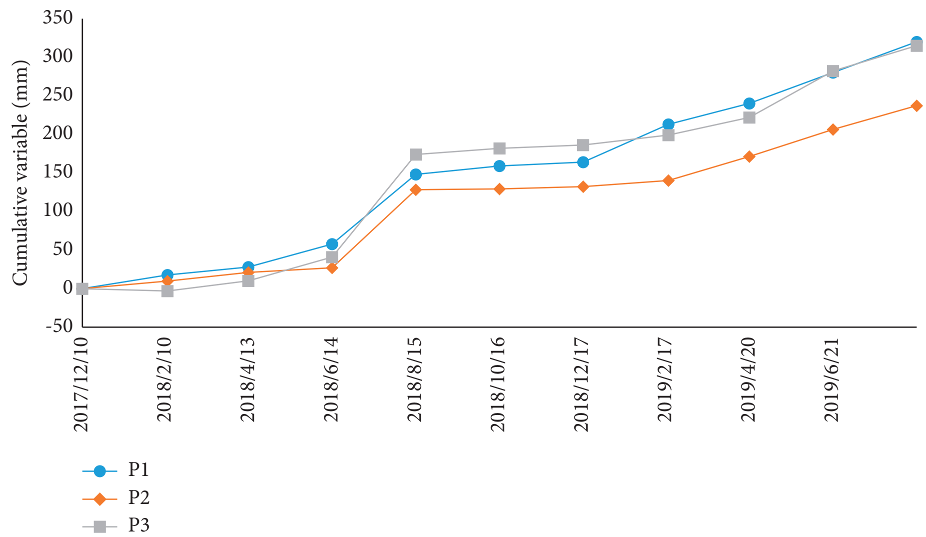

Figure 6: Cumulative deformation.

Table 1: Evaluation factor information scale.

Primary impact factor	Secondary impact factor	Information quantity value (I)	Primary impact factor	Secondary impact factor	Information quantity value (I)
Elevation (unit: m)	<1500	1.527912	Earthquake intensity	VI	−1.018517
	1500–2000	1.878802		VII	−0.305413
	2000–2500	1.217833		VIII	0.371931
	2500–3000	0.069574		IX	2.395062
	3000–3500	−1.16868	Average annual rainfall (unit: mm)	<560	−0.647191
	>3500	−3.18195		560–590	−0.162065
Slope (unit: °)	0–10	−0.19465		590–620	0.1848005
	10–20	−0.60147		620–650	−0.363789
	20–30	0.160048		>650	−0.604173
	30–40	0.060803	Rivers (distance from rivers in km)	<0.5	1.1197684
	40–50	−0.13246		0.5–1	−0.020673
	>50	−0.76925		1–1.5	−1.642546
Aspect of slope	North, northeast	−0.57554		>1.5	−1.944394
	East, southeast	0.34215	Road (distance from road, unit: m)	<200	1.9516436
	South, southwest	0.292185		200–600	1.2565791
	West, northwest	−0.37974		600–1000	0.8739286
Geological structure (distance from fault, unit: km)	<3	0.577263		1000–1400	−0.224026
	3–6	0.176452		1400–1800	−0.668493
	6–9	0.025197		>1800	−1.106742
	>9	−0.68012	Topographic relief (unit: m)	0–100	0.553517
Vegetation coverage	<50%	−0.1233		100–200	0.230892
	50%–60%	0.006014		200–300	−0.339274
	60%–70%	0.392581		300–400	−0.134666
	70%–80%	0.964443		400–500	0.33332
	>80%	0.420331		>500	−2.133569
Stratigraphic lithology	T	−0.04822			
	DCWZE	0.268584			
	CPQ	0.004012			

amount of the secondary influencing factors in the table is less than 0, it means that, in the area where the secondary influencing factors are distributed, the ease of developing geological disasters under the influence of this factor is below the overall development level of mountain disasters affected by this factor in the study area.

4.1.3. Improved Analytic Hierarchy Process. Using the analytic hierarchy process to calculate the weights of evaluation factors, the hierarchical structure model is constructed, as shown in Figure 7. Eleven evaluation factors, including stratum lithology (C1), slope (C2), river (C3), topographic relief (C4), vegetation coverage (C5), average annual rainfall

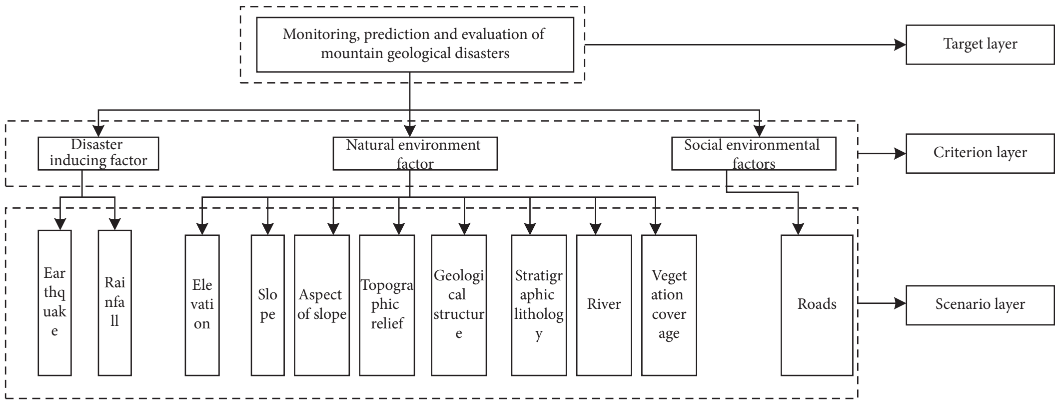

Figure 7: Hierarchical model.

Table 2: Judgment matrix.

	C1	C2	C3	C4	C5	C6	C7	C8	C9	C10	C11
C1	1	2	3	3	4	5	6	7	8	9	9
C2	1/2	1	2	3	4	4	5	7	7	8	9
C3	1/3	1/2	1	2	3	4	5	6	7	7	8
C4	1/3	1/3	1/2	1	2	3	4	5	6	7	7
C5	1/4	1/4	1/3	1/2	1	2	3	5	5	6	6
C6	1/5	1/4	1/4	1/3	1/2	1	2	4	5	6	6
C7	1/6	1/5	1/5	1/4	1/3	1/2	1	3	3	5	5
C8	1/7	1/7	1/6	1/5	1/5	1/4	1/3	1	2	4	3
C9	1/8	1/7	1/7	1/6	1/5	1/5	1/3	1/2	1	2	3
C10	1/9	1/8	1/7	1/7	1/6	1/6	1/5	1/3	1/2	1	2
c11	1/9	1/9	1/8	1/7	1/6	1/6	1/5	1/3	1/3	1/2	1

(C6), geological structure (C7), elevation (C8), earthquake intensity (C9), road (C10), and slope aspect (C11), are selected, and the ranking of factors represents the importance to the formation of geological disasters. The judgment matrix constructed by using the above evaluation factors is shown in Table 2.

The weights of each evaluation factor calculated by geometric average method, arithmetic average method, and eigenvector method are represented by $W1$, $W2$, and $W3$, respectively, and the average value W is calculated as the final weight, as shown in Table 3.

4.2. Verification of Evaluation Results. By getting the information quantity of each evaluation factor, the weight of each evaluation factor is obtained, and the total information quantity of each evaluation unit is obtained when the improved AHP-information quantity method is adopted.

According to the calculation results, the lowest total information value of risk assessment in this area is -1.03541, and the highest is 0.6739. According to the total information value of each evaluation unit obtained in the study area, the natural breakpoint method is used to classify it. The region is divided into four regions, and the information value ranges are low-risk area [−1.03541, −0.5475], medium-risk area (−0.5475, −0.2482], high-risk area (0.2482, 0.0874), and extremely high-risk area (0.0874, 0.6739).

ROC (Receiver Operating Characteristic) curve is a common method widely used to test the accuracy of geological hazard zoning assessment in recent years. In the ROC curve, the vertical axis represents the true positive rate, and in the geological hazard risk assessment, the cumulative percentage of the area from high to low in the study area is used as the ordinate. The horizontal axis represents the false positive rate, i.e., 1−specificity, and the cumulative percentage of the number of real historical geological disasters corresponding to each risk level in the study area is used as the abscissa in the geological disaster risk assessment. By calculating the AUC (Area under Curve) under the ROC curve, the evaluation accuracy of the geological hazard evaluation model is measured.

The value range of AUC is [0, 1], and the higher the value, the better the prediction effect of the model. Usually, we use AUC range (0.5, 0.7], (0.7, 0.8), (0.8, 0.9), (0.9, 1) to indicate low, fair, good, and excellent prediction accuracy, respectively. Figure 8 shows a ROC graph, in which gray lines represent the dividing line with AUC value of 0.5. The AUC values of the improved AHP-information method before and after calculation are 0.812 and 0.854, respectively, and their values are between (0.8, 0.9), indicating that the two models have good effects on the risk assessment and classification of geological disasters. The improved AHP-information model improves the prediction credibility, and the evaluation results can reflect the difficulty of mountain geological disasters in the study area.

Table 3: Weight calculation.

Evaluation factor	W_1	W_2	W_3	W
Stratigraphic lithology	0.2531	0.2512	0.2555	0.2532
Slope	0.2024	0.1962	0.2021	0.2003
River	0.1556	0.1512	0.1553	0.1545
Topographic relief	0.1165	0.1144	0.1145	0.1158
Vegetation coverage	0.0846	0.0855	0.0832	0.0849
Average annual rainfall	0.0643	0.06853	0.0643	0.065
Geological structure	0.0452	0.0492	0.0458	0.0463
Elevation	0.023	0.0291	0.026	0.0277
Earthquake intensity	0.0213	0.0231	0.0210	0.0224
Roads	0.0158	0.0176	0.0158	0.0163

According to the average random consistency index table, RI is 1.52, CI is 0.0842, and CR is 0.05539 < 0.1, passing the consistency test.

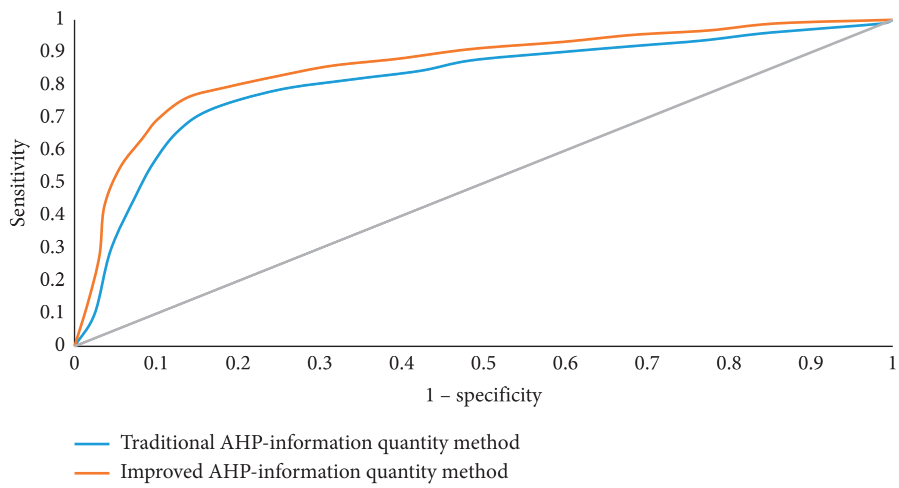

Figure 8: ROC curve.

5. Conclusion

In this paper, the evaluation factors are obtained according to the existing research results and the actual situation. Then, the traditional analytic hierarchy process using a single method to calculate the weights is improved, the geometric average method, arithmetic average method, and eigenvector method are selected to obtain the weights, and the average value is determined as the final weight. In this paper, the improved AHP-information method is used to classify the risk of mountain geological disasters in the study area. Finally, the evaluation results are verified, which proves that the improved AHP-information method is reliable, and its mountain geological disaster monitoring and prediction evaluation effect is better than the traditional AHP-information method. There is no in-depth research on target recognition accuracy, so it is necessary to combine multi-sensor data with SAR data such as images for comprehensive analysis, which can improve the monitoring effect and application value of mountain geological disasters.

Data Availability

The experimental data used to support the findings of this study are available from the corresponding author upon request.

Conflicts of Interest

The authors declare that they have no conflicts of interest regarding this work.

References

[1] M. Rao and S. A. Gillani, "Active surface deformation from DEM based surface dynamics in upstream of mangla reservoir and eastern potwar plateau," *International Journal of Innovations in Science & Technology*, vol. 2, no. 2, pp. 51–60, 2020.

[2] J. W. Goodge, "Geological and tectonic evolution of the Transantarctic Mountains, from ancient craton to recent enigma," *Gondwana Research*, vol. 80, pp. 50–122, 2020.

[3] C. Xiong, F. Ji, C. Zhou, and Y. Pan, "Investigation and motion characteristics analysis of dangerous rock in high and steep slope based on UAV," *IOP Conference Series: Earth and Environmental Science*, vol. 569, Article ID 012002, 2020.

[4] M. Yu and J. Chao, "Remote sensing investigation of geological hazards in xingguo county, jiangxi province," *E3S Web of Conferences*, vol. 131, no. 5, Article ID 01056, 2019.

[5] Z. Hu, B. Li, Y. Liu, and X. Niu, "Research on quality improvement method of deformation monitoring data based on InSAR," *Journal of Visual Communication and Image Representation*, vol. 64, Article ID 102652, 2019.

[6] Y. Yang, Y. Sun, S. Wu et al., “Surface deformation monitoring of a section of gongyu expressway based on SBAS-InSAR technology,” *E3S Web of Conferences*, vol. 233, no. 4, Article ID 01149, 2021.
[7] A. M. Ruiz-Armenteros, M. Marchamalo-Sacrsitán, M. Bakoň et al., “Monitoring of an embankment dam in southern Spain based on Sentinel-1 Time-series InSAR,” *Procedia Computer Science*, vol. 181, no. 3, pp. 353–359, 2021.
[8] L. Teixeira, M. R. Oswald, M. Pollefeys, and M. Chli, “Aerial single-view depth completion with image-guided uncertainty estimation,” *IEEE Robotics and Automation Letters*, vol. 5, no. 2, pp. 1055–1062, 2020.
[9] Y.-s. Tang, Z.-z. Yin, L.-g. Zhang, Q.-j. Guo, J.-z. Cao, and J.-j. Tong, “The application of the DEM-based burnup construction method in the pebble burnup history analysis in HTR-10,” *Nuclear Engineering and Design*, vol. 349, no. AUG, pp. 1–7, 2019.
[10] R. Zhang, C. Meng, C. Wang, and Q. Wang, “Compressed sensing reconstruction of radar echo signal based on fractional fourier transform and improved fast iterative shrinkage-thresholding algorithm,” *Wireless Communications and Mobile Computing*, vol. 2021, no. 2, pp. 1–15, 2021.
[11] R. Zhang, Z. Tang, D. Luo, H. Luo, S. You, and T. Zhang, “Combined multi-time series SAR imagery and InSAR technology for rice identification in cloudy regions,” *Applied Sciences*, vol. 11, no. 15, p. 6923, 2021.
[12] D. Bekaert, A. L. Handwerger, P. Agram, and D. B. Kirschbaum, “InSAR-based detection method for mapping and monitoring slow-moving landslides in remote regions with steep and mountainous terrain: an application to Nepal,” *Remote Sensing of Environment*, vol. 249, no. 1, Article ID 111983, 2020.
[13] J. Widodo, Y. Izumi, A. Takahashi, H. Kausarian, D. Perissin, and J. T. Sri Sumantyo, “Detection of peat fire risk area based on impedance model and DInSAR approaches using ALOS-2 PALSAR-2 data,” *IEEE Access*, vol. 7, pp. 22395–22407, 2019.
[14] G. Wang, Y. Wang, X. Zang, J. Zhu, and W. Wu, “Locating and monitoring of landslides based on small baseline subset interferometric synthetic aperture radar,” *Journal of Applied Remote Sensing*, vol. 13, no. 4, p. 1, 2019.
[15] K. Konagai, “More than just technology for landslide disaster mitigation: signatories to the Kyoto Landslide Commitment 2020—No. 3,” *Landslides*, vol. 18, no. 1, pp. 1951–1957, 2021.
[16] I. Abdulrahman and G. Radman, “Power system spatial analysis and visualization using geographic information system (GIS),” *Spatial Information Research*, vol. 28, no. 4, pp. 101–112, 2019.
[17] U. Goel, K. P. Gupta, and R. Manrai, “Analyzing the factors that affect the adoption of payments banks services in India: an Analytic Hierarchy Process (AHP) approach,” *International Journal of Business Information Systems*, vol. 1, no. 1, p. 1, 2020.
[18] F. Imron and M. Rum, “Modernization readiness analysis of Belitang irrigation system at region level using analytic hierarchy process (AHP) method,” *IOP Conference Series: Earth and Environmental Science*, vol. 644, no. 1, Article ID 012070, 2021.
[19] X. Ning, K. Gong, W. Li, L. Zhang, X. Bai, and S. Tian, “Feature refinement and filter network for person re-identification,” *IEEE Transactions on Circuits and Systems for Video Technology*, vol. 31, no. 9, pp. 3391–3402, 2021.
[20] S. Qi, X. Ning, G. Yang et al., “Review of multi-view 3D object recognition methods based on deep learning,” *Displays*, vol. 69, no. 1, Article ID 102053, 2021.
[21] Y. Jiang, J. Zou, X. Hu et al., “Study on optimal laminographic tilt angle: a method for analyzing quantity information gained in projections,” *IEEE Access*, vol. 8, pp. 38164–38173, 2020.

Hindawi
Scientific Programming
Volume 2022, Article ID 5336786, 18 pages
https://doi.org/10.1155/2022/5336786

Research Article

Design and Optimization of Children's Education Online Monitoring System Based on 5G and Internet of Things

Wu Lv [1] and Qiuju Zhong [2]

[1]School of Preschool Education, Jiangsu Second Normal University, Nanjing 210013, China
[2]School of Education Science, Nanjing Normal University, Nanjing 210024, China

Correspondence should be addressed to Wu Lv; lvwu@mail.bnu.edu.cn

Received 19 September 2021; Revised 4 November 2021; Accepted 6 November 2021; Published 17 January 2022

Academic Editor: Le Sun

At present, the problem of children's education informationization is becoming more and more prominent. With the strengthening of national education, children's online education has become one of the main forms. In order to educate children online, this paper proposes an online education system based on 5G technology and Internet of Things technology, which mainly solves the problems existing in current education. The results show the following: (1) UI test results basically meet the requirements of users; for the pursuit of personalized users, further development and improvement are needed. (2) Compared with children's module, the response time of manager module increased by 12%, and all the response times did not exceed 10s, so the user experience was very good. The access success rate of children's module is 99%, and that of managers' module is 98%. It is necessary to further study what factors interfere with the success rate, which leads to the failure of 100% success. (3) After optimization, the total energy consumption is the lowest compared with NOMA and TDMA, which is the best energy efficiency optimization method to solve the communication of Internet of Things. The simulation of the system is in good condition, and the follow-up research work of developers will take this system as the core to improve more details, hoping to put it into market operation formally.

1. Introduction

Children's education has always been the focus of education departments and industries. China's online education industry has experienced more than 20 years of development, which is closely related to modern information technology. However, the online education content for children's education is uneven, which brings about many worries and worries school parents. Relevant state departments and parents need a high-quality online monitoring system to monitor. As we all know, children's education is a key topic that even the whole world pays attention to. It is a very effective way to improve the national quality to carry out high-quality education for children in a country. Young children's brains are not fully developed when they are growing up. At this time, if the relevant state departments and parents do not give good guidance, coupled with the impact of the online world, they will miss the best time to educate children. Compared with younger children, older children are easily affected by electronic devices. At this time, if there is no effective system to monitor, educate, and standardize children's behavior online, children will probably be exposed to bad information in advance or accept negative influences from society. These two situations will be disastrous and devastating to children's development and growth. Therefore, this paper carries out the research on online monitoring of children's education in order to get an excellent system that can guarantee children's safety and education quality and help schools and families reduce their burdens. The literature [1] survey considers the Internet to be a tool to support schools and provide children with opportunities for informal learning, literacy, communication, and participation. Literature [2] uses Internet to educate teenagers about osteoporosis. Literature [3] identifies a series of potential daily concepts to educate children on network security in the early stage of Internet. Literature [4] develops a game system connected to the Internet of Things platform to record children's game activities for fine stimulation of children aged five to six years. Literature [5] developed and tested an early counseling system for children with developmental disorders by using the Internet. Literature [6] shows how children between the ages of nine and twelve years use different models to describe the Internet and talk about reliability. Literature [7] implements the practice and management system of "children's science education" by using remote Internet video conference. Literature [8] systematizes children's ecological and art education under the background of national cultural tradition through teaching modeling method and establishes a consistent theoretical basis. Literature [9] discusses children's education in a safe guardianship environment, hoping to achieve a global understanding of effective policies and practices. Literature [10] discusses exploring ways to promote the integrated development of children's technical thinking and humanistic thinking, virtual thinking and realistic thinking, and divergent thinking and convergent thinking in the era of "Internet plus." Literature [11] carries out systematic robot education for children through cooperative and robot-based learning. Literature [12] studies the QoE-aware resource allocation mode provided by 5G tactile industrial Internet of Things, which is applied to medical care, manufacturing, mining, education, automatic driving, and other fields. Literature [13] investigates various optimization methods to solve the resource problems of 5G and Internet of Things from the technical level. Literature [14] proposes key technologies for applying MEC to 5G and Internet of Things, such as cloud computing, network function virtualization, information-centric network, intelligent devices, network slicing, and computing offload. Literature [15] studies the Internet of Things intelligence and 5G network to establish sports and health big data system to solve some open problems. Better promoting the digital and intelligent transformation of education industry can better promote the rapid development of online education, meet the increasing needs of people, and help schools and families reduce their burdens. Establishing a system can be conveniently used by parents, teachers, and children. Through the division of labor and cooperation between the manager module and the children module, the educational content suitable for children can be screened and avoided from the source, and the physical condition, positioning, and social interaction of children can also be supervised, which is convenient for parents and teachers to find children's problems as soon as possible and sort out and guide them in time. In order to build a modern online monitoring system suitable for children's education, according to the capital cost and various needs of children's education, we choose to link the Internet of Things with distributed systems and use Java as a programming language to realize a distributed architecture system based on 5G Internet of Things communication.

2. Theoretical Basis

2.1. 5G Technology. In recent years, new high-quality technologies have emerged continuously, rising in many computer network fields, which not only changes people but also facilitates people's lives and habits. Mobile communication technology has been developing from 1G, 2G, 3G, and 4G. After years of development, it has continuously broken through the technical constraints and now successfully developed into the fifth-generation mobile communication technology. We usually simplify this name to 5G technology [16], which all comes from a simple formula [17].

$$c_{(\text{speed})} = \lambda_{(\text{wavelength})} \nu_{(\text{frequency})}. \tag{1}$$

Conduct 5G 28 GHz frequency band test according to international standards [18]:

$$\begin{aligned} \text{wavelength} &= \frac{\text{speed}}{\text{frequency}} \\ &= \frac{300,000,000\,\text{m/s}}{28,000,000,000\,\text{Hz}} \approx 10.7\,\text{mm}\,(\text{millimeter}). \end{aligned} \tag{2}$$

The method of communication technology to disseminate information and data [19] is shown in Figure 1.

It has powerful functions of more efficiency and convenience and lower delay than 4G, and it is also a powerful network infrastructure guarantee for us to realize the new era of interconnection among people, things, and machines (Internet of Everything). The coverage area comparison is shown in Figure 2.

5G technology will help researchers provide key technical knowledge in the fields of industry, education, medical care, unmanned driving, energy, and so forth, so that there can be newer technological breakthroughs in these fields, as shown in Figures 3 and 4.

2.2. Internet of Things Technology. Internet of Things (IoT) [20] is a new technology in the 21st century which can realize the Internet of Everything. It is an effective crossing and integration of virtual world and real world, and its development trend in China is good. With the development of time, it has gradually become an important symbol for China to enter the information age in an all-round way. Internet of Things (IoT) relies on sensors and other devices to collect information and then realizes the function of information exchange with the help of network (this paper chooses to use more efficient 5G network). The future ubiquitous network [21] is the embodiment of the Internet of Things at a higher level. Here, it is briefly mentioned that it is the prospect of the future direction of the Internet of Things. As shown in Table 1, it is the development standard table of Internet of Things technology [22].

Here, we explain the system framework of the Internet of Things as shown in Figure 5.

The Internet of Things architecture is divided into three layers: application layer, network layer, and

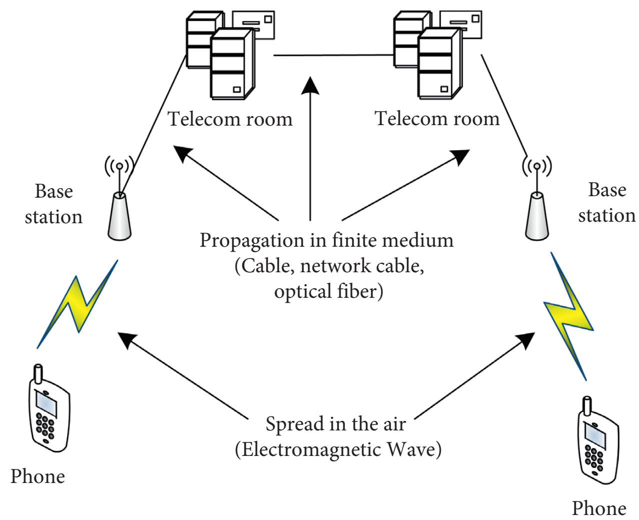

Figure 1: Communication technology propagation diagram.

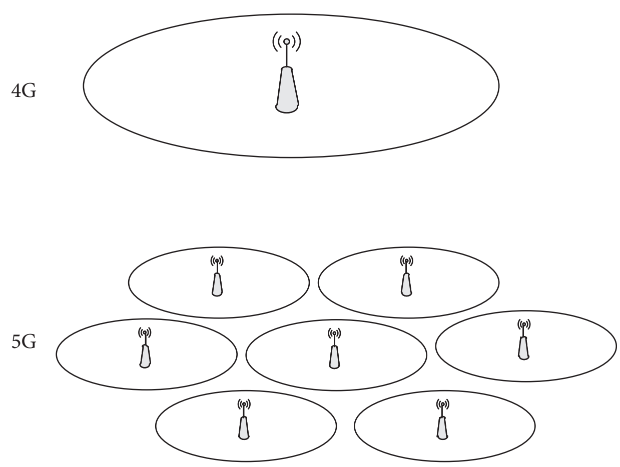

Figure 2: Comparison between 4G and 5G.

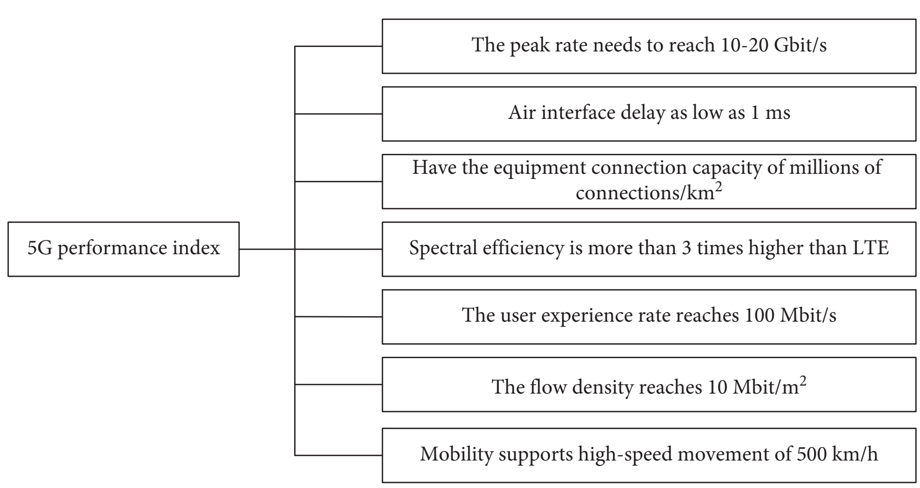

Figure 3: 5G performance indicators.

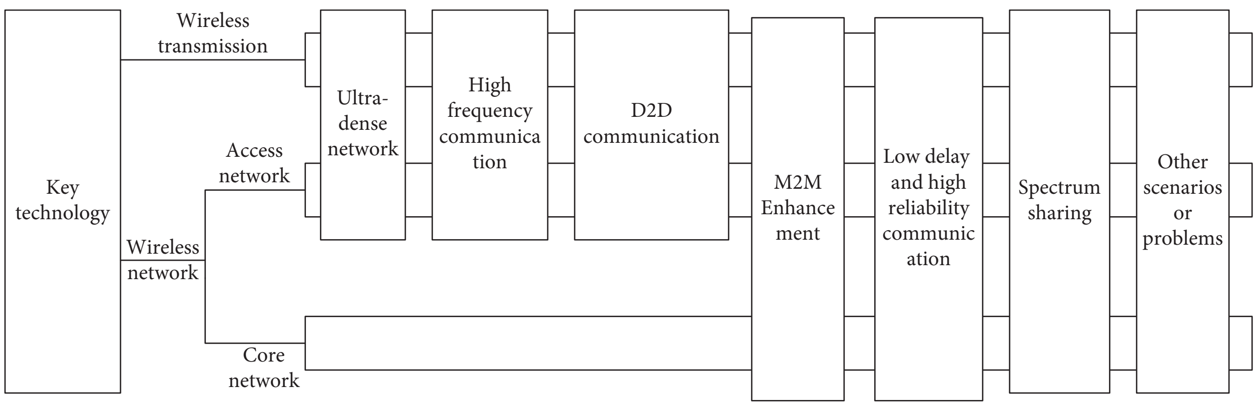

Figure 4: Overall framework of 5G key technologies.

Table 1: Standards and standards organizations.

Abbreviation	Full name	Standards being developed
Automatic identification laboratory	Automatic identification center	Networked Radio Frequency Identification and Emerging Sensing Technology
EPCglobal	Electronic product code technology	Standard using EPC (EPC coding) technology
FDA	US Food and Drug Administration	UDI (Unique Device Identification) system for different identifiers of medical devices
IEEE	Institute of Electrical and Electronics Engineers	Underlying communication technology standards, such as IEEE 802.15.4
IETF	Internet Engineering Working Group	Standards that include TCP/IP
OMA	Open Mobile Alliance	OMA DM and OMA LW2M for IoT device management, and GotAPI for IoT application security framework

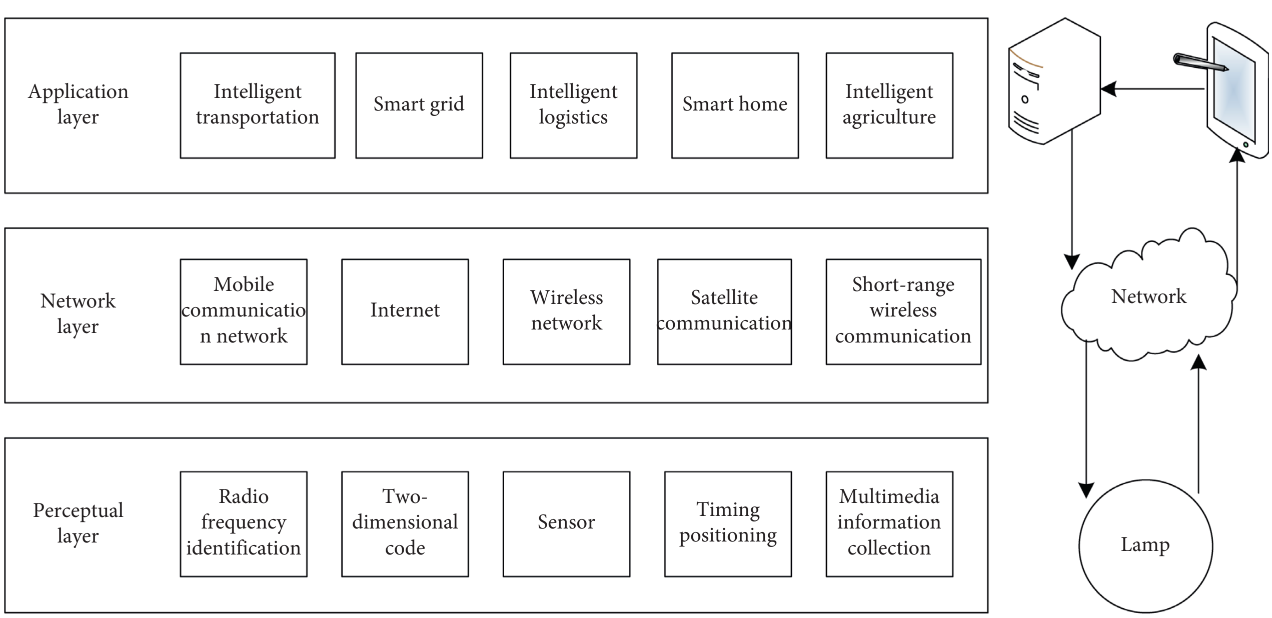

Figure 5: Schematic diagram of Internet of Things architecture.

perception layer. Perception layer is responsible for information collection and information transmission between objects. The network layer uses wireless and wired networks to encode, authenticate, and transmit the collected data. The mobile communication network is the infrastructure to realize the Internet of Things, forming a collaborative awareness network. The application layer provides specific applications and combines the Internet of Things technology with the needs of industry informationization.

2.3. Distributed Systems. In the early development of the system, there was a high demand for servers, the cost of software was very high, and it was very troublesome to expand and upgrade. Figure 6 shows a schematic diagram of the centralized system [23].

Therefore, due to the limitation of funds and core technologies, we choose a distributed system that simplifies the logical structure of the host and can be included in the scope of system use without highly configured computers. It is a multiprocessor computer system with independent hardware and unified software, which is easy to upgrade and expand, and its availability is often higher than that of centralized systems. Figure 7 shows a schematic diagram of the distributed system [24].

2.4. Children's Educational Concept. The ultimate goal of the concept of children's education is for children to grow up healthily and smoothly into the plastic talents of the country. Children are the flowers cultivated in the greenhouse of the motherland, and we should create a safe and reliable environment for children, which is isolated from all external dangers and suitable for seedlings to thrive. Here, children will be nourished by sunshine, rain, and fertilizer and can be well cultivated both materially and spiritually.

2.5. Research Methods. In this paper, we need to take some methods to collect and sort out the opinions and needs of schools, parents, and children, so as to understand what kind of effect our system should achieve, what functions it needs to have, and whether it can meet the real needs of schools, parents, and children. (1) Literature research method [25]: We selectively refer to many documents, not only Chinese documents but also foreign documents, and obtain materials from various academic websites such as China Academic Journal Network, Baidu Academic, and China Knowledge Network. After careful screening, these documents are the scientific theoretical basis of this study. (2) Questionnaire: We use questionnaires to distribute 1000 questionnaires to the relevant respondents (students, parents, and teachers) and collect 963 questionnaires. We use SPSS 19.0 to input and count the data (without showing). We can get the expectations and wishes of the respondents for the system from these questionnaires, and our design will be designed and improved based on their ideas. Only a system that meets the wishes of the demander is a qualified and good system.

3. Design and Optimization of the System

3.1. Design Objectives and Feasibility Analysis. The design goal of this study is to build a modern online monitoring system suitable for children's education. According to the capital cost and various needs of children's education, we choose to link the Internet of Things with distributed systems and use Java as a programming language to realize a distributed architecture system based on 5G Internet of Things communication.

(1) Economic feasibility. 5G and Internet of Things technologies are mature and are widely used in China. The related industrial chain is also relatively perfect, and the cost of application will not be too much. Because of its own characteristics, the distributed system has lower requirements for related computer configuration, which also saves a lot of money in disguise. So we say that this system is economically feasible.

(2) Technical feasibility. Internet technology is changing with the international trend, and its development is very mature, and it has been widely used in various fields. Therefore, this study is technically feasible and reliable.

(3) Feasibility of social environment. For schools and parents, it is the most difficult for a child with immature mind to judge his thinking. The complexity of society (especially on the Internet) is difficult for young children who have no independent thinking ability to cope with, and children are easily hurt. Therefore, for the social environment, it is necessary and feasible to design this system.

3.2. Architecture Design of the System. We choose Apache Mina technology for this system, and the system framework is shown in Figure 8.

Remote control uses ActiveMQ to transmit messages to instruction forwarding module, which is the consumer of messages. After receiving messages, it forwards them to the corresponding session and sends them to the equipment through this channel to realize bidirectional communication of data. Because the information security of a system is very important, especially in the education of children, the system needs to prevent the invasion of global criminals through malicious attacks, tampering, destruction, and so forth and strictly refuse any individual or computer that has not been accessed through formal channels. Figure 9 shows a schematic diagram about electronic security technology:

3.3. Functional Design of the System. The various functions of this system are carefully designed according to the results of the questionnaire, which are mainly divided into manager module and children module. The system covers children's humanistic education, safety education, thinking education, health education, and so on. Because of the particularity of this system, when visiting the system for the first time, the school or parents must log in, authenticate, and grant permission, and children can use the specific services of this system and will be guided and monitored by parents or teachers in the process of learning online.

3.3.1. Manager Module. The administrator module is mainly used by school teachers or parents, and the available functions are shown in Figure 10.

(1) The data information function is to give it to the system to determine whether it is qualified for

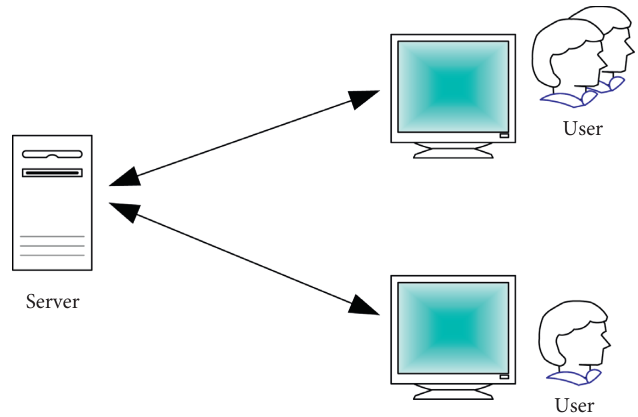

Figure 6: Centralized system.

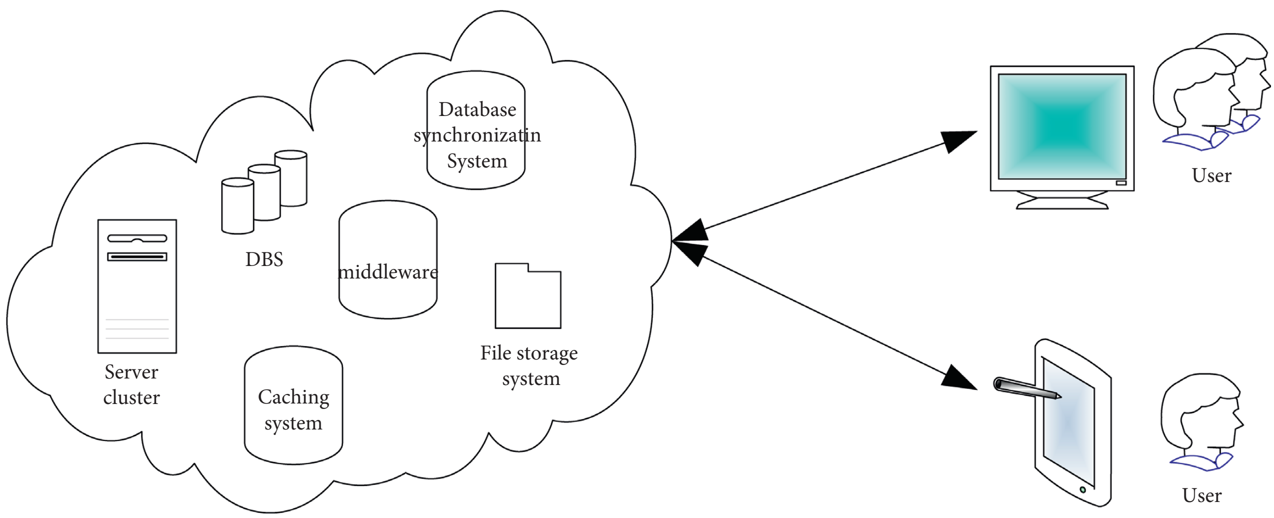

Figure 7: Distributed system.

identity authentication and register an account for children. The flow chart is shown in Figure 11.

(2) The child positioning system is to monitor the position of children and ensure that children are in a safe guardianship range. Figures 12 and 13 show an overall block diagram of positioning and a flow chart of positioning monitoring.

(3) The lock management function is set to prevent children from indulging in the online world and facilitate parents or teachers to manage. Children's equipment can be controlled by turning on or off this function directly in the system.

(4) The function of learning data status is to facilitate parents or teachers to monitor children's specific learning progress at any time, generate reports to parents or teachers at any time, *and adjust children's education programs at any time according to data results. The health*-related management function is to monitor children's health status at any time, generate reports to parents or teachers, and find and treat problems as soon as possible. The flow chart of obtaining the report is shown in Figure 14.

(5) Home/school equipment control is to facilitate parents or teachers to efficiently manage the equipment around children, as shown in Figure 15.

(6) The emergency function is to contact parents or teachers at any time if children are in any danger, and parents and teachers can make relevant treatment quickly.

(7) Feedback and opinions are to provide parents or teachers with reasonable feedback channels to help developers maintain, update, and optimize the system.

3.3.2. Children's Module. This module aims to help children receive various kinds of education, pay attention to the process of children's healthy development and happy growth, and give children a happy childhood experience. The specific functions are shown in Figure 16.

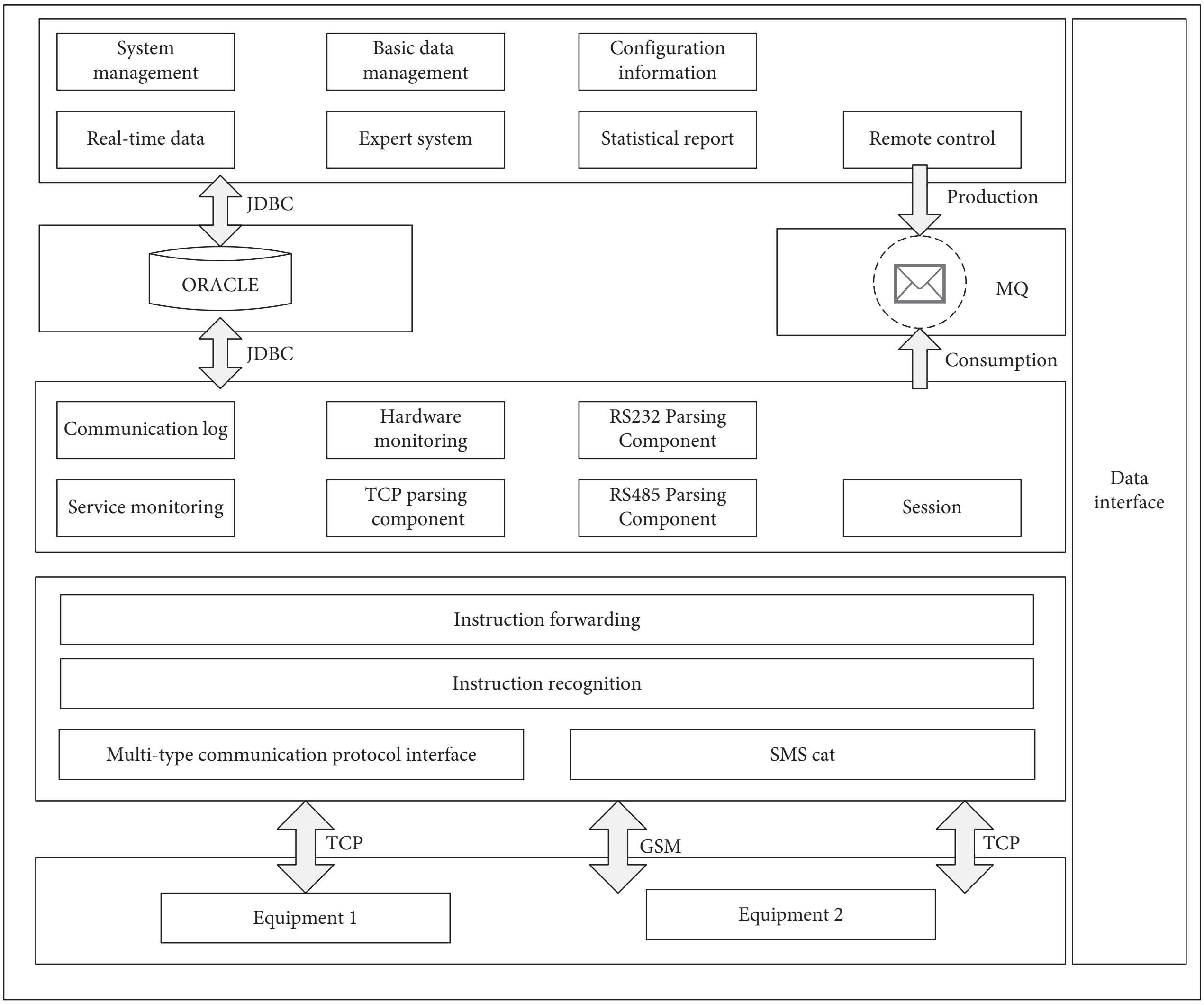

Figure 8: Distributed architecture of Internet of Things.

(1) Humanistic education is the education of basic simple subject knowledge. Art education is to cultivate children's hobbies, such as piano, painting, dance, and calligraphy. Traditional culture education is based on our national cultural characteristics, explaining our customs, etiquette, diet, and other contents. Traffic safety education is to popularize traffic signs, traffic rules, emergency calls, and so on. Network security education is to teach children how to surf the Internet safely and protect personal privacy. Health education is to teach children not to be picky eaters and learn to describe uncomfortable places, health knowledge, simple food nutrition and health, and so forth.

(2) Educational robot is an application layer device that can connect with children's system and share information. Children can use educational robots to learn directly, and robots will send relevant data back to children's systems, which is convenient for data recording.

(3) Puzzle games are designed for children, which are entertaining, so that children can learn useful knowledge imperceptibly while entertaining.

(4) Systems can be connected with each other, so that children of the same age can know each other and develop social skills.

(5) Child location monitoring is a passive function, and children cannot turn off this function directly. When the manager module makes positioning requirements, the system will automatically collect information and send it to the manager module.

(6) Physical condition data is a device worn by children, which is connected to the children's system to record the data.

(7) Emergency contact function is a function used by children in emergency or danger, which can immediately contact school teachers or parents and connect remote video calls.

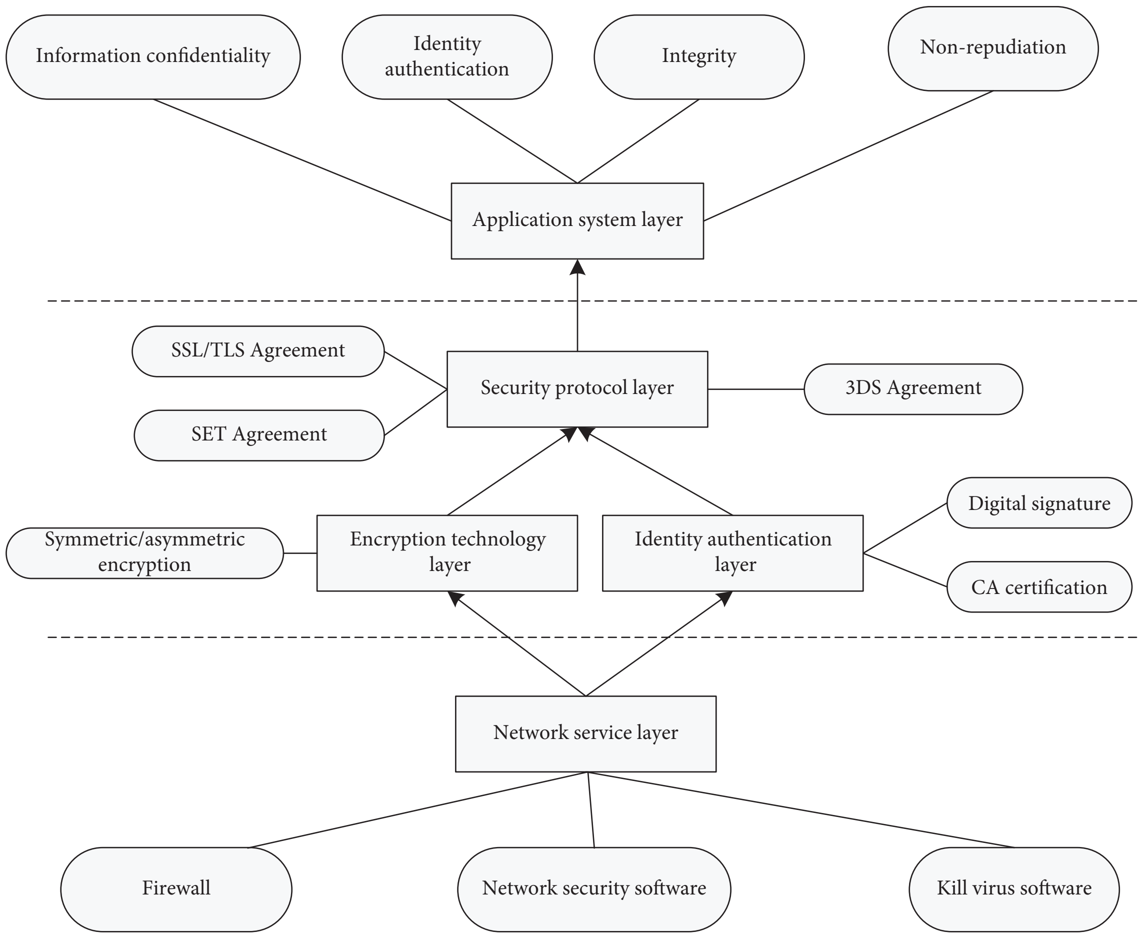

Figure 9: Electronic security technology.

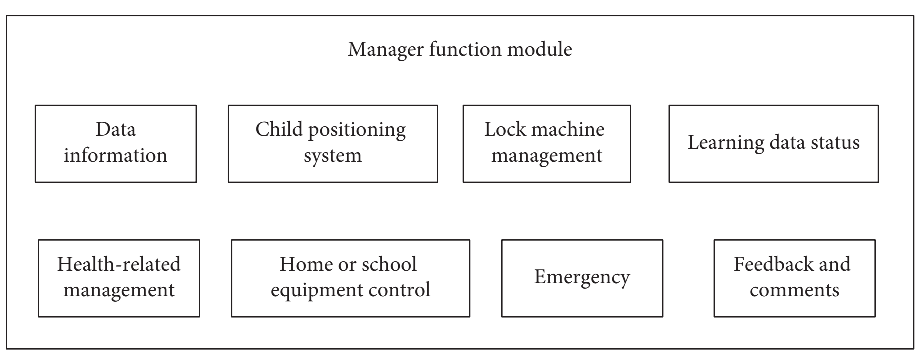

Figure 10: Introduction of manager module function.

3.4. Technical Optimization. When optimizing the system, we can use tools that can help locate system performance problems, but it should be noted that there are some system problems that cannot be detected by the tools, or we need to use other methods for optimization operations. The related tools are shown in Table 2.

3.4.1. Optimization of Code Quality. Efficient and excellent code usually has comments and code. The quality and logic of the code are very important, which can save developers unnecessary work and trouble. When doing some optimization work, we should carefully modify our code. In many cases, a little change can improve performance. Therefore, it is proposed that we should not optimize too early or over-optimize, for example, slow query caused by modifying SQL statements and frequent creation or replication of large objects.

3.4.2. Optimization of Internet of Things Communication. The optimization of energy efficiency is a very important issue. We will use a series of formulas for optimization.

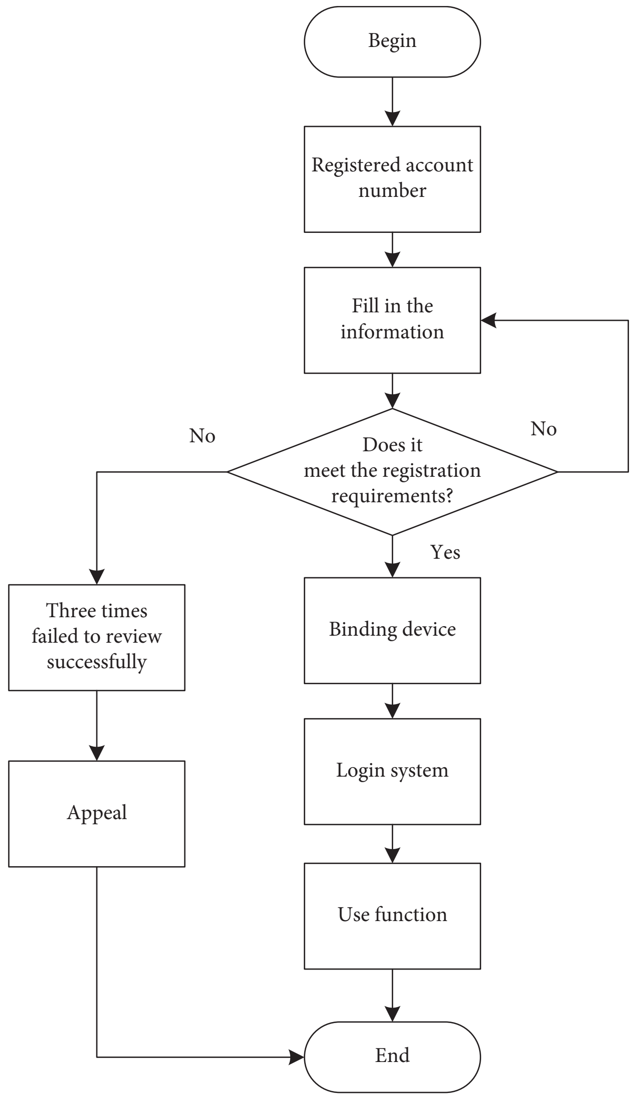

FIGURE 11: Flow chart of data information authentication.

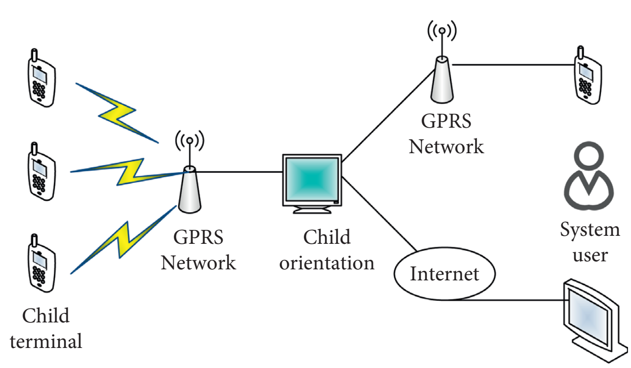

FIGURE 12: Child positioning system.

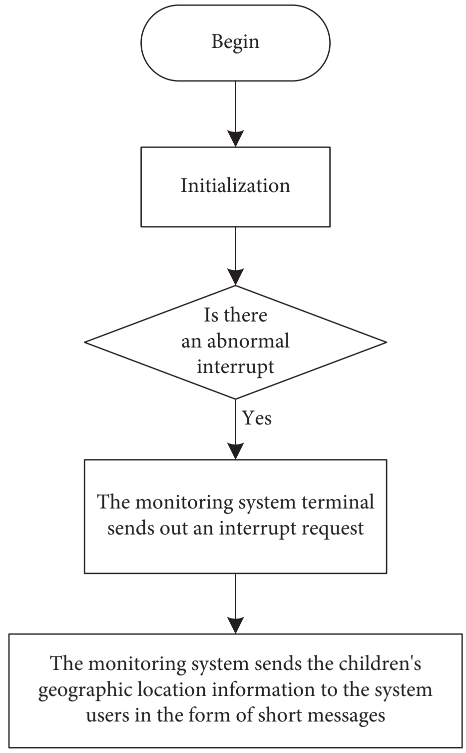

FIGURE 13: Flow chart of positioning monitoring.

(1) System model:

(1) The problem of SDN to UE:
The SDN is allocated to each UE, and the allocation factor A_{ij} is calculated.

$$A_{ij} = \frac{U_i}{d_{ij}}. \tag{3}$$

The transmission time meets the conditions:

$$\sum_{i=1}^{N} t_i \le T_i. \tag{4}$$

Received signal:

$$y_i = \sum_{j=J_{i-1}+1}^{J_i} h_{ij} \sqrt{p_j} s_j + n_i. \tag{5}$$

Achieve data throughput:

$$r_{ij} = Bt_i \log_2\left(1 + \frac{\left|h_{ij}\right|^2 p_j}{\sum_{l=j+1}^{J_i} \left|h_{ij}\right|^2 p_l + \sigma^2}\right). \tag{6}$$

Energy minimization problem from SDN_s to UEs:

$$\min_{p,t} \sum_{i=1}^{N} t_i \sum_{j=J_{i-1}+1}^{J_i} p_j. \tag{7}$$

(2) UE to base station problem:
Signal received by antenna:

$$y_l = \sum_{i=S_{l-1}+1}^{S_l} h_{li} \sqrt{q_i} m_i + n_i. \tag{8}$$

Achieve data throughput:

$$r_{il} = B_{SC} t_j \log_2\left(1 + \frac{\left|h_{li}\right|^2 q_i}{\sum_{k=i+1}^{S_l} q_k \left|h_{lk}\right|^2 + \sigma^2}\right). \tag{9}$$

UE_s to BS energy minimization problem:

$$\min_{Q,t} \sum_{j=N+1}^{N+L} t_j \sum_{i=S_{l-1}+1}^{S_i} q_i. \tag{10}$$

(2) Energy efficiency optimization:

(1) Optimization from SDN to UE:
Transmit power:

$$p_j = \frac{\sigma^2}{\left|h_{ij}\right|^2} \sum_{m=j}^{J_i} \prod_{k=m}^{J_i} \left(e^{(\ln 2) D_{j_i+j-k}/Bt_i - 1}\right). \tag{11}$$

Substituting formula (11) into (7) yields

$$\min_{t} \sum_{i=1}^{N} \sum_{j=J_{i-1}+1}^{J_i} \frac{\sigma^2 t_i}{\left|h_{ij}\right|^2} \sum_{m=j}^{J_i} \prod_{k=m}^{J_i} \left(e^{(\ln 2) D_{j_i+j-k}/Bt_i - 1}\right). \tag{12}$$

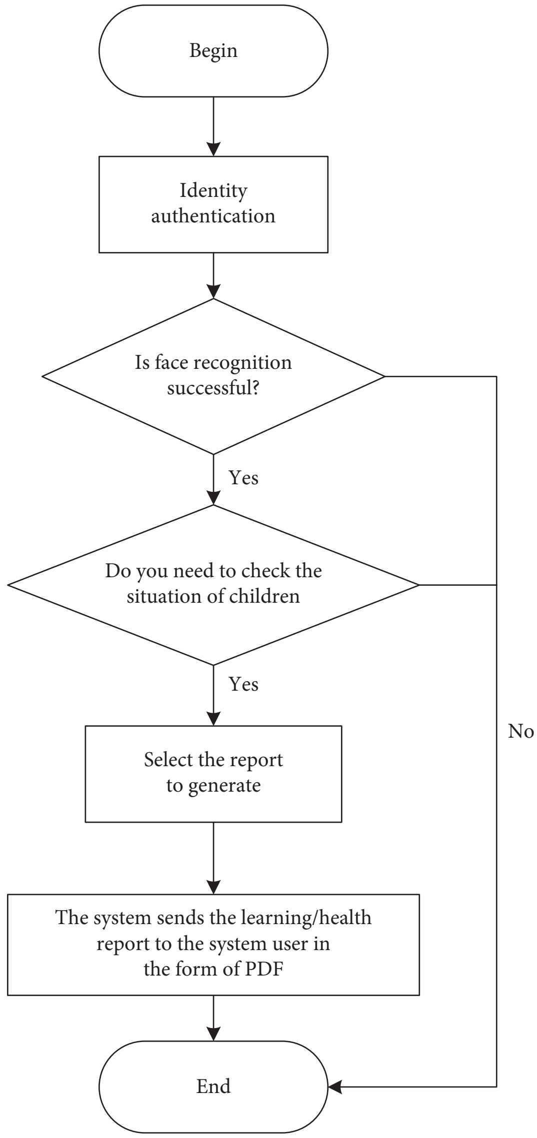

Figure 14: Learning and health report acquisition flow chart.

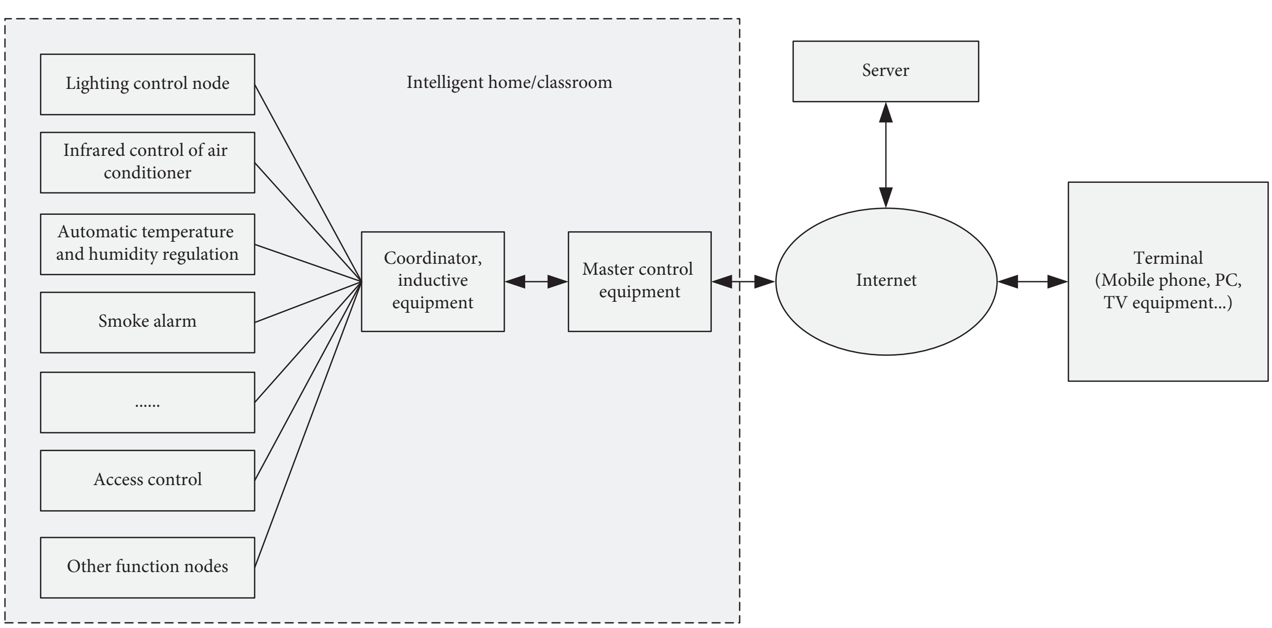

Figure 15: Equipment control structure diagram.

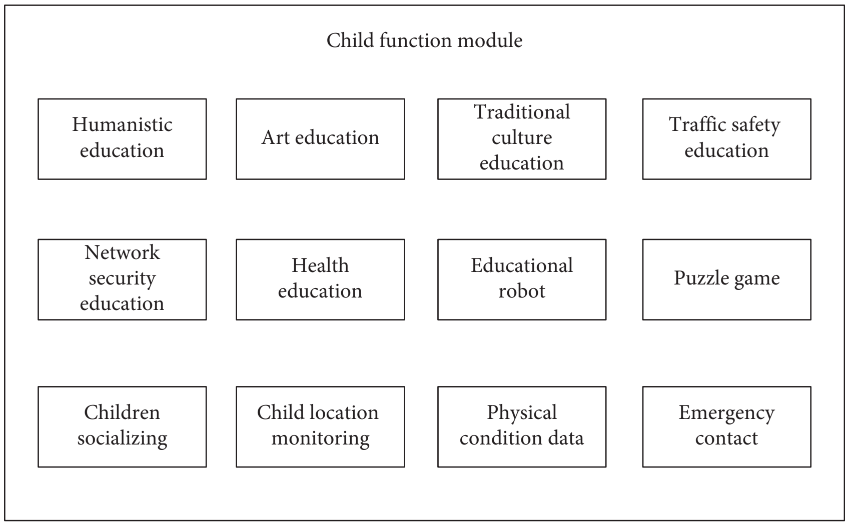

Figure 16: Introduction of children's module function.

Table 2: Tools for locating performance issues.

Type	Problem	Tools
Network	Network connection	Ping, netstat, traceroute, tcpdump
Disk	Read and write performance	IOTOP, IOSTAT
Memory	Memory leak	Valgrind, Purify
Memory	Memory swap	Free, top

Lagrange function:

$$L(t,\lambda) = \sum_{i=1}^{N} \sum_{j=J_{i-1}+1}^{J_i} \frac{\sigma^2 t_i}{\left|h_{ij}\right|^2} \sum_{m=j}^{J_i} \prod_{k=m}^{J_i} \left(e^{(\ln 2) D_{j_i+j-k}/Bt_i}\right) + \lambda\left(\sum_{i=1}^{N} t_i - T_1\right). \tag{13}$$

The optimal solution should satisfy

$$\frac{\partial L}{\partial t_i} = 0. \tag{14}$$

(2) Optimization from UE to BS:

$$\min_t \sum_{l=1}^{L} \sum_{i=S_{l-1}+1}^{S_l} \frac{\sigma^2 t_l}{\left|h_{li}\right|^2} \sum_{m=i}^{S_l} \prod_{k=m}^{S_l} \left(e^{(\ln 2) E_{S_l+i-k}/Bsct_l - 1}\right). \tag{15}$$

3.4.3. Distributed Optimization Algorithm

(1) Distributed problem description:

$$\begin{cases} \min f(x) = \sum_{i=1}^{n} f_i(x_i), \\ \text{s.t. } x_1 = x_2 = \cdots = x_n. \end{cases} \tag{16}$$

Single integrator system:

$$\dot{x}_i = u_i. \tag{17}$$

(2) DGD continuous time form:

$$\dot{x}_i = -Lx - \alpha \nabla f(x). \tag{18}$$

(3) EXTRA continuous time form:

$$\begin{aligned} \dot{x} &= -Lx - \alpha \nabla f(x) + y, \\ \dot{y} &= -Lx. \end{aligned} \tag{19}$$

(4) Classical primal-dual algorithm:

Distributed problem description:

$$\begin{cases} \min f(x) = \sum_{i=1}^{n} f_i(x_i), \\ \text{s.t. } D^T x = 0. \end{cases} \tag{20}$$

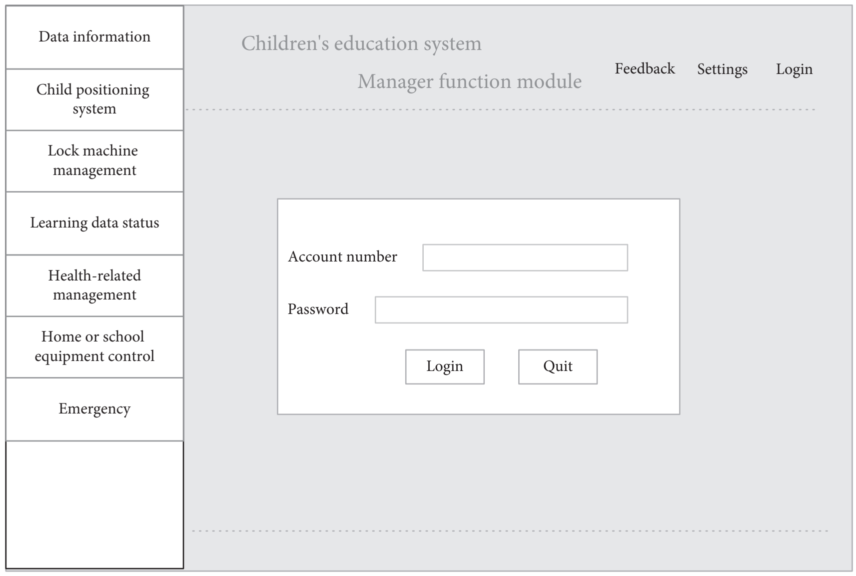

Figure 17: Manager module.

Constructing augmented Lagrange function:

$$L(x, y) = f(x) + \frac{1}{\alpha} y^T D^T x + \frac{1}{2\alpha} x^T L x. \tag{21}$$

Solve with primal-dual algorithm:

$$\begin{aligned} \dot{x} &= -Lx - \alpha \nabla f(x) - Dy, \\ \dot{y} &= D^T x. \end{aligned} \tag{22}$$

(5) DGT:

$$\begin{aligned} \dot{x} &= -Lx - \alpha y, \\ \dot{y} &= -Ly + \nabla^2 f(x) \dot{x}. \end{aligned} \tag{23}$$

(6) Global objective function:

$$\min_{x \in R^n} \sum_{i=1}^{N} f_i(x). \tag{24}$$

(7) Convex analysis: convex functions:

$$f(\theta x + (1-\theta) y) \le \theta f(x) + (1-\theta) f(y). \tag{25}$$

Strongly convex function:

$$(\nabla f(y) - \nabla f(x))^T (y - x) \ge \mu \|y - x\|^2. \tag{26}$$

Smooth function:

$$\|\nabla f(y) - \nabla f(x)\| \le L \|y - x\|. \tag{27}$$

4. Implementation and Test of the System

4.1. Development Platform and Environment. This system is mainly developed in Windows 10 operating system environment, using Java programming language, MYSQL database management, and Apache Mina technology to design the system framework. The development platform is Visual Studio 2018, the processor is AMD Athlon (TM) II P360 Dual-Core Processor 2.30 GHz, the running memory is 8G, and the simulation platform is MATLAB.

4.2. System Interactive Interface. The interface of children's education online monitoring system is shown in Figures 17 and 18, respectively.

4.3. System Simulation Test

4.3.1. UI Testing. First the basic function preparation test is carried out; if the system operation interface is reasonable, then the deeper function is tested; if the UI test does not meet the requirements, the system is directly redeveloped. After testing, there is no abnormality in the UI interface. We invited ten volunteers who are familiar with UI testing and made statistics on satisfaction recognition, as shown in Figure 19.

UI test results basically meet the requirements of users, but because everyone has personalized requirements, it is impossible to fully meet the requirements, and the UI interface needs to be improved in detail. It mainly depends on the tester's judgment feeling. UI test points are as follows: (1) the overall style of the page is unified, the layout is coordinated, the header and footer contents are complete and consistent, and the page framework is clear; 2) the fonts of the page are unified and coordinated, displayed normally, and have good effect; 3) the display of the page navigation bar and the content distribution spacing are reasonable; 4) the page organizes and designs the line thickness; 5) the page picture size, position, resolution, and horizontal and vertical directions are not stretched; and 6) the page reads normal pictures and correct addresses.

4.3.2. Performance Test. For users, they do not care about how the system works behind them, and they only care about

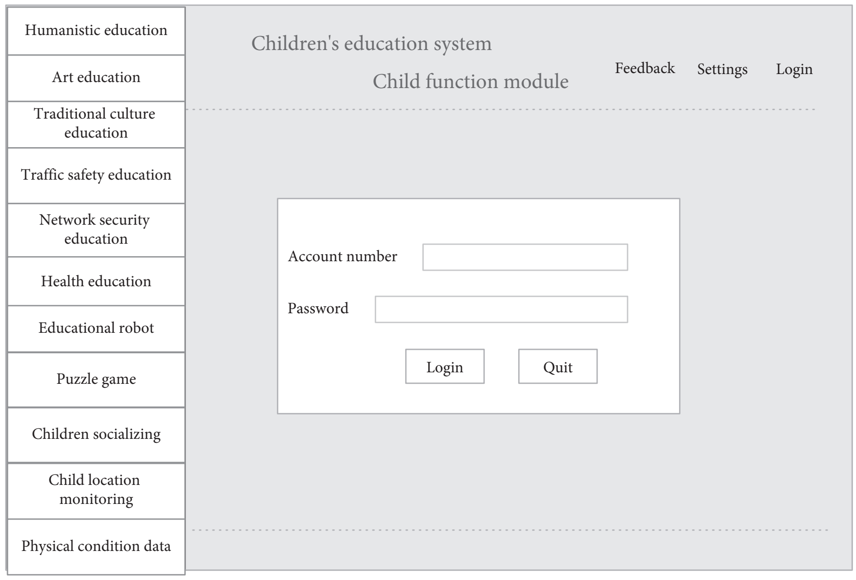

Figure 18: Children's module.

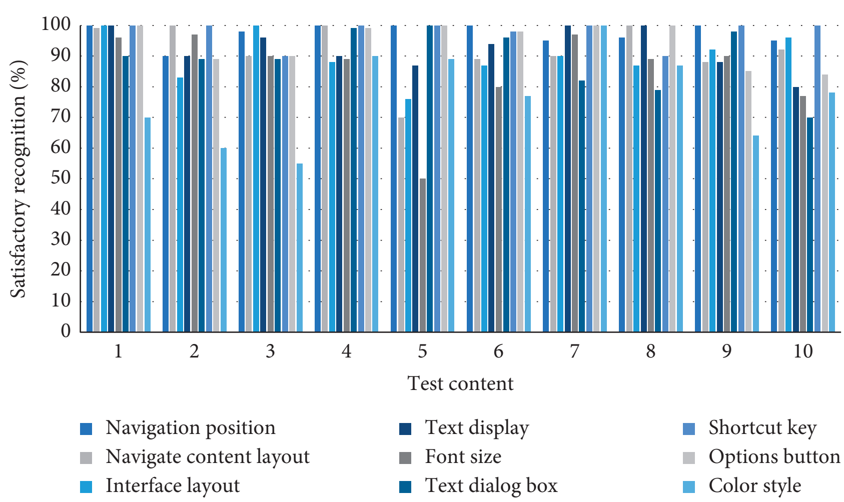

Figure 19: UI test results.

whether the system is "fast or not"; that is, the response time of the system is much less. In particular, for the vast majority of people, giving a response within 2 s is the best experience and the user is the most happy; giving a response within 5 s is a "fairly OK" experience; once the system response exceeds 10 s, the user experience is failed and uncomfortable. This test mainly tests the access time of the system, and the relevant calculation formula is as follows:

$$\begin{aligned}
&\text{network transmission time} = N_1 + N_2 + N_3 + N_4,\\
&\text{apply server processing time} = A_1 + A_3,\\
&\text{database server processing time} = A_2,\\
&\text{response time} = N_1 + N_2 + N_3 + N_4 + A_1 + A_3 + A_2.
\end{aligned} \tag{28}$$

We set the numbers of visits requesting access to the system at the same time to 1000, 2000, 3000, 4000, and 5000. In the online monitoring system for children's education designed by us, the response time of the manager module and the children module is tested, respectively, and finally the submodules of the two systems are compared, as shown in Figure 20.

According to the results, we can find that the average response time of each request of children's module is about 725 ms, and that of managers is about 812 ms, which is about 12% higher than that of children's module. With more visits requested, especially more than 3000 times, the success rate of visits decreases greatly. The access success rate of children's module is 99%, the access success rate of manager module is 98%, and the response time is not more than 10 s. The user experience is very good.

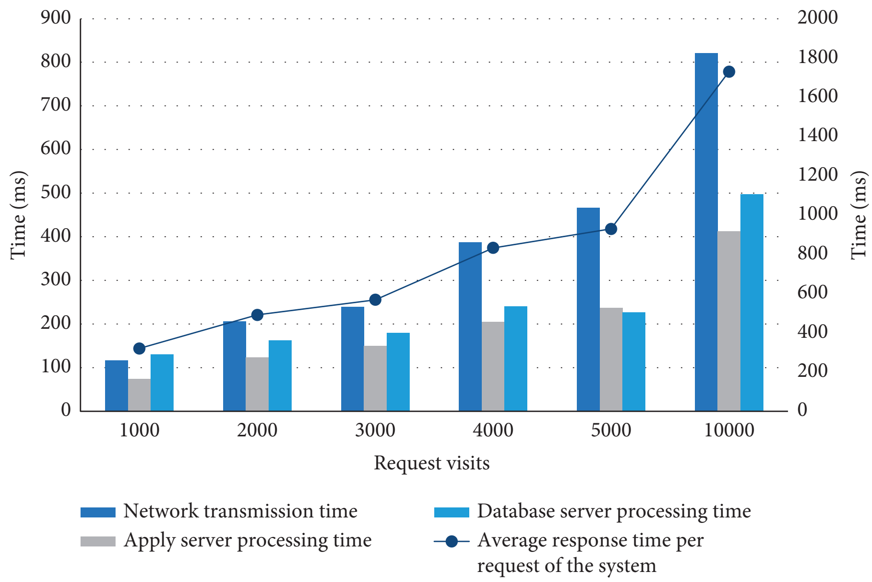

(a)

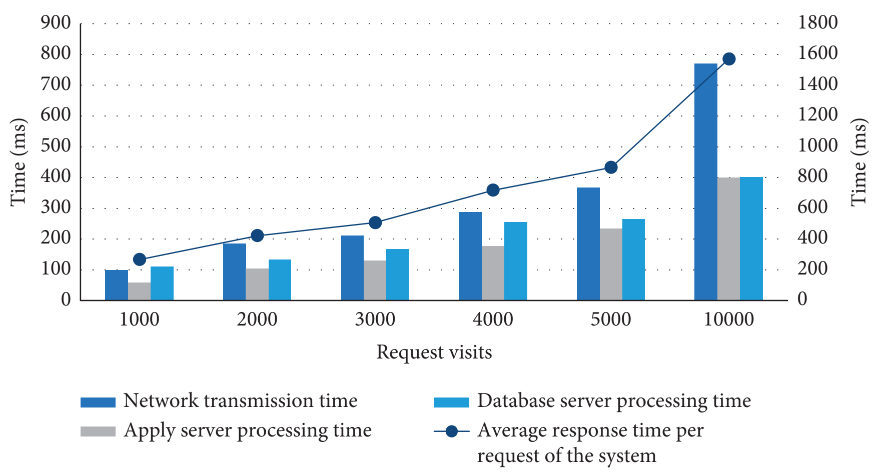

(b)

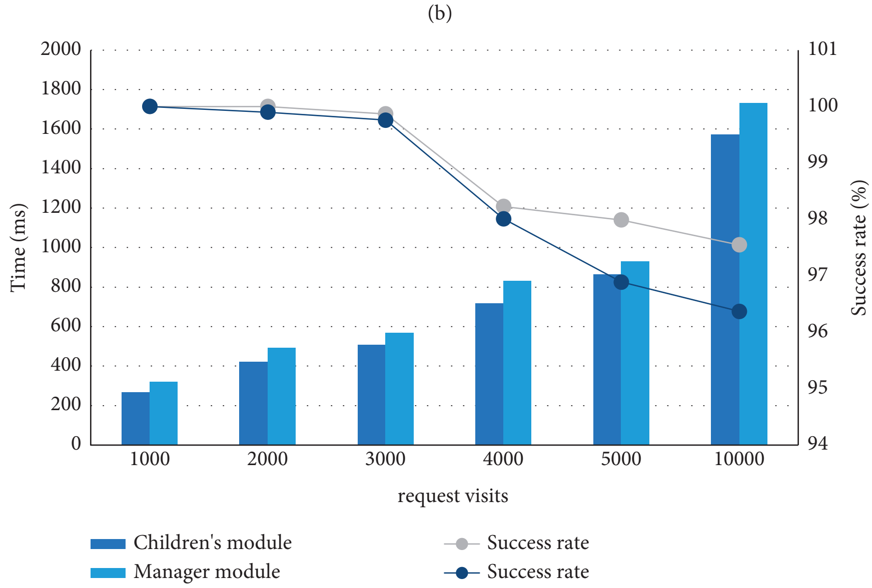

(c)

FIGURE 20: Response time test results. (a) Manager module. (b) Children's module. (c) Comparison of two submodules.

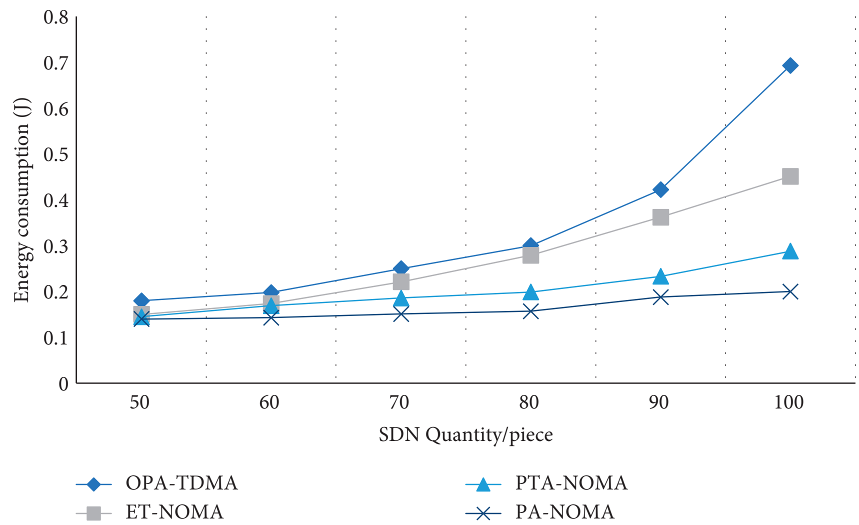

Figure 21: Comparison of optimized energy consumption with NOMA and TDMA.

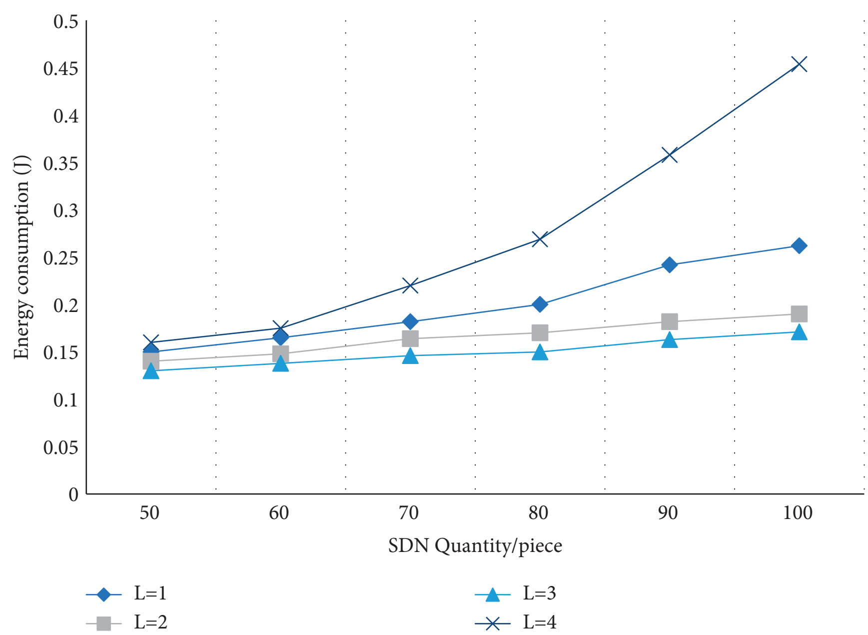

Figure 22: Relationship between optimized energy consumption and number of subchannels.

4.3.3. Optimization Test

(1) After the test optimization, the total energy consumption is shown in Figure 21.

According to the results, the energy consumption of PA-NOMA, ET-NOMA, and PTA-NOMA is greater than that of OPA-TDMA of TDMA when the amount of SDN increases. Compared with ET-NOMA, PA-NOMA greatly reduces energy consumption. Compared with PTA-NOMA, it can reduce the energy efficiency by more than 6%.

(2) After the test optimization, the total energy consumption and the number of subchannels allocated are shown in Figure 22.

According to the results, we find that when $L = 1$, the unmolecular channel is the same as PTA-NOMA. The total energy consumption at $L = 2$ is lower than that at $L = 1$; when $L = 3$, the total energy consumption is the lowest; when $L = 4$, the energy consumption is the largest. Therefore, the optimized energy consumption is the lowest, which can also verify the conclusion of Figure 21.

5. Conclusion

To sum up, the system designed in this paper for online monitoring of children's education has been developed, using the fifth-generation mobile communication technology, Internet of Things technology, distributed system development, and other technologies. According to the needs of schools, parents, and children, the practical application of children's education concept is carefully studied. The system is well developed and the simulation test results are good.

The results show the following: (1) UI test results basically meet the requirements of users; for the pursuit of personalized users, further development and improvement are needed. (2) Compared with children's module, the response time of manager module increased by 12%, and all the response times did not exceed 10 s, so the user experience was very good. The access success rate of children's module is 99%, and that of managers' module is 98%. It is necessary to further study what factors interfere with the success rate, which leads to the failure of 100% success. (3) After optimization, the total energy consumption is the lowest compared with NOMA and TDMA, which is the best energy efficiency optimization method to solve the communication of Internet of Things.

Therefore, our system can be further improved and updated and can be gradually put into market testing according to market research. In the follow-up, the developers' research work will focus on this system to improve more details, hoping to put it into market operation as soon as possible and bring about new technology convenience to children's education.

Data Availability

The experimental data used to support the findings of this study are available from the corresponding author upon request.

Conflicts of Interest

The authors declare that they have no conflicts of interest regarding this work.

References

[1] S. Livingstone and M. Bober, "Taking up online opportunities? children''s uses of the internet for education, communication and participation," *E-Learning*, vol. 1, no. 3, pp. 395–419, 2010.

[2] E. Randi Schoenfeld, P. Ng, and K. Henderson, "Using the internet to educate adolescents about osteoporosis: application of a tailored web-education system," *Health Promotion Practice*, vol. 11, no. 1, pp. 104–111, 2010.

[3] S. Edwards, A. Nolan, M. Henderson, A. Mantilla, L. Plowman, and H. Skouteris, "Young children''s everyday concepts about the internet: implications for cyber-safety education in the early years," *British Journal of Educational Technology*, vol. 49, no. 1, 2018.

[4] S. Shonia, N. A. Suwastika, and R. Yasirandi, "Bag toss game based on internet of education things (IoET) for the development of fine motor stimulation in children 5-6 Years old," *EMITTER International Journal of Engineering Technology*, vol. 8, pp. 326–345, 2020.

[5] Y. Tamekawa, H. Seki, S. Hashimoto, A. Hayashi, K. Ikeda, and A. Kanno, "Development and trials of the internet consultation system for children with developmental disabilities," *Ieice Technical Report Education Technology*, vol. 102, no. 594, pp. 41–46, 2003.

[6] A. B. Enochsson, "Children's models of the internet," *Information Technology in Childhood Education Annual*, vol. 2004, no. 1, pp. 5–23, 2004.

[7] T. Tajima, Y. Tsuji, M. Nishiokau, and K. Okuda, "The practice and the management system of "the child science classroom" via internet," *Computer & Education*, vol. 22, pp. 113–118, 2007.

[8] O. A. Kireeva, "Theoretical model of children''s ecological and artistic education system in the context of ethno-cultural traditions," *Problems of Modern Education (Problemy Sovremennogo Obrazovaniya)*, vol. 5, no. 5, pp. 153–162, 2020.

[9] A. A. Shafi, R. Little, and S. Case, "Children''s education in secure custodial settings: towards a global understanding of effective policy and practice," *International Journal of Educational Development*, vol. 82, no. 12, Article ID 102379, 2021.

[10] L. Zhang and S. Ni, "The integrated development of children''s thinking mode in the\\ "internet +\\" era%\\ "internet plus\\" era," *Journal of Shaanxi Institute of Education*, vol. 35, no. 9, pp. 12–16, 2019.

[11] I. Jawaid, M. Y. Javed, M. H. Jaffery, and A. Akram, "Robotic system education for young children by collaborative,roject-based learning," *Computer Applications in Engineering Education*, vol. 28, no. 1, 2019.

[12] M. Aazam, K. A. Harras, and S. Zeadally, "Fog computing for 5G tactile industrial internet of things: QoE-aware resource allocation model," *IEEE Transactions on Industrial Informatics*, vol. 15, pp. 3085–3092, 2019.

[13] B. S. Awoyemi, A. S. Alfa, and B. Maharaj, "Resource optimisation in 5G and internet-of-things networking," *Wireless Personal Communications*, vol. 111, no. 4, pp. 2671–2702, 2020.

[14] Y. Liu, M. Peng, G. Shou, Y. Chen, and S. Chen, "Towards edge intelligence: multi-access edge computing for 5G and internet of things," *IEEE Internet of Things Journal*, vol. 7, no. 8, pp. 6722–6747, 2020.

[15] K. Zhan, "Sports and health big data system based on 5G network and internet of things system," *Microprocessors and Microsystems*, vol. 80, no. 2, Article ID 103363, 2020.

[16] P. Yu, M. Yang, A. Xiong et al., "Intelligent-driven green resource allocation for industrial internet of things in 5G heterogeneous networks," *IEEE Transactions on Industrial Informatics*, vol. 18, no. 99, p. 1, 2020.

[17] M. N. Mahdi, A. R. Ahmad, Q. S. Qassim, H. Natiq, M. Subhi, and M. Mahmoud, "From 5G to 6G technology: meets energy, internet-of-things and machine learning: a survey," *Applied Sciences*, vol. 11, no. 17, p. 8117, 2021.

[18] S. Li, "The 5G/6G enabled future internet of things," *EAI Endorsed Transactions on Internet of Things*, vol. 6, no. 22, Article ID 166349, 2020.

[19] R. Kanehisa, F. Barbosa, and A. D. Castro, "5G energy efficiency for Internet of Things," *Academic Journal on Computing Engineering and Applied Mathematics*, vol. 1, no. 2, pp. 14–23, 2020.

[20] R. Khdhir, "5G LTE-A cognitive multiclass scheduling scheme for internet of things," *International Journal of Advanced Trends in Computer Science and Engineering*, vol. 8, no. 5, pp. 2485–2491, 2019.

[21] A. Durak and H. Kaygin, "Parental mediation of young children''s internet use: adaptation of parental mediation scale and review of parental mediation based on the demographic

variables and digital data security awareness," *Education and Information Technologies*, vol. 25, no. 3, pp. 2275–2296, 2020.

[22] H. Bai and Q. Zhang, "English smart classroom teaching system based on 5 network and internet of things," *Microprocessors and Microsystems*, vol. 2020, Article ID 103421, 2020.

[23] R. Hassan, F. Qamar, M. K. Hasan, A. Aman, and A. Ahmed, "Internet of things and its applications: a comprehensive survey," *Symmetry*, vol. 12, no. 1674, 2020.

[24] J. Chen and B. Yang, "Optimization of construction and management of practical education system based on system analysis," *Laboratory Research and Exploration*, vol. 32, no. 10, pp. 241–244, 2013.

[25] S. Titarenko, "Multimedia technologies usage to optimize motor activity of kindergarten children," *Open Educational E-Environment Of Modern University*, vol. 8, no. 8, pp. 147–153, 2020.

Hindawi
Scientific Programming
Volume 2022, Article ID 7861157, 10 pages
https://doi.org/10.1155/2022/7861157

Research Article

Application and Analysis of Education and Teaching Mode Based on 5G and Smart Technology

Ran Yan

School of Marxism, Zhengzhou Railway Vocational & Technical College, ZhengZhou 451460, China

Correspondence should be addressed to Ran Yan; 11110@zzrvtc.edu.cn

Received 5 November 2021; Revised 6 December 2021; Accepted 14 December 2021; Published 13 January 2022

Academic Editor: Le Sun

The development of information technology has brought tremendous changes to our country's education. Based on the 5G + Internet, the article proposes a brand-new intelligent education model and proposes an ST analysis method, which mainly studies the teacher and students in the classroom. Class performance, based on Yebes network, proposed a learning decision method and application. The research results of the article show the following: (1) The article compares the monthly test scores of three variables under two different teaching modes. The results show that the performance of the online teaching mode is generally better than that of the traditional teaching mode, and the performance of the experimental class has increased more, with an average growth score of 4.83, indicating that there are significant differences in students' learning and cognitive abilities under different teaching models. (2) The article compares the students' knowledge mastery under two different teaching modes. The results show that under the traditional teaching mode, the students' knowledge mastery is low, and the complete mastery rate is only 15%. In the network multimedia teaching mode, the students' knowledge mastery rate has been greatly improved, the complete mastery rate is as high as 45%, and the students' mastery of knowledge has been extremely improved, indicating that the network multimedia teaching mode can stimulate students' learning interest more, improve learning efficiency. (3) Studying the differences in the source of curriculum resources of three different types of teachers, and the results show that the proportion of curriculum resources downloaded through the Internet is the largest; in the investigation of the impact of multimedia teaching on the classroom, the cooperation rate of students when multimedia teaching is not used, classroom practice accuracy and classroom completion rate are low, but after using multimedia teaching, students' cooperation rate and classroom practice accuracy rate have been greatly improved, among which the accuracy rate of the experimental class is as high as 62.4%, and the students' thinking ability is also good. Great improvement.

1. Introduction

Information technology has brought tremendous changes to China's education. 5G technology has provided a better guarantee for the sharing of curriculum resources. In the face of the extreme shortage of education resources in China, limited educational resources, and unlimited higher education development needs the contradiction between them is becoming more and more prominent. How to effectively realize the resource sharing among various universities has become a problem that must be considered in the development of talents in major universities. Literature [1] explores teaching models suitable for teaching activities. Literature [2] describes the implementation process of the model in educational statistics and SPSS courses. The article analyzes the implementation process of the teaching model from the aspects of experiment and evaluation and puts forward the problems and solutions in the application process of the model. Literature [3] constructs a smart classroom teaching model that conforms to the development of the times by analyzing the connotation and technical characteristics of smart classrooms. Network technology has gradually replaced traditional learning methods. Some e-learning platforms have also received more and more people's favor. Some educational structures are also taking full advantage of the advantages of e-learning to attract more people. Literature [4] mainly describes how to identify and analyze factors that contribute to the design of e-learning applications. Literature [5] mainly discusses the application of modern educational technology in computer teaching. On university campuses, using the convenience of 5G and the Internet, they have gradually formed a model of curriculum education resource sharing, which can share teaching resources, as well as the sharing of teacher resources, curriculum resources, and advanced teaching facilities. Literature [6] is based on the DBR educational research paradigm and verifies the original concept through practical exploration in real situations. Literature [7] conducted a series of data analyses and research on the application of data mining technology in student performance. Analyzed the internal relations and teaching rules between the various courses. With the advent of the Internet age, the use of big data analysis technology has become a method and technology used in many fields, and big data has also promoted the reform and innovation of various universities. With the development of science and technology and the prevalence of Internet technology, compared with traditional networks, 5G networks have the advantages of low coverage, low energy consumption, and high capacity in hot spots. It can carry out data dissemination very well. According to the current state of extreme scarcity of educational resources, some places do not have advanced teaching resources, and it is necessary to use the convenience of the Internet to communicate and share on the Internet. Literature [8] starts from the design concept of the smart campus and studies the application of data mining technology in the smart campus system under the background of big data. Literature [9] analyzes the characteristics and advantages of the university listening and speaking teaching mode under the network environment. Literature [10] analyzed the advantages of the experimental teaching platform in terms of hardware and software and designed the application mode of the PBL teaching method in the experimental teaching platform. Literature [11] conducts a rational analysis of the application of information technology in education, based on the mainstream technological phenomenology of the current philosophy of technology. With the development of Internet technology, the demand for technical talents is also increasing. In order to cultivate more professional talents, a model of integration of production and education can be implemented. Literature [12] makes a general analysis of the application of intelligent technology in teaching mode at the present stage in China and discusses the current situation of the application of talent training mode. Literature [13] analyzes the sports teaching mode based on multimedia information technology and the advantages of multimedia teaching from the perspective of 5G and the internet of things technology. Literature [14] investigates the education mode of a university and analyzes the teaching elements of innovative teaching of numerical control technology application from the teaching case analysis. Literature [15] proposed a new mobile platform for micro-English education and learning based on mobile 5G technology.

2. Basic Theory

2.1. The Application of 5G Smart Technology in Education. 5G is the foundation of the intelligent Internet. In the teaching process, it is equipped with information technology such as remote interaction and artificial intelligence, which is deeply integrated with course teaching, enriches classroom teaching, allows students to participate in teaching, and enhances students' interest in learning. Teachers can teach students in accordance with their aptitude through real-time interaction with students. Many excellent teaching resources can be shared on the Internet; through the Internet, students can study outside of class, check deficiencies, and realize the universalization of education. Even in the most remote rural areas, as long as they have the Internet, they can enjoy rich and high-quality education. Resources, to achieve the sharing of educational resources. In the field of education, 5G + Al will give birth to intelligent education, embodying a people-oriented teaching model. Through the close integration of Al and big data technology, under the support of 5G network, the teaching data related to the teaching behavior of the teacher in the classroom and the student's listening effect are captured in real-time through the intelligent teaching terminal, and the method and method of the teacher's teaching in the teaching are extracted by using big data analysis technology. Based on the unstructured behavior data generated by the students' listening state, the extracted unstructured data is effectively analyzed and summarized with the help of AI algorithms, cloud computing, etc., and finally using data visualization technology, according to the data results generated by teachers and students, teaching managers, teachers, and students provide scientific behavior analysis reports, which are displayed to relevant teaching management institutions and class teachers to assist teaching management and improve teaching quality. For parents, they can observe students' learning conditions online, realize online tutoring, and protect their children's healthy growth. The application of 5G in the education industry is shown in Figure 1:

5G and intelligent technology have brought a lot of convenience to the work and study of teachers and students. Intelligence means that the campus has a scientific research cloud, intelligent classroom, campus security, and other platforms. Teachers can read papers online and evaluate oral English. Students can also learn online, and parents can tutor online; the platform will introduce student information and teaching resources into the platform. The intelligent technology + education will further extend the information interconnection from the breadth to the colleges and universities, from the depth to the organization of colleges and universities, and smooth informatization.

2.2. Construction of Intelligent Education Model. The development model of the smart education resource innovation ecosystem is the progression and deepening of the "Internet +" education development model and is the product of smart technology + education resources. Internet education takes communication and social interaction as the

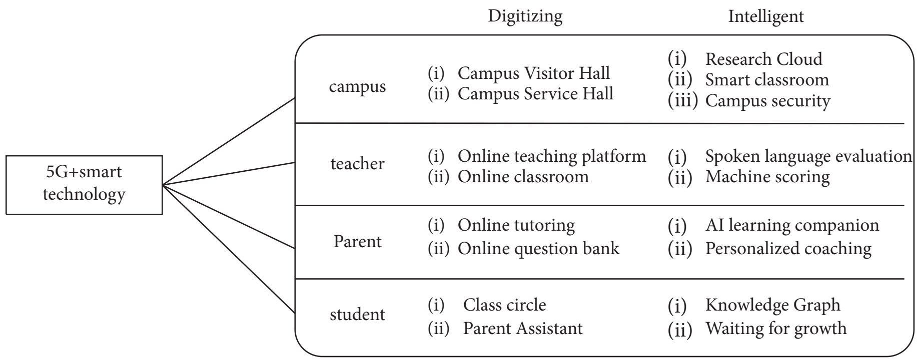

Figure 1: 5G + smart technology helps education.

core content, realizes the connection between learners, and establishes a learning website, connects learners and campus services, that is, establishes external connections between learners and campus, and makes the campus service information communicated to learners more efficiently and quickly. The intelligent technology + education will further extend the information interconnection from the breadth to the various colleges and universities, from the depth to the internal organization of the colleges, and smooth informatization, so that the school can reorganize the learning elements and the needs of the learners. The management operation mode, so as to achieve efficient coordination between learners and school management operations, and more efficient matching of information supply and demand. The intelligent education model diagram is shown in Figure 2:

The development mode of the intelligent education resources innovation ecosystem is progressive and deepening of the "Internet +" education development mode and is the product of intelligent technology + education resources. Internet education takes communication and social interaction as the core content, realizes the connection between learners, and establishes a learning website to connect learners and campus services, that is to establish the external connection between learners and campus so that the service information of campus can be more efficiently and quickly conveyed to learners. The new ecosystem of intelligent education provides services for learners. Learners feedback data to the new ecosystem of intelligent education, and the information fed back can generate educational resources through the new ecosystem.

2.3. Analysis of Intelligent Teaching Mode. Based on the 5G mobile network, it is possible to achieve lectures by famous teachers in the near-end classrooms, interaction, auditing, and commenting in the remote classrooms, and to achieve smooth listening and free evaluation in campus scenarios such as remote recording and broadcasting classrooms, dual-teacher classrooms, and smart classroom delivery. Classes, centralized control, 5G remote listening, and evaluation classes have greatly improved in response speed, image quality, feedback timeliness, and evaluation effectiveness. Realize online patrol realize the diversification of teaching evaluation. Supported by the 5G network environment, teaching evaluation collects a full range of data through the observation of learners' online or offline learning process, discovers their participation in learning behavior patterns, excavates their thinking process to complete tasks, discovers problems in real-time, and solves the process. In order to realize the real-time and accurate evaluation of the problems encountered in the process and the formulation of intervention methods, the realization of multimodal learning data collection, full-scene demand analysis, and three-dimensional evaluation, and realization of guidance and improvement based on the results of learning evaluation. The intelligent education model diagram is shown in Figure 3:

2.3.1. Personalized Learning Mode. Teaching should pay attention to teaching students in accordance with their aptitude because each student's learning methods and mastery of knowledge are different. Personalized education is based on the current learning status of each student to implement education in a targeted manner. With more and more student and learning data recorded by the system, it is more difficult to achieve targeted and personalized education. Intelligent teaching solves this problem very well. The system will conduct a test on the students' learning situation and difficult points, and the test results will be transmitted to the teacher's computer. The teacher can customize the learning plan according to each person's situation. Students can also master their learning situation, so as to carry out targeted exercises, and truly teach students in accordance with their aptitude.

2.3.2. Diversified Learning Modes. The traditional teaching method is basically in a fixed place, teaching according to fixed textbooks, and teachers will teach fixed content according to the requirements of the school. This traditional teaching mode will be restricted by time, place, and space. With the development of science and technology, the new educational model can break the shackles of this traditional teaching concept. Teaching is not limited by time and place and realizes "learning all the time." Students can choose to learn effectively according to their own learning progress and learning intensity. Learning should be people-oriented

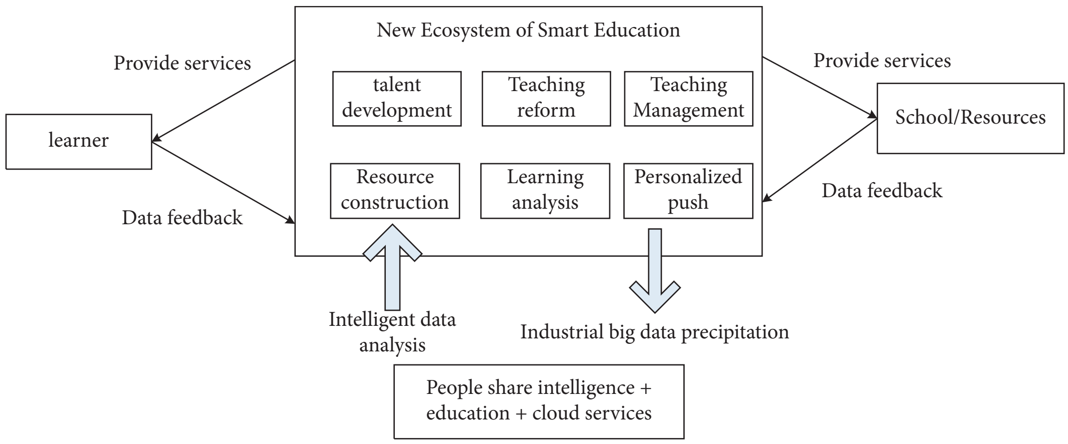

Figure 2: Smart education system model diagram.

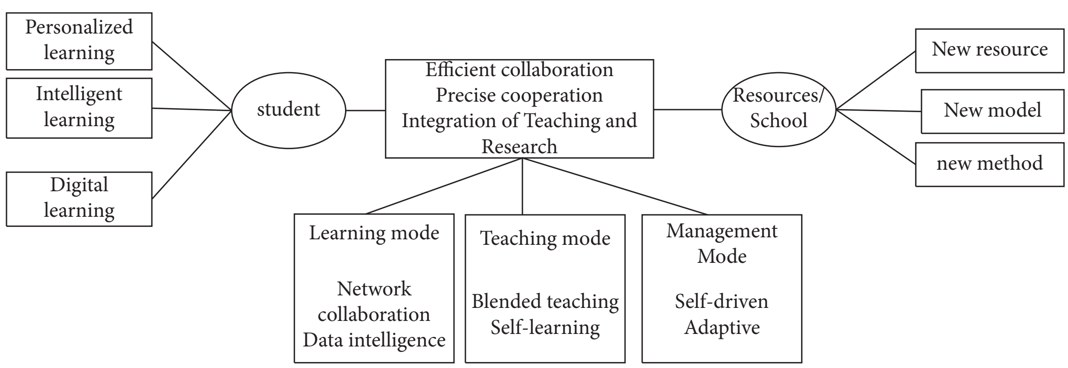

Figure 3: Smart education model diagram.

and focus on content rather than form, so as to keep pace with the times.

Differentiated learning is an individualized teaching method, in which teachers adjust the teaching process and products according to students' learning willingness, interest, and learning style. Its learning plan focuses on content, while the learning content of all students remains the same. It is a school- and curriculum-centered approach that attempts to modify the way that is content is taught to meet student needs, differing strengths, and general readiness. Personalized learning looks at the learner, thinking about the question, "What does this student need to know, and how best to do that?" It is a student-centered approach to learning that is built around recognizing the vast differences between students, not only in literacy or diagramming abilities but also in the real needs of students.

3. Method

3.1. Classroom Teaching Analysis

3.1.1. S-T Analysis Method. S stands for student and T stands for the teacher. It mainly studies the classroom observation methods of teacher and student behavior in the classroom. The number of S behaviors is recorded as N_s, and the number of T behaviors is recorded as N_t [16], and the formula is

$$N = N_s + N_t. \tag{1}$$

The teacher behavior share R_t is

$$\begin{aligned} R_t &= \frac{N_t}{N} \\ &= \frac{(N - N_s)}{N} \\ &= 1 - \frac{N_s}{N}. \end{aligned} \tag{2}$$

The formula for calculating behavioral conversion rate Ch is

$$\mathrm{Ch} = \frac{g - 1}{N}. \tag{3}$$

Ch is the behavior conversion rate indicates the interactivity in teaching. The larger the Ch, the more frequent the switching between student and teacher behaviors.

3.1.2. Classroom Video Feature Extraction. The convolutional layer is the most common method for deep neural networks to process pictures, which mainly compresses and extracts features [17]; its mathematical formula is

$$S(m,n) = (f * g)(m,n) = \sum_{i=-\infty}^{\infty} \sum_{j=-\infty}^{\infty} f(i,j) g(m-i, n-i). \tag{4}$$

The convolution in the neural network is

$$S(m,n) = (I * K)(m,n) = \sum_{i} \sum_{j} I(m+i, n+i) K(i,j). \tag{5}$$

Logical function

$$s(x) = \frac{1}{1+e^{-x}}. \tag{6}$$

The hyperbolic tangent function is

$$\tanh(x) = \frac{e^{x} - e^{-x}}{e^{-x} + e^{-x}}. \tag{7}$$

The linear rectification function is

$$\mathrm{ReLU}(x) = \begin{cases} 0, & x < 0, \\ x, & x \geq 0. \end{cases} \tag{8}$$

The function of the normalized index layer is to complete the calculation of the normalized index function in most linear classifiers [18], the specific algorithm input vector is

$$X = (x_1, x_2, \ldots, x_n). \tag{9}$$

Calculate n scalar values

$$y_k = \frac{e^{x_k}}{e^{x_1} + \cdots + e^{x_n}}. \tag{10}$$

Spliced into

$$Y = (y_1, y_2, \ldots, y_n). \tag{11}$$

The pros and cons of the face detection algorithm and the face detection system performance are mainly evaluated by the following main performances [19], the detection rate is

$$\mathrm{DR} = \frac{m_1}{M_1}. \tag{12}$$

False detection rate is

$$\mathrm{FAR} = \frac{m_2}{M_2}. \tag{13}$$

Missed detection rate is

$$\mathrm{FRR} = \frac{m_3}{M_3}. \tag{14}$$

3.2. Research on the Learning Method of Bayesian Network

3.2.1. Definition of Bayesian Network. Given a directed acyclic graph G, the variable nodes in the graph are a set of discrete variables [20]

$$U = \{X_i, X_2, \ldots, X_n\}. \tag{15}$$

The value range of each variable X_i is expressed as

$$\mathrm{Val}(X_i) = \{x_i^1, x_i^2, \ldots, x_i^m\}. \tag{16}$$

The conditional probability corresponding to the variable X_i is

$$\theta_i = \prod_{i} p(x_i \mid pa(x_i)), \tag{17}$$

where $pa(x_i)$ is the direct parent node of x_i, and the joint probability distribution is p [21]

$$p(x_i, x_2, \ldots x_n) = \prod_{i} p(x_i \mid x_1, x_2, \ldots, x_{n-1}) = \prod_{i} p(x_i \mid pa(x_i)). \tag{18}$$

The pair $\langle G, \Theta \rangle$ formed by the directed acyclic graph G and the parameter set $\Theta = \{\theta_1, \theta_2, \ldots, \theta_n\}$ becomes a Bayesian network [22].

3.2.2. Bayesian Network Structure Learning. The K2 algorithm mainly solves the problem of network structure learning with unknown structures and complete data [23]. The scoring method is expressed as follows:

$$\max_{Bs}[P(Bs, D)] = C \prod_{i=1}^{n} \max \prod_{i} \left[\prod_{j=1}^{q_j} \frac{((r_i - 1))!}{(N_{ij} + r_i - 1)!} \prod_{k=1}^{r_i} N_{ijk}! \right]. \tag{19}$$

The $B\ De$ scoring formula is

$$p(G \mid D) = p(G) \prod_{i=1}^{n} \prod_{j=1}^{q_j} \frac{\left(\sum_k N_{ijk}'\right)}{\left(\sum_k N_{ijk}' + N_{ij}\right)} \prod_{k=1}^{r_i} \frac{\left(\sum_k N_{ijk}' + N_{ijk}\right)}{\left(\sum_k N_{ijk}'\right)}. \tag{20}$$

The score of a Bayesian network structure is expressed as [24]

$$DL(G, D) = DL_{\mathrm{stru}}(G) + DL_{\mathrm{tab}}(G) + DL_{\mathrm{data}}(D \mid G). \tag{21}$$

In

$$\begin{cases} DL_{\mathrm{stru}}(G) = \sum_{i=1}^{n} (\log n + \log(n, Pa_i) \mid), \\ DL_{\mathrm{tab}}(G) = \frac{1}{2} \sum_{i=1}^{n} |Pa_i| * (r_i - 1) \log N, \\ DL_{\mathrm{data}}(D \mid G) = N \sum_{i=1}^{n} H(X_i \mid Pa_i). \end{cases} \tag{22}$$

According to Bayesian principle $\log P(G \mid D)$, it is expressed as

$$\log(G^s \mid D) = \log P(D \mid G^s) + \log P(G^s). \tag{23}$$

The approximate expression of the score obtained by the integral is

$$\log(G \mid D) \approx \log P(D \mid \tilde{\theta}_G, G) - \frac{d}{2} \log N. \tag{24}$$

This dimension is expressed for the Bayesian network as

Table 1: Statistics of traditional teaching samples.

Class	Class size	Average (E)	Standard deviation	Mean standard error
Experimental class	42	68.67	15.422	2.380
Control class	42	67.69	15.045	2.322
Standard class	42	65.78	15.012	2.314

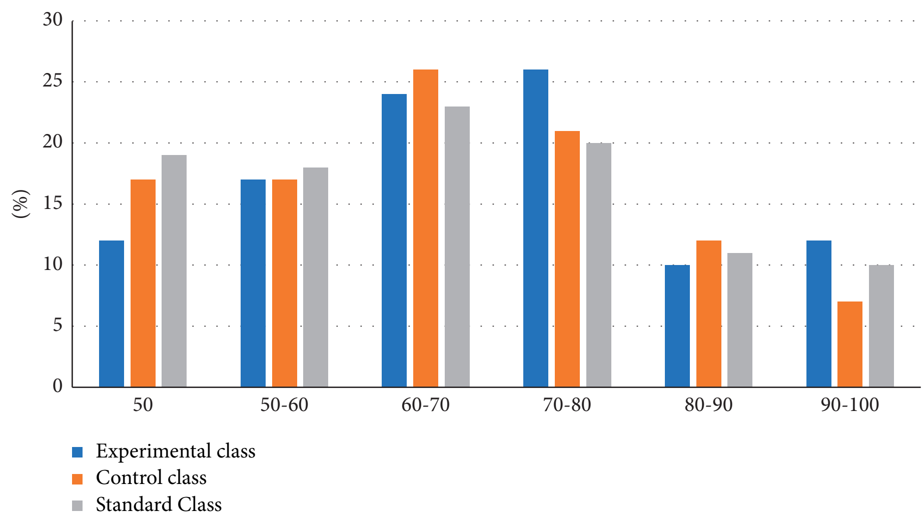

Figure 4: Traditional teaching mode results.

$$d = \sum_{i=1}^{n} |Pa_i|\left(|X_i| - 1\right). \quad (25)$$

MCMC the algorithm transfers from the i^{th} network structure Bs to the new network structure Bs, the reception probability is [25]

$$\alpha(Bs, Bs') = \min\{1, R_\alpha\},$$
$$R_\alpha = \frac{\#(\text{nbd}(Bs))P(Bs' \mid D)}{\#(\text{nbd}(Bs'))P(Bs \mid \mid D)}. \quad (26)$$

4. Simulation Experiment

4.1. Analysis of Student Performance

4.1.1. Traditional Teaching Mode. The score analysis data are shown in Table 1 and Figure 4:

4.1.2. Network Multimedia Teaching Mode. The score analysis data are shown in Table 2 and Figure 5:

From Tables 1 and 2, we can see that the monthly test scores of the experimental class, the control class, and the standard class under the standard teaching mode are 68.67, 67.69, and 65.78, respectively, and the scores under the network multimedia teaching mode are 73.50, 72.27, and 70.24, respectively. The results of the online teaching model are generally higher than those of the traditional teaching model. Among them, the performance of the experimental class has a higher degree of increase, with an average increase of 4.83, indicating that there are significant differences in the learning and cognitive abilities of students under different teaching models.

4.2. Analysis of Students' Knowledge Mastery. In order to test the students' mastery of knowledge under the two different teaching modes, we issued questionnaires to the students in the experimental class, the control class, and the standard class under the two different teaching modes, and compared the results obtained. The experimental conditions are shown in Figures 6 and 7.

From Figures 3 and4, we can see that under the traditional teaching mode, students have a low degree of knowledge mastery, with a complete mastery rate of only 15%. Under the network multimedia teaching mode, the student's knowledge mastery rate has been greatly improved. The complete mastery rate is as high as 45%, and the students' mastery of knowledge has been excellently improved, indicating that the network multimedia teaching mode can stimulate students' interest more in learning and improve learning efficiency.

4.3. Comparative Study of Teaching Design. Under the traditional teaching method, teachers generally use the textbooks issued by the school to teach. The traditional teaching methods will inevitably have some shortcomings. In the online teaching mode, the teacher will make the key content of the classroom into a PPT and display it in the classroom, which is not only convenient for the students, we understand the key points of the classroom, and it is also convenient for

Table 2: Sample statistics of online teaching mode.

Class	Class size	Average (E)	Standard deviation	Mean standard error
Experimental class	42	73.50	11.677	1.756
Control class	42	72.27	14.357	2.215
Standard class	42	70.24	14.258	2.122

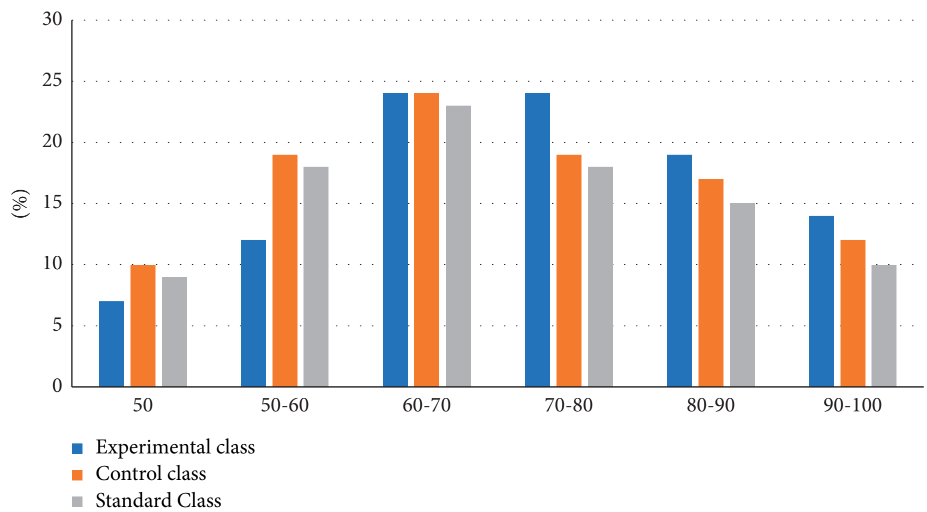

Figure 5: Network multimedia teaching mode results.

Figure 6: Knowledge mastery survey.

students to save and review later. In order to study the differences in the sources of teachers' lesson preparation resources, we have investigated the sources of lesson preparation resources of three different types of teachers, as shown in Table 3:

From the survey results in Table 3 and Figure 8, we can conclude that the three different types of teachers have the largest proportion of downloading course resources through the Internet; we have conducted research and investigation on whether to use courseware in class and the performance of students in class. The survey results are shown in Tables 4 and 5.

From the research results in Figures 9 and 10, we can conclude that when multimedia teaching is not used, students' cooperation rate, classroom practice accuracy rate, and classroom completion rate are low. However, these

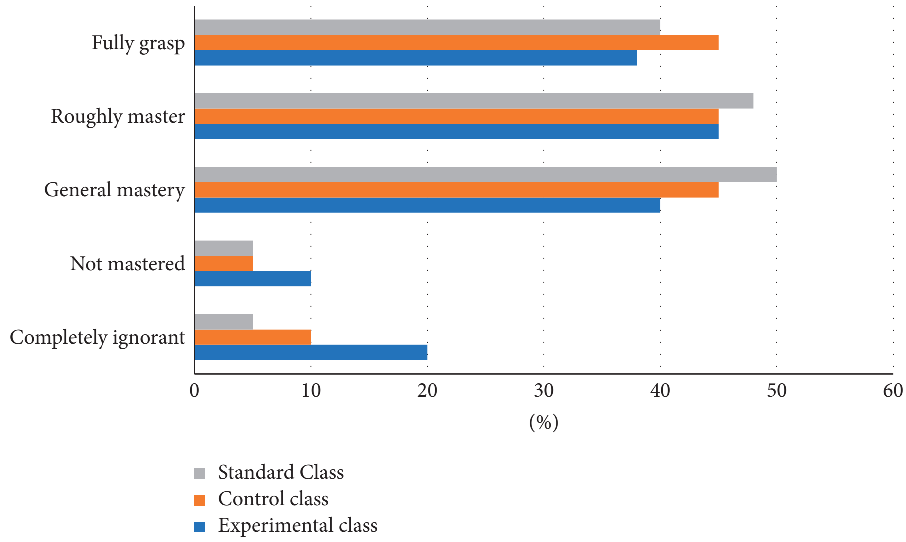

Figure 7: Knowledge mastery survey.

Table 3: Statistical table of sources of teaching resources.

	Excellent teacher lesson plan (%)	Teaching reference (%)	Online download (%)	Write your own (%)	Other (%)
Expert	18.8	28.1	36.5	17.5	1.2
Proficient	16.7	27.2	40.1	15.6	2.6
Novice	26.2	35.7	46.7	11.9	2.4

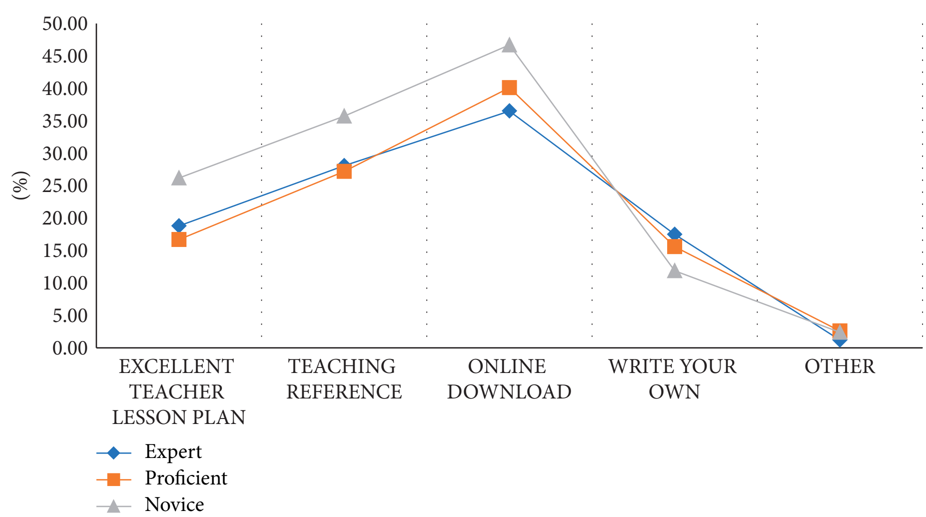

Figure 8: Statistics of sources of teaching resources.

problems have been improved after multimedia teaching is used. The cooperation rate of students and the accuracy of classroom exercises have been greatly improved. The accuracy rate of the experimental class is as high as 62.4%, and the thinking ability of students has also been greatly improved.

Table 4: Class performance without multimedia.

	Students actively cooperate (%)	Successfully complete the teaching plan (%)	Classroom practice accuracy (%)	Improve students' thinking ability (%)
Standard class	11.5	6.3	30.6	13.5
Control class	12.1	16.7	35.2	15.9
Experimental class	13.9	21.4	42.2	19.4

Table 5: Use of multimedia classroom performance.

	Students actively cooperate (%)	Successfully complete the teaching plan (%)	Classroom practice accuracy (%)	Improve students' thinking ability (%)
Standard class	22.5	16.9	41.6	23.5
Control class	35.1	27.6	55.3	17.9
Experimental class	33.9	32.5	62.4	21.4

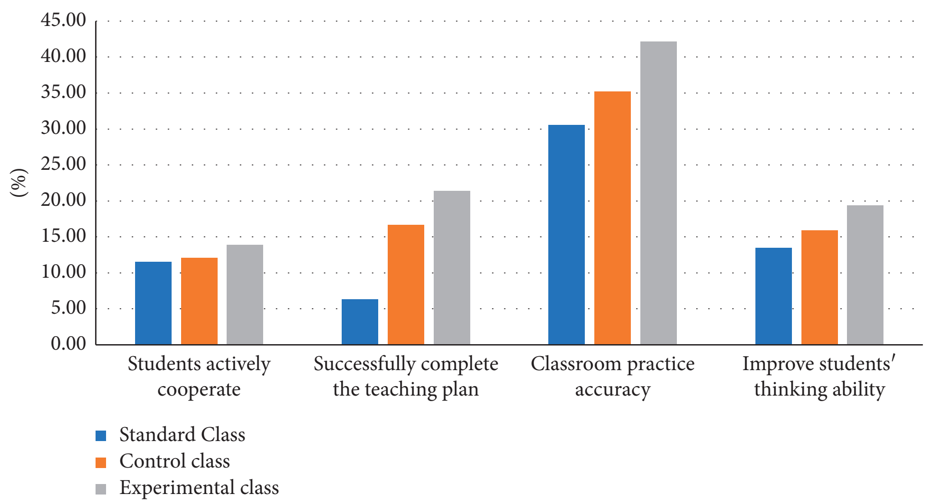

Figure 9: Non-use of multimedia classroom performance statistics chart.

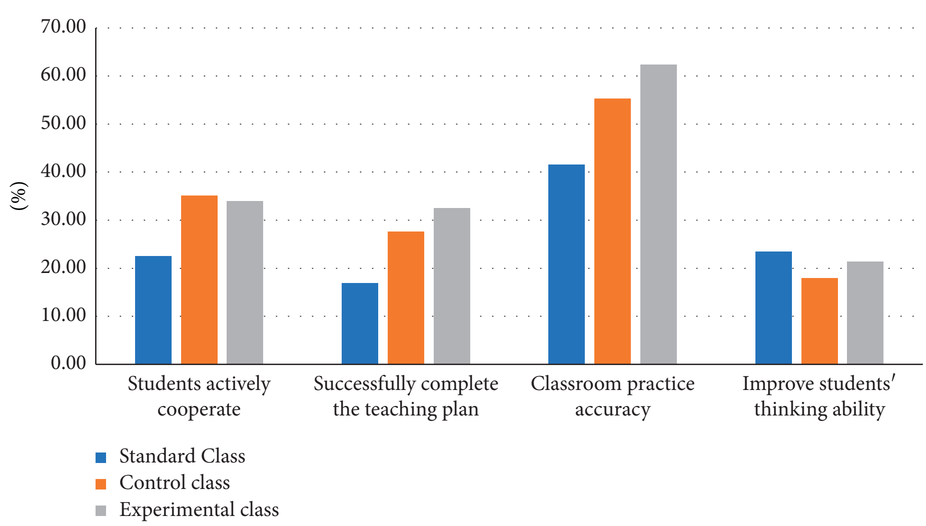

Figure 10: Using multimedia classroom performance statistics.

5. Conclusion

Artificial intelligence empowers education reform, and the superiority of technology is vividly reflected. However, although all countries have achieved good results, the shortcomings of artificial intelligence empowerment are gradually exposed. In order to guide the development of artificial intelligence-enabled education, it is necessary to analyze the international experience and current problems and propose new directions for future artificial intelligence-enabled education. Make education fairness a reality and achieve the highest quality educational resources in the shortest time.

Data Availability

The experimental data used to support the findings of this study are available from the corresponding author upon request.

Conflicts of Interest

The author declares that there are no conflicts of interest regarding this work.

References

[1] X. N. Guo, "Analysis and exploration of computer teaching mode based on modern education technology," *Computer Knowledge and Technology*, vol. 23, no. 5, pp. 17–23, 2014.

[2] G. Liu, "The application of the mixed teaching mode based on SPOC in the course of education statistics and SPSS," *Modern Information Technology*, vol. 09, no. 12, pp. 141–167, 2018.

[3] Y. Wang, "Research on the construction and application of college smart classroom based on education informationization," in *Proceedings of the 2018 8th International Conference on Education, Management, Computer and Society(EMCS 2018)*, pp. 258–262, Shenyang, China, December 2018.

[4] M. Veeramanickam, N. M. Sundaram, and L. S. Kumar, "Analysis of smart E-learning application based on various design aspects in IoT and ANN model," in *Proceedings of the 2019 PhD Colloquium on Ethically Driven Innovation and Technology for Society (PhD EDITS)*, pp. 1–4, Bangalore, India, August 2019.

[5] F. Li, "The analysis of computer teaching mode based on modern educational technology," in *Proceedings of the 2018 International Conference on Educational Research, Economics, Management and Social Sciences(EREMS 2018)*, pp. 1184–1188, Changchun, China, February 2018.

[6] X. Zhang, Y. Wang, and S. Sharma, "Design and analysis of flipped classroom experiment teaching based on DBR in information technology environment," *International Journal of System Assurance Engineering and Management*, vol. 09, no. 13, pp. 17–26, 2021.

[7] W. Jian, Z. Lu, W. Wu, and Y. Li, "The application of data mining technology based on teaching information," in *Proceedings of the 2012 7th International Conference on Computer Science & Education (ICCSE)*, pp. 652–657, IEEE, Melbourne, Australia, July 2012.

[8] J. Y. Zeng, "The research and application of smart campus system based on big data in data mining technology," *Journal of Guiyang University (Natural Sciences)*, vol. 07, no. 20, pp. 17–21, 2018.

[9] L. Liu, "Analysis of college listening and speaking teaching mode based on network environment," *Journal of Jilin Institute of Architecture & Civil Engineering*, vol. 06, no. 23, pp. 19–26, 2011.

[10] X. Xu, "Analysis on application mode of PBL teaching method based on experimental teaching platform," *Experimental Technology and Management*, vol. 8, no. 21, pp. 113–125, 2014.

[11] L. Wang, "An analysis of the application and limitation of information technology in education based on ihde's phenomenology of technology," *Modern Distance Education Research*, vol. 9, no. 4, pp. 105–113, 2012.

[12] B. Ge, "Analysis on professional integration of production and education personnel training mode in mobile application technology," vol. 08, no. 13, pp. 78–85, 2017.

[13] H. Zhao, Y. Fei, and C. Li, "Empirical analysis on aerobics multimedia teaching based on interactive mode," *Applied Mechanics and Materials*, vol. 380-384, pp. 2901–2905, 2013.

[14] J. Shao, "Innovative numerical control technology application teaching mode analysis," in *Proceedings of the 2016 International Conference on Modern Education Technology (MET2016)*, pp. 589–594, Sanya, China, November 2016.

[15] C. Yu, "Research on the application mode of mobile learning in English education based on 4G technology," in *Proceedings of the 2016 International Conference on Education, Sports, Arts and Management Engineering*, pp. 5–9, Xi'an, China, March 2016.

[16] G. Chen, X. Xie, and S. Li, "Research on complex classification algorithm of breast cancer chip based on SVM-RFE gene feature screening," *Complexity*, vol. 2020, Article ID 1342874, 12 pages, 2020.

[17] B. He, "5G acceleration will drive economic output of 10.6 trillion yuan," *Science Grand View Garden*, vol. 07, no. 13, pp. 50–55, 2019.

[18] L. Li, "Research on the integration of 5G+VR technology and ideological and political education——taking the first VR ideological and political education training room in Jiangsu as an example," *Education Modernization*, vol. 6, no. 12, pp. 21–25, 2019.

[19] M. Sharples and J. Domingue, "The blockchain and kudos: a distributed system for educational record, reputation and reward,"vol. 9891, pp. 490–496, in *Proceedings of the European Conference on Technology Enhanced Learning*, vol. 9891, Springer, Lyon, France, September 2016.

[20] M. B. Hoy, "An introduction to the b and its implications for libraries and medicine," *Medical Reference Services Quarterly*, vol. 36, no. 3, pp. 273–279, 2017.

[21] D. J. Skiba, "The pb in education and health care," *Nursing Education Perspectives*, vol. 38, no. 4, pp. 220-221, 2017.

[22] C. F. Wu and L. P. Huang, "Developing the environment of information technology education using cloud computing infrastructure," *American Journal of Applied Sciences*, vol. 8, no. 9, pp. 864–871, 2011.

[23] X. Wang, G. Han, X. Du, and J. J. P. C. Rodrigues, "Mobile cloud computing in 5G: e," *IEEE Network*, vol. 29, no. 2, pp. 4-5, 2015.

[24] L. N. Tuan, H. M. Arif, I. Amirul, D. Y. Kim, Y. J. Choi, and Y. J. Men, "Survey of promising tech-nologies for 5G networks," *Mobile Information Systems*, vol. 08, no. 12, pp. 1–25, 2016.

[25] G. Sun, C.-C. Chen, and S. Bin, "Study of cascading failure in multisubnet composite complex networks," *Symmetry Plus*, vol. 13, no. 3, p. 523, 2021.

Hindawi
Scientific Programming
Volume 2022, Article ID 1313819, 11 pages
https://doi.org/10.1155/2022/1313819

Research Article

Colour Recognition Algorithm Based on Colour Mapping Knowledge for Wooden Building Image

Siyi Jia and Heng Chen

Guangxi Arts University, Nanning 530022, China

Correspondence should be addressed to Heng Chen; 20030022@gxau.edu.cn

Received 15 November 2021; Revised 3 December 2021; Accepted 7 December 2021; Published 12 January 2022

Academic Editor: Le Sun

In the cross-media image reproduction technology, the accurate transfer and reproduction of colour between different media are an important issue in the reproduction process, and the colour mapping technology is the key technology to effectively maintain the image details and improve the level of colour reproduction. Wooden structure in the image colour and colour piece is different, the image of each colour of visual perception is not independent, and every colour in the image pixels is affected by the surrounding pixels, but in the process of image map, without thinking of the pixel space, adjacent pixels of mutual influence in particular, do not let a person particularly be satisfied with the resulting map figure. In the process of image processing by traditional colour mapping algorithm, the colour distortion caused by colour component is ignored and the block diagram of colour mapping system is constructed. With the continuous development of mapping recognition algorithms, the maximum and minimum brightness values in the image are mapped to the maximum and minimum brightness values of the display device by linear mapping algorithm according to the flow of the established recognition algorithm. By establishing the colour adjustment method of the colour mapping image, the processing effect of the mapping algorithm is analysed. The results show that the brightness deviation of the image is reduced and the colour resolution is improved by the colour brightness compensation.

1. Introduction

The 21st century is the information age. Computer technology changes with each passing day, and people's access to information, processing information, and the way of transmitting information also have a qualitative development. 83% of the information acquired by human beings comes from the visual system, and the image is the carrier of visual information, so the image plays an important role in information transmission. Image processing is to use computer to process the image information, so as to achieve the desired effect. Image processing technology can make people understand the world more objectively and accurately. In many cases, the image people get is fuzzy; through image enhancement, blurred image can be made clear. Image processing technology has achieved rapid development; all kinds of digital images are also widely used in various fields of production and life. Usually, digital image in the used process will involve the image data processing, such as image information acquisition and transmission. In these processes, the quality of the image itself must be guaranteed to meet the requirements of use [1]. Pattern recognition technology can identify the target in the image and retrieve and classify the image. Colour mapping is to solve the problem of large contrast attenuation to transform the brightness of the scene to the range that can be displayed, while maintaining the image details and colour information which is very important for the performance of the original scene. The colour mapping algorithm maps the range of the image to the range that the general display device can display. On the one hand, the mapping of high dynamic range images must map large range to display device range through compression, which will inevitably lead to the loss of details. On the other hand, it is necessary to enhance the detail information in order to keep the high light and low dark, which will lead to the contradiction between the compression of scope and the enhancement of detail, and easily cause visual defects, such as halo phenomenon and gradient inversion. Just because of these contradictions and difficulties, image colour mapping algorithm has always been the focus of image processing and display research.

With the rapid development of human science and technology, a variety of buildings with different styles, materials, and uses have emerged. So many architectural landscapes not only enrich human life but also provide a broad space for choice. However, in today's highly developed human civilization, humanistic thought has received great attention, which has invisibly increased human troubles. We explore from the perspective of image, use image processing knowledge and computer technology to get valuable data, and find the essential difference hidden behind the image. Although there are a large number of articles with similar purposes in previous studies, the analysis of various architectural images is rarely done. In the field of image processing, the analysis results of architectural images are mainly applied in image retrieval and image classification [2]. With the rapid development of database system and computer vision, basic low-level features, such as colour, line, and texture, are generally selected for image classification based on image features. In daily life, all the wonderful visual presentation comes from colour. Colour is an important language and factor in architectural design. Cleverly applying the rules of colour emotion in the design and giving full play to the implication of colour can attract extensive attention and interest of the public and easily produce various associations and imaginations. As an independent subject, chronology has its basic laws and attributes. Although colour perception varies from person to person, it has a common side. When people are opposite calorific experience and understanding mix after complex thought feeling and rich life experience, colour becomes rich human nature and emotional appeal. Architectural colour, as an important factor of urban landscape, directly affects people's visual and spiritual feelings. Different colour can produce different psychological feeling, and the association that colour place introduces and feeling concern the creation of environmental atmosphere directly. The same colour can also produce different psychological feelings in different architectural environments. Orderly architectural colour collocation not only can bring people a pleasant and unforgettable feeling but also makes the city more unique charm. Otherwise, the chaotic architectural colour can only bring colour pollution; in the long run, it will cause people's visual fatigue but also cause damage to the image of the city.

Architectural colour, as an important factor of urban landscape, directly affects people's visual and spiritual feelings. Different colour can produce different psychological experience, and the association that colour place introduces and feeling, the creation that concerns environmental atmosphere directly. The same colour can also produce different psychological feelings in different architectural environments. Orderly architectural colour collocation not only can bring people a pleasant and unforgettable feeling but also makes the city more unique charm. Otherwise, the chaotic architectural colour can only bring colour pollution; in the long run, it will cause people's visual fatigue but also cause damage to the image of the city. The information conveyed by colour plays an irreplaceable role. People no longer only stay in the visual level but begin to pay more attention to the impact of colour on people's spiritual world [3]. Under the impetus of lacquer craft development, wooden structure utensils represented by black and red eventually replaced bronze utensils and were widely used. For the purpose of protecting wood, with the development of lacquer technology and colouring technology, Chinese wood structure architecture slowly presents rich colours. Wooden structure building gradually from the original colour to a variety of colour development, from architectural colour to material colour, as well as architectural colour painting, reflect a huge difference. The main colours of traditional wooden structure buildings reflect two extremes due to different architectural functions, namely, "low-key and elegant" and "rich and colourful." Under the influence of the view of nature, Chinese traditional wooden structure buildings also reflect the characteristics of respecting nature. Wooden structure residential buildings often use local materials and make use of the colour of building materials themselves. Due to the difference of natural environment, human environment, and social background, the application of colour in Chinese traditional wooden structure architecture reflects different characteristics in different air. The traditional wooden structure architecture has experienced thousands of years of development. Under the interweaving of regional culture and national culture with different characteristics in China, the colour system of wooden structure architecture with national characteristics has been developed, and its differences are reflected in different wooden structure architecture. Wood construction is a kind of art, image colour regulation is also an important part of architectural art, and how to obtain real colour through colour regulation has become the primary problem to be solved at present.

2. Related Work

Colour mapping algorithm will use different mapping functions for different local areas of the image according to the neighbourhood information of the image pixels in the process of mapping. In the process of local colour mapping, the values of two pixels with the same gray value may be different after mapping, and the values of two pixels with different gray value may be the same after mapping. This can enhance the local contrast of the image, but there may be visual defects such as gradient inversion and halo phenomenon. Fan et al. proposed a multiscale Retinex colour mapping algorithm based on human visual model. The algorithm can achieve dynamic range compression of images by eliminating the influence of illumination to obtain the reflected images reflecting the essential features of images. However, this method will produce halo phenomenon at the high-contrast edge of the image. Colour mapping using multiscale algorithm can reduce the halo phenomenon but will not completely eliminate it [4]. Haindl and Mikes proposed a colour mapping algorithm that is processed in the gradient domain. Firstly, the gradient domain of image brightness component is calculated, and then the larger gradient in the attenuation gradient domain is worth the modified gradient domain. Finally, the compressed image is obtained by solving the Poisson equation. This method can effectively compress the dynamic range of images and avoid visual defects such as gradient inversion and halo phenomenon, but it does not consider the accuracy of human visual system. Areas that are too dark become lighter or areas that are too bright become darker. The scale selection of the local area of the algorithm has a great influence on the mapping result and is prone to halo [5]. Zheng proposed a colour mapping algorithm based on fast bilateral filtering. Fast bilateral filtering is an improvement of bilateral filtering, which greatly improves the time efficiency. Fast bilateral filtering is obtained by piecewise linear approximation and spatial downsampling in the intensity domain of bilateral filtering. Fast bilateral filter is used to divide the image into basic layer and detail layer. Dynamic range compression is performed on the basic layer, and then it is added to the detail layer for subsequent processing to obtain the image after dynamic range compression [6]. Colour mapping using bilateral filtering is easy to produce visual defects such as halo and gradient inversion. Bilateral filter which can effectively filter out image details while preserving image edges is called edge preserving filter. Colour mapping algorithms based on edge preserving filter have been developed vigorously in the following years. This algorithm first transforms the image into a brightness channel and then scales it with an edge preserving filter. The filtering result of the original image is the basic layer, and the difference between the original image and the basic layer is the detail layer. The dynamic range of the base layer is compressed, and the dynamic range of the detail layer is enhanced. Finally, after combining the basic layer and detail layer, colour restoration is carried out to get the image after colour mapping.

In the colour mapping algorithm, it is necessary to maintain the spatial relationship of the image as a basic principle, that is, the details obtained by the filter must be returned to the image by certain technical means. The colour mapping algorithm based on edge preserving filter has a very good image effect. Spreitzer et al. proposed the weighted least squares filter, which is an edge-preserving filter based on the weighted least squares framework, which can extract details of any scale while preserving edges and avoid halo effect and gradient inversion [7]. Masaoka et al. proposed the guidance filter, which processes the input image through a guidance image, so that the output image is similar to the input image in general but similar to the guidance image in texture. Guided filtering can overcome the problem of gradient inversion of bilateral filtering, but image processing will have halo phenomenon [8]. Sikudova et al. proposed the 0L smoothing filter, which performs edge preservation and smoothing on the image under the constraint of the minimum norm of 0L [9]. Lee et al. proposed the local edge-preserving filter, which defined the prominent edge as a relatively large local gradient, defined the detail as the local extreme value of the image, and then calculated the filtered value through energy function operation [10]. Pytlarz et al. proposed the gradient domain guided filter, which is an edge-preserving filter based on the guided filter and combined with explicit first-order edge perception constraints. The gradient domain guided filtering can maintain the edge of the image better than the guided filtering and reduce the halo phenomenon in the image [11]. Wan et al. proposed a local colour mapping algorithm based on photographic model while proposing a global colour mapping algorithm based on average logarithmic brightness. They partitioned the dynamic range of the scene and the display device. Firstly, the dynamic range of the display device was divided into 11 regions, and then the average log value of the scene brightness was corresponding to region 5, and the dynamic range of the scene was divided into regions according to the maximum and minimum brightness values in the scene [12]. At present, there are many filtering technologies, but there is still no one to achieve a wide range of applications, so the problem that needs to be considered is how to enhance the adaptive filter, so that the filter noise elimination effect is improved and tends to be stable. The edge structure filtering technique can eliminate the noise and save the structure information of the image, which is beneficial to the subsequent processing of the image. The edge preserving filtering technique is such a filtering method that can best preserve edge and detail while removing noise.

Masaoka et al. proposed a colour mapping algorithm based on histogram, which can maintain visibility in various scenes with high dynamic range. This algorithm adds a new histogram adjustment technique on the basis of local adaptive brightness of scene. The luminance histogram is first created, and then the cumulative probability density function is calculated, which is mapped according to the maximum and minimum luminance after histogram and mapping. At the same time, the algorithm combined the human contrast sensitivity, glare, spatial sensitivity, and colour sensitivity models to make the mapped image have a better visual experience [13]. Zhang et al. proposed a global colour mapping algorithm based on mean logarithmic compression. The method first calculates the average logarithmic brightness value of the image. In practice, they find that the average pixel brightness is always mapped to 18% of the average scene display range, thus establishing the compression equation. Then the image is linearly compressed, and the dynamic range of the image is mapped to the dynamic range that can be displayed by the display device [14]. Xu et al. proposed an adaptive logarithmic colour mapping algorithm based on base number. Human eyes have a similar sensitivity to luminance changes as logarithmic function, so logarithmic mapping can achieve good results. The algorithm simulates the human eye's response to light and compresses the luminance logarithmically. The deviation energy function is used to change the logarithmic base adaptively so that the mapped image has good detail information and contrast. Meanwhile, gamma correction was used to enhance the contrast of dark areas [15]. Poppiel et al. proposed a colour mapping algorithm based on linear mapping and histogram equalization, which combined linear mapping and histogram equalization, taking into account both the pixel value of the image and the pixel distribution of the image, achieving good results.

Firstly, global histogram mapping is used to compress the dynamic range; then the image is segmented, and the local area of the image is adjusted adaptively to enhance the local contrast, so as to obtain better image quality [16]. Xu et al. proposed a colour mapping algorithm based on histogram and human visual model. The algorithm uses brightness histograms to build lookup tables for colour mapping. Firstly, the high dynamic range image is transformed into brightness channel, and then the histogram is constructed according to the threshold and intensity curve of human visual model. At the same time, in order to avoid excessive compression and excessive enhancement, the improved histogram is obtained by removing the pixels in the histogram that cannot be distinguished by HVS in consideration of the visual contribution of each pixel in the histogram. Combined histograms are obtained by weighting original histograms and improved histograms. Finally, LUT is created and the mapping process and colour restoration are carried out to obtain the corresponding low dynamic range image. Colour mapping algorithms based on histogram and human visual model are relatively simple and efficient and can produce visually pleasing colour mapping images [17]. Kim et al. proposed an image adjustment method based on Gaussian pyramid. By calculating the average difference and standard deviation of RGB images; the colour emission equation is constructed to compensate the colour and complete the colour adjustment of the image [18].

This paper will study how to extract the colour features of the building image and analyse the processing effect of the mapping algorithm by establishing the colour mapping image colour adjustment method to provide reference for the subsequent research. It overcomes the phenomenon of colour distortion caused by ignoring colour component guide in traditional colour mapping algorithm.

3. Research on Colour Mapping Knowledge Recognition Algorithm

3.1. Overview of Colour Map Recognition Algorithm. Colour mapping compresses the high dynamic range of the real world so that it can be optimally displayed on low dynamic range devices. Colour mapping is established from high dynamic range to low dynamic range, and the compressed dynamic can optimize the brightness information of the actual scene, which is displayed on the common low dynamic range equipment, giving the observer a matching observation experience. This is the essence of all colour mapping algorithms. It can be defined mathematically as follows:

$$T\colon\ L_d = T\left(L_w\right), L_d \in D, L_w \in W. \tag{1}$$

In the above formula, T represents the colour mapping operator, namely TMO; D is the set of luminance values of the display device; W is the set of luminance values of the actual scene; L_d and L_w represent the luminance values of the display device and the actual scene, respectively.

The colour mapping framework based on image detail preservation firstly uses image filtering technology to filter the input image, which is decomposed into low frequency image corresponding to image edge contour information (also known as base layer image) and high frequency image corresponding to image texture detail information (also known as detail layer image). The first mapping results are added, and the final mapping result is obtained by the second mapping of the merged image. The two-colour mapping processes in the framework all use colour mapping methods, and different algorithms can be selected according to the actual mapping effect. Figure 1 shows a block diagram of a typical colour mapping system.

Colour mapping algorithms can be divided into two types: one is spatial invariant algorithm, also known as global dynamic range compression. This algorithm applies the same transformation curve to each pixel when transforming the dynamic range of the image [19]. The transformation curve can be specified in advance or obtained according to the content of the image. Exponential transformation or logarithmic transformation are commonly used, because these two kinds of curves are more consistent with the human visual model curve. Different visual effects can be obtained according to different transformation curves. This mapping algorithm is relatively simple and efficient. Compared with traditional mapping algorithms, it uses the same transformation curve for each pixel in the image, which is actually a point processing that separates each pixel without considering the influence of the neighbourhood on the pixel. Fixed transformation curve cannot adapt to different regions of the image, resulting in a certain loss of detail, brightness, and colour of the mapped image. The other is spatial correlation algorithm, also known as local dynamic range compression algorithm. This kind of algorithm is not for a single pixel processing, but according to the pixel neighbourhood different transformation. When transforming the gray value of a point in the image, the spatial information of the point is also taken into account. Therefore, two pixels with the same value in an image may have different mapping values after mapping, and originally different pixel values may be mapped to the same value after mapping.

3.2. Identify the Flow of Algorithms. The recognition algorithm firstly transforms the high dynamic range image into luminance channel and takes logarithm and normalization for preprocessing. Then, scale decomposition process, using filter for filtering, get the basic layer and the details of the corresponding layer, using the basic layer recognition algorithm based on histogram and the method of human visual model to create dynamic range compression, both efficient and effective compression basic layer, and accord with human visual characteristic, making the compressed image contrast effect very good; it is superior to other s-shaped curves for basic layer compression. The detail layer is enhanced by S-curve processing, which not only stretches the contrast but also conforms to human visual characteristics [20]. At the same time, there is no gradient inversion, which makes the detail information of the resulting image richer. The treated basic layer and detail layer are combined

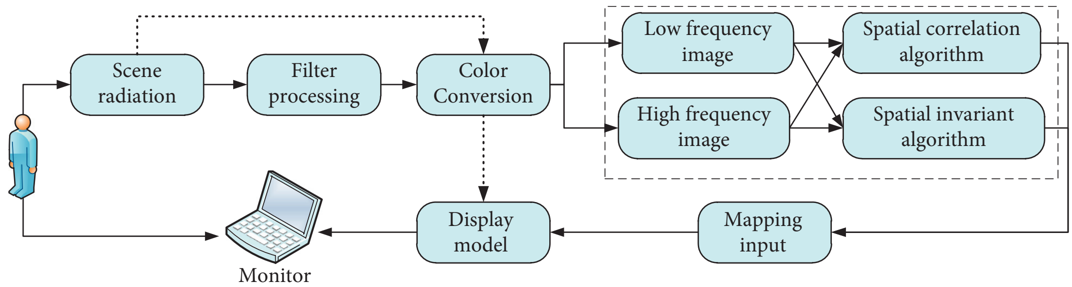

FIGURE 1: Tone mapping system framework diagram.

to obtain the treated brightness channel value. At last, after postprocessing, abnormal pixels were removed to remove noise; normalization and colour correction were carried out to obtain the low dynamic range image. The process of identifying the algorithm is shown in Figure 2.

In the colour mapping algorithm, independent dynamic range compression for R, G, and B channels can produce better colour reproduction and mapping results. The local colour mapping algorithm compresses the three channels independently, which leads to colour distortion. Therefore, the local colour mapping algorithm can effectively separate the colour information and brightness information of the image, while preserving the colour information of the image. For the preprocessing of the algorithm, we first transform it into grayscale image, then perform a preliminary logarithmic compression transformation, and finally normalize the brightness channel.

3.3. Linear Mapping Algorithm. Linear mapping is the simplest mapping method, which maps the maximum and minimum brightness values in the high dynamic image to the maximum and minimum brightness values of the display device, respectively, and the brightness values in the middle are mapped to this range according to the corresponding mapping relationship [21]. A linear transformation method is given in this paper. The transformation formula used is as follows:

$$L_d = mL_w, \tag{2}$$

$$m = \left[\frac{1.219 - L_d^{0.4}}{1.219 - L_w^{0.4}}\right]^{2.5}. \tag{3}$$

L_d and L_w indicate the brightness that can be represented by the display device and the illumination value of the actual scene, respectively.

In the implementation of this system, two linear mapping operators are compared. One is to set m in formula (2) as a constant, which is valued as 150 here, and the other is to use the following linear mapping operators:

$$\xi = \frac{\log\xi_h - \log\xi_h^{\min}}{\log\xi_h^{\max} - \log\xi_h^{\max}} \times 255. \tag{4}$$

The above mapping operator is to map all the brightness values of the actual scene to and then multiply to restore to the dynamic range of the common display device.

Linear mapping operator has a small amount of calculation, and this algorithm can achieve good results when the dynamic range of the scene is not much different from that of the display device. However, for high dynamic images, many highlights and dark scene details will be lost. In addition, this method does not consider the absolute radiation intensity of the scene at all, so it may lead to the same image mapped to the same scene under sunlight in the day and weak light at night, and the overall impression information of brightness of the scene is lost.

Because the change of logarithmic relation is very close to the pattern of human eye's response to the change of light intensity, the logarithmic relation equation can be used to compress the data of high dynamic range image to achieve a better effect. This paper proposes a logarithmic mapping relation:

$$L_d = \frac{\log(L_w - 1)}{\log(L_{w\max} - 1)}. \tag{5}$$

For each pixel, L_d is the light intensity displayed by the display device, L_w is the light intensity of the actual scene, and $L_{\max}$ is the maximum light intensity in the actual scene. This mapping ensures that no matter what the dynamic range of the actual scene is, the highest light intensity is always mapped (white) and the rest of the light intensity is smoothly mapped onto the display device. This method is good for high dynamic range images with high contrast, but it cannot reproduce very dark and very bright image scenes simultaneously. Therefore, this mapping operator is suitable for high dynamic images without extreme brightness scenes.

This paper improved the formula and proposed a new logarithm equation:

$$L_d = \frac{L_{d\max} \times 0.01}{\log(L_{w\max} - 1)} \times \frac{\log(L_w - 1)}{\log(2L_w + L_{w\max})}. \tag{6}$$

The equation is adaptive and the mapping factor varies with the brightness pairwise relationship. The basic idea is to use a user control parameter to control the shape of the mapping factor curve and the corresponding brightness range. If there is extreme brightness scene in high dynamic image, the user can adjust the appropriate control parameters according to the characteristics of the image and also get ideal results. In the above formula, $L_{w\max}$ is the maximum brightness value of the actual scene, and $L_{d\max}$ is the maximum brightness value that can be displayed by the display device and is used as the quantization parameter for display. Generally, L_w is the brightness value of the actual scene.

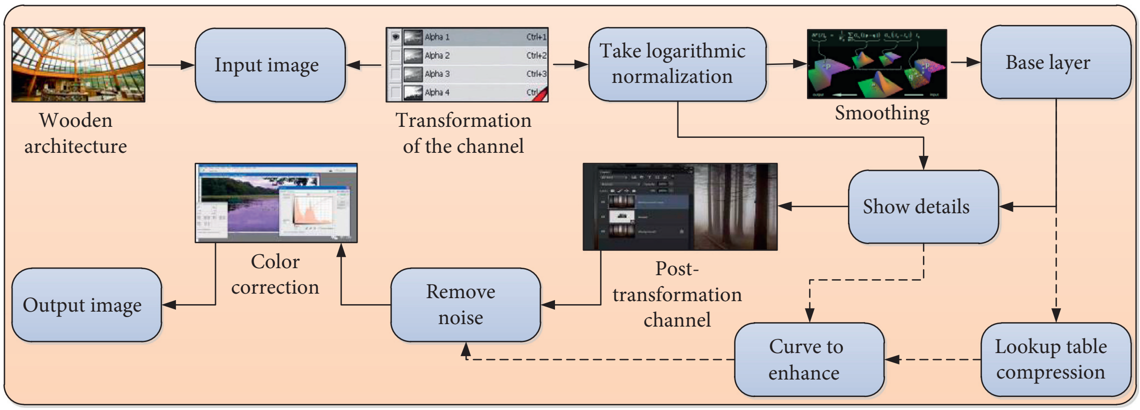

FIGURE 2: Identify the flow chart of the algorithm.

In order to enable the algorithm to automatically adjust the radix of the logarithm equation for brightness values of different pixels and make it change between 2 and 10, the algorithm adopts an adaptive logarithm radix calculation equation:

$$S(t) = t^{\log(b)/\log(0.5)}. \tag{7}$$

Here is the parameter that can be adjusted by user B, which has a significant influence on the bright area and dark area of the image. The recommended value range is 0.5–1.0.

Another point to note about this algorithm is that the data used to map highly dynamic images is done in colour space. In the algorithm, firstly, to the input of high dynamic image data from colour space conversion, for the space in the space, the channel value is the brightness of the original image; the channel into the formula (6) to calculate the value of the generation Y compressed the brightness values of high dynamic, and then brightness value data is converted to RGB colour space; you can get the final output effect.

3.4. Colour Mapping Image Colour Adjustment Method. On the basis of the image correction results, the response curves of channels R, G, and B were set, and the illuminance value of each image pixel point in the corresponding channel was obtained through the response curve [9, 10]. The gain coefficient was extracted from the illuminance value by the colour mapping algorithm, and the colour adjustment was completed through the gain parameters. The specific process is as follows. The global colour mapping algorithm is adopted to compress the illumination value of the wooden building into the gray value of the image:

$$D(E) = (D_{\max} - D_{\min}) \times \frac{\log(E_{\min} - 1)}{\log(E_{\max} - 1)}. \tag{8}$$

In the formula, E represents the illuminance value of wood-framed buildings, and D represents the Gray value of wood-framed buildings. $E_{\max}$ represents the maximum illuminance of wood structure buildings, and $E_{\min}$ represents the minimum illuminance of wood structure buildings. $D_{\max}$ represents the maximum and $D_{\min}$ the minimum of wood construction gray scale.

According to the above formula, the average illuminance can be obtained as

$$\overline{E} = \exp\left[\frac{1}{N}\sum_{x,y}\log - E(x, y)\right], \tag{9}$$

where N represents the total number of pixel points in the image and E (x, y) represents the illuminance value of a certain point.

Determine the median value as shown in

$$k = A \times B^{[\log E_{\max} - \log E]}, \tag{10}$$

where the value of k is [0,1] and A and B represent constants.

The offset at the solution of formula (10) is calculated by Newton iteration method:

$$k = \frac{\log(\overline{E} - \tau) - \log(E_{\min} - \tau)}{\log(\overline{E}_{\max} - \tau) - \log(E_{\min} - \tau)}, \tag{11}$$

where τ represents the offset. Colour level mapping is performed by offsets of retro architectural images:

$$DR = DR_{\max} - DR_{\min}. \tag{12}$$

Extract the level mapping image of the colour channel:

$$k_r = \frac{\sum_{i=1}^{M}\sum_{j=1}^{N} R_{ij} + \sum_{i=1}^{M}\sum_{j=1}^{N} G_{ij} + \sum_{i=1}^{M}\sum_{j=1}^{N} B_{ij}}{\sum_{i=1}^{M}\sum_{j=1}^{N} R_{ij}}. \tag{13}$$

Use gain coefficient to adjust colour:

$$\begin{cases} DR' = DR \times k_r, \\ DG' = DG \times k_g, \\ DB' = DB \times k_b. \end{cases} \tag{14}$$

4. Research and Analysis of Colour Mapping Knowledge Recognition Algorithm for Wooden Building Image

4.1. Image Brightness Deviation. In order to prove the effectiveness of the proposed method of automatic colour adjustment of wooden building image based on colour

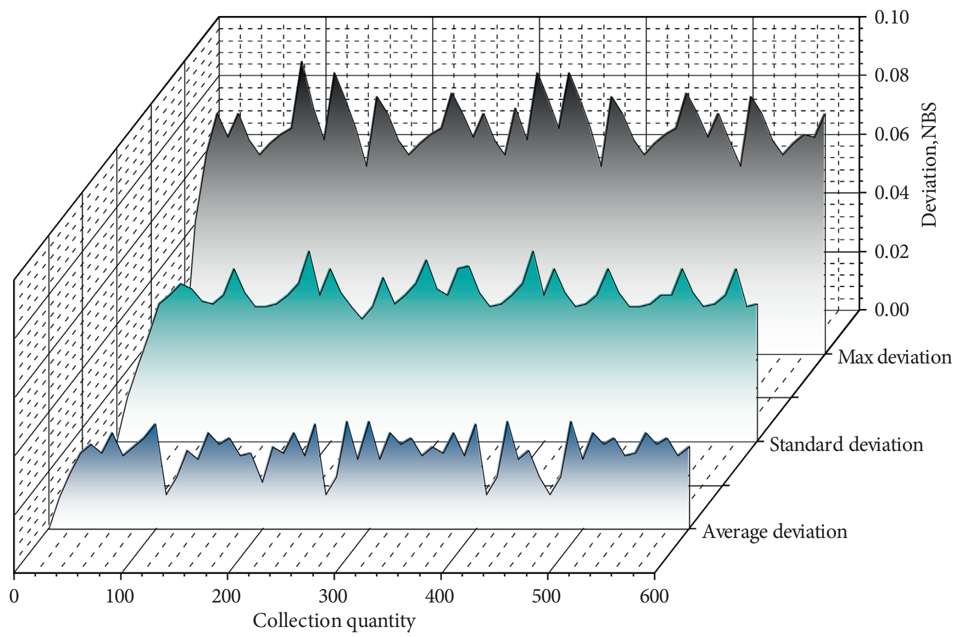

Figure 3: Result diagram of automatic colour adjustment method for wooden building image.

mapping algorithm, a simulation is needed. The simulation environment is as follows. The platform of MATLAB R2015b is used, and the experimental data is OTB-50 standard dataset. The brightness deviation of the proposed colour mapping algorithm was compared with that of the gradient region segmentation method. The results of automatic colour adjustment method for wood-frame building image based on colour mapping algorithm are shown in Figure 3. The result of colour regulation method based on gradient region segmentation is shown in Figure 4.

It can be seen from the figure that the brightness deviation of the image colour adjustment method based on the colour mapping algorithm is relatively low. When the number of experiments is 30, the brightness deviation of the proposed method is 0.29 cd/m^2, and that of the colour adjustment method based on the gradient region segmentation is 0.78 cd/m^2. The proposed method compensates the brightness of the colour. The image brightness deviation is reduced and the colour resolution is improved. The colour adjustment method based on colour mapping is obviously superior to the colour adjustment method based on gradient region segmentation in terms of average and maximum chromatic aberration. Image solving colour correction function reduces colour distortion so that the original image retains the structural characteristics and improves the colour node effect. Through intuitive visual experience and integrated image details, the algorithm in this chapter has well expanded the dynamic range of the image, made the image have more details, and performed well in colour without colour deviation.

4.2. Colour Adjustment Time. A large number of experiments were conducted on 40 wood-framed building images, and the traditional colour adjustment method and colour mapping recognition algorithm were used to conduct the colour adjustment time. The statistical results are shown in Figure 5.

As can be seen from the figure, the average time of the proposed image colour adjustment method based on colour mapping algorithm is 3.25 s, the shortest colour adjustment time is 2.98 s, and the longest colour adjustment time is 3.34 s. Compared with traditional algorithms, the proposed method can effectively reduce the time of colour adjustment by correcting the image colour.

4.3. Peak Signal-to-Noise Ratio. In the process of system testing, 40 wooden building images were selected for a large number of experiments, and several building colour template coefficients were obtained. After the relevant template is obtained, the colour component can be encoded, and the obtained colour component can be inverted to obtain the reconstructed image, which is matched with each feature region, and the peak signal-to-noise ratio can be calculated. The calculation formula is as follows:

$$P = \lg \frac{255^2}{\delta}, \tag{15}$$

where δ represents the mean square error of the original image. The sample pattern was analysed and its peak signal-to-noise ratio was compared. The analysis results of the statistical system are shown in Figure 6.

It can be seen from the figure that the results of peak SNR analysed by traditional system and this paper differ greatly in different feature areas of wood-frame building images, and the fundamental reason lies in the coding elements corresponding to the correlation template coefficients. In the traditional system, there is no step to encode the image, which leads to high channel pressure. The mean square error of the encoded region and the original region becomes

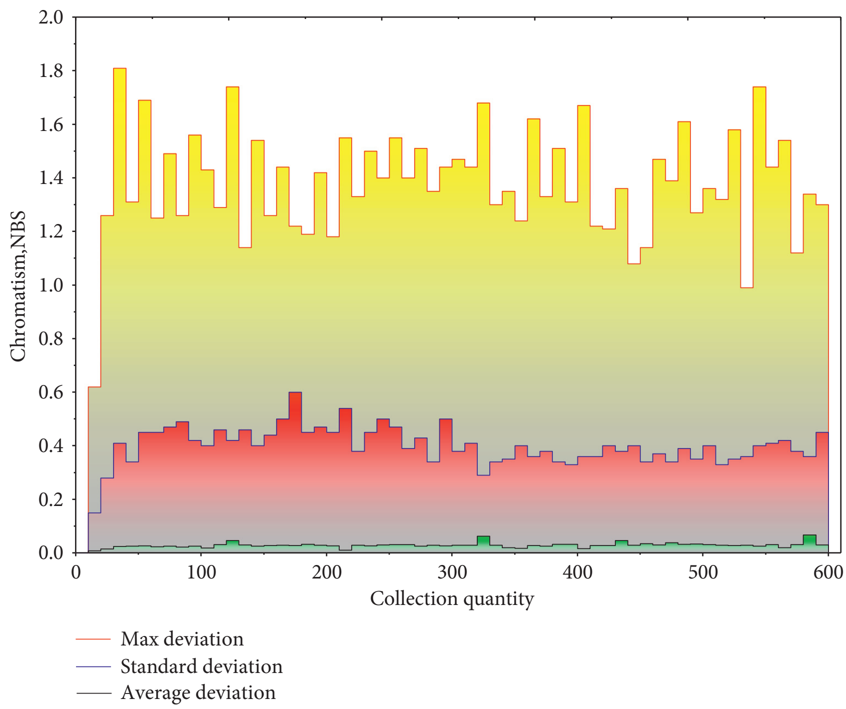

Figure 4: Results of colour regulation method based on gradient region segmentation.

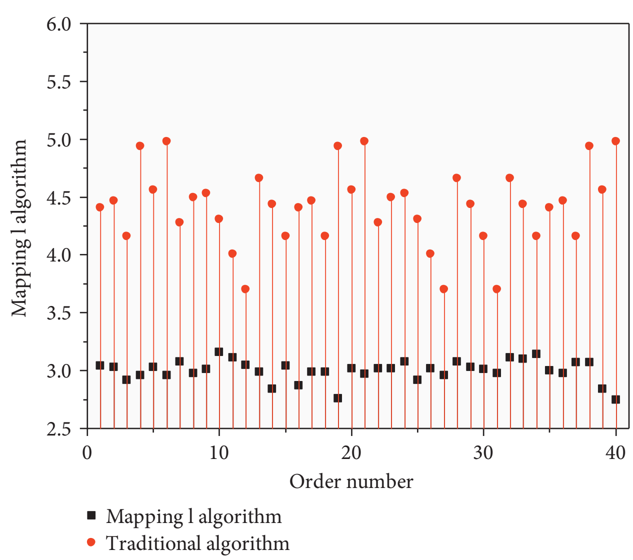

Figure 5: Results of colour regulation method based on gradient region segmentation.

smaller, and the signal-to-noise ratio after coding will be higher, and the mining degree of visualization of colour attribute information of wooden buildings will be higher.

4.4. Quality Factor. In order to more objectively compare the application effect of the traditional algorithm with that of the algorithm in this paper, 10 classical wood-framed building pictures are used for the experiment, and the results obtained are shown in Figure 7.

As can be seen from the figure, the average value of the obtained images is the highest, indicating that the image quality after the algorithm mapping is the best. The time complexity of guided filtering is low, but some images after mapping have halo phenomenon. On the basis of guided filtering, filtering can better maintain the image edge and reduce the halo phenomenon. The efficiency of the mapping algorithm is improved by 50%, especially the efficiency of the large image. The recognition algorithm can effectively maintain the details of the image, have good brightness and

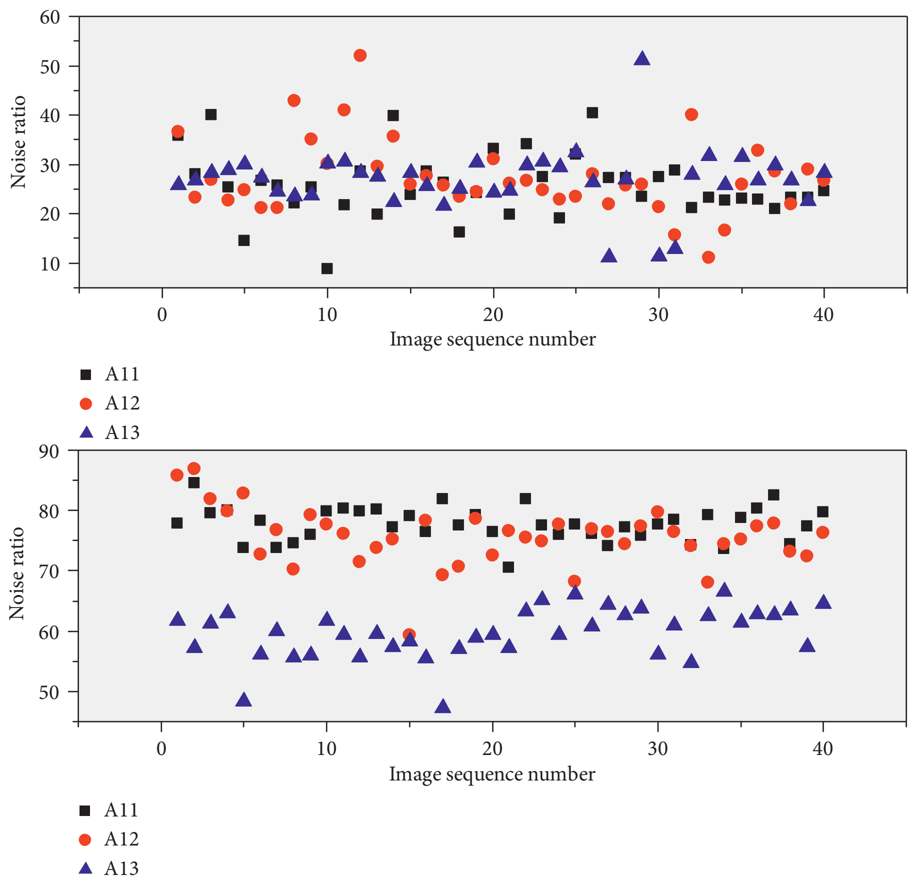

Figure 6: Peak signal to noise ratio statistical analysis result diagram.

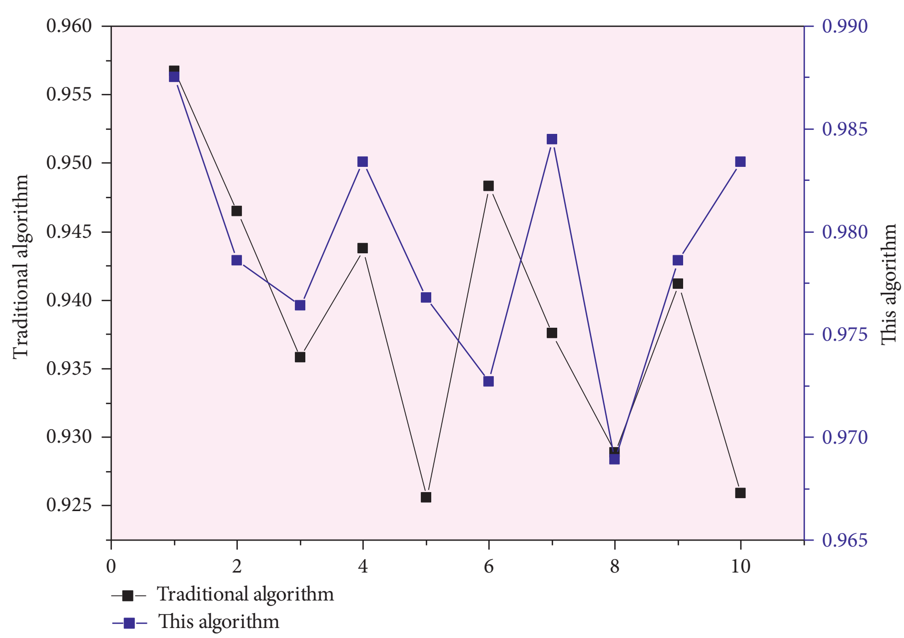

Figure 7: Comparison diagram of application effect between traditional algorithm and this algorithm.

contrast, display the information of the image highlighting and low dark at the same time, and obtain good image quality.

5. Conclusion

With the update and iteration of multimedia equipment, more and more image capture equipment can capture the high dynamic range of natural scenes more accurately. Colour mapping algorithm emerges as The Times require. Colour mapping is a key technology in cross-media image replication. Images store nearly real scene information with rich details and can truly represent various rich information in the natural world. In this paper, the hue mapping algorithm is implemented to enable the mapped image to be displayed on the monitor. In the process of colour mapping, we should try to keep more details, enhance the information with small contrast, keep the corresponding cooler information, and avoid visual defects such as halo. Through the analysis of the tone-mapping algorithm for wooden building image, the effectiveness of the algorithm is verified by subjective and objective experiments. The existing image colour mapping algorithm is studied in detail from the realization principle and application effect of the algorithm. By using the method of colour mapping image colour adjustment, the time of colour adjustment can be reduced effectively. The efficiency of the mapping algorithm is improved by 50%, especially the efficiency of the large image. The recognition algorithm can effectively maintain the details of the image, compared with the traditional algorithm which has better brightness and contrast, while displaying the image highlighting and low dark information, and obtain good image quality. Compared with traditional mapping, algorithm is improved and achieved great success, but the colour mapping algorithm remains a technical problem; how to maintain the effect of improving the efficiency of the algorithm, how to enlarge the scope of the same kind of algorithm, and making it in different brightness of the image can produce good effect, where it is also needed to follow up on constant innovation and improvement.

Data Availability

The labeled dataset used to support the findings of this study is available from the corresponding author upon request.

Conflicts of Interest

The authors declare that there are no conflicts of interest.

Acknowledgments

This study was sponsored by Guangxi Arts University.

References

[1] M. Arashpour, T. Ngo, and H. Li, “Scene understanding in construction and buildings using image processing methods: a comprehensive review and a case study,” *Journal of Building Engineering*, vol. 33, Article ID 101672, 2021.

[2] M. Alam, D. Toslak, J. I. Lim, and X. Yao, “Color fundus image guided artery-vein differentiation in optical coherence tomography angiography,” *Investigative Opthalmology & Visual Science*, vol. 59, no. 12, pp. 4953–4962, 2018.

[3] C. Liu, S. Shirowzhan, S. M. E. Sepasgozar, and A. Kaboli, “Evaluation of classical operators and fuzzy logic algorithms for edge detection of panels at exterior cladding of buildings,” *Buildings*, vol. 9, no. 2, p. 40, 2019.

[4] L. Fan, L. Chen, and C. Zhang, “Collaborative three-dimensional completion of color and depth in a specified area with superpixels,” *IEEE Transactions on Industrial Electronics*, vol. 66, no. 8, pp. 6260–6269, 2018.

[5] M. Haindl and S. Mikeš, “A competition in unsupervised color image segmentation,” *Pattern Recognition*, vol. 57, pp. 136–151, 2016.

[6] D. Zheng, “A new method for automatic separation of fabric color,” *Textile Research Journal*, vol. 85, no. 14, pp. 1520–1538, 2015.

[7] G. Spreitzer, J. Tunnicliffe, and H. Friedrich, “Large wood (LW) 3D accumulation mapping and assessment using structure from Motion photogrammetry in the laboratory,” *Journal of Hydrology*, vol. 581, Article ID 124430, 2020.

[8] K. Masaoka, Y. Kusakabe, T. Yamashita, Y. Nishida, T. Ikeda, and M. Sugawara, “Algorithm design for gamut mapping from UHDTV to HDTV,” *Journal of Display Technology*, vol. 12, no. 7, pp. 760–769, 2016.

[9] E. Sikudova, T. Pouli, and A. Artusi, “A gamut-mapping framework for color-accurate reproduction of HDR images,” *IEEE computer graphics and applications*, vol. 36, no. 4, pp. 78–90, 2015.

[10] D. Dohyoung Lee and K. N. Plataniotis, “Towards a full-reference quality assessment for color images using directional statistics,” *IEEE Transactions on Image Processing*, vol. 24, no. 11, pp. 3950–3965, 2015.

[11] J. Pytlarz, K. Thurston, D. Brooks, P. Boon, and R. Atkins, “Realtime cross-mapping of high dynamic range images,” *SMPTE Motion Imaging Journal*, vol. 126, no. 3, pp. 37–44, 2017.

[12] Y. Wan, Y. Cao, C. Chen et al., “Active phase error suppression for color phase-shifting fringe projection based on hue pre-correction,” *Optics & Laser Technology*, vol. 118, pp. 102–108, 2019.

[13] K. Masaoka, T. Yamashita, Y. Nishida, and M. Sugawara, “Color management for wide-color-gamut UHDTV production,” *SMPTE Motion Imaging Journal*, vol. 124, no. 3, pp. 19–27, 2015.

[14] T. Zhang, H.-M. Hu, and B. Li, “A naturalness preserved fast dehazing algorithm using HSV color space,” *IEEE Access*, vol. 6, Article ID 10644, 2018.

[15] L. Xu, B. Zhao, and M. R. Luo, “Color gamut mapping between small and large color gamuts: part II gamut extension,” *Optics Express*, vol. 26, no. 13, Article ID 17335, 2018.

[16] R. R. Poppiel, M. P. C. Lacerda, R. Rizzo et al., “Soil color and mineralogy mapping using proximal and remote sensing in midwest Brazil,” *Remote Sensing*, vol. 12, no. 7, p. 1197, 2020.

[17] L. Xu, B. Zhao, and M. R. Luo, “Colour gamut mapping between small and large colour gamuts: Part I gamut compression,” *Optics Express*, vol. 26, no. 9, Article ID 11481, 2018.

[18] S. Kim and D. S. Han, “Real time traffic light detection algorithm based on color map and multilayer HOG-SVM,” *Journal of Broadcast Engineering*, vol. 22, no. 1, pp. 62–69, 2017.

[19] Y. Wan, Y. Cao, C. Chen, G. Fu, Y. Wang, and C. Li, “Single-shot real-time three dimensional measurement based on hue-

height mapping," *Optics Communications*, vol. 416, pp. 10–18, 2018.

[20] T. H. Khan, S. K. Mohammed, and M. S. Imtiaz, "Color reproduction and processing algorithm based on real-time mapping for endoscopic images," *SpringerPlus*, vol. 5, no. 1, pp. 1–16, 2016.

[21] B. K. Kim, R. H. Park, and S. Chang, "Tone mapping with contrast preservation and lightness correction in high dynamic range imaging," *Signal, Image and Video Processing*, vol. 10, no. 8, pp. 1425–1432, 2016.

Hindawi
Scientific Programming
Volume 2022, Article ID 5011804, 10 pages
https://doi.org/10.1155/2022/5011804

Research Article

A Cognitive Diagnosis Method in Adaptive Learning System Based on Preconceptions

Jue Wang [1] and Kaihua Liang [2,3]

[1]School of Foreign Languages, Northeast Normal University, Changchun, Jilin 130024, China
[2]School of Education, Shaanxi Normal University, Xi'an, Shaanxi 710062, China
[3]Ordos Educational Technology Center, Ordos, Inner Mongolia 017010, China

Correspondence should be addressed to Kaihua Liang; liangkaihua@snnu.edu.cn

Received 28 October 2021; Revised 6 December 2021; Accepted 14 December 2021; Published 10 January 2022

Academic Editor: Hai Dong

One advantage of an adaptive learning system is the ability to personalize learning to the needs of individual users. Realizing this personalization requires first a precise diagnosis of individual users' relevant attributes and characteristics and the provision of adaptability-enabling resources and pathways for feedback. In this paper, a preconcept system is constructed to diagnose users' cognitive status of specific learning content, including learning progress, specific preconcept viewpoint, preconcept source, and learning disability. The "Force and Movement" topic from junior high school physics is used as a case study to describe the method for constructing a preconception system. Based on the preconception system, a method and application process for diagnosing user cognition is introduced. This diagnosis method is used in three ways: firstly, as a diagnostic dimension for an adaptive learning system, improving the ability of highly-adaptive learning systems to support learning activities, such as through visualization of the cognition states of students; secondly, for an attribution analysis of preconceptions to provide a basis for adaptive learning organizations; and finally, for predicting the obstacles users may face in the learning process, in order to provide a basis for adaptive learning pathways.

1. Introducing the Problem

Diagnosing user attributes and providing appropriate feedback based on these results is fundamental to realizing personalized learning support functions in data-driven learning systems. Traditional cognitive diagnostic methods utilize discrete representation methods, such as "mastered/not mastered" to express a learner's cognitive status in relation to pieces of knowledge, and then use this data as a foundation for estimating the user's skill or ability level. This approach to diagnosis inevitably weakens diagnostic precision; the learning outcomes from a data-driven environment will decline correspondingly.

A few issues inhibit the effectiveness of the traditional approach. One is that this type of measurement does not accurately reflect the user's cognitive patterns. The learning process cannot be reduced simply to "yes or no." This discrete descriptive method ignores the actual cognitive processes of the user as well as the problems the user needs to resolve in the learning process. From the perspective of cognitive development patterns, the process of user gaining new knowledge is in fact a process of conceptual transformation. Reductive quantifiable diagnostic results do not capture why a user has not yet grasped an aspect of knowledge, meaning that the system cannot provide precise adaptive feedback. Second, in terms of methodology, this approach represents a "qualitative-quantitative-qualitative" approach. As such, information loss during transmission is inevitable, reducing the accuracy of diagnosis. Reduced accuracy of the diagnosis system means that the quality of feedback provided, including visualization of the user's knowledge and skills, will be reduced as the effectiveness of adaptive support mechanisms built on diagnostic results is reduced. Third, in terms of practical pedagogy, conducting transformative instruction based on a single preconceptual perspective leads to poor learning results. Since users have their own naïve theory framework [1–8] to explain everyday life, naïve concepts are not separated from one another in their minds. If transformation is applied to only one conceptual point in the framework, cognitive dissonance will emerge between the conceptual point and the overall framework. When users experience cognitive dissonance, they tend to adjust the concept to be consistent with the overall naïve theory framework, rendering prior conceptual transformation useless. Another possibility is that users will classify concepts according to different application scenarios, so that the same knowledge points can sometimes only be used to correctly solve related problems. Effective pedagogy needs not only the conceptual transformation of individual preconceptions, but also the conceptual transformation of preconceptions related to the relevant naïve theoretical framework, so as to attribute them from the perspective of specific concepts.

Based on the three issues described above, the authors of this paper analyze users' true cognitive processes based on preconception research, designing a cognitive diagnosis method for data-driven learning environments. The method described enhances the precision of system diagnosis to meet the needs of users in learning and teaching activities. The topic of "Force and Movement" from junior high school physics is used as a topic to explain this diagnostic method.

2. Preconception Definition Differentiation and Analysis

The concept of "preconception" can be traced back to Piaget (*The Child's Conception of the World,* 1929) and Ausubel (*Meaningful Learning Theory*, 1960s). These scholars suggested that, prior to formal learning, users produce their own concepts, perspectives, and ideas regarding occurrences in life. These prior knowledge structures play an important role in later learning. From the 1970s, research on the conceptual transformation from preconception to scientific conception started to emerge [9–13]. Based on four different perspectives, researchers emphasized the following: this conceptual transformation begins prior to formal learning; it is different from scientific concepts; and it has its origins in everyday life. Research was primarily conducted with children of ages 5–17. Details are shown in Table 1.

This paper focuses on diagnosing the cognitive states of users. The authors believe that using the term "preconception" to describe the characteristics of users is most suitable. For the purposes of this paper, the term is characterized as follows:

(1) *Preconceptions Occur in Daily Life and Typically Deviate from Scientific Concepts.* For a user, engaging in learning involves a process of transforming preconceptions into scientific conceptions. In other words, learning involves transforming daily experience into standard scientific knowledge and abstract symbols.

(2) *Differences between Eastern and Western Definitions of "Preconception" May Lead to Deviations in Understanding.* Regarding the English term "preconception," the root of the word "conception" has an objective meaning, but is also associated with subjective scholarly perspectives and ideas.

(3) *The Difficulty of Transforming Preconceptions into Scientific Conceptions Is Higher Due to the Cognitive Patterns of Users.* Previously, the author investigated 185 students from two schools in J province. The topics considered include thermodynamics, electricity, and force. It is found that prejudice constitutes an obvious obstacle to learning in the process of physics learning. The author also finds that bias still exists even after classroom teaching. For example, question 3 in the survey requires students to compare the brightness of two small bulbs in a closed series circuit. Students show two classic biased views in their answers. One bias is that students believe that a current, similar to water flow, will lose strength when reaching an obstacle, resulting in a brighter bulb closer to the positive pole. Another view is that the second bulb will collect the power supply and the current from the first bulb, which means that the second bulb will receive more current than the first bulb, so it will be brighter. See Table 2.

(4) *The "Pre" in Preconception Does Not Refer to the Time Dimension, but Rather the User's Current Conceptual Processing and the State of the User prior to Learning Scientific Concepts.* Some preconceptions appear in the learning process, such as when instructors explain "concepts in electrical currents" using water currents as an analogy to aid student understanding. In such a scenario, preconceptions will emerge when students consider problems related to electrical currents. At the same time, acceptance of cognitive approaches similar to using "water currents analogous to electrical currents" to learn new scientific concepts is also a preconception.

Only by constructing a preconception system and establishing the connections between preconceptions can preconceptions be properly attributed and predicted, enabling personalized learning. Below, the authors will describe the methodology used and a case study for the construction of a preconception system using the topic of "Force and Movement."

3. Process and Methodology for Constructing a Preconception System

Constructing a system requires analyzing the components of the system and then exploring the connections between those components. The specific preconception perspectives of users are the components of preconception systems, while the connections between those preconception perspectives comprise the structure of preconception systems.

Table 1: Four perspectives on defining preconception.

Terminology	Perspective
Preconception; preunderstanding; precognitive structure	Emphasis on origins prior to formal learning
Alternative; conceptions\frameworks; misconception	Emphasis on differentiation from scientific concepts
Nature conceptions; naive conceptions	Emphasis on origins in everyday life
Children's; conceptions\ideas\knowledge	Research focuses on subjects in childhood, ages 5–17

Table 2: Comparison of common incorrect preconceptions before and after learning.

Common incorrect preconceptions	Eight grade (prelearning)		Ninth grade (postlearning)	
The first bulb the current passes through will be brighter	Number of respondents selecting (individuals)	Percentage of students in grade (%)	Number of respondents selecting (individuals)	Percentage of students in grade (%)
	29	26.66	9	12.68
The bulb receiving the current twice will be brighter; the circuits and currents flow into each other	Number of respondents selecting	Percentage of students in grade	Number of respondents selecting	Percentage of students in grade
	12	10.62	1	1.41

3.1. Methods for Extracting Preconception System Components. Preconceptions emerge from the experiences and perceptual structures of users, representing their understanding, perspectives, and explanations regarding scientific knowledge. Ultimately, preconceptions represent the mapping of objective knowledge by subjective individuals. Extracting the preconception perspectives of users requires diagnosing how users understand scientific knowledge and explain scientific phenomena when learning specific content. Common methodologies include interviews, the think-aloud method, and two-stage diagnostic surveys. As this study required the calculation and analysis of a large sample set, a two-stage objective diagnostic survey was used.

The two-stage diagnostic questionnaire is an effective method for diagnosing the preconceptions of respondents. Unlike regular questionnaires, two-stage questionnaires include two parts in each question. The first part asks respondents to make a judgment on the question; the second part asks them to explain the reasoning behind their judgment. Using a two-stage diagnostic questionnaire enables researchers to obtain the users' perspectives on explanations of the questions. Developing a two-stage objective diagnostic questionnaire enables the diagnosis of large numbers of users, while simplifying data compilation and analysis [14–19].

3.2. Method for Examining Preconception System Structure. Understanding scientific content is a concept-level reason for the emergence of preconception viewpoints. Explaining scientific phenomena involves the application of concepts in understanding phenomena; in other words, it is the "dependent" variable. As such, preconception systems are necessarily hierarchical structures.

As a causal relationship exists between the comprehension layer of the concepts and cognitive phenomena, in situations with sufficient sample sizes, the significant correlations between preconception errors in the understanding of scientific concepts and other preconceptions will be more numerous than those among other preconceptions. Accordingly, a hierarchical structure for preconceptions can be constructed. Bayesian probability can be used to derive correlations between various preconceptions and to map internal relationships within the preconception system.

3.3. Process of Constructing a Preconception System. Preconception systems are an important component of the user cognition diagnosis method introduced in this paper. Users' preconception systems must be constructed based on specific learning content based on the following stages: steps and methods. The construction process can be divided into three stages: preconception perspective extraction; preconception hierarchy division; and preconception correlation calculation. The process, stages, and methods for constructing a preconception system are described below using the "force and movement" unit from junior high school as a case study.

3.3.1. Preconception Perspective Extraction. Extracting the preconception viewpoints of students on specific learning content is the most fundamental and important stage for constructing a preconception system. The objective is to extract users' preconceptions of specific knowledge points, in other words specific preconception viewpoints, using a two-stage diagnostic questionnaire. This stage consists of four steps: analysis of knowledge points for the tested content; design and distribution of a two-stage subjective diagnostic questionnaire; analysis and summary of the two-stage subjective diagnostic questionnaire; and analysis of specific preconception viewpoints.

(1) Analyzing Knowledge Points for the Tested Content. Using People's Education Publishing curriculum, the authors selected knowledge points from the "Force and Movement" unit for analysis [18]. Concepts in "Force and Movement" include movement [20], force, Newton's First Law of Motion, gravity, and friction. Knowledge points were further divided into specific content and coded as Movement–M, Force–F, Newton's First Law of Motion–N, Gravity–G,

Friction–C. Specific knowledge points were arranged in order, e.g., F1—definitions of the three elements of force and F2—definitions of interactions among forces.

(2) Two-Stage Subjective Diagnostic Questionnaire

(1) *Questionnaire Design.*

Preconceived information about the subject content was gathered through a review of relevant literature and interviews with faculty and students. Then this information was used to design subjective questions. Then the questions are compared with the knowledge points of the test to ensure that the questions designed cover all the knowledge points of the test content. At this stage, all questions in the questionnaire are subjective and open-ended.

(2) *Questionnaire Testing.*

The questionnaire was then distributed for testing. Teachers and students provided feedback for editing. The most common issues were that question phrasing was unclear, that questions and answers lacked tight logic, and that diagrams were incomprehensible.

(3) *Formal Survey Testing.*

The updated edition of the survey was distributed and retrieved in person.

(3) Analysis and Summary of the Two-Stage Subjective Diagnostic Survey

(1) *Questionnaire Analysis.*

Qualitative and quantitative analysis were conducted for the retrieved surveys. The main answers for each question were summarized, and students were interviewed to identify the reasoning behind their answers. The results of summary and analysis are shown in Table 3 below, ensuring that all possible responses are included.

(2) *Questionnaire Summary.*

(a) The results of some questions were not comprehensive enough; additional questions need to be added to those knowledge points to obtain more detailed conclusions

(b) The answers of respondents to these two questions will form the backbone of objective questionnaire answers in the next step

(c) New preconception viewpoints were obtained through the summary, such as respondents believing that a taller object is subject to greater gravity

(d) Design and distribution of the two-stage objective diagnostic questionnaire

(3) Questionnaire Design

The analysis results of subjective questionnaires are used as the basis for the answer choices of objective questions. The second part of each question contains an open-ended option that allows students to provide new answers or explanations.

Questions in subjective questionnaires with poor measurement results were redesigned or decomposed into new detailed questions.

(4) Questionnaire Distribution

Questionnaires were distributed and then retrieved in person.

(4) Preconception Viewpoint Analysis. As shown in Table 4, respondents' answers represent their judgment of the questions as well as their reasons for making those judgments, i.e., preconception viewpoints in their minds. Each answer combination was analyzed. A total of 41 specific preconception viewpoints (L1-L41) from the "Force and Movement" unit are summarized below.

Specific preconceptual views are associated with corresponding knowledge points. For example, for the interviewee who chose A for the two subquestions in question 1, A indicates that the interviewee has A preconceived view L12: inanimate objects cannot apply force. This preconceived view is the knowledge point related to Newton's first law of knowledge, indicating that interviewees have a wrong understanding of F2's fourth preconceived concrete content "F2—the definition of the three elements of force." Preconceptions and how they relate to knowledge points are shown in Figure 1.

3.3.2. Dividing the Preconception Hierarchy into Stages. Dividing the preconception hierarchy into stages primarily involves using sample data to establish connections between the various preconception viewpoints and to build the preconception system structure. There are different connections between various knowledge content and preconceptions, potentially leading to different structures. Defining the structure of preconcept is the basis of designing preconcept attribution algorithm.

(1) Obtaining Connections between Preconception Viewpoints through Sample Data. Regression analysis for the various preconception viewpoints related to the "force and movement" topic was conducted using SPSS software, yielding significant correlations for preconception viewpoints. The table below lists significant correlations for all preconception viewpoints, represented by constructing vectors. For example, specific preconception viewpoint L1 is significantly correlated with L2, L4, L12, and L33, establishing correlation vector R1 (L1, L2, L4, L12, L33), as shown in Table 5. It can be seen that significant correlation among some preconception viewpoints is significantly higher than the average.

(2) Analyzing Reasons for Data Results and Establishing a Preconception System Structure. A number of commonalities and attributes can be observed from preconception viewpoints with a greater number of significant correlations amongst themselves. These preconception viewpoints show that students waver in their understanding of scientific concepts; these misunderstandings are the root cause of preconceptions. The other preconception

Table 3: Example subjective questionnaire analysis.

Question	Summary and analysis
As shown in the figure below, if an additional book is placed on top of the table and the books from the previous question, does the book at the top exert pressure on the table top?	Summary of answers *A*. Exerts pressure; *B*. Does not exert pressure; *C*. Unknown *A*. Since there are two books on the table, the book on top exerts pressure on the table through the book below it *B*. Since every book exerts pressure, the additional book exerts pressure on the table *C*. Since the book on top has no contact with the table, it does not exert pressure on the table *D*. Since the book on top is not heavy enough, it does not exert pressure on the table

Table 4: Answer options from objective questionnaire and corresponding specific preconception viewpoints.

Question	Analysis	Associated knowledge point
	BC—correct answer	
	Aa—L12: lifeless objects cannot exert force	F2(4)
2	AB—L8: incorrect definition of pressure	F2(3)
	AD—L10: incorrect understanding of force, lacking understanding of how to define size of force	F2(1)
	CD—L10; incorrect understanding of force, lacking understanding of how to define size of force	F2(1)

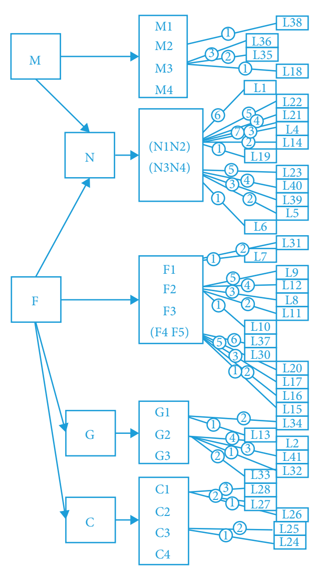

Figure 1: Diagram depicting correspondence between preconceptions and knowledge points.

Table 5: List of significant correlations.

Specific preconception viewpoint	Preconception viewpoints with significant correlation	Correlation vector
L1	L2, L4, L12, L33	R1
L2	L1, L7	R2
L3	L9, L19, L22, L30, L32, L35, L38	R3
. . .		. . .

viewpoints represent the preconceptions of users in explaining specific physical phenomena. At the same time, preconceptual views that can be analyzed can be divided into two levels. The top layer is the ontology layer, which refers to the user's preconceptions about the specific content of scientific concepts, which may be because the user has not yet learned the scientific concepts or has difficulty remembering or understanding them. The bottom layer is the cognition level, referring to users' preconceptions in understanding questions and understanding phenomena, which can arise for many different reasons. See Table 6 below for specifics.

It should be pointed out that preconceptions also exist in mathematics, chemistry, and biology. Some preconceptions therein also necessarily deal with concept ontology and application of concept ontology. As these fields differ in their knowledge content and attributes, however, they will exhibit different correlations and hierarchical structures.

3.3.3. Calculation of Preconception Correlation. Calculation of preconception correlation was conducted using SPSS analysis of sample data to obtain the correlation coefficients for preconception viewpoints with significant correlation, thereby realizing the attribution and prediction functions of this diagnosis method.

As can be seen from Table 5, there is a significant correlation between some preconceptions. Therefore, statistical methods can be used to calculate correlation coefficients of preconcepts with significant correlation using Bayesian probability formulas.

The formula for Bayesian probability is as follows:

$$P(AB) = P(B) * P(A|B) = P(A) * P(B|A). \tag{1}$$

In this formula, P(AB) is the joint probability of event AB; $P(A)$ is the probability of event A; $P(B)$ is the probability of event B; P(A|B) represents conditional probability, indicating the probability A under conditions of B; and P(B|A) represents conditional probability, indicating the probability of B under conditions of A.

It can be seen that, under conditions of sufficient samples,

$$\begin{aligned} P'(LxiLxj) &\approx P(LxiLxj) \\ P'(Lxi) &\approx P(Lxi) \\ P'(Lxj) &\approx P(Lxj) \end{aligned} . \tag{2}$$

Therein, P' is the sampling probability $\{Lxi, Lxj \in S(o) \cup S(f),\ 1 \le xi \le 41,\ 1 \le xj \le 41\}$.

When $Lxi, Lxj \in Si$, the two preconception viewpoints are significantly correlated:

$$\begin{aligned} P(Lxi|Lxj) &= \frac{P'(LxiLxj)}{P'(Lxj)}, \\ P(Lxj|Lxi) &= \frac{P'(LxiLxj)}{P'(Lxi)}. \end{aligned} \tag{3}$$

Therein, the correlation coefficient of Lxi and $'(LxiLxj)$ can be observed. The Bayesian probability function can be used to predict other preconception viewpoints and to guide the adjustment of pedagogical strategies.

In summary, by conducting statistical analysis and calculation of preconception viewpoints, a preconception system with significant correlations between preconceptions, consisting of specific preconception viewpoints, can be made and an ontology level and cognition level can be constructed.

4. Method for Conducting Cognition Diagnosis for Users Using Preconception System

In a quantified learning system, the preconception system can be used to describe the preconception states and cognitive states of users, enabling attribution and prediction of learning obstacles. This information also provides a basis for system feedback and improvement of pedagogical quality. The algorithms are described as follows.

4.1. Preconception Attribution Algorithms. Attributing cause to preconceptions involves two dimensions: first, preconception viewpoints generated by errors in understanding scientific concept ontologies; second, preconception viewpoints generated due to application of preconceptions, rather than scientific concepts in explaining scientific phenomena.

4.1.1. Concept Ontology Dimension. As shown in Table 7, students responded to a two-stage objective diagnostic survey. Each answer corresponded to a preconception viewpoint Lxi. If $Lxi \in S(o)$, then the preconception viewpoint is rooted in the ontology level; in other words, the student does not have an adequate understanding of the scientific concept itself, which can be directly traced to the knowledge point corresponding to Lxi. For example, in diagnosing a student as having preconception viewpoint L6, an instructor can use Figure 1 and Table 3 to figure out that the student does not have a proper understanding of "Knowledge point N2: when an object is subject to a nonzero combined force, its state of movement changes."

4.1.2. Conceptual Cognition Dimension. If $Lxi \in S(f)$, then the preconception viewpoint is rooted in the cognition level. In other words, the student's preconception viewpoint is generated in the cognitive process, influenced by one or more preconceptions. The naïve theoretical framework in the student's mind is reflected in this field. Attribution can be conducted by backtracking to derive the relevant preconception viewpoints.

As shown in Table 5, Rxi is defined as a significant one-dimensional correlation vector that exists between Lxi and other preconceptions. There exists $r[xi][0] = Lxi$, $r[xi]\ [1] = L(xi + t1)$, $r[xi]\ [2] = L(xi + t2)$. . . . . .$r[xi][n] = L(xi + tn)$, where $1 \le xi + t1$, $xi + t2$, $xi + tn \le 41$, $t1$, $t2$, $tn \ne 0$, indicating the various preconceptions viewpoints significantly related to Lxi. n represents the number of preconception viewpoints related to Lxi. When the diagnostic result $LXi \in S(f)$, the naïve theoretical framework generated by Lxi should be attributed.

(1) In determining Rxi, test for whether $\mathrm{L(xi + tm)} \in S(\mathrm{o})$, where $1 \le \mathrm{xi + tm} \le 41$, $1 \le \mathrm{tm} \le n$. If it exists, L(xi + tm) is a preconception viewpoint in the naïve framework, Frame = { L(xi + tm)}.

Table 6: Two-level concept viewpoint.

Level	Preconception viewpoint	Example
Ontology layer S(o)	L1, L3, L6, L7, L10, L13, L19, L27, L28, L30, L33, L35, L36, L37	L33: When at rest, objects are not subject to gravity
Cognition layer S(f)	L2, L4, L5, L8, L9, L11, L12, L14, L15, L16, L17, L18, L20, L21, L22, L23, L24, L25, L26, L29, L31, L32, L34, L38, L39, L40, L41	L34: Because objects naturally fall, objects are only subject to gravity when they rise

Table 7: Visualization of student cognitive state.

Student_ID: 8559601		
Student name: James May		
Learning path: M (M1 ⟶ M4) ⟶ F (F1 ⟶ F5) ⟶ N (N1) ⟶ G (G1 ⟶ G2)		
Specific preconcepts	Level of preconcepts	Related knowledge point or cognitive framework
L6		N2
L7	LXi ∈ S(o)	F1
L16		F4
. . .		. . .
LX		{L(x + tm), L[x + tm][tm], . . ., L[x + tm][tm]n}
Ly	LXi ∈ S(f)	{L(y + tm), L[y + tm][tm], . . ., L[y + tm][tm]n}
. . .		. . .
Latent preconception	Related knowledge point	Probability (%)
Lxj	C1	25
	. . .	. . .
. . .	. . .	. . .
LXz	F3	70
	. . .	. . .

(2) If L(xi + tm) ∉ S(o), the various r in R(xi + tm) are determined.

(3) As in (1), determine whether L[xi + tm][tm] ∈ S(o) in R(xi + t1), R(xi + t2) ……R(xi + tn). If yes, L [xi + tm][tm] is a preconception viewpoint in the naïve framework. Frame = {L(xi + tm), L[xi + tm][tm]}. If no, then repeat Step (2).

(4) Based on iterations, there must be L[xi + tm][tm] n ∈ S(o), as specific preconception viewpoints are based on a misunderstanding of the knowledge point. As a result, attribution procedures will ultimately converge on one or more preconception viewpoints at the ontology level. As such, Lxi is attributed to the naïve theoretical framework:

$$\text{Frame} = \{L(xi + tm), L[xi + tm][tm], \ldots\ldots, L[xi + tm][tm]n\}. \tag{4}$$

Taking a real example, in diagnosing student Xiaoming as holding the preconception viewpoint L41, L41 ∈ S(f), then diagnosis can begin from R41.

(1) R41 = (L41, L17, L39), L17 ∈ S(f), L39 ∈ S(f)

(2) R17 = (L17, L10, L27, L39, L41), R39 = (L39, L17, L27, L41), L10 ∈ S(o), L27 ∈ S(o), then Frame = {L10, L27}

It can be seen that the student holds the preconception viewpoint L41, as they hold the naïve cognition framework Frame = {L10, L27}.

4.2. Learning Obstacle Prediction Algorithm.

Once the user's current preconceptions are known, the user's future learning can be predicted.

It can be seen from the previously derived formulas that when Lxi, Lxj ∈ Si, the two preconception viewpoints are significantly related:

$$\begin{aligned} P(Lxi|Lxj) &= \frac{P'(LxiLXj)}{P'(Lxj)}, \\ P(Lxj|Lxi) &= \frac{P'(LxiLxj)}{P'(Lxi)}. \end{aligned} \tag{5}$$

Sampling P′(LxiLxj), P′(Lxi), P′(Lxj) can be known. When the diagnosed student holds preconception, the probability of each specific preconception viewpoint significantly related to Lxi can be obtained for Rxi:

$$P_0(Lxj|Lxi) = \frac{P'(LxiLxj)}{P'(Lxi)}. \tag{6}$$

These calculation results indicate that the probability P_0(Lxj|Lxi) of each related preconception viewpoint occurring can be used to predict learning obstacles emerging in the learning process. Performing ranking based on likelihood enables instructors to select appropriate learning paths.

4.3. Example of Personal Cognition Diagnosis Output Results.

In summary, by constructing a preconception system to conduct preconception attribution and prediction, individuals can be diagnosed. The following information can be visualized: basic information, student ID, name, learning path, codes for preconception viewpoints currently held by the student, the level of the preconception, the reasons the student holds these preconception viewpoints, latent preconceptions the student may hold, the possibility those preconceptions exist, and the reasons those latent preconceptions may exist. The process of the cognitive diagnosis method is illustrated in Figure 2, and one example of method results is illustrated in Table 7.

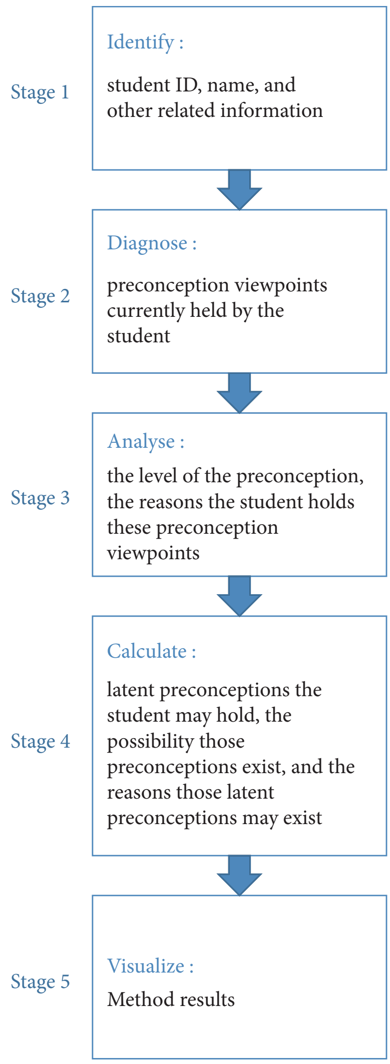

FIGURE 2: The process of the cognitive diagnosis method works in adaptive learning system.

5. Conclusions and Vision

By developing a preconception system for diagnosing users, the user cognition diagnostic method developed in this study produces outputs, including a description of the cognitive states of users, and also describes and attributes current preconception viewpoints, enabling the prediction of potential preconceptions in the learning process.

5.1. Satisfying E-Learning Requirements for Actual Pedagogy and Learning. The persistence and invisibility of preconceptions have consistently been a troubling issue in physics education. The diagnostic method in this study was developed directly based on pedagogical strategies, enabling visualization of the user's preconceptions and their origins, as well as potential future learning difficulties. The method, offered to both instructors and teachers, facilitates the design of pedagogical activities effective in driving conceptual transformation.

The outputs of the diagnostic method developed in this study do not only represent how well a student does or does not understand a knowledge point, guessing at the level of familiarity or confidence for that knowledge point. The diagnostic method in this study was developed based on the design and application of students' actual cognitive development processes. By taking into consideration the actual cognitive development of students during the learning process, as well as specific difficulties faced in the learning process, this method enables the visualization of users' specific cognitive states, their difficulties, and the origins of those difficulties.

5.2. Low Design Difficulty, Easy Development. The design thinking and process for the cognitive diagnosis method introduced in this study were based on specific questions, allowing for easy understanding by developers. The design approach herein represents a commonplace research method that is also easy for instructors to learn and apply. At the same time, the research carrier in this diagnosis method is based on specific learning content, requiring less content to be analyzed and reducing the required sample sizes and workload. The difficulty of development is decreased. Correspondingly, satisfying the needs of users for more learning activities requires higher development costs. The application of this diagnosis method requires the designers of quantified learning systems to make wise, nimble choices based on actual needs.

5.3. Increasing the Precision of Adaptive Learning System Diagnosis. The purpose of adaptive learning systems is to meet the individualized learning needs of users in an adaptive way, which includes the following: supporting learning automation; diagnosing personal characteristics, pushing learning resources and increasing the precision of learning path selection; and supporting the personalization of learning for different users.

5.3.1. Increasing Diagnosis and Feedback Precision through Smart Design. By constructing a preconception system, the diagnosis method introduced in this study can accurately and realistically describe the current cognitive state of users, as well as trace the origins of current learning obstacles and preconceptions. The system can also predict future learning obstacles and visualize the results of automated diagnosis on the cognitive states of users. At the same time, the diagnosis method produces individualized diagnosis results based on the answers of different users. Based on these diagnostic results and in accordance with conceptual transformation theory, instructors can design learning activities and develop targeted learning resources, offering feedback rules for the adaptability of the adaptive learning system, guaranteeing the precision and accuracy of learning support. As such, this diagnosis method can provide information for developers to apply smart design in increasing the performance of the adaptive learning system.

5.3.2. Diagnostic Precision Increases with Sample Sizes. This study draws on data mining and machine learning concepts. Using statistical and probabilistic methods, one can view the preconceptual system as a structured training model. In the process of development and application, with the increase of sample size and the enrichment of training, the accuracy is also improved. The authors intend to increase sample sizes in future studies. There are two primary routes to increasing sample sizes. One is to increase sample sizes during the process of designing diagnosis methods, thus increasing accuracy. The second is to increase sample sizes during pedagogical processes applying this diagnosis method, increasing the precision of the correlation coefficients of preconception systems.

5.4. New Perspective on User Diagnosis. Currently, adaptive learning systems primarily diagnose the cognitive levels and capabilities of users. In other words, they focus on what the user is capable of doing and how the user's recent development has progressed. This study was based on a different set of issues: what the user is not capable of and where learning obstacles lie; which knowledge points have not been grasped or where a user's understanding is actually tenuous; and which knowledge points the user fails to grasp due to misunderstandings arising from preconceptions. This approach represents a new paradigm for developing adaptive learning systems. Its design, based on the diagnostic dimension of preconceptions, is an augmentation of existing adaptive diagnosis.

Data Availability

The labeled datasets used to support the findings of this study are available from the corresponding author upon request.

Conflicts of Interest

The authors declare no conflicts of interest.

Acknowledgments

This paper was funded by Research on the Construction of Precision Learner Model in Intelligent Learning Environment; a project supported by the Ministry of Education of Humanities and Social Science Project (grant no. 18YJCZH169); Research on the Construction of Precision Learner Model in Intelligent Learning Environment Based on Cognitive Development Theory; a project supported by the Youth Fund Project of Northeast Normal University in Philosophy and Social Sciences (Fundamental Research Funds for the Central Universities) (grant no. 18XQ005); Research on the Construction and Representation Method of Precision Learner Model in Intelligent Learning Environment; and a project funded by China Postdoctoral Science Foundation (grant no. 2019M651189).

References

[1] C. Osterhaus, A. C. Brandone, S. Vosniadou, and N. Ageliki, "Editorial: the emergence and development of scientific thinking during the early years: basic processes and supportive contexts," *Frontiers in Psychology*, vol. 12, 2021.

[2] I. G. N. Darmawan, S. Vosniadou, M. J. Lawson, P. Van Deur, and M. Wyra, "The development of an instrument to test preservice teachers' beliefs consistent and inconsistent with self-regulation theory," *British Journal of Educational Psychology*, vol. 90, no. 4, pp. 1039–1061, 2020.

[3] H. Khosravi, S. Sadiq, and D. Gasevic, "Development and adoption of an adaptive learning system: reflections and lessons learned," in *Proceedings of the 51st ACM Technical Symposium on Computer Science Education*, pp. 58–64, Portland, OR, USA, March 2020.

[4] G.-J. Hwang, H.-Y. Sung, S.-C. Chang, and X.-C. Huang, "A fuzzy expert system-based adaptive learning approach to improving students' learning performances by considering affective and cognitive factors," *Computers & Education: Artificial Intelligence*, vol. 1, Article ID 100003, 2020.

[5] E. G. Nihad, K. Mohamed, and E. N. El Mokhtar, "Designing and modeling of a multi-agent adaptive learning system (MAALS) using incremental hybrid case-based reasoning (IHCBR)," *International Journal of Electrical and Computer Engineering*, vol. 10, no. 2, pp. 1980–1992, 2020.

[6] T. Wambsganss, C. Niklaus, and M. Cetto, "An adaptive learning support system for argumentation skills," in *Proceedings of the 2020 CHI Conference on Human Factors in Computing Systems*, pp. 1–14, Honolulu, HI, USA, April 2020.

[7] I. Tnazefti Kerkeni, H. Bélaïd, and B. Talon, "An adaptive learning system based on tracking," in *Proceedings of the CSEDU*, no. 2, Prague, Czech Republic, May 2020.

[8] H. Elmunsyah, W. N. Hidayat, S. Patmanthara, F. A. Dwiyanto, W. M. Utomo, and K. Kusumadyahdewi, "Adaptive learning system in open educational resource digital sharing community as a media for learning autonomous students," *IOP Conference Series: Materials Science and Engineering*, vol. 732, no. 1, Article ID 012110, 2020.

[9] M.-L. Li, S. Chen, and J. Chen, "Adaptive learning: a new decentralized reinforcement learning approach for cooperative multiagent systems," *IEEE Access*, vol. 8, pp. 99404–99421, 2020.

[10] C. Troussas, A. Krouska, and C. Sgouropoulou, "A novel teaching strategy through adaptive learning activities for computer programming," *IEEE Transactions on Education*, vol. 64, no. 2, pp. 103–109, 2020.

[11] C. Mu, K. Wang, and Z. Ni, "Adaptive learning and sampled-control for nonlinear game systems using dynamic event-triggering strategy," *IEEE Transactions on Neural Networks and Learning Systems*, 2021.

[12] F. Sense, M. van der Velde, and H. van Rijn, "Predicting university students' exam performance using a model-based adaptive fact-learning system," *Journal of Learning Analytics*, vol. 8, no. (3), pp. 1–15, 2021.

[13] M. Marienko, Y. Nosenko, A. Sukhikh, V. Tataurov, and M. Shyshkina, "Personalization of learning through adaptive technologies in the context of sustainable development of teachers education," 2020, https://arxiv.org/abs/2006.05810.

[14] T. Wilschut, F. Sense, M. van der Velde, Z. Fountas, S. C. Maass, and H. V. Rijn, "Benefits of adaptive learning transfer from typing-based learning to speech-based learning," *National Center for Biotechnology Information*, vol. 4, 2021.

[15] T. Wilschut, M. van der Velde, F. Sense, Z. Fountas, and H. van Rijn, "Translating a typing-based adaptive learning model to speech-based L2 vocabulary learning," in *Proceedings of the 29th ACM conference on user modeling, Adaptation and Personalization*, pp. 245–250, Utrecht, The Netherlands, June 2021.

[16] L. Zhang, L. Wang, and D. F. Treagust, “Discipline-specific cognitive factors that influence grade 9 students’ performance in chemistry,” *Chemistry Education: Research and Practice*, vol. 22, no. 4, pp. 813–841, 2021.
[17] F. J. García-Peñalvo, *Innovative Trends in Flipped Teaching and Adaptive Learning*, Sein-Echaluce, M. Luisa, and A. Fidalgo-Blanco, Eds., IGI Global, Hershey, PA, USA, 2019.
[18] Y. Gu, D. Yang, Q. Huang, W. Yang, and H. Liu, “Robust EMG pattern recognition in the presence of confounding factors: features, classifiers and adaptive learning,” *Expert Systems with Applications*, vol. 96, pp. 208–217, 2018.
[19] A. W. Subiantoro and D. F. Treagust, “Development and validation of an instrument for assessing high-school students’ perceptions of socio-scientific issues-based learning in biology,” *Learning Environments Research*, vol. 24, no. 2, pp. 223–237, 2021.
[20] Matovu, D. Ungu, and M. Won, “Walking into a protein molecule together: university students’ exploration of an enzyme-substrate interaction in immersive virtual reality,” in *Proceedings of the Australian Conference on Science and Mathematics Education*, vol. 39, Sydney, Australia, September 2021.

Hindawi
Scientific Programming
Volume 2022, Article ID 1384589, 11 pages
https://doi.org/10.1155/2022/1384589

Research Article

Movie Special Effects Processing Based on Computer Imaging Technology

Yidong Cheng and Yi Wang

Sejong University, Seoul 05006, Republic of Korea

Correspondence should be addressed to Yidong Cheng; 16115291@bjtu.edu.cn

Received 23 November 2021; Revised 9 December 2021; Accepted 16 December 2021; Published 10 January 2022

Academic Editor: Le Sun

The film space is the image of social life represented on the screen, which determines that the form of the film and television picture is a plane model, and it can only use a two-dimensional plane space to express an objective scene with a three-dimensional space. In order to improve the effects of special effects processing in movies, this paper applies computer imaging technology to the processing of movie characteristics. When performing specific scene simulations, the specific structure of each computer imaging particle system is derived on the basis of the general structure of the computer imaging particle system. In addition, this paper combines the improved algorithm to carry out several case analyses, and the reliability of this method is verified through simulation experiments, which promotes the application and promotion of computer imaging technology in movie special effects processing.

1. Introduction

With the development of the economy and the advancement of science and technology, computers have gradually become small and compact from giants. Gradually, ordinary people can also purchase computers, which were very high-tech machines in the past. The gradual popularization of computers has quietly changed the development direction of all walks of life. The film special effects modeling industry eager for new technologies quickly absorbed the fresh blood of computer technology and began to develop in a new direction, and film special effects came into being [1]. Before being impacted by digital special effects, physical special effects prevailed, and all the characters imagined by people need to be realized by the technical means of physical sculpture. However, after the prevalence of computer technology, special effects technology gradually made special effects modeling virtual, and special effects scenes and characters completed the transition from realization to virtualization. This has a certain inevitability. Before computer technology took shape, the physical special effects of entities had been very strenuous in order to satisfy people's powerful imagination, and the physical special effects could no longer satisfy people's increasingly romantic and exaggerated imagination of movies. Moreover, excellent physical effects studios such as Winston Studio seem to have achieved the ultimate in physical effects, so it is difficult to have new possibilities [2]. At this time, the emergence of computer special effects is just right for the film special effects industry.

Movie is a kind of audiovisual art expressed through pictures, and pictures are the basic elements of movies. The sense of space of the screen is particularly important in the modeling of the film and television screen and the three-dimensional space of the screen scene [3].

The reason why film and television can become an art is that it can use various methods and means to overcome its own shortcomings and show itself more perfectly. People have determined the direction of space according to the direction of the sun, and the east, south, west, north, southeast, northeast, southwest, and northwest are collectively referred to as all directions. We call the depth of space. In reality, the space we are in is a three-dimensional space. Objects can be stationary in a fixed position in space, or they can change their own position by moving in any direction in all directions of spatial location. This kind of spatial position movement will cause changes in the spatial distance when moving away from the viewpoint or approaching the viewpoint. The spatial form refers to the length, width, and height of the space occupied by an object when it is in a three-dimensional space. When the specific values of these three dimensions are determined, then the specific spatial form of the object is also determined. In reality, people's perception of external objects is specific and tangible. In the absence of specific and accurate three-dimensional values, one can still determine its spatial form by perceiving the three-dimensional proportions of external objects based on existing experience.

The form of an object in space can be divided into two- and three-dimensional spatial forms. Two-dimensional space is usually a flat surface, and the displayed objects have only length and width. From this point of view, the film screen is a two-dimensional spatial form, which belongs to graphic art. The real objective world is a three-dimensional space. The objects in this world represent the three-dimensional space form. The biggest difference from the two-dimensional plane form is that the three-dimensional space form has spatial depth. Therefore, graphic arts such as paintings and photographs are suitable for expressing things in two-dimensional space, and objects with spatial depth need to be expressed in a three-dimensional space. What film art needs to do is to accommodate objects in three-dimensional spatial form on a limited two-dimensional space plane and to express the three-dimensional visual characteristics of the object to be photographed on the two-dimensional plane.

This paper applies computer imaging technology to the process of film characteristics processing and studies the essence of film special effects processing, which provides a theoretical reference for the further development of subsequent film special effects processing technology.

2. Related Work

Three-dimensional technology is a product of the combination of graphic calculus and art school rapid expression [4]. It is more expressive and more attractive than traditional two-dimensional animation art. With the rapid development of science and technology, the tastes of the audience continue to improve. This method is obviously more in line with the aesthetic characteristics and advantages of modern people [5]. Therefore, it has to be admitted that Disney's 3D animation films have more vitality and market appeal than traditional 2D animations. The development of animation film special effects and the development of computers are inseparable. The traditional two-dimensional animation is to first draw the characters in action on paper according to the action scene cartoon animator and then copy them to the top of the cartoon characters [6].

The development of plane technology and the formation of application software in the computer three-dimensional effect, so far, have gone through several decades. With the rapid development of computer hardware and computer-intensive computer graphics technology, computer-generated false scenes and special effects are no longer a fantasy [7]. The subtle performance of animation technology perfectly expresses the artistic beauty, art, and technology as a solid foundation; technology and art are constantly sublimated. The computer can generate a virtual world that is enough to be fake [8]. This depends on the modeling, rendering, and animation technology related to computer animation expertise and motion control synthesis technology [9]. Although many software has advanced to other technical levels, higher requirements have been put forward for the flexibility and controllability of the scene movement. The LED is more of an animation design-type technology; at the same time, due to its simplicity and compatibility, there is a widespread concern in the polygonal mesh model of the computer animation system [10].

Literature [11] studied the real-time lighting rendering of nonuniform participating media and proposed a real-time lighting rendering method for participating media in a virtual indoor environment. In terms of the specific implementation, by using 3D textures to organize nonuniform participating media, real-time rendering is realized: combining shadow mapping, volume shadowing, and light stepping technologies; a method of object volume shadowing considering the role of participating media is described hybrid drawing methods. Literature [12] studied the rendering of scattering materials and proposed an efficient algorithm based on Woodcock tracking.. First, the traditional light stepping (ray marching algorithm) was implemented, and multiple comparison experiments were performed to verify the implementation, including the comparison of homogeneous participating media (homogeneous) and nonuniform participating media (heterogeneous), single scattering, and multiple subscattering. Then a more efficient Woodcock tracking algorithm is implemented, and the rendering efficiency and rendering effect of the two algorithms are compared. Literature [13] proposed a variant algorithm. It can use any selected cross-section. It is not the main cross-section of the entire system to sample the free flight distance. This technique avoids the main shortcomings of traditional Woodcock sampling and shows the theoretical derivation of heterogeneous media. Literature [14] proposed a one-dimensional analysis and numerical model. It is used for the basic optimization study of free sampling parameters and demonstrates the application case description using GPU-based Monte Carlo code for radiotherapy.

In computer graphics, participatory media is usually described as a collection of scattering microscopic particles (although described as particles, fluid media is also applicable to these theories. For the convenience of introduction, the explanation of the theory will be continued later. Following the term "particles"), due to the small size of these particles and the characteristics of random distribution, we generally do not describe the interaction of individual particles but consider the probabilistic behavior of the entire collection of particles [15]. When a photon passes through a medium composed of a group of microscopic particles, it may not collide with any particles at all and continue to travel freely (just like in a vacuum), or it may interact with some of the particles, thereby affecting the transmission of light [16]. The probability of interaction between photons and particles depends on the extinction coefficient of the medium, also known as the attenuation coefficient, which is represented by a variable named sigIllaT. The size of the extinction coefficient depends on the density of the medium and other physical characteristics. It is the result of the interaction of two types of illumination: when a photon interacts with a particle, the photon is either absorbed by the particle or scattered to another direction [17].

3. Computer Molding Technology

At present, it is an era of digital information processing. Under the condition of limited bandwidth resources, people have higher and higher requirements for signal sampling rate and processing speed. Information processing in the traditional sense is to compress after a large amount of sampling, thereby reducing the pressure of signal transmission and storage. This method often causes a large amount of waste of sampling information.

We assume that the discrete signal in an n-dimensional domain space is $x \in R^n$ and an orthonormal basis in the space is $\psi \in R^{m\times n}$, and the signal x can be uniquely linearly represented by the basis matrix ψ as follows [18]:

$$x = \psi\alpha, \tag{1}$$

where α is the linear representation coefficient of the signal x on the base matrix A. If there are many items that are equal to or have values close to zero in the representation coefficients obtained by using the above transformation on the signal, then it can be said that the signal has sparseness under the base matrix. In particular, when the number of nonzero elements in the coefficient vector α is k, the signal x is called a sparse signal representing k on the basis matrix ψ.

The above x and α can be regarded as representations of the same signal in different domains, and there may be cases where the signal x is not compressible in the domain space α but is compressible in the domain space ψ. This characteristic of the signal is used in many applications, such as wavelet transform in image processing. The value of each pixel in the original image is almost nonzero in the spatial domain, but it is very sparse in the wavelet domain representation, and there are only a few nonzero coefficients. In the image restoration process, only the limited nonzero coefficients are needed to approximate the original image well. However, in traditional signal processing, transform coding only exists in the signal compression process, and a large amount of sampling information is still needed in the sampling stage, which causes a serious waste of sampling information.

Compressed sensing theory proposes to compress the sparse signal x in formula (1), that is, it uses a random measurement matrix $\Phi \in R^{m\times n}$ that is not correlated with the base matrix ψ or has little correlation to sample x. In the process of sampling, data compression is completed, and the number of sampling is $m_c \geq k\ \log(n/k)\ (m_c \ll n)$, thus greatly reducing the waste of sampling information. The sampling result is expressed as follows [19]:

$$y = \Phi x, \tag{2}$$

where $y \in R^n$ is called the observed value, which is not the signal itself but the projection value of the signal from high to low dimensions. When the sparse representation of x is incorporated into the above formula, we can get:

$$y = \Phi x = \Phi\psi\alpha. \tag{3}$$

Finally, the original signal x can be recovered approximately by reconstructing the observed value y. The specific method is in the known base matrix ψ, by solving the optimization problem [20]:

$$\begin{aligned} &\underset{\{\alpha\}}{\text{minimize}}\ \|\widehat{\alpha}\|_0 \\ &\text{subject to}\ \|y - \Phi\psi\widehat{\alpha}\|_2 \leq \varepsilon. \end{aligned} \tag{4}$$

We get a $\widehat{\alpha}$ with the smallest number of nonzero values and recover the original signal $x \approx \widehat{x} = \psi\widehat{\alpha}$, where ε is the threshold of the fitting error.

The sparse characteristic of the signal itself or the sparse representation in a certain transform domain is the basis for the application of compressed sensing. For the definition of signal sparsity, when the number of nonzero elements in the coefficient vector of the signal in the base matrix is k, the signal is called a k-sparse signal. When the coefficient vector of the signal under the base matrix satisfies the equation [21]:

$$\|\alpha\|_p = \left(\sum_i |\alpha_i|^p\right)^{1/p} \leq R. \tag{5}$$

The signal is sparse, and the range of p and R in the formula is $0<p<2$ and $R>0$. In general, the degree of sparse representation of the signal under different base matrices ψ is not the same. Therefore, in practical engineering applications, the most appropriate sparse representation base needs to be selected. Usually, in signal processing, a large number of transform bases are used in the frequency domain, such as Fourier transform bases, discrete cosine transform bases, and wavelet transform bases. By using them, the original signal can be projected into the corresponding new space, and the processing that the signal cannot achieve in the original domain, such as spectrum analysis and frequency domain filtering, can be completed. In addition, the commonly used basis matrices include curvelet basis, Gabor basis, and so on.

The representation of the measurement matrix is $\Phi \in R^{m\times n}$, and $m \ll n$. The effect of the above measurement matrix can be expressed mathematically as follows:

$$y = \Phi x = \Phi\psi\alpha \text{ or } y = \Phi\alpha = \Phi\psi^T x. \tag{6}$$

That is, the signal or the sparse representation coefficient vector of the signal is projected to obtain the measured value $\psi \in R^m$. The ultimate goal of compressed sensing is to recover the signal x or its sparse representation coefficient vector α through the measured value y. In fact, it is to solve equation (6). This process is a mapping process from a low-dimensional signal (m-dimensional) to a high-dimensional signal (n-dimensional), which solves an underdetermined system of equations. In theory, this underdetermined problem has an infinite number of solutions, but the signal processed by compressed sensing is sparse. The signal x is a k-sparse signal ($k \ll m$), so formula (6) is solvable under this premise.

For any signal x with a sparsity of k, if the equation is satisfied:

$$(1-\delta_k)\|k\|_{l_2}^2 \leq \|\widetilde{\Phi}\xi\|_{l_2}^2 \leq (1+\delta_k)\|x\|_{l_2}^2, \delta_k \in [0,1], \quad (7)$$

where $\widetilde{\Phi} = \Omega\psi$ (or $\Phi\psi^T$) is the compressed sensing matrix; then $\widetilde{\Phi}$ at this time satisfies the constraint equidistance condition. In practical applications, it is very difficult to select the measurement matrix through the principle of formula (7), and solving it is a problem of combinatorial complexity. When the measurement matrix Φ is not related to the base matrix ψ, the compressed sensing matrix $\widetilde{\Phi}$ satisfies the constraint equidistance condition with a high probability. The uncorrelation at this time means that the measurement matrix and the base matrix cannot be sparsely represented by each other. When the irrelevance is stronger, the more the information of the signal x carried in the measurement value y, the higher the success rate of signal reconstruction.

Therefore, when designing the measurement matrix, it is necessary to consider the constraint equidistance condition or the principle of noncorrelation. At present, the commonly used measurement matrices are random matrices, such as random Gaussian matrix, random Bernoulli matrix, random Toplitz matrix, and so on.

The third key part of compressed sensing is the signal reconstruction algorithm. A good reconstruction algorithm will improve the efficiency and accuracy of signal reconstruction.

The signal reconstruction algorithm needs to solve the problem of recovering the signal x from the measurement result y described in equation (3) or (6). The signal optimization problem described by equation (4) can be expressed as a Lagrangian equation. In the solution process, the signal reconstruction error and the coefficient sparsity level are weighed into consideration, expressed as follows:

$$\underset{\{\alpha\}}{\text{minimize}} \|y - \Phi\psi\widehat{\alpha}\|_2 + \lambda\|\widehat{\alpha}\|_0. \quad (8)$$

Equations (4) and (8) are essentially underdetermined equations. The ℓ_0-norm problem in the equation is a nondeterministic polynomial hard (NP-hard) problem. Two types of methods commonly used to solve such problems are greedy methods and convex relaxation methods.

The greedy method has low computational complexity and fast execution speed in sparse signal reconstruction, but its accuracy is relatively low. Contrary to the convex relaxation method, the accuracy of signal approximation is greatly improved. The core idea of this kind of method is to replace the ℓ_0-norm that causes NP-hardness in the original problem with the convex ℓ_1-norm so as to transform the NP-hard problem into a related convex problem. Studies have proved that this kind of replacement is possible with a high probability.

When the basis pursuit (BP) in the convex relaxation method solves the convex problem, the ℓ_0 norm in (4) is replaced with the ℓ_1 norm, and the measured value y is constrained by the equation, expressed as follows:

$$\underset{\{\alpha\}}{\text{minimize}} \|\widehat{\alpha}\|_0 \text{ subject to } y = \Phi\psi\widehat{\alpha}. \quad (9)$$

When the number of samples meets $m_c \geq k\log(n/k)$, base tracking can get good results. The basis tracking denoising (BP denoising; BPDN), which is similar to basis tracking, can well suppress the noise signal in the process of solving. The problem it deals with can be expressed as follows:

$$\underset{\{\alpha\}}{\text{minimize}} \|\widehat{\alpha}\|_0 \text{ subject to } \|y - \Phi\psi\widehat{\alpha}\|_2 \leq \varepsilon. \quad (10)$$

Unlike equation (9), it uses an inequality to constrain the measured value y. These two methods for solving convex problems can be summarized as: minimizing the sparsity of coefficient vectors while satisfying the approximation error. In addition, methods for solving convex problems include the lasso algorithm (Lasso), the interior point method, and so on.

The convex relaxation method can obtain the global optimal approximation result, and the solution accuracy is high, but the calculation time is longer than that of the greedy method. Therefore, in practical applications, we can choose a suitable signal reconstruction algorithm according to specific requirements.

The object displayed in the light-field three-dimensional display can be regarded as composed of many three-dimensional points, and the light field can be expressed as a five-dimensional plenoptic function: $L = L_{O_1}(x_i, y_i, z_i, \theta, \phi)$. This chapter uses the two-plane parameterization method to parameterize the light field in the analysis process of calculating the light field collection. The specific description is: in the free space without occlusion, the intensity of light will not attenuate during the propagation process. The five-dimensional plenoptic function L can be reduced to four-dimensional and mathematically described as the flow of light energy along the light in the three-dimensional space. It is produced by the diffuse reflection, specular reflection, and ambient light from the surface of the object to the light emitted by the light source. For visualization purposes, light rays can be described as a line connecting them with the intersection of two parallel planes separated by a unit distance, that is, the line connecting the first plane point pair $u = \{u_i, v_i\}$ and the second plane point pair $s = \{s_i, t_i\}$ shown in Figure 1. The light field at this time is the collection of all rays in the scene, which can be expressed as $I\{u_i, v_i, s_i, t_i\}$, which is a four-dimensional representation. In the rest of this chapter, the light field is abbreviated as $l(u, s)$.

In the two-plane parameterization method of the light field, a plane can be placed at infinity, and the light at this time can be parameterized as a point plus a direction. This kind of parameterization is very useful for constructing the

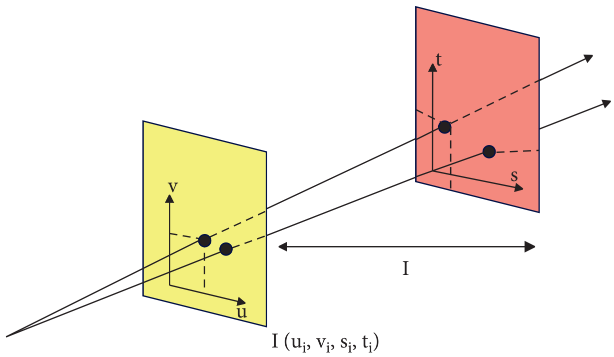

Figure 1: Two-plane parameterization of the four-dimensional light field.

light field because the light field at this time can be regarded as a set of images within a certain angle of view. In addition, the geometric operation efficiency of this parameterization method is very high. The specific performance is that the process of light mapping to plane points and the process of inverse mapping of image pixels to light are linear problems, which can be realized by multiplying by a matrix.

We analyze in advance the phenomena that occur during the propagation of the light field and the corresponding changes in the light field after the phenomena occur. For the two-plane parameterized light field $l(u, s)$, its Fourier transform is expressed as follows:

$$L = (f_u, f_s) = \int_{u=-\infty}^{\infty} \int_{s=-\infty}^{\infty} l(u, s) e^{(-2i\pi f_u u)} e^{(-2i\pi f_s s)} \mathrm{d}u\mathrm{d}s. \tag{11}$$

When the light field propagates in free space, the intensity of the light will not change, but its angular dimension (direction dimension) and spatial dimension will change. Therefore, the process of light field propagation is actually the reparameterization of the light field. If it is assumed that z is the distance traveled by the light field $l(u, s)$, the light field at this time can be expressed as follows:

$$l_0(u, s) = l(u - zs, s). \tag{12}$$

The corresponding Fourier transform is as follows:

$$\begin{aligned} L_0(f_u, f_s) &= \int_{u'=-\infty}^{\infty} \int_{s=-\infty}^{\infty} l_0(u', s) e^{(-2i\pi f_u (u'+2s))} e^{(-2i\pi f_s s)} \mathrm{d}u' \mathrm{d}s \\ &= \int_{u'=-\infty}^{\infty} \int_{s=-\infty}^{\infty} l_0(u', s) e^{(-2i\pi f_u u')} e^{(-2i\pi (f_s + z f_u))} \mathrm{d}u' \mathrm{d}s \\ & L(f_u, f_s + z f_u), \end{aligned} \tag{13}$$

where $L_0(f_u, f_s)$ and $L(f_u, f_s)$ represent the Fourier transform corresponding to $l_0(u, s)$ and $l(u, s)$, respectively. It can be clearly seen from $L_0(f_u, f_s)$ that the spectrum after propagation has undergone shear along the f_s dimension, and the longer the propagation distance, the more obvious the shear.

When the light is occluded, its intensity value is equivalent to multiplying by an occlusion function and becomes:

$$l_0(u, s) = l(u, s) O(u, s). \tag{14}$$

When it is completely occluded, the occlusion function $O(u, s) = 0$; $O(u, s) = 1$ is the case of no occlusion. When $0 < O(u, s) < l$, it is occluded to varying degrees. The position where the light is blocked depends entirely on the spatial dimension u. The Fourier transform form of the occlusion process is as follows:

$$L_0(f_u, f_s) = L(f_u, f_s) * O(f_u, f_s). \tag{15}$$

In general, the occluder will affect the spatial dimension u and the angular dimension s of the light at the same time, and the influence on the angular dimension is related to the depth range of the occluder. In particular, when the occluder is a plane occluder and is perpendicular to the light, its occlusion function is a constant in the angular dimension s, and the corresponding Fourier transform is a unit pulse.

4. Movie Special Effects Processing Based on Computer Imaging Technology

When simulating a specific scene, we derive the specific structure of each computer imaging particle system on the basis of the general structure of the computer imaging particle system. The general structure of the computer imaging particle system is shown in Figure 2. The computer imaging particle system is generally composed of computer imaging particle management, computer imaging particle storage, and computer imaging particle rendering.

In the computer imaging particle system, each computer imaging particle must undergo three life courses: birth, dynamic change, and extinction. The algorithm framework of the computer imaging particle system is shown in Figure 3.

In order to simplify the calculation, the distribution area can be replaced by a rectangular parallelepiped in front of the viewpoint without affecting the realism of the graphics. The normal vector of a certain surface of the rectangular parallelepiped passes through the viewpoint, and the initial distribution area of the computer imaging particles is a

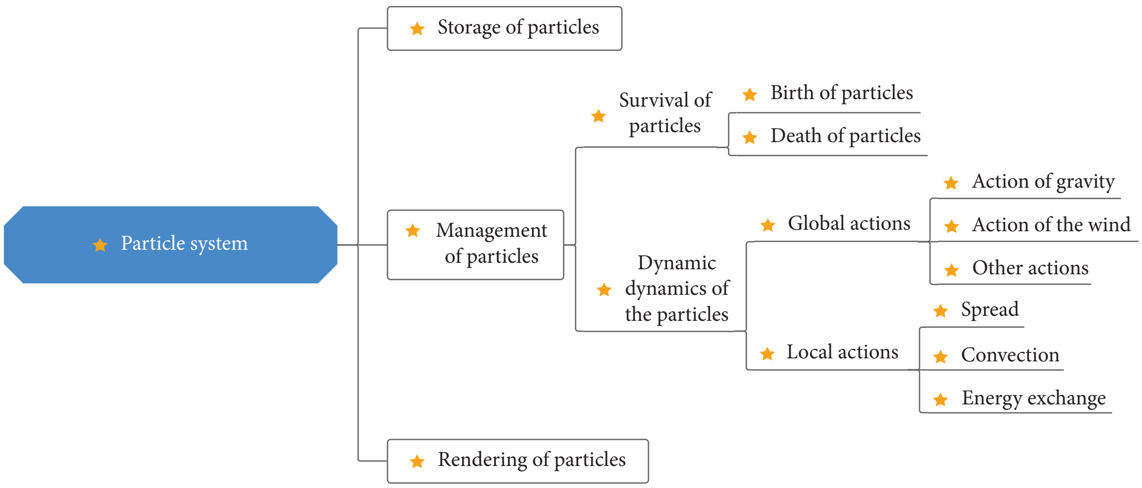

Figure 2: General structure of computer imaging particle system.

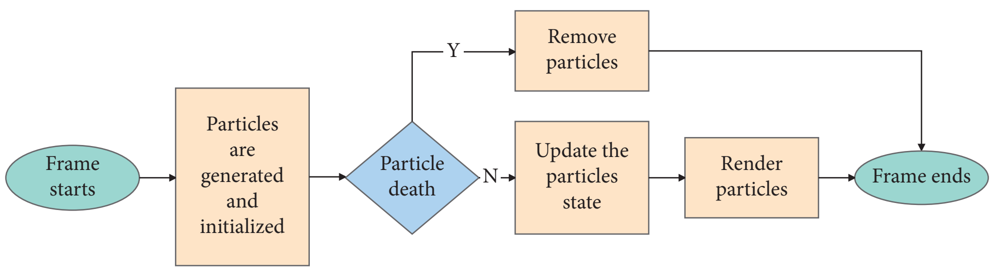

Figure 3: Algorithm framework of computer imaging particle system.

surface parallel to the XOZ surface in the rectangular parallelepiped, and its normal is facing downwards. The schematic diagram of the distribution area is shown in Figure 4.

When setting the spatial location properties of raindrops, the algorithm still takes the principle of not affecting the real effects of raindrops, and the main goal is to maximize the number of particles in computer imaging. Moreover, it also designs the spatial position distribution area of the raindrop computer imaging particles in a deep area within the viewing cone. However, because the raindrop itself is greatly affected by gravity, the initial spatial position of the raindrop can be distributed on a quarter of a sphere with the viewpoint as the center of the sphere, including the viewing cone, as shown in Figure 5.

The fountains seen in real life consist of spraying hair out of the body of water, and under certain water pressure, a column of water is emitted upwards and then spreads around to form fountains of different shapes. The entire fountain body can be regarded as multiple parabolic water columns emitted from the surrounding by the central nozzle, and each water column is composed of multiple water columns, as shown in Figure 6. The fountain model is special. The special feature is that the computer imaging particles of water droplets in the fountain water are not independent individuals, but the computer imaging particles of water droplets have a certain adhesive force between them, which makes the computer imaging particles of water droplets stick together to form larger water droplets.

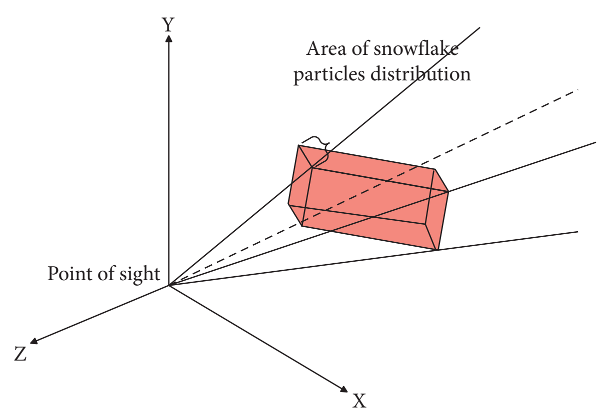

Figure 4: Schematic diagram of the computer imaging particle distribution area of snowflake.

The implementation modules of the system are divided into the following two categories in terms of function. The first is the basic function module, which is composed of two modules, a memory management module and a mathematical basic module, mainly to provide memory and data operation support for the system. The other is the system core module, which consists of four modules: system control module, scene management module, computer imaging particle system management module, and graphics

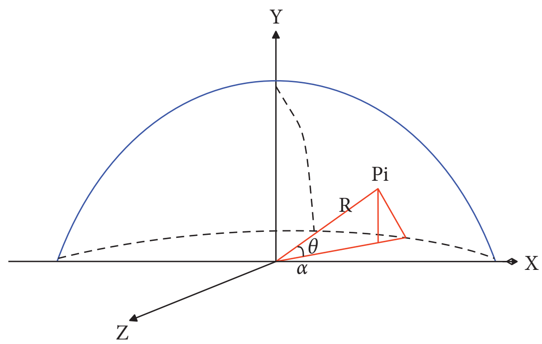

Figure 5: Schematic diagram of the computer imaging particle distribution area of raindrops.

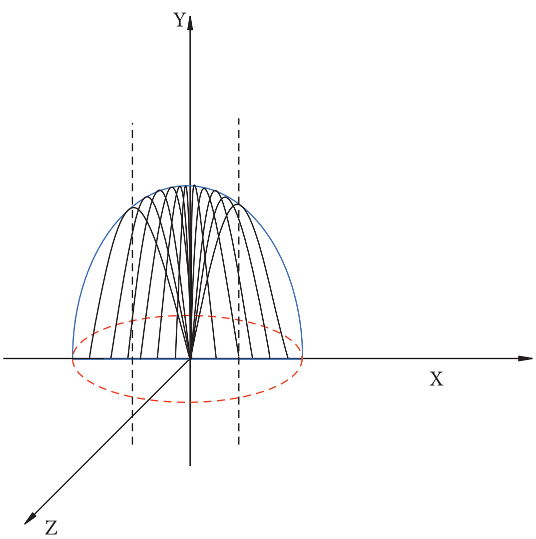

Figure 6: Fountain model diagram.

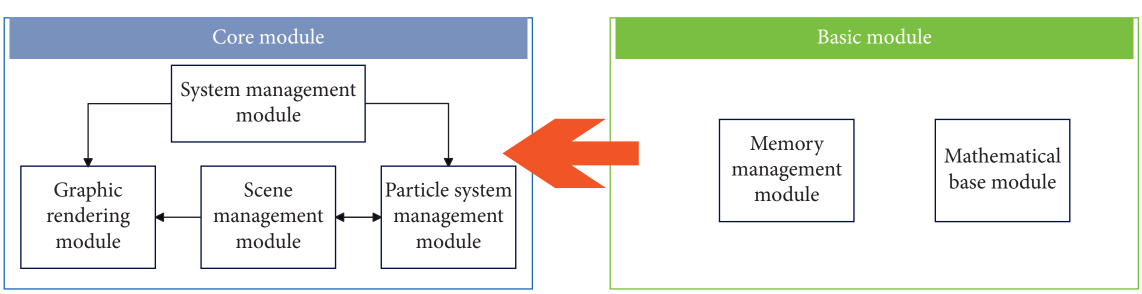

Figure 7: Macroscopic architecture diagram of 3D computer imaging particle special effects system.

rendering module. The system architecture of the 3D computer imaging particle special effects system is shown in Figure 7.

On this basis, we need to clarify the processing flow of the system. Figure 8 shows the brief processing flow of the system.

In order to better simulate various irregular sceneries with complex shapes and strengthen the management of natural sceneries, object-oriented thinking is adopted, and the concept of the hierarchical structure of computer imaging particle systems is introduced. The hierarchical structure of the computer imaging particle system is shown in Figure 9:

The processing flow of the control submodule is shown in Figure 10:

After constructing the system, the system is simulated and studied; TV special effects processing is simulated; and the computer imaging effects and film special effects processing effects of the system in this paper are evaluated, and the results are shown in Table 1 and Figure 11 are obtained.

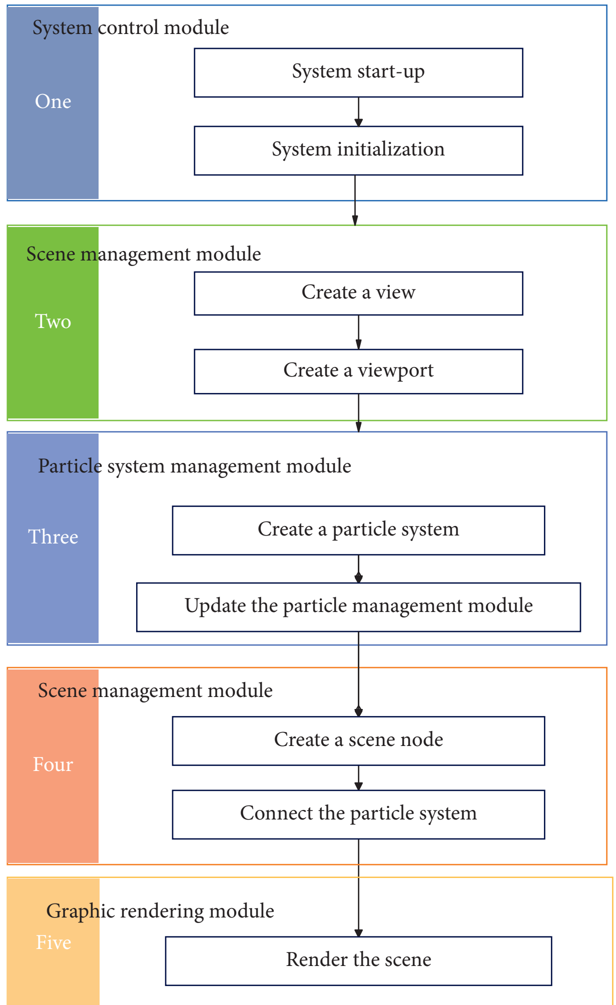

Figure 8: Process flow chart of computer imaging particle system.

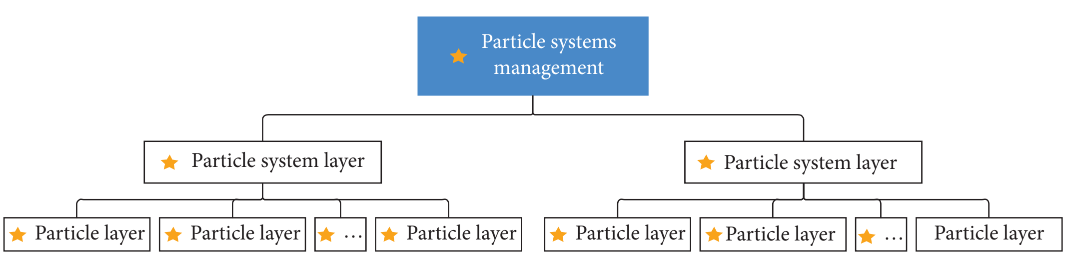

Figure 9: The hierarchical structure of computer imaging particle system.

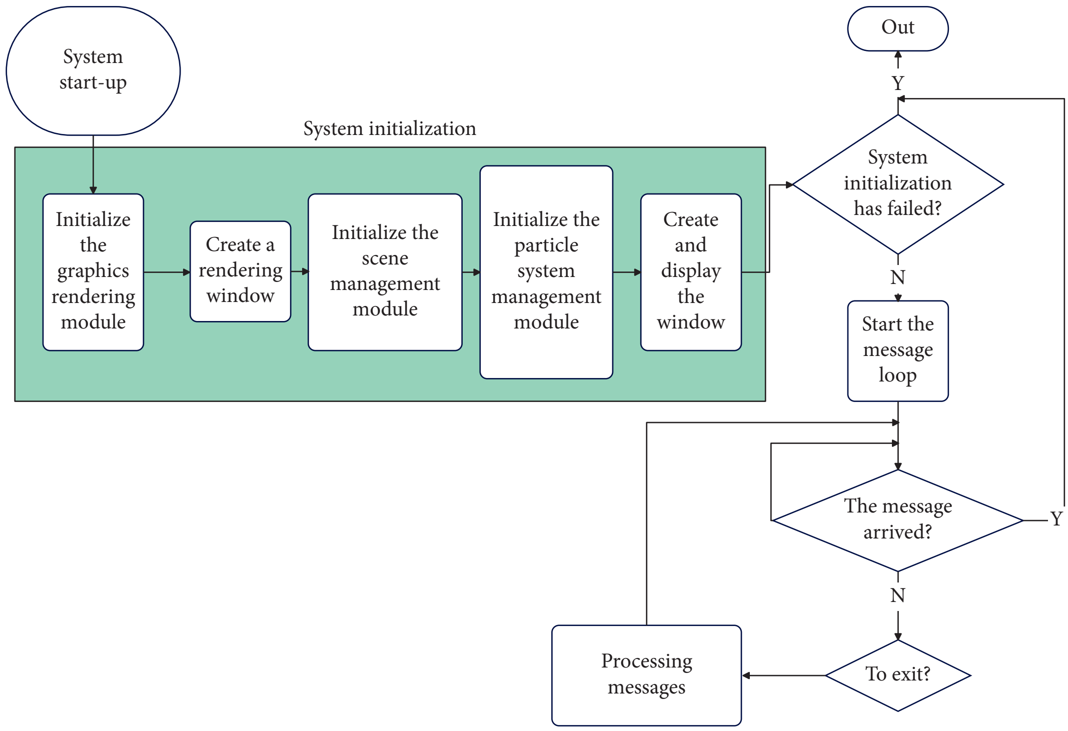

Figure 10: The execution flow chart of the control submodule.

Table 1: Evaluation of movie special effects processing effect based on computer imaging technology.

No.	Imaging effect	Special effects processing	No.	Imaging effect	Special effects processing
1	94.14	89.25	18	92.21	88.19
2	92.52	90.12	19	91.96	88.28
3	92.45	92.24	20	95.61	87.34
4	93.16	89.99	21	95.29	84.26
5	92.46	84.91	22	95.22	89.47
6	94.43	89.30	23	91.11	85.78
7	95.75	88.45	24	93.10	86.96
8	94.18	90.84	25	95.09	85.82
9	94.83	92.19	26	94.96	86.86
10	92.03	91.79	27	93.40	91.15
11	94.23	85.58	28	95.77	92.96
12	91.25	88.28	29	91.71	86.70
13	95.94	88.41	30	94.54	92.83
14	95.03	85.08	31	93.39	90.28
15	92.38	85.13	32	93.44	91.84
16	92.19	91.22	33	93.85	86.98
17	95.90	87.43	34	91.20	88.88

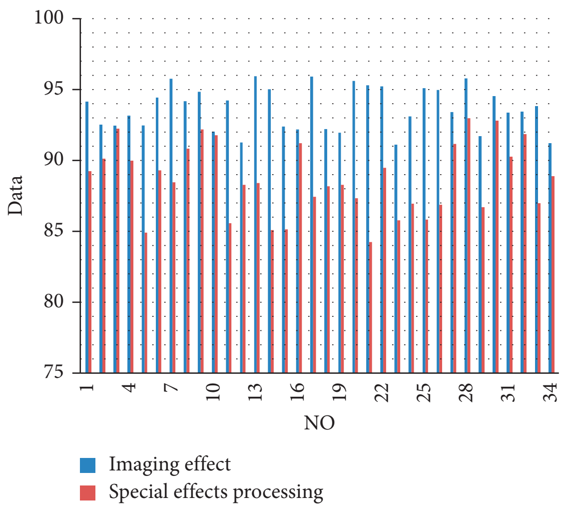

Figure 11: Statistical diagram of system performance.

Through the above experimental research, it can be seen that the film special effects processing method based on computer imaging technology proposed in this paper has good practical effects, and the computer imaging effects and film special effects processing effects are very good.

5. Conclusion

The construction of the film and television picture is in the same vein as the composition of the painting, so naturally, it is necessary to pay attention to the sense of space in the picture. The sense of space of the movie screen is formed by the combination of the composition of the screen, the perspective relationship of objects, and the visual illusion of people. Filmmakers must focus on the cross-composition of two-dimensional screen planes and three-dimensional projection elevations to develop the thinking of film space through the selection of film specifications and picture formats, the skills of framing and composition, and the processing of in-depth scheduling so as to realize the space design of the film screen up, down, left, and right. The truth of the picture depends on the understanding of the picture space. This paper applies computer imaging technology to the process of film characteristics processing and studies the essence of film special effects processing. The experimental results show that the movie special effects processing method based on computer imaging technology proposed in this paper has good practical effects, and the computer imaging effects and movie special effects processing effects are very good.

Data Availability

The labeled data set used to support the findings of this study is available from the corresponding author upon request.

Conflicts of Interest

The authors declare that there are no conflicts of interest.

Acknowledgments

This study was sponsored by Sejong University.

References

[1] L.-C. Cheng and C.-L. Huang, "Exploring contextual factors from consumer reviews affecting movie sales: an opinion mining approach," *Electronic Commerce Research*, vol. 20, no. 4, pp. 807–832, 2020.

[2] I. Spielvogel, B. Naderer, and J. Matthes, "Again and again: exploring the influence of disclosure repetition on children's cognitive processing of product placement," *International Journal of Advertising*, vol. 39, no. 5, pp. 611–630, 2020.

[3] J. Steffens, "The influence of film music on moral judgments of movie scenes and felt emotions," *Psychology of Music*, vol. 48, no. 1, pp. 3–17, 2020.

[4] G. Schalk, C. Kapeller, C. Guger et al., "Facephenes and rainbows: causal evidence for functional and anatomical specificity of face and color processing in the human brain," *Proceedings of the National Academy of Sciences*, vol. 114, no. 46, pp. 12285–12290, 2017.

[5] S. Han, B. Liu, R. Wang, Y. Ye, C. D. Twigg, and K. Kin, "Online optical marker-based hand tracking with deep labels," *ACM Transactions on Graphics*, vol. 37, no. 4, pp. 1–10, 2018.

[6] D. Stawarczyk, M. A. Bezdek, and J. M. Zacks, "Event representations and predictive processing: the role of the midline default network core," *Topics in Cognitive Science*, vol. 13, no. 1, pp. 164–186, 2021.

[7] A. G. Sares, N. E. V. Foster, K. Allen, and K. L. Hyde, "Pitch and time processing in speech and tones: the effects of musical training and attention," *Journal of Speech, Language, and Hearing Research*, vol. 61, no. 3, pp. 496–509, 2018.

[8] A. K. Fishell, T. M. Burns-Yocum, K. M. Bergonzi, A. T Eggebrecht, and J. P Culver, "Mapping brain function during naturalistic viewing using high-density diffuse optical tomography," *Scientific Reports*, vol. 9, no. 1, pp. 11115–11211, 2019.

[9] E. Peters and C. Muñoz, "Introduction to special issue Language learning from multimodal input," *Studies in Second Language Acquisition*, vol. 42, no. 3, pp. 489–497, 2020.

[10] C. Li, Z. Wang, Y. Lu, X. Liu, and L. Wang, "Conformation-based signal transfer and processing at the single-molecule level," *Nature Nanotechnology*, vol. 12, no. 11, pp. 1071–1076, 2017.

[11] N. Molinaro and M. Lizarazu, "Delta(but not theta)-band cortical entrainment involves speech-specific processing," *European Journal of Neuroscience*, vol. 48, no. 7, pp. 2642–2650, 2018.

[12] Y. Deldjoo, M. F. Dacrema, M. G. Constantin et al., "Movie genome: alleviating new item cold start in movie recommendation," *User Modeling and User-Adapted Interaction*, vol. 29, no. 2, pp. 291–343, 2019.

[13] R. Piryani, V. Gupta, and V. K. Singh, "Movie Prism: a novel system for aspect level sentiment profiling of movies," *Journal of Intelligent and Fuzzy Systems*, vol. 32, no. 5, pp. 3297–3311, 2017.

[14] T. Alexopoulou, M. Michel, A. Murakami, and D. Meurers, "Task effects on linguistic complexity and accuracy: a large-scale learner corpus analysis employing natural language processing techniques," *Language Learning*, vol. 67, no. S1, pp. 180–208, 2017.

[15] S. De Jans, D. Van de Sompel, L. Hudders, and V. Cauberghe, "Advertising targeting young children: an overview of 10

years of research (2006-2016)," *International Journal of Advertising*, vol. 38, no. 2, pp. 173–206, 2019.

[16] F. M. Schneider, "Measuring subjective movie evaluation criteria: conceptual foundation, construction, and validation of the SMEC scales," *Communication Methods and Measures*, vol. 11, no. 1, pp. 49–75, 2017.

[17] M. A. Mizher, A. A. Mazhar, M. C. Ang, and M. A. Mizher, "A review of video falsifying techniques and video forgery detection techniques," *International Journal of Electronic Security and Digital Forensics*, vol. 9, no. 3, pp. 191–208, 2017.

[18] J. T. Fisher, J. R. Keene, R. Huskey, and R. Weber, "The limited capacity model of motivated mediated message processing: taking stock of the past," *Annals of the International Communication Association*, vol. 42, no. 4, pp. 270–290, 2018.

[19] V. Grech, "The application of the mayer multimedia learning theory to medical powerpoint slide show presentations," *Journal of Visual Communication in Medicine*, vol. 41, no. 1, pp. 36–41, 2018.

[20] J. Black, M. Barzy, D. Williams, and H. Ferguson, "Intact counterfactual emotion processing in autism spectrum disorder: evidence from eye-tracking," *Autism Research*, vol. 12, no. 3, pp. 422–444, 2019.

[21] P. Tashman, V. Marano, and J. Babin, "Firm-specific assets and the internationalization-performance relationship in the U.S. movie studio industry," *International Business Review*, vol. 28, no. 4, pp. 785–795, 2019.

Hindawi
Scientific Programming
Volume 2022, Article ID 7314599, 12 pages
https://doi.org/10.1155/2022/7314599

Research Article

A Cross-Modal Image and Text Retrieval Method Based on Efficient Feature Extraction and Interactive Learning CAE

Xiuye Yin [1] and Liyong Chen [2]

[1]*School of Computer Science and Technology, Zhoukou Normal University, Henan, Zhoukou 466001, China*
[2]*School of Network Engineering, Zhoukou Normal University, Henan, Zhoukou 466001, China*

Correspondence should be addressed to Xiuye Yin; 20111036@zknu.edu.cn

Received 10 November 2021; Revised 1 December 2021; Accepted 9 December 2021; Published 10 January 2022

Academic Editor: Le Sun

In view of the complexity of the multimodal environment and the existing shallow network structure that cannot achieve high-precision image and text retrieval, a cross-modal image and text retrieval method combining efficient feature extraction and interactive learning convolutional autoencoder (CAE) is proposed. First, the residual network convolution kernel is improved by incorporating two-dimensional principal component analysis (2DPCA) to extract image features and extracting text features through long short-term memory (LSTM) and word vectors to efficiently extract graphic features. Then, based on interactive learning CAE, cross-modal retrieval of images and text is realized. Among them, the image and text features are respectively input to the two input terminals of the dual-modal CAE, and the image-text relationship model is obtained through the interactive learning of the middle layer to realize the image-text retrieval. Finally, based on Flickr30K, MSCOCO, and Pascal VOC 2007 datasets, the proposed method is experimentally demonstrated. The results show that the proposed method can complete accurate image retrieval and text retrieval. Moreover, the mean average precision (MAP) has reached more than 0.3, the area of precision-recall rate (PR) curves are better than other comparison methods, and they are applicable.

1. Introduction

With the advancement of digitalization, more and more people use the Internet to obtain the information they need. How to make users accurately and quickly search for the information they need has become a hot issue [1]. In the era of mobile Internet, each of us is receiving massive amounts of information from the Internet, while at the same time generating massive amounts of multimedia information, that is, multimodal data [2]. The original form of cross-modal retrieval is similar to that of single-mode retrieval. With the growth of multimodal data, it is more difficult for users to retrieve the information they are interested in efficiently and accurately [3]. There are many retrieval methods so far, most of which are based on a single modality, such as searching for articles by text, searching for pictures by pictures, or multimodal search on the surface. In fact, it is in the form of search keywords to query and request the most matching content among many resources on the Internet.

In order to meet people's actual needs and provide better retrieval services, scholars are committed to the research on relevant methods and practice in the field of cross-modal retrieval. Therefore, the cross-modal retrieval method has a wide range of application scenarios and research significance. How to mine the effective information in these multimodal data is an important problem in the research field of cross-modal retrieval.

Researchers found a semantic gap between the low-level features of data and high-level semantics, and the data of different modalities are heterogeneous [4, 5]. It can be seen that the core of cross-modal retrieval research is to mine the associated information between different modal data. How to mine this associated information has become the key to the research of cross-modal retrieval technology.

In recent years, with the rapid development of deep learning technology, people have become more and more capable of solving more complex machine learning problems and have made great progress in analyzing and processing multimodal data [6]. Multimodal content analysis has broad application prospects in various fields such as smart cities, smart homes, and smart transportation. Based on the breakthrough progress in the application research of deep learning in the monomodal field, it is applied to the theoretical research of cross-modal retrieval tasks, and technical practice is provided at the same time [7].

The current cross-modal retrieval system modelling mainly solves two problems: one is how to complete the unified mapping of different modal information features and the second is how to ensure the retrieval rate on the basis of improving the retrieval rate of retrieval models [8]. These two problems are interdependent. Due to the diversity and heterogeneity of different modal information, the feature extraction method and unified representation form of each modal become the key to solving the problem [9, 10]. In addition, the corpus with three modalities and above is less researched, and the corpus with two modalities is more common. In particular, the corpus with the modal alignment of images and text is more common.

2. Related Research

Because there is a huge heterogeneous gap in different modal data, how to effectively measure the content similarity of different modal data has become a major challenge [11]. Nowadays, many cross-modal retrieval methods have been proposed [12].

2.1. Real-Valued Cross-Modal Retrieval Method. Cross-modal retrieval methods based on real-valued representation can generally be divided into two categories: canonical correlation analysis (CCA) and deep learning [13]. CCA uses different modal data to form sample pairs, learns a projection matrix, and projects different modal data to a common latent subspace, and then in the subspace, measures the similarity between modal data [14]. Reference [15] proposed a new multilabel kernel canonical correlation analysis (ml-KCCA) method for cross-modal retrieval, which uses the high-level semantic information reflected in multilabel annotations to enhance the kernel CCA. Reference [16] proposed cross-media correlation learning with deep canonical correlation analysis (CMC-DCCA). It can better mine the complex correlation between cross-media data and achieve better cross-media retrieval performance. However, the performance of its feature extraction algorithm highly depends on the size of the sample set, and it is difficult to obtain training samples for noncooperative targets in actual situations. How to efficiently set the parameter range still needs further exploration.

The cross-modal retrieval method based on deep learning makes full use of the powerful feature extraction capabilities of deep learning models, learns the feature representation of different modal data, and then establishes semantic associations between modalities at a high level [17]. Reference [18] proposed a two-stage deep learning method for supervised cross-modal retrieval, extending the traditional norm-related analysis from 2 views to 3 views and conducting supervised learning in two stages. The evaluation results on two publicly available datasets show that the proposed method has a better performance. However, there is still room for optimization for the detection accuracy of complex retrieval environments. At present, the dimensionality obtained by the representation learning model when automatically extracting features is relatively high. Particularly for the cross-modal retrieval model based on deep learning, the sample feature dimension obtained in the representation stage is usually not less than 4096, and the final feature dimension is still too high [19]. Reference [20] proposed an image retrieval method combining deep Boltzmann machine (DBM) and CNN to extract high-order semantic features of the image.

2.2. Cross-Modal Retrieval Method Based on Hash Transformation. The cross-modal retrieval method based on real-valued representation has the problems of time-consuming calculation and large demand space when facing large-scale data. Therefore, an information retrieval method based on hash transformation appears. This method is based on the paired sample pairs of different modal data, learns the corresponding hash transformation, maps the corresponding modal data features to the Hamming binary space, and then realizes faster cross-modal retrieval in this space [21]. The premise of hash transformation is that the hash codes of similar samples are also similar. Reference [22] proposed a method called DNDCMH. This algorithm uses binary vectors specifying the existence of specific facial attributes as input queries to retrieve relevant facial images from the database. Secondly, the dimension reduction methods such as principal component analysis (PCA) can reduce the feature dimension to a certain extent, but under the premise of maintaining the necessary retrieval accuracy, the dimension that can be reduced is quite limited and lacks efficient and reasonable retrieval mechanism that can adapt to large-scale image sets [23]. Reference [24] proposed a new self-supervised deep multimodal hashing (SSDMH) method. However, cross-modal retrieval still only realizes the matching of image content and subject words, ignoring a large amount of content-based, subtle, and important image information [25]. Reference [26] proposed a deep hashing method that can combine stacked convolutional autoencoders with hash learning and hierarchically map the input image to a low-dimensional space. Some additional relaxation constraints are added to the objective function to optimize the hash algorithm. Experimental results on ultra-high-dimensional image datasets show that the proposed method has good stability in cross-modal retrieval, but the detection timeliness needs to be optimized. However, various models have their specific adaptation targets, advantages, and limitations. How to combine the advantages of models and various algorithms in practical applications to construct a universal cross-modal retrieval model is one of the urgent problems to be solved in the current cross-modal retrieval research.

2.3. Other Cross-Modal Retrieval Methods. In addition to the above classical methods, there are some other methods. For example, Feng et al. [27] proposed an automatic encoder

(Corr-AE) model, which is characterized by using two autoencoder networks to encode image vectors and text vectors with each other to obtain two correlation loss terms for model training. Reference [28] proposed a retrieval method based on multimodal semantic autoencoder. This method uses an encoder decoder to learn projection and preserve feature and semantic information while ensuring embedding. The 2-way net model proposed in [29] also applies the idea of autoencoder, which is optimized in more detail than Corr-AE. Reference [30] proposed a graphic matching method based on semantic concepts and order (SCO), which is characterized by introducing a multilabel classification mechanism when retrieving images. Specifically, SCO performs a multilabel classification operation for each candidate image extracted by the target detection network so that each candidate image can not only carry entity category information but also add some attribute labels.

According to the above analysis, (1) in CCA method, the single-mode feature representation of different data is extracted first, and then associated learning is carried out. This two-stage method cannot ensure that the extracted single-mode feature is the effective representation required by associated learning. (2) In the deep learning method, most networks use shallow networks to model the association learning part, ignoring the high-level semantic association between modes. (3) In the deep hashing method, some information will be lost when it converts the modal representation to hash coding.

Therefore, effective feature extraction and feature association learning are key to improving the accuracy of cross-modal retrieval. In order to make better association learning between different modal data, a cross-modal image and text retrieval method combining efficient feature extraction and interactive learning convolutional autoencoder (CAE) is proposed in this paper. The innovations of the proposed method are as follows:

(1) Image feature extraction: The new convolution kernel constructed by 2DPCA is integrated into the image feature extraction based on residual network, which avoids the complex operation of traditional PCA and reduces the dimension of image spatial features.

(2) Cross-modal CAE architecture: Based on the traditional multimodal CAE architecture, a feature association module (i.e., joint public representation) is integrated to associate the representations of each mode to realize interactive learning, make the learned intermediate representation of each mode contain the association relationship between modes, and improve the accuracy of cross-modal retrieval.

3. Method Framework

3.1. Overall Framework. In order to make full use of the advantages of complementary information of multimodal data, in the training stage, the proposed method takes image data and text data as the input of the network at the same time, carries out interactive learning of image and text features through multimodal CAE model, and generates the classification model of the retrieval system. In the test stage, the image or text features are input into the classification model for discrimination, and the retrieval results are obtained. The overall architecture of the proposed method is shown in Figure 1.

Among them, the image data use the residual network as the image feature extractor and introduce two-dimensional principal component analysis (2DPCA) to construct a new convolution kernel. The text data use word2vec and long short-term memory (LSTM) network as the text feature extractor. The network fusion layer is designed using cross-modal convolution CAE based on interactive learning, and the two modal data features are fused and sent to the next fully connected layer. In order to learn the nonlinear mapping from the image-text data feature space to the semantic label space and prevent overfitting, the Batch Norm layer and the ReLU layer are added to the fully connected layer. The output dimension of the final fully connected layer is consistent with the data dimension of the real label. The proposed method takes full advantage of the complementary information of different modal data for multimodal data-image data and text data.

3.2. Improved Image Feature Extraction of Convolution Kernel

3.2.1. Convolution Neural Network Is Used to Extract Image Features. For the extraction of image features, a very mainstream residual network, which is more suitable for image features, is selected. The network has five convolution stages, each of which has a corresponding pooling operation. After inputting a piece of image data, it is processed in layers of convolution, and the size of the output image feature map is $7 \times 7 \times 2048$, which can be processed according to the needs of subsequent machine learning tasks.

Image modal data have high dimensionality and rich content information. The selection of a deep convolutional neural network will extract effective visual monomodal representation features. Using W_x to simplify the model parameters of the entire embedded subnetwork, the feature output h_x of the image modal data after passing through this network is

$$h_x = f_x(X; W_x), \tag{1}$$

where X is the input image modal data.

3.2.2. Constructing a New Convolution Kernel by Introducing 2DPCA. PCA is a linear analysis method to extract the main features of data in high-dimensional space and transform it into low-dimensional vector space. 2DPCA directly utilizes the two-dimensional information of the image, avoiding the complicated calculations brought about by PCA's row and column vector conversion while retaining the spatial characteristics of the image. Assuming that there are M images $I = \{I_1, I_2, \ldots, I_M\}$ of size $w \times h \times c$, the average image of the sample can be expressed as

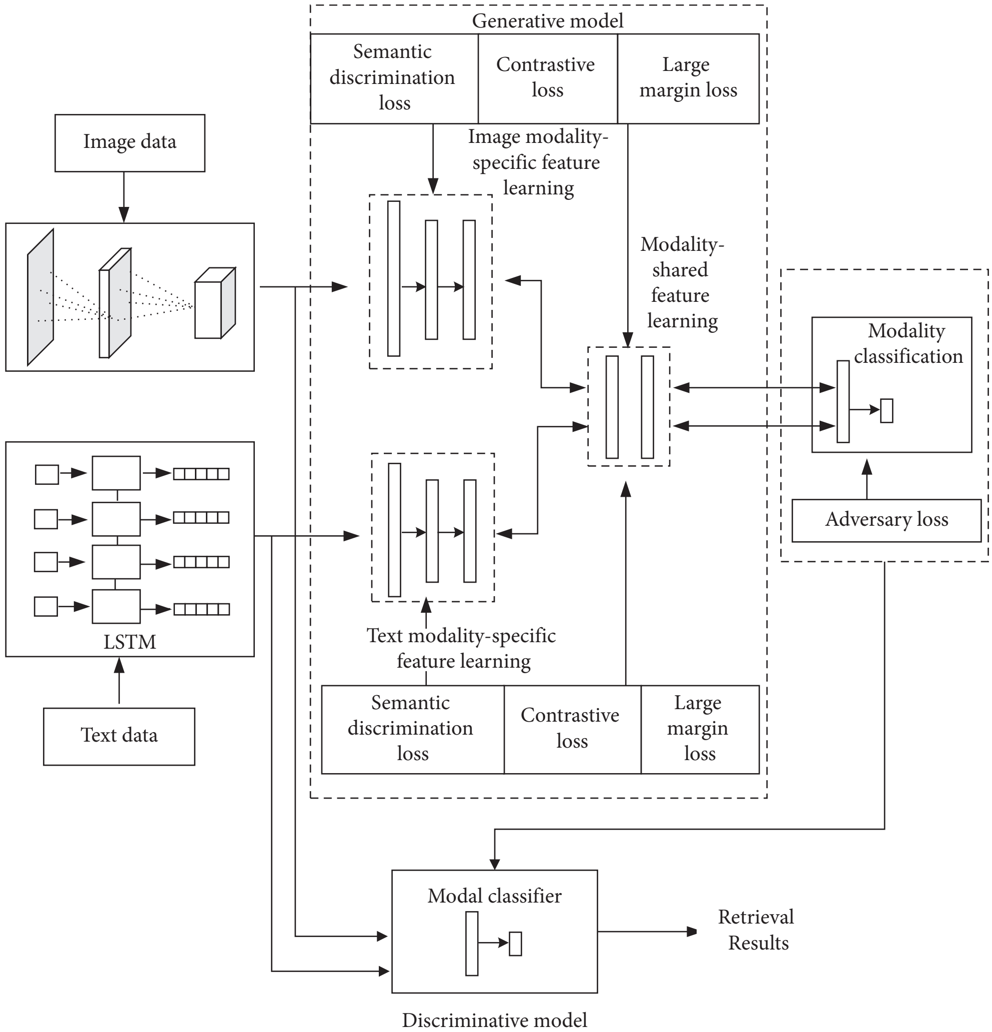

Figure 1: Overall framework of the proposed method.

$$\bar{I} = \frac{1}{M}\sum_{i=1}^{M} I_i. \tag{2}$$

The difference image between each sample and the average image is

$$Z(i) = I_i - \bar{I}. \tag{3}$$

The required covariance matrix is

$$C_{n\times n} = \frac{1}{M}\sum_{i=1}^{M} \left(I_i - \bar{I}\right)^T \left(I_i - \bar{I}\right). \tag{4}$$

The optimal projection subspace $U = \{\eta_1, \eta_2, \ldots, \eta_d\}$ can be constructed using the orthogonal eigenvectors corresponding to the first d eigenvalues of the covariance matrix. Mapping the original image to the projection space can obtain the feature image $T_i = Z_i U$ after dimensionality reduction. The flow of the 2DPCA algorithm is shown in Figure 2.

3.3. Text Feature Extraction. In the multimodal dataset used, the text modal data are mainly in the form of long text, so a reasonable representation that matches its characteristics is used for text feature extraction.

Short sentences: the text representation of short sentences is simpler than long sentences. It is represented by word vector (word2vec); that is, words are converted into vectors that can be accepted by machine learning tasks.

Long sentences: The representation of long sentences is more complicated because the words of the sentence are related to each other. The first or several words will affect the understanding of the following sentence, so the sentence's meaning should be grasped from the whole. In order to retain the previous information in the text, the LSTM network is used to first represent each word in the sentence by a word vector $Y = \{y_1, y_2, \ldots, y_c\}$, and c represents the number of words in the sentence, so each sentence is represented as a 300-dimensional word vector sequence.

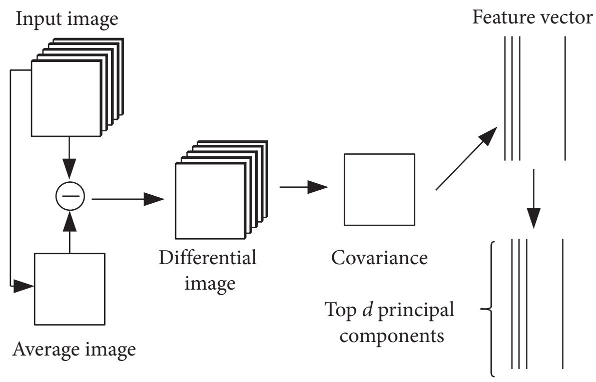

Figure 2: The flow of the 2DPCA algorithm.

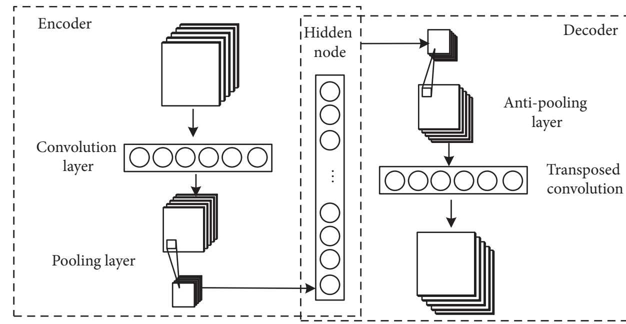

Figure 3: CAE model.

4. Cross-Modal Convolutional Autoencoder

4.1. Classical Convolutional Autoencoder (CAE). An autoencoder (AE) is an unsupervised learning algorithm that makes the output close to the input by learning data representation. AE extracts data features through an encoder and then decodes the acquired features through a decoder to realize the reconstruction of input data. CAE is based on unsupervised AE, combining the convolution and pooling operations of CNN to convolve the encoder and decoder to achieve better feature extraction [31]. The single-layer CAE network model is shown in Figure 3. The coding part is composed of a convolutional layer and a maximum pooling layer.

Given M_{C1} feature maps $I = \{I_1, I_2, \ldots, I_{C1}\}$, after convolution operation, a set of F_{C2} feature maps is obtained

$$g_n(i,j) = a\left(\sum_{u=-k}^{k}\sum_{v=-k}^{k} F_n^{(1)}(u,v) * I(i-u, j-v) + b_n^{(1)}\right), \quad (5)$$

where $g_n(i,j)$ is the activation value at pixel (i,j) in the activation map of the n-th channel and $a(\cdot)$ is a nonlinear activation function. The size of the filter is $F_{C2} = 2k+1$. $F_n^{(1)}$ is the weight of the convolution filter in the encoding process, and the number of channels of each filter is the same as that of the input sample. $b_n^{(1)}$ is the offset of the encoder convolutional layer to the activation map of the n-th channel.

The convolutional layer of the convolutional encoding part outputs a feature map of size $(O_{C1} - F_{C2}/S_{C2} + 1)^2 \times M_{C2}$. After the maximum pooling operation, the final output of the encoding part is obtained. Among them, $O_{C1} = ((w - F_{C1} + S_{C1})/S_{C1}F_{P1})$ is the output feature map size of the convolution module $C1$.

The decoding process is the process of reconstructing the original image from the feature activation map. CAE is a fully convolutional network, so the decoding process is mainly realized through deconvolution operation. Considering that the size of the feature activation map obtained after encoding is smaller than the original image, the size information of the original image cannot be reconstructed only through the transposed convolution of the decoding process. Therefore, it is necessary to perform zero padding operation on the input feature map to decode later; a reconstructed image with the same size as the original image can be reconstructed. The convolution output of the encoding part is used as the input of the decoder and then convolved with the convolution filter $F^{(2)}$ to obtain the reconstructed image:

$$\tilde{I} = f\left(G * F_n^{(2)} + b_n^{(2)}\right), \quad (6)$$

where G is the set of feature maps obtained by encoding and $b_n^{(2)}$ is the offset of the activation map of the n-th channel corresponding to the decoder deconvolution layer.

4.2. Cross-Modal CAE Based on Interactive Learning. Different from the existing multimodal CAE models [32, 33], while learning the representations of different modes, respectively, this method generates some association between the representations of each mode through a feature association module (i.e., joint public representation) after the hidden layer, to realize interactive learning. Therefore, the intermediate representation of each mode contains the correlation between modes, which helps to improve the accuracy of cross-modal retrieval. The proposed dual-mode interactive learning CAE architecture is shown in Figure 4.

The input text and image data are, respectively, passed through the convolution layer and the pooling layer to obtain the data representation. Then, through an intermediate interaction layer, the feature representation of text and image data is interactively learned to obtain a new joint public representation feature data. The original input can be obtained by deconvolution of the feature data [34–36].

In order to train the dual-mode interactive learning CAE, it is necessary to construct the objective function in the training stage. In classical CAE training, the objective function is usually to minimize the reconstruction error. However, in the dual-mode interactive learning CAE model, the interactive learning between multimodal features is integrated to improve the accuracy of model retrieval. Therefore, the objective function needs to include the goal of maximizing the correlation between the two modal features in the hidden layer.

The given input is $z_i = \{x_i; y_i\}$, where z_i is the associated representation of the input views x_i and y_i. Self-reconstruction loss and cross-reconstruction loss are defined as

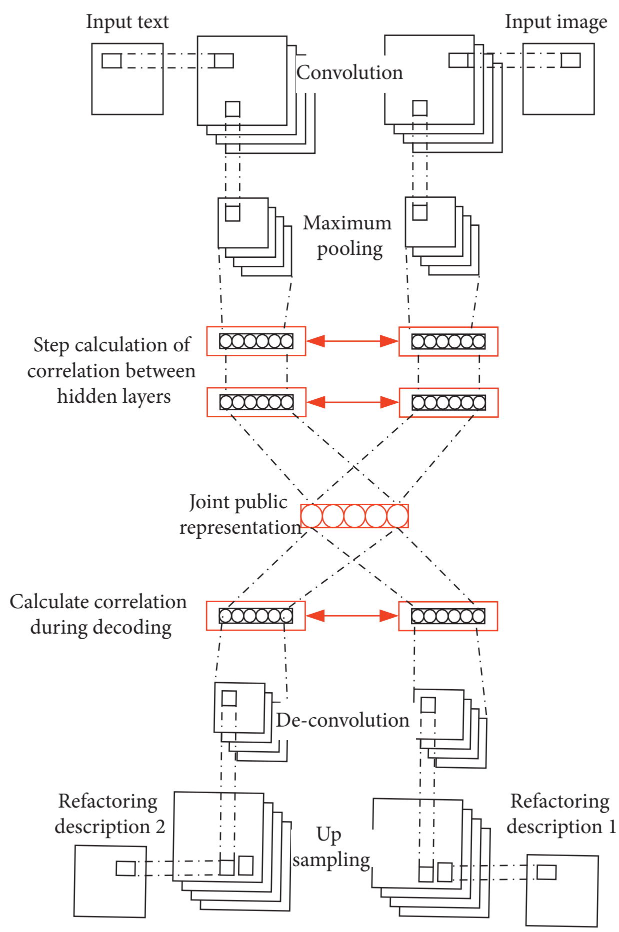

Figure 4: Dual-mode interactive learning CAE architecture.

$$\begin{aligned}
L_1 &= \sum_{i=0}^{N} L\left(z_i, g\left(h\left(z_i\right)\right)\right),\\
L_2 &= \sum_{i=0}^{N} L\left(z_i, g\left(h\left(x_i\right)\right)\right),\\
L_3 &= \sum_{i=0}^{N} L\left(z_i, g\left(h\left(y_i\right)\right)\right),\\
L_4 &= \sum_{k=0}^{K}\sum_{i=0}^{N} L\left(h\left(x_i\right)^k, h\left(y_i\right)^k\right),\\
L_5 &= \sum_{i=0}^{N} L\left(g\left(h\left(x_i\right)\right), g\left(h\left(y_i\right)\right)\right),
\end{aligned} \tag{7}$$

where g, h are the nonlinearity generally regarded as ReLU, $g(h(x_i^k))$ and $g(h(y_i^k))$ are the representations of the k^{th} intermediate hidden layer ($K = 2$), and L is the error function. In the loss L_2 and L_3 (for cross reconstruction), the 0 vector is used instead of another view to calculate x_i and y_i.

Finally, in order to enhance the interaction between the two modal features, the objective function of correlation loss is expressed as follows:

$$\begin{aligned}
L_6 &= \lambda \operatorname{corr}\left(h(X), h(Y)\right),\\
L_7 &= \sum_{k=0}^{K} \lambda_k \operatorname{corr}\left(h(X)^k, h(Y)^k\right),
\end{aligned} \tag{8}$$

where $h(X)$ and $h(Y)$ are the projections of the combined model (the projections of the joint public representation in Figure 4). X and Y are the representation of two modal features. λ_k is the relative regularization hyperparameter used for each k^{th} intermediate encoding step (similarly using λ in the decoding stage). In the encoding process, a convolution layer and two intermediate layers ($K = 2$) are used. For decoding, the deconvolution layer and an intermediate layer ($K = 1$) are used for reconstruction. λ affects the complexity of model training. When it is too small, the model is easy to overfit. When the value is large, it is easy to cause underfitting. Considering the search results on each dataset, $\lambda_1 = 0.004$ and $\lambda_2 = 0.05$ in item L_7 and $\lambda = 0.02$ in item L_6 are uniformly set here.

The correlation between the two views $h(X)$ and $h(Y)$ is

$$\operatorname{corr}(h(X), h(Y)) = \frac{\sum_{i=1}^{n}\left(h(x_i) - \overline{h(X)}\right)\left(h(y_i) - \overline{h(Y)}\right)}{\sqrt{\sum_{i=1}^{n}\left(h(x_i) - \overline{h(X)}\right)^2 \sum_{i=1}^{n}\left(h(y_i) - \overline{h(Y)}\right)^2}}, \tag{9}$$

where $\overline{h(X)}$ and $\overline{h(Y)}$ are the mean vectors of the hidden representations of the two views. $h(x_i)$ and $h(y_i)$ are hidden layer representations of a single modal view.

Integrate all objective functions to build a total objective function, which is expressed as follows:

$$L(\theta) = \sum_{i=1}^{5} L_i - \sum_{j=6}^{7} L_j, \tag{10}$$

where θ is the model parameter. The above formula minimizes self-reconstruction and cross-reconstruction and maximizes the association between views.

5. Experiment and Analysis

5.1. Experimental Dataset. In order to verify the performance of the proposed method, the effectiveness of the method is verified on three commonly used real cross-modal graphic retrieval datasets: Flickr30K dataset, MSCOCO dataset, and Pascal VOC 2007 dataset.

(1) Flickr30K: The Flickr30K dataset contains 31,783 images, and the English description of the images is 158,915 sentences. That is, each image corresponds to 5 sentences with different description sentences. The sentence descriptions of these images are obtained through manual annotation. The Flickr30K dataset is divided into three parts: 1000 images and corresponding descriptions as the verification dataset, 1000 images and corresponding descriptions as the test dataset, and the remaining part as the training dataset.

(2) MSCOCO: The MSCOCO dataset contains 123287 images, and each image also corresponds to 5 different description sentences. This dataset is divided into four parts, including 82783 images as the training dataset, 5000 images as the verification dataset, 5000 as the test dataset, and 30504 images as the reserved dataset.

(3) Pascal VOC 2007: The Pascal VOC 2007 dataset contains 5011 image-annotation pairs for training and 4952 image-annotation pairs for testing, all from the Flickr website. Each sample pair is labeled as one of 20 semantic categories. This dataset is randomly divided into three subsets: training set, test set, and validation set, which contain 800, 100, and 100 samples, respectively.

The experimental running environment is a PC configured with Intel Core i7-7700 CPU and Nvidia GTX1070Ti 8G video memory GPU. The deep learning framework used is PyTorch, and the development language is Python.

5.2. Performance Index and Comparison Method. The evaluation indexes commonly used in the cross-modal retrieval field are selected to compare and analyse the proposed methods: the mean average precision (MAP) and the precision-recall (PR) curve. Among them, MAP can effectively evaluate the experimental results through the positions of positive samples and negative samples in the search results. AP represents the average accuracy of each specific search, calculated as follows:

$$\mathrm{AP} = \frac{\sum_{k=1}^{n} (P(k) \times \varphi(k))}{N}, \tag{11}$$

where N represents the total number of search results that belong to the same semantic category as the query. n is the number of all results returned by the search. k is the position index in the search result sequence. $P(k)$ is the accuracy of the first k search. $\varphi(k)$ indicates whether the k th search result and the query have the same semantic category (the same value is 1, and the value is 0 if they are different).

The value of MAP is the average of AP values corresponding to multiple searches:

$$\mathrm{MAP} = \frac{\sum_{q=1}^{Q} \mathrm{AP}(q)}{Q}, \tag{12}$$

where Q represents the total number of searches.

Use MAP@R to indicate that given a query, sort the top R results with the highest similarity according to the similarity. The accuracy of these R results was averaged:

$$\mathrm{MAP@R} = \frac{\sum_{k=1}^{R} P(k) \times \varphi(k)}{N}. \tag{13}$$

The PR curve is the curve of the accuracy rate changing with the recall rate, which is used as the performance evaluation index in cross-modal retrieval.

In the experiment, the three selected datasets have two modes: image and text. This model is compared with the reference model on two retrieval tasks, namely, retrieving text with images and retrieving images with text. For example, when retrieving images based on text, the proposed method selects each text in the test set to retrieve all images in the test set and finally obtains the retrieval result.

In order to verify the effectiveness of the proposed method, it is compared with two classical methods: CCA and deep hashing method. The corresponding research is a multilabel kernel canonical correlation analysis (ml-KCCA) method proposed in [15] and a cross-modal hashing retrieval method (DNDCMH) proposed in [22]. In addition, in order to highlight the effectiveness of the interactive learning CAE model proposed in this paper, it is compared with other methods based on the CAE model, such as the text retrieval method based on multimodal semantic automatic encoder (SCAE) proposed in [28].

5.3. Cross-Modal Retrieval Example

5.3.1. Image-Text Retrieval Analysis. The image-text retrieval results obtained by the proposed method and [22] retrieval method are shown in Table 1. It is the text retrieval

Table 1: Comparison of text retrieval.

Retrieving images	Methods	Text retrieval results (top 5)
	Reference [22] (Flickr30K)	**1. A man wearing a black sweater cook food in a pan while standing in a cluttered kitchen.** **2. A man cooking food on the stove.** **3. A man is cooking on a stove in a kitchen, using wooden utensil.** 4. A cook is posing for a camera while cooking. 5. Man with a white T-shirt and black rimmed glasses cooking a pot of food on the stove.
	The proposed method (Flickr30K)	1. **A man preparing food in his kitchen.** 2. **A man wearing a black sweater cook food in a pan while standing in a cluttered kitchen.** 3. **A man cooking food on the stove.** 4. **A man is cooking on a stove in a kitchen, using wooden utensil.** 5. A man stirring a pot of liquid in this kitchen.

result of the image on the Flickr30K test set. The text in bold is the correct recall text, and the text without bold is the wrong recall text.

It can be seen from Table 1 that the proposed method has better retrieval results in terms of recall index. Specifically, in the text retrieval task, the proposed method uses image search to find the correct text sorting more advanced. These visually presented phenomena more intuitively illustrate the effectiveness of the proposed method. In [22], DNDCMH is used to achieve text retrieval. Due to the lack of image feature extraction effect, the correct text is less.

5.3.2. Text-Image Retrieval Analysis. In order to compare the performance of the proposed method and the comparison method [15, 22, 28], in text-image retrieval, the 'car' is used as the query text to retrieve the image on the Pascal VOC 2007 dataset. The top 5 images retrieved by various methods are shown in Figure 5.

It can be seen from Figure 5 that compared to other comparison methods, the text retrieval results of the proposed method are more reasonable. Since the proposed method uses word2vec and LSTM network for text feature extraction, the extraction effect is better. Therefore, the retrieval images obtained through the CAE network of interactive learning are more accurate.

5.4. Performance Comparison. In order to demonstrate the retrieval performance of the proposed method in the three datasets, it is compared with the methods in [15, 28] and [22]. The MAP values of the first 50 results of the four methods are shown in Table 2.

It can be seen from Table 2 that, in the two retrieval tasks of retrieving images by text and retrieving text by images, the proposed method has significantly improved MAP on these three datasets compared with other comparison methods. Since the Pascal VOC 2007 dataset has the largest magnitude, the proposed method has the most significant improvement on Pascal VOC 2007. On Flickr30K, MSCOCO, and Pascal VOC 2007, three cross-modal graphic retrieval domain datasets, the average MAP on the two retrieval tasks of the proposed method are 0.359, 0.334, and 0.309, respectively. Compared with [15], it increased by 58.85%, 44.59%, and 58.46%; compared with [28], by 14.14%, 9.57%, and 10.69%; and compared with [22], by 16.56%, 12.46%, and 24.10%.

In addition, with different methods on the Flickr30K dataset, the PR curves for two different retrieval tasks of image retrieval and text retrieval are shown in Figure 6. The ordinate represents the precision, and the abscissa represents the recall. Similarly, the PR curves of two different retrieval tasks on MSCOCO and Pascal VOC 2007 datasets with different methods are shown in Figures 7 and 8, respectively.

It can be seen from Figure 6 that whether it is image retrieval text or text retrieval image, the area of the PR curve of the proposed method is larger than other comparison methods. Because it adopts the cross-modal retrieval method of image and text interactive CAE and incorporates 2DCPA into the feature extraction, the accuracy of retrieval is improved. Reference [15] proposed a ml-KCCA method to achieve cross-mode retrieval, but the retrieval performance is low due to poor feature extraction. Reference [28] combined low-level features and high-level semantic information to learn feature representation. Although it solves the problem of feature representation, due to the lack of feature interaction, the retrieval accuracy for complex environments still needs to be improved. Reference [22] used the DNDCMH method to complete cross-modal retrieval. However, this method has poor universality, so the retrieval performance is inferior to the proposed method.

It can be seen from Figure 7 that the retrieval performance of the proposed method is better than other comparison methods in the two retrieval tasks of image retrieval text and text retrieval image. When the recall is 0.2, the accuracy of each method reaches the maximum, and the recall increases and decreases continuously. Since the MSCOCO dataset has relatively few samples, the area composed of PR curves of different methods has increased compared to the Flickr30K dataset.

It can be seen from Figure 8 that, like the first two datasets, the retrieval performance of the proposed method on the Pascal VOC 2007 dataset is better than other comparison methods. The proposed method uses the residual network to extract image features and introduces 2DPCA to construct a new convolution kernel. At the same time, using

FIGURE 5: An example of image retrieval with text "car."

TABLE 2: MAP ($R = 50$) values of different methods on three datasets.

Datasets	Methods	MAP values Image query	Text query	Average
Flickr30K	Reference [15]	0.215	0.237	0.226
	Reference [28]	0.304	0.312	0.328
	Reference [22]	0.281	0.335	0.308
	The proposed method	0.338	0.379	0.359
MSCOCO	Reference [15]	0.198	0.264	0.231
	Reference [28]	0.293	0.319	0.301
	Reference [22]	0.275	0.318	0.297
	The proposed method	0.324	0.343	0.334
Pascal VOC 2007	Reference [15]	0.192	0.198	0.195
	Reference [28]	0.279	0.295	0.262
	Reference [22]	0.251	0.247	0.249
	The proposed method	0.306	0.311	0.309

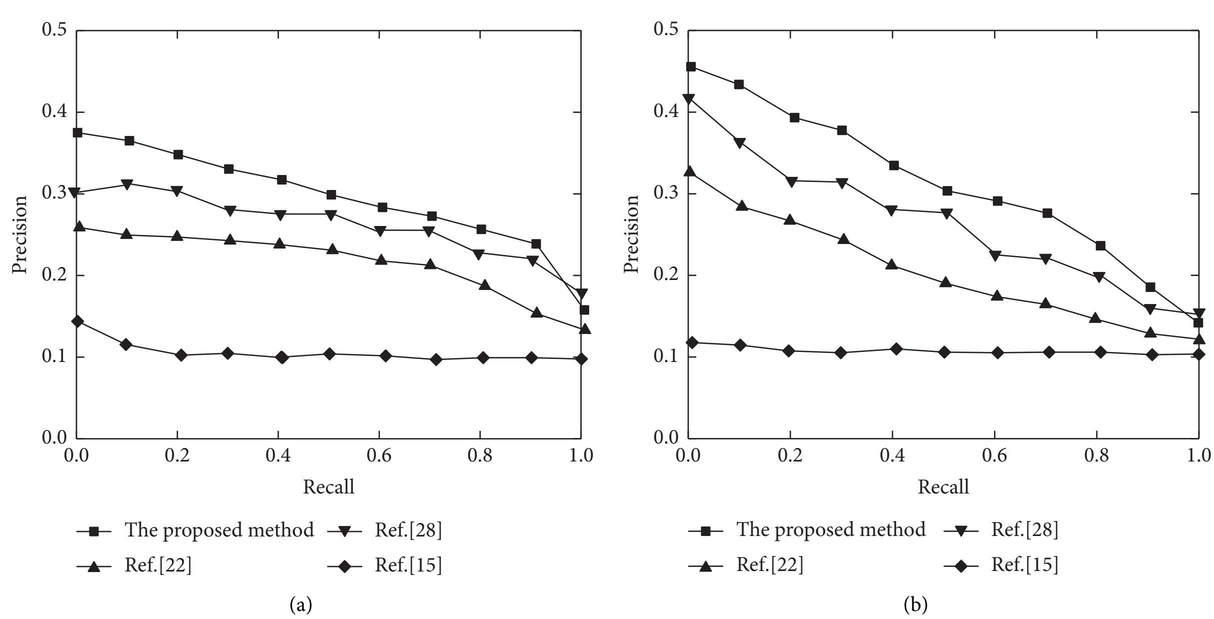

FIGURE 6: PR curves on Flickr30K datasets. (a) Retrieving text with images. (b) Retrieving images with text.

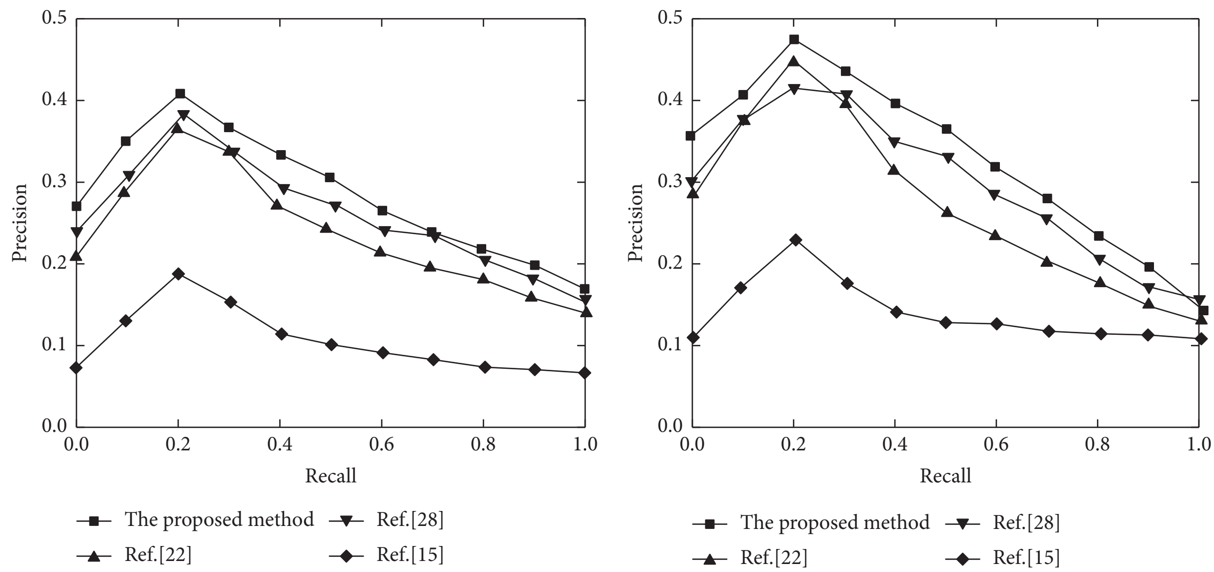

(a) (b)

Figure 7: PR curves on the MSCOCO datasets. (a) Retrieving text with images. (b) Retrieving images with text.

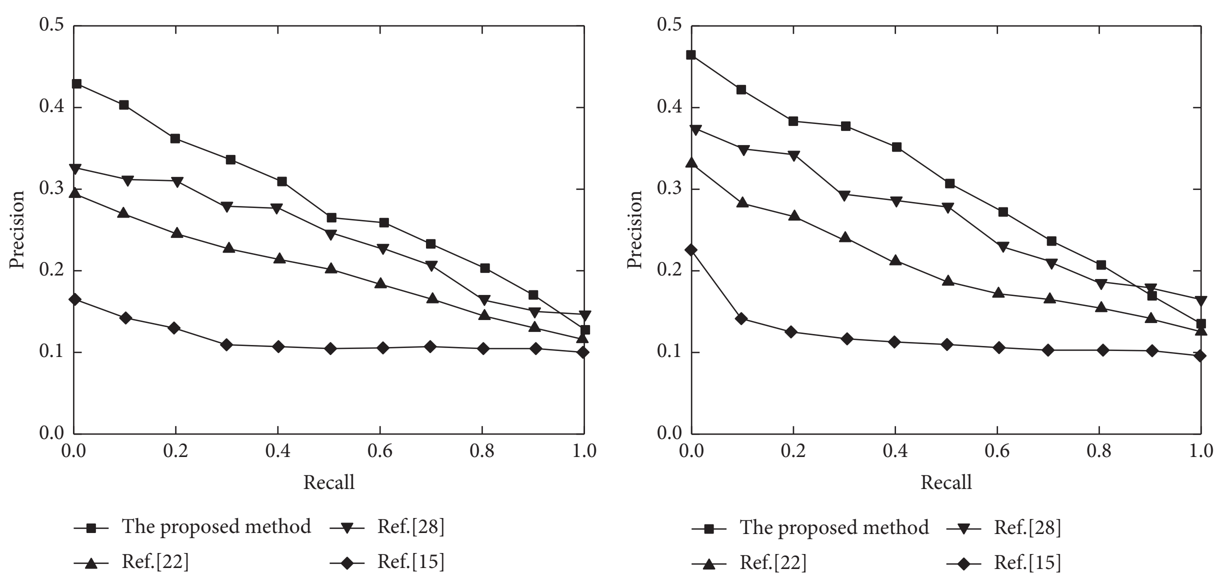

(a) (b)

Figure 8: PR curves on Pascal VOC 2007 datasets. (a) Retrieving text with images. (b) Retrieving images with text.

word2vec and LSTM network for text feature extraction, feature extraction is more efficient. It is better than [15] using existing label information and [22] using specific images. In addition, [28] used the semantic CAE method to learn multimodal mapping and projected multimodal data into low dimensional space to retain feature and semantic information and improve retrieval accuracy. However, the proposed method uses the CAE model with interactive learning, and the fusion effect of image and text feature learning is better, so the retrieval performance is more ideal.

In summary, it can be seen from the PR curves on different datasets that the proposed method shows the best results under different recall. This proves that the deep interactive learning method constructed by it is effective.

6. Conclusion

Cross-modal retrieval technology meets people's more diverse retrieval needs and solves the problems of heterogeneous gap and semantic gap between different modal data. However, the retrieval accuracy still needs to be improved. For this reason, a cross-modal image retrieval method combining efficient feature extraction and interactive learning CAE is proposed. The residual network convolution kernel is improved by incorporating 2DPCA to extract image features, and text features are extracted through LSTM and word vectors to obtain image and text features. After that, the two features are input into the cross-modal CAE of interactive learning, and through the interactive learning of the middle layer, the image-text retrieval is realized. In addition, the proposed method is experimentally demonstrated based on the Flickr30K, MSCOCO, and Pascal VOC 2007 datasets. The results show that the proposed method can complete accurate image retrieval and text retrieval. Moreover, the average MAP on the two retrieval tasks is 0.359, 0.334, and 0.309, which are higher than other comparison methods. The same is true for the area formed by the PR curve.

At present, the method proposed in this paper is only suitable for cross-modal retrieval between text and image, but there are many types of multimodal data on the network. Next, more data of different media types such as audio and video will be expanded to meet people's broader retrieval needs.

Data Availability

The data included in this paper are available without any restriction.

Conflicts of Interest

The authors declare that there are no conflicts of interest regarding the publication of this paper.

Acknowledgments

This work was supported by the National Natural Science Foundation of China (61402350, 61103143, U1404620, and U1404622), the Key Scientific and Technological Project of Henan Province (182102310034, 172102310124, and 212102210400), and the Key Research Projects of Henan Provincial Department of Education (20A520046).

References

[1] L. Ma, H. Li, F. Meng, Q. Wu, and K. N. Ngan, "Global and local semantics-preserving based deep hashing for cross-modal retrieval," *Neurocomputing*, vol. 312, no. 10, pp. 49–62, 2018.

[2] Y. Wu, S. Wang, and Q. Huang, "Online fast adaptive low-rank similarity learning for cross-modal retrieval," *IEEE Transactions on Multimedia*, vol. 22, no. 5, pp. 1310–1322, 2020.

[3] L. Mou and X. X. Zhu, "Vehicle instance segmentation from aerial image and video using a multitask learning residual fully convolutional network," *IEEE Transactions on Geoscience and Remote Sensing*, vol. 56, no. 11, pp. 6699–6711, 2018.

[4] J. Zhang and Y. Peng, "Multi-pathway generative adversarial hashing for unsupervised cross-modal retrieval," *IEEE Transactions on Multimedia*, vol. 22, no. 1, pp. 174–187, 2020.

[5] Y. Tao, K. Xiangwei, Y. Lianshan, T. Wenjing, and T. Qi, "Efficient discrete supervised hashing for large-scale cross-modal retrieval," *Neurocomputing*, vol. 385, no. 04, pp. 358–367, 2020.

[6] D. Xie, C. Deng, C. Li, X. Liu, and D. Tao, "Multi-task consistency-preserving adversarial hashing for cross-modal retrieval," *IEEE Transactions on Image Processing*, vol. 29, no. 02, pp. 3626–3637, 2020.

[7] X. Yuan, H. Zhong, Z. Chen, F. Zhong, and Y. Hu, "Multimedia feature mapping and correlation learning for cross-modal retrieval," *International Journal of Grid and High Performance Computing*, vol. 10, no. 3, pp. 29–45, 2018.

[8] P. Hu, D. Peng, X. Wang, and Y. Xiang, "Multimodal adversarial network for cross-modal retrieval," *Knowledge-Based Systems*, vol. 180, pp. 38–50, 2019.

[9] H. Chen, G. Ding, Z. Lin et al., "ACMNet: adaptive confidence matching network for human behavior analysis via cross-modal retrieval," *ACM Transactions on Multimedia Computing, Communications, and Applications*, vol. 16, no. 1, pp. 1–21, 2020.

[10] C. Ushasi, B. Biplab, B. Avik, and D. Mihai, "A deep learning based model for cross-modal retrieval in remote sensing," *Pattern Recognition Letters*, vol. 131, no. 03, pp. 456–462, 2020.

[11] G. Guanghua, L. Jiangtao, L. Zhuoyi, H. Wenhua, and Z. Yao, "Joint learning based deep supervised hashing for large-scale image retrieval," *Neurocomputing*, vol. 385, no. 93, pp. 348–357, 2020.

[12] Y. Fang, H. Zhang, and Y. Ren, "Unsupervised cross-modal retrieval via multi-modal graph regularized smooth matrix factorization hashing," *Knowledge-Based Systems*, vol. 171, no. 05, pp. 69–80, 2019.

[13] C. Jing-Jing, P. Lei and N. Chong-Wah, Cross-modal recipe retrieval with stacked attention model," *Multimedia Tools and Applications*, vol. 77, no. 22, Article ID 29457, 2018.

[14] A. Jiang, H. Li, Y. Li, and M. Wang, "Learning discriminative representations for semantical crossmodal retrieval," *Multimedia Systems*, vol. 24, no. 1, pp. 111–121, 2018.

[15] Y. Jia, L. Bai, S. Liu, P. Wang, J. Guo, and Y. Xie, "Semantically-enhanced kernel canonical correlation analysis: a multi-label cross-modal retrieval," *Multimedia Tools and Applications*, vol. 78, no. 10, Article ID 13169, 2019.

[16] S. Wang and Z. Shi, "Cross-media semantic retrieval with deep canonical correlation analysis," *Journal of University of ence and Technology of China*, vol. 48, no. 4, pp. 322–330, 2018.

[17] Y. Liu, K. Cai, C. Liu, and F. Zheng, "Csrncva: a model of cross-media semantic retrieval based on neural computing of visual and auditory sensations," *Neural Network World*, vol. 28, no. 4, pp. 305–323, 2018.

[18] J. Shao, Z. Zhao, and F. Su, "Two-stage deep learning for supervised cross-modal retrieval," *Multimedia Tools and Applications*, vol. 78, no. 12, Article ID 16615, 2019.

[19] Y. Yu, S. Tang, K. Aizawa, and A. Aizawa, "Category-based deep CCA for fine-grained venue discovery from multimodal data," *IEEE Transactions on Neural Networks and Learning Systems*, vol. 30, no. 4, pp. 1250–1258, 2019.

[20] Q. Wu, "Image retrieval method based on deep learning semantic feature extraction and regularization softmax[J]," *Multimedia Tools and Applications*, vol. 79, no. 13, pp. 9419–9433, 2020.

[21] Z. Xie, L. Li, X. Zhong, Y. He, and L. Zhong, "Enhancing multimodal deep representation learning by fixed model reuse," *Multimedia Tools and Applications*, vol. 78, no. 21, Article ID 30769, 2019.

[22] F. Taherkhani, V. Talreja, M. C. Valenti, and N. M. Nasrabadi, "Error-corrected margin-based deep cross-modal hashing for

facial image retrieval," *IEEE Transactions on Biometrics, Behavior, and Identity Science*, vol. 2, no. 3, pp. 279–293, 2020.
[23] Z. Xi, L. Hanjiang, and F. Jiashi, "Attention-aware deep adversarial hashing for cross-modal retrieval," in *Proceedings of the European Conference on Computer Vision*, pp. 614–629, Munich, Germany, September 2018.
[24] G. Wu, J. Han, Z. Lin, G. Ding, B. Zhang, and Q. Ni, "Joint image-text hashing for fast large-scale cross-media retrieval using self-supervised deep learning," *IEEE Transactions on Industrial Electronics*, vol. 66, no. 12, pp. 9868–9877, 2019.
[25] M. Zhang, H. Zhang, J. Li, Y. Fang, L. Wang, and F. Shang, "Multi-modal graph regularization based class center discriminant analysis for cross modal retrieval," *Multimedia Tools and Applications*, vol. 78, no. 19, Article ID 28285, 2019.
[26] M. Zareapoor, J. Yang, D. K. Jain, P. Shamsolmoali, N. Jain, and S. Kant, "Deep semantic preserving hashing for large scale image retrieval," *Multimedia Tools and Applications*, vol. 78, no. 17, Article ID 23831, 2019.
[27] F. Feng, X. Wang, and R. Li, "Cross-modal retrieval with correspondence autoencoder," in *Proceedings of the ACM International Conference on Multimedia*, pp. 7–16, New York, NY, USA, November 2014.
[28] Y. Wu, S. Wang, and Q. Huang, "Multi-modal semantic autoencoder for cross-modal retrieval," *Neurocomputing*, vol. 331, no. 28, pp. 165–175, 2019.
[29] A. Eisenschtat and L. Wolf, "Linking image and text with 2-way nets," in *Proceedings of the IEEE Conference on Computer Vision and Pattern Recognition (CVPR)*, Honolulu, HI, USA, July 2017.
[30] Y. Huang, Q. Wu, and L. Wang, "Learning Semantic Concepts and Order for Image and Sentence matching," 2017, https://arxiv.org/abs/1712.02036.
[31] C. Zhou, L. M. Po, W. Y. F. Yuen et al., "Angular deep supervised hashing for image retrieval," *IEEE Access*, vol. 7, no. 99, Article ID 127521, 2019.
[32] G. Wu, J. Han, Y. Guo et al., "Unsupervised deep video hashing via balanced code for large-scale video retrieval," *IEEE Transactions on Image Processing*, vol. 28, no. 4, pp. 1993–2007, 2018.
[33] S. Basavaraju and A. Sur, "Multiple instance learning based deep CNN for image memorability prediction," *Multimedia Tools and Applications*, vol. 78, no. 24, Article ID 35511, 2019.
[34] Y. Li, L. Wan, T. Fu, and W. Hu, "Piecewise supervised deep hashing for image retrieval," *Multimedia Tools and Applications*, vol. 78, no. 17, Article ID 24431, 2019.
[35] Y. Gu and J. Yang, "Densely-connected multi-magnification hashing for histopathological image retrieval," *IEEE Journal of Biomedical and Health Informatics*, vol. 23, no. 4, pp. 1683–169, 2019.
[36] H. Hu, K. Wang, C. Lv, J. Wu, and Z. Yang, "Semi-supervised metric learning-based anchor graph hashing for large-scale image retrieval," *IEEE Transactions on Image Processing*, vol. 28, no. 2, pp. 739–754, 2018.

Hindawi
Scientific Programming
Volume 2022, Article ID 6201367, 11 pages
https://doi.org/10.1155/2022/6201367

Research Article

Design and Implementation of Intelligent Vehicle Control System Based on Internet of Things and Intelligent Transportation

Zhihui Hu and Hai Tang

Hubei University of Automotive Technology, Shiyan 442002, Hubei, China

Correspondence should be addressed to Zhihui Hu; hzh@huat.edu.cn

Received 16 October 2021; Revised 6 November 2021; Accepted 9 November 2021; Published 10 January 2022

Academic Editor: Le Sun

With the improvement of urbanization and the continuous expansion of transportation scale, traffic problem has become an important problem in our life. How to ensure traffic safety has become the key issue for the government to implement social management. Nowadays, Internet of Things (IOT) technology is widely used in the industrial technology field. It will have a great impact on human production and life. Intelligent transportation system is a research field involving many high and new technologies. This paper proposes an intelligent transportation system based on Internet of Things technology. This paper presents the optimal design structure of intelligent transportation system based on Internet of Things technology. The experimental results show that the intelligent transportation system can effectively realize the information interaction between the vehicle and the control center and understand the road conditions in advance. At the same time, the intelligent transportation system can improve the driving speed of vehicles on the road, make effective use of resources, reduce economic losses during vehicle operation, and reduce air pollution caused by gasoline emission.

1. Introduction

With the development of urbanization, more and more vehicles have flooded into our life and work. In the process of social and economic development, people will pay more attention to traffic problems. At present, the number of motor vehicles in our country is as high as more than 200 million, and the traffic flow and the number of vehicles have a close relationship; how to avoid traffic congestion to ensure smooth traffic has become a hot topic [1]. In order to better control traffic problems, the emergence of intelligent system can be said to have a great significance. Intelligent traffic control system using Internet of Things technology can bring great benefits, such as reducing traffic pollution, easing traffic congestion, and reducing energy consumption [2].

As a newly proposed emerging technology, the Internet of Things (IoT) has experienced rapid development from its first appearance to the present. The emergence of WSN and RFID, two core technologies of the Internet of Things, has laid a foundation for realizing intelligent monitoring and remote intelligent identification by using them. Through the above technologies, the Internet of Things seamlessly connects the Internet, devices, and people together. Through the Internet of Things technology, we can effectively connect small smart devices and even personal computers to a variety of networks, so that anyone can enjoy high-quality information services, no matter where and when [3, 4]. Through the intelligent expert system, people can timely and effectively receive the status information of the goods they care about and make timely decisions, so as to achieve the effect of energy saving and emission reduction. It is becoming more and more urgent to introduce high technology to control traffic. Therefore, due to the emergence of the Internet of Things, intelligent identification and management can be realized through relevant technologies, so as to solve or alleviate the abovementioned social contradictions [5].

Intelligent transportation is another typical application of IOT. Because of the high social value of realizing intelligent transportation through Internet of Things technology, intelligent transportation can become one of the two typical applications of Internet of Things. Because of this, the research on the related technologies of intelligent transportation is particularly important [6]. It can promote the development of the whole social industrial chain, drive the relevant social and economic progress, and make a significant contribution to the realization of a harmonious society. Intelligent transportation is to apply many cutting-edge technologies to traffic management, so as to realize real-time, accurate and effective transportation management and integrated control system [7]. As an important branch of the Internet of Things, intelligent transportation can generate many related value-added services. The Internet of Vehicles is a new branch of the Internet of Things defined by Chinese people under such background. The so-called Internet of Vehicles refers to the application of the Internet of Things in intelligent transportation [8]. The main roads on Beijing are all clogged, so the government has issued the policy of limiting car license plate purchase and driving. This not only restricts the development of national economy but also seriously affects the normal life of ordinary people.

This paper fully investigated the key technologies of intelligent transportation in the Internet of Things environment, designed an intelligent system, and studied the two core technologies of intelligent transportation in view of the two core problems of transportation. It also summarizes the intelligent transportation system under the Internet of Things environment proposed in the paper and makes a summary for some of the problems and makes a plan and outlook for the existing related problems, puts forward improvement measures, and makes a work plan [9].

Internet of Things (IOT) refers to the real-time collection of any object or process that needs monitoring, connection, and interaction through various information sensors, radio frequency identification technology, global positioning system, and other devices and technologies, so as to realize the ubiquitous connection between things and people and realize the intelligent perception of things and processes through various possible network access identification and management [10]. The Internet of Things is an information carrier based on the Internet and traditional telecommunication networks. It allows all ordinary physical objects that can be independently addressed to form an interconnected network. The system also provides an adaptive cruise control system based on distance detection. At the same time, the system will give an audio and visual alarm if the distance detected by neighboring vehicles is less than the safe distance.

The main contributions of this paper can be described as follows:

(1) We deeply study the intelligent transportation technology, Internet of Things technology, and the main characteristics and application fields of these technologies. We have studied the main ways of the application of Internet of Things technology in the field of intelligent transportation.

(2) We introduce the Internet of Things technology into intelligent transportation filed, and we give the experiments which can verify the good performance of this method.

The structure of the rest of this paper is described as follows: Section 2 gives the overview for the Internet of Things. Section 3 gives the overview of intelligent transportation systems. Section 4 describes intelligent transportation system in the Internet of Things environment. Section 5 gives the conclusion.

2. Overview for the Internet of Things

The Internet of Things (IoT) is regarded as a major development and change opportunity in the field of information, and it will be widely used in many fields. Sensor network, transmission network, and application network constitute the Internet of Things system. In the sensor network, we arrange a large number of various sensors and related wireless communication nodes around the monitoring target regularly or irregularly [11]. The environmental parameters of the monitored target or its surroundings can be sensed through current, voltage, or digital sensors. In the transmission network, the perceived data are transmitted to the wireless communication device as the sink node through the wireless communication device as the terminal in a single hop or after multiple hops. Several sink nodes are combined to aggregate all the perceived data to the gateway device together [12, 13]. Data aggregated to a gateway device can be transmitted to a cluster server over multiple types of networks such as Internet, GSM, and 3G. In the application network, including many terminal devices, through the Internet and other external networks can read the data and status of the entire network, and according to the feedback information further reverse control of the operation of the entire network. Through intelligent decision-making and manual decision-making, information acquisition and reverse control can be carried out through terminals such as computers and mobile phones. The architecture diagram of the Internet of Things is shown in Figure 1.

Figure 2 shows a complex wireless sensor network, typically consisting of a data awareness network, a data transmission network, and a data processing and intelligent decision management center. In the wireless sensor network, the network topology is particularly important. So, we will take a comprehensive look at its properties. In a communication network, the main parameters to measure its performance are service packs and QoS for propagating messages. QoS refers to message delay, arrival time, bit error rate, packet loss rate, economic cost and transmission power, etc. Several basic network topologies is described in Figure 3. Generally speaking, the specific form of network topology is always in accordance with QoS considerations, combined with installation environment, economic considerations, and application applications. A communication network is composed of many nodes with computing power and bidirectional communication ability of sending and receiving data, as shown in Figure 3. A basic network topology has various forms of expression, such as star, ring, bus, tree, fully connected, and network [14]. A single network may consist of a number of interrelated subnets of different topologies. Networks can be further divided into local area networks (LANs) and wide area networks (WANs).

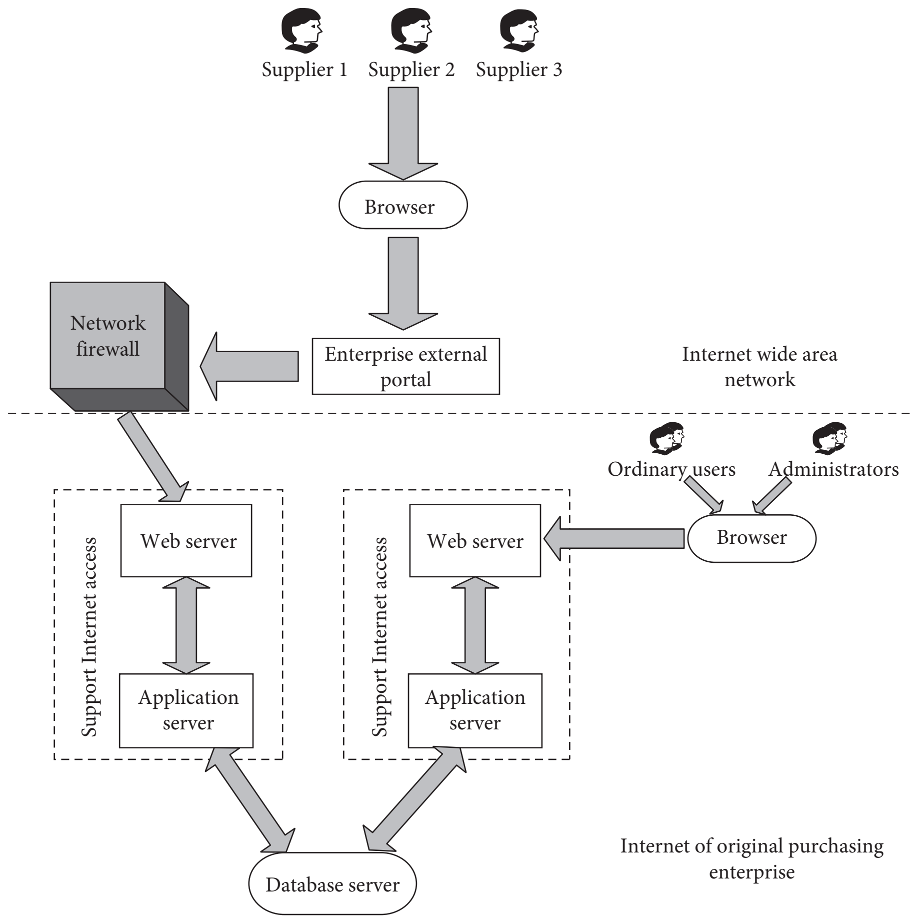

Figure 1: Architecture of the Internet of things.

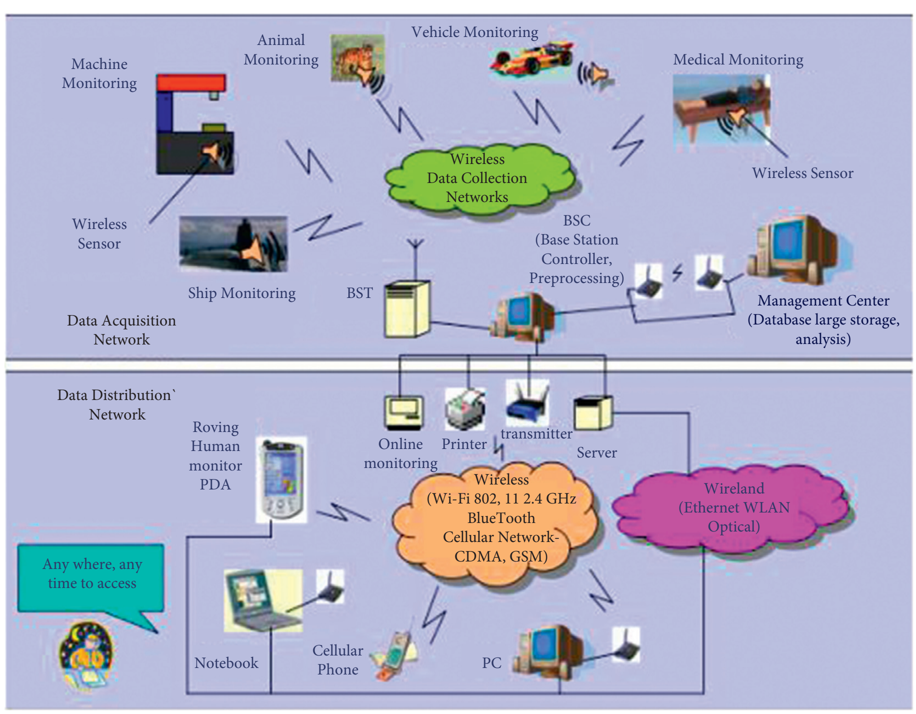

Figure 2: Structure of wireless sensor.

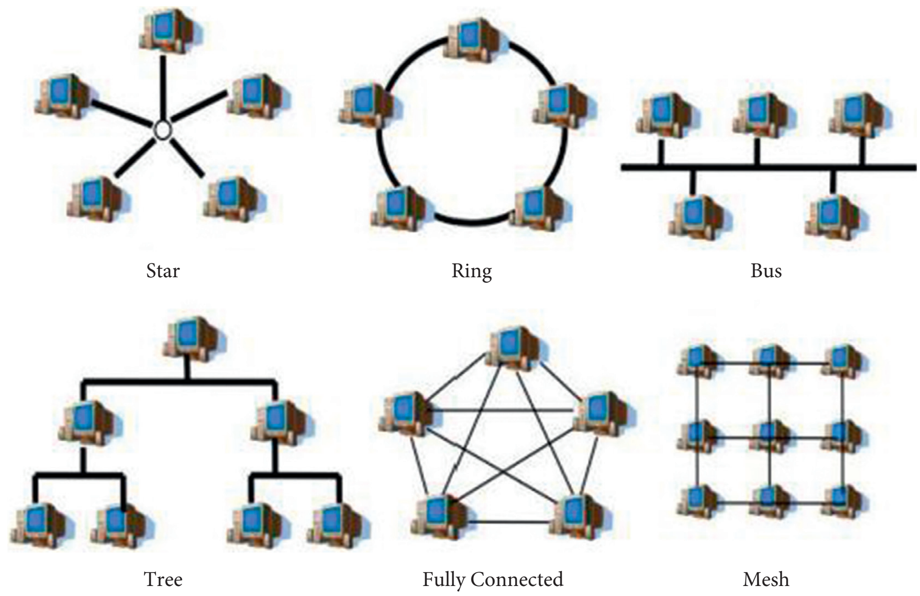

Figure 3: Structure network topology. (a) Star. (b) Ring. (c) Bus. (d) Tree. (e) Fully connected. (f) Mesh.

Radio frequency identification (RFID) is an integral part of our life, and its emergence has increased productivity and brought convenience to our life [15, 16]. It realizes digital information communication between a fixed position and a moveable object or a moveable object through short-range radio technology. The tag usually reads the stored data in its internal memory and changes the encoding loaded on the tag antenna so that it can be used to store the data. Figure 4 shows the main components of the new electronic tag, including the storage and memory function, display function, automatic reading function, positioning function, and input and output function of the new electronic tag.

The reason why the Internet of Things and the concept of Smart Earth can be realized is that the world has already stepped into the era of 3I, namely, instrumented, interconnected, and intelligent. We only need "a hundred steps on the road, one step further" enables the IoT world to be implemented anywhere, anytime and in any way [17]. Typical applications of the Internet of Things are reflected in the following aspects: urban management, such as intelligent transportation, intelligent energy conservation, intelligent buildings, cultural relics protection, digital museums, real-time monitoring of ancient trees, digital libraries and digital archives, digital home, positioning and navigation, modern logistics management, food safety management, retail, digital medical, and anti-intrusion system. From these typical applications of the Internet of Things, we can see that the intelligent transportation system is an application demonstration that can be used as a typical environment. At the same time, we can apply multiple intelligent transportation systems to public facilities and then form a community to form an intelligent community of information, thus paving the way for realizing the lofty goal of a smart city [18].

3. Overview of Intelligent Transportation Systems

Under the control of the Internet of Things, the intelligent transportation system realizes the interaction between people and information in the traffic system. Through various sensing technologies, the acquired object information is analyzed and processed, and the final conclusions are transmitted to the object, making it more convenient and fast for the object to travel in traffic [19, 20]. The intelligent transportation model of the Internet of Things includes three layers: the perception layer, the transmission layer, and the application layer. The sensing layer includes tools such as sensors and terminal devices [21]. FRID technology has been applied to the perceptual layer and has been successfully applied to the electronic nonstop toll collection system in China. The role of the transport layer is to transfer information, and there are communication networks and gateways. The role of the application layer is the application software at the receiver and publisher of the message. The structural model composed of three layers is called DCM three layers. Overall framework of the IOT is shown in Figure 5.

The occurrence of traffic accidents and the number of vehicles, the skills of the driver, has a great relationship, especially on the highway, and driving inexperience is easy to happen traffic accidents; traffic accidents once cannot be solved in time, will cause a second accident, threatening the lives and property of drivers and drivers [22]. Usually, video image processing technology is used to detect traffic accidents. Video technology can intuitively collect the vehicle information of the accident. However, video technology may be affected by weather conditions, and the monitoring may lose its function in serious cases. In addition to video image processing technology, acoustic technology can also be used

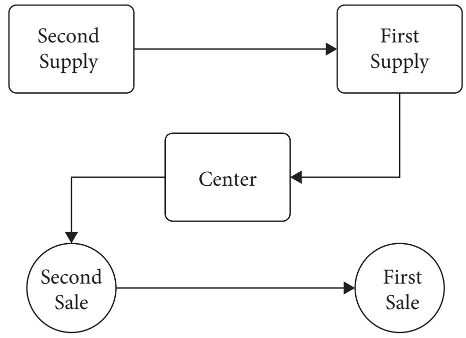

Figure 4: Overall framework of the new electronic tag.

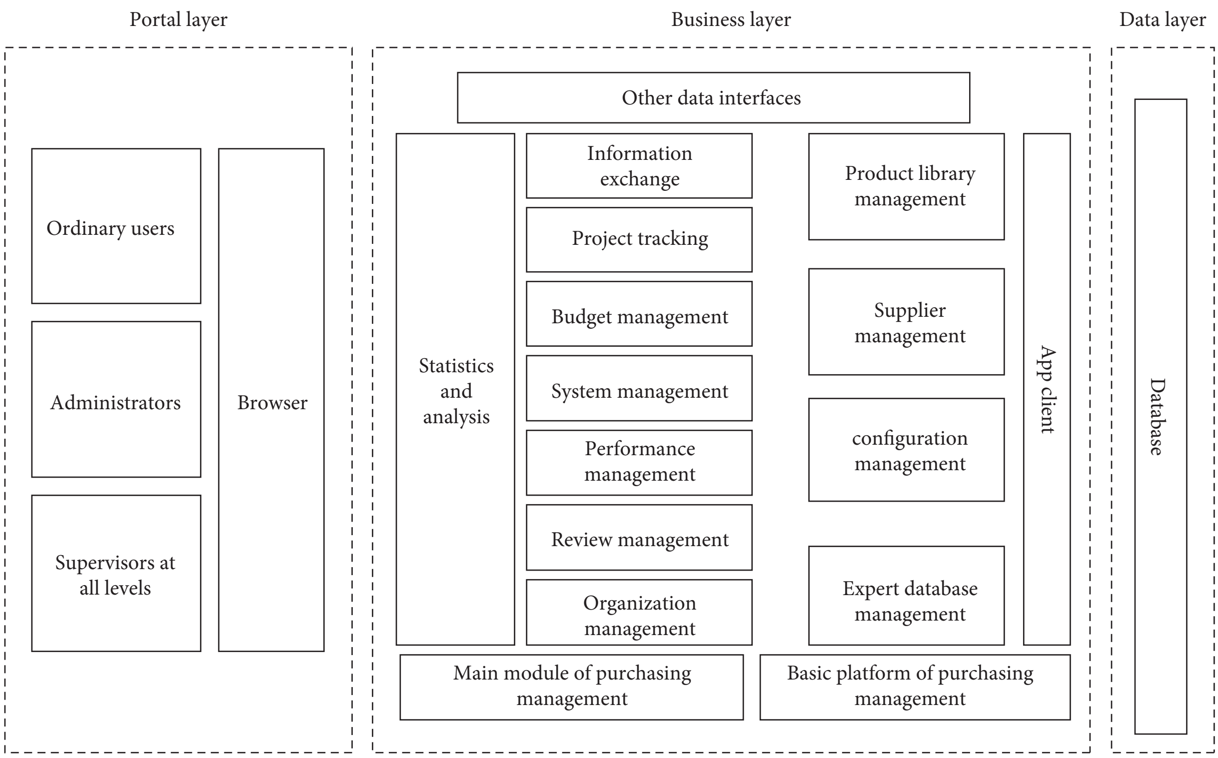

Figure 5: Overall framework of the IOT.

to detect vehicle accidents. When a collision occurs, the vehicle will emit impact noise, and its high frequency part has obvious characteristics. The frequency resolution of the wavelet transform decreases with the increase of the frequency in the time-frequency plane. Wavelet packet characteristics can be used to reflect the system state of the feature vector, using the method of pattern recognition to identify and classify the features, can be in the shortest time to seek help, reduce the occurrence of secondary accidents, effective detection, and treatment of vehicle accidents [23].

Each vehicle in the IoT intelligent transportation system is equipped with a FRID tag, which is designed to detect the vehicle in various aspects. The vehicle information collected by FRID is relayed to a reader, which decodes the data and relayed it to a data center. The reader can then identify the vehicle's origin, brand and traffic conditions, calculate the exact traffic flow, and develop management and control measures. FRID sensing detection can save the workload of vehicle inspection and improve the work efficiency. When FRID is used in conjunction with other automatic control systems, it can be used to organize vehicles that do not have permission to enter a certain area or vehicles with violation records to enter a certain road section. The efficient management improves the quality of service while greatly reducing labor costs [24].

Intelligent transportation systems can provide accurate and fast information through the Internet, facilitating travel. In addition, it can also be used to inform impending dangers and possible delays, while improving efficiency and reducing waste of fuel. Intelligent transportation systems can produce safer, more efficient, and more environmental friendly vehicle movements. Because of the rapid development of intelligent transportation, advanced intelligent transportation assistant

(ADAS) and intelligent vehicle type detection system have been promoted. Intelligent transportation assistant refers to the integration, such as cars, trucks, bus arrangement of sensors, and control systems, the aim is, through the collection of sensor technology and algorithm of vehicle network, to help the driver away or warning of potential risks better help driver to provide advice, effectively avoid the occurrence of traffic accidents, at the same time can get road vehicle information. It provides the basis for intelligent decision of traffic system.

4. Intelligent Transportation System in the Internet of Things Environment

Referring to the newly proposed Internet of Vehicles (IoV) technology, in this chapter, we realized the vehicle type identification based on the acoustic sound system by using the embedded technology and the integration of KPCA and SVM. The uniqueness of this algorithm is that it uses KPCA to identify vehicles. The outcomes indicated that it can accurately distinguish vehicle types.

In this chapter, based on the previous research, we put forward an innovative feature extraction algorithm: kernel complex discrimination algorithm, which can be widely used in the intelligent transportation assistant by combining with the embedded platform of low power consumption and high efficiency and verify its effectiveness. In the next step, more environmental factors (such as reflections, bad weather, and differences in light intensity at different times) will be taken into account to make the system more robust.

4.1. Brief Introduction of Intelligent Transportation System in the Environment of Internet of Things. Intelligent transportation combines many advanced technologies in today's world. Among them, there are not only low-level data awareness technology but also middleware data communication technology and network technology. There are not only the upper level of big data processing technology but also reverse automatic control technology and information release technology. In the course of establishing and perfecting the information and accurate transportation and management system, the integration of the abovementioned technologies has laid a solid foundation for the emergence of the system. It is the expansion of wireless sensor network in the field of transportation and the perception and processing ability of computer system to data. It can carry on the information monitoring and management and also can release the real-time traffic information to the drivers and passengers in the car and can carry on the emergency warning.

Internet of Vehicles, as an important part of intelligent transportation system, has been widely concerned by people since its appearance. From the rise of the Internet of Things in the late 1990s to the subsequent concept of smart city and smart Earth, these concepts are derived into the transportation system and hence the emergence of smart transportation and the Internet of Vehicles. The Internet of Things is transformed and evolved from the sensor network. The rapid development of IoT-related industries, especially the rapid integration in the field of transportation, promotes the emerging direction of intelligent transportation—Internet of Vehicles. A simple description of the Internet of Vehicles is that different types of sensors, such as temperature and humidity sensors, light sensors, or cameras, are arranged on the "car," or the abovementioned sensors are deployed in the surrounding environment of the "car," so as to realize the information interaction between cars and cars, and between cars and people. It is the expansion of wireless sensor network in the field of transportation and the perception and processing ability of computer system for the century. Through the Internet of Vehicles, it can effectively realize the rapid dispatch of cars and people, and at the same time, it can monitor and manage their information. In addition, through a powerful integrated information service system, real-time traffic information can be released to the drivers and passengers in the car, and the emergency warning can be carried out. In terms of policy, the Internet of Vehicles and related projects have also received strong support from governments around the world. A car will also be connected to the Internet and its related industry in China as a national major project research projects, car networking as breakthrough point of the Internet of things, and improve people's livelihood of major science and technology application, getting priority support in terms of economy; it provides capital for the vigorous development of car networking support, believe in the following the development of science and technology, will certainly come to the fore.

4.2. Two Key Technologies. The two core problems of traffic are traffic congestion and traffic safety. As the traffic system becomes more and more complex, the traffic management will develop to the precision, information, and intelligence. Experience-based traffic management will no longer fit the current needs, and there is an urgent need to introduce high technology to control traffic. The emergence of vehicle network and Internet of Things has laid a theoretical foundation for it. This paper studies the intelligent vehicle statistics system and the intelligent traffic assistant system in the intelligent transportation and provides solutions for the two core problems mentioned above in the traffic.

The occurrence of traffic accidents and the number of vehicles and the skills of the driver has a great relationship, especially on the highway; driving inexperience is easy to happen traffic accidents; traffic accidents once cannot be solved in time will cause a second accident, threatening the lives and property of drivers and drivers. Usually, video image processing technology is used to detect traffic accidents. Video technology can intuitively collect the vehicle information of the accident. However, video technology may be affected by weather conditions, and the monitoring may lose its function in serious cases. In addition to video image processing technology, acoustic technology can also be used to detect vehicle accidents. When a collision occurs, the vehicle will emit impact noise, and its high frequency part has obvious characteristics. Wavelet packet characteristics can be used to reflect the system state of the feature vector, using the method of pattern recognition to identify and classify the features, and can be in the shortest time to seek help and reduce the occurrence of secondary accidents, effective detection, and treatment of vehicle accidents.

Each vehicle in the IoT intelligent transportation system is equipped with a FRID tag, which is designed to detect the vehicle in various aspects. The vehicle information collected by FRID is relayed to a reader, which decodes the data and relayed it to a data center. The reader can then identify the vehicle's origin, brand, and traffic conditions, calculate the exact traffic flow, and develop management and control measures. FRID sensing detection can save the workload of vehicle inspection and improve the work efficiency. When FRID is used in conjunction with other automatic control systems, it can be used to organize vehicles that do not have permission to enter a certain area or vehicles with violation records to enter a certain road section. The efficient management improves the quality of service while greatly reducing labor costs.

In this paper, we design and develop a signal processing system based on sound feature matching on an integrated module. The main hardware system includes an integrated processor and a wireless transmission module. In terms of software, we chose KPCA as the feature extraction method and support vector machine as the classifier because of its nonlinearity. This system can detect a moving car and determine its type. By building a test platform, we compare this method (KPCA + SVM) with other traditional methods and find that this method is more accurate than other methods. In this paper, we also designed an integrated signal processing embedded system, as the system can use image features to classify vehicles, better help drivers to provide driving advice, and effectively avoid traffic accidents. We choose the kernel identification method based on Fourier transform (FKD) as the feature extraction algorithm; because of its high-precision nonlinear ability, we can realize the image preprocessing by selecting the best frequency band and then choose the nearest neighbor classifier (NNC) to identify the image. The system also uses embedded devices to detect the distance between vehicles, effectively helping vehicles avoid collisions.

4.3. Designing Systems. With the development of transportation industry, the length of roads is increasing. We can detect different information on different roads by using the intelligent transportation system. Static information refers to the object information of vehicles or detection points, while dynamic information refers to the road traffic conditions, abnormal traffic events, and environmental information. Collecting dynamic information is the basis of traffic control and management. The main information collected includes density, flow, vehicle type, vehicle speed, and other traffic environment information. In the process of building an intelligent transportation system, it is not only necessary to collect traffic operation information in a timely manner but also to transmit information in a timely manner. Intelligent transportation should learn to use advanced technology to transform and connect the wireless access network and the core network to meet the requirements of power consumption of the sensing layer. Now, we should pay more attention to FRID, 4G networks, and sensor networks, and closely integrate wired networks and wireless networks to address each other's shortcomings and effectively improve the standardization and compatibility of network transmission.

At present, the traffic management and dispatching system in China can timely and accurately collect and process information. IoT Intelligent transportation system is a combination of multiple traffic management subsystem, such as video monitoring system and traffic detection system, as well as the good visual interface, which can realize the control center and information to accept good interaction between objects, effectively improve the efficiency of work, and eventually reach good scheduling results. Intelligent traffic management and scheduling system based on Web GIS has a wide range of access, which can manage and collect data sources. Users in the system can access the database through web browser at any time and realize remote data sharing, which is conducive to drivers' timely understanding of traffic conditions. At the same time, the intelligent traffic management and scheduling system based on web GIS also makes full use of the network resources, the server side distributes the basic work, the client side completes the operation with small data volume, effectively balances the computing load, and seamlessly integrates other information services, which is conducive to the addition and upgrading of the following sequence modules and functions.

One of the core problems to be solved is traffic congestion, so the acquisition of vehicle information on the road is particularly important. By using the data of vehicle type, speed and basic information of vehicle and people in operation, reasonable postregulation, and road information analysis can be carried out, so as to solve or alleviate the traffic congestion problem. Therefore, the statistics of vehicle types has become a hot topic in the research of the Internet of Vehicles. There are many ways to identify different types of vehicles by identifying different types of signals, such as vehicle detection and identification using magnetic fields, images, and sounds. To sum up, we choose to transmit acoustic signals through wireless sensor network for vehicle identification. The movement of vehicles on the ground affects the environment in different ways. Suppose similar vehicles under the same operating conditions produce the same sound. In view of this, we can classify vehicles according to their sound. This has led to research on how best to obtain the sound of each type of vehicle and extract the best feature description. In this chapter, a novel sound signal acquisition and feature extraction method based on KPCA is proposed, and the method is compared with other techniques. Support vector machine (SVM) is used as a classifier to detect recognition rate.

Compared with the traditional sound perception system, the embedded speech perception system has the advantages of greater amplification, faster processing speed, and higher recognition rate than the ordinary sound perception system. With a perceived CC2430 voice transmission system and a ARM11 processing system

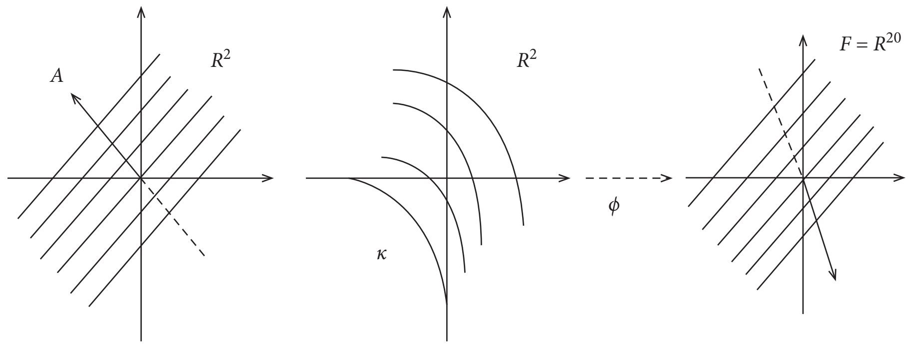

Figure 6: PCA.

composed of voice identification system is compared, we found that more than sound perception transmission system, a sound perception transmission system consisting of two sensors and a signal transmission components) compared with a single voice transmission system perception, collected a better and more full of voice. It provides an accurate signal source for the subsequent feature extraction system, thus obviously improving the sound recognition rate. Multisensor system can identify the sound perceived by each sensor.

Vehicle characteristics refer to the process of developing a vehicle's characteristics for use in classification. Usually, the processing of this feature is done using a general-purpose computer. Suppose there are M cars, all of which are target classification systems, and let V_j, $j = 1, \ldots, K$ is the sound of the JTH car. A collection of sound samples is called a training group. The training set classifier is then used to tag each vehicle generated. The V_j training sample refers to the sound sample collected from the jth vehicle. The training samples are used as classifier training and will generate a marker for each vehicle. Through the nonlinear mapping, the KPCA algorithm converts the sound signal from the data space to the feature space, in the feature space, and then using the principal component analysis, we can calculate the best projection direction and get the nonlinear feature. PCA is shown in Figure 6.

In the higher dimensional feature space, we do the kernel PCA transformation of the sound signal, just as we do the PCA transformation in the input space. So, it becomes nonlinear when the input space is projected onto the main eigenvector. More importantly, for KPCA, it does not actually map into F space, but performs kernel function K calculations in the input space. To sum up, we carry out the KPCA transformation by introducing the nonlinear transformation function, and each sound sample vector X_k is projected from the input space onto the higher dimensional feature space F. Then, from the feature space F, combined with the existing PCA algorithm, we can obtain the main features of the target.

4.4. Analysis of System Experiment Results. In our experimental platform, we induced RRS from a number of experiments. All experiments are carried out in a quiet area, where there is no abnormal noise such as wind noise. Because we do not know if there is an effective algorithm for mixed sound recognition, this case was not included in our experiment. Because the different sound samples of training vehicles will affect the recognition rate, we adjust the number of training samples appropriately. Our sound database includes 40 samples from six different types of cars. First of all, under the condition of using ML classifier, we conducted relevant experiments on the influence of different training samples on the recognition rate. Then, we change the classifier type, using KNN classifier and SVM classifier to do relevant experiments. The number of training samples increased from 4 to 12, with a step of 1. Figures 7–10 show the recognition rate distribution diagrams of different feature extraction methods and different classifier combinations. In order to verify the performance, we give the comparison of the methods of FFT, PSD, PCA, and FPCA.

Fourier transform was carried out on the collected car images, and the related points' location can be shown in Figure 11.

The image resolution ($800 * 640$) is 30 frames per second. As shown in Figure 11, the intranet system for crude oil trade procurement is grouped into three major components, namely, portal, business, and data layer. The portal layer is mainly responsible for accessing registered users to the system. All administrators with authority may access the enterprise internal network through any browser, and before entering the intranet, the web server shall process the access request, encapsulate the request, and send the request to the server. The main task of the business layer is to handle the requests from the web server and support the whole business layer by using the APP terminal. Function layer used to realize the functions of the intranet system, including the basic part of procurement management, the main part of procurement management, and the interface function with other systems.

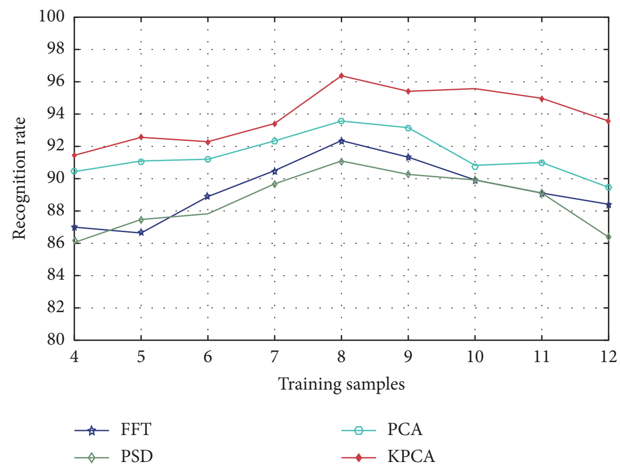

Figure 7: ML classifier.

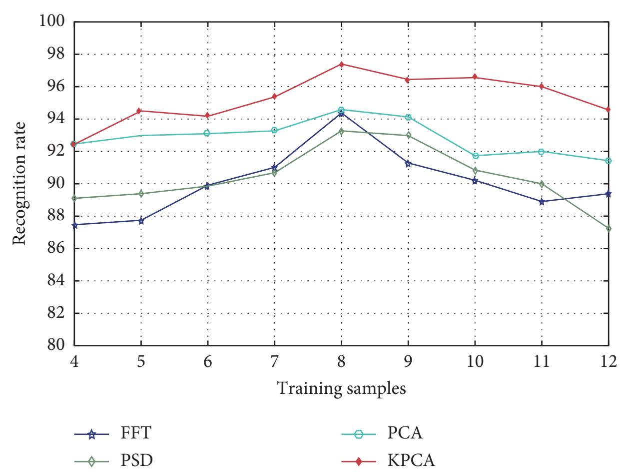

Figure 8: KNN classifier.

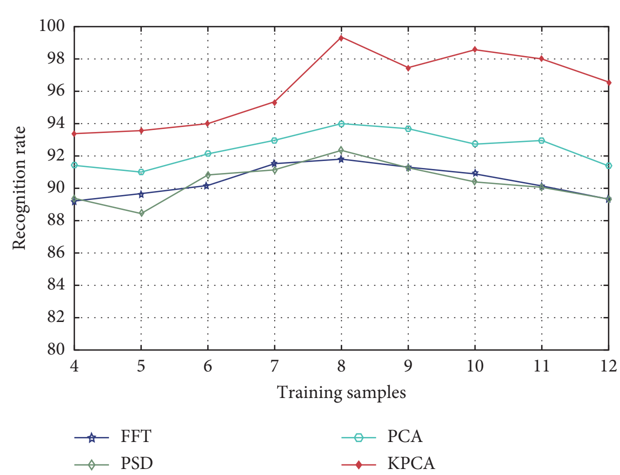

Figure 9: SVM classifier.

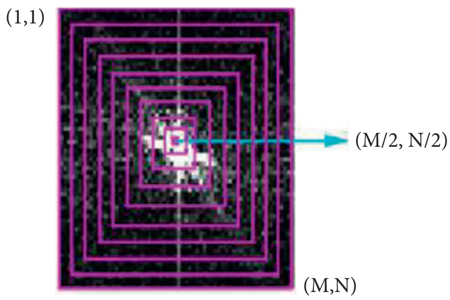

Figure 10: The case of F Translation.

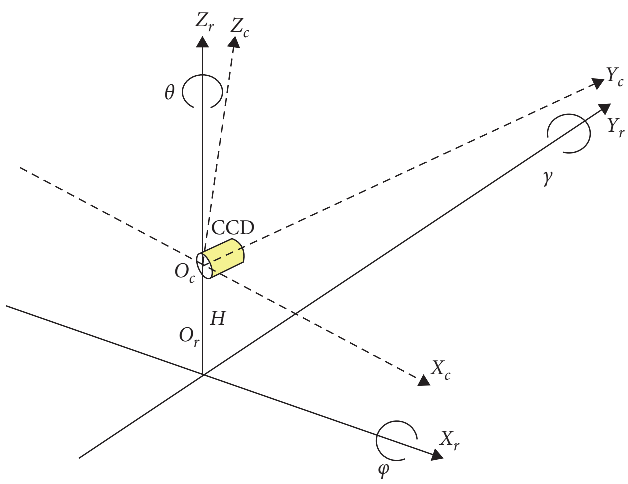

Figure 11: The camera corresponds to the coordinate system.

5. Conclusion

In this paper, a novel feature extraction algorithm, kernel complex discrimination algorithm, is proposed, which can be widely used in intelligent transportation assistant by combining with embedded platform with low power consumption and high efficiency. The system also provides an adaptive cruise control system based on distance detection. At the same time, the system will give an audio and visual alarm if the distance detected by neighboring vehicles is less than the safe distance. According to the method proposed in this paper, the amount and cost of calculation will be large. So, in the future, we will conduct further research mainly in the following aspects:

(1) The intelligent energy saving system under the environment of the Internet of Things proposed in this paper is only running in a single test environment. If it is promoted, how to realize big data processing and distributed computing is a challenge and requires in-depth study.

(2) The test environment of the intelligent vehicle statistics system based on voice recognition and kernel principal component analysis proposed in this paper is in the absence of other noise interference, while the real environment is far worse than this, so how to eliminate interference is the focus of the following research of this topic.

(3) The test environment of intelligent traffic assistant system based on verification authentication proposed in this paper is completed on the basis of no light interference. However, in the real operation, there are often many light interferences, and how to solve the light interference is the core of the following research of this topic.

Data Availability

The data used to support the findings of this study are available from the corresponding author upon request.

Conflicts of Interest

The authors declare that there are no conflicts of interest.

Acknowledgments

This work was supported by the Science and Technology Plan Project of Shiyan, Hubei Dongfeng Light Engine Co. Ltd., MES system key technology research (19Y134), Research Project of Hubei Provincial Department of Education, Research on Active Safety Technology for Antislip Rolling of Vehicles in Curved Roads (B2018070), Key Laboratory of Automotive Power Train and Electronics Hubei University of Automotive Technology, and Research on Active Safety Technology System for Vehicle Curved Driving (ZDK1201603).

References

[1] L. Liu, G. Han, Z. Xu, J. Jiang, L. Shu, and M. M. Garcia, "Boundary tracking of continuous objects based on binary tree structured SVM for industrial wireless sensor networks," *IEEE Transactions on Mobile Computing*, vol. 5, no. 99, p. 1, 2020.

[2] Z. Zhang and Y. Zhang, "Application of wireless sensor network in dynamic linkage video surveillance system based on Kalman filtering algorithm," *The Journal of Supercomputing*, vol. 75, no. 9, pp. 6055–6069, 2019.

[3] W. Wang and M. Zhang, "Self-adaptive gathering for energy-efficient data stream in heterogeneous wireless sensor networks based on deep learning," *IEEE Wireless Communications*, vol. 27, no. 5, pp. 74–79, 2020.

[4] T. Wang, H. Xiong, H. Ding, and L. Zheng, "TDOA-based joint synchronization and localization algorithm for asynchronous wireless sensor networks," *IEEE Transactions on Communications*, vol. 68, no. 5, pp. 3107–3124, 2020.

[5] S. M. Chowdhury and A. Hossain, "Impact of error control code on characteristic distance in wireless underground sensor networks," *IET Communications*, vol. 12, no. 13, pp. 1540–1549, 2018.

[6] B. J. Fan, Y. R. Li, and Y. Z. Liu, "The study on the controller of aviation switched reluctance starter/generator integrated system," *Computer Simulation*, vol. 36, no. 1, pp. 102–107, 2019.

[7] N. N. Tang, X. F. Zheng, J. Z. Wu, H. Chen, and H. X. Li, "Design of off-line led control system based on 4G-LTE," *Chinese Journal of Liquid Crystals and Displays*, vol. 33, no. 1, pp. 55–60, 2018.

[8] B. H. Xiao, B. Q. Pei, and N. Wu, "Design of manned centrifuge control system based on motion controller,"

Space Medicine and Medical Engineering, vol. 31, no. 1, pp. 32–36, 2018.

[9] K. Khoshraftar and B. Heidari, "A hybrid method based on clustering to improve the reliability of the wireless sensor networks," *Wireless Personal Communications*, vol. 113, no. 2, pp. 1029–1049, 2020.

[10] Q. Liu, "Coverage reliability evaluation of wireless sensor network considering common cause failures based on d–s evidence theory," *IEEE Transactions on Reliability*, vol. 70, no. 99, pp. 1–15, 2020.

[11] Y. Cui, L. Zhang, Y. Hou, and G. Tian, "Design of intelligent home pension service platform based on machine learning and wireless sensor network," *Journal of Intelligent and Fuzzy Systems*, vol. 40, no. 2, pp. 2529–2540, 2021.

[12] Z. Ying, J. Wang, and G. Hao, "An autonomous connectivity restoration algorithm based on finite state machine for wireless sensor-actor networks," *Sensors*, vol. 18, no. 2, p. 153, 2018.

[13] X. Yu, H. Lu, X. Yang, Y. Chen, and W. Shi, "An adaptive method based on contextual anomaly detection in internet of things through wireless sensor networks," *International Journal of Distributed Sensor Networks*, vol. 16, no. 5, p. 155, 2020.

[14] Y. Yang, S. Wang, W. Xu, and K. Wei, "Reliability evaluation of wireless multimedia sensor networks based on instantaneous availability," *International Journal of Distributed Sensor Networks*, vol. 14, no. 11, p. 155, 2018.

[15] Q. Xu, Q. Guo, C. X. Wang et al., "Network differentiation: a computational method of pathogenesis diagnosis in traditional Chinese medicine based on systems science," *Artificial Intelligence in Medicine*, vol. 118, no. 7724, Article ID 102134, 2021.

[16] M. Li, H. Jiang, H.. Yule et al., "A systematic review on botany, processing, application, phytochemistry and pharmacological action of Radix Rehmnniae," *Journal of Ethnopharmacology*, vol. 4, Article ID 114820, 2021.

[17] Y. Qi, C. Ma, H. Yu, and X. Bian, "A key pre-distribution scheme based on μ-PBIBD for enhancing resilience in wireless sensor networks," *Sensors*, vol. 18, no. 5, p. 1539, 2018.

[18] Y. Zhou, R. Zhao, Q. Luo, and C. Wen, "Sensor deployment scheme based on social spider optimization algorithm for wireless sensor networks," *Neural Processing Letters*, vol. 48, no. 1, pp. 71–94, 2018.

[19] R. Sharma, V. Vashisht, and U. Singh, "WOATCA: a secure and energy aware scheme based on whale optimisation in clustered wireless sensor networks," *IET Communications*, vol. 14, no. 8, pp. 1199–1208, 2020.

[20] J. Wang, R. Zhu, S. Liu, and Z. Cai, "Node location privacy protection based on differentially private grids in industrial wireless sensor networks," *Sensors*, vol. 18, no. 2, p. 410, 2018.

[21] S. Yang, Z. Gong, K. Ye, Y. Wei, Z. Huang, and Z. Huang, "EdgeRNN: a compact speech recognition network with spatio-temporal features for edge computing," *IEEE Access*, vol. 8, Article ID 81468, 2020.

[22] J. Zhang and D. Tao, "Empowering things with intelligence: a survey of the progress, challenges, and opportunities in artificial intelligence of things," *IEEE Internet of Things Journal*, vol. 8, no. 10, pp. 7789–7817, 2021.

[23] M. S. Hossain and G. Muhammad, "An audio-visual emotion recognition system using deep learning fusion for a cognitive wireless framework," *IEEE Wireless Communications*, vol. 26, no. 3, pp. 62–68, 2019.

[24] A. Facchinetti, L. Gasparetto, and S. Bruni, "Real-time catenary models for the hardware-in-the-loop simulation of the pantograph-catenary interaction," *Vehicle System Dynamics*, vol. 51, no. 4, pp. 499–516, 2013.

Hindawi
Scientific Programming
Volume 2022, Article ID 7289661, 13 pages
https://doi.org/10.1155/2022/7289661

Research Article

Smart City Public Art Planning and Design in a Multimedia Internet of Things Environment Integrating Scene Elements

Congcong Tang and Lei Zhao

School of Architecture and Art Design, Hebei Academy of Fine Arts, Shijiazhuang 050700, China

Correspondence should be addressed to Congcong Tang; standardtcc@hbafa.edu.cn

Received 18 November 2021; Revised 9 December 2021; Accepted 14 December 2021; Published 10 January 2022

Academic Editor: Le Sun

Public art planning and design in the context of smart cities need to keep pace with the times, but the integrity of the original scene needs to be maintained in the process of public art design. Therefore, this paper combines the elements of the scene and integrates the Internet of Things smart city to conduct public art planning and design research. Moreover, based on the multimedia Internet of Things environment, this paper analyzes the effects of virtual reality technology in urban public art planning and design and gives the overall optimization ideas for the organization and rendering of VR scene data. Then, this paper studies the organization and rendering optimization methods of the terrain scene model and the scene model, respectively. The experimental research results show that the smart city public art planning and design system under the multimedia Internet of Things environment designed in this paper has a good smart city public art planning and design effect.

1. Introduction

In recent years, public art that has emerged from the West has gradually spread and flourished globally, and various forms of public art works are displayed in front of the world. Public art design should actually be called public space art design. It is actually a general term for environmental landscape design, public sculpture art, mural art, ornament decoration design, craft design, video media design, and so on. Public art is also an emerging art category in my country. In recent years, it has gradually prospered, many new artists continue to emerge, and many outstanding public art works are also presented in front of people [1].

The content of public art is quite extensive. In a broad sense, all visual and auditory art that has an artistic relationship with the public in time or space should belong to the category of public art, such as drama, film, dance, and performance art. However, due to the differences in the cultural history and reality of various nationalities, different countries, regions, and nationalities often have different focuses when implementing public art design, so public art does not have a clear theoretical concept [2]. The full name of "Public Art" is "Public Space Art Design." The role of public art in urban public space is not only a materialized structure but also the catalyst of urban cultural spirit of events, performances, plans, festivals, and occasional or derived urban stories [3].

Public art design plays an important role in beautifying the city. Its decorative function has never disappeared from ancient times to the present. The foundation of any art form is inseparable from decoration. First, the decoration of the layout: when painting, we pay attention to the coordination and completeness of the picture to produce a reasonable composition, make the picture produce different effects, and give people different visual feelings. The same is true for public art. When conceiving and designing a public space, the first thing to consider is a reasonable spatial layout, such as a stable horizontal layout, a solemn vertical layout, an elegant curved layout, a sharp triangular layout, a tensioned radial layout, and a clear theme. The central layout, the progressive layout with a sense of rhythm, the free three-point layout, and so on can make the public space decorative and bring people a different visual experience. Secondly, the decorativeness of the expression technique: whether it is a black-and-white painting or decorative painting, different expressions are needed to display it to achieve its decorativeness, and public art also needs it. Different colors bring different psychological feelings to people. Public art expresses the effect of decoration through the change of colors or the attributes of materials.

Public art planning and design in the context of smart cities need to keep pace with the times, but the integrity of the original scene needs to be maintained in the process of public art design. Therefore, this paper combines the elements of the scene and integrates the Internet of Things smart city to conduct public art planning and design research.

2. Related Work

In the practice of urban public art, there are various problems. In the implementation of urban construction, it is necessary to face up to the many practical issues that must be solved. For example, it is necessary to safeguard the comprehensive interests of the local and even the country in the political, economic, and cultural fields, and it is necessary to respect the customs and customs that reflect the geography, history, and reality. The spatial order and functions that are suitable for the established or planned city need to follow the aesthetic laws, technical requirements, and evaluation standards of the art itself. It is necessary to establish rules including decision-making and public opinion exchanges, qualification identification and authority norms of the creative subject, conventional procedures, related laws and regulations, the whole set of operating mechanisms within, and so on [4]. With the development of society and the improvement of urban economic strength, my country's cities have taken on a new look, and the quality of urban public has been greatly improved. However, compared with developed countries, there are still big gaps and many problems in urban public art design in my country [5]. For example, some urban public and landscape have improved, but the overall urban public quality has declined. There have been many destructive constructions, resulting in new visual pollution. Urban public art design emphasizes construction and neglects protection, and many historical and cultural heritages have been destroyed. Urban public construction emphasizes surface, neglects substance, is eager for quick success and instant benefits, and so on [6].

Literature [7] believes that public art is a concept with strong sociology and culture, rather than a concept of pure art. Although in recent years, critics and artists have raised the issue of the publicity of art, public art in the strict sense has not appeared in China. Literature [8] believes that public art is not equal to urban sculpture and landscape art. The core of public art is the publicity of art. The premise of publicity is respect for the individual, and at the same time, publicity means communication and communication, emphasizing the common social order and personal social responsibility. Literature [9] proposes that, in a broad sense, all artworks in public spaces can be called public art. As for public art, it may be limited to works under percentage for art programs. Document [10] mentioned that public art refers to art located in public space, which can reflect the characteristics of the base and express the surrounding environment; it is given the task of conveying social and cultural information and meaning, making it for the general public understand; at the same time, it also stimulates the vitality and vitality of the area or place and promotes the production of activities. In other words, the activities of daily life, the emotions of people, and the environment can all be conveyed through the medium of public art. Document [11] proposes that public art can be discussed in the following four areas: (1) Placed in a public space, through the existence of artworks, it emphasizes the importance of public welfare. (2) The artist will directly face an unspecified third party. (3) The process of consciousness formation (from top to bottom or bottom to top). (4) Decision-making should include the concept of "user participation." Through the above four methods, the definition of public art is staggered. Literature [12] mentions that public art has the following characteristics: (1) Public art is an artistic creation that emphasizes teamwork, and it must work with architects, landscape architects, engineers, and so on. Collaborate with other professionals. (2) Public art aims at serving the public and is an artistic creation involving the public. (3) Public art has a closer relationship with people. Everyone has the opportunity to appreciate and contact. It is almost a part of people's daily life. It is an art of living. (4) Public art often needs to be created in accordance with the location of the furnishings, sometimes even part of the overall environment, and has an indispensable characteristic. (5) The content and materials of public art are diversified, and there are no set factors that limit the content of creation. (6) Public art initially aims at beautifying the environment and focusing on visual aesthetics, which can be one of the tools of government construction. (7) One of the characteristics of public art is that it never stands for politicians. It is not the essence of the past social elites. It is contemporary civilian art.

3. Smart City Public Art Planning and Design Technology

Height map is a storage method that uses the gray value to represent terrain elevation information, and it has a wide range of applications in virtual simulation modeling. Using height maps to build terrain is a common method for VR platforms, so choosing a height map to build terrain scenes has higher efficiency.

The following is the height map production process, as shown in Figure 1[13].

(1) First of all, the DEM data is converted into coordinates, which is converted from WGS84 coordinates to rectangular coordinates to match the coordinate format under the VR platform. The following formula is used to convert the WGS84 latitude and longitude coordinates of the northern hemisphere China into rectangular coordinates. The specific conversion formula is as follows:

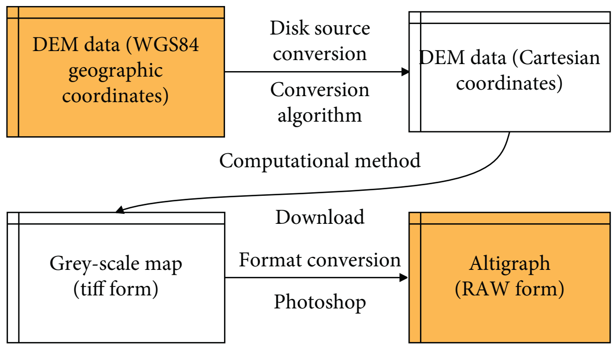

Figure 1: Height map production process.

$$\begin{cases} X = (N + H)\cos B \cos L, \\ Y = (N + H)\cos B \sin L, \\ Z = \left(\dfrac{Na^2}{b^2} + H\right)\sin B. \end{cases} \quad (1)$$

Among them, X, Y, and Z are the converted rectangular coordinates, L, B, and H are the longitude, latitude, and height in the WGS84 coordinate system, N is the radius of the unitary circle, and a and b are the semimajor axis and semiminor axis of the reference ellipsoid respectively. The calculation formula is as follows:

$$N = \frac{a}{\sqrt{1 - e^2 \sin^2 B}}. \quad (2)$$

Among them, e is the first eccentricity of the reference bin ball, and the calculation formula is

$$e^2 = \frac{a^2 - b^2}{a^2}. \quad (3)$$

Using ArcGIS and other types of software can generate data that satisfies the terrain modeling of the VR platform.

(2) The DEM data of the converted coordinate system is used to make a grayscale image. The grayscale value of the grayscale image corresponds to the elevation of the terrain. The specific corresponding relationship is shown in formula 4 [14]:

$$H_{\text{grid}} = \frac{H_{\max} - H_{\min}}{\varphi_{\max} - \varphi_{\min}} \varphi_{\text{grid}}. \quad (4)$$

Among them, H_{grid} is the actual elevation value of the DEM grid, $H_{\max}$ and $H_{\min}$ represent the maximum and minimum actual elevation values of the DEM grid, max and min represent the maximum and minimum gray values in the grayscale image, and grid represents the gray value of the DEM grid. Using the above formula, the relationship between the DEM data and the grayscale image can be established, and the production of the grayscale image can be realized.

(3) Finally, since the initial grayscale image format is tiff and the format required by the VR platform is the height map in RAW format, the format needs to be converted. This paper chooses to use the commercial software Photoshop to convert the above two formats, and no data is lost in the conversion process.

In the VR platform, the steps of using the height map to construct the terrain include height map importing, setting parameters, generating terrain, and texture mapping. The specific steps are shown in Figure 2. The process is described in detail.

First of all, the height map that has been made is imported into the VR platform. At the same time, according to the actual attributes of the terrain, related parameters are set to avoid changing the actual size of the terrain, mainly including depth, terrain size, width, and height. Among them, the size of the terrain is set according to the length and width of the actual terrain. Then, use the VR platform to read the grid and its value of the height map to automatically generate a terrain model. Finally, the texture mapping relationship is established according to the height map index, the terrain texture map is completed, and the urban public art VR terrain scene is constructed.

3.1. Principle of Mask Test. Mask testing occurs in the stage of GPU chip-by-chip operation. This stage is the last step of the rendering pipeline. Among them, one of the most important tasks is to determine the visibility of each element, which involves a series of tests, including pixel ownership test, crop test, alpha test, mask test, depth test, and so on. The complete process is shown in Figure 3. In this process, only after the fragment data has passed all the tests, can the newly generated fragments be mixed with the colors of the pixels already in the buffer and finally written into the buffer for rendering. This fusion display method is to use template testing to discard the fusion area fragments in order to achieve the purpose of fusion display of urban building openings and terrain. The specific process of the template test is described in detail in the following.

Template testing is a more complicated process, the details of different graphics interfaces are different, and it is usually used to limit the area of rendering. When the template is tested, the GPU will first read the template value of the fragment position in the template buffer. Then, it compares the value with the read reference value, and the developer can specify a comparison function, such as discarding the fragment when it is less than the reference value. If the fragment data does not pass the mask test, the fragment will be discarded and will not enter the following depth test. At the same time, the color value of the fragment and the color already stored in the color buffer will not be merged, thereby achieving the effect of limiting rendering. The process of mask testing is shown in Figure 4.

3.2. Calculation Method of Fusion Area

(1) The curved wall section is shown in Figure 5, and its outer contour is composed of a straight line and a

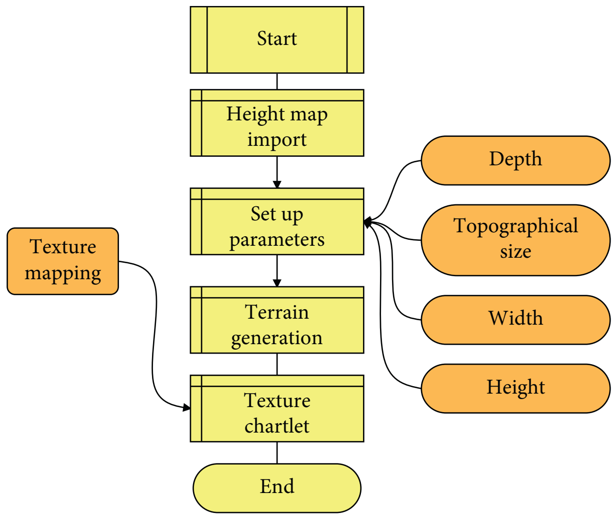

FIGURE 2: The process of using height maps to build terrain.

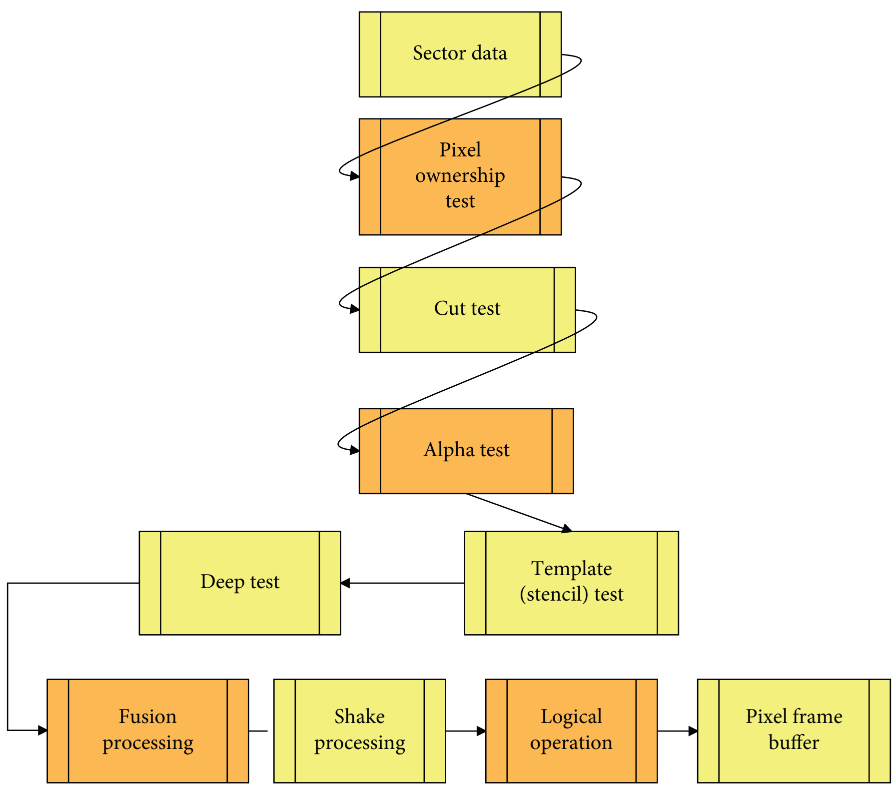

FIGURE 3: GUP segment-by-segment operation process.

circular arc. The points on the straight line P and Pn + z are easy to draw and will not be described in detail here.

The coordinate system XOY is established based on the urban building center lines O and P; then, any point P(X, Y) on the outer contour of the urban building can be calculated by formula 5 [15].

$$\begin{cases} X_i = X_0 + d + R\cos\,\alpha_i, \\ Y_i = Y_0 + d + R\sin\,\alpha_i. \end{cases} \tag{5}$$

(2) The straight wall section is shown in Figure 6. Its outer contour includes straight and curved sections. The points on the straight line $P_0P_{n+1}, P_{n+1}P_{n+2}, P_{n+2}P_n$ are easy to calculate.

d is the distance between o and O, H is the distance between point P and point Pn + z, R is the radius of the arc, point P is any point on the arc, and αx is the coordinate azimuth angle of the two points o1 and Pi. We establish the coordinate system XOY based on the centerline of the city buildings O and P; then, any point $P_i(X_i, Y_i)$ on the outer

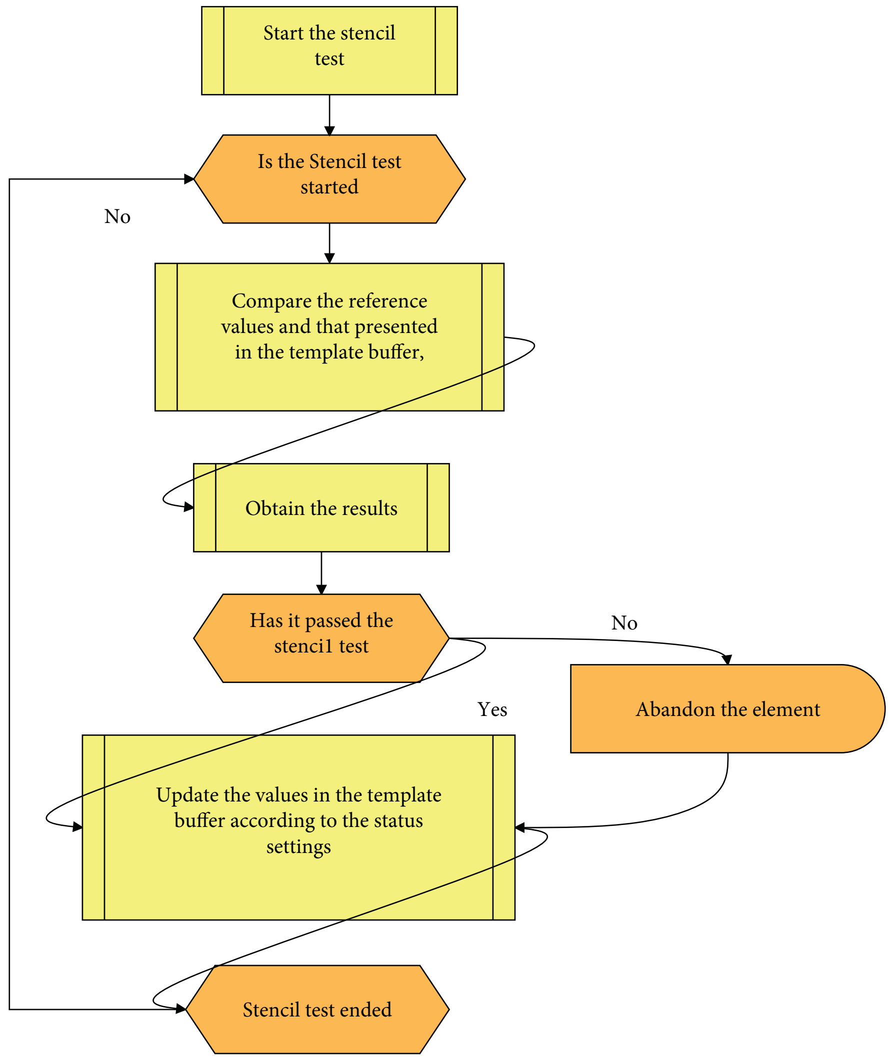

FIGURE 4: Mask testing process.

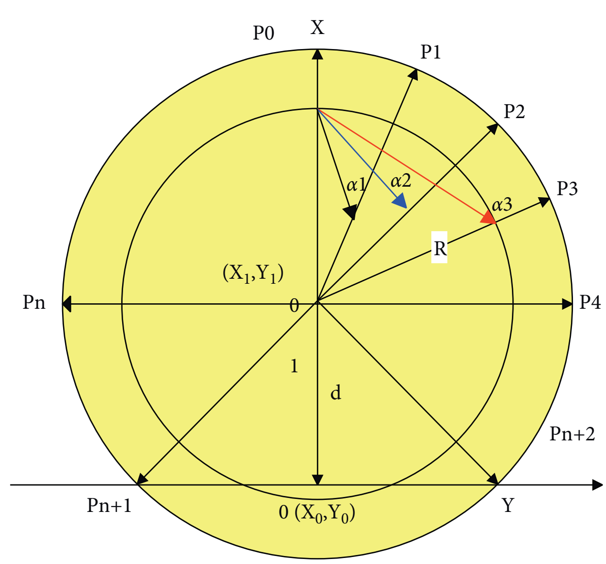

FIGURE 5: Schematic diagram of single heart curved wall section.

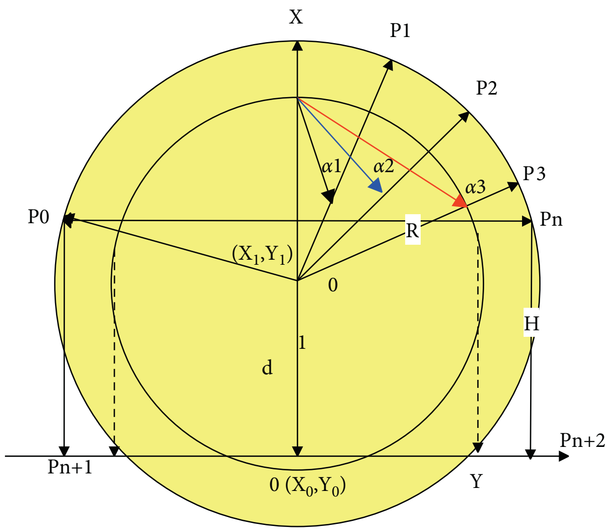

Figure 6: Schematic diagram of the vertical wall section.

contour of the city building can be calculated by formula 6 [16].

$$\begin{cases} X_i = X_0 + d + R\cos\alpha_i, \\ Y_i = Y_0 + d\sin\alpha_i + H - d. \end{cases} \quad (6)$$

After obtaining the plane coordinates of any point on the outer contour of the city building's cross section, it is also necessary to calculate the Z-axis coordinate value of the cross section. According to the orthogonal relationship between the cross section and the terrain slope, the Z value can be calculated by projecting the cross section of the city building in the orthogonal direction, as shown in Figure 7 [17].

We take the orthogonal direction of the urban building's cross section as the Z-axis direction and obtain the slope s of the urban building's slope according to the design data. Then, the Z value of point P can be calculated according to formula 7.

$$Z_p = Y_p \cdot S. \quad (7)$$

The above can obtain the intersection area of the urban building entrance and the terrain, that is, the fusion area, and then realize the restriction on the terrain rendering of the fusion area based on the template test principle and achieve the integrated display of the urban building entrance.

The urban building entrance fusion display is generally divided into three aspects: fusion area calculation (the area where the urban building opening and the terrain intersect), template testing, and updated terrain rendering. The specific steps are shown in Figure 8.

First, before starting the fusion display, it is necessary to judge whether it needs fusion according to the name and location information of the model. If fusion is not required, it ends the fusion display. If fusion is needed, it calculates the topographic grid of the fusion area according to the calculation method of the fusion area and the slope parameters of the urban building opening. Then, establish a reference value in the fusion area. When it is used in the template test,

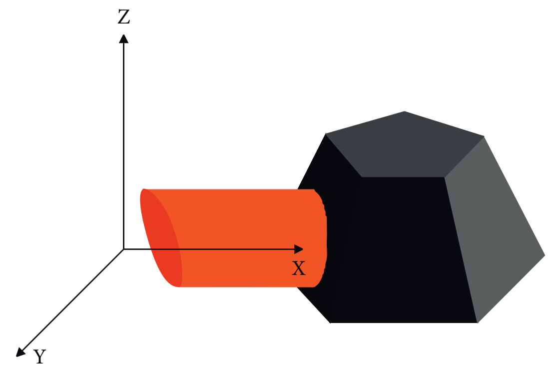

Figure 7: Schematic diagram of the topographic intersection of the city's construction entrance.

the template value of the topographic fragment is compared with the reference value of the fusion area to determine whether the topographic fragment is in the fusion area. If it is, it discards the terrain patch metadata. If it is not, it retains the terrain fragment. Finally, the rendering of the terrain of the fusion area is precisely limited to realize the dynamic fusion display of the urban building opening.

The viewing frustum refers to the range of the cone visible to the camera in the scene. Based on the terrain scheduling of the camera frustum, the range of the frustum must be calculated in real time according to the camera position, and the terrain bounding box under the node must be determined. Then, it performs real-time detection of whether the bounding box is within the camera's field of view to determine the terrain data that can be retrieved. The following describes the frustum calculation and bounding box detection separately.

3.2.1. Frustum Calculation. Figure 9 shows a schematic diagram of the camera frustum. The viewing frustum is the space visible to the camera, which is composed of top, bottom, left, right, near-cut planes, and far-cut planes. The four sides (upper, left, lower, and right) forming the viewing frustum correspond to the four boundaries of the screen, respectively. In order to prevent the object from getting too close to the camera, set the near-cut surface. At the same time, in order to prevent objects from being too far away from the camera to be visible, we set a far-cut plane, and only objects within 6 planes can be rendered. The calculation method of the frustum section is described in detail in the following [18].

The first step is to obtain the camera's opening angle in the vertical direction, that is, the vertical opening angle shown in Figure 9. The second is to calculate the aspect ratio (aspect in Figure 9). The specific calculation formula is shown in Figure 9. Then, the parameter f_Y is calculated, which is used to represent the offset between the upper and lower sides of the viewing frustum and the XZ plane. The calculation method is as public 8. In the same way, the f parameter is calculated to indicate the offset between the left

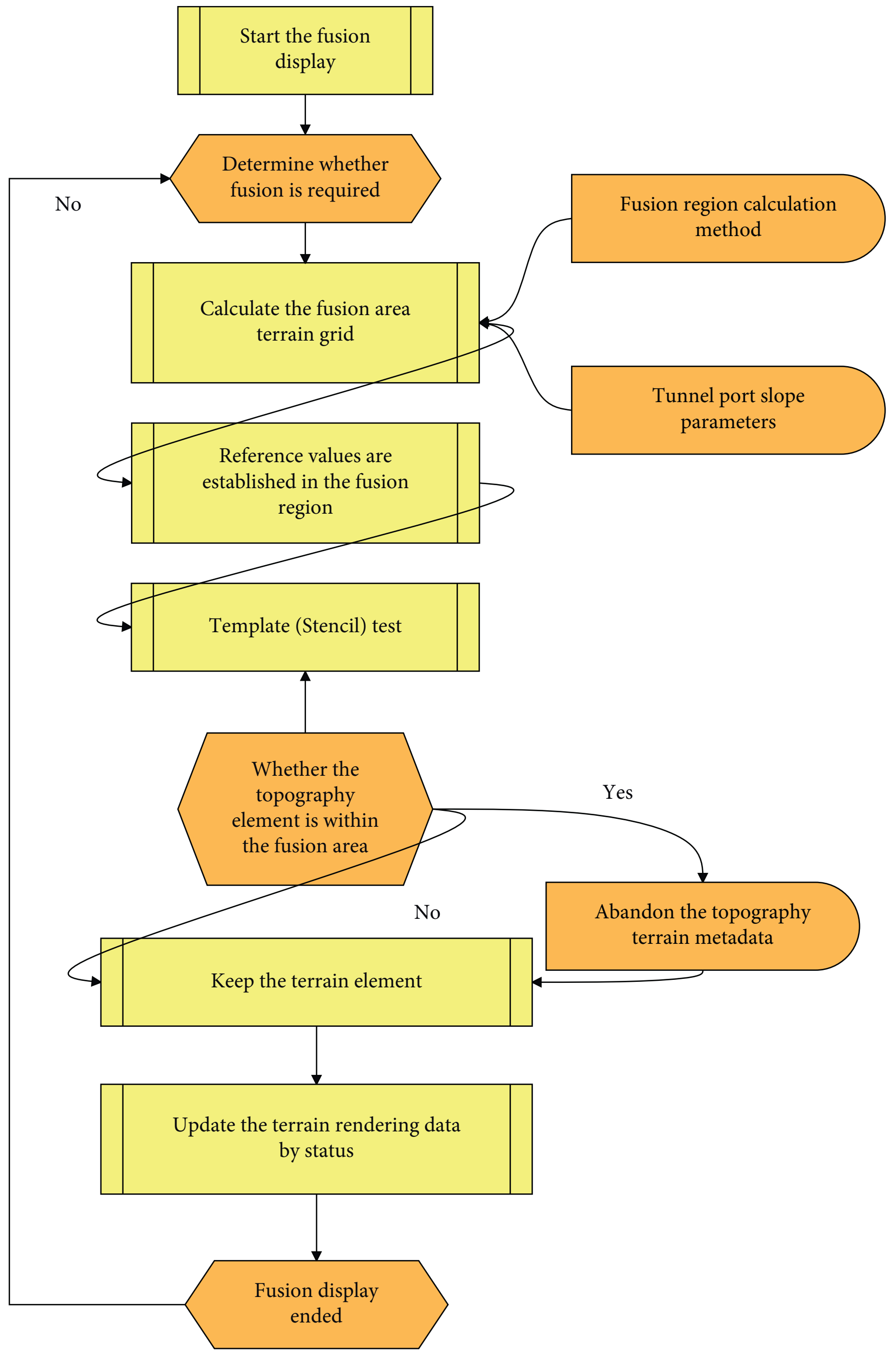

Figure 8: The steps of urban architectural integration display.

and right sides of the viewing cone and the YZ plane, as shown in formula 9.

The calculation formula for the offset of the XZ plane is as follows:

$$f_Y = \tan \frac{f_v}{2}. \tag{8}$$

The calculation formula for the offset of the XY plane is as follows:

$$f_X = f_Y * \text{Aspect}. \tag{9}$$

In the formula, f_v represents the vertical opening angle, and the unit is radians. Since the camera's vertical angle f_v has an angle of $f_v/2$ up and down centered on the XZ plane, it must be divided by 2. Aspect is the ratio of width to height, that is, the ratio of the amount of offset calculation in the horizontal and vertical directions.

Finally, the three-dimensional coordinates of the 8 vertices of the viewing cone are calculated as shown in formulas 11 and 12.

The calculation formula of the side direction vector is as follows [19]:

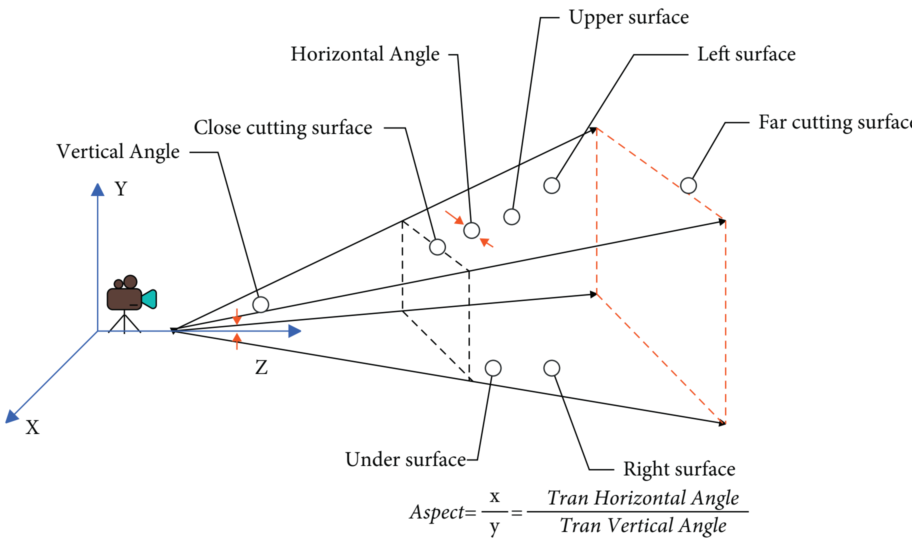

Figure 9: Schematic diagram of the frustum.

$$\begin{cases} \overrightarrow{f_0} = \text{Matix} * \begin{bmatrix} -f_X \\ -f_Y \\ 1 \end{bmatrix}, \\ \overrightarrow{f_1} = \text{Matix} * \begin{bmatrix} -f_X \\ f_Y \\ 1 \end{bmatrix}, \\ \overrightarrow{f_2} = \text{Matix} * \begin{bmatrix} f_X \\ -f_Y \\ 1 \end{bmatrix}, \\ \overrightarrow{f_3} = \text{Matix} * \begin{bmatrix} f_X \\ f_Y \\ 1 \end{bmatrix}. \end{cases} \tag{10}$$

The formula for calculating the vertices of the far-tangent plane is as follows:

$$\begin{cases} V_1 = P_c + d_{\text{far}} * f_0, \\ V_2 = P_c + d_{\text{far}} * f_1, \\ V_3 = P_c + d_{\text{far}} * f_2, \\ V_4 = P_c + d_{\text{far}} * f_3. \end{cases} \tag{11}$$

The calculation formula for the vertex of the near-cut surface is as follows:

$$\begin{cases} V_5 = P_c + d_{\text{near}} * f_0, \\ V_6 = P_c + d_{\text{near}} * f_1, \\ V_7 = P_c + d_{\text{near}} * f_2, \\ V_8 = P_c + d_{\text{near}} * f_3. \end{cases} \tag{12}$$

In the formula, Matix is the matrix for transforming local coordinates to world coordinates, f_X is the offset of the XY plane, f_Y is the offset of the XZ plane, P is the three-dimensional coordinates of the camera, and $\overrightarrow{f_0}, \overrightarrow{f_1}, \overrightarrow{f_2}, \overrightarrow{f_3}$ is the direction vector of the four sides. d_{far} is the distance from the camera to the far-tangent plane, d_{near} is the distance from the camera to the near-tangent plane, V_1, V_2, V_3, V_4 are the coordinates of the lower-left vertex, upper-left vertex, lower-right vertex, and upper-right vertex of the far-tangent plane, respectively, and V_5, V_6, V_7, V_8 are the coordinates of the lower-left vertex, upper-left vertex, lower-right vertex, and upper-right vertex of the near-tangent plane, respectively.

3.2.2. Bounding Box Detection. The function of bounding box detection is to determine the terrain data to be rendered, and it is a key issue to determine whether the terrain node is inside the frustum. The space plane equations of the six faces of the viewing cone can be established according to the calculated vertices of the viewing cone (such as formula 13), and the point on the bounding box is determined by formula 14 on which side of the viewing cone. If it is ①, the point is on the plane. If it is ②, the point is on one side of the plane. If it is ③, the point is on the other side of the plane. Through the comprehensive judgment of the six faces of the viewing frustum, it can be concluded whether the point on the bounding box is inside the viewing frustum [20].

$$aX + bY + cZ = 0, \tag{13}$$

$$\begin{cases} aX_1 + bY_1 + cZ_1 = 0, \\ aX_1 + bY_1 + cZ_1 < 0, \\ aX_1 + bY_1 + cZ_1 > 0. \end{cases} \tag{14}$$

By judging all the vertices on the bounding box, it can be concluded whether the node is in the frustum, including the following three situations:

(1) If all vertices are within the viewing cone, the bounding box of the node to be judged must be within the viewing cone.

(2) If some of the vertices are within the viewing cone, the bounding box of the node to be judged intersects with the viewing cone. This situation is considered visible.

(3) If all the vertices are not within the range of the viewing cone, the bounding box of the node to be judged may be outside the viewing cone, but there is an exception; that is, the viewing cone is within the node bounding box, which is distinguished by setting a threshold at this time.

Figure 10 is a flowchart of octree bounding box detection and terrain scheduling. In order to improve efficiency, first determine whether it is the first determination. If it is, the root node of the entire scene will start to find the left and right largest nodes in the frustum and save them in the terrain node library. If it is not the first judgment (when the viewpoint is moving), first look up the largest node contained in the viewing cone from the recorded terrain nodes, and then search for other nodes on this basis and record this node for updating the node database. At the same time, the terrain data in the frustum saved in the node library is drawn in real time.

Model scheduling based on VR ray collision detection mainly includes three contents: VR ray creation, model collision detection, and model scheduling, which will be explained separately in the following:

(1) Creating a ray: it refers to the generation of a ray from the camera to the viewing cone. The end of the ray is the farthest position that the viewpoint can see. By using the function RayCast, a uniform-density ray is created. The ray is created with the center of the camera as the origin and the viewing cone as the boundary.

(2) Model collision detection: the key to model collision detection is to determine whether a model intersects with each ray in the direction. Since the constituent unit of the three-dimensional model is a triangle, judging whether the model intersects the ray is judging that the ray intersects the triangle. In this paper, the method of solving the ray and the triangle is used to determine whether the ray and the triangle intersect. The formula is as 3–8. The left side of the equation is the parametric equation of the ray, and the right side of the equation is the parametric equation of the triangle [21].

$$0 + DI = (1 - u - v)U_0 + uU_1 + vU_2. \tag{15}$$

Among them, 0 is the starting point of the ray, D is the direction, and U_0, U_1, U_2 are the three vertices of the triangle. The coefficients of l, u, and v can be obtained by using Cramer's law. Use the RaycastHit class to save some information on the collision detection model so that the model can be scheduled based on this information. The information is mainly the distance between the ray origin and the collision model and the three-dimensional coordinates of the model position.

(3) Model scheduling: the main idea of model scheduling is to dynamically schedule the scene model to the rendering pipeline for rendering according to the results of VR ray collision detection, as shown in Figure 11. According to the information obtained from collision detection, it is judged whether the model is inside the frustum.

The solid red line in Figure 11 represents the VR ray. Model scheduling based on collision detection results includes several situations. It is not in the viewing frustum, and collision does not occur; the model does not perform scheduling and drawing. It is occluded in the viewing frustum, collision does not occur, and the model is not scheduled and drawn. It is not occluded in the viewing frustum, the collision occurs, and the model is scheduled and drawn.

4. Smart City Public Art Planning and Design in a Multimedia Internet of Things Environment Integrating Scene Elements

Smart city public art is the product of the combination of design language such as the form, color, quality of the product entity, and the way of setting it in the space. Its connotation cannot be created out of thin air without the facility entity and space. Moreover, it mainly refers to the existence of values that can be perceived, read, and arouse people's emotional resonance on the spiritual level of the city image, city spirit, and public emotion attached to the material entity of the facility product. When new fashion trends enter the daily life of the public in the form of styles and concepts, the connotation of facilities usually presents new forms and styles. The facility reflects the emotional needs of the contemporary public by integrating multiple cultural elements and provides new vitality for the formation of new art types and the extension and expansion of the connotation and expansion of the fashion field. Figure 12 shows the planning and design of smart city public art in a multimedia Internet of Things environment that integrates scene elements.

In this study, 20 sets of image adjectives are evaluated on public art modeling samples. After the process of factor analysis, the 20 sets of image adjectives are reduced to two sets of image adjectives. Moreover, this paper has renamed it based on the meaning and characteristics of two factors, namely, "innovative factors" and "affinity factors." Next, we will use these two new factors to construct the relationship position of each sample in the image perception space coordinates and discuss the relative relationship between each sample based on the distance in space. It is hoped that we can better understand the perception and meaning of images presented by each modeling sample. The image recognition map of public art modeling is shown in Figure 13 [22].

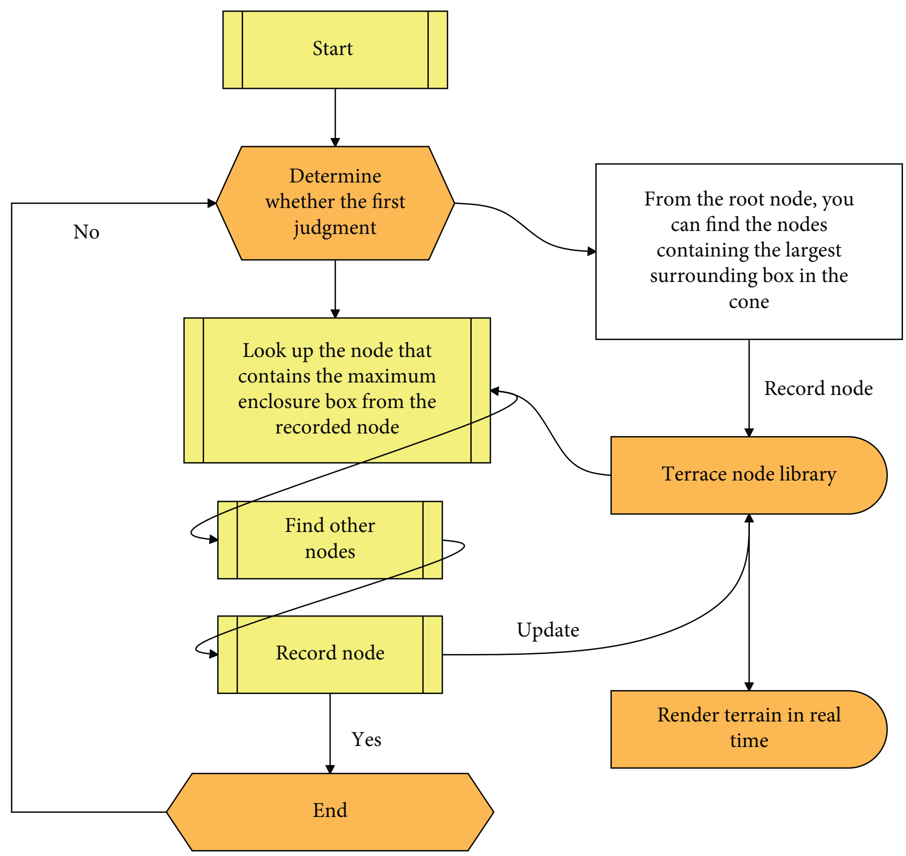

Figure 10: Bounding box detection and terrain scheduling.

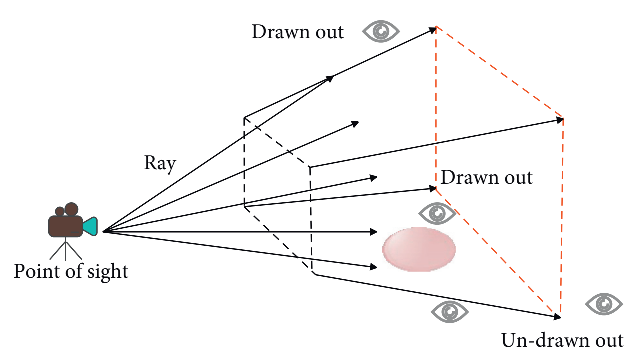

Figure 11: Schematic diagram of model scheduling based on VR ray collision detection.

On the basis of the above model, the effect of this model in public art planning and design is studied. First, the effect of scene element fusion is evaluated, and the result shown in Figure 14 is obtained.

Through the above research, we can know that the smart city public art planning and design system in the multimedia Internet of Things environment designed in this paper has a good integration effect of scene elements. After that, the effect of the smart city public art planning and design of the system in this paper is evaluated, and the results shown in Figure 15 are obtained.

Through the above research, it can be known that the smart city public art planning and design system under the multimedia Internet of Things environment that integrates

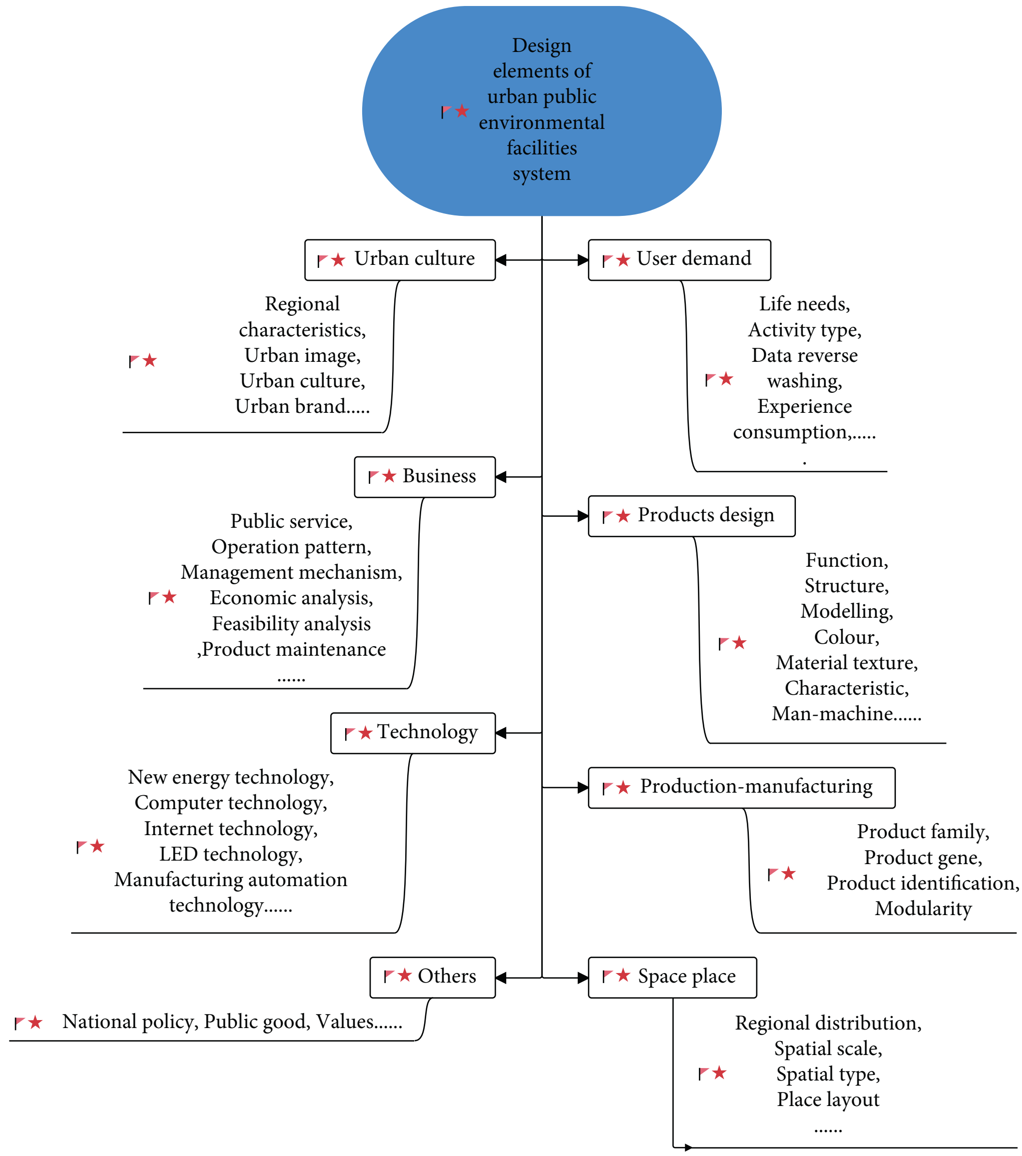

FIGURE 12: Planning and design of smart city public art in a multimedia IoT environment integrating scene elements.

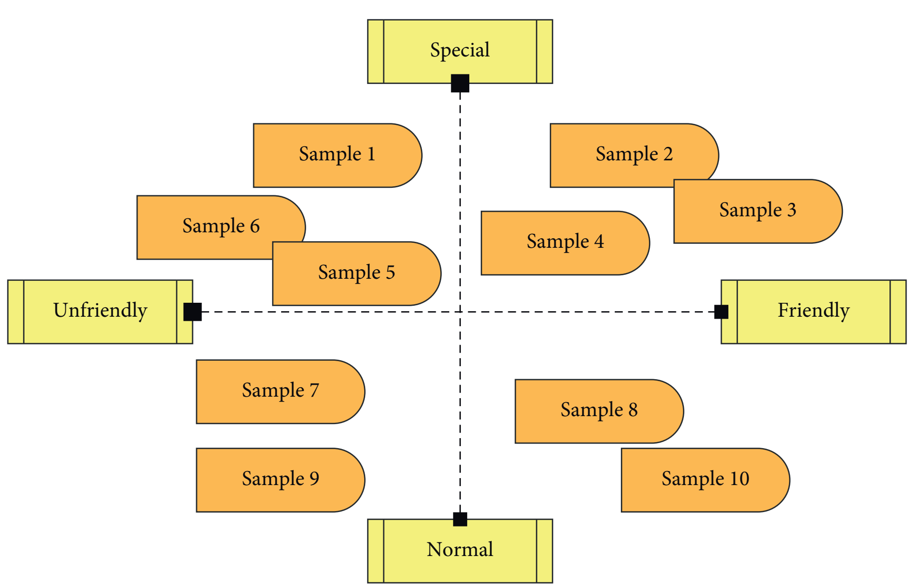

FIGURE 13: Image recognition of public art modeling.

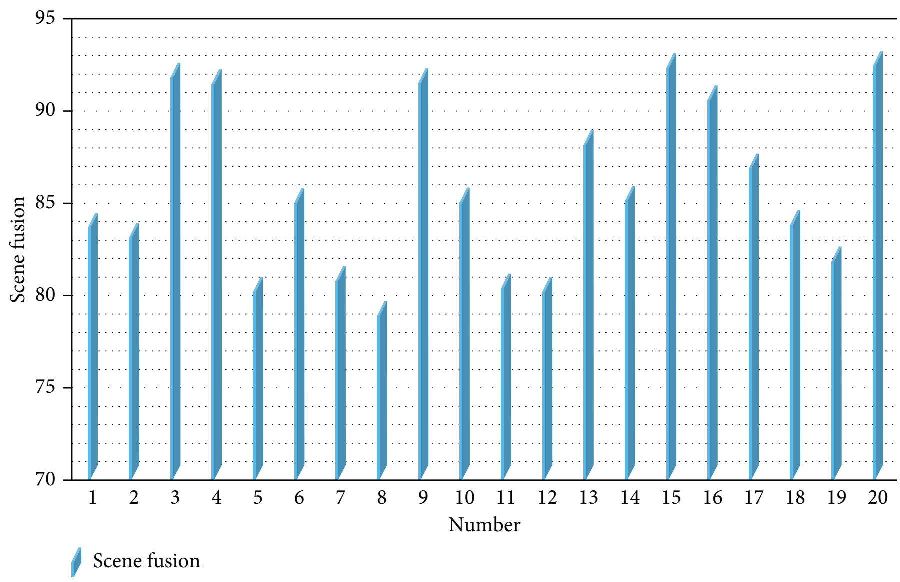

Figure 14: Fusion effect of scene elements.

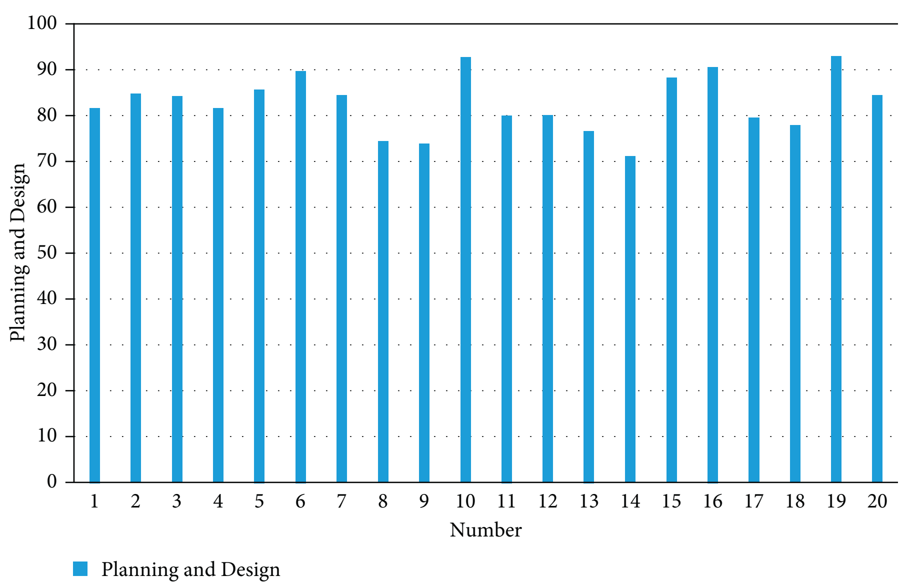

Figure 15: The effect of smart city public art planning and design.

scene elements designed in this paper has a good smart city public art planning and design effect.

5. Conclusion

The practicality of public art can be divided into two categories: public landscape and indoor landscape, which are distributed in every corner of the urban space. Large and small sculptures, installations, and plant shapes are scattered all over the streets and alleys, and signs and floor coverings also cover the walls and floors of public places. Bionics is a design method often used in public landscapes. With the help of a certain biological feature, the designer uses this feature to express in the design of public service facilities in the public space on the basis of imitating the shape so as to increase the sense of interest while being practical. In addition, a simple relief or floor covering can also be a group of visual guides. It uses labeling to guide the vision, which not only beautifies the public space environment but also fully reflects the practical function of public art. Based on the integration of scene elements, this paper combines the Internet of Things smart city to conduct public art planning and design research. The experimental research results show that the smart city public art planning and design system under the multimedia Internet of Things environment that integrates scene elements proposed in this paper has a good effect on smart city public art planning and design.

Data Availability

The labeled dataset used to support the findings of this study is available from the corresponding author upon request.

Conflicts of Interest

The authors declare no conflicts of interest.

Acknowledgments

This study was sponsored by Hebei Academy of Fine Arts.

References

[1] N. McCartney and J. Tynan, "Fashioning contemporary art: a new interdisciplinary aesthetics in art-design collaborations," *Journal of Visual Art Practice*, vol. 20, no. 1-2, pp. 143–162, 2021.

[2] J. Lockheart, "The importance of writing as a material practice for art and design students: a contemporary rereading of the Coldstream Reports," *Art, Design & Communication in Higher Education*, vol. 17, no. 2, pp. 151–175, 2018.

[3] G. Sachdev, "Engaging with plants in an urban environment through street art and design," *Plants, People, Planet*, vol. 1, no. 3, pp. 271–289, 2019.

[4] Y. M. Andreeva, V. C. Luong, D. S. Lutoshina et al., "Laser coloration of metals in visual art and design," *Optical Materials Express*, vol. 9, no. 3, pp. 1310–1319, 2019.

[5] Z. Nebessayeva, K. Bekbolatova, K. Mussakulov, S. Zhanbirshiyev, and L. Tulepov, "Promotion of entrepreneurship development by art and design by pedagogy," *Opción*, vol. 34, no. 85-2, pp. 729–751, 2018.

[6] D. Mourtzis, "Simulation in the design and operation of manufacturing systems: state of the art and new trends," *International Journal of Production Research*, vol. 58, no. 7, pp. 1927–1949, 2020.

[7] K. W. Klockars, N. E. Yau, B. L. Tardy et al., "Asymmetrical coffee rings from cellulose nanocrystals and prospects in art and design," *Cellulose*, vol. 26, no. 1, pp. 491–506, 2019.

[8] M. Hermus, A. van Buuren, and V. Bekkers, "Applying design in public administration: a literature review to explore the state of the art," *Policy & Politics*, vol. 48, no. 1, pp. 21–48, 2020.

[9] J. Calvert and P. Schyfter, "'What can science and technology studies learn from art and design? reflections on "'," *Social Studies of Science*, vol. 47, no. 2, pp. 195–215, 2017.

[10] J. A. Greene, R. Freed, and R. K. Sawyer, "Fostering creative performance in art and design education via self-regulated learning," *Instructional Science*, vol. 47, no. 2, pp. 127–149, 2019.

[11] B. Bafandeh Mayvan, A. Rasoolzadegan, and Z. Ghavidel Yazdi, "The state of the art on design patterns: a systematic mapping of the literature," *Journal of Systems and Software*, vol. 125, no. C, pp. 93–118, 2017.

[12] A. Thorpe and E. Manzini, "Weaving people and places: art and design for resilient communities," *She Ji: The Journal of Design, Economics, and Innovation*, vol. 4, no. 1, pp. 1–10, 2018.

[13] M. Sclater and V. Lally, "Interdisciplinarity and technology-enhanced learning: reflections from art and design and educational perspectives," *Research in Comparative and International Education*, vol. 13, no. 1, pp. 46–69, 2018.

[14] V. Kinsella, "The use of activity theory as a methodology for developing creativity within the art and design classroom," *International Journal of Art & Design Education*, vol. 37, no. 3, pp. 493–506, 2018.

[15] C. Liu, S. Chen, C. Sheng, P. Ding, Z. Qian, and L. Ren, ""The art of a hydraulic joint in a spider"," *Journal of Comparative Physiology A*, vol. 205, no. 4, pp. 491–504, 2019.

[16] Z. Luo and J. Dai, "Synthetic genomics: the art of design and synthesis," *Sheng Wu Gong Cheng Xue Bao= Chinese Journal of Biotechnology*, vol. 33, no. 3, pp. 331–342, 2017.

[17] E. Knight, J. Daymond, and S. Paroutis, "Design-led strategy: how to bring design thinking into the art of strategic management," *California Management Review*, vol. 62, no. 2, pp. 30–52, 2020.

[18] D. Jordan and H. O''Donoghue, "Histories of change in art and design education in Ireland: towards reform: the evolving trajectory of art education," *International Journal of Art & Design Education*, vol. 37, no. 4, pp. 574–586, 2018.

[19] T. Bastogne, "Quality-by-design of nanopharmaceuticals - a state of the art," *Nanomedicine: Nanotechnology, Biology and Medicine*, vol. 13, no. 7, pp. 2151–2157, 2017.

[20] K. Maras, "A realist account of critical agency in art criticism in art and design education," *International Journal of Art & Design Education*, vol. 37, no. 4, pp. 599–610, 2018.

[21] M. S. Ravelomanantsoa, Y. Ducq, and B. Vallespir, "A state of the art and comparison of approaches for performance measurement systems definition and design," *International Journal of Production Research*, vol. 57, no. 15-16, pp. 5026–5046, 2019.

[22] K. C. Tsai, "Teacher-student relationships, satisfaction, and achievement among art and design college students in Macau," *Journal of Education and Practice*, vol. 8, no. 6, pp. 12–16, 2017.

Hindawi
Scientific Programming
Volume 2022, Article ID 5798625, 12 pages
https://doi.org/10.1155/2022/5798625

Research Article

Destruction Feature Extraction of Prefabricated Residential Building Components Based on BIM

Peili Zhao,[1] Xiaohong Liu,[2] and Zhisheng Liang[2]

[1]*Department of Management Engineering, Guangxi Polytechnic of Construction, Nanning 530007, China*
[2]*School of Information and Management, Guangxi Medical University, Nanning 530021, China*

Correspondence should be addressed to Zhisheng Liang; liangzhsh@stu.gxmu.edu.cn

Received 4 November 2021; Revised 29 November 2021; Accepted 7 December 2021; Published 7 January 2022

Academic Editor: Le Sun

In order to improve the damage feature extraction effect of prefabricated residential building components and improve the structural stability of prefabricated residential components, this paper applies BIM technology to the structural feature analysis of prefabricated residential components. Moreover, this paper adopts the simple superposition method and combines the first strength theory of material mechanics to derive the formula for calculating the cracking torque of prefabricated residential building components under compound torsion. In addition, based on the variable-angle space truss model, this paper uses a simple superposition method to derive the calculation formula for the ultimate torque of composite torsion of fabricated residential building components and applies it to the BIM fabricated residential model. Finally, this paper constructs an intelligent BIM prefabricated residential building construction damage characteristic monitoring system. Through experimental research, it can be seen that the intelligent BIM prefabricated residential building construction damage feature monitoring system proposed in this paper can monitor the damage characteristics of prefabricated residential building construction and can predict the evolution of subsequent building features.

1. Introduction

Compared with low-rise buildings, high-rise buildings change from mainly resisting vertical loads to simultaneously bearing vertical and horizontal loads. High-rise buildings have more design requirements in terms of strength, stiffness, and ductility. This is because under the action of horizontal load, if the high-rise building structure has insufficient resistance to lateral deformation or low lateral stiffness, it will cause excessive lateral deformation. Under the combined action of vertical loads, additional internal forces will be generated, which will cause cracks or deformations in infill walls and building decoration, and structural damage will occur in serious cases [1]. Therefore, high-rise buildings must not only have sufficient strength during the design, but also have reasonable stiffness to ensure that the lateral deformation generated under the horizontal load meets the requirements of the code. At the same time, high-rise buildings must meet the requirements of the seismic code for “small earthquakes are not bad, moderate earthquakes can be repaired, and large earthquakes cannot fall.” The conventional structure is a frame-shear wall structure in terms of load-bearing system. The new structure is a box-type multitube structure, which is also a frame-shear wall structure in terms of load-bearing system. Frame-shear wall structure refers to adding an appropriate amount of shear walls to the frame structure, and they work together through the floor slab to meet the lateral requirements of the building [2]. In the case of little impact on the use function of the building, adding a proper amount of shear walls to the frame can significantly improve the lateral stiffness and bearing capacity of the structure. Therefore, the structural system has the advantages of both the frame and the shear wall structure and has strong applicability [3].

In this paper, BIM technology is applied to the damage feature extraction of prefabricated residential building construction. This method can effectively improve the reliability and construction effect of residential buildings, can prevent and eliminate residential risk factors in time, and can improve the safety of residential buildings.

2. Related Work

The literature [4] used a three-dimensional laser scanner to create a virtual 3D model of the Mevlana Museum of Konya History in Turkey. Literature [5] proposed a reconstruction method of historical building information model based on 3D laser scanning technology and digital pictures. In order to maintain the integrity of historical buildings, literature [6] proposed a method combining ground laser scanners and red-hot exterior images to obtain the detection of the protection status of historical buildings. Aiming at the insufficiency of digital technology in prefabricated residential buildings and the "secondary damage" caused by contact measurement to buildings, the literature [7] proposed a research idea of integrated internal and external three-dimensional modeling combining three-dimensional laser scanning technology and modern measurement methods, which provides high-precision data benchmarks for the future development, protection, maintenance, restoration, and reconstruction of cultural heritage of prefabricated residential buildings. The literature [8] applied three-dimensional laser scanning technology to complete three-dimensional data collection of ancient buildings. Literature [9] uses the massive point cloud data obtained by 3D laser scanning as an example to study the detailed process of point cloud data acquisition and processing in the 3D reconstruction of prefabricated residential buildings.

Oblique photography modeling is to use aerial camera to shoot images of buildings from different angles and then use data processing software for three-dimensional modeling and finally output the model [10]. Oblique photography modeling is a new type of surveying and mapping method with a wide range of applications, and the final result is also very real. Literature [11] uses oblique photography and ITS technology to perform 3D modeling of the city, showing the ability of oblique photography technology to be able to model large-scale three-dimensional modeling. Literature [12] uses oblique photography technology to perform 3D modeling of the ancient city of Rome, and the output results truly reflect the magnificence of the ancient city of Rome on the computer. Oblique photography technology started late in our country, but there are many research results in this area. Literature [13] uses oblique photography technology to establish a three-dimensional model and evaluates the progress. Literature [14] uses oblique photography technology to perform three-dimensional reconstruction of prefabricated residential buildings. Although oblique photography technology can carry out large-scale 3D reconstruction of buildings, its modeling cost is high and the amount of data is huge. However, prefabricated residential buildings have many components. Aerial photography cannot capture all of the complete prefabricated residential buildings and will be affected by the obstruction of objects around the building. The original appearance of the prefabricated residential buildings cannot be completely preserved. It also takes a lot of manpower to modify the built model, so the oblique photography technique cannot be applied to the technical method of batch modeling of Hakka prefabricated residential buildings.

Manual geometric modeling is to use SketchUp, 3DMax, unity3D, CAD, and other modeling software to perform 3D modeling of prefabricated residential buildings based on the drawings and data of prefabricated residential buildings. It has not formed a mature modeling system for 3D modeling of prefabricated residential buildings. And frameworks, among them, manual geometric modeling, 3D laser scanning modeling, and other modeling technology methods, are all three-dimensional modeling for a single prefabricated residential building, and the digital data of the prefabricated residential building can be used for virtual simulation and digital media display. In [15], the oblique photography technology has high modeling cost and large amount of data. Therefore, there is no technical means for prefabricated residential buildings that can be used universally and can be used for batch three-dimensional modeling. In order to solve the problem of rapid 3D modeling of mass prefabricated residential buildings, 3D modeling technology based on CGA grammar rules has gradually become the current research focus. Literature [16] uses the CityEngine platform to design the CGA rules for the three-dimensional modeling of Fujian Tulou and establishes a three-dimensional model of prefabricated residential buildings. Literature [17] analyzes the characteristics of prefabricated residential buildings and conducts three-dimensional modeling of its roof and its CGA Grammar optimization research. Literature [18] uses CityEngine to study the 3D modeling method of Lanzhou furnished residential buildings. Literature [19] uses CityEngine to model 3D prefabricated residential buildings, which provides a scientific and reasonable basis for the protection of the core old city landscape pattern. Literature [20] uses CityEngine's CGA rule modeling technology to achieve the establishment of a three-dimensional model of prefabricated residential buildings.

3. Research on the Damage Characteristics of Residential Building Construction

In this paper, the force mechanism, failure characteristics, stiffness, energy dissipation, ductility and torsion bearing capacity calculation formulas of reinforced concrete members under pure torsion, compression torsion, bending torsion, and shear torsion are studied in depth.

3.1. Space Truss Model. After the component cracks, the concrete cracks along a 45-degree angle with the longitudinal axis and forms a spiral diagonal strut. Moreover, it works in conjunction with longitudinal ribs and stirrups to form a space truss that relies on the shear flow on the pipe wall to resist torque. The schematic diagram of the model is shown in Figure 1. The basic assumptions of the space truss model are shown in Table 1.

The force mechanism of this model is clear, and the formula is simple and easy to calculate. However, at the same time, it also has the following problems. (1) The model

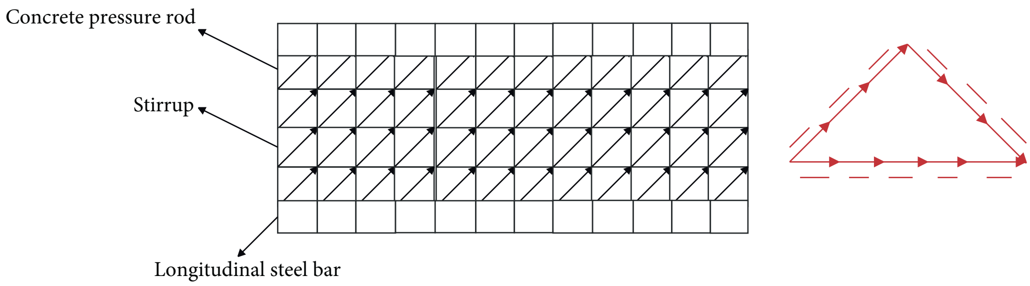

Figure 1: Space truss model.

Table 1: Basic assumptions of the space truss model.

Basic assumption type	Basic assumption content
Basic assumption 1	The longitudinal bars and stirrups and the concrete diagonal struts are hinged at the nodes to form a space truss structure
Basic assumption 2	It is only considered that the concrete diagonal compression rod bears the axial pressure, and the shear capacity is ignored
Basic assumption 3	Longitudinal bars and stirrups only bear tensile force and do not consider the bolting effect of steel bars
Basic assumption 4	It ignores the torsion resistance of the concrete in the core area

ignores the torsion resistance of the concrete. After the component is cracked, the steel bar and the concrete at the edge of the crack still interact, which can limit the development of the crack, so the calculation of the torsion bearing capacity of the component is conservative. (2) The model does not consider that the strength ratio of stirrups and longitudinal reinforcements will affect the torsion bearing capacity of components. Moreover, it assumes that the amounts of longitudinal reinforcement and stirrup are equal and ignores the influence of redundant longitudinal reinforcement and stirrup on the torsional bearing capacity of the member, which directly causes the increase in the amount of reinforcement and increases the production cost. (3) For reinforced concrete members with a higher reinforcement ratio, because the members cannot all reach yield, a higher estimate of the torsion bearing capacity of the steel bars makes the calculation structure unsafe.

3.2. Theoretical Model of Oblique Bending Failure. An oblique bending failure model is proposed on the basis of the combined bending, shear, and torsion test. The schematic diagram is shown in Figure 2. The model considers that the failure of the component occurs at the space section created by the spiral crack. With the change of cross-sectional shape, torsion ratio, and reinforcement ratio, the position of the compression zone of the failure surface will also change, which can be on the bottom, top, or side of the cross section. The model believes that the torsion member forms a space-deflection failure section through a compression surface and three tension surfaces. The oblique bending failure model uses the internal and external moments of the neutral axis of the failure surface to use the balance of the internal and external moments to derive the calculation formula of the ultimate torsion bearing capacity.

After idealizing the failure section, another calculation model is proposed. It is considered that the failure section is at a 45-degree angle to the beam axis and a 90-degree angle to the wide face of the beam. The failure surface does not intersect the short-leg stirrups, and the impact of the short-leg on the torsional bearing capacity is not considered. The conclusions drawn according to these assumptions are consistent with the fact that the short-leg stirrup stress is relatively small in the experiment. In addition, this model also considers the pinning effect of concrete and longitudinal reinforcement in the compression zone and the shearing effect of concrete.

3.3. Variable-Angle Space Truss Model. In the space truss model, the inclination angle θ of the concrete oblique strut is a constant, while the variable-angle space truss model considers the inclination θ of the concrete oblique strut to be a variable, and the size of θ is determined by the relative magnitude of the yield stress of the stirrup and the longitudinal reinforcement. In the design process, we determine the size of θ according to the most economic ratio of the amount of stirrup and longitudinal reinforcement. The schematic diagram of the variable-angle space truss model is shown in Figure 3. The variable-angle space truss model also has four basic assumptions, as shown in Table 2.

3.4. Baroclinic Field Calculation Model. Based on the space truss model, the geometric deformation conditions and static equilibrium conditions of the members are considered at the same time, and this theory is applied to prestressed concrete structures. This model assumes that, after the component cracks, the concrete no longer resists the pulling force, and the torsion is completely resisted by the diagonal struts. The inclination angle of the reinforced concrete

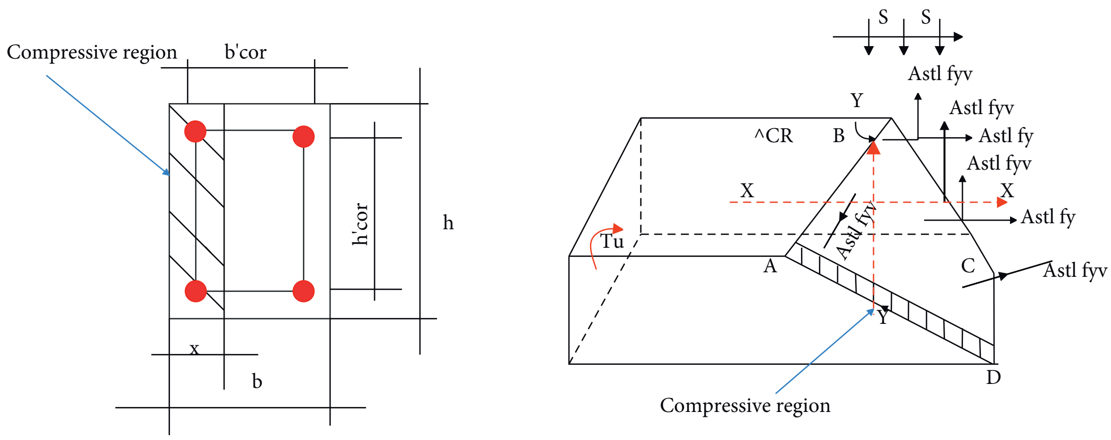

Figure 2: Calculation model of oblique bending theory.

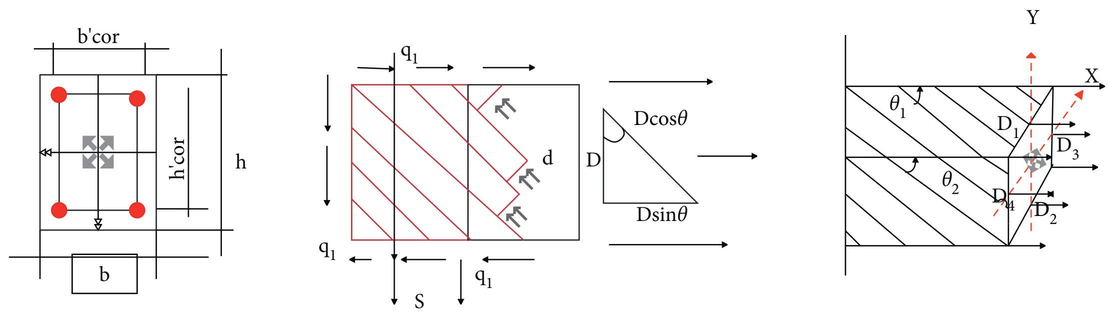

Figure 3: Variable-angle space truss model.

Table 2: Basic assumptions of the variable-angle space truss model.

Basic assumption type	Basic assumption content
Basic assumption 1	The oblique concrete rod formed by the spiral crack only bears pressure, and the inclination angle is θ
Basic assumption 2	The stirrups are regarded as the web members of the space truss, and the longitudinal ribs are regarded as the chords of the space truss, which only bear pressure
Basic assumption 3	It ignores the torsion effect of the concrete in the core area
Basic assumption 4	Under the action of torque, a constant shear flow is formed along the side wall of the box section

oblique beam can be determined by the coordinated conditions of the torsion of the reinforced concrete member. At the same time, it also took the concrete protective layer withdrawal work as the starting point to reduce the area of the concrete core area, adjust the position of the shear flow, and adjust the space truss model's defect that the torsion bearing capacity is too high.

3.5. Coordinated Pressure Field Calculation Model. The "softened space truss model" believes that the development direction of cracks is perpendicular to the direction of the main tensile stress of the concrete, and there is no shear stress in the section where the crack occurs. The direction of the main compressive stress of the concrete directly determines the direction of the concrete diagonal compression bar. The model ignores the influence of shear stress at the crack section on the torsional bearing capacity of the member and only considers the contribution of the steel frame to the torsional bearing capacity of the member.

Because the strain of the steel bar before cracking of the reinforced concrete member is small, the influence of the steel bar can be ignored when calculating the cracking torque of the reinforced concrete member under pure torsion.

Under the action of torque, torsional shear stress τ_i will be generated in the section of plain concrete member, and the calculation formula of τ_i is shown as follows:

$$\tau_i = \frac{T}{W_t}. \tag{1}$$

In the formula, Wt is the torsional plastic resistance moment of the section.

The torque generated by the component before it cracks is very small. Approximately analyze the stress distribution of the plain concrete member's section according to the elastic theory.

When torque acts on a rectangular section, the maximum shear stress will be generated at the midpoint of the long side of the rectangular section, and a principal tensile stress equal to the torsional shear stress will be generated in the direction at 45° to the longitudinal axis of the section. When the main tensile stress reaches the concrete tensile strength, the surface concrete cracks, and the development direction of the cracks forms an angle of 45° with the longitudinal axis. Using the elastic theory, the formula for the cracking torque of concrete under pure torsion is obtained:

$$T = \alpha f_t b h^2. \tag{2}$$

In the formula, α is related to the ratio of long side b and short side h of the section, which can be obtained by looking up the table, f_t is the tensile strength of concrete, and b and h are the long side and the short side of the component section.

When calculating the cracking torque of concrete members according to plastic theory, it is assumed that concrete is an ideal plastic material. As the torque increases, the cross section of the component begins to enter the plastic state from part to the full plastic state. At this time, the concrete stress on the cross section of the component all reaches the tensile strength of the concrete, and the cross section of the component is cracked. At this time, the plastic torsion resistance moment W_t of the cross section of the member can be obtained according to the sand pile analogy method. The sand pile analogy method is shown in Figure 4.

$$\begin{aligned} V &= \frac{1}{12}\tau_t b^2 (3h - b), \\ \tau_i &= T = 2V \\ &= \frac{1}{6} b^2 (3h - b). \end{aligned} \tag{3}$$

The formula for calculating the cracking torque of the component is

$$\begin{aligned} T_\sigma &= f_t W_t \\ &= f_t \frac{1}{6} b^2 (3h - b). \end{aligned} \tag{4}$$

Concrete is an elastoplastic material between plastic and elastic materials. For reinforced concrete members under pure torsion, at the initial stage of torque, the stress distribution of the cross section can be approximated by elastic theory analysis. However, the stress distribution of the cross section gradually enters the elastoplastic stage as the torque increases. If calculated completely according to the plastic theory, the cracking torque of the component will be overestimated. If calculated completely according to the elastic theory, the cracking torque of the component will be underestimated, especially as the strength of the concrete increases, the brittleness of the concrete increases. In order to facilitate the calculation, we use the ideal plastic theory to approximate the cracking torque of reinforced concrete members, but the tensile strength of concrete should be

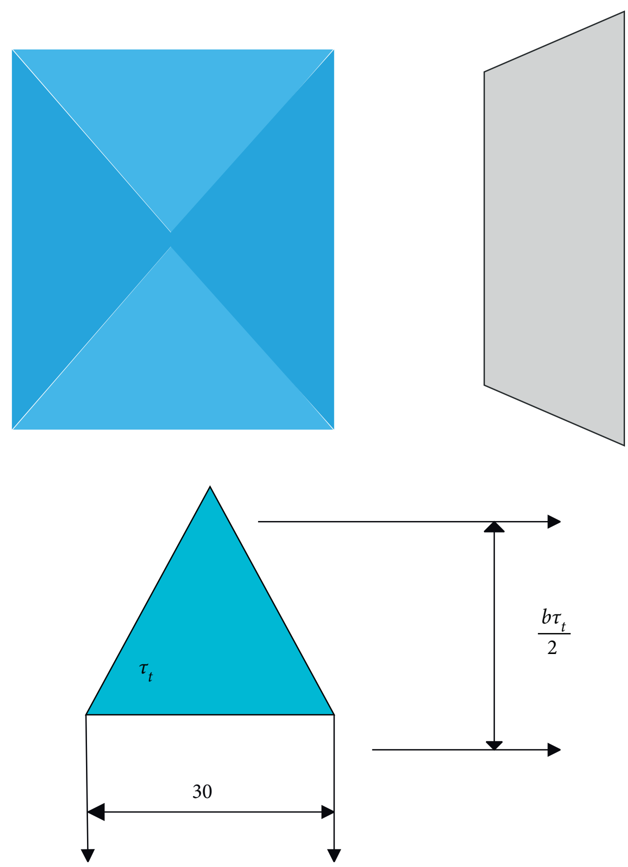

Figure 4: Schematic diagram of sand pile analogy method.

appropriately reduced. When calculating the cracking torque of reinforced concrete members under pure torsion, China's "Code for Design of Concrete Structures" (GB50010-2010) stipulates that a reduction factor should be multiplied on the basis of plasticity theory. The calculation formula is as follows:

$$T_\sigma = \gamma_t f_t W_t. \tag{5}$$

In the formula, γ_t is the reduction factor, which is 0.8 for high-strength concrete and 0.7 for low-strength concrete.

We select a stress element at the middle edge of the column for research and obtain the principal tensile stress of the stress element according to the Moiré strength theory. When the principal tensile stress reaches the tensile strength of the concrete, it is considered that the concrete is cracked, namely:

$$\sigma\{\sigma(N, M), \tau(T, V)\} = f_t. \tag{6}$$

(1) The normal stress on the stress element is

$$\sigma(N, M) = \sigma_N + \sigma_M. \tag{7}$$

For the convenience of calculation, we assume that the deformations of reinforced concrete and section steel are coordinated. At the same time, considering the role of longitudinal reinforcement, the axial pressure of the reinforced concrete part can be expressed as

$$\begin{aligned}N_1 &= \frac{f_c A + f_y A_s}{f_c A + f_y A_s + f_a A_a} \\ &= \alpha_1 N.\end{aligned} \tag{8}$$

The compressive stress generated by the shaft pressure is

$$\sigma_N = \frac{N_1}{A}. \tag{9}$$

For H-shaped steel, before the concrete cracks, the strain of the steel flange is small. For simple calculation, all the bending moment is borne by the reinforced concrete and then the compressive stress generated by the bending moment is as follows:

$$\sigma_M = \frac{M}{W}. \tag{10}$$

In the formula, A is the cross-sectional area of the member, A = bh; W is the section flexural modulus of the component, and rectangular section is $W = bh^2/6$.

(2) The shear stress on the stress element is

$$\tau(T, V) = \tau_T + \tau_V. \tag{11}$$

According to the shear stiffness, the shear force borne by the concrete part and the section steel part is distributed, and the shear force borne by the concrete part is

$$\begin{aligned}V_1 &= \frac{\tau_c bh}{\tau_c bh + \tau_a t_w b_w} V \\ &= \alpha_2 V.\end{aligned} \tag{12}$$

The shear stress generated by the shear force is

$$\tau_V = \frac{V_1 S}{b I_0}. \tag{13}$$

In the formula, τ_c and τ_a are the shear strength of concrete and section steel; t_w and b_w are the thickness and width of section steel web; S is the static moment of cross section; and I_0 is the moment of inertia of the cross section on the neutral axis.

It is the same as the steel-concrete component under pure torsion; regardless of the influence of the steel on the cracking torque, the torque is all borne by the concrete part. Then, the shear stress generated by the torque is

$$\tau_T = \frac{T_{cr}}{W_t}. \tag{14}$$

According to the formula of Mohr's strength theory, under the action of compressive stress σ and shear stress t, the main tensile stress is

$$\sigma_t = \frac{\sigma_M - \sigma_N}{2} + \sqrt{\left(\frac{\sigma_M - \sigma_N}{2}\right)^2 + \tau^2}. \tag{15}$$

If $\sigma_t = f_t$, then

$$f_t = \frac{\sigma_M - \sigma_N}{2} + \sqrt{\left(\frac{\sigma_M - \sigma_N}{2}\right)^2 + \tau^2}. \tag{16}$$

Through sorting, we can get

$$T_{cr} = f_t W_t \left(\sqrt{1 + \frac{\alpha_1 N}{f_t A} - \frac{M}{f_t W}} - \frac{\alpha V}{f_t b I_0}\right). \tag{17}$$

γ is the influence coefficient considering the axial pressure, bending moment, and shear force on the cracking torque of steel reinforced concrete members under combined torsion; then,

$$\begin{aligned}\gamma &= \sqrt{1 + \frac{\alpha_1 N}{f_t A} - \frac{M}{f_t W}} - \frac{\alpha V}{f_t b I_0} \\ T_{cr} &= \gamma f_t W_t.\end{aligned} \tag{18}$$

With the decrease of the torsion-bending ratio, the failure mode of steel reinforced concrete members gradually changes from torsion failure to bending failure. When the first crack appears at the neutral axis of the shear superimposed surface, the influence of the bending moment on the cracking torque of the component can be ignored. When the first crack appears on the curved tensile surface, it is necessary to consider the influence of bending moment, shear force, and axial pressure on the cracking torque of the component at the same time.

According to observations, the first crack in this test generally appears in the middle of the shear superimposed surface. At this time, the bending deformation of the steel reinforced concrete member is very small, and the crack is generally located at the neutral axis, and the bending moment can be approximately regarded as zero. Taking into account that concrete is an elastoplastic material and its softening properties at failure, it is multiplied by the torque reduction coefficient K on the right side of (19) to obtain the formula:

$$\begin{aligned}T_{cr} &= K\gamma f_t W_t \\ &= K f_t W_t \left(\sqrt{1 + \frac{\alpha_1 N}{f_t A} - \frac{M}{f_t W}} - \frac{\alpha_2 V}{f_t b I_0}\right).\end{aligned} \tag{19}$$

Under pure torsion, the external reinforced concrete bears most of the torque. Because the external concrete restricts the deformation of the internal steel, the calculation of the torsional bearing capacity of the internal steel is more complicated. In the actual engineering design, the relationship between the effective wall thickness of the torsion member and the thickness of the steel reinforced concrete protective layer should be considered first. When the thickness of the steel reinforced concrete protective layer is large, the effect of the internal steel can be ignored, and only the torsion bearing capacity of the reinforced concrete members can be calculated. The empirical formula of the ultimate torque obtained from the test of reinforced concrete members in China is

$$T_{RC} = 0.35 f_t W_t + 1.2\sqrt{\xi}\, \frac{A_{sv} f_{yv} A_{cor}}{s}. \tag{20}$$

In the formula, f_t is the concrete tensile strength; W_t is the torsional plastic resistance of the section; ξ is the reinforcement strength ratio considering the influence of section steel, $0.6 \le \xi \le 1.7$; $f_{yv}{}' A_{sv}$ is the design value of the tensile strength of the torsion stirrup and the cross-sectional area of the torsion stirrup; A_{cor} is the area of the core area of concrete components; and s is the stirrup spacing.

When the thickness of the protective layer of steel section concrete is small, the ultimate torque of section steel-concrete members can be obtained by superimposing the respective torques borne by section steel and concrete, and the concrete part can be obtained from the above formula. The full plastic torque of H-shaped steel can still be divided into two parts: warping torsion and free torsion. In this case, the simple superposition method can be used for calculation; the formula is as follows:

$$T_{SRC} = T_{BC} + T_a = T_{RC} + T_u + T_w \tag{21}$$

In the formula, T_{RC} is the torque borne by a reinforced concrete part; T_u is the free torsion torque of section steel; and T_{w} is the warping torque of the section steel.

Substituting the full plastic free torsion torque T_u and the full plastic warping torsion torque T_{w} into the formula, we get

$$T_{SRC} = 0.35 f_t W_t + 1.2\sqrt{\xi}\ \frac{A_{sv} f_{yv} A_{cor}}{s} + \frac{f_y}{\sqrt{3}}\left[bt^2\left(1 - \frac{t}{3b}\right) + h_0\frac{t_w^2}{2} + \frac{t_w^2}{6}\right] + \frac{2M_{fp}h_0}{L}. \tag{22}$$

When the member is in the limit state, the warping torsion torque is generally 22–033 of the free torsion torque, and the free torsion torque increase coefficient α of the section steel is introduced, and then (23) is obtained on the basis of (22):

$$T_{SRC} = 0.35 f_t W_t + 1.2\sqrt{\xi}\ \frac{A_{sv} f_{yv} A_{cor}}{s} + \alpha\frac{f_y}{\sqrt{3}}\left[bt^2\left(1 - \frac{t}{3b}\right) + h_0\frac{t_w^2}{2} + \frac{t_w^2}{6}\right]. \tag{23}$$

Based on the spatial variable-angle analysis frame model, the strength-related equations of reinforced concrete members under bidirectional compression, bending, shear and torsion are obtained:

$$\frac{T_1^2}{T_0^2} + \frac{V_x^2}{v_{0X}^2} + \frac{V_Y^2}{v_{0Y}^2} + \frac{M_x}{M_{0x}} + \frac{M_y}{M_{0y}} - \frac{N_1}{N_0} = 1. \tag{24}$$

This experiment is the analysis of the unidirectional compression, bending, shear, and torsion force of steel reinforced concrete members. The equation is simplified as

$$\frac{T_1^2}{T_0^2} + \frac{V_1^2}{V_0^2} + \frac{M_1}{M_0} - \frac{N_1}{N_0} = 1. \tag{25}$$

In the formula,

$$\begin{aligned} T_0 &= 2A_{\mathrm{cor}}\sqrt{\frac{f_y A_{stl}}{u_{\mathrm{cor}}}\cdot\frac{A_{sv} f_{yv}}{s}},\\ V_0 &= \frac{A}{t_2 + t_4}\sqrt{2\cdot\frac{f_y A_{stl}}{b_{\mathrm{cor}}}\cdot\frac{A_{sv} f_{yv}}{s}},\\ N_0 &= \frac{A_{stl} f_y}{\beta_N},\\ M_0 &= \frac{3A_{stl} f_y b\prime}{8}. \end{aligned} \tag{26}$$

According to Figure 3, we take

$$\begin{aligned} t_1 &= t_3 = \frac{b}{5},\\ t_2 &= t_4 = \frac{h}{5}. \end{aligned} \tag{27}$$

Then,

$$\begin{aligned} \beta_N &= \frac{A}{A}\\ &= 1 - \frac{(b - t_1 - t_3)(h - t_2 - t_4)}{bh}\\ &= 0.64\\ V_0 &= \sqrt{\frac{125 b f_y A_{stl} f_{yv} A_{sv}}{8}},\\ N_0 &= \frac{f_y A_{stl}}{0.64},\\ M_0 &= 0.3 b f_y A_{stl}. \end{aligned} \tag{28}$$

T1, V1, M1, and N1 are, respectively, the torque, shear force, bending moment, and axial pressure of the reinforced concrete part under the action of compression, bending, shear, and torsion, which are distributed according to the following formula.

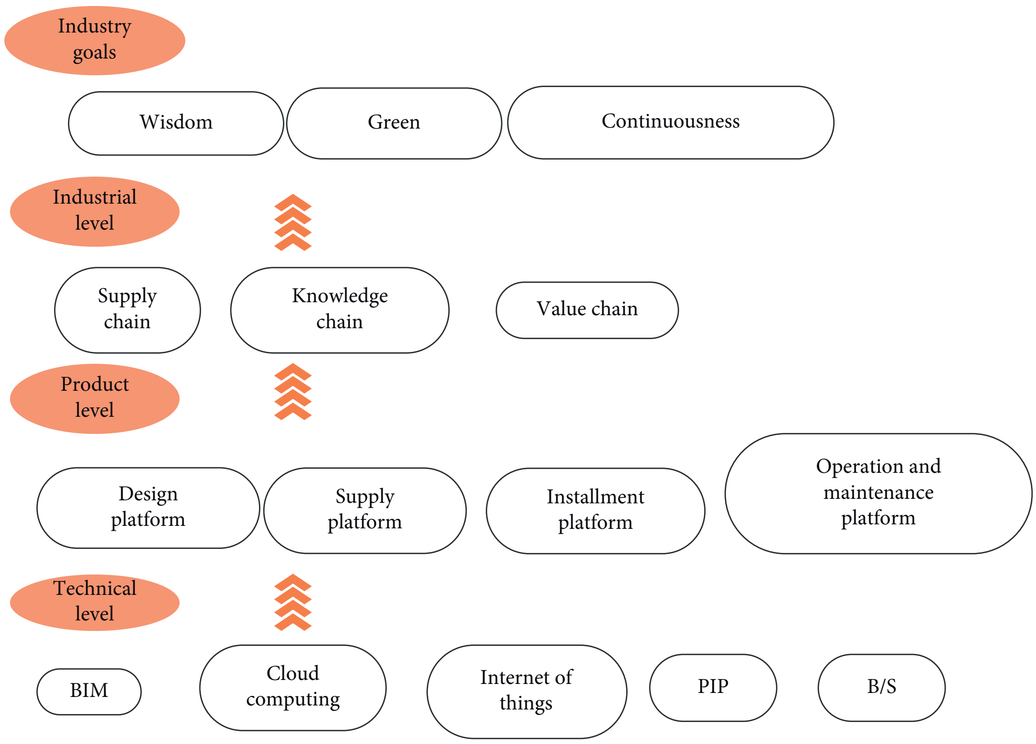

FIGURE 5: Roadmap of the R&D technology of the integrated management platform.

3.5.1. Torque Distribution. According to (23), referring to formulas (20) and (21), the torsion bearing capacity of steel-concrete members under pure torsion is superimposed according to the torque borne by the reinforced concrete part and the torque borne by the steel part:

$$T_1 = \frac{T_{RC}}{T_{RC} + T_a} = \alpha_1 T. \tag{29}$$

In the formula, α_1 is the percentage of torque borne by the reinforced concrete part.

3.5.2. Shear Force Distribution.

$$V_1 = \frac{\tau_c bh}{\tau_c bh + \tau_a t_w b_w} V = \alpha_2 V. \tag{30}$$

In the formula, τ_c and τ_a are the shear strength of concrete and section steel; t_w and b_w are the thickness and width of the profiled steel web; $\alpha 2$ is the percentage of shear force borne by the reinforced concrete part.

3.5.3. Bending Moment Distribution.

$$M_1 = \frac{f_y A_s h\prime}{f_y A_s h\prime + f_a A_{af} h\prime\prime} = \alpha_3 M. \tag{31}$$

In the formula, h' is the distance from the point of action of tensile longitudinal bars to the point of action of compressed longitudinal bars; h' is the center distance of the steel flange; A_s is the area of the longitudinal ribs on the bending and tensile side; A_{Af} is the area of a single steel flange; and α_s is the percentage of bending moment borne by the reinforced concrete part.

3.5.4. Axial Force Distribution.

$$N_1 = \frac{f_c A_c + f_y A_{stl}}{f_s A_c + f_y A_{stl} + f_a A_a} = \alpha_4 N. \tag{32}$$

α is the percentage of axial pressure borne by the reinforced concrete part.

Substituting (29), (30), (31), and (32) into (25), the strength-related equations of H-shaped steel-concrete members are obtained.

The ultimate bearing capacity T of steel reinforced concrete members under composite torsion is

$$\left(\frac{\alpha_1 T}{T_0}\right)^2 + \left(\frac{\alpha_2 V}{V_0}\right)^2 + \frac{\alpha_3 M}{M_0} + \frac{\alpha_4 N}{N_0} = 1. \tag{33}$$

Substituting (19) for the ultimate torque of reinforced concrete members under pure torsion into (34), we get

$$T_u = \frac{T_0}{\alpha_1}\sqrt{1 - \left(\frac{\alpha_2 V}{V_0}\right)^2 - \frac{\alpha_3 M}{M_0} + \frac{\alpha_4 N}{N_0}}. \tag{34}$$

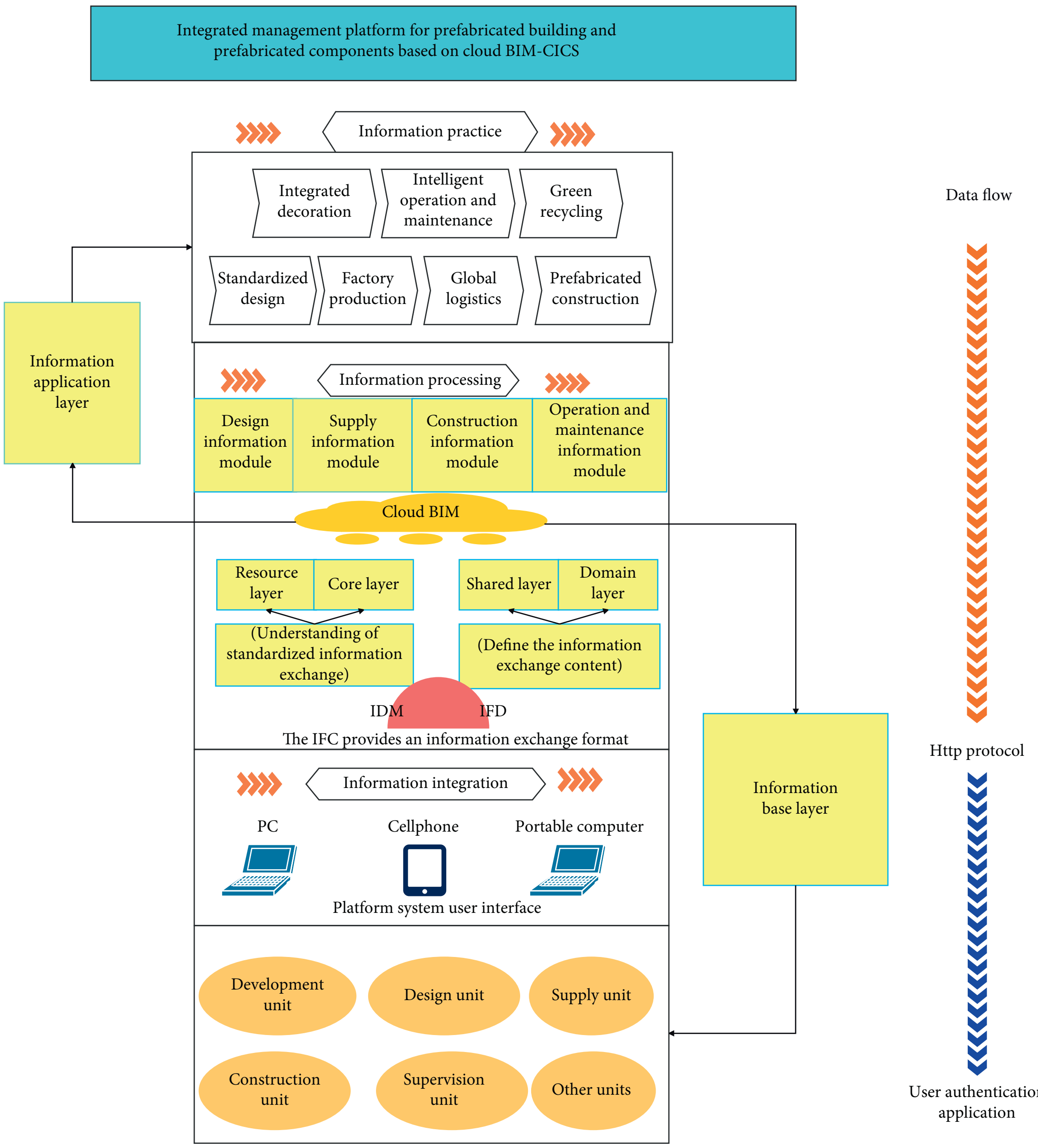

Figure 6: Architecture diagram of integrated management platform for prefabricated components.

4. Construction Damage Feature Extraction of Prefabricated Residential Buildings Based on BIM

The development of an integrated management platform for prefabricated building components based on cloud BIM-CICS integrates technologies such as cloud BIM, Internet of Things, networks, and databases. Based on the design idea of the integrated management platform, this paper is oriented to the business points of prefabricated component management of prefabricated buildings and determines the R&D technical route of the platform, as shown in Figure 5.

Based on the cloud BIM technology and the characteristics of China's prefabricated component management and the goals of the platform, this paper determines the prefabricated component integrated management platform architecture of the prefabricated building based on cloud BIM-CICS, as shown in Figure 6. The platform realizes the integrated management of industry chain information, allows production information to "flow," realizes effective sharing of information in various links such as component design, supply, installation, operation, and maintenance, and improves project management efficiency.

Combined with the demand for extraction of damage characteristics of prefabricated residential buildings, this paper constructs an intelligent BIM prefabricated residential building construction damage feature monitoring system as shown in Figure 7.

After the above intelligent system is constructed, the damage feature monitoring effect of the system in this paper

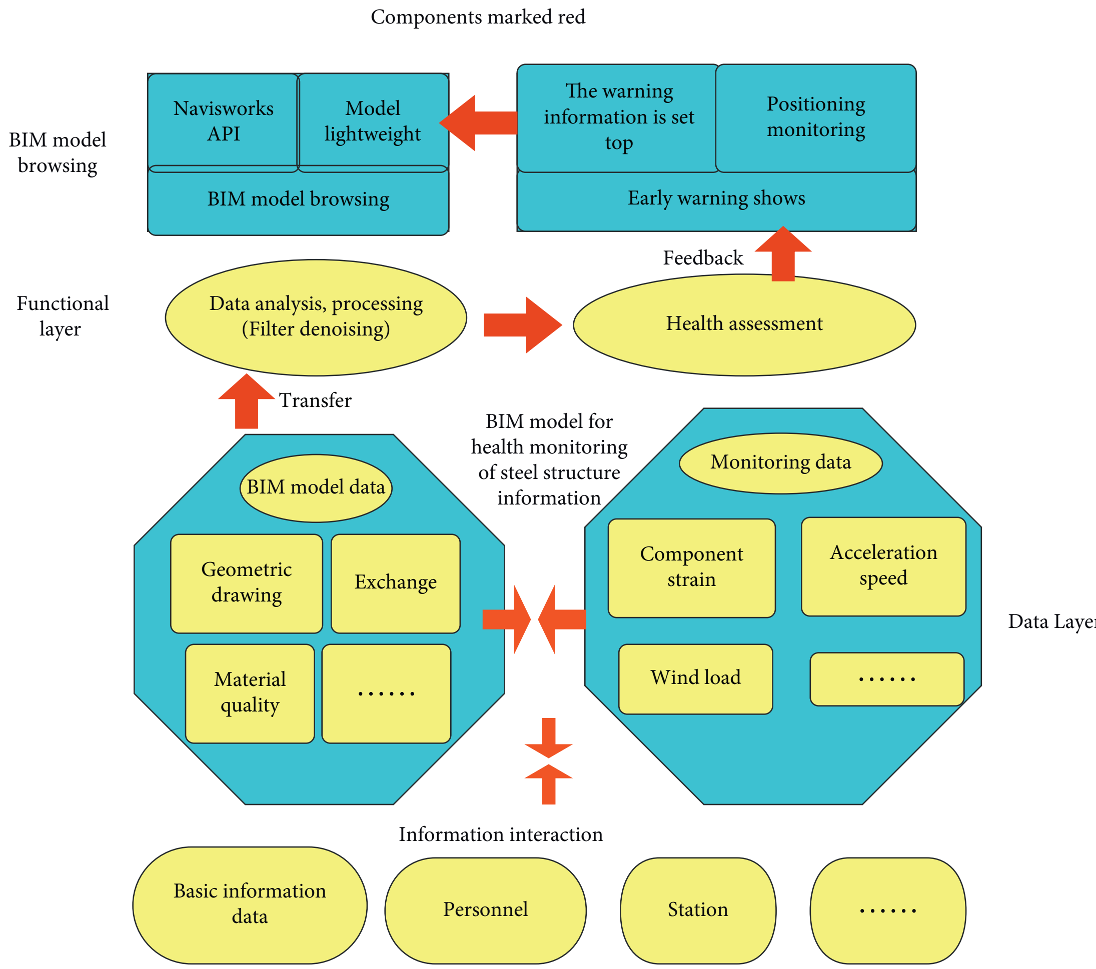

Figure 7: Intelligent BIM prefabricated residential building construction damage feature monitoring system.

Table 3: The monitoring effect of residential building damage feature of intelligent BIM prefabricated residential building construction damage feature monitoring system.

No.	Feature monitoring	No.	Feature monitoring	No.	Feature monitoring
1	86.7	20	78.3	39	87.7
2	75.3	21	86.4	40	75.7
3	79.5	22	88.7	41	80.8
4	78.4	23	76.4	42	84.5
5	89.2	24	77.2	43	82.7
6	93.9	25	81.7	44	75.0
7	89.2	26	74.7	45	90.5
8	87.9	27	80.6	46	76.9
9	86.9	28	81.1	47	87.1
10	91.3	29	74.1	48	82.8
11	86.9	30	75.6	49	78.4
12	78.1	31	90.5	50	78.8
13	84.1	32	76.8	51	86.6
14	90.0	33	83.8	52	81.9
15	88.7	34	91.8	53	83.6
16	75.6	35	81.0	54	85.7
17	76.2	36	89.9	55	93.8
18	91.6	37	92.6	56	79.7
19	78.2	38	74.9		

Table 4: The prediction effect of residential building component features of intelligent BIM prefabricated residential building construction damage feature monitoring system.

No.	Feature prediction	No.	Feature prediction	No.	Feature prediction
1	85.2	20	71.0	39	81.6
2	71.5	21	78.9	40	73.3
3	77.9	22	68.4	41	68.0
4	68.7	23	78.4	42	83.8
5	70.9	24	82.6	43	70.0
6	80.0	25	83.7	44	81.4
7	79.8	26	84.6	45	68.1
8	78.4	27	79.7	46	67.3
9	87.3	28	75.7	47	87.9
10	74.3	29	75.7	48	83.9
11	86.8	30	73.0	49	80.0
12	78.4	31	70.5	50	69.1
13	74.3	32	86.1	51	87.4
14	81.2	33	79.2	52	83.7
15	82.5	34	78.0	53	81.3
16	79.5	35	83.1	54	87.9
17	67.7	36	75.9	55	71.7
18	79.7	37	70.6	56	75.6
19	83.2	38	67.1		

and the component feature prediction effect of the system in this paper are evaluated by simulation tests, and the results are shown in Tables 3 and 4.

From the above research, it can be seen that the intelligent BIM prefabricated residential building construction damage feature monitoring system proposed in this paper can monitor the damage characteristics of the prefabricated residential building construction and can predict the evolution of subsequent building features.

5. Conclusion

With the rapid development of the residential building industry, the structure and calculation theory of residential building structures are constantly improving and perfecting. In particular, the strength of steel has been greatly improved, which has further promoted the development of structural members in the direction of thin walls. In high-rise residential buildings, the lateral force resistance system transmits the horizontal load (wind, earthquake, and so on) that the house bears to the foundation. The high-rise residential building as a whole is regarded as a cantilever beam under the action of vertical and horizontal forces. As the height of the residential building increases, the vertical force at the bottom of the structure increases linearly, and the bending moment and lateral displacement of the bottom floor increase in an exponential curve. Therefore, as the height increases, the horizontal load will gradually become the dominant factor in the structural design, and the selection and composition of the lateral force-resistant structural system have become the primary consideration and decision-making focus of the structural design of high-rise residential buildings. In most cases, it is unified with the vertical load transfer system. In this paper, BIM technology is applied to the failure feature extraction of prefabricated residential building construction. This method can effectively improve the reliability and construction effect of residential buildings, can prevent and eliminate residential risk factors in time, and can improve the safety of residential buildings.

Data Availability

The labeled datasets used to support the findings of this study are available from the corresponding author upon request.

Conflicts of Interest

The authors declare that there are no conflicts of interest.

Acknowledgments

This study was sponsored by the Research Foundation of Young and Middle-aged Teachers in Guangxi Universities + Research on the Flexural Properties of Prefabricated Reinforced Concrete Partial Composite Plates (2020KY35019); 2020 Guangxi Vocational Education Teaching Reform Research Project (GXGZJG2020B053) Curriculum Reform and Practice of "Construction Project Management" under PC factory + Smart Site mode.

References

[1] D. Chakraborty and H. Elzarka, "Advanced machine learning techniques for building performance simulation: a comparative analysis," *Journal of Building Performance Simulation*, vol. 12, no. 2, pp. 193–207, 2019.

[2] O. Guerra-Santin and S. Silvester, "Development of dutch occupancy and heating profiles for building simulation," *Building Research & Information*, vol. 45, no. 4, pp. 396–413, 2017.

[3] T. Dodd, C. Yan, and I. Ivanov, "Simulation-based methods for model building and refinement in cryoelectron

microscopy," *Journal of Chemical Information and Modeling*, vol. 60, no. 5, pp. 2470–2483, 2020.

[4] T. Abuimara, W. O'Brien, B. Gunay, and J. S. Carrizo, "Towards occupant-centric simulation-aided building design: a case study," *Building Research & Information*, vol. 47, no. 8, pp. 866–882, 2019.

[5] P. Remmen, M. Lauster, M. Mans, M. Fuchs, T. Osterhage, and D. Müller, "TEASER: an open tool for urban energy modelling of building stocks," *Journal of Building Performance Simulation*, vol. 11, no. 1, pp. 84–98, 2018.

[6] N. Endo, E. Shimoda, K. Goshome, T. Yamane, T. Nozu, and T. Maeda, "Simulation of design and operation of hydrogen energy utilization system for a zero emission building," *International Journal of Hydrogen Energy*, vol. 44, no. 14, pp. 7118–7124, 2019.

[7] M. I. Beausoleil, "Learning the fundamentals of building performance simulation through an experiential teaching approach," *Journal of Building Performance Simulation*, vol. 12, no. 3, pp. 308–325, 2019.

[8] C. Xiong, J. Huang, and X. Lu, "Framework for city-scale building seismic resilience simulation and repair scheduling with labor constraints driven by time-history analysis," *Computer-Aided Civil and Infrastructure Engineering*, vol. 35, no. 4, pp. 322–341, 2020.

[9] A. D. Black, "Wor(l)d-Building: simulation and metaphor at the mars desert research station," *Journal of Linguistic Anthropology*, vol. 28, no. 2, pp. 137–155, 2018.

[10] K. Hanson, L. Hernandez, and J. A. Banaski, "Building simulation exercise capacity in Latin America to manage public health emergencies," *Health security*, vol. 16, pp. S-98–S-102, 2018.

[11] E. K. Wati and N. Widiansyah, "Design of learning media: modeling & simulation of building thermal comfort optimization system in building physics course," *Jurnal Pendidikan IPA Indonesia*, vol. 9, no. 2, pp. 257–266, 2020.

[12] C. W. Lee and S.-J. Cho, "The development of converting program from sealed geological model to gmsh, COMSOL for building simulation grid," *Journal of the Korean Earth Science Society*, vol. 38, no. 1, pp. 80–90, 2017.

[13] C. Miller, D. Thomas, J. Kämpf, and A. Schlueter, "Urban and building multiscale co-simulation: case study implementations on two university campuses," *Journal of Building Performance Simulation*, vol. 11, no. 3, pp. 309–321, 2018.

[14] X. Xie and Z. Gou, "Building performance simulation as an early intervention or late verification in architectural design: same performance outcome but different design solutions," *Journal of Green Building*, vol. 12, no. 1, pp. 45–61, 2017.

[15] A. I. Adilkhodjayev, I. M. Mahamataliev, and S. S. Shaumarov, "Theoretical aspects of structural and simulation modeling of the macrostructure of composite building materials," *Journal of Tashkent Institute of Railway Engineers*, vol. 14, no. 2, pp. 3–14, 2019.

[16] S. Imam, D. A. Coley, and I. Walker, "The building performance gap: are modellers literate?" *Building Service Engineering Research and Technology*, vol. 38, no. 3, pp. 351–375, 2017.

[17] J.-S. Pei, B. Carboni, and W. Lacarbonara, "Mem-models as building blocks for simulation and identification of hysteretic systems," *Nonlinear Dynamics*, vol. 100, no. 2, pp. 973–998, 2020.

[18] A. Brunelli, F. de Silva, A. Piro et al., "Numerical simulation of the seismic response and soil-structure interaction for a monitored masonry school building damaged by the 2016 central Italy earthquake," *Bulletin of Earthquake Engineering*, vol. 19, no. 2, pp. 1181–1211, 2021.

[19] P. Andrio, A. Hospital, J. Conejero et al., "Bioexcel building blocks, a software library for interoperable biomolecular simulation workflows," *Scientific Data*, vol. 6, no. 1, pp. 169–178, 2019.

[20] G. Petrou, A. Mavrogianni, P. Symonds et al., "Can the choice of building performance simulation tool significantly alter the level of predicted indoor overheating risk in London flats?" *Building Service Engineering Research and Technology*, vol. 40, no. 1, pp. 30–46, 2019.

Hindawi
Scientific Programming
Volume 2022, Article ID 4223295, 10 pages
https://doi.org/10.1155/2022/4223295

Research Article

Animation Character Detection Algorithm Based on Clustering and Cascaded SSD

Yuan Wang

School of Design and Art, Xijing University, Xi'an, Shaanxi 710123, China

Correspondence should be addressed to Yuan Wang; 20070045@xijing.edu.cn

Received 25 November 2021; Accepted 11 December 2021; Published 7 January 2022

Academic Editor: Le Sun

With the evolution of the Internet and information technology, the era of big data is a new digital one. Accordingly, animation IP has been more and more widely welcomed and concerned with the continuous development of the domestic and international animation industry. Hence, animation video analysis will be a good landing application for computers. This paper proposes an algorithm based on clustering and cascaded SSD for object detection of animation characters in the big data environment. In the training process, the improved classification Loss function based on Focal Loss and Truncated Gradient was used to enhance the initial detection effect. In the detection phase, this algorithm designs a small target enhanced detection module cascaded with an SSD network. In this way, the high-level features corresponding to the small target region can be extracted separately to detect small targets, which can effectively enhance the detection effect of small targets. In order to further improve the effect of small target detection, the regional candidate box is reconstructed by a k-means clustering algorithm to improve the detection accuracy of the algorithm. Experimental results demonstrate that this method can effectively detect animation characters, and performance indicators are better than other existing algorithms.

1. Introduction

In recent years, IP (intellectual property) has ushered in the outbreak of various forms of industry, such as literature, music, games, animation, and film and television industries. In addition, the development of related industries with IP as the core also promotes the cross-border integration of different industries. All kinds of enterprises in the whole industrial chain have started cross-industry and cross-industry new exploration in different forms. Various IP resources are utilized to promote operation and development [1]. Big data has strong functionality in the era of network science and technology with highly developed information sharing. However, the transformation of big data as new thinking will be missed out if we only see the functionality of big data. Therefore, animation circles can apply the function and thinking of big data to promote the development of animation IP [2].

Among all kinds of IP, animation IP has received more and more attention with the continuous development of the domestic and international animation industry, such as the birth of "Nezha's Devil boy" and "the big fish Begonia" in China, and "the pirate king" and "spider man" in foreign countries. In addition to creating high-quality works in this field, such excellent animation IP often extends to a variety of surrounding industries. Borrowing the mature IP of the industry, it has made more profits in the pan entertainment field and expanded its influence [3]. Therefore, the intelligent detection and recognition of animation characters and their surroundings (such as Cosplay) can help cultivate users' interest in animation characters, encourage users to consume products around animation characters, and realize pan entertainment of animation IP.

Object detection is one of the basic tasks of computer vision, which is widely used in the fields of unmanned driving, safety systems, and defect detection. Target detection technology is mainly divided into three research directions. The first target detection direction is the traditional target detection method. In this method, feature descriptors are constructed to extract features, and then classifiers are used to classify features to achieve target detection [4]. Typical representatives are HOG, LBP, and Haar.

The second target detection direction is a two-step target detection algorithm, which first recommends regions and then classifies targets. Typical representatives are regions with volatile neural network features (R-CNN) and fast R-CNN. R-CNN framework and Fast R-CNN framework were proposed by Girshick to improve the accuracy of target detection [5, 6]. After that, Ren et al. proposed a Faster R-CNN network, in which the candidate regions were proposed by RPN (region proposal network). In the final feature map, the objects in the original image are much smaller and difficult to locate. Therefore, Faster R-CNN cannot solve the problem of small object detection [7]. At the same time, a complete convolutional network (FCN) has been proposed and proved to be good at semantic segmentation tasks. FCN combines convolution and pooling networks to receive image and output feature maps. Feature map uses deconvolution layer to obtain output image with the same size as input image [8].

The third target detection direction is end-to-end target detection, which uses a deep learning network for one-step detection. Its typical representatives are You Only Look Once (YOLO), SSD, etc. Redmon has proposed the YOLO algorithm, which is an end-to-end network architecture. The input of the network is image content, and the output is the information of boundary box and related class probability. Yolov3 [9], the third version of Yolo, connects the high-level network with the low-level network to obtain more meaningful semantic information from the fine-grained information in the high-level function and early function diagrams [10].

In the end-to-end single-stage target detection algorithm, SSD (single shot multibox detector) uses a layered detection method. SSD has good detection speed and accuracy, being one of the best target detection algorithms in industrial production. SSD algorithm takes into account the detection speed of the YOLO algorithm and the detection accuracy of the fast RCNN algorithm [11]. However, the effect of small target detection is general [12] since SSD uses Conv4_ 3 when a low-level feature is applied to small target detection. Besides, the number of low-level feature convolution layers is small, and there is the problem of insufficient feature extraction. In response to this problem, researchers have made many improvements to the SSD algorithm. For example, DSSD adds context information to the algorithm. The improved algorithm uses the deconvolution operation to a one-way fusion of high and low-level features, which improves the overall target detection effect and also improves the detection of small targets [13]. RSSD integrates the characteristics of different layers through rainbow concatenation. While increasing the feature map relationship between different layers, it also increases the number of feature maps in different layers, which improves the overall target detection effect and also improves the detection of small targets [14].

Although the above algorithm has achieved good detection results, there are still some shortcomings. The original SSD algorithm is not good for small target detection, which is mainly caused by three reasons. The first reason is that the training samples are unbalanced. The second reason is that the underlying feature representation ability is weak, and it is difficult to accurately classify small targets. The third reason is that the feature of a small target area is very small, which cannot be detected in a high-level feature detector. However, DSSD and RSSD adapt feature fusion, resulting in large network parameters and more calculation, which makes the detection speed very slow. In order to solve the problems in the above methods, this paper proposes a target detection algorithm based on clustering and cascaded SSD. The advantages of the algorithm are as follows:

(1) To solve the problem of unbalanced training samples, the proposed method designed an improved loss function based on Focal Loss and Truncated gradient (TG). It makes the training more focused on the samples with large loss values that are not easy to classify. The trained model can better detect the target.

(2) Aiming at the problem that the underlying feature representation ability is not enough and cannot be classified accurately, a small target enhancement detection module is designed to cascade with the SSD network. The module detects small targets in high-level features with sufficient position information and representation ability.

(3) To solve the problem that the feature of a small target area is too small to be detected in the high-level feature detector, the upsampling method of the bicubic interpolation algorithm is adopted. It samples the bottom feature of the small target area to the size of the original bottom feature so that the small target can be detected in the top feature detector.

(4) For real-time detection needs fast detection speed, this paper uses phased detection to detect the target, making the computation of the network not increase much. And the real-time performance is good.

(5) In order to solve the problem of low accuracy when selecting the default box, the k-means clustering algorithm is used to reconstruct the regional candidate box to improve the detection accuracy of the algorithm.

2. Related Work

2.1. Classic SSD Algorithm. SSD algorithm, proposed by Wei Liu, is one stage class algorithm. The algorithm is characterized by fast detection speed and good detection accuracy, which can meet the general industrial needs. It is one of the most widely used detection algorithms. The SSD algorithm combines the regression ideas in the YOLO algorithm and the Anchor mechanism in the Faster-RCNN algorithm. It uses multiscale regions at various locations in the entire image for regression, which not only maintains the fast characteristics of the YOLO algorithm but also ensures that the window prediction is as accurate as the Faster-RCNN algorithm. The core of the SSD algorithm is to use convolution kernels on feature maps of different scales to predict the category and coordinate offset of a series of Default Bounding Boxes.

The network adopts a layered detection mode. A low level detects a small target, and a high level detects a big target. Finally, the redundant boundary boxes are removed through NMS (nonmaximum suppression) to obtain the final detection result. Since the semantic information of a small target is not enough at the bottom level, and the location information at the high level is not enough as well, the SSD has a good effect on big target detection. However, the detection effect of small targets is relatively poor, and there are some deficiencies in the target detection task with more small targets.

The algorithm in this paper uses layered detection mode for reference. The detection is divided into two stages. In the first stage, the trained model is used to extract the high-level features of the image and detect the target, respectively, to obtain the small target area with an unknown specific category and the big target border with a known specific category. In the second stage, the small target enhancement detection module is cascaded with the SSD network. The high-level features corresponding to the small target area are extracted separately to detect the small target. This kind of detection adopts the phased form, which can improve the detection effect and has good real-time performance.

2.2. Focal Loss. Focal Loss is a new loss function for target detection proposed by Kaiming and RB. The loss function is mainly used to deal with the imbalance of training samples. By reducing the weight of easy-to-classify samples, Focal Loss makes the model pay more attention to hard-to-classify samples in training. In this way, the training effect is enhanced and the detection result is improved. Taking the second classification as an example, the specific formula is as follows:

$$\mathrm{FL}(u) = \begin{cases} -(1-u)^{\delta}\log(u), & y = 1, \\ -u^{\delta}\log(1-u), & \text{otherwise}, \end{cases} \tag{1}$$

where u is the prediction probability of the network to the sample. δ is the added suppression parameter, which is greater than 0 and is used to suppress the weight of easy-to-classify samples. y is the actual category.

For example, when $\delta = 2$, for normal samples, the prediction result of 0.9 is definitely a simple sample. So $(1-0.9)^{\delta}$ will be very small, and then the loss function value will become smaller. However, the sample with a prediction probability of 0.3 has a relatively large loss. The same is true for negative samples. The predicted result of 0.1 should be much smaller than the predicted sample loss of 0.7. Therefore, the training will focus on samples that are difficult to classify.

The SSD algorithm uses the cross entropy loss function as the classification loss function. Hard negative mining is adopted for the sample imbalance problem, ignoring the influence of more negative samples with low loss value on training. The emphasis of network training depends on the loss value gap between them. Compared with the cross entropy loss function, the loss value of difficult samples in Focal Loss is reduced, but the easy-to-classify samples are reduced more. Based on this, the algorithm in this paper integrates the Truncated Gradient idea on the basis of Focal Loss, which makes the training more focused on hard-to-classify samples and makes the training effect better.

3. Animation Characters' Target Detection Algorithm Based on Clustering and Cascaded SSD

3.1. Anime Character Data Set Construction. The training of intelligent recognition model of animation characters requires a large number of animation characters' images and labels of the characters in the images. Table 1 shows some classic animation characters and objects.

Each animation character needs at least 500 pictures of different angles and shapes for the training set. In addition, no less than 30% of the samples in the training set should be prepared as the test set. Pictures of animation characters used as training samples should be jpg, jpeg, bmp, and png. The resolution of the picture is not less than $640 * 480$. The training data source flow is shown in Figure 1.

The source data is mainly video and picture data, and the sources are mainly divided into the following categories:

(1) Relevant video and picture data acquired in the content management platform.

(2) Related video and picture data crawled and downloaded from the Internet.

(3) Operators upload relevant video and picture data.

(4) Data enhancement.

3.2. Target Detection Algorithm Based on Clustering and Cascaded SSD. In this paper, the algorithm adopts an improved classification loss function for the bottom detector during training, which makes the training more inclined to samples that are difficult to classify. In this way, a better model for small target position detection can be obtained. The forecast is divided into two stages. In the first stage, the features of each layer of the picture are extracted by the trained model and the targets are detected separately. In this stage, the small target border Pb_s with unknown category and the big target border B_b with known specific category can be obtained. In the second stage, the small target enhancement detection module is designed to cascade with the SSD network. In this stage, it is necessary to extract high-level features of Pb_s and then detect them. In this way, a small target detection result B_s is obtained. Then nonmaximum suppression (NMS) is applied to B_b and B_s, and the final detection result B_{fr} is obtained. Finally, the k-means clustering algorithm is used to reconstruct the regional candidate box to improve the detection accuracy of the algorithm. The algorithm is mainly divided into four parts, which are small target position detection module, big target detection module, small target enhancement detection module, and k-means clustering algorithm reconstruction region candidate box module. The specific network structure of is shown in Figure 2.

Table 1: List of animation characters and objects.

Content name	Character	Content name	Character	Content name	Character
Prince of Tennis	Ryoma dragon horse	Naruto	Lillock	Inuyasha	Inuyasha
The magic bucket quickly	Criminal kid	Naruto	Yu Zhibo Sasuke	Inuyasha	Platycodon Grandiflorum
Detective Conan	Maori Kogoro.	Dragon ball	Sun WuKong	Inuyasha	Kagome
Detective Conan	Conan Edogawa	Sea king	Robin	Inuyasha	Sesshomaru
Detective Conan	The Maori orchid	Sea king	Nami	Inuyasha	Qibao

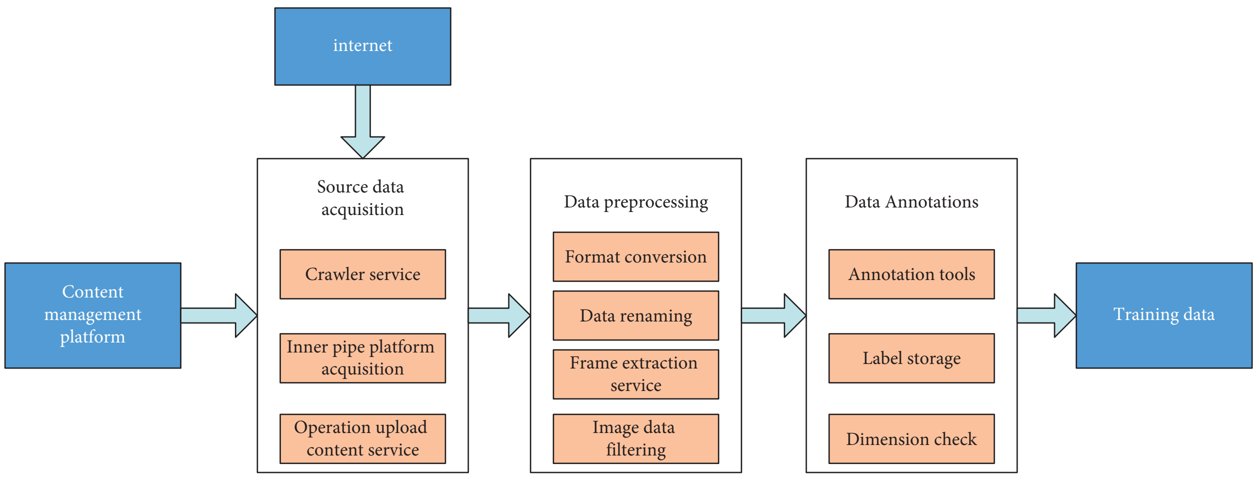

Figure 1: Training data generation flow.

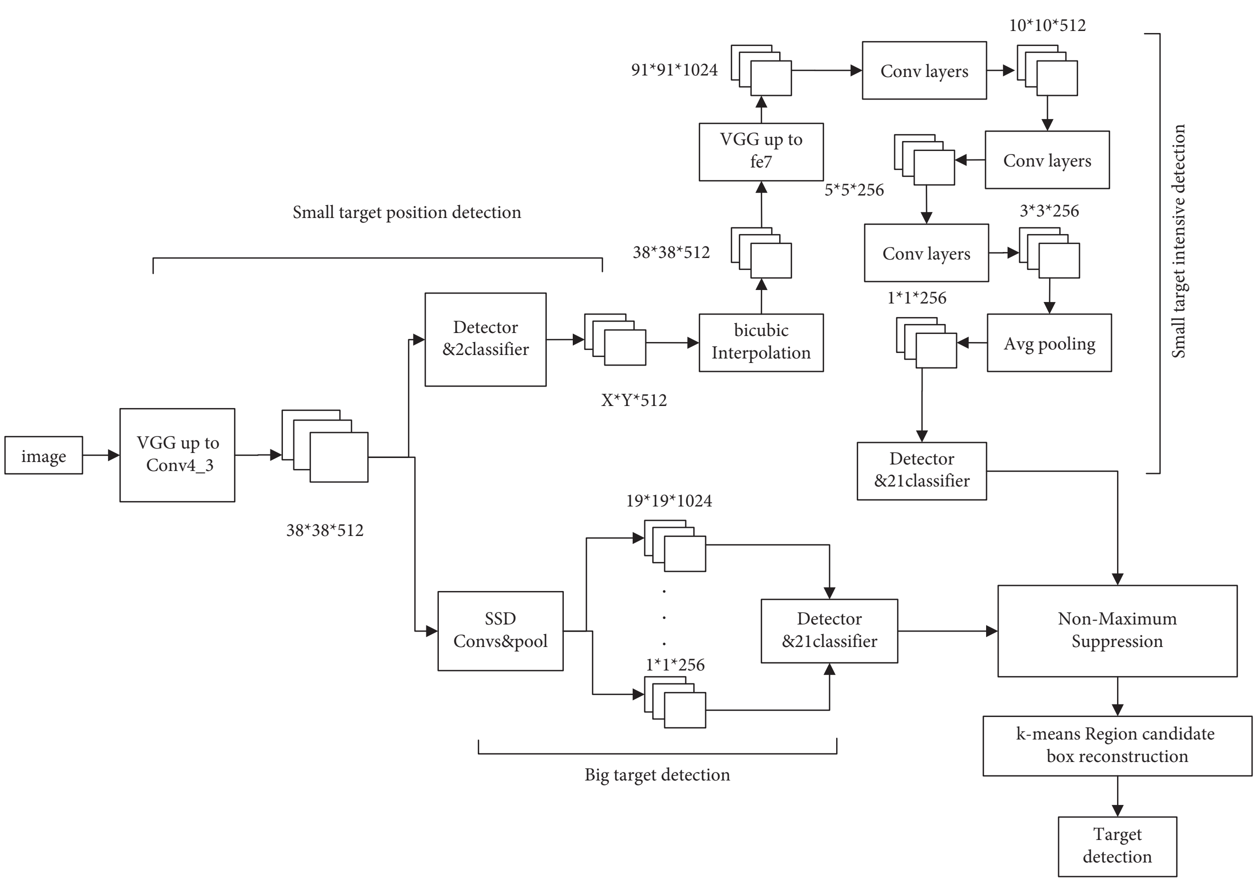

Figure 2: The specific network structure of this algorithm.

3.2.1. Small Target Position Detection Module. At the initial stage of the whole network, a small target position detection module is set up. VGG16 is used as the basic feature extraction network. The image is convolved several times after input to layer Conv4_3. The features of this layer are detected as the bottom feature map of the picture. At this time, the detector used is 2 classification and position regression, which only detects the position of the small target without detecting the specific category of the small target. The border of the small target position is obtained without knowing the specific category. The main tasks of this module are as follows:

(1) Improve the classification loss function Enhanced Focal Loss to replace the original cross entropy loss function and improve the network detection effect.

(2) Design a new small target detector to detect the small target position to improve the network detection effect and reduce the network computation.

In the training stage of the network, the imbalance between easy-to-classify samples and hard-to-classify samples will have a great influence on the training results. Easy-to-classify samples refer to the samples that are easy to be detected by the network. Generally, they refer to the samples with the prediction probability $p > 0.6$. The network prediction probability of the other sample is $p \leq 0.6$, which is difficult to predict accurately. Network learning this kind of fuzzy sample is more difficult, which is called a difficult sample. If samples are not balanced, the difficult samples have little influence on the weights generated in the network learning process. With the network training, difficult samples may be taken as background and then ignored.

The original SSD network adopts the cross entropy loss function as the classification loss function. It uses hard negative mining to select negative samples for the sample imbalance problem. The positive and negative sample ratio is 1 : 3. However, the negative samples are sorted according to the loss value of samples, and the negative samples with larger loss are selected as the negative samples for training. But in this way, negative samples with less loss are ignored. Although the loss of these negative samples is small, the number and the combined loss are large. Based on the ideas of Focal Loss and Truncated Gradient, this paper proposes an improved classification loss function, Enhanced Focal Loss, to replace the original cross entropy loss function. The advantage is that the influence of a large number of negative samples with a small loss value on the training is considered, and the network training is more obviously biased towards samples that are difficult to classify. The function is mainly divided into the following four parts:

(1) Based on the original cross entropy loss function, it describes the distance between the actual output u (the prediction probability of the network to the sample) and the expected output (the actual category of the sample). The smaller the value of cross entropy is, the smaller the loss value is, and the more accurate the network prediction is.

$$\mathrm{CE}(u, y) = -\log(u_n),$$
$$u_n = \begin{cases} u, & \text{if } y = 1, \\ 1 - u, & \text{otherwise,} \end{cases} \tag{2}$$

where u_n is the overall cross entropy loss function. u is the output probability. y is the actual category.

(2) The equilibrium coefficient β is added to optimize the imbalance of positive and negative samples.

$$\mathrm{CE}(u_n) = -\beta_n \log(u_n),$$
$$\beta_n = \begin{cases} \beta, & \text{if } y = 1, \\ 1 - \beta, & \text{otherwise,} \end{cases} \tag{3}$$

where β_n is the balance coefficient. β is a balance parameter to be set by yourself, which is used to control the weight of positive and negative samples. y is the actual category of the sample. u_n is the sample output probability.

(3) Focal Loss idea is incorporated and inhibition coefficient $(1 - u_n)^\delta$ is added to make network training slightly biased to hard-to-classify samples.

$$\mathrm{FL}(u_n) = \begin{cases} -\beta (1 - u_n)^\delta \log(u_n), & y = 1, \\ -(1 - \beta)(1 - u_n)^\delta \log(u_n), & \text{otherwise,} \end{cases} \tag{4}$$

where $(1 - u_n)^\delta$ is the suppression coefficient. δ is a suppression parameter to be set by yourself to suppress the weight of easy-to-classify samples. y is the actual category of the sample. u_n is the sample output probability.

(4) Incorporating Truncated Gradient and adding truncation coefficient $\varepsilon(u_n)$. In this way, the influence of a large number of negative samples with a small loss value on the training is considered, which makes the network training greatly biased towards the samples that are difficult to classify.

$$\varepsilon(u_n) = \begin{cases} (1 - u_n)^\delta, & u_n > 0.6, \\ \delta \cdot (1 - u_n), & \text{otherwise.} \end{cases} \tag{5}$$

Formula (5) defines the truncation coefficient as u_n calculating the loss value in sections for the cut-off point. δ is a parameter that needs to be set by yourself to suppress the weight of easy-to-classify samples. u_n is the prediction probability of the network to the sample.

$$\mathrm{EFL}(u_n) = \begin{cases} -\beta \cdot (1 - u_n)^\delta \cdot \log(u_n), & y = 1,\ u_n > 0.6, \\ -\beta \cdot \delta \cdot (1 - u_n) \cdot \log(u_n), & y = 1,\ \leq 0.6, \\ -(1 - \beta) \cdot (1 - u_n)^\delta \cdot \log(u_n), & y \neq 1,\ u_n > 0.6, \\ -(1 - \beta) \cdot \delta \cdot (1 - u_n) \cdot \log(u_n), & y \neq 1,\ u_n \leq 0.6. \end{cases} \tag{6}$$

Formula (6) is a global Enhanced Focal Loss function. β is a balance parameter to be set by yourself, which is used to control the weight of positive and negative samples.

The network can better extract the underlying features of the picture in the prediction stage after using the Enhanced Focal Loss as the loss function. It is input to the detector for detection after extracting the bottom feature map used to detect the small target. The original bottom feature detector is to directly carry out 21 classifications and position regression. Some areas containing targets can be detected in this way in that the location information of the low-level feature map is sufficient. However, due to insufficient semantic information, it is difficult to achieve accurate classification, which will eventually be abandoned. It leads to poor detection effects for small targets. Based on this, this paper designs a small target detector to carry out 2 classifications and position regression. The small target detector only detects the small target area but does not detect the specific category of this small target. Thus, a better detection effect of a small target position is obtained. At the same time, this method changes the classification from 21 to 2, which reduces the network parameters and computation. The specific steps of the detector are as follows:

(1) The original picture x is input into the detection network, and the underlying feature map $\mathrm{FM}_1 = H_4(H_3(\cdots H_1(x))$ for detecting small targets is extracted, where x represents the original drawing. $H_1(x)$ represents the features extracted after the first convolution.

(2) 2-classification detection and position regression are performed on the feature map FM_1, and $pb_s = (\mathrm{Detector}_1(\mathrm{FM}_1))$ is obtained, where FM_1 represents the bottom feature map for detecting small targets, and $\mathrm{Detector}_1$ is a small target detector.

These borders pb_s are subject to nonmaximum suppression, which can suppress some overlapping or incorrect borders. After that, we can get the small target position frame $Pb_s = \mathrm{NMS}(pb_s)$ without knowing the specific category, but with an accurate position, where pb_s represents all small target frames obtained by the small target detector. $\mathrm{NMS}(pb_s)$ means to perform nonmaximum suppression operation on pb_s.

3.2.2. Big Target Detection Module. Based on the idea of the original SSD, big target detection will use multiple detectors to detect on multiple high-level feature maps and get specific types of l big target detection frames. The location information and semantic information of the big target on the high-level feature map are sufficient, and the specific category and location can be directly detected. Therefore, all high-level detectors are 21-classification detection and position regression. The specific detection steps of this module are as follows.

(1) The original image x is input into the detection network, and the bottom feature image FM_1 used to detect small targets is extracted.

(2) The feature map FM_1 is convolved for three times, and the first high-level feature map for detecting big targets is obtained. $\mathrm{FM}_2 = H_7(H_6(H_5(\mathrm{FM}_1)))$, where FM_1 is the bottom feature map. $H_5(\mathrm{FM}_1)$ is the fifth convolution of FM_1.

(3) Similar to the operation in the second step, backward convolution and pooling are continued to obtain the following four feature graphs FM_3, FM_4, FM_5, and FM_6 for detecting big targets.

(4) For these high-level feature maps, their corresponding detectors are used to obtain multiple big target frames $b_b = \mathrm{Detector}_2(\mathrm{FM}_2) + \cdots + \mathrm{Detector}_6(\mathrm{FM}_6)$, where $\mathrm{Detector}_n(\mathrm{FM}_n)$ indicates that the detector corresponding to the feature map is used for detection.

(5) These frames b_b are subjected to nonmaximum suppression processing, and some overlapping or incorrect frames are suppressed so as to obtain a big target frame $B_b = \mathrm{NMS}(b_b)$ with a specific category and accurate position. In which b_b represents a plurality of big target frames obtained by the big target detector. $\mathrm{NMS}(b_b)$ represents nonmaximum suppression operation for b_b.

$$\begin{aligned} b_b &= \mathrm{Detector}_2(\mathrm{FM}_2) + \cdots + \mathrm{Detector}_6(\mathrm{FM}_6)B_b \\ &= \mathrm{NMS}(b_b)B_b = \mathrm{NMS}(b_b). \end{aligned} \tag{7}$$

3.2.3. Small Target Enhancement Detection Module. When small targets are detected on the underlying feature map, the underlying semantic information is not enough to detect specific categories. When detecting on the high-level feature map, the small target with a very small size does not have enough position information among the features with enough high-level semantic information, making it impossible to detect small targets. Based on this, a small target enhancement detection module and SSD cascade are designed to detect the specific category and accurate location of the small target frame B_s.

The module is divided into two parts. The first part is to transform small target detection into big target detection. The bottom feature of the small target location is sampled to the size of FM_1 of the bottom feature of the original image, so the small target detection problem is transformed into a big target detection problem. The second part is to extract high-level features and detect them and learn the advantages of the original SSD network in detecting big targets. The subsequent stage of this module is to extract high-level features from the upsampled feature map and then detect it. At this time, the network layer similar to the original SSD network is used to extract high-level features, and the last high-level features are used for target detection. The main steps of this module are as follows:

(1) The small target position frame Pb_s obtained from the small target position detection module is input. Based on the principle of translation invariance of CNN (Convolutional Neural Network), the bottom

feature FM_s of the position corresponding to pbs is obtained from the bottom feature map FM_1.

(2) These small target bottom features FM_s are upsampled by a bicubic interpolation algorithm, and the small target bottom feature map BFM_s with the same size as the original bottom feature map FM_1 is obtained.

$$BFM_s = FM_s \uparrow s, \tag{8}$$

where $\uparrow s$ represents the upsampling operator.

(3) Then, the low-level feature map BFM_s of small targets is convolved and pooled for many times, its high-level feature UFM_s is extracted. The high-level feature UFM_s is classified by 21 and its position is detected, so as to obtain a plurality of small target frames b_s.

$$\begin{aligned} UFM_s &= P\left(H_{10}\left(H_9\left(\cdots H_5\left(UFM_s\right)\right)\right)\right),\\ b_s &= \text{Detector}_6\left(UFM_s\right), \end{aligned} \tag{9}$$

where $P(\cdot)$ represents the average pooling operation. $H(\cdot)$ represents the convolution operation. Detector_6 is the detector.

(4) Finally, these frames b_s are suppressed by non-maxima. Some overlapping or incorrect frames are suppressed, so as to obtain the big target frames B_s with specific categories and accurate positions.

$$B_s = NMS\left(b_s\right), \tag{10}$$

where b_s represents a plurality of small target frames detected from the high-level features of small targets. $NMS(b_s)$ represents nonmaximum suppression operation for b_s.

3.2.4. Reconstruction of Regional Candidate Box Based on k-Means Clustering. The performance of a deep learning target detection algorithm largely depends on the quality of feature learning. Feature learning is driven by training data, which in the SSD target detection task is the area candidate box. When the intersection union ratio (IOU) of the region candidate frame and the real frame is greater than the threshold, it is marked as a positive sample. On the contrary, it is marked as a negative sample. The formula of candidate box parameters is as follows:

$$F_z = F_{\min} + \frac{F_{\max} - F_{\min}}{w-1}(z-1), \tag{11}$$

where the value range of z is $[1, w]$. w is the characteristic layer number. $F_{\min}$ and $F_{\max}$ represents the minimum and maximum characteristic layer scale, respectively, and the corresponding default values are generally 0.2 and 0.9. The middle characteristic layer is evenly distributed in scale. As shown in Figure 3, the region candidate algorithm based on clustering can generate four candidate boxes, including two squares (red dotted lines) and two rectangles (black dotted lines).

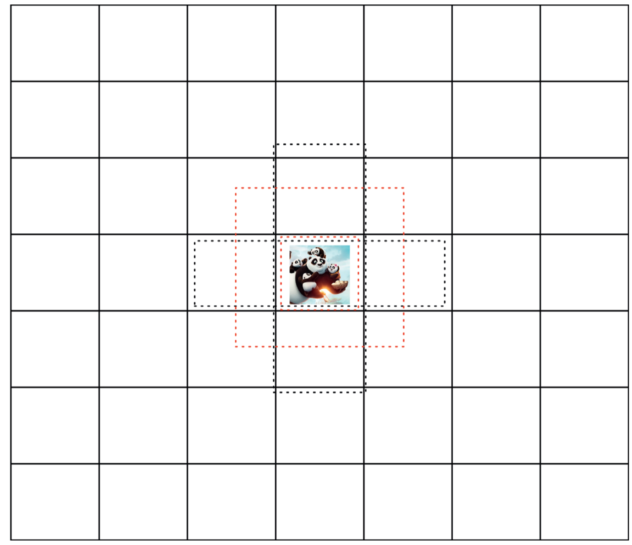

Figure 3: Schematic diagram of candidate box.

In the past tests, most of them set the size and proportion of candidate boxes according to experience. During the training process, the network will adjust the candidate box. If the appropriate size and proportion of candidate boxes can be found in advance before training, better prediction results will be obtained. In this paper, the k-means clustering algorithm is used to predict the size and proportion of candidate frames. The distance measurement formula used in this paper is as follows:

$$\begin{aligned} d(\text{box}, \text{center}) &= 1 - IOU(\text{box}, \text{center}),\\ d(\text{box}, \text{center}) &= 1 - IOU\left[\left(x_q, y_q, w_q, h_q\right), \left(x_p, y_p, W_p, H_p\right)\right], \end{aligned} \tag{12}$$

where center is the clustering center. *box* is the callout box. When calculating, the value of IOU can only be calculated if the center point of each annotation box coincides with the center point of the cluster center. (x_q, y_q) is the center point of the callout box. (w_q, h_q) is the width and height of the callout box. (W_p, H_p) is the width and height of the cluster center. $q \in \{1, 2, \ldots\ldots N\}$, $p \in \{1, 2, \ldots\ldots K\}$. N is the number of annotation boxes. K is the number of clusters. According to the above formula, the annotation box is assigned to the nearest cluster center. After all annotation boxes are allocated, the cluster center points are recalculated for each set.

$$\begin{aligned} W_i' &= \frac{1}{N_i} \sum_{w_i},\\ H_i' &= \frac{1}{N_i} \sum h_i. \end{aligned} \tag{13}$$

Find the average width and height of all annotation boxes in the set, and then repeat the above steps until the cluster center changes little. In the experiment, $K = \{1, 2, 3, 4, 5, 6, 7, 8, 9, 10\}$ is set for the experiment, and the marked boxes were clustered separately. The experimental results show that when $K < 6$, the average intersection ratio increases greatly. When $K > 6$, it tends to be flat basically. Combined with the algorithm, $K = 6$ is selected. When $k = 6$, the aspect ratio (AR) of candidate frames is [0.59, 0.89, 1.18, 1.84, 1.9, 2.84]. Reconstruct the candidate box with this AR.

Cascade SSD algorithm uses six feature maps to generate candidate boxes with different sizes. If the size of the feature graph is $M * N$, the corresponding feature graph is divided into $M * N$ grids. Then H candidate boxes are generated with the center point of each grid as the center. The number of candidate boxes generated by each feature graph is $M * N * H$. In this algorithm, the AR of six feature maps is set to {1, 2, 3}. The number of H is {6, 6, 6, 6, 6, 6}. Table 2 shows the setting of the candidate box of the algorithm area.

When the algorithm is used for target detection in this paper, the final detection result is related to the prediction of the regional candidate box. However, the regression of the prediction frame of the regional candidate has a great relationship with the samples in a certain range around it. Therefore, an appropriate threshold value should be selected when reconstructing the region candidate box. Experiments were carried out under different thresholds to select a suitable threshold. The experimental results show that the optimal threshold is 0.45.

4. Experiment and Analysis

4.1. Experimental Environment and Data Set. The operating system of the experimental software environment is Ubuntu14.04, using the TensorFlow deep learning framework. The training environment settings are shown in Table 3.

The animation character material pictures used for detection can be obtained from the screenshots in the video library, with abundant sources and a large amount of data. 80% of the training set and 20% of the test set are used to divide the training set and testing set. The animation character material pictures are obtained by searching the cosplay pictures of specific characters from the Internet. The amount of data is meager. Therefore, training and test sets are divided into 85% training set and 15% test set during training.

4.2. Evaluation Criteria. In this paper, mAP (mean average precision) is adopted to evaluate the detection performance of the algorithm. The detection speed is used to evaluate the detection speed of the algorithm, and its unit is fps. Detection speed refers to the number of pictures that can be processed per second. Detection speed comparison needs to be done on the same hardware. mAP refers to the accuracy of all kinds of objects on all graphs, and its calculation formula is as follows:

$$\mathrm{mAP} = \frac{\sum \mathrm{Precision}_{\mathrm{Aver}}}{N}, \tag{14}$$

where $\mathrm{Precision}_{\mathrm{Aver}} = \sum \mathrm{Precision}_C / N_{\mathrm{Images}}$ represents the average precision sum of all categories. N means all categories.

4.3. Experimental Analysis. In order to verify the detection effect of this algorithm, experiments will be carried out from the following aspects. To verify that the loss function Enhanced Focal Loss designed in this paper is more effective than the cross entropy loss function and Focal Loss in this algorithm, these three loss functions are applied to the training of this algorithm, respectively. The selection of training samples, function composition, and comparison of detection accuracy of the three functions are shown in Table 4.

As shown in Table 4, the original cross entropy loss function selects positive samples and negative samples with large loss values as training samples. In this way, a large number of negative samples with a small loss value are lost, which is obviously unfavorable to network training. Finally, the detection accuracy of this algorithm is 78.73%. Focal Loss selects all the samples as training samples, including a large number of negative samples with small loss values, and added suppression coefficient to control the loss of hard-to-classify samples and easy-to-classify samples. This makes the loss of easy-to-classify samples greatly reduced, and the loss of difficult-to-classify samples slightly reduced. On the whole, the weight of hard-to-classify samples increased slightly, which made the network training biased towards hard-to-classify samples. Finally, the detection accuracy of Focal Loss in this algorithm is 78.8%. The Enhanced Focal Loss used in this paper is integrated with Truncated Gradient thought, which makes the loss of easily classified samples decrease. The loss of hard-to-classify samples increases and the overall weight of hard-to-classify samples increases significantly, making network training more obviously biased towards hard-to-classify samples. Finally, the detection accuracy of this algorithm is 78.94%.

Some existing SSD improved algorithms are trained and predicted on relevant data sets, and the training and prediction results are compared with the target detection algorithm in this paper. The comparison results are shown in Table 5.

Analysis of Table 5 shows that compared with the improved SSD algorithm, the detection accuracy of the improved algorithm proposed in this paper is obviously improved. The real-time detection performance of the algorithm is well maintained. Especially, the detection speed of this algorithm is nearly three times faster than DSSD.

Some existing target detection algorithms are trained and predicted on the experimental design data set. The training and prediction results are compared with the target detection algorithm in this paper. The comparison results are shown in Figure 4.

As can be seen from Figure 4, the accuracy of this paper in animation character detection is larger than other algorithms. The predicted mAP of the proposed algorithm is 79.7%, which is 15.7% higher than that of YOLO. That's a 2.1% increase over DSSD. It can be verified that in the object detection of cartoon characters, the clustering and cascaded SSD algorithm proposed in this paper not only has a faster detection speed but also significantly improves the detection quality.

Table 2: Setting of candidate box of algorithm area in this paper.

Characteristic diagram	Conv4_3	Fc7	Conv6_2	Conv7_2	Conv8_2	Conv9_2
M∗N	38 ∗ 38	19 ∗ 19	10 ∗ 10	5 ∗ 5	3 ∗ 3	1 ∗ 1
Quantity	8664	2166	600	150	54	6
Total			8664 + 2166 + 600 + 150 + 54 + 6 = 11640			

Table 3: Configuration of training environment.

Serial number	Package	Model
1	CPU	Intel(R) Xeon(R) CPU E5-2620 v3 2.4 GHz 12 core
2	Internal storage	128 GB
3	Hard disc	2 ∗ 200 GB SSD + 2 ∗ 1.2 TB SAS
4	Display card	NVIDIA (R)GTX (R)1080TI
5	System kernel	Ubuntu 18.04.5 LTS (GNU/Linux 4.15.0–135-generic x86_64)

Table 4: Comparison of loss functions.

Loss function	Positive samples	Negative samples (big loss)	Negative samples (small loss)	Inhibition coefficient	Truncated gradient	mAP (%)
Cross entropy	✓	✓	✗	✗	✗	78.73
Focal loss	✓	✓	✓	✓	✗	78.8
Enhanced focal loss	✓	✓	✓	✓	✓	78.94

Table 5: Comparison between MPa and detection speed of SSD-related improved algorithms.

Target detection algorithm	Training MAP (%)	Predication MAP (%)	Detection speed (fps)
Method in [15]	76.1	74.8	54
Method in [16, 17]	74.7	73.9	58
DSSD	74.1	72.6	19
RSSD	76.3	75.1	58
FSSD	74.3	73.7	56
Our method	78.4	76.5	59

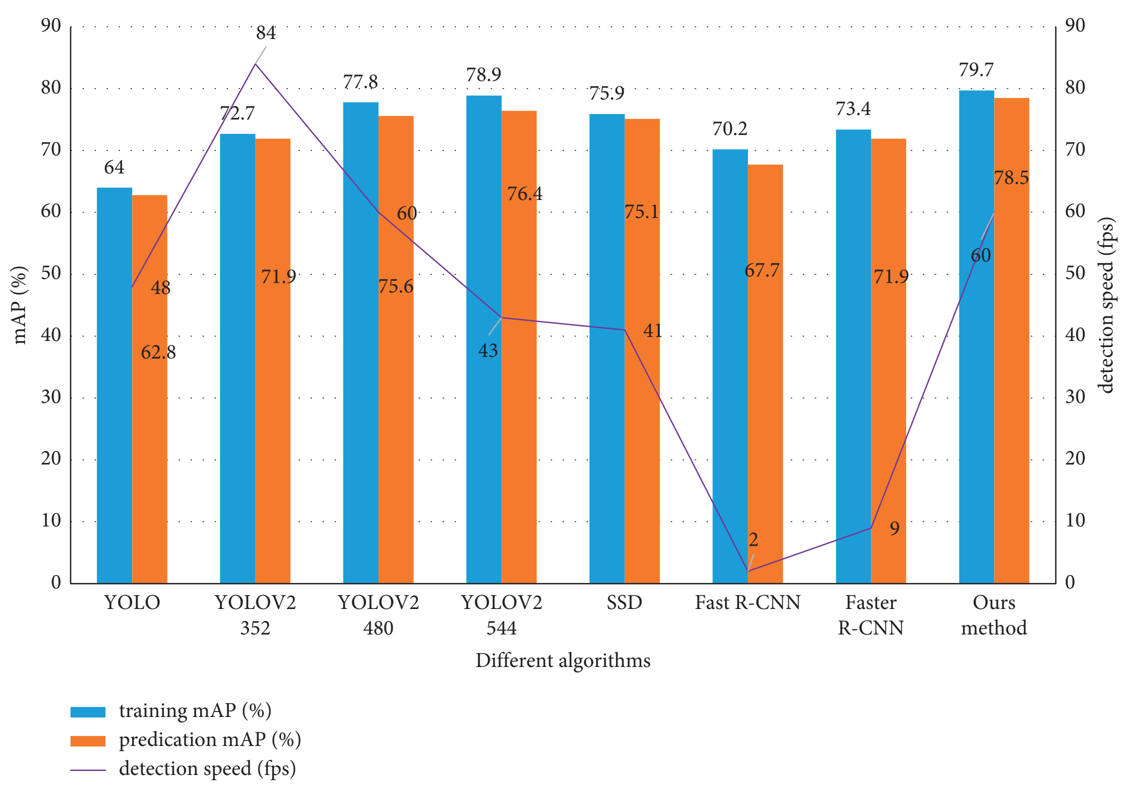

Figure 4: Comparison of target detection algorithms MPa and detection speed.

5. Conclusion

Aiming at the problem of animation character detection, this paper proposes a novel method based on clustering and cascaded SSD. A new loss function is designed to solve the problem of unbalanced training samples for small targets. The algorithm extracts the features of each layer of the image through the trained model and detects the target, respectively. In this way, the small target border of an unknown specific category and the big target border of the known specific category can be obtained. Then, a small target enhancement detection module, which is cascaded with an SSD network, is designed by the algorithm. Additionally, the high-level features corresponding to the small target area can be extracted separately to detect small targets. It can be seen that this algorithm is superior to other existing algorithms via the final experimental comparison. The future work is to improve the upsampling method and enhance the positioning ability of small targets.

Abbreviations

abrIP: Intellectual property
SSD: Single shot multibox detector.

Data Availability

The labeled dataset used to support the findings of this study is available from the corresponding author upon request.

Conflicts of Interest

The author declares no competing interest.

Acknowledgments

This paper was supported byXijing University Research Fund "one belt one road directive" under the background, Innovative design of cartoon image of door God in Shanxi Province of Fengxiang Province" (No. XJ160207).

References

[1] M. Pellitteri, "The European experience with Japanese animation, and what it can reveal about the transnational appeal of anime," *Asian Journal of Communication*, vol. 31, no. 1, pp. 21–42, 2021.
[2] K. Liu and X. Q. Sun, "Research on the development and innovation of animation industry in jilin Province in the Internet big data era," in *Proceedings of the IOP Conference Series: Earth and Environmental Science*, vol. 619, no. 1, Article ID 012073, Changchun, China, August 2020.
[3] J. H. Yan, B. C. Lee, and T. Yun, "A study on the elements of Chinese animation IP (intellectual property) development based on the pan-entertainment industry," *International Journal of Internet, Broadcasting and Communication*, vol. 13, no. 1, pp. 168–179, 2021.
[4] J. Zhang, X. Hu, Z. Ning et al., "Energy-latency tradeoff for energy-aware offloading in mobile edge computing networks," *IEEE Internet of Things Journal*, vol. 5, no. 4, pp. 2633–2645, 2018.
[5] P. Sun, R. Zhang, Y. Jiang et al., "Sparse r-cnn: end-to-end object detection with learnable proposals," in *Proceedings of the IEEE/CVF Conference on Computer Vision and Pattern Recognition*, June 2021, Article ID 14454.
[6] Z. Y. Chen and I. Y. Liao, "Improved fast r-cnn with fusion of optical and 3d data for robust palm tree detection in high resolution uav images," *International Journal of Machine Learning and Computing*, vol. 10, no. 1, pp. 122–127, 2020.
[7] Z. Ning, X. Hu, Z. Chen et al., "Obaidat, A cooperative quality-aware service access system for social Internet of vehicles," *IEEE Internet of Things Journal*, vol. 5, no. 4, pp. 2506–2517, 2017.
[8] Z. Shao, W. Zhou, X. Deng, M. Zhang, and Q. Cheng, "Multilabel remote sensing image retrieval based on fully convolutional network," *IEEE Journal of Selected Topics in Applied Earth Observations and Remote Sensing*, vol. 13, pp. 318–328, 2020.
[9] L. Zhao and S. Li, "Object detection algorithm based on improved YOLOv3," vol. 9, no. 3, pp. 537–548, 2020.
[10] L. Fu, Y. Feng, J. Wu et al., "Fast and accurate detection of kiwifruit in orchard using improved YOLOv3-tiny model," *Precision Agriculture*, vol. 22, no. 3, pp. 754–776, 2021.
[11] C. Chakraborttii and H. Litz, "Improving the accuracy, adaptability, and interpretability of SSD failure prediction models," in *Proceedings of the 11th ACM Symposium on Cloud Computing*, pp. 120–133, ACM, Times Square, NY, USA, October 2020.
[12] B. Hu, G.-P. Gao, LeLe He, X.-D. Cong, and J.-N. Zhao, "Bending and on-arm effects on a wearable antenna for 2.45 GHz body area network," *IEEE Antennas and Wireless Propagation Letters*, vol. 15, pp. 378–381, 2016.
[13] Y. Yang, J. Yu, and T. Kurihara, "Immature Yuzu Citrus Detection Based on DSSD Network with Image Tiling approach," in *Proceedings of the 2021 60th Annual Conference of the Society of Instrument and Control Engineers of Japan (SICE)*, pp. 1128–1133, IEEE, Tokyo, Japan, September 2021.
[14] S. Wang, R. Inkol, and B. R. Jackson, "Relationship between the maximum likelihood emitter location estimators based on received signal strength (RSS) and received signal strength difference (RSSD)," in *Proceedings of the 2012 26th Biennial Symposium on Communications (QBSC)*, pp. 64–69, IEEE, Kingston, ON, Canada, May 2012.
[15] J. W. Wen, Y. W. Zhan, C. H. Li, and J. Lu, "Design of atrous filter to strengthen small object detection capability of SSD," *Application Research of Computers*, vol. 36, no. 3, pp. 861–865, 2019.
[16] X. Hu, J. Cheng, M. Zhou et al., "Emotion-Aware cognitive system in multi-channel cognitive radio ad hoc networks," *IEEE Communications Magazine*, vol. 56, no. 4, pp. 180–187, 2018.
[17] W. Wei, B. Zhou, D. Polap, and M. Wozniak, "A regional adaptive variational PDE model for computed tomography image reconstruction," *Pattern Recognition*, vol. 92, pp. 64–81, 2019.

Hindawi
Scientific Programming
Volume 2022, Article ID 4456150, 16 pages
https://doi.org/10.1155/2022/4456150

Research Article

Supply Chain Governance of Agricultural Products under Big Data Platform Based on Blockchain Technology

Wei Guo [1] and Kai Yao [2]

[1] *Department of Business Administration, Anhui Business College, Wuhu 241002, Anhui, China*
[2] *School of Management, Fudan University, Shanghai 200433, China*

Correspondence should be addressed to Wei Guo; guowei@abc.edu.cn

Received 25 October 2021; Revised 15 November 2021; Accepted 23 November 2021; Published 6 January 2022

Academic Editor: Le Sun

The present work serves to improve the stable cooperation relationship among subjects of supply chain such as enterprises, farmers, intermediary organizations, and retailers and enhance the governance and optimization of agricultural product supply chain, thus strengthening the competitiveness of China's agricultural industry. The supply chain governance of agricultural products is taken as the research object. Initially, the stabilities of two supply chain organization modes, "company and farmer" and "company, intermediary organization and farmer," are analyzed by static game analysis. Then, based on the above analysis and the characteristics of blockchain institutional technology, a detailed analyzation is made on the mechanism of supply chain of agricultural products governance based on blockchain technology. Finally, the functional framework of agricultural supply chain governance is designed based on the basic framework of blockchain technology, and analyzation is made on the trust mechanism and contract mechanism of agricultural supply chain governance based on blockchain technology. The research results show that problems such as information and cognitive constraints in agricultural supply chain governance cannot be completely solved only through the evolution of blockchain organizational structure and the supply of governance mechanism, and speculative behavior will still appear. Optimizing the governance of supply chain of agricultural products based on blockchain technology can realize the transformation of its governance scenario. Meanwhile, the blockchain technologies such as deintermediation, demistrust, and intelligent contract play an important role in the process of agricultural supply chain governance, which can make it change in many aspects such as organization mode, application operation, and governance mechanism. The rapid development of new generation information technologies such as blockchain, the Internet of Things, and computer technology makes it possible to comprehensively digitize economic activities such as production and transaction in the supply chain of agricultural products. The present work combines the technical logic of blockchain digital governance with the institutional logic of agricultural product supply chain governance and tries to solve the instability problems caused by imperfect organization, lack of trust, and incomplete contract in agricultural product supply chain governance with the characteristics of blockchain such as deintermediation, demistrust, and intelligent contract.

1. Introduction

Under the rapid development of free market economy, in order to realize the modernization of China's agricultural field, society must keep up with the pace of reform and opening up. With the constant industrialization of agriculture, the agricultural economic form has changed to some extent. New forms of agricultural products supply chain emerge such as strategic alliance and cooperative production. Under the organization modes of "company and farmer" and "company, intermediary organization and farmer," the supply chain of agricultural products is constantly developing and growing [1, 2]. Establishing a stable cooperative relationship among the participants in the agricultural supply chain and strengthening the governance of the agricultural supply chain can effectively improve the competitive advantage of China's agriculture. In recent years, a variety of agricultural products supply chain models, such as "farmers and companies," "family farms and companies," and "farmers, supermarkets, and rural cooperatives" have emerged constantly, and the participants are also growing [3]. On the whole, through the governance and optimization of supply chain of agricultural products, the cooperative relationship in supply chain of agricultural products has become relatively stable. Its organizational structure has gradually changed from loose to tight. However, there are still some problems to be solved in China's agricultural supply chain for a long time, such as the difficulty in ensuring the quality of agricultural products, the high default rate when farmers and companies cooperate, and the difficulty in reaching long-term cooperative relations [4–6].

By consulting relevant references, results turn out that many researchers attribute the change of the relationship of supply chain of agricultural products to the change of system. Based on the relevant theories under the new system, study and discussion are made on the formation and evolution of supply chain of agricultural products. On the governance of agricultural supply chain, some relevant scholars have compared the governance mechanism and transaction relationship in different agricultural products circulation channels through actual case analysis. The research results show that the long-term transaction relationship of "order industry" has the highest performance level, which verifies that trust relationship is beneficial to improving industry performance [7]. In the follow-up development process, some researchers also used case analysis and model empirical method to analyze the causal relationship of the relationship governance elements between vegetable growers and companies. The results show that there are the two following causal chains during the transaction between vegetable growers and companies. "Farmers' perception of enterprise behavior determines whether farmers trust the enterprise, which in turn determines the cooperative relationship between farmers and companies." "Farmers' trust in companies will affect the degree of cooperation between farmers and companies, which in turn determines the certainty of farmers' transactions" [8].

At present, there are many researches on the governance optimization of supply chain of agricultural products globally, but most of them are focused on how to alleviate the effectiveness of opportunistic risks through the optimization of governance models and mechanisms, while there are relatively few researches on the governance optimization of supply chain of agricultural products based on blockchain embedding. Therefore, based on blockchain digital governance technology, optimization is made on the governance of agricultural supply chain, and solutions are given for the unstable problems caused by low trust between companies and farmers and imperfect organization and management system based on the characteristics of blockchain, such as deintermediation, demistrust, and intelligent contract.

2. Literature Review

The research on the organization and governance of agricultural product supply chain mainly evolved from the research on agricultural industrial organization. Li and Zhang (2021) [9] concluded that vertical integration of agricultural supply chains had a positive impact on the safety of agricultural products through the analysis of economic models. With the improvement of vertical integration of agricultural products supply chain, wholesalers and suppliers have improved the security of agricultural products, reduced the circulation cost of agricultural products, and decreased the sales price of agricultural products. To promote the close integration of agricultural product supply chain, Zhou and Metawea (2021) [10] proposed a computer simulation model of agricultural product supply chain based on multiagent system. Through a series of simulation experiments, detailed discussion was made on the evolution of the organizational structure of agricultural supply chain under different government regulations and its impact on the quality and safety of agricultural products. The simulation results revealed that the more long-term contracts between farmers and retailers, the more conducive to the improvement of the quality and safety of agricultural products, and the scholars put forward corresponding countermeasures and suggestions. Qiu (2017) [11] studied retailers' pricing and ordering strategies based on real-time value loss information of agricultural products. Considering the influence of technology application on the circulation of fresh agricultural products, the scholars constructed the profit model of two stages of fresh agricultural products supply chain and analyzed three key parameters. The results indicated that the upstream and downstream parts of the supply chain had the consistent investment interval of technology label cost; under certain conditions, upstream suppliers bore the cost of technical labels, and wholesale and retail prices were determined by incremental delivery.

By comparing the relevant literature, it can be found that, in terms of theoretical research, Chinese researchers still focus on the theory of new institutional economics. The research on transaction governance and relationship governance based on transaction cost economics has just started. The research on agricultural product supply chain from the perspective of transaction cost economics in foreign countries has been relatively mature, which is also more in-depth and detailed, and is gradually expanded to the combination of various theories.

3. Methods

3.1. Blockchain Data Structure and Functional Framework of the Blockchain System

3.1.1. Blockchain Data Structure. Figure 1 signifies the data structure of the blockchain system.

Figure 1 illustrates that the blockchain is composed of a block header and a block body, and the block header also includes a timestamp, a random number, a target hash, and a Merkle root. The Merkle root is generated by the data structure of Merkle tree and counted in the head of the block, of which the value is unique. The blocks are connected in time sequence to form a blockchain. Each blockchain is connected by the address information of the previous block in the block header, and each transaction can be recorded in

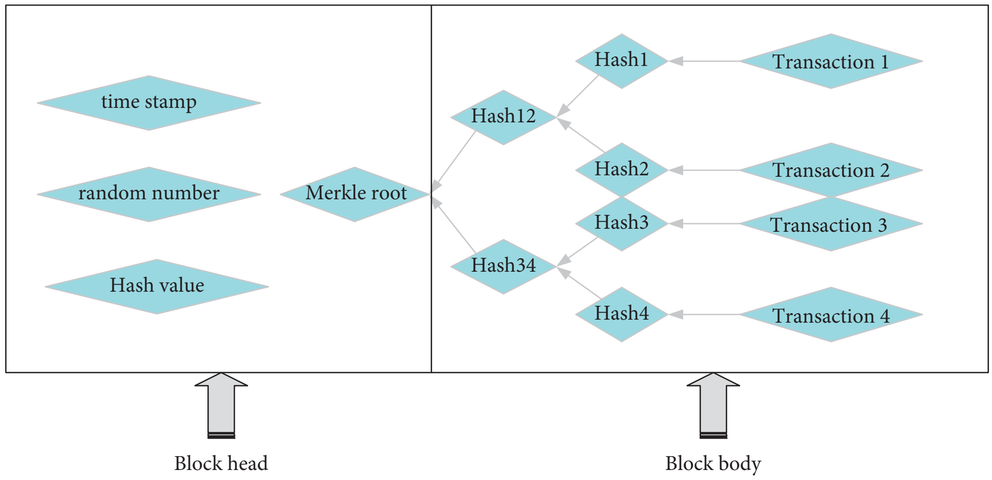

FIGURE 1: Blockchain data structure.

the block body by the Merkle tree structure key, finally forming a data chain with comprehensive transaction records [12, 13].

3.1.2. Overall Functional Architecture of the Blockchain System. With the continuous development of digital technology, the data structure of blockchain is constantly being updated. From the earliest distributed accounting system to Ethereum to the current alliance chain, it can be found that blockchain is constantly being merged with digital technology. Although there are some differences in specific applications among different blockchains, their overall architectures are basically the same [14]. Figure 2 shows the overall functional framework of the system.

3.2. Stability Analysis of Supply Chain of Agricultural Products under Different Organizational Modes

3.2.1. Stability Game Analysis under the Organization Mode of "Company and Farmer". Under this mode, the company signs long-term contracts with farmers. Based on the "company and farmers" mode, it can not only solve the supply problem of raw materials for agricultural products but also increase the sales volume of farmers' agricultural products. However, there are some problems that need to be solved urgently, such as the low trust between companies and farmers, which leads to frequent defaults between both parties. In this mode, the game relationship between the two parties is very obvious, and the trust relationship between the two parties will directly affect the development of the company and farmers [15]. This problem will be analyzed in detail below. Before the concrete analysis, it is assumed that when farmers and companies conduct transactions, both parties of the transaction are rational transactions, the purpose of which is to enable them to obtain greater benefits. Before trading, the quantity of agricultural products traded by both parties has been stated in the contract, which is set as V, and the prices of agricultural products will fluctuate accordingly different market conditions. The prices of agricultural products in good and better market conditions are set as P_g and P_b, respectively. The price in the purchase of agricultural products of farmers is set as P_f, the production cost of farmers in the production of agricultural products is expressed as C_1, and the logistics cost of companies is represented by C_2. Farmers will hand over the quantity V of agricultural products to companies for processing and sales, and finally the money profits obtained by companies are referred to by M, where $P_g > P_f > P_b$. The probability of default by both parties and the amount of compensation to be paid after default are set as R and L, respectively [16]. As the default of an enterprise in the transaction process will have a certain impact on the reputation of the enterprise, the loss brought by the subsequent development of the enterprise is set as D. When the market develops well, the benefits of both parties of the transaction are as shown in Figure 3 [17].

As Figure 3 displays, when the overall development of the market is good, companies will make greater profits by choosing to abide by the contract, while farmers will make their choices by comparing the benefits they have obtained under the conditions of abiding by the contract and breaching the contract. The situation arises as

$$VP_f - C_1 > VP_g - C_1 - Lr. \tag{1}$$

Namely,

$$Lr > V\left(P_g - P_f\right). \tag{2}$$

In equations (1) and (2), V expresses the amount of agricultural products; P_f represents the order price of agricultural products; C_1 denotes the production cost of farmers; P_g refers to the price of agricultural products when there is more benefit in the market; L stands for the compensatory payment for breaching of contract; r accords with the rate that compensatory payment will be paid.

Then, the farmers' profit from breach of contract is greater than that from keeping the contract. Hence, farmers will choose to default.

When the overall development of the market is poor, the benefits of both parties to the transaction are as shown in Figure 4.

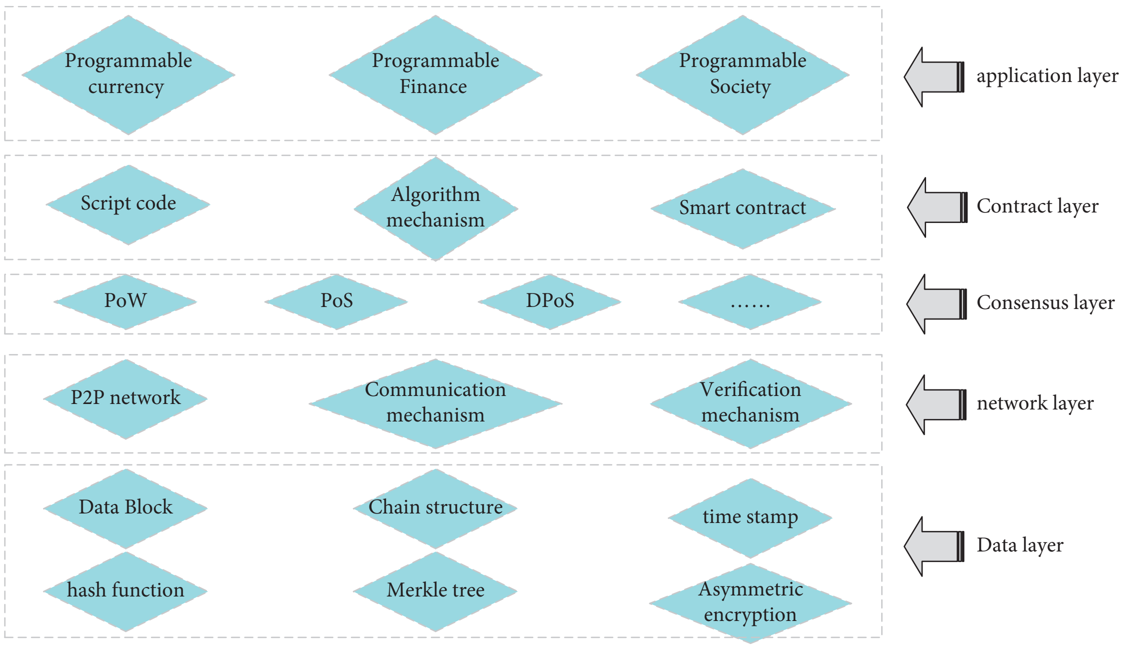

FIGURE 2: Overall functional framework of the blockchain system.

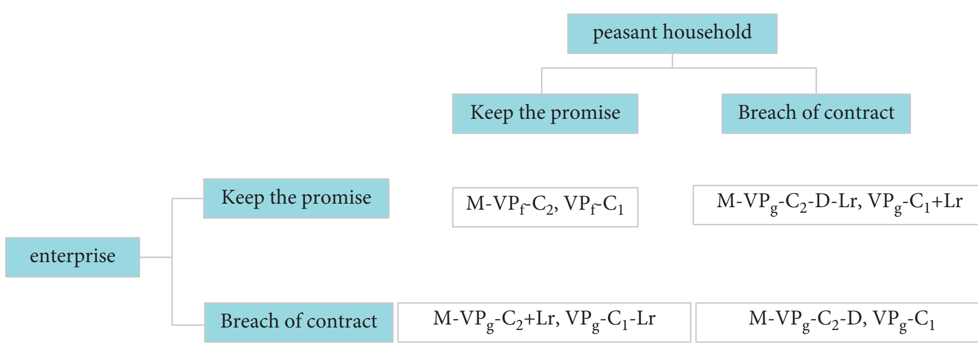

FIGURE 3: Benefits of both parties to the transaction when the market develops well.

As Figure 5 signifies, in the case of poor overall market development, farmers will make greater profits by choosing to keep the contract, while companies will make their choice by comparing the benefits obtained by keeping the contract and breaching the contract. The situation arises as follows:

$$M - VP_f - C_2 < M - VP_b - C_2 + Lr. \tag{3}$$

Namely,

$$V\left(P_f - P_b\right) > D + Lr. \tag{4}$$

In equations (3) and (4), M represents the gain of processing and selling V agricultural products; C_2 expresses the logistic and production cost of enterprises; P_f refers to the order price of agricultural products; P_b refers to the price of agricultural products when there is less benefit in the market; L stands for the compensatory payment for breach of contract; r accords with the rate that compensatory payment will be paid; D expresses the future discount losses, which will be led by the reputational losses suffered by enterprises, if they breach the contract.

Then, if the profit obtained by the enterprise's breach of contract is greater than the profit obtained by keeping the contract, the enterprise will choose to default.

The above analysis illustrates that the following aspects will influence the cooperative relationship between companies and farmers: first, the price fluctuation of agricultural products, and second, the cost of default, such as the probability of compensation and the amount of loss after default. The price fluctuation of agricultural products is mainly affected by the external environment, namely, market environment. From that perspective of default cost, because the number of farmers is large but the scale of their property is small, once the amount to be paid for breach of contract exceeds the scope of farmers' acceptance, farmers will think passively before participating in the supply chain organization, so the default amount should not be too large. Additionally, the value of compensation probability r is mainly affected by transaction costs such as negotiation ability and litigation cost of both parties. However, because the price of agricultural products is relatively low, the value of agricultural products is often lower than the transaction

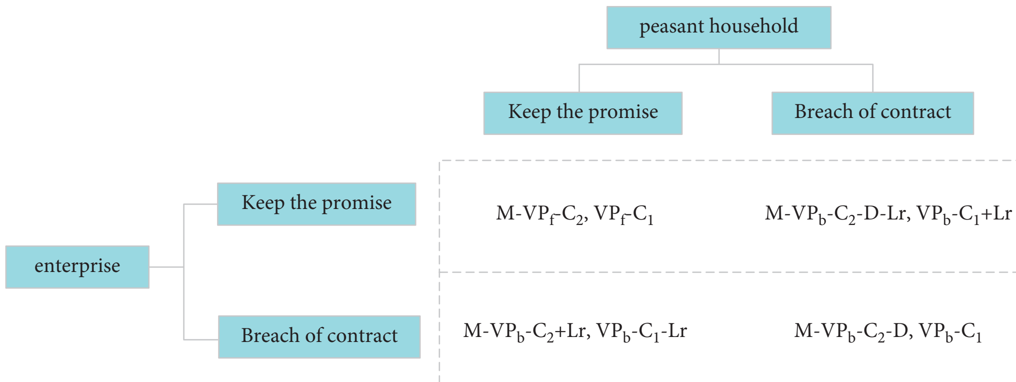

Figure 4: Income of both parties to the transaction subject when the market development is poor.

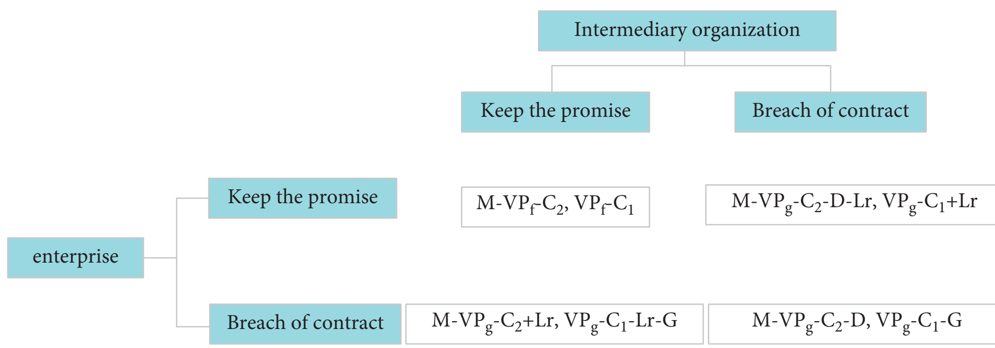

Figure 5: Benefits of companies and intermediary organizations when the market develops well.

execution cost, and both parties to the transaction will consider this factor and give up default during the transaction, so the probability of compensation is very low. Generally speaking, the stability of the organization mode of "farmers and companies" is relatively poor.

Time Impression Company, also known as Shaanxi Time Impression Electronic Commerce Co., Ltd., is engaged in online sales of agricultural and sideline products, storage, sales, and industrial information services of kiwifruit, as well as special products and dry fruit and fresh fruit acquisition and sales business. The operation mode of the enterprise is "company + farmer." It mainly cooperates with farmers in signing of planting acquisition contracts, where the enterprise puts forward a series of crop process requirements for farmers. Farmers grow products according to requirements of the enterprise, and the latter finally purchases products at market prices in the acquisition. The whole process from orchard to market is divided into several stages, and the scope of responsibility is delimited. Time Impression Company began to implement cooperation with farmers from 2010, mainly in the way of order acquisition during 2010-2011; in the way of order acquisition, technical training, and demonstration guidance during 2011–2013; and in the way of brand building, marketing, and integrated service system during 2014–2016.

3.2.2. Stability Game Analysis under the Organizational Mode of "Company, Intermediary Organization, and Farmer". The members of intermediary organizations in this mode are mostly local farmers, so the trust between intermediary organizations and farmers is high. Therefore, when analyzing this mode, the game relationship between farmers and intermediary organizations is ignored intentionally, and analyzation is made only on the game between companies and intermediary organizations [18].

Before the analysis, the following assumptions are made: in order to ensure that both parties can get the maximum benefits, both parties are rational in the transaction process. The number of agricultural products traded is set as V, the price of agricultural products is represented by P_f, and the prices of agricultural products are referred to by P_g and P_b, when the market environment is good or bad, respectively, where $P_g > P_f > P_b$. The cost of the intermediary organization is C_1, and the cost of the enterprise in the transportation process is C_2. Farmers hand over V quantity of agricultural products to the enterprise for processing and sales, and finally the money profit obtained by the enterprise is set as M, and the probability of default and the amount of compensation to be paid after default by both parties are set as R and L, respectively. The losses caused to the development of companies or intermediary organizations are set as D and G. Figure 5 indicates the benefits of both intermediary organizations and companies, when the overall market development is good [19].

As Figure 5 presents, when the overall development of the market is good, companies will make greater profits by choosing to abide by the contract, while intermediary organizations will make their choices by comparing the benefits obtained under the two situations of abiding by the contract and breaching the contract. The situation arises as equations (5) and (6) [20] show

$$VP_f - C_1 < VP_g - C_1 - Lr - G. \quad (5)$$

Namely,

$$Lr + G < V\left(P_g - P_f\right). \quad (6)$$

In equations (5) and (6), V refers to the amount of the agricultural products; P_f indicates the price of agricultural products in the contract; P_g represents the price of agricultural products when there is more benefit in the market; C_1 denotes the cost of the agricultural products purchased by intermediary organizations; L expresses the compensatory payment for breach of contract; r accords with the rate that compensatory payment will be paid; G stands for the future discount losses, which will be led by the reputational losses suffered by intermediary organizations with certain size. The profit obtained by the intermediary organization's breach of contract is greater than the profit obtained by keeping the contract, so the enterprise will choose to default.

When the overall market development is poor, the benefits of both intermediary organizations and companies are presented in Figure 6.

Through the above analysis, the results show that the three following aspects will affect the cooperative relationship between companies and intermediary organizations: first, the price fluctuation range of agricultural products, second, the probability of compensation, and third, the loss caused by reputation damage after default to the future development of companies and intermediary organizations. The price fluctuation of agricultural products is mainly affected by the external environment. Compared with the organization mode of "company and farmer," the number of orders has been greatly increased due to the addition of intermediary organizations, and the order value has exceeded the cost required by default litigation, so the probability of winning compensation has been greatly improved.

3.3. Mechanism Analysis on Governance Optimization of Agricultural Products Supply Chain Based on Blockchain Technology. According to the analysis of " company and farmer" and "company, intermediary organization, and farmer" in Section 2 and the understanding of new institutional economics, it can be found that the agricultural products supply chain is constantly evolving in the way illustrated in Figure 7.

Institutional factors such as asset specificity, uncertainty, and transaction frequency play an important role in the organizational structure of agricultural products supply chain.

Figure 8 displays three important factors of governance of agricultural products supply chain based on blockchain data technology.

3.3.1. Blockchain Optimizes the Network Organization Structure of Supply Chain of Agricultural Products. Supply chain of agricultural products is a very complicated business system, and its main components include consumers, farmers, companies, supervision institutions, and cooperatives. Business entities not only have certain dynamics and randomness but also have certain constraints [21, 22]. Therefore, certain requirements for the governance structure of blockchain are also put forward, so that it can be coupled with the governance structure of agricultural supply chain. Figure 9 signifies the specific structure.

As a decentralized and distributed database technology under collective maintenance, blockchain can save a lot of intermediary costs in reality. This peer-to-peer trading method with equal rights and obligations for each node eliminates the hierarchical relationship derived from the traditional central governance structure to the surrounding radiation. Therefore, the advantage of blockchain embedding in traditional organizations is to guide the "deintermediation" of traditional intermediaries and transaction settlement systems, improve transaction efficiency, and reduce transaction costs.

The traditional agricultural supply chain is a distributed network chain structure composed of enterprises, farmers, distributors, regulators, consumers, and other participating entities. Due to the characteristics of agriculture, the participants of agricultural supply chain are distributed in space and time dimension, and the traditional centralized transaction structure can easily add the cost of information processing and the degree of information asymmetry, resulting in higher transaction costs. The distributed and decentralized characteristics of blockchain are coupled with the distributed network organization of agricultural product supply chain. The agricultural product supply chain embedded in the blockchain can use the point-to-point information and value transmission network architecture based on the blockchain P2P network to trade, thereby changing the centralized governance of agricultural product supply chain governance. Blockchain technology embedding can transform the original "series" organizational governance structure of agricultural product supply chain into a flat "parallel" organizational governance structure. The participants can realize the direct exchange of economic factors in the agricultural product supply chain system based on blockchain and form the technical support of "deintermediation" in the agricultural product supply chain organization, thus further reducing the transaction cost.

The governance of agricultural product supply chain includes complex contents, such as the docking of external market transactions, the collaboration among organizational members, and the hierarchical governance within members. The blockchain can be divided into public chain, alliance chain, and private chain according to the degree of openness. Public chain refers to the blockchain where anyone can join, read data, participate in the consensus process, send transactions, and obtain effective confirmation at any time; alliance chain refers to the blockchain where consensus process is controlled by preselected nodes, allowing only designated node users to account for and modify blockchain data, which can be regarded as a "partially decentralize" blockchain; private chain refers to the blockchain that the written permissions are controlled by an organization or institution, whose data processing speed is far better than

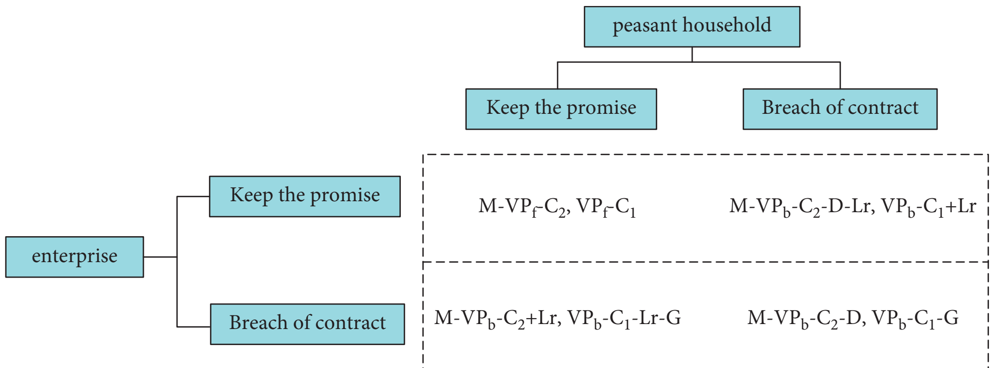

Figure 6: Income of companies and intermediary organizations when market development is poor.

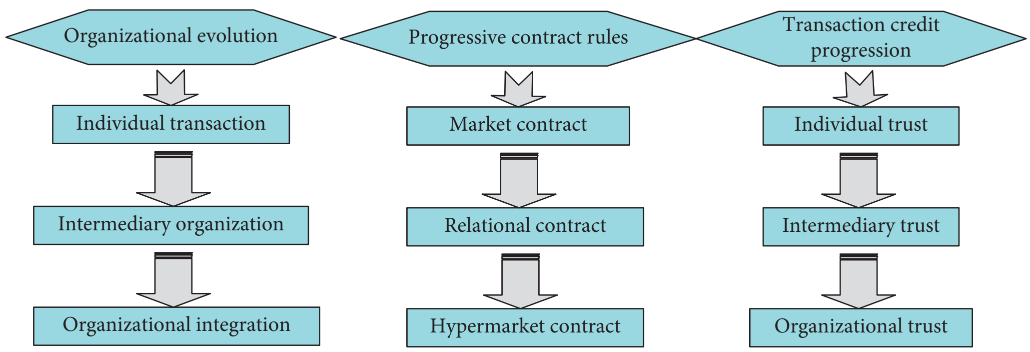

Figure 7: Evolution of organizational governance of agricultural supply chain.

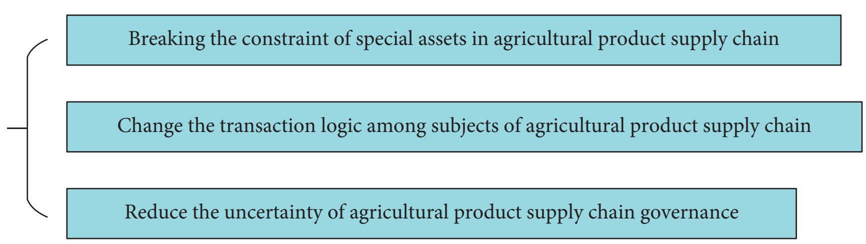

Figure 8: Blockchain embeddedness affects three important factors of agricultural supply chain governance.

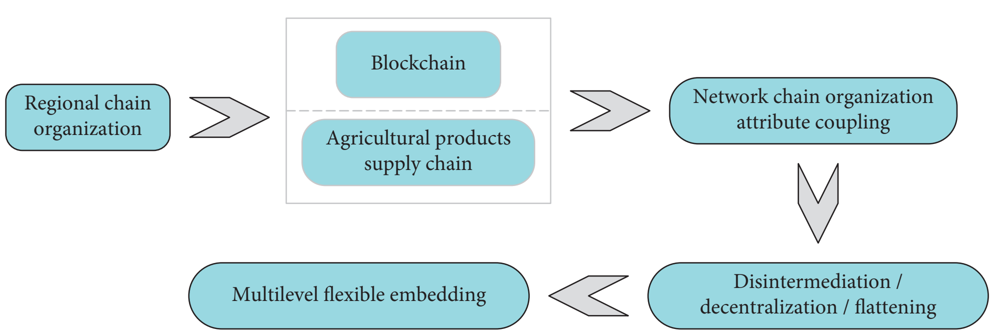

Figure 9: Blockchain optimizing the organization structure of agricultural products supply chain network chain.

public chain and alliance chain. Considering the processing speed and the privacy of book access, many enterprises choose private chain technology at the level of corporate governance. Agricultural products supply chain can flexibly use cross-chain, public chain, alliance chain, private chain, hierarchical cloud mechanism, and other technologies to deal with the participants of agricultural products supply chain dynamically and form a more matching blockchain and the network chain coupling mapping of agricultural products supply chain.

3.3.2. Blockchain Improves the Contract Completeness of Supply Chain of Agricultural Products. When constructing the contract theory, the relevant scholars found that there were some differences in the information about the quality and sales volume of agricultural products owned by both parties to the contract, and, in the whole process of transactions between both parties, irrational transactions might occur between both parties. Therefore, it is very difficult to clarify all the rights and obligations that both parties need to perform when conducting transactions through the clauses in the contract, and this will increase transaction costs [23, 24]. Therefore, incomplete contracts are ubiquitous in the transaction process of both parties, and the main transaction costs brought by incomplete contracts include the three following points: First, because there are relatively many trading subjects involved in the supply chain of agricultural products, the cost of signing contracts is relatively high. Second, because there are few "objects" contents to be standardized when the subject of agricultural products trade enters into a contract, the cost to supervise the implementation of the contract is higher than the trading target of agricultural products. Third, natural disasters and market risks will have a great impact on the production of agricultural products, and both natural disasters and market risks have unpredictability, resulting in higher information and cognitive costs [25].

Incomplete contracts and transaction costs are the sources of organizational and governance problems, while a considerable number of scholars believe that, when solving the problems caused by incomplete contracts, a new generation of technologies such as blockchain can be embedded. Figure 10 explains the specific structure.

3.3.3. Blockchain Optimizes Organizational Trust of Supply Chain of Agricultural Products. The root cause of the breach of contract between the two parties is not the incomplete contract but the speculative behavior. Companies, farmers, intermediary organizations, and other participants in the supply chain of agricultural products may realize their own goals by relying on other parties violating the rules in order to realize their own interests in the transaction process, and the stronger the asset specificity is in the supply chain of agricultural products, the more likely the trading subject is to be "locked up," and the more likely it is to have speculative behavior.

All the problems in the supply chain of agricultural products, such as high uncertainty, speculative behavior, and limited rationality of trading subjects, will lead to the emergence of organizational and governance problems. An effective way to overcome speculative behavior and enable the trading subjects to cooperate for a long time is to improve the trust of both parties. Interpersonal trust can solve problems such as difficulty in quantifying transaction costs and unclear property rights in supply chain of agricultural products caused by incomplete contracts.

Blockchain based on digital technology can not only make the transaction information transparent but also make it automatically execute the contract contents through intelligent contracts, to avoid the speculative behavior that the transaction subjects improve their own interests by deception in the transaction process. Figure 11 shows the specific structure.

3.3.4. The Principle of the Agricultural Product Supply Chain Governance. Agricultural product supply chain governance is a very interdisciplinary subject, which can be divided into aspects of agricultural products, supply chain, and governance. Different combinations, different perspectives, and different focuses of the three aspects influence each other, infuse with each other, and then derive the ever-changing researches and results. From the perspective of agricultural products, the different biochemical characteristics of agricultural products, regional agricultural production, farmers' different preferences, and cultural attributes of different aspects of the change factors into the subject of agricultural supply chain governance will form a new perspective of research. Therefore, with the deepening of research, scholars' researches show gradually more specific trends, such as focusing on the supply chain management of some agricultural products, comparative analysis of supply chain management of different agricultural products, the impact of agricultural production brought by regional characteristics on the supply chain management of agricultural products, and the impact of farmers' various preferences on the supply chain management of agricultural products, and these studies show different research results through different research methods and models. In the past few decades, with the development of globalization, industrialization, and technology, supply chain has experienced multiple stages of development, including logistics management stage, value-added stage, network chain stage, and emerging supply chain business stage, and both its external form and internal mechanism have undergone great changes. From the perspectives of supply chain logistics, capital flow, and information flow, the research on agricultural product supply chain governance derives many research topics such as agricultural product supply chain finance, agricultural product quality and safety governance, and information sharing under agricultural product supply chain. From the perspective of governance, researches are more consistent with the development logic of new institutional economics. With the continuous enrichment of the content of new institutional economics, the research contents, and achievements of agricultural product supply chain organization, contract regulation and relationship governance are also constantly enriched.

4. Results and Discussion

4.1. Analysis of China's Total Output Value and Total Import and Export Volume of Agricultural Products. As a big agricultural producer, China's gross agricultural output value has exceeded the trillion yuan mark at the end of last century. With the steady growth of gross agricultural output

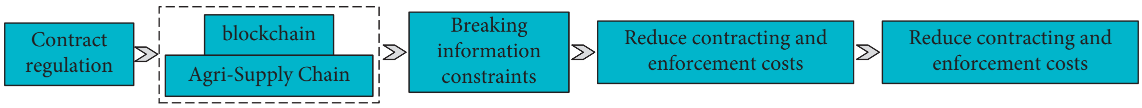

FIGURE 10: Blockchain optimizing contract regulation of supply chain of agricultural products.

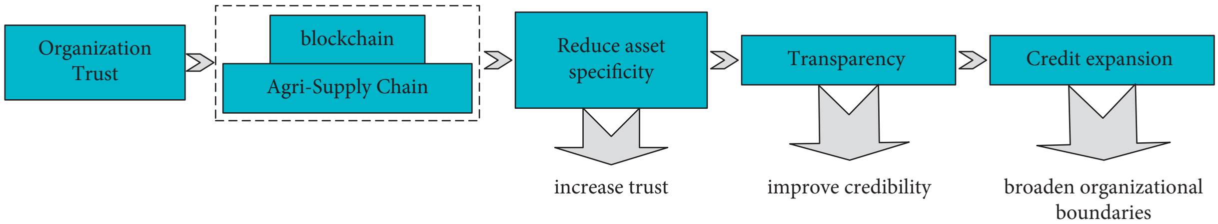

FIGURE 11: Blockchain strengthening organizational trust in agricultural supply chain.

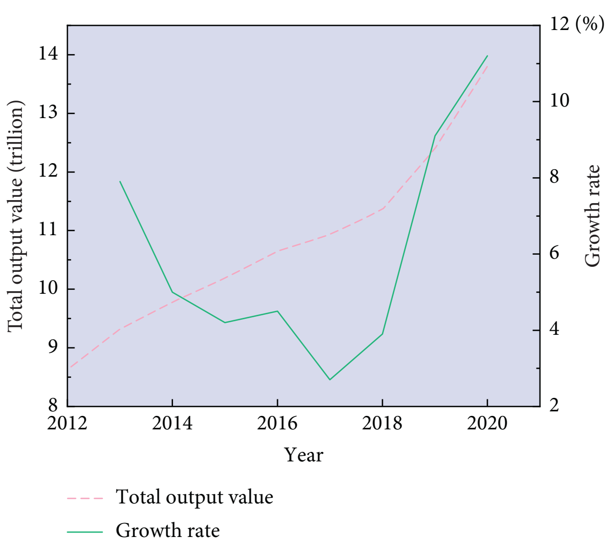

FIGURE 12: Gross output value and growth rate of agricultural products in China from 2012 to 2020.

value, China's agricultural production and management level are also steadily improving. Figure 12 presents the total output value and growth rate of China's agricultural products in recent years.

As Figure 12 shows, China's gross agricultural products have been increasing since 2012, with the gross agricultural products of China reaching 11.36 trillion yuan in 2018 and 12.4 trillion yuan in 2019, up 9.1% year-on-year. China, as an important global producer and consumer of agricultural products, has increased the proportion of agricultural products trade in the world agricultural products trade year by year. It is playing an increasingly important role in the world's agricultural trade. With the rapid growth, the structure of China's agricultural trade is constantly changing as shown in Figure 13.

Figure 13 describes that the total of import and export of agricultural products in China showed a declining trend from 2014 to 2017. From 2017, the total of import and export of agricultural products in China began to rise continuously. In 2018, the total of import and export of agricultural products was $228.43 billion, and, in 2019, it was $228.43 billion, an increase of 5.7% year-on-year.

4.2. Functional Framework of Supply Chain Governance of Agricultural Products under the Blockchain Technology Path. In the process of rapid development of digital technology, blockchain technology has been continuously integrated with digital technology to provide more effective solutions for optimizing the organizational governance system. By combining different digital technologies, different technical characteristics can be brought to blockchain products. However, each blockchain product can be divided into data layer, network layer, consensus layer, contract layer, and application layer on the technical path of systematic functional architecture. On the basis of consulting relevant literature, the overall functional framework of agricultural products supply chain is reconstructed in view of the existing problems in the current supply chain of agricultural products, which can be divided into five parts as shown in Figure 14.

In order to intelligently identify and track and monitor the processes and subjects in the supply chain of agricultural products, the physical layer in Figure 14 is set up, which includes various digital technologies such as intelligent remote sensing and laser scanning. Through the integration with these technologies, the planting, processing, and logistics information in the supply chain of agricultural products can be collected. For example, if the sensor is installed on the agricultural seed machine, the position information provided by GPS can be used to photograph the growth of farmland crops, which can be input into the computer system for further processing and storage of relevant data.

The data layer mainly includes many data technologies such as asymmetric encryption, hash function, and Merkle tree to store the data in the process of agricultural supply chain governance. Asymmetric encryption can encrypt data through a pair of public key and private key; the public key is open to the whole network, while the private key can only be used by individuals. This method can not only protect personal data privacy and ensure the information stored by users safely but also clarify the boundaries between the two parties in the supply chain. Hash function has the characteristics of noninterference and being one-way. Based on these characteristics, it can ensure that the data in the supply chain of agricultural products will not be easily tampered

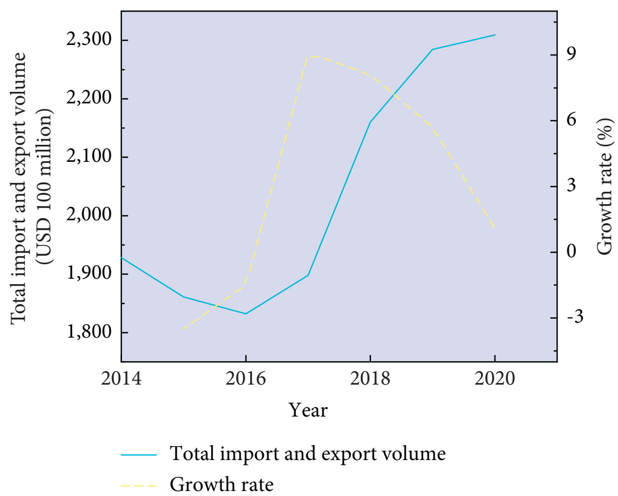

Figure 13: Total of import and export volume and growth rate of China's agricultural products from 2014 to 2020.

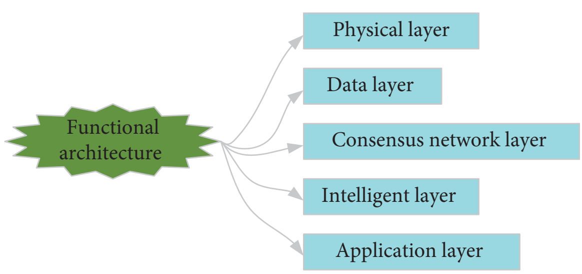

Figure 14: The overall functional framework of supply chain governance of agricultural products.

and ensure the authenticity of the recorded data. Merkle tree is an essential technology when building the block data structure of blockchain. Its branch nodes can store the calculated hash value, and the root value corresponds to the last hash value in recursive calculation, which is recorded in the block data structure together to ensure that the previous data can be traced back. Therefore, this technology can be used when constructing the data traceability system of supply chain of agricultural products and building the relational database based on the trading network.

The consensus network layer includes cross-chain technology for connecting different blockchains, consensus algorithms such as DPoS and PoW, and P2P network technology. The network layer frames the data verification structure, information dissemination mechanism, and network formation mode among the trading subjects of supply chain of agricultural products and reshapes the organization mode of supply chain of agricultural products. Among them, DPoS, PoW, and other blockchain consensus algorithms can ensure that the number of general ledgers is consistent when the bookkeeping rights of each node in the supply chain of agricultural products organization are the same. The distributed ledger formed based on this algorithm can improve the trust between transaction subjects and make the organizations in the supply chain of agricultural products form mutual trust. P2P network technology can ensure that the trading statuses of each subject equal each other in supply chain of agricultural products. In this case, the intervention of third-party intermediary is not needed, and the point-to-point trading structure among trading subjects is realized, thus effectively reducing the transaction cost.

Intelligent contract layer includes Multisignature Technology, Programmable Script Technology, and Turing Complete Technology. It can transform contracts in supply chain of agricultural products into computer protocols in blockchain data structure through program codes. This protocol adopts self-verification method and automatically performs tasks without intervention of intermediary. In order to make the information exchange, asset management, and value transfer between trading entities more efficient and convenient, various data and assets can be flexibly embedded in smart contracts. It can also be embedded with intelligent prediction machines and various intelligent algorithms involved in transactions to build an intelligent system that can analyze the environment and make corresponding decisions.

The application layer contains various application cases and scenarios in the supply chain of agricultural products, which are applied to the specific production process based on the functions of the above layers. For example, the organizational credit system of supply chain of agricultural products is constructed, and the data of the participants' demand and financial supply are analyzed. Through the above analysis, the intelligent functional framework of agricultural products supply chain based on blockchain can be obtained as in Figure 15.

4.3. Mechanism Optimization of Supply Chain Governance of Agricultural Products under Blockchain Technology Path. All participants in the supply chain of agricultural products can sign contracts before trading, so that the interests of both parties can be effectively guaranteed. The clearer the terms in the contracts, the more stable the cooperative relationship between both parties. At present, the commonly used formal governance mechanism is shown in Figure 16.

In the governance mechanism of agricultural supply chain, it includes not only formal governance mechanisms such as contracts but also informal governance mechanisms such as agreements and exchanges, as shown in Figure 17.

4.3.1. Blockchain Embedding Optimizes the Trust Mechanism of Supply Chain of Agricultural Products. Because the supply chain of agricultural products is greatly influenced by the natural environment, the investment risk is high, the establishment of trust relationship between trading subjects can avoid opportunistic behavior to a great extent, and the improvement of trust between trading subjects can improve the stability of the supply chain of agricultural products. By encrypting and transparentizing the data and information, the distrustful factors in the blockchain can be removed, and the influence degree of the organization can be reduced by "information without doubt." Blockchain can encrypt data information to ensure the authenticity and reliability of data and reduce the influence of personal feelings on trust. In order to effectively deal with the limited rationality among

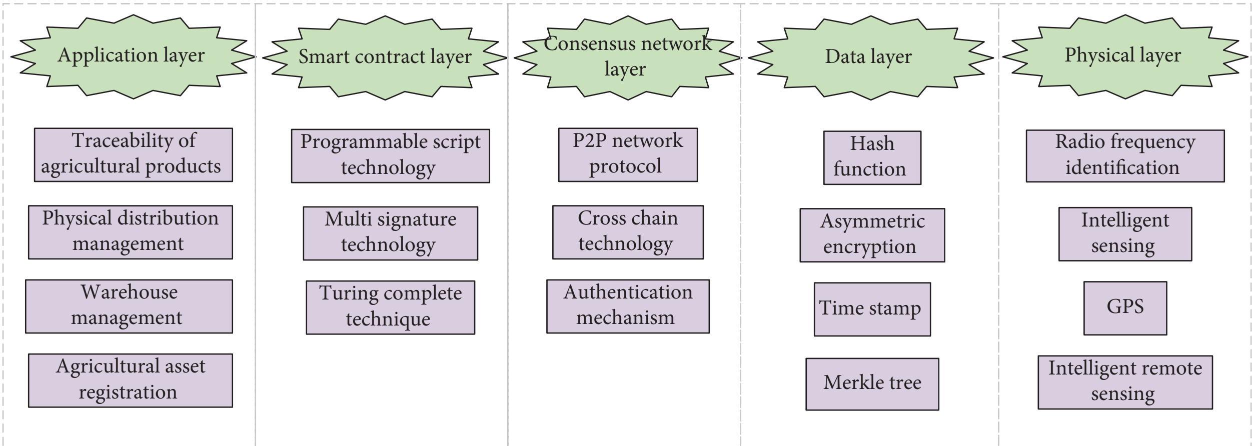

Figure 15: Functional framework of supply chain governance of agricultural products based on blockchain.

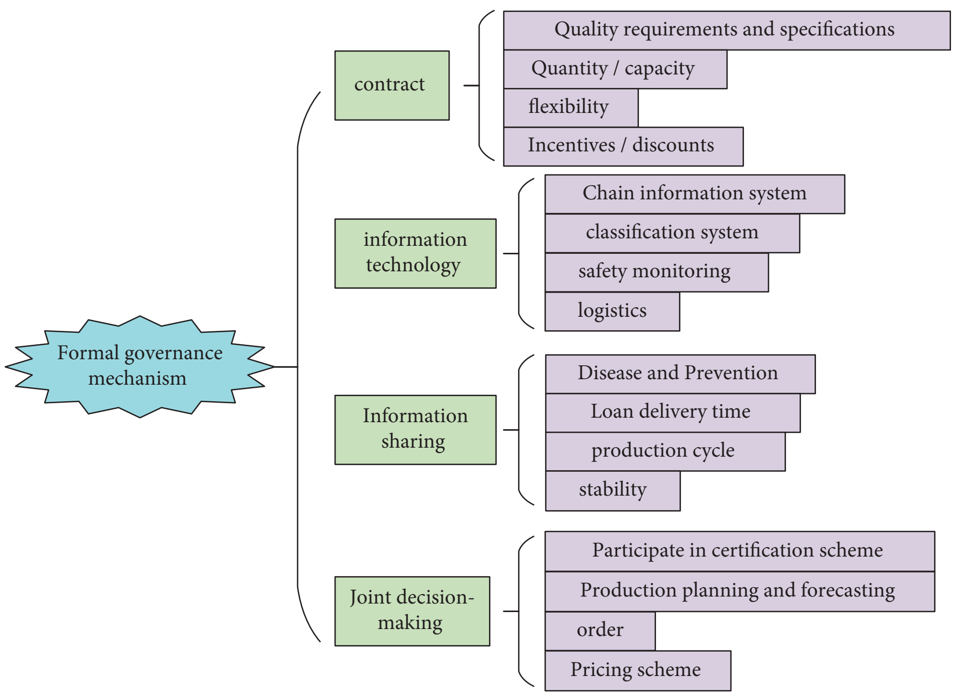

Figure 16: Formal governance mechanism of supply chain of agricultural products.

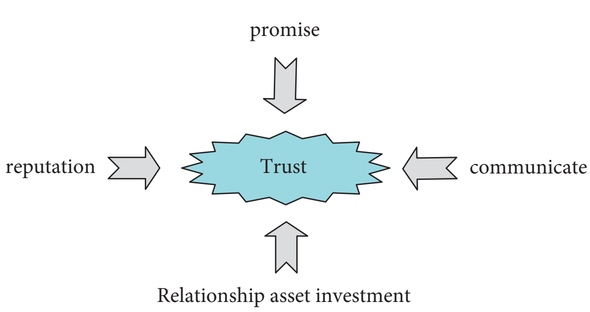

Figure 17: Informal governance mechanism of supply chain agricultural products.

the trading subjects, there are two main ways to realize "information without doubt" based on the technology of blockchain: first, construct the infrastructure of "information without doubt" based on new information technology; second, build the digital trust mechanism to improve the enthusiasm of trading subjects such as companies, farmers, and intermediary organizations.

Figure 18 signifies the "information without doubt" technology constructed according to the above contents.

4.3.2. Blockchain Optimizes the Contract Mechanism of Agricultural Supply Chain Governance. Contract mechanism is similar to smart contract, which is realized by computer programming. Based on reducing costs, its application scope is broader, and the transparency of the implementation process greatly reduces the probability of default by both parties. The smart contract based on blockchain technology can be divided into broad sense and narrow sense. The broad sense smart

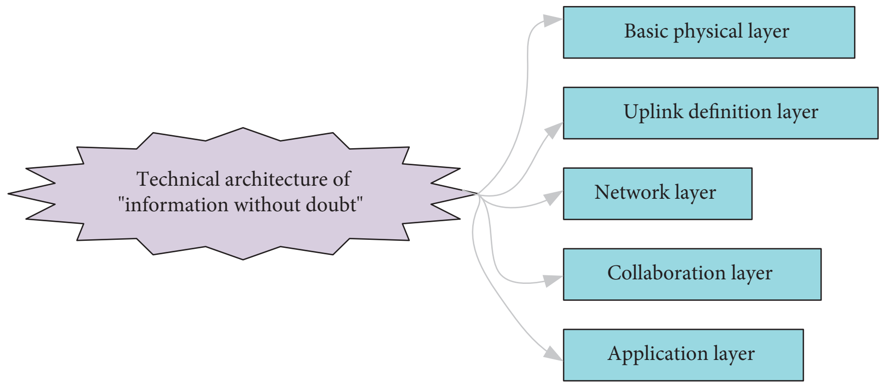

Figure 18: Technical architecture of “information without doubt.” In addition, the application of blockchain technology can optimize the trust generation and guarantee mechanism in supply chain of agricultural products, illustrated in Figure 19.

contract does not consider the influence of intermediary organizations. It can consciously carry out relevant activities according to the contents of the contract and play a supplementary or even alternative role to the existing rules and regulations.

In the supply chain of agricultural products based on blockchain technology, transactions among companies, intermediary organizations, farmers, and other trading entities can be transformed into codes by computer algorithms and then evolved into programs, forming computer protocols and storing them. Economic activities such as identity authentication and contract transactions can be completed through intelligent contracts. Figure 20 shows the specific functional architecture.

4.4. Case Analysis

4.4.1. Case Description. Based on the high-quality black land of ”BEIDAHUANG Group,” “Shan Liang Taste” integrates a new generation of information technologies such as Internet of Things, blockchain, and big data to serve the whole supply chain and creates the first rice supply chain system in China based on blockchain in the form of “consumers + logistics system + trading platform + production base + farmers.” “Shan Liang Taste” implements the digitization of agricultural assets. The supply chain is split into 1639 business nodes, spanning 3 farms, 9 administration areas, and 33 workstations, signing 249 plots (a total of 24318.98 mu), and covering 1477 plots (a total of 271223.03 mu), and single land has 17 conventional digital attributes. “Shan Liang Taste” links the contracted agricultural land to the network platform, forming the corresponding programmable assets. Relying on the modernized, standardized, and mechanized production management mode of the “BEIDAHUANG Group,” various intelligent devices are embedded in all aspects of the supply chain such as rice planting, production, sales, and after-sales. Collection is made on a series of data such as soil environment, fertilizer and water use, seedling information, rice deep processing, storage and transportation, and sales and distribution in the process of rice planting. After process screening and algorithm screening, the data are uploaded to the blockchain to ensure the objective authenticity of the data.

Based on this, “Shan Liang Taste” realizes the comprehensive data mapping of the participants, production, and circulation, agricultural assets, and trading system of the rice supply chain in the blockchain network, breaks the data island, and forms the consistent database of the rice supply chain based on the blockchain. Specifically, “Shan Liang Taste” uses blockchain to create a closed-loop autonomous system and develops APP and digital equipment based on blockchain in the production and logistics links of rice supply chain for digital governance.

In the transaction of rice supply chain, on the one hand, ”Shan Liang Taste” makes the best of the financial and technological characteristics of blockchain to organically combine the circulation of digital assets of farm land with bulk grain transactions. In the blockchain environment, ”Shan Liang Taste” forms a confirmed agricultural product by anchoring with the land of “Shan Liang Farm,” thus creating a brand grain futures trading scene based on blockchain “Grain Exchange.” “Shan Liang Taste” anchors the digital assets of agricultural land with the “Shan Liang blockchain grain ticket,” a tradeable and mortgageable digital planting order produced by the plot. Grain ticket is the only certificate for grain physical delivery in “Grain Exchange,” and farmland asset securitization is completed by anchoring grain ticket and real grain.

On the other hand, “Shan Liang Taste” implements e-commerce sales for consumers. Consumers can delimit a part of the farm through cloud farms, order one season of rice produced on the land, and generate orders online with one button. Farmers can contract the production orders of land anchored by “Shan Liang Blockchain Grain Ticket” online through “Farmer Treasure,” thus forming blockchain futures products of shared farms. After that, through the closed-loop channel construction and traceability certification process of “Shan Liang Taste,” the high-quality grain with “geographical stamp, time stamp, and quality stamp” is sent to consumers by express delivery. In June 2018, “Shan Liang Taste” cooperated with Tencent and issued a “Shan Liang Blockchain Order” corresponding to the land through WeChat, which was sold online at the price of CNY 8,000 per mu of land and 500 kg of high-quality rice to support online crowdfunding consumption. Ten people could make group reservations and the goods would be delivered by express

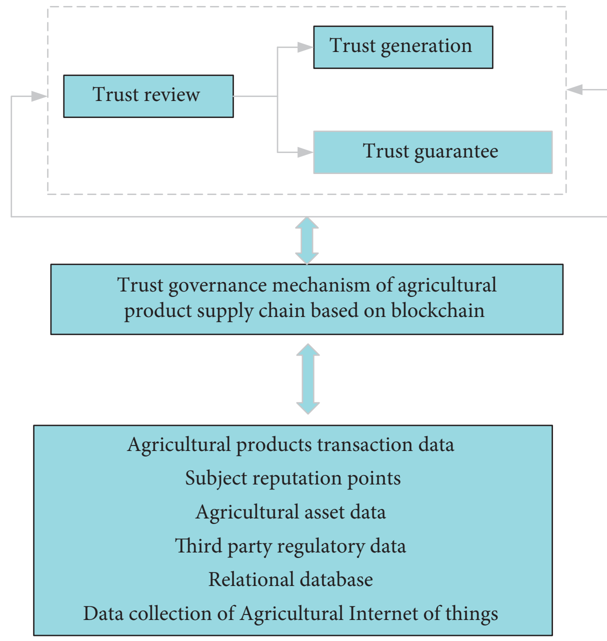

Figure 19: Trust mechanism structure of supply chain of agricultural products based on blockchain.

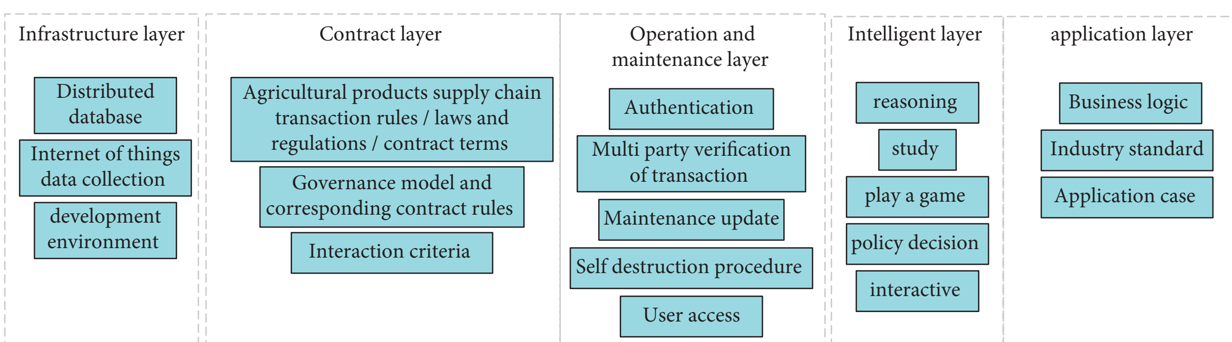

Figure 20: Functional architecture of intelligent contract mechanism of supply chain of agricultural products based on blockchain.

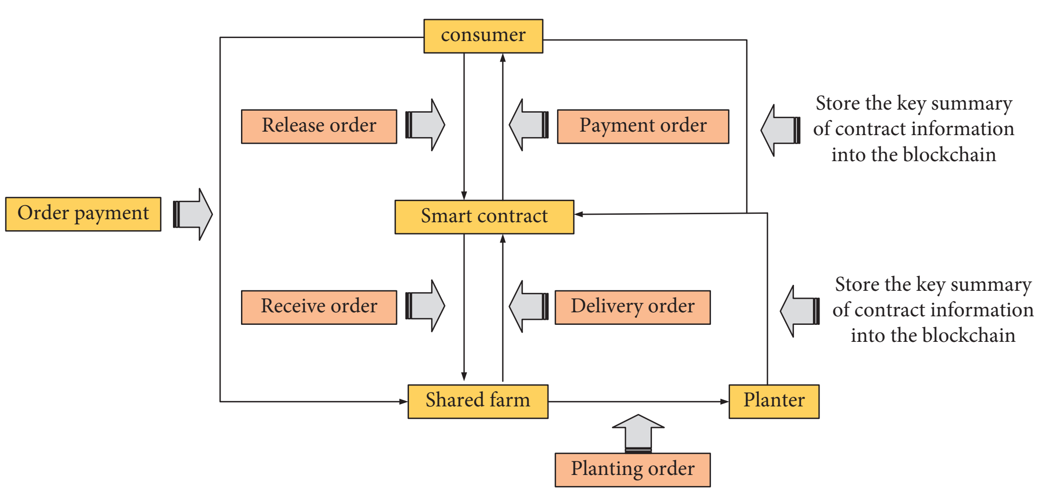

Figure 21: Ordering flow of “Shan Liang Taste Sharing Farm.”

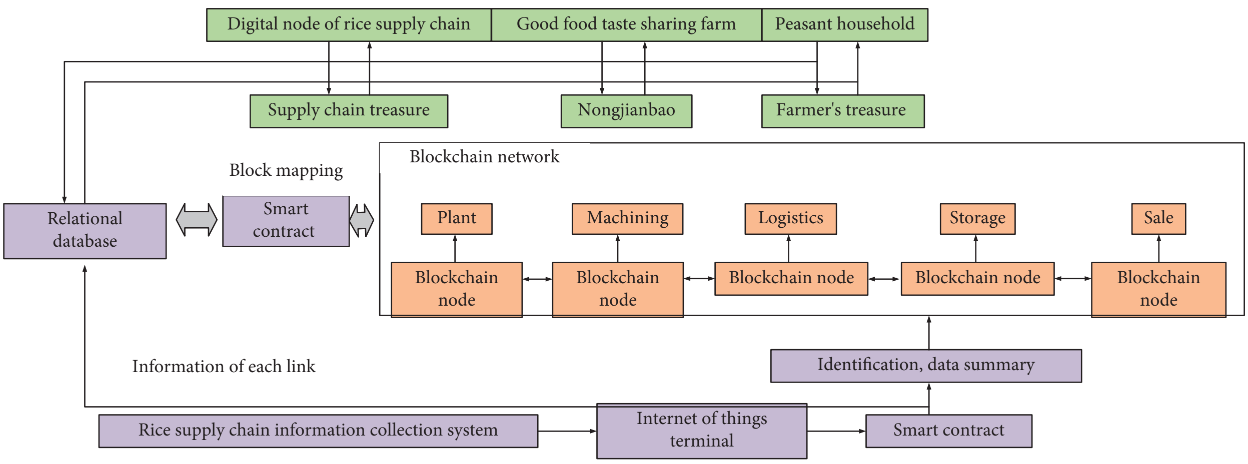

Figure 22: Scheme of the "Shan Liang Taste" blockchain network architecture.

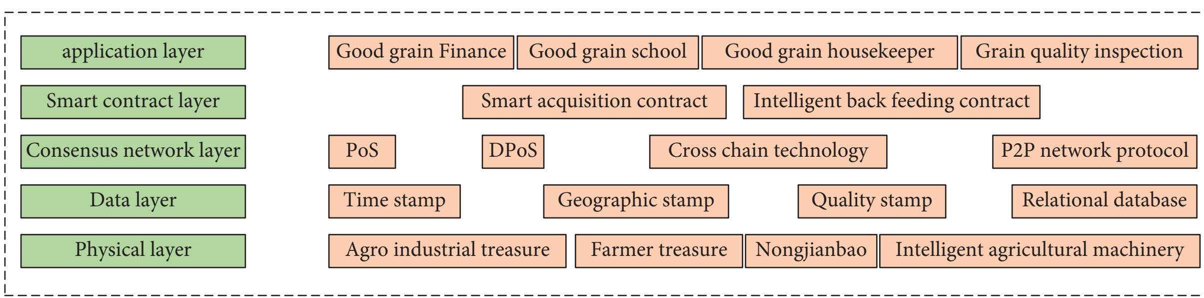

Figure 23: System functional framework based on blockchain governance for "Shan Liang Taste."

delivery four months later. Figure 21 illustrates the ordering flow of "Shan Liang Taste Sharing Farm."

Whether it is the blockchain-based commodity trading or consumer-oriented online orders, "Shan Liang Taste" uses blockchain-based smart contracts. "Shan Liang Taste" digitizes and programmes the order through script code. Once the system triggers the threshold, the contract terms will be automatically executed, and none of participants of the contract unilaterally have right to cancel or prevent the contract execution, which effectively solves the contract credit problem faced by the original rice supply chain. "Shan Liang Taste" releases the rights, responsibilities, and benefits of all aspects of the agricultural supply chain transparently and open in the form of blockchain-based smart contract terms. Once an order happens in the sales end, intelligent contracts will automatically allocate revenue to each supply chain link. The rice supply chain based on blockchain has formed a systematic, digital, and intelligent benefit distribution mechanism. The originally fragmented supply chain subjects have formed efficient coordination and positive incentives through algorithms.

"Shan Liang Taste" relies on a new generation of information technology to create a variety of integrated applications for specific scenarios of rice supply chain at the platform level, for example, relying on BEIDAHUANG Group standardized production, integrated services, and digital management to create "Shan Liang Stewards," to provide integrated services for supply chain participants, unified breeding, agricultural procurement, production planning, warehousing acquisitions, logistics, and distribution services; developing "Shan Liang School" to spread farming skills and knowledge and providing all-round skills services such as fertilizer and pesticide use and pest control technology for the new farmers who contracted rice production tasks; cooperating with financial institutions to create "Shan Liang New Finance" and forming a consistent database based on blockchain with financial institutions. Based on the big data analysis of the production, processing, logistics, trading, and consumption of the rice supply chain, financial services such as borrowing, asset securitization, and insurance are carried out to solve the problems of opaque financial information in the agricultural supply chain, redundant intermediaries, and complex business processes and provide effective protection for the financial needs of farmers and SMEs in the rice supply chain. Figure 22 demonstrates the scheme of the "Shan Liang Taste" blockchain network architecture.

4.4.2. Optimization of Agricultural Products Supply Chain Governance from the Perspective of Blockchain Embedding. Blockchain is the technology to solve the problem of rice supply chain. Besides, the underlying technical logic of decentralization, trust, intelligent contract, and consensus sharing of blockchain is the core of guiding the project of "Shan Liang Taste." "Shan Liang Taste" uses blockchain as the underlying functional architecture to integrate Internet of Things, big data, artificial intelligence, visualization, and other technologies into the framework to optimize the governance of rice supply chain. According to the functional framework design of agricultural product supply chain governance based on blockchain, “Shan Liang Taste” also adopts similar functional architecture on the technical path: basic physical layer, data layer, consensus network layer, intelligent contract layer, and application layer.

The basic physical layer integrates technologies such as the Internet of Things, mobile Internet, big data, remote control, and data processing. Each node in the rice supply chain contains much data. These data are collected through various technologies and terminals in the physical layer and uploaded to the system with communication protocols. The whole process mapping of the rice supply chain is completed in the physical layer. “Shan Liang Taste” relies on the same cultivation of rice standard with BEIDAHUANG Group and uses the Internet of Things, mobile Internet, and other technologies to realize the whole process of data collection in the preparation, production, and receiving links. The data layer integrates hash function, distributed database technology, timestamp, cloud database, Merkle tree, and other technologies to receive data from the basic physical layer and unify data format, which is stored in the “Shan Liang Taste” system. The consensus network layer adopts the common consensus algorithms such as PoS and DPoS and the hybrid consensus mechanism of joint consensus. The intelligent contract layer encapsulates the business logic and transaction logic of the code-programmed “Shan Liang Taste” system, which is a complete intelligent contract. The application layer encapsulates the application logic of specific cases in the “Shan Liang Taste” rice supply chain based on the functions of each layer. The API interface provided by the underlying blockchain can call the distributed data of each layer and the resources for consumers, enterprises, regulators, and trusted service providers to realize the governance requirements of specific system applications, such as user authentication, quality inspection and detection, product traceability, monitoring and early warning, supply chain finance, and other specific application scenarios. Figure 23 signifies the system functional framework based on blockchain governance for “Shan Liang Taste.”

5. Conclusion

Because the information owned by the trading subjects in the agricultural supply chain is not completely consistent and not necessarily completely rational in the trading process, there is instability in the governance of the agricultural supply chain, which will lead to speculative behavior of the trading subjects. According to the new institutional economics theory of blockchain technology and agricultural supply chain governance, the governance of supply chain of agricultural products is discussed through literature research, executive analysis, and interdisciplinary research. The results are as follows: By analyzing the organizational structure and stability of two organizational models, “company and farmer” and “company, intermediary organization, and farmer,” a deep discussion is made on the relationship, organizational structure, and manifestation of trading subjects in the supply chain of agricultural products. With the rapid development of the new generation of information technology, such as blockchain, Internet of Things, and computer technology, it is possible to comprehensively digitize economic activities such as production and transaction in the supply chain of agricultural products.

Data Availability

The labeled datasets used to support the findings of this study are available from the corresponding author upon request.

Conflicts of Interest

The authors declare no conflicts of interest.

Acknowledgments

This work was supported by the project of Education Science Planning in Anhui Province, the Research on the Talent Training and the Countermeasures of Higher Vocational Education in Connection with Agricultural Modernization, under JG14016, and Key Research Project of Humanities and Social Sciences of Anhui Provincial Department of Education, Research on the Transformation and Development of China’s Retail Industry under the New Retail Normal, under SK2016A0353.

References

[1] S. Cheng and M. López, “Synergy analysis of agricultural economic cycle fluctuation based on ant colony algorithm,” *Open Physics*, vol. 16, no. 1, pp. 978–988, 2018.

[2] X. He, L. Dong, J. Huang, and K. Hu, “Agricultural climate change and agricultural economic sustainability based on resource scheduling algorithm,” *Arabian Journal of Geosciences*, vol. 14, no. 15, pp. 1–19, 2021.

[3] J. Gao, “Two echelon supply chain model of agricultural products based on stochastic fuzzy process of cost demand,” *International Journal of Reasoning-Based Intelligent Systems*, vol. 9, no. 3-4, pp. 149–156, 2017.

[4] U. S. Sakalli, “Optimization of production-distribution problem in supply chain management under stochastic and fuzzy uncertainties,” *Mathematical Problems in Engineering*, vol. 2017, no. 10, pp. 1–29, 2017.

[5] X. Chen and Y. Yun, “Optimization of a green supply chain network with various transportation types for tire industry in korea,” *Journal of the Korean Society of Supply Chain Management*, vol. 19, no. 2, pp. 91–106, 2019.

[6] D. Delfitriani, “A supply chain risk management for dadih product by pricing optimization,” *SEAS (Sustainable Environment Agricultural Science)*, vol. 2, no. 1, p. 41, 2018.

[7] J. Zhao, K. Gerasimova, Y. Peng, and J. Sheng, “Information asymmetry, third party certification and the integration of organic food value chain in China,” *China Agricultural Economic Review*, vol. 12, no. 1, pp. 20–38, 2019.

[8] Y. Sun, X. Yuan, and K. Shi, “Research on decision of supply chain of fresh agricultural products based on altruism preference,” *Systems Engineering-Theory & Practice*, vol. 37, no. 5, pp. 1243–1253, 2017.

[9] Y. Li and C. J. Zhang, "Vertical Integration of Agricultural products supply chain and quality Safety of Agricultural products," *E3S Web of Conferences*, vol. 275, no. 4, p. 2048, 2021.
[10] W. Zhou and M. S. Metawea, "Quality safety of agricultural products in supply chain-computer simulation based on multi-agent system," *Journal of Intelligent and Fuzzy Systems*, vol. 5, no. 2, pp. 1–8, 2021.
[11] L. Qiu, "Research on RFID investment decision and coordination of fresh agricultural products supply chain based on fixed price," *Revista de la Facultad de Ingenieria*, vol. 32, no. 14, pp. 342–347, 2017.
[12] M. Muzammal, Q. Qu, and B. Nasrulin, "Renovating blockchain with distributed databases: an open source system," *Future Generation Computer Systems*, vol. 90, no. JAN, pp. 105–117, 2019.
[13] J. Thatcher, "Improving visibility and transparency with blockchain," *APIC*, vol. 27, no. 3, p. 16, 2017.
[14] L. Ismail, H. Materwala, and A. Hennebelle, "A scoping review of integrated blockchain-cloud (BcC) architecture for healthcare: applications, challenges and solutions," *Sensors*, vol. 21, no. 11, p. 3753, 2021.
[15] M. S. Cheruvu, C. V. Cheruvu, and A. D. Farmer, "Oesophageal emergencies," *Medicine*, vol. 47, no. 4, pp. 224–227, 2019.
[16] Q. Li, X. Chen, and Y. Huang, "The stability and complexity analysis of a low-carbon supply chain considering fairness concern behavior and sales service," *International Journal of Environmental Research and Public Health*, vol. 16, no. 15, p. 2711, 2019.
[17] Z. Huang and L. Qiao, "Agricultural organizations and the role of farmer cooperatives in China since 1978: past and future," *China Agricultural Economic Review*, vol. 10, no. 1, p. 25, 2018.
[18] Y. Bo, X. H. Wu, Y. Bing, and Y.-W. Zhang, "Three-level supply chain coordination of fresh agricultural products in the Internet of Things," *Industrial Management and Data Systems*, vol. 117, no. 9, pp. 1842–1865, 2017.
[19] F. Özen, "On the intermediary effect of organizational policy: the effect of perceived ethical climate on corruption behavior of teachers," *Journal of Education and Training Studies*, vol. 6, no. 8, p. 52, 2018.
[20] J. Scholz, A. De Meyer, A. S. Marques et al., "Digital technologies for forest supply chain optimization: existing solutions and future trends," *Environmental Management*, vol. 62, no. 6, pp. 1108–1133, 2018.
[21] B. Yan, G. Liu, X. Wu, and J. Wu, "Decision-making on the supply chain of fresh agricultural products with two-period price and option contract," *Asia Pacific Journal of Operational Research*, vol. 38, no. 01, pp. 93–107, 2021.
[22] L. Popov and N. Yanneils, "Industrialization and the evolution of enforcement institutions," *Economic Theory*, vol. 69, no. 3, pp. 1–44, 2020.
[23] B. Lopez-Martin and D. Perez-Reyna, "Contracts, firm dynamics, and aggregate productivity," *Journal of Economic Dynamics and Control*, vol. 130, no. 3, p. 104190, 2021.
[24] J. Lehner and J. Sametinger, "Verwendung von Blockchain und Custom Tokens zur Projektkoordination - ein Pilot versuch," *HMD Praxis der Wirtschaftsinformatik*, vol. 55, no. 6, pp. 1285–1296, 2018.
[25] L. Song, X. Wang, P. Wei, Z. Lu, X. Wang, and N. Merveille, "Blockchain-based flexible double-chain architecture and performance optimization for better sustainability in agriculture," *Computers, Materials & Continua*, vol. 68, no. 1, pp. 1429–1446, 2021.

Hindawi
Scientific Programming
Volume 2022, Article ID 2167874, 10 pages
https://doi.org/10.1155/2022/2167874

Research Article

Research on the Trust Mechanism of Individual Consumers in Rural Financial Markets Based on the Dynamic CGE Model

Fang Lin [1] and Wenxiang Chen [2]

[1]School of Economics and Management, Fujian Vocational College of Agriculture, Fuzhou 350002, China
[2]State-Owned Assets Management Office, Fujian Agriculture and Forestry University, Fuzhou 350002, China

Correspondence should be addressed to Wenxiang Chen; chenwenxiang@fafu.edu.cn

Received 16 October 2021; Revised 9 November 2021; Accepted 13 November 2021; Published 4 January 2022

Academic Editor: Hai Dong

In order to obtain the complete equilibrium state of rural financial market and ensure the stable development of rural financial consumer market, this paper introduces CGE model and analyzes the dynamic trust mechanism of individual consumers in rural financial market. In this paper, the single variable evolutionary fuzzy clustering algorithm is used to analyze the orthogonal eigenvector solutions of individual consumers; the big data of individual consumers under the mode of perceived trust is automatically clustered, so as to obtain the fuzzy analogy function of individual consumers in the rural financial market; and finally the prediction value of consumer trust is obtained. The results show that trust, customer satisfaction, and service quality are positively correlated. Under the same sample expectation constraints, the dynamic CGE model is more robust, and the individual consumer trust mechanism of rural financial market in the study area has higher advantages.

1. Introduction

Since the late 1990s, in order to meet the challenges of domestic and foreign banking industry, commercial banks, especially the Agricultural Bank of China, have significantly accelerated the pace of building modern commercial banks. The operation has obviously turned to the direction of commercialization, a large number of township institutions have been merged, and loans tend to be large customer groups [1]. Not only make it appear fault in rural financial services, but also make a large number of rural funds have turned to the city, so that the supporting role of commercial finance on rural economy is weakening. In fact, the rural financial field is also a promising field. The rural financial market should not become a wasteland of commercial finance. Although China has been an agricultural policy bank for more than ten years, the current agricultural development bank has a single source of funds and a heavy burden of nonperforming assets. Rural financial consumption refers to the behavior that rural residents purchase financial products provided by financial institutions in order to meet their own consumption needs and enjoy financial services. The construction and improvement of rural financial consumption market are closely related to the overall development pattern of China's financial industry [2]. Building a stable rural financial consumer market is of great practical significance for expanding the domestic demand and promoting the stable development of rural economic and financial market. Based on the stable development of the market, consumer trust plays an important role in the rural financial consumption market. From the perspective of relationship marketing, trust plays an important role in strengthening relationships. Keeping trust with consumers is the most effective way for enterprises to carry out relationship marketing. In the case of uncertainty, high risk, and lack of contract and guarantee, the establishment of consumer trust has far-reaching significance for enterprises, which helps to establish stable customer relationship and maintain market share [3].

CGE model is essentially a micro model of multiple sectors and multiple markets; it also contains a lot of macroeconomic content. CGE model can make feedback adjustment and spontaneous decision by setting the optimal decision of decision-makers, so it has obvious advantages over other research methods in analyzing the effect of policy changes. Using CGE model to analyze the trust mechanism of individual consumers in rural financial market dynamically, we can classify and refine the production sector or individual consumption factors, link the resources and environment variables with relevant departments, and obtain the production function or consumption function without changing the basic assumptions and structure of the model. This paper analyzes the formation and evolution of individual consumer trust mechanism in rural financial market and puts forward some suggestions for its development.

CGE is a model based on general equilibrium theory, which can calculate the equilibrium solution, involving three aspects of interpretation.

Computability means taking the real economic data as the input and calculating the equilibrium solution.

Generality means multiple industries and multiple subjects, such as government, family, industry, and trading partners; general behavior equation, utility maximization, and profit maximization.

Equilibrium means demand = supply. Through price changes, the product and factor markets can be cleared.

Because of the above characteristics of CGE, this method can be easily applied to research on the trust mechanism of individual consumers in rural financial. According to the CGE method, we analyze the constraints of the rural financial consumer market and then introduce the trust mechanism of individual consumers in the financial market, extending the CGE model. Besides, we analyze the relationship between rural customers' perception of financial service quality, customer satisfaction, and customer trust and set the variables and conditions of the CGE extended model to judge whether the rural financial consumer market is in a stable development state. This paper determines the credit risk evaluation index, introduces the improved analytic hierarchy process, evaluates the credit risk of individual consumers in rural financial market, determines the advantages of the trust mechanism of individual consumers in rural financial market, and makes a dynamic analysis of the trust mechanism of individual consumers in rural financial market.

The contributions of this paper can be described as follows:

(1) In this paper, the single variable evolutionary fuzzy clustering algorithm is used to analyze the orthogonal eigenvector solutions of individual consumers; the big data of individual consumers under the mode of perceived trust is automatically clustered, so as to obtain the fuzzy analogy function of individual consumers in the rural financial market; and finally the prediction value of consumer trust is obtained.

(2) This paper analyzes the constraints of the rural financial consumer market, introduces the trust mechanism of individual consumers in the financial market, extends the CGE model, and analyzes the relationship between rural customers' perception of financial service quality, customer satisfaction, and customer trust.

(3) This paper determines the credit risk evaluation index, introduces the improved analytic hierarchy process, evaluates the credit risk of individual consumers in rural financial market, and determines the advantages of the trust mechanism of individual consumers in rural financial market.

The remainder of this paper is organized as follows. Section 2 introduces the perceived trust model of individual consumers in rural financial market. Section 3 discusses the dynamic CGE model of individual consumer trust mechanism in rural financial market. Section 4 discusses experiment and analysis. Section 5 presents the conclusions of the study.

2. The Perceived Trust Model of Individual Consumers in Rural Financial Market

The steady improvement of the overall income level of rural residents, the continuous increase of disposable financial consumption income, and the continuous updating of consumption concept set higher requirements for the diversification of rural financial consumption products and financial services [4]. However, the products in the market are uneven, which requires consumers to have perception and trust in the rural financial market, so it is necessary to improve the quality of products. In this paper, single variable evolutionary fuzzy clustering algorithm is used to analyze the orthogonal eigen vector solutions of individual consumers. Assuming a single component of individual consumers' perceived trust ε_k, the individual consumer feature $x(t_{n+1})$ decomposition model is obtained:

$$\begin{aligned} VV^T &= I_M, \\ \sum &= \operatorname{diag}(\sigma_1, \sigma_2, \ldots, \sigma_m) \in R^{m\times m}, \\ VV^T &= I_M, \\ \sum &= \operatorname{diag}(\sigma_1, \sigma_2, \ldots, \sigma_m) \in R^{m\times m}, \end{aligned} \tag{1}$$

where $R^T R$ represents the continuous statistical characteristic quantity of the personal consumer information sampling sequence $R^{m\times m}$. Since there is a surplus probability in the statistical process, the size of the distribution characteristic value of the personal consumer is ranked:

$$\sigma_1 > \sigma_2 > \sigma_3 > \cdots > \sigma_{s+1} > \sigma_m. \tag{2}$$

Under the evolutionary game, the new characteristic sequence of individual consumers in rural financial market is as follows:

$$X_{m+1}(m) = X_{k+1}(m) \pm \sqrt{\left(d_m(0)e^{\lambda_1}+\right)^2 - \sum_{i=1}^{m-1}\left[X_{m+1}(i) - X_{k+1}(i)\right]^2}. \tag{3}$$

Under the condition of local stability analysis, the quantitative prediction value of individual consumers is obtained as follows:

$$x(t_{n+1}) = X_{m+1}(m). \tag{4}$$

The expected value$R^T R$ and standard deviation ε_k in the Gaussian self-similar process of individual consumer sequence are set as$R^T R = 0$, $D_0 = 1, = 1$, and $k = 1, 2, \ldots, n-1$, respectively. After reconstructing the phase space of the evolution data sequence of individual consumer, the fuzzy clustering method is used to automatically cluster the big data of individual consumer under the perceptual trust mode, and a group of new time series that replace individual consumer are mined, The results are as follows:

$$\begin{aligned} D_k &= \frac{D_{k-1} - N_{k-1}^2}{D_{k-1}}, \\ \phi_{kk} &= \frac{N_k}{D_k}, \\ \phi_{kj} &= \phi_{k-1,j} - \phi_{kk} \cdot \phi_{k-1,k-j}. \end{aligned} \tag{5}$$

In the Gaussian distribution N(0,1) of individual consumers, an initial value of x_0 is generated. Based on the initial value, the trust perception is iteratively calculated. Suppose that the discrete characteristic component of individual consumers' demand information in the perceived trust mode is $s_i = (x_i, x_{i+\tau}, \ldots, x_{i+(m-1)\tau})^T$, and the above formula is a short-term discrete information distribution set, which is embedded in the embedded space of individual consumers in the rural financial market. The distribution function of the state set of individual consumers in the rural financial market under the mode of perceived trust is obtained as follows:

$$\frac{\mathrm{d}\mathbf{z}(t)}{\mathrm{d}t} = F(\mathbf{z}). \tag{6}$$

In order to ensure that the effective probability density of individual consumers in rural financial market is high, the appropriate $s_i = (x_i, x_{i+\tau}, \ldots, x_{i+(m-1)\tau})^T$ and $s_i = (x_i, x_{i+\tau}, \ldots, x_{i+(m-1)\tau})^T$ are selected according to the above formula:

$$R_1 = \{X_1, X_2, X_3, \ldots, X_d\}^T. \tag{7}$$

Through multiple comparison analysis, the correlation function of individual consumers in rural financial market is obtained as follows:

$${R_1}^T R_1 = \{X_1, X_2, \ldots, X_m\}\{X_1, X_2, \ldots, X_m\}^T. \tag{8}$$

A pre-estimator is set to calculate the best decomposition value V_1^T of individual consumers in rural financial market:

$${R_1}^T R_1 = V_1 \sum V_1^T. \tag{9}$$

Assuming that $\mathbf{x}_j$ is an $\mathbf{x}_i$ nearest neighbor function, this paper uses earnings management method to make fuzzy prediction of individual consumers from $L+1$ to $2L$ dimensions. In this process, X_m in the phase space is taken as the central point, and the fuzzy analogy of individual consumers in the rural financial market under the mode of perceived trust is as follows:

$$\begin{aligned} R_2^T R_2 &= V_2 \sum_2 V_2^T, \\ R_2 &= \{X_{d+1}, X_{d+2}, \ldots X_{d+m}\}^T, \\ R_2^T R_2 &= \{X_{d+1}, X_{d+2}, \ldots X_{d+m}\}\{X_{d+1}, X_{d+2}, \ldots X_{d+m}\}^T. \end{aligned} \tag{10}$$

In the formula, the wide area characteristic component of individual consumers in rural financial market is as follows:

$$V = [V_1, V_2, \ldots, V_m] \in R^{m\times m}. \tag{11}$$

Through univariate analysis of variance, according to the evolution characteristics of predicted values X_m and X_k, the predicted values of consumer trust are X_{m+1} and X_{k+1}.

3. Dynamic CGE Model of Individual Consumer Trust Mechanism in Rural Financial Market

3.1. Dynamic Analysis of Trust Mechanism of Individual Consumers. The traditional CGE model is based on the pure economic system, so SAM accounting framework, as the database of CGE model, only describes the pure economic aspects of production, consumption, and other activities, excluding the resource and environmental losses caused by economic activities and corresponding protection activities [5]. In fact, if we make proper use of resources and environment in economic activities and take timely measures to protect rural resources and control pollution, the interaction between resources, economy, and environment will be in a virtuous circle. Therefore, a completely balanced state is the stable development of rural financial consumption market. However, there are still many restrictive factors in the rural financial consumption market, like the following:

(1) It is difficult for low coverage of rural financial services and relatively single financial products to meet the diversified needs of rural consumer groups for financial services. First, the service coverage of financial institutions is relatively narrow. Rural financial service coverage refers to the level and degree of financial services such as deposit, loan, settlement, and financial management provided by financial institutions for enterprises and farmers in rural areas. It is the main quantitative index to evaluate the status of rural financial services. Due to the fact that quite a number of banking financial institutions have realized the strategic transfer from villages and towns to large- and medium-sized cities, the underdeveloped rural areas have become the areas with extremely weak financial strength. Second, there are few kinds of suitable financial service products. The design of financial consumer products for rural residents by rural financial institutions is far behind

the current needs. Relying on the villages and towns, the financial services of financial institutions in the vast rural areas still stay at the level of traditional business such as deposit, means of production loan, and general settlement, which makes the financial supply and farmers' demand unable to smoothly connect, thus restricting the normal start of rural financial consumer market. Third, the appropriate financial products are not yet mature. Financial consumer products lack proper standards and mislead financial consumers to buy financial products from time to time.

(2) The low efficiency and fairness of rural financial services cannot meet the diversified needs of rural consumer groups. One is the restriction of loan approval authority [6]. A considerable number of rural financial institutions lack sufficient approval authority due to the collection of loan authority, which makes it more difficult for rural financial consumers to raise funds, thus missing the best opportunity for investment or production. The second is the restriction of financial resources allocation. Quite a number of banking financial institutions lack sufficient attention to all kinds of loans in rural areas for their own economic interests and credit risk prevention [7, 8]. The third is the restriction of payment and settlement system. Due to the backward construction of rural financial payment and settlement service system, the low level of rural financial services, and the lack of financial consumer products and financial publicity, farmers have less knowledge and use of modern financial knowledge and investment and financial products, and it is difficult for the relatively weak rural financial consumer groups to enjoy modern financial services [9].

Therefore, in order to highlight the coverage of rural financial services and the role of efficiency and fairness of rural financial services in farmers' production activities, we introduce the trust mechanism of individual consumers in the financial market and expand the CGE model; that is, besides land, capital, and labor, we introduce the virtual element of "individual consumer trust," as shown in Figure 1.

In the multilayer nested structure shown in Figure 1, the first level first synthesizes the intermediate input and initial factor input (added value) of nonindividual consumer trust into the total output of the department in the form of CES function. In the second level, the intermediate input of nonindividual consumer trust is decomposed into various intermediate inputs according to Leontief structure; that is, there is no substitutability between inputs, and the added value of the same level is decomposed into labor force and generalized capital (including capital, land, individual consumer trust, and natural endowment) according to CES structure. In the third level, labor force is further decomposed into agricultural labor force, industrial workers, and technicians with CES structure, and generalized capital is further decomposed into individual consumer trust and capital land endowment with CES structure. In the fourth level, the individual consumer trust is divided into the input of various individual consumer trust products. The model assumes that there is a certain substitution possibility between different individual consumer trust inputs (such as the substitution of coal, oil, and natural gas), so all kinds of individual consumer trust inputs synthesize individual consumer trust with CES structure. At the same time, capital land endowment is decomposed into capital land and natural endowment. As a necessary and irreplaceable input factor, natural endowment enters the equation in a fixed proportion and is combined with capital land in the form of Leontief function. Finally, capital land is decomposed into capital and land in CES structure (this study is from the perspective of individual consumers and does not involve the issue of energy output).

3.2. Variable Setting and Reduction Conditions of CGE Extended Model. Customers with trust can bring profit growth. With the successive establishment of rural banks and the increasing number of rural financial outlets of banks and credit enterprises, the competition in rural financial market will be fiercer and fiercer [10–12]. Therefore, how to improve the quality of rural financial services, promote the trust of rural customers, and retain customers is an important issue for financial enterprises. Therefore, it is necessary to start from the relationship between whether the customer has trust, customer satisfaction, and service quality and establish the relationship model of rural customers' perception of financial service quality, customer satisfaction, and customer trust according to the existing theoretical research results and relevant research experience, as shown in Figure 2.

The income of rural residents mainly comes from the factor income of labor and capital, as well as the transfer payment of government, enterprises, and foreign countries. After paying personal income tax, residents use disposable income for saving and consumption, which is reflected in commodity market equilibrium, factor market equilibrium, government budget equilibrium, balance of international payments, and balance of savings and investment, mainly describing nominal and real GDP and social welfare. In the dynamic module, capital accumulation, population, and labor force changes are introduced to make the model dynamic. From the macro point of view, in order to make the model achieve a stable and balanced growth path [13, 14], this paper sets the growth rate of the main exogenous variables to be consistent with the population growth rate

$$H_K = \frac{(1 - \mathrm{dep}_t) \cdot K \cdot K_a + \mathrm{ENTSAV}_t}{\sum_t K^{t+1} \cdot W^{\mathrm{zeta}} \cdot K^t}, \tag{12}$$

where K^{t+1} is the capital supply in t+1 period, dep_t is the composite investment price K_a in t period, $w_k t$ is the capital price in t period, *zeta* is the elastic parameter of investment distribution, ENTSAV_t is the household savings in t period, and K^t is the labor supply in t period.

Because the approximate conditions of the model are that the variable is stable and balanced, it is dynamic. If the

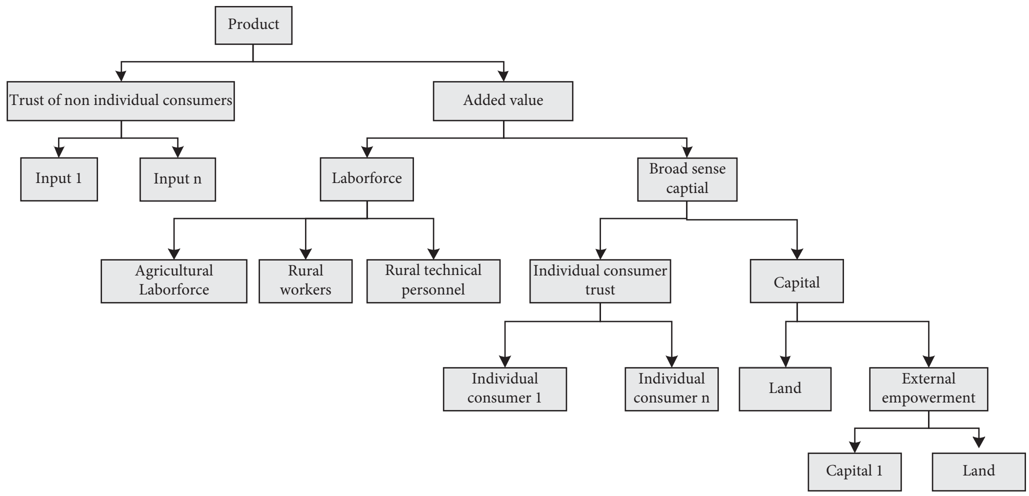

Figure 1: CGE extended structure.

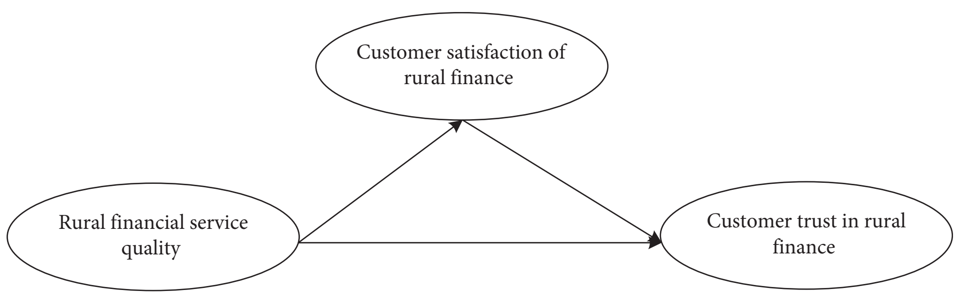

Figure 2: The relationship between rural customers' perception of financial service quality, customer satisfaction, and customer trust.

model has only one solution, it can be judged that the rural financial consumption market in the region is developing steadily.

3.3. Credit Risk Assessment of Individual Consumers in Rural Financial Market. There are two basic relationships in human economic activities: the relationship between man and nature and the relationship between man and man. There are both cooperation and conflict between people. In order to effectively resolve conflicts, promote cooperation, and improve the welfare level of social members, human beings have invented various systems to regulate their own economic behavior in the long-term evolutionary game. In any transaction, if the buyer does not trust the quality and quality of the products provided by the seller, or the seller does not trust the buyer's means of payment, there is no way to conduct the transaction. In this sense, without trust, there will be no transaction and no market [15]. However, trust must be mutual. Therefore, after determining the degree of trust of individual consumers in the market, it is necessary to determine the degree of trust of the market subject, that is, the enterprise to individual consumers, that is, to determine the credit risk of consumers.

The enterprise is to determine the credit risk evaluation index as the premise to evaluate the credit risk of customers. Credit risk index can comprehensively evaluate the comprehensive level of customers and credit management. Customer credit risk assessment indicators follow the principles of comprehensiveness, scientificity, practicability, and operability and the combination of quantitative and qualitative. It mainly investigates customer credit status from the aspects of trading environment, mortgage, ethics, capital, and rural financial market capabilities The specific level is shown in Table 1.

In Table 1, regarding environment, the law of social and economic development and the special changing market transactions in a certain region affect the solvency of customers, mainly selecting the macro environment and medium environment that affect enterprises. With respect to mortgage, customers use their assets as guarantee for repayment, and the main indicators are mortgage and guarantee under customer market transactions. As for morality, the possibility of payment commitment to market transaction is evaluated according to customer's previous credit record. Because of the special needs of enterprises, the index is directly selected by obtaining the information resources of customer market transactions. Concerning capital, the financial status of customers is analyzed according to the financial statements of enterprises, which is the basic guarantee for the repayment ability of customers' market transactions. In respect of ability, the customer's market transaction payment ability is judged according to the customer's business status and asset status. The main selected indicators are financial indicators reflecting the profitability and solvency of enterprises.

Table 1: Credit risk assessment index system.

Target layer	Criterion layer	Index layer
Credit risks	Environment	Enterprise development prospects, technical factors, social and cultural factors, economic factors, industry nature, political factors, legal factors, and other factors.
	Mortgage	Customer mortgage.
	Capital and capacity	Speed ratio, cash ratio, asset liability ratio, return on assets, net profit rate of sales, etc.
	Character	Public information, litigation for breach of contract, execution and scheduling, illegal transactions, on-time repayment rate of loans, cumulative arrears ratio, average payment days, and arrears ratio.

Taking the credit risk in Table 1 as the judgment index, this paper introduces the improved AHP method (analytic hierarchy process) to evaluate the credit risk of individual consumers in rural financial market, that is, customers. The algorithm uses the concept of optimal transfer matrix to improve AHP, so that it can naturally meet the consistency requirements and directly calculate the weight value, that is, the credit risk value. The specific steps are as follows:

(a) Set up credit risk evaluation index system based on market transaction. According to the customer credit evaluation index system, set up the evaluation index set; refer to Table 1.

(b) The judgment matrix is established. After establishing the matrix according to the credit risk evaluation index system, the weight of each level index in the customer credit risk evaluation index system is determined by AHP. By comparing the two elements, the importance of the elements in the hierarchy relative to a certain factor in the upper level is clarified, and the judgment matrix of comparing the two factors is constructed. The judgment matrix of two factors for a certain criterion is calculated as follows:

$$B = \left(b_{ij}\right)_{\min},$$
$$b_{ij} = \frac{b_{jk}}{b_{jk}}, \quad i, j, k = 1, 2 \ldots, n, \tag{13}$$

Where b_{ij} is the proportional scale of the importance of factors B_i and B_i relative to criterion U.

C. Based on the improved AHP method, calculate the weight of each level evaluation index. After using the improved AHP method to calculate the index weight, there is no need to do consistency test. Firstly, the established judgment matrix is transformed to obtain the quasi-optimal matrix B^* (as shown in Figure 3). The square root method is used to solve the eigenvector of the modified B^*. Multiply the elements of the judgment moment by lines to get the following formula:

$$N_i = \prod_{j=1}^{n} b_{ij}, \quad i = 1, 2, 3 \ldots n. \tag{14}$$

Open the n-th root of the product to calculate $P_i = N_i^{1/n}$. Normalize the root vector $P = [P_1, P_2, \ldots, P_n]^Q$ to get the ranking weight vector P.

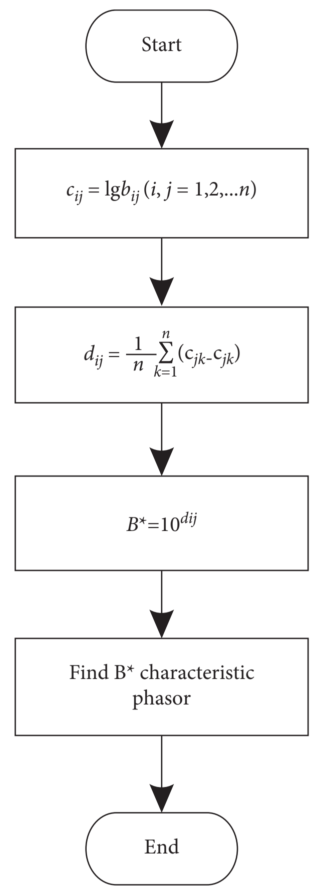

Figure 3: Credit risk assessment process of individual consumers in rural financial market.

Credit risk assessment process of individual consumers in rural financial market is shown in Figure 3.

$$p = \frac{P_i}{\sum_{j=1}^{n} P_j}. \tag{15}$$

At this time, P means the credit risk value of individual consumers in rural financial market. The higher the risk value is, the lower the trust degree of enterprises in individual consumers is. The abovementioned CGE expansion model has many variables, and the trust mechanism of individual consumers in the rural financial market is limited. On the contrary, the trust mechanism of individual consumers in the rural financial market is more superior.

4. Experimental Analysis

4.1. Data Sources and Basic Information. This study takes the customers of rural commercial banks, credit cooperatives, some rural banks, and other financial service institutions in a province as the survey objects. The descriptive statistical data obtained show that the basic characteristics of the survey objects, such as age, sex ratio, education level, and family income, are consistent with the reality, with a normal distribution, and their Cronbach's alpha coefficient is 53.53%. The rotation factor load of each index item exceeded 0.7, and the scale had good validity ($P \leq 0.001$). The Pearson correlation coefficients of the three dimensions were lower than 0.5, and there was no serious collinearity between the dependent variable and the independent variable.

Based on this, this paper uses SPSS17.0 software to test the relationship between trust, customer satisfaction, and service quality. The test results are shown in Table 2.

Table 2 shows that from the F value of regression equation, they all reached the extremely significant degree ($P < 0.001$). In rural financial services, customer's attitude satisfaction is significantly positively affected by rural financial service's tangibility, responsiveness, certainty, and empathy; result satisfaction is significantly positively affected by rural financial service's tangibility and responsiveness; process satisfaction is significantly positively affected by rural financial service's tangibility, reliability, and responsiveness. Environmental satisfaction is significantly positively affected by the tangibility and certainty of rural financial services, while capability satisfaction is significantly positively affected by the tangibility, responsiveness, and certainty of rural financial services, Empathy has a positive impact on attitude satisfaction, which makes customers have trust.

Using the descriptive statistical analysis method in Table 1, this paper makes a linear analysis of individual consumer trust in rural financial market under the mode of perceived trust.

Using p_i, one of the above samples belongs to the possibility of available C_i, and s_i/s is used to estimate it. Suppose that the set v with attribute A and v different values can be equally divided into subsets A by attribute A, in which S_j includes such part of the samples in S, and all of them have the same value of a_j on A. Then, when A is selected as the test attribute, some subsets will correspond to the node branches of set S. If s_{ij} is the specific number of samples of class C_i in subset s_j, then according to the expected value information formula divided into subsets by A, there is

$$E(A) = \frac{\sum\left(s_{1j} + \cdots + s_{mj}\right) * I\left(s_{1j} + \cdots + s_{mj}\right)}{s}. \tag{16}$$

Thus, under different sample models from 2011 to 2020, with the same sample expectation as the constraint, the analysis results of individual consumer trust in rural financial market are obtained, as shown in Table 3.

According to the analysis results of trust bias distribution and descriptive comparison in Table 1, the above experimental results are available, and the dynamic CGE model of individual consumer trust mechanism in rural financial market is more robust.

4.2. Discussion and Suggestions

(1) Most dimensions of rural financial service customer satisfaction are positively correlated with customer trust. Specifically, the degree of customer's attitude trust in rural financial services is mainly positively affected by attitude satisfaction and result satisfaction, and the degree of behavior trust is mainly positively affected by environment satisfaction and ability satisfaction. This shows that the more satisfied the rural customers are with the service attitude of financial services, the more consistent the service result is with the customer's expectation, and the stronger the customer's preference for the service provider is. The more satisfied the customers are with the service environment and serviceability of financial institutions, the higher the degree of trust is, and the more willing the customers are to choose the products and services they want to build again. From the perspective of the effect of rural financial service quality on customer loyalty, rural customers' attitude trust is positively affected by the tangible benefits and responsiveness of financial services, and their behavior trust is mainly affected by reliability and certainty, while rural financial customers' cognitive trust is not significantly affected by service quality.

(2) There is a positive correlation between financial service quality and customer trust. Specifically, the impact of customer attitude loyalty is mainly customers' perception of financial service tangibility and responsiveness, and the impact of behavior loyalty is mainly customers' perception of financial service reliability. This shows that the better the hardware facilities of rural financial enterprises are, the higher the service efficiency is, and the easier the customers will have a good reputation for the financial service providers. The more stable the financial products and reliable the services provided by rural financial enterprises are, the more customers tend to choose the enterprise repeatedly and recommend it to others.

The steady development of the rural financial consumer market is inseparable from the service and support of the rural finance, and also inseparable from the protection of financial consumers' rights and interests by government functional departments. The protection of financial consumers' rights and interests highlights the cultivation and perfection of the rural financial consumer market, and the development of the rural financial consumer market can promote the prosperity and stability of the rural financial industry, which have a positive impact on each other.

4.2.1. Market

(1) We will improve the rural financial service system and expand the coverage of rural financial services. Based on the existing organizational framework of rural financial institutions, we should speed up the construction of a modern rural financial service

Table 2: Test results of the relationship between trust, customer satisfaction, and service quality.

Variable	The results are satisfactory	Process satisfaction	Satisfied with the environment	Ability satisfaction	Satisfied with attitude
Gender	0.048	0.123	−−0.007	0.013	0.022
Age	−0.001	−0.017	−0.017 ****	0.045	0.017
Degree of education	−0.07	−0.069	0.069	0.069	0.069
Income	0.046	0.046	0.046	0.046	0.046
The tangibility of financial services	0.289****	−0.335****	−0.135**	−0.250****	−0.205****
Reliability of financial services	0.179	0.07	0.217****	−−0.07	−−0.07
Responsiveness of financial services	0.117****	0.017	0.117***	−0.017	−0.017
Certainty of financial services	0.169 ***	−0.069	0.069	0.059	0.049
Empathy of financial services	27.152****	16.045****	19.486***	14.546****	13.146****
F	0.635	0.525	0.515	0.545	0.485
R	0.357	−−0.257	−−0.217	−−0.227	−−0.210

*represents $P < 0.05$, **represents $P < 0.01$, **represents $P < 0.005$, and **represents $P < 0.001$.

Table 3: Analysis results of individual consumer trust in rural financial market.

Year	2011–2015	2016–2018	2019–2020
2011–2015	1		
2016–2018	0.0455	1	
2019–2020	0.0452**	0.0523*	1

*means significant at the level of 0.05.

system with sound functions, reasonable layout, orderly competition, and efficient services. First, further improve the rural financial service system, clear positioning, strengthen supervision, and encourage the development of various ownership financial organizations. We should continue to cultivate and develop new rural financial institutions such as rural banks, enhance the ability of sustainable support for agriculture, and constantly improve the coverage of financial services in rural areas. Second, accelerate the development of various forms of new rural financial organizations and regional small- and medium-sized banks mainly serving rural areas, and vigorously develop microfinance and microfinance services. At the same time, small rural financial organizations are allowed to integrate funds from formal financial institutions. Third, we should further improve the legal system of rural finance, standardize the nongovernmental financial behavior, absorb social capital and nongovernmental funds, and meet the needs of rural economic development.

(2) Standardize rural financial consumer products to meet the multilevel consumption needs of rural areas. There are not only differences in urban and rural financial consumption, but also different levels of consumption. Urban financial services can provide housing, vehicles, and personal consumption loans for urban residents, while rural finance is very weak in this aspect. To standardize rural financial consumer products, it is necessary to introduce a third-party evaluation agency to evaluate the risk of rural financial consumer products. When promoting financial products, we should follow the principle of risk matching, prohibit promoting or misleading rural financial consumers to buy financial products that are inconsistent with their risk tolerance, and effectively protect the rights and interests of financial consumers. In order to meet the diversified needs of rural residents for financial consumer products, rural financial institutions can combine the actual situation of local rural areas to launch simple and practical financial consumer products.

(3) With the development of rural economy and the acceleration of the process of urban-rural integration, the financial service needs of rural residents are increasingly diversified and specialized. To improve the rural financial consumption system and expand the rural financial consumption market, we should relax the market access conditions and encourage the emergence and growth of various types of financial consumption, especially the development of durable consumer goods credit. Second, we should make full use of the opportunity of "finance going to the countryside," actively carry out the propaganda of financial consumption knowledge, enhance the financial consumption awareness of rural residents, update the traditional consumption concept, and transform the potential consumption awareness into the actual consumption behavior. Third, we should tap the market potential and broaden the field of financial consumption services. Financial institutions should establish the overall concept and development concept and extend the field of financial consumption services from the city to the vast rural areas so that the vast number of rural residents can enjoy equal financial consumption services with urban residents. Fourth, we should improve the management of financial consumption, introduce financial support and guarantee mechanisms, and

give financial assistance to specific types of financial consumption.

5. Consumers

(1) We will improve the laws related to the protection of financial consumers' rights and interests. First, improve the relevant laws, further clarify the rights and obligations of financial consumers and financial institutions, and introduce measures related to the rights and interests of rural financial consumers. Second, put consumers' rights and interests into the regulatory objectives, and establish the legal status of financial regulators in the protection of financial consumers' rights and interests. Third, to further improve the information disclosure system, it is necessary for financial institutions to comprehensively, accurately, and timely disclose their product and service information.

(2) Establish financial consumer protection institutions. First, strengthen coordination of rights protection. Set up special financial consumer protection institutions in the regulatory department and corresponding organizations in the financial industry association. Through multilevel organizations, it plays an active role in rural financial consumer education, consumer risk warning, and handling financial consumer complaints. Second, strengthen the education of safeguarding rights. It is necessary for regulatory authorities, industry associations, and financial institutions to actively carry out various forms of financial knowledge publicity and education for rural financial consumers. While enriching the financial knowledge of rural consumer groups, we should further improve the legal awareness of rural financial consumers.

(3) Improve the financial consumer complaints platform. The protection and maintenance of the rights and interests of rural financial consumers need an appropriate complaint and handling platform. First, set up a special department for handling consumer complaints. Establish a consumer complaint database; classify, investigate, and mediate in consumer complaints; and regularly analyze information to identify potential problems, to provide a reference for the formulation of relevant laws and regulations. Second, establish consumer self-discipline organizations in the banking industry to coordinate disputes. Third, improve the compensation and punishment system. Give consumers the right to recover from financial institutions after the event, and improve the compensation to consumers and the punishment to financial institutions.

6. Conclusion

This paper introduces the CGE model, uses the fuzzy clustering algorithm of univariate evolution, obtains the fuzzy analogy function of individual consumers in the rural financial market, and combines them with the improved AHP method to analyze the relationship between rural customers' perception of financial service quality, customer satisfaction, and customer trust, to determine the superiority of the trust mechanism of individual consumers in the rural financial market. The dynamic analysis of the trust mechanism of individual consumers in the rural financial market provides new ideas for the steady development of rural financial consumer market.

7. Future Research Directions

(1) In this paper, the elements of the consumer trust-building mechanism need to be refined and supplemented. For example, when consumers purchase products, the calculation of the benefits brought by the products they choose and the risks brought by the failure of choice should also belong to a new mechanism. In this way, the study of consumer trust mechanisms will be more perfect.

(2) The consumer trust mechanism studied in this paper is based on the research background of China's home appliance industry, but in fact many industries similar to the home appliance industry have great similarities. The process and conclusion of this study, to a certain extent, are also applicable to these industries. Based on the research method of this paper, it is feasible to study the consumer trust mechanism of other similar industries.

Data Availability

The data used to support the findings of this study are available from the corresponding author upon request.

Conflicts of Interest

The authors declare that they have no conflicts of interest.

Acknowledgments

This work was supported by the Education and Scientific Research Project of Young and Middle-Aged Teachers of Fujian Department of Education (Social Science) (Grant no. JAS19578).

References

[1] R. Sousa, C. Horta, R. Ribeiro, and E. Rabinovich, "How to serve online consumers in rural markets: e," *Business Horizons*, vol. 63, no. 3, pp. 351–362, 2020.

[2] L. Yan, K. Hong, K. Chen, H. Li, and L. Liao, "Benefit distribution of collectively-owned operating construction land entering the market in rural China: a multiple principal–agent theory-based analysis," *Habitat International*, vol. 109, no. 2, Article ID 102328, 2021.

[3] T. Potocki and M. Cierpiał-Wolan, "Factors shaping the financial capability of low-income consumers from rural regions of Poland," *International Journal of Consumer Studies*, vol. 43, no. 2, pp. 187–198, 2019.

[4] E. Krivosheya, “The role of financial innovations in consumer behavior in the Russian retail payments market,” *Technological Forecasting and Social Change*, vol. 161, no. 7, Article ID 120304, 2020.
[5] X. Li, X. Yao, Z. Guo, and J. Li, “Employing the CGE model to analyze the impact of carbon tax revenue recycling schemes on employment in coal resource-based areas: evidence from Shanxi,” *The Science of the Total Environment*, vol. 720, no. 10, Article ID 137192, 2020.
[6] L. J. Brown, G. M. Jones, and M. J. Bond, “E.-health: Psychosocial challenges for South Australian rural mental health consumers,” *Rural and Remote Health*, vol. 19, no. 3, pp. 174–184, 2019.
[7] M. R. Mohapatra, N. S. Moirangthem, and P. Vishwakarma, “Mobile banking adoption among rural consumers: evidence from India,” *American Business Review*, vol. 23, no. 2, pp. 300–315, 2020.
[8] X. Cui, J. J. Xiao, and J. Yi, “Employment type, residential status and consumer financial capability: evidence from China household finance survey,” *Singapore Economic Review*, vol. 64, no. 1, pp. 57–81, 2019.
[9] K. Mahasuar and S. Patnaik, “Strategic innovations in distribution channels - an emerging market perspective and case studies from consumer packaged goods (CPG) industry of India,” *Strategic Direction*, vol. 35, no. 1, pp. 13–16, 2019.
[10] B. Rokicki, E. A. Haddad, J. M. Horridge, and M. Stpniak, “Accessibility in the regional CGE framework: the effects of major transport infrastructure investments in Poland,” *Transportation*, vol. 26, no. 48, pp. 747–772, 2020.
[11] P. Qin, P. Chen, X.-B. Zhang, and L. Xie, “Coal taxation reform in China and its distributional effects on residential consumers,” *Energy Policy*, vol. 139, no. 15, Article ID 111366, 2020.
[12] I. Opitz, F. Zoll, I. Zasada, A. Doernberg, R. Siebert, and A. Piorr, “Consumer-producer interactions in community-supported agriculture and their relevance for economic stability of the farm - an empirical study using an Analytic Hierarchy Process,” *Journal of Rural Studies*, vol. 68, no. 5, pp. 22–32, 2019.
[13] Y. Weng, S. Chang, W. Cai, and C. Wang, “Exploring the impacts of biofuel expansion on land use change and food security based on a land explicit CGE model: a case study of China,” *Applied Energy*, vol. 236, pp. 514–525, 2019.
[14] R. Langarita, R. Duarte, G. Hewings, and J. Sánchez-Chóliz, “Testing European goals for the Spanish electricity system using a disaggregated CGE model,” *Energy*, vol. 179, pp. 1288–1301, 2019.
[15] B. Lin and Z. Jia, “Economic, energy and environmental impact of coal-to-electricity policy in China: a dynamic recursive CGE study,” *The Science of the Total Environment*, vol. 698, no. 1, Article ID 134241, 2019.

Hindawi
Scientific Programming
Volume 2023, Article ID 9795181, 1 page
https://doi.org/10.1155/2023/9795181

Retraction

Retracted: Economic Market Fluctuation Model Based on Internet of Things Technology

Scientific Programming

Received 1 August 2023; Accepted 1 August 2023; Published 2 August 2023

This article has been retracted by Hindawi following an investigation undertaken by the publisher [1]. This investigation has uncovered evidence of one or more of the following indicators of systematic manipulation of the publication process:

(1) Discrepancies in scope
(2) Discrepancies in the description of the research reported
(3) Discrepancies between the availability of data and the research described
(4) Inappropriate citations
(5) Incoherent, meaningless and/or irrelevant content included in the article
(6) Peer-review manipulation

The presence of these indicators undermines our confidence in the integrity of the article's content and we cannot, therefore, vouch for its reliability. Please note that this notice is intended solely to alert readers that the content of this article is unreliable. We have not investigated whether authors were aware of or involved in the systematic manipulation of the publication process.

Wiley and Hindawi regrets that the usual quality checks did not identify these issues before publication and have since put additional measures in place to safeguard research integrity.

We wish to credit our own Research Integrity and Research Publishing teams and anonymous and named external researchers and research integrity experts for contributing to this investigation.

The corresponding author, as the representative of all authors, has been given the opportunity to register their agreement or disagreement to this retraction. We have kept a record of any response received.

References

[1] L. Zhai, "Economic Market Fluctuation Model Based on Internet of Things Technology," *Scientific Programming*, vol. 2022, Article ID 2296823, 11 pages, 2022.

Hindawi
Scientific Programming
Volume 2022, Article ID 2296823, 11 pages
https://doi.org/10.1155/2022/2296823

Research Article

Economic Market Fluctuation Model Based on Internet of Things Technology

Lu Zhai

Shenyang Normal University, Shenyang 110034, China

Correspondence should be addressed to Lu Zhai; zhailu@synu.edu.cn

Received 11 October 2021; Revised 11 November 2021; Accepted 26 November 2021; Published 4 January 2022

Academic Editor: Le Sun

In order to explore the impact of the Internet of Things technology on economic market fluctuations and the analysis effect of the Internet of Things technology on economic market fluctuations, this paper uses the Internet of Things algorithm to improve the economic fluctuation model. Moreover, this paper uses the Internet of Things algorithm to locate economic transactions and performs data processing to optimize the intelligent network system to improve the operating effect of the economic system. In addition, this paper improves the sensor node algorithm and proposes to use the weighted value of network node density to balance the positioning problem caused by the unbalanced distribution of network nodes in the detection area. Finally, this paper analyzes the market economy volatility model through the Internet of Things technology, combined with simulation experiments to explore the application of the Internet of Things technology in the economic market volatility model. Through experimental research, it can be known that economic market fluctuation models based on Internet of Things technology can play an important role in market economic analysis.

1. Introduction

In the face of the following development status: weak investment growth, lack of new consumption hotspots, poor international markets, and the existence of hidden risks in some areas, the extensive economic development model is no longer applicable. Therefore, the development of the national economy urgently needs to seek new economic growth points, and the transformation and upgrading of industries brooks no delay. The Internet of Things industry is just such a new economic growth point, which hides the impetus to reform the future economic form [1]. At the World Internet of Things Expo in November 2016, the Deputy Minister of Industry and Information Technology stated that China's economy is currently undergoing in-depth adjustments and reforms, and the manufacturing industry is accelerating toward mid-to-high end, and the Internet of Things will become a weapon to help Chinese manufacturing turn around. At present, China's manufacturing industry has completed a huge change from scratch and from a small path. It is currently becoming bigger and stronger. This process requires the support of various forces including material technology, information technology, and artificial intelligence. The Internet of Things uses sensor technology to connect with objects to identify products, optimize production processes, change warehousing and sales models, and improve management. This new technology will open up a new growth point and boost the improvement of the company's core competitiveness. As the Made in China 2025 strategy continues to advance and the 5G era is getting closer, the Internet of Things application field will be wider and the economic value will be greater and greater, which provides a powerful means for the transformation and transformation of traditional enterprises. Therefore, the development of the Internet of Things industry has become the main thrust of my country's economy to leapfrog the L-shaped growth stage [2].

Under the contemporary political, economic, and cultural background, the development of the Internet of Things industry has shown great vitality and competitive advantages and has been valued by many countries and regions. As the result of a new revolution in information technology, it further optimizes the production, distribution, exchange, and consumption of information resources, breaks through the time and space constraints of social production, and is a transformation from an industrial economy to a digital economy and an information economy. The Internet of Things technology penetrates into all aspects of the economy and society, which is conducive to the adjustment of the theoretical paradigm, existing mechanisms, policy trends, and actual operations of the original industry and is conducive to the emergence of new economic growth points and the formation of new economic forms of growth points on the basis of Internet of things [3].

The Internet of Things industry is a high value-added industry that is talent-intensive, knowledge-intensive, and technology-intensive, and its own development is in line with the advancement of the industrial structure. Vigorously developing the Internet of Things industry can achieve a higher level of industrial restructuring, optimization, and upgrading. At the same time, the Internet of Things industry occupies a higher position in the value chain with two core elements of information and technology and extends the industrial value chain through powerful radiation effects, penetrating and integrating with traditional industries. As a result, traditional industries have been given certain characteristics of the Internet of Things industry, which will help to improve the technical level, production efficiency, and product added value of traditional industries, so that the traditional industrial structure will continue to evolve to a higher level of industrial structure, and the industrial structure will be realized optimization and upgrade.

The development of the Internet of Things technology will cause mobile fluctuations in the economic market, so this paper analyzes the fluctuations of the Internet of Things technology on the economic market, and builds a corresponding intelligent model to provide a theoretical reference for subsequent economic forecasting and analysis.

2. Related Work

After combing through the research literature of the Internet of Things industry, it is found that due to the fact that the Internet of Things industry has not been standardized for a long time and related statistical data are relatively lacking, there has been no systematic research on the impact of the development of the Internet of Things industry on economic growth. However, the research on related aspects of the Internet industry has been relatively mature. Scholars have analyzed the mechanism of the Internet industry on economic growth from a theoretical and empirical perspective and measured the influence of the Internet industry on economic growth. The literature [4] empirically analyzed the pulling and supporting effects of the Internet industry on the national economy. The literature [5] conducted the cointegration test and the Granger causality test on the relationship between the information industry and economic growth and established a corresponding error correction model. Based on the unit root test and the cointegration test, the literature [6] used panel data of per capita real GDP to construct an individual time-point two-way fixed effect model to conduct an empirical analysis of the relationship between the development of the Internet industry and economic growth. The literature [7] used the spatial weight matrix of inter-regional trade correlation to systematically measure the spillover effect of the Internet industry on the production level, export level, and wage level of other regions. The results show that the development of the Internet industry has a positive effect on the growth of this region and other regions.

Literature [8] discusses the development status and development trend of the key technologies of the Internet of Things and, based on this, divides the Internet of Things industry into 4 development stages. The first stage is the initial application of radio frequency identification technology in the logistics, retail, and pharmaceutical fields; the second stage is the connection of things; the third stage is semi-intelligence; and the fourth stage is comprehensive intelligence. Literature [9] conducts theoretical research on the business model under the conditions of the Internet of Things, the Internet of Things industry and its operations, and the impact of the Internet of Things on traditional economics. Literature [10] believes that: “Internet of Things Economics is a science that studies how to obtain greater economic, ecological, and social benefits with a small investment.” Literature [11] takes the SCP paradigm in the theory of industrial organization as the Internet of Things in my country The analysis framework of the industry analyzes the market structure of the Internet of Things industry from four aspects: overall market characteristics, market concentration, entry and exit barriers, and product differentiation. Literature [12] analyzes the competitiveness of the Internet of Things industry from the perspectives of industrial policy, current situation, industrial chain, capital operation, market share and development space, and industrial promotion model. Literature [13] makes a theoretical and empirical analysis of the driving factors affecting the development of the Internet of Things industry with the help of the “Diamond Model” based on panel data from eight major cities. Literature [14] shows that the main driving factors affecting the development of the Internet of Things industry are the Internet of Things Industry supply and demand factors, government support factors, scale factors, development potential factors, and related industry factors.

3. Application Improvement of Internet of Things Algorithm in Economic Fluctuation Model

This article uses the Internet of Things algorithm to improve the economic fluctuation model. Internet of Things algorithms can not only locate economic transactions but also perform data processing, while optimizing intelligent network systems.

In the economic fluctuation model, the random distribution of network nodes will cause the distribution of network nodes in the target area to not meet the expected effect, and the distribution of nodes in the network will directly affect the positioning effect of DV-Hop in practical applications. The number of neighbors of a node in the network can reflect the local distribution of network nodes. From the local distribution of the network, the distribution of the entire network can be inferred. Furthermore, the distribution of neighbors of network nodes is also one of the factors reflecting the positioning effect. In general, the calculated value of the estimated distance between neighbor nodes can be reflected in two aspects: the total number of neighbor nodes and the total number of all neighbor nodes. The closer the nodes in the monitoring area are, the greater the number of nodes in common with each other, and the greater the ratio of the number of shared nodes to the number of nodes within the single-hop range of each other. On the contrary, the nodes within the single-hop range are more reliable. The farther, the fewer the number of shared nodes between each other, and the smaller the ratio of the number of shared nodes to the number of nodes within the communication radius of the two nodes. Based on the above analysis of the DV-Hop algorithm error, the DV-Hop algorithm will be further improved based on the previous research results of the researchers. The distribution of nodes in the target area in the network is used to assist in improving the positioning effect. The concepts of weighted value of network node density and distance correction factor are proposed. The weighted value of network node density refers to the ratio of the number of shared nodes between neighbor nodes in the network to the total number of nodes. The distance between neighbor nodes is calculated according to the weighted value of the node density of the node, and the distance between all nodes in the entire network is estimated through an iterative cumulative calculation method. Finally, the specific network node is obtained through an improved particle swarm algorithm.

In order to improve the positioning effect of the network and the accuracy of network node positioning as much as possible, this paper combines the existing improvement methods of traditional DV-Hop and the proposed network node density weighting value to improve the positioning effect of DV-Hop.

Since most WSNs are deployed in dangerous places, almost all large-scale WSNs use the method of randomly deploying nodes to initialize the entire network, and they are generally deployed by dedicated machines. The random deployment mechanism of the network creates a series of problems for the positioning of network nodes. In order to solve the problem of poor positioning effect caused by uneven distribution of network nodes, the network will calculate the node credibility of each beacon node. The credibility of anchor nodes is based on the actual number of hops between anchor nodes, the actual distance between anchor nodes, and the communication radius of the nodes to calculate the credibility between anchor nodes, and then all hop distances are weighted to obtain the final node credibility. The improved beacon reliability schematic diagram is shown in Figure 1.

The hop distances of all nodes to be located in the network are to be weighted based on the average hop distance of the beacon nodes. In order to reduce the error impact of the hop distance of the beacon nodes in the network on the network positioning, a further weighted adjustment will be made to the average hop distance of the anchor nodes in the network. As shown in Figure 2, the actual number of hops from anchor node A to anchor nodes B, C, and D is 2, 3, and 3, and the actual distance from beacon node A to beacon nodes B, C, and D is a, b, and c. The formula for calculating the credibility of the beacon node A is shown in the below formula:

$$R(A) = \frac{(a/2 + b/3 + c/3)}{R}. \tag{1}$$

By analogy, the general expression of the credibility of anchor node i in the network is given in the following formula:

$$\mathrm{Re}(i) = \frac{\sum_1^n \mathrm{Dis}(n)/R/\mathrm{Hop}_{AN}}{N}. \tag{2}$$

All beacon nodes in the network can rely on their own hardware advantages to achieve positioning. The distance between the beacon nodes can be the actual distance to each other according to the Euclidean formula. Then, the average hop distance HopDis of each anchor node in the network is obtained according to the calculation formula; that is, the actual distance is divided by each other's minimum hops. Finally, the modified average hop distance HopDis' of the anchor node is obtained according to the weighted value, and the calculation formula is shown in the following formula:

$$\mathrm{Hop\,Dis}' = \mathrm{Hop\,Dis} \times \mathrm{Re}. \tag{3}$$

In the classic DV-Hop, the node to be located takes the saved last hop distance information packet as the average hop distance, and the positioning error caused by this value method is still relatively large. In order to improve this situation, in the section, the average hop distance of the node to be located does not use a single beacon node as the reference node to calculate the hop distance of the node. Instead, a weighted average of all average hop distances within 3 hops of the node is used to determine the final hop distance. In order to highlight the importance of beacon nodes within the single-hop range of nodes, in the weight ratio, beacon nodes that can communicate directly account for 50% of the average hop distance during the calculation process, and the remaining nodes also account for 50%. The jump distance expression is given in the following formula:

$$\mathrm{Hop\,Dis}_A = \sum_1^n \frac{\mathrm{Hop\,Dis}(n)}{2n} + \sum_1^i \frac{\mathrm{Hop\,Dis}(i)}{2i}, \tag{4}$$

where $\mathrm{Hop\,Dis}_A$ is the average hop distance of the node to be located, HopDis(n) is the average hop distance of the neighbor nodes of unknown node A, and n means the number of anchor nodes within the single hop range of unknown node A.

After optimizing the average hop distance using the credibility weight obtained by the packet data, in order to reduce the positioning error of the algorithm, the characteristics of random deployment of network nodes are taken into consideration.

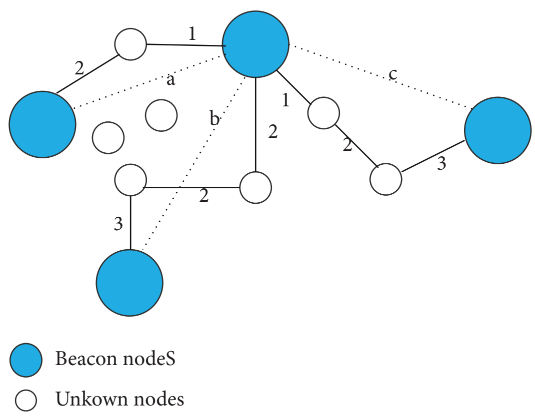

Figure 1: Route diagram from beacon node to each beacon node.

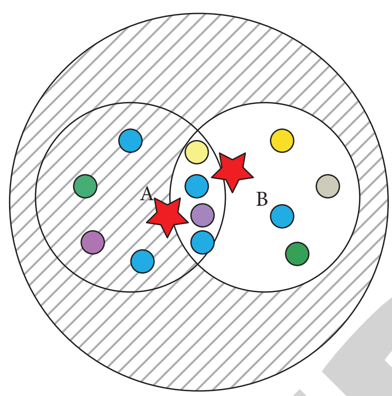

Figure 2: Distribution of neighbor nodes.

Node density represents the density of local nodes in the entire network. In the network, the area with the greater the density of nodes, the closer the broadcast path of the node is to a straight line, the higher the accuracy of the algorithm's positioning. In terms of node density, the classic DV-Hop also divides the node to be located and the nearest beacon node into the same type of node density. Their default node density is the same, and the hop distances derived from each other are also the same. It is proposed to use the weighted value of network node density De to balance the positioning problem caused by the unbalanced distribution of network nodes in the detection area. The weighted value of network node density refers to the ratio of the number of nodes that can be directly communicated in the network to the total number of nodes that can be directly communicated in the network Figure 2.

The node density-weighted value De(A,B) expressions of nodes A and B and the expressions of the distance correction factor are shown in equations (5) and (6):

$$De(A,B) = \frac{(N_A \cap N_B)}{\text{sum}(N_A, N_B)}, \tag{5}$$

$$De(A,B) = \frac{(1 - De(A,B))}{(1 + De(A,B))}, \tag{6}$$

where N_A and N_B, respectively, represent the number of nodes within the single hop range of nodes A and B, $N_A \cap N_B$ is the common neighbor node between nodes A and B, and $\text{sum}(N_A, N_B)$ represents the total number of neighbor nodes of nodes A and B. Neighbor nodes in the network can modify the estimated distance according to the weighted value of node density, thereby avoiding the same estimated distance between nodes in DV-Hop.

The nodes in the network are powered by batteries, and the limited energy of their own is taken into account. In the process of positioning, nodes should avoid complex calculations. When the energy of the node is limited, this calculation will greatly consume the energy carried by the node itself, thereby reducing the life of the node. The failure of a node will cause the topology of the network to change, and the routing of nodes between networks will also change accordingly. This change will lead to a change in the positioning effect, which is unacceptable for the entire network. In order to further reduce the energy loss caused by the node positioning, the linear calculation formula (7) with a smaller calculation amount is adopted when the inertia weight of the particle swarm algorithm is improved:

$$w = w_{\max} - t \times (w_{\max} - w_{\min}) \times (T_{\max} + t). \tag{7}$$

In the experiment, the inertia weight setting value is $w_{\max} = 0.95$, and $w_{\min} = 0.4$ is the ideal setting. The relationship between w and t in the formula is shown in Figure 3. The inertia weight of the network is linearly positively related to the number of experimental simulations. The update speed of the particles during the entire optimization process is the same, but the linear method can reduce the energy consumption during the arithmetic operation of the nodes.

In the RDD positioning algorithm, the algorithm uses the communication radius of the node to locate the node. The weighting factor is determined according to the node density within one hop range of the node. The network first calculates the density-weighted value of neighboring nodes in the network, multiplies the communication radius by the node density-weighted value to obtain the estimated distance between all neighboring nodes in the network, and then calculates the number of hops between nodes in the network according to the formula and the optimal path estimated distance for 2 hops. Finally, it calculates the estimated distance of all nodes in the network according to the iterative accumulation method. The specific steps are as follows:

(1) Neighbor node model:

In order to further use the network node density to improve the positioning accuracy of the algorithm, this paper proposes an RDD distance model, as shown in Figure 4.

When the nodes can communicate directly with each other, the distance between nodes i and j is shown in Formula (8) [15]:

$$\text{Distance}(i,j) = R \times \frac{(1 - R\,DD(i,j))}{(1 - R\,DD(i,j))}. \tag{8}$$

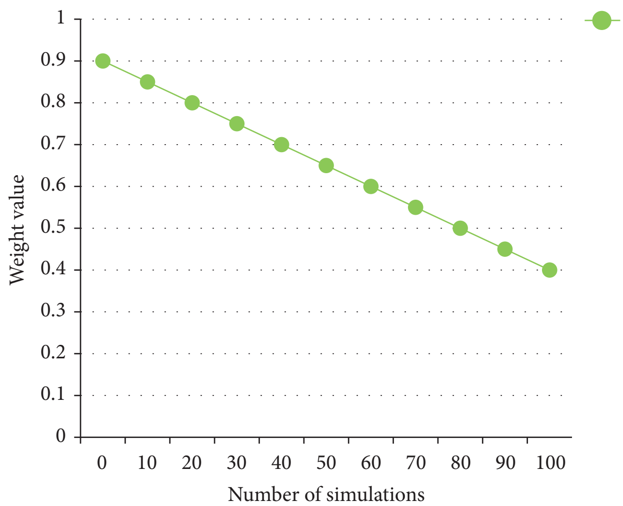

Figure 3: The relationship between simulation times and inertia weight.

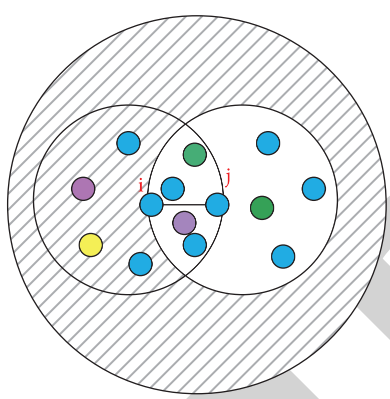

Figure 4: Neighbor node model.

Distance $(i.j)$ is the distance between node i and j, R is the communication radius of the node, and RDD$(i.j)$ is the density-weighting coefficient of nodes i and j. The value of RDD(i, j) is equal to the number of public sensing units within the communication radius of i, j divided by the total number of nodes within the communication radius of i, j. The calculation formula is as shown in the following formula:

$$\mathrm{RDD}(i, j) = \frac{\left(N_i \cap N_j\right)}{\mathrm{sum}\left(N_i, N_j\right)}. \tag{9}$$

N_i, N_j are the number of nodes within one hop of node i and j, $N_i \cap N_j$ is the number of public nodes within one hop of node i and j, and sum(N_i, N_j) is the total number of nodes within one hop of node i and j [16].

(2) Two-hop distance model between nodes:

When the distance between nodes i and j is two hops, this paper considers two distance calculation methods. The calculation formulas of the two methods are shown in formula (10). First, the intersection of nodes within one hop of node i and j is used to find the relay node set a, but the two methods adopt different methods for the selection of relay node α. The analysis results are as follows:

$$\begin{aligned}\mathrm{Distance}(i, j) = {} & R \times \mathrm{RDD}(i, a) \\ & + R \times \mathrm{RDD}(a, j).\end{aligned} \tag{10}$$

According to Figure 5(a), the number of hops between i and j is 2. The dotted line is a path where the distance between two hop nodes can communicate with each other, the relay node is a, and the circle of the dotted line is the range of the communication radius of the relay node set α. The first method is to select a. When there are multiple a in the shortest route of the network, the relay node a with the largest number of nodes $(N_i \cap N_a + N_a \cap N_j)$ among the three nodes i, j, and a is selected.

According to Figure 5(b), the number of hops between i and j is equal to 2, and the relay node is a. When the second method is to select a, if there are multiple routing methods to choose from the network, the shortest route to i is selected.

After experimental simulation analysis, it is found that the first method is more suitable for the algorithm proposed in this paper, and the second method causes a greater positioning error. The possible reason is that the separation of one hop and two hops in the first method can reduce the accumulation of errors caused by multiple hops between network nodes. The second method has a greater impact on the subsequent multihop iterations in this paper.

(3) Multihop distance model between nodes:

When the distance between nodes is multihop (Hop$(ij) > 2$), as shown in Figure 6. When the number of hops is equal to 3 hops, if it is assumed that the number of hops between a and i is one hop, and the distance between the relay node b and nodes a and j is one hop, this paper uses one hop plus two hops to find the three-hop distance. The calculation formula is shown in formula (11) [17]:

$$\begin{aligned}\mathrm{Distanice}(i, j) = {} & \mathrm{Distance}(i, b) \\ & + R \times \mathrm{RDD}(b, j).\end{aligned} \tag{11}$$

RDD(b, j) is the density-weighted value from node i to node b, and node b to node j. When there are multiple relay nodes b, the minimum value of $\mathrm{Distance}(i, b) + R \times \mathrm{RDD}(b, j)$ is selected as the relay node. For the case where the number of hops between nodes i and j is n $(n > 2)$ hops, Hop$(i, b) = n - 1$ is selected and b with Hop$(b, j) = 1$ is used as the transit unit. When the number of qualified transit units in the network is greater than 1, the minimum value of $\mathrm{Distance}(i, b) + \mathrm{Distance}(b, j)$ is selected as the distance between nodes i and j [18].

The formula for the distance between each node is shown as follows:

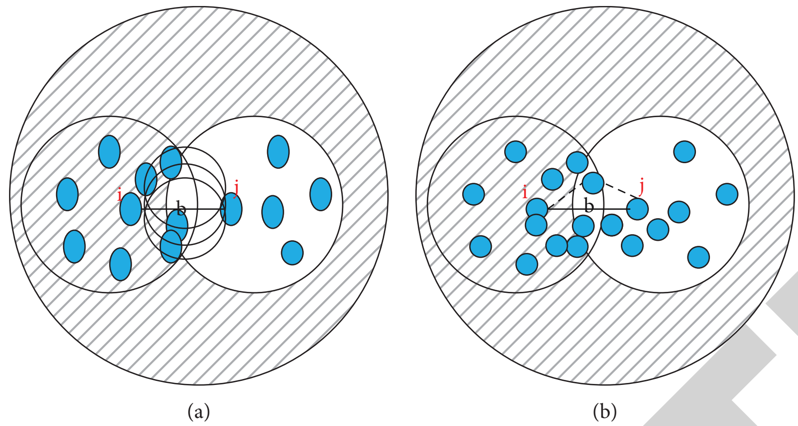

Figure 5: Two-hop routing selection method between nodes. (a) Two-hop routing mode a between nodes. (b) Two-hop routing mode b between nodes.

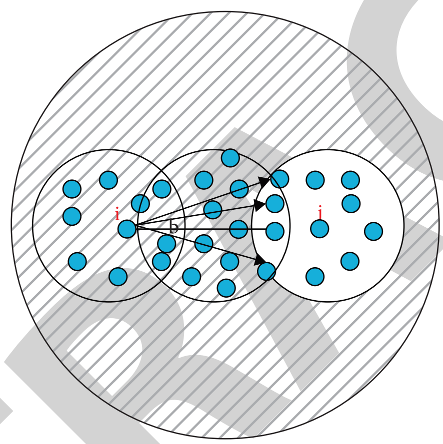

Figure 6: Multihop distance model between nodes.

$$\text{Distance}(i, j) = \begin{cases} R \times \text{RDD}(i, j), & \text{Hop}(i, j) = 1, \\ R \times (\text{RDD}(i, a) + \text{RDD}(a, j)), & \text{Hop}(i, j) = 2, \\ \text{Distance}(i, b) + R \times \text{RDD}(b, j), & \text{Hop}(i, j) \geq 3. \end{cases} \tag{12}$$

(4) The anchor node is used to correct the estimated distance:

A node density correction factor $\phi_{\text{rdd}}(i)$ is introduced, and the calculation formula for $\phi_{\text{rdd}}(i)$ is given below:

$$\phi_{\text{rdd}}(i) = \frac{\sum_{i \neq j, i, j \in N} (D(i, :))}{\sum_{i \neq j, i, j \in N} \text{Distance}(i, :)}. \tag{13}$$

In formula (10), i and j are beacon nodes, N is the set of beacon nodes, and $D(i, :)$ and $\text{Distance}(i, :)$, respectively, represent the Euclidean distance and the estimated distance from i to each anchor node. The distance calculation formula is (14) [19]:

$$\text{Distance}(i, j) = \text{Distance}(i, j) \times \phi_{\text{rdd}}(i). \tag{14}$$

The third stage of DV-Hop algorithm and RND algorithm adopts the trilateration estimation method for positioning, which depends on the accuracy of network ranging, while the least square method is affected by hardware conditions when determining the position of the node to be located. Intelligent algorithms are used to optimize positioning to avoid accumulation of errors and obtain satisfactory results. Compared with other intelligent algorithms, the particle swarm optimization algorithm has the advantages of low algorithm complexity, easy network implementation, and good optimization capabilities. At the end of this paper, an improved PSO is used to replace the trilateration estimation method to correct the positioning of network nodes.

In the improved PSO used in this paper, if it is assumed that the number of particles is N, the search space dimension is equal to M, the position of the ith particle is $x_i = (x_{i1}, x_{i2}, x_{i3}, \ldots\ldots, x_{iN})$, the velocity is $v_i = (v_{i1}, v_{i2}, v_{i3}, \ldots\ldots, v_{iN})$, the historical optimal position of particle

i is $\text{pbx}_i = (p_{i1}, p_{i2}, p_{i3}, \ldots\ldots, p_{iN})$, and the global historical optimal position is $\text{gbx} = (p_{g1}, p_{g2}, p_{g3}, \ldots\ldots, p_{gN})$. The update formulas of the velocity $v_{i\,d}$ and position x_{id} of the particle i are Equations (15) and (16) [20]:

$$v_{i\,d}(T+1) = w \times v_{i\,d}(T) + c_1 \times r(N,2) \times (\text{pbx} - x_{i\,d}(T)) + c_2 \times r(N,2) \times (\text{gbx} - x_{i\,d}(T)), \tag{15}$$

$$x_{i\,d}(T+1) = x_{i\,d}(T) + v_{i\,d}(T+1). \tag{16}$$

Among them, i represents the ith particle, w is the inertia weight, and $r(N.2)$ is a random number uniformly distributed in the interval [0, 1]. At the same time, c_1, c_2 are learning factors, and T represents the number of iterations.

(1) Improved inertia weight:

The proper inertia weight used by the algorithm can not only prevent the algorithm from falling into premature but also avoid falling into the local optimum. In order to obtain a better optimization effect, this paper uses an exponential decreasing function to improve the value of the inertia weight w, and the improved formula is as follows:

$$w = w_{\max} - 0.5 \times (w_{\max} - w_{\min}) \times e^{\left(\sqrt{T/T_{\max}}\right)}. \tag{17}$$

Among them, T is the current iteration number, $T_{\max}$ is the maximum iteration number, and $w_{\max}$ and $w_{\min}$ are the largest and smallest inertia weights, respectively. When the inertia weight is $w_{\max} = 0.95$ and $w_{\min} = 0.4$, an ideal positioning range can be obtained. The relationship between w and T is shown in Figure 7.

(2) The process of particle swarm optimization for positioning optimization:

The process of particle swarm optimization to optimize the positioning of network nodes is as follows:

(1) The network provides the coordinates of the beacon node, the distance from the node to be located to the beacon node, the number of hops from the node to be located to the beacon node, the number of beacon nodes, and the total number of nodes as the initialization parameters of the particle swarm algorithm.
(2) The algorithm initializes the reference expressions of the particle i's velocity $x_i = (x_{i1}, x_{i2}, x_{i3}, \ldots\ldots, x_{iN})$, velocity $v_i = (v_{i1}, v_{i2}, v_{i3}, \ldots\ldots, v_{iN})$, and the optimal position pbx_i of the particle itself (10). The fitness F value of the population particles is calculated, and gbx_i is set to the optimal position of the initial population, $T = 0$.
(3) $T = T + 1$, according to formula (10), the velocity and position of the particles are updated.
(4) The fitness F value of the particle is compared to update the optimal position of the particle.
(5) If the particle position meets the set conditions, the optimal solution of the equation is output. Otherwise, it is judged whether the algorithm has completed the iterative process. If so, the algorithm outputs the particle coordinates. Otherwise, it returns to steps 3 to 5 and loops to find the best point of the network.

The RDD algorithm process is as follows:

(1) The network performs flood broadcasting.
(2) The network obtains the anchor node distance matrix and the minimum node hop matrix based on the information data of the flood broadcast in the first stage.
(3) The node obtains the number of nodes and their labels within the single-handed range according to the broadcast data packet.
(4) The algorithm calculates the distance within the single hop range of the node according to the radius R multiplied by the density-weighted value.
(5) The algorithm finds the distance between nodes with a 2-hop distance.
(6) The algorithm uses the iterative accumulation method to multihop the distance between nodes.
(7) The algorithm calculates the distance between the node to be located and the anchor node and uses the improved PSO to obtain the coordinates of the further optimized node.

The RDD algorithm flowchart is shown in Figure 8.

4. Market Economy Fluctuation Model Based on Internet of Things Technology

At present, Internet of Things providers in the Internet of Things market distribute different data centers in different areas in order to provide the best Internet of Things to meet the needs of different groups of users. However, in order to better meet the service needs of users, it is necessary to coordinate the amount of service resources from different service providers in the market to balance market supply and demand. Therefore, it is necessary to coordinate market supply and demand. Figure 9 depicts a market transaction mechanism for the Internet of Things. In this mechanism, the cloud broker coordinates the service requirements of all parties and conducts reasonable allocation and balanced

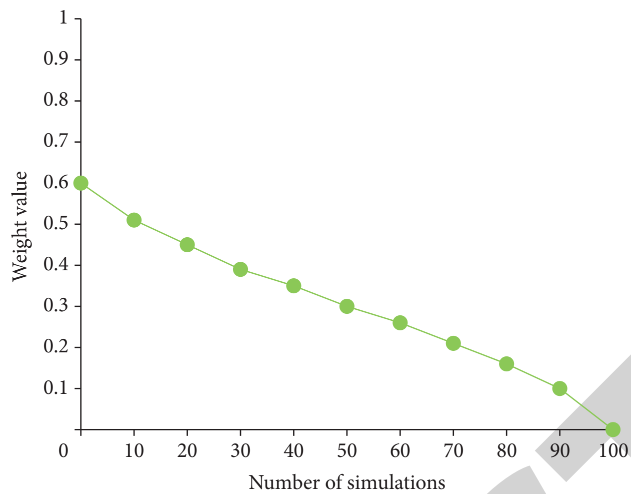

FIGURE 7: Weight value and simulation times.

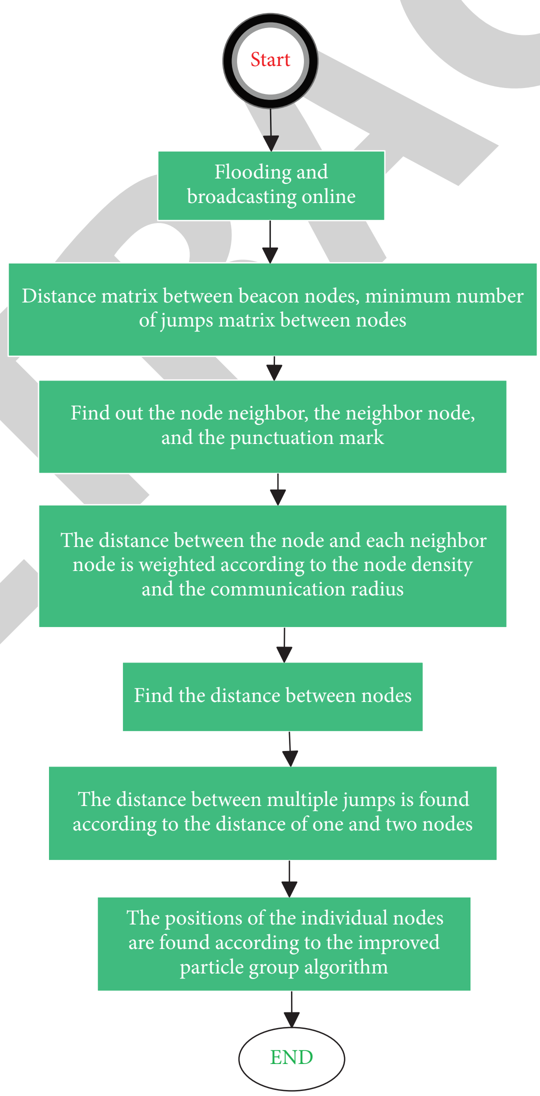

FIGURE 8: RDD algorithm flowchart.

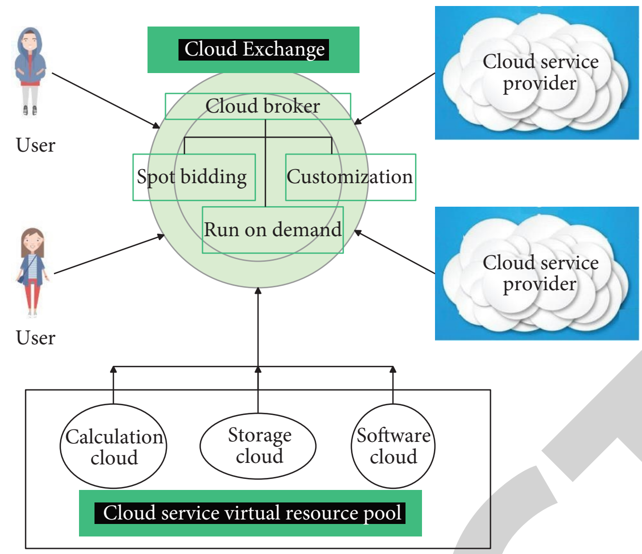

Figure 9: Market transaction system based on the Internet of Things.

Table 1: Data processing effect of market economy fluctuation model based on Internet of Things.

Number	Positioning effect	Data processing	Number	Positioning effect	Data processing
1	91.82	88.14	19	91.31	88.79
2	94.55	92.21	20	96.90	88.79
3	95.10	88.20	21	93.75	92.60
4	94.03	94.46	22	92.50	92.57
5	95.38	92.37	23	93.71	94.65
6	94.29	88.74	24	95.80	88.03
7	93.62	91.44	25	92.45	89.73
8	95.60	91.70	26	96.64	92.54
9	95.80	94.81	27	93.77	90.03
10	91.56	89.40	28	93.03	93.96
11	91.27	88.30	29	91.82	94.65
12	94.98	89.02	30	92.25	94.25
13	92.08	91.70	31	93.58	92.59
14	92.14	90.28	32	91.19	90.00
15	96.68	92.69	33	92.75	91.31
16	96.17	88.50	34	92.95	92.44
17	95.70	89.64	35	92.44	91.04
18	94.16	88.35	36	95.00	92.40

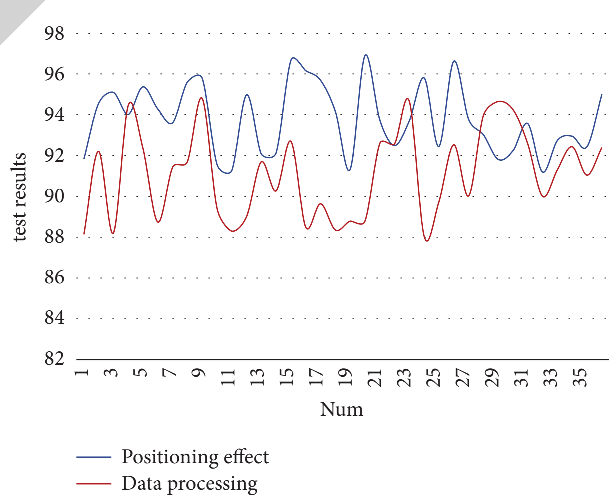

Figure 10: Statistical diagram of the data processing effect of the market economy fluctuation model based on Internet of Things.

Table 2: Market fluctuation analysis effect of market economy fluctuation model based on Internet of Things technology.

Number	Evaluation results	Number	Evaluation results	Number	Evaluation results
1	90.95	13	82.34	25	82.58
2	81.48	14	80.64	26	82.73
3	89.45	15	81.28	27	89.63
4	85.68	16	91.10	28	90.61
5	90.36	17	85.53	29	85.05
6	86.93	18	81.04	30	89.08
7	90.76	19	81.10	31	83.79
8	89.86	20	82.33	32	83.68
9	83.06	21	89.09	33	84.39
10	86.33	22	88.69	34	89.64
11	83.06	23	91.38	35	90.92
12	84.84	24	88.74	36	86.42

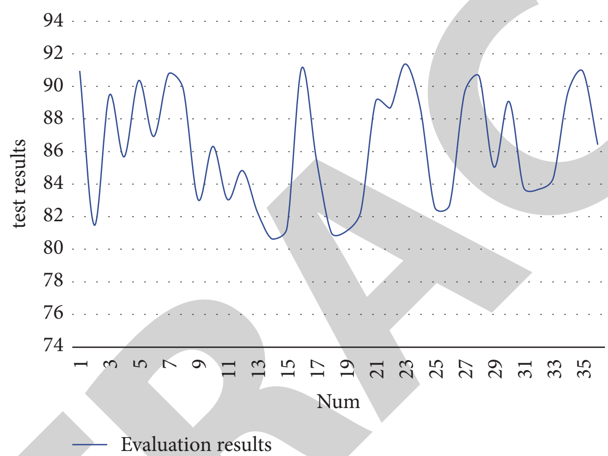

Figure 11: Statistical diagram of the model's practical effect.

coordination of market demand services. Figure 9 describes the distribution of a collaborative development type of Internet of Things transaction system. It can bring considerable economic benefits to market transaction participants.

This article analyzes the market economy volatility model through the Internet of Things technology, combined with simulation experiments, and explores the application of the Internet of Things technology in the economic market volatility model. First, this paper explores the effect of market economy fluctuation model based on Internet of Things technology through simulation experiments, and the results are shown in Table 1 and Figure 10.

From the above research, we can see that the method proposed in this paper can realize accurate positioning of the economic market transaction location, and can process economic data at the same time. On this basis, this paper judges the effect of the Internet of Things technology in the analysis of market economic fluctuations and presents the results by scoring, as shown in Table 2 and Figure 11.

From the above analysis, it can be seen that the market economy fluctuation model based on Internet of Things technology can play an important role in market economy analysis.

5. Conclusion

The Internet of Things has a long industrial chain and forms a wider coverage. In the process of penetration and integration with different industries, it will expand the space for economic development and stimulate economic growth. The manufacturing industry represented by the manufacturing of chips, sensors, and terminal equipment in the upstream of the IoT industry chain has formed a forward relationship with the secondary industry, especially the manufacturing industry. The downstream information transmission, software industry, cloud computing technology application and the financial industry, transportation industry and information communication industry and other tertiary industries have formed a backward relationship. It can be said that the application field of the Internet of Things extends almost to all categories of existing national economic industries. For example, industries such as smart transportation, environmental monitoring, public safety, smart logistics, precision agriculture, industrial safety monitoring, entertainment and education, and medical and health care all involve the use of IoT technology. Relying on the advantages of the Internet of Things industry, a new profit growth space has emerged in all walks of life in the national economy, which has

Hindawi
Scientific Programming
Volume 2022, Article ID 5333346, 9 pages
https://doi.org/10.1155/2022/5333346

Research Article

Energy Efficiency Analysis of e-Commerce Customer Management System Based on Mobile Edge Computing

Wenxing Chen[1] **and Bin Yang**[2]

[1]*Henan Quality Polytechnic, Pingdingshan 467000, China*
[2]*Henan University of Urban Construction, Pingdingshan 467000, China*

Correspondence should be addressed to Wenxing Chen; sun20211120@163.com and Bin Yang; 20210001@hncj.edu.cn

Received 22 November 2021; Revised 8 December 2021; Accepted 16 December 2021; Published 3 January 2022

Academic Editor: Le Sun

Energy efficiency optimization of mobile edge computing e-commerce clients and reasonable management of server computing resources are worth further study. The participant of the algorithm game model proposed in this paper is mobile e-commerce customer management. The decision space is a two-dimensional space composed of unloading decision and power control, and the benefit function is the energy efficiency function and delay function. The existence and uniqueness of the multidimensional game model are proved theoretically. The simulation results show that the proposed multidimensional game based energy efficiency optimization algorithm of mobile edge computing can reduce the energy consumption and delay of mobile terminals and improve the energy efficiency of unloading calculation under the same task compared with the game scheme without considering power consumption control when the number of e-commerce customer management is larger. This paper deduces the optimal load migration decision of mobile e-commerce customer management and the optimal pricing strategy of mobile edge cloud service providers and proves that the optimal decision and optimal pricing constitute the Starkberg equilibrium. The semidistributed and decentralized task transfer decision-making mechanisms are designed, respectively, and the management decision-making behaviors of mobile e-commerce customers in the mobile edge cloud energy trading market are studied by numerical analysis, as well as the time efficiency of the two mechanisms.

1. Introduction

Mobile edge is defined as the technology by the European Telecommunications Standards Institute (ETSI), providing service environments, within wireless access networks and in the vicinity of mobile users [1]. ETSI on mobile edge computing is considered to be an important emerging technology and an important part of the next generation of networks.

The video stream from the monitoring device is processed and analyzed on the MEC server, and the meaningful data is extracted from the video stream. You can transfer valuable data that are inherently cooperative in data, edge computing, and data transfer in the prediction link. Data processing can be performed on a wooden MEC server rather than a centralized server to provide a good user experience. The Internet of Things generates additional messages over telecommunications networks, requiring gateways to aggregate messages and ensure low latency and security. We introduce a new architecture for collecting [2, 3], classifying, and analyzing IoT data flows using MEC servers that manage various protocols, message distribution, and analytical processing. A vibrant ecosystem creates new opportunities for mobile operators, applications, and content providers.

With the rapid development of e-commerce in today's society, customers also have a great impact on the development of e-commerce enterprises. Firstly, in the e-commerce environment, customers can browse, understand, and purchase products and services through the network; through realization, such as customer purchasing power, and customer loyalty; then through network communication and other ways to timely contact customers; and through care and other marketing means to obtain more customer support. The development of e-commerce enterprises needs the support of an e-commerce customer relationship management system, which provides a scientific basis for enterprises to make scientific decisions and market development strategies.

2. Related Work

In e-commerce customer relationship management systems, data mining technology is integrated to realize the analysis of existing customer data, establish an analysis model for customers, analyze customers through the data model, classify customers, and find more potential customers [4, 5]. The e-commerce customer relationship management system in the domestic market system is not perfect but also made some achievements. Earlier construction of e-commerce customer relationship management systems includes telecom and mobile companies, the banking industry, and aviation. Customer relationship management not only includes the addition, deletion, and modification of customer information but also includes the analysis of customer data, understanding customers' hobbies, timely finding which customers are easy to lose, and vigorously digging potential customer markets. Domestic theoretical research in these aspects has achieved initial results, such as the use of the genetic algorithm, artificial neural network, and other classification acquisition methods for customer data analysis and prediction. The system structure of domestic e-commerce customer relationship management system is relatively simple, the function is relatively simple, and most of the management systems are only to achieve the management of customer basic information data. Compared with foreign countries, the development and research of China's e-commerce customer relationship management system are still relatively backward and single [6, 7]. All in all, abroad and at home, now the common development of the world economy is not a good customer relationship management system support; it is not a successful future business, helps the customer management and analysis, and enhances the working efficiency of the enterprise; the Lord will help improve the position and role of enterprise in the market.

Among them, the energy efficiency optimization of mobile edge computing e-commerce customer relationship management system includes a well-designed task unloading scheme, communication channel allocation, and transmission power control. In literature [8], an effective MEC system calculation model is proposed to combine computing and communication cooperation to optimize system energy efficiency. In literature [9], dynamic voltage scaling technology is used to jointly optimize the computing speed, transmission power, and unloading ratio of mobile devices to improve energy efficiency. In literature [10], transmission power control and unloading decision of MEC systems under single user conditions are studied. As an improvement, the authors of literature [11] extended the conclusions in literature to multiuser MEC systems, and combined with resource allocation, they optimized the energy efficiency of multiuser MEC systems through Lyapunov. In [12], an integrated framework for computational unloading is proposed, which takes into account unloading decisions, to optimize energy efficiency. However, in literature [13], intercustomer interference of e-commerce is not taken into account when the unloading decision of mobile users is determined. Studies show that effective power control can effectively suppress intercustomer interference of e-commerce in a small e-commerce customer network [5, 14]. Therefore, some MEC algorithms based on transmission power control are proposed. For example, the transmission power control algorithms proposed in the literature [15, 16] and the algorithms proposed in the literature [17] are effective in multiuser MEC systems, but they are centralized and not always effective in distributed systems. As the computing resources of the MEC server are limited, more and more terminal devices will connect to the server in the future when the number of mobile devices is increasing exponentially. Therefore, how to reasonably manage computing resources has become a significant research direction. Literature [18] proposed a branch and bound algorithm (VF-BNB) based on variable fusion to optimize computing resources. The model in literature [19] is a mobile edge computing system with a large number of low-power mobile terminals. Therefore, reasonable allocation of computing resources is the key to achieving system performance. The problem of computing resource allocation in the upstream MEC system under the minimum to maximum fairness criterion is studied. Literature [20] uses the Lagrange multiplier method with a predetermined resource allocation strategy to solve the problem of computing resource allocation. The above literature conducts quantitative analysis from the perspective of limited computing resources and then completes resource management through carefully designed algorithms but ignores the mobility of terminal devices. If the user continues to move, the original request discharge calculation of the server may not be able to timely send the result in the user's next position. User mobility prediction distribution and which server to use are studied in the literature [21]. Literature [22] studies a kind of virtual machine migration strategy based on the Markov decision process; in the literature [23], congestion in the network virtual machine migration strategy is studied.

However, the commonly used assumptions in the above algorithms for energy efficiency optimization of e-commerce CRM systems based on MEC mobile edge computing have certain limitations: the computing resources of MEC servers are limited, and unloading a large number of tasks will bring considerable queuing delay. In the scenario of ultradense networks (UDN), interference between e-commerce customers can significantly affect data rates and lead to unexpected transmission delays, which can lead to low energy efficiency and long delays. Therefore, interference and queuing problems cannot be ignored in reality. Although MEC has many benefits, the energy efficiency of its mobile terminal cannot be ignored. Game theory is a powerful distributed mechanism design tool. In order to maintain the balance of the system and consider the interests of each user, it is of great significance to use game theory as a tool to study energy efficiency in the MEC system. In the MEC system, virtual machine migration is usually adopted for user movement, but for some applications with high instantness requirements and small task volume, the migration cost is too large. Although mobility prediction is carried out, the model is an ideal case of uniform motion. In general, the user's movement has acceleration, so there is room for further study of this scheme.

3. Mobile Edge Computing for e-Commerce Customer Management Energy Efficiency Optimization Framework and Key Technology Analysis

3.1. System Architecture. Enabling MEC applications to be realized as pure software entities running on MEC hosts, mobile edge platforms provide the base needed to run applications. MEC applications are run as virtual machine VMS on top of a virtualized infrastructure that includes a data platform that enforces traffic rules received by mobile edge platforms and routes traffic between the application forest network and the external network. In host level management including mobile platform edge and virtualization infrastructure, the former is responsible for the management of electronic commerce application of life cycle and rule requirements, including e-commerce customer management system business license, flow rule, and the domain name system conflict resolution, which is responsible for the allocation, management, and releasing the visualization of virtualization infrastructure (computing, storage, and network resources). The architecture diagram is shown in Figure 1.

As shown in Figure 2, the framework of the e-commerce customer management system of edge computing is divided into mobile edge computing level, mobile edge e-commerce customer system host level, and network-level entity. The host layer of the mobile edge e-commerce customer system is the basic part of the framework, which consists of mobile edge host and host management. Virtualization infrastructure can provide ME with the application with computing, storage, and network resources and can provide ME with the application with persistent storage and access to relevant information; it includes a data forwarding plane, used to receive from ME platform data forwarding rules, as well as between each application, service, and network flows. The ME platform receives traffic forwarding rules from the ME platform manager, ME applications, or ME services and sends instructions to the forwarding plane based on the forwarding rules. In addition, the ME platform supports the configuration of local domain name system (DNS) proxy servers to redirect data traffic to corresponding applications and services. The ME platform can also communicate with other ME platforms through Mp3 reference points, which can serve as the basis for interconnecting different ME platforms in the collaboration mechanism of distributed MEC systems.

Among them, intelligent service is based on the model-driven unified service framework, which realizes the coordination of development and deployment intelligence through the development service framework and deployment operation service framework, and can realize the consistency of software development and deployment operation automation. Intelligent business orchestration defines end-to-end business flows through business support capabilities to achieve business agility. Connected computing achieves a minimalist architecture, shielding services from the complexity of edge intelligent distributed architecture, realizing automation and visualization of operation, information and communication technology infrastructure deployment and operation, and supporting intelligent collaboration between edge computing resource services and industry business needs. Intelligent Edge computing node (ECN) is compatible with a variety of heterogeneous connections, supports real-time processing and response, and provides hardware and software integration security. The three-tier model is mainly for scenarios where services are deployed to one or more scattered regions, and the business flow in each region is small, such as smart street lamps, smart elevators, and smart environmental protection. After the intelligent asset is processed locally, multiple types of service data are aggregated to the intelligent gateway along the north-south direction. The intelligent gateway processes real-time service requirements locally and aggregates non-real-time data and sends it to the cloud for processing.

3.2. Research on Key Technology of Energy Efficiency Optimization. An important part of calculating unload is deciding whether to unload, whether all or part of it applies, what to unload, and how to unload. The uninstall decision depends on the application model categorized according to three criteria. In the task execution schedule, we need to know how to select the task execution sequence to reduce the task execution time, and so on. For optimization problems with equality and inequality constraints, the general form is

$$\min_{x} h(x),\ f_i(x) \leq 0, \quad i = 1, \ldots, n. \tag{1}$$

In the optimization problem-solving algorithm, the KKT condition is the necessary and sufficient condition for the convex optimization problem to obtain the optimal solution, and the KKT condition is

$$\delta h(x) + \sum_{i=1}^{n} u_i f_i(x) + \sum_{j} v_j = 0. \tag{2}$$

The in-memory data grid technology is adopted, and improvements are made in storing lightweight and high-performance access, forming a lightweight and high-performance edge service catalog. On this basis, considering the influence of the mobile edge computing environment and the dynamic change of directory nodes, the synchronization and consistency guarantee technology of the edge service directory is studied. The core methods to solve this problem include the following three aspects: (1) taking into account the synchronization modes such as upstream and downstream synchronization and peer synchronization, the problem of information service sharing can be solved by flexibly selecting suitable directory synchronization mode,

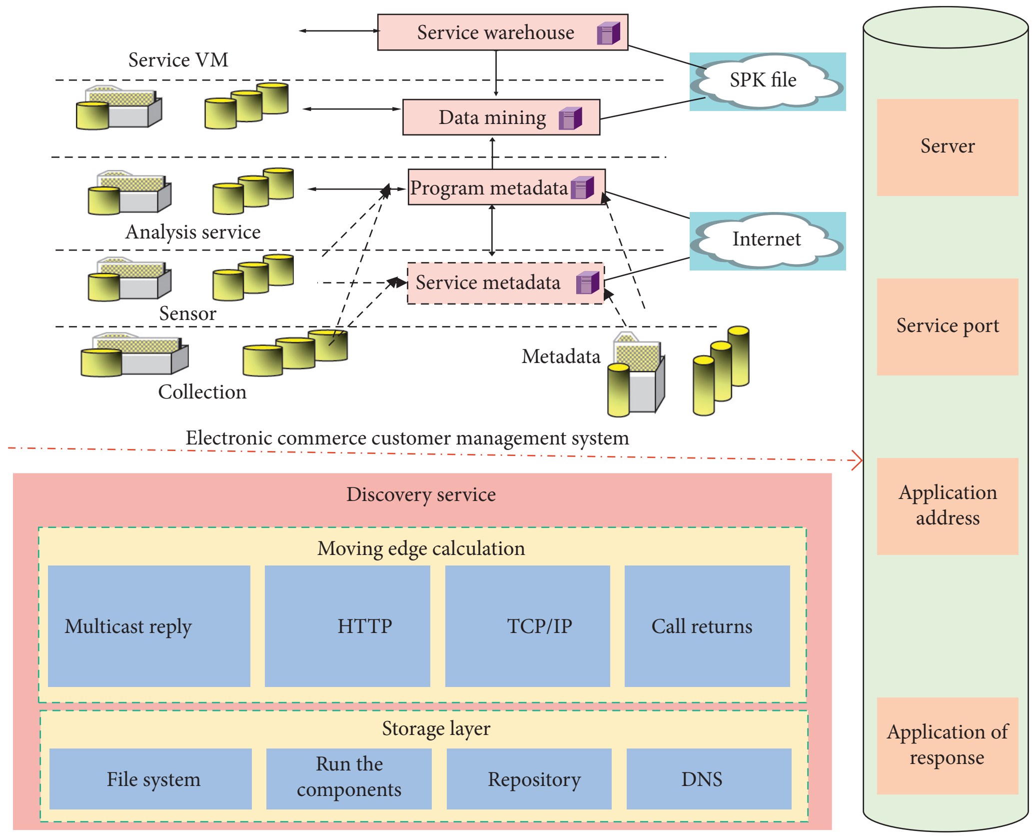

Figure 1: Optimized e-commerce customer management architecture for mobile edge computing energy efficiency.

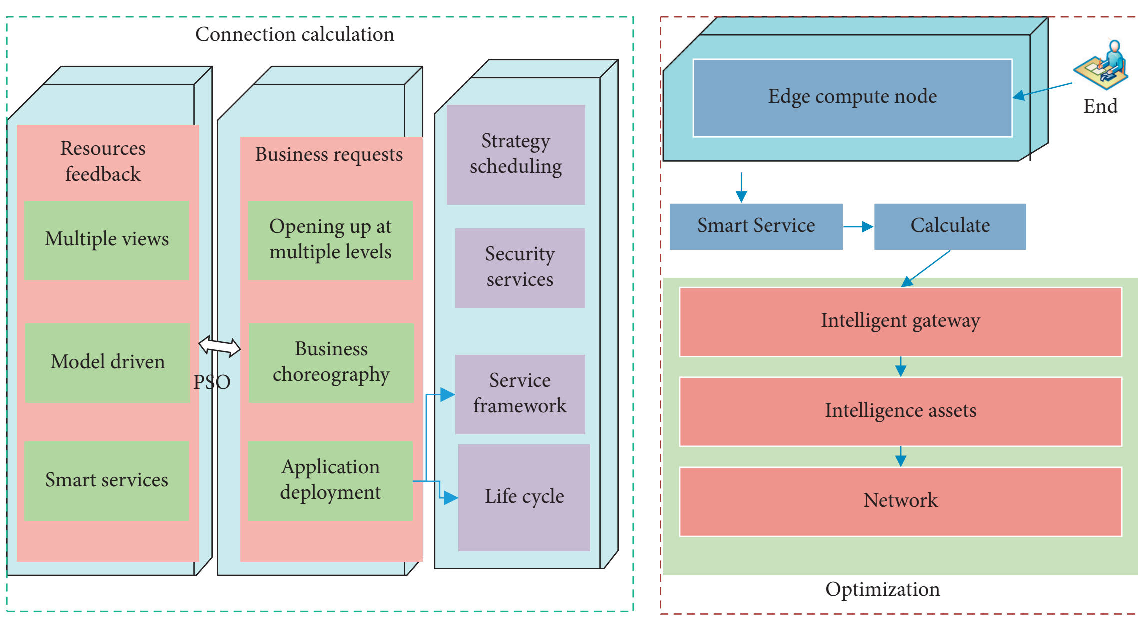

Figure 2: Energy efficiency optimization architecture of mobile edge computing for e-commerce customer management.

supporting dynamic discovery, flexible networking, and service sharing among nodes, and realizing the dynamic collaborative operation of service catalog; (2) we adopt the updating mechanism of active monitoring to ensure that the service information recorded in the decentralized edge service catalog is consistent, real-time, and effective and improve the availability of services built on the distributed structure; (3) a new distributed consistency algorithm based on state machine replication is proposed. By sorting and executing the uncoupling consensus protocol and the operation commands, the operation commands can be concurrently submitted for all backups at any time without determining the order of the operation commands and can be executed in the same order on all backups. The structure of the service catalog can be divided into three layers, namely, catalog summary layer, catalog middle layer, and service instance layer. The aggregation layer of the service catalog and the directory area of the middle layer have a central service catalog sharing model, which is mainly used in the service catalog. The directory services use the directory equivalent middle layer region sharing service model. The mobile edge computing service catalog model architecture is shown in Figure 3.

The existing microservice system mainly adopts a rule-based routing policy to realize the routing function of the service based on the service catalog information provided by the service registry and the service status information reported by the service agent. However, the mobile edge computing environment is complex and changeable and has significant dynamic characteristics. If a simple and rules-based routing strategy is directly adopted, the system performance cannot be optimized. Therefore, how to select the service invocation path intelligently according to the service quality, service invocation history, dynamic use of system resources, and other information in the current application environment, as well as the historical service routing strategy, is the key problem of edge service routing address.

4. Energy Efficiency Optimization Algorithm for e-Commerce Customer Management Based on Mobile Edge Computing

In the two-dimensional space composed of decision-making, interference between users can be reduced through the reasonable design of transmitting power size, the upper limit of MEC server computing resources can be set, queuing delay of the mobile terminal is added, optimization target is energy consumption and delay of the mobile terminal, and game model is established. The core idea is to select the most suitable unloading decision and transmitting power for each user under the current situation through the game, so as to reduce interference so that more users can have the opportunity of unloading computing and improve the energy efficiency of the mobile terminal. The purpose of using the game algorithm is to select the most suitable decision so as to optimize the energy consumption and delay function:

$$\min_{i} f_i\left(s_{in}, -s_{in}\right). \tag{3}$$

This algorithm is a multiuser system, which uses parallel time slots, and each user calculates its own optimal response decision in each time slot. During initialization, the user's decision is to uninstall the MEC server for calculation, and the upload power is randomly selected. In each time slot, the user collects energy efficiency information: other e-commerce customers need to uninstall the MEC server computing the number of users, their choice of channel, and according to the information transmission rate calculation, each channel interference, and the total number of users, in MEC server to determine whether the user needs to line up. From these parameters, the optimal response, namely, the unload decision (whether to unload) and the upload power size, can be calculated. In the process of inference in means—purpose with an online autonomous learning algorithm to realize the optimal strategy of child intent, intention to achieve group, and the agent need to consider its own state—action value function updates for other agent update value functions can be without a second thought, thus greatly reducing the space complexity of the algorithm and improving the learning speed. The algorithm flow is shown in Figure 4.

Customer Relationship Management (CRM) system is a business strategy of an enterprise. It divides and effectively organizes enterprise resources according to customer conditions and cultivates customer-centered operation behavior and customer-centered business process, so as to improve enterprise profitability, increase revenue, and improve customer satisfaction. The development of e-commerce requires enterprises to transform all internal and external business processing mechanisms into "customer satisfaction" service subjects and use new measures and technologies to reduce internal consumption and cost so that the business processing capacity of enterprises constantly meets the needs of Internet customers' rapid operation. One of the purposes of establishing a customer relationship management system is to improve the quality of customer service, depending on the customer service management module, which can effectively achieve customer service and improve customer trust in enterprises and products.

The function module has a customer service console, customer service event record, customer complaint management, and consultation library. The customer service console provides quick inquiries for customer service personnel and provides assistance for customer service personnel. For example, customer service personnel can quickly check the handling of complaints through this module, timely contact customers to solve the unresolved complaints, or carry out customer care and return visits for customers classified as easy to lose, so as to reestablish the trust between customers and enterprises. According to the optimal pricing strategy of customer and demand, the mobile edge energy efficiency mechanism is designed by semidistributed method and decentralized method respectively. See Table 1.

5. Example Verification

This part analyzes the behavior of mobile users with five user scenarios. These five users are named U1, U2, U3, U4, and U5, respectively, and the number of CPU cycles for each user task is set. The task is sorted in descending order of energy efficiency. Figure 5 shows the trend of users' load migration decisions as energy efficiency pricing strategy changes. When energy efficiency pricing is low, all users migrate their load tasks to energy efficiency for processing. After that, as energy efficiency pricing increases, users will gradually reduce the proportion of tasks migrating to energy efficiency. When energy efficiency pricing reaches a certain level, the lower bound of optimal energy efficiency pricing, user U5 will begin to reduce its load migration ratio. As energy efficiency pricing increases further, other users will respond

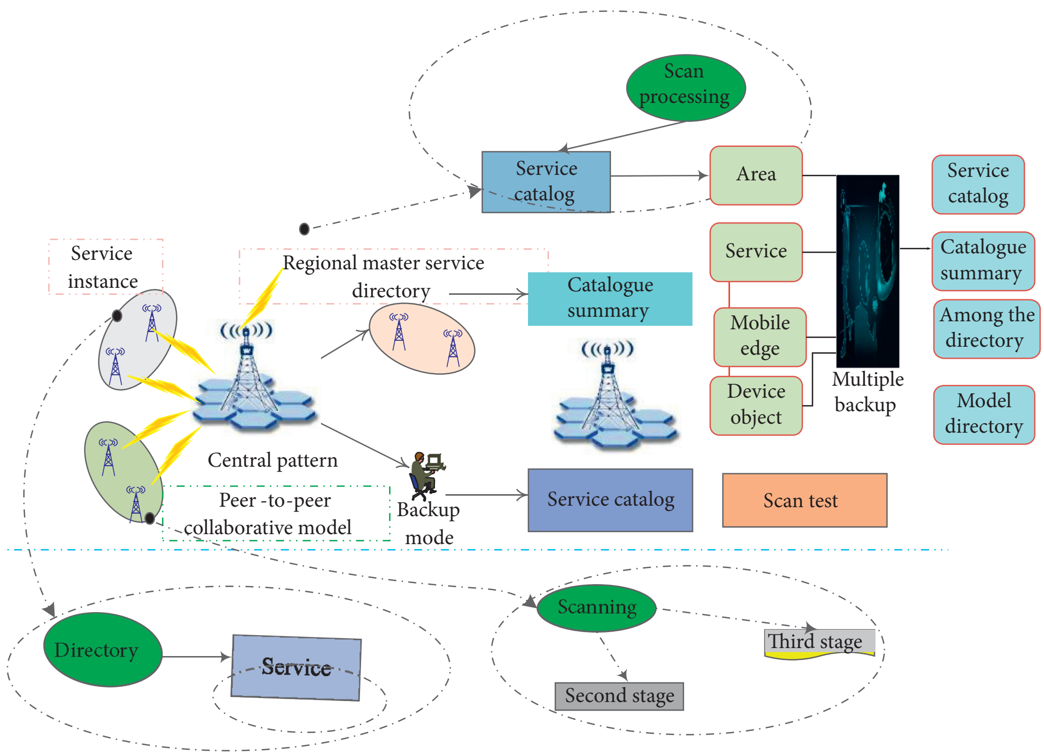

FIGURE 3: Mobile edge computing service catalog model architecture.

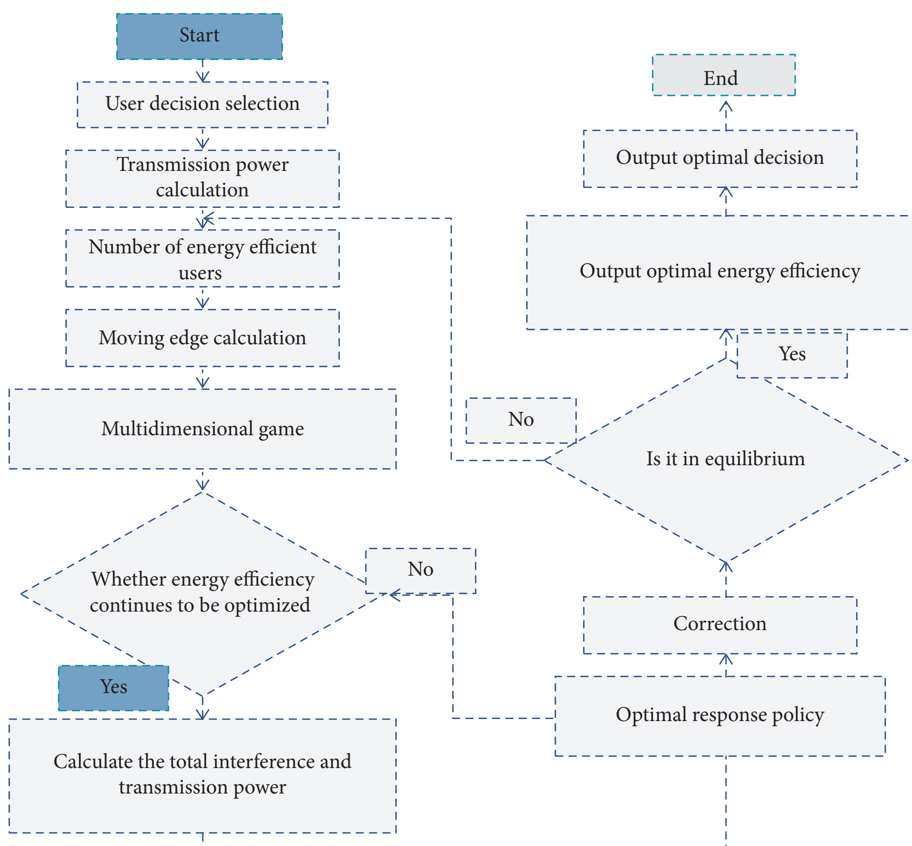

FIGURE 4: Flow chart of energy efficiency optimization algorithm for moving edge computing based on a multidimensional game.

Table 1: Design of energy efficiency mechanism of moving edge by the decentralized method.

On each mobile user's side
1: if $E_i \geq 0$, then
2: user I sends the load migration information to the customer
3: waiting for price P
4: end if
5: each user calculates the optimal load migration policy based on the received customer demand P
6: each user loads some tasks to energy efficiency f and locally calculates the remaining tasks on the demand side
7: waiting for user information
8: arrange all user information in descending order of energy efficiency f
9: calculate P and broadcast it to all users
10: wait for the user load migration task to be executed

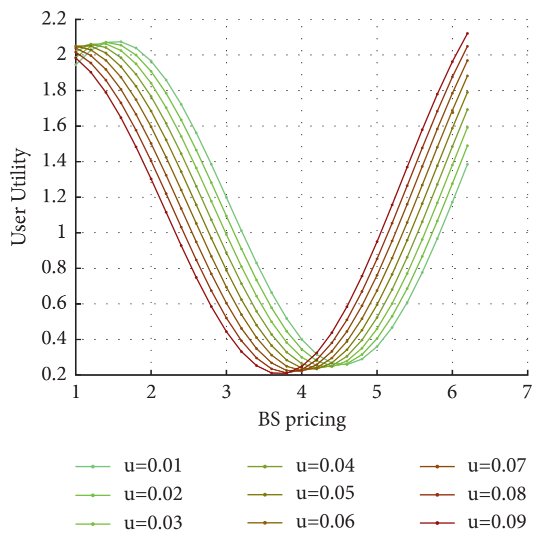

Figure 5: Decision analysis of energy efficiency change of e-commerce management at mobile user edge.

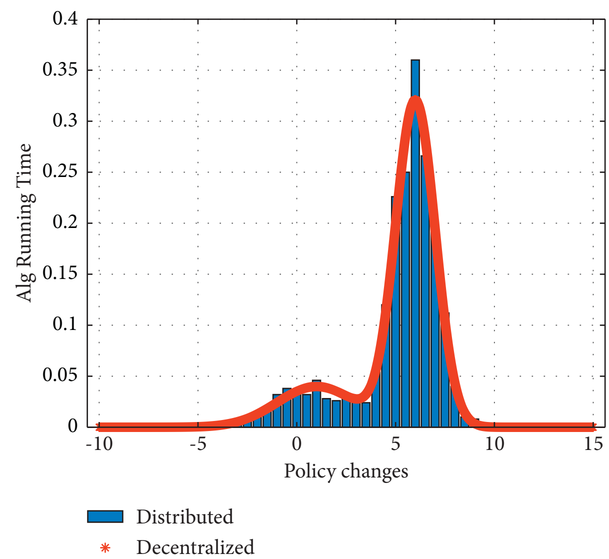

Figure 6: Time efficiency of mobile edge cloud energy consumption optimization algorithm.

to the price and reduce the proportion of load transfer tasks. When the price of energy efficiency reaches a high level, the upper bound of optimal pricing strategy for energy efficiency), no user migrates tasks to energy efficiency for processing. Obviously, when energy efficiency pricing is lower than or higher than the lower bound of its optimal pricing strategy, energy efficiency cannot obtain optimal utility benefits. At the same time, in the game of energy-efficient computing resources among users, users with higher energy efficiency, that is, high efficiency of task transfer, have a stronger tendency of task transfer.

For all users, the computing power of load migration is evenly distributed in the interval. For the decentralized algorithm, its operating efficiency is related to the initial pricing strategy set by the algorithm. When evaluating the efficiency of the algorithm, the average number of iterations under the two conditions is taken as the number of iterations of the algorithm. The time efficiency of the two algorithms is shown in Figure 6. The solid blue line represents the algorithm time of this distributed algorithm, and the dotted red line represents the number of iterations of the decentralized algorithm. For the decentralized algorithm, the number of iterations of the algorithm is independent of the number of users participating in the game because the algorithm is mainly searching the feasible region of the pricing strategy. For the semidistributed algorithm, the relationship between the algorithm complexity and the number of users is superlinear, which also leads to the increase of the number of users participating in the game; the algorithm strategy will produce a certain amount of algorithmic calculation pressure on the base station.

As shown in Figure 7, when the initial speed is $V = 60$ km/h and $a = 1.5$ m/s^2, the success rate increases with the increase in the number of MEC servers, because the increase in the number of servers means that the number of available servers is increasing. As the speed increases, the user moves more distance, and the MEC server has a limited range of connections; the success rate decreases as the number of tasks increases. Moreover, with the expansion of the mobile range, it can be seen that the success rate of CRMAEKF is better than PA.

Figure 8 shows the comparison of total system energy consumption and delay of the two algorithms, namely, the sum of all users and the comprehensive consideration of energy consumption and delay, so the unit is not considered. The higher the energy consumption and delay are, the lower the energy efficiency is. As shown in Figure 8, as the number of users increases, both MQO and ODPC show an increasing trend, but MQO has lower energy consumption and delay

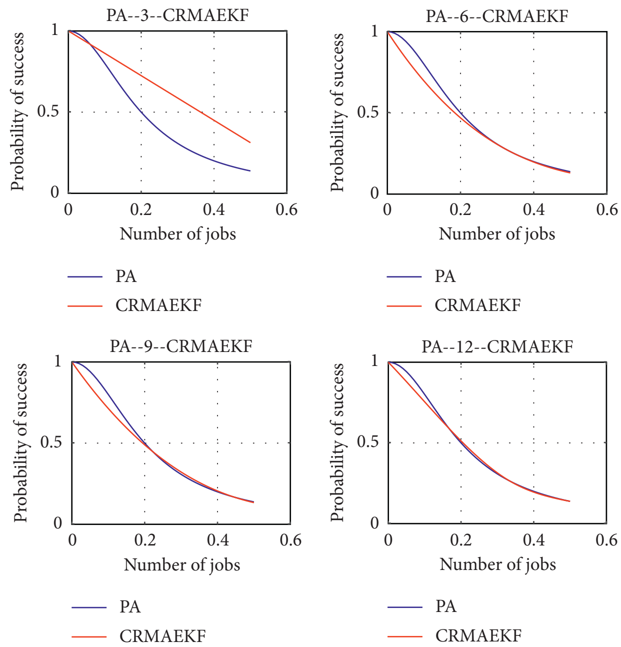

Figure 7: Success rate of different tasks at initial velocity $V = 60\,\text{km/h}$ and $A = 1.5\,\text{m/s}^2$.

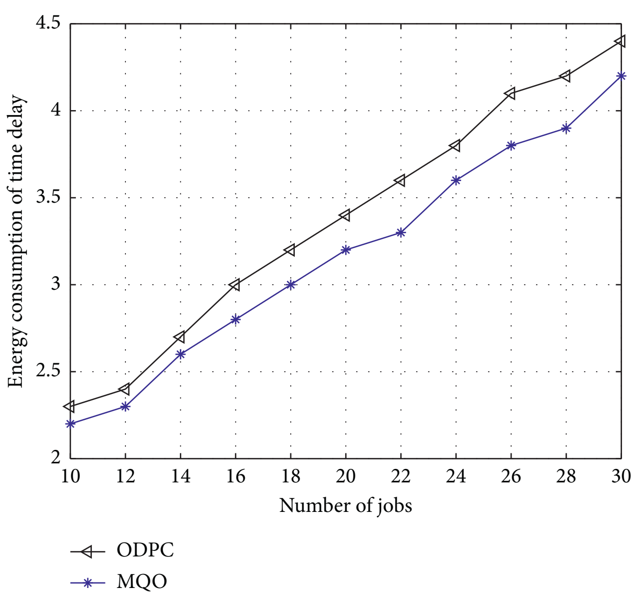

Figure 8: User energy consumption and delay of different numbers of e-commerce customers.

than ODPC. As the number of e-commerce customers increases, so does the number of users. As more and more users choose to unload computing, the queuing delay and interference increase significantly. Under the control of unloading quantity, the energy consumption and delay of MQO are lower than those of ODPC, which proves that the optimization of energy consumption and delay of MQO is superior to that of ODPC.

This paper studies the energy efficiency optimization of the mobile terminal using a game in a multiuser system and proposes an energy efficiency optimization algorithm of mobile edge computing based on multidimensional game. The decision of the game model is a two-dimensional space, which consists of an unloading decision and power control. MEC server computing resources are limited. If the MEC server is overloaded, queuing delay will be introduced. The existence and uniqueness of Nash equilibrium are proved by theoretical deduction. According to this algorithm, the energy consumption and delay of the mobile terminal can be reduced, and the smaller the energy consumption is, the higher the energy efficiency is. And because transmitting power is considered jointly in the decision space, the number of users in unloading calculation can be increased by controlling transmitting power to reduce interference.

6. Conclusion

This paper proposes an energy efficiency optimization algorithm of mobile edge computing based on multidimensional game. Aiming at the energy efficiency optimization problem of the mobile terminal in the multiuser system, this paper aims to improve the energy efficiency of the mobile terminal, establish a communication model and calculation model, set upper limit for MEC server computing resources, and add queuing delay. The multidimensional game model is constructed based on game theory, in which the game decision is a two-dimensional space composed of an unloading decision and power control. It is proved that the Nash equilibrium of this multidimensional game model exists and is unique through theoretical deduction, and the Nash equilibrium solution is finally obtained. The simulation experiment proves that the proposed energy efficiency optimization algorithm of mobile edge computing based on multidimensional game can improve the energy efficiency of mobile terminal compared with the one-dimensional game scheme without power control and reduce interference by controlling transmission power so that more users can unload tasks to MEC server for computing processing. The development of e-commerce and the management of customer relationships should be rationally and effectively combined. The development of e-commerce has promoted the research of customer management and improved the importance of customer relationships. The improvement of customer relationships is helpful for e-commerce enterprises to seize the high-end market, expand business development, and make scientific development strategies. The two complement each other.

Data Availability

The data used to support the findings of this study are available from the corresponding author upon request.

Conflicts of Interest

The authors declare that they have no conflicts of interest.

Acknowledgments

This study was sponsored by HeNan Quality Polytechnic.

References

[1] Y. Yang, Z. Mei, and B. Zheng, "Design of enterprise management system based on edge computing architecture," *Mobile Information Systems*, vol. 2021, no. 10, 12 pages, Article ID 5512958, 2021.

[2] Z. Zheng and X. Zhou, "Design and simulation of ship energy efficiency management system based on data analysis," *Journal of Coastal Research*, vol. 94, no. sp1, pp. 552–567, 2019.

[3] R. Gopi, S. T. Suganthi, R. Rajadevi, P. Johnpaul, N. Bacanin, and S. Kannimuthu, "An enhanced green cloud based queue management (GCQM) system to optimize energy consumption in mobile edge computing," *Wireless Personal Communications*, vol. 117, no. 4, pp. 3397–3419, 2021.

[4] J. Sun, "Research on resource allocation of vocal music teaching system based on mobile edge computing," *Computer Communications*, vol. 160, no. 2, pp. 345–365, 2020.

[5] H. Sun, F. Zhou, and R. Q. Hu, "Joint offloading and computation energy efficiency maximization in a mobile edge computing system," *IEEE Transactions on Vehicular Technology*, vol. 68, no. 3, pp. 3052–3056, 2019.

[6] T. Wang, G. Zhang, and X. Yang, "A trusted and energy efficient approach for cluster-based wireless sensor networks," *International Journal of Distributed Sensor Networks*, vol. 4, pp. 131–143, 2016.

[7] T. Le Tan, "Successful factors of implementation electronic customer relationship management (e-CRM) on E-commerce company," *American Journal of Software Engineering and Applications*, vol. 6, no. 5, pp. 121–127, 2017.

[8] Z. Di, Z. Zhenyu, and Z. Zhengyu, "Energy efficiency analysis of ICN assisted 5G IoT system," *Wireless Communications and Mobile Computing*, vol. 2017, Article ID 6579467, 9 pages, 2017.

[9] P. Wumin and M. Rui, "Research on improvement of China mobile customer relationship management system based on apriori algorithm," *Boletin Tecnico/Technical Bulletin*, vol. 55, no. 19, pp. 520–526, 2017.

[10] W. Sun and Y. Gao, "The design of university physical education management framework based on edge computing and data analysis," *Wireless Communications and Mobile Computing*, vol. 2021, no. 2, 8 pages, Article ID 5537471, 2021.

[11] S. Azeem, N. Nasir, and S. Kousar, "Impact of E-commerce investment and enterprise performance based on customer relationship management," *International Journal of Psychosocial Rehabilitation*, vol. 24, no. 9, pp. 9–31, 2020.

[12] H. Jiang, Y. Wang, and X. Yue, "Performance analysis of NOMA-based mobile edge computing with imperfect CSI," *EURASIP Journal on Wireless Communications and Networking*, vol. 2020, no. 1, 138 pages, 2020.

[13] S. Zhou, W. Jadoon, and J. Shuja, "Machine learning-based offloading strategy for lightweight user mobile edge computing tasks," *Complexity*, vol. 2021, no. 3, 11 pages, Article ID 6455617, 2021.

[14] Y. Sun, C. Song, S. Yu, Y. Liu, H. Pan, and P. Zeng, "Energy-efficient task offloading based on differential evolution in edge computing system with energy harvesting," *IEEE Access*, vol. 9, Article ID 16383, 2021.

[15] P. Corcoran, "Mobile-edge computing and Internet of Things for consumers: Part II: energy efficiency, connectivity, and economic development," *IEEE Consumer Electronics Magazine*, vol. 6, no. 1, pp. 51-52, 2016.

[16] M. Xia, Z. Huang, L. Tian et al., "SparkNoC: an energy-efficiency FPGA-based accelerator using optimized lightweight CNN for edge computing," *Journal of Systems Architecture*, vol. 115, no. 4, Article ID 101991, 2021.

[17] S. Han, X. Xu, S. Fang et al., "Energy efficient secure computation offloading in NOMA-based mMTC networks for IoT," *IEEE Internet of Things Journal*, vol. 6, no. 3, pp. 5674–5690, 2019.

[18] Q. Wang, S. Guo, J. Liu, and Y. Yang, "Energy-efficient computation offloading and resource allocation for delay-sensitive mobile edge computing," *Sustainable Computing: Informatics and Systems*, vol. 21, no. MAR., pp. 154–164, 2019.

[19] X. Liu, J. Yang, and C. Zou, "Collaborative edge computing with FPGA-based CNN accelerators for energy-efficient and time-aware face tracking system," *IEEE Transactions on Computational Social Systems*, vol. 4, no. 9, pp. 12–27, 2021.

[20] D. Zhang, C. Gong, and T. Zhang, "A new algorithm of clustering AODV based on edge computing strategy in IOV," *Wireless Networks*, vol. 27, no. 4, pp. 13–31, 2021.

[21] R. Tatiara, A. N. Fa Jar, and B. Siregar, "Analysis of factors that inhibiting implementation of information security management system (ISMS) based on ISO 27001," *Journal of Physics Conference*, vol. 978, Article ID 12039, 2017.

[22] Y. Bian, M. Hu, Y. Wang, and H. Xu, "Energy efficiency analysis of the economic system in China during 1986-2012: a parallel slacks-based measure approach," *Renewable and Sustainable Energy Reviews*, vol. 55, pp. 990–998, 2016.

[23] S. Z. Zhao and L. Zhang, "Analysis of enterprise management information system based on cloud computing," *Journal of Physics: Conference Series*, vol. 1533, Article ID 22038, 2020.

Hindawi
Scientific Programming
Volume 2021, Article ID 5969446, 10 pages
https://doi.org/10.1155/2021/5969446

Research Article

New Media Advertising Communication Analysis Model Based on Extension Neural Network

Zhe Zhang

School of Humanities and Law, North China University of Technology, Beijing 100144, China

Correspondence should be addressed to Zhe Zhang; zhangzhe@ncut.edu.cn

Received 15 November 2021; Revised 8 December 2021; Accepted 15 December 2021; Published 29 December 2021

Academic Editor: Le Sun

In order to improve the effect of new media advertising communication analysis, this paper combines the scalable neural network to construct the new media advertising communication analysis model. Moreover, this paper analyzes in detail the basic theories of fuzzy neural network and extension evaluation, the structure design and learning algorithm, and classification of fuzzy neural network. In particular, this paper summarizes the optimization algorithms and methods of neural network structure. In addition, this paper improves the algorithm to meet the needs of new media advertising data analysis and builds an intelligent system framework. The experimental verification shows that the new media advertising communication analysis model based on the extension neural network proposed in this paper meets the new media advertising communication analysis effect.

1. Introduction

With the increasing innovation and popularization of Internet applications, a large number of information and people have gathered in the Internet time and space, and rich digital network media and applications have become an indispensable communication tool in public life. The new public attention points have formed a variety of new media, which show the characteristics of strong interaction, precise positioning, and topic segmentation [1]. From application tools to social and cultural carriers, the Internet is increasingly showing its media attributes. In particular, the emergence of the Internet, mobile phones, and a large number of new outdoor media has made the development of the "new media" industry prosperous. At present, rich media forms and rich media information surround the people's living space. For a time, the term "new media" has become a popular vocabulary familiar to the public. From the perspective of natural science or social science, the birth of "new media" is of great significance [2]. However, due to the surging development of the "new media" industry, new technological changes are coming. Due to the endless emergence of new media and new applications, as well as the impetuous mentality of media commercial applications, the theoretical community's understanding and research on "new media" has shown a multipolarity [3].

The process of digitization has brought about tremendous changes in the communication pattern and the media itself: not only have the information (computer) industry, telecommunications industry, and mass media industry presented a new trend of business intersection of triple play, but also cross-domain enterprises have emerged, with questions about mergers and acquisitions and integration. Digital media has changed the characteristics of mass communication in the past and enabled the characteristics of "focus" and "niche" to be carried forward. For example, digital media technology makes radio, television media, and scarce channel resources called rich resources [4]. Digital media has also changed the one-way media communication in the past. The status of the "audience" that can only passively receive information has been greatly changed, and the initiative of receiving information is increasingly shifted to the audience [5]. Digital media has changed the traditional feature that audiences must be synchronized when listening to and watching radio and television and has achieved asynchrony; that is, audiences can listen and watch at any time selected, and they can listen and watch repeatedly if they are interested [6]. Whether newspapers and periodicals are printed in different places through satellite transmission or distributed through the Internet, or digital satellite broadcasting and satellite TV, they are all characterized by covering intercontinental and even the world, pursuing international influence and competing for share in the international media market.

This thesis combines the scalable neural network to construct the new media advertising communication analysis model and conducts research on the new media advertising communication analysis.

2. Related Work

Some scholars combine changes in communication methods with technological updates and call new media "interactive digital composite media" [7]. Literature [8] provided a more comprehensive and objective summary of new media advertising. It believes that "new media advertising refers to the brand communication behavior and form that is reflected in the multimedia video based on digital transmission, which can realize instant interaction of information, and the terminal appears as a network link and is conducive to the communication of information between advertisers and target audiences." Literature [9] believed that new media advertising extends in the direction of "immediate, mobile, request, and concise." It collects, produces, processes, compresses, stores, and applies "advertising information" into various forms of advertising expression. Literature [10] believed that the forms of new media advertising mainly include outdoor new media, mobile new media, and mobile phone new media. Among them, outdoor new media include outdoor video, outdoor touch, and outdoor projection, etc., while mobile new media is realized through mobile TV, car TV, and subway TV. Literature [11] believed that homepage advertising occupies an important position in new media advertising. The reason is that homepage advertisements can not only spread the image and culture of the company, but also convey information about the company's products. Moreover, many companies have e-commerce platforms, so homepage advertisements play a direct role in the sales of their products. Literature [12] divides online advertising into portal advertising and interactive advertising. Literature [13] classified online advertising as follows: banner advertising, button advertising, e-mail advertising, wallpaper advertising, sponsored advertising, competition and promotion advertising, interstitial advertising, interactive game advertising, commercial service advertising, full-screen advertising, banner advertising, picture-in-picture advertising, streaming advertising, interstitial advertising, instant pop-up advertising, mobile advertising, hover advertising, etc.

3. Extension Neural Network Model

3.1. The Concept of Matter Element. People and things are collectively called things. Things have various characteristics, and each characteristic can be characterized by a corresponding value. Therefore, the name, characteristics, and value of things are the basic elements to describe things, called the three elements of matter-element. Matter element is the basic element for formal description of matter. It is represented by an ordered triplet consisting of the name of the object, the feature (feature name for short), and the corresponding value, that is, the matter element (thing, feature name, and value).

The concept of matter element correctly reflects the relationship between the quality and quantity of things and the dynamics of things and can more closely describe the changing process of objective things. It studies things, characteristics, and corresponding values as a whole and provides a formal tool for solving contradictory problems by combining qualitative and quantitative methods.

3.2. Definition of Matter Element. We set the thing N, and it is about the value v of the feature c, and the basic element of the thing can be described by the ordered triple $R = (N, c, V)$, referred to as the matter element. Since V can be determined by N and c, the matter element can also be expressed as [14]

$$R = (N, c, V(N)). \tag{1}$$

The array with n features and corresponding n magnitudes is [15]

$$R = \begin{pmatrix} & c_1 & v_1 \\ N & c_2 & v_2 \\ & \vdots & \vdots \\ & c_n & v_n \end{pmatrix} = \begin{pmatrix} R_1 \\ R_2 \\ \vdots \\ R_n \end{pmatrix}. \tag{2}$$

R is an n-dimensional matter element, denoted as $R = (N, c_i, V_i)$, $i = 1, 2, \ldots, n$. Each dimensional matter element R_i is called a divided matter element.

Extension sets are just a new concept in response to requirement. It could describe the mutual transformation between right and wrong and the degree to which things have certain properties.

U is the universe of discourse, u is any element in U, k is a mapping from U to the real domain I, and $T = (T_U, T_k, T_u)$ is a given transformation:

$$\widetilde{E}(T) = \{(u, y, y') | u \in T_U U, y = k(u) \in T_k(T_u u) \in I\}, \tag{3}$$

g is an extension set on the universe U, $y = k(u)$ is the correlation function of $\widetilde{E}(T)$, and $y' = T_k k(T_u u)$ is the extension function of $\widetilde{E}(T)$. Among them, T_U, T_k, T_u are the transformation of the universe U, the correlation quasi-function k, and the element u, respectively [16].

Extension sets are based on set theory and described by correlation functions, which can be used as a tool to quantitatively describe the quantitative and qualitative changes of things. The value range of the correlation function is the entire real number axis. The value of the correlation function can describe not only the degree to which different things have the same nature, but also the degree to which things in mediation have certain properties, and it can also describe the degree of difference between different things with opposite properties. Algebraic expressions are used to express the correlation function of extension sets, which makes it possible to quantify the process of solving incompatible problems.

In the extension set, the concept of correlation function is established, and the concept of distance and place value is also established which serves as the basis for expanding the qualitative description to the quantitative description.

3.2.1. Definition of Distance. x is a point on the real axis, $X_0 = (a, b)$ is an interval on the real field [17]:

$$\rho(x, X_0) = \left| x - \frac{a+b}{2} \right| - \frac{b-a}{2}, \tag{4}$$

is the distance between point x and interval X_0. Among them, (a, b) is either an open interval, a closed interval, or a half-open and half-closed interval.

3.2.2. Definition of Location. In practical problems, in addition to the positional relationship between points and intervals, the positional relationship between intervals and intervals and a point and two intervals must also be considered.

Then the bit value of point x with respect to the interval set consisting of intervals X_0 and X is specified as

$$D(x, X_0, X) = \begin{cases} \rho(x, X) - \rho(x, X_0), & x \notin X_0, \\ -1, & x \in X_0. \end{cases} \tag{5}$$

$D(x, X_0, X)$ is positional relationship between point x and the interval set composed of X_0 and X, referred to as position value.

Describe the difference in the position of a point in the interval according to the difference of the value of the distance. The concept of distance describes the positional relationship between points and intervals, which makes people develop from “the same within a class” to a quantitative description with a degree of difference within the class.

On the basis of distance and position, the elementary correlation function is established [18]:

$$K(x) = \frac{\rho(x, X_0)}{D(x, X_0, X)}, \tag{6}$$

and is used to calculate the degree of correlation between points and interval sets. Among them, $X_0 \subset X$ and there is no public endpoint. The value of correlation function is $(-\infty, +\infty)$, and the above is to express the correlation function in the extension set, and the thing with “property P” is extended from the qualitative description to the quantitative description of “the degree of property P.”

For a certain evaluated object N, if there is an index SI that measures the pros and cons and the range of the required value is X, the allowable value range of the value is X. The establishment of the correlation function $K(n)$ represents the degree to which the object N meets the requirements, which is called the correlation degree of N with respect to SI.

N is the correlation degree of SI on the measurement index $K(n)$; then [19]

$$k = \begin{cases} \dfrac{K_i(N_j)}{\max\limits_{x \in X_0} K_i(x)}, & K_i(N_j) > 0, \\[2ex] \dfrac{K_i(N_j)}{\max\limits_{x \notin X_0} K_i(x)}, & K_i(N_j) < 0, \end{cases} \tag{7}$$

is called the standard relevance of N to SI.

If a certain evaluated object is N, the measurement index set is SI = {SI, SI, . . ., SI,}, the normative correlation degree of N to SI is k_i ($i = 1, 2, \ldots, n$), the weight coefficient of SI is a_i, and $0 \le a_i \le 1$. a_i represents the relative importance of SI.

The extension evaluation method evaluates the research object from the perspective of feasibility and optimization and is a combination of qualitative and quantitative ones. It uses the extension of matter elements for qualitative calculations and uses extension set theory to perform quantitative calculations through correlation functions. Extension evaluation takes matter-element theory and extension mathematics as the theoretical basis and realizes the transformation of evaluation methods by establishing matter-element models.

In this paper, this method is applied to the evaluation and screening of schemes. The purpose of the screening is to remove the inferior and save the superior. The screening process is shown in Figure 1.

The criteria for evaluating the pros and cons of an object N_j ($j = 1, 2, \ldots, n$) is $\mathrm{SI}_1, \mathrm{SI}_2, \ldots, \mathrm{SI}_n$.

There are majorities, and the weight coefficients are used to express the importance of each indicator. For the indicators that must be met, they are represented by the indicator input, and for other measurement indicators, values between [0, 1] are assigned. The weight coefficient is recorded as [20]

$$\alpha = (\alpha_1, \alpha_2, \ldots, \alpha_n). \tag{8}$$

Since the selection of measurement indicators directly affects the evaluation results, the selection of measurement indicators must be cautious. Generally, indicators that meet the evaluation purpose, are representative, are easy to evaluate, and have relatively regular changes should be selected as the measurement indicators.

The selection of measurement conditions should pay attention to the following points:

(1) Purpose. We first attend the purpose of the evaluation and the evaluation object. The measurement conditions selected when evaluating different types of programs are different.

(2) Comprehensiveness. Goodness evaluation method is a comprehensive evaluation. In order to ensure this, the selection of measurement conditions must be representative. From the requirements of technology, economy, society, resources, environment, and development, select the most representative indicators that play an important role in achieving the goals of the plan.

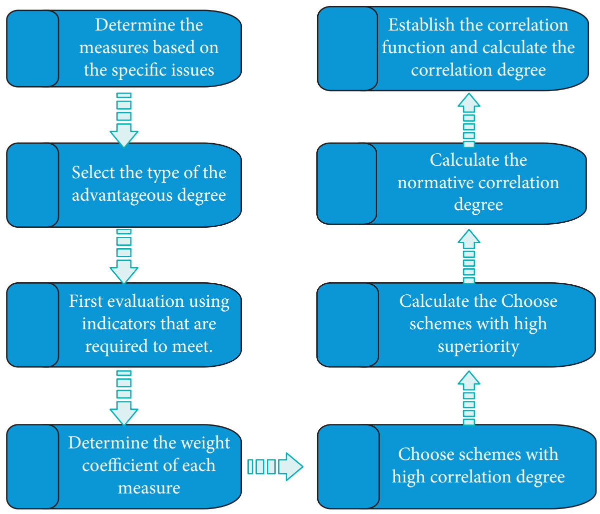

Figure 1: Basic flow of goodness evaluation method.

(3) Feasibility. The selected measurement conditions should be representative and usable for evaluation. Moreover, the data for the measurement conditions should be easy to obtain, and the data can be of high quality, truthfulness, and reliability.

(4) Stability. The selected measurement conditions should change more regularly.

Regarding the determination of the measurement condition SI, the following points should be paid attention to:

(1) It should be based on the actual situation of social as well as economic state and based on the spatial range data and historical data related to the evaluated object.

(2) It is necessary to pay attention to the development of social and economic state.

(3) The determination of the value range should have regulatory as well as management functions. The planned value of the national (regional, department) social and economic management can be considered as the boundary of the value range.

Among them, we set $\alpha_{i_0} = \Lambda$; then [21]

$$\sum_{\substack{k=1 \\ k \neq i_0}}^{n} \alpha_k = 1. \tag{9}$$

The size of the weight coefficient has a pivotal effect on the degree of goodness. Different weight coefficients cause a change in the order of the evaluated objects. Moreover, the analytic hierarchy process can be used to determine the relative importance order between the measurement indicators, thereby determining the weight coefficient.

After determining the weight coefficient of each measurement indicator, we use the indicators that must be met to filter and perform the following steps on the objects that have met the condition.

The measurement index set is $\mathrm{SI} = \{\mathrm{SI}_1, \mathrm{SI}_2, \ldots, \mathrm{SI}_n\}$, where $\mathrm{SI}_i = (c_i, V_i)$, $i-1,2,\ldots,n$, and the weight coefficient is assigned as [22]

$$\alpha = (\alpha_1, \alpha_2, \ldots, \alpha_n). \tag{10}$$

According to the requirements of each measurement index, the correlation function $K_1(x_1), K_2(x_2), \ldots, K_n(x_n)$ is established.

(1) If V_i is a finite interval X_{0i} or an infinite interval, the algorithm takes the correlation function $K_i(x_i)$.

$$K_i(x_i) = \frac{\rho(x, X_{0i})}{|X_{0i}|}, \quad i = 1, 2, \ldots, n. \tag{11}$$

(2) If V uses X and X_i (XEX) to form an interval set description without a common end point, and the best point of this index is at point x_{0i}, then the algorithm takes the elementary correlation function as

$$K_i(x_i) = \frac{\rho(x_i, x_{0i}, X_{0i})}{D(x_i, x_{0i}, X_{0i})}. \tag{12}$$

The correlation function of the object N_j with respect to each measurement index SI_i is abbreviated as $K_i(x_j)$; then the correlation degree of each object $N_1, N_2, \ldots, N_m$ with respect to SI_i is [23]

$$K_i = (K_i(N_1), K_i(N_2, \ldots, K_i(N_m))), \quad i = 1, 2, \ldots, n,$$
$$k = \begin{cases} \dfrac{K_i(N_j)}{\max\limits_{x \in X_0} K_i(x)}, & K_i(N_j) > 0 \\[2ex] \dfrac{K_i(N_j)}{\max\limits_{x \notin X_0} K_i(x)}, & K_i(N_j) < 0 \end{cases},$$
$$i = 1, 2, \ldots, , j = 1, 2, \ldots, m. \tag{13}$$

The canonical correlation degree of each object $N_1, N_2, \ldots, N_m$ with respect to SI_i is

$$k_i = (k_{i1}, k_{i2}, \ldots, k_{iM}), \quad i = 1, 2, \ldots, n. \tag{14}$$

The canonical correlation degree of object N_j with respect to each measurement index $\mathrm{SI}_1, \mathrm{SI}_2, \ldots, \mathrm{SI}_n$ is [24]

$$K(N_j) = \begin{bmatrix} k_1 \\ k_2 \\ k_3 \\ \vdots \\ k_n \end{bmatrix}, \quad j = 1, 2, \ldots, m. \tag{15}$$

According to the different requirements of actual problems, the superiority of object N can be divided into three situations:

(1) If in actual problems, the comprehensive relevance of all measurement indicators is required to be greater than 0 before the object N is considered to meet the requirements, then the goodness is defined as

$$C(N_j) = \sum_{i=1}^{m} \alpha_i k_i = (\alpha_1, \alpha_2, \ldots, \alpha_n) \begin{bmatrix} k_{1j} \\ k_{2j} \\ \vdots \\ k_{nj} \end{bmatrix}, \quad j = 1, 2, \ldots, m. \tag{16}$$

(2) If in actual problems, as long as the comprehensive correlation degree of a certain measurement index is greater than 0, it is considered that the object N meets the requirements, then the goodness is defined as

$$C(N_j) = \bigcup_{i=1}^{n} k_{ij}, \quad j = 1, 2, \ldots, m. \tag{17}$$

(3) If in actual problems, the correlation degree of all measurement indicators is required to be greater than 0 before the object N is considered to meet the requirements, then the degree of goodness is defined as

$$C(N_j) = \bigcap_{i=1}^{n} k_{ij}, \quad j = 1, 2, \ldots, m. \tag{18}$$

According to actual problems, we first evaluate the evaluation object with "indicators that must not be satisfied." For all objects that meet the requirements, we use one of the above three kinds of goodness to calculate its goodness and compare the goodness of N. If

$$C(N_0) = \max_{j=\{1,2,\ldots,m\}} \{C(N_j)\}, \tag{19}$$

then object N_0 is better.

The essence of the extensional neural network that can analyze things qualitatively and evenly is derived from the quantitative analysis ability of the correlation function. However, extenics is single-threaded, and there is no multithreaded, parallel operation and computing power. Neural networks can overcome this shortcoming of extenics. Therefore, extenics and neural networks are combined to learn from each other. On the one hand, visualization technology is used to construct a new neural network structure. On the other hand, the learning mechanism of the network is combined with the extension matter element, and the sample data is learned and trained on this basis to achieve the purpose of improving the learning efficiency and the correctness of the classification. The extension neural network is shown in Figure 2.

It belongs to a two-layer structure, including an input layer and an output layer, with the connection weight of the input neuron and the output neuron. Each node in the input layer is a different feature of the multidimensional matter element. The number of neurons in the input layer depends on the number of input parameter vectors. Each neuron in the input layer and each neuron in the output layer are bidirectionally connected with weights. The basic unit of connection is the minimum value of the feature vector field and the maximum value of the feature vector.

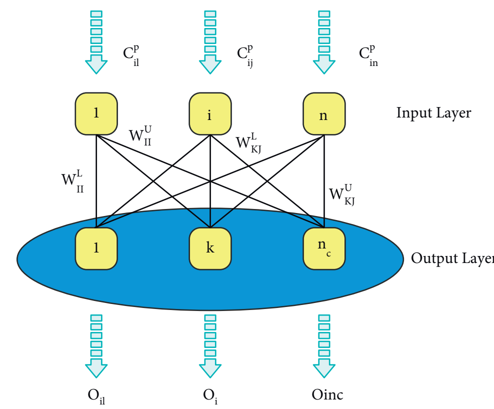

Figure 2: Extension neural network model structure.

4. New Media Advertising Communication Analysis Model Based on Extension into the Network

The consumer decision-making process gives a good description of the correlation between consumers and brands. This process also describes in more detail the process of consumers from having a purchase demand to generating a purchase action to achieving mutual trust, and it also studies how to influence consumer behavior in this process. The consumer decision-making process has also gone through six stages, which are mainly divided into consideration, evaluation, purchase, experience, mutual fans, and mutual trust, as shown in Figure 3.

Based on the theory of consumer decision-making process, the author also summarized the structure of the communication mode under mobile advertising from the perspective of consumer psychology based on the reality under the background of the mobile Internet era (Figure 4).

The advertising communication model established in this paper is different from the general advertising communication model. It combines complex network theory and advertising communication theory to construct an advertising communication model that can quantify the effect of communication. The channels of advertising communication in this paper are divided into two types: mass communication and interpersonal communication. Moreover, this paper proposes a two-layer network topology structure of the advertising dissemination network, as shown in Figure 5.

From a logical point of view, it is easier to understand the two-layer structure of the advertising dissemination network. As shown in Figure 5, the first-level interpersonal communication network reflects the relationship between user nodes. There are friend relationships between edge-connected nodes, and both parties can transmit information. Therefore, for user nodes, it is important for

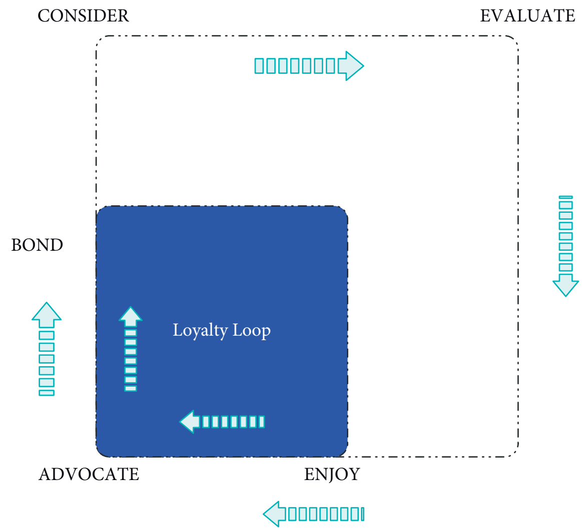

Figure 3: Consumer decision-making process.

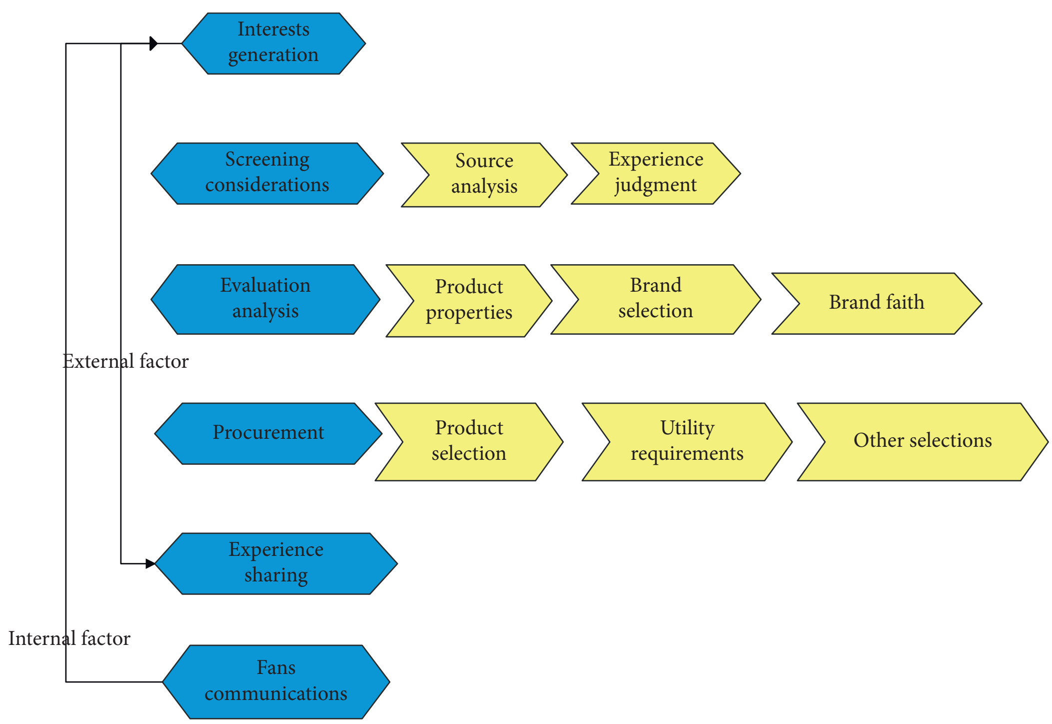

Figure 4: Improved model of mobile advertising communication mode.

advertising. Information attitudes and behaviors are affected by their friends' nodes; the second-tier mass communication network is a network composed of mass communication media used in advertising, and the mass communication network includes several specific media networks, each of which is specific The media network refers to the network composed of user nodes owned by the media and reflects the relationship between the user nodes and the media.

The establishment of advertising communication network is the necessary foundation and prerequisite for the follow-up simulation to proceed smoothly. Next, the Nanjing area will be used as the target of advertising, and the two-layer network model of advertising will be used to construct an advertising communication network model. First, build the first layer of interpersonal network. Since the first-level network reflects the interpersonal relationship between people, it is necessary to build an interpersonal network. From the well-known phenomenon of "six degrees of separation," each node in the interpersonal network can also be connected indirectly through several individual nodes in the network; that is, the interpersonal network has obvious small world characteristics, so randomization will be used in this article. The method of

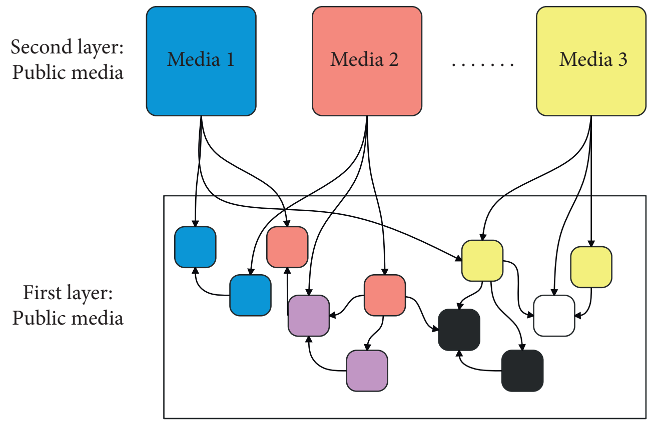

Figure 5: Structure diagram of advertising dissemination network.

adding edges constructs a NW small world network as the interpersonal network in the advertising communication network, that is, the first-layer network of advertising communication.

Generally, the scale of the interpersonal communication network is set to 1000, and the node degree distribution and clustering coefficient of the interpersonal network constructed according to the NW network construction method are shown in Figures 6 and 7, respectively.

The number of user nodes when advertisement propagation reaches a steady state is represented by a table as shown in Table 1.

It can be seen from Table 1 that when the propagation process reaches a stable state, the number of nodes in the final unknown state is the least, and television media is the least, followed by newspapers, networks, radio stations, and magazines. From the perspective of the final purchase status alone, television media is the most, followed by newspapers, Internet, radio, and magazines. In terms of the number of neglected states alone, newspaper media is the largest, followed by the Internet, TV, magazines, and radio. After knowing the situation of their respective advertisements, the comparative changes of their advertisements' spread are shown in Figure 8.

Through the above analysis, the effect of the model proposed in this paper is verified, multiple sets of advertisements are obtained through the Internet, and the effect of the model of this paper is verified. First, the analysis effect of the model of this paper on the advertising data is verified, and the results shown in Table 2 and Figure 9 below are obtained.

From the above analysis, it is verified that the new media advertising communication analysis model based on extension network can play a certain role in advertising data analysis. On this basis, this paper conducts the

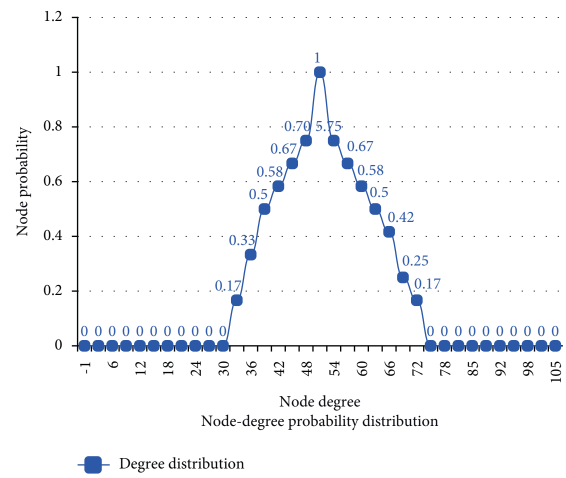

Figure 6: Probability distribution of network node degree.

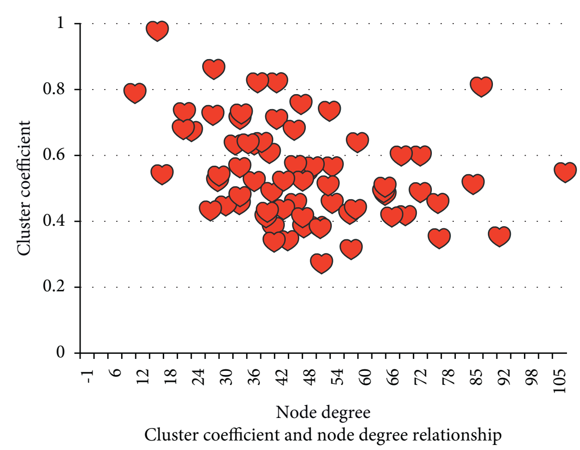

Figure 7: The relationship between network clustering coefficient and node degree.

Table 1: Proportion of nodes in various states when the propagation reaches a steady state.

	Unknown state	Known state	Desired state	Purchase state	Ignore state
Magazine	0.770	0.000	0.000	0.160	0.070
Radio station	0.700	0.000	0.000	0.250	0.050
The Internet	0.450	0.000	0.000	0.440	0.110
Newspaper	0.240	0.000	0.000	0.620	0.150
Television	0.140	0.000	0.000	0.750	0.110

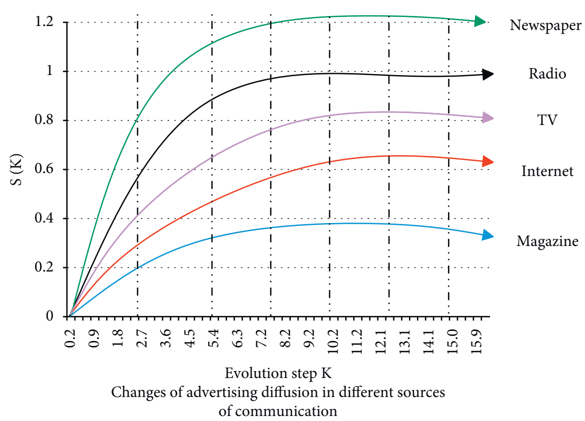

Figure 8: Changes in the diffusion degree $s(k)$.

Table 2: The analysis effect of the model on advertising data.

Number	Advertising data analysis	Number	Advertising data analysis	Number	Advertising data analysis
1	79.75	11	84.99	21	92.31
2	88.38	12	79.95	22	86.31
3	85.78	13	85.75	23	84.67
4	84.66	14	90.10	24	80.06
5	87.40	15	87.34	25	83.38
6	81.86	16	85.14	26	80.30
7	87.74	17	88.44	27	90.80
8	90.40	18	79.99	28	89.61
9	81.94	19	87.51	29	81.35
10	92.27	20	87.73	30	91.95

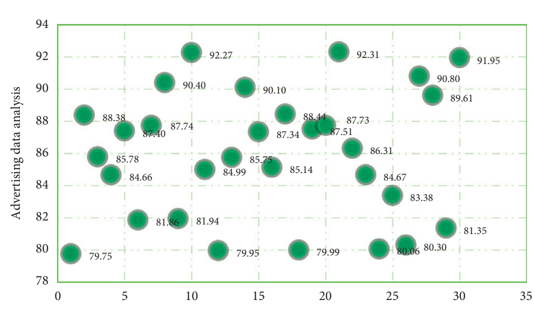

Figure 9: Statistical diagram of advertising data analysis test.

performance verification of the new media advertising communication analysis, and the expert evaluation method is used to verify the results shown in Table 3 and Figure 10 below.

From the above experimental verification, it can be seen that the new media advertising communication analysis model based on the extension of the network proposed in this paper meets the new media advertising communication analysis effect.

Table 3: Performance verification of new media advertising communication analysis.

Number	Communication effect analysis	Number	Communication effect analysis	Number	Communication effect analysis
1	78.16	11	76.96	21	85.91
2	73.08	12	82.13	22	85.67
3	87.20	13	76.68	23	88.62
4	81.40	14	83.71	24	73.60
5	77.14	15	76.92	25	80.63
6	76.21	16	77.67	26	80.53
7	73.80	17	88.90	27	88.12
8	77.57	18	78.24	28	78.42
9	87.52	19	86.02	29	74.30
10	75.83	20	72.63	30	88.07

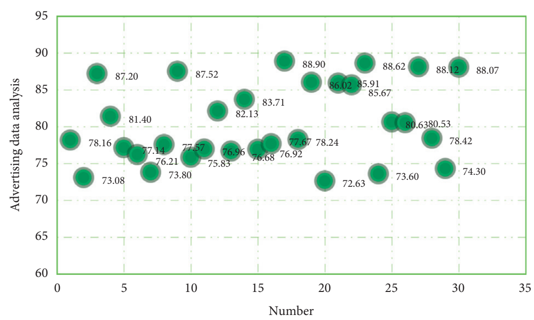

Figure 10: Advertising communication performance analysis.

5. Conclusion

The media is the platform and support for advertising and dissemination, and the relationship between advertising and the media is close and inseparable. A certain understanding of media, especially emerging digital media and communication knowledge, is a necessary foundation for advertising activities. The development of communication technology has caused media competition to become fierce. Although mass communication media occupies a large market share and competitiveness, the lack of communication characteristics of traditional media makes the communication effect unsatisfactory. Network media has the new characteristics of media communication, such as large amount of information, diverse forms, being rapid and timely, global communication, easy copying, easy retrieval, freedom, and interaction, which undoubtedly fill the deficiencies of traditional media. On the other hand, with the increasingly obvious trend of consumer market segmentation and increasingly fierce competition in the advertising market, these factors have provided a hotbed for rapid development of online advertising as the main pillar of the advertising industry. This thesis combines the scalable neural network to construct the new media advertising communication analysis model and conducts research on the new media advertising communication analysis. The experimental verification shows that the new media advertising communication analysis model based on the extension of the network proposed in this paper meets the new media advertising communication analysis effect.

Data Availability

The data used to support the findings of this study are available from the corresponding author upon request.

Conflicts of Interest

The authors declare that there are no conflicts of interest.

Acknowledgments

This work in this article was supported by North China University of Technology.

References

[1] F. Guo, G. Ye, L. Hudders, W. Lv, M. Li, and V. G. Duffy, “Product placement in mass media: a review and bibliometric analysis,” *Journal of Advertising*, vol. 48, no. 2, pp. 215–231, 2019.

[2] A. Yadi Yaakop, S. A. Ismail, S. Aishah Ismail, and Z. Zainal Ariffin, “Breaking through clutter: analysis of mobile political advertising in Malaysia,” *International Journal of Social Science and Humanities*, vol. 9, no. 2, pp. 26–30, 2019.

[3] U. U. Akpan, “Print media management and ethical advertising under r,” *Journal of Media Management and Entrepreneurship*, vol. 3, no. 1, pp. 1–11, 2021.

[4] A. R. Condeza Dall’Orso, P. Matus Lobos, and E. Vergara Leighton, “Stereotypes and sexualization of girls and adolescent girls in Chilean advertising: a case study,” *Tripod*, vol. 50, no. 50, pp. 187–204, 2021.

[5] C. Kolo and F. Haumer, “Social media celebrities as influencers in brand communication: an empirical study on influencer content, its advertising relevance and audience expectations,” *Journal of Digital and Social Media Marketing*, vol. 6, no. 3, pp. 273–282, 2018.

[6] R. L. Gruner, A. Vomberg, C. Homburg, and B. A. Lukas, “Supporting new product launches with social media communication and online advertising: sales volume and profit implications,” *Journal of Product Innovation Management*, vol. 36, no. 2, pp. 172–195, 2019.

[7] H. Li, “Visual communication design of digital media in digital advertising,” *Journal of Contemporary Educational Research*, vol. 5, no. 7, pp. 36–39, 2021.

[8] Y. Wang and E. N. Remchukova, “Development of the advertising specialty in higher education in Russia and China,” *RUDN Journal of Psychology and Pedagogics*, vol. 18, no. 3, pp. 532–554, 2021.

[9] H. A. M. Voorveld, "Brand communication in social media: a research agenda," *Journal of Advertising*, vol. 48, no. 1, pp. 14–26, 2019.

[10] E. Pancaningrum and W. A. Rahayu, "The effectiveness of Facebook as an advertising strategic method using EPIC: a case study of Mie Jupe Jombang," *Chinese Business Review*, vol. 16, no. 7, pp. 309–315, 2017.

[11] H. Li, "Special section introduction: artificial intelligence and advertising," *Journal of Advertising*, vol. 48, no. 4, pp. 333–337, 2019.

[12] T. Arora, B. Agarwal, and A. Kumar, "A study of millennials's preferences for social media advertising in Delhi NCR," *Indian Journal of Marketing*, vol. 49, no. 10, pp. 34–51, 2018.

[13] S. Ali, "Women objectification and advertising: an analysis of sexually objectified portrayal of women in television advertising in Pakistan," *Global Media Journal*, vol. 16, no. 31, pp. 1–9, 2018.

[14] T. Arora and B. Agarwal, "An empirical study on determining the effectiveness of social media advertising," *International Journal of E-Business Research*, vol. 16, no. 2, pp. 47–68, 2020.

[15] A. Ujică and R. Băbuţ, "Female stereotypes in Romanian advertising: an interpretative content analysis," *Studia Universitatis Babes-Bolyai Oeconomica*, vol. 66, no. 2, pp. 25–37, 2021.

[16] E. N. Malyuga, E. V. Ponomarenko, and A. V. Minayeva, "Stylistic devices as means of forming discursive features of advertising minitexts (exemplified by English economic and political media sources)," *Vestnik of Samara University. History, Pedagogics, Philology*, vol. 26, no. 4, pp. 82–87, 2020.

[17] D. Datta and A. K. Choudhury, "Economics OF health care service sector related public service outdoor media advertising IN Tripura, India," *International Journal on Recent Trends in Business and Tourism*, vol. 3, no. 3, pp. 35–48, 2019.

[18] M. Guardino and D. Snyder, "The capitalist advertising and marketing complex and the US social order: a political-materialist analysis," *New Political Science*, vol. 39, no. 4, pp. 588–608, 2017.

[19] H. Jin and F. Yang, "A strategic study on customer engagement improvement from the perspective of short video advertising: take douyin as an example," *International Journal of Engineering and Management Research*, vol. 4, no. 3, pp. 6–8, 2020.

[20] T. Dummanonda and C. Nuangjamnong, "The influence of social media advertising value on consumer behavior in renting apartment rooms in bangkok, Thailand," *International Research E-Journal on Business and Economics*, vol. 6, no. 1, pp. 13–27, 2021.

[21] B. Yoosefy, H. Honari, A. Ghobadi Yeganeh, and V. N. Palangard, "The effect of sport fandom and general attitude towards advertising on the credibility of sports advertising," *Communication Management in Sport Media*, vol. 7, no. 3, pp. 33–42, 2020.

[22] A. Yazdanparast, I. Naderi, N. Spears, and R. O. Fabrize, "Advertising and pseudo-culture," *Journal of Macromarketing*, vol. 38, no. 2, pp. 185–205, 2018.

[23] R. Winks and K. Cresen, "Impact OF language frames IN advertising effectiveness," *International Journal of Linguistics*, vol. 1, no. 1, pp. 28–33, 2021.

[24] X. Yu and T. Natori, "Scientific mapping for advertising in recent decades: a citespace bibliometric analysis," *International Journal of Japan Association for Management Systems*, vol. 12, no. 1, pp. 103–110, 2020.

Hindawi
Scientific Programming
Volume 2021, Article ID 9485654, 14 pages
https://doi.org/10.1155/2021/9485654

Research Article

Design and Implementation of Intelligent Educational Administration System Using Fuzzy Clustering Algorithm

Fang Liu

Scientific Research Department, Xijing University, Xi'an, Shaanxi 710123, China

Correspondence should be addressed to Fang Liu; sunrain110312@163.com

Received 24 October 2021; Revised 17 November 2021; Accepted 25 November 2021; Published 29 December 2021

Academic Editor: Le Sun

The present work aims to solve the problems that the traditional educational administration management system has, such as low efficiency in analyzing big data, and the analysis results have low value, which is based on manual rules definition in big data analysis and processing. The work proposes a student achievement prediction model FCM-CF based on Fuzzy C-means (FCM) and Collaborative Filtering (CF). The work also introduces it into the research of educational administration management to construct an intelligent educational administration management system. At the beginning, the FCM-CF model is described in detail. Then, the system requirements and specific design methods are described in detail. Eventually, with the students' performance prediction as an example, the performance of the system is tested by designed simulation experiments. The result shows that the students' achievement in study is closely related to their daily study performance such as preparation before class, classroom performance, attendance, extracurricular study, and homework completion. Generally, the examination scores of students are significant to their daily performances. Under the same experimental conditions, the prediction error of the FCM-CF model proposed here is less than 10.8% of that of other algorithms. The model has better prediction performance and is more suitable for the prediction of middle school students' examination scores in educational administration management system. The innovation of intelligent educational administration management system is that, in addition to the basic information management function, it also has two other functions: students' performance prediction analysis and teacher evaluation prediction. It can provide data support for improving teaching quality. The research purpose is to provide important technical support for more intelligent educational administration and reduce the loss of human resources in educational administration.

1. Introduction

In recent years, with the continuous development of computer technology, people's life has entered a highly information-based era. Whether it is personal identity information, consumption information, or travel information, while bringing great convenience to people, they have been familiar by people. Of course, this convenience is also reflected in the education industry, especially in colleges. The use of information technology has been very mature. In daily teaching, the application of computer-aided instruction (CAI) breaks the rigid traditional teaching mode and makes the lecture vivid and flexible [1]. In the aspect of campus management, the application of information technology makes the management of colleges become intelligent, which greatly reduces the waste of related manpower. The educational administration management system in colleges is the embodiment of this utilization. As the center of college management, educational administration management system manages a series of actions and plans of the college, including the students' status information, students' online course selection, teachers' annual teaching plan, teaching materials, ability test of each semester, statistical entry and query of test results, and management of teachers' evaluation of teaching [2].

Nasir et al. investigated the influencing factors of self-regulated academic performance of students majoring in management in the College of Teacher Training and Science Education. The results showed that students with higher academic performance would have stronger self-regulation ability [3]. Lv et al. designed the scheme of intelligent building indoor environment measurement, and the control system based on cyber-physical systems (CPS) included four basic modules: detection, control, execution, and communication. CPS and artificial intelligence (AI) were studied to promote their application in the construction industry. It is believed that the research on the combination of CPS and AI in the construction industry can provide theoretical basis for the development of intelligent building industry [4]. Xie et al. claimed that deep learning (DL) had shown great potential in disease prediction and drug response prediction, summarized the DL prediction methods for different diseases, pointed out a series of problems in current disease prediction, and proved the high correlation between DL and the future development of medical field [5]. Lv et al. built a smart city constructing model with the support of Internet of things, cloud computing, and Internet and stimulated the vertical market system of smart city from an economic perspective. The results suggested that the system had good stability. From the perspective of vertical market, self-operated retailers have more advantages, which can provide experimental reference for future smart city construction and economic development [6].

With the expansion of scales of colleges and enrolment, the number of students and teachers is increasing. The large quantity of personnel information data brings difficulties to school management. However, most colleges and universities do not pay attention to the innovation of educational administration management. Their management systems are still designed by technical personnel directly through the definition of rules according to the actual situation and needs of the school. These systems can provide information query, adding and deleting functions, but cannot be used to analyze data. Therefore, the school enrolment plan analysis, teacher personnel management, teaching management, and asset equipment management need to be carried out by manual analysis and processing, and the efficiency is very low. Based on this, the present work proposes a student achievement prediction model-FCM-CF based on Fuzzy C-means (FCM) and Collaborative Filtering (CF) and introduces it into the research of educational administration management to construct an intelligent educational administration management system. Primarily, the FCM-CF model is described in detail. Then, the system requirements and specific design methods are illustrated. Ultimately, taking the student performance prediction as an example, the performance of the system is tested by designed simulation experiments. The powerful data mining ability of FCM can also make colleges better deal with the real-time situation of education and make a certain contribution to the development and optimization of educational administration in colleges. The research purpose is to provide important technical support for more intelligent educational administration and reduce the loss of human resources in educational administration.

2. Model Construction and System Design

2.1. Students' Scores Prediction Model Based on FCM-CF. Clustering analysis is the process of using mathematical methods to study and process the given objects, and distinguishing and classifying them according to the similarity between things. With the establishment of fuzzy theory, people begin to use fuzzy methods to deal with clustering problems, namely, the fuzzy clustering analysis. Fuzzy clustering can be applied to deal with many objects whose attribute distinction is not obvious in practice. It uses membership function to express the similarity between samples. Since fuzzy clustering obtains the uncertainty degrees of number of samples and each category, it expresses the intermediary of the sample category; that is, it establishes the description of the uncertainty of the sample for the category, which can more objectively reflect the real world. Generally, the fuzzy clustering method based on objective function is used to cluster the targets [7]. Equation (1) represents the sample set $X = \{x_1, x_2, \ldots, x_n\}$.

$$\sum_{j=1}^{c} \mu_{jk} = 1. \tag{1}$$

In equation (1), $j = 1, 2, \ldots, c$, $k = 1, 2, \ldots, n$. Parameter $c\,(2 \le c \le n)$ is the number of categories of sample X transferred. Parameter $\mu_{jk} \in [0, 1]$ means the membership degree of sample k to the class j.

The fuzzy partition matrix U is defined as

$$U = \left\{ \begin{matrix} \mu_{11}\mu_{12}\cdots\mu_{1n} \\ \mu_{21}\mu_{22}\cdots\mu_{2n} \\ \vdots\ \vdots\ \mu_{jk}\ \vdots \\ \mu_{c1}\mu_{c2}\cdots\mu_{cn} \end{matrix} \right\}. \tag{2}$$

In equation (2), $\mu_{jk}\,(1 \le j \le c, 1 \le k \le n)$ represents the membership degree of sample x_k to the class j. At present, the most widely used FCA is Fuzzy C-means (FCM), which mainly obtains the membership degree of each sample point to all class centers by optimizing the objective function, to determine the class of sample points to achieve the purpose of automatic classification of sample data. Each sample is given a membership function belonging to each cluster, and the samples are classified by the membership value. Its objective function J_f is

$$J_f = \sum_{j=1}^{c} \sum_{k=1}^{n_j} \mu_{jk}^{b} \left\| x_k^{(j)} - m_j \right\|^2. \tag{3}$$

In equation (3), b refers to a weighted index, $b > 1$, which is used to describe the fuzzy degree of clustering results. The best empirical values are adopted, of which $b = 2$. Parameter x_k stands for sample k in the X, m_j refers to the cluster center, and μ_{jk} is a membership function.

To make J_f minimum, equations (1)–(3) are transformed into equation (4) to solve the problem of constraint optimization.

$$\left\{ \min \sum_{j=1}^{c} \sum_{k=1}^{n_j} \mu_{jk}^{b} \left\| x_k^{(j)} - m_j \right\|^2, \text{s.t.} \sum_{j=1}^{c} \mu_{jk} = 1. \right. \tag{4}$$

In equation (4), b represents a weighted index, x_k stands for the sample k in X, m_j is the cluster center, and μ_{jk} refers to a membership function. The Lagrange multiplier method is used to solve the problem as

$$L = \sum_{j=1}^{c}\sum_{k=1}^{n}\mu_{jk}^{b}\left\|x_k - m_j\right\|^2 - \sum_{k=1}^{c}\lambda_k\left[\sum_{j=1}^{c}\mu_{jk} - 1\right]. \quad (5)$$

In equation (5), b refers to a weighted index, x_k stands for sample k in X, m_j represents the cluster center, and μ_{jk} is a membership function , L denotes the Lagrange multiplier method , and λ_k refers to a multiplier of the function. Then, the partial derivatives of L about m_j, μ_{jk}, λ_k are set to zero as follows:

$$\mu_{jk} = \frac{\left\|x_k - m_j\right\|^{2/1-b}}{\sum_{l=1}^{c}\left\|x_k - m_l\right\|^{2/1-b}}. \quad (6)$$

In equation (6), μ_{jk} represents a membership function, b refers to a weighted index, x_k stands for sample k in X, and m_j represents the cluster center.

$$m_j = \frac{\sum_{k=1}^{n}\mu_{jk}^{b}x_k}{\sum_{k=1}^{n}\mu_{jk}^{b}}. \quad (7)$$

In equation (7), m_j is the cluster center, b refers to a weighted index, x_k stands for sample k in X, and μ_{jk} represents a membership function. Figure 1 demonstrates the concrete steps of FCM.

First, parameter c is set as the number of categories of fuzzy clustering, b as a weighted index, I as the number of iterative operations, and ε as the threshold to stop iteration. Second, the clustering center is initialized. Third, iterative operation is carried out, the membership function is updated by equation (6), and the clustering center is updated by equation (7) until the result converges, so that the final result of clustering center and fuzzy partition matrix can be obtained [8].

Applying the fuzzy clustering technology to the educational management system, valuable information and its inherent laws can be excavated from the large amount of data in the educational management system. It helps improve the efficiency of school enrolment and employment management, teacher personnel management, educational management, student growth guidance and management, and asset and equipment management, to better understand students, optimize teaching, strengthen management, and improve relevant systems.

CF algorithm is a technology in information filtering and information system. It is used to analyze the users' interest, find the similar user of the specified user in the user group according to his or her interest, synthesize the evaluation of these similar users on a certain information, and form a system to predict the preference of the specified user for this information. The prediction of students' performance can be understood as the "recommendation" of students' performance, and the more similar the situation or factors between students, the more closer the students' examination scores. Predicting a student' s performance can use the historical student data to find similar students to be predicted.

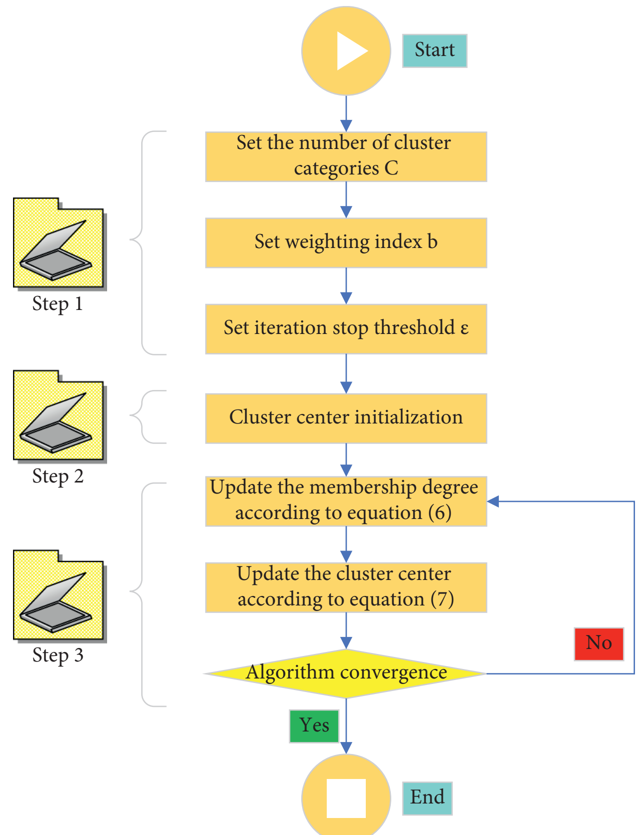

Figure 1: The concrete steps of FCM.

Students correspond to similar users in the collaborative filtering data set. These similar students' historical results can be integrated to predict the performance of the designated students. The present work combines FCM-CF to propose a student achievement prediction model based on FCM-CF. Figure 2 displays the structure of the model.

Initially, the fuzzy clustering technology is used to cluster the historical students' achievement data, and the membership matrix of each student in each cluster is obtained. Then, the prediction of each cluster to predict students' performance is calculated, according to the distribution of each student belonging to each cluster and the collaborative filtering method based on students. Eventually, the final prediction results are obtained by weighting the distribution of the target students belonging to each cluster. Specific prediction algorithms are as follows:

Through subordinate matrix- U and the situation of each student belonging to each clustering center, the performance of student-$s\prime$ in cluster-c can be calculated [9] as

$$\mathrm{per}\left(C_j\right) = \frac{\sum_{i=0}^{m-1}u_{ij}P_{in-1}}{\sum_{i=0}^{m-1}u_{ij}}. \quad (8)$$

In equation (8), u_{ij} refers to the element in U, P_{in-1} represents the performance of student s' under the $n-1$ influencing factors, m denotes the number of students, and $\mathrm{per}(C_j)$ means performance of student-s' in cluster- c.

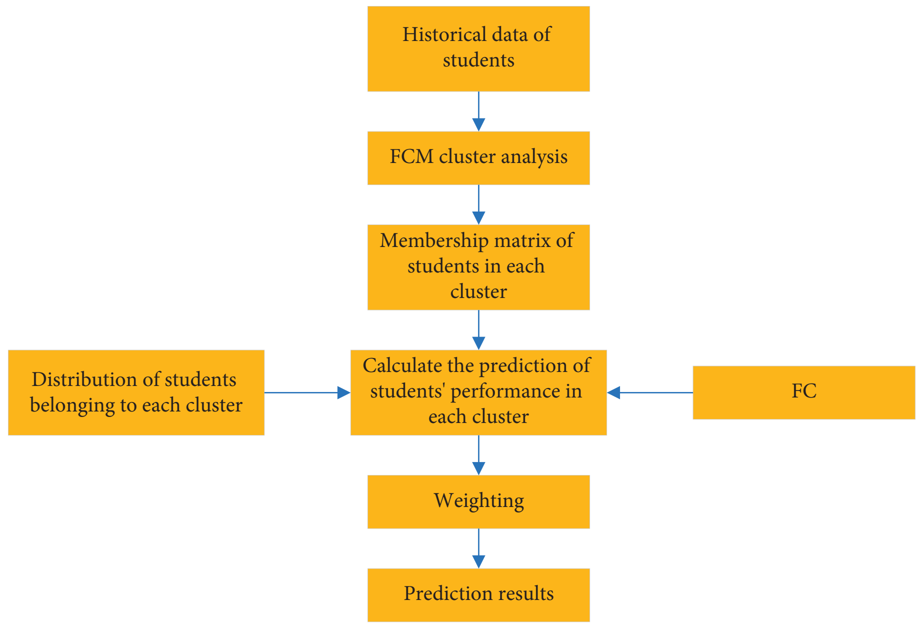

Figure 2: Structure of FCM-CF model.

Performance of s' under the factor n can be obtained according to which cluster the students is subordinate.

$$\mathrm{FCMCF}\left(s', n\right) = \sum_{j=0}^{c-1} u_{mj} \mathrm{per}\left(C_j\right). \tag{9}$$

In equation (9), u_{mj} refers to an element in U, and $\mathrm{FCMCF}\left(s', n\right)$ stands for performance of the target student-s' under the factor n.

2.2. Analysis of System Design. The development of technologies and the continuous advancement of informatization tremendously influence people's life, including the convenience brought by information technology and the troubles brought by information leakage. To keep up with the pace of the time, the requirements for modernization of all walks of life are increasing day by day. Informatization does not completely represent modernization. However, the realization of modernization must be inseparable from the development of informatization [10]. For modern college education, information technology is an indispensable method and a common used tool in the trend of educational reform. With the application of computer and other information technologies, teaching and learning in higher education have broken through the limitations of traditional teaching mode and become more flexible and controllable. With the advancement of educational informatization, in the continuous development, colleges inevitably face the situation that massive educational information needs to be processed. Although the information management systems of colleges are constantly improved, the current educational administration management system is still facing enormous challenges [11]. Using FCM to manage the educational information can provide data support for colleges to improve teaching quality. Additionally, the powerful data mining ability of FCM can also make colleges better handle the real-time situation of education, thus providing theoretical basis for the management decision-making of colleges [12].

The original intention of the educational administration management system is to manage the teaching work in colleges, and its functions need to meet the daily operation needs of colleges [13]. The requirements of the functions of education management system mainly include:

(1) Construction and management of academic status database, and input and editing of academic information.

(2) Formulating overall education plan for the institute, releasing teaching syllabus for the institute, and making teaching plan for teachers and reviewing on teaching plan from academic administration.

(3) Input, inquiry, editing, and statistic of the academic materials.

(4) Releasing information of curriculum from academic administration, inquiry, and selecting courses by students, integrating the information of courses selection, and reselecting courses.

(5) Arrangement of location and time of examination, selection and determination of the invigilator, and other inquiry of related information.

(6) Input and editing of the students' scores by teachers, statistical analysis on the students' personal performance by system automatically, and inquiry and complaints from students.

(7) Accomplishing self-evaluating of teachers, evaluation from students, colleagues, and leaders, and statistic analysis of the evaluation information.

The design of the system is aimed at improving the educational management level of colleges, which makes the educational management work systematic, standardized, and intelligent, and reducing the manpower consumption required for information management in colleges. As a conclusion, the design of educational administration management system has five basic principles [14] as displayed in Figure 3.

(1) The principle of management institutionalization: The design of educational administration management system must be consistent with the educational administration management system of colleges. And the corresponding educational standards and systems should be taken as the benchmark to ensure the practicability of the system.

(2) The principle of openness and sharing of the system: To share information and data and facilitate users to operate across platforms, the design of the system should be kept open.

(3) The principle of simple and quick operation: Most of the time, the management of educational administration is relatively trivial. Therefore, the operation of the system must be simple and quick to facilitate the management of managers.

(4) The principle of convenient updating and upgrading: The complexity and diversity of information data require that the educational administration management system be convenient for updating, upgrading, and facilitating the subsequent improvement of the system.

(5) The principle of safety and reliability: As a tool of educational management in colleges, the educational management system must have a high degree of safety and stability. On the premise of ensuring that confidential information will not be leaked, the system cannot easily collapse with the operation.

2.3. Design of Educational Administration Management System

2.3.1. Design of Hardware of the System. The educational management system of college is composed of server, client, and network equipment. The system constructed here has two servers, namely, database server and network server. The former provides users with data query and instruction submission services, and the latter provides network connection services [15]. The instructions submitted by users are transmitted to the server through the network server, switches, firewalls, and route routers. After the server processes the instructions, the information is fed back to the user client [16]. Figure 4 displays the specific hardware architecture of the system.

2.3.2. Microsoft SQL Server 2008 Database. Microsoft SQL Server is a comprehensive database platform released by Microsoft, which has advantages such as great convenience and flexibility, and is very practical and highly integrated with other software [17]. Microsoft SQL Server 2008 is the most powerful and comprehensive version of Microsoft SQL Server, which has characteristics as following:

(1) Credibility: this characteristic makes application software of enterprise safe, reliable and expandable when carrying out important missions.

(2) High effectiveness: this characteristic reduces the time and cost when enterprise conduct developing and managing on infrastructure of data

(3) Intelligence: the development platform can provide related data for users, as a comprehensive and flexible platform [18]

Microsoft SQL Server 2008 has 4 kinds of core components as following:

(1) Database engine: mainly used to storage, manage, and control the access and other handling on the data

(2) Analysis service: providing supports for online analytical processing and data mining based on existing database

(3) Reporting service: presenting the generated classified information based on existing data in the reports, thus making users can access the reports and the data

(4) Integrating service: integrating data, processed results, and processing reports of the core component to realize the integration of the data

Figure 5 demonstrates the architecture of Microsoft SQL Server 2008.

2.3.3. Structure Design of the System. The Client-Server (C/S) mode takes the server as the center, which can make full use of the hardware advantages of the server and the client, allocate tasks reasonably, and reduce the communication time of the system. The client can access the server to obtain the required network resources, and the information uploaded by the client can be stored on the server. Figure 6 manifests the structure of C/S system.

Browser-Server mode (B/S) is an improvement of C/S, which belongs to three-layer C/S structure. B/S structure only needs a browser to fix the problem that the traditional way must use special software to solve, which greatly saves costs and simplifies the development, maintenance, and use of the system. It is a new software system construction technology. This model unifies the client and concentrates the core part of the system function realization on the server. Data interaction can be achieved by installing a browser on the client and a database on the web server [19]. Figure 7 signifies the structure of B/S system.

The system or software using B/S structure can have the server to complete the installation, modification, and maintenance functions. The biggest advantage of B/S structure is that whenever and wherever users want a computer that can connect to the Internet, they can achieve the purpose of zero maintenance of the client without installing special software. Both structures have their own

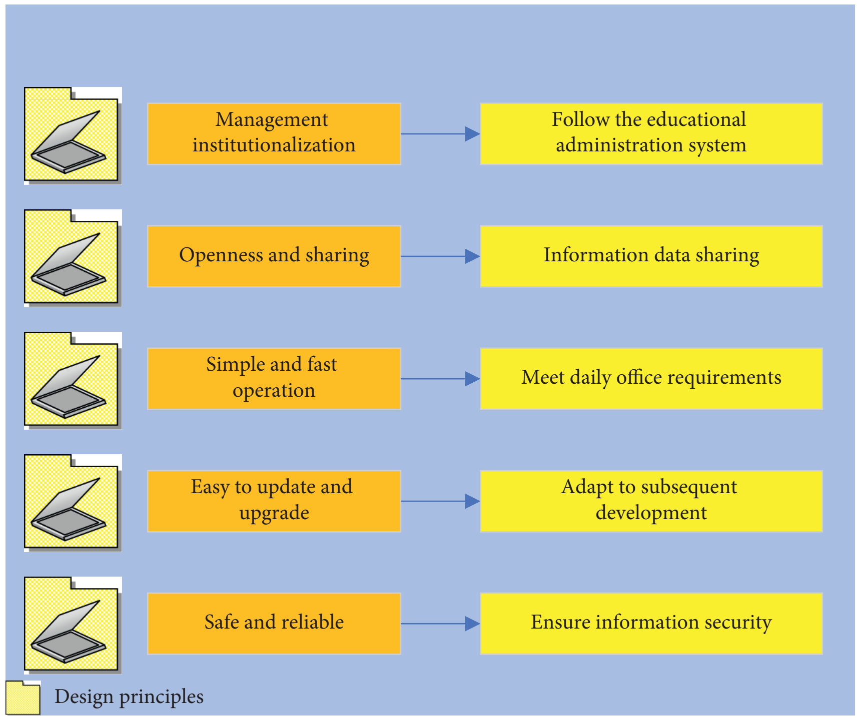

Figure 3: Design principles of educational administration management system.

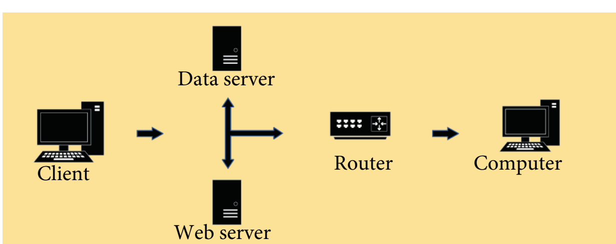

Figure 4: Hardware architecture of educational management system.

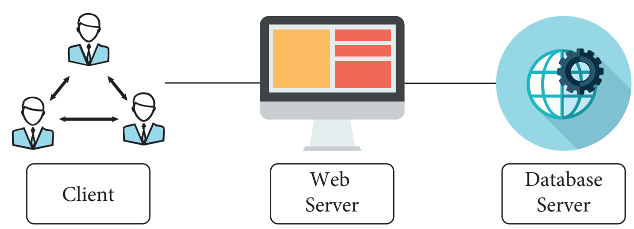

Figure 6: Structure of C/S system.

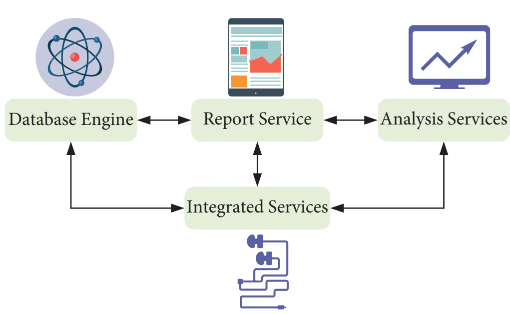

Figure 5: Architecture of Microsoft SQL Server 2008.

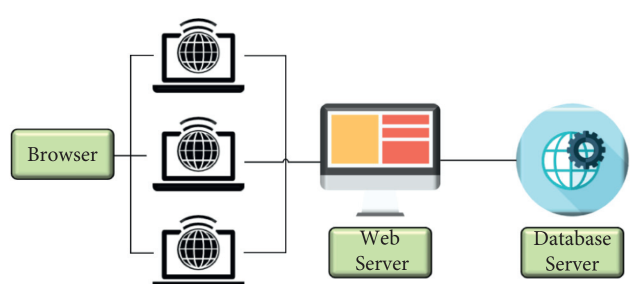

Figure 7: Structure of B/S system

advantages and disadvantages [20], as shown in Figures 8 and 9.

In view of the advantages and disadvantages of B/S structure and C/S structure, the present work mainly discusses the integration of the two architectures. At present, there are two ways for C/S and B/S mixed model: one is called "inquiry/modifying" model, and the other is called "inside/outside" model.

In the B/S and C/S mixed software architecture of the "Inquiry/modifying" model, regardless of the way users are connected to the system via Internet or LAN, the C/S architecture is used if maintenance and modification of data operations are required. If only general query and browsing operations are performed, the B/S architecture is used.

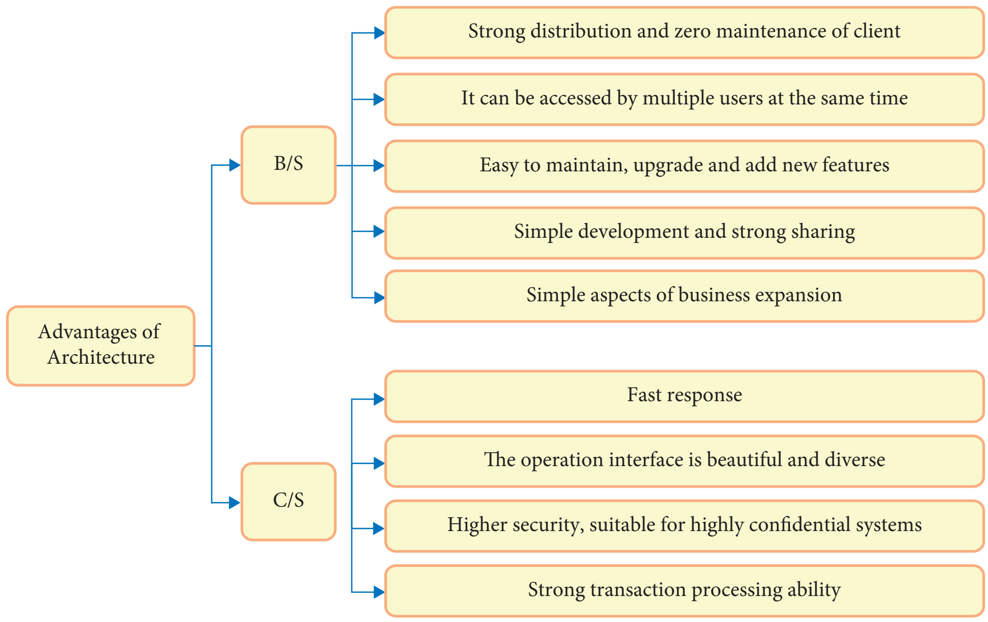

Figure 8: Comparison between advantages of B/S structure and C/S structure.

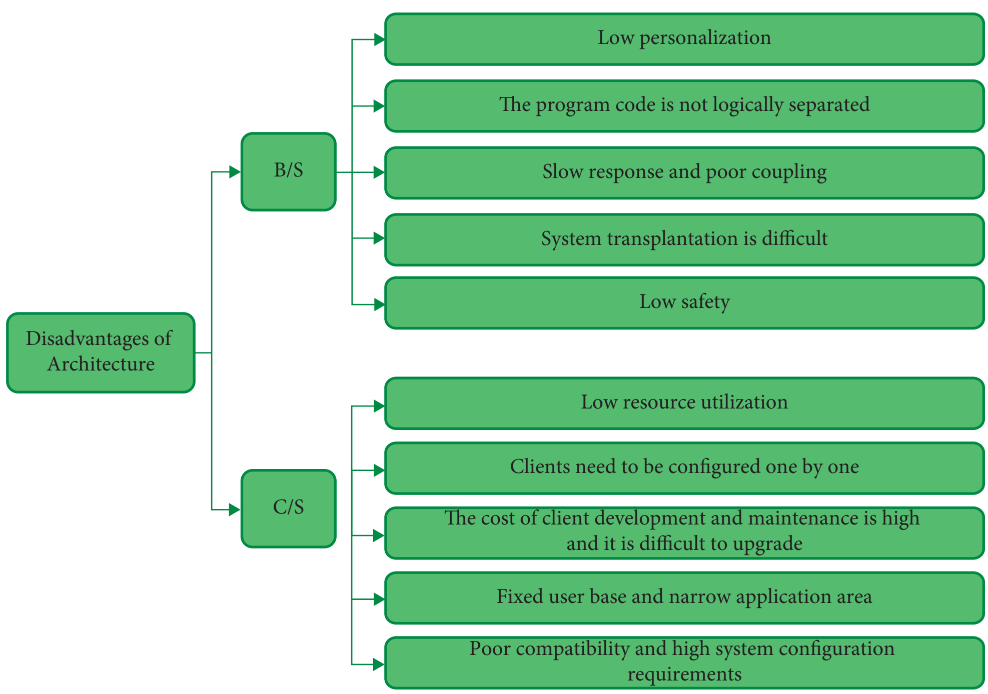

Figure 9: Comparison between disadvantages of B/S structure and C/S structure.

In the "inside/outside" model of B/S and C/S mixed software architecture, the outside users of enterprise access network server through Internet and then access database server through network server. The internal users of the enterprise directly access the database server through the LAN, and the software system adopts the C/S architecture.

The software architecture of the educational administration management system constructed is combined with Browser\Server (B\S) and Client\Server (C\S), and the internal LAN is used to store, manage, and maintain the educational administration information [21]. Different roles correspond to different management paths. Students and teachers need functions such as inquiring and entering educational information, while the Academic Affairs Office needs functions such as reviewing and maintaining educational information [22]. Figure 10 signifies the specific software architecture.

Based on the functional requirements of the system mentioned in the previous section, the seven main

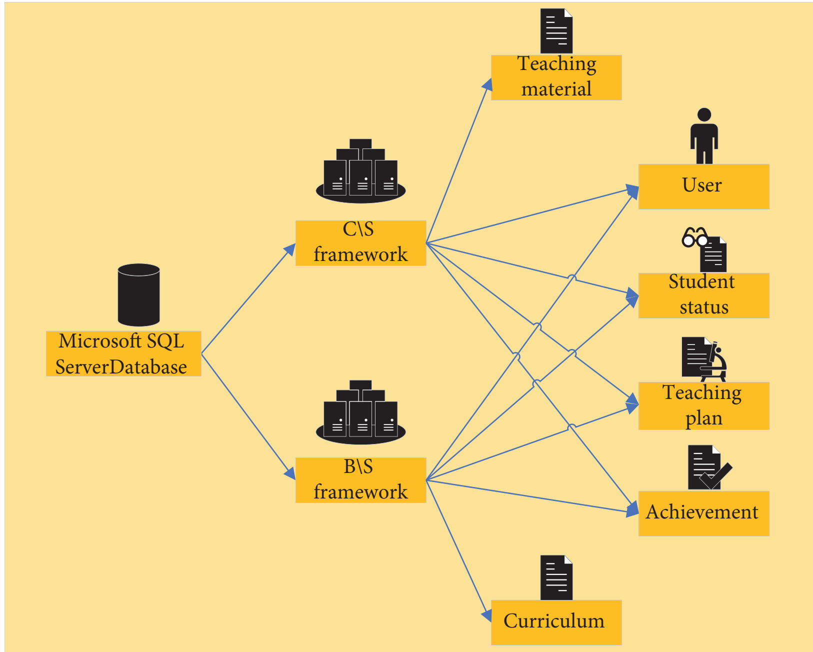

FIGURE 10: Software architecture of educational administration system.

functions are designed for the educational administration management system, which are student status information, annual teaching plan, teaching materials, online course selection for students, ability test for each semester, statistical entry and query of test results, and evaluation management for teachers [23]. Figure 11 illustrates the specific operation flow.

Figure 12 demonstrates the main functions of the 7 modules of educational management system.

Academic status information management includes three parts: information management, daily management, and affairs management. The management of the teaching plan mainly refers to the fact that the academic administration formulates and publishes the overall teaching plan of the academic year through the system, and the teachers formulate and upload the teaching plan according to the syllabus and teaching tasks. The teaching material management module is used for collecting of teaching material demand information and the input of teaching material purchase and distribution records; students' online course selection management mainly provides the selection and confirmation functions of compulsory courses and elective courses; semester test management is mainly used for inquiry, affirming, arranging, and releasing examination time, examination room information, and invigilator information; the performance management module provides the functions of input, query, and complaints of test scores. Present work applies the FCM-CF algorithm to this module, which can realize the prediction of students' future scores based on students' historical scores. Teachers' evaluation and management module is mainly used to input and edit information related to teachers' evaluation.

2.4. System Simulation Experiment Design

2.4.1. Selection of Dataset and Transition of Data. The present work mainly takes student achievement prediction as an example to carry out the performance test research of prediction model. Students' academic performance is related to many factors. Extracurricular learning is as important as in-class learning. Students' personal interest in learning, learning ability, and learning methods directly affect students' examination scores. The investigation of students' extracurricular learning provides a more comprehensive grasp of the factors affecting students' performance. The present work takes the survey results collected by the "C language programming" course of Computer Science and Application specialty and students' examination scores of the course as an example and selects the fields that have a greater impact on academic performance, such as preclass preparation, classroom performance, attendance rate, extracurricular learning, and homework completion of students, to predict their examination scores of the course. Table 1 lists the specific data.

For the convenience of statistics, the preclass preparation, classroom performance, attendance, extracurricular study, and homework completion in Table 1 are converted into corresponding scores (0~10). The students' exam scores are divided by 10, for example, 60 points into 6.

A dataset contains all the students' scores. The dataset is divided into training set and test set to verify the effect of each prediction method.

2.4.2. Specific Design of Experiment Flow. According to the educational management system constructed above, FCM-CF model is used to predict students' exam scores.

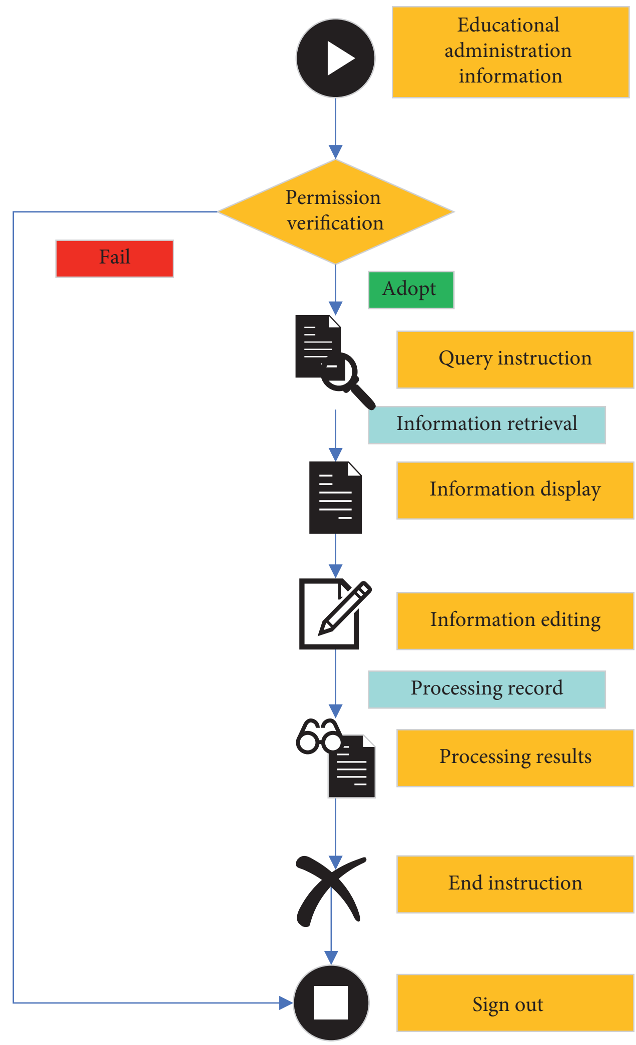

FIGURE 11: Operation flow of educational administration information management.

To verify the validity of the model, *K*-Means clustering (*K*-Means) is selected to replace the FCM-CF model to form a comparison. The historical performance data set of students is used to predict the performance of students, and the prediction results are compared and analyzed. When the two algorithms are used for prediction, the number of cluster (parameter c) needs to be determined first. In this process, the data set is temporarily divided into training set and test set in a ratio of 9 : 1. Simultaneously, it is necessary to determine the number K of the nearest neighbor in KNN algorithm. In the experiment, the K value is initially taken as 10% of the size of the training set and increased at an interval of 5%.

In the FCM-CF prediction model, the whole training set refers to the students whose exam scores are to be predicted, and data of all students are divided into different clusters according to different probabilities of the prediction results. Accordingly, different weights are used to predict the students' scores. Hence, the present work explores the best proportion of training set to data set when using FCM-CF prediction model. Figure 13 shows the specific process.

2.4.3. Evaluation Indexes. The mean absolute error (MAE) is used as the standard of prediction and evaluation [24]. The smaller the value of MAE, the higher the prediction accuracy. Equation (10) shows the calculation.

$$\mathrm{MAE} = \frac{\sum_{i=1}^{N} \left| \hat{r}_{ui} - r_{ui} \right|}{N}. \tag{10}$$

In equation (10), $\hat{r}_{ui}$ refers to prediction score of user- u to project- i, namely, the prediction score of the target students' test scores by the prediction method. Parameter r_{ui} stands for actual score of user-u to project -i, namely, the actual test scores of the target students. N represents the number of scores, which user-u makes on the project -i 3.

3. Results of Simulation Experiment

3.1. Display of Forecast Data. Figure 14 demonstrates the transition results of students' exam scores.

Figure 14 shows that the students' final achievement is closely related to their daily study performance. Whether to prepare before class, listen carefully in class, attend every

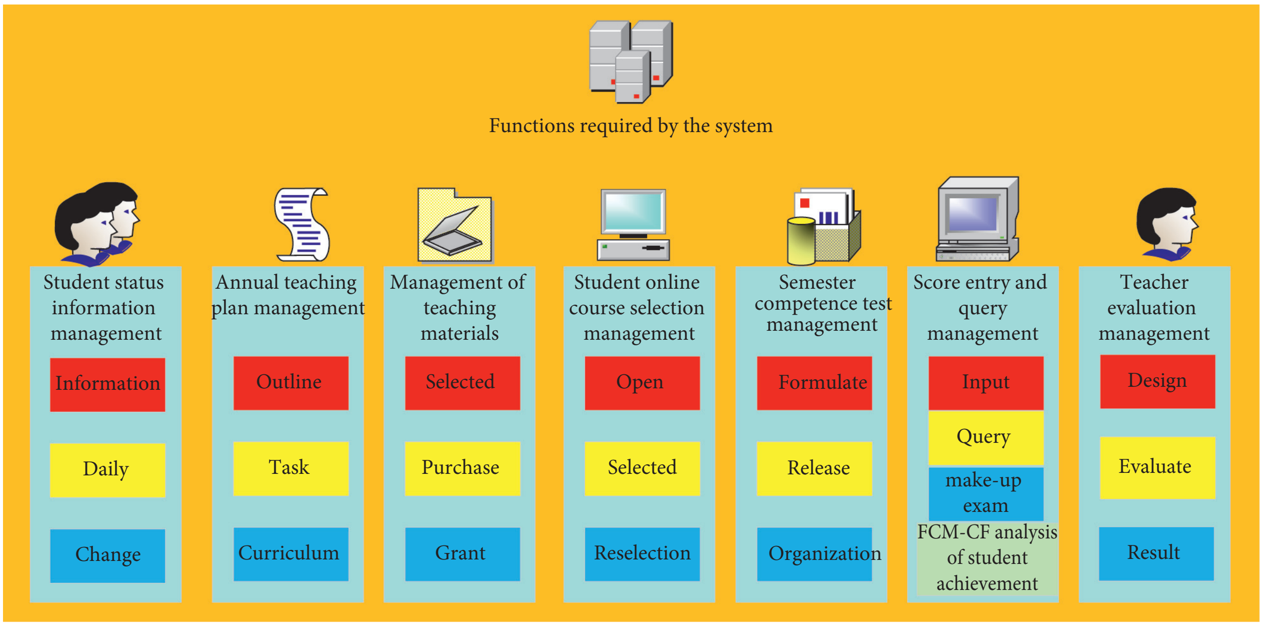

Figure 12: Main functions of each module in the educational management system.

Table 1: Students' performance prediction results.

Student number	Preview before class	Classroom performance	Attendance	Out-of-class activities	Operation	Exam score
1	Basically not	Very bad	Poor	Basically not	Very bad	27
2	Complete preview	Excellent	Good	Occasionally	Excellent	90
3	Basic preview	Commonly	Good	Occasionally	Secondary	68
4	Good preview	Good	Excellent	Often	Good	81
5	Partial preview	Commonly	Commonly	Very seldom	Secondary	86
6	Basic preview	Poor	Excellent	Often	Poor	59
...	...	...	...	...	...	...

class, carry out related study after class, complete homework, etc. will directly affect the students' final achievement. Under normal circumstances, students' scores corresponding to these performances will be similar; that is, students who have prepared well before class will perform very well in class, their attendance rate will be relatively high, and their extracurricular study time will be longer. Meanwhile, the completion of their homework is also very good, and correspondingly, their exam scores will be satisfactory. On the contrary, students who do not preview before class will perform poorly in class, and their attendance rate will be relatively low. They will not study after class, the quality of their homework will be poor, and their final exam results will be unsatisfactory.

3.2. Determination of the Indexes of KMCF Model and FCM-CF Model

3.2.1. Determination of the Indexes of the Model. Figure 15 reveals the variation trend of the predicted mean absolute error (MAE) of the KMCF model as the number of clusters c in the K-means clustering changes from 1 to 25, and K takes 10% to 40% of the training set.

Figure 15 reveals that it is the optimal, when the number of clusters is 10, and the K value is 20% of the training set. When the number of clusters is 1, that is, when all students are in the same cluster, the K-means clustering is not taken to cluster students. As the number of clusters increases, and the number of clusters is relatively small, more students in the same cluster with the students whose scores are to be predicted will be given higher authority, and students being in the same cluster can be considered to have higher similarity. However, when the number of clusters is too large, even when each student is a cluster, clustering should not be taken under this situation.

With the increase of the nearest neighbor size K, more students similar to the students to be predicted are divided into the nearest neighbor set, which will improve the accuracy of prediction. However, the K value continues to increase to be even equivalent to that of the entire training set, and students who are very different from the students to be predicted are also divided into the KN set, thus reducing the accuracy of KMCF prediction method. When the FCM-CF model is used for prediction, the number of clusters c in the clustering is kept as 10 of the KMCF model.

3.2.2. Determination of Training Set Ratio of FCM-CF Model. Figure 16 illustrates the variation trend of MAE along with the change of training set ratio.

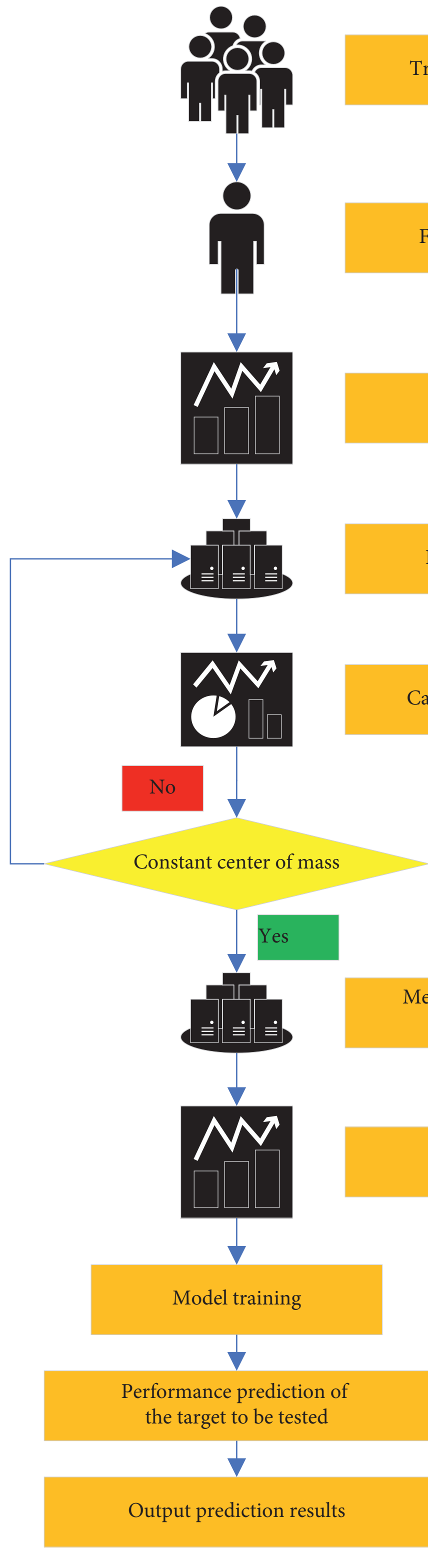

Figure 13: Clustering of students' scores and flow of predictions.

Figure 16 indicates that when the FCM-CF is adopted to carry out prediction, the prediction error of the model increases with the increase of the proportion of the training set. When the proportion of the training set is 90%, the error of the model reaches the minimum. This is because when the size of the training set increases, more data of students' performance will be involved in the prediction, avoiding some accidental factors, so that the smaller the MAE value of the test set, the better the prediction effect. Therefore, the proportion of training set in data set is set to 90%.

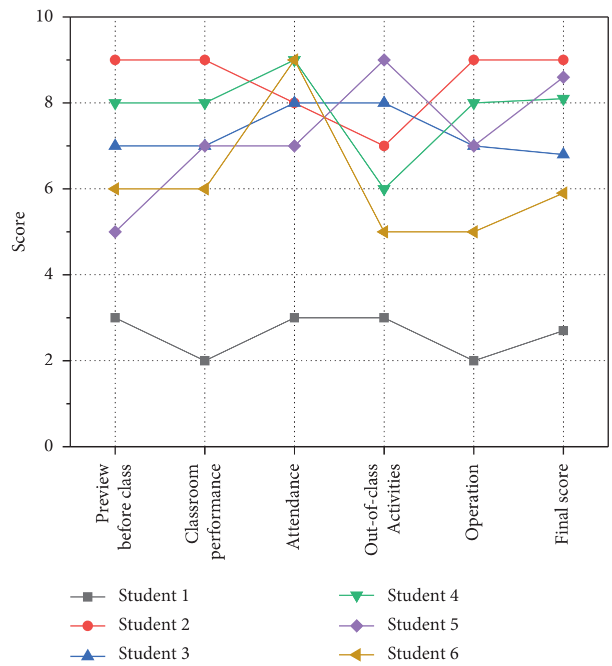

FIGURE 14: Students' scores prediction curve.

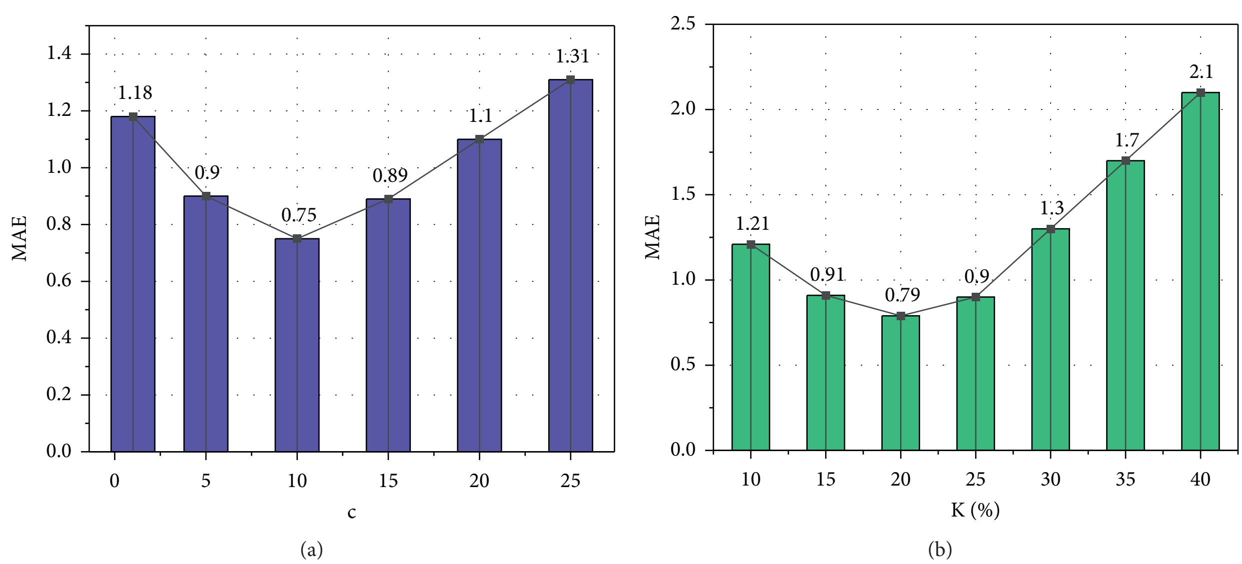

FIGURE 15: Clustering of students' scores and flow of predictions. (a) Variation trend of MAE with the change of the number of cluster c; (b) variation of MAE with the change of closest neighbor K.

3.3. Comparative Analysis of Prediction Performance of Models. To get a clearer comparison between KMCF and FCM-CF models, comparisons are made on the MAE results predicted by the two models under different training set ratio. Figure 17 denotes the comparison results.

Figure 17 implies that the prediction MAE of KMCF and FCM-CF models declines with the growth of the proportion of training set to data set, and the models have the lowest prediction MAE when the proportion of training set is 90%. The average MAE predicted by KMCF model is 0.939. The average MAE of FCM-CF model is 0.838, lower than that of

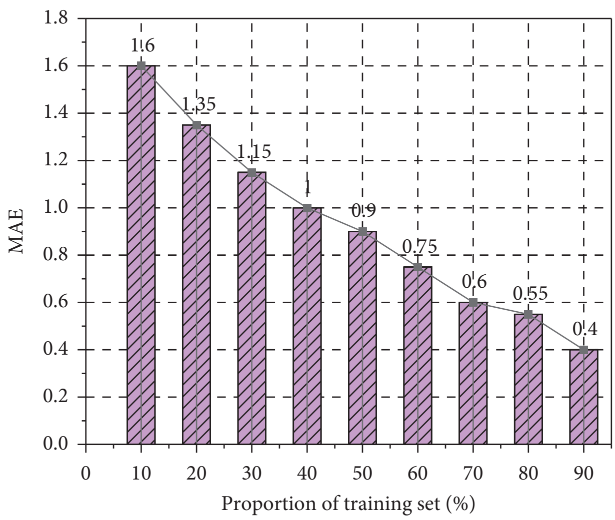

Figure 16: Variation trend of MAE along with the change of training set ratio.

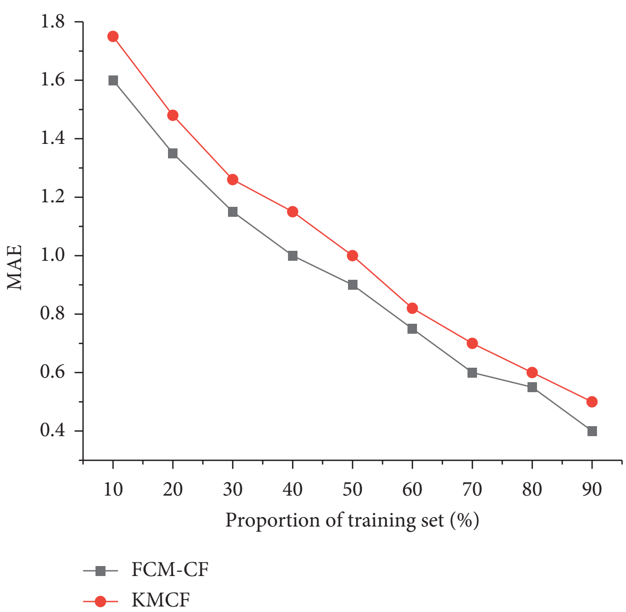

Figure 17: Variation trend of MAE along with the change of the training set size.

KMCF model 10.8%. Therefore, under the same conditions, the prediction error of FCM-CF model is lower, which is more suitable for the prediction of middle school students' performance in educational management system.

4. Conclusion

With the progress of the times, colleges are inevitably faced with the situation that massive educational information needs to be processed in the continuous development, and the educational administration of colleges is in urgent need of being made further intelligent. The present work proposes a student achievement prediction model based on FCM-CF, introduces it into the research of educational management, and constructs an intelligent educational management system. Initially, the FCM-CF model is described in detail. Next, the system requirements and specific design methods are expounded. Eventually, taking the student performance prediction as an example, the performance of the system is tested by designed simulation experiments. The results show that students' exam scores are closely related to their daily learning performance. Under the same experimental conditions, the prediction error of FCM-CF model proposed here is less than 10.8% of other algorithms, which has better prediction performance and is more suitable for the prediction of middle school students' scores in educational administration management system. The innovation is to introduce FCM-CF algorithm into the educational administration system model, giving it the function of data mining and intelligent performance prediction. There are some shortcomings, such as incomplete coverage of the factors affecting students' grades. Additionally, there is room for optimization of the operation efficiency of the algorithm provided. Subsequent research will solve the above problems. The research purpose is to provide important technical support for the educational management of colleges to be more intelligent and reduce the waste of manpower.

Data Availability

The labeled dataset used to support the findings of this study is available from the corresponding author upon request.

Conflicts of Interest

The author declares no competing interests.

References

[1] R. Shang, C. Chen, G. Wang, L. Jiao, M. A. Okoth, and R. Stolkin, "A thumbnail-based hierarchical fuzzy clustering algorithm for SAR image segmentation," *Signal Processing*, vol. 171, Article ID 107518, 2020.

[2] D. Mújica-Vargas, "Superpixels extraction by an intuitionistic fuzzy clustering algorithm," *Journal of Applied Research and Technology*, vol. 19, no. 2, p. 141, 2021.

[3] S. Nasir, N. Nurhidayah, and A. Suprianto, "Effect of self-regulated learning on academic achievement of Puangrimaggalatung university educational administration study program students," *International Journal of Educational Management and Innovation*, vol. 1, no. 3, p. 205, 2020.

[4] Z. Lv, D. Chen, R. Lou, and A. Alazab, "Artificial intelligence for securing industrial-based cyber-physical systems," *Future Generation Computer Systems*, vol. 117, pp. 291–298, 2021.

[5] Z. Ning, X. Hu, Z. Chen et al., "A cooperative quality-aware service access system for social internet of vehicles," *IEEE Internet of Things Journal*, vol. 5, no. 4, pp. 2506–2517, 2018.

[6] Z. Lv, D. Chen, and J. Li, "Novel system design and implementation for the smart city vertical market," *IEEE Communications Magazine*, vol. 59, no. 4, pp. 126–131, 2021.

[7] N. Mahata and J. K. Sing, "A novel fuzzy clustering algorithm by minimizing global and spatially constrained likelihood-based local entropies for noisy 3D brain MR image segmentation," *Applied Soft Computing*, vol. 90, Article ID 106171, 2020.

[8] J. Li, Y. Ning, Z. Yuan, and C. Yang, "Research on medical image segmentation based on fuzzy clustering algorithm," *Matrix Science Pharma*, vol. 3, no. 1, p. 9, 2019.

[9] I. Oplatka, "School leadership for refugees' education: social justice leadership for immigrant, migrants, and refugees," *Journal of Educational Administration and History*, vol. 53, no. 1, pp. 1–3, 2020.

[10] N. Ibrahim Fantoukh, M. Maher Ben Ismail, and O. Bchir, "Automatic determination of the number of clusters for semi-supervised relational fuzzy clustering," *International Journal of Fuzzy Logic and Intelligent Systems*, vol. 20, no. 2, pp. 156–167, 2020.

[11] H. Xu, R. Hou, J. Fan, L. Zhou, and J. Liu, "The unordered time series fuzzy clustering algorithm based on the adaptive incremental learning," *Journal of Intelligent and Fuzzy Systems*, vol. 38, no. 1, pp. 1–9, 2020.

[12] X. Hu, J. Cheng, M. Zhou et al., "Emotion-aware cognitive system in multi-channel cognitive radio ad hoc networks," *IEEE Communications Magazine*, vol. 56, no. 4, pp. 180–187, 2018.

[13] Y. Zhang, Y. Zhang, and R. Zhang, "Text information classification method based on secondly fuzzy clustering algorithm," *Journal of Intelligent and Fuzzy Systems*, vol. 38, no. 1, pp. 1–12, 2020.

[14] N. Y. Pehlivan and I. B. Turksen, "A novel multiplicative fuzzy regression function with a multiplicative fuzzy clustering algorithm," *Romanian Journal of Information Science and Technology*, vol. 24, no. 1, pp. 79–98, 2021.

[15] D. Tan, W. Zhong, C. Jiang, X. Peng, and W. He, "High-order fuzzy clustering algorithm based on multikernel mean shift," *Neurocomputing*, vol. 385, no. 8, pp. 63–79, 2020.

[16] L. H. Wen, Z. H. Shi, and H. Y. Liu, "Research on risk assessment of natural disaster based on cloud fuzzy clustering algorithm in Taihang mountain," *Journal of Intelligent and Fuzzy Systems*, vol. 37, no. 4, pp. 1–9, 2019.

[17] Z. Hayat and T. R. Soomro, "Implementation of Microsoft SQL server using 'AlwaysOn' for high availability and disaster recovery without shared storage," *International Journal of Experiential Learning and Case Studies*, vol. 3, no. 1, pp. 9–17, 2018.

[18] B. C. Gabriel and L. G. Kabari, "Hybridized concurrency control technique for transaction processing in distributed database system," *International Journal of Computer Science and Mobile Computing*, vol. 9, no. 9, pp. 118–127, 2020.

[19] Y. Li, L. Chen, D. Yu, and R. Gao, "Research and developing of evaluation information system using B/S structure and SQL server technology," *Journal of Physics: Conference Series*, vol. 1952, no. 4, Article ID 042088, 2021.

[20] S. K. Singh and A. K. Tiwari, "Design and implementation of secure computer based examination system based on B/S structure," *International Journal of Applied Engineering Research*, vol. 11, no. 1, pp. 312–318, 2016.

[21] F. Zhao, C. Li, H. Liu, and J. Fan, "A multi-objective interval valued fuzzy clustering algorithm with spatial information for noisy image segmentation," *Journal of Intelligent and Fuzzy Systems*, vol. 36, no. 6, pp. 5333–5344, 2019.

[22] Y. Yang, J. Yu, Y. Fu, and J. Hu, "Research on geological hazard risk assessment based on the cloud fuzzy clustering algorithm," *Journal of Intelligent and Fuzzy Systems*, vol. 37, no. 2017, pp. 1–8, 2019.

[23] D. Sivaganesan, "Optimized wireless sensor node multidimensional routing using fuzzy clustering and chaotic gravitational search algorithm," *IRO Journal on Sustainable Wireless Systems*, vol. 3, no. 1, pp. 40–48, 2021.

[24] H. Peng, B. Hu, Q. Shi et al., "Removal of ocular artifacts in EEG-an improved approach combining DWT and ANC for portable applications," *IEEE Journal of Biomedical and Health Informatics*, vol. 17, no. 3, pp. 600–607, 2013.

Hindawi
Scientific Programming
Volume 2023, Article ID 9878754, 1 page
https://doi.org/10.1155/2023/9878754

Retraction

Retracted: Application of Intelligent Sensor Algorithm in Student Management Information Fusion

Scientific Programming

Received 1 August 2023; Accepted 1 August 2023; Published 2 August 2023

This article has been retracted by Hindawi following an investigation undertaken by the publisher [1]. This investigation has uncovered evidence of one or more of the following indicators of systematic manipulation of the publication process:

(1) Discrepancies in scope
(2) Discrepancies in the description of the research reported
(3) Discrepancies between the availability of data and the research described
(4) Inappropriate citations
(5) Incoherent, meaningless and/or irrelevant content included in the article
(6) Peer-review manipulation

The presence of these indicators undermines our confidence in the integrity of the article's content and we cannot, therefore, vouch for its reliability. Please note that this notice is intended solely to alert readers that the content of this article is unreliable. We have not investigated whether authors were aware of or involved in the systematic manipulation of the publication process.

Wiley and Hindawi regrets that the usual quality checks did not identify these issues before publication and have since put additional measures in place to safeguard research integrity.

We wish to credit our own Research Integrity and Research Publishing teams and anonymous and named external researchers and research integrity experts for contributing to this investigation.

The corresponding author, as the representative of all authors, has been given the opportunity to register their agreement or disagreement to this retraction. We have kept a record of any response received.

References

[1] Y. Li, "Application of Intelligent Sensor Algorithm in Student Management Information Fusion," *Scientific Programming*, vol. 2021, Article ID 3053538, 12 pages, 2021.

Hindawi
Scientific Programming
Volume 2021, Article ID 3053538, 12 pages
https://doi.org/10.1155/2021/3053538

Research Article

Application of Intelligent Sensor Algorithm in Student Management Information Fusion

Yanan Li

Basic Medical College, Chifeng University, Chifeng 024000, China

Correspondence should be addressed to Yanan Li; jcyxyliyn@cfxy.edu.cn

Received 18 November 2021; Accepted 9 December 2021; Published 29 December 2021

Academic Editor: Le Sun

In order to improve the effectiveness of college student management and promote the integration of college student management information, this paper applies intelligent sensor algorithms to student management. Moreover, this paper combines uncertainty theory with multisensor data fusion technology to establish a complete set of multisensor data processing tools for student information and provides a complete mathematical theoretical framework for the principles of student management information fusion. In addition, in view of the problem of comparing a large number of mixed data of information sources, it is necessary to transfer the information fragments obtained by each sensor to a common set so that the information fragments expressed in different sets can be integrated. Finally, this paper constructs an intelligent student management model and conducts research in combination with simulation experiments. Through simulation research, it can be known that the method proposed in this paper can effectively improve the effect of student management.

1. Introduction

Higher education is the highest level of China's education system, and it directly affects the level of China's training of high-level talents. In recent years, as the pace of reform in various industries in our country has accelerated, the reform of higher education has also been accelerating year by year, the scale of enrollment has been increasing, and the number of students has also increased steadily. The level of high-level talent training should not only be expressed in quantity, but more importantly, in high standards of quality. This inevitably puts forward higher requirements on management. Many colleges and universities across the country have researched and developed their own student information management systems, but there is no very flexible and practical student information management system software on the market. Therefore, the student information management system based on intelligent sensor algorithms studied in this paper has a certain market value.

Management Information System (MIS) is a system composed of people, computers, and other peripheral equipment. It can collect, transmit, store, process, maintain, and use information. The main task of the system is to use computer and network communication technology to maximize the information management of the enterprise. Moreover, it obtains true and accurate data through the investigation and analysis of the resource conditions of the enterprise's human, financial, material, equipment, and technology, which are processed and compiled into various information materials to provide a decision-making basis for managers [1].

The design and development of any software system must follow the general rules of software development in order to ensure better software quality and obtain higher development efficiency [2]. The general process of typical software system development can be divided into five stages: system requirements analysis, design, programming, testing, and maintenance. System requirement analysis is the first stage of software system development, and it is also a very important stage. The result of requirement analysis is the basis of the other four stages, and the analysis result directly affects software system development [3]. The main task of the requirement analysis stage is to put forward the goal that the system is going to achieve and the complete, clear, and specific requirements of the software system that need to be constrained in terms of function, performance, and design [4]. Requirements analysis includes two aspects: functional requirements analysis and nonfunctional requirements analysis. Functional requirements refer to the functions that the software must complete and are business requirements. Through the functions provided by the software system, users can complete established tasks. Nonfunctional requirements are good expectations for system safety and operating status, including development constraints of software systems, response time, continuous working time, error recovery time, and error prompts [5].

With the gradual transformation of China's higher education from "elite education" to "mass education," higher education has developed rapidly. The number of enrolled students in colleges and universities has continued to increase, and the scale of running schools has continued to expand. The number of students in the school has grown from a few thousand at the beginning to tens of thousands of people now. The increase in the number of students has also increased the management pressure of the school on various management affairs. In addition, the expansion of the school scale has made the limited educational resources of the school even more scarce. Only by establishing an effective management mechanism, uniformly deploying existing educational resources, and increasing the utilization rate of resources can the needs of school development be met. The student integrated information management system can realize the information and scientific comprehensive management of all aspects of student management, which not only improves the efficiency of school management but also creates opportunities for the efficient scheduling of school education resources and the improvement of management quality.

Based on the abovementioned analysis, this paper combines the intelligent sensor algorithm to construct the student management information system, analyzes the information fusion process of the intelligent sensor algorithm to propose an improved algorithm, and verifies the performance of the system in this paper.

2. Related Work

In the era of the information society and the knowledge economy, the construction of informatization and digital campuses is a hot spot in the construction of universities at home and abroad. The concept of a digital campus was first proposed by the Massachusetts Institute of Technology in the 1970s. After years of hard work, a more mature digital campus model has been constructed. Generally, foreign universities have their own correspondingly stable technical teams for information systems. The users provide services and technical support. As a branch of the educational administration and teaching management system, the student information management system is relatively mature in terms of business and technical performance [6]. In addition, foreign universities have always paid attention to the establishment of laws and regulations in the process of building management systems. Software designers have their own copyrights. By assigning different permissions to different software applications, users can legally share information to improve work efficiency and reduce software costs [7]. Among them, the representative research result is the SIF (schools interoperability framework) education information technology standard. It was originally initiated and formulated by some American companies and related educational organizations. The goal is to solve the current resource sharing problem in American universities. Educational information technology standard solutions enable different application programs of various university management to be operated by each other and achieve the purpose of data resource sharing through this authorized interactive operation [8].

Although the management level of student information has gradually transitioned to computer software system management and some colleges and universities have corresponding material inputs and have arranged special personnel for management, they lack supporting software development, and software management is often a mere formality. Other colleges and universities are committed to independent research and development, and actively set up special departments to be responsible for the development and promotion of the school's internal management software. Although the developed software has powerful functions and can fully meet the needs of student information management, due to the lack of communication and coordination with various functional departments in the school, the developed software cannot adapt to the specific management of each functional department requirements, resulting in software being abandoned by managers after a period of use, and formalism, which to a large extent caused a waste of resources [9]. The theory of digital campus has been deeply rooted in the hearts of the people. Colleges and universities have begun to invest in the construction of various hardware equipment and software systems according to their actual needs, including the construction of campus wired and wireless networks; various teaching, scientific research, office management, and other application system software development and introduction have formed their own informatization construction systems [10].

Literature [11] uses Visual Basic 6.0 as the program development language and the Access database as the realization of a relational database. It has developed a set of features for teaching and student management in colleges and universities. The functions include student employment management, grade management, course management, student status management, and a student information management system for class management. Literature [12] designed a set of postgraduate information management systems, using Microsoft's NET technology and XML-based mature technology as the technical guarantee; SQL Server000 as the system database; different users are assigned different roles to improve management efficiency, and standardize the purpose of graduate student information management. Literature [13] adopts a multilayer application software architecture and a development route based on distributed object technology and component technology. IBM or SUN's UNIX platform-based server is the school's central database server, and the database system adopts the ORACLE8i of the American ORACLE company and realized the teaching management information system of Shanghai Jiaotong University. At present, the key structure and some subsystems have been developed, and the inspiring new look brought by the new architecture and technology to the management information system is beginning to appear, and it also provides new ideas for the design of the information system. Literature [14] uses the MVC design pattern to design and implement a student management system on the J2EE platform and uses the popular open source framework Struts for development. Literature [15] through the research on the college student management system based on the C/S and B/S mixed modes, realized college student status management, student daily management, student-related management, counselor management, office management, student information query and statistics. It expounds the advantages of the C/S and B/S hybrid development models, and puts forward the idea of "establishing a university student management data center shared by the whole school."

The analysis of the abovementioned data found that for the university student management system, the successful experience can only be used as a reference and reference. It is not feasible to copy a certain advanced experience and management system completely. It is necessary for each university to develop a suitable one according to its actual situation. The management information system based on its own management mode is also the purpose of the development of this system.

3. Research on the Multisensor Data Fusion Method of Student Management Information

The essence of students' daily information management is actually the integrated navigation of multiple students. The essence of integrated navigation is multisensor data fusion, which realizes accurate positioning of the carrier position through the loose and tight coupling of MIMU/GPS, MEMS inertial sensor, magnetometer, and GPS combination ways to achieve accurate measurement of the carrier's attitude. Common sensor data fusion methods are mainly based on filtering.

For the comparison of a large number of mixed data sources, it is necessary to transfer the student management information fragments obtained by each sensor to a common set, so that the student management information fragments expressed in different sets can be integrated. Before processing student management information fragments, it is necessary to use a function to project the provided knowledge fragments into a different collection, and then it is necessary to connect these collections and express their relationships.

Combine two sets of operations through the subdivision and coarsening, adjustment, and imbalance of the recognition frame, the student management information fragment can be transferred between any two sets of credibility $Pl(\cdot)$. The following will focus on introducing a special extended operation based on these two types of operations. Similarly, this extension can also transfer the credibility of any recognition framework to other recognition spaces.

Specific steps are as follows:

(1) The algorithm determines an incompletely defined likelihood function $Pl_e(.)$ within the scope of the recognition frame E.

(2) The algorithm calculates $Pl_s(./B \subseteq E_e)$, that is, the incomplete likelihood function on c when subset B of E_e is truly valid.

(3) The algorithm calculates E_r, $E_r \subseteq E_e$, which belongs to a set of element E_e and is associated with any given element of E_s. Elements in E_s that are incompatible with E_e are eliminated through $Pl_s(./B \subseteq E_e) = 0$. Conversely, elements in E_e that are incompatible with E_s are identified by $E_e - E_r$.

(4) With the conclusion data of the first three steps, the algorithm begins to build an extended operation, which is divided into three steps. First, the algorithm uses the formula [16]:

$$Pl_{sr}(A \times B) = Pl_s(./B \subseteq E_e)\frac{Pl_e(B)}{Pl_e(E_r)}. \tag{1}$$

To find the value of the likelihood function $Pl_{sr}(A \times B)$ of $E_s \times E_r$. Then, a specific algorithm is used to determine the mass function $m_{sr}(.)$ with the least specificity corresponding to its likelihood value. Finally, the formula is used [17]:

$$m_s(A) = \sum_{B \subseteq E_r} m_{sr}(A \times B). \tag{2}$$

To determine the mass distribution function $m_s(.)$ on the recognition frame Es.

The essence of the algorithm with the smallest specific mass function is to determine the mass function $m(.)$ associated with the incompletely defined likelihood function $Pl(.)$ on the recognition space E. Because of the uncertainty of this quality function, it is necessary to find the function with the highest evidence strength. We define the specific function Sp (m) as

$$sp(m) = \sum_{B \subseteq E_r} \frac{m(A)}{|A|}. \tag{3}$$

In order to limit student management information outside the facts, it is necessary to find the smallest Sp (m). The algorithm update flowchart is shown in Figure 1 [18].

During the update process, it should be noted that the initialization $m(.)$ process must make $m(E) = 1$. After processing a likelihood subset, $m(E)$ needs to be set to an uncertain partial quality. When choosing $B_j \subset E$, we need to consider the order in order to reduce the cardinality. If the cardinality of the two sets is equal, it will not be considered first. When $\Delta_j > 0$ is judged, it is necessary to examine the main element [19] A of $m(.)$, which must satisfy formula (3).

$$\begin{cases} A_i \cap B_j \neq \varnothing, \\ A_i - B_j \neq \varnothing, \\ \left|A_i - B_j\right|^{-1} - \left|A_i\right|^{-1} = \min. \end{cases} \tag{4}$$

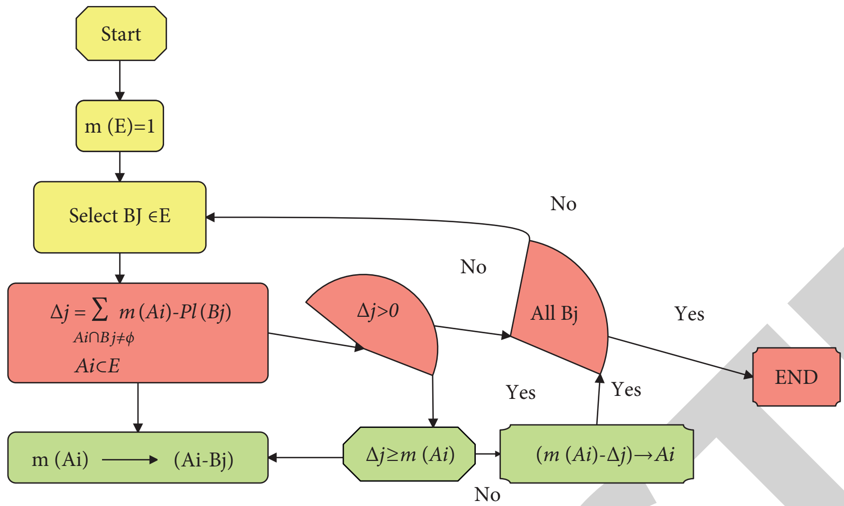

Figure 1: The smallest specific m (.) algorithm.

Finally, it is worth noting that the solutions derived from different problem conditions are not unique. The process of student information recognition is set as the recognition frame E_c is as follows:

$$E_c = \{H_1, H_2, H_3, H_4, H_5, H_6\}. \tag{5}$$

Among them,

$$\begin{cases} H_1 = \{\text{Stationary state}\}, \\ H_2 = \{\text{cceleration/deceleration}\}, \\ H_3 = \{\text{Slow moving state, straight walking}\}, \\ H_4 = \{\text{Slow moving state, curve walking}\}, \\ H_5 = \{\text{Fast moving state, straight line}\}, \\ H_6 = \{\text{Fast moving state, curve}\}. \end{cases} \tag{6}$$

According to the abovementioned identification framework, Hi ($i = 1$–6) is the situational variable. Now, it is necessary to determine the attribute uj corresponding to each scenario variable. The attributes are the longitude, latitude, altitude, roll angle, pitch angle, and yaw angle of the carrier, a total of six variables, which are recorded as follows [19]:

$$\mu_j = \{\lambda, \phi, h, \text{roll}, \text{pitch}, \text{yaw}\}\,(j = 1 \sim 6). \tag{7}$$

The collection is as follows:

$$\begin{cases} \lambda = \{\lambda_1, \lambda_2, \lambda_3, \ldots, \lambda_n\}, \\ \varphi = \{\varphi_1, \varphi_2, \varphi_3, \ldots, \varphi_n\}, \\ h = \{h_1, h_2, h_3, \ldots, h_n\}, \\ \text{roll} = \{\text{roll}_1, \text{roll}_2, \text{roll}_3, \ldots, \text{roll}_\text{n}\}, \\ \text{pitch} = \{\text{pitch}_1, \text{pitch}_2, \text{pitch}_3, \ldots, \text{pitch}_\text{n}\}, \\ \text{yaw} = \{\text{yaw}_1, \text{yaw}_2, \text{yaw}_3, \ldots, \text{yaw}_\text{n}\}. \end{cases} \tag{8}$$

In the set, n represents the n kinds of calculation methods, which are selected according to the actual situation. Each attribute may have less than or equal to n kinds of solution methods, and some attributes are still coupled for a certain solution method. For the convenience of building the model, the dimension is uniformly set to n. It is worth noting that taking the largest dimension does not violate the actual situation, because each attribute is directly or indirectly coupled.

In addition, we identify several important vectors [20]:

$$\begin{cases} A_c = \{C_x, C_y, C_z\}, \\ A_g = \{g_x, g_y, g_z\}, \\ A_o = \{O_x, O_y, O_z, O_B\}, \\ A_r = \{\lambda, \varphi, h, v_x, v_y, v_z\}. \end{cases} \tag{9}$$

Among them, A_c is the student management information of the three-axis magnetometer; A_g is the student management information of the three-axis accelerometer; A_o is the student management information of the three-axis gyroscope; and A_r is the student management information of the GPS satellite receiver.

Start with the observation data. The vector A_c, A_g, A_o, A_r itself is not a set, so it is necessary to transform the four sets of vectors into a set. The abovementioned four sets of vectors can be transformed to the set (8), that is, each single element in the set is composed of four sets of vectors calculated by the navigation algorithm.

This section mainly analyzes the collection management. The research object is the collection (8). The application of the four sets of vectors of the collection (9) will be explained in detail in the next section. We use the attribute λ as an example.

Step 1. The algorithm calculates the likelihood function of each subset λ_i. The specific calculation is shown as follows [21]:

$$Pl(\lambda_i) = \frac{|\lambda_i - [\lambda]|}{\sum|\lambda_i - [\lambda]|} \quad (i = 1 \sim n). \tag{10}$$

In the formula, $[\lambda]$ is the standard value. Because this value cannot be collected in real time, one or more sensors with the highest reliability can be determined in advance according to the way of scenario simulation, and the $[\lambda]$ calculated by using these reliable sensors is the standard output.

The second step is as follows: according to the reliability analysis of each sensor variable, the algorithm removes the unreliable sensor attributes; the mass function $m_{ij}(.)$ of each set is calculated according to the minimum specific mass function method, and the reliability is eliminated.

The third step is as follows: the algorithm updates the student management information. When the student management information λ_k at the previous moment is transformed into the student management information λ_{k+1} at the next moment, the student management information at the two moments needs to be merged. Among them, simple weighting is one way. After that, we solve the expansion operation which is as follows:

(1) E_k is the collection of student management information at the previous moment
(2) E_{k+1} is the collection of student management information x.z at a later time
(3) $Pl_k(.)$ is the Bayesian simple integration of the likelihood function distribution at the previous moment
(4) $Pl_{k+1}(./B \subseteq E_k)$ is the distribution of the likelihood function at a later time of Bayesian simple integration, which may have a value of 0 or 1
(5) According to the mass distribution function of the specific set of attributes, the algorithm determines the corresponding conversion model

The reliability management of knowledge fragments is an important foundation in the process of sensor data fusion. For the problem of ensuring the stability (robustness) of the output signal in the solution process of the integrated navigation system, the reliability management of the student management information is extremely important. The combination stage usually encourages the use of a simple weighted combination of the management information of each sensor student, but the shortcomings are also obvious. It is very sensitive to the selected parameters, which often leads to low robustness of the output signal and susceptibility to external interference.

In the reliability function theory, if the source identification frame is E_e, then the mass function on E_e is $m\ (A)$, where $\forall A \subset E_e$. If the reliability of the source is known $q \in [0,1]$, the unreliable part can be eliminated to obtain

$$\begin{cases} m^q(A) = qm(A)\forall A \subset E_e, \\ m^q(E_e) = 1 - q(1 - m(E_e)). \end{cases} \tag{11}$$

The function of reliability function rejection is to reduce the performance of the uncertainty part of the sensor by a factor $(1-q)$. That is, it reduces the mass distribution of all elements and redistributes the mass on the recognition frame. Moreover, the overall credibility is reduced by $(1-q)$, so the uncertainty of the overall Ee is increased. This elimination operation retains the original evaluation and improves the evaluation between total uncertainties. In addition, for the likelihood function, a similar method is used here, as shown in the following formula:

$$Pl^q(B) = 1 - q(1 - Pl(B)). \tag{12}$$

Here is the application process of multisensor student management information reliability management in the overall system, as shown in Figure 2.

If the MTI data is ax, y, or o, and the IMU data is ae, ay, or loz, the reliability expression is as follows:

$$q_{ij} = \frac{\left|E(\tilde{\omega}_x - \omega_x)\right|}{E\left(\left|\tilde{\omega}_x\right|\right)} \quad (i = 1 \sim 6,\ j = 1 \sim 16). \tag{13}$$

Among them, i represents the student management information sequence, and j represents the sensor sequence. The essence of this kind of reliability expression is the expression of the accuracy of the sensor under the management information of different students when the sensor is not damaged. Therefore, the expression defects are also obvious:

(1) It can only bind offline, and it is difficult to guarantee the accuracy of the binding. The first point is that when the reliability database is used for binding, the accuracy of the expression itself cannot be measured according to formula (13), that is, the reliability of the algorithm needs to be verified.
(2) When it is applied, it must be searched by the interpolation method, and the accuracy is further degraded.
(3) The most important point is that it is impossible to determine the true operating status of the sensor, which introduces hidden dangers to the update of student management information in a real application environment.

There is no doubt that how to optimally combine student management information from different sensors is the core content of data fusion, but this function is also the most difficult part to achieve. The influencing factors mainly include the following: the difference of sensors, the diversity of the identification framework that can express the available student management information, the rigorous mathematical modeling expression of the problem, and the handling of conflicts between signal sources. Numerous identification frameworks provide a large number of combination rules. Therefore, how to select the optimal combination has become the most difficult and most critical problem.

Here, the D-S evidence theory is used for synthesis, and this synthesis rule reflects the combined effect of evidence. We give several trust functions based on different evidence on the same identification framework. If several batches of evidence are incompletely conflicting, you can use the D-S evidence theory to calculate a new trust function.

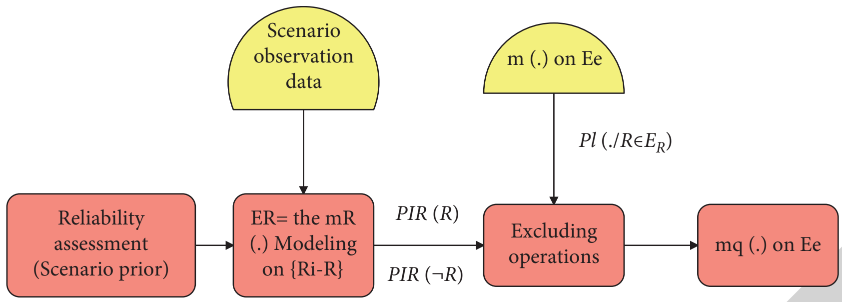

FIGURE 2: Flowchart of comprehensive management of reliability.

This trust function can be used as the trust function under the joint action of the several batches of evidence, and the trust function is called the orthogonal sum of the original trust functions.

$$m(A) = \begin{cases} \sum\limits_{\cap A_i = A} \prod\limits_{1 \le j \le n} \dfrac{m_i(A_i)}{(1-K)}, & A \neq \varnothing, \\ 0 A = \varnothing, \end{cases} \tag{14}$$

where

$$K = \sum_{\cap A_i = A} \prod_{1 \le j \le n} m_i(A_i). \tag{15}$$

The factor K is called the conflict coefficient, which represents the inconsistency of data fusion, that is, a measure of the degree of conflict between different quality functions.

We assume that the set E_k of student management information at the previous moment and the set E_{k+1} of student management information A_{k+1} at the next moment are two different independent signal sources and that the two sets of signal sources can determine the reliability distribution of the signal.

The identification framework is as follows: $E_k = \{\lambda_{1k}, \lambda_{2k}, \lambda_{3k}, \ldots, \lambda_{nk}\}$, $E_{k+1} = \{\lambda_{1k+1}, \lambda_{2k+1}, \lambda_{3k+1}, \ldots, \lambda_{nk+1}\}$;

The mass function assignment is m_k: $m_k(\{\lambda_{1k}\}), m_k(\{\lambda_{2k}\}), m_k(\{\lambda_{3k}\}), \ldots, m_k(\{\lambda_{1k}\}), m_k(\{\lambda_{nk}\}), m_k(\{\lambda_{1k}, \lambda_{2k}\}), m_k(\{\lambda_{1k}, \lambda_{3k}\}), m_k(\{\lambda_{1k}, \lambda_{4k}\}), \ldots, m_k(\{\lambda_{1k}, \lambda_{4k}\}), \ldots, \{\lambda_{1k}, \lambda_{2k}, \lambda_{3k}, \ldots, \lambda_{nk}\}$ m_{k+1}: $m_k(\{\lambda_{1k+1}\}), m_k(\{\lambda_{2k+1}\}), m_k(\{\lambda_{3k+1}\}), \ldots, m_k(\{\lambda_{1k+1}\}), m_k(\{\lambda_{nk+1}\}), m_k(\{\lambda_{1k+1}, \lambda_{2k+1}\}) m_k(\{\lambda_{1k+1}, \lambda_{3k+1}\}), m_k(\{\lambda_{1k+1}, \lambda_{4k+1}\}), \ldots, m_k(\{\lambda_{1k+1}, \lambda_{4k+1}\}), \ldots, \{\lambda_{1k+1}, \lambda_{2k+1}, \lambda_{3k+1}, \ldots, \lambda_{nk+1}\}$

According to Dempster combination rules (14) and (15), the probability assignment of each attribute is calculated as follows: $m(\{\lambda_i\})$

$$K = \sum_{\cap A_i = A} \prod_{1 \le j \le n} m_i(A_i),$$

$$m(A) = \begin{cases} \sum\limits_{\cap A_i = A} \prod\limits_{1 \le j \le n} \dfrac{m_i(A_i)}{(1-K)}, & A \neq \varnothing, \\ 0 A = \varnothing. \end{cases} \tag{16}$$

Finally, the calculated $m\ (A)$ is the basic probability assignment (BPA) of attribute 3.

The overall framework of the established model is shown in Figure 3.

The model summarizes the contents of the first three sections, and the overall framework is divided into two ways. The first path is the real-time observation value sj, and the possibility C_{tj} under the hypothetical H condition is calculated from the real-time measurement value and expressed as the mass function mv (.). mvg (.) is only related to the recognition frame $E = \{H, -H\}$.

Because mvgy (.) is the quality function of C_{ij}, the general conventions are as follows:

$$Pl_{\mathrm{vij}}(H_i) = C_{ij}. \tag{17}$$

Equation (17) accurately describes the classic problem of classification, that is, affirming that the measurement result is similar to the learning of H. However, it has uncertainty and may be similar to another hypothesis, and only considers the smallest specific mass function on H, which is called "model 1":

$$\begin{cases} mv_{ij}(H_i) = 1 - C_{ij}, \\ mv_{ij}(E_i) = C_{ij}. \end{cases} \tag{18}$$

In particular, C_{ij} is a symbol of meaning. When the value is 0, it is believed that H_i cannot be authenticated, and when the value is 1, it is sure that H_i is authenticated. At this point, we need to add conditions:

$$Pl_{vij}(H_i) = 1 - C_{ij}. \tag{19}$$

By combining formulas (17) and (18), inferences can be made, which is called "model 2."

$$\begin{cases} mv_{ij}(H_i) C_{ij}, \\ mv_{ij}(H_i) = 1 - C_{ij}. \end{cases} \tag{20}$$

Model 1 has the smallest specificity. Model 2 is not used under special circumstances. The data modeling in the integrated navigation system will be discussed further. Here, because of the uncertainty of sensor data, Model 1 is preferred.

In addition, when the model 2 is selected, the C_{ij} measurement method is sj, and the learning data method is $p(\mu_j / H_i)$, then C_{ij} is transformed into the following:

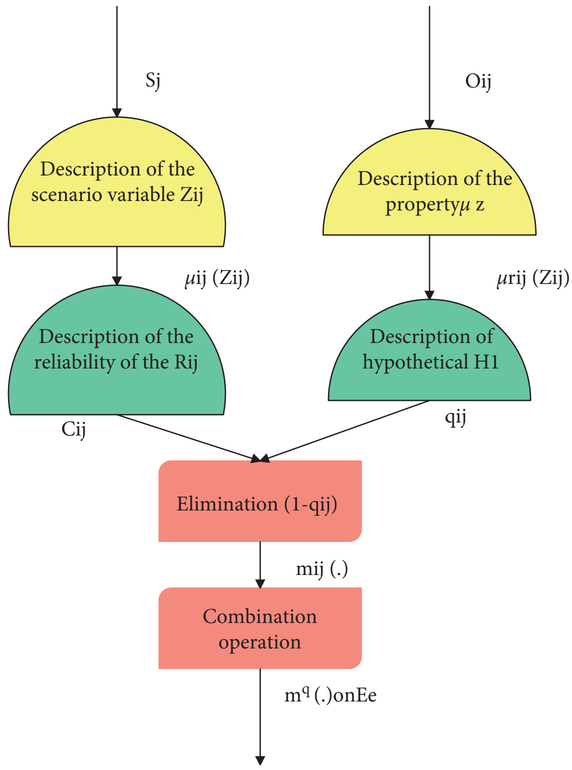

Figure 3: Overall framework of the model.

$$\begin{cases} C_{ij} = R_i p \dfrac{p\left(\mu_j/H_i\right)}{\left(1 + R_j p\left(\mu_j/H_i\right)\right)}, \\ R_j \in \left[0, \left(\max\left(p\left(\mu_j/H_i\right)\right)\right)^{-1}\right]. \end{cases} \tag{21}$$

4. Application of an Intelligent Sensor Algorithm in Student Management Information Fusion

In the entire school, the overall plan for the daily management of all classes is as follows: student work managers (including the school's student office administrators and the student department administrators of various departments), head teachers, and teachers complete the maintenance of the basic data required by the system in the management system, including the addition, modification, and deletion of all basic data. The teacher business flowchart is shown in Figure 4.

According to the daily management of the school's head teacher's work and business processes and the requirements of all system functions, the data flow is analyzed, the specific functional modules are divided, and the relationships and connections between them are clarified. The layer 1 data flow diagram of the management information system is shown in Figure 5.

It is further refined to form the data flow diagram of the second layer, as shown in Figures 6 and 7.

Shown in Figure 8 is the basic data flow diagram of the class teacher's management of the class in the class teacher's management information system. Among them, the relevant regulations of the school and the department are strictly enforced to evaluate the students in the class, and the reward and punishment information is recorded and provided to all users for easy inquiries.

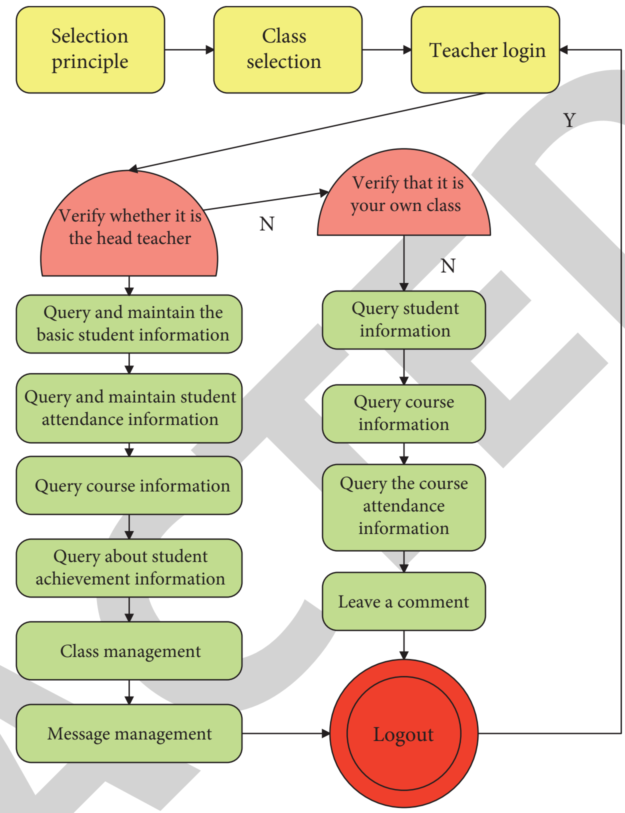

Figure 4: Teacher business flowchart.

Users can learn more about the information of each student during their schooling through the inquiry of modules such as attendance management, teaching management, dormitory management, reward and punishment management, and student information management. Among them, attendance information, dormitory information, and performance information can more accurately and concretely show the pros and cons of each student. Moreover, it can enable the head teacher and subject teachers to discover the problems of each student in a relatively short period of time and take immediate measures to control the spread of the problems. At the same time, all queries are open to students so that all students can grasp their true situation. With the help of all teachers, they can control their words and deeds during school so as to gradually cultivate personal self-discipline and learn to abide by rules. The information in the system can also be notified to parents of students in time through the home-school communication system, so that parents can keep track of their children's performance at school. This is convenient to enhance the understanding of students and is more conducive to communication with the head teacher and the school. In addition, with the information provided by the system, teachers, students, and parents can communicate in a timely manner, thereby avoiding unnecessary disputes in the later period.

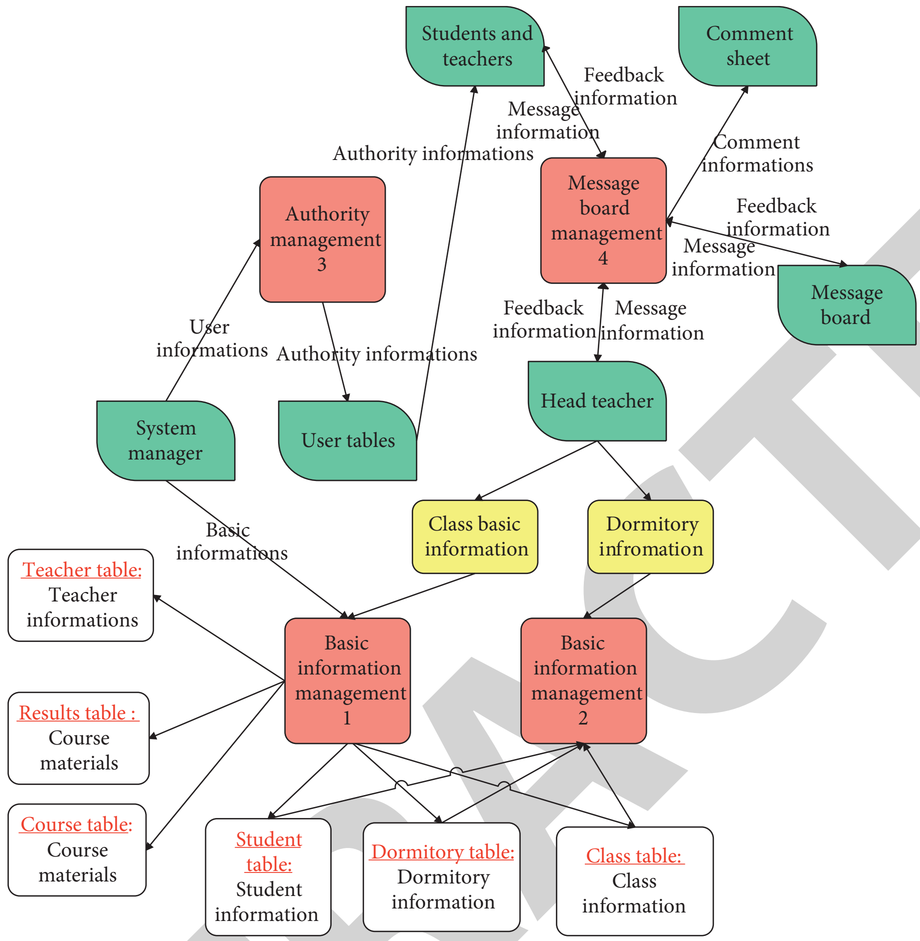

Figure 5: Data flow diagram of the management information system.

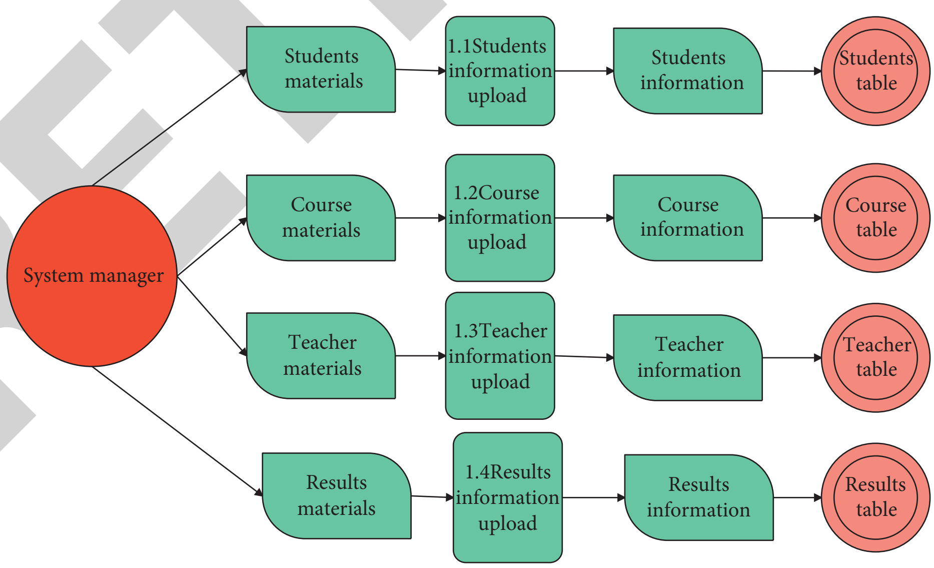

Figure 6: Data flow diagram of basic information management.

The user table is used to store basic user information, including user ID, user name, student ID or teacher ID, student card number, teacher user password, and user type, as shown in Table 1.

The student basic information table is used to store the basic personal information of students, mainly including student name, student number, card number, gender, political outlook, telephone number, class, dormitory number,

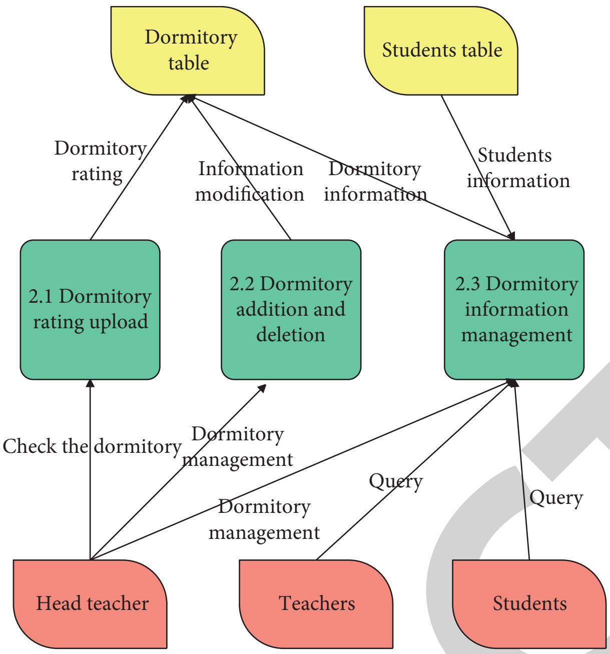

FIGURE 7: Data flow diagram of dormitory management.

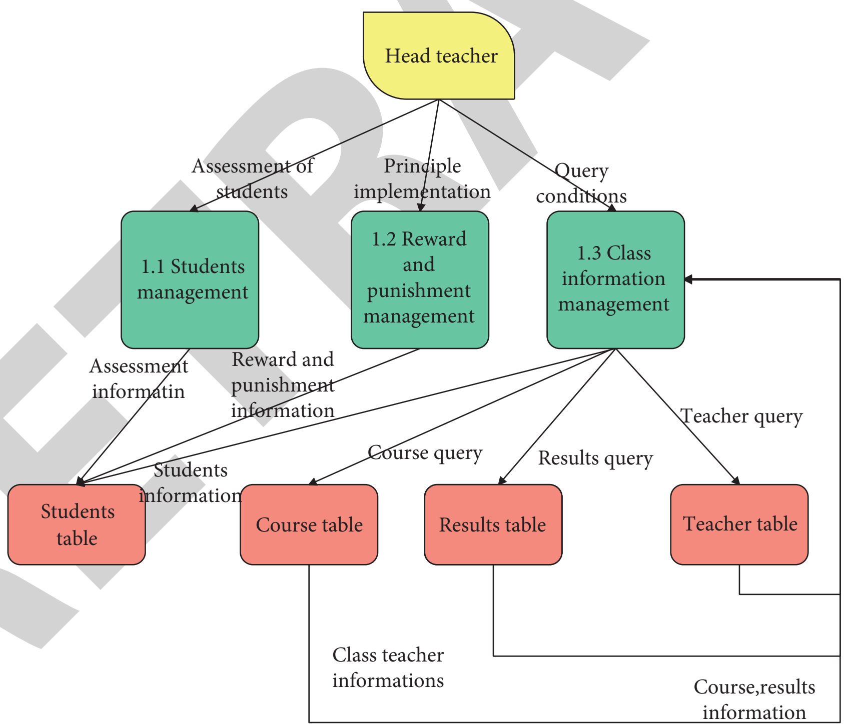

FIGURE 8: Data flow diagram of class management.

bed number, reward and punishment information, ID number, home address, and parent contact number, as shown in Table 2.

On the basis of the above-built system, through multiple sets of data, this paper uses the system proposed in this paper to fusion processing student information and performs data processing with the support of intelligent sensing algorithms. The results are shown in Figure 9.

As can be seen from the above figure, the smart sensor algorithm proposed in this paper can effectively promote the integration of student management information and has an important supporting role in the processing of college student management information. On this basis, the effect of the student assistance management of this system is evaluated, and the results are shown in Figure 10.

Table 1: User table.

Field name	Type of data	Annotation
User_ID	Int	User ID
User_Num	Varchar	Teacher employee number or student number
Card_num	Varchar	Student card number
User_Name	Varchar	Username
User_Pwd	Varchar	User password
User_Acc	Int	User rights

Table 2: Student basic information table.

Field name	Type of data	Annotation
Stu_ID	Int	Student ID
Stu_Num	Varchar	Student ID
Card_Num	Varchar	Student card number
Class_ID	Int	Class number
Stu_Name	Varchar	Student name
Stu_Sex	Varchar	Student gender
Stu_Rem	Varchar	Student rewards and punishments information
Stu_Adr	Varchar	Student's home address
Stu_HKLX	Varchar	Student account type
Stu_XSGZ	Logic	Whether the student enjoys the national bursary
Stu_XSDB	Logic	Whether the student enjoys the urban subsistence allowance
Stu_Zzmm	Varchar	Student political outlook
Stu_Sfc	Varchar	Student ID number
Stu_Csny	Date	Student's date of birth
Stu_Tel	Varchar	Student phone
Stu_Fqtel	Varchar	Student father phone
Stu_Mqtel	Varchar	Student mother phone
SS_ID	Int	Dormitory number

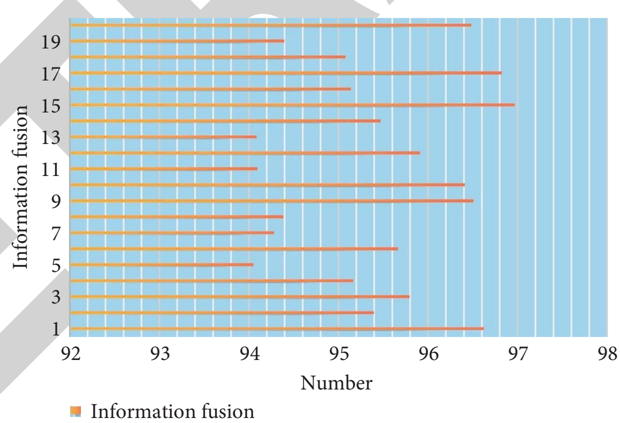

Figure 9: Information fusion processing results.

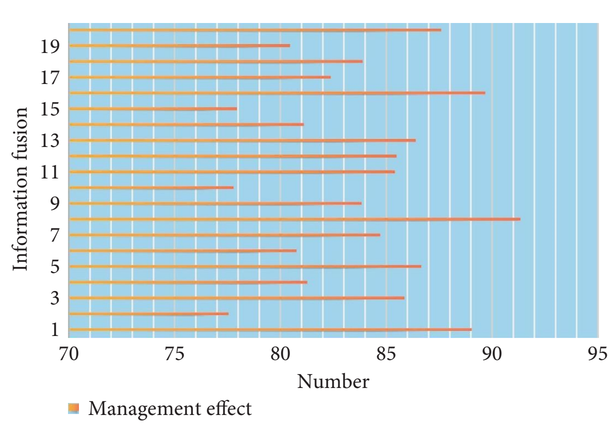

Figure 10: Student management effect.

It can be seen from the above figure that the method proposed in this paper can effectively improve the effect of student management and has an important role in promoting student information management in colleges and universities.

5. Conclusion

When colleges and universities conduct student management under the traditional management mode and the stand-alone mode of computer information systems, most of the time of each stage of the work of the management personnel is used to manually search for data and statistical information from various tables. Even if a computer information system is used in management work, it is limited to simple data processing, and there is no connection between different management tasks on the computer. Moreover, the role of the computer only improves the efficiency of management staff in handling daily business. The data of management work is communicated in a static way, and the data is completely relied on manual mutual verification and collaborative work, which causes the school's management links to be disconnected from each other and affects the overall management order of the school. This paper combines the intelligent sensor algorithm to construct the student management information system, analyzes the information fusion process of the intelligent sensor algorithm, proposes an improved algorithm, and verifies the performance of the system in this paper. Through simulation research, we can see that the method proposed in this paper can effectively improve the management effect of students.

Data Availability

The labeled dataset used to support the findings of this study are available from the corresponding author upon request.

Conflicts of Interest

The author declares no conflicts of interest.

Acknowledgments

This study was sponsored by Chifeng University.

References

[1] V. Rodriguez-Galiano, M. Sanchez-Castillo, M. Chica-Olmo, and M. Chica-Rivas, "Machine learning predictive models for mineral prospectivity: an evaluation of neural networks, random forest, regression trees and support vector machines," *Ore Geology Reviews*, vol. 71, no. 3, pp. 804–818, 2015.

[2] C. W. Coley, R. Barzilay, T. S. Jaakkola, W. H. Green, and K. F. Jensen, "Prediction of organic reaction outcomes using machine learning," *ACS Central Science*, vol. 3, no. 5, pp. 434–443, 2017.

[3] A. Chowdhury, E. Kautz, B. Yener, and D. Lewis, "Image driven machine learning methods for microstructure recognition," *Computational Materials Science*, vol. 123, no. 8, pp. 176–187, 2016.

[4] S. Basith, B. Manavalan, T. H. Shin, and G. Lee, "SDM6A: a web-based integrative machine-learning framework for predicting 6mA sites in the rice genome," *Molecular Therapy - Nucleic Acids*, vol. 18, no. 6, pp. 131–141, 2019.

[5] C. Voyant, G. Notton, S. Kalogirou et al., "Machine learning methods for solar radiation forecasting: a review," *Renewable Energy*, vol. 105, no. 2, pp. 569–582, 2017.

[6] H. Li, O. L. Kafka, J. Gao et al., "Clustering discretization methods for generation of material performance databases in machine learning and design optimization," *Computational Mechanics*, vol. 64, no. 2, pp. 281–305, 2019.

[7] L. Cheng, N. B. Kovachki, M. Welborn, and T. F. Miller, "Regression clustering for improved accuracy and training costs with molecular-orbital-based machine learning," *Journal of Chemical Theory and Computation*, vol. 15, no. 12, pp. 6668–6677, 2019.

[8] S. K. Mydhili, S. Periyanayagi, S. Baskar, P. M. Shakeel, and P. R. Hariharan, "Machine learning based multi scale parallel K-means++ clustering for cloud assisted internet of things," *Peer-to-Peer Networking and Applications*, vol. 13, no. 6, pp. 2023–2035, 2020.

[9] M. Mirmozaffari, A. Boskabadi, G. Azeem et al., "Machine learning clustering algorithms based on the DEA optimization approach for banking system in developing countries," *European Journal of Engineering Research and Science*, vol. 5, no. 6, pp. 651–658, 2020.

[10] M. Chegini, J. Bernard, P. Berger, A. Sourin, K. Andrews, and T. Schreck, "Interactive labelling of a multivariate dataset for supervised machine learning using linked visualisations, clustering, and active learning," *Visual Informatics*, vol. 3, no. 1, pp. 9–17, 2019.

[11] A. Nandi, J. M. Bowman, and P. Houston, "A machine learning approach for rate constants. II. Clustering, training, and predictions for the O(3P) + HCl ⟶ OH + Cl reaction," *The Journal of Physical Chemistry A*, vol. 124, no. 28, pp. 5746–5755, 2020.

[12] S. Dotsenko, O. Illiashenko, S. Kamenskyi, and V. Kharchenko, "Integrated security management system for enterprises in industry 4.0," *Information and security: an international journal*, vol. 43, no. 3, pp. 294–304, 2019.

[13] N. Y. Kim, S. Rathore, and J. H. Ryu, "A survey on cyber physical system security for IoT: issues, challenges, threats, solutions," *Journal of Information Processing Systems*, vol. 14, no. 6, pp. 1361–1384, 2018.

[14] S. U. Hani and A. T. Alam, "Software development for information system - achieving optimum quality with security," *International Journal of Information System Modeling and Design*, vol. 8, no. 4, pp. 1–20, 2017.

[15] M. Sun, I. Konstantelos, and G. Strbac, "A deep learning-based feature extraction framework for system security assessment," *IEEE Transactions on Smart Grid*, vol. 10, no. 5, pp. 5007–5020, 2018.

[16] K.-K. R. Choo, M. M. Kermani, R. Azarderakhsh, and M. Govindarasu, "Emerging embedded and cyber physical system security challenges and innovations," *IEEE Transactions on Dependable and Secure Computing*, vol. 14, no. 3, pp. 235-236, 2017.

[17] D. Li, Z. Cai, L. Deng, Y. Xiang, and H W. Harry, "Information security model of block chain based on intrusion sensing in the IoT environment," *Cluster Computing*, vol. 22, no. 1, pp. 451–468, 2019.

[18] A. Safi, "Improving the security of internet of things using encryption algorithms," *International Journal of Computer and Information Engineering*, vol. 11, no. 5, pp. 558–561, 2017.

Hindawi
Scientific Programming
Volume 2021, Article ID 3074167, 12 pages
https://doi.org/10.1155/2021/3074167

Research Article

Production Efficiency Prediction of Pig Breeding Industry by Optimized LSTM Computer Algorithm under Environmental Regulation

Yunfei Jia, Zhaohui Zhang, Zejun He, Panpan Zhu, Yibei Zhang, and Tianhua Sun

Institute of Economics and Management, Henan Agricultural University, Zhengzhou, Henan 450046, China

Correspondence should be addressed to Zejun He; ndxbjyf@henau.edu.cn

Received 11 October 2021; Revised 28 October 2021; Accepted 3 November 2021; Published 26 December 2021

Academic Editor: Le Sun

The study aims to improve the economic income of pig breeding industry under environmental regulation and control the environmental pollution caused by pig breeding. Long short-term memory (LSTM) neural network combined with environmental regulation is proposed to forecast the price of live pigs, to reduce the cost of environmental pollution control and improve the production efficiency of pig breeding. Primarily, analyses are made on the industrial structure and pollution of pigs in China, and studies are carried out on the inevitability of large-scale and intensive pig breeding. Then, pig breeding and environmental pollution are coordinated under the environmental regulation. From the perspective of green total factor productivity, calculation is made on the profit of pig breeding and the cost of environmental pollution control. Next, the LSTM neural network is used to predict the price of live pigs, thus effectively controlling the scale of pig breeding and making timely decisions that conform to market rules. The results show that with the increase of feed and land prices, the advantages of large-scale pig breeding gradually become prominent, which leads to the small- and medium-sized scale farmers withdrawing from the market. Compared with other similar models, the designed model can better simulate the future trend of hog price, of which the prediction accuracy is over 80%. When combined with environmental regulations, the prediction accuracy of the model for different data sets reaches 83%, so the designed model can better predict the changing trend of the price of live pigs, thus improving the production efficiency of large-scale pig farmers.

1. Introduction

Pig breeding industry is an important part of China's rural economic system. With the rapid increase of people's demand for pork in recent years, pig breeding industry has developed rapidly [1]. China is the largest country in pork consumption in the world. From 2010 to 2018, Chinese consumed more than 50 million tons of pork every year. Therefore, pork is the main source of meat for Chinese and plays an important role in dietary structure of Chinese, which shows that there is a huge market demand for pork in the domestic market. However, since 2019, under the combined influence of environmental protection policies, large-scale breeding trend, and "swine fever," the slaughter rate of Chinese pigs has decreased, resulting in a severe decline in pork production. However, the intensive and large-scale pig breeding model also poses a challenge to the carrying capacity of the natural environment, which becomes an important agricultural pollution source. Therefore, in the process of agricultural economic development, the government began to pay attention to the sustainable development of pig breeding industry and formulated relevant environmental regulation policy system to centrally control the environmental pollution caused by large-scale pig breeding in rural areas. Under environmental regulation, pig breeding industry requires optimizing regional layout, changing production mode, and promoting green sustainable development [2].

Nevertheless, the increasingly perfect breeding environment regulation policy system cannot effectively curb the environmental pollution of pig industry. With the increasingly serious problems of resources and environment, the traditional extensive, high-pollution, and high-yield economic development model cannot meet the standards of social development. Green total factor productivity is an important indicator to measure production efficiency. From the aspect of the growth, the indicator includes green technology progress and green technology efficiency [3]. Green total factor productivity is put forward based on traditional total factor productivity, which refers to the ratio of total output to total production factor input in a system. The improvement of green technology progress and green technology efficiency will lead to the continuous improvement of green total factor participation rate. The harm to the environment in the process of development should be avoided to ensure the sustainable development of the pig breeding industry. By analyzing the influencing factors in green total factor productivity growth of pig breeding under environmental regulation and analyzing the main influencing factors, construction of a perfect environmental protection policy system of pig breeding industry is finished; it improves green total factor productivity and promotes the sustainable development of pig breeding industry [4].

In view of the development of pig breeding industry under environmental regulation, global experts and scholars have done a lot of research. Biddle (2021) studied the regular analysis of statistical samples to predict the supply of various agricultural products and compared it with the actual situation, which proved the effectiveness of regular forecasting in solving practical problems [5]. Xie et al. (2021) studied the application of artificial intelligence technology in the medical field, compared it with the prediction of diseases and drug reactions through deep learning technology, established a framework based on deep learning, and analyzed the prediction methods corresponding to different diseases [6]. The current related research suggests that the development of pig breeding industry under the agricultural environmental regulation has become an important economic variable and academic research hotspot under the new development concept. There are many research works on green total factor productivity of pig industry breeding, combined with the research of China's macroeconomic development and environmental regulation measurement [7]. However, there is a lack of those on the relationship between environmental regulation and green total factor productivity of pig breeding. Therefore, analyses are made on the production efficiency of pig industry under environmental regulation by combining factors such as pig breeding scale, pig price, and environmental control cost. The changing trend of pig price is predicted through neural network model. Studies are released on the relationship between green total factor productivity of pigs and environmental regulation by using panel data combined with environmental control cost, aimed at looking for the inflection point of the optimal agricultural environmental regulation intensity under different pig breeding scales. From these results, the most suitable pig breeding scale can be obtained to realize the green and sustainable development of pig breeding industry and further improve farmers' income.

2. Environmental Regulation and Production Efficiency of Pig Breeding Industry

2.1. Industrial Structure of Pig Scale Breeding and Environmental Pollution under Environmental Regulation. With the accelerated consumption of resources and the deteriorating social environment, resource and environmental problems have become an important factor affecting residents' life and social development in China. Therefore, more and more scholars have introduced natural resources and environmental factors into the process of economic growth and put forward the green economic growth theory [8]. Combined with the sustainable development theory, the green economic growth theory is put forward. The theory believes that green economic growth is an economic development model which ensures that natural resources can continue to provide various resources and environmental services for people's happiness, reduces environmental risks and scarcity of ecological resources, and then promotes positive economic growth and development [9]. For a long time, China's pig breeding industry has been dominated by the scattered breeding, with a low degree of scale breeding. However, in recent years, affected by the increase of opportunity cost and environmental protection supervision, retail investors began to withdraw from the pig breeding industry, and the scale of domestic pig breeding is further improving [10]. Moreover, in order to regulate China's pork production, many policy documents have been issued to promote the development of pig industry; promote the pig breeding industry from the perspectives of land, subsidies, and environmental protection; stabilize the supply of pork production, further promote the transformation, upgrading, and development of pig industry; and promote the optimized development of pig breeding industry to a strategic development position [11]. Figure 1 indicates the structure of pig breeding industry chain.

The essence of green economic growth theory is to realize the coordinated development of resources, environment, and economy with the least resource consumption and the least environmental cost. Therefore, the application of green economic growth to pig breeding industry emphasizes adjusting the speed of pig breeding economic growth and ensuring the quality of economic growth, to realize the coordinated development between economy, resources, and environment of pig breeding industry and maximize the comprehensive social welfare. The Market Failure Model holds that some obstacles in the real market make it difficult to allocate resources only by the price mechanism to achieve the Pareto Optimum, and there is a certain loss of efficiency [12]. Therefore, the method of resource allocation in the market is completely generated by the structure of market competition, and also under the influence of external obstacles such as monopoly, information asymmetry, and public goods, the price mechanism will be limited. Merely through the market resource allocation, the resource allocation efficiency cannot achieve the Pareto Optimum, which is manifested as the failure of market mechanism.

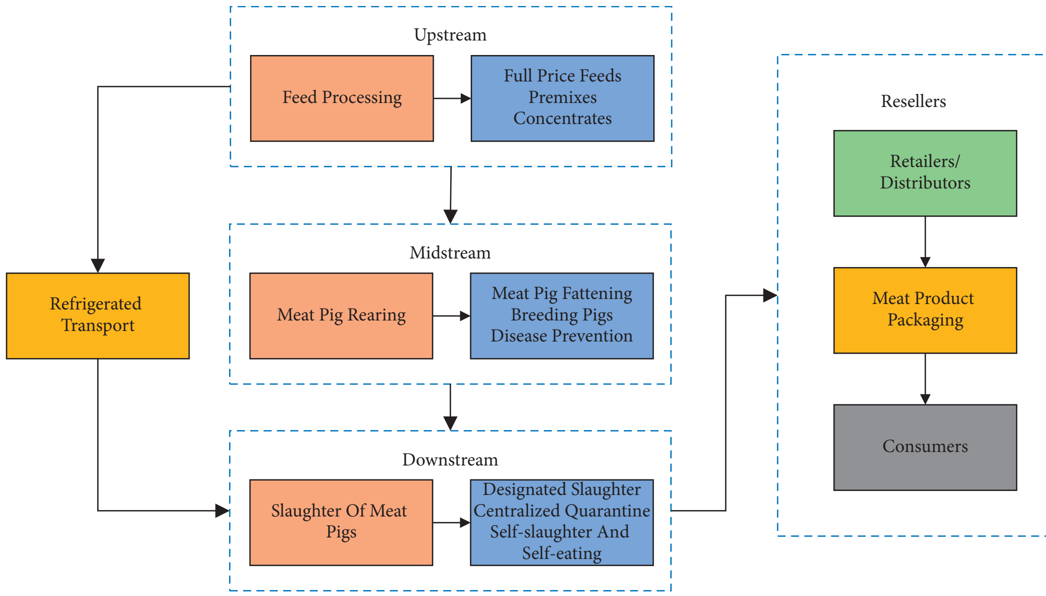

Figure 1: Pig breeding industry chain.

Environmental pollution is the most important embodiment of economic externality. When the business entity produces pollution discharge to the environment in the process of production and business activities, but it does not compensate timely for environmental pollution, it will produce environmentally external economy. From the perspective of private interests, to maximize profits, it is necessary for the business entities to minimize the production cost while ensuring their established income. Therefore, there will be business entities that will transfer the cost of environmental pollution to the society, so that the society will jointly bear the cost of environmental pollution control brought by the entities. Environmental regulation is the environmental binding of the regulation subject to the regulation object. Environmental regulation is generally accepted as the direct intervention of the government in the organization or individual environment that operates business, through the formulation of prohibitions and environmental standards. The main feature is that the government implements environmental norms by forcible means to achieve the protection of the environment. In the research process, by comparing the cost-benefit, environmental pollution and green total factor productivity of the pig breeding industry at different times, regions, and production scales, there can be more understanding of the actual situation of pig breeding to provide a practical basis for the subsequent optimization of production mode, reducing environmental pollution and promoting the transformation of pig breeding industry. The impact of environmental regulation on the green total factor productivity of pig breeding industry is analyzed [13].

After a long period of development, China's pig breeding industry has become an intensive means of production input industry that relies on factors such as capital and labor. Although the overall economic aggregate of the pig breeding industry is increasing, the profits of the industry are generally low and are constrained by resources, environment, and environmental regulations, so the pig breeding industry needs dynamic and green transformation from the original extensive economic growth model to the intensive economic growth model. A new green economic growth industry should be guided by green total factor productivity [14]. As a coordination mechanism combining environment, resources, and economic development, environmental regulation plays an important guiding role in the direction of green economy development. The environmental regulation can inhibit the pollution of pig breeding industry to a certain extent, but it will also affect the economic growth efficiency of pig breeding industry as well [15].

2.2. Calculation of Pig Breeding Profit and Environmental Pollution Control Cost. However, from the perspective of the overall development model, environmental regulation can realize the green economic growth of pig breeding industry, promote the emission reduction of pig breeding industry, and improve the efficiency of pig breeding industry. By analogy with the impact of industrial environmental regulation on industrial pollution emission, industrial environmental regulation can not only reduce industrial pollution emission, but also promote the efficiency of economic growth [16]. Compared with the pollution caused by industrial production, due to the small-scale and periodic operation, the environmental pollution produced by the pig breeding industry presents the problems of dispersion, concealment, and difficult monitoring, which increases the difficulty of controlling the environmental pollution of the pig breeding industry [17]. In the macroeconomic system, the total output includes expected output such as economic output value and unexpected output such as environmental pollution cost. When constructing the theoretical model of productivity, it is necessary to consider the traditional means of production such as capital, labor, and land, in addition to the resource and environmental factors, especially the environmental pollution factors [18]. By referring to the definition of green total factor productivity, the green total factor productivity of pig breeding is defined, which represents the expected output, such as economic output value in the process of pig breeding, and the proportion of undesired output such as environmental pollution in the input of production factors such as capital, labor, and land. Further, what can be obtained is the ratio between increase of the expected output such as economic output value and the decrease of unexpected outputs such as environmental pollution, in a specific direction under the given input [19].

Compared with the traditional calculation of total factor productivity, resource and environmental factors are focused by green total factor productivity based on input and output, so it is necessary to introduce environmental pollution evaluation indexes such as chemical oxygen demand (COD), total nitrogen (TN), and total phosphorus (TP). Nonparametric estimation methods, such as data inclusion analysis (DEA), are often used to calculate green total factor productivity. The advantage of the single method lies in its handy calculation and unnecessity of environmental pollution values to be considered. In addition, it does not depend on the specific form of the production function and does not need an assumed specific form of the production function beforehand, so it can be applied to measurement directly by using the linear programming method [20]. Combined with previous studies, the Fixed-Window-Malmquist–Luenberger (FWML) index is used to measure the green total factor productivity (GTFPCH) of pig breeding industry. Green total factor productivity is divided into two parts: green technology efficiency (GEFFCH) and green technology progress (GTECHCH). Equations (1) and (2) provide the specific calculation.

$$\mathrm{GTFPCH}_w^{\mathrm{fixed}} = \frac{1 + \overrightarrow{D}_w^{\mathrm{fixed}}\left(x^t, y^t, b\right)^t}{1 + \overrightarrow{D}_w^{\mathrm{fixed}}\left(x^{t+1}, y^{t+1}, b^{t+1}\right)}, \tag{1}$$

$$\mathrm{GEFFCH}_w^{\mathrm{fixed}} = \frac{1 + \overrightarrow{D}_w^{t}\left(x^t, y^t, b^t\right)}{1 + \overrightarrow{D}_w^{t+1}\left(x^{t+1}, y^{t+1}, b^{t+1}\right)}, \tag{2}$$

$$\mathrm{GTECHCH}_w^{\mathrm{fixed}} = \frac{1 + \overrightarrow{D}_w^{\mathrm{fixed}}\left(x^t, y^t, b^t\right)}{1 + \overrightarrow{D}_w^{t}\left(x^t, y^t, b^t\right)} \times \frac{1 + \overrightarrow{D}_w^{t+1}\left(x^{t+1}, y^{t+1}, b^{t+1}\right)}{1 + \overrightarrow{D}_w^{\mathrm{fixed}}\left(x^{t+1}, y^{t+1}, b^{t+1}\right)}. \tag{3}$$

In (1) and (2), $\overrightarrow{D}_w^{t+1}$ stands for the production reference set based on directional distance function in $t+1$ period under a fixed window, $\overrightarrow{D}_w^{t}$ refers to the production reference set based on directional distance function in t period under a fixed window, x means input elements, y represents the expected output element, and b is set to be the unexpected output element. The non-angle SBM function is selected as the directional distance function [21].

With panel data, the impact of environmental regulation on the total factors of green productivity, green technology efficiency, and green technology progress of pig breeding is investigated. The panel bidirectional fixed effect model and tool variable method are used to understand the influence and mechanism of green total factor productivity under environmental regulation. The Moran index and the spatial effect brought by spatial Doberman model are used [22, 23]. Combined with the influencing factors of environmental regulation on pig breeding, (4) shows the established empirical model (in (4), i stands for provinces, t refers to time, *GTFPCH* is the abbreviation of the green total factor productivity of pig breeding, *GEFFCH* represents the green technical efficiency of pig breeding, *GTECHCH* means the green technology progress of the pig breeding industry, *ERI* stands for the environmental regulation intensity, *NATRES* is the resource endowment status, *ECODEV* is the economic development level, *INDFOU* refers to industrial basic status, *MARECO* stands for the market economy condition, *TRAINF* stands for the transportation infrastructure, μ_{area} stands for the regional effect, μ_{year} denotes the time effect, and ε stands for the random disturbance term [24]):

$$\begin{aligned}\mathrm{GTFPCH}_{i,t} = {} & \alpha_0 + \alpha_1 \mathrm{ERI}_{i,t} + \beta_1 \sum \mathrm{NATRES}_{i,t} + \beta_2 \sum \mathrm{ECODEV}_{i,t} \\ & + \beta_3 \sum \mathrm{INDFOU}_{i,t} + \beta_4 \sum \mathrm{MARECO}_{i,t} + \beta_5 \sum \mathrm{TRAINF}_{i,t} + \mu_{\mathrm{area}} + \mu_{\mathrm{year}} + \varepsilon_{i,t}.\end{aligned} \tag{4}$$

To help better understand the influence mechanism of green total factor productivity of pig breeding under environmental regulation, the green total factor productivity is decomposed into green technical efficiency and green technical progress as shown in the following equations:

$$\begin{aligned}\mathrm{GEFFCH}_{i,t} = {} & \alpha_0 + \alpha_1 \mathrm{ERI}_{i,t} + \beta_1 \sum \mathrm{NATRES}_{i,t} + \beta_2 \sum \mathrm{ECODEV}_{i,t} \\ & + \beta_3 \sum \mathrm{INDFOU}_{i,t} + \beta_4 \sum \mathrm{MARECO}_{i,t} + \beta_5 \sum \mathrm{TRAINF}_{i,t} + \mu_{\mathrm{area}} + \mu_{\mathrm{year}} + \varepsilon_{i,t},\end{aligned} \tag{5}$$

$$\begin{aligned}\mathrm{GTECHCH}_{i,t} = {} & \alpha_0 + \alpha_1 \mathrm{ERI}_{i,t} + \beta_1 \sum \mathrm{NATRES}_{i,t} + \beta_2 \sum \mathrm{ECODEV}_{i,t} \\ & + \beta_3 \sum \mathrm{INDFOU}_{i,t} + \beta_4 \sum \mathrm{MARECO}_{i,t} + \beta_5 \sum \mathrm{TRAINF}_{i,t} + \mu_{\mathrm{area}} + \mu_{\mathrm{year}} + \varepsilon_{i,t}.\end{aligned} \tag{6}$$

2.3. Relationship between Pig Price and Breeding Scale. The fluctuation of pig price is due to many reasons, which has an impact on pig production and consumption. In China, the pork price is mainly regulated by a dual-track system, which combines the guidance price with the market-regulated price. With the steady improvement of social and economic level, people's income level is constantly improving. People's consumption level and quality of life are constantly improving, which leads to a further increase in the demand for pork, which makes the price of pork constantly increasing. However, with the increasing supply of beef, mutton, fish, and poultry and the increasing pork demand, the price of pork exceeds the per capita consumption level of people; the pork supply is excessive [25]. Figure 2 shows the periodic fluctuation law of pork price.

The majority of small- and medium-sized retail investors in the early pig breeding industry easily lose money in the pig market when the pig price is high and the column is low, resulting in the production capacity of pigs being consistent with the change trend of pig prices. The long-term average price of pork pigs depends on the price of live hogs and is affected by the relationship between market supply and demand in the short term. When breeders expect the price of pork to rise, they will increase the number of sows and stocks, resulting in oversupply in the market; when they expect pork prices to fall, they will reduce the number of sows and stocks, resulting in the market supply of pork short of the demand. The pork price will also be alternated in the fluctuation caused by the two methods, resulting in the continuous fluctuation of pork price. Moreover, China is further banning the retail pig breeding, to ensure the steady prices of pork. However, the intensive and large-scale pig breeding also leads to the gradual formation of a monopoly trend among slaughtering enterprises and intervenes in the purchase price of pigs and the wholesale price of pork. Table 1 shows the classification criteria of pig breeding scale.

The most intuitive economic benefits brought by pig breeding are reflected in the pork price. The fluctuation of the price of pig is as regular as other commodities. The periodic price fluctuation is mainly affected by the relationship between market supply and demand, and the two factors also affect each other. Since 2006, the fluctuation cycle of China's pig price is generally 3~4 years, and the pork price shows a trend where it is low in the middle of the curve and high in the two ends of the curve in one year. Specifically, the pork price is high from January to February in every year. It decreases from March and reaches the lowest point from May to July. Then, it begins to recover slowly and reach the peak of a new round before the Spring Festival. However, with the development of social economy, some changes have taken place in the price law of pig market. Judging by the fluctuation of pig price, the overall supply trend of the market, the reluctance of farmers to sell, the scale of pig breeding, and the pig transportation have impacted and restricted the import and terminal demand of pigs [26]. Figure 3 illustrates the influencing factors in pig prices.

2.4. Prediction Model of Pig Price and Yield Based on LSTM. Artificial neural network simulates the ability of human brain to process information from the perspective of information processing. Thus, what is established is a network model composed of different connection modes. The neural network contains many neuron nodes, which are interconnected to form an operation model, and each neuron node represents a specific output function. The connection between two nodes represents the weight of the connection signal [27]. The internal connection mode of neural network determines the output result of the network, which can be divided into forward network and feedback network according to the characteristics of network topology. Figure 4(a) shows the structure of the forward neural network, and Figure 4(b) reveals the structure of the feedback neural network. Artificial neural network is characterized by strong self-learning ability, associative storage ability, and ability to find the optimal solution.

The recurrent neural network (RNN) includes input units, output units, and hidden units. After data being put into the neural network and processed, the data of hidden layer and output layer are obtained. The hidden layer plays an important role in RNN. Figure 5(a) indicates the structure of RNN, and Figure 5(b) illustrates the network expansion. Every neuron structure will be used over and over again [28]. Parameter x_t represents the input at time t, o_t refers to the output at time t, and s_t means the memory at time t. Parameter s_t can be calculated according to the output of the input layer and the state of the hidden layer as shown in the following equation:

$$s_{\mathrm{I}} = f\left(U - x_{\mathrm{T}} + W - s_{r-1}\right). \tag{7}$$

Parameter f represents a nonlinear activation function. When calculating the hidden layer state of the word s_0, s-1 does not exist in fact, which needs to be used. The result is impossible to predict directly with single matrix, so it is necessary to introduce a weight matrix V. When prediction begins, o_t stands for the output at time t, and the equation is

$$o_r = \mathrm{softmax}\left(V \cdot s_r\right). \tag{8}$$

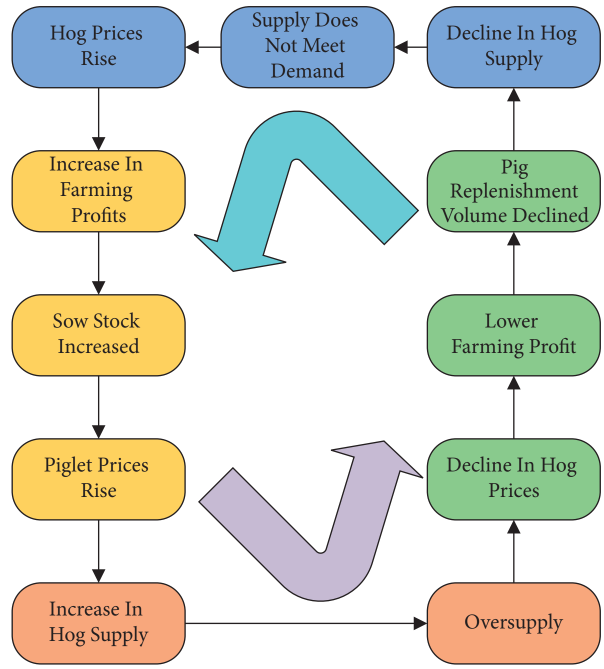

Figure 2: Periodic fluctuation law of pork price.

Table 1: Classification standard of pig breeding scale.

	Farrow-to-finish	Piglet feeding	Breeding piglets
Retail investors	Scale base: sows <10, commercial pigs <160/year	Scale base: sows = 0, commercial pigs <160/year	Scale based sows <10, piglets <160/year
Small-scale industries	Scale base: sows <100, commercial pigs <1600/year	Scale base: sows = 0, commercial pigs <1600/year	Scale base: sows <100, piglets <1600/year
Medium-scale industries	Scale base: sows <1000, commercial pigs <10000/year	Scale base: sows = 0, commercial pigs <10000/year	Scale base: sows <1000, piglets <10000/year
Large-scale industries	Scale base: sows >3000, commercial pigs >50000/year	Scale base: sows = 0, commercial pigs >50000/year	Scale base: sows <3000, piglets <50000/year

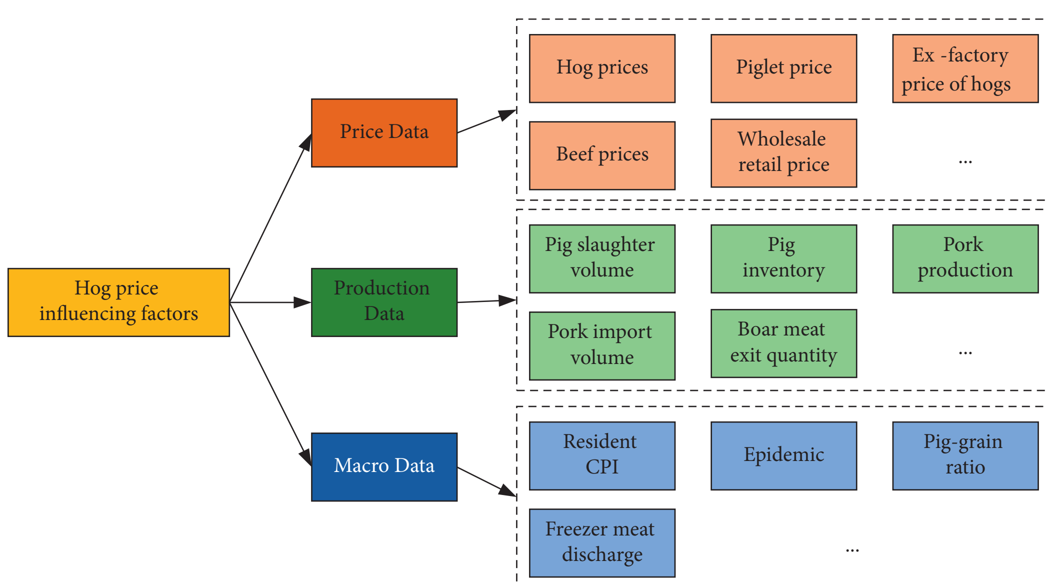

Figure 3: Table of influencing factors in pig price.

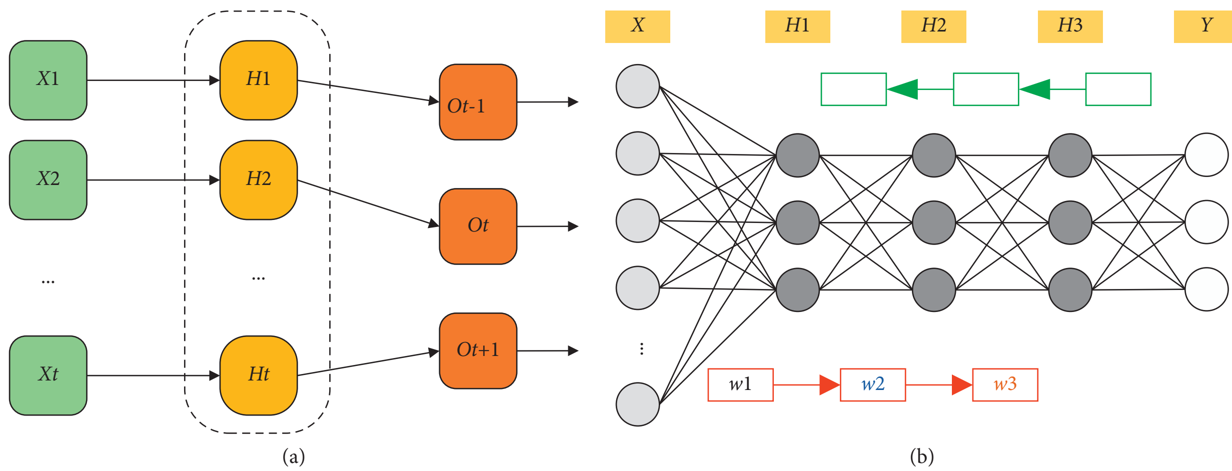

Figure 4: Structure of feedforward neural network (a) and feedback neural network (b).

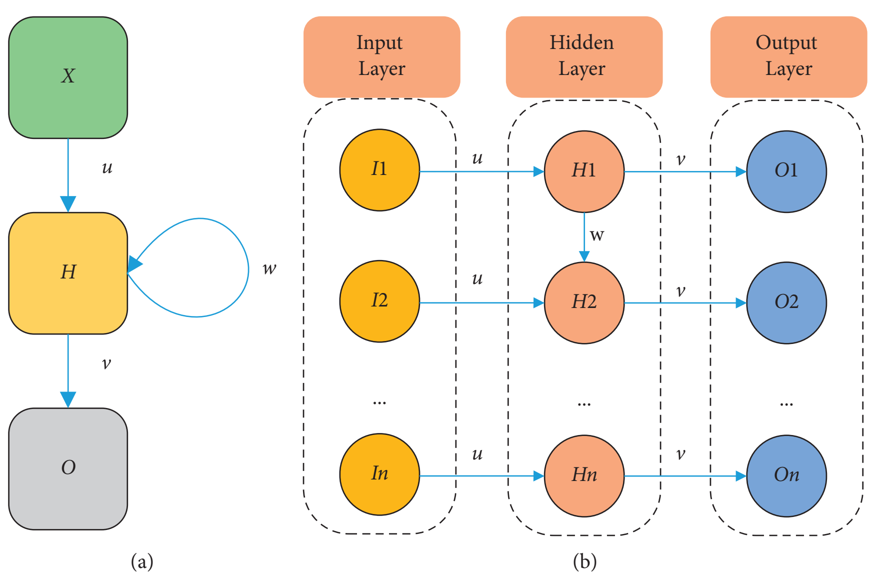

Figure 5: Structure of cyclic neural network: (a) RNN structure; (b) RNN deployment structure.

Figure 5 shows that each memory unit in the network shares a set of parameters (u, v, w), which greatly reduces the amount of calculation of the neural network. However, the neurons are independent of each other; ideal results cannot be obtained when dealing with timing problems. Furthermore, in the process of network training, there is also the problem of gradient disappearance or explosion, which cannot solve the problem of long-term dependence. However, the long short-term memory (LSTM) network solves these problems well. Compared with the cyclic neural network, it has the function of long-term memory [29]. Therefore, it is suitable for processing and predicting the events with relatively long interval and delay in time series. Figure 6 shows the deformed structure of LSTM network. Based on the structure of ordinary cyclic neural network, it adds memory units to each neural unit of hidden layer, to make the memory information on time series controllable. Each time data is transmitted between each unit of hidden layer, it passes through several controllable gates (forgetting gate, input gate, candidate gate, output gate), which can control the memory degree of previous information and current information.

The memory block in the LSTM network structure includes three parts: forgetting gate, input gate and output gate, and a memory unit. The first step of the LSTM neural network is to decide, through the forgetting gate and the sigmoid function, and to control which information can pass through the memory unit [30]. According to the output h_{t-1} at the previous moment and the current input x_t, a value of f_t from 0 to 1 is generated to decide whether to let the information C_{t-1} learned at the previous moment pass or partially pass:

$$f_t = \sigma\left(W_f\left[h_{t-1}, x_t\right] + b_f\right). \tag{9}$$

The second step is to generate the updated information, including two values generated by the input layer and the

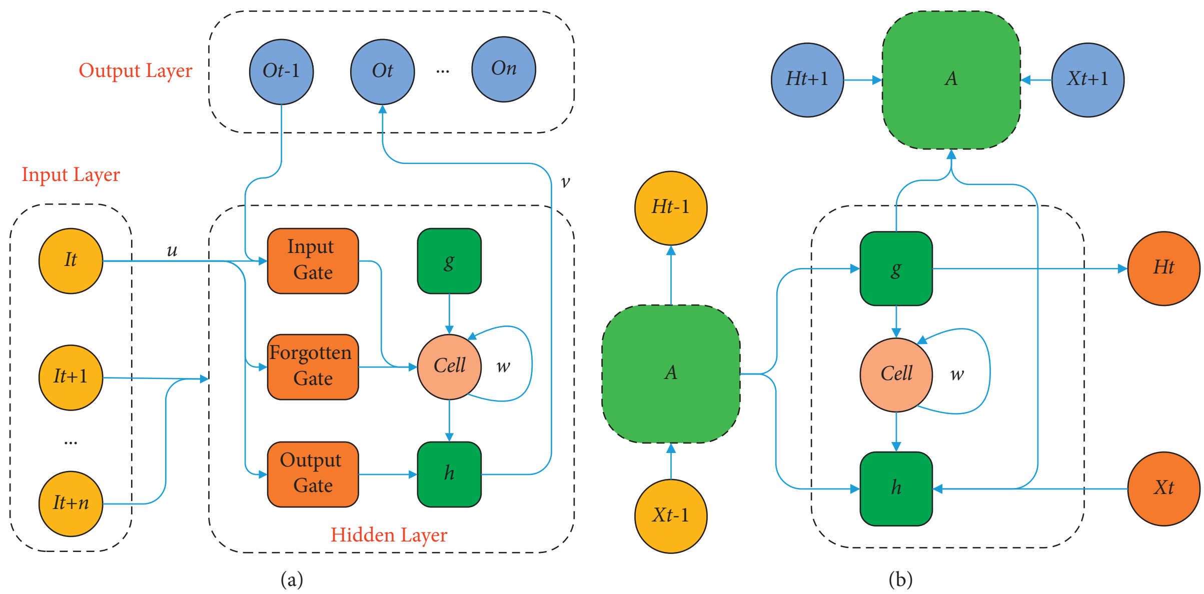

FIGURE 6: LSTM memory network: (a) LSTM neural network; (b) expansion of LSTM neural network.

tanh, which will be used as candidate values of the hidden layer and added to the memory unit. The equation is

$$i_t = \sigma\left(W_i\left[h_{t-1}, x_t\right] + b_i\right), \quad (10)$$

$$\widetilde{C}_t = \tanh\left(W_c\left[h_{t-1}, x_t\right] + b_c\right). \quad (11)$$

After the information generated by the previous memory unit is multiplied with f_t, i_t is added to multiply the candidate value to generate a new candidate value. The combination of the two can make the unnecessary information forgotten. Equation (12) illustrates the process of adding new information:

$$C_t = f_t \cdot C_{t-1} + i_t \cdot \widetilde{C}_t. \quad (12)$$

The last step is to determine the output of the model. An initial output is obtained through the sigmoid layer, and then the value of Ct is scaled to [−1, 1] by using tanh and then multiplied by the output obtained by sigmoid one by one. Thus, the final output of the model is obtained as shown in the following equations:

$$o_t = \sigma\left(W_o\left[h_{t-1}, x_t\right] + b_o\right), \quad (13)$$

$$h_t = o_t \cdot \tanh\left(C_t\right). \quad (14)$$

2.5. Experimental Methods and Data Sets. The data are selected from the panel data of pig breeding industry in cities of 6 provinces: Heilongjiang, Hebei, Shaanxi, Hunan, Zhejiang, and Guangdong, from 2005 to 2019. Under the consideration of the changes of pig price caused by the differences of provinces in different regions, the model of different provinces is trained to predict the prices of "Shunfeng Pork." In the research process, due to the lack of research data in some provinces, the Difference Method is used to supplement the missing data on the basis of the established research, to improve the research efficiency and comparability of data. The web crawler is used to obtain the transaction price of the Chinese pig market, the quotation of employees, and the pig price of the trading website and save them as an Excel file. To ensure the accuracy of the obtained data, the pig prices of the Statistical Yearbook published by the National Bureau of Statistics is used as the standard price of pigs. In the study, the data of pigs from 2005 to 2015 are selected as the training set and the data from 2016 to 2019 are selected as the test set. The input and parameter selection of the model have a great impact on the results obtained by the model. Therefore, the pig prices of the collected data from the above sources are used as the input of the model, to obtain the real relationship between the collected data and pork price. Figure 7 illustrates the calculation process.

In the process of evaluating the models, the following evaluation criteria are adopted, including four evaluation indexes: Mean Absolute Error (MAE), Mean Absolute Percent Error (MAPE), Mean Square Error (MSE), Root Mean Square Error (RMSE), and Trend Accuracy (TAR).

(1) MAE:

$$\mathrm{MAE} = \frac{1}{N}\sum_{t=1}^{N}\left|\widehat{y}_t - y_t\right|. \quad (15)$$

(2) MAPE:

$$\mathrm{MAPE} = \frac{1}{N}\sum_{t=1}^{N}\left|\frac{\widehat{y}_t - y_t}{y_t} \times 100\%\right|. \quad (16)$$

(3) MSE:

$$\mathrm{MSE} = \frac{1}{N}\sum_{t=1}^{N}\left(\widehat{y}_t - y_t\right)^2. \quad (17)$$

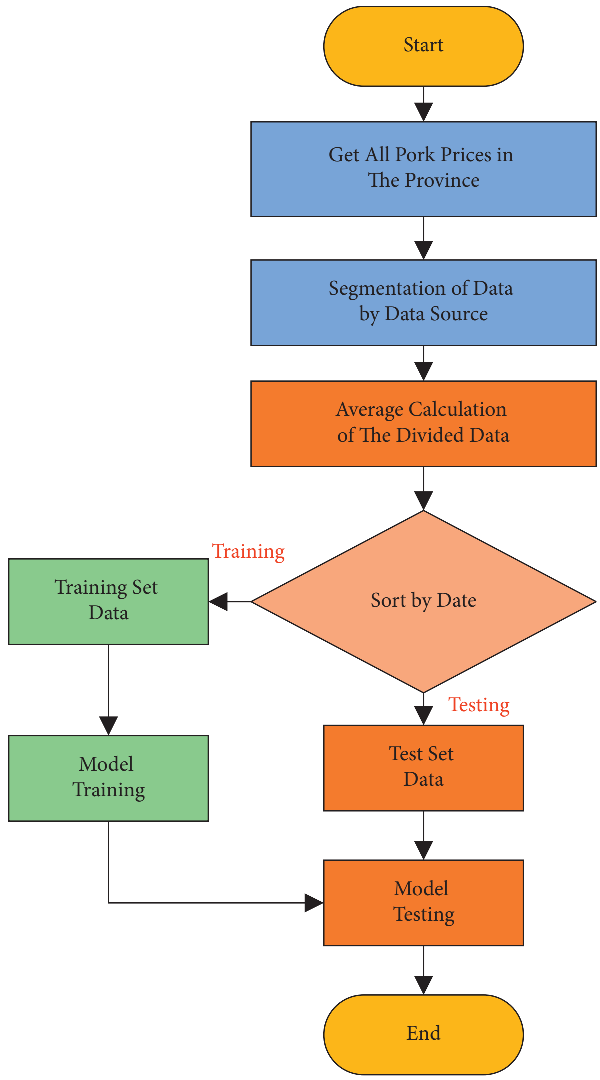

Figure 7: Calculation process of pork prices in different places.

(4) RMSE:

$$\mathrm{RMSE} = \sqrt{\frac{1}{N}\sum_{t=1}^{N}\left(\hat{y}_t - y_t\right)^2}. \quad (18)$$

In (15)–(18), y_t represents the true value, $\hat{y}t$ stands for the predicted value, and N refers to the total number of values.

3. Model Test and Prediction Results of Pig Breeding

3.1. Changes in Pig Breeding Costs. The cost of pig breeding is analyzed from two aspects of different scales and different structures combined with relevant pig breeding data, to give a better understanding of the change of the cost and benefit of pig breeding, Figure 8(a) shows the change trend of the cost of different scales of pig breeding. Figure 8(b) shows the change trend of structural cost of pig breeding industry.

Figure 8(a) reveals that with the increase of pig breeding scale, the cost of pig breeding gradually decreases. From 2005 to 2011, the cost of small-scale pig breeding is less than the total cost of total scale breeding; from 2009 to 2019, the total cost of small-scale pig breeding is greater than that of medium-scale pig breeding; from 2005 to 2007, the cost of small-scale pig breeding is less than that of large-scale pig breeding; from 2009 to 2019, the total cost of small-scale breeding is higher than that of large-scale breeding. Therefore, there are advantages in the feeding cost of small-scale pig breeding from 2005 to 2010, but with the increase of feed and land prices, the cost advantage of small-scale pig breeding disappears. Therefore, in this process, the advantages of large-scale and intensive pig breeding have been gradually reflected. Figure 8(b) illustrates that the various costs and expenses of pig breeding industry are increasing, which also leads to the increase of feeding costs borne by small-scale pig breeders, the decrease of their income, and the acceleration of small-scale breeders withdrawing from the market. The cost of piglets shows volatile changes, which may be due to the fluctuation of

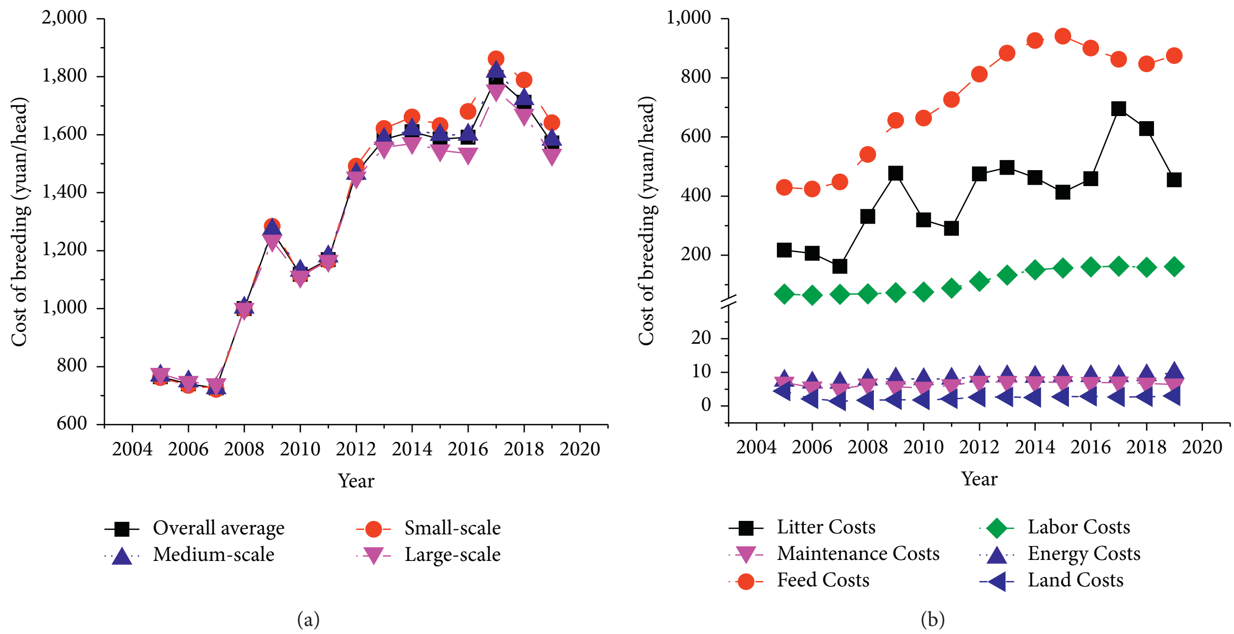

Figure 8: Cost of pig breeding industry: (a) different scale cost of pig breeding industry; (b) structural cost of pig breeding industry.

the number of piglets caused by the impact of pig breeding prices in the previous year, which in turn affects the cost of piglets in the next year. Figure 8(a) demonstrates that the price of pigs also fluctuated in 2008, which may be due to the influence of the price of piglets in 2008, and the change of the price of pigs in the next few years is similar to the fluctuation form of the price of piglets. Due to the influence of other factors, the total breeding cost shows an upward trend.

3.2. Model Prediction Results. The prices of live pigs during a total of 31 days in August of 2018 in Shaanxi Province are randomly chosen to test the predicting accuracy of the model designed here. The orange line in Figure 9 indicates the actual price curve of the market price of live pigs. Comparison is made between the results of BP neural network (BPNN), support vector regression algorithm (SVR), and convolutional neural networks (CNN), and Figure 9 displays the results.

Figure 9 shows that the real price of pigs in August has experienced rising, falling, and rising again. However, generally speaking, the pork price shows an upward trend. Compared with the experimental results of several prediction algorithms, the overall trend of BP neural network is relatively stable. Results of SVR algorithm and CNN show an upward trend of pork price, while the results of the LSTM algorithm are relatively stable. The reason may be that LSTM algorithm can retain the correlation information in the historical data of pig price, while other algorithms can only retain the short-term information in the iterative process, which affects the prediction results of the model. The model based on LSTM neural network can predict the pork price well.

To verify the effectiveness of the designed algorithm, LSTM algorithm, CNN algorithm, and BP algorithm are

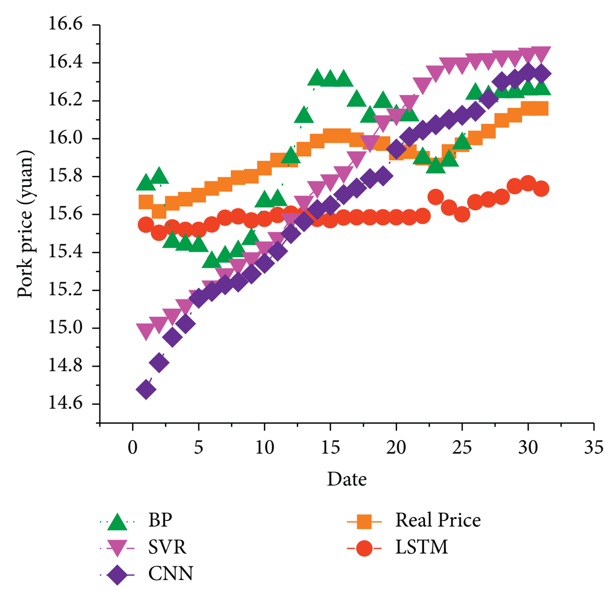

Figure 9: Model simulation results.

tested with three different pig price data sets: state price, market price, and website price. Figure 10 shows the results.

Figure 10 reveals that the prediction accuracy of the designed LSTM algorithm on different data sets is over 80.1%, higher than that of BP algorithm and CNN algorithm. Therefore, after processing based on the LSTM model, the algorithm can effectively predict the change of the future hog price.

3.3. Performance of Model Prediction under Environmental Regulation. In Section 2.3, study is made on the total factor productivity of pig breeding under environmental

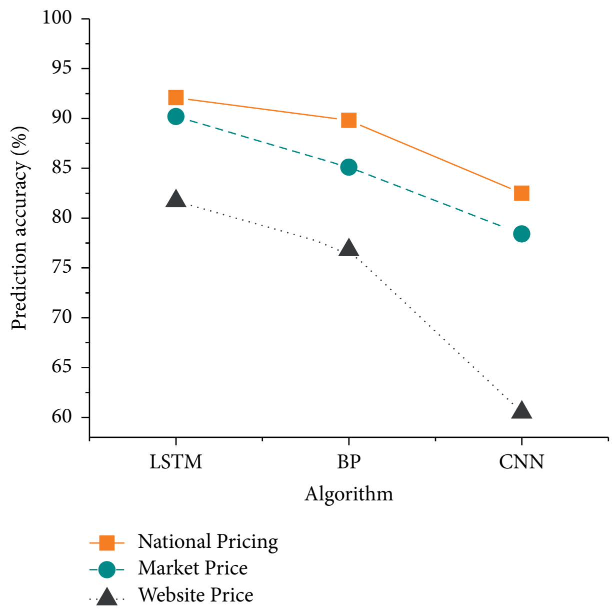

Figure 10: Comparison of face recognition results.

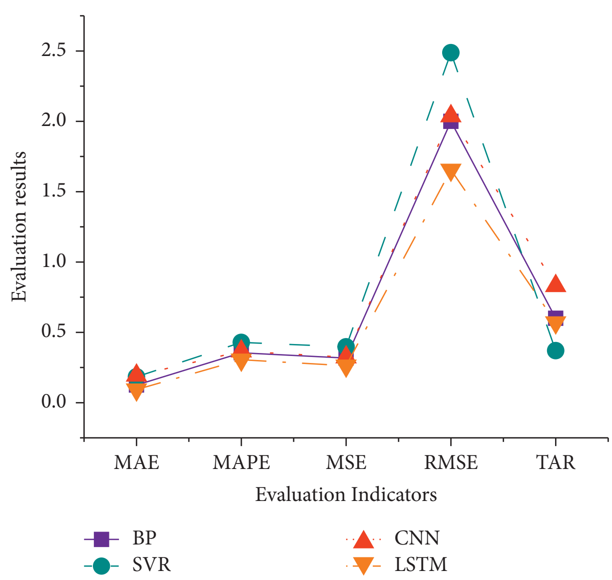

Figure 11: Comparative analysis of model performance.

regulation. Combined with the existing research results, analysis is made on the prediction effect of the model under environmental regulation. In addition, comparison is made between the experimental results of BPNN, SVR, and CNN algorithms. Figure 11 displays the experimental results.

Figure 11 reveals that the prediction performance of LSTM model is the best in four of the five indexes and that the average absolute error is around 0.1. Comparing the difference between the predicted price and the real price, we find that the absolute error of BPNN model is the maximum. Compared with LSTM neural network, other models have larger deviation in prediction results. Moreover, the LSTM model has a prediction accuracy of 0.83 for the price trend of live pigs, which has the final stable trend prediction result.

4. Conclusion

This study is focussed on the production efficiency of pig breeding industry under environmental regulation. What is predicted with LSTM neural network is the pig price. The research process, firstly, analyzes the development of pig breeding industry and the environmental pollution caused by it and, then, introduces green total factor productivity to analyze the profit of pig breeding and the cost of environmental pollution under environmental regulation. The experimental results show that with the increase of breeding cost, small-scale pig breeding is gradually eliminated, and intensive and large-scale pig breeding is the development trend in the future, which makes the control of environmental pollution caused by pig breeding harder. The designed model can accurately predict the price of pigs; namely, the designed model can well solve the problem of pig breeding production efficiency under environmental regulation.

However, there are still some deficiencies. There are many aspects of the impacts of environmental regulation on pig breeding. Only the influencing factors of environmental pollution control were considered, while the change of pig price is also affected by many influencing factors. The study is only carried out on several important influencing factors. Therefore, various influencing factors will be comprehensively considered in follow-up research to better solve these deficiencies and use better algorithm to predict factors such as pork cost and profit.

Data Availability

The labeled data set used to support the findings of this study are available from the corresponding author upon request.

Conflicts of Interest

The authors declare no conflicts of interest.

Acknowledgments

This work was supported in part by the Key Consulting and Research Project of Chinese Academy of Engineering in 2020 (No. 2020-XZ-19), the Consulting and Research Project of Henan Academy of Engineering in 2021 (No. 2021HENZDA04), the General Project of Educational Science of Henan Province (No. 2021YB0050). Henan Science and Technology Think Tank Project (No. HNKJZK-2022-21B), and 2021 Strategic Research Project of the Education and Science Commission of the Ministry of Education (No. 29).

References

[1] Y. Xue, W. Luan, H. Wang, and Y. J. Yang, "Environmental and economic benefits of carbon emission reduction in animal husbandry via the circular economy: case study of pig farming in Liaoning, China," *Journal of Cleaner Production*, vol. 238, Article ID 117968, 2019.

[2] Y. Lam, J. P. Fry, and K. E. Nachman, "Applying an environmental public health lens to the industrialization of food

animal production in ten low-and middle-income countries," *Globalization and Health*, vol. 15, no. 1, pp. 1–20, 2019.

[3] R. Espinosa, D. Tago, and N. Treich, "Infectious diseases and meat production," *Environmental and Resource Economics*, vol. 76, no. 4, pp. 1019–1044, 2020.

[4] K. Ye, Y. Piao, K. Zhao, and X. Cui, "A heterogeneous graph enhanced LSTM network for hog price prediction using online discussion," *Agriculture*, vol. 11, no. 4, p. 359, 2021.

[5] J. Biddle, "Statistical inference in economics in the 1920s and 1930sThe crop and livestock forecasts of the US department of agriculture," *History of Political Economy*, vol. 26, pp. 53–80, 2021.

[6] S. Xie, Z. Yu, and Z. Lv, "Multi-disease prediction based on deep learning: a survey," *CMES-Computer Modeling in Engineering and Sciences*, vol. 127, no. 3, pp. 1–34, 2021.

[7] D. Pan, J. Tang, L. Zhang, M. He, and C.-C. Kung, "The impact of farm scale and technology characteristics on the adoption of sustainable manure management technologies: evidence from hog production in China," *Journal of Cleaner Production*, vol. 280, Article ID 124340, 2021.

[8] D. Xie, L. Zhuo, P. Xie, Y. Liu, B. Feng, and P. Wu, "Spatiotemporal variations and developments of water footprints of pig feeding and pork production in China (2004–2013)," *Agriculture, Ecosystems & Environment*, vol. 297, Article ID 106932, 2020.

[9] Y. Woonwong, D. Do Tien, and R. Thanawongnuwech, "The future of the pig industry after the introduction of African swine fever into Asia," *Animal Frontiers*, vol. 10, no. 4, pp. 30–37, 2020.

[10] M. Costantini, J. Bacenetti, G. Coppola, L. Orsi, A. Ganzaroli, and M. Guarino, "Improvement of human health and environmental costs in the European Union by air scrubbers in intensive pig farming," *Journal of Cleaner Production*, vol. 275, Article ID 124007, 2020.

[11] Z. Ni, J. I. Chen, and J. Ding, "Pig farmers' willingness to recover their production under COVID-19 pandemic shock in China–Empirical evidence from a farm survey," *Journal of Integrative Agriculture*, vol. 19, no. 12, pp. 2891–2902, 2020.

[12] Y. Yang, S. Xing, Y. Chen et al., "Profiles of bacteria/phage-comediated ARGs in pig farm wastewater treatment plants in China: association with mobile genetic elements, bacterial communities and environmental factors," *Journal of Hazardous Materials*, vol. 404, Article ID 124149, 2021.

[13] C. Secco, L. M. D. Luz, E. Pinheiro et al., "Circular economy in the pig farming chain: proposing a model for measurement," *Journal of Cleaner Production*, vol. 260, Article ID 121003, 2020.

[14] J. Johnston and L. Cushing, "Chemical exposures, health, and environmental justice in communities living on the fenceline of industry," *Current environmental health reports*, vol. 7, no. 1, pp. 48–57, 2020.

[15] Y. Takahashi, H. Nomura, and C. T. Son, "Manure management and pollution levels of contract and non-contract livestock farming in Vietnam," *The Science of the Total Environment*, vol. 710, Article ID 136200, 2020.

[16] B. Yan, J. Yan, W. Shi, and Y. Li, "Study on the comprehensive comparative advantages of pig production and development in China based on geographic information system," *Clean Technologies and Environmental Policy*, vol. 22, no. 1, pp. 105–117, 2020.

[17] E. Nie, G. Zheng, and C. Ma, "Characterization of odorous pollution and health risk assessment of volatile organic compound emissions in swine facilities," *Atmospheric Environment*, vol. 223, Article ID 117233, 2020.

[18] K. W. R. Chan and G. Enticott, "The Suzhi farmer:Constructing and contesting farming Subjectivities in post-Socialist China," *Journal of Rural Studies*, vol. 67, pp. 69–78, 2019.

[19] Z. I. Kimera, G. Frumence, L. E. G. Mboera, M. Rweyemamu, S. E. Mshana, and M. I. N. Matee, "Assessment of drivers of antimicrobial use and resistance in poultry and domestic pig farming in the msimbazi river basin in Tanzania," *Antibiotics*, vol. 9, no. 12, p. 838, 2020.

[20] A. H. Bukhari, M. A. Z. Raja, M. Sulaiman, S. Islam, M. Shoaib, and P. Kumam, "Fractional neuro-sequential ARFIMA-LSTM for financial market forecasting," *IEEE Access*, vol. 8, Article ID 71326, 2020.

[21] T. Kuhn, D. Schäfer, K. Holm-Müller, and W. Britz, "On-farm compliance costs with the EU-Nitrates Directive: a modelling approach for specialized livestock production in northwest Germany," *Agricultural Systems*, vol. 173, pp. 233–243, 2019.

[22] Q. Liang and X. Wang, "Cooperatives as competitive yardstick in the hog industry? - evid?:ence from China," *Agribusiness*, vol. 36, no. 1, pp. 127–145, 2020.

[23] E. Hsu, "Cost-benefit analysis for recycling of agricultural wastes in Taiwan," *Waste Management*, vol. 120, pp. 424–432, 2021.

[24] Y. Wang, J. Zhang, Y. Li et al., "Methane production from the co-digestion of pig manure and corn stover with the addition of cucumber residue: role of the total solids content and feedstock-to-inoculum ratio," *Bioresource Technology*, vol. 306, Article ID 123172, 2020.

[25] C. Zhou, Z. Fang, X. Xu et al., "Using long short-term memory networks to predict energy consumption of air-conditioning systems," *Sustainable Cities and Society*, vol. 55, Article ID 102000, 2020.

[26] M. Wang, "Short-term forecast of pig price index on an agricultural internet platform," *Agribusiness*, vol. 35, no. 3, pp. 492–497, 2019.

[27] F. Zhang and F. Wang, "Prediction of pork supply via the calculation of pig population based on population prediction model," *International Journal of Agricultural and Biological Engineering*, vol. 13, no. 2, pp. 208–217, 2020.

[28] V. Gundu and S. P. Simon, "PSO–LSTM for short term forecast of heterogeneous time series electricity price signals," *Journal of Ambient Intelligence and Humanized Computing*, vol. 12, no. 2, pp. 2375–2385, 2021.

[29] J. Klomp, "The impact of Russian sanctions on the return of agricultural commodity futures in the EU," *Research in International Business and Finance*, vol. 51, Article ID 101073, 2020.

[30] H. Jahangir, H. Tayarani, and S. S. Gougheri, "Deep learning-based forecasting approach in smart grids with microclustering and bidirectional LSTM network," *IEEE Transactions on Industrial Electronics*, vol. 68, no. 9, pp. 8298–8309, 2020.

Hindawi
Scientific Programming
Volume 2021, Article ID 2689029, 8 pages
https://doi.org/10.1155/2021/2689029

Research Article

Improved Facial Expression Recognition Method Based on GAN

Junhuan Wang

School of Computer Science, Guangdong University of Education, Guangzhou 510303, Guangdong, China

Correspondence should be addressed to Junhuan Wang; wangjunhuan06@163.com

Received 10 November 2021; Revised 26 November 2021; Accepted 30 November 2021; Published 21 December 2021

Academic Editor: Le Sun

Recognizing facial expressions accurately and effectively is of great significance to medical and other fields. Aiming at problem of low accuracy of face recognition in traditional methods, an improved facial expression recognition method is proposed. The proposed method conducts continuous confrontation training between the discriminator structure and the generator structure of the generative adversarial networks (GANs) to ensure enhanced extraction of image features of detected data set. Then, the high-accuracy recognition of facial expressions is realized. To reduce the amount of calculation, GAN generator is improved based on idea of residual network. The image is first reduced in dimension and then processed to ensure the high accuracy of the recognition method and improve real-time performance. Experimental part of the thesis uses JAFEE dataset, CK + dataset, and FER2013 dataset for simulation verification. The proposed recognition method shows obvious advantages in data sets of different sizes. The average recognition accuracy rates are 96.6%, 95.6%, and 72.8%, respectively. It proves that the method proposed has a generalization ability.

1. Introduction

Recognizing facial expressions can provide a more comprehensive understanding of people's inner world [1]. It has many applications in medicine, transportation, culture, and education [2–5]. Therefore, the recognition and analysis of facial expressions have important research significance and value.

At present, certain researchers have carried out research on image expression recognition, the purpose of which is to accurately classify and recognize seven basic emotional expressions in facial images [6, 7] including anger, disgust, fear, happy, sad, surprise, and neutrality.

Traditional facial expression feature extraction uses mathematical methods to calculate and process facial expression images. Mainly, it can be divided into two situations for processing static images and dynamic images. Statistical methods, Gabor wavelet, and local binary method belong to the feature extraction of static images [8, 9]. Geometric method, optical flow method, and model method belong to the feature extraction of dynamic images [10–12]. However, there are diversity and complexity in image acquisition. Traditional facial expression recognition methods face the problem of nonlinear uncertainty of sample data. The features selected in facial expression feature extraction have no good representation ability [13] and need to be extracted manually according to people's experience. These problems will have a great impact on the recognition accuracy of the model, resulting in the poor generalization ability.

It should be noted that for facial expression recognition research, its essence is to optimize and analyze massive data [14, 15]. Benefiting from the development of artificial intelligence and big data technology, the deep network model can effectively extract effective image features from massive multidimensional image data through continuous iterative learning of multilayer network. And based on its strong learning ability, compared with the traditional facial expression recognition method, it can classify the facial expression more accurately and quickly [16–19]. Reference [20] analyzed the facial expression information of time series based on the part-based hierarchical bidirectional recurrent neural network and extracts facial temporal features in dataset. It can comprehensively analyze facial expressions. Reference [21] proposed a method based on fusion of deep belief network (DBN) and local features. This method extracts eyebrows, eyes, and mouth with rich expression information as local expression images. It also combines the Log-Gabor feature with texture information and the second-order histogram with the gradient direction feature of shape information to realize facial expression recognition. Reference [22] combined spatio-temporal features and used deep residual networks to extract feature. Reference [23] used three channels to extract feature of expression images, respectively. Then, extracted features are connected and sent to the next layer for processing.

Considering the previous work, the network designed in this paper mainly has the following innovations:

(1) Through continuous confrontation training of generator and discriminator in GAN, the deep extraction of the features of processed expression dataset is realized thereby improving performance of corresponding facial expression classification and recognition.

(2) The performance and speed of network are improved. The idea of adding residual network to the generator network improves the operation efficiency while ensuring accuracy.

In addition, the second section introduces related theoretical methods. The third section introduces the improved network and explains the structure of the discriminator and generator in the network. The fourth section introduces the experimental results and analysis based on different datasets. The fifth section is the conclusion.

2. Related Methods and Theories

2.1. General Steps. Face recognition technology includes four steps. They are face detection, face alignment, face representation, and face matching, as shown in Figure 1. Face detection module is used to detect position of face in input image. The face alignment module automatically locates key points around the face according to the input such as eyebrows, eyes, corner points of mouth, nose tip, and contour points. Face characterization is to locate a face picture from the above two steps, extract from it, or convert it into a feature vector. In the face matching part, the extracted feature vector will be used to compare with these in database. Based on the similarity between the two, it is possible to determine whether they belong to the same person in the database.

The image needs to be preprocessed to improve accuracy of judgment [24]. The advantages of traditional face key point detection algorithms are clear architecture and easy to understand. However, the operation efficiency is not high, and it is not suitable for processing a large number of images.

For face characterization processing and analysis, the data feature vector often contains information such as the position of eyebrows, nose, and eyes and even additional information such as contour and shape. The more classic methods include HOG method, Haar wavelet method, and eigenface method. However, traditional methods are used to extract the front of a human face, but the effect is not good enough for the side [25].

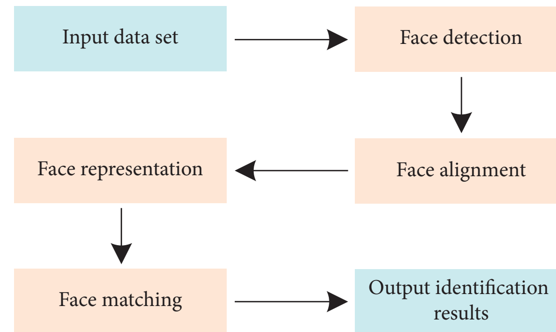

Figure 1: The step of face recognition.

Face matching generally compares the extracted face feature vector with these in database. If the distance of feature vector is close, identity information is output. If there is no match for all faces in database, output cannot be recognized.

2.2. Convolutional Neural Network (CNN). CNN is good at processing images [26]. Traditional face recognition methods show poor results when facing complex scenes. CNN-based deep learning methods can automatically extract features based on a large amount of image data and perform well in complex scenes.

The CNN model is essentially a deep feedforward model, which updates parameters through backpropagation. To obtain better results, it generally needs to design the cores of convolutional layer and pooling layer. And they will be continuously combined to obtain better image characteristics.

2.3. Generative Adversarial Network. Due to its multilayer network structure, the convolutional neural network also has too many problems in its network parameter settings, which makes the CNN face recognition training process very fragile [27]. For face recognition research and analysis, subtle changes in the CNN structure or a little adjustment of parameters will lead to deviations in the recognition results.

As a deep learning model that is widely used in current image analysis, GAN can solve the problem of instability in the training process through adversarial learning methods.

A typical GAN consists of two part, namely, generator G and discriminator D. During training, these two subnetworks play a game, as shown in Figure 2.

First, the generated image and real image are input into discriminator at the same time, and the discriminator is trained. As the training process progresses, the pictures generated by the generator become more and more realistic, and the classification ability of the discriminator is gradually improved. Finally, the training process reaches a state of convergence. The discriminator cannot identify the true and false of the input image, and the image generated is also the same as the real image; that is, the Nash equilibrium state is reached. The training process of the entire game can be described in the following value function $V(D, G)$:

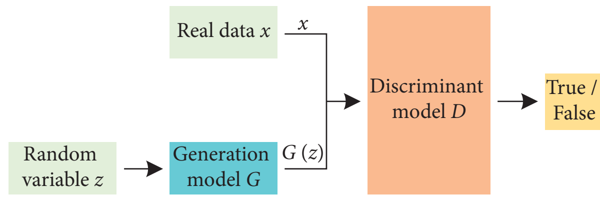

Figure 2: Schematic diagram of generative adversarial networks.

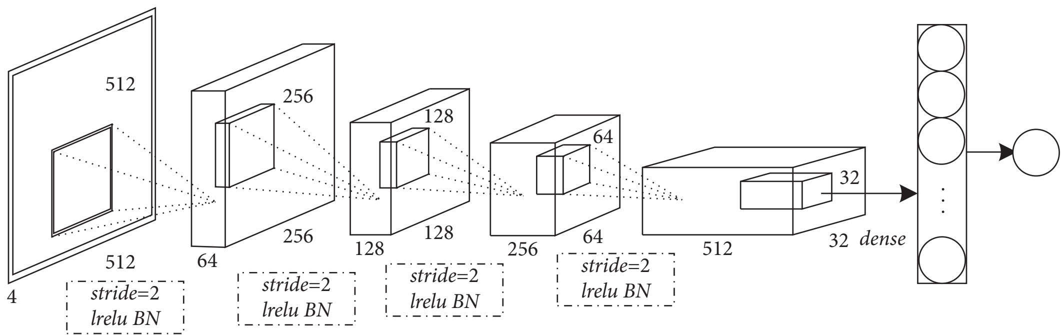

Figure 3: Discriminator network structure.

$$\min_G \min_D V(D,G) = E_{x\sim P\,da\,ta(x)}[\log D[x]] + E_{Z\sim P_{z(z)}}[\log(1-D(G(z)))], \quad (1)$$

where $E_{x\sim P\,da\,ta(x)}$ and $E_{Z\sim P_{z(z)}}$ are the expected functions; x is the real image; z is the image of input generator. G converts the variable z into the probability $G(z)$ that the image generated by the converter is a real image. The variable z is basically a sample from the distribution p_z. The ideal distribution p_z should converge to the data distribution $p_{da\,ta}$. Practice has proved that in the generator, maximizing the logarithm $\log(D(G(z)))$ is better than minimizing the logarithm $\log(1-D(G(z)))$.

Since the GAN network has two models, the loss of discriminator is as follows:

$$\min_D V(D,G) = E_{x\sim P\,da\,ta(x)}\{[\log D(x)]\} + E_{x\sim P_{G(x)}}\{\log\{1-D[G(z)]\}\}. \quad (2)$$

When training loss function of generator, default discriminator has the best ability. The $E_{x\sim P\,da\,ta(x)}\{[\log D(x)]\}$ part is a constant, so the loss of generator is as follows:

$$\min_G V(D,G) = E_{x\sim P_{G(z)}}\{\log 1 - D[G(z)]\}. \quad (3)$$

3. Method

3.1. Discriminator Network. For the discriminator network in the GAN, this paper uses the VGG-16 network as backbone network structure [28], and the network structure is shown in Figure 3. Using $\{x_i, y_i\}_{i=1}^N$ or $\{x_i, G(x_i)\}_{i=1}^N (x_i \in X, y_i \in Y)$ as input, $x \in R^{512\times512\times3}$ and $y \in R^{512\times512\times1}$. When the input is $\{x_i, y_i\}$, correct output of discriminator is 1 and the correct output of input $\{x_i, G(x_i)\}$ discriminator is 0. Leaky-ReLU is used as a nonlinear activation function in each convolutional layer in the discriminator.

First, two convolution and pooling operations are performed on the image, and each operation includes two convolutions and one maximum pooling. Then, three convolution and pooling operations are performed, and each operation includes three convolution operations and a maximum pooling operation. Finally, there are three fully connected layers and one Softmax layer. Similar to traditional generative confrontation network, the discriminator mainly judges the authenticity of input discriminator image. Input image has same size and dimension as the generated image, and both are $3\times48\times48$. The adversarial loss $E_{a\,dv}$ is defined as follows:

$$E_{a\,dv}(\theta_f,\theta_h,\theta_d) = \sum_{i=1,2,\ldots,N}(1-L_d(G_d(x_i;\theta_d))) + \sum_{i=1,2,\ldots,N} L_d(G_d(G_h(G_f(x_i;\theta_f);\theta_h);\theta_d)), \quad (4)$$

where x_i is the real image, G_f is the feature extractor, θ_f is the parameter of feature extractor, G_h is a feature synthesizer, θ_h is the parameter of feature synthesizer, G_d is the discriminator, θ_d is the parameter of discriminator, and L_d is the loss calculation function of discriminator. Then, the total loss function E_{total} is as follows:

$$E_{\text{total}}(\theta_f,\theta_h,\theta_c,\theta_d) = E_c(\theta_f,\theta_c) + E_{\text{adv}}(\theta_f,\theta_h,\theta_d). \quad (5)$$

3.2. Generator Network. The generator network in GAN uses $x \in R^{w\times h\times c}$as the input image, where $w = n = 512$, $c = 3$, The network structure is shown in Figure 4. Some previous segmentation methods use encoder-decoder [29]. This structure first down-samples and then gradually up-samples.

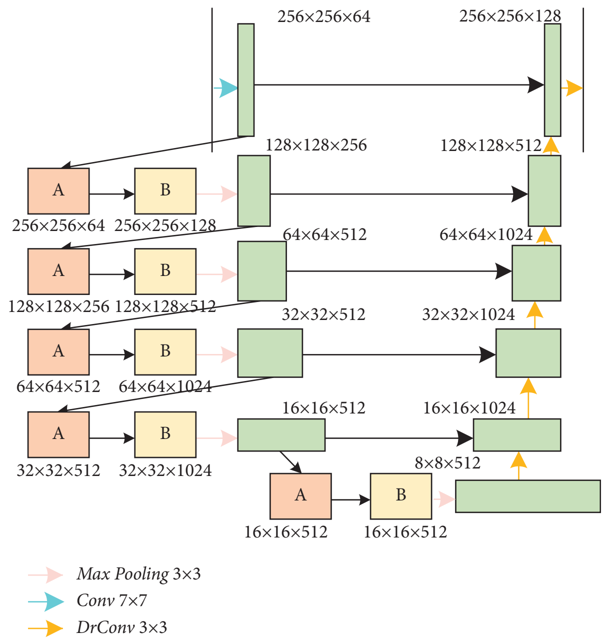

Figure 4: Generator network structure.

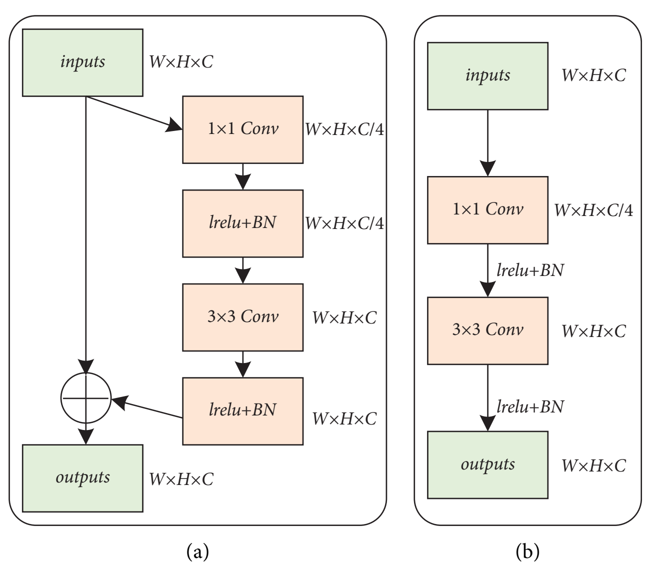

Figure 5: Different variant of convolutional.

This paper uses a U-shaped structure for the generator. The feature extractor is used to extract the feature of input image. Image input resolution is $3 \times 48 \times 48$, and the backbone network uses ResNet-18 [30]. Unlike the traditional generative confrontation network, the generator input is not random noise but a facial expression image. First, the feature extractor performs a 3×3 convolution operation on the input image $x_i\ (i = 1, 2, \ldots, n)$ with a step size of 1. Then, there are batch normalization and ReLU. Second, convolution operation of 4 modules is performed, respectively. Then, the average pooling operation is performed after convolution, and window size is 2×2. Dropout is used after the average pooling operation. Finally, the extracted features are input to two fully connected layers and one Softmax layer. The 512-dimensional feature vector is classified into 7 types of facial expressions, and the facial expression recognition results are obtained. The classification loss E_c of classifier is defined as

$$E_c\left(\theta_f, \theta_c\right) = \sum_{i=1,2,\ldots,N} L_c\left(G_c\left(G_f\left(x_i; \theta_f\right); \theta_c\right), y_i\right), \tag{6}$$

where x_i is the original input image, θ_f is the parameter of feature extractor, G_f is the feature extractor, θ_c is the parameter of classifier, G_c is the classifier, y_i is the real label, and L_c is the classification loss.

At the same time, this paper adds a residual module to generator, and it is shown in Figure 5(a). The structure of the forward propagation convolution unit is shown in Figure 5(b).

Through the confrontation training between the generator and the discriminator, the feature extractor's ability to extract features and the discriminator's recognition ability are improved. The feature synthesizer is a symmetrical structure to the feature extractor and is mainly composed of a convolutional layer and an upsampling layer. After continuous convolution and upsampling operations, the generated output image is restored to the original size.

4. Experimental Results and Analysis

The experiment uses TensorFlow framework to implement network model training on simulation dataset. To ensure quality of the experiment, *Python* is used as the programming language. And NVIDIA CUDA 9.0 is used for GPU accelerated computing. The specific system development environment of the face recognition simulation experiment is shown in Table 1.

4.1. Parameter Setting. When the face recognition network is trained, the optimization method uses SGD, momentum parameter is set to 0.9, and weight decay rate is 10^{-4}. Learning rate is a reduction strategy of multiplying the initial $lr = 3 \times 10^{-3}$ by $(1\text{-}current\_iter/max\_iter)^{power}$ where $power = 0.9$, $current\_iter$ is the current number of iterations, and max_iter is the maximum number of iterations in training process. For the discriminant network, the Adam optimization method is used, $betas \in (0.9,\ 0.99)$, and the initial $lr = 1 \times 10^{-4}$. The learning rate reduction strategy is the same as the method of training the segmentation network. Taking into account the GPU memory limitation, the image size in the experiment is set to 348×348 pixels.

4.2. Evaluation Index. To measure performance of identification our method, an objective and fair evaluation index should be used. Accuracy (AC), precision (*P*), and recall (*R*) are commonly used indicators in big data image classification research, which can be used to analyze performance of face recognition results. The calculation formulas are shown in formulas (7)–(9).

P represents how many of the samples that the model predicts to be positive are true categories. *R* is expressed as how many of the model's predicted categories are positive examples in the samples where the true category is positive.

$$\text{AC} = \frac{\text{TP} + \text{TN}}{\text{TP} + \text{FN} + \text{TN} + \text{FP}}, \tag{7}$$

$$\text{Precision} = \frac{\text{TP}}{\text{TP} + \text{FP}}, \tag{8}$$

$$\text{Recall} = \frac{\text{TP}}{\text{TP} + \text{FN}}. \tag{9}$$

Table 1: System development environment.

Hardware environment	Software environment
CPU: AMD 7 4800H 2.9 GHz	Operating system: Windows 10
Graphics card: NVIDIA CUDA 9.0	Development tool: TensorFlow
Memory card: 16 G	Development language: *Python*

Table 2: Confusion matrix.

Real situation	Forecast result	
	Positive	Negative
Positive	TP	FN
Negative	FP	TN

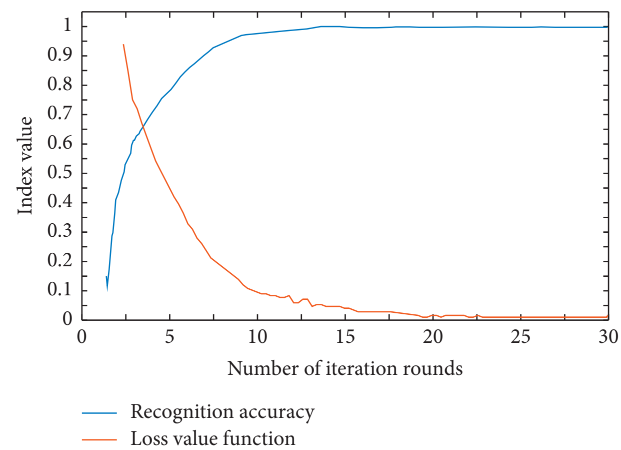

Figure 6: Convergence of the proposed method under multiple iterations.

For classification problems, the combination of the model prediction result and the true category of the sample can be divided into true positive (TP), true negative (TN), false positive (FP), and false negative (FN).

The precision and recall rate can be represented by a confusion matrix, as shown in Table 2.

At the same time, the loss value function c is used to evaluate the model and to measure the quality of the training performance of the GAN model. The appropriate number of iterations is determined in the process of training discrimination. In this paper, cross-entropy loss is used to express probability of predicting which type of input sample belongs to, and its expression is as follows:

$$c = -\frac{1}{n} \sum [y \ln a + (1 - y) \ln (1 - a)], \tag{10}$$

where y is the true classification value, a is the predicted value, and c represents the loss value.

4.3. Training Process. We analyze recognition and classification performance of the GAN model for face collection data and explore the convergence of collection data training

Table 3: Identification performance based on JAFFE dataset.

	Average recognition accuracy (%)	Running time (s)
The proposed method	96.6	54.23
Reference [21]	95.7	54.53
Reference [22]	93.5	55.32
Reference [23]	94.3	56.32

Table 4: Identification performance based on CK + dataset.

	Average recognition accuracy (%)	Running time (s)
The proposed method	95.6	84.23
Reference [21]	91.7	89.53
Reference [22]	90.5	88.32
Reference [23]	90.3	84.32

process. Figure 6 shows the convergence performance of the training process for the expression dataset.

In the 10th iteration, recognition accuracy of training set samples has reached 95%. At the end of 15 iterations, the accuracy is approximately close to 100%. At the same time, through the numerical analysis of the loss function of each iteration, it can be known that the training set has been quickly and effectively attenuated before the 10th iteration. At the 18th iteration, the loss function value is close to 0. In summary, the improved expression recognition method of GAN has good convergence performance.

4.4. Simulation Analysis of General Experimental Dataset. The experimental simulation analysis is carried out using the methods proposed in references [21–23] and this paper. To verify generalization performance of the proposed recognition method on data sets of different sizes, the small, medium, and large experimental simulation data sets are selected as JAFEE dataset, CK + dataset, and FER2013 dataset in turn.

The JAFFE dataset was created by the Michael Lyons team. The image data collected in this dataset contain the expressions of 10 Japanese female participants, with a total of 213 facial images. The JAFEE dataset contains 7 types of basic expressions: anger, happy, sad, surprise, fear, disgust, and neutral.

The CK + dataset comes from the Patrick Lucey team's expansion in the Cohn–Kanade dataset. The CK + dataset collected 123 facial expression images of different people, a total of 593 expression sequences and 951 image samples. The image pixel size is $3 \times 48 \times 48$.

The FER 2013 dataset comes from the Kaggle competition and consists of 35886 facial expression pictures. There are 28708 test sets, 3589 public verification sets, and 3589 private verification sets. Each image is composed of 48×48 grayscale images.

4.4.1. JAFFE Dataset Experiment. This paper chooses JAFFE dataset as a small dataset to simulate and verify performance of the proposed GAN facial expression recognition method. Table 3 shows the stability results based on JAFFE dataset under different methods.

It can be seen from Table 3 that in terms of facial expression recognition for JAFFE dataset, accuracy of our method is 96.6%. It is 0.9%, 2.1%, and 2.3% higher than references [21–23]. The proposed method has no obvious advantage over the comparative method in terms of simulation runtime. Therefore, we believe that when performing expression recognition on small data sets, the method proposed in this article can be selected for efficient discrimination.

4.4.2. CK + Dataset Experiment. The CK + dataset is used as a medium-sized data set for facial expression recognition in this article, and different methods are also used for comparative analysis with our method. The face recognition performance of the CK + dataset under different methods is shown in Table 4.

It can be seen from Table 4 that our method has the accuracy of 95.6% for CK + dataset, which is 5.3% higher than that in reference [23]. The PCNN used in reference [23] has more network layers. There is the problem of the disappearance of the network gradient during training, which causes a large gap in the recognition accuracy compared with our method. The simulation time of the identification method in this paper is 84.23 s, which is 5.3 s shorter than that in reference [21]. Compared with reference [23], the simulation time is relatively close, but reference [23] does not have an advantage in recognition accuracy. Therefore, it is proved that GAN has good accuracy and real-time performance for facial expression recognition of medium-sized volume data sets.

4.4.3. FER2013 Dataset Experiment. Table 5 shows the simulation analysis results of large datasets using different facial expression recognition and classification methods.

From Table 5, the accuracy of expression classification and recognition of all methods for the FER2013 dataset is both below 75%. This is because there are a certain number of error labels in the FER2013 dataset. All of this results in a lower accuracy of the recognition method. However, our method has the highest accuracy of 72.8%. The running time of our method is 134.23 s, which is shortened by more than 10 s

Table 5: Identification performance based on FER2013 dataset.

	Average recognition accuracy (%)	Running time (s)
The proposed method	72.8	134.23
Reference [21]	67.8	145.53
Reference [22]	69.5	144.32
Reference [23]	65.3	146.32

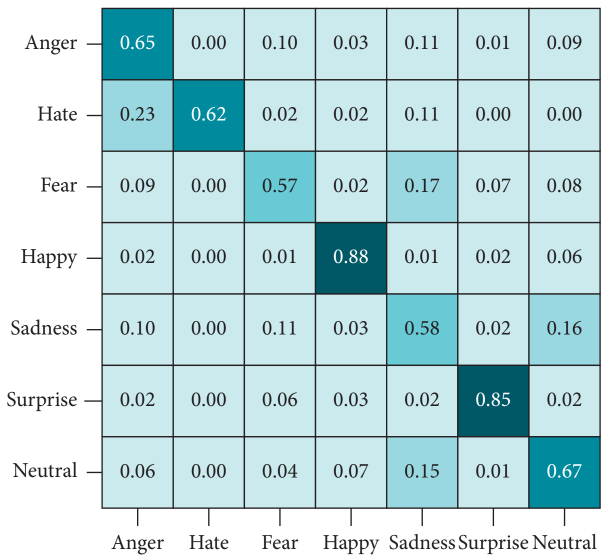

Figure 7: Schematic diagram of the confusion matrix of FER2013 dataset.

compared with references [21–23]. Therefore, the improved expression recognition method of GAN proposed in this paper can also be used for large-scale data set analysis.

To further illustrate recognition performance, a confusion matrix is used to display and illustrate the recognition results obtained by our method, as shown in Figure 7. The accuracy of the method for the recognition of anger, disgust, fear, happiness, sadness, surprise, and neutral expressions is 65%, 62%, 57%, 88%, 58%, 85%, and 67%, respectively.

Figure 7 shows that the method performs well in identifying "happy" and "surprised," with accuracy rates reaching 88% and 85%, respectively. In addition, it can be noticed that the ability to recognize "fear" facial expressions of generating confrontation network is low, with an accuracy rate of 57%. This is because the labeling in the FER 2013 dataset is not good.

In summary, compared with other methods, our method has higher accuracy and operating efficiency for different volume data sets. It shows that our method has excellent generalization ability.

5. Conclusion

This paper proposes a facial expression recognition method based on GAN. This method is based on continuous confrontation training between generator structure and discriminator structure in GAN, which realizes the accurate extraction of data set features and ensures the accurate recognition of facial expressions. By improving the generator structure in GAN network, the residual network is combined with image processing technology. Thus, the amount of calculation for identifying the network model is reduced. Finally, based on general datasets of different sizes, our method is validated for the efficient performance of facial expression recognition. It is proved that our method has obvious advantages in recognition accuracy and processing speed.

In the future, we also plan to add an attention mechanism to the network to further improve accuracy and prune the network to improve efficiency and strive to achieve industrialization.

Data Availability

The data included in this paper are available without any restriction.

Conflicts of Interest

The author declares that there are no conflicts of interest regarding the publication of this paper.

Acknowledgments

This work was supported by the "Software Engineering" (Key Subjects' Construction Project) in Guangdong University of Education.

References

[1] I. Gogic, M. Manhart, I. S. Pandzic, and J. Ahlberg, "Fast facial expression recognition using local binary features and shallow neural networks," *The Visual Computer*, vol. 36, no. 1, pp. 97–112, 2020.

[2] J. Lee, S. Kim, S. Kim, and K. Sohn, "Multi-modal recurrent attention networks for facial expression recognition," *IEEE Transactions on Image Processing*, vol. 29, no. 1, pp. 6977–6991, 2020.

[3] Y. Yan, Y. Huang, S. Chen, C. Shen, and H. Wang, "Joint deep learning of facial expression synthesis and recognition," *IEEE Transactions on Multimedia*, vol. 22, no. 11, pp. 2792–2807, 2020.

[4] A. R. Dores, F. Barbosa, C. Queirós, I. P Carvalho, and M. D Griffiths, "Recognizing emotions through facial expressions: a l experimental study," *International Journal of Environmental Research and Public Health*, vol. 17, no. 20, pp. 1–13, 2020.

[5] L. Yan, "Application of face expression recognition technology in skilled unsupervised course based on ultra-wide regression network," *Journal of Intelligent and Fuzzy Systems*, vol. 38, no. 6, pp. 7167–7177, 2020.

[6] G. Ali, A. Ali, F. Ali et al., "Artificial neural network based ensemble approach for multicultural facial expressions analysis," *IEEE Access*, vol. 8, no. 1, pp. 134950–134963, 2020.
[7] Y. T. Su, M. M. Wang, J. Liu, Y.P Fei, and X. He, "Micro expression recognition algorithm based on multi motion feature fusion," *Progress of laser and optoelectronics*, vol. 57, no. 14, pp. 353–358, 2020.
[8] T. Chen, T. Gao, and X. Zhao, "Single sample description based on Gabor fusion," *IET Image Processing*, vol. 13, no. 14, pp. 2840–2849, 2020.
[9] F. Kong, "Facial expression recognition method based on deep convolutional neural network combined with improved LBP features," *Personal and Ubiquitous Computing*, vol. 23, no. 3-4, pp. 531–539, 2019.
[10] M. H. Kabir, M. S. Salekin, M. Z. Uddin, and M. Abdullah-Al-Wadud, "Facial expression recognition from depth video with patterns of oriented motion flow," *IEEE ACCESS*, vol. 5, no. 1, pp. 8880–8889, 2017.
[11] X. Jia, X. Ben, H. Yuan, K. Kpalma, and W. Meng, "Macro-to-micro transformation model for micro-expression recognition," *Journal of computational science*, vol. 25, no. 1, pp. 289–297, 2018.
[12] E. Zangeneh and A. Moradi, "Facial expression recognition by using differential geometric features," *The Imaging Science Journal*, vol. 66, no. 8, pp. 463–470, 2018.
[13] N. Y. Zheng, H. Zhang, B. Y. Song, W. Liu, Y. Li, and A. M. Dobaie, "Facial expression recognition via learning deep sparse autoencoders," *Neurocomputing*, vol. 273, no. 1, pp. 643–649, 2018.
[14] J. Guo, K. Shan, H. Wu, R. Bie, W. You, and D. Lu, "Research on facial expression recognition technology based on convolutional-neural-network structure," *International Journal of Software Innovation*, vol. 6, no. 4, pp. 103–116, 2018.
[15] J. H. Lu, S. M. Zhang, and J. L. Zhao, "Facial expression recognition based on deep learning," *Computer application research*, vol. 37, no. 04, pp. 966–972, 2020.
[16] Y. He and S. X. Chen, "Person-independent facial expression recognition based on improved local binary pattern and higher-order singular value decomposition," *IEEE ACCESS*, vol. 8, no. 1, pp. 190184–190193, 202.
[17] Z. Zhang, C. Lai, H. Liu, and Y.-F. Li, "Infrared facial expression recognition via Gaussian-based label distribution learning in the dark illumination environment for human emotion detection," *Neurocomputing*, vol. 409, no. 1, pp. 341–350, 2020.
[18] A. T. Lopes, E. de Aguiar, A. F. De Souza, and T. Oliveira-Santos, "Facial expression recognition with Convolutional Neural Networks: c," *Pattern Recognition*, vol. 61, no. 1, pp. 610–628, 2017.
[19] X. L. Peng, H. X. Zhang, and Q. Y. Hu, "Face/facial paralysis expression recognition method based on multi task deep convolution neural network," *Journal of Northwest University*, vol. 49, no. 2, pp. 187–192, 2019.
[20] K. Zhang, Y. Huang, Y. Du, and L. Wang, "Facial expression recognition based on deep evolutional spatial-temporal networks," *IEEE Transactions on Image Processing*, vol. 26, no. 9, pp. 4193–4203, 2017.
[21] L. L. Wang, J. H. Liu, and X. M. Fu, "Facial expression recognition based on local features and deep belief networks," *Progress in laser and optoelectronics*, vol. 55, no. 1, pp. 204–212, 2018.
[22] Y. H. Ma, R. J. Zhang, C. Wu, and J.S Qu, "Expression recognition of image sequence based on deep residual network and LST," *Journal of Chongqing University of Posts and Telecommunications (NATURAL SCIENCE EDITION)*, vol. 32, no. 5, pp. 874–883, 2020.
[23] L. L. Xu, S. M. Zhang, and J. L. Zhao, "Expression recognition algorithm based on parallel convolutional neural network," *Chinese Journal of image and graphics*, vol. 24, no. 2, pp. 227–236, 2019.
[24] W. Zhang and Y. T. Qian, "Streamlined face landmark detection network with global constraint," *Journal of Signal Processing*, vol. 35, no. 3, pp. 507–515, 2019.
[25] M. Annalakshmi, S. M. M. Roomi, and A. S. Naveedh, "A hybrid technique for gender classification with SLBP and HOG features," *Cluster Computing*, vol. 22, no. 1, pp. 11–20, 2019.
[26] T. Nishime, S. Endo, K. Yamada, N. Toma, and Y. Akamine, "Feature acquisition from facial expression image using convolutional neural networks," *Journal of Robotics, Networking and Artificial Life*, vol. 3, no. 1, pp. 9–12, 2016.
[27] L. Zhu, Y. Chen, P. Ghamisi, and J. A. Benediktsson, "Generative adversarial networks for h image classification," *IEEE Transactions on Geoscience and Remote Sensing*, vol. 56, no. 9, pp. 5046–5063, 2018.
[28] D. Chun, T. S. Kim, K. Lee, and H.-J. Lee, "Compressed video restoration using a generative adversarial network for subjective quality enhancement," *IEIE Transactions on Smart Processing & Computing*, vol. 9, no. 1, pp. 1–6, 2020.
[29] C. Tao, H. Wang, J. Qi, and H. Li, "Semisupervised v generative adversarial networks for h image classification," *IEEE Journal of Selected Topics in Applied Earth Observations and Remote Sensing*, vol. 13, no. 1, pp. 914–927, 2020.
[30] L. Ma, R. Shuai, X. Ran, W. Liu, and C. Ye, "Combining DCGAN with ResNet for blood cell image classification," *Medical, & Biological Engineering & Computing*, vol. 58, no. 6, pp. 1251–1264, 2020.

Hindawi
Scientific Programming
Volume 2021, Article ID 5042286, 9 pages
https://doi.org/10.1155/2021/5042286

Research Article

Research on Recommendation of Personalized Exercises in English Learning Based on Data Mining

Lina Zhou and Chunxia Wang

Baotou Medical College, Baotou 014040, China

Correspondence should be addressed to Chunxia Wang; 102002066@btmc.edu.cn

Received 16 October 2021; Revised 14 November 2021; Accepted 19 November 2021; Published 21 December 2021

Academic Editor: Hai Dong

Aiming at the problems of traditional method of exercise recommendation precision, recall rate, long recommendation time, and poor recommendation comprehensiveness, this study proposes a personalized exercise recommendation method for English learning based on data mining. Firstly, a personalized recommendation model is designed, based on the model to preprocess the data in the Web access log, and cleaning the noise data to avoid its impact on the accuracy of the recommendation results is focused; secondly, the DINA model to diagnose the degree of mastery of students' knowledge points is used and the students' browsing patterns through fuzzy similar relationships are clustered; and finally, according to the clustering results, the similarity between students and the similarity between exercises are measured, and the collaborative filtering recommendation of personalized exercises for English learning is realized. The experimental results show that the exercise recommendation precision and recall rate of this method are higher, the recommendation time is shorter, and the recommendation results are comprehensive.

1. Introduction

Educational data mining is an important research direction of personalized teaching assistance. In recent years, network video teaching, especially the rise of online classroom at home and abroad, has rapidly accumulated a large number of pure electronic educational data, which provide rich materials for educational data mining research [1]. Exercise training is an important part of education, and its personalized recommendation is of great significance. According to the personalized situation of different students, targeted exercise recommendation can effectively improve the teaching quality [2]. However, personalized exercise recommendation still faces great challenges. First of all, how to accurately obtain students' knowledge mastery and knowledge points that have not been mastered according to students' history learning behavior, so as to accurately model students, still has a huge room for improvement [3]. Secondly, how to make a reasonable electronic modeling of the knowledge points that students need to master, and make a reasonable personalized exercise recommendation according to the students' cognitive level model, so that students can more quickly and accurately check deficiencies and fill gaps, which is also one of the key concerns of researchers [4].

In view of the above problems, relevant scholars have conducted in-depth research and achieved some results. Among them, reference [5] proposed a personalized test question recommendation method based on deep self-encoder and secondary collaborative filtering; firstly, considering the students' cognition of knowledge points, the secondary collaborative filtering test question recommendation based on knowledge points is carried out, and then, the project response theory and depth self-encoder are applied to predict the students' scores and comprehensive scores related to recommended knowledge points in the recommended test questions. Finally, the prediction results are jointly judged and the difficulty of the final personalized recommended test questions is controlled, generating a final list of recommended questions. Through comparative experiments, this method can realize the personalized recommendation of test questions. Reference [6] proposes a literature personalized recommendation model based on three dimensions, which identifies users' points of interest through the collaboration of three dimensions: expert weight dimension, user dimension, and context perception dimension. The recommendation model uses the analytic hierarchy process and entropy weight method to quantify expert opinions and uses the potential Dirichlet distribution and KL divergence to calculate quantitative user similarity. Through the user's social annotation behavior, search behavior, and browsing behavior, the user's emotional tendency is obtained, and the time factor is introduced to quantify the user's emotion. Finally, the "maximum frequency value" is introduced to determine the recommendation index of each dimension, and the literature comprehensive recommendation index is obtained by weighted calculation. Taking the university library as the experimental platform, the method is verified. The experimental results show that the method has good recommendation performance. Reference [7] proposes a personalized exercise recommendation method combining in-depth knowledge tracking model and collaborative filtering method. This method first models students' knowledge with in-depth knowledge tracking model, then combines collaborative filtering method to calculate students' correct probability of exercises, and recommends exercises within a certain difficulty range to students according to this probability. This method refers to the personal knowledge level and the nearest neighbor information of students in similar situations at the same time, has better model accuracy, and can recommend suitable content according to the difficulty range. Finally, the effectiveness of this method is verified by experiments.

Although the above traditional methods realize the recommendation function, they still have some room for improvement in precision, recall, recommendation time, and comprehensiveness. Therefore, this study proposes a personalized exercise recommendation method for English learning based on data mining. The main research contents of this method are as follows:

(1) A personalized recommendation model is designed to preprocess the data;
(2) Cleaning the data to reduce the influence of noise data on the recommendation result is focused;
(3) The Dina model is used to diagnose students' mastery of knowledge points, and the fuzzy similarity relationship is used to cluster students' browsing patterns;
(4) The similarity measurement is carried out, and the collaborative filtering recommendation of personalized exercises in English learning is realized according to the measurement results; and
(5) Through comparative experimental verification, the advantages of this method are obtained and its application value is verified.

Our contribution is threefold:

(1) Aiming at the problems of traditional method of exercise recommendation precision, recall rate, long recommendation time, and poor recommendation comprehensiveness, this study proposes a personalized exercise recommendation method for English learning based on data mining.
(2) We design a personalized recommendation model, based on the model to preprocess the data in the Web access log, and focus on cleaning the noise data to avoid its impact on the accuracy of the recommendation results.
(3) The experimental results show that the exercise recommendation precision and recall rate of this method are higher, the recommendation time is shorter, and the recommendation results are comprehensive.

The remainder of this study is organized as follows: Section 2 introduces the personalized recommendation model design; Section 3 discusses the recommendation method of personalized exercises for English learning based on data mining; Section 4 discusses simulation experiment and analysis; and Section 5 presents the conclusions of the study.

2. Personalized Recommendation Model Design

The current network teaching platform system structure generally consists of three parts, namely education resource library, learning platform, and users. The educational resource library is a media server that stores various types of educational resources; users are students; the learning platform is a Web server that displays teaching resources to users through the Web, and users can freely choose learning resources. The personalized network teaching platform improves the learning platform in the original teaching platform and introduces a personalized service module here, so that the network teaching platform can recommend exercise resources for students in a targeted manner according to their personality characteristics. The schematic diagram of the personalized recommendation model is shown in Figure 1.

The function of the personalized recommendation model is to track changes in students' interest in the network teaching system, use the knowledge obtained from data mining to dynamically recommend teaching resources to students from teaching resources, and provide customized teaching resources for users according to the resource interest characteristics described by users. The model includes 6 main modules, and they are preprocessing module, association rule mining module, personalized customization module, user feature extraction module, personalized computing module, and personalized extraction module. There are also 4 resource libraries in the model [8], namely Web access transaction library, teaching resource library, frequent item set library, and user feature library. The following is a detailed analysis of the various modules of the recommended model.

2.1. Preprocessing Module. The main function of the preprocessing module is to clean and filter the server-side access logs, with the purpose of obtaining transaction data that

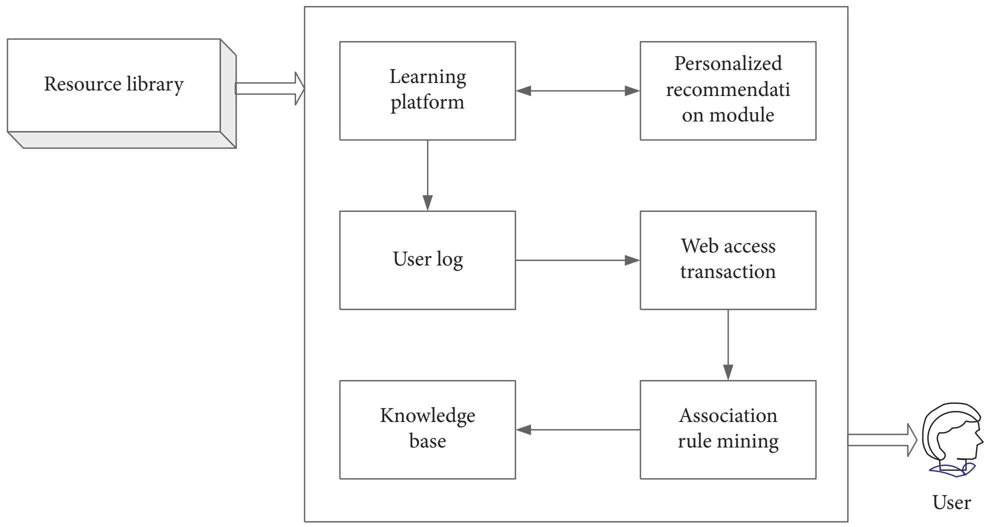

Figure 1: Schematic diagram of personalized recommendation model.

meet the requirements of association rule mining. The preprocessing work is mainly divided into four parts: data cleaning, user authentication, session authentication, and sequence identification.

(1) Data cleaning: the spam in the server's original log is filtered out, such as invalid access records embedded in HTML files. These access records are meaningless entries for mining. What is really needed in the recommendation is to contain teaching content HTML access record [9];

(2) User authentication: the task of user authentication is to obtain a collection of all paths accessed by the same client;

(3) Session authentication: the access sets of the identified users are distinguished, and the different sessions of the proposed user are found out; and

(4) Sequence identification: the purpose of sequence identification is to find the user's meaningful access subsequences. The result of session authentication is a collection of user access sequences, and sequence identification is to find a number of meaningful subsequences in this collection. The multiple relatively independent access subsequences for the user in a session are formed.

2.2. Association Rule Mining Module. The function of the association rule mining module is to find out all the Web access rules based on the Web access transaction database. The work done by this module has nothing to do with the business domain. The method used is the classic Apriori algorithm. The output of this module is Web access frequent item sets, and these frequent item sets are knowledge reflecting the learning trajectory of students [10].

2.3. Personalized Customization Module. The personalized customization module provides students with customized page content based on the user's selected teaching resource classification, course options, discussion topics, and other interest characteristics. For example, the user will select the content of three courses in the online teaching platform and fill in other field interest options, so that every time a student logs in, the system can provide the student with the teaching content of these three courses and exercise data in other fields. When new teaching resources in these fields are generated, the system will promptly renew.

2.4. User Feature Extraction Module. The purpose of user feature extraction is to extract access interest information from each session of the user. The user interest feature is described through the student submodel, which defines the user's basic information and interest feature information. After each user logs in, the system starts to record the user's access tracks and filter out nonteaching contents (such as navigation and reference pages) from these access tracks and stops this recording until the end of the user's access session. The result of this module is the students' access interest characteristics. These characteristics describe the sequence sets of teaching resources accessed by the students in the last session. These access sequence sets are written into the user feature library at the end of the students' current session.

2.5. Personalized Computing Module. The personalized computing module inputs the visit sequence of the user's most recent session into the recommendation algorithm, finds out the strong rules for Web visits by matching the corresponding frequent item sets, and stores the consequence of this rule in the user feature database as the recommended set. It recommends users the next time they log in. In this way, at the beginning of each new conversation, the students will get the system-tailored recommended content, and the function of recommending relevant content to the students is completed through the personalized recommendation algorithm.

2.6. Personalized Extraction Module. The personalized extraction module extracts personalized content from the user feature library every time a user logs in. These personalized contents are obtained by the personalized computing module using the interest features of the user when they log in last time.

3. Recommendation Method of Personalized Exercises for English Learning Based on Data Mining

3.1. Data Preprocessing. The main data source of data mining is the original records of a large number of user visits stored in the Web access log, but it is meaningless to conduct frequent pattern mining directly from these data, because there are a lot of noise data in the Web access log. The existence of noisy data will interfere with the accuracy of data mining. Therefore, before using data mining algorithms to mine Web access logs, it must be preprocessed to obtain user access sequence information that meets the requirements of data mining.

Web log preprocessing is roughly divided into five steps: data cleaning, user authentication, session authentication, path integration, and sequence identification. Since most customer information is shielded under the proxy server, it is necessary to distinguish different customer records under the same proxy server. Each user may have several visits, and it is necessary to distinguish different sessions of the same user. Customers may go back, forward, and refresh the page while browsing. The user access sequence obtained from the log file needs to be path integrated to get a complete user access path. The session generated by the user during one visit contains not only one sequence, but also may have several relatively independent visit sequences. Therefore, sequence identification is required. The process of data preprocessing is shown in Figure 2.

In data preprocessing, a large amount of data need to be processed. In this process, more interference data will be generated. Therefore, data cleaning is a very important part of it. Data cleaning refers to the removal of redundant records in the Web access log. Each webpage on the Web server is specified through a separate link. When a user sends an access request for a page, the graphics, scripts, images, and other resources contained in the page will be automatically downloaded and written into the access log, and these contents are noise data for data mining. The data cleaning process is shown in Figure 3.

3.2. Diagnosis of Students' Knowledge of Mastery. To obtain the student's learning status (student personality status), on the basis of data preprocessing and data cleaning, the DINA model [11] is used to diagnose the degree of mastery of students' knowledge points.

Assume each student P as a knowledge point mastery degree vector $K = \{k_1, k_2, \ldots, k_n\}$, where each dimension corresponds to a knowledge point, $k_n = 1$ represents that student P has knowledge point n, and $k_n = 0$ represents that student P has not mastered knowledge point $n\prime$.

Given student P's knowledge point master vector K, for student P unanswered test question A_i, the potential answer of student P to test question A_i can be obtained according to the following formula:

$$f_{ik} = \prod_{i=1}^{n} \xi_i^u \times A_i, \tag{1}$$

where ξ_i^u represents the student's test score matrix; $f_{ik} = 0$ represents that student P cannot answer test question A_i correctly; and $f_{ik} = 1$ represents that student P can answer test question A_i correctly.

In addition, the DINA model also introduces test question parameters (error rate) and guessing rate to model students' answering conditions in the real state. Specifically, student P's response to test question A_i is expressed by the following formula:

$$P(A_i) = E_k\left(1 - M_{li} \times M_{lj}\right), \tag{2}$$

where E_k represents all the knowledge points examined in the test question set; M_{li} represents the student's record of doing the questions; and M_{lj} represents the relationship between the test questions and the knowledge points.

Because the relationship between knowledge points is considered to be "connected" in the DINA model, the error rate D_z is defined as the probability that a student who has mastered all the skills required for the test question will still be unable to answer the test question A_i correctly; the guess rate D_c is defined as the probability that a student who has not mastered all the skills required to answer the question A_i correctly.

The DINA model uses the EM algorithm [12] to maximize the edge likelihood of formula (2), thereby obtaining the parameter estimates of D_z and D_c. The knowledge point mastery vector K of student P can be determined by maximizing the posterior probability of the student's test score, so as to obtain the student's dichotomous knowledge point mastery vector. The formula for calculating the posterior probability of student test score is as follows:

$$\begin{aligned} \widehat{K} &= \sum_{i,j=1}^{n} \left(\alpha_i - \alpha_j\right)\left(\varphi\left(x_i\right), \varphi\left(x_j\right)\right), \\ &= \sum_{i,j=1}^{n} \left(\alpha_i - \alpha_j\right)^2 \\ &= \arg\max \mathrm{K}\left(P \mid K, D_z, D_c\right), \end{aligned} \tag{3}$$

where α_i represents the potential feature vector of students; α_j represents the potential feature vector of test questions; $\varphi(x_i)$ represents the potential factors of students; and $\varphi(x_j)$ represents the potential factors of test questions.

After obtaining the mastery of students' knowledge points, students' browsing patterns can be clustered and used for exercise recommendation in combination with the mastery of students' knowledge points and the examination of knowledge points of the test questions to be recommended.

3.3. Clustering Algorithm of Student Browsing Patterns Based on Fuzzy Similarity Relations. In the online learning mode, the process of student learning is the process of activities in

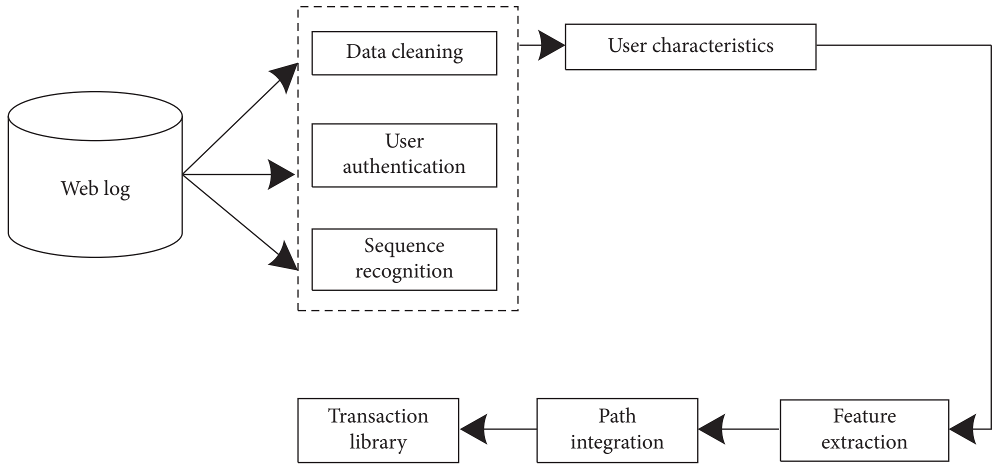

Figure 2: Data preprocessing flow chart.

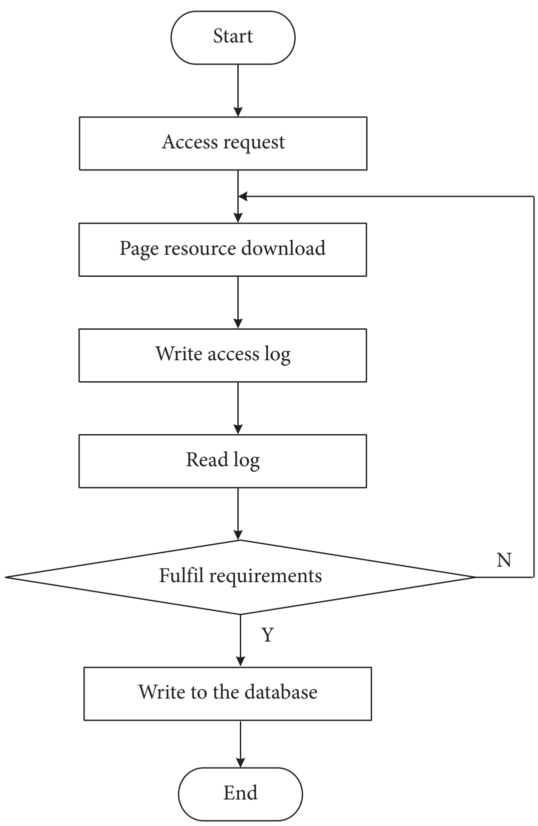

Figure 3: Data cleaning flow chart.

the distance education website. Each activity of the student is a click operation on a page object on the learning website, and these click operations are completely recorded in the log file middle. Through data mining of the log files left by students visiting the learning website, we can find the hidden patterns, reveal students' preference for access paths, find the trends and laws of students' access paths, and help understand students' learning behavior, so as to improve the structure of the site and provide personalized services for students.

According to the actual situation, in relation to a criterion or a certain method, a number in the interval [0, 1] is assigned to each element in the universe of G, which is called the similarity coefficient, and its size indicates that the two elements are each other, degree of closeness or similarity [13].

Let S_{ij} denote the similarity coefficient between elements u_i and u_j, where

$$\begin{aligned} u_i &= \{u_{i1}, \ldots, u_{iN}, \ldots, u_{iM}\}, \\ u_j &= \{u_{j1}, \ldots, u_{jN}, \ldots, u_{jM}\}, \end{aligned} \tag{4}$$

where $N = 1, 2, \ldots$; $M = 1, 2, \ldots$.

$S_{ij} = 0$ means that u_i and u_j are completely different and have no similarities; $S_{ij} = 1$ means that u_i and u_j are exactly the same.

The methods to determine S_{ij} include data accumulation method, correlation coefficient method, and distance method. After calibration, for a set Y with a capacity of r, $n \times n$ numbers representing the degree of similarity between elements can be obtained, and the set obtains a matrix V as follows:

$$V = \begin{bmatrix} v_{11} & v_{12} & v_{1n} \\ v_{21} & v_{22} & v_{2n} \\ v_{n1} & v_{n2} & v_{nr} \end{bmatrix}. \tag{5}$$

Corresponding to $V = (S_{ij})$, let $V = (\mu S_{ij})$, where

$$S_{ij} = \left\{ \begin{matrix} 1, & S_{ij} \geq \mu, \\ 0, & \text{other.} \end{matrix} \right\}. \tag{6}$$

Then, V_μ is called the cutoff matrix of $\mu-$. Obviously, it is a Boolean matrix. The element in the V matrix is a symmetrical binary variable, which describes the similarity between objects.

Since V defined in this way is an equivalent relationship on set Y, then V can uniquely determine a division of set Y, and it can also classify set Y according to its $\mu-$ section relationship. Different section relationships can get a different classification.

Clustering can divide the pattern set into several classes, but there may not be a clear boundary between classes, which means that there is overlap between classes. A model may belong to multiple classes with different membership degrees. In addition, the log file on the web server contains the access sequence of specific students accessing the web page, which is not a real value vector, and the length of different sequences is different, so it is transformed into a real value vector of equal length by using the method of fuzzy mathematics. Forms are easy to compare the degree of similarity between patterns, so as to cluster student behavioral affairs.

Student behavior affairs are a data collection of multiple student browsing behaviors. Assuming there are M students, there is transaction set H, which contains m different student affairs, and its representation is as follows:

$$H = \{h_1, h_2, \ldots, h_m\}, \tag{7}$$

where h_i represents the sequence of the ith student.

Assume δ is a complete collection of pages clicked by different students, and its representation is as follows:

$$\delta = \{\delta_1, \delta_2, \ldots, \delta_n\}. \tag{8}$$

Each $h_i \in H$ is a non-empty subset of δ.

To better measure the similarity between any two objects, each student's behavioral affair is first converted into the form of a real-valued vector with equal length.

For any student behavior transaction $h \in H$, it can be expressed as a real-valued vector, and its form can be expressed as follows:

$$h_x = \{f_1, f_2, \ldots, f_r\}. \tag{9}$$

Of which

$$f_r = \begin{cases} 1, & f_r \in h, \\ 0, & \text{other}. \end{cases} \tag{10}$$

In this way, each student transaction is represented as a vector with equal length, and each element in the vector is 1 or 0, so as to realize student behavior transaction clustering.

3.4. Similarity Measure. Based on the clustering results of the student browsing mode, the exercises to be recommended are referred to by matrix J. The rows in the matrix represent the students, and the columns represent the recommended exercises. The matrix scoring value in a certain range of values reflects the differences in the recommended exercises by the students. The degree of preference, if there is only 1 or 0 in the matrix data, means that the user has only two choices: like or dislike. The following matrix is used to describe students' interest and preference for exercises:

$$J_P = \begin{bmatrix} j_{1,1} & j_{1,2} & \cdots & j_{1,p} \\ j_{2,1} & j_{2,2} & \cdots & j_{2,p} \\ \vdots & \vdots & \cdots & \vdots \\ j_{p,1} & j_{p,2} & \cdots & j_{p,n} \end{bmatrix}. \tag{11}$$

For the exercise data unknown to students, if want to accurately predict students' interests and preferences, cosine similarity is used to measure the similarity between neighborhood exercises [14].

The exercise data as the word frequency vector and the student's score as $N\prime$ vector are set. The angle cosine between the two word frequency vectors is used to describe the degree of similarity between the exercises. The angle cosine between the two exercise vectors can reflect the difference between the exercises, and degree of similarity. If the student does not give a score for the problem data, the score value is 0.

Given that two students are P_1 and P_2, and their scores on the exercises are ϖ_1 and ϖ_2, the cosine similarity $\text{sim}(P_1, P_2)$ between the exercises is calculated as follows:

$$\text{sim}(P_1, P_2) = \frac{P_1 \times P_2}{\|P_1\|^2 * \|P_2\|^2}, \tag{12}$$

where $\|P_1\|^2$ and $\|P_2\|^2$ represent the scores of students P_1 and P_2 on the exercises.

Considering that there are certain differences in students' scoring standards, the cosine similarity calculation method is optimized, and the average score of the exercises is removed to reduce the degree of scoring difference.

Based on the corresponding problem sets P_1 and P_2 scored by students I_u and I_v, and the intersection I_c of the exercises scored by the two students, the following formula for calculating the improved cosine similarity $\text{sim}(I_u, I_v)$ is constructed:

$$\text{sim}(I_u, I_v) = \sum_{u,v=1}^{n} (R_u - R_v) \times (\overline{R}_u - \overline{R}_v), \tag{13}$$

where R_u and R_v represent the number of exercises in the problem sets I_u and I_v, respectively; $\overline{R}_u$ and $\overline{R}_v$ represent the average scores of students P_1 and P_2, respectively.

To obtain the similarity more accurately with respect to the problem I_c that was scored by the two students, the following similarity expression can be used:

$$\text{sim}(I_c) = \sqrt{\sum_{c=1}^{n} (R_c - \overline{R}_c)^2}, \tag{14}$$

where R_c and $\overline{R}_c$ both represent the student's score for problem I_c.

3.5. Collaborative Filtering Recommendation of Personalized Exercises for English Learning. According to the measured student similarity and the simultaneous exercise similarity relationship, combined with the similarity relationship between the fuzzy attribute characteristics of the exercises, the comprehensive similarity between the exercises is solved by weighted fusion. The calculation formula is shown in the following equation:

$$\text{sim}(I_d) = \omega_1 \text{sim}(I_u, I_v) + \omega_2 \text{sim}(I_c), \tag{15}$$

where ω_1 represents the cooperative similarity value of exercises under the scoring matrix; ω_2 represents the similarity value of exercises based on fuzzy attribute characteristics. $\omega_1 + \omega_2 = 1$, according to the sparsity of scoring data, and ω_1 and ω_2 can be clarified.

Assuming that set S_u is the neighborhood set of exercise I_u, and S_v is the neighborhood set of exercise I_v, through the similarity between the exercises and the sets S_u and S_v, combined with the score results of the neighborhood user set, the estimated score $\Phi_{u,v}$ of exercises I_u and $I_v$is solved, and the calculation formula is as follows:

$$\Phi_{u,v} = \left(\overline{R}_u + \overline{R}_v\right) \times \frac{\sum_{u,v=1}^{N} \mathrm{com\_sim}\left(I_u, I_v\right)}{\sum_{u,v=1}^{N} \left|\mathrm{com\_sim}\left(I_u, I_v\right)\right|^2}, \tag{16}$$

where the comprehensive similarity between the two exercises is $\mathrm{com\_sim}\left(I_u, I_v\right)$, based on the average scores $\overline{R}_u$ and $\overline{R}_v$ of exercises I_u and I_v, to complete the collaborative filtering recommendation of personalized exercises for English learning [15].

4. Simulation Experiment

A simulation experiment is designed to verify the effectiveness of the personalized exercise recommendation method for English learning based on data mining. Taking the personalized test question recommendation method based on deep self-encoder and secondary collaborative filtering and the literature personalized recommendation model based on the three-tier dimension as the comparative method, this study makes a comparative analysis with the method in this study and draws the corresponding conclusions.

4.1. Data Set Description. To verify the feasibility and accuracy of the recommendation method of personalized English learning exercises based on data mining, this article uses an exercise data set, which is a university "C language programming" course exercises and the course examination answer records in the past 5 years.

Exercise data set is composed of the following data: (1) the exercise database of C language programming course, which marks knowledge points according to expert knowledge, contains 1653 exercises including multiple-choice questions, blank filling questions, judgment questions, program questions, and programming questions, involving 237 knowledge points, and each question is marked by 1~6 knowledge points; (2) the examination answer records of the course in recent 5 years contain 1069 answer data. In this study, the answer data are normalized and preprocessed, the answer scores of objective questions and subjective questions are mapped to [0, 1], also known as score ratio, and 1069 answer records are randomly divided into 3 copies. 10 experiments are carried out by means of cross-validation, and the average value is taken as the experimental result. The exercise data set is described in Table 1.

The experiment uses Windows 7 64 bit operating system, the CPU is Intel® Core™ i7-4700MQ, the memory size is 16 GB, the hard disk size is 2 TB, and the experiment language is MATLAB R2012a version.

4.2. Analysis of Experimental Results

4.2.1. Precision and Recall/%. In recommendation research, precision and recall are two commonly used evaluation indicators, which are different from common e-commerce recommendation methods. Exercise recommendation focuses on digging out students' knowledge of knowledge points. The table is the evaluation index to compare different methods.

$$\begin{aligned} \text{precision} &= \frac{\theta_a}{\theta_a + \theta_b}, \\ \text{recall} &= \frac{\theta_a}{\theta_a + \theta_c}, \end{aligned} \tag{17}$$

where θ_a represents the number of correct recommendations; θ_b represents the number of actual recommendations; and θ_c represents the number of incorrect recommendations.

Exercises to target students are recommended, and the recommended precision and recall rates to obtain comparative experimental results are used. The experimental results are shown in Table 2.

It can be seen from the results in Table 2 that in terms of exercise recommendation precision and recall, this method is superior to the personalized test recommendation method based on deep self-encoder and secondary collaborative filtering and the literature personalized recommendation model based on the three-tier dimension. The highest precision and recall rates reach 98.1% and 90.2%, respectively. This method uses the Dina model to diagnose the mastery degree of students' knowledge points and has an in-depth understanding of students' learning situation. It can not only reflect students' learning situation, but also improve the quality of exercise recommendation. It verifies that this method has high pertinence of knowledge points and the accuracy of exercise recommendation.

4.2.2. Recommended Time/S. Next, a comparative experiment is conducted on the recommended time of individualized exercises for English learning under the three methods. 1400 pieces of data information are randomly selected from the exercise data set, and the recommended time is used as the evaluation standard. The comparison result is shown in Figure 4.

It can be seen from Figure 4 that the exercise recommendation time of the method in this study is significantly lower than that of the personalized test question recommendation method based on deep self-encoder and secondary collaborative filtering and the literature personalized recommendation model based on the three-tier dimension. Although the recommendation time of the three methods shows a gradual increasing trend with the increase in data information, however, the increasing trend of this method is significantly lower than that of traditional methods. The maximum recommended time of this method is only 6.5 s, while the maximum recommended time of the two traditional methods is 12.0 s and 15.0 s, respectively. It can be seen that this method speeds up the recommendation speed of exercises.

4.2.3. Recommended Comprehensiveness. To further test the application value of the recommendation method, the comprehensiveness of exercise recommendation as the

Table 1: Details of exercise data set.

Data set number	Number of students/person	Number of questions/piece	Number of exercises submitted/time
1	3528	204	254698
2	2706	1127	321486
3	1983	580	367190

Table 2: Comparison of precision and recall.

Data set	Method of this article		Personalized test question recommendation method based on deep self-encoder and secondary collaborative filtering		Literature personalized recommendation model based on three dimensions	
	Precision	Recall	Precision	Recall	Precision	Recall
1	97.5	89.7	90.2	79.5	85.2	75.2
2	98.1	86.3	89.6	78.1	84.1	76.4
3	97.6	90.2	87.4	78.0	86.3	77.0

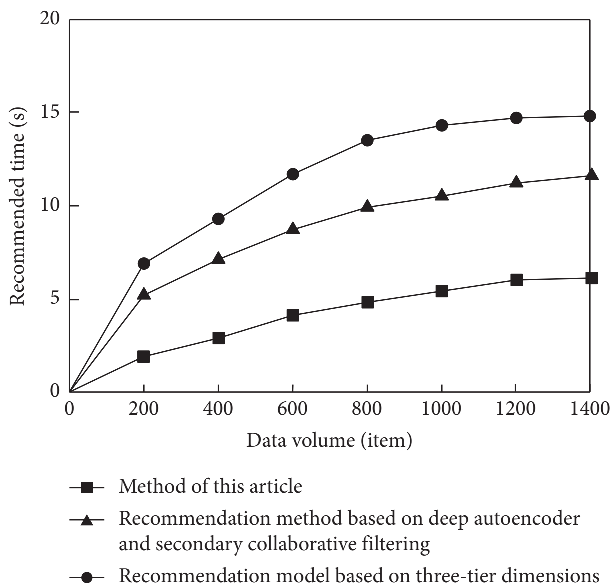

Figure 4: Comparison of recommended time for exercises.

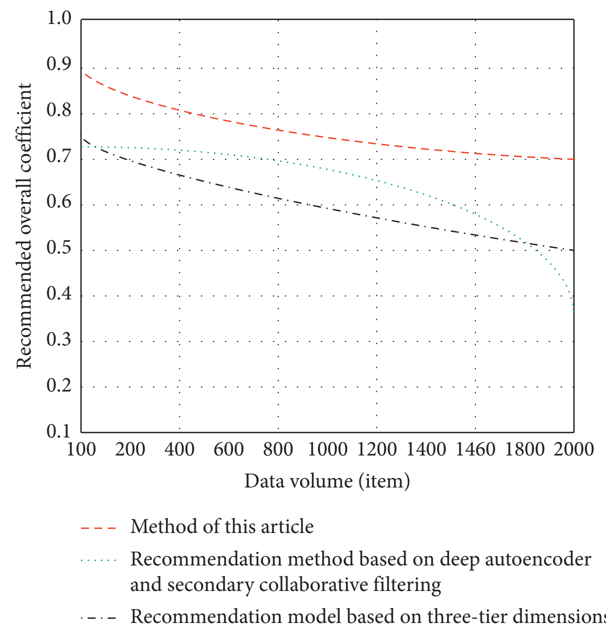

Figure 5: Comprehensiveness of exercise recommendations.

evaluation index is taken, and different methods are compared. The results are shown in Figure 5. Among them, the comprehensiveness of recommendation is expressed by numerical value, specifically 0.1–1.0. The larger the value is, the more comprehensive the recommendation result is.

By analyzing the data in Figure 5, it can be seen that when the data information is 100, the recommended comprehensive coefficient of the method in this study is 0.9, and the recommended comprehensive coefficients of the personalized test question recommendation method based on deep self-encoder and secondary collaborative filtering and the literature personalized recommendation model based on the three-tier dimension are 0.72 and 0.75, respectively; when the data information is 2000 pieces, the recommendation overall coefficient of this method is 0.7, the recommendation overall coefficients of personalized test question recommendation method based on deep self-encoder and secondary collaborative filtering and literature personalized recommendation model based on the three-tier dimension are 0.38 and 0.5, respectively. The comparison shows that the recommendation of this method is more comprehensive, which shows that this method can recommend more comprehensive exercise resources for students and help students practice better.

5. Conclusion

To solve the problems of low precision, recall, long recommendation time, and poor comprehensiveness of exercise recommendation in traditional methods, this study proposes a personalized exercise recommendation method for English learning based on data mining. The main innovations of this method are as follows:

(1) Design a personalized recommendation model, preprocess the data in the Web access log, clean the

data to avoid the impact of noise data on the recommendation results, and improve the accuracy of the recommendation results;

(2) iagnose the degree of mastery of students' knowledge points by the Dina model, and cluster the browsing patterns of students by fuzzy similarity relationship; and

(3) Measure the similarity, including the similarity between students and exercises, and finally, realize the collaborative filtering recommendation of personalized exercises in English learning.

The experimental results show that the highest accuracy and recall rates of exercise recommendation in this method are 98.1% and 90.2%, respectively, and the highest recommendation time is only 6.5 s, and the comprehensiveness coefficient of exercise recommendation is high, indicating that the recommendation effect of this method is good. In the future work, we can further optimize the information storage mode, query mode, and resource management, to conduct accurate query in the case of complex data.

Data Availability

The data used to support the findings of this study are available from the corresponding author upon request.

Conflicts of Interest

The authors declare that they have no conflicts of interest.

Acknowledgments

This study was supported by the Project of the Federation of Social Sciences of Inner Mongolia Autonomous Region: A Study on the Ideological and Political Teaching Model of College English Course based on "online and offline" Hybrid Teaching (No. 20WY15) and 2022 University Scientific Research Project of Inner Mongolia Autonomous Region: Student Behavior Analysis of English online education from the perspective of big data (No. NJSY22064).

References

[1] L. F. Daghestani, L. F. Ibrahim, R. S. Al-Towirgi, and H. A. Salman, "Adapting gamified learning systems using educational data mining techniques," *Computer Applications in Engineering Education*, vol. 28, no. 3, pp. 568–589, 2020.

[2] M.-C. Chiu, J.-H. Huang, S. Gupta, and G. Akman, "Developing a personalized recommendation system in a smart product service system based on unsupervised learning model," *Computers in Industry*, vol. 128, no. 10, Article ID 103421, 2021.

[3] F. Prathama, W. F. Senjaya, B. N. Yahya, and J. Z. Wu, "Personalized recommendation by matrix Co-factorization with multiple implicit feedback on pairwise comparison," *Computers & Industrial Engineering*, vol. 152, no. 1, Article ID 107033, 2020.

[4] M. Gupta and P. Kumar, "Recommendation generation using personalized weight of meta-paths in heterogeneous information networks," *European Journal of Operational Research*, vol. 284, no. 2, pp. 660–674, 2020.

[5] H. J. Xiong, Y. F. Song, P. Zhang, and L. B. Liu, "Personalized question recommendation based on autoencoder and two-step collaborative filtering," *Computer Science*, vol. 46, no. 2, pp. 182–187, 2019.

[6] S. Sheng and Y. Lu, "Personalized literature recommendation model based on three-layer dimension," *Information Science*, vol. 37, no. 2, pp. 19–24, 2019.

[7] X. R. Ma, Y. Xu, and Q. X. Zhu, "Personalized exercises recommendation method based on deep knowledge tracing," *Journal of Chinese Computer Systems*, vol. 41, no. 5, pp. 990–995, 2020.

[8] Z. Alavikia and A. Ghasemi, "Pool resource management based on early collision detection in random access of massive MTC over LTE," *Ad Hoc Networks*, vol. 91, no. 8, Article ID 101883, 2019.

[9] T. Zhang, Y. J. Zhang, X. S. Huang, and T. T. Zhang, "Network data encryption transmission information protection method simulation," *Computer Simulation*, vol. 36, no. 8, pp. 280–283, 2019.

[10] L. Dey and A. Mukhopadhyay, "Biclustering-based association rule mining approach for predicting cancer-associated protein interactions," *IET Systems Biology*, vol. 13, no. 5, pp. 234–242, 2019.

[11] Y. Chen, Y. Liu, S. A. Culpepper, and Y. Chen, "Inferring the number of attributes for the exploratory DINA model," *Psychometrika*, vol. 22, no. 4, pp. 30–64, 2021.

[12] B. Tan, J. Guo, G. Chang, and Q. Xu, "Estimation and detection of a weak magnetic dipole signal with a latent variable based on a non-probability-distribution EM algorithm," *Journal of Intelligent and Fuzzy Systems*, vol. 36, no. 6, pp. 6669–6684, 2019.

[13] M. Diering, K. Dyczkowski, and A. Hamrol, "Rating system Analysis in quality engineering based on fuzzy similarity," *Journal of Multiple-Valued Logic and Soft Computing*, vol. 32, no. 3-4, pp. 277–292, 2019.

[14] S. Samanta, S. O'Hagan, N. Swainston, T. J. Roberts, and D. B. Kell, "VAE-sim: a novel molecular similarity measure based on a variational autoencoder," *Molecules*, vol. 25, no. 15, p. 3446, 2020.

[15] J. Das, S. Majumder, P. Gupta, and K. Mali, "Collaborative recommendations using hierarchical clustering based on K-d trees and quadtrees," *International Journal of Uncertainty, Fuzziness and Knowledge-Based Systems*, vol. 27, no. 4, pp. 637–668, 2019.

Hindawi
Scientific Programming
Volume 2021, Article ID 3406612, 11 pages
https://doi.org/10.1155/2021/3406612

Research Article

Research on Traffic Detection Method of Secure Transmission Industrial Internet of Things Based on Computer Vision

Donghui Yang

Department of Business Administration, Kunlun Tourism College, Heilongjiang Institute of Technology, Harbin 150000, China

Correspondence should be addressed to Donghui Yang; yangdonghui1998@s.hrbcu.edu.cn

Received 20 October 2021; Revised 24 November 2021; Accepted 3 December 2021; Published 20 December 2021

Academic Editor: Le Sun

In recent years, the process of industrial modernization has intensified, traditional industrial control has been improved and rapidly developed, industrial automation and intelligent unmanned production lines have become a new development trend, and the Internet of Things has become the basic direction of industrial development. In order to improve the effect of safe transmission and industrial IoT traffic detection, this study uses a neural network to improve the industrial IoT traffic detection algorithm. In order to improve the visualization effect of monitoring, this study uses computer vision technology to construct a traffic detection system of secure transmission industrial Internet of Things and builds an intelligent detection model. Finally, this study combines experimental research to verify the performance of the system. From the statistical point of view, it can be seen that the system's security detection and traffic detection effects are very good.

1. Introduction

In an industrial production environment, IoT sensor devices are often used to capture data to monitor and adjust the production operation process. The data generated by these devices are collected and organized in different ways and used for various purposes [1]. The transmission speed of IoT sensors is very fast, and the application of a large number of sensor devices will definitely lead to a substantial increase in the output of industrial data. The Internet of Things and big data are closely linked, and the data generated by sensors can also be processed by the big data platform [2]. Industrial Internet of Things and big data are different from internet big data. In addition to the general characteristics of big data, they also have strong relevance and timing. Therefore, traditional Internet big data processing methods are not fully applicable, and new solutions need to be designed specifically to properly analyze IoT data and extract more important information from IoT monitoring equipment. The proposal of "Industry 4.0" [3] has promoted the rapid development of global industries toward intelligence. In order to comply with the intelligent development of the new generation of industries, the number of IoT devices used in industrial production environments is also increasing. Moreover, the amount of data collected by sensors is exponentially increasing [4], so it is necessary to find more effective processing methods for these large-scale industrial data.

Usually, data analysis needs to move a subset of data to a data warehouse, and the speed of data analysis in Hadoop is very slow. However, with the development of SQL query engines, big data technology can already be used in business analysis scenarios. By building a data model in Hadoop or other databases, the original data are turned into meaningful indicators, and the large-scale historical data accumulated and stored for a long time are used in the big data processing system for information mining. The main purpose of adopting a distributed query strategy and using a memory-based computing method is to quickly query information in massive data, give timely feedback to users, and improve query efficiency.

Based on the above analysis, this study combines computer vision to conduct research on safe transmission and industrial Internet of Things traffic detection methods to further improve industrial production safety and enhance the application effect of the Internet of Things in the industry.

2. Related Work

Led by the transformation and upgradation of the manufacturing industry, a new round of industrial revolution has started around the world [5]. The application of industrial big data will greatly promote and optimize industrial production efficiency and management. In order to provide better services to users, industrial production should save and mine these data. For industrial information with high data volume and updated speed characteristics, data acquisition and analysis will face certain difficulties. In the processing of industrial IoT big data, various application frameworks have been mentioned in many documents. The literature [6] proposed an industrial big data ingestion and analysis platform (IBDP), which integrates HDFS, Spark, Hive, HBase, Flume, Sqoop, OpenStack, etc., and is suitable for industrial data ingestion and analysis. The literature [7] proposed and developed a smart city system based on the Internet of Things using Hadoop ecosystem use and big data analysis technology and combined with Spark over Hadoop to achieve the efficiency of big data processing. The literature [8] proposed the use of the Hadoop software environment, including data collection, data storage, data normalization and analysis, and data visualization components to realize the parallel processing of large heterogeneous data for IoT network security monitoring. The value of industrial big data has been globally recognized. Therefore, how to combine big data processing technology to store, manage, and analyze industrial big data is a topic of widespread concern for domestic and foreign researchers. In the development of big data in the industrial Internet of Things, China still has shortcomings in terms of format specification, platform technology integration, informatization strategy, and security. In order to better promote the development of industrial big data, it is necessary to realize the unification of data standardization, big data collection, multisource data processing, and information mining analysis and realize the visualization of data in the industrial production process and increase the usability of industrial data. There are many unknown possibilities for the integration between the Industrial Internet of Things and big data technologies, and the corresponding platform framework and technical support are not unique. Through more scientific and in-depth research, and constantly changing needs, the industrial IoT big data operating platform will also be continuously improved due to technological progress [9].

As products have higher and higher requirements for production equipment and processes, making production equipment and production lines more and more complex, remote intelligent control and supervisory analysis become more and more important [10]. The Internet of Things remote data transmission system can automatically upload equipment operating data to the Internet, finally, collect, process, and store in the database in the Internet data service center, then transform and disassemble the data information, and finally use intuitive graphs and line graphs, Pie charts, and tables, etc., so that engineering supervisors can quickly obtain data transmission information and accurately control the production and operation of machinery and equipment. Engineering monitoring personnel can view the status of production equipment through the remote data transmission system of the Internet of Things. In addition, the system can set functions such as abnormal prompts, fault alarms, and preliminary cause investigation [11]. The modern industrial Internet of Things remote data transmission system is mainly composed of a remote monitoring center, a mobile device data transmission terminal, a wireless transmission module, and an intelligent collection terminal. Each module is connected through the Internet, mobile communication base stations, GPRS networks, local wireless transmission equipment, and sensors and connected and communicated with smart collection terminals [12].

However, in dealing with the problems of multivariate and big data in the industry, many data quality problems are often encountered, which will greatly affect the effect of analysis and processing. Traditional machine learning methods are often at a loss for this. In comparison, the application of ensemble learning in this area highlights a huge advantage. Gradient boosting decision tree [13] (GBDT) is a decision tree algorithm based on iterative construction in integrated learning. It has an excellent performance in the practice of processing industrial data. Literature [14] studies the gradient boosting decision tree algorithm, using a large amount of collected power load data for model training, generating a new decision tree above the negative direction of the loss function gradient, and optimizing the prediction accuracy of short-period negative power load. XGBoost (Extreme Gradient Boosting) is based on the optimization of the GBDT algorithm [15]. It can make full use of the CPU's multithreading to perform parallel calculations and, at the same time, optimize and improve the algorithm to a certain extent, which improves the accuracy of the model. XGBoost combines many single decision tree models with low classification accuracy to form a tree model with relatively high classification accuracy. Each time a single weak learner is trained, the weight of the last residual is first increased, then the learning of the current learner is performed, then the previous residual is adjusted by adding a new weak learner, finally, the weight of multiple learners is calculated, and the final result is predicted. Literature [16] uses the XGBoost algorithm to improve the accuracy of rolling bearing fault diagnosis; literature [17] applies the algorithm to the quality inspection stage of the manufacturing industry to achieve the purpose of accurately predicting product quality.

3. Traffic Detection of Secure Transmission Industrial Internet of Things

In the case of unsupervised and undesired output, the self-organizing competitive network is a neural network based on unsupervised learning. It is mainly through observing, analyzing, and comparing the characteristics of objective things, prompting the inner law by itself, and classifying according to the similarity of this characteristic. This kind of network is similar to the learning mode of the biological neural network in the human brain, which both accurately discover the type of sample through the extraction of features and adjust the network parameters through the corresponding learning algorithm.

Competitive networks are generally divided into the input layer and the competition layer. Its network structure is shown as in Figure 1.

We assume that the input layer and the competition layer of the network each have I and C neurons, the link weight between the two layers of nodes is $\omega_{ij}\,(i = 1, 2, 3, \ldots, I\,; j = 1, 2, 3, \ldots, C)$, and the arithmetic sum of the ownership values is 1, that is, $\sum_{i=1}^{N} \omega_{ij} = 118$.

The input samples of the competitive network are all binary vectors (O or 1). Only one neuron in each input sample wins and assigns its corresponding label. Different competing layer neurons represent different classifications. The calculation method of the competitive layer neuron j is as follows:

$$S_j = \sum_{i=1}^{N} \omega_{ij} x_i. \qquad (1)$$

When a neuron in the competition layer has the largest weight value, the neuron wins. According to the corresponding strategy, the input of the winning neuron is 1, and the rest are 0. As shown in the formula,

$$a_k = \begin{cases} 1, & S_k > S_j,\ \forall j,\ k \neq j, \\ 0, & \text{else}. \end{cases} \qquad (2)$$

The neuron that wins the competition will be trained and learned according to the input vector. For all the input layer neuron i, there is the following formula:

$$\omega_{ij} = \omega_{ij} + a\left(\frac{x_i}{m} - \omega_{ij}\right). \qquad (3)$$

In the formula, a is the learning rate, which generally satisfies $0 < a << l$, and m is the total number of neurons whose output is 1 in the input layer and satisfies $m = \sum_{i=1}^{N} x_i$. This formula shows that if x_i is active, its corresponding i-th weight will increase; otherwise, it will decrease [19].

The self-organizing feature map model SOM (self-organizing feature map) makes nearby neurons compete with each other to solve the problem of external information forming concepts in the self-organization of the human brain. For a system, it is to solve the corresponding expression of internal self-organization when a system accepts external roles. This is expressed as the adjustment of the weight coefficient in the artificial neural network.

The SOM network can be multidimensional. For the convenience of description, a two-dimensional planar competition layer array is taken as an example. The n neurons in the input layer are fully connected with the axb neurons in the competition layer. Additionally, axb neurons in the competition layer are also directly or indirectly connected, and neurons in adjacent areas inhibit each other. Its network structure is shown in Figure 2.

The data that enter the SOM network through the input layer will be selectively given the corresponding response by the network through the corresponding strategy. The specific steps are as follows.

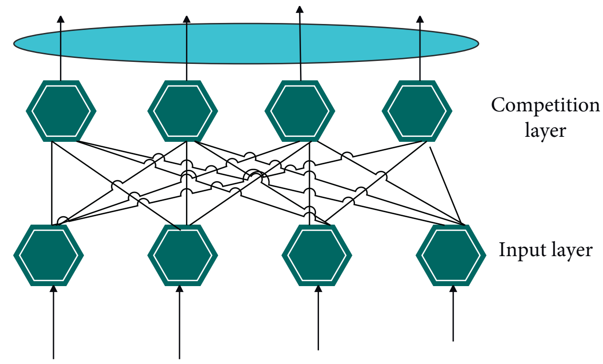

Figure 1: Self-organizing competition network topology diagram.

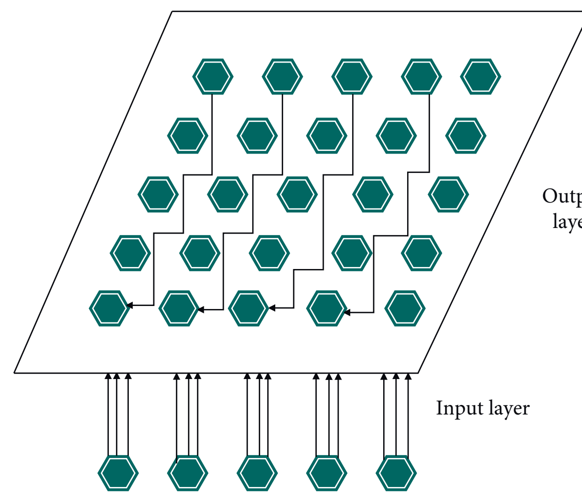

Figure 2: SOM neural network topology diagram.

3.1. Network Initialization. The weight is randomly assigned to the initial value of the weight, which is usually small. SJ is a group of J-neighboring neurons, that is, the number of adjacent neurons continues to decrease.

3.2. Calculating the Euclidean Distance between the Weight Vector of the Mapping Layer and the Input Vector. In the competition layer, the algorithm calculates the Euclidean distance between the weight vector of each neuron and the input vector. The distance between the j neuron and the input vector is as follows:

$$d_j = \left\| X - W_j \right\| = \sqrt{\sum_{i=1}^{m} \left(x_i(t) - \omega_{ij}(t)\right)^2}. \qquad (4)$$

The algorithm takes the neuron with the smallest distance obtained as the winning neuron and records it as j^*. For any competitive layer neuron j, there is a specific k that satisfies $d_k = \min(d_j)$.

3.3. Learning of Weights. According to the input vector, the algorithm trains the weights of j^* and its neighboring neurons as follows:

$$\Delta\omega_{ij} = \omega_{ij}(t+1) - \omega_{ij}(t) = \eta(t)\left(x_i(t) - \omega_{ij}\right). \quad (5)$$

Among them, the value of η is $0 < \eta < 1$. As time increases, its value gradually approaches 0.

3.4. Calculating Output O_k

$$o_k = f\left(\min_j \left\| X - W_j \right\|\right). \quad (6)$$

Among them, $f(^*)$ is a linear function.

3.5. If the Expected Setting Is Not Reached, the Algorithm Returns to Step (2). The data collected by the model in this study are stored in a sliding queue-based buffer set by the cluster head node, as shown in Figure 3. In the entire interactive cycle, feature sampling is performed on the interactive data stream, and the length of the sliding queue n is determined by the two factors discussed above. Once the queue length is exceeded, the element at the head of the queue is taken out of the queue. Figure 3 details this process.

The algorithm evaluates the collected feature values, including repetition rate evaluation, time regularity evaluation, and abnormal data change ratio evaluation.

3.5.1. Evaluation of Data Repetition Rate. In general, normal nodes will not continuously send data with a higher repetition rate. The higher the data repetition rate (rep), the smaller the evaluation will be with the increase in rep, and the rate of change should rise. That is, when the rep is getting closer and closer to the critical value of 0, its evaluation is getting lower and lower. This changing trend can be expressed by an exponential function with a base greater than 1, as shown in the following formula [20]:

$$R_1 = \begin{cases} 2 - \beta^{\text{rep}}, & \text{rep} < \theta, \\ 0, & \text{rep} > \theta. \end{cases} \quad (7)$$

Among them, $2 - \beta^{\text{rep}} > 0$, and the critical value 0 is determined by the specific network.

3.5.2. Time Regularity Evaluation. The regularity of time is evaluated here. ti represents the i-th time interval and normalizes each time interval. This study considers the dispersion of time intervals. The greater the dispersion, the less regularity, and the lower the possibility of it being a malicious node. The smaller the dispersion, the stronger the regularity of the time interval, and it may be a malicious node. The formula is as follows:

$$R_2 = \frac{\sum_{i=1}^{n-1}\left(t_i - \mu\right)}{n-1}. \quad (8)$$

When $n = 1$, there is only one interval, which means there is no regularity; then, $R_2 = 1$.

3.5.3. Evaluation of Abnormal Data Parameter Change Ratio. Without loss of generality, the abnormal data parameter here can be a variety of parameters, including the number of streams corresponding to the substream, the number of packets, the number of bytes, and other parameters. According to different application scenarios or network conditions, it can set one or more parameters to participate in the evaluation. We assume that the parameter at this time uses the number of bytes sent. If a DoS attack is sent during node interaction, a relatively large change will inevitably occur in the amount of data. DoS attacks must continue to attack to achieve results. However, the current DoS attack methods are endless. In order to conceal the attack behavior, it will mix the attack data stream with the normal data stream, which is difficult to be found. The data change rate X is its ratio to the previous data change. It is calculated as follows:

$$X = \frac{|m - \overline{m}|}{m_{\text{var}}}. \quad (9)$$

We assume that m is the feature parameter of the new queue node. There are k historical records in front of it, $\overline{m}$ is the expectation of the previous k historical data, and m_{var} represents the average value of the previous k data changes. It is calculated as follows [21]:

$$m_{\text{var}} = \sum_{i=1}^{k} \frac{\left|m_i - \overline{m}\right|}{k}. \quad (10)$$

The algorithm determines the interval of the parameter under normal conditions according to specific application scenarios and normal interaction data and sets the critical value σ. The algorithm calculates the number of n data parameters that does not exceed σ and uses its proportion as an evaluation of the change ratio of abnormal data parameters.

$$R_3 = 1 - \frac{x}{n}. \quad (11)$$

On the basis of obtaining the above evaluation indicators, the algorithm performs weighted aggregation on them. The algorithm uses weighting coefficients $W1$, $W2$, $W3$, and $W1 + W2 + W3 = 1$. At this point, the node behavior evaluation is as follows:

$$R = W_1 R_1 + W_2 R_2 + W_3 R_3. \quad (12)$$

When the core layer information management center of the Internet of Things network receives the service request sent by the user, it sends the request data to the subordinate management node, and the subordinate agent node has individual requirements for the type of service.

To select and authorize the sensor layer nodes, for the trust management module studied in this study, the basis of authorization is the evaluation of trust. It includes two types of trust factor-historical statistical trust value and recommended trust value. The algorithm calculates the static trust degree of this interaction through the weighted synthesis of two types of trust factors and decides whether to authorize or not according to the security policy by comparing with the threshold.

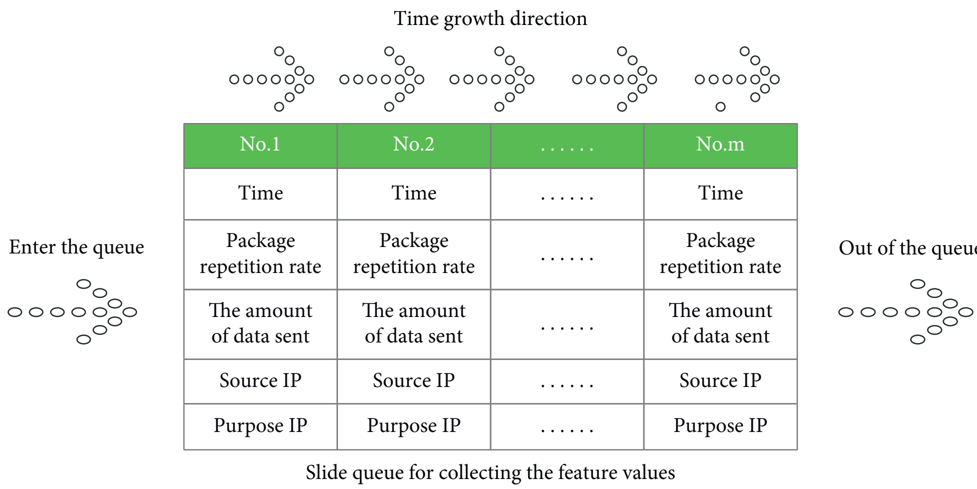

FIGURE 3: Sliding queue.

Step l. The algorithm reads the historical trust sequence H_{all} locally stored in the cluster head. We assume that Qb is the trust history record of the target node B. That is, $H_b = \{q_1, q_2, q_3, \ldots, q_{dn}\}$, and n is the number of historical interactions. Among them, any element qi $(i > n)$ contains information such as flag, time, comprehensive trust, behavior evaluation value, and the address of the interactive node.

Step 2. The algorithm checks whether the flag of q is 0. If it is 0, it means that the trust management center has not processed the abnormal node and directly discards the node. If it is not 0, the algorithm continues.

Step 3. The algorithm performs attenuation synthesis for each record. The degree of attenuation is represented by the time function $\theta(t) = Q_t + e^{-N_t(t-t_i)}$. Among them, Q_t and N_t are both parameters greater than 0, and they are mainly determined according to the requirements of specific applications. t is the current time, and t_i is the time when h_i occurred.

In summary, the historical comprehensive trust of node A to node B is

$$T^{\text{his}}(A \longrightarrow B) = \sum_{i=1}^{n} \frac{\theta(t_i)}{\sum_{j=1}^{n} \theta(t_j)} \left[\lambda \text{hist}_i + (1-\lambda) R_i\right], \quad n > 0,\ 0 < \lambda < 1. \tag{13}$$

In the formula, hist_i represents the historical interaction satisfaction stored at the i-th time, and R_i represents the behavior evaluation value of the i-th interaction.

When there is locally no interactive record, this means that, for unfamiliar nodes, the trusting subject cannot determine whether their behavior is normal or abnormal. To a certain extent, this is similar to the habits of human society.

According to the clusters of the interactive nodes of both parties, it can be divided into intracluster recommendation and intercluster recommendation:

(1) The recommended trust in the cluster is as follows: the subject node and the target node belong to the same cluster, but the subject node A recorded in the cluster head did not interact with the target node B many times or even had no interaction. At this time, the cluster head node selects nodes with a higher reputation value to form the sequence $H_{\text{rec}} = \{h_1, h_2, h_3, \ldots, h_{rn}\}$, and H_{rec} meets the condition and has multiple interaction records with the target node B. The algorithm takes the trust record in the H sequence as the recommended trust data as $T^{\text{rec}}(A \longrightarrow B)$.

(2) The recommended trust between clusters is as follows: the subject node and the target node are in different clusters. Nodes in different clusters need to pass through the cluster head node to interact. Therefore, compared with the recommendation trust relationship within the cluster, the recommendation trust relationship between clusters is transformed into an indirect relationship, that is, the mutual evaluation between the cluster heads of the two clusters.

The key to recommendation trust calculation is to obtain the trust degree of the main node for the recommendation data. The calculation steps of recommended trust are as follows:

Step 4. The cluster head node selects the recommended node from the cluster, and the recommended node C satisfies the following conditions: it has interacted with the main node A, has a high degree of trust, and also has an interaction record with the target node B.

Step 5. The algorithm first judges whether the target node B and the subject node A are in the same cluster. If it gets a positive response, the algorithm skips this step and continues to step 3. If it is a different cluster node, the algorithm adds the trust value between clusters as the data for the recommended trust calculation. The trust transfer method between clusters takes the cluster head node of the cluster where the main node is located as the new main node and the cluster head of the cluster where the target node is located as the recommended node. Then, we substitute the corresponding data into the recommendation trust calculation formula, namely, formula (2) in step 3.

Step 6. The algorithm selects the recommended node set $H_{\text{rec}} = \{h_1, h_2, h_3, \ldots, h_{rn}\}$ according to the record, and the recommended trust degree sequence $H_{rt} = \{m_1, m_2, m_3, \ldots, m_{rn}\}$ for the target node B. rn is the number of recommended nodes, m_i is the recommendation trust degree of the corresponding recommended node to the target node, and $0 < i < rn$. Taking the recommended node C in the cluster as an example, the calculation formula of m_i corresponding to the recommended node C is as follows:

$$m_i = T_i^{\text{his}}(A \longrightarrow C) \times T_i^{\text{his}}(C \longrightarrow B), \quad 0 < i < rn. \tag{14}$$

Step 7. The algorithm weights and aggregates the recommended trust value provided by each recommended node to obtain the recommended trust value. Considering that malicious nodes deliberately uplift or downgrade the target node to form cooperative deception, the model in this study uses the dispersion of the expected and actual value of the recommended trust degree as the weight to reduce the influence of outliers on the trust evaluation. The reason is that it is almost impossible that most of the recommended nodes are malicious nodes. The formula is as follows:

$$T^{\text{his}}(A \longrightarrow B) = \sum_{i=1}^{rn} \omega_1 \times m_i, \quad 1 < i < rn. \tag{15}$$

Among them, ω_i is the dispersion degree between the recommendation trust degrees provided by the i-th recommendation node and the overall recommendation trust degree expectation, and it is used as the weight coefficient in formula (3). It can reduce the weight of outlier data in recommendation trust to a certain extent, thereby reducing the impact of malicious recommendation.

$$\omega_i = \frac{1 - \left|E_r(m) - m_i\right|}{\sum_{i=1}^{rn}\left(1 - \left|E_r(m) - m_i\right|\right)}, \quad 0 < i \leq rn, \tag{16}$$

where $E_r(m_i)$ is the mathematical expectation of overall recommendation trust.

$$E_r(m) = \frac{m_1 + m_2 + \cdots + m_{rn}}{rn}. \tag{17}$$

The historical statistical trust value T^{his} and the recommended trust value T^{rec} obtained by the above calculation and their weighted combination can get the authorized trust value T^{out}. By comparing it with the preset threshold, we arrive at a decision and grant corresponding permissions based on specific network security policies. For nodes with hierarchical authorization, higher-level nodes can be allowed to access and use more resources, and lower-level nodes cannot be accessed beyond authority.

$$T^{\text{out}} = \alpha T^{\text{his}} + (1 - \alpha) T^{\text{rec}}. \tag{18}$$

Among them, ∂ represents the historical statistical trust weight, which is obtained by the following formula:

$$\xi = \frac{\left(1/D_h(\text{hist})\right)}{\left(1/D_h(\text{hist})\right) + \left(1/D_r(m)\right)} = \frac{D_r(m)}{D_h(\text{hist}) + D_r(m)}. \tag{19}$$

$D(x)$ is the variance function, which is used to represent the dispersion of the data. For the weight α, the general trust model is often determined by means of expert experience and simulation experiment results. Moreover, the result of doing so often lacks science, flexibility, and adaptability.

4. Computer Vision-Based Traffic Detection Method of Secure Transmission Industrial Internet of Things

The Internet of Things system comprehensively uses diversified data sensors, radio frequency identification technology, laser scanning equipment, and other tools to collect information on monitored objects, uses the network as a connection to realize data sharing and analysis, and intelligently manages things. This study uses computer vision technology to construct a traffic detection system for the secure transmission of the industrial Internet of Things. The overall layout is shown in Figure 4.

The data service backend, more formally called "middleware," is located between sensing devices and applications. It is the center of providing services for devices and users and is also the core part of our entire IoT remote monitoring system. Its characteristics are shown in Figure 5.

In order to ensure the reliability of transmission, this system adopts TCP-based socket data transmission technology. By analyzing the performance of the transmission framework, a two-tier socket framework is designed, and JSON is used as the message transmission format. Finally, this system uses RSA encryption and integrity verification to achieve reliability and security during data transmission. A detailed explanation of the socket communication process is shown in Figure 6.

It uses a two-layer frame design, as shown in Figure 7. The first layer is N receiving threads to receive client data. The second layer corresponds to N worker threads (processing threads), which process the data received in the receiving threads.

This study adopts a sliding window serial method of abnormal traffic detection with mixed dimensions of time and space. That is, this study first uses the sliding window method based on the time dimension to extract the features of the dataset. After forming several window instances and marking them, this study uses machine learning algorithms for preliminary screening and classification. The purpose of preliminary screening is mainly to locate and find windows with malicious traffic and screen out benign windows. In the second step, this study uses a sliding window method based on spatial dimensions to perform a second accurate detection of the traffic of the malicious window classified for the first time. Moreover, this study re-extracts the features and

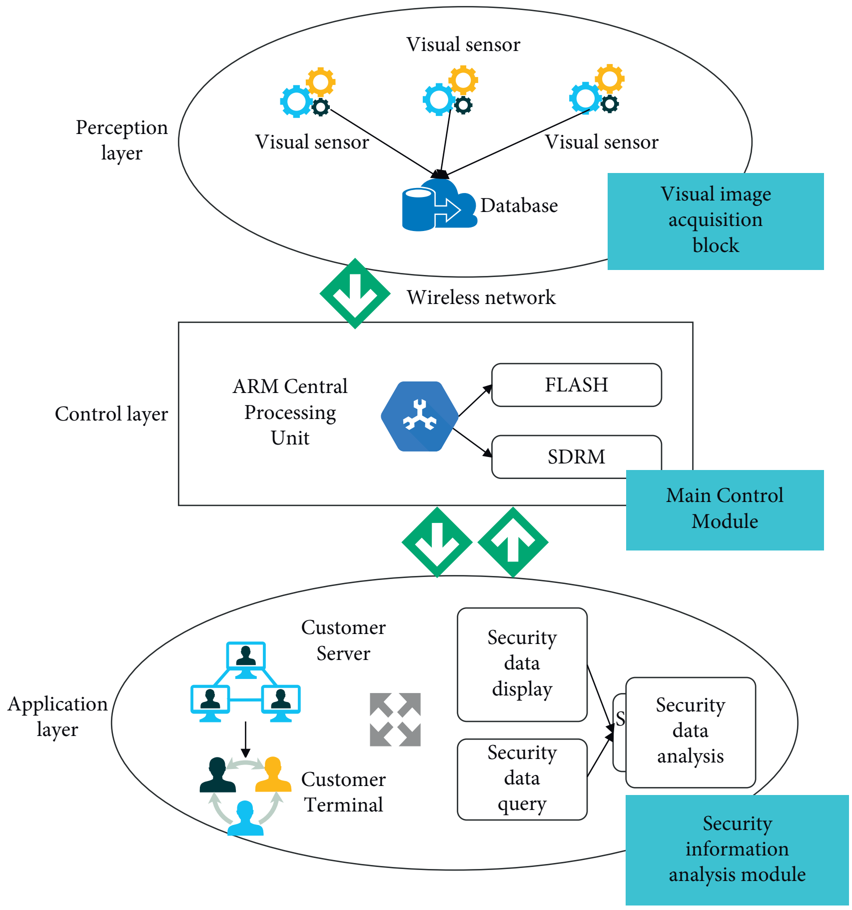

Figure 4: The overall layout of the traffic detection system of secure transmission industrial Internet of Things.

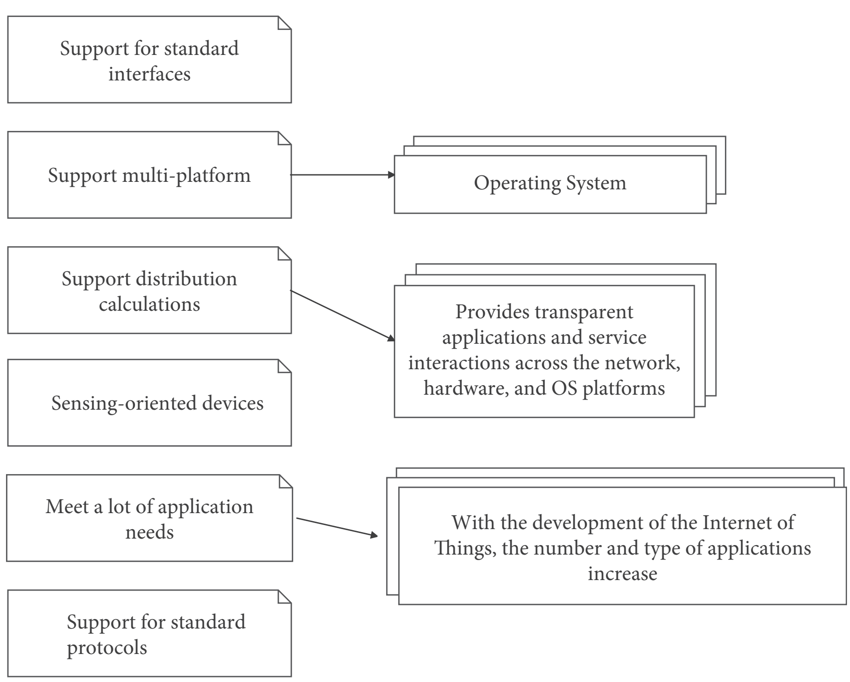

Figure 5: Features of middleware.

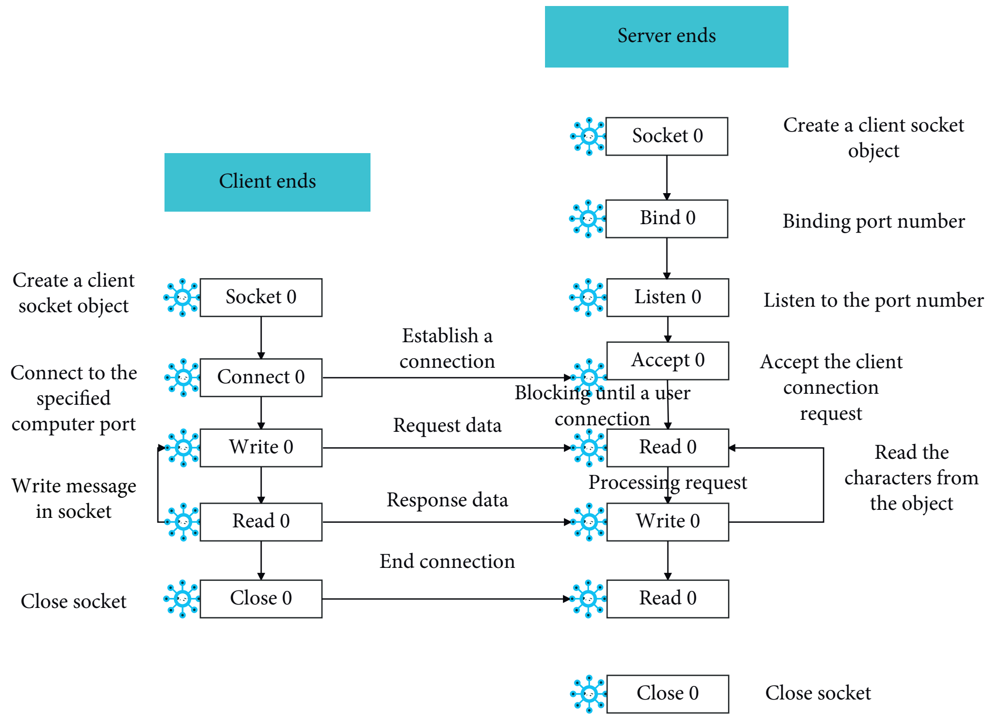

Figure 6: Detailed explanation of the socket communication process.

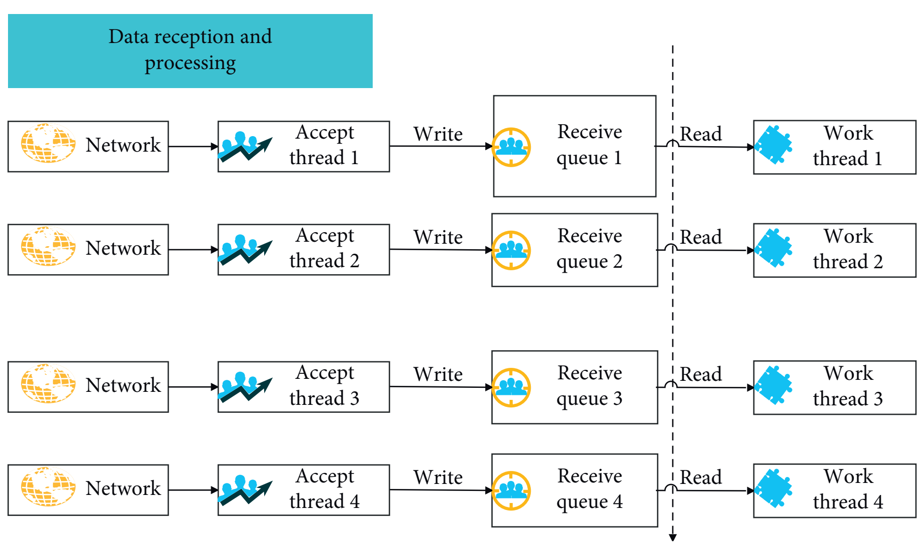

Figure 7: Socket frame design.

marks the flow of this type of window and uses the neural network detection algorithm for fine screening. Figure 8 shows the specific architecture.

Figure 9 shows the overall architecture of the program. The detection scheme is mainly divided into a flow acquisition module, a sliding window abnormal flow detection module based on the time dimension, and a sliding window abnormal flow detection module based on the space dimension.

After constructing the above model, the performance of the model is verified. Under the condition of ensuring that it is not interfered with by other external factors, this study constructs a simulation system of the industrial Internet of Things, performs security detection and flow detection on the system, and uses multiple sets of data to detect and calculate the test results, as shown in Table 1.

It can be seen from the above research that the effects of security detection and traffic detection are very good, so the traffic detection method of computer vision-based secure transmission industrial Internet of Things proposed in this study is very effective.

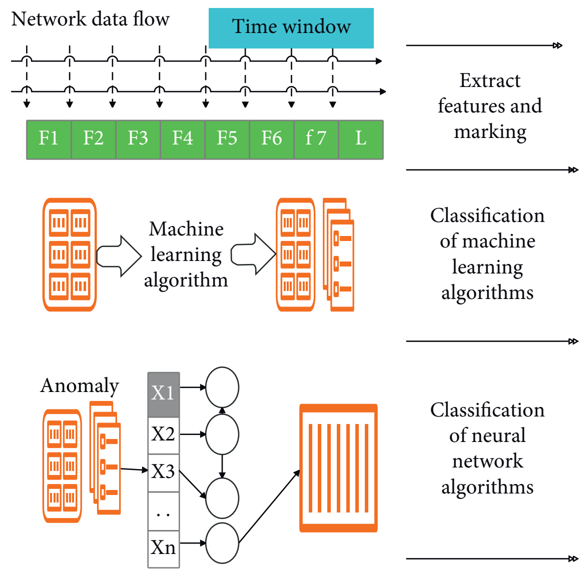

Figure 8: Abnormal traffic detection architecture.

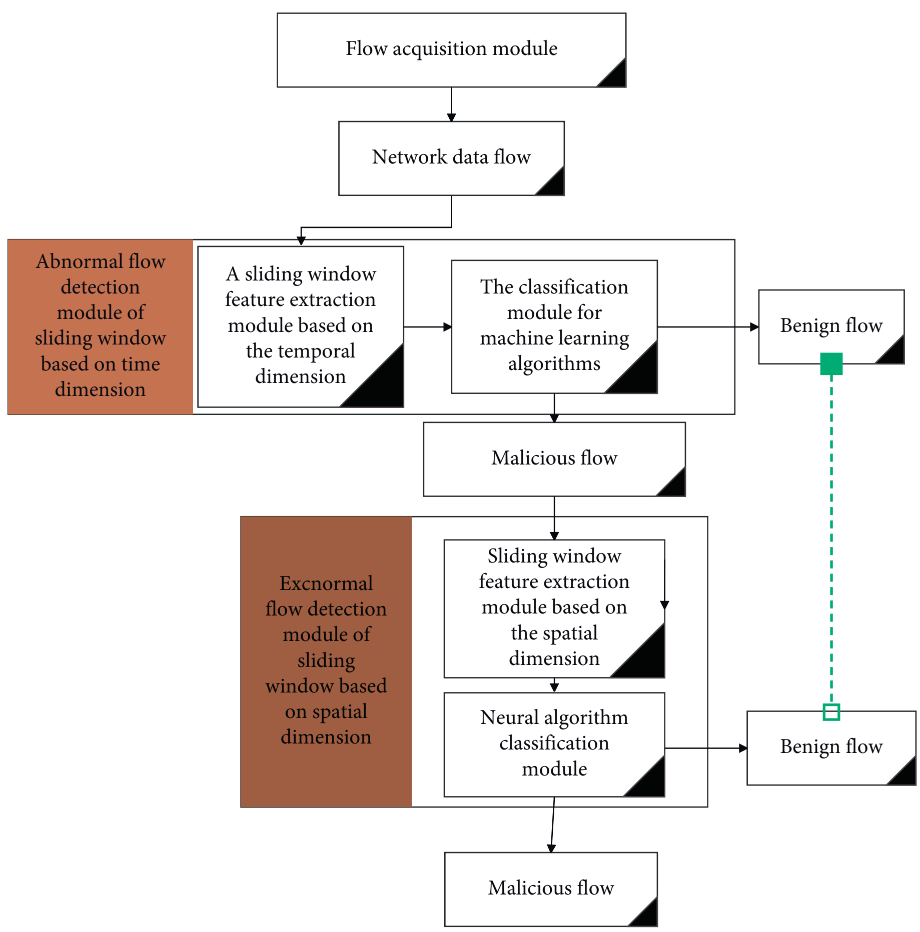

Figure 9: Overall structure diagram.

Table 1: Security detection and flow detection.

Number	System security	Flow detection	Number	System security	Flow detection	Number	System security	Flow detection
1	81.9	88.0	19	82.1	96.2	37	84.7	92.7
2	79.4	89.0	20	84.9	90.3	38	84.8	89.7
3	86.7	94.3	21	89.1	85.0	39	89.3	88.6
4	91.2	95.4	22	87.6	96.2	40	91.5	92.9
5	92.2	85.8	23	86.8	88.2	41	86.5	95.8
6	83.3	90.1	24	85.4	87.6	42	89.5	92.4
7	80.1	90.1	25	80.2	86.6	43	87.8	87.4
8	79.3	86.8	26	79.2	95.1	44	92.0	90.7
9	93.3	94.8	27	88.1	90.9	45	86.1	94.2
10	83.9	85.5	28	82.8	85.4	46	82.6	91.1
11	86.8	87.8	29	90.6	86.1	47	84.0	94.7
12	91.3	96.7	30	85.5	92.0	48	79.3	86.9
13	86.3	91.7	31	84.6	85.1	49	84.4	95.0
14	86.2	91.4	32	92.8	87.5	50	84.6	89.1
15	84.0	88.5	33	89.8	92.6	51	93.1	86.4
16	84.4	86.2	34	88.0	96.8	52	82.7	88.2
17	81.2	89.1	35	79.7	90.9	53	89.3	85.6
18	89.8	91.8	36	90.2	90.4	54	83.4	90.5

5. Conclusions

Currently, the application of big data processing and analysis technology is mostly focused on the Internet field, but there is a lack of rational use of massive industrial data in industrial production scenarios. Therefore, it is necessary to use the existing big data technology to design a better data processing platform suitable for industrial IoT big data. In order to improve the analysis efficiency of industrial Internet of Things data, it is necessary to implement a low-latency query system based on a Hadoop data warehouse, which can handle a large number of concurrent query requests and a single query can return results faster, thereby improving the efficiency of data processing and analysis. This study combines computer vision to conduct research on safe transmission and industrial Internet of Things traffic detection methods to further improve industrial production safety. Moreover, this study constructs an intelligent model to verify the performance of the system combined with experimental research. From the data statistics point of view, the model's security detection and flow detection effects are very good, so the computer vision-based security transmission industrial Internet of Things flow detection method proposed in this study is very effective.

Data Availability

The labeled dataset used to support the findings of this study is available upon request to the author.

Conflicts of Interest

The author declares no conflicts of interest.

Acknowledgments

This work was sponsored by the Kunlun Tourism College, Heilongjiang Institute of Technology.

References

[1] J. H. Abawajy and M. M. Hassan, "Federated internet of things and cloud computing pervasive patient health monitoring system," *IEEE Communications Magazine*, vol. 55, no. 1, pp. 48–53, 2017.

[2] D. He, R. Ye, S. Chan, M. Guizani, and Y. Xu, "Privacy in the internet of things for smart healthcare," *IEEE Communications Magazine*, vol. 56, no. 4, pp. 38–44, 2018.

[3] P. P. Ray, "Internet of things for smart agriculture: technologies, practices and future direction," *Journal of Ambient Intelligence and Smart Environments*, vol. 9, no. 4, pp. 395–420, 2017.

[4] Y. A. Qadri, A. Nauman, and Y. B. Zikria, "The future of healthcare internet of things: a survey of emerging technologies," *IEEE Communications Surveys & Tutorials*, vol. 22, no. 2, pp. 1121–1167, 2020.

[5] B. H. Dobkin, "A rehabilitation-internet-of-things in the home to augment motor skills and exercise training," *Neurorehabilitation and Neural Repair*, vol. 31, no. 3, pp. 217–227, 2017.

[6] J. Yao and N. Ansari, "Caching in energy harvesting aided Internet of Things: a game-theoretic approach," *IEEE Internet of Things Journal*, vol. 6, no. 2, pp. 3194–3201, 2018.

[7] J. E. Siegel, S. Kumar, and S. E. Sarma, "The future internet of things: secure, efficient, and model-based," *IEEE Internet of Things Journal*, vol. 5, no. 4, pp. 2386–2398, 2017.

[8] M. A. Abd-Elmagid, N. Pappas, and H. S. Dhillon, "On the role of age of information in the Internet of Things," *IEEE Communications Magazine*, vol. 57, no. 12, pp. 72–77, 2019.

[9] A. Sheth, U. Jaimini, and H. Y. Yip, "How will the internet of things enable augmented personalized health?[J]," *IEEE Intelligent Systems*, vol. 33, no. 1, pp. 89–97, 2018.

[10] G. J. Joyia, R. M. Liaqat, A. Farooq, and Rehman, "Internet of Medical Things (IOMT): applications, benefits and future challenges in healthcare domain," *Journal of Communication*, vol. 12, no. 4, pp. 240–247, 2017.

[11] N. Kshetri, "The evolution of the internet of things industry and market in China: an interplay of institutions, demands and supply," *Telecommunications Policy*, vol. 41, no. 1, pp. 49–67, 2017.

[12] S. Siboni, V. Sachidananda, and Y. Meidan, "Security testbed for Internet-of-Things devices," *IEEE Transactions on Reliability*, vol. 68, no. 1, pp. 23–44, 2019.
[13] Y. Yang, M. Zhong, H. Yao, and Yu, "Internet of things for smart ports: technologies and challenges," *IEEE Instrumentation and Measurement Magazine*, vol. 21, no. 1, pp. 34–43, 2018.
[14] M. Mayer and A. J. Baeumner, "A megatrend challenging analytical chemistry: biosensor and chemosensor concepts ready for the internet of things," *Chemical Reviews*, vol. 119, no. 13, pp. 7996–8027, 2019.
[15] M. Saez, F. P. Maturana, and K. Barton, "Real-time manufacturing machine and system performance monitoring using internet of things," *IEEE Transactions on Automation Science and Engineering*, vol. 15, no. 4, pp. 1735–1748, 2018.
[16] V. Jagadeeswari, V. Subramaniyaswamy, R. Logesh, and V. Vijayakumar, "A study on medical Internet of Things and Big Data in personalized healthcare system," *Health Information Science and Systems*, vol. 6, no. 1, pp. 1–20, 2018.
[17] S. Smys, A. Basar, and H. Wang, "Hybrid intrusion detection system for internet of things (IOT)," *Journal of ISMAC*, vol. 2, no. 4, pp. 190–199, 2020.
[18] I. Butun, P. Österberg, and H. Song, "Security of the internet of things: vulnerabilities, attacks, and countermeasures," *IEEE Communications Surveys & Tutorials*, vol. 22, no. 1, pp. 616–644, 2019.
[19] T. Qiu, N. Chen, K. Li, and M. Zhao, "How can heterogeneous internet of things build our future: a survey," *IEEE Communications Surveys & Tutorials*, vol. 20, no. 3, pp. 2011–2027, 2018.
[20] A. Heiskanen, "The technology of trust: how the Internet of Things and blockchain could usher in a new era of construction productivity," *Construction Research and Innovation*, vol. 8, no. 2, pp. 66–70, 2017.
[21] M. Wolf and D. Serpanos, "Safety and security in cyber-physical systems and internet-of-things systems," *Proceedings of the IEEE*, vol. 106, no. 1, pp. 9–20, 2017.

Hindawi
Scientific Programming
Volume 2021, Article ID 4751263, 11 pages
https://doi.org/10.1155/2021/4751263

Research Article

Game Teaching Method in Preschool Education Based on Big Data Technology

Rui Bai

School of Education, YuLin University, Yulin, China

Correspondence should be addressed to Rui Bai; bairui@yulinu.edu.cn

Received 20 October 2021; Revised 3 November 2021; Accepted 30 November 2021; Published 16 December 2021

Academic Editor: Le Sun

The traditional preaching way of imparting knowledge can only stifle children's imagination, creativity, and learning initiative a little bit, which is harmful to children's healthy and happy growth. This paper combines big data technology to evaluate the effect of game teaching method in preschool education, analyzes the teaching effect of game teaching method in preschool education, and combines big data technology to find problematic teaching points. Based on the collaborative filtering algorithm of preschool children, this paper estimates the current preschool children's score for the game by referring to the scores of neighbor preschool children on the predicted game and constructs an intelligent model. Finally, this paper combines experimental research to verify the model proposed in this paper. From the experimental research, it can be seen that the method proposed in this paper has a certain effect.

1. Introduction

The continuous development of information technology and network terminal technology has given mobile phones and other life tools great entertainment. The time required for games and the cost of money have been continuously reduced, and digital games have gradually entered various households. Whether it is young and middle-aged parents or the elderly taking care of children, they cannot avoid preschool children from coming into contact with games. The magic of this kind of game can make a crying child stop immediately, can make the child sit quietly in the corner and wait, and can be a variety of rewards for parents. However, this "game-style trick" can only bring more problems such as more eyesight and distracted attention, and seriously, it also causes communication barriers for preschoolers. While the digital age brings convenience to people's lives, there are also risks that cannot be underestimated [1]. As practitioners of preschool education, when seeing children with lively, smart, and witty nature being increasingly eroded by digital games, they deeply feel the crisis in preschool education and child development. It is the nature of children to like to play games, and games are also the best way for children to learn. Games cannot be discarded in the growth of preschool children. Based on such concerns, they began to think about how to construct a digital game curriculum suitable for the development of preschool children and implement it in real preschool education activities. Compared with traditional outdoor games for children, the design and implementation of digital games are easier to add elements that are conducive to the development of children's cognitive development and mathematical logic. It can be said that making good use of digital games is of great benefit to the development of preschool children [2]. Here, how to take the essence of digital games and remove the dross of digital games is extremely important [3].

This paper combines big data technology to evaluate the effect of game teaching method in preschool education and analyzes the teaching effect of game teaching method in preschool education. Moreover, this paper combines big data technology to discover problematic teaching points and, on this basis, further enhance the teaching effect of preschool education.

2. Related Work

Information multimedia technology is developing at a speed beyond people's imagination. The entire society is in a critical period of transition from an industrialized society to an informationized society. Informationization has become a common trend in the world's economic and social development. At present, many developed countries have paid attention to the cultivation of the information quality of the next generation, and all countries in the world are accelerating the informatization process of basic education [4]. Educational informatization has a comprehensive impact on preschool education. It has changed the educational goals, educational structure, educational content, educational methods, and even teaching evaluation [5].

The United Kingdom no longer stacks computers but moves them into the class to make it a gaming area. Computer education is called information technology education in British kindergartens. Almost every kindergarten class is equipped with a computer and learning software that matches the model [6]. Computers can not only teach children English, mathematics, and science but also teach them to sing, draw, play chess, and walk through mazes. The more entertaining software can greatly arouse children's interest in learning computer and through the intervention of multimedia, such as sound, image, text, animation, and so on,, make children feel the endless joy of learning. The educational software associated with the teaching of various subjects can play a role in assisting education. Through the method of entertaining and teaching, children can learn easily and happily and increase their intelligence [7]. The method of computer education mainly adopts the game method, that is to say, computer education starts from the game. The game activity stimulates the children's learning interest and thirst for knowledge, and the children never get tired of it. Japanese families can receive a set of video tapes, books, and magazines every month to encourage parents to help their children play cartoon characters, text, and digital games, and open a hotline [8]. In the United States, computers are now popularized in all kindergartens. Under the guidance of full-time computer teachers, three- or four-year-old children "touch the future" in front of the keyboard and mouse. In addition to playing computer games, the community also provides gamification and information technology–teaching activities [9]. In Canada, kindergartens have opened "virtual schools" for teaching activities. Australia has a computer game group, New Zealand has a computer game center, and France and Sweden have also incorporated computers and networks into their preschool education plans. It should be said that the computer entering kindergarten is another development trend of today's kindergarten curriculum[10].

Literature [11] elaborated on the influence of multimedia computer-assisted teaching MCAI in children's teaching and mentioned the combination of multimedia computer-assisted teaching and the use of game courseware to carry out mathematics education. Practice has proved that children learn best in a game environment, and what they learn can be quickly applied to more abstract and formal situations. The action thinking in the game can solve their more disciplinary problems in the future. The formation of abilities, such as mind image and recording, lays a solid foundation. Therefore, it is feasible to carry out research on gamification theme teaching in kindergartens, and it has significant effects. The main research content of the literature [12] is how to build a kindergarten modern education environment, strengthen teacher information technology training, pay attention to teaching research and practice under the information technology environment, and establish a comprehensive evaluation system for kindergarten information technology education. The process evaluation, stage evaluation, and comprehensive evaluation here have given me a lot of enlightenment and provided a reference for the monthly stage evaluation standard selection and formulation. Literature [13] studies the informatization of environmental education and integrates the element of information technology into environmental education, making environmental education with the characteristics of informatization. The two are interactive and two-way integration. This integration is not a simple application of courseware for demonstration auxiliary teaching, but the integration of modern information technology methods and courses, and it is no longer just a demonstration of media or tools. More abstract environmental knowledge and problems are more visualized, promote children's environmental protection emotions, and trigger the use of information technology to present a holographic learning environment for environmental education, so that children can be in the information world and deeply feel the application of information technology [14].

3. Game Teaching Method in Preschool Education Based on Big Data Recommendation Algorithm

The recommendation algorithm is one of the cores of the recommendation system because it is directly related to the accuracy of the recommendation system and the satisfaction of preschoolers. A tag is a kind of keywords used to describe information without hierarchical structure. It can be used to describe the semantics of the game and the interests of preschoolers, and to connect the two. As shown in Figure 1, there are three main ways to source tags in the recommendation system. (1) Preschoolers use labels to describe their personal interests. (2) The administrator uses tags to describe the game features when creating the game. (3) Preschool children use several tags to describe the game. Figure 1 also shows the relationship between preschoolers, tags, and games. When the tags used by the preschool children match the tags added by the game, to a certain extent, the preschool children and the game have a set of potential consumption relationships. The tags used by preschoolers here include tags for preschoolers to describe personal interests and tags for preschoolers to describe games.

Therefore, the process of tag-based recommendation algorithm is as follows:

(1) The algorithm calculates the common labels of each preschooler, and the number of times the preschoolers have used these labels.

(2) The algorithm calculates the number of times each game has been hit by each tag. The more times a game is described by a tag, the more relevant the game is to that tag.

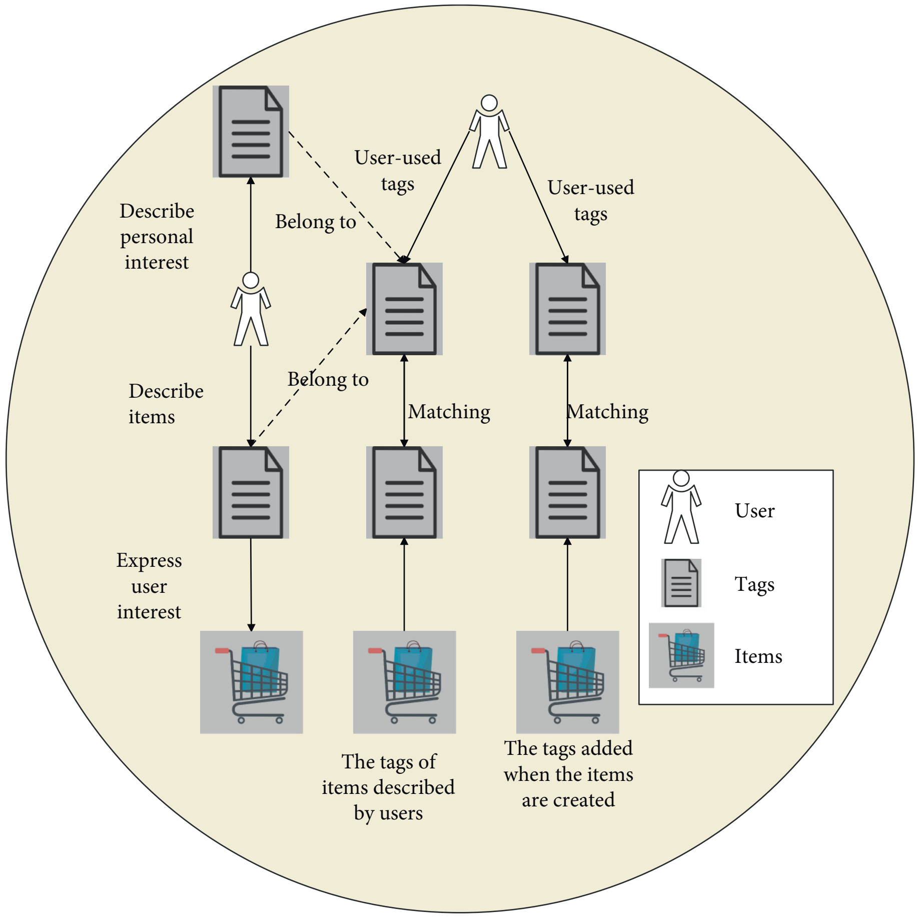

FIGURE 1: The relationship between preschoolers, tags, and games.

(3) When recommending for a preschooler, the algorithm associates the preschoolers' common labels with the most relevant games described by these labels and recommends them to the preschoolers according to the correlation, as shown in formula (1) [15]:

$$P(u,i) = \sum_{t\in T(u)} n_{u.t} n_{t.i}. \tag{1}$$

Among them, $P(u, i)$ represents the degree of interest of the preschooler u in the game i and T(u) is the set of tags used by the preschooler u. $n_{u.t}$ is the number of times the preschooler u has used the label t, and $n_{t.i}$ is the number of times the label t is used to describe the game i.

In practical applications, certain tags will be used many times by preschoolers, and tags of certain popular games will also be used repeatedly by preschoolers when evaluating the game. The algorithm described in formula (1) will be overly inclined to popular tags and popular games for preschool children in terms of results. The main problem is that the algorithm cannot distinguish which labels are popular labels and which labels are personalized labels for preschoolers. Therefore, we borrow the idea of TF-IDF5. Considering how many different preschoolers use each tag and how many different preschoolers describe each game with tags, we use these two to punish popular tags and popular games. The improved algorithm (TFIDF Tag Based) is shown in formula (2) [16]:

$$P(u,i) = \sum_{t\in T(u)} \frac{n_{u.t}}{\log\left(1+n_t^{(n)}\right)} \frac{n_{t.i}}{\log\left(1+n_i^{(u)}\right)}. \tag{2}$$

Among them, $n_t^{(n)}$ indicates how many different preschoolers have used the label t, and $n_i^{(u)}$ indicates how many different preschoolers have used the label to describe the game i.

In response to this problem, the solution used in this paper is to extend the original label. The original tags include tags used by preschool children or tags that have been described in games, while the expanded tag set includes the original tags and the tag set with higher similarity to the original tags. Measuring the similarity between two tags can be simplified to calculate the proportion of the number of games that have been described by the two tags at the same time to the total number of games that have been described by the two tags. The Jaccard formula can be used to calculate the similarity between tags t1 and t2, as shown in formula (3) [17]:

$$\mathrm{sim}(t_1,t_2) = \frac{\left|I(t_1)\cap I(t_2)\right|}{\left|I(t_1)\cup I(t_2)\right|}. \tag{3}$$

Among them, $I(t)$ represents the set of games described by the label r. In addition, the cosine similarity formula can also be used to calculate the similarity between tags t_1 and t_2:

$$\operatorname{sim}(t_1, t_2) = \frac{\sum_{i\in I(t_1)\cap I(t_2)} n_{t_1,i}^{(u)} n_{t_2,i}^{(u)}}{\sqrt{\sum_{i\in I(t_1)\cap I(t_2)} n_{t_1,i}^2 n_{t_2,i}^2}}. \quad (4)$$

Among them, $n_{t,i}^{(u)}$ is the number of preschool children who have described game i with the label t.

The accuracy of the tag-based recommendation algorithm has a lot to do with the quality of the tag itself. The quality here refers to whether the label is descriptive, whether it is distinguishable, whether it follows the standard grammar, and so on. The quality of the labels in the recommendation system is mainly guaranteed through low-quality label cleaning and high-quality label recommendation.

The entire cleaning process is shown in Figure 2. The nonreferenced tags are primarily screened by identifying commonly used stop words and defining and expanding the stop dictionary. After that, we can let preschoolers mark useless labels through feedback from preschoolers. Tags with high-text content similarity can be identified and processed through regular expressions and string edit distance algorithms.

To describe the collaborative filtering algorithm, this paper introduces the following symbols: U represents the set of preschool children in the recommendation system; I represents the set of all recommended candidate games; R represents the set of score records in the system; a score record is a triple set of preschool children, games, and scores; and S represents the range of scores (e.g. $S = \{1,2,3,4,5\}$, $S =$ {interest, not interested). At the same time, we assume that any preschooler $u \in U$ can only have at most one score for each game $i \in$ I, and this score is recorded as $R_{\mathrm{u,i}}$. U_i represents the subset of preschoolers who have evaluated game i, and $I_{u,v}$ represents the subset of games evaluated by preschooler u. I_u means preschooler u and preschooler v [18].

The intersection of the reviewed items is $I_{u,v} = I_u \cap I_v$, $U_{i,j}$ represents the set of preschoolers who have reviewed both game i and game j, that is, $U_{i,j} = U_i \cap U_j$.

The collaborative filtering algorithm based on preschool children estimates the current preschool children's score for the game by referring to the scores of neighbor preschool children on the predicted game. The neighbor preschoolers here refer to a collection of preschoolers with similar scoring patterns to the current preschoolers. The calculation of preschooler u's prediction score for game ü is shown in formula (5) [19]:

$$P(u,i) = \frac{\sum_{v\in N_i(u)} \operatorname{sim}(u,v) R_{v,i}}{|\operatorname{sim}(u,v)|}. \quad (5)$$

Among them, $N_i(u)$ is the preschooler's neighbor set composed of K preschoolers who have evaluated game i and have the highest similarity with preschooler u, sim(u,v) represents the similarity between preschooler u and preschooler v.

Based on the game-based collaborative filtering algorithm, we estimate the current preschool children's score for the game by referring to the score records of the preschool children's games with the neighbors of the predicted game. The neighbor game here refers to a game that is highly similar to the predicted game. The calculation of preschooler u's prediction score for game i is shown in formula (6) [20]:

$$P(u,i) = \frac{\sum_{v\in N_i(i)} \operatorname{sim}(i,j) R_{v,i}}{\sum_{v\in N_i(i)} \operatorname{sim}(i,j)}. \quad (6)$$

Among them, $N_u(i)$ is the game neighbor set composed of K games with the highest similarity to game i among the games evaluated by preschooler u, and sim(i,j) represents the similarity between preschooler i and preschooler j.

Commonly used similarity measurement methods in collaborative filtering algorithms mainly include Cosine Similarity and Pearson Correlation. The cosine similarity method is often used in game-based collaborative filtering algorithms. This method represents objects as vectors and obtains the similarity between objects by calculating the cosine angle between the vectors:

$$\operatorname{sim}(i,j) = \frac{\sum_{u\in U_{i,j}} R_{u,i} R_{u,j}}{\sqrt{\sum_{u\in U_{i,j}} R_{u,j}^2 \sum_{u\in U_{i,j}} R_{u,j}^2}}. \quad (7)$$

Since this similarity measurement method does not consider the difference between preschool children's scores and their average scores, we use Adjusted Cosine Similarity, as shown in formula (8) [21]:

$$\operatorname{sim}(i,j) = \frac{\sum_{u\in U_{i,j}} \left(R_{u,i} - \overline{R_u}\right)\left(R_{u,j} - \overline{R_u}\right)}{\sqrt{\sum_{u\in U_{i,j}} \left(R_{u,i} - \overline{R_u}\right) \sum_{u\in U_{i,j}} \left(R_{u,j} - \overline{R_u}\right)}}. \quad (8)$$

Among them, $\overline{R_u}$ represents the average value of the sum of u scores of preschool children. It shows that adjusting the cosine similarity is more suitable for use in game-based methods than the Pearson correlation coefficient. In contrast, the Pearson correlation coefficient has better results in the method based on preschool children, which is shown in formula (9) [22]:

$$\operatorname{sim}(i,j) = \frac{\sum_{u\in I_{iu,v}} \left(R_{u,i} - \overline{R_u}\right)\left(R_{v,j} - \overline{R_u}\right)}{\sqrt{\sum_{u\in I_{u,v}} \left(R_{u,i} - \overline{R_u}\right) \sum_{u\in I_{u,v}} \left(R_{v,j} - \overline{R_u}\right)}}. \quad (9)$$

In the actual scoring process, the evaluation criteria of each preschool child are different. Some preschool children are more relaxed and tend to give most games 4 or even 5 points, and some preschool children are stricter and more cautious and tend to give most games less than 3 points. In other words, if a score record is 4 points, it does not necessarily mean that preschoolers like the game. For relaxed preschoolers, maybe 5 points are really liked. However, for strict preschool children, a score of 4 has already indicated the preschool children's tendency to be interested or like it. Therefore, the average score of preschool children is introduced here to measure whether a certain preschool child's score record is a positive or negative tendency score, as shown in formula :

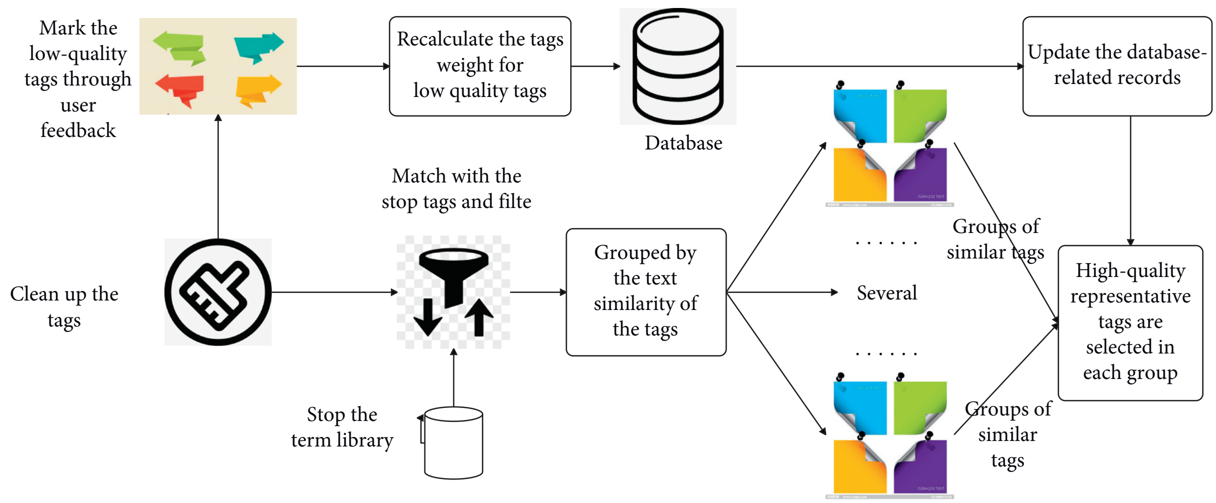

FIGURE 2: Label cleaning process.

$$P(u,i)=\overline{R_u}+\frac{\sum_{v\in N_i(u)}\mathrm{sim}(u,v)\left(R_{v,i}-\overline{R_v}\right)}{\sum_{v\in N_i(u)}\mathrm{sim}(u,v)}. \tag{10}$$

Game-based methods can also be similarly processed by introducing average game scores, as shown in formula :

$$P(u,i)=\overline{R_t}+\frac{\sum_{v\in N_u(i)}\mathrm{sim}(i,j)\left(R_{u,j}-\overline{R_j}\right)}{\sum_{v\in N_u(i)}\mathrm{sim}(i,j)}. \tag{11}$$

In the practical application of the recommender system, the total number of score records is much smaller than the product of preschool children and the number of games. The score matrix for preschool children and games contains a large number of zero-value elements (indicating that preschool children have not rated the game or preschool children have not purchased the game). Such a scoring matrix has the problem of data sparsity. The definition of the sparsity of the scoring matrix is shown in formula :

$$\mathrm{Sparsity}\left(M_R\right)=\frac{|R|}{|U||I|}. \tag{12}$$

When calculating the similarity of preschoolers based on a sparse scoring matrix, it is likely that only a few scores are involved. When these scores are exactly similar or even equal, this group of preschool children will be considered completely similar (the similarity is close to 1). In fact, because the number of common scores is too small, this phenomenon may be just a coincidence, but it will cause dissimilar preschoolers to have too high recommendation weights in the recommendation calculation process, and ultimately unreliable recommendation results.

Aiming at the data sparsity problem in the collaborative filtering algorithm, a feasible solution strategy is to reduce the similarity obtained by only a small number of scores. The improved similarity of preschool children is shown in formula :

$$\mathrm{sim}\prime(u,v)=\frac{\min\left\{\left|I_{u,v}\right|,\gamma\right\}}{\gamma}\times\mathrm{sim}(u,v). \tag{13}$$

Similarly, the improved game similarity is shown in formula :

$$\mathrm{sim}'(u,v)=\frac{\min\left\{\left|I_{u,v}\right|,\gamma\right\}}{\gamma}\times\mathrm{sim}(u,v). \tag{14}$$

This method penalizes the similarity calculated involving the number of ratings less than the specified number y. The y value varies according to the data set, and cross-validation is required to determine the best y value.

This paper proposes another solution to the data sparsity problem, which increases the number of available scores by improving the similarity calculation process. Carefully analyze the calculation process of the similarity of preschool children. No matter which similarity calculation formula is used, the accuracy bottleneck lies in the size of the $|I_{u,v}|$. In the traditional similarity calculation method, the calculation of $I_{u,v}$ is done by exact matching, that is, only those games that match exactly in the game set evaluated by preschooler u and preschooler v will be used to calculate the similarity between the two spend. Now, we consider the following situation: preschooler u rated game i with 5 points, preschooler v rated game j with 5 points, preschooler u did not rate j, and preschooler v did not rate game i. There is no score intersection between u and preschooler v. It is known that the similarity between game i and game j is 0.9 (very similar). According to the aforementioned description, because the exact match result of the game is an empty set, the traditional similarity calculation method cannot calculate the similarity between the preschooler u and the preschooler v.

The set of high-scoring games for preschool children u is the User Favorite Item Set (User Favorite Item Set). By accumulating the similarity between each group of successfully matched game pairs and taking the average, the result is the set similarity between $I^+{}_u$ and $I^+{}_v$. To get closer to the similarity of the real game set, try to avoid the situation where the same game is matched multiple times (as shown in Figure 3). Especially, when the game similarity is calculated based on the collaborative filtering similarity algorithm, the similarity between popular games and other games is

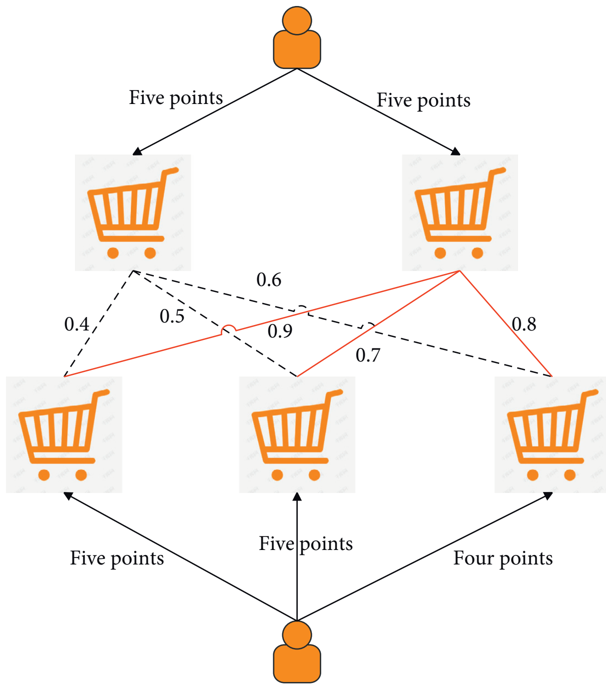

FIGURE 3: An example where a game is matched multiple times in the calculation of set similarity.

generally high, which will cause the calculated set similarity to not well reflect the preschool children's degree of similarity between interests.

Therefore, the weight reduction penalty should be imposed on games that have been matched more than once. Considering that the result range of cosine similarity or Pearson's correlation coefficient is [-1,1], different penalty mechanisms are adopted for positive and negative similarity, although in theory it is difficult for games with negative correlation to be the best match. The penalty strategy is to reduce all similarities related to the game when calculating the similarity according to the number of times the game has been matched.

In addition, for each game i, the game i^* that is most similar to game i in the set of scored games for each preschooler u can be calculated, that is, $\left\{i^* \in I_u, \operatorname{sim}(i, i^*) = \max_{i \in I_u} \operatorname{sim}(i, i^*)\right\}$. The collaborative filtering method based on preschool children can be extended with formula :

$$P(u,i) = \frac{\sum_{v \in N_i(i)} \operatorname{sim}(u,v) \operatorname{sim}(i,j) R_{v,j}}{\sum_{v \in N_i(i)} |\operatorname{sim}(u,v)| |\operatorname{sim}(i,j)|}. \quad (15)$$

The advantage of using this expansion formula to calculate is that for different prediction games, even if the number of reliable neighbors for preschoolers is insufficient, we can expand enough neighbors and scores by looking for approximate games, thereby solving data sparseness to a certain extent. Improve the reliability of prediction results.

4. Analysis of Game Teaching Method in Preschool Education Based on Big Data Technology

Users can obtain information based on their existing knowledge, perception, and thinking through the intuitive interactive interface provided by the machine and react through the interactive interface. The machine processes the received information and then transmits it to the user through the man-machine interface or makes other forms of feedback. The human–computer interaction process can be summarized as consisting of four basic functions: information receiving function, information storage function, information processing and decision-making function, and execution function, as shown in the following Figure 4:

The memory storage model is the three-level memory model of memory. This model divides the process of memory into three stages according to the time sequence of memory. Sensory memory is the initial stage, followed by short-term memory, and finally long-term memory. The model can be shown in Figure 5:

It can be seen from the model in Figure 5 that people first obtain information from the environment through sensory memory, such as vision and hearing. Some information will be lost in this process. Then, when the information gets attention, the human brain begins to perform the next stage of memory, which is short-term memory. When performing short-term memory, the human brain processes and reorganizes information and responds. To achieve this process, the human brain also needs to call up the knowledge in long-term memory. When the information is retold and strengthened, the information can be stored in long-term memory. The arrows on the way indicate the flow of information.

The human–computer interaction function diagram clearly describes the flow of information: information input, reception, processing, storage and output, and so on can know the goal and structure of the information, but does not reflect the roles of the three modules of the user's memory. In the process of using handheld mobile devices, in addition to the user's memory, the three modules affect all aspects of the information circulation process, the interactive design of the device, the difficulty of game tasks, and the user's information cognitive ability also affect the effect of information transmission. Based on the mutual influence of the aforementioned elements, a design model of instructional games supported by mobile devices has been researched, as shown in Figure 6.

The multisensory and multidimensional interactive virtual reality environment composed of sensors-controllers (chips)-virtual worlds (computers) will have a better immersive effect than virtual reality where computers are solely used as visual and auditory output. This research will combine the multisensory and multidimensional

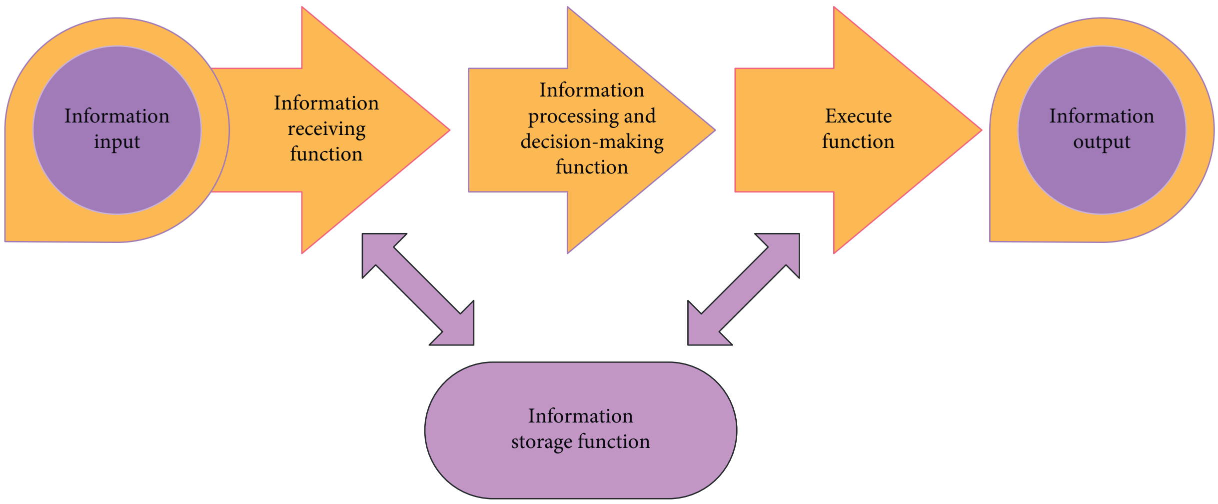

Figure 4: Basic functions of human-computer interaction.

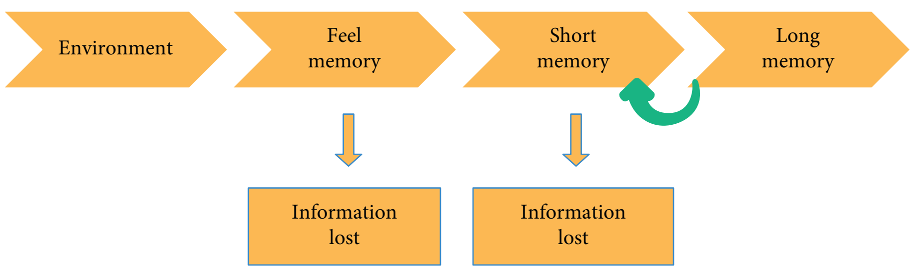

Figure 5: Three-storage model of memory.

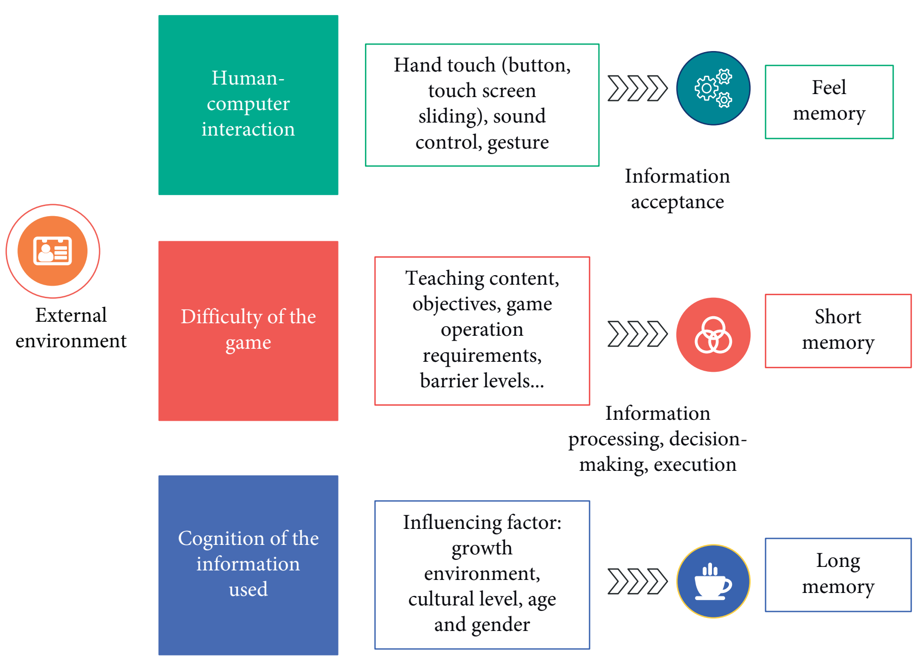

Figure 6: Teaching game design model supported by mobile devices.

interaction concept of sensor-controller (chip)-virtual world (computer) to design a virtual reality psychological relaxation game suitable for preschool students, as shown in Figure 7.

After constructing the aforementioned model, the performance of the model is verified. The model built in this paper is mainly used in preschool education, and it uses big data recommendation algorithms to recommend

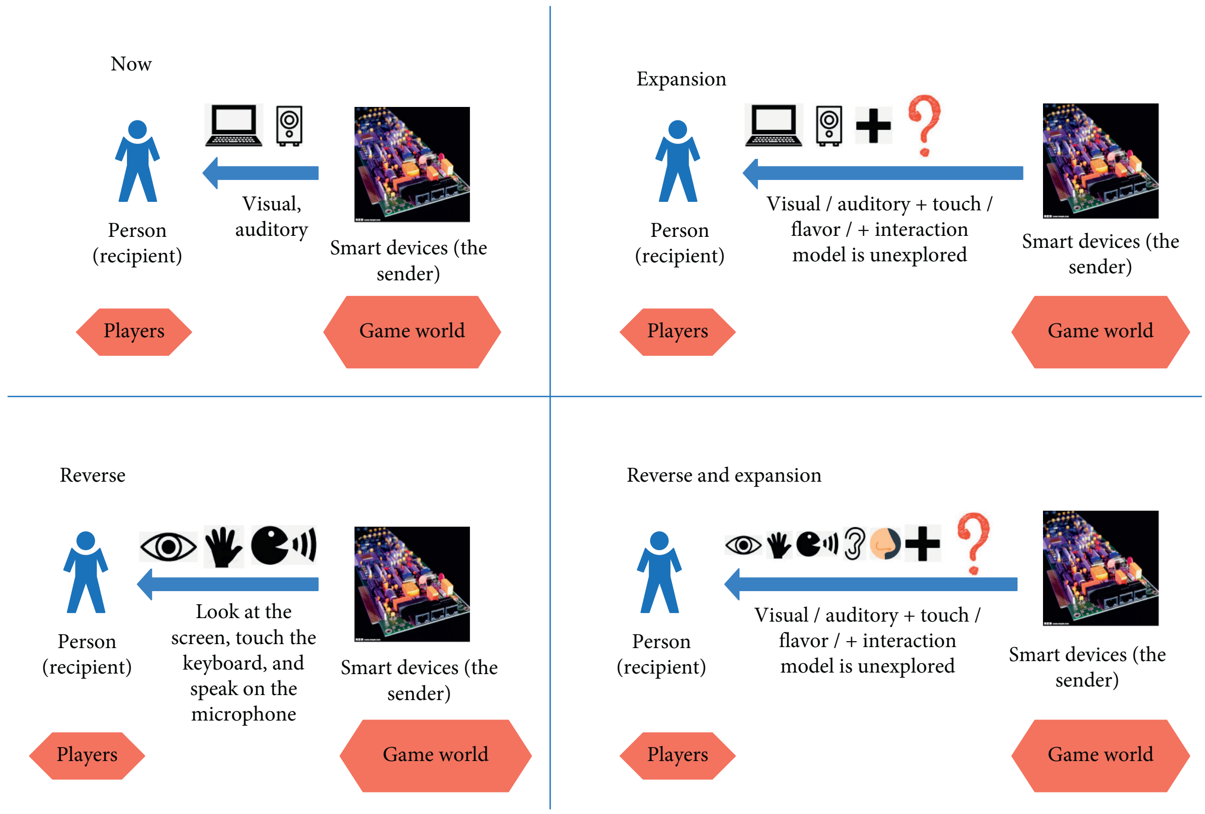

Figure 7: Game teaching mode in preschool education.

Table 1: Preschool education data mining and game recommendation effects.

Number	Data mining	Game recommendation
1	92.6	80.0
2	85.5	85.7
3	93.9	77.6
4	89.2	90.0
5	82.3	84.5
6	85.1	90.0
7	84.9	87.3
8	81.7	88.4
9	88.3	89.5
10	91.3	88.9
11	89.6	78.2
12	89.5	84.9
13	82.7	76.8
14	86.2	88.7
15	90.9	76.3
16	86.8	90.8
17	88.1	82.0
18	89.2	82.8
19	84.2	89.2
20	83.0	87.5
21	93.1	76.9
22	92.3	87.9
23	82.1	87.4
24	90.5	81.9
25	90.8	88.1
26	87.1	76.9
27	89.3	83.1
28	82.5	84.5

Table 1: Continued.

Number	Data mining	Game recommendation
29	89.7	87.9
30	81.9	79.3
31	89.2	90.8
32	88.1	88.8
33	85.8	89.1
34	82.7	88.4
35	93.9	88.1
36	90.6	85.0
37	87.0	81.4
38	93.2	76.5
39	90.0	76.1
40	92.7	87.9
41	89.5	76.4
42	87.3	82.3
43	86.6	88.0
44	84.0	76.4
45	89.9	78.9
46	82.7	90.2

Table 2: Evaluation of the teaching effect.

Number	Teaching effect
1	91.3
2	89.8
3	88.2
4	87.1
5	80.8
6	85.9
7	90.1
8	80.9
9	88.5
10	81.5
11	85.3
12	80.9
13	92.0
14	88.6
15	87.4
16	81.6
17	85.1
18	86.7
19	81.9
20	82.5
21	80.7
22	89.7
23	81.2
24	88.4
25	88.9
26	86.9
27	91.6
28	81.6
29	86.4
30	88.2
31	89.2
32	86.7
33	82.6
34	84.1
35	82.2
36	92.3
37	85.7

Table 2: Continued.

Number	Teaching effect
38	86.5
39	84.3
40	85.8
41	89.3
42	88.8
43	92.1
44	89.3
45	87.2
46	90.1

appropriate games and uses data mining algorithms to mine students' learning conditions and improve real-time teaching.

Therefore, this paper first designs experiments to conduct preschool education data mining and game recommendation effect verification and obtain relevant experimental data through multiple sets of simulation data. The results are shown in Table 1 below.

From the experimental results in Table 1, the game teaching method in preschool education based on big data technology proposed in this paper can effectively conduct preschool education data mining and can recommend suitable games for preschool education. After that, this paper evaluates the teaching effect, and the results are shown in Table 2.

From the above research, the game teaching method in preschool education based on big data technology proposed in this paper has good teaching effects and can play a certain role in preschool education.

5. Conclusion

Games and teaching are two important means of modern preschool education practice, and there is a close relationship between them. The implementation of preschool game education must be based on a scientific understanding of the relationship between the two. With the continuous reform and development of preschool education, the kindergarten preschool education has undergone earth-shaking changes, including adjustments to educational content, teaching methods, and educational goals. In particular, it emphasizes that kindergarten education should be based on games. This adjustment not only conforms to the children's physical and mental development law and age characteristics but also realizes the teaching mode of "children as the main body and teachers as the leading" in the game. Modern educational psychology research shows that children's learning is a proactive process of knowledge construction, and teachers should pay full attention to children's subjective status. This paper combines big data technology to evaluate the effect of game teaching method in preschool education, analyzes the teaching effect of game teaching method in preschool education, and combines big data technology to discover problematic teaching points, so as to further improve the teaching effect of preschool education.

Data Availability

The labeled dataset used to support the findings of this study are available from the corresponding author upon request.

Conflicts of Interest

The author declares no competing interests.

Acknowledgments

This work was supported by YuLin University.

References

[1] S. F. M. Alfalah, "Perceptions toward adopting virtual reality as a teaching aid in information technology," *Education and Information Technologies*, vol. 23, no. 6, pp. 2633–2653, 2018.

[2] G. Cooper, H. Park, Z. Nasr, L. P. Thong, and R. Johnson, "Using virtual reality in the classroom: preservice teachers' perceptions of its use as a teaching and learning tool," *Educational Media International*, vol. 56, no. 1, pp. 1–13, 2019.

[3] J. Zhao, X. Xu, H. Jiang, and Y. Ding, "The effectiveness of virtual reality-based technology on anatomy teaching: a meta-analysis of randomized controlled studies," *BMC Medical Education*, vol. 20, no. 1, pp. 127–210, 2020.

[4] S. J. Bennie, K. E. Ranaghan, H. Deeks et al., "Teaching enzyme catalysis using interactive molecular dynamics in virtual reality," *Journal of Chemical Education*, vol. 96, no. 11, pp. 2488–2496, 2019.

[5] S. F. M. Alfalah, J. F. M. Falah, T. Alfalah, M. Elfalah, N. Muhaidat, and O. Falah, "A comparative study between a virtual reality heart anatomy system and traditional medical teaching modalities," *Virtual Reality*, vol. 23, no. 3, pp. 229–234, 2019.

[6] M. Reymus, A. Liebermann, and C. Diegritz, "Virtual reality: an effective tool for teaching root canal anatomy to undergraduate dental students - a preliminary study," *International Endodontic Journal*, vol. 53, no. 11, pp. 1581–1587, 2020.

[7] V. L. Dayarathna, S. Karam, R. Jaradat et al., "Assessment of the efficacy and effectiveness of virtual reality teaching module: a gender-based comparison," *International Journal of Engineering Education*, vol. 36, no. 6, pp. 1938–1955, 2020.

[8] O. Hernandez-Pozas and H. Carreon-Flores, "Teaching international business using virtual reality," *Journal of Teaching in International Business*, vol. 30, no. 2, pp. 196–212, 2019.

[9] V. Andrunyk, T. Shestakevych, and V. Pasichnyk, "The technology of augmented and virtual reality in teaching children with ASD," *Econtechmod: Scientific Journal*, vol. 4, no. 7, pp. 59–64, 2018.

[10] R. Mayne and H. Green, “Virtual reality for teaching and learning in crime scene investigation,” *Science & Justice*, vol. 60, no. 5, pp. 466–472, 2020.

[11] M. Taubert, L. Webber, T. Hamilton, M. Carr, and M. Harvey, “Virtual reality videos used in undergraduate palliative and oncology medical teaching: results of a pilot study,” *BMJ Supportive & Palliative Care*, vol. 9, no. 3, pp. 281–285, 2019.

[12] K. E. McCool, S. A. Bissett, T. L. Hill, L. A. Degernes, and E. C. Hawkins, “Evaluation of a human virtual-reality endoscopy trainer for teaching early endoscopy skills to veterinarians,” *Journal of Veterinary Medical Education*, vol. 47, no. 1, pp. 106–116, 2020.

[13] X. Xu, P. Guo, J. Zhai, and X. Zeng, “Robotic kinematics teaching system with virtual reality, remote control and an on-site laboratory,” *International Journal of Mechanical Engineering Education*, vol. 48, no. 3, pp. 197–220, 2020.

[14] P. W. Chang, B. C. Chen, C. E. Jones, K. Bunting, C. Chakraborti, and M. J. Kahn, “Virtual reality supplemental teaching at low-cost (VRSTL) as a medical education adjunct for increasing early patient exposure,” *Medical Science Educator*, vol. 28, no. 1, pp. 3-4, 2018.

[15] J. Zhang and Y. Zhou, “Study on interactive teaching laboratory based on virtual reality,” *International Journal of Continuing Engineering Education and Life Long Learning*, vol. 30, no. 3, pp. 313–326, 2020.

[16] R. Ramlogan, A. U. Niazi, R. Jin, J. Johnson, V. W. Chan, and A. Perlas, “A virtual reality simulation model of spinal ultrasound,” *Regional Anesthesia and Pain Medicine*, vol. 42, no. 2, pp. 217–222, 2017.

[17] Y.-C. Hsu, “Exploring the learning motivation and effectiveness of applying virtual reality to high school mathematics,” *Universal Journal of Educational Research*, vol. 8, no. 2, pp. 438–444, 2020.

[18] J. D. Anacona, E. E. Millán, and C. A. Gómez, “Aplicación de los metaversos y la realidad virtual en la enseñanza,” *Entre ciencia e ingeniería*, vol. 13, no. 25, pp. 59–67, 2019.

[19] P. Calvert, “Virtual reality as a tool for teaching library design,” *Education for Information*, vol. 35, no. 4, pp. 439–450, 2019.

[20] J. Morimoto and F. Ponton, “Virtual reality in biology: could we become virtual naturalists?” *Evolution: Education and Outreach*, vol. 14, no. 1, pp. 1–13, 2021.

[21] D. Checa and A. Bustillo, “Advantages and limits of virtual reality in learning processes: briviesca in the fifteenth century,” *Virtual Reality*, vol. 24, no. 1, pp. 151–161, 2020.

[22] B. Sung, E. Mergelsberg, M. Teah, B. D’Silva, and I. Phau, “The effectiveness of a marketing virtual reality learning simulation: a quantitative survey with psychophysiological measures,” *British Journal of Educational Technology*, vol. 52, no. 1, pp. 196–213, 2021.

Hindawi
Scientific Programming
Volume 2021, Article ID 7613511, 9 pages
https://doi.org/10.1155/2021/7613511

Research Article

Network Course Recommendation System Based on Double-Layer Attention Mechanism

Qianyao Zhu

Education Information Network Center, Guizhou Education University, Guiyang, Guizhou 550018, China

Correspondence should be addressed to Qianyao Zhu; zhuqianyao@gznc.edu.cn

Received 20 October 2021; Revised 3 November 2021; Accepted 9 November 2021; Published 16 December 2021

Academic Editor: Le Sun

In view of the lack of accurate recommendation and selection of courses on the network teaching platform in the new form of higher education, a network course recommendation system based on the double-layer attention mechanism is proposed. First of all, the collected data are preprocessed, while the data of students and course information are normalized and classified. Then, the dual attention mechanism is introduced into the parallel neural network recommendation model so as to improve the model's ability to mine important features. TF-IDF (term frequency-inverse document frequency) based on the student score and course category is improved. The recommendation results are classified according to the weight of course categories, so as to construct different types of course groups and complete the recommendation. The experimental results show that the proposed algorithm can effectively improve the model recommendation accuracy compared with other algorithms.

1. Introduction

At present, online learning has become a common way of learning. Students do not have to be limited by the physical classroom; instead, they can break through the traditional time and space free choice of learning [1]. Online learning platforms emerge one after another, bringing great convenience to people. In the context of the new form of intelligent education [2, 3], the teaching platform that recommends online courses through the analysis of historical behavioral data has become the mainstream of the "Internet + education" model [4].

In the online learning environment, students need to spend tremendous time searching and browsing to confirm whether they are interested in the resources. Therefore, the problem of knowledge overload inevitably arises. An effective way to solve the problem of knowledge overload is to use a personalized recommendation algorithm [5]. After years of development, the performance of the recommendation system has greatly improved. Currently, recommendation algorithms are mainly divided into the collaborative filtering-based recommendation algorithm [6], content-based recommendation algorithm [7], and hybrid recommendation algorithm [8]. The recommendation algorithm based on collaborative filtering finds similar users by acquiring their historical behavior and rating data and by capturing the likes and dislikes of similar users and recommending items that users have not seen before. Content-based recommendation algorithms are mainly based on the items or ratings that users have selected and also based on the user's historical behavior information to find similar projects to recommend. The hybrid recommendation algorithm will fuse different recommendation algorithms and then recommend to get better recommendation effect. As data grow, so do the types of data. Traditional recommendation algorithms cannot learn the deep features of users or projects. How to make full use of multisource heterogeneous data to improve the performance of recommendation system has become a hot topic of recommendation system research [9].

In recent years, deep learning has its own strong learning ability and has been widely applied in image recognition [10, 11], speech recognition [12, 13], natural language processing [14, 15], and other fields [16]. Deep learning is good at mining and learning the deep features of multisource heterogeneous data. By combining it with the recommendation system, the hidden features of user and project attributes can be learned more efficiently [17]. Therefore, more and more researchers apply deep learning to the recommendation system. Although the application of neural network to the recommendation system can effectively improve the recommendation performance, not all feature interactions can contribute to the prediction results. For example, learning user or project features interacting with useless features may introduce noise and thus affect the performance of the recommendation system [18].

The teaching recommendation system algorithm is mainly based on content recommendation and collaborative filtering recommendation. For example, Yao et al. [19] introduced the application of three-dimensional biased weight tensor decomposition in teaching recommendation. Jie-Guang et al. [20] introduced a teaching optimization and research mode of rectangular neighborhood structure. Hou et al. [21] introduced WebGIS course teaching evaluation based on the dynamic adaptive teaching and learning optimization algorithm. Guan et al. [22] introduced the design and implementation of an open platform for dynamic mathematical and digital resources.

In view of the lack of accurate recommendation and selection of courses on online teaching platforms, the main work and innovations of this paper are as follows:

(1) An online course recommendation system based on the double-layer attention mechanism is proposed. By introducing the double-layer attention mechanism into the parallel neural network recommendation model, the model's ability to mine important features is improved.

(2) Reset the weight of the preprocessed course text information. The student feature vectors and course feature vectors learned by a multilayer fully connected neural network were input into the second-layer attention mechanism, and the multilayer perceptron was used to parameterize the attention score.

Finally, the curriculum attribute dataset is used to conduct curriculum recommendation experiments, and the accuracy of the proposed method in curriculum recommendation is compared and verified.

The structure of this paper is as follows. Section 2 focuses on the proposed algorithm model in this paper. Section 3 describes the experiment and analysis. Section 4 lists the conclusion.

2. The Proposed Model

A neural collaborative filtering (NCF) model uses a parallel neural network to learn user and project potential feature vectors, respectively [23]. In the prediction layer, the implicit vector is mapped to the predicted value by a multilayer perceptron (MLP). The NCF model uses the MLP to extract higher order feature information to improve the recommendation ability of the model. In the process of feature interaction, not all feature interactions can contribute to the prediction results, and the different effects of items in the historical interaction sequence on the current prediction are ignored. Therefore, this paper introduces the attention mechanism into the neural network to assign personalized weight to the items of historical interaction sequence and improves the model.

On the basis of the NCF recommendation model, attribute information of students and online courses is taken as input data u: $\{u_1, u_2 \ldots {}_2u_n\}$ and v: $\{v_1, v_2 \ldots v_n\}$, respectively. The algorithm model architecture of this paper is shown in Figure 1.

A double-layer attention mechanism is introduced, and the first layer is used to combine with the convolutional neural network (CNN) to build a subnetwork so that the CNN can learn the key content in the online course text. The other layer takes student and online course feature vectors as input data and uses the attention mechanism to assign personalized weight to the students' history interactive online course. Then, the effect of different online courses on the current prediction preference can be obtained. The recommendation results are grouped and shown to students in the form of the online course group to enhance the order of the recommendation content.

2.1. Learning the Underlying Characteristics.

To solve the problem of sparse data in the recommendation system, the attribute information of students and online courses is used to predict scores. After data preprocessing, the attribute information of students and online courses is input into the embedded layer to encode the attribute information. The embedding layer maps the input sparse vector to a dense low-dimensional embedding vector and obtains the embedding representations ρ_u and σ_v of student and online course attributes. At the beginning of the training, the embedding is simply selected randomly. As the training goes on, each embedded vector will be updated to help the neural network perform its task.

The embedding vectors ρ_u and σ_v of students and online courses are input into the parallel multilayer fully connected neural network to learn the potential feature vectors of nontext attributes of students and online courses, respectively:

$$\begin{aligned}\widehat{\rho}_u &= f\left(w_{u2} f\left(w_{u1}\rho_u + d_{u1}\right) + d_{u2}\right),\\ \widehat{\sigma}_v &= f\left(w_{v1}\rho_v + d_{v1}\right),\end{aligned} \tag{1}$$

where $f(\cdot)$ is the tanh activation function and w_v and d_u are the weight matrix and bias to be learned, respectively.

2.2. Convolutional Neural Network with Attentional Mechanism.

The text information of the attributes of online courses includes the title of online courses. In order to enhance the network's ability to learn the key content in the text, the attention mechanism is combined with the CNN to form a subnetwork to extract text features. The text convolutional neural network is composed of an attention layer, a convolutional layer, a pooling layer, and a full connection layer, as shown in Figure 2.

The attention layer assigns attention weight to the word vector matrix of each online course text to obtain the

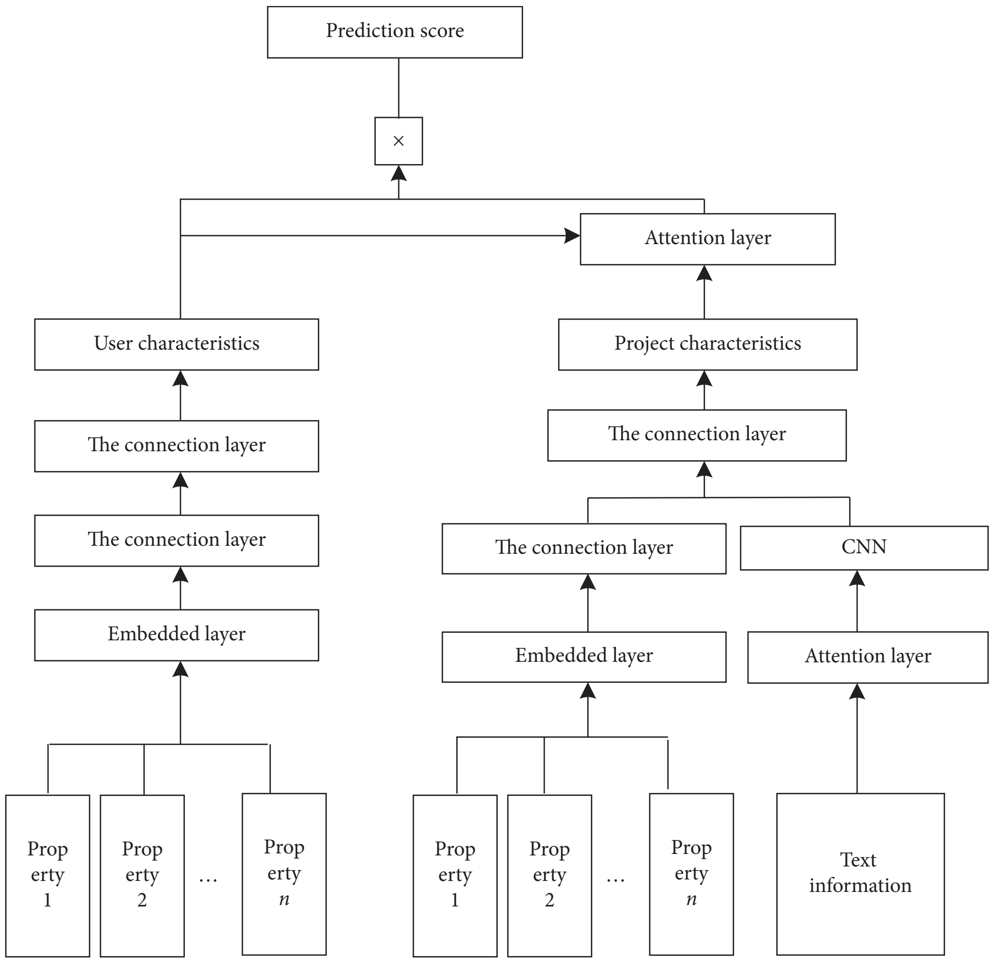

Figure 1: Architecture of the proposed algorithm in this paper.

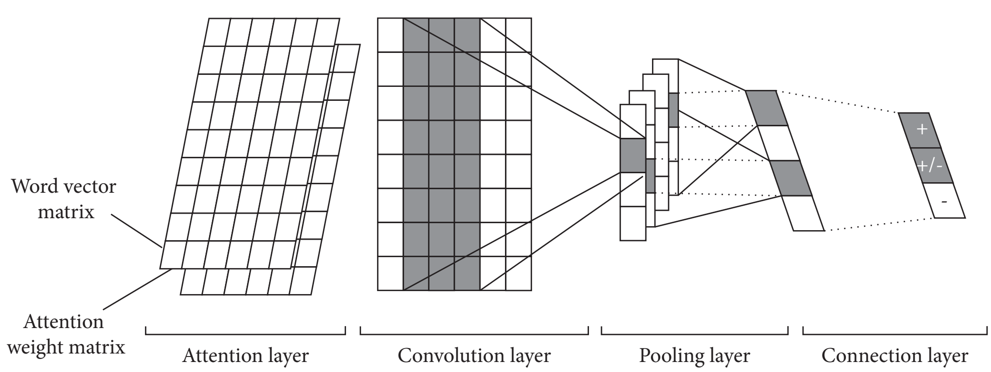

Figure 2: Text convolutional neural network.

updated word vector matrix. The word vector matrix $E \in \mathbb{R}^{n\times k}$ is obtained by embedding the text content of online course. K is the dimension of word vector, that is, every word is mapped to a K-dimensional vector $\alpha_x \in \mathbb{R}^k$. n is the number of words. $F \in \mathbb{R}^{n\times k}$ represents the word vector matrix of the text information carried by all the online courses browsed by the target student u_x. α_x is the word vector of the ith word indicating $\alpha_x \in \mathbb{R}^k$. The word vector representation α_x of each word in the word vector matrix F of target students and the attention score of each word α_x in the word vector matrix E of all texts of online courses are calculated:

$$c\left(\alpha_x, \alpha_y\right) = v_c^T R\left(w_c\left[\alpha_x \oplus \alpha_y\right]\right), \tag{2}$$

where v_c^T and w_c are training parameters.

The attention score of $c(\alpha_x, \alpha_y)$ is normalized by Softmax function, and the attention weight aiJ corresponding to each word vector is obtained:

$$c_{xy} = s\left(c\left(\alpha_x, \alpha_y\right)\right) = \frac{\exp\left(c\left(\alpha_x, \alpha_y\right)\right)}{\sum_{y=1}^{n} \exp\left(c\left(\alpha_x, \alpha_y\right)\right)}, \tag{3}$$

where $c_{xy} \in C^{s\times k}$ is the attention weight value. The vector splicing operation of the attention weight matrix $C^{s\times k}$ and original word vector matrix F is carried out. The updated network course word vector matrix M_{att} will be obtained as the input matrix of the convolutional neural network:

$$M_{att} = C \odot F. \tag{4}$$

In the convolution layer, each neuron slides from the leftmost of the matrix F_{att} to the right along the direction of the sentence by the convolution kernel $F \in \mathbb{R}^{k\times m}$. The window size of convolution kernel F_y is set to m, and the feature representation of each word in the sentence is obtained after the convolution operation. Feature graphs are formed by activation functions. The y-th neuron produces features as shown in the following equation:

$$H_y = f\left(M^{s\times k} * F_y + d_y\right), \tag{5}$$

where $*$ is the convolution operation, d_y is the offset term, and f is the nonlinear activation function ReLU; the nonlinearity of the convolutional neural network is enhanced through the activation function f:

$$R(\alpha) = \max(0, \alpha). \tag{6}$$

Select maximum pooling to pool the output results of the convolution layer. The feature graph is divided into several rectangular regions, and the maximum value is output for each subregion. Maximum pooling removes unimportant or repetitive features in each subarea for the current task and retains information that can express text features. The pooling result of the y-th convolution kernel is shown in the following equation:

$$h_y' = \max\left\{h_1, h_2, h_3, \ldots, h_y^{k-m+1}\right\}. \tag{7}$$

The pooled output is input to the full connection layer, multiplied by the weight matrix of the full connection layer, and added with a bias sum. Classification output is obtained after ReLU activation function; the hidden features of online course text information are as follows:

$$\sigma_{\text{text}} = R\left(w_y h_y' + d_y\right), \tag{8}$$

where w_y is the weight coefficient of the full connection layer and d_y is the offset term. Assume that the nontext attribute feature vector $\widehat{\sigma}_v$ of online courses can be connected to the text feature vector σ_{text} to obtain the online course feature $\widehat{\sigma}_y$:

$$\widehat{\sigma}_y = h\left(\widehat{\sigma}_v, \sigma_{\text{text}}\right). \tag{9}$$

2.3. Prediction Score. Traditional recommendation models typically perform the interaction between the implicit representation of $\widehat{\rho}_u$ of student characteristics and $\widehat{\sigma}_y$ of online course characteristics to obtain the final predicted grade. Due to the lack of customized optimization of the recommendation task, the equal treatment of all the history online courses will limit the representation ability of the model. The traditional neural network recommendation model ignores that different online courses of student history play different roles in predicting the next online course, so the accuracy is low.

In the prediction layer of the algorithm model in this paper, a neural attention network is used to distinguish the importance of history network courses to overcome the limitations of the traditional neural network recommendation model. Learn the tacit representation of $\widehat{\rho}_u$ of student characteristics and $\widehat{\sigma}_y$ of online course characteristics as the input of the attention layer. The attention of target students to different online courses has different effects on predicting the next online course. The attention score of the student u_x to the online course v_y is shown in the following equation:

$$s_h\left(\widehat{\rho}_u, \widehat{\sigma}_y\right) = R_e\left(w_1\left(\widehat{\rho}_u \odot \widehat{\sigma}_y\right) + d_1\right), \tag{10}$$

where w_1 and d_1 are the weight matrix and bias term to be learned. The nonlinear relation of the current online course to predict the next online course is obtained by Re activation function. $s_h(\widehat{\rho}_u, \widehat{\sigma}_y)$ indicates that the student u_x pays more attention to the online course v_y. The online course v_y plays an important role in predicting the next online course. Softmax function was used to normalize the attention score $\widehat{c}_{xy}$:

$$\widehat{c}_{xy} = \frac{\exp\left(s_h\left(\widehat{\rho}_u, \widehat{\sigma}_y\right)\right)}{\sum_{y\in R(u)} \exp\left(s_h\left(\widehat{\rho}_u, \widehat{\sigma}_y\right)\right)}, \tag{11}$$

where $\widehat{c}_{xy}$ is the contribution degree of online course v_y to students' u_x preference curve and $R(u)$ indicates the historical interactive network course set of the student u_x. The weight of $\widehat{\sigma}_y$ is implicitly reassigned to course characteristics as follows:

$$\widehat{\sigma}_x = \sum_{y\in R(u)} \widehat{c}_{xy} \widehat{\sigma}_y. \tag{12}$$

As the inner product of student bearing $\widehat{p}$up^u and online course bearing $\widehat{\sigma}_x$ is calculated, the predicted score can be obtained as shown in the following equation:

$$\widehat{\beta}_{ux} = \widehat{\rho}_u^T \widehat{\sigma}_x. \tag{13}$$

The mean square error (MSE) was used as a loss function to minimize the gap between the real score and the predicted score during the training of the model:

$$L_{\text{sqr}} \geq \sum_{(u,\lambda)\in R(u)} \left(\beta_{ux} - \widehat{\beta}_{ux}\right)^2, \tag{14}$$

where β_{ux} marks students' real online courses and $\widehat{\beta}_{ux}$ estimates the scores students have for online courses. The objective function was optimized by using the stochastic gradient descent method to minimize the loss function, and the weight w_n and bias d_n of each layer were optimized by using the backpropagation algorithm. After the neural network training is completed by the algorithms above, the model is used to predict students' grading of ungraded online courses. Recommendations are made to target students according to the predicted score size. The recommendation results are used for subsequent grouping to realize online course group recommendation.

2.4. Improved TF-IDF Method. TF-IDF is often used for text classification and information retrieval. TF-IDF generally considers only the number of documents and the frequency with which keywords appear in documents. When words have score data, they cannot make full use of score data to calculate TF-IDF values more accurately. The scoring data are introduced into the TF-IDF method to avoid losing words with high scores while evaluating the importance of words. The improved TF-IDF method is shown in the following equation:

$$S_{u_y,w_x} = \frac{\sum_{s=1}^{n} r_{u_y v_s^{v_x}}}{\sum_{s=1}^{n} r_{u_y,v_s}} lb \frac{|K|}{\left|\left\{y\colon w_x \in k_y\right\}\right|}, \quad (15)$$

where S_{u_y,w_x} is the importance of w_x to student u_y, ranging from 0 to 1; $\sum_{s=1}^{n} r_{u_y v_s^{v_x}}$ is the score of the file containing the words w_x; $\sum_{s=1}^{n} r_{u_y,v_s}$ is the score sum of all files; $|K|$ is the total number of files in the database; and $|\{y\colon w_x \in k_y\}|$ is the number of all files. According to the dataset of the online course, scoring data are determined and obtained as r_{u_y,v_s}. S_{u_y,w_x} is calculated based on the score data of the history online courses of the designated students in the training set. The improved TF-IDF is used to calculate the TF-IDF value of the types of online courses contained in the recommendation results, and the group recommendation of online courses is realized by obtaining students' preference for different types.

The first part of equation (15) is term frequency calculation of TF-IDF. The predicted score was used to calculate the score of online courses containing file WI and its proportion in the total file score sum. When the number is large, it indicates that the score of the file containing w_x is higher, which reflects the importance of w_x to some extent. The second part is the inverse document frequency of TF-IDF. The more the number of files contain words w_x in the total number of database files, the more weak the importance of TF will be w_x. S_{u_y,w_x} is obtained by multiplying the two parts, and the w_x value indicates students' preference for the word.

Based on the improvement of the TF-IDF algorithm, this paper analyzes the types of online courses in the recommendation results, obtains the importance of different types of online courses to students, and realizes the automatic grouping of recommendation results. The same online courses from the top-N recommendation results were placed into the same group. Students' favorite type of online courses will be recommended first, so that students can quickly find content that matches their interests. The specific implementation steps of the improved TF-IDF algorithm are as follows:

Step 1: calculate the word frequency in the specific file k_y, including the word w_x score of the online course and the proportion of the score and sum of all online courses in the students' browsing history:

$$\mathrm{TF}_{y,x} = \frac{\sum_{s=1}^{n} r_{u_y v_s^{w_x}}}{\sum_{s=1}^{n} r_{u_y,v_s}}. \quad (16)$$

Step 2: calculate the reverse file frequency index. Divide the number of centralized online courses by the number of online courses containing the word w_x and then take the logarithm of the quotient:

$$\mathrm{IDF}_x = lb \frac{|K|}{\left|\left\{y\colon t_x \in k_y\right\}\right|}. \quad (17)$$

Step 3: multiply word frequency and reverse file word frequency to obtain the TF-IDF value of w_x in the file S_{u_y,w_x}:

$$S_{u_y,w_x} = \mathrm{TF}_{y,x} \times \mathrm{IDT}_x. \quad (18)$$

The improved TF-IDF uses score data to reflect the proportion of word w_x in the file k_y when calculating word frequency.

2.5. Grouping the Recommended Results. The improved TF-IDF method was used to obtain students' preference for different types of online courses. Taking online course recommendation as an example, the CourseLens dataset is used to test the algorithm. The word frequency information of online course types is shown in Table 1. First of all, N online courses are recommended to students. Second, the online course information document $M = \{m_1, m_2, \ldots, m_N\}$. Extract the network course types contained in the network course information documents and establish the network course type information documents $G = \{g_1, g_2, \ldots, g_N\}$. Finally, the word frequency statistics of online course type documents are made to obtain the word frequency information of online course type in the recommended results.

When the recommended online course m_s contains the online course type, the value of Rm_s, g_x is 1. Otherwise, the value is 0. The improved TF-IDF is used to analyze the word frequency information of online course types and predict students' preference for different online course types, as shown in the following equation:

$$S_{u_y,g_x} = \frac{\sum_{s=1}^{n} r_{u_y,m_s} \times R_{m_s,g_x}}{\sum_{s=1}^{n} r_{u_y,m_s}} lb \frac{N}{\sum_{s=1}^{n} R_{m_s,g_x}}, \quad (19)$$

where r_{u_y,m_s} is the scores of the student u_y on the online course m_s, R_{m_s,g_x} indicates whether the online course m_s contains type g_x, N is the number of online courses with recommended results, and S_{u_y,g_x} is students' preference for different types of online courses.

The types of online courses are arranged in descending order according to their preference degree S_{u_y,g_x}, and the first

Table 1: Word frequency information of course types.

Course	Type			
	g_1	g_2	...	g_x
m_1	Rm_1, g_1	Rm_1, g_2	...	Rm_1, g_x
m_2	Rm_2, g_1	Rm_2, g_2	...	Rm_2, g_x
...	...	...		...
m_s	Rm_s, g_1	Rm_s, g_2	...	Rm_s, g_x

K types are taken as the group name of the online course group to be recommended, namely, $L = \{L_1, L_2 \ldots, L_K\}$, where L represents the set of online course groups to be recommended. Add D online courses of the same type to each online course group. The online courses in L_K are derived from the recommendation results generated by the algorithm model in this paper. The online courses in the online course group are arranged in descending order according to the predicted score. Finally, K online course groups are formed, and each online course group contains online course group recommendation of the same type of online course in part D.

3. Experiment

3.1. Experimental Environment and Dataset. The experiment was carried out in PyCharm integrated development environment on a 64 bit Windows 10 system. Versions of Python and TensorFlow deep learning frameworks are 3.7.9 and 1.8.0. The CPU of the computer is 3.50 GHz Intel Core i7-7800, and the memory is 32 GB.

The experiment used data from an online learning platform. Through collection and collation, the dataset of 500 students, 700 online courses, and 35,000 scoring records was finally formed. As the collected data have both structured and unstructured data, it is necessary to preprocess the data. First of all, the data are classified, and different processing methods are selected for different classification using group student ID, online course ID, the number of studies, and grade value. As the types of students, grades, and categories of online courses are classified information, they are classified as one class. Then, the values of each field are digitized. Since the name and description information of online courses are both text information and cannot be quantified, they are classified as one class.

There are three stages to realize the recommendation: the first stage is data preprocessing, the second stage is the construction and training of deep neural networks, and the third stage is the generation of the recommendation list.

(1) Data preprocessing. Since the data used are not all of digital form, such as the type of students and the category of online courses, these data cannot be directly input into the network; instead, they need to be transformed into vector representation.

(2) Building and training the network model. First, a deep neural network is constructed. On this basis, the data processed in the previous step are divided into training sets and test sets. In this experiment, 80% of the datasets are used as training sets and 20% of the datasets are used as test sets.

(3) Generating a recommendation list. The trained model was used to predict scores. Finally, the top-N online courses are recommended for students according to the rank of scoring value.

3.2. Evaluation Indicators. There are many evaluation indexes based on the top-N recommendation algorithm. The HR (hit ratio), NDCG (normalized discount cumulative gain), RMSE (root mean square error), and MAE (mean absolute error) will be used in this experiment.

The calculation equation of HR is as follows:

$$\mathrm{HR}(N) = \frac{\left|\rho \in \text{testset} \,\&\, \rho \in R_N\right|}{|\text{testset}|}, \tag{20}$$

where P represents the online courses in the test set, $\rho \in \text{testset}\&\rho \in R_N$ indicates that online courses in the test set are also in the top-N recommended set, and testset indicates the number of test sets.

The NDCG is widely used in the evaluation tasks of recommendation ranking and information index ranking. It is a kind of evaluation index sensitive to ranking position. The more relevant the ranking is, the bigger the corresponding NDCG will be. First, the DCG is introduced, and its calculation equation is as follows:

$$\mathrm{DCG}_n = \sum_{x=1}^{n} \frac{2^{\mathrm{rel}_x - 1}}{\log_2(x+1)}, \tag{21}$$

where rel_x is the relevance of the first online course to students. In this experiment, if the online course is a positive sample, the correlation degree is 1, while the negative sample has a correlation degree of 0. If more relevant online courses are ranked later, the overall DCG will be smaller.

Each student's recommendation is ranked by an ideal value, which is ranked from most relevant to least relevant. This is the minimum IDCG that each student can calculate. Thus, the NDCG can be calculated by the following equation:

$$\mathrm{NDCG}_n = \frac{\mathrm{DCG}_n}{\mathrm{IDCG}_n}. \tag{22}$$

The NDCG has a value between 0 and 1, and the larger the value, the better the recommendation effect.

The RMSE and MAE are calculated as follows:

$$\begin{aligned} \mathrm{RMSE} &= \sqrt{\frac{\sum_{u,x\in T}\left(r_{ux} - \hat{r}_{ux}\right)^2}{|T|}}, \\ \mathrm{MAE} &= \frac{\sum_{u,x\in T}\left|r_{ux} - \hat{r}_{ux}\right|}{|T|}, \end{aligned} \tag{23}$$

where T is the number of online courses with scoring records in the test set.

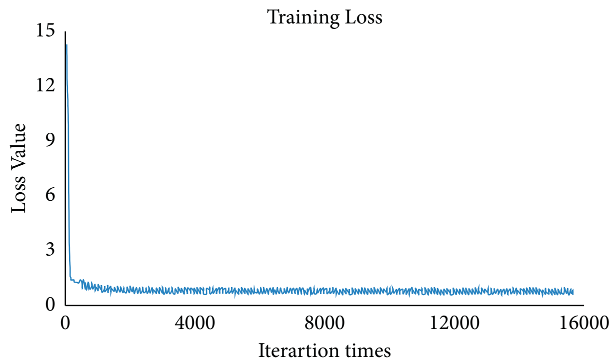

Figure 3: Loss value of the proposed method.

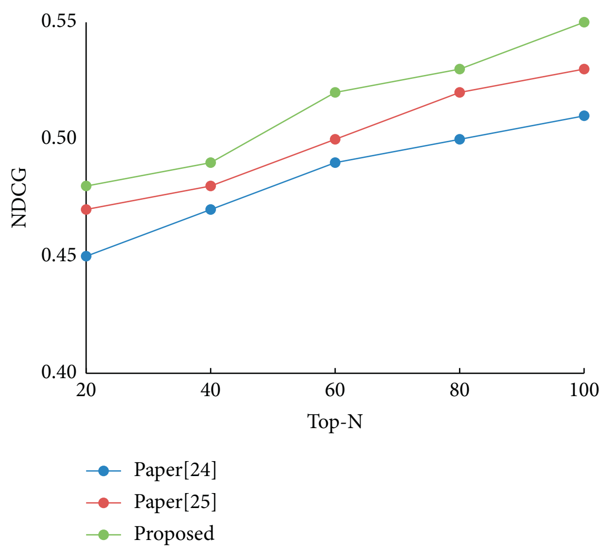

Figure 4: Comparison results of the NDCG index.

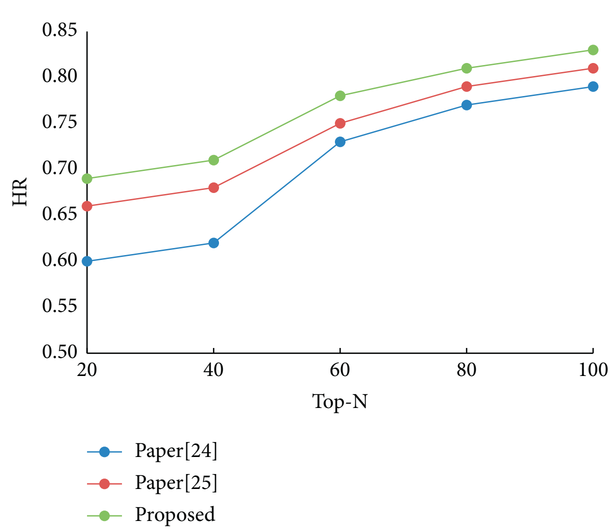

Figure 5: Comparison results of the HR index.

3.3. Experimental Results and Analysis. In order to verify the effectiveness of the algorithm in this paper, MAE function was used for training in the experiment. It can be seen from the Figure 3 that, with the increase of iteration times, the MAE value gradually decreases to 0.69. The algorithm model in this paper, which combines student attributes, online course attributes, and content description information, has more complete data and tends to reduce errors. Therefore, the model in this paper has certain validity (Figure 3).

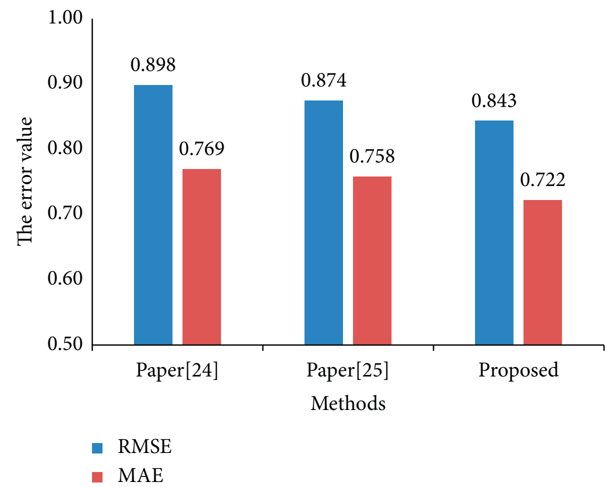

Figure 6: Comparison results of RMSE and MAE indexes.

Next, the algorithm in this paper is analyzed and compared with other algorithms [24, 25]. In order to test the influence of top-N number on the recommendation effect, the values of N were set as 20, 40, 60, 80, and 100, respectively. The NDCG and HR were analyzed, respectively. The experimental results are shown in Figures 4 and 5. It can be seen that, with the increase of top-N number, NDCG and HR indicators of these three algorithm models are constantly improved. The performance indexes of the proposed algorithm are all higher than those of other algorithm models, indicating that the proposed algorithm model has a better recommendation effect.

The comparison of the RMSE and MAE between online course group recommendation and other recommendation algorithms is shown in Figure 6. The RMSE and MAR values of the proposed algorithm are higher than those of other algorithms. This further indicates that the proposed algorithm can improve the accuracy of the recommendation algorithm by extracting implied features of students and online courses after referring to the attention mechanism.

4. Conclusion

This paper proposes a kind of online course recommendation system based on the double-layer attention mechanism, aiming to solve the problem of lack of precise guided course selection in the existing network platform. The feature extraction ability of the convolutional neural network is improved by introducing the two-level attention mechanism into the convolutional neural network. Different preference weights are assigned to curriculum features to achieve a recommendation method more in line with students' preferences. In course recommendation to target students, score data and network course type data are combined to complete the grouping of recommendation results. The experimental results show that the system achieves better performance in the NDCG, HR, RMSE, and MAE, which provides necessary theoretical support for the accurate selection of course guidance on the network platform. The analysis and optimization of algorithm efficiency is the direction of further research.

Data Availability

The labeled datasets used to support the findings of this study are available from the author upon request.

Conflicts of Interest

The author declares that there are no conflicts of interest.

Acknowledgments

This work was supported by the study on the Practice of Improving Information Technology Application Ability of College Teachers in the Context of Education Informatization 2.0 (no. 20190202047069) and in part by the study on the Measurement Model of Teaching Proximity in Online Courses in Higher Education (no. 19GZQN26).

References

[1] L. Dunlop, L. Clarke, and V. McKelvey-Martin, "Free-choice learning in school science: a model for collaboration between formal and informal science educators," *International Journal of Science Education, Part B*, vol. 9, no. 1, pp. 13–28, 2019.

[2] S. Ali, B. H. Payne, R. Williams, and C. Breazeal, "Constructionism, ethics, and creativity: developing primary and middle school artificial intelligence education," in *Proceedings of the International Workshop on Education in Artificial Intelligence K-12 (EDUAI'19)*, pp. 1–4, Austria, Hungary, 2019.

[3] K. Kim, "An artificial intelligence education program development and application for elementary teachers," *Journal of the Korean Association of Information Education*, vol. 23, no. 6, pp. 629–637, 2019.

[4] K. Ren and Y. Bai, "Research on innovative methods of college students' sports teaching based on internet education technology," *Educational Sciences: Theory and Practice*, vol. 18, no. 5, p. 2486, 2018.

[5] X. Xiaoli, H. Hui, W. Mengmeng, L. Yu, Y. Ziheng, and W. Yingfeng, "Development of personalized learning resources recommendation system based on knowledge graph," *International Journal of Educational Technology and Learning*, vol. 10, no. 2, pp. 68–72, 2021.

[6] L. Wu, X. He, X. Wang, and K. Zhang, "A survey on neural recommendation: from collaborative filtering to content and context enriched recommendation," 2021, https://arxiv.org/abs/2104.13030.

[7] J. Shu, X. Shen, H. Liu, B. Yi, and Z. Zhang, "A content-based recommendation algorithm for learning resources," *Multimedia Systems*, vol. 24, no. 2, pp. 163–173, 2018.

[8] Y. Tian, B. Zheng, Y. Wang, Y. Zhang, and Q. Wu, "College library personalized recommendation system based on hybrid recommendation algorithm," *Procedia CIRP*, vol. 83, pp. 490–494, 2019.

[9] A. M. Elkahky, Y. Song, and X. He, "A multi-view deep learning approach for cross domain user modeling in recommendation systems," in *Proceedings of the 24th International Conference on World Wide Web*, pp. 278–288, Florence, Italy, May 2015.

[10] J. Huixian, "The analysis of plants image recognition based on deep learning and artificial neural network," *IEEE Access*, vol. 8, Article ID 68828, 2020.

[11] T. Shen, C. Gao, and D. Xu, "The analysis of intelligent real-time image recognition technology based on mobile edge computing and deep learning," *Journal of Real-Time Image Processing*, vol. 18, no. 4, pp. 1157–1166, 2021.

[12] A. Santhanavijayan, D. Naresh Kumar, and G. Deepak, "A semantic-aware strategy for automatic speech recognition incorporating deep learning models," in *Advances in Intelligent Systems and Computing*, pp. 247–254, Springer, Berlin, Germany, 2021.

[13] H. Veisi and A. Haji Mani, "Persian speech recognition using deep learning," *International Journal of Speech Technology*, vol. 23, no. 4, pp. 893–905, 2020.

[14] A. Torfi, R. A. Shirvani, Y. Keneshloo, N. Tavaf, and E. A. Fox, "Natural language processing advancements by deep learning: a survey," 2020, https://arxiv.org/abs/2003.01200.

[15] D. W. Otter, J. R. Medina, and J. K. Kalita, "A survey of the usages of deep learning for natural language processing," *IEEE Transactions on Neural Networks and Learning Systems*, vol. 32, no. 2, pp. 604–624, 2020.

[16] Q. Yuan, H. Shen, T. Li et al., "Deep learning in environmental remote sensing: achievements and challenges," *Remote Sensing of Environment*, vol. 241, Article ID 111716, 2020.

[17] S. Minaee, N. Kalchbrenner, E. Cambria, N. Nikzad, M. Chenaghlu, and J. Gao, "Deep learning--based text classification," *ACM Computing Surveys*, vol. 54, no. 3, pp. 1–40, 2021.

[18] H. J. Xue, X. Dai, and J. Zhang, "Deep matrix factorization models for recommender systems," in *Proceedings of the International Joint Conferences on Artificial Intelligence (IJCAI 2017)*, vol. 17, pp. 3203–3209, Melbourne. Australia, August 2017.

[19] D. H. Yao, L. I. Shi-Jun, and H. U. Ya-Hui, "A three-dimensional partial weight tensor model for teaching recommendation," *Journal of University of Electronic Science and Technology of China*, vol. 46, no. (5), pp. 747–754, 2017, https://doi.org/10.3969/j.issn.1001-0548.2017.05.018.

[20] H. E. Jie-Guang, Z. P. Peng, W. H. Lin, and D. L. Cui, "A teaching-learning-based optimization algorithm with rectangle neighborhood structure," *Acta Electronica Sinica*, vol. 47, no. 8, pp. 1768–1775, 2019.

[21] J.-w. Hou, K.-l. Jia, and X.-j. Jiao, "Teaching evaluation on a WebGIS course based on dynamic self-adaptive teaching-learning-based optimization," *Journal of Central South University*, vol. 26, no. 3, pp. 640–653, 2019.

[22] H. Guan, X. Qin, and Y. Rao, "Research and design of dynamic mathematical digital resources open platform," *Journal of Harbin Institute of Technology*, vol. 51, no. 5, 22 pages, 2019.

[23] X. He, L. Liao, H. Zhang, and L. Nie, “Neural collaborative filtering,” in *Proceedings of the 26th International Conference on World Wide Web*, pp. 173–182, Perth, Australia, April 2017.

[24] X. He, Z. He, J. Song, Z. Liu, Y.-G. Jiang, and T.-S. Chua, “NAIS: neural attentive item similarity model for recommendation,” *IEEE Transactions on Knowledge and Data Engineering*, vol. 30, no. 12, pp. 2354–2366, 2018.

[25] Y. Zhu, H. Lu, P. Qiu, K. Shi, J. Chambua, and Z. Niu, “Heterogeneous teaching evaluation network based offline course recommendation with graph learning and tensor factorization,” *Neurocomputing*, vol. 415, pp. 84–95, 2020.

Hindawi
Scientific Programming
Volume 2021, Article ID 4774140, 13 pages
https://doi.org/10.1155/2021/4774140

Research Article

Application of Data Mining in the Evaluation of Enterprise Lean Management Effect

Jinpeng Yang [1] and Ying Liu [2]

[1]School of Harbin Institute of Technology, Harbin 150001, China
[2]School of Business, Jinggangshan University, Jian 343009, China

Correspondence should be addressed to Ying Liu; liuying1979@jgsu.edu.cn

Received 31 October 2021; Revised 16 November 2021; Accepted 22 November 2021; Published 16 December 2021

Academic Editor: Le Sun

In order to improve the effect of enterprise lean management, this study proposes a lean data mining algorithm based on the characteristics of lean data in enterprise management. This study connects data mining and lean production to study the data of enterprise management operation, proposes an intelligent data processing model suitable for modern enterprise management, and constructs the model function module in combination with the enterprise operation management process. Moreover, this study constructs an evaluation system for the effect of enterprise lean management based on data mining. The system provides a human-computer interaction interface, and operators can use various functions and services provided by the system through a visual interface. Through experimental research, it can be known that the enterprise lean effect evaluation system based on data mining proposed in this study can play an important role in enterprise lean management.

1. Introduction

With the formation of China's position as the world's manufacturing center, the problem of how to improve the utilization of manufacturing resources and improve production efficiency has become increasingly prominent, and lean production has received increasing attention as a management method to eliminate waste and improve efficiency. In-depth promotion of the practice of lean production objectively requires some support from the related theoretical research of lean production [1]. It can be seen that both objective practice and theoretical circles need to further deepen lean-related research. In the 21st century, the methods and experience of achieving lean have become more abundant and mature. During this period, digital manufacturing has provided more powerful tools for the realization of lean and expanded the scope of application of lean thinking in manufacturing enterprises. In the past, we emphasized quality, efficiency, and cost control in the manufacturing process. However, in fact, the design process also needs to pursue high quality, high efficiency, and low cost. That is, we need to extend the "lean" thinking from manufacturing to design and use the best solution as much as possible in every link, step, and process of design. At the same time, it can accurately control and optimize the design process and state in the design activity, so as to achieve the highest product value and the lowest cost [2]. It is based on this demand that lean thinking is applied to the design stage, and the problems that may arise in the future operation of the enterprise will be eliminated from the design stage. This mode of operation can avoid the fundamental elimination of waste in the enterprise and avoid the "remedy" practice of improving after problems arise in the operation of the enterprise [3].

The continuous and dynamic economic and social competitive environment has intensified competition among enterprises and brought challenges to the survival and development of enterprises. How to deal with the dynamic changes of the current economic and social competitive environment has become one of the hot issues that academia and business circles pay attention to. It is generally believed that innovation is a powerful weapon for companies to survive and develop in a continuous dynamic environment. If companies want to occupy a favorable position in fierce competition, they must continue to innovate. Although the academic circles have different understandings of the innovation system, they all agree that management innovation and technological innovation are the indispensable content of the enterprise innovation system, and they are also the two cores of enterprise innovation. However, enterprise innovation is a systematic project, which requires not only technological innovation but also continuous promotion of management innovation.

Enterprises, especially manufacturing enterprises, as the engine of the country's industrialization and modernization, are the production departments with complex technology and the most advanced technologies. More than 7% of the scientific research funds in developed countries are used for the construction and research of manufacturing technology. It can be seen that technological innovation is of the importance of enterprises (especially manufacturing). However, because technological innovation can be clearly reflected in products, managers in enterprises pay too much attention to technological innovation and neglect management innovation, causing many enterprises to encounter bottlenecks in the middle of their development. The proposal of enterprise innovation tasks, the organization of power, the allocation of resources, the incentive and coordination of the process, etc., are inseparable from the management's strategic vision, innovation guidance, and mechanism support. Therefore, it can be said that management innovation is the locomotive of enterprise innovation. Many Chinese companies can design and trial produce advanced samples, but it is more difficult to ensure the quality of their mass production, and the unit consumption of resources is much higher than the international level, and the waste is large. At the same time, the personnel involved in innovation are also less, and these problems are also the main problems faced by most companies that adopt the strategy of in-line and external expansion to become stronger and bigger, because these companies are not facing the pressure of external expansion, but the pressure of in-line lean management innovation. The lean management idea with "full participation, continuous improvement, elimination of waste, creation of value, and stimulation of positive energy" as the core is derived from lean production and is a production organization based on the Toyota Production System (TPS) as a prototype. Based on this method, lean management is derived, that is, the use of lean thinking to manage various activities of the enterprise. This method provides an idea for enterprises to effectively solve management problems in the process of in-line development and promote enterprise management innovation.

2. Related Work

The literature [4] has conducted an in-depth study on the essence of Toyota's production management and found that if the company does not fully integrate lean thinking into the enterprise, the organization's cost management cannot find lean thinking. Based on the TOC theory and accounting system, an analysis model that combines the basic operating characteristics of lean production methods with the practical application of the enterprise management information system is proposed to achieve the goal of the lowest cost of the enterprise. The literature [5] puts forward the concept of lean accounting, which is based on the comparison of standard cost and value stream cost. The literature [6] proposed that value stream cost management can make enterprise cost decisions more accurate, so it has very important significance for lean enterprises.

Literature [7] designed a lean cost management system with wider applicability based on the Toyota cost accounting system. As a result, lean cost management began to prevail all over the world. Literature [8] proposes how to conduct cost management under the lean accounting system: cost management with value flow as the core does not require annual budgets, and the calculation of performance appraisal indicators is not based on historical data but is oriented to the future status of the enterprise. Literature [9] reviewed the development process of lean management and explained its connotation and proposed that lean cost management is based on the correct understanding of value flow, and the smooth flow of value flow is guaranteed. The vitality of lean cost management comes from continuous improvement and the pursuit of perfection. The key to this is that customers should act as the driving force of the value stream. Literature [10] puts forward the theoretical framework of lean cost management, aiming at low-cost, high-efficiency, and high-quality production, with just-in-time production and the self-consciousness of personnel as the pillars, to eliminate all waste from point to surface and be uninterrupted based on the improvement activities. Literature [11] puts forward the five basic principles of lean cost management: customers determine the product value structure, eliminate waste in the industrial value chain, turn batches and queues into a continuous flow, drive the value chain by customer demand, and pursue perfection. Literature [12] puts forward a lean accounting viewpoint that is different from the previous accounting viewpoints. Its goal is customer value, the core of management is value flow, and the ultimate goal is to eliminate waste. Taking value stream costing analysis and assessment as the entry point, the implementation process of lean accounting is discussed in depth and detail, which provides a highly operational guiding framework for lean enterprise cost management. From the perspective of lean management accounting, literature [13] explains the obstacles, such as corporate culture obstacles, financial role transition obstacles, educational background obstacles, and employee personal obstacles, encountered when applying lean accounting theory to implement cost management. Literature [14] summarizes the basic content of lean accounting, including value stream costing, analysis, and management and proposes the principles of lean accounting: group work, self-responsibility, and regular improvement. Literature [15] pointed out the inapplicability of the traditional accounting indicator system to lean organizations, thereby constructing a new performance measurement indicator system for lean organizations. The indicator system includes the value stream level and the production unit level and fully combines the characteristics of lean production. Literature [16] demonstrates the four-level structure model of lean cost management, lean basis, lean functions, lean methods, and lean objectives. Literature [17] believes that lean cost management can help Chinese companies effectively cope with the economic crisis and pointed out that lean cost management with the elimination of waste as the core embodies the spirit of innovation, shows corporate culture, and contains social responsibility. Literature [18] proposes that in the process of implementing lean cost management, enterprises must adhere to the four principles of combination: refinement, simplification and quantification, revenue increment and waste elimination, stock revitalization and incremental optimization, and local optimization and overall coordination. Literature [19] starts with the shaping of lean cost values and explains the importance and feasibility of lean construction. Literature [20] constructed a cost management system that focuses on value stream cost management, including cost decision-making, cost accounting, cost analysis, and cost assessment. Literature [21] proposes that lean cost management can effectively reduce waste in the production and operation of enterprises, has conducted research on improving the operation process of lean enterprises and the efficient use of lean cost management, and has provided operable applications for enterprises in management practice methods.

3. Lean Management Data Mining Algorithm

The time series is $X_1, X_2, \ldots, X_N$ with N-ordered observations that can be regarded as a part of the random process $\{X_t \mid t = 0, \pm 1, \pm 2\}$, and the observation value of the time series is $x_1, x_2, \ldots, x_N$.

Stationarity is the following: if the time series is $X_1, X_2, \ldots, X_N$, it can be called weakly stationary or second-order stationary. The following conditions need to be met: the mean value of X_t (mathematical expectation) does not change with time. That is, for any t, $E(X_t) = \mu$ (where μ is a constant). Moreover, for any lag period τ, the correlation coefficient between X_t and $X_{(t+\tau)}$ is $\mathrm{Cov}(X_t, X_{(t+\tau)}) = \gamma_t$, that is, the correlation coefficient only depends on τ and has nothing to do with time t. Obviously, the variance of a stationary time series is also a constant: $\mathrm{Var}(X_t) = \gamma_0$. In general practical applications, it is enough to focus on weak stationarity.

The backshift operator is as follows: B is defined as $By_t = t_{(t-1)}$. Obviously, $\nabla = 1 - B$. Among them, ∇ is the difference operator, and there is $\{X_1, X_2, \ldots, X_N\}$ for the sequence $\nabla_s X_t = X_t - X_{(t-s)}$. The backshift operator has the following properties:

$$\begin{aligned} B^s y_t &= y_{(l-s)}, \\ \frac{1}{(1-\alpha B)} y_t &= \left\{1 + \alpha B + \alpha^2 B^2 + \cdots\right\} y_t \\ &= y_t + \alpha y_{(t-1)} + \alpha^2 y_{(t-2)} + \cdots \text{ or } |\alpha < 1|. \end{aligned} \tag{1}$$

White noise is as follows: if all observations of sequence $\{w_t\}$ are independent and identically distributed, and other mean μ and variance σ^2 are finite constants, it is called white noise or pure random process. The definition of white noise is represented by the symbol:

$$w_t = ii\ d\left(\mu, \sigma^2\right). \tag{2}$$

If the distribution of white noise is a normal distribution with a mean value of 0, $\{w_t\}$ also becomes Gaussian white noise.

The MA model is as follows: it is assumed that $\{w_t\}$ is a white noise sequence with a mean value of 0 and a variance of σ^2. If the sequence $\{X_t\}$ satisfies,

$$X_t = \mu + w_t + \theta_1 w_{(t-1)} + \cdots + w_{(t-q)}. \tag{3}$$

Then, it is called the q-order MA process, that is, the q-order moving average process (moving average process), denoted as MA(q). If $\theta(B) = 1 + \theta_1 B_1 + \cdots + \theta_2 B^2 + \cdots + \theta_q B^q$, the model is

$$X_t = \mu + \theta(B) w_t. \tag{4}$$

AR model is as follows: the hypothesis is a white noise sequence with a $\{w_t\}$ mean value of 0 and a variance of σ^2. If the sequence $\{X_t\}$ satisfies,

$$X_t = \theta_1 X_{(t-1)} + \cdots + \theta_p X_{(t-p)} + w_t. \tag{5}$$

Then, it is called the p-order AR process, that is, the p-order autoregressive process (moving average process), denoted as AR(p). If the X_t mean value is not 0, the above equation is equivalent to

$$X_t = \alpha + \phi_1 X_{(t-1)} + \cdots + \phi_p X_{(t-p)} + w_t. \tag{6}$$

In the formula, $\alpha = (1 - \phi_1 + \cdots + \phi_p)\mu$. If $\phi(B) = 1 - \phi_1 B^1 - \phi_2 B^2 + \cdots - \phi_p B^p$, the model is

$$\phi(B) X_t = \alpha + w_t. \tag{7}$$

If we consider B as a complex variable,

$$\phi(B) = 0. \tag{8}$$

It is called the characteristic equation of the AR model.

The ARMA model is as follows: if the expectation of X is $\mu = 0$, then the autoregressive average process ARMA(p, q) is defined as

$$X_t = \phi_1 X_{(t-1)} + \cdots + \phi_p X_{(t-p)} + w_t + \theta_1 w_{(t-1)} + \cdots + \theta_p w_{(t-p)}, \tag{9}$$

or $\phi(B) X_t = \theta(B) w_t$ and $\theta(B) = 1 + \theta_1 B + \cdots - \theta_p B^q$. If it is expected that μ is not equal to 0, the above definition can be written as

$$\begin{aligned} X_t = \phi_0 + \phi_1 X_{(t-1)} + \cdots + \phi_p X_{(t-p)} + w_t + \theta_1 w_{(t-1)} \\ + \cdots + \theta_p w_{(t-p)} \end{aligned} \tag{10}$$

and $\phi_0 = (1 - \phi_1 - \ldots - \phi_p)\mu$.

We assume that $\{w_t\}$ is a white noise sequence with variance σ^2, and we consider an ARMA sequence with a mean of 0.

$$\phi(B)X_t = \theta(B)w_t. \tag{11}$$

The sequence can be written as

$$X_t = \frac{\theta(B)}{\phi(B)}w_t = \psi(B)w_t = w_t + \psi_1 w_{(t-1)} + \psi_2 w_{(t-2)} + \cdots. \tag{12}$$

Our goal is to predict the future value q of m steps based on the past $(X_n, X_{(n-1)}, \ldots, X_1)$ up to n hours. The predicted value is $X_{(n+m)}$. In ntm, there are

$$X_{(n+m)} = \sum_{j=0}^{\infty}\psi_j w_{(n+m-j)} = \sum_{j=0}^{m-1}\psi_j w_{(n+m-j)} + \sum_{j=m}^{\infty}\psi_j w_{(n+m-j)}. \tag{13}$$

Among them, $\sum_{j=0}^{m-1}\psi_j w_{(n+m-j)}$ represents the future w, and $\sum_{j=m}^{\infty}\psi_j w_{(n+m-j)}$ represents the past w. We want to express $\widehat{X}_n(m)$ as a linear combination of these $w_1, w_{(n-1)}, \ldots$.

$$\widehat{X}_n(m) = \psi_m^* w_n + \psi_{(m+1)}^* w_{(n-1)} + \psi_{(m+2)}^* w_{(n-2)} + \cdots. \tag{14}$$

Therefore, it is necessary to find the coefficient ψ_j^* that minimizes the mean square error, and the mean square error is

$$E\left(X_{n+m} - \widehat{X}_n(m)\right)^2. \tag{15}$$

$$E\left(X_{n+m} - \widehat{X}_n(m)\right)^2 = \sigma^2\sum_{j=0}^{m-1}\psi_j^2 + \sigma^2\sum_{j=0}^{\infty}\left(\psi_{(m+j)} - \psi_{(m+j)}^*\right). \tag{16}$$

Therefore, we require

$$\frac{\partial E\left(X_{n+m} - \widehat{X}_n(m)\right)^2}{\partial\psi^*} = -2\sigma^2\sum_{j=0}^{\infty}\left(\psi_{(m+j)} - \psi_{(m+j)}^*\right) = 0. \tag{17}$$

This results in $\psi_{(m+j)} = \psi_{(m+j)}^*$, that is,

$$\widehat{X}_n(m) = \psi_m w_n + \psi_{(m+1)}w_{(n-1)} + \psi_{(m+2)}w_{(n-2)} + \cdots. \tag{18}$$

From another perspective, $X_{(n+m)}$ can be expressed as

$$X_{(n+m)} = \sum_{j=0}^{\infty}\psi_j w_{(n+m-j)} = \sum_{j=0}^{m-1}\psi_j w_{(n+m-j)} + \sum_{j=0}^{\infty}\psi_j w_{(n-j)}. \tag{19}$$

We know that when past information $I_n = \{X_n, X_{n-1}, \ldots\}$ is given, the best prediction for $X_{(n+m)}$ is

$$E\left(X_{(n+m)} \mid I_n\right) = E\left(\sum_{j=0}^{m-1}\psi_j w_{(n+m-j)}|I_n\right) + E\left(\sum_{j=0}^{\infty}\psi_j w_{(n-j)}|I_n\right) = 0 + \sum_{j=0}^{\infty}\psi_j w_{(n-j)}. \tag{20}$$

Therefore,

$$\widehat{X}_n(m) = E\left(X_{(n+m)} \mid I_n\right)^2 = \sum_{j=0}^{\infty}\psi_j w_{(n-j)}. \tag{21}$$

We get the prediction error

$$P_n(m) = X_{(n+m)} - \widehat{X}_n(m) = \sum_{j=0}^{m-1}\psi_j w_{(n+m-j)} = w_{(n+m)} + \psi_1 w_{(n-k+m)} + \cdots + \psi_{(m-1)}w_{(n+1)}. \tag{22}$$

This is an MA $(m-1)$ process with a mean of 0 and a variance of $\sigma^2\sum_{j=0}^{m-1}\psi_j^2$. $P_n(m)$ is relevant for $m > 1$, and it is

$$P_{n-k}(m) = \sum_{j=0}^{m-1}\psi_j w_{n-k+m-j} = w_{n-k+m} + \psi_1 w_{n-k+m-1} + \cdots + \psi_{m-1}w_{n-k+1}. \tag{23}$$

Therefore, the covariance of the prediction error is

$$\operatorname{cov}\left(P_n(m), P_{(n-k)}(m)\right) = \sigma^2 \sum_{l=n+1}^{n+m-k} \psi_{(l-n)}\psi_{(l-n-k)}, \quad k < 1. \tag{24}$$

The basic idea of the ARMA forecasting model is to assume that the corresponding sequence $\{y_t\}$ and the input variable sequence (independent variable sequence) $\{x_t\}(u = 1, 2, \ldots, k)$ are both stationary. It first builds a regression model of the response sequence and the input variable sequence. Since both $\{y_t\}$ and $\{x_t\}(u = 1, 2, \ldots, k)$ are stationary, and the linear combination of stationary series is also stationary, the residual series $\{\varepsilon_t\}$ is a stationary series $\{\varepsilon_t\}$. Subsequently, it uses the ARMA model to continue to extract the residual sequence $\{\varepsilon_t\}$. Finally, the model can be obtained as equation (22). The prediction process is shown in Figure 1.

The basic ARMA model uses the unary time series analysis method. In reality, many time series are affected by other time series in addition to their own changing laws. The introduction of relevant time series can increase the fit of the ARMA model. If the input sequence is a leading indicator, the lag of the ARMA forecast will be improved, and the forecast value of the model will be more accurate.

The ARMAX model improves the prediction of the input sequence by using the historical information of the output sequence and its related input sequence, and it has the following structure:

$$\left\{ y_t = \mu + \sum_{l=1}^{k} \frac{\Theta_l(B)}{\Phi_l(B)} B^{l_1} x^{lt} + \varepsilon_t \varepsilon_t = \frac{\Theta_l(B)}{\Phi_l(B)} w_t. \right. \tag{25}$$

In the formula, $\Phi_l(B)$ represents the autoregressive coefficient polynomial of the ith input variable, $\Theta_l(B)$ represents the average coefficient polynomial of the ith input variable, $1i$ represents the delay order of the ith input variable, and $\{\varepsilon_t\}$ represents the regression residual sequence. $\Theta_l(B)$ represents the autoregressive coefficient polynomial of the residual sequence, $O(B)$ represents the moving average coefficient polynomial of the residual sequence, and $\{w_t\}$ represents the zero-mean white noise sequence.

The basic idea of the ARMAX forecasting model is to assume that the corresponding sequence $\{y_t\}$ and the input variable sequence (independent variable sequence) $\{x_t\}(u = 1, 2, \ldots, k)$ are both stationary. First, it constructs a regression model of the response sequence and the input variable sequence. Since both $\{y_t\}$ and $\{x_t\}(u = 1, 2, \ldots, k)$ are stationary, and the linear combination of stationary sequences is also stationary, the residual sequence $\{e,\}$ is the stationary sequence $\{\varepsilon_t\}$. Subsequently, it uses the ARMA model to continue to extract the residual sequence $\{\varepsilon_t\}$. Finally, the model can be obtained as equation (22), and the prediction process is shown in Figure 2.

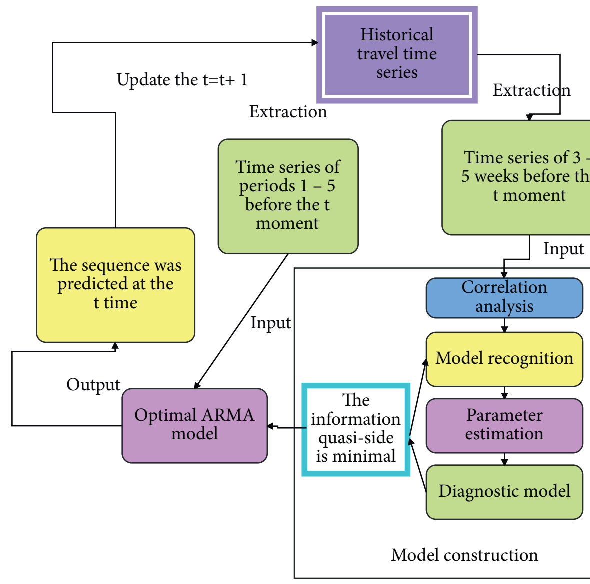

Figure 1: ARMA predictive model process.

4. Evaluation of the Effect of Enterprise Lean Management Based on Data Mining

For a manufacturing system, the demand for raw materials or parts is closely related to the demand for finished products and cannot be simply regarded as an independent demand. Moreover, the manufacturing method has experienced the evolution from handmade to mass production and then to lean production and as shown in Figure 3.

Lean production is a comprehensive technological system that encompasses a variety of manufacturing technologies and management technologies. The composition of lean production mainly includes the following: kanban-based production control, total quality management, participation of all employees in decision-making, and supplier collaboration. Lean production strictly organizes production according to orders through the kanban control method, transmits material demand information between processes through kanban, and uses kanban to delegate production control to the subsequent processes of each process. The technical system structure of lean production is shown in Figure 4.

The planning level of the batch production model in the small-batch environment of the variety is shown in the following Figure 5.

Figure 6 shows the hardware composition model of the lean production management system. The monitoring system adopts the B/S model in architecture. System software and related databases only need to be installed on the server side. Moreover, the computers connected by various departments do not need to be installed as clients and only need to use a browser to use the production monitoring system. Using this hardware composition model has the following advantages: ① investment is low. In addition to purchasing computers, hardware equipment of the original network system is basically used. ② In the process of system

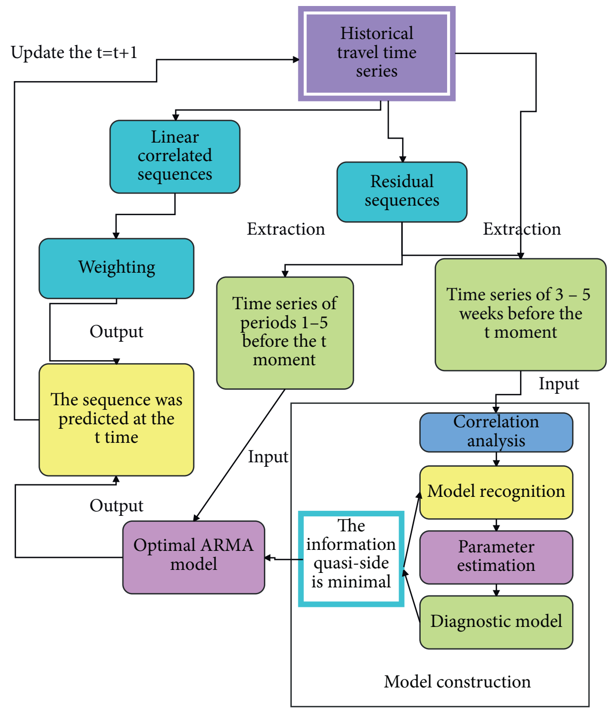

FIGURE 2: ARMAX prediction model process.

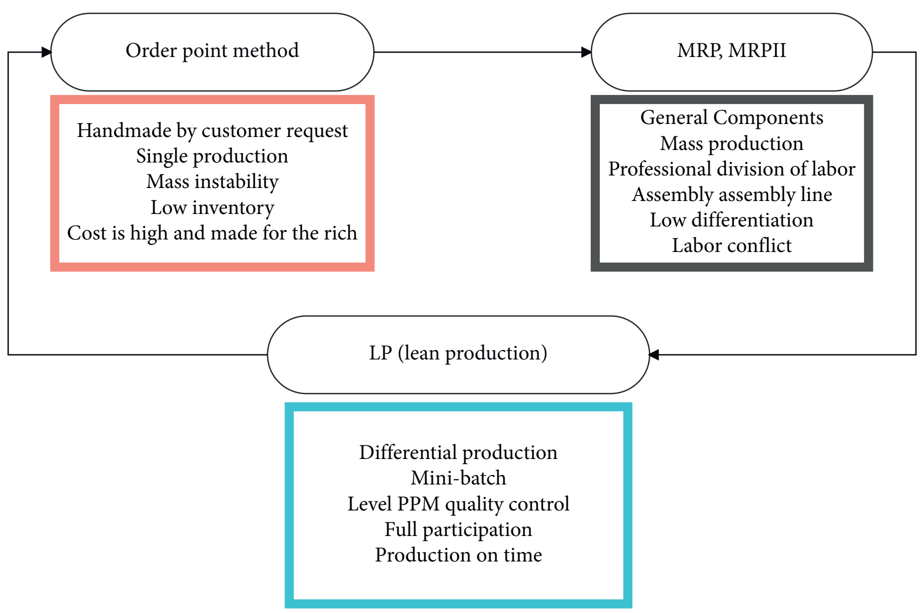

FIGURE 3: Evolution of manufacturing methods.

transformation, production can normally proceed without being affected at all. ③ Data are uniformly processed on the server side of the production management system. The front-end program browser is only responsible for displaying the feedback information of the server program, so the computer configuration requirements for each department's access are not high. ④ When the lean production management system needs to be upgraded, it only needs to update the server-side program installed on the production management server and does not need to reinstall the front-end application program, which facilitates the system upgrade.

With the development of internet technology, computing technology is changing from an application system based on the C/S (client/server) model to an application system based on the B/S (browser/server) model. In the B/S model, the core point is to replace the original client program with a general-purpose browser. All configuration work is concentrated on the server side, the security of the system is improved, and it also brings convenience to the

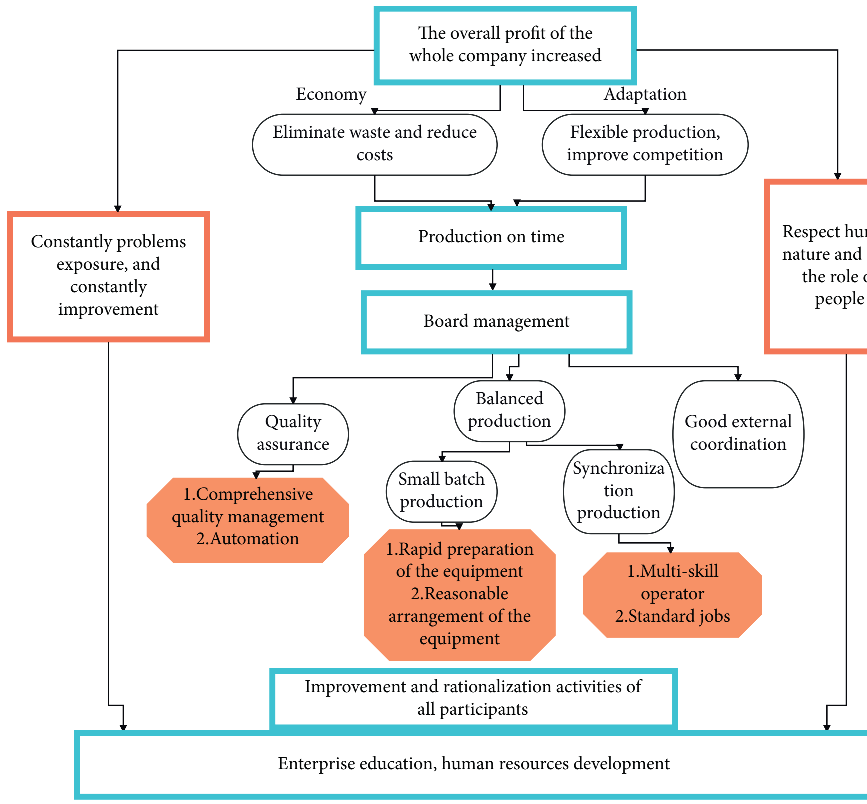

Figure 4: Lean production manufacturing system structure.

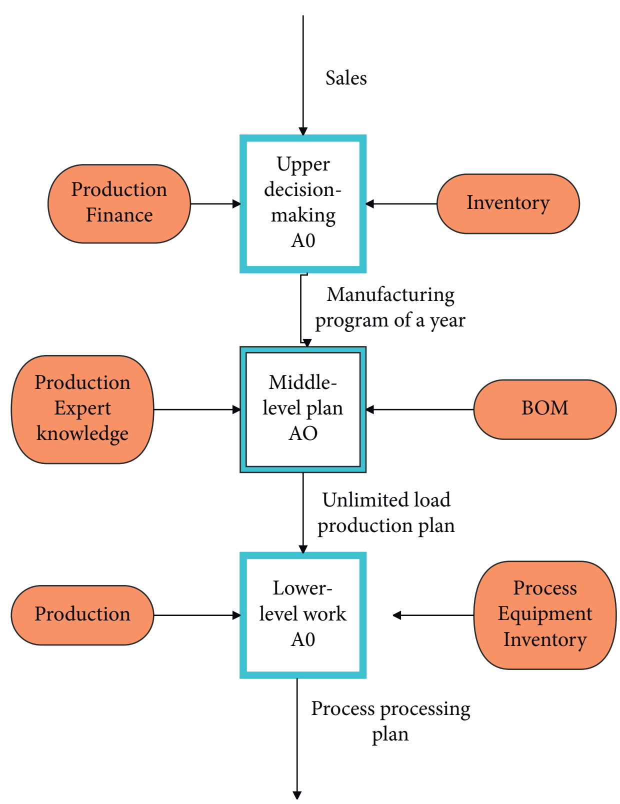

Figure 5: Production planning hierarchy.

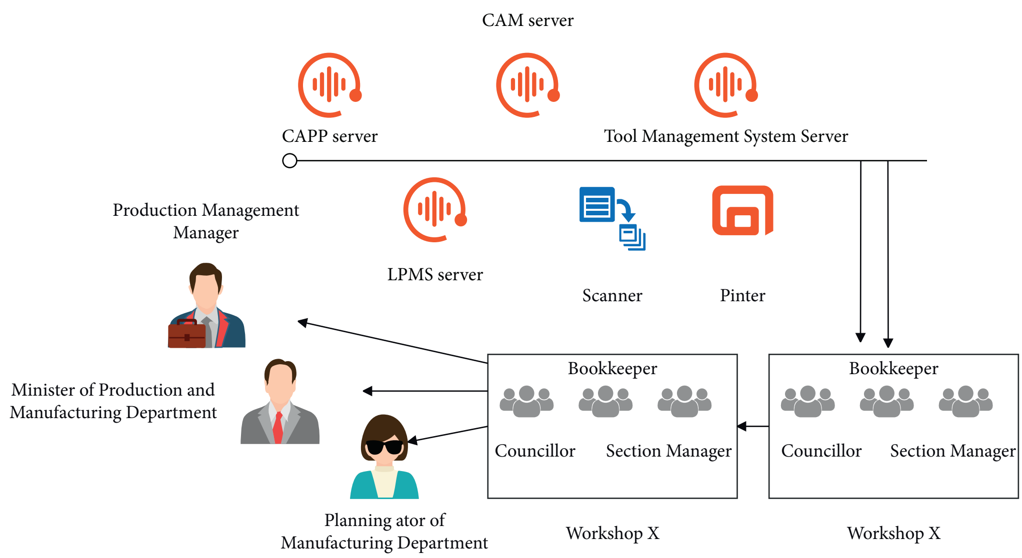

Figure 6: The hardware composition model of the lean production management system.

deployment, upgradation, and maintenance of the program. This study uses B/S application architecture based on J2EE technology to build a lean production management system. In the field of software engineering, in order to reduce the degree of module coupling and improve the reusability of modules, layering has always been a widely adopted method. Layering can also enable developers to focus on a certain layer for development and make the division of software development finer and improve production efficiency. An enterprise level, the J2EE application is usually divided into the following three layers: UI layer, business logic layer, and data persistence layer. A brief introduction to these layers is given below. (1) The UI layer is responsible for interacting with the user, including accepting the user's request and returning the processing result to the user. (2) The business logic layer is mainly responsible for specific business processing. (3) The data persistence layer is mainly responsible for dealing with the underlying database.

The web application in this study is divided into 3 layers in terms of responsibilities, and these three layers are presentation, business, and persistence. Figure 7 is a schematic diagram of the system architecture. Each layer should have a clear responsibility for processing procedures and should not be functionally mixed with other layers, and each layer should be separated from other layers, but a communication interface should be placed between them.

The traditional lean production theory is only applied to the partial implementation process and organizational scope, and its effect can only be reflected in the field and operation level. Therefore, the lean production management system based on VSM will implement lean improvement from
project ⟶ plan ⟶ task ⟶ improvement ⟶ abnormal.
This method is an optimization of the traditional lean production theory, and it is a holistic lean improvement process, rather than applied to the local implementation process and organizational scope. Moreover, its effect will also be reflected in the entire process of lean improvement, rather than just reflected in the field and operation level. The improvement process of the VSM-based lean production management system is shown in Figure 8.

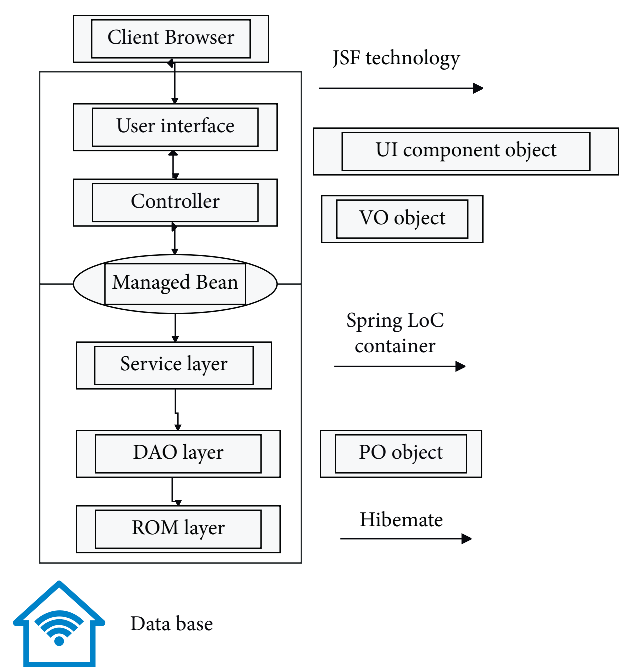

Figure 7: B/S three-tier system structure.

Project management rules are the supporting framework of the project management model. Project management rules are composed of five modules: project formulation, project review, project monitoring, project statistics, and project summary. The project formulation module is composed of survey information and project details. The survey information includes three aspects of field data, resource allocation, and market conditions. The project details include parameters such as project ID, project name, project constraints, project type, and project content. Constraints

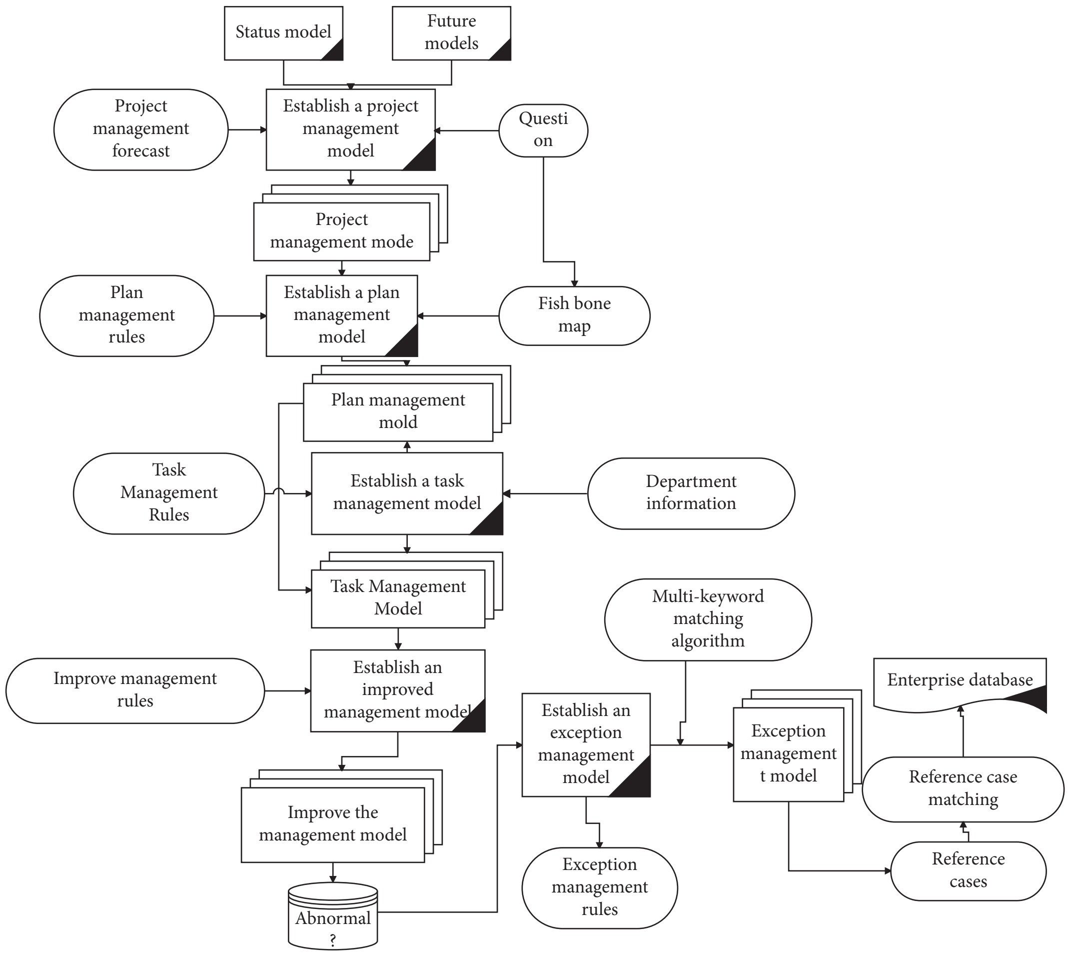

Figure 8: The improvement process of the lean production management system based on VSM.

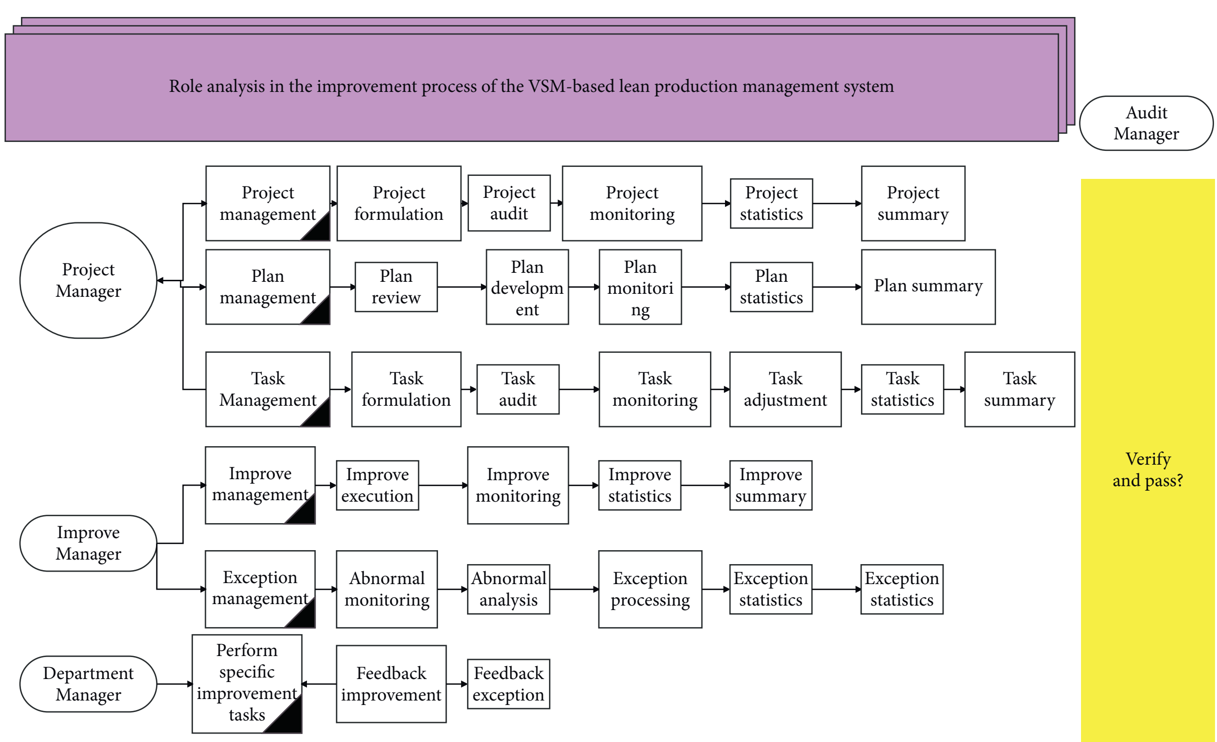

Figure 9: Role analysis in the improvement process of the lean production management system based on VSM.

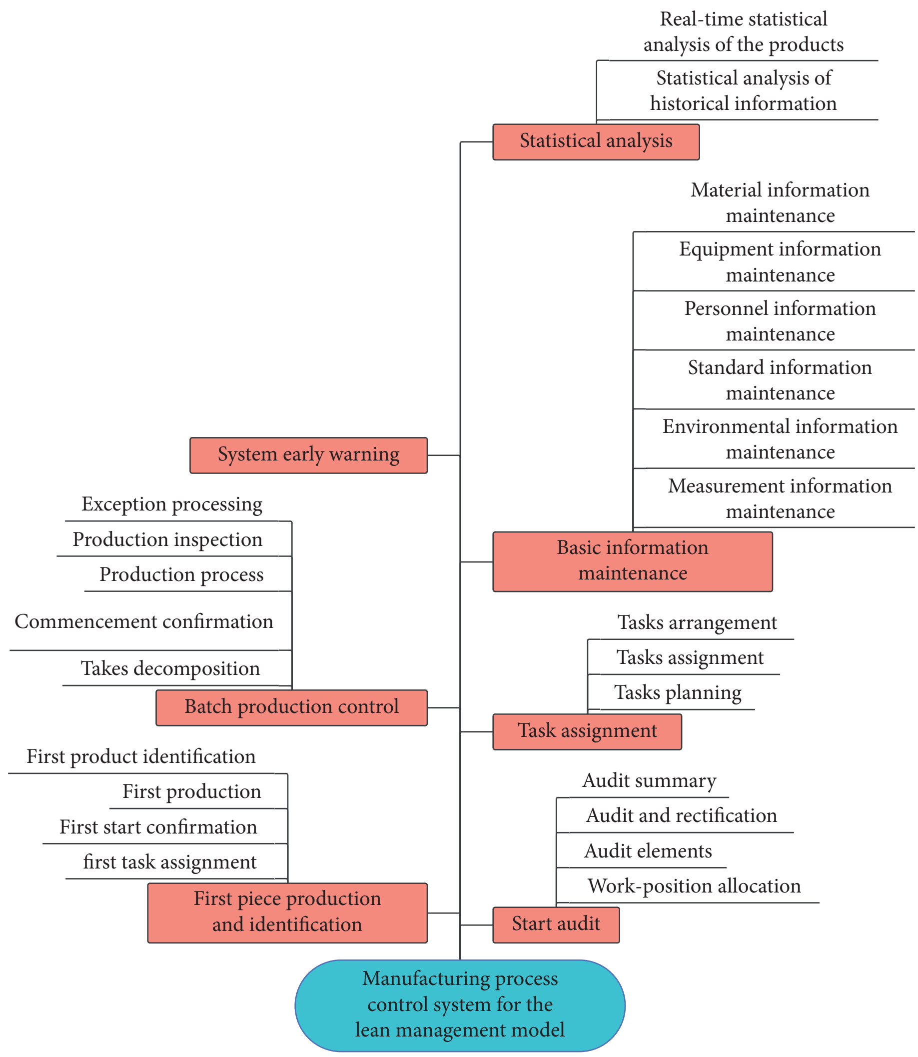

Figure 10: System hierarchy function diagram.

refer to the constraints on the implementation of projects such as expected time limit and budget funds. The second is the project review module. The project review module is mainly for project details, including two points: review content and review results. The review content refers to the project information reviewed, and the review result refers to the evaluation of the project content. The project monitoring module is responsible for real-time monitoring of project implementation, including parameters such as project name, project content, project progress, and project completion. The project statistics module is responsible for information statistics during project execution, including project name, project content, number of employees, time consumption, material consumption, capital consumption, and completion status. In addition, the project management rules also include a project summary module, which is responsible for the reflection and summary of the project implementation process.

Four roles are set up in the improvement process of the VSM-based lean production management system. After the setting of roles and the analysis of their functions, customers no longer only refer to the final customers but also include other participants in the production of the enterprise. Moreover, it allows everyone to participate in the lean improvement process and solves the defect that traditional lean production theory ignores in enterprise production participants. The following will introduce the functional analysis and definition of the four roles in this method. The role analysis in the improvement process of the VSM-based lean production management system is shown in Figure 9.

It can be seen from the previous analysis that a top-down analysis method is adopted. The system can be abstracted into subsystems such as start-up review, task allocation, first-article production and appraisal, basic data maintenance, mass production process control, system early warning, and statistical analysis. Moreover, each subsystem can be divided into several modules according to its function. The hierarchical functional structure of the system is shown in Figure 10.

On the basis of the above models, combined with data mining algorithms, an evaluation model for the effect of enterprise lean management is constructed. In order to

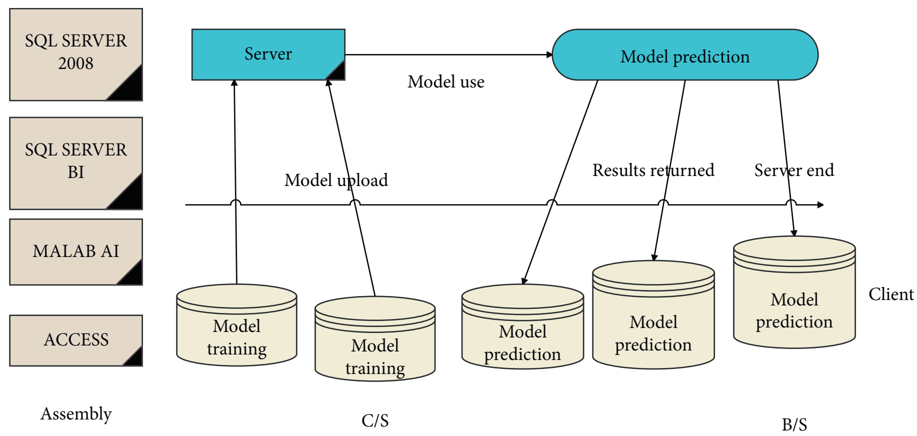

Figure 11: Quality prediction system based on data mining.

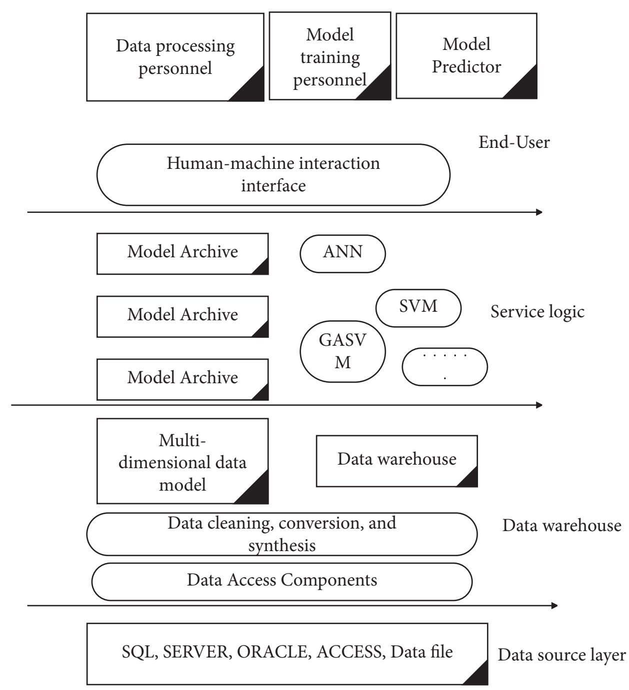

Figure 12: The evaluation model of enterprise lean management effect based on data mining.

facilitate deployment and rational use of system resources, the system adopts C/S and B/S hybrid architecture model for development. The model training client uploads the model file to the server, and the model prediction client directly returns the result calculated on the server. Due to the need to call some computing components, the server and the model training client take up a lot of system resources (as shown in Figure 11). The system ultimately faces three types of users: data processing personnel, model training personnel, and model prediction personnel. The data processing personnel perform data loading and data cleaning operations, and the model training personnel are responsible for the training of the model. They upload the models that meet the conditions to the server for use. Model forecasters can directly use the model files on the server through a browser. Therefore, the system provides a human-computer interaction interface, and operators use various functions and services provided by the system through a visual interface, as shown in Figure 12.

After constructing an enterprise lean effect evaluation system based on data mining, we evaluate the lean data mining, problem discovery, data processing, and management evaluation of the system in this study. The results are shown in Table 1 and Figure 13.

From the above research, the enterprise lean effect evaluation system based on data mining proposed in this study can play an important role in enterprise lean management.

Table 1: Performance verification of enterprise lean effect evaluation system based on data mining.

Number	Data mining	Problem discovery	Data processing	Management evaluation
1	91.72	86.52	87.32	81.72
2	89.62	92.94	95.63	80.96
3	86.47	76.87	89.13	89.16
4	85.41	85.30	75.77	88.42
5	82.85	88.68	77.70	82.62
6	93.30	84.73	85.45	93.49
7	93.86	84.09	89.38	93.31
8	90.76	92.79	83.83	96.97
9	82.87	86.12	91.24	88.86
10	87.92	87.77	94.58	91.48

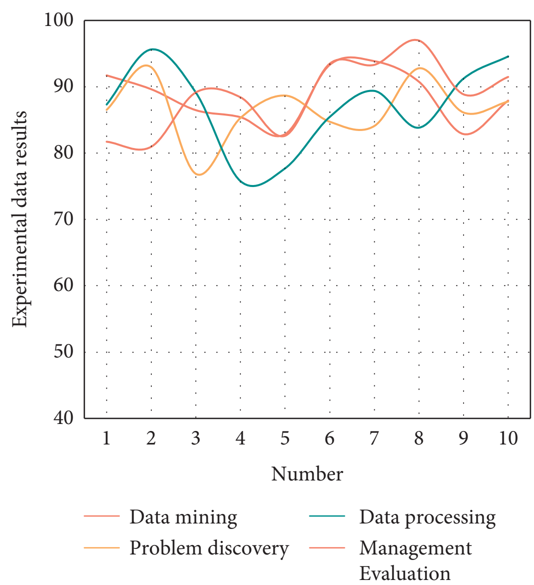

Figure 13: Statistical diagram of system performance test data results.

5. Conclusions

The secret of lean production is that it is not only a production method but also reflects an advanced management idea. It uses product production processes as clues to organize closely related supply chains. On the one hand, it reduces transaction costs in enterprise collaboration, and on the other hand, it ensures stable demand and timely supply and takes the entire mass production system as the optimization goal. As the application of database management systems becomes more and more widespread, the scale of the database is constantly expanding, and people have accumulated massive amounts of business data, such as customer data, transaction history data, sale records, and so on. These databases contain a lot of valuable business information. At present, although the applied database system can efficiently realize data entry, query, statistics, and other functions, it cannot find the relationships and rules existing in the data and cannot predict the future development trend based on the existing data. Therefore, this study links data mining and lean production to build a data mining-based enterprise lean management effect evaluation system, which improves the efficiency of enterprise lean management.

Data Availability

The labeled dataset used to support the findings of this study is available from the corresponding author upon request.

Conflicts of Interest

The authors declare no conflicts of interest.

Acknowledgments

This work was supported by Jinggangshan University.

References

[1] S. Amershi, M. Cakmak, W. B. Knox, and T. Kulesza, "Power to the people: the role of humans in interactive machine learning," *AI Magazine*, vol. 35, no. 4, pp. 105–120, 2014.

[2] S. Basith, B. Manavalan, T. H. Shin, and L. Gwang, "SDM6A: a web-based integrative machine-learning framework for predicting 6mA sites in the rice genome," *Molecular Therapy–Nucleic Acids*, vol. 18, no. 6, pp. 131–141, 2019.

[3] A. Chowdhury, E. Kautz, B. Yener, and D. Lewis, "Image driven machine learning methods for microstructure recognition," *Computational Materials Science*, vol. 123, no. 8, pp. 176–187, 2016.

[4] C. W. Coley, R. Barzilay, T. S. Jaakkola, W. H. Green, and K. F. Jensen, "Prediction of organic reaction outcomes using machine learning," *ACS Central Science*, vol. 3, no. 5, pp. 434–443, 2017.

[5] H. Darabi, B. Choubin, O. Rahmati, A. T. Haghighi, B. Pradhan, and B. Kløve, "Urban flood risk mapping using the GARP and QUEST models: a comparative study of machine learning techniques," *Journal of Hydrology*, vol. 569, no. 5, pp. 142–154, 2019.

[6] P. Feng, B. Wang, D. Li Liu, C. Waters, and Q. Yu, "Incorporating machine learning with biophysical model can improve the evaluation of climate extremes impacts on wheat yield in south-eastern Australia," *Agricultural and Forest Meteorology*, vol. 275, no. 3, pp. 100–113, 2019.

[7] K. Kourou, T. P. Exarchos, K. P. Exarchos, M. V. Karamouzis, and D. I. Fotiadis, "Machine learning applications in cancer prognosis and prediction," *Computational and structural biotechnology journal*, vol. 13, no. 5, pp. 8–17, 2015.

[8] A. Rajkomar, J. Dean, and I. Kohane, "Machine learning in medicine," *New England Journal of Medicine*, vol. 380, no. 14, pp. 1347–1358, 2019.

[9] V. Rodriguez-Galiano, M. Sanchez-Castillo, M. Chica-Olmo, and M. Chica-Rivas, "Machine learning predictive models for

mineral prospectivity: an evaluation of neural networks, random forest, regression trees and support vector machines," *Ore Geology Reviews*, vol. 71, no. 3, pp. 804–818, 2015.

[10] C. Voyant, G. Notton, S. Kalogirou et al., "Machine learning methods for solar radiation forecasting: a review," *Renewable Energy*, vol. 105, no. 2, pp. 569–582, 2017.

[11] L. Ward, A. Agrawal, A. Choudhary, and C. Wolverton, "A general-purpose machine learning framework for predicting properties of inorganic materials," *npj Computational Materials*, vol. 2, no. 1, pp. 1–7, 2016.

[12] Y. Xin, L. Kong, Z. Liu et al., "Machine learning and deep learning methods for cybersecurity," *IEEE Access*, vol. 6, no. 1, Article ID 35365, 2018.

[13] C. Folberth, A. Baklanov, J. Balkovič, R. Skalský, N. Khabarov, and M. Obersteiner, "Spatio-temporal downscaling of gridded crop model yield estimates based on machine learning," *Agricultural and forest meteorology*, vol. 264, no. 4, pp. 1–15, 2019.

[14] J. Sieg, F. Flachsenberg, and M Rarey, "In Need of bias control: evaluating chemical data for machine learning in structure-based virtual screening," *Journal of Chemical Information and Modeling*, vol. 59, no. 3, pp. 947–961, 2019.

[15] F. Thabtah and D. Peebles, "A new machine learning model based on induction of rules for autism detection," *Health informatics journal*, vol. 26, no. 1, pp. 264–286, 2020.

[16] F. A. Narudin, A. Feizollah, N. B. Anuar, and A. Gani, "Evaluation of machine learning classifiers for mobile malware detection," *Soft Computing*, vol. 20, no. 1, pp. 343–357, 2016.

[17] Q. Yao, H. Yang, R. Zhu et al., "Core, mode, and spectrum assignment based on machine learning in space division multiplexing elastic optical networks," *IEEE Access*, vol. 6, no. 6, Article ID 15898, 2018.

[18] D. Bzdok and A. Meyer-Lindenberg, "Machine learning for precision psychiatry: opportunities and challenges," *Biological Psychiatry: Cognitive Neuroscience and Neuroimaging*, vol. 3, no. 3, pp. 223–230, 2018.

[19] M. Chen, Y. Hao, K. Hwang, L. Wang, and L. Wang, "Disease prediction by machine learning over big data from healthcare communities," *Ieee Access*, vol. 5, no. 1, pp. 8869–8879, 2017.

[20] L. Itu, S. Rapaka, T. Passerini et al., "A machine-learning approach for computation of fractional flow reserve from coronary computed tomography," *Journal of Applied Physiology*, vol. 121, no. 1, pp. 42–52, 2016.

[21] K. K. F. Tsoi, N. B. Chan, K. K. L. Yiu, S. K. S. Poon, B. Lin, and K. Ho, "Machine learning clustering for blood pressure variability applied to systolic blood pressure intervention trial (SPRINT) and the Hong Kong community cohort," *Hypertension*, vol. 76, no. 2, pp. 569–576, 2020.

Hindawi
Scientific Programming
Volume 2023, Article ID 9790230, 1 page
https://doi.org/10.1155/2023/9790230

Retraction

Retracted: Research on Students' Adaptive Learning System Based on Deep Learning Model

Scientific Programming

Received 1 August 2023; Accepted 1 August 2023; Published 2 August 2023

This article has been retracted by Hindawi following an investigation undertaken by the publisher [1]. This investigation has uncovered evidence of one or more of the following indicators of systematic manipulation of the publication process:

(1) Discrepancies in scope
(2) Discrepancies in the description of the research reported
(3) Discrepancies between the availability of data and the research described
(4) Inappropriate citations
(5) Incoherent, meaningless and/or irrelevant content included in the article
(6) Peer-review manipulation

The presence of these indicators undermines our confidence in the integrity of the article's content and we cannot, therefore, vouch for its reliability. Please note that this notice is intended solely to alert readers that the content of this article is unreliable. We have not investigated whether authors were aware of or involved in the systematic manipulation of the publication process.

Wiley and Hindawi regrets that the usual quality checks did not identify these issues before publication and have since put additional measures in place to safeguard research integrity.

We wish to credit our own Research Integrity and Research Publishing teams and anonymous and named external researchers and research integrity experts for contributing to this investigation.

The corresponding author, as the representative of all authors, has been given the opportunity to register their agreement or disagreement to this retraction. We have kept a record of any response received.

References

[1] X. Yang, Z. Zhou, and Y. Xiao, "Research on Students' Adaptive Learning System Based on Deep Learning Model," *Scientific Programming*, vol. 2021, Article ID 6593438, 13 pages, 2021.

Hindawi
Scientific Programming
Volume 2021, Article ID 6593438, 13 pages
https://doi.org/10.1155/2021/6593438

Research Article

Research on Students' Adaptive Learning System Based on Deep Learning Model

Xi Yang[1], **Zhihan Zhou**[1], **and Yu Xiao**[2]

[1]*School of Economics, Peking University, Beijing 100871, China*
[2]*School of Software and Microelectronics, Peking University, Beijing 100871, China*

Correspondence should be addressed to Xi Yang; 1701110928@pku.edu.cn

Received 13 October 2021; Revised 11 November 2021; Accepted 26 November 2021; Published 16 December 2021

Academic Editor: Le Sun

With the rapid development of deep learning in recent years, recommendation algorithm combined with deep learning model has become an important direction in the field of recommendation in the future. Personalized learning resource recommendation is the main way to realize students' adaptation to the learning system. Based on the in-depth learning mode, students' online learning action data are obtained, and further learning analysis technology is used to construct students' special learning mode and provide suitable learning resources. The traditional method of introducing learning resources mainly stays at the level of examination questions. What ignores the essence of students' learning is the learning of knowledge points. Students' learning process is affected by "before" and "after" learning behavior, which has the characteristics of time. Among them, bidirectional length cyclic neural network is good at considering the "front" and "back" states of recommended nodes when recommending prediction results. For the above situation, this paper proposes a recommendation method of students' learning resources based on bidirectional long-term and short-term memory cyclic neural network. Firstly, recommend the second examination according to the knowledge points, predict the scores of important steps including the accuracy of the recommended examination of the target students and the knowledge points of the recommended examination, and finally cooperate with the above two prediction results to judge whether the examination questions are finally recommended. Through the comparative experiment with the traditional recommendation algorithm, it is found that the student adaptive learning system based on the deep learning model proposed in this paper has better stability and interpretability in the recommendation results.

1. Introduction

With the advent of the era of big data, combining the educational big data generated in the field of education with the deep learning model [1] can find internal characteristics from a large number of educational data, thus optimizing the educational model and carrying out more efficient teaching activities. The essence of education big data is big data in the field of education. Its data sources include not only learners' learning data, but also all people's behavior data in daily educational activities. It has the characteristics of multitheme, multielement, and multiform. If we deviate from the adaptive learning of educational big data, we can solve the problems of unbalanced educational resources and educational model planning in traditional education, pay attention to students themselves, and realize personalized learning. On the basis of the continuous development of information technology, distance education to overcome the limitation of time and space began to appear [2]. Adaptive learning system dynamically adjusts the generation of learning resources according to students' learning conditions, which overcomes the problems of unbalanced distribution of educational resources and single educational model in Chinese traditional education, and is of great significance to the realization of high-quality education. However, compared with foreign countries, there are more mature systems, such as Moodle Learning Management System and Knewton Personalized Learning Platform [3]. In China, the research on students' adaptive learning system is still in the theoretical stage. The research, design, development, and implementation of adaptive learning system are one of the research hotspots in the future education field.

With the rise of artificial intelligence, more and more people use data and machine learning to help and assist students to learn, which is used to detect emotional state and transfer negative state. We propose to use multimodal sensor data and machine learning system, which can improve the learning speed and keep the learner in the optimal emotional state [4]. Adaptive learning rate algorithm is an automatic method to set learning rate manually. We study Barzilai–Borwein step size method and extend it to adaptive learning rate problem. Through experiments, it is found that this method has great advantages in the learning speed and generalization performance compared with other methods [5]. With the popularity of the Internet, people are increasingly accepting online learning. It can provide learners with various learning materials and acquire knowledge in various fields. Based on the adaptive learning management system based on real-time personalization and personalized page ranking algorithm, we complete the skill test evaluation report and use Navies Bayes classifier to classify the learners' test results. Jagadeesan and Subbiah [6] provided learning content according to the level differences of learners and combined different learning methods and time for effective management.

Each learner has different abilities and preferences, which leads to the lack of a good way to support learners' needs in online education system, which is a challenge we face. Therefore, we adjust the teaching decisions according to the different needs of learners and develop an adaptive learning system that can generate learning paths according to learners' personal data. Q-learning algorithm is a reinforcement learning technique in this system, which provides learners with necessary contents and courses based on learners' feedback [7]. Adaptive learning management system can solve this problem by choosing suitable learning methods according to learners' learning conditions. This system can create courses with customized content and update them constantly during learning. The learning materials come from the knowledge base, which is searched, updated, and ranked for relevance by using the network. In order to verify its effectiveness, we test and evaluate the system, and the results show that the real-time test of the system shows its most advanced performance [8].

2. Recommendation Algorithm Based on Deep Learning

2.1. Traditional Recommendation Algorithm

2.1.1. Recommendation Algorithm Based on Popularity. Popularity-based recommendation algorithm is the simplest and most direct recommendation algorithm, which is widely used in various sites. It is mainly recommended to sort items based on PV, UV, and other data [9], where PV is page view. Its advantage is that it has no cold start problem and is suitable for new users. The disadvantage is that it cannot be customized for users.

2.1.2. Collaborative Filtering Recommendation Algorithm. At present, the cooperative filter recommendation algorithm is the most successful and widely used recommendation algorithm, mainly including user-based common filtering recommendation algorithm and project-based common filtering recommendation algorithm. The common filter recommendation algorithm based on users first analyzes the evaluation records between users and items, calculates the similarity between users based on the evaluation records, and then selects *M* users who are most similar to the current users. Finally, the similar user group has the highest evaluation and selects the target users not to use *N* items in the records to recommend. The project-based joint filter recommendation algorithm firstly analyzes the evaluation records of users and projects, calculates the similarity of each project according to the evaluation records, and finally finds out *N* projects with the highest similarity of the projects evaluated by target users for recommendation. The principle of filtering recommendation algorithm is simple, and the evaluation indexes such as accuracy and recall rate are also very good. However, there is also the problem of relying too much on user ratings. When there are few records of cold start, new projects, and new users, the recommendation effect is poor.

2.1.3. Content-Based Recommendation Algorithm. Its principle is to analyze the content of the items used by the user to generate the content selection of the user's preference and recommend other items with high similarity of the items used [10]. Its advantage is to solve the problem of cold start, but its disadvantage is that users directly recommend items closely related to reading content, and the recommended content is more single.

2.1.4. Model-Based Recommendation Algorithm. Make a model to predict the user's score according to which is recommended [11]. The greatest advantage of this recommended method is that it is correct and fast. The disadvantage is that in order to maintain a better recommendation effect, the online recommendation mode is often maintained and updated to adapt to the changes of users and projects.

2.1.5. Hybrid Recommendation Algorithm. Recommendation methods have their own advantages and disadvantages. In order to get better recommendation results, hybrid recommendation strategies are often used in the real world [12]; there are often mixed recommendation strategies, such as conversion, crowding, and so on. Crowding is to return the recommendation results of various recommendation technologies to users for selection.

2.1.6. Comparison of Recommendation Algorithms. A comparison of the advantages and disadvantages of the above recommended algorithms is shown in Table 1.

2.2. Recommendation Algorithm Based on Deep Learning Model. Deep learning can directly extract features from content, process noise data, have better noise resistance [13],

Table 1: Comparison of the commonly used recommendation algorithms.

Recommended technology	Advantages	Disadvantages
Recommendation algorithm based on popularity	Simple and easy to operate, without the problem of cold start	Unable to make personalized recommendations
Collaborative filtering recommendation algorithm	Simple and easy to implement, with high recommendation accuracy	Too much reliance on user ratings; cold start; low project coverage
Content-based recommendation algorithm	No cold start problem	The recommended content is relatively simple
Model-based recommendation algorithm	Fast and accurate, especially suitable for high real-time business	Models need to be maintained frequently

and can realize dynamic or sequential data modeling. Because of the characteristics of this neural network, it is also very effective to import the recommendation system.

2.2.1. Recommendation Model Based on Multilayer Perceptron. The MLP network structure of a three-tier structure is shown in Figure 1.

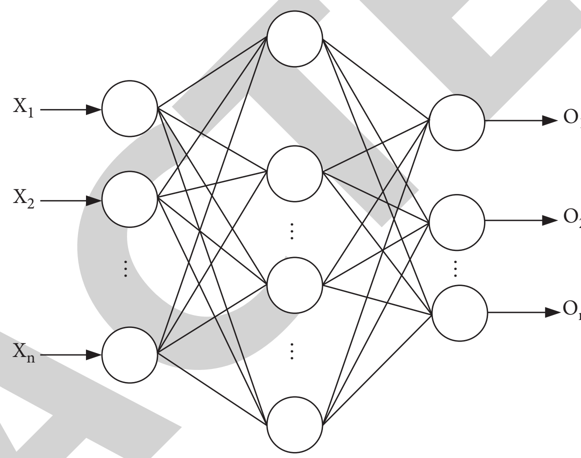

Figure 1: Multilayer perceptron network structure.

2.2.2. Recommendation Model Based on Automatic Encoder. The data conversion from the input layer to the hidden layer is a program φ after decoding the data conversion from the hidden layer to the output layer, and the calculation method is as shown in the following formulas:

$$\phi\colon X \longrightarrow Z\colon x \mapsto \phi(x) = \sigma(Wx + b) = z, \tag{1}$$

$$\varphi\colon Z \longrightarrow X\colon z \mapsto \phi(z) = \sigma(\widetilde{W}z + \widetilde{b}) = x. \tag{2}$$

The first layer of the encoder can learn the primary features of the original input, and the second layer can learn the secondary features corresponding to the primary features.

2.2.3. The Model Based on Convolution Neural Network. It is assumed that the neural network is an I input unit and a K output unit, the implicit layer is a layer, and the J unit is shared. The formula for the sum of squared errors is as follows:

$$E = \frac{1}{2}\sum_{k=1}^{k}\left(d_k - o_k\right)^2. \tag{3}$$

Among them, the following hold:

$o_k = f(net_k)$ is the actual output value of neuron k in the output layer.

d_k is the desired output value of the output layer neuron k.

y_j is the output value of hidden layer neuron j.

For the E-value, in order to achieve the goal of the ideal value, it is necessary to change the weight value of the network. First, adjust the connection weights between the implicit layer and the output layer.

$$w_{kj}(t+1) = w_{kj}(t) + \Delta w_{kj}. \tag{4}$$

In the above formula, the value obtained by the gradient method is the adjusted value of the connection weight between the implicit layer and the output layer.

$$\Delta w_{kj} = -\eta\frac{\partial E}{\partial w_{kj}} = \eta\left(d_k - o_k\right)f'\left(net_k\right)y_j. \tag{5}$$

In the above formula, η is the normal value, which is expressed as the iteration step.

In a similar manner, you can adjust the connection weights between the input layer and the implicit layer. Formula adjustment:

$$v_{ji}(t+1) = v_{ji}(t) + \Delta v_{ji}. \tag{6}$$

In the above formula, Δv_{ji} is the adjustment amount for determining the connection weight between the input layer and the implicit layer by the gradient method. It can be obtained from the following formula:

$$\Delta v_{ji} = -\eta\frac{\partial E}{\partial v_{ji}} = \eta\sum_{k=1}^{k}\left(d_k - o_k\right)f'\left(net_k\right)w_{kj}f'\left(net_j\right)x_i. \tag{7}$$

When there are samples, if there are P training samples, the total error sum form of the above calculation method is

$$E_p = \frac{1}{2}\sum_{p=1}^{P}\sum_{k=1}^{K}\left(d_k - o_k\right)^2. \tag{8}$$

As long as the operation is repeated for P samples as described above, Ep reaches the minimum requested value, and the algorithm ends.

The workflow is shown in Figure 2.

2.2.4. Recommendation Model Based on Recurrent Neural Network. Recent progress shows that RNN can effectively solve this part of the problem. Unlike feedforward neural networks, RNN has previous calculations, such as LSTM and GRU, which are usually used to overcome gradient disappearance in practical use.

2.2.5. Recommendation Model Based on Deep Semantic Similarity Model. In this model, different items are projected into a common low-dimensional space, and the similarity of items is calculated by cosine similarity calculation method. The details are shown in Figure 3.

2.2.6. Emerging Methods: Neural Autoregressive Distribution Estimation and Generative Countermeasure Network. Compared with other recommendation models based on deep learning, these two methods can obtain the best recommendation accuracy and good recommendation effect.

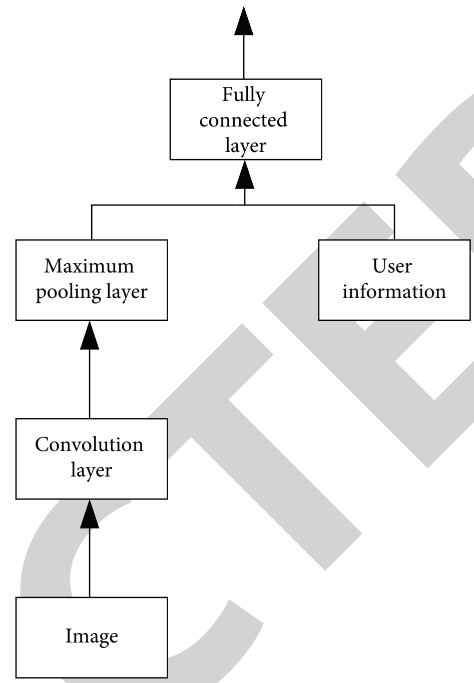

Figure 2: Workflow chart of attention-based convolution neural network recommendation model.

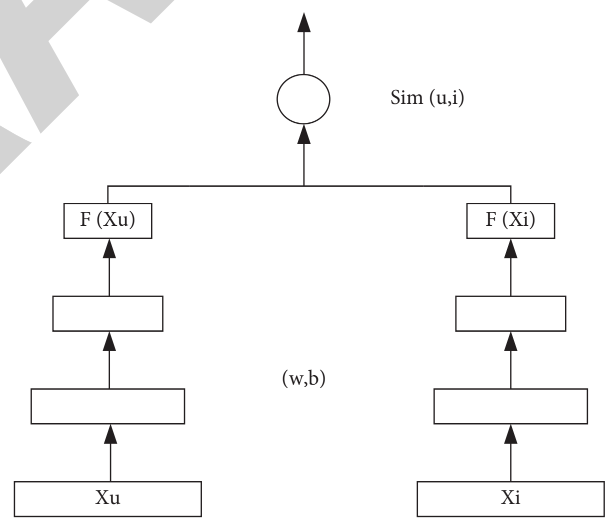

Figure 3: DSSM workflow chart.

3. Research on Adaptive Learning System Based on Personalized Learning Resource Recommendation Algorithm

3.1. Personalized Learning Resource Recommendation Algorithm Based on Deep Learning Model. This section proposes a personalized learning resource recommendation algorithm based on deep learning. Specifically, the algorithm [14, 15] does not simply carry out TOP-N recommendation, but considers students' learning progress and current situation, predicts students' actions according to time information, and recommends learning resources.

3.1.1. Problem Description. The purpose of the introduction of personality test questions is to analyze students' logs, obtain students' learning status, and provide high-quality test questions exercises with personality so as to help students get rid of monotonous and repeated mechanical exercises.

Howard Gedina, an American educator, believes that quality intelligence can be developed and that anyone's intelligence can be improved by learning. When introducing personalized examination questions, students' learning situation and cognitive ability should be considered, and corresponding recommendations should be made according to their actual conditions. If the difficulty of the problem is not set properly, it is the students' "cognitive loss." Appropriate organization of learning resource sequence can stimulate students' learning enthusiasm and learning efficiency. It is extremely important to determine the difficulty of learning resources and the sequence of the most effective learning resources in students' learning process, which is also called the principle of procedure. Therefore, when making exam recommendations, we should bravely jump out of the comfort zone of the target students and cannot practice between the knowledge points we have been learning. Proper development can improve students' enthusiasm and initiative.

3.1.2. Algorithm Framework. Figure 4 shows the framework of the algorithm proposed in this paper.

The main flow of the method proposed in this paper is defined:

(1) Analyze the data set, obtain the interactive records between students and exam questions, and construct

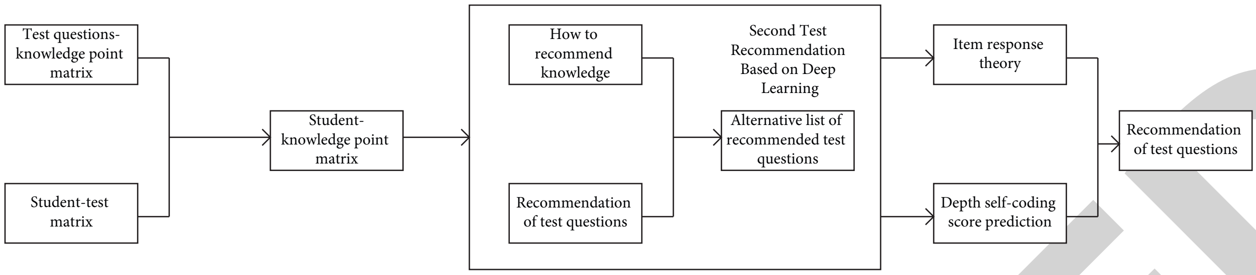

Figure 4: Personalized test recommendation algorithm framework.

the correlation matrix between questions and knowledge points.

(2) This paper introduces the detection problem of quadratic cooperative filter based on knowledge points. Firstly, knowledge points are recommended according to the knowledge point matrix of students, and then test questions containing recommended knowledge points are introduced on the basis of recommended knowledge points.

(3) According to the structural prediction model of IRT, judge whether the steps of using this knowledge point in the recommended examination are correct.

(4) Predict the recommended test questions according to the scores and judge the correct rate of each test question.

(5) Determine the final test question introduction list, control the difficulty range of the recommended test, and the final recommended test questions are not difficult.

3.1.3. Algorithm Implementation

Constructing Student-Knowledge Matrix. Firstly, the students' learning log is processed, and the interactive records between students and examination questions are obtained. The data format of each line of the student-exam question record seems to be "studentuid: probemuid: ratimestamp". Use the correct rate of exam questions to express students' grasp of this problem. A question contains many knowledge points, so students' exercises on examination questions are classified as exercises on students' knowledge points. The mapping relationship between student-examination question matrix and examination question-calculation knowledge point matrix is obtained, and the interactive matrix related to student-knowledge points is standardized and uniformly processed, and the interactive records are integrated. Students use the correct rate of all questions including a certain knowledge point to express their mastery of the knowledge point and record it as a time stamp of dialogue with the knowledge point in the maximum time, and finally get the student-knowledge point column. The interactive record of student-examination questions is further changed into the interactive record of student-knowledge point, and "studentuid: kcuid: ratimestamp" is recorded. Finally, according to the chapters with knowledge points, ECharts is used to show the processed results. Organize the knowledge points of learning and understand the overall grasp of the situation.

Bi-LSTM Collaborative Filtering. The Long Short-Term Memory Network (LSTM) [16, 17] is a special RNN of the network structure shown in Figure 5. LSTM model is used to overcome the increase of long-term storage calculation index of RNN. Besides the basic structure of RNN, valve nodes of each layer are added to determine whether the model storage state is added to the calculation of this layer.

In LSTM model training, the state transfer is carried out from the back direction to one direction, but in some problems, the output of the current time is not only related to the previous state, but also related to the subsequent state. In this case, a bidirectional LSTM (Bi-LSTM) model is needed. Bi-LSTM is composed of two parts of one-way LSTM. The basic flow of secondary recommendation based on knowledge points using Bi-LSTM is as follows:

(1) Raw data conversion

Generate a model training data set. After the data set is thermally encoded separately, sparse data with m binary features will be formed. By using single hot coding, the problem that the classifier cannot deal with attribute data well can be overcome.

(2) Confirmation and adjustment of network model structure

After a series of experimental studies, we can determine the Bi-LSTM network model [18], determine the obsolescence rate of each layer, the repeated updating mode of weighting parameters, and the best model training including epoch and batch size. Finally, we decided to recommend the most effective Bi-SLSTM network model structure for personalization problems [19].

(3) Prediction of model training results

In the recommended method of submitting test questions, firstly, knowledge points are recommended according to the interaction records between students and knowledge points. In addition, on the basis of recommending knowledge points, according to the alternate records of students and examination questions, personalized examination questions based on knowledge points are recommended, and the candidate recommendation list of personalized examination based on knowledge points is determined.

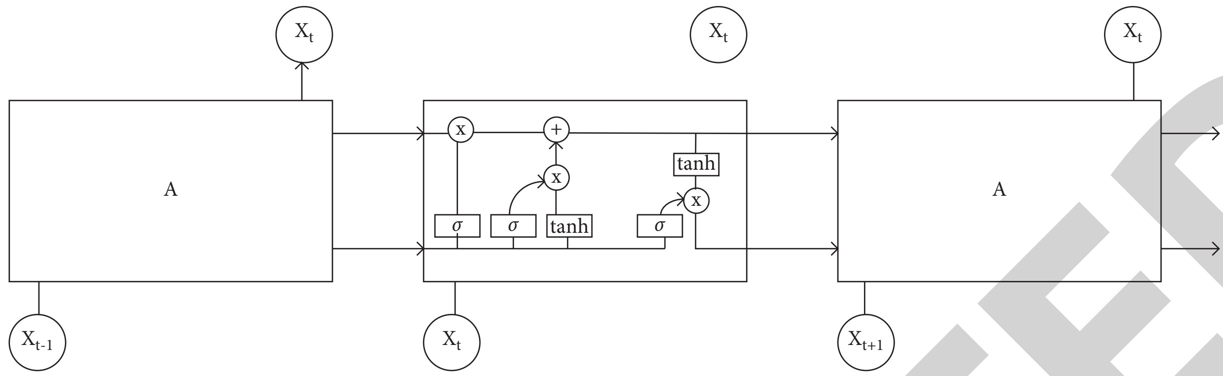

FIGURE 5: LSTM model structure diagram.

Item Response Theory Model. The original data is processed to obtain cognitive diagnosis data set. In the case of model training, weights are assigned to each sample data, and these weights constitute vector D. The error rate calculation method is defined as follows [20]:

$$\varepsilon = \frac{\text{Number of samples incorrectly classified}}{\text{Number of all samples}}. \tag{9}$$

The change formula of error sample weight is as follows:

$$D_i^{(t+1)} = \frac{D_i^{(t)} e}{\text{Sum}(D)}. \tag{10}$$

The correct sample weight is changed as follows:

$$D_i^{(t+1)} = \frac{D_i^{(t)} e^{-a}}{\text{Sum}(D)}. \tag{11}$$

t is the current classifier and i indicates the ith sample. Then, the updated sample weight training is used to repeat the above process. The weighting calculation formula of classifier is as follows:

$$a = \frac{1}{2} \ln\left(\frac{1-\varepsilon}{\varepsilon}\right). \tag{12}$$

Use the last trained model to predict students' learning resources in Figure 6.

3.2. Students' Adaptive Learning System. Adaptive learning system is divided into online learning subsystem, individual test subsystem, learning information analysis subsystem, and resource management subsystem according to business functions. In the online learning subsystem, students order and study courses according to their needs, and when they learn to a certain stage, they can take the exams published by the course teachers to achieve the purpose of consolidating exercises in Figure 7.

Business service model is a module that provides substantive operations and applies specific business operation processes. The course management mainly depends on the business service module to process and supplement the business service. The storage side is the efficiency of storing and submitting data management for related data.

4. Experiment

4.1. Data Collection and Processing. Table 2 is the record data, which contains a series of question record information, such as student ID, question grade, and question name. According to the problem log information, the cognitive status of students' knowledge points is obtained.

Data sets are processed and analyzed through deep learning model. On the other hand, by extracting the information recorded for each problem, the right and wrong information of students' knowledge points and steps corresponding to specific problems can be obtained. According to the statistics of knowledge points, understand the knowledge points of students (correct rate). Finally, through the interaction between students and the knowledge points, the timestamp information can be recorded, and the students and examination questions, knowledge points, cognitive status, and timestamp information can be obtained. On the other hand, by processing the whole data set based on knowledge points, we can obtain the relevant information that the number of occurrences of knowledge points represents the weight of knowledge points. It is important to express the error rate of students' knowledge points.

4.1.1. Precision. Accuracy is one of the important indexes of students' adaptive learning system. Introductory problems applied to individualized learning problems. That is, it represents the ratio of the number of questions hit practiced by the user in the test set to the total number of recommended tests R.

$$\text{Precision} = \frac{\text{hit}}{R}. \tag{13}$$

4.1.2. Recall. Recall rate is another important indicator for evaluating students' adaptive learning system, and it is suitable for recommending questions of personality test questions. That is, it represents the ratio of the number of questions hit practiced by the user to the number of questions T practiced by the user in the test question. Specific definition formula is

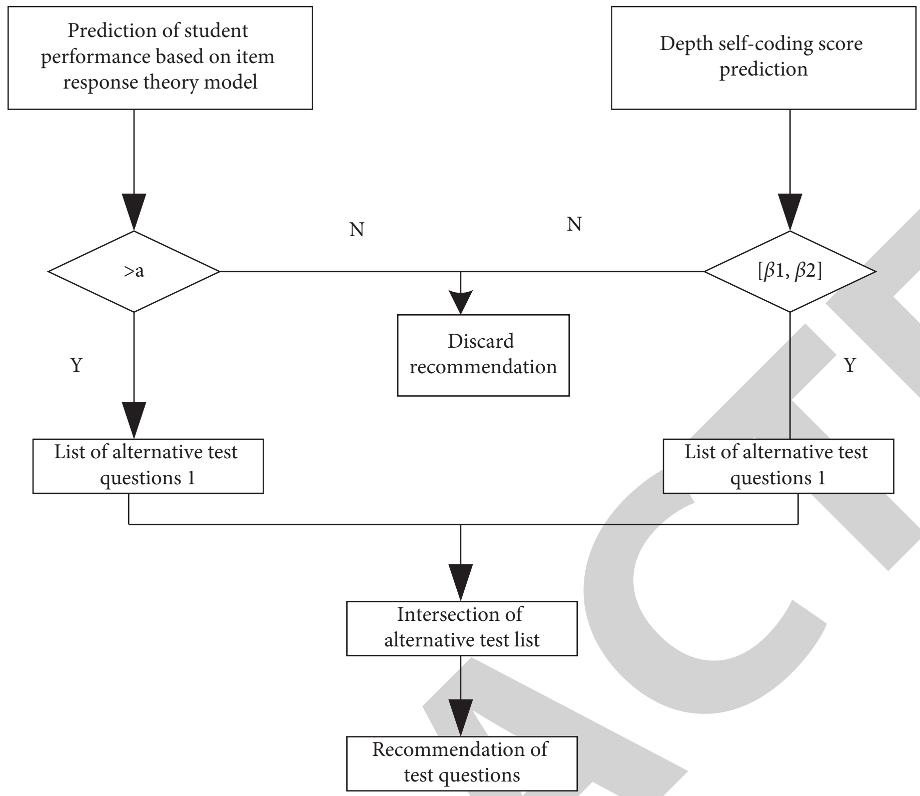

Figure 6: Flowchart of determining the recommended list of test questions.

$$\text{recall} = \frac{\text{hit}}{T}. \tag{14}$$

4.1.3. Item_Coverage. Project coverage is to measure the mining ability of the final project recommendation system. Excellent recommendation improves the user experience, improves the possibility of users using the project to achieve their goals, and should have the opportunity to recommend each project in the system as much as possible. Item_Coverage is numerically equal to the total number of recommended different items.

4.1.4. Average Difficulty (AD). Different from the introduction of traditional movies and music, the essence of the problem is the actual grasp of knowledge points introduced by students. Therefore, only using the evaluation parameters (correct rate, recall rate, and $F1$) based on the previous TOP-N or evaluation prediction idea is not comprehensive enough. Therefore, in order to evaluate the recommendation results of test questions, this paper puts forward the average difficulty of test questions AD.

$$\text{AD} = \frac{\sum_{i=1}^{n} D}{n}, \tag{15}$$

where D is the difficulty of each test question and n is the number of recommended test questions. AD indicates the average difficulty of the test question, but the smaller the AD value, the simpler the recommended test, and the purpose of practice cannot be achieved. If the AD value is small, it is difficult to recommend the exam, which means that the correct rate of students is low. The AD value of the recommended result should be kept within an appropriate range.

4.2. Comparison of Algorithms. In this paper, the proposed test problem recommendation method is verified by comparative experiments, including user-based collaborative filtering recommendation algorithm, potential trajectory modeling recommendation method, and Markov chain comparison. User-based common filtering recommendation algorithm is one of the most classical recommendation algorithms. Markov chain is a recommendation algorithm based on classical sequence. In addition, the recommendation method of personalized test questions based on deep learning proposed in this paper is also the recommendation of test questions based on sequential questions. The selection of Markov chain can better show the efficiency of the recommended method proposed in this paper.

4.2.1. User-Based Collaborative Filtering Recommendation Algorithm (UserCF).

$$sim(u, v) = \sum i \in (Pu \cap Pv) \frac{\left(R_{u,i} - \overline{R}_t\right) \times \left(R_{v,i} - \overline{R}_t\right)}{\sqrt{\left(R_{u,i} - \overline{R}_t\right)^2} \times \sqrt{\left(R_{v,i} - \overline{R}_t\right)^2}}, \tag{16}$$

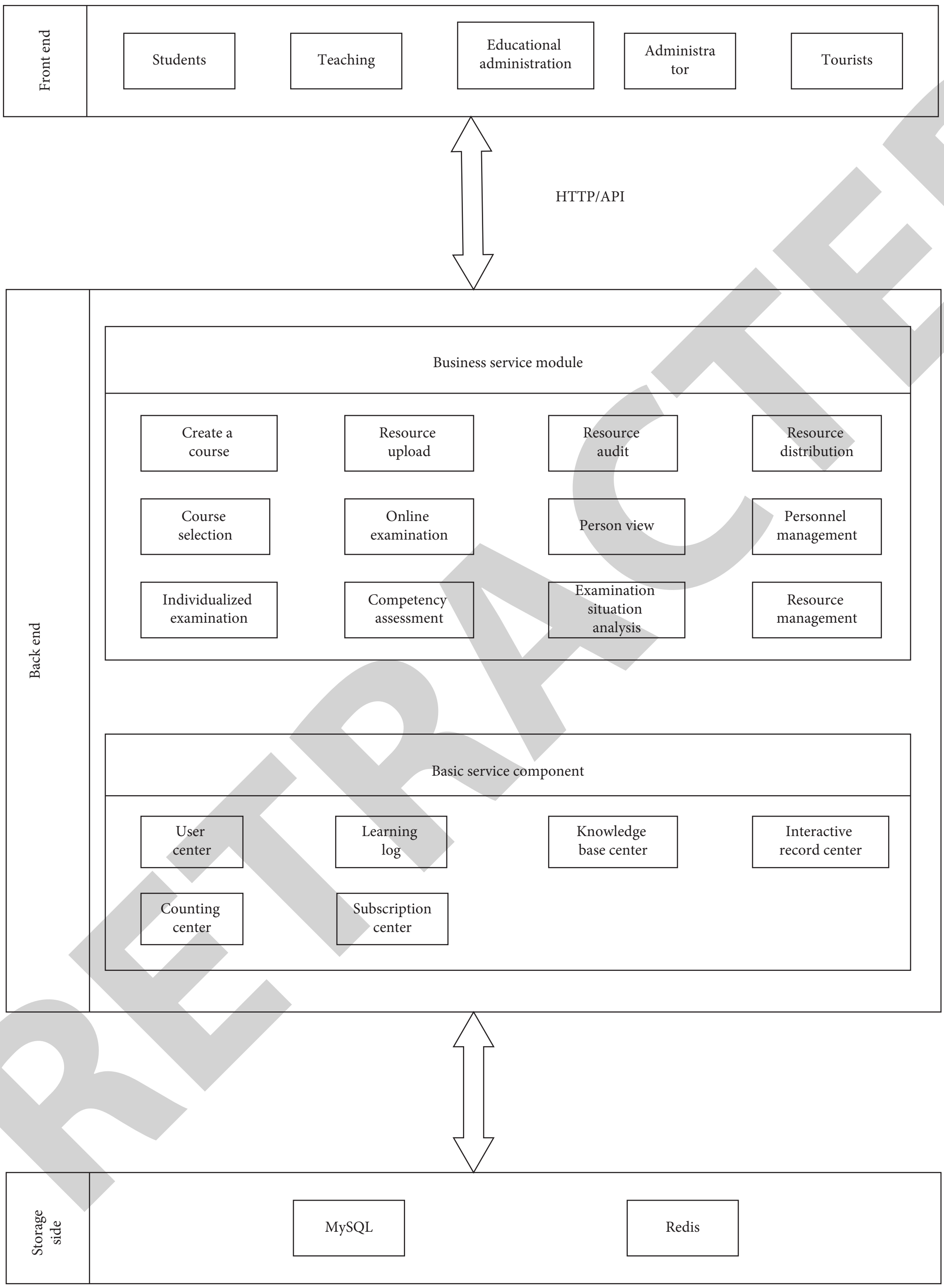

Figure 7: Architecture diagram of students' adaptive learning system.

Table 2: Data set field description.

Field name	Remarks	Field name	Remarks
Anon student ID	Student ID	Step duration	Step time
Problem hierarchy	Chapter	Correct step duration	Correct step time
Problem name	Test questions	Error step duration	Error step time
Problem view	Number of problems encountered	Correct first attempt	First attempt time
Step name	Step name	Incorrects	Number of errors

where P_u is the set of exercise questions for student u; P_v is the set of exercise questions for student v; and $R_{u,i}$ is the score of student u on test i.

After determining the similar student groups of the target students, the performance of the test questions of the target students is predicted according to the weighting of the similar student groups and the scores of the test questions, and the test questions recommendation list is obtained to recommend the test questions.

4.2.2. Latent Trajectory Modeling Recommendation Algorithm (LTM). Latent trajectory modeling (LM) recommendation algorithm is an effective method to introduce time element into the recommendation method.

4.2.3. Markov Chain Prediction Algorithm (MarkovChain). First of all, model the practice records of students' examination questions, make examination questions with different states, and write X1, X2, X3, and X4.... The value of X_n is a matter of practice at time n. $X_n + 1$ is a function of the conditional probability of the past state X_n. The calculation formula is as follows:

$$P\left(X_{n+1} = x \mid X_1 = x_1, X_2 = x_2, \ldots, X_n = x_n\right) = P\left(X_{n+1} = x \mid X_n = x_n\right). \tag{17}$$

According to the Markov chain test questions, the test questions that predict the students' next state and practice are recommended.

4.3. Result Analysis. Firstly, the Bi-LSTM model is adjusted, including learning rate, dropout, and batch size. The quality of the model is judged from four angles: recall rate, sps, project coverage, and ndcg, and the structure of the model is finally determined.

4.3.1. Learning Rate (learning_rate). Learning rate determines whether the training of deep learning model can converge to local minimum and convergence speed. In order to select the best learning rate, 1, 0.1, 0.01, 0.001, and 0.0001 were selected in turn for comparative experiments. Experimental results (Figure 8) show the evaluation of experimental results of learning_rate.

It can be observed through Figure 8 that when the learning rate is 0.0001, the training mode is obviously dominant in the recall rate, and with the training, the recall rate is significantly improved. When the learning rate is 0.001 and 0.0001, although the growth trend of sps, item_coverage, and ndcg is the same, the performance of 0.0001 learning rate is better than 0.001. On the other hand, when the learning rate is 1, 0.1, and 0.01, the other evaluation indexes have no obvious improvement with the training. Therefore, 0.0001 is the learning rate of the final model.

4.3.2. Dropout. In order to avoid the overfitting phenomenon in deep learning mode training, that is, the trained model shows excellent performance in training data, but due to poor performance and low accuracy of test data, the method of adjusting Dropout parameters is adopted. In this adjustment of Dropout, a comparative experiment was performed using 0.4, 0.5, 0.6, 0.7, and 0.8, and the experimental results are shown in the evaluation of experimental results of Dropout in Figure 9.

It can be seen from Figures 9(a)–9(d) that with the training, recall, sps, item_coverage, and ndcg have similar changes when dropout is 0.4, 0.5, 0.6, 0.7, and 0.8. But dropout was unstable at 0.7 and 0.8. Combining the performances of recall, sps, item_coverage, and ndcg, the final dropout is determined to be 0.5.

4.3.3. batch_size. batch_size is one of the important parameters of deep learning. Appropriate batch_size can improve memory utilization, while inappropriate batch_size will lead to slow convergence and other problems. Choose 16, 32, 64, 128, and 256 for comparative experiments, and the experimental results are shown in Figure 10.

As can be seen from Figures 10(a)–10(d), with the training, batch_size tends to change like recall, sps, and dcg at 16, 32, 64, 128, and 256. The item_cover with batch_size of 256 performs well at the start of the training and has a steady tendency thereafter. When batch_size is 16,256, the performance of recall, sps, item_cover, and ndcg is fluctuating. Combining all the results and their stability, the value of batch_size is finally determined to be 32.

The data set is divided into 0.6, 0.7, 0.8, and 0.9 for training, and the segmentation results are displayed in the experimental data set in Table 3.

Specific comparative experimental results are shown in Figure 11; with the increase of training groups, the accuracy of the previous UserCF began to decrease significantly, the accuracy of LTM has been at a low level, MC and the method proposed in this paper are relatively stable, and the comparison has been improved to a certain extent. According to Figure 11(b), the recall values of UserCF and MC methods change obviously with the increase of the proportion of training groups, but although the recall values of the methods proposed in this paper and LTM are low, the values are always stable. As can be seen from MC method (Figure 11(c)), with the expansion of training set, item_coverages decreases like a cliff, which is not conducive to new learning resources. The project coverage of this method has always maintained stable and excellent performance. As can be seen from Figure 11(d), the examination question resources of the method proposed in this paper are relatively stable, and it has better applicability considering whether

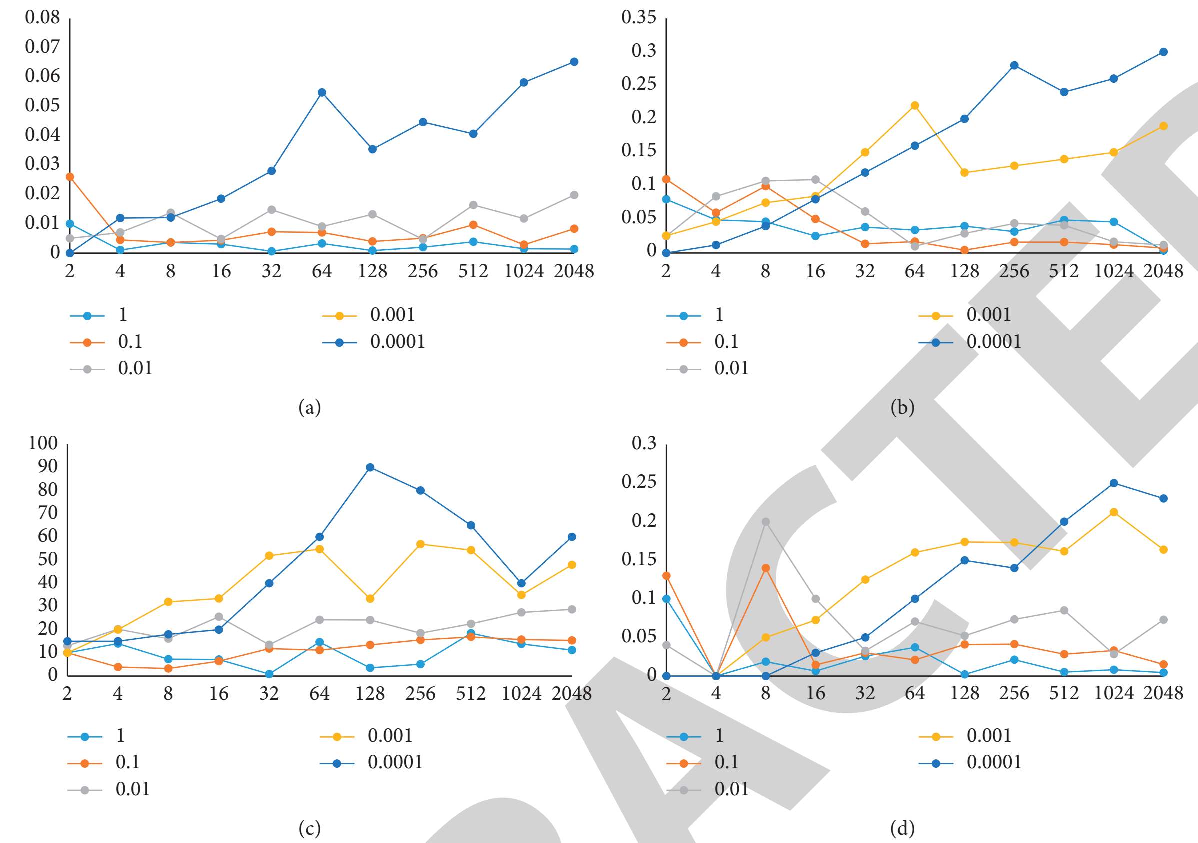

FIGURE 8: Evaluation of learning_rate experimental results. (a) Recall. (b) sps. (c) item_coverage. (d) ndcg.

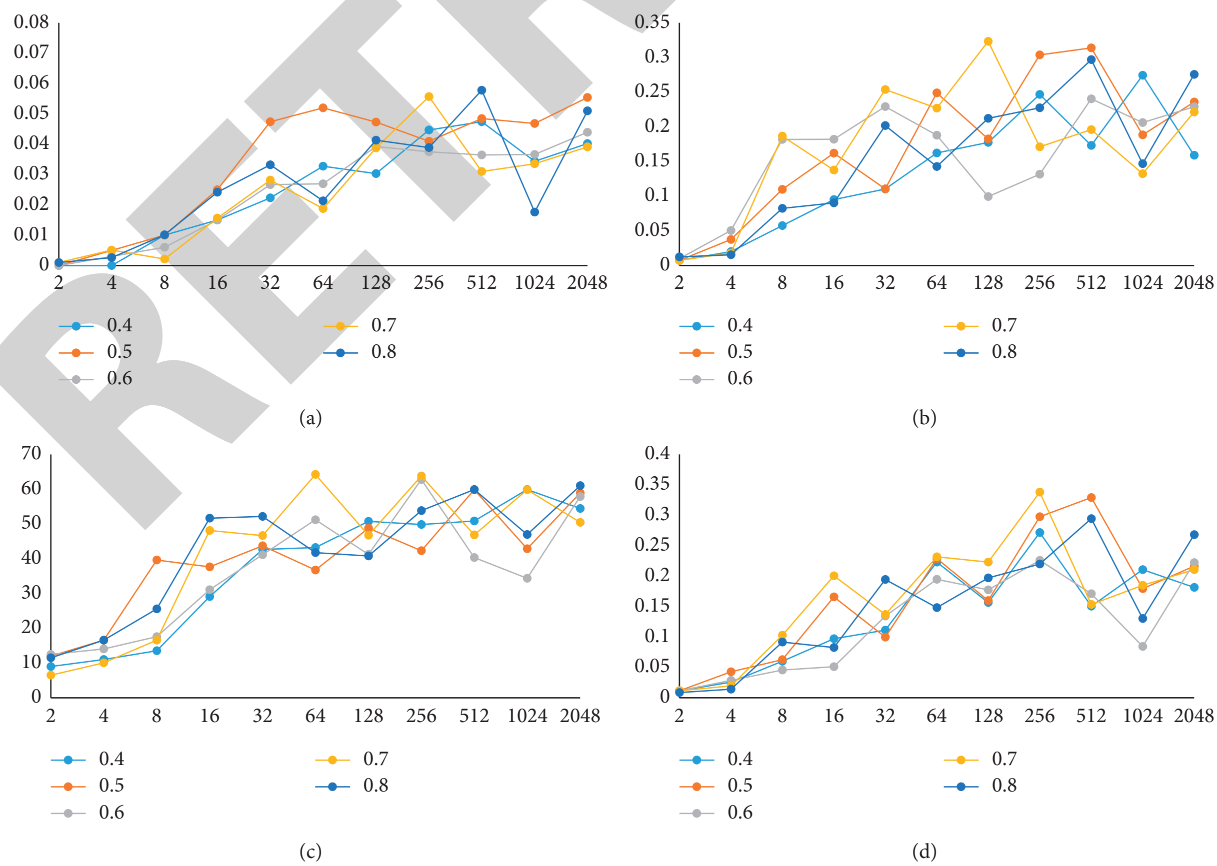

FIGURE 9: Evaluation of Dropout experimental results. (a) Recall. (b) sps. (c) item_coverage. (d) ndcg.

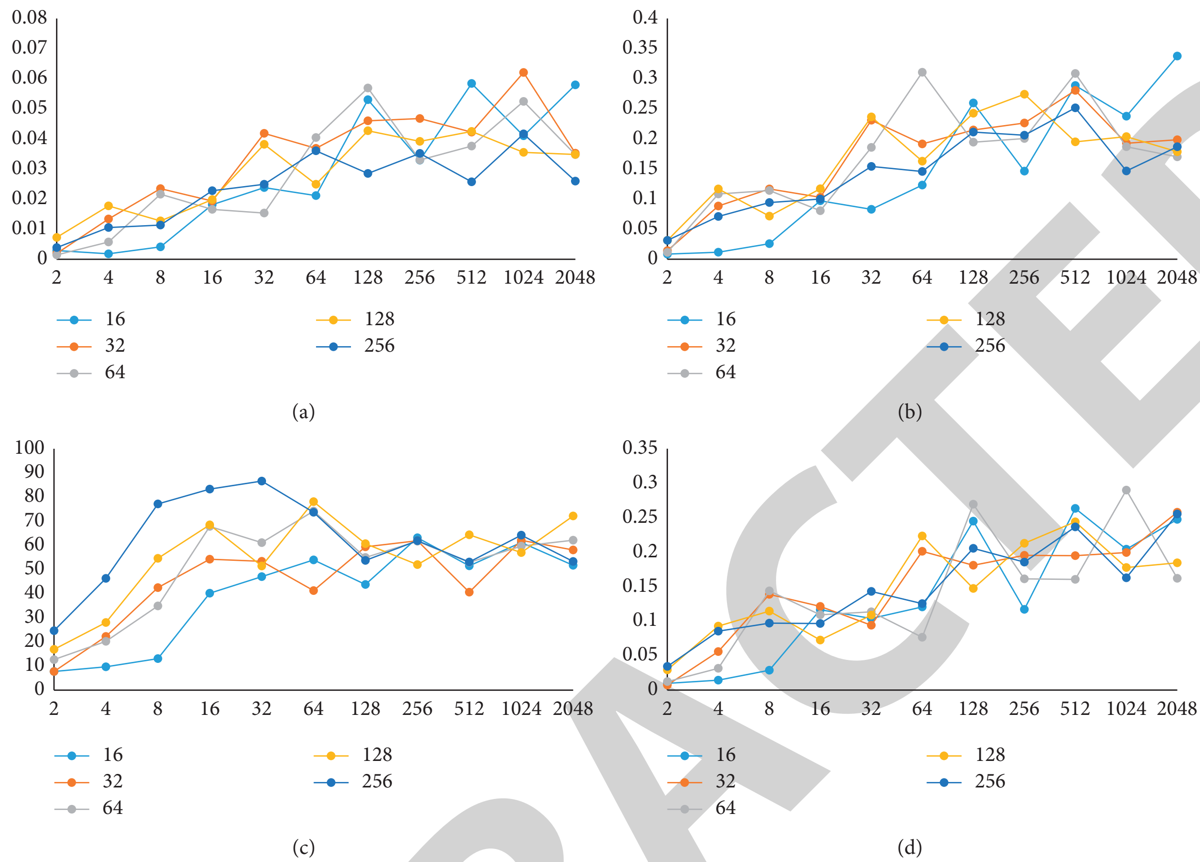

Figure 10: Evaluation of batch_size experimental results. (a) Recall. (b) sps. (c) item_coverage. (d) ndcg.

Table 3: Experimental data set.

Training set ratio	0.6			0.7			0.8			0.9		
	Full	Train	Test	Full	Train	Test	Full	Train	Test	Full	Train	Test
Users	2913	1874	1040	2913	2121	793	2915	2364	552	2912	2915	274
Items	15046	15028	12984	15045	15042	11807	15044	15044	9920	15043	15044	9982
Interaction	418291	265417	152873	418291	302817	115473	418291	338273	80019	418291	418291	39488

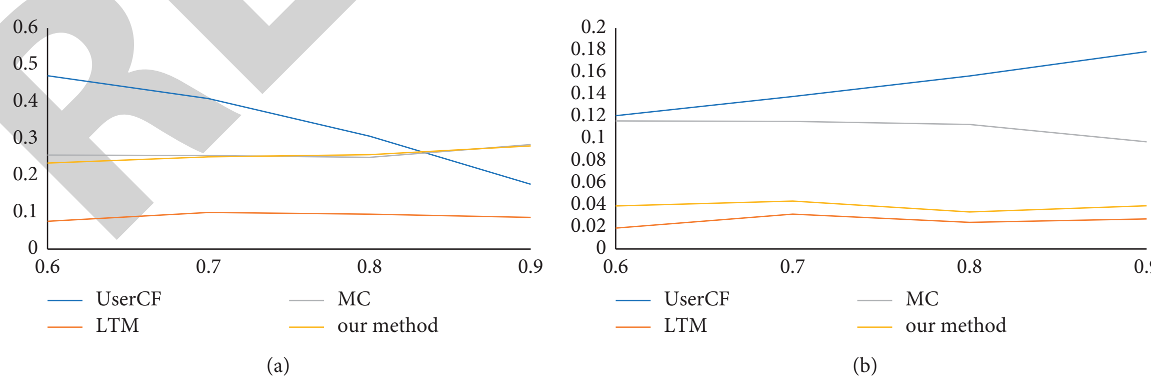

Figure 11: Continued.

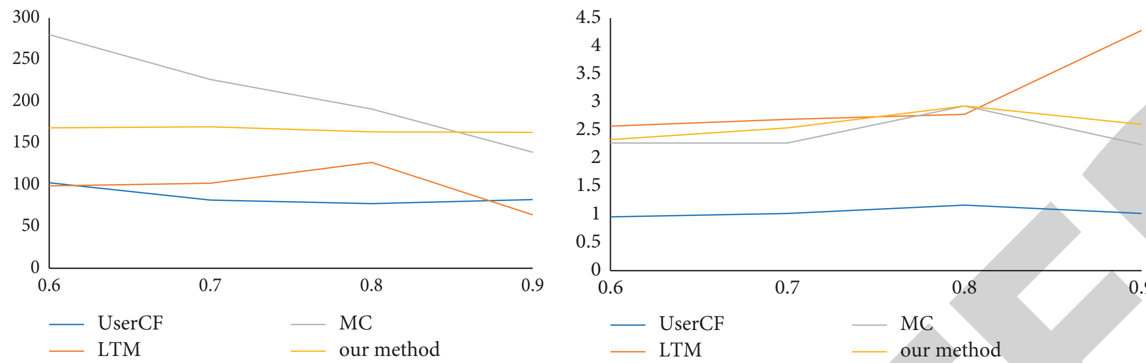

(c) (d)

Figure 11: Evaluation of comparative experimental results. (a) Precision. (b) Recall. (c) item_coverage. (d) AD.

students adapt or not. The topics recommended by UserCF are not practical. The Markov Chain Prediction Algorithm is not more practical because of its unstable difficulty in the test questions recommended by the Markov Chain Prediction Algorithm. According to the above analysis, the recommendation method of personalized learning resources based on deep learning proposed in this paper has high stability even if the training data are different in size and can recommend corresponding topics to students with personality. The recommendation results can be further explained.

5. Conclusion

This paper discusses some disadvantages of Chinese traditional education and introduces students' self-adaptive learning system to solve these problems by understanding the definition, principle, research status, and key technologies of adaptive learning system. By studying the core part of personalized recommendation in adaptive learning system, a personalized learning resource recommendation algorithm based on deep learning model is proposed. The effectiveness of recommending learning resources is proved by comparative experiments, and it is integrated into students' adaptive learning system. At the same time, personalized learning in the field of education is one of the hot research topics at present, but it is still in the stage of theoretical research and faces many problems. The key research work in the future is to study the personalized recommendation methods for individual learners. Different behaviors, interests, and habits can improve the accuracy of recommendation.

Data Availability

The experimental data used to support the findings of this study are available from the corresponding author upon request.

Conflicts of Interest

The authors declare that they have no conflicts of interest regarding the publication of this work.

References

[1] Z. Wang and H.-T. Liao, "Towards the eco-design of Artificial Intelligence and Big Data applications: a bibliometric analysis of related research," *IOP Conference Series: Materials Science and Engineering*, vol. 806, no. 1, 5 pages, Article ID 012039, 2020.

[2] W. Duarte and L. Bernal, "Teaching-Learning Ergonomics in Virtual and Distance Education: Bibliometric Review," in *Proceedings of the Advances in Intelligent Systems and Computing,Advances in Human Factors in Training, Education, and Learning Sciences*, pp. 112–117, USA, 2020.

[3] M. Li and L. Wang, "A Survey on Personalized News Recommendation Technology," *IEEE Access*, vol. 7, pp. 145861–145879, 2019.

[4] M. Taheri, "An evaluation of an adaptive learning system based on multimodal affect recognition for learners with intellectual disabilities," *British Journal of Educational Technology*, vol. 51, no. 5, pp. 1748–1765, 2020.

[5] J. Liang, Y. Xu, C. Bao, Y. Quan, and H. Ji, "Barzilai-Borwein-based adaptive learning rate for deep learning," *Pattern Recognition Letters*, vol. 128, pp. 197–203, 2019.

[6] S. Jagadeesan and J. Subbiah, "Real-time personalization and recommendation in adaptive learning management system," *Journal of Ambient Intelligence and Humanized Computing*, vol. 11, no. 11, pp. 4731–4741, 2020.

[7] A. Mb, B. Bh, and A. Me, "Towards an adaptive E-learning system based on Q-learning algorithm - ScienceDirect," *Procedia Computer Science*, vol. 170, pp. 1198–1203, 2020.

[8] S. Sridharan, D. Saravanan, A. K. Srinivasan, and B. Murugan, "Adaptive learning management expert system with evolving knowledge base and enhanced learnability," *The Journal*, vol. 26, pp. 5895–5916, 2021.

[9] X. Fang, J. Wang, and D. Seng, "Recommendation algorithm combining ratings and comments," *AEJ - Alexandria Engineering Journal*, vol. 60, no. 6, pp. 5009–5018, 2021.

[10] W. Liu, Z. Lin, H. Zhu, and J. Wang, A. K. Sangaiah, Attention-based adaptive memory network for recommendation with review and rating," *IEEE Access*, vol. 8, Article ID 113953, 99 pages, 2020.

[11] C. H. Lai, D. R. Liu, and K. S. Lien, "A hybrid of XGBoost and aspect-based review mining with attention neural network for user preference prediction," *International Journal of Machine Learning and Cybernetics*, vol. 12, no. 5, pp. 1–15, 2021.

[12] B. Cai, X. Zhu, and Y. Qin, "Parameters optimization of hybrid strategy recommendation based on particle swarm

Hindawi
Scientific Programming
Volume 2021, Article ID 4872947, 11 pages
https://doi.org/10.1155/2021/4872947

Research Article

Research on Sports and Health Intelligent Diagnosis Based on Cluster Analysis

Zhiqiang Lian, Shanyun Liu, Jieming Lu, and Luxing Zhou

Tianjin University of Sport, Tianjin 301617, China

Correspondence should be addressed to Zhiqiang Lian; 201920200005@stu.tjus.edu.cn

Received 21 October 2021; Revised 5 November 2021; Accepted 18 November 2021; Published 14 December 2021

Academic Editor: Le Sun

In order to explore the relationship between sports and health and improve the scientific nature of sports, this paper uses cluster analysis algorithm as the basis, adopts the entropy estimation method for small sample sets to estimate the information entropy value, and improves the mutual information estimation to propose a mutual information estimation method based on entropy estimation. Moreover, this paper uses a clustering algorithm to combine sports and health intelligent diagnosis requirements to construct a system structure. The system recommends better sports suggestions to the user according to the user's physical condition, makes sports plans according to the user's health, and can also analyze the user's sports process. In addition, on the basis of demand analysis, this paper designs experiments to test the performance of the system constructed in this paper. From the experimental statistical results, it can be seen that the system constructed in this paper can basically meet the actual needs of sports and health intelligent diagnosis. At the same time, this paper proves that there is a strong correlation between sports and health.

1. Introduction

In the modern city, people's physical labor is less and less and mental work and work pressure are more and more, so people's physical function according to the current mode of life is gradually declining. Therefore, the defense ability of the whole body should be improved through sports, including muscle, bone, and the whole internal organs system and body circulation system. Therefore, it is necessary to study the benefits of aerobic metabolism sports on menopausal women health.

Exercise therapy is the application of sports in medicine. It is a treatment method based on kinematics, biomechanics, and neurodevelopment, and its main goal is to improve the physical, physiological, psychological, and spiritual dysfunction, and its main factor is force and reaction. Exercise therapy includes both active physical activity training and passive physical activity training, and its functions include improving blood circulation, metabolism, and nerve control of sports tissues (muscles, bones, joints, and ligaments), promoting neuromuscular function, improving muscle strength, endurance, cardiopulmonary function, and balance function, and alleviating abnormalities [1].

Moderate and active sports can make people feel comfortable, relaxed, and happy, thus weakening the pressure brought by the fast-paced modern life. After sports, people can also be relaxed due to the end of muscle contraction or hormone secretion. Although sports can not completely eliminate the pressure source and also face pressure and tension after sports, it can temporarily reduce pressure and remove harmful energy substances to the human body. When people face pressure again in a comfortable and happy mood, they will face the challenge of pressure with a positive and confident attitude [2].

The idea that sports is medicine (ELM) has existed for a long time. In 2007, the American Sports Medicine Association formally proposed ELM as a health promotion action to solve global public health problems, which has been widely responded to and promoted in many countries and regions. The aim of ELM is that doctors, fitness professionals, and other health care providers apply scientific evidence and policies on the relationship between sports and health in practice and apply evidence of sports science research to public health practice in the form of laws or illegal legal policies, so as to promote the globalization of EIM. EIM suggests that the level of physical activity should be taken as a basic vital sign and included in the content system of doctor consultation. Clinicians and health managers should actively participate in preventive health services to promote the improvement of the level of physical activity and advocate a positive and healthy lifestyle. EIM is a global public health practice based on evidence.

Based on the above analysis and clustering analysis algorithm, this paper constructs an intelligent diagnosis system of motion and health based on cluster analysis, studies the relationship between motion and health, and verifies the performance of the system.

2. Related Work

By studying the influence of Taijiquan Exercise on human physical health, literature [3] found that different frequencies of Taijiquan sports have a positive impact on the human respiratory system and cardiovascular system and can also improve the flexibility of the human body. Through the study of the influence of sports on human physical health, literature [4] found that long-term sports has a good effect on human body shape, especially on the weight index, and can play the role in weight loss. The research of literature [5] shows that the effect of sports on the vital capacity of boys and girls is different; that is, it can significantly improve the vital capacity of boys but can only maintain the original vital capacity of girls. The research of literature [6] shows that sports can significantly improve the strength of boys' upper limbs, but it has no obvious effect on girls' upper limb strength, but it also has a certain effect, and sports can improve the quality of human speed and endurance. In the study of the effect of aerobic sports on human cardiopulmonary function in literature [7], it was found that aerobic sports has a benign effect on the cardiopulmonary function of the human body, can improve the myocardial function, make the blood circulation supply capacity more smooth, and increase the vital capacity, can improve the aerobic metabolism ability of the body, and also can improve the contractile ability of the heart and the relaxation tension of the blood vessels, enhance the elasticity of the blood vessels, promote the blood lipid metabolism, effectively prevent arteriosclerosis, and thus reduce the blood pressure and improve the cardiovascular function when the body is quiet. By studying the influence of different elective courses on human physical health, literature [8] found that different elective courses have different degrees of influence on human physical health.

There are internal and external factors and subjective and objective factors that affect human physical health, and the internal and external factors are mainly congenital inheritance and acquired. The subjective factor mainly includes their own personality characteristics and cognition of physical health [9]. By studying the relationship between subjective factors and human physical health, literature [10] concluded that the subjective factors affecting human physical health are mainly the cognition of physical health, and the degree of cognition of physical health is an important factor affecting human physical health. In addition, people's own personality characteristics also have a great impact on physical health. The physical condition of extroverted people is much better than that of introverted people. Literature [11] believed that the physical health status of people with lively and extroverted personality and high enthusiasm is significantly better than that of people with introverted personality and low enthusiasm. Through the investigation of people's sports lifestyle, literature [12] found that sports lifestyle and habits are the important reasons for affecting physical health and finally concluded that a good sports lifestyle is an important factor affecting people's physical condition. Literature [13] analyzed the relationship among obesity rate, family income, and physical health status through relevant research on the influence of obesity rate on physical health status in colleges and universities. The results show that family economic status has a significant impact on male obesity, which is basically proportional to the relationship, while female obesity is less affected by family income status, which is not significant or linear. The analysis of literature [14] shows that there are many factors that affect the physical fitness of the masses in China. Among them, the main social reason is online games, which makes the human body ignore the awareness of sports. Second, the school ignoring the importance of fitness is one of the important factors, so that the campus cannot form a good fitness atmosphere, resulting in poor physical health of students.

With the development of social science and technology, Internet technology has been widely used in society, which provides a new platform for sports health control and management system [15]. We can install a control terminal on the detection equipment and use Internet technology to control the terminal to collect the data of the detection equipment and upload the data to the background cloud computing server of the sports health control and management system, so as to avoid the inconvenience of user manual input and improve the efficiency [16].

3. Information Entropy Estimation of Sports and Health

In the estimation of information entropy, the general method is to use the discrete probability of variables and usually use the histogram method to estimate the probability density of discrete random variables. When the sample set is large enough, the estimated value of information entropy tends to its true value. However, in the case of small sample size, if we still use the simple method to replace the probability in the histogram with the observed frequency, the statistical fluctuation will make the distribution look less uniform, which will lead to the underestimation of information entropy. In this case, the estimation of information entropy will be biased, which will affect the accuracy of information entropy calculation. At present, a lot of research work has put forward relevant suggestions on how to estimate the deviation in order to reduce the deviation of information entropy estimation. Similarly, in the estimation of continuous and discrete variables, there is the problem of estimation bias.

In the histogram method, a given discrete random variable X contains N results $X = \{X_1, X_2, \ldots, X_n\}$. And the corresponding number of occurrences is $x_i = \{n_1, n_2, \ldots, n_N\}$, $i \in (1, N)$ which has the following formula:

$$n = |X| = \sum_{i=1}^{N} n_i,$$
$$\widehat{p}(x_i) = \frac{|x_i|}{|X|} = \frac{n_i}{n}. \tag{1}$$

The following results can be derived:

$$\begin{aligned} H(X) &= -\sum_{i=1}^{N} p(x_i)\log\, p(x_i) \\ &= -\sum_{i=1}^{N} \frac{n_i}{n}\log\frac{n_i}{n} = \sum_{i=1}^{N}\frac{n_i}{n}\left(\log\, n - \log\, n_i\right) \\ &= \log\, n\sum_{i=1}^{N}\frac{n_i}{n} - \frac{1}{n}\sum_{i=1}^{N} n_i \log\, n_i \\ &= \log\, n - \frac{1}{n} n_i \log\, n_i. \end{aligned} \tag{2}$$

Formula (2) is called the naive entropy estimation, and the information entropy is estimated by counting the frequency of discrete values in the sample set.

The relevant literature explains the deviation of the naive estimation method. If the real entropy value of the random variable is assumed to be H, then the expected value of the entropy value estimated using formula (2) is as follows [17]:

$$E\left[H_E\right] = H - \frac{N-1}{2n} - \frac{1}{12n^2}\left(1 - \sum_{i=1}^{N}\frac{1}{p(x_i)}\right) + O\left(n^{-3}\right). \tag{3}$$

Miller proposed the Miller correction term to correct the deviation of the primary term $(N-1)/2n$, which is called Miller correction, and designed an entropy estimation method that takes into account the deviation in the entropy estimation process. The Miller-adjust entropy estimation method is defined as follows [18]:

$$H_M(X) = H(X) + \frac{N-1}{2n}. \tag{4}$$

Formula (4) corrects the deviation of the naive estimation method in the primary term, so that the estimated entropy value is relatively closer to the true entropy value, and further improves the accuracy of the entropy estimation method. The Miller-adjust method only corrects the deviation of the first term in formula (3). However, the quadratic and higher-order terms in formula (3) all depend on the true probability density function value, so it is usually difficult to estimate and correct.

Hierarchical clustering of mutual information based on the Grassberger entropy estimation method is as follows.

Grassberger proposed a series of entropy estimation methods by considering the deviation in entropy estimation. They all have the following basic forms but differ in the expression of the $\Phi(x_i)$ term [19].

$$H_\Phi = \log\, n - \frac{1}{N}\sum_{i=1}^{N} n_i \Phi(x_i). \tag{5}$$

If we approximate $\Phi(x_i)$ in the formula to $\log\, n_i$,

$$\Phi(x_i) = \log\, n_i. \tag{6}$$

Formula (5) will be transformed into formula (2); that is, the abovementioned entropy estimation method will be transformed into the Naive entropy estimation method by substituting formula (6). If Grassberger assumes that the probability density $p(x_i)$ is much less than 1, then the sample set will follow a Poisson distribution. Therefore, the q-order Renyi entropy can be defined as follows:

$$H(q) = \frac{1}{1-q}\log\sum_{i=1}^{N} p^q(x_i). \tag{7}$$

When q infinitely tends to 1, formula (7) is transformed into Shannon entropy. $p^q(x_i)$ in formula (7) can be estimated by the following formula:

$$p^q(x_i) = \frac{1}{n^q}\frac{N!}{(N-q)!}. \tag{8}$$

Among them, n represents the number of samples and N represents the number of random variables with different values in the sample set. In a study by Grass Gerber, the Γ function is used to replace the factorial operation in formula (8), and the following formula is used to define the Shannon entropy [20]:

$$H_\psi = \sum_{i=1}^{N}\frac{n_i}{n}\left(\log\, n - \psi(n) - \frac{(-1)^n}{n_i(n_i+1)}\right). \tag{9}$$

When $p(x_i)$ is smaller, this method has higher accuracy than Miller entropy estimation.

Grassberger proposed a more effective method in the subsequent entropy estimation research:

$$H_G = \log\, n - \sum_{i=1}^{N} n_i G(n_i). \tag{10}$$

Among them, $G(n_i)$ is expressed as follows:

$$G(n_i) = \psi(n_i) + \frac{1}{2}(-1)^{n_i}\left(\psi\left(\frac{n_i+1}{2}\right) - \psi\left(\frac{n_i}{2}\right)\right), \tag{11}$$

where ψ represents the dual gamma function. From formula (11), it can be concluded that when n_i approaches infinity, $G(n_i)$ will approach the log function, which is transformed into a naive entropy estimation method, thereby making the entropy estimation approach the theoretical value. However, in actual estimation, it is difficult for n_i to reach infinity due to the limitation of sample size. Therefore, the Grassberger entropy estimation method is more accurate than the Naive entropy estimation method in the case of small samples.

In the research, this article first obtains the estimation formula of mutual information through the relationship between the concepts of information entropy:

$$I(X;Y) = H(X) - H(X|Y) = H(X) - \sum_{y\in\gamma} p(y)H(X|y). \tag{12}$$

Then, the Grassberger entropy estimation formula is brought into the mutual information estimation formula so that the mutual information estimation method based on Grassberger entropy estimation can be deduced by the following formula:

$$I_G(X;Y) = H_G(X) - \sum_{y\in\gamma} p(y)H_G(X|y). \tag{13}$$

In this part, by introducing the Grassberger entropy estimation method, the mutual information estimation method based on the Grassberger entropy estimation is derived. Because Grassberger entropy estimation can accurately estimate information entropy when the sample size is small, the calculated deviation is smaller than that calculated by the Naive entropy estimation method. Nuwozin also proved in the research that Grassberger entropy estimation can effectively reduce the deviation of information entropy estimation compared with the Miller entropy estimation method. Therefore, the mutual information estimation method based on Grassberger entropy estimation deduced in this paper can effectively estimate the mutual information between random variables in a finite sample set, making the estimation of mutual information more accurate and more applicable than the estimation using ordinary methods.

In this paper, the derived method of mutual information estimation based on Grassberger entropy estimation is used in agglomerated hierarchical clustering analysis, and a new mutual information hierarchical clustering algorithm based on Grassberger entropy estimation is proposed. The basic idea of the G-MIHC algorithm is to first treat each sample point as a cluster, so that each cluster contains only one sample point, and then use the similarity metric based on mutual information to calculate the distance between the clusters and build a distance matrix. In this process, the mutual information estimation method based on Grassberger entropy estimation is used to calculate the mutual information value. Second, the algorithm finds the two closest clusters according to the minimum distance criterion and merges these two clusters to form a new cluster, then updates the distance matrix again, and deletes the distance between the original two clusters and other clusters from the distance matrix. The mutual information distance between the new cluster and all other clusters is calculated, and it is put into the distance matrix. The distance information between other clusters remains unchanged during the update process. Finally, the algorithm judges whether the number of clusters meets the termination condition; if not, it continues to merge clusters and updates the distance matrix. If the set termination condition is reached, it stops clustering and returns the clustering result.

The algorithm flow chart of G-MIHC is shown in Figure 1.

In terms of setting the number of clusters, there are usually two selection methods. First, when the number of clusters is small, the experiment usually enumerates 1 to N and then uses the evaluation index to measure the optimal situation. The other is that when the number of clusters is relatively large, the algorithm can use the learning method to use the previous state to modify the number of clusters in the current state. Because the biomedical dataset used in this article contains prior category information, this experiment directly uses the number of dataset categories as the parameter setting for the number of clusters.

When estimating information entropy, the general method is to use the discrete probability of the variable to bring in information entropy, and the histogram method is usually used to estimate the probability density of the discrete random variable. When the sample set is large enough, the estimated value of information entropy approaches its true value. However, in the case of a small sample size, if we still use the naive method to simply replace the probability in the histogram with the observed frequency, the statistical fluctuation will make the distribution look less uniform, which will lead to a loss of information entropy. This situation will bias the estimation of information entropy, thereby affecting the accuracy of information entropy calculation. A lot of research work has put forward relevant suggestions on how to estimate the deviation to reduce the deviation of information entropy estimation. Similarly, the problem of estimation bias appears in the estimation process of continuous and discrete variables.

4. Sports and Health Intelligent Diagnosis System Based on Cluster Analysis

According to the design concept of cluster analysis, the flow chart of the push mechanism of sports health management messages is shown in Figure 2.

The system algorithm mainly calculates according to the user's physical condition to recommend better diet and sports suggestions to the user. Because there is no way to give all users professional and targeted advice one by one, we look for relevant information about healthy sports to customize the algorithm and calculate the user's record data to give a reasonable diet and sports recommendation feedback. The user data analysis process is shown in Figure 3.

According to the judgment result of the user's sports and diet situation in the recent period, the corresponding decision is selected from the decision table of many situations preset in the system and recommended to the user. The corresponding process is shown in Figure 4.

Similar functions should be placed in a large module as much as possible, the classification should be reasonable, the main function should be prominent, the level should not be too many, and it is better not to exceed four levels, and we need to think about the layout of the function from the perspective of the user. After the previous analysis and research, the final system module structure is shown in Figure 5.

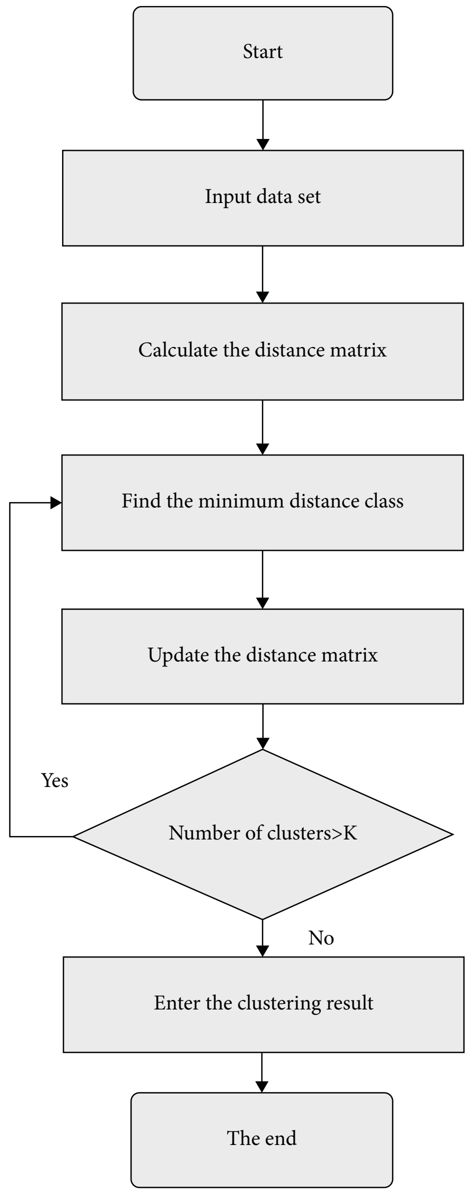

Figure 1: Flow chart of the G-MIHC algorithm.

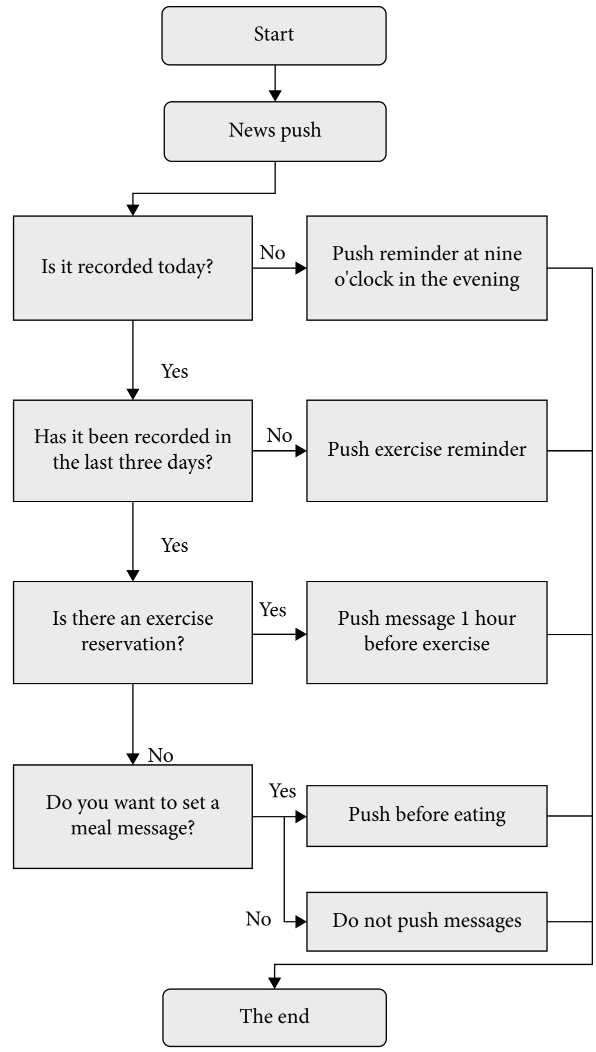

Figure 2: Flow chart of message push.

Based on the analysis of functional requirements and the overall structure design, the health and sports management system is divided into functional modules, as shown in Figure 6.

When the user enters the health sports management system for the first time, in order to make the user have a better experience in the future, the user needs to set some basic information of his own. In this way, data applicable to each user can be better pushed in future use. Figure 7 is an operation flowchart when the user enters the system.

5. Sports and Health Intelligent Diagnosis Analysis Based on Cluster Analysis

This article combines cluster analysis to construct a sports and health intelligent diagnosis and analysis system, which can make sports plans according to the user's health and can also analyze the user's sports process. After that, this paper verifies the performance of the sports and health intelligent diagnosis system constructed in this paper through experiments. This paper selects users from the society, connects the system with users through wearable devices, and obtains 81 sets of valid data through health diagnosis. The scores of the health diagnosis effect of the system are shown in Table 1 and Figure 8.

From the above analysis, it can be seen that the sports and health intelligent diagnosis system based on cluster analysis constructed in this paper has a good effect on human health diagnosis. On this basis, this article studies the effects of the system constructed in this article on human health and sports recommendation. The results are shown in Table 2 and Figure 9.

From the above analysis, it can be seen that the sports and health intelligent diagnosis system based on cluster analysis constructed in this article meets the expected functional requirements, can make sports plans based on human health, and also proves that there is a clear correlation between sports and health.

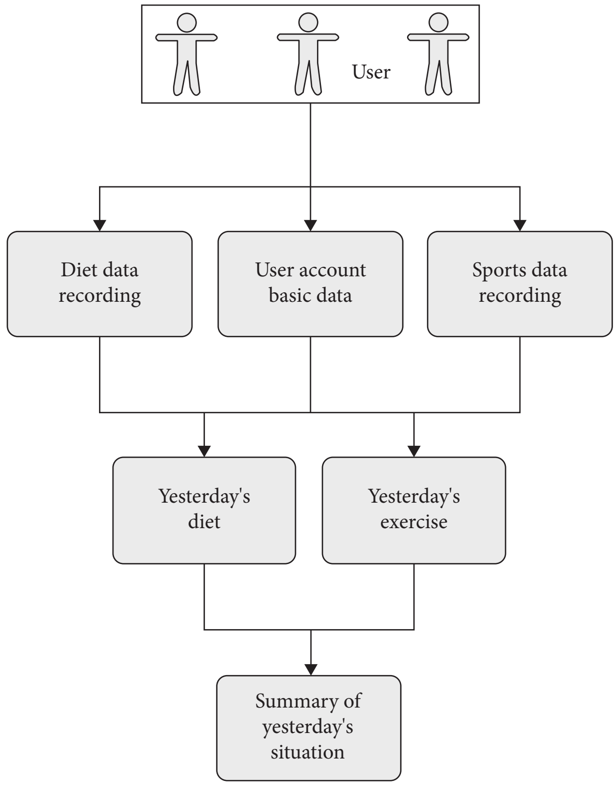

Figure 3: User data analysis process.

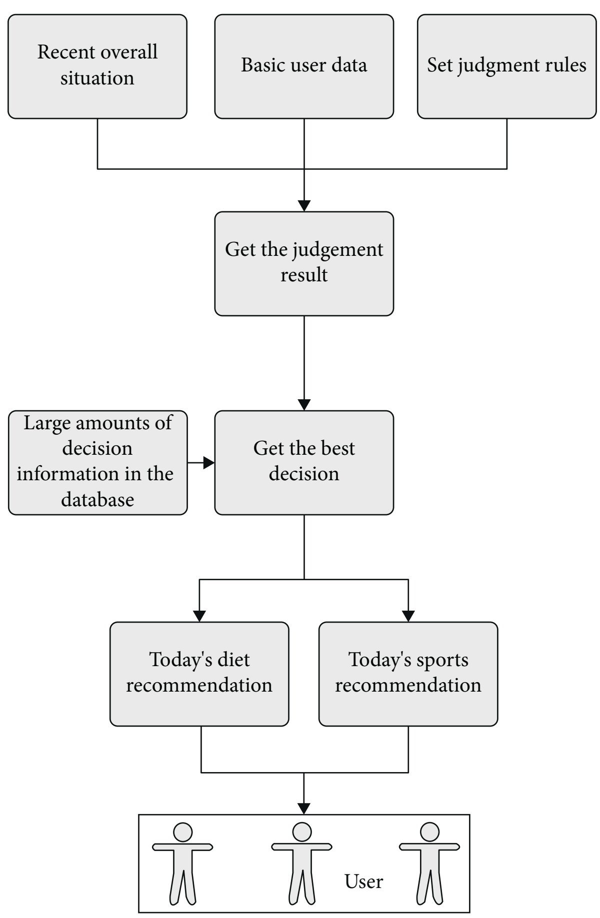

Figure 4: Evaluation and decision-making selection recommendation process.

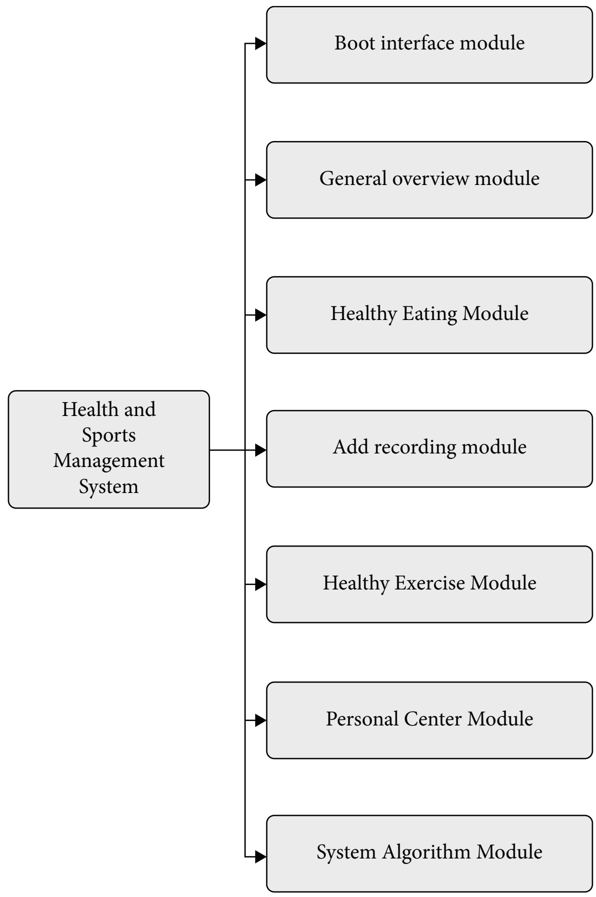

Figure 5: Structure diagram of the system module.

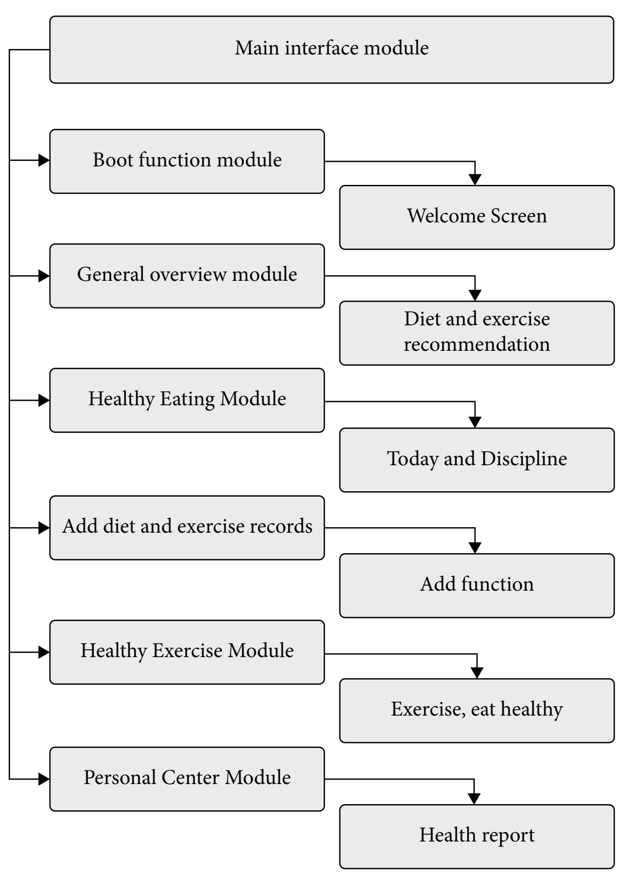

Figure 6: Detailed function division diagram of the system.

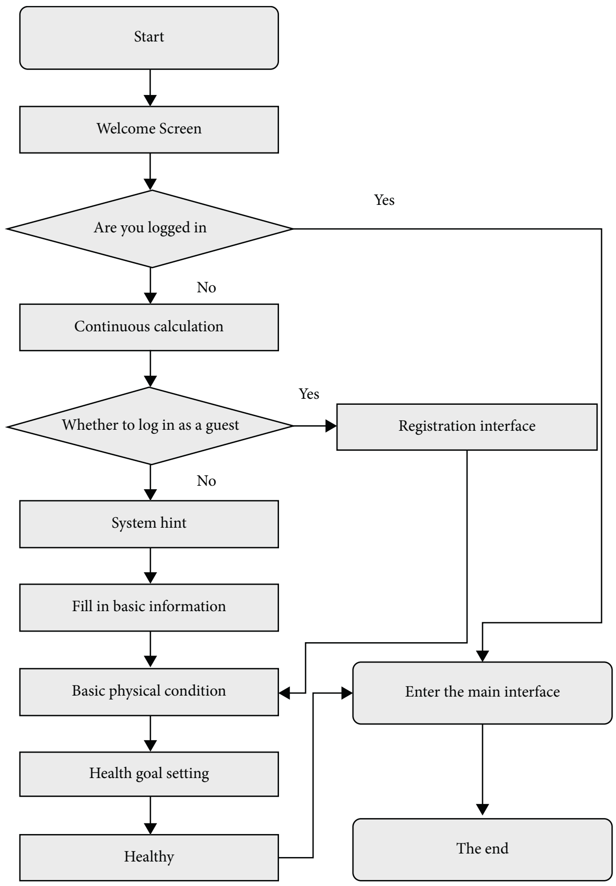

Figure 7: Operation flowchart when the user enters the system.

Table 1: Statistical table of the health diagnosis effect of the sports and health intelligent diagnosis system based on cluster analysis.

No.	Health diagnosis effect	No.	Health diagnosis effect	No.	Health diagnosis effect
1	79.3	28	86.6	55	87.9
2	81.1	29	90.2	56	83.5
3	89.4	30	85.4	57	85.1
4	80.3	31	80.0	58	79.5
5	90.8	32	80.4	59	91.1
6	84.6	33	87.5	60	82.6
7	87.9	34	88.1	61	88.2
8	87.4	35	88.7	62	80.7
9	90.0	36	84.3	63	87.0
10	90.6	37	89.7	64	79.0
11	83.8	38	79.5	65	89.4
12	86.4	39	83.2	66	85.7
13	85.3	40	79.4	67	79.7
14	80.9	41	80.6	68	89.2
15	85.3	42	84.7	69	82.3
16	89.5	43	87.6	70	83.5
17	79.7	44	83.0	71	82.1
18	89.4	45	81.9	72	79.0
19	91.9	46	86.7	73	89.1
20	86.6	47	82.6	74	89.7
21	90.3	48	83.5	75	81.2
22	86.5	49	82.8	76	86.7
23	83.7	50	81.0	77	90.5
24	86.7	51	80.7	78	79.1
25	86.6	52	91.1	79	85.0
26	80.9	53	88.0	80	89.6
27	88.9	54	83.7	81	79.5

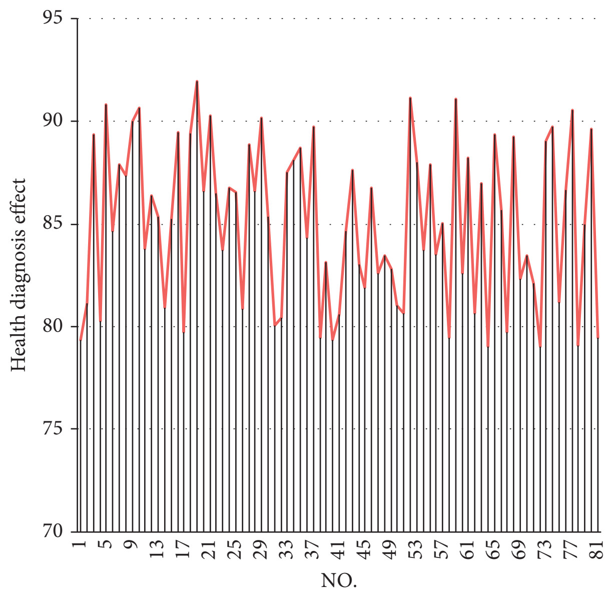

FIGURE 8: Statistical diagram of the health diagnosis effect of the sports and health intelligent diagnosis system based on cluster analysis.

TABLE 2: Statistical table of sports recommendation effect of the sports and health intelligent diagnosis system based on cluster analysis.

No.	Health diagnosis effect	No.	Health diagnosis effect	No.	Health diagnosis effect
1	79.2	28	85.5	55	79.4
2	76.5	29	83.0	56	78.2
3	78.5	30	82.9	57	71.5
4	85.1	31	74.8	58	71.3
5	77.0	32	76.4	59	75.8
6	71.7	33	85.4	60	72.4
7	81.2	34	81.5	61	84.0
8	79.3	35	77.9	62	81.3
9	82.5	36	81.3	63	84.7
10	79.4	37	81.9	64	82.9
11	74.1	38	78.2	65	71.6
12	71.0	39	80.7	66	84.2
13	75.7	40	76.3	67	81.7
14	72.3	41	76.0	68	80.6
15	82.9	42	74.8	69	81.8
16	74.9	43	71.4	70	71.5
17	81.0	44	77.2	71	84.4
18	75.7	45	74.7	72	78.1
19	80.6	46	73.0	73	85.6
20	85.7	47	75.8	74	76.1
21	80.0	48	83.6	75	80.6
22	82.6	49	82.2	76	84.5
23	84.0	50	80.7	77	72.8
24	83.0	51	75.0	78	82.6
25	79.7	52	79.5	79	74.1
26	75.9	53	80.0	80	82.3
27	84.8	54	83.7	81	76.9

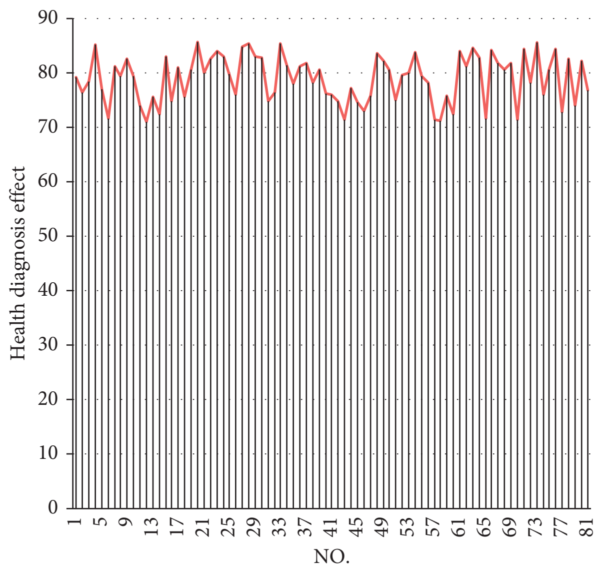

Figure 9: Statistical diagram of sports recommendation effect of the sports and health intelligent diagnosis system based on cluster analysis.

6. Conclusion

Scientific sports can prevent many diseases and can also be used to treat some diseases. What we need is a reasonable and targeted sports guidance method; otherwise, it will often produce unfavorable effects. Moreover, personal errors or unreasonable sports are not only harmful to the physical condition but may also aggravate some health risks. The analysis of the combination of basic personal body data and sports data to provide users with suitable health plans and sports programs and to guide people to perform more reasonable fitness will help our body's health and disease prevention. This article combines the clustering analysis algorithm to construct a sports and health intelligent diagnosis system based on the clustering algorithm, sets the functional modules of the health diagnosis system based on actual needs, and verifies the performance of the system. From the research results, the system constructed in this paper has a certain effect.

Data Availability

The labeled dataset used to support the findings of this study is available from the corresponding author upon request.

Conflicts of Interest

The authors declare that there are no conflicts of interest.

Acknowledgments

This study was sponsored by Tianjin University of Sport.

References

[1] L. J. Ferguson, K. T. Carlson, and D. Rogers, "Moving towards reconciliation through sport: sharing our process of exploring team saskatchewan experiences at the North American Indigenous Games," *Journal of Exercise, Movement, and Sport*, vol. 51, no. 1, p. 99, 2019.

[2] K. Kimasi, V. Shojaei, and M. R. Boroumand, "Investigation of safety conditions at gymnasia in different organizations," *Journal of Humanities Insights*, vol. 3, no. 2, pp. 70–74, 2019.

[3] C. Abanazir, "E-sport and the EU: the view from the English bridge union," *The International Sports Law Journal*, vol. 18, no. 3, pp. 102–113, 2019.

[4] A. Gerke, K. Babiak, G. Dickson, and M. Desbordes, "Developmental processes and motivations for linkages in cross-sectoral sport clusters," *Sport Management Review*, vol. 21, no. 2, pp. 133–146, 2018.

[5] C. Abanazir, "E-sport and the EU: the view from the English Bridge Union," *The International Sports Law Journal*, vol. 18, no. 3, pp. 102–113, 2019.

[6] D. C. Ilies, R. Buhas, M. Ilies et al., "Sport activities and leisure in Nature 2000 protected area-Red Valley, Romania," *Journal of Environmental Protection and Ecology*, vol. 19, no. 1, pp. 367–372, 2018.

[7] A. I. Pogrebnoy and I. O. Komlev, "Sport institutions reporting to Ministry of Sport of Russian Federation: intellectual property, invention activity, patenting and legal consulting service analysis," *Theory and Practice of Physical Culture*, vol. 2, no. 2, pp. 2–10, 2018.

[8] R. Giulianotti and D. Numerato, "Global sport and consumer culture: an introduction," *Journal of Consumer Culture*, vol. 18, no. 2, pp. 229–240, 2018.

[9] A. I. Kondrukh, "Practical shooting sport in Russian sport system: essential specifications and features," *Theory and Practice of Physical Culture*, vol. 5, pp. 27–33, 2017.

[10] M. Mountjoy, A. Costa, R. Budgett et al., "Health promotion through sport: international sport federations' priorities, actions and opportunities," *British Journal of Sports Medicine*, vol. 52, no. 1, pp. 54–60, 2018.

[11] J. J. Pulido, D. Sánchez-Oliva, P. A. Sánchez-Miguel, D. Amado, and T. G. Calvo, "Sport commitment in young soccer players: a self-determination perspective," *International Journal of Sports Science & Coaching*, vol. 13, no. 2, pp. 243–252, 2018.

[12] J. Cristiani, J. C. Bressan, B. L. Pérez, L. Galatti, and R. Reverdito, "Clubs SOCIO-deportivos en UN municipio brasileño: ESPACIO, EQUIPOS Y CONTENIDOS [Sport clubs in Brazil: facilities, equipment and content in][Clubes socio-esportivos em município brasileiro: espaço, equipamentos e conteúdos]," *E-Balonmano.com: Revista de Ciencias del Deporte*, vol. 13, no. 2, pp. 105–112, 2017.

[13] E. Happ, M. Schnitzer, and M. Peters, "Sport-specific factors affecting location decisions in business to business sport manufacturing companies: a qualitative study in the Alps," *International Journal of Sport Management and Marketing*, vol. 21, no. 1-2, pp. 21–48, 2021.

[14] M. Castro-Sánchez, F. Zurita-Ortega, and R. Chacón-Cuberos, "Motivation towards sport based on sociodemographic variables in university students from Granada," *Journal of Sport and Health Research*, vol. 11, no. 1, pp. 55–68, 2019.

[15] S. M. Hadlow, D. Panchuk, and D. L. Mann, "Modified perceptual training in sport: a new classification framework," *Journal of Science and Medicine in Sport*, vol. 21, no. 9, pp. 950–958, 2018.

[16] J. H. Du Plessis and M. Berteanu, “The importance of prosthetic devices in sport activities for Romanian amputees who compete in Paralympic competitions,” *Medicina Sportiva: Journal of Romanian Sports Medicine Society*, vol. 16, no. 1, pp. 3197–3204, 2020.
[17] M. Stylianou, A. Hogan, and E. Enright, “Youth sport policy: the enactment and possibilities of ‘soft policy’ in schools,” *Sport, Education and Society*, vol. 24, no. 2, pp. 182–194, 2019.
[18] S. A. Richmond, A. Donaldson, A. Macpherson et al., “Facilitators and barriers to the implementation of iSPRINT: a sport injury prevention program in junior high schools,” *Clinical Journal of Sport Medicine*, vol. 30, no. 3, pp. 231–238, 2020.
[19] B. J. Ruihley, T. C. Greenwell, Y. Mamo, T. Greenwell, and P. S. Damon, “Increase customer retention: an examination of quality and its effects on the retention of sport participants,” *Journal of Sport Behavior*, vol. 42, no. 3, pp. 365–388, 2019.
[20] J. P. DiFiori, G. Green, W. Meeuwisse, M. Putukian, G. S. Solomon, and A. Sills, “Return to sport for North American professional sport leagues in the context of COVID-19,” *British Journal of Sports Medicine*, vol. 55, no. 8, pp. 417–421, 2021.

Hindawi
Scientific Programming
Volume 2021, Article ID 2648352, 9 pages
https://doi.org/10.1155/2021/2648352

Research Article

Ideological and Political Education Recommendation System Based on AHP and Improved Collaborative Filtering Algorithm

Nan Wang

School of Xingjian Academy, Xijing University, Xi'an, Shaanxi 710123, China

Correspondence should be addressed to Nan Wang; 13991115103@163.com

Received 26 October 2021; Revised 11 November 2021; Accepted 18 November 2021; Published 14 December 2021

Academic Editor: Le Sun

Aiming to solve the problem that ideological and political education courses in universities are not targeted enough and cannot form personalized recommendations, this paper proposes an ideological and political education recommendation system based on analytic hierarchy process (AHP) and improved collaborative filtering algorithm. Firstly, considering the time effect of student scoring, the recommendation model is transformed into Markov decision process. Then, by combining the collaborative filtering algorithm with reinforcing learning rewards and punishments, an optimization model of student scoring based on timestamp information is constructed. To quantify the degree of students' preference for courses, the analytic hierarchy process is used to convert the students' behavior data into the preference value of courses. To solve the problem of data scarcity, the missing values are predicted by the prediction score rounding filling and the optimization boundary completion method. Experimental results show that the feasibility of the proposed system is verified, and the system has vital accuracy and convergence performance. The ideological and political education recommendation system proposed in this paper has important reference significance for promoting ideological and political education in the era of big data.

1. Introduction

As the main channel to carry out ideological and political work in colleges and universities, ideological and political education curriculum is a critical way to practice the mechanism of education in colleges and universities. Ideological and political education courses run through the whole process of higher education teaching and are an essential system for universities to cultivate high-quality talents [1]. At present, ideological and political education in colleges and universities mostly adopts the way of large classes and open classes for collective teaching. There are many problems in this way, such as single form, weak pertinence, lack of synergistic effect, and being unable to form personalized collaborative education mechanism. Therefore, combining with the characteristics of students, it is of great significance to carry out personalized recommendations of ideological and political education courses.

With the continuous development of network and information technology, the amount of network information data of ideological education courses is also increasing exponentially. Faced with a variety of ideological education courses, how to carry out personalized recommendations needs to be systematically studied. Personalized recommendation can effectively filter unwanted information by analysing users' behavioural preferences through various recommendation algorithms [2]. Recommendation system can actively provide personalized information for users. At present, personalized recommendation has been widely used in social networking [3], news, music, books, and movies [4], such as cloud music [5] and online shopping product recommendation [6].

Recommendation algorithms are mainly divided into the following three categories [7]. In the first category, collaborative filtering recommendation algorithm makes recommendations based on users' intentions [8, 9]. It has achieved significant improvement in recommendation accuracy. However, their interpretation of recommendation results is often not intuitive [10]. In the second category, content-based recommendation algorithm conducts feature modeling through various available content information [11, 12]. Because the content of an item is easier for the user to understand, it is often intuitive to explain to the user why the item is being recommended. Collecting the required content information under different recommendation backgrounds is a time-consuming task, which becomes the bottleneck of content-based recommendation algorithms. However, the construction of knowledge map can reduce the workload of extracting content information. Therefore, knowledge graph, as an emerging auxiliary data, is attracting the attention of researchers [13]. Deep learning also brings innovative ideas for recommendation system [14]. However, the existing recommendation algorithm based on deep learning only considers the rating data by using matrix decomposition, which inhibits the recommendation effect [15]. In the third category, hybrid recommendation algorithm [16, 17] can often achieve better recommendation effect by combining the advantages of multiple recommendation algorithms.

As a typical recommendation algorithm, collaborative filtering technology mainly includes memory-based and model-based algorithms [18]. The former calculates the similarity by analysing the user-item score matrix and makes the prediction and recommendation based on the similarity. The latter trains a prediction model through the user's network history, operation, and other data. It then uses this prediction model to predict the project score. Many studies have optimized the recommendation effect by improving collaborative filtering algorithms, such as restricted Boltzmann machine [19], K-nearest neighbour algorithm [20], and singular value decomposition (SVD) [21] algorithm. Not only is SVD a mathematical problem, but also it has been successfully applied in many engineering applications. In the recommendation system, it is easy to obtain the full rank decomposition of any matrix by using SVD. Then, it can realize data compression and dimensional reduction. SVD++ [22] further integrates implicit feedback information on the basis of SVD and adopts implicit preference to optimize SVD model with better performance. However, SVD++ and SVD do not consider the impact of time timestamp on recommendation performance, and the actual recommendation effect is related to timestamp to a certain extent. For example, the ratings of users ten years ago on a certain product are different from those of current users, so it is necessary to improve it and optimize the prediction effect.

Considering the time effect of student rating, the recommendation model is transformed into Markov decision process. Then, in order to quantify the degree of students' preference for courses, the analytic hierarchy process is used to convert the students' behaviour data into the preference value of courses. Finally, the accuracy of the recommendation model is improved by constructing a student scoring optimization model integrating timestamp information.

To solve the problem that ideological and political education courses in universities are not targeted enough and cannot form personalized recommendations, this paper proposes an ideological and political education recommendation system. The contribution of our paper is summarized, which is grouped into the following three points.

(a) The recommendation model is transformed into Markov decision process considering the time effect of student scoring.
(b) An optimization model of student scoring based on timestamp information is constructed by combining the collaborative filtering algorithm with the process of reinforcing learning rewards and punishments.
(c) To quantify the degree of students' preference for courses, the analytic hierarchy process is used to convert the students' behavior data into the preference value of courses.

The rest of the paper is organized as follows. In Section 2, modeling for the system is introduced first, and then the process of training and prediction is introduced. Section 3 gives the experimental results and discussion. At last, Section 4 draws a conclusion of this paper.

2. The Proposed Recommendation System

2.1. Modeling for the System. Firstly, the curriculum recommendation system of ideological and political education is modelled, and the high-dimensional sparse matrix is decomposed into low-dimensional matrix by singular value decomposition method. Then, students' behaviour data are converted into course preference values through analytic hierarchy process (AHP). Finally, the recommendation model is transformed into Markov decision process by establishing model mapping.

2.1.1. Singular Value Decomposition. In real life, the student-course matrix is large, but due to the limited interests of students. The grading data of individual students on courses are often small. The core idea of SVD is to decompose a high-dimensional sparse matrix into two low-dimensional matrices. Compared with eigenvalue decomposition, it can only be used for symmetric matrices. SVD can perform full rank decomposition on any $M \times N$ matrix to achieve data compression. However, before SVD is used to decompose the matrix, blank items in the matrix need to be filled to get a dense matrix. Assuming that the matrix before filling is R and after filling is R$'$, the calculation formula is as follows:

$$R' = URV^T. \tag{1}$$

The calculation formula of SVD algorithm is as follows:

$$\hat{r}_{px} = \mu + d_p + d_x + v_x^T u_p, \tag{2}$$

where $\hat{r}_{px}$ represents the predicted score value, μ represents the average value of the score, d_p and d_x represent the offset amount of student p and course x, respectively, v_x and u_p correspond to the feature vectors of courses and students on each hidden trait, respectively, and T superscript stands for transpose.

If a student scores a course, it means he has seen it. Such behaviour contains certain information, so it can be inferred that the behaviour of grading reflects students' preferences. Accordingly, this preference can be reflected in the model in the form of implicit parameters to obtain a more accurate model SVD++.

The calculation formula of SVD++ model is as follows:

$$\hat{r}_{px} = \mu + d_p + d_x + v_x^T \left(u_p + \frac{1}{\sqrt{|T(p)|}} \sum_{y \in T(p)} j_y \right), \quad (3)$$

where $T(p)$ is the collection of all courses browsed and evaluated by student p, j_y bias for hidden student-course J's personal preferences, and the preference degree of student p consists of explicit feedback pu and implicit feedback $1/\sqrt{|T(p)|}\sum_{y \in T(p)} j_y$.

2.1.2. Preference Calculation Method Based on AHP. To analyze the hidden bias of students' preference for courses, the data of students' browsing course introduction, collecting course, and learning course were firstly collected. Then, the analytic hierarchy process (AHP) is used to calculate the value of students' preference for courses. The questions favoured by students are divided into goal layer, criterion layer, and program layer. Use browsing course profiles, bookmarking courses, and studying courses as criteria for making decisions. The hierarchical model of student interest calculation is shown in Figure 1.

The judgment matrix C is constructed by pairwise comparison of different factors. It is more important to bookmark the course than to browse the course introduction. Learning the course content is more important than collecting the course. Therefore, the scale is set as follows: the ratio of collection course to browsing course is 3; the ratio of learning course to browsing course is 5; the ratio of learning course to collection course is 3. Therefore, the judgment matrix C is

$$C = \begin{bmatrix} 1 & \frac{1}{3} & \frac{1}{5} \\ 3 & 1 & \frac{1}{3} \\ 5 & 3 & 1 \end{bmatrix}. \quad (4)$$

The maximum eigenvalue of the matrix is

$$\lambda = 3.0414. \quad (5)$$

The eigenvector m of the matrix is

$$m = (0.11, 0.26, 0.63)^T. \quad (6)$$

EX of consistency indicator is

$$EX = \frac{3.0414 - 3}{3 - 1} = 0.0207, \quad (7)$$

and Table 1 shows that the average random consistency index RX is

$$RX = 0.52. \quad (8)$$

The size of the calculated consistency ratio ER is

$$ER = \frac{EX}{RX} = \frac{0.0207}{0.52} = 0.0398 < 0.1. \quad (9)$$

The final result passes the consistency ratio test. Therefore, the weight of browsing course profiles is 0.11. The weight of collecting courses is 0.26, and the weight of learning courses is 0.63.

The degree of students' preference for course operation is quantified. The calculation formula of students' preference intention is as follows:

$$V = 0.11^* U1 + 0.26^* U2 + 0.63^* U3. \quad (10)$$

U1 here browses the course introduction for students. U2 has a collection of lessons for students. U3 studied the course for students. Therefore, the analytic hierarchy process (AHP) is used to convert student behaviour data into course preference values.

2.1.3. Markov Decision-Making Process. Markov decision process is an intuitive and basic construction model in decision theoretic programming, reinforcement learning, and stochastic domain. In this model, the environment is modelled through a set of states and actions that can be used to execute the state of the control system. The goal of controlling the system in this way is to maximize a model's performance criteria. At present, many problems have been successfully modelled by Markov decision process, such as multiagent problem, robot learning control, and game playing problem. Therefore, Markov decision process has become a standard method to solve timing decision problems.

A general Markov decision process is represented by A quintuple, as shown in Figure 2, where S_n represents the state, c_n represents the action, and r_n represents the return function. The agent senses the state information in the current environment and chooses to perform some actions according to the current state. The environment sends a reward or punishment signal to the agent based on the selected action. Based on this reward and punishment signal, the agent moves from one state to the next.

To optimize SVD++ recommendation model by reinforcement learning method, the mapping relationship between recommendation prediction model and Markov decision process should be established first. In order to construct Markov decision process, students' preference scores for courses under different time stamps are converted into quintuples. The following is the mapping relationship between course scoring designed in this paper and Markov decision process.

(1) For state space S, in this paper, student p scores the course at time n as state $S_n^{(p)}$. Because the score of students on courses in the data set is 5 integers within the range [1, 5], the range of $S_n^{(p)}$ is [1, 5]. The state $S_n^{(p)}$ under all timestamps constitutes the state space S.

(2) For action space C, student U looks at the course under time n and gives a grade $S_n^{(p)}$, which will affect

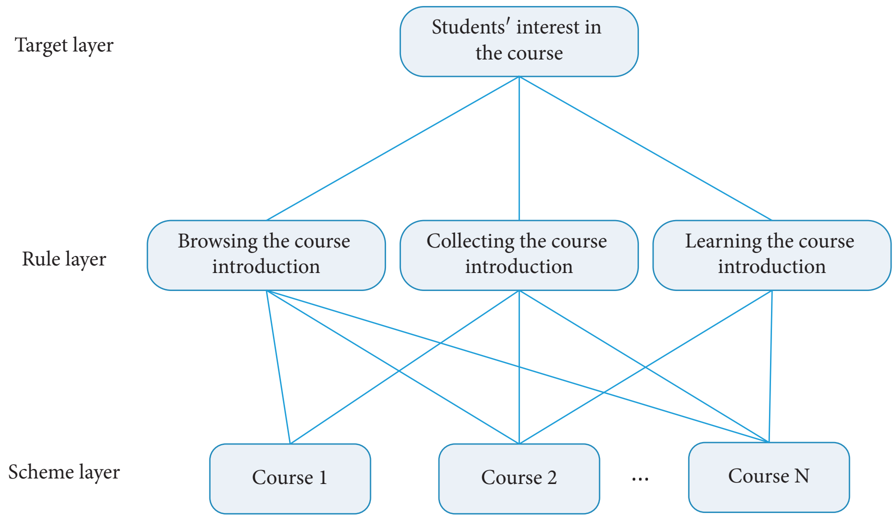

Figure 1: The hierarchical model of student interest calculation.

Table 1: Reference table of average random uniformity index RX value.

Order number	RX
1	0
2	0
3	0.52
4	0.89
5	1.12

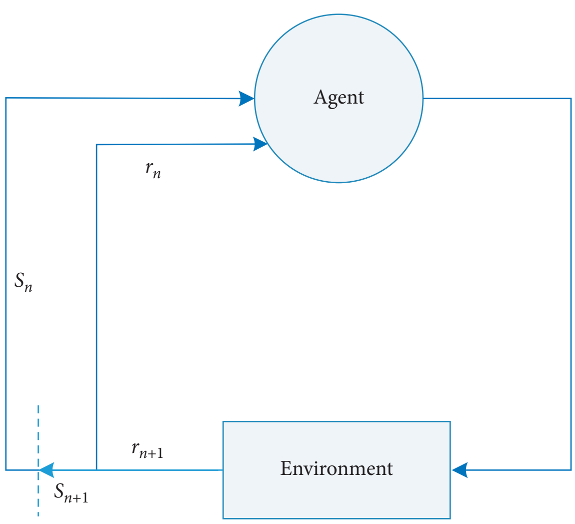

Figure 2: Markov decision process.

his grade $S_{n+1}^{(p)}$ for the course under time n. Therefore, write $C_n^{(p)}$ as the action from $S_n^{(p)}$ to $S_{n+1}^{(p)}$, as shown in the following equation. The action $C_{n+1}^{(p)}$ at all times constitutes the action space C:

$$S_n^{(p)} \xrightarrow{c_n^{(p)}} S_{n+1}^{(p)}. \tag{11}$$

(3) For state transition probability U, the action $C_n^{(p)}$ taken by student p under state $S_n^{(p)}$ is determined by the timestamp. Once the action $C_n^{(p)}$ is determined, the next state $S_n^{(p)}$ is also determined. At this point, the transition probability between states is determined; that is, $C_n^{(p)} = S_{n+1}^{(p)}$, $U = 1$. The value range of the action $C_n^{(p)}$ is [1, 5].

(4) For discount factor ?, in the model, each action generates a corresponding reward. However, the same student's viewing time will have different influences on the selection of the next course, and γ is a factor reflecting this influence. The later the reward, the greater the discount, and the return is always limited. Therefore, set $0 \le \gamma < 1$.

(5) For reward and punishment function R_{gm}, the punishment and reward function values represent the reward for completing an action in a state. This paper defines the reward and punishment function values R_{gm} as follows:

$$R_{gm}\left(s_n^{(p)}, c_n^{(p)}\right) = s_{n+2}^{(p)} - \hat{r}_{px}, \tag{12}$$

where $s_{n+2}^{(p)}$ is the course score of student p when $(n+2)$. px represents the predicted grade of student p for course x calculated using an SVD or SVD++ model. R_{gm} represents the reward and punishment value obtained by student p taking the action $C_n^{(p)}$ under state $S_n^{(p)}$, and the corresponding reward and punishment table can be obtained according to the reward and punishment function.

According to the Markov decision process mentioned above, the action of transferring from one state to the next state corresponds to the score of the course at the next time. Although the name and type of course are ostensibly ignored, students' preferences for the course are implicitly reflected in the timestamp. This process processes the course data set into the form shown in Table 1, where the first number in parentheses reflects the grade given by the students in the corresponding row to the courses in the corresponding column. The second number reflects the timestamp information or chronological order in which students in the corresponding row watched the courses in the corresponding column. For example, row 1, column 1 (4, 3rd) indicates that student 1 watches course 1 in the third chronological order. So, the timestamp $n = 3$ and student 1 scored 4 for course 1. NaN said the students did not watch the course.

Sort the data in Table 2 by timestamp, and the generated state transition path is as follows:

$$\begin{gathered} 4 \longrightarrow 5 \longrightarrow 4 \longrightarrow 2 \\ 3 \longrightarrow 3 \\ 2 \longrightarrow 4 \longrightarrow 5 \longrightarrow 2 \\ 4 \longrightarrow 4 \longrightarrow 3 \\ 3 \longrightarrow 2 \longrightarrow 3 \longrightarrow 5 \end{gathered} \tag{13}$$

According to Table 2, the rules of the state transfer path are obtained, and the first example is used for illustration. The state transition path 4⟶5⟶4⟶2 in line 1 reflects that student 1 is watching course 3 when timestamp $n = 1$. Its grade for course 3 is 4. If you look at course 2 at $n = 2$, you give course 2 a grade of 5. If you look at course 1 at $n = 3$, you give course 1 a grade of 4. If you look at course 5 at $n = 4$, you give course 5 a grade of 2. The other four transfer paths were obtained in a similar way.

This state transition path represents the state transition in Markov decision-making process and guides the updating direction of V table.

2.2. Training and Prediction Process. The recommendation algorithm proposed in this paper includes two parts: training and prediction. During the training, SVD++ algorithm is first used for model training on the training set, and SVD++ recommended model is obtained, as shown in formula (3). Then, the reinforcement learning model is trained, and the reward and punishment function shown in (12) is used to calculate the reward and punishment value R_{gm} of state transfer. The reinforcement learning table is updated for the

Table 2: Data evaluation table.

Student	Course 1	Course 2	Course 3	Course 4	Course 5
Student 1	(4, 3rd)	(5, 2nd)	(4, 1st)	NaN	(2, 4th)
Student 2	(3, 1st)	NaN	NaN	NaN	(3, 2nd)
Student 3	NaN	(2, 1st)	(2, 4th)	(5, 3rd)	(4, 2nd)
Student 4	(4, 2nd)	(4, 1st)	NaN	(3, 3rd)	NaN
Student 5	(3, 1st)	NaN	(5, 4th)	(2, 2nd)	(3, 3rd)

optimization model of SVD++ recommendation scoring. During the prediction, the prediction score value is firstly obtained according to SVD++ recommendation model. Then, the optimization model designed in this paper is used to optimize the prediction score, and the final prediction score is obtained. The optimization model designed in this paper is expressed as follows:

$$\hat{r}'_{px} = \hat{r}_{px} + V\left(S^{(p)}_{n-2}, c^{(p)}_{n-2}\right), \tag{14}$$

where $\hat{r}_{px}$ is the predicted score of student p for the x course calculated by SVD++ recommendation model. $S^{(p)}_{n-2}$ is the grade of student p watching the course when the timestamp is (n-2) before watching course x. $c^{(p)}_{n-2}$ is the timestamp $(n-2)$ to see the grade of the course. $V\,(S^{(p)}_{n-2}, C^{(p)}_{n-2})$ is the value of V table in $(S^{(p)}_{n-2}, C^{(p)}_{n-2})$ coordinates. It requires reinforcement learning algorithm and prediction score based on SVD++ recommendation model. It is used to optimize the final predicted score. If the value of $(S^{(p)}_{n-2}, c^{(p)}_{n-2})$ does not exist, the mean value of the current V table is taken. $\hat{r}'_{px}$ is the prediction score after optimization.

2.2.1. Training Process. Firstly, the training set is trained through (3), and the SVD++ recommended model is obtained. Then, the reinforcement learning model was trained. Formula (12) is used to calculate R_{gm} of reward and punishment values, and then R_{gm} is used in the updating process of V value in q-learning Algorithm 1. V table update formula is as follows:

$$V\left(s^{(p)}_{n+1}, c^{(p)}_{n}\right) = V\left(s^{(p)}_{n}, c^{(p)}_{n}\right) + \alpha\left[R_{gm}\left(s^{(p)}_{n}, c^{(p)}_{n}\right) + \gamma \underset{c'_x}{\mathrm{wci}}\, V\left(\delta\left(s^{(p)}_{n}, c^{(p)}_{n}\right), c^{(p)}_{n}\right) - V\left(s^{(x)}_{n}, c^{(x)}_{n}\right), \right. \tag{15}$$

where $V\,(s^{(p)}_{n}, c^{(p)}_{n})$ is a 5×5 V table, $V\,(s^{(p)}_{n}, c^{(p)}_{n})$ starts at 0, $V\,(s^{(p)}_{n}, c^{(p)}_{n})$ is the value of V at the coordinates $(s^{(p)}_{n}, c^{(p)}_{n})$, $R_{gm}\,(s^{(p)}_{n}, c^{(p)}_{n}) + \gamma\, \underset{c''}{wci}\, V\,(\delta\,(s^{(p)}_{n}, c^{(p)}_{n}), c^{(p)}_{n}) - V\,(s^{(x)}_{n}, c^{(x)}_{n})$ is the reward or punishment for choosing the next move, α is learning rate, and γ is discount factor. The higher the V value is, the more the reward you get for performing the next action, and the less the reward you get for performing the next action.

2.2.2. Prediction Process. The prediction process is based on the prediction score obtained by SVD++ recommendation model and combined with V table of training to predict the score of student p on course x. At the same time, it can predict the courses that student p has not watched but other students have watched.

In addition, $s^{(p)}_{n-1}$ is not used in the prediction score optimization model shown in (13) for the following reasons. If $s\,(p)/n-1$ is used, the optimization model will become $\hat{r}_{px}{}' = \hat{r}_{px} + V\,(s^{(p)}_{n-1}, c^{(p)}_{n-1})$. Because $c^{(p)}_{n-1} = s^{(p)}_{n-1}$ and $s^{(p)}_{n-1}$ is the score $\hat{r}_{px}{}'$ that needs to be predicted, $s^{(p)}_{n-2}$ is chosen.

The data set used in this paper has a default value, that is, there is no graded course information. According to the construction idea of the optimization model in this paper, the scoring information of ungraded courses should be used in the subsequent optimization process. This will lead to the possibility of missing s or c values in $V\,(s^{(p)}_{n-2}, c^{(p)}_{n-2})$, which will invalidate the optimization model. To avoid this

```
Input:
  The number of students N, the courses that students have graded W, the learning rate α, and the discount factor γ
Output:
  V(s,c)
S1: Initialize V(s,c) = 0 for any s ∈ S, c ∈ C
S2: Training SVD++ model, calculate r̂_px from equation (3)
S3: Get the initial state S and action A from the data.
S4: For each episode x = 1: T do
  For z = 1: Wx do
    S5: Calculate the reward and punishment functions according to equation (8).
    S6: Apply the calculated punishment and reward functions to equation (10)
    S7: Update the V table.
  end for
end for
```

Algorithm 1: The pseudocode of proposed algorithm training process.

situation, SVD++ model is adopted in this paper to predict missing values and then fill them to solve the problem of sparse data.

In addition, when $n = 1, 2$, the boundary $s_{n-2}^{(p)}$ and $c_{n-2}^{(p)}$ will exceed the subscript range, and there will be no corresponding value. Therefore, the prediction score of the last two columns is used as the prediction score data of column -1 and column 0 in this paper to ensure data integrity.

3. Experiment and Analysis

3.1. Experimental Data Set. To verify the actual effect of the algorithm in this paper on the recommendation model of ideological and political courses in colleges and universities, sklearn library based on *Python* 3.6.5 kernel provided by GitHub open source platform is adopted. The main library packages used are numpy-1.14.3, NetworkX-2.3, Keras-2.0.5, and sklearn-0.20.0. The experiment was conducted in ubuntu-16.04 environment. Multidimensional constraints such as scale, feature, target, and noise are set by programming, and sklearn library is used to generate simulated data sets that meet the conditions. The simulated data set of the experiment in this paper contains information of 570 ideological and political education courses, information of 13,000 college students, and information of 50,000 college students' operation and grading of courses.

3.2. Performance Indexes. To evaluate the recommended performance of the proposed algorithm, MAE and RMSE were used as evaluation indexes.

MAE represents the average absolute error between the predicted value and the true value. The smaller the MAE is, the higher the recommendation accuracy is. It is defined as follows:

$$M_{\mathrm{MAE}} = \frac{\sum_{x,y}\left|\hat{r}_{xy} - r_{xy}\right|}{t}. \tag{16}$$

RMSE represents the square root of the sum of the squares of the deviation between the predicted value and the true value and the ratio of the predicted number t. RMSE reflects the dispersion degree of samples, and the smaller the RMSE, the higher the recommendation accuracy. It is defined as follows:

$$R_{\mathrm{RMSE}} = \sqrt{\frac{\sum_{x,y}\left(\hat{r}_{xy} - r_{xy}\right)^2}{t}}, \tag{17}$$

where $\hat{r}_{xy}$ is the predicted score value, r_{xy} is the true value, and t is the number of predicted scores.

3.3. Feasibility Analysis. Since the learning rate α and discount factor γ can be adjusted dynamically, it is necessary to study the influence of the changes of α and γ in the algorithm in this paper on the prediction performance. The experimental results are shown in Figure 3. As can be seen from Figure 3, when α is constant, γ increases from 0.4 to 0.6, and RMSE of the proposed algorithm decreases continuously. The results were best when $\alpha = 0.000003$ and $\gamma = 0.6$. At this time, RMSE can reach 0.81948, which is 0.0086 lower than before. Thus, the feasibility of the proposed algorithm is proved. This configuration is used for comparison in subsequent experiments.

3.4. Comparison Experiment. To verify the effectiveness of the algorithm in this paper, representative matrix decomposition algorithm [23], direct trust matrix decomposition algorithm [24], and indirect social relationship matrix decomposition algorithm [25] were selected for comparison in the experiment. All experiments were carried out for 10 times, and the experimental results were averaged.

Tables 3 and 4 show the error values of different algorithms. By observing the data in the table, it can be seen that the error value of the algorithm in this paper is lower than that of other comparison algorithms, and the error comparison becomes more obvious with the increase of training sets. According to Tables 3 and 4, the more the training sets, the lower the error rate of the algorithm. Compared with the algorithm [23], the algorithm [24] reduces the error value due to the introduction of direct social relations. On the basis of the algorithm [24], the algorithm [25] established

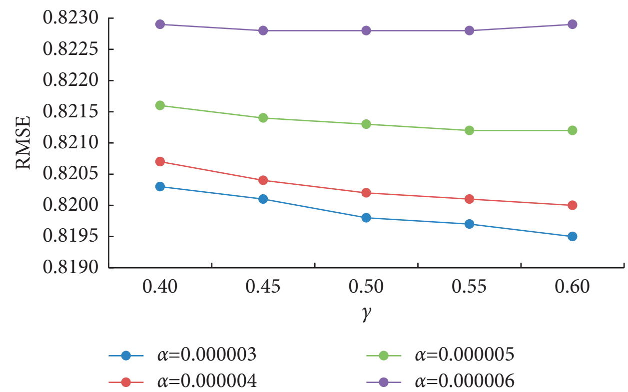

Figure 3: Influence of γ variation on RMSE at constant α.

Table 3: Comparison of error values with MAE.

Training set (%)	Index	Paper [23]	Paper [24]	Paper [25]	Proposed
40	MAE	1.0207	0.9841	0.8656	0.8324
60	MAE	1.0179	0.9588	0.8492	0.7810
80	MAE	1.0069	0.9406	0.8354	0.7500

Table 4: Comparison of error values with RMSE.

Training set (5%)	Index	Paper [23]	Paper [24]	Paper [25]	Proposed
40	RMSE	1.3489	1.2718	1.1151	1.1024
60	RMSE	1.3443	1.2429	1.1333	1.0663
80	RMSE	1.3223	1.2066	1.1890	1.0029

indirect social relations by considering the degree of influence between each student. This relationship includes both direct and indirect connections between students, so the error value is further reduced. However, these algorithms only analyze the degree of influence among students, ignoring the potential connection between courses and the difference of influence degree of different neighbours on different nodes. The algorithm in this paper constructs preference vector and feature vector, respectively, according to the influence degree of scoring and behaviour from different perspectives of students and courses. At the same time, considering the time effect of student scoring, the recommendation model is transformed into Markov decision process. Therefore, the proposed algorithm has a higher recommendation rate than other algorithms.

To verify whether the algorithm in this paper can reduce the iterative convergence times, the original data set is taken as the training set, and the experimental results are shown in Figure 4. It can be seen that compared with other comparison algorithms, the iteration times of the algorithm in this paper quickly reach convergence. Moreover, the recommendation efficiency of the proposed algorithm is significantly higher than other algorithms. This is because the algorithm in this paper fully mines the potential connections between them from the perspectives of students and courses, so it not only improves the recommendation efficiency but also reduces the convergence times.

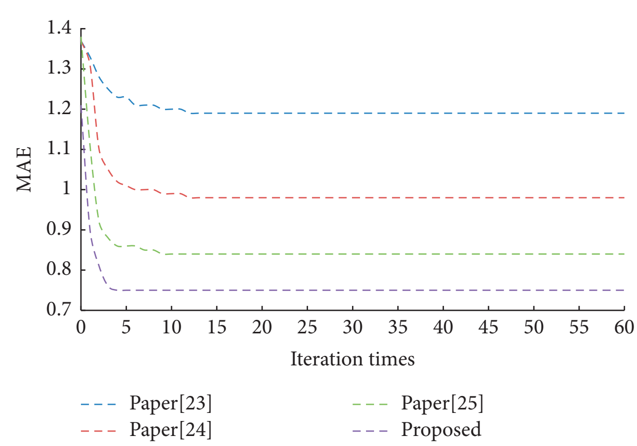

Figure 4: Comparison of iterative convergence times.

At the beginning of iteration, the error value of comparison algorithm is about 1.38. By observing Figure 4, it can be seen that the error value of the zeroth iteration of the algorithm in this paper is lower than 1.38. As the number of iterations increases, the algorithm [23] achieves convergence and maximum error only after 20 iterations. However, the algorithm in [24] and the algorithn [25] indirectly corrected the preference vector of students, and reached convergence after 15 iterations, followed by recommendation efficiency.

Because the algorithm in this paper optimizes the preference vector and feature vector from the two aspects of students and courses, respectively, convergence has been achieved and the error value is small at the fourth time. Experimental results further verify the proposed algorithm's recommendation accuracy and convergence performance.

4. Conclusion

Ideological and political education curriculum runs through the whole process of higher education teaching and is an essential system for universities to cultivate high-quality talents. To realize personalized recommendations of ideological and political education courses, this paper proposes a recommendation algorithm based on the analytic hierarchy process and an improved collaborative filtering algorithm. The action of students scoring courses under different time stamps is transformed into Markov decision process. Through analytic hierarchy process, the student behavior data is converted into course preference value. The collaborative filtering algorithm is combined with the reinforcement learning reward and punishment process, and the prediction effect was improved by adjusting the influence factors. Experimental results show that the feasibility of the proposed system is verified, and the system has good accuracy and convergence performance. In the case of insufficient training set data, how to improve the accuracy of the algorithm is the future research work.

Data Availability

The labeled dataset used to support the findings of this study is available from the corresponding author upon request.

Conflicts of Interest

The authors declare that they have no conflicts of interest.

References

[1] G. Gong, "The Integration of Ideological and Political Education in Colleges and Universities and Employment of College Students," *DEStech Transactions on Social Science, Education and Human Science*, 2017, https://www.dpi-proceedings.com/index.php/dtssehs/article/view/13031.

[2] J. Zhang, X. Hu, Z. Ning et al., "Energy-latency tradeoff for energy-aware offloading in mobile edge computing networks," *IEEE Internet of Things Journal*, vol. 5, no. 4, pp. 2633–2645, 2018.

[3] L. G. Xing, I. A. Abiodun, C. W. Khuen, and B. T. Teik, "A Personalized Recommendation Framework with User Trajectory Analysis Applied in Location-Based Social Network (LBSN)," in *Proceedings of the IEEE 3rd International Conference on Engineering Technologies and Social Sciences (ICETSS)*, pp. 1–6, IEEE, Bangkok, Thailand, August 2017.

[4] X. Yang, Z. Huan, Y. Zhai, and T. Lin, "Research of personalized recommendation technology based on knowledge graphs," *Applied Sciences*, vol. 11, no. 15, p. 7104, 2021.

[5] D. Xu, "Research on music culture personalized recommendation based on factor decomposition machine," *Personal and Ubiquitous Computing*, vol. 24, no. 2, pp. 247–257, 2020.

[6] R. Alaa, M. Gawich, and M. Fernández-Veiga, "Personalized Recommendation for Online Retail Applications Based on Ontology Evolution," in *Proceedings of the 2020 6th International Conference on Computer and Technology Applications*, pp. 12–16, Bogotá, Colombia, April 2020.

[7] W. Zhu, W. Liu, and Z. Liu, "News personalized recommendation based on event ontology," *Computer Engineering*, vol. 45, no. 6, pp. 267–272, 2019.

[8] H. Zarzour, Z. Al-Sharif, M. Al-Ayyoub, and Y. Jararweh, "A New Collaborative Filtering Recommendation Algorithm Based on Dimensionality Reduction and Clustering techniques," in *Proceedings of the 9th International Conference on Information and Communication Systems (ICICS)*, pp. 102–106, IEEE, Irbid, Jordan, April 2018.

[9] Z. Cui, X. Xu, F. Xue et al., "Personalized recommendation system based on collaborative filtering for IoT scenarios," *IEEE Transactions on Services Computing*, vol. 13, no. 4, pp. 685–695, 2020.

[10] X. Hu, J. Cheng, M. Zhou et al., "Emotion-Aware cognitive system in multi-channel cognitive radio ad hoc networks," *IEEE Communications Magazine*, vol. 56, no. 4, pp. 180–187, 2018.

[11] A. Suglia, C. Greco, and C. Musto, "A Deep Architecture for Content-Based Recommendations Exploiting Recurrent Neural networks," in *Proceedings of the 25th Conference on User Modeling, Adaptation and Personalization*, pp. 202–211, Bratislava, Slovakia, July 2017.

[12] M. Oppermann, R. Kincaid, and T. Munzner, "Vizcommender: computing text-based similarity in visualization repositories for content-based recommendations," *IEEE Transactions on Visualization and Computer Graphics*, vol. 27, no. 2, pp. 495–505, 2020.

[13] X. Wang, X. He, and Y. Cao, "Kgat: knowledge graph attention network for recommendation," in *Proceedings of the 25th ACM SIGKDD International Conference on Knowledge Discovery & Data Mining*, pp. 950–958, Anchorage AK, USA, August 2019.

[14] M. Naumov, D. Mudigere, H. J. M. Shi, and J. Huang: Deep Learning Recommendation Model for Personalization and Recommendation Systems, 2019.

[15] R. Mu, "A survey of recommender systems based on deep learning," *Ieee Access*, vol. 6, pp. 69009–69022, 2018.

[16] G. Manogaran, R. Varatharajan, and M. K. Priyan, "Hybrid recommendation system for heart disease diagnosis based on multiple kernel learning with adaptive neuro-fuzzy inference system," *Multimedia Tools and Applications*, vol. 77, no. 4, pp. 4379–4399, 2018.

[17] Z. Ji, H. Pi, W. Wei, B. Xiong, M. Wozniak, and R. Damasevicius, "Recommendation based on review texts and social communities: a Hybrid model," *IEEE Access*, vol. 7, Article ID 40416, 2019.

[18] J. L. Herlocker, J. A. Konstan, L. G. Terveen, and J. T. Riedl, "Evaluating collaborative filtering recommender systems," *ACM Transactions on Information Systems*, vol. 22, no. 1, pp. 5–53, 2004.

[19] X. Wu, X. Yuan, C. Duan, and J. Wu, "A novel collaborative filtering algorithm of machine learning by integrating restricted Boltzmann machine and trust information," *Neural Computing & Applications*, vol. 31, no. 9, pp. 4685–4692, 2019.

[20] R. Ahuja, A. Solanki, and A. Nayyar, "Movie Recommender System Using K-Means Clustering and K-Nearest Neighbor," in *Proceedings of the 9th International Conference on Cloud Computing, Data Science & Engineering (Confluence)*, pp. 263–268, IEEE, Noida, India, January 2019.

[21] C. Bakir, “Collaborative filtering with temporal dynamics with using singular value decomposition,” *Tehnički Vjesnik*, vol. 25, no. 1, pp. 130–135, 2018.

[22] R. Kumar, B. K. Verma, and S. S. Rastogi, “Social popularity based SVD++ recommender system,” *International Journal of Computer Application*, vol. 87, no. 14, 2014.

[23] C. Chen, M. Zhang, Y. Zhang, Y. Liu, and S. Ma, “Efficient neural matrix factorization without sampling for recommendation,” *ACM Transactions on Information Systems*, vol. 38, no. 2, pp. 1–28, 2020.

[24] G. Guo, J. Zhang, and N. Yorke-Smith, “Trustsvd: collaborative filtering with both the explicit and implicit influence of user trust and of item ratings,” in *Proceedings of the AAAI Conference on Artificial Intelligence*, vol. 29, no. 1, Austin, TX, USA, January 2015.

[25] T.-w. Zhang, W.-p. Li, L. Wang, and J. Yang, “Social recommendation algorithm based on stochastic gradient matrix decomposition in social network,” *Journal of Ambient Intelligence and Humanized Computing*, vol. 11, no. 2, pp. 601–608, 2020.

Hindawi
Scientific Programming
Volume 2021, Article ID 7557175, 12 pages
https://doi.org/10.1155/2021/7557175

Research Article

Analysis of Spatial and Temporal Distribution Characteristics of Land Desertification Based on GIS and Remote Sensing Images

Li Cui

School of Prospecting and Surveying Engineering, Changchun Institute of Engineering, ChangChun 130021, China

Correspondence should be addressed to Li Cui; gcrz2019ch@ccit.edu.cn

Received 21 September 2021; Accepted 9 November 2021; Published 13 December 2021

Academic Editor: Hai Dong

Due to the complex geographical situation in China, in this paper, the area of land desertification is 98.5% of the total land desertification area in China. Based on the measured data of GIS and remote sensing images, we will discuss the spatial and temporal distribution characteristics of land desertification in China by calculating standardized precipitation evapotranspiration index (SPEI) and normalized vegetation index and establishing the CA model. The results show the following. (1) The trend of desertification in China has decreased as a whole, and the percentage of nondesertification has increased from 36.91% in 1991 to 44.46% in 2020, an increase of 7.55%. Extremely severe desertification increased from 21.72% to 24.25%, an increase of 2.53%. (2) The drought situation in the study area gradually improved, and the change trend of SPEI decreased by 74%. (3) In recent ten years (2011–2020), the vegetation grew well gradually, and it was in the best state in 2018. The NDVI index value increased by 5.9% compared with the average value in this decade. (4) The model designed by us works very well, and the results of simulating and testing the Three Rivers Source region are very little different from the actual situation, which meets our research requirements.

1. Introduction

The Earth, on which human beings depend, is facing severe environmental challenges, such as air pollution, soil erosion, and garbage disposal, which threaten human survival and cause continuous and bad effects. Due to the vast territory and complex natural geography in China, the problem of land desertification is particularly prominent in some areas of China, and the desertified land accounts for 27.2% of the national area. It is precisely because the population affected by desertification in China is the largest, and people are deeply eroded by wind and sand, so the research methods and prevention means of land desertification in China are relatively mature. GIS and remote sensing images are commonly used technologies. By analyzing the spatial and temporal distribution characteristics of land desertification, we can choose a more optimized method to guide the desertification control. Remote sensing monitoring of desertification land in northern China in 2000 showed that desertification land developed rapidly [1], and desertification land in some dry farming areas and farming-pastoral ecotone areas was obviously reversed. Land cover, normalized difference vegetation index, cropland, woodland, and grassland maps were developed using remote sensing data and GIS monitoring [2]. In reference [3], GIS was used to evaluate land desertification, and wetness index, windy days, soil texture, and surface vegetation coverage were selected as evaluation factors of desertification sensitivity. Literature [4] found that desertification is serious from TM images of GIS, which is related to physical factors and differences in land use patterns. Literature [5] described the structural changes and development characteristics of desertification in Yanchi in detail through GIS and database. Literature [6] obtained the data of temporal and spatial change and differentiation model of desertification land around Qinghai and predicted the development trend of desertification in the next 20 years. Literature [7] described a GIS-based software tool for qualitative assessment of desertification risk. Through RS and GIS dynamic monitoring [8], it is found that land desertification is widespread in Longyangxia reservoir area of Qinghai Province. Literature [9] used Google Maps API, data cache, and other technologies to demonstrate the desertification situation in Lurgai area. Gad and Lotfy [10] produced ETM satellite imagery and geological and soil maps of the whole of Egypt, with a scale of 1 : 1000000. Literature [11] used GIS and ecosystem models to assist in assessing and mapping desertification. Literature [12] interpreted TM remote image of oasis lake area to analyze desertification evolution and simulated desertification dynamics by arc object module and cellular automata model. The spatial analysis function of ArcGIS 9.3 software [13] is used to evaluate the desertification index in southern Iraq, and the integrated remote sensing and GIS are used to evaluate the desertification environmentally sensitive areas. Literature [14] studied the dynamics of desertification and examined the accuracy of non-out-of-scope classification methods. According to RS and GIS information of Yijinhuoluo County in Muwu Sandy Land, Xu [15] established the estimation model of vegetation coverage rate and biomass. Desertification exists in some areas. This paper discusses the spatial and temporal distribution characteristics of land desertification in China by using the measured data of GIS and remote sensing images, calculating standardized precipitation evapotranspiration index (SPEI) and normalized vegetation index and establishing the CA model. Through the analysis of spatial and temporal distribution characteristics of land desertification, a more optimized method is selected to guide the desertification control.

2. Study the Relevant Theoretical Basis

Geographic Information System (GIS) uses GIS tools (or platforms) to display these data in the form of intuitive and effective maps and to display and describe its geographic analysis functions. GIS [16] is usually complementary to GPS technology [17] and satellite remote sensing technology [18]. It helps people in need to complete a series of work such as modeling, prediction, and detection. Now, GIS is no longer a distant "high-tech" product; it is quietly gradually into the public life. Everyone can easily use GIS service [19] to obtain geographical knowledge and data.

Remote sensing technology [20] is not a new detection technology in recent years. As early as 1960s, this technology has been produced and put into use in the exploration and monitoring of the Earth, which is used to obtain a large number of resources and environmental information. Because of the maturity of technology and the cheapness, convenience, and richness of obtaining data, it has been widely used in agriculture, forestry, ocean, geography, and other fields, which is closely related to people. Remote sensing technology uses photography to obtain images [21] to improve the accuracy of GIS and reduce the map update cycle [22]:

(1) With the help of ternary wavelet transform [23], the formula is as follows:

$$DA(x,y)\langle DB(x,y), DA(x,y)\rangle DB(x,y),$$
$$R(x,y) = \begin{cases} A(x,y) \\ B(x,y) \end{cases} \tag{1}$$

(2) Remote sensing images are corrected geometrically [24] to reduce the effects of distortion. The general flow of geometric correction is shown in Figure 1.

In Figure 1, because the remote sensing image will be geometrically deformed by the imaging lens, almost all kinds of remote sensing images need to be geometrically corrected to reduce the influence of distortion on data acquisition and generate more accurate maps or graphics that meet the requirements.

The geometric registration [25] formula is as follows:

$$\begin{cases} X = a_0 + a_1x + a_2x + a_3x + \cdots\cdots, \\ Y = b_0 + b_1x + b_2x + b_3x + \cdots\cdots. \end{cases} \tag{2}$$

2.1. Introduction to ERADS Software. ERADS IMAGINE V9.2 developed by American ERADS Company is a powerful and easy-to-operate ERADS IMAGINE V9.2 product. This software product is technically mature and integrates the geographic information system (GIS) and remote sensing image processing. A great feature of this software is that it has a good and sufficient interface, which can communicate stably with other software (such as ARC/INFO, Dbase, and Autocad), share functions and data, and greatly improve the usability of this product. Software versions are constantly updated and maintained, including the latest image processing algorithms, and adaptability is extremely strong. The functional system of the product is shown in Figure 2.

2.2. Cellular Automata (CA). Cellular automaton is a dynamic system.

Represent a model with a formula as follows:

$$A = (C, S, N, R). \tag{3}$$

Represent models in sets as follows:

$$S^{t+1} = f\left(S^t, N\right). \tag{4}$$

Formula (5) is a function that can explain the basic principle of cellular automata (CA). We use sets to express the cellular automata (CA) model. This expression is concise and clear, and the model is more intuitive. In particular, S is a finite set, which also represents cell state, N is the cell domain, variable t represents the time, and letter f represents the local transformation rule.

The structure diagram of the model is shown in Figure 3.

2.3. Drought Evaluation Indicators

2.3.1. Standardized Precipitation Evapotranspiration Index (SPEI). Standardized precipitation evapotranspiration index (SPEI) can help us to analyze the dynamic process of land desertification at different levels, which is of great significance to the study of this paper. The formula for SPEI is as shown in equation (5) where $w = \sqrt{-2\ \ln(P)}$, $C_0 = 2.51552$, $C_1 = 0.80285$, $C_2 = 0.01033$, $d_1 = 1.43279$, $d_2 = 0.18927$, and $d_3 = 0.00131$:

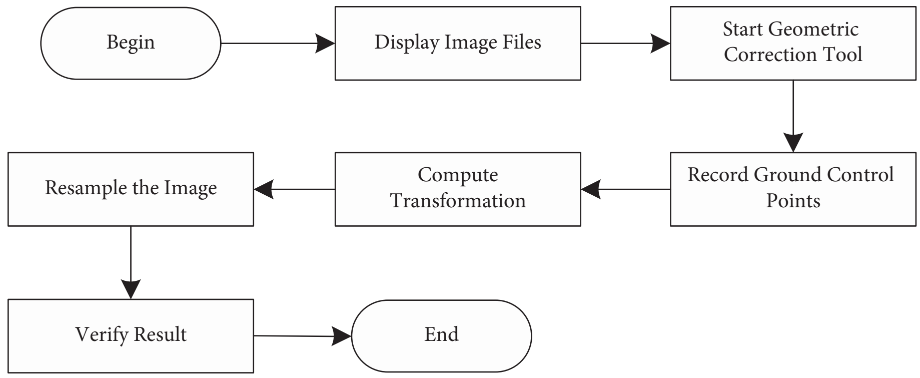

Figure 1: Image geometric correction.

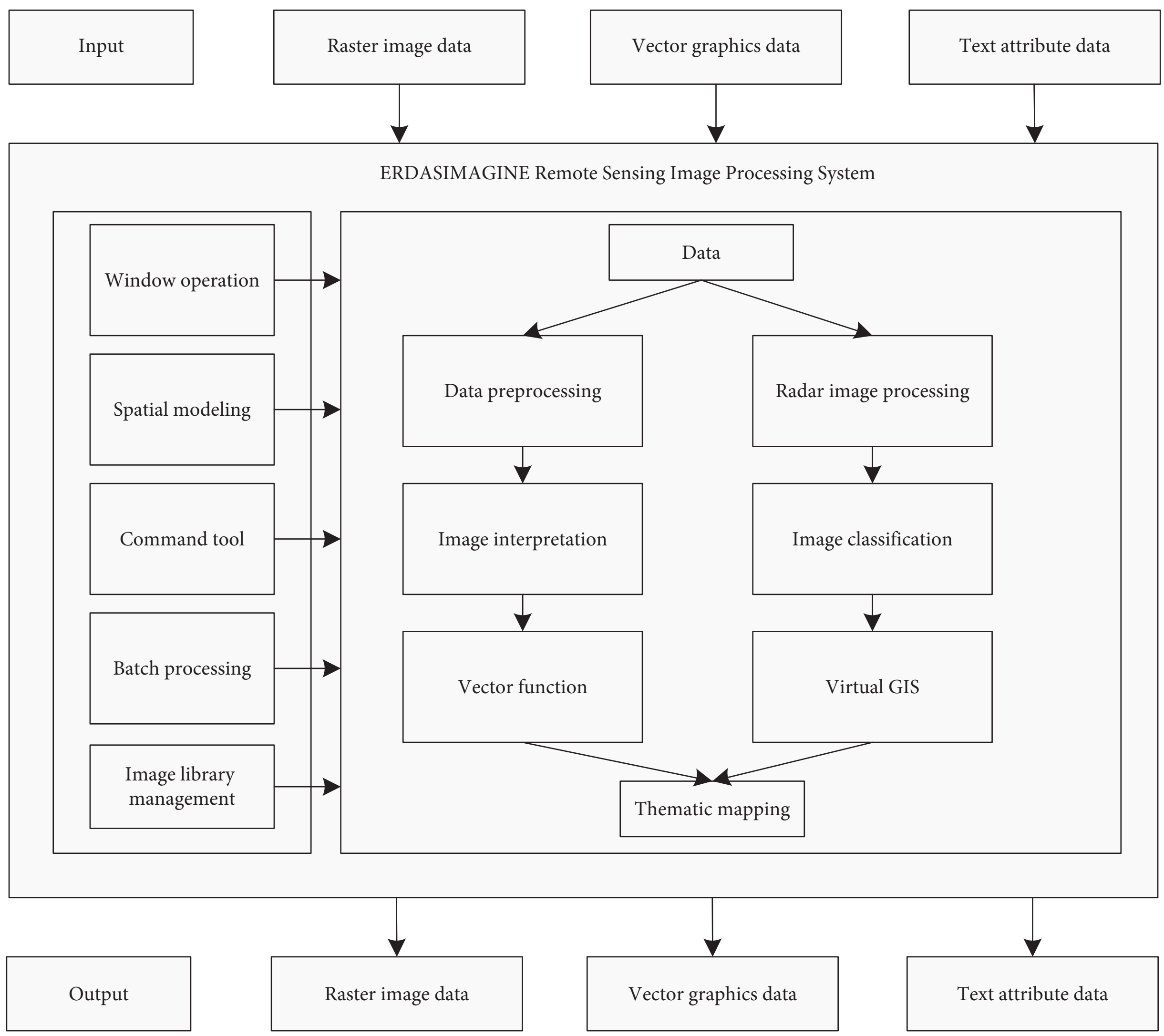

Figure 2: Block diagram of ERADS IMAGINE V9.2.

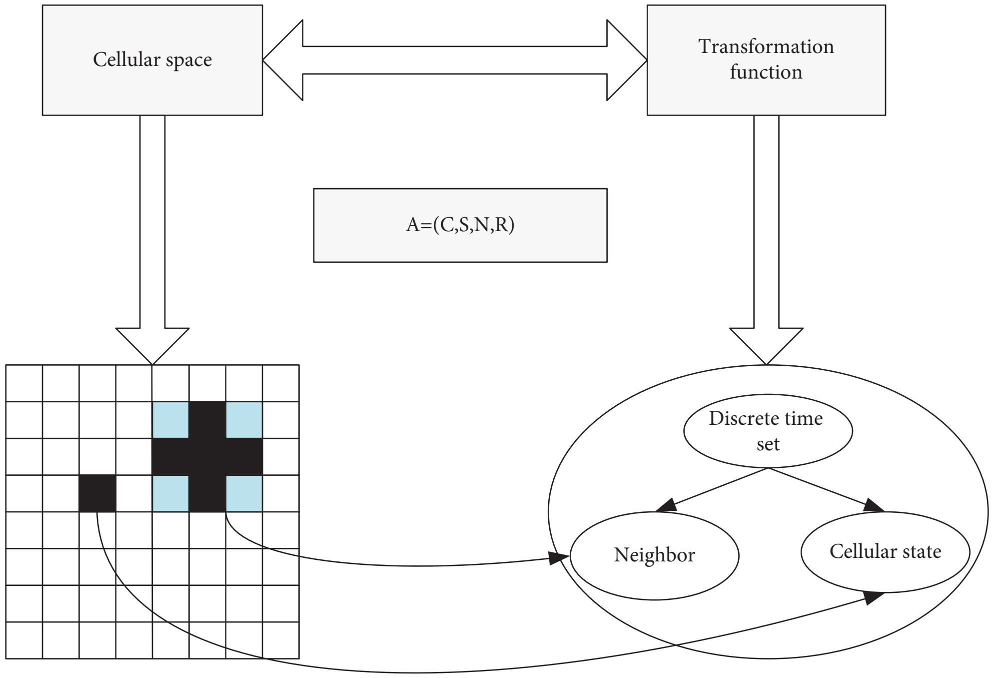

Figure 3: Composition of the cellular automata (CA) model.

$$\mathrm{SPEI} = w - \frac{C_0 + C_1 w + C_2 w^2}{1 + d_1 w + d_2 w^2 + d_3 w^3}. \tag{5}$$

When $P > 0.5$, P is replaced by $1-P$, and the value is reversed positively and negatively. $F(x)$ is a function of water surplus and deficiency:

$$P = 1 - F(x),$$
$$F(x) = \left[1 + \left(\frac{\alpha}{x-\gamma}\right)\beta\right]^{-1}. \tag{6}$$

Potential evapotranspiration is calculated by the following formula:

$$E_d = \frac{0.408\Delta(R_n - G) + \gamma 900/T_a + 273u_2(e_s + e_a)}{\Delta + \gamma(1 + 0.34u_2)}. \tag{7}$$

2.3.2. Ratio of Drought Stations (P_j). The calculation formula of arid station frequency ratio is as follows:

$$P_j = \frac{m_j}{M} \times 100\%. \tag{8}$$

2.3.3. Drought Intensity (S_j). Drought intensity can evaluate the severity of drought. The larger the *SPI* value in the formula, the more serious the drought it represents. The specific calculation formula is shown as follows:

$$S_j = \left|\frac{1}{m}\sum_{i=1}^{m} \mathrm{SPI}_i\right|. \tag{9}$$

2.4. Normalized Vegetation Index (NDVI). Using remote sensing image data and GIS, this study can obtain the spatial distribution map of vegetation growth in China's land desert areas, then calculate the normalized vegetation index (NDVI), and then analyze and map it. We can analyze the desertification and ecosystem in China according to the monitored vegetation coverage and growth, which is of great significance. The greater the NDVI, the denser the vegetation; the smaller the NDVI, the more sparse the vegetation. The calculation formula is shown as follows:

$$\mathrm{NDVI} = \frac{\mathrm{Band2} - \mathrm{Band1}}{\mathrm{Band2} + \mathrm{Band1}}. \tag{10}$$

China has a vast territory and a complex and changeable geographical situation. Due to the actual situation and technical reasons, this study cannot fully discuss the national land desertification situation. Therefore, we mainly choose the northern region of China as the study area, and the land desertification in the northern region accounts for 98.5% of the total land desertification area in China, namely, Shaanxi, Ningxia, Hebei, Gansu, Qinghai, Inner Mongolia, Xinjiang, and Tibet. These provinces have high research value in terms of geography and climate, and the rest provinces account for 1.5%, which are classified into one category because they are too scattered, so they only do brief discussion and research. The specific distribution map of 8 provinces of land desertification is shown in Figure 4.

The data obtained in this study include land use map, basic statistical data, and second-hand data. The specific data processing specifications are shown in Table 1.

Figure 4: Main land desertification provinces.

Table 1: Data processing specifications.

Time series	Spatial distribution rate (m)	Storage form	Model data format
Year	30	Grid	Binary data (ASCII code format)

3. Analysis of Land Desertification Degree

3.1. Analysis of Various Land Types. We obtain the land type change data of desertification in northern China, and we can find that the land vegetation types are basically divided into desert, Gobi, bare land, sandy land, grassland, cultivated vegetation, meadow, alpine vegetation, coniferous forest, and broad-leaved forest. Desertification land accounts for the heaviest proportion in the figure. The details are shown in Figure 5.

There are basically five types of land use, as shown in Figure 6.

3.2. Classification and Classification System of Desertification. In the study, the land desertification classification in the study area is convenient for researchers to make reasonable judgments and can quickly determine the degree and current situation of desertification in the region. We introduce Feng Yusun's evaluation system to classify desertification, as shown in Table 2.

The desertification classification system is shown in Table 3.

3.3. Temporal and Spatial Variation Characteristics of Desertification Land. We divide the period 1991–2020 into three time periods: 1991–2000, 2001–2010, and 2011–2020. The specific desertification situation is shown in Table 4.

According to the above table, the general trend of land desertification in northern China is gradually decreasing, and the percentage of nondesertification has increased from 36.91% in 1991 to 44.46% in 2020, an increase of 7.55%. However, the extremely severe desertification increased from 21.72% to 24.25%, an increase of 2.53%. This shows that the ecological environment in desertification areas in China is gradually improving, but it is inevitable that some areas are not only not improving but also aggravating the trend of land desertification, which deserves the attention of local relevant departments, and more control and prevention should be given to land desertification. We need to assess the situation of land desertification from multiple angles and aspects, instead of measuring it with one or two unilateral factors.

3.3.1. Regional Drought Dynamics. Drought is a serious meteorological disaster. Due to the greenhouse effect and the influence of various human activities, the economic loss

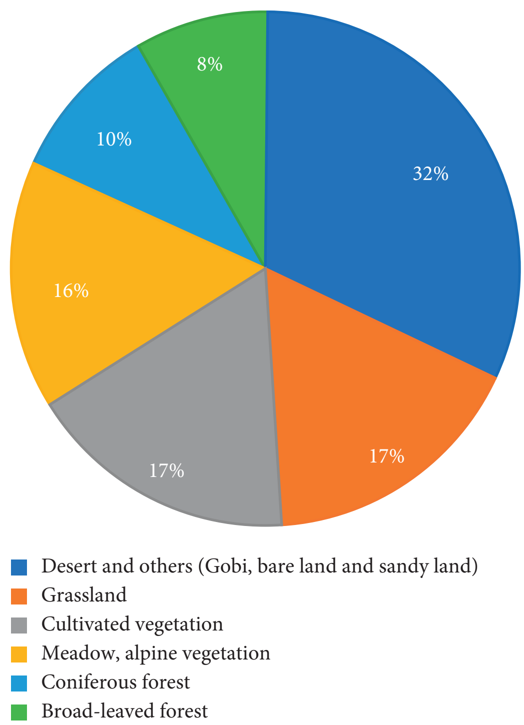

Figure 5: Various land types in northern China.

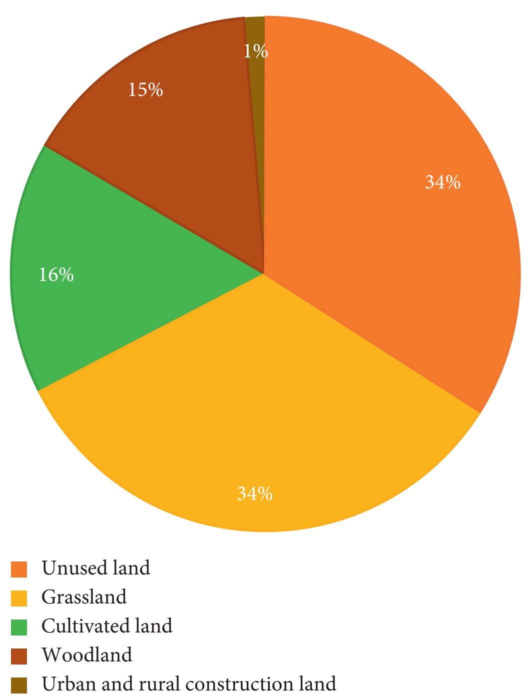

Figure 6: Land use types in northern China.

caused by drought disasters in the world is as high as 43% every year, which accounts for the largest proportion of all natural disaster losses.

(1) The annual and seasonal changes of SPEI in the northern study area decreased as a whole, with a decrease area of 74% and a significant decrease area of 43%. In some areas, the increase area is 26%, and the significant increase area is 6%.

As shown in Table 5, it is a statistical table of SPEI and drought grade change trend in northern study area.

(2) Drought stations in different dry and wet areas from 1966 to 2020 are shown in Figure 7.

We can find from the figure that the distribution of arid station frequency ratio in humid area is uneven, and the arid station frequency ratio is the least in some regional droughts. The ratio of drought stations and drought intensity in humid and semi-humid areas showed an increasing trend. The ratio of arid stations and drought intensity in arid and semiarid areas showed a decreasing trend.

(3) The tendency rate of SPI in different dry and wet areas from 1966 to 2020 is shown in Figure 8.

According to the analysis of SPI propensity rate in the line chart, we can obviously observe that SPI propensity rate increases in different dry and wet areas in different seasons.

3.3.2. Changes in Desertification Vegetation Growth. Figure 9 shows the average NDVI trend chart.

As shown in Figure 10, it is a change map of the vegetation index.

Vegetation in desertification areas has gradually grown well in recent ten years. In 2018, the state was the best, and the NDVI index value increased by 5.9% compared with the average value in this decade. The ecosystem of desert areas in northern China has gradually improved, and the trend of desertification has been gradually controlled.

3.3.3. Dynamic Simulation Analysis of Desertification in the Source Region of the Three Rivers. Because of the vast land in northern China, the development status of each region is different, so it is difficult to carry out dynamic simulation and prediction analysis uniformly. Considering the money cost, time cost, and difficulty of data extraction, we choose Sanjiangyuan region, which is located in the south of Qinghai Province and the hinterland of Qinghai-Tibet Plateau, as a regional dynamic simulation and prediction analysis of land desertification. As shown in Figure 11, it is the geographical location map of the Sanjiangyuan region.

3.4. Data Preparation and Preprocessing. To simulate the evolution of desertification, we need to collect various spatial data and statistical data, use ERADS software to preprocess the original data, extract important data from GIS and remote sensing images, and standardize the data after processing. This processing can effectively prevent the original data measured by us from being affected by interference factors such as human factors and equipment factors and ensure the accuracy of experimental results.

There are two data standardization methods when preprocessing data.

Table 2: Feng Yusun's desertification classification system.

Characteristic	Serious	Strongly developing	In development	Potential
Proportion of desertification land	>50%	25–50%	5–25%	<5%
Expansion rate of desertification land	>40%	40–20%	5–20%	<5%
Dune type	Large area crescent dunes or dune chains	Beam-shaped dunes are dominant and crescent-shaped dunes occasionally appear	Beam-shaped sand dunes, shrub sand piles, and sand ridges intersect	There is basically no quicksand distribution
Relative height of dune undulation (M)	>25	10–25	5–10	<5
Degree of dune activity	Mobile dune	Semimobile dune	Semifixed dune	Fixed dune
Vegetation coverage on sand dunes	<15%	15–30%	30–50%	>50%

Table 3: Classification system of land desertification in northern China.

Types of desertification	Vegetation coverage	Wind erosion thickness of land (cm)	Aeolian deposition of land (cm)	Soil erosion ($1/hm^2 \cdot y$)	Population overload rate (%)	Livestock overload rate (%)
Mild desertification	40–60%	<5	<5	<0.5	−50~31	−50~31
Moderate desertification	25–40%	5~10	5~10	0.5~1.0	−31~0	−31~0
Severe desertification	10–25%	10~20	10~20	1.0~3.0	0~31	0~31
Extremely severe desertification	<10%	>20	>20	>3.0	>31	>31

Table 4: Desertification land area and percentage of different grades from 1991 to 2020.

Type	1991–2000		2001–2010		2011–2020	
	Area ($10^4\,km^2$)	Percentage (%)	Area area/$10^4\,km^2$	Percentage (%)	Area area/ $10^4\,km^2$	Percentage (%)
Nondesertification	196.12	36.91	213.73	40.23	236.22	44.46
Mild desertification	67.99	12.80	60.57	11.40	50.24	9.46
Moderate desertification	50.21	9.45	45.69	8.60	42.84	8.06
Severe desertification	101.17	19.04	94.22	17.73	72.98	9.46
Extremely severe desertification	115.40	21.72	116.93	22.01	128.84	24.25

Table 5: SPEI and statistics of drought change trend.

Project	Variation trend of SPEI in years and seasons					Variation trend of different drought grades		
	Year (%)	Spring (%)	Summer (%)	Autumn (%)	Winter (%)	Mild (%)	Moderate (%)	Extreme (%)
Increasing trend	26	19	36	33	48	78	81	69
Significant increase	6	0	1	1	6	17	38	4
Reducing trend	74	81	64	67	52	22	19	31
Significant reduction	43	43	12	17	7	0	0	1

(1) Min-max standardization method is as follows:

$$y_i = \frac{x_i - x_{\min}}{x_{\max} - x_{\min}}. \tag{11}$$

(2) Z-score standardization method is as follows:

$$y_i = \frac{x_i - u}{s}. \tag{12}$$

In this paper, the min-max standardization method is adopted, as shown in Table 6, which is partially standardized data.

The CA model selected in this study is based on raster data. The realization of the CA model should first define the state and type of land, then monitor the desertification land in the source region of the Three Rivers, and comprehensively judge the influence degree of desertification by various indicators. We select the data in 2000 to run the model, compare the simulated desertification results in 2018 with the actual land desertification distribution in 2018, then constantly adjust and run the model, and finally select the more suitable model parameters for evolutionary simulation analysis.

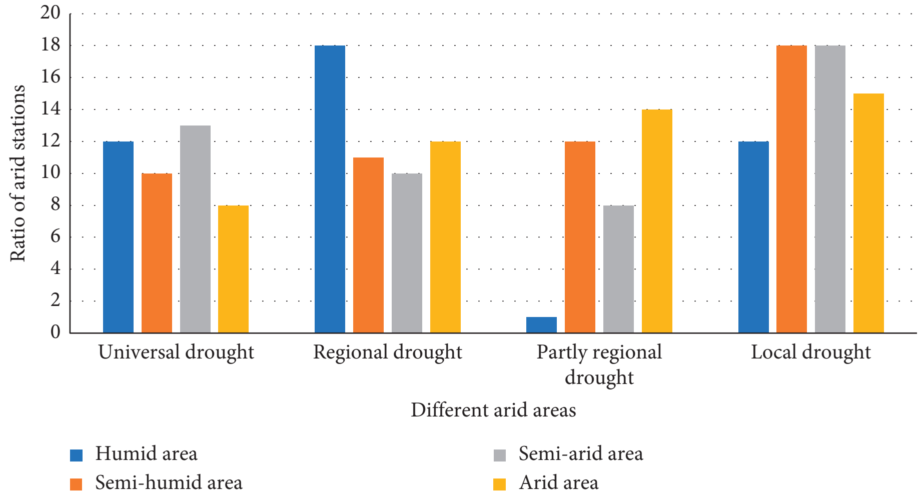

Figure 7: Ratio of arid stations in different dry and wet areas from 2006 to 2020.

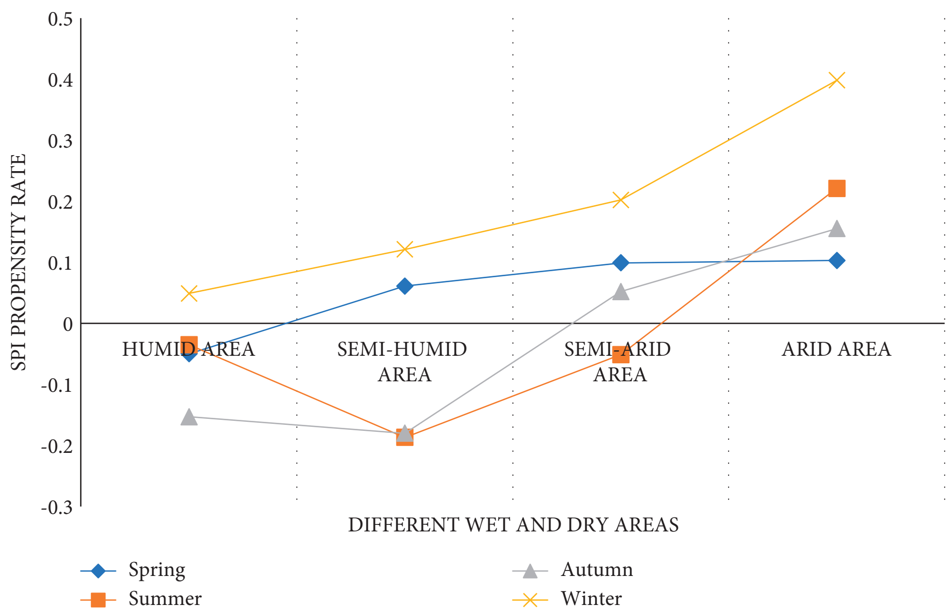

Figure 8: SPI tendency rate in different dry and wet areas in four seasons.

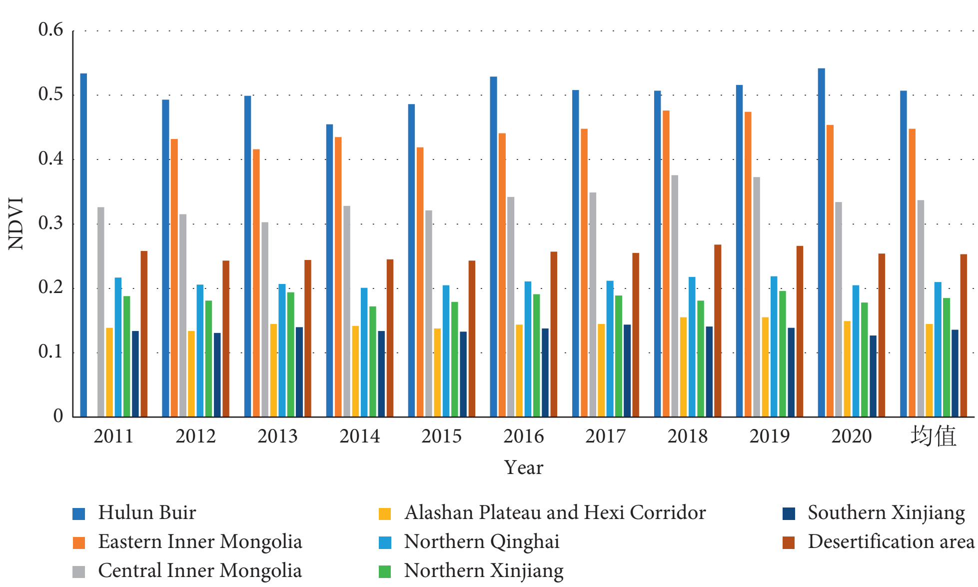

Figure 9: Analysis of the change trend of average NDVI in recent 10 years.

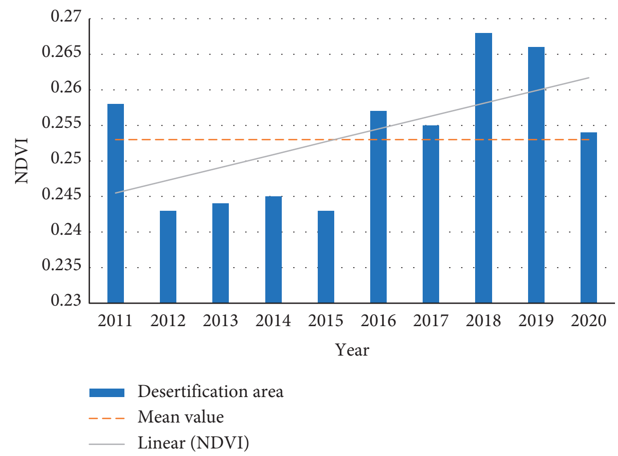

Figure 10: Changes of vegetation index in recent 10 years.

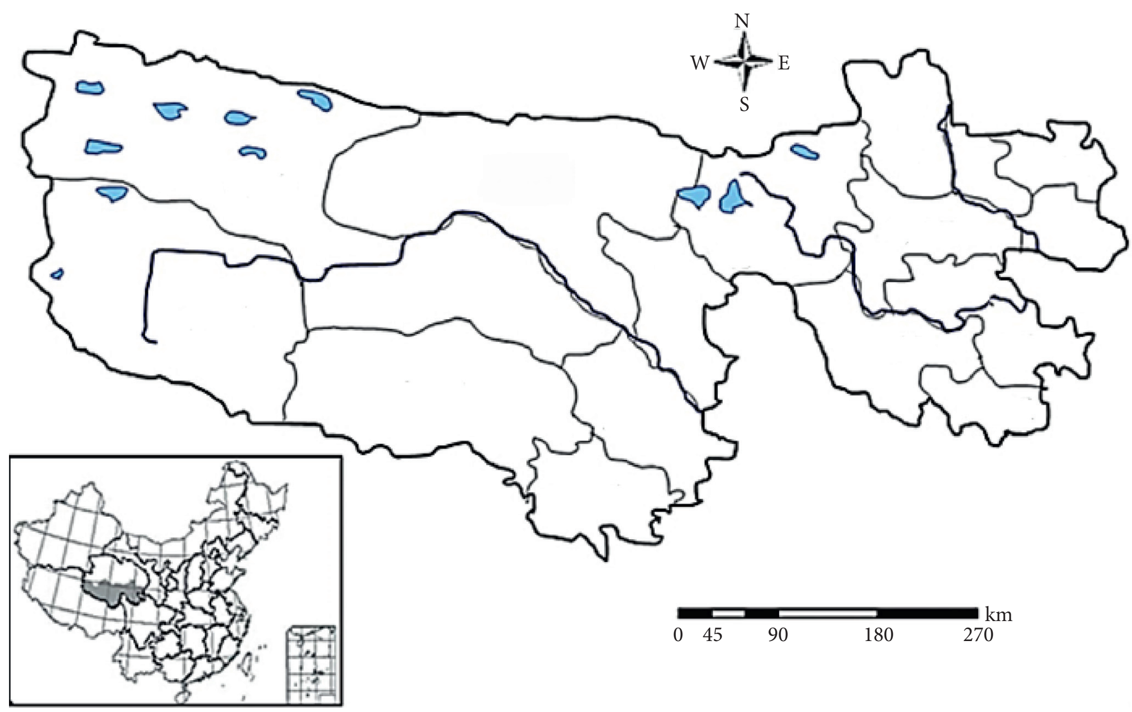

Figure 11: Geographic map of position.

Taking the land desertification in the source region of the Three Rivers in 2000 as the initial state, the model is run. The accuracy is tested by Kappa, and the calculated result is 0.864, and the simulation result is ideal.

$$\text{Kappa} = \frac{\left(P_0 - P_c\right)}{\left(P_p - P_c\right)}. \tag{13}$$

The goal is to unify the specifications, facilitate data processing, and avoid more troubles caused by the confusion of various data formats.

In equation (8), the ratio of drought stations can be used to evaluate the size and severity of drought range, M refers to the total number of weather stations in the study area in the north, J refers to different years, and MJ refers to the number of weather stations with drought in J year.

In equation (10), Band1 is the reflectivity in red band and Band2 is the reflectivity in near infrared band. The greater the calculated NDVI value, the greater the vegetation density. The smaller the *NDVI* value, the smaller the vegetation density. In particular, the NDVI value ranges from −1 to 1.

In equation (13), P_0 is the ratio of correct simulation, P_c is the ratio of expected correct simulation in random case, and P_p is the ratio of correct simulation in ideal classification case. $Kappa > 0.75$ indicates that the accuracy of the model is good.

3.5. Simulation Results

3.5.1. Types of Land Ecosystems. As shown in Figure 12, most of the Sanjiangyuan region is grassland. Desertification land accounts for 9% of the total area.

Table 6: Partially standardized data.

Month	NDVI	Precipitation	Temperature
2000-01	0.085106	0.003344	0.124879
2000-02	0.085106	0.041033	0.396034
2000-03	0.271277	0.211556	0.683783
2000-04	0.558511	0.184884	0.898734
...	...	...	...

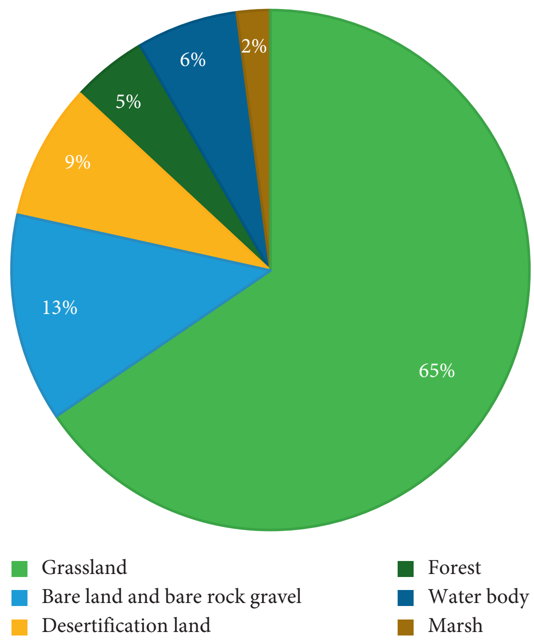

Figure 12: Statistical table of ecosystem type area in Sanjiangyuan.

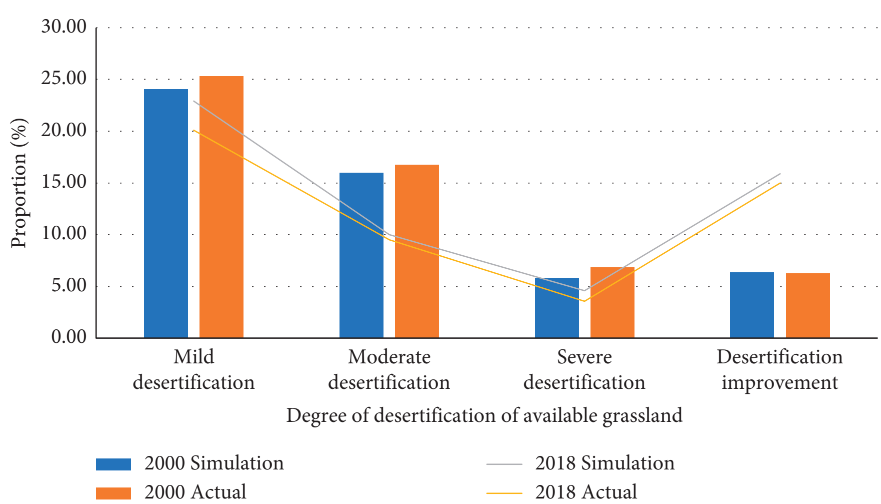

Figure 13: Desertification degree of available grassland.

3.5.2. Simulation Test Comparisons. In recent years, the ecosystem of Sanjiangyuan has been seriously damaged. Besides desertified land, nearly 70% of grassland is gradually desertified, and the annual desertification rate is maintained at 2.3%.

(1) Land Desertification in Sanjiangyuan Region. We compare the desertification situation in 2000 and 2018 tested by the model with the actual desertification situation in 2000 and 2018. It can be found that the results tested by our simulation system are not much different from the actual results. The average difference between the simulation test in 2000 and the actual monitoring results is 0.78, while the average difference between the simulation test and the actual monitoring results in 2018 is 1.31. The specific desertification statistics of available grassland are shown in Figure 13.

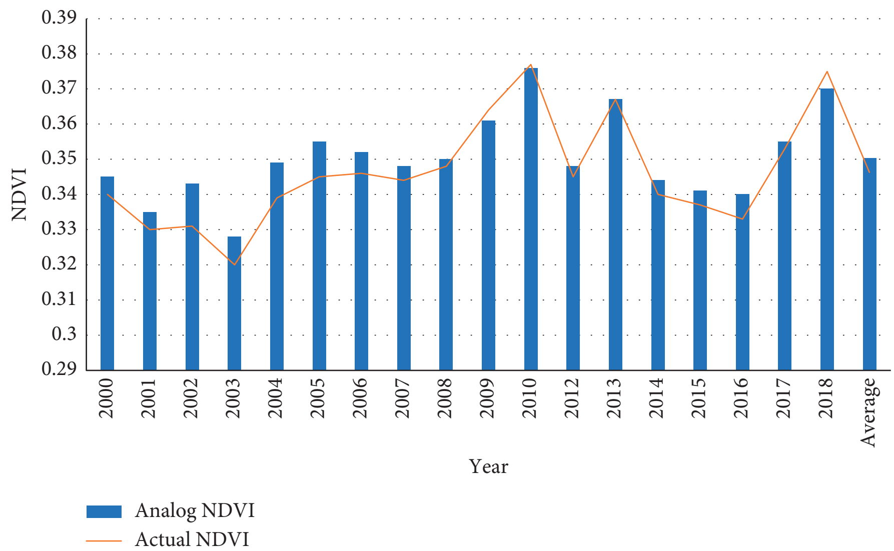

Figure 14: Interannual variation of NDVI.

(2) Interannual Variation of NDVI in the Source Region of the Three Rivers. The interannual changes of NDVI in 2000 and 2018 tested by the model are compared with the actual situation. It can be found from the figure that from 2000 to 2008, the simulated situation is quite different from the actual situation, and the difference from 2009 to 2018 is very small. The average annual NDVI in the simulation test is 0.350, and the average annual NDVI in actual situation is 0.346. The details are shown in Figure 14.

The model designed by us runs very well and has little difference with the actual situation, which meets our research requirements.

4. Conclusion

(1) Most of the study area is covered by desert. In the past 10 years, the general trend of desertification has gradually decreased, and the ecological environment has gradually improved. The percentage of non-desertification has increased from 36.91% in 1991 to 44.46% in 2020, an increase of 7.55%. Extremely severe desertification increased from 21.72% to 24.25%, an increase of 2.53%.

(2) The annual and seasonal variation trend of SPEI in the northern study area decreased as a whole, with a decrease area of 74%. The drought situation in the study area gradually improved.

(3) In recent ten years (2011–2020), the vegetation in China's land desertification areas has gradually grown well, and it is in the best state in 2018. The NDVI index value has increased by 5.9% compared with the average value in the past ten years. Land desertification has been controlled in China.

(4) The simulation test of land desertification in the source region of the Three Rivers has a good performance, and the difference between the test results and the actual results is basically very small, and the overall desertification trend in the source region of the Three Rivers is controlled.

The above data and methods in this paper are suitable for studying the spatial and temporal distribution characteristics of land desertification, but there are still some shortcomings and needs to be refined.

Data Availability

The experimental data used to support the findings of this study are available from the corresponding author upon request.

Conflicts of Interest

The author declares that there are no conflicts of interest regarding this work.

Acknowledgments

This work was sponsored by Jilin Provincial Department of Education (JJKH20191267KJ).

References

[1] T. Wang, W. Wu, and X. Xue, "Time-space evolution of desertification land in northern China," *Journal of Desert Research*, vol. 23, no. 3, pp. 24–29, 2003.

[2] Y. Zhang, Z. Chen, B. Z. X. Luo et al., "Land desertification monitoring and assessment in Yulin of Northwest China using remote sensing and geographic information systems (GIS)," *Environmental Monitoring and Assessment*, vol. 147, no. 1-3, pp. 327–337, 2008.

[3] K. Liu, W. H. Xu, Z. Y. Ouyang, and A. W. Jing, "GIS-based assessment on sensitivity to land desertification in Gansu province," *Bulletin of Soil and Water Conservation*, vol. 22, no. 5, pp. 29–31, 2002.

[4] L. Zhang, L. Yue, and B. Xia, "The study of land desertification in transitional zones between the MU US Desert and the Loess

Plateau using RS and GIS?a case study of the Yulin region," *Environmental Geology*, vol. 44, no. 5, pp. 530–534, 2003.

[5] Y. Qi, Y. M. Wang, J. H. Wang, and C. Z. Yan, "Analysis on desertification dynamics based on remote sensing and GIS-exampled in Yanchi county, Ningxia," *Journal of Desert Research*, vol. 30, no. 4, pp. 862–880, 2003.

[6] H. U. Meng-Jun, L. H. Tian, D. S. Zhang, and Z. Na, "Study on dynamic changes of aeolian desertification lands around Qinghai lake in recent 30Years based on remote sensing and GIS," *Journal of Desert Research*, vol. 32, no. 4, pp. 901–909, 2012.

[7] M. Santini, G. Caccamo, A. Laurenti, S. Noce, and R. Valentini, "A multi-component GIS framework for desertification risk assessment by an integrated index," *Applied Geography*, vol. 30, no. 3, pp. 394–415, 2010.

[8] Z. J. Sha, Y. N. Zeng, L. Q. Li, M. H. Zhou, G. C. Cao, and P. Yang, "Dynamic monitoring of land desertification by RS and GIS - a case study in Longyangxia Reservoir area," *Arid Land Geography*, vol. 2013, no. 1, pp. 274–278, 2000.

[9] X. W. Liu et al., "A Web GIS application of desertification status of Ruoergai area," *Advanced Materials Research*, vol. 2014, pp. 838–841, 2014.

[10] A. Gad and I. Lotfy, "Use of remote sensing and GIS in mapping the environmental sensitivity areas for desertification of Egyptian territory," *Earth Discussions*, vol. 3, no. 2, pp. 654–660, 2008.

[11] J. Grunblatt, W. K. Ottichilo, and R. K. Sinange, "A GIS approach to desertification assessment and mapping," *Journal of Arid Environments*, vol. 23, no. 1, pp. 81–102, 1992.

[12] D. M. Song, G. X. Wang, C. Shen, and J. Wang, "Desertification evolution prediction for lake area of Minqin oasis based on integration of GIS and cellular automata," *Science of Cold and Arid Regions (English Version)*, vol. 4, no. 3, pp. 222–228, 2012.

[13] A. S. Hadeel, M. T. Jabbar, and X. Chen, "Application of remote sensing and GIS in the study of environmental sensitivity to desertification: a case study in Basrah Province, southern part of Iraq," *Applied Geomatics*, vol. 2, no. 3, pp. 101–112, 2010.

[14] X. L. Mao, P. X. Zhao, D. X. Wang, W. Z. Li, and S. M. Liu, "Nonsupervising digital classification and GIS in the dynamic monitoring of soil desertification application," *Journal of Northwest Forestry University*, vol. 20, no. 3, pp. 6–9, 2005.

[15] W. Xu, "Quantitative estimation of desertification degree based on RS and GIS in mu us sandland, inner Mongolia," *Scientia Silvae Sinicae*, vol. 43, no. 5, pp. 48–53, 2007.

[16] C. S. Jarnevich, T. R. Holcombe, D. T. Barnett, T. J. Stohlgren, and J. T. Kartesz, "Forecasting weed distributions using climate data: a GIS early warning tool," *Invasive Plant Science and Management*, vol. 3, no. 4, pp. 365–375, 2017.

[17] C. Leake and J. Malczewski, "GIS and multicriteria decision analysis," *Journal of the Operational Research Society*, vol. 51, no. 2, p. 247, 2000.

[18] J. Hansen, R. Ruedy, J. Glascoe, and M. Sato, "GISS analysis of surface temperature change," *Journal of Geophysical Research: Atmosphere*, vol. 104, no. D24, pp. 30997–31022, 1999.

[19] M. Wheatley, J. T. Fisher, K. Larsen, L. Joseph, and B. Stan, "Using GIS to relate small mammal abundance and landscape structure at multiple spatial extents: the northern flying squirrel in Alberta, Canada," *Journal of Applied Ecology*, vol. 42, no. 3, pp. 577–586, 2010.

[20] A. Facchinelli, E. Sacchi, and L. Mallen, "Multivariate statistical and GIS-based approach to identify heavy metal sources in soils," *Environmental Pollution*, vol. 114, no. 3, pp. 313–324, 2001.

[21] G. Cmara, R. C. M. Souza, U. M. Freitas, M. F. Ubirajara, and G. Juan, "SPRING: integrating remote sensing and GIS with object-oriented data modelling," *Computers & Graphics*, vol. 15, no. 6, pp. 13–22, 1996.

[22] L. ü a Guo-Nian, G. Z. Ping, S. H. Sheng, and N. X. Su, "GIS-based logistic regression for landslide susceptibility mapping of the Zhongxian segment in the Three Gorges area, China," *Geomorphology*, vol. 115, no. 1–2, pp. 23–31, 2010.

[23] J. Malczewski, "GIS-based multicriteria decision analysis: a survey of the literature," *International Journal of Geographical Information Science*, vol. 20, no. 7, pp. 703–726, 2006.

[24] M. Stuiver, P. M. Grootes, and T. F. Braziunas, "The GISP2 δ18O climate record of the past 16,500 years and the role of the sun, ocean, and volcanoes," *Quaternary Research*, vol. 44, no. 3, pp. 341–354, 1995.

[25] G. Dc, "Manipulating cattle distribution with salt and water in large arid-land pastures: a GPS/GIS assessment," *Applied Animal Behaviour Science*, vol. 73, no. 4, pp. 251–262, 2001.

Hindawi
Scientific Programming
Volume 2021, Article ID 5984306, 9 pages
https://doi.org/10.1155/2021/5984306

Research Article

The Mechanism of Evolution and Balance for e-Commerce Ecosystem under Blockchain

Fengqin ZhuanSun, Jiaojiao Chen, Wenlong Chen, and Yan Sun

School of Management, Wuxi Institute of Technology, Wuxi 214000, China

Correspondence should be addressed to Fengqin ZhuanSun; zhsfq@wxit.edu.cn

Received 15 October 2021; Revised 9 November 2021; Accepted 13 November 2021; Published 13 December 2021

Academic Editor: Hai Dong

With the development of society, e-commerce competition has become increasingly intense and has ascended to the level of the ecosystem. Therefore, it is extremely significant to study the mechanism of evolution and balance for the e-commerce ecosystem. Simultaneously, blockchain technology is essentially a consensus mechanism, the core idea of which is decentralization, but it is actually the deconstruction of privileges and authority. Especially, the influence on the e-commerce ecosystem cannot be underestimated. Blockchain technology ultimately changes not only technology, but a comprehensive reconstruction of various industries. Building an e-commerce information ecosystem based on blockchain can promote the healthy and sustainable development of e-commerce information ecology. This work combines the definition and technical characteristics of blockchain, discusses the blockchain-based e-commerce information ecosystem model, and discusses how to achieve the ecological balance and system evolution of e-commerce under the background of blockchain. According to the internal problems of the e-commerce ecosystem, three evolutionary paths are proposed in this work. First, consider the timeliness of the information and construct a full-process information channel. Second, remove central nodes and build a safe and efficient block payment. Third, solve the blind zone in the field of logistics and create efficient and transparent intelligent logistics. This work can provide an effective reference for the development of e-commerce.

1. Introduction

With the development of society, the Internet has ushered in a brand-new business era and the era of e-commerce. e-Commerce can be regarded as another industrial revolution after the agricultural revolution and the industrial revolution. It has become the business trend of the 21st century and an important means to promote economic development and management progress [1–6].

With the rapid development of e-commerce, it is imperative to build a balanced and sustainable e-commerce information ecosystem. At the same time, the emergence of digital currency represented by Bitcoin, the underlying technology of the digital cryptocurrency system, and the blockchain has also attracted widespread attention from the academic community [7–12]. Blockchain technology is regarded as another disruptive technological innovation in the computing paradigm after the Internet. The application of blockchain technology has gradually penetrated into many fields such as network financial services, the Internet of Things, online education industry, and network sharing economy. Its rapid development is expected to lead the transformation of the Internet economy from an application-driven innovation model to a technology-driven innovation model. Blockchain technology is a complete, distributed, and nontamperable ledger database technology maintained by a multicenter consensus. It is ordered data composed of distributed storage, decentralization, cryptography, consensus mechanism, and smart contracts. The overall characteristics of blockchain and blockchain technology are embodied in the immutability of data, collective maintenance of data, and multicentralized decision-making.

The business ecosystem refers to the interaction between individuals and organizations [13–16], whose members include core enterprises, consumers, market intermediaries, suppliers, and risk-takers. The internal members of the system constitute a value chain, and different value chains are intertwined. As a significant value network, each subject in the system has its own function and at the same time is interdependent. Material, energy, and information flow and circulate among alliance members through a specific value network. The importance of e-commerce in the process of economic development continues to increase, and the research of e-commerce ecosystem has gradually become a hot spot. The e-commerce ecosystem mainly includes e-commerce platforms, merchants, consumers, suppliers, logistics companies, third-party payment companies, drainage companies, consumer finance, supply chain finance, and these organic enterprises and individuals within the system, i.e., internal system. The information flow, capital flow, and logistics generated by the communication between living organisms together constitute the e-commerce ecosystem. The e-commerce ecosystem is characterized by diversification and complexity [17–19]. Most of the professional e-commerce companies prefer using a cooperative model to achieve the value creation [20]. The imperfect coordination mechanism between the subjects of the e-commerce ecosystem has led to problems, such as the lack of online transaction data between consumers and merchants [21], and the obvious lack of coordination between e-commerce and logistics [22].

As a dynamic and open business ecosystem, the e-commerce ecosystem always exchanges energy and material with the external environment. The external environment is the basis for the existence of the e-commerce ecosystem. There are also interactions between different subjects within the e-commerce ecosystem. The specific manifestation is the flow of information flow, capital flow, and logistics in the entire e-commerce ecosystem. Information flow, capital flow, and logistics are the core of the e-commerce ecosystem. In order to study the utility of information flow, capital flow, and logistics in the entire e-commerce ecosystem, the subjects in e-commerce are divided into different populations, and the e-commerce system is explained by studying the interaction between different populations and different subjects for evolution and balance mechanism. The main research method is synergetics in evolutionary economics, and it is used to study the collaboration within the e-commerce ecosystem to achieve the balance of the system.

The contribution of this work can be summarized as follows: according to the internal problems of the e-commerce ecosystem, three evolutionary paths are proposed in this work: (1) consider the timeliness of the information, and construct a full-process information channel. (2) Remove central nodes, and build a safe and efficient block payment. (3) Solve the blind zone in the field of logistics, and create efficient and transparent intelligent logistics. This work can provide an effective reference for the development of e-commerce.

2. Related Work

Looking at the foreign literature, the application research based on blockchain technology shows that a hundred flowers bloom and a hundred schools of thought are contending. As far as the field of e-commerce is concerned, the research of blockchain focuses on the innovation of specific things in e-commerce. The evolution and balance mechanism of the e-commerce ecosystem in the context of blockchain is a new topic that needs to be studied urgently. Bilgihan and Gen [23] analyzed the importance of e-commerce companies maintaining a good reputation from the perspective of consumers. Trust is the prerequisite for consumers to maintain online shopping loyalty. Yu et al. [24] believed that e-commerce business processes adopt a structure of multiple participants, including shopping customers, merchants, third-party payment platforms, and banks. The communication between these participants relies on web services and application programming interfaces. The complex interactions between multiple participants will bring new security challenges. Min [25] thought that the blockchain was considered to be a peer-to-peer information network technology. The use of distributed account books to store digital asset transaction records can reduce the intervention of intermediaries, reduce external risks, and improve the flexibility of supply chain management. Robert et al. [26] believed that information will be in the process of transforming new energy for enterprise development to an open innovation ecosystem, and it is necessary to ensure that data owners can better control their own data and privacy and independently choose whether to share and with whom to share and exchange specific data streams, as well as regions. The degree to which blockchain technology meets these requirements. Angelis and Ribeiro da Silva [27] discussed the relationship between the characteristics of blockchain technology and its potential value drivers. The value drivers of blockchain are mainly reflected in transactions, smart contracts, and distributed applications. These studies have discussed issues such as information asymmetry, information security, supply chain management, user privacy, and information sharing in e-commerce companies, and we believe that the application of blockchain technology is conducive to solving the above problems. The above studies all study the impact of blockchain technology on e-commerce from a single perspective, but there is a lack of research on the evolutionary impact of blockchain on the e-commerce ecosystem from a systematic perspective. Dennis and Owenson [28] constructed a platform merchant credit rating system based on blockchain technology, which eliminates the inauthenticity of online rating information. Schaub et al. [29] further expanded the application of blockchain in the credit rating system of merchants, realizing real online reviews of merchants under the condition of high privacy of buyer information.

Different from the foreign research studies, the domestic research of e-commerce ecosystem is mainly concentrated in the fields of financial currency, medical care, sharing economy, education, and energy. Wang [30] discussed the feasibility of blockchain currency as legal tender. Zhang [31] cited the case of Philips Medical to illustrate that blockchain technology could realize the authentication and privacy protection of patient medical records. Li et al. [32] realized distributed learning record storage and credit banking services by the blockchain technology. Zhang et al. [33] studied the typical application of blockchain technology in the energy Internet. Based on the consensus mechanism of the blockchain and the core idea of decentralization, Dan [34] launched the analysis of the reconstruction of the e-commerce ecosystem by the blockchain. Zhang and Li [35] discussed the electronic commerce in the context of the blockchain. The collection of business value-added tax has been explored, and the conclusion that blockchain is universal in the collection of e-commerce value-added tax has been arrived, and relevant suggestions have been given. Chen [36] conducted research on the corporate credit information sharing model based on the blockchain technology, aiming at China's corporate credit information industry being in the primary stage of development, and the credit coverage rate of the credit reporting system is not high, especially the lack of credit information for small and micro-enterprises. It is difficult for small and micro-enterprises to raise funds and propose a proposal to build a corporate credit information sharing model based on blockchain technology. Liu [37] from the perspective of ecology used business ecosystem theory, evolutionary economics, and evolutionary games theory, and the theory and methods of ecology and collaborative evolution were introduced into the field of cross-border e-commerce research, and a platform-based cross-border e-commerce ecosystem is proposed and constructed. Zhang et al. [38] researched by building an e-commerce ecosystem user perception model. It was believed that the factors that affect user perception can be divided into three categories: self-organization factors, internal relationship factors, and health factors, and they have different degrees of influence on the online shopping experience.

3. Analysis between Blockchain and E-Commerce Ecosystem

In this section, the relationship between blockchain and e-commerce ecosystem will be dissected from two aspects: the fit between blockchain and e-commerce as well as the e-commerce information ecological model based on blockchain.

3.1. Analysis of the Fit between Blockchain and E-Commerce

3.1.1. Sharing Mechanism Fits. Blockchain technology is a distributed shared database technology. All nodes in the network share data and information, and each node stores a complete account book. This method is different from the traditional centralized network structure. The data information in the blockchain network is mutually backed up between different nodes, and the data update and maintenance are completed by multiple nodes in the system. e-Commerce is a new networked economic activity in which suppliers, distributors, customers, e-commerce platforms, third-party payment, logistics companies, and other entities realize resource sharing through information sharing. Blockchain technology and distributed management of e-commerce information resources are both based on the development concept of information sharing, relying on the data network development space to engage in various operations such as data exchange, transfer, and storage. From this, it can be seen that the two have a consistent relationship in the information sharing mechanism, as shown in Figure 1.

3.1.2. Trust Mechanism Fits. The blockchain network has a high degree of trust. Compared with the traditional trust mechanism, its trust is built on technical endorsement, not a centralized credit institution. This mechanism ensures that the data interaction between distributed nodes can be carried out without mutual trust and trust guarantees from central institutions. It can be seen that there is a close relationship between the two in the trust mechanism, as shown in Figure 2.

3.1.3. Coordination Mechanism Fits. The information verification, exchange, update, and maintenance of the blockchain database are completed by the cooperation of distributed nodes. Relying on the network service platform, e-commerce optimizes the cooperative relationship among suppliers, logistics, distributors, customers, financial payment institutions, and the government to ensure the smooth flow of information among various entities. It can be seen that the two have a coherent relationship in the coordination mechanism, as shown in Figure 3.

3.1.4. Security Mechanism Fits. The internal data structure of the blockchain network has the characteristics of security, transparency, nontampering, and traceability. Its distributed redundant storage mode means high data security, which is beneficial to avoid large-scale data loss due to the collapse of the central organization. E-Commerce data security involves website information security, transaction information security, and user information security. The blockchain data security mechanism helps to enhance the construction of an e-commerce information security protection system. It can be seen that the two have a close relationship in the security mechanism, as shown in Figure 4.

3.1.5. Contract Mechanism Fits. The blockchain system has a complete smart contract function. The intelligent contract built into the block can be run in the virtual machine environment of the blockchain after being compiled. Therefore, once an event triggers the execution conditions premade by the state machine, the system will automatically execute the contract. e-Commerce uses smart contracts to replace operating, transaction, and legal terms, which can not only ensure the automatic execution of system rules, but also avoid malicious interference caused by human factors, improve execution efficiency, and reduce resource waste. It

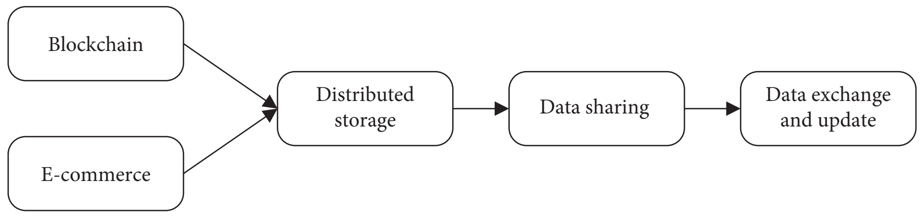

Figure 1: Sharing mechanism fits.

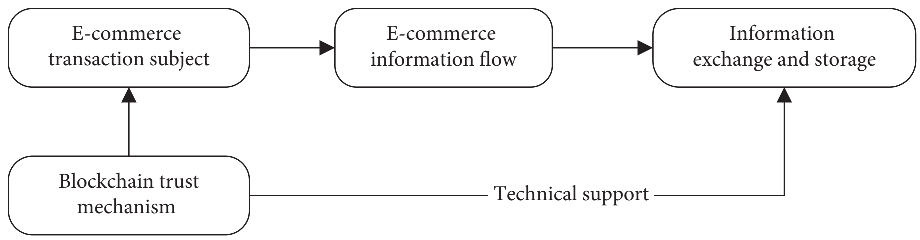

Figure 2: Trust mechanism fits.

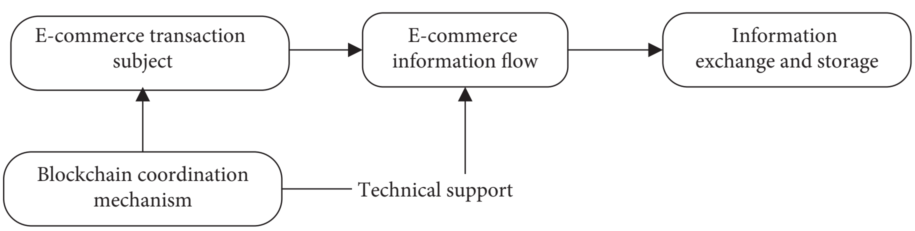

Figure 3: Coordination mechanism fits.

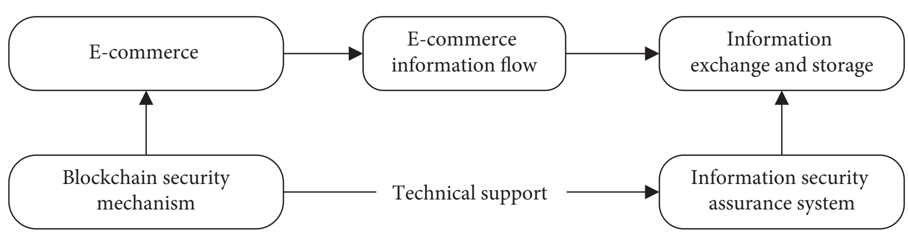

Figure 4: Security mechanism fits.

can be seen that the two have a close relationship in the contract mechanism, as shown in Figure 5.

3.2. E-Commerce Information Ecological Model Based on Blockchain

3.2.1. E-Commerce Information Ecological Chain. In the Internet business environment, the e-commerce information ecological chain is an important content to ensure the high-speed circulation of online business information. It is mainly based on information technology, combined with information sharing and main body collaboration, and in accordance with the actual development of the enterprise itself and its respective functional characteristics, a network structure that maximizes the benefits of the enterprise while obtaining valuable information to achieve gains. E-Commerce information ecological chain is mainly composed of information, information transmitter, information environment, and information technology. Among them, information is the foundation, the information transmitter is the core, the information environment is the medium for information circulation, and information technology is the support for operation, which provides technical guarantee for realizing the high-speed circulation of information and ensuring the information security of e-commerce websites.

Information subjects in the e-commerce information ecological chain play different roles in real life. They are not only information producers, but also information transmitters and consumers. They transform and depend on each other between different roles. In the information flow of the entire ecological chain, the information producer is the starting point (suppliers, merchants), and its main job is to provide information and collect information. In the ecological chain, the information transmitter (certification center, credit agency) is an internal link, and the main work is to transmit and process information, and to process and arrange information. Consumers are the end of the

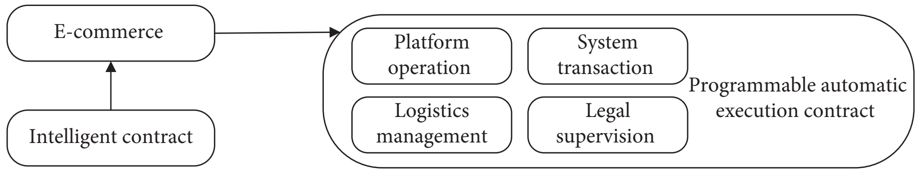

Figure 5: Contract mechanism fits.

information flow of the ecological chain, which mainly include website managers and customers. Information decomposers (government, scientific research institutions) mainly filter and feedback information. In the ecological chain, various subjects will interact and cooperate to achieve healthy competition and mutual benefit and win-win, make the development environment of the ecological chain more harmonious, and maintain the balance of the information ecology to a certain extent.

During the normal operation of the e-commerce information ecological chain, the main body will not only exchange certain information, but also maintain communication with the external environment, realize information exchange and energy exchange, and will also be affected by the ecological environment and the information environment. Therefore, it is necessary to continuously coordinate the various internal elements to achieve coordinated development and allow them to form a relatively stable self-regulation mechanism.

According to the decentralized characteristics of the blockchain, the blockchain is used as the lowest technology in the e-commerce ecological chain. It can be known that the main basic models are divided into data layer, virtual network layer, core consensus layer, value incentive layer, intelligent contract layer, and real-world applications. Among them, the data layer includes network and chain structures such as information flow and logistics, as well as technologies such as time stamps. Connect the blocks in the corresponding chronological order to form the main chain. Through the use of timestamps, encryption technology, the goals of data security, and traceability can be achieved. Designing P2P networking methods, verification protocols, and related verification mechanisms in the virtual network layer can make the status of each information block equal and form a flat topology structure, so that the connection between blocks can be realized without hindrance when a new block is formed, the whole network broadcast method can be used to enable each node to undertake the corresponding obligations of spreading and verifying the new block. The decentralized structure makes the degree of information sharing between information subjects continue to increase, so that the flow of information, logistics, and capital will not be interrupted due to the damage of some nodes, and the value of information has been increased. With the help of platform sharing in the block, the final ecological value stream can be formed. The blockchain-based e-commerce information ecological chain is shown in Figure 6.

3.2.2. E-Commerce Information Ecosystem. The dynamic interactive relationship between information subjects and the information environment, using information as a link, is called the e-commerce information ecosystem. In this type of ecosystem, it mainly focuses on e-commerce companies, sellers, customers, and other information subjects to carry out related e-commerce activities. The information ecosystem is divided into five levels: core, technology, media, extension, and periphery.

In the e-commerce information ecosystem, the core layer includes e-commerce companies, sellers, and customers. The technical layer includes blockchain-based seller-customer interaction software, product recommendation system, and online evaluation system. The media layer includes third-party payment, logistics companies, advertising companies, search websites, and other service providers. The extension layer includes government, scientific research, and educational institutions. The outer layer includes political, social, cultural, legal, economic, and other environments. The e-commerce information ecosystem constructed by blockchain technology is shown in Figure 7.

3.2.3. E-Commerce Information Ecosystem Model Based on Blockchain. Based on the abovementioned research on the blockchain-based e-commerce information ecological chain and the blockchain-based e-commerce information ecosystem, this part proposes the theoretical framework of the blockchain-based e-commerce information ecosystem model. It has ecological characteristics such as data sharing, transparency, antitampering, open data platform, consensus and collaboration of various subjects, dynamic intelligent evolution, and value appreciation, which can promote the stable, sustainable, and healthy development of e-commerce information ecosystem. The e-commerce information ecosystem model based on blockchain is shown in Figure 8.

In traditional e-commerce, the supervision of the e-commerce platform population and the complaints of the consumer population are mainly used to ensure the integrity of the business [39]. Consumers in e-commerce under the blockchain can use the product traceability mechanism to detect the validity of the product, generate full trust in the information of the purchased product, and then trust in the merchant and e-commerce platform. This kind of strong endorsement of credit relies on data precipitation. It is a completely different model from traditional e-commerce companies relying on their own reputation and volume to gain consumer trust. What e-commerce merchants under the blockchain need to pay attention to is no longer consumer trust issues, but consumer preferences and product quality, not to mention worrying about the opportunistic behavior of other businesses. The regulatory pressure on e-commerce platforms under the blockchain will be greatly reduced, and the reputation of e-commerce platforms will

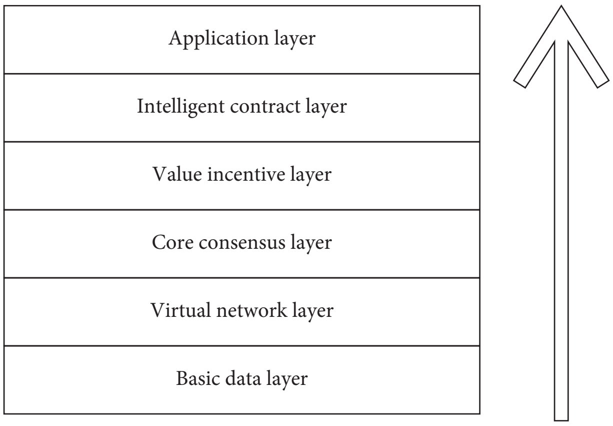

Figure 6: E-Commerce information ecological chain.

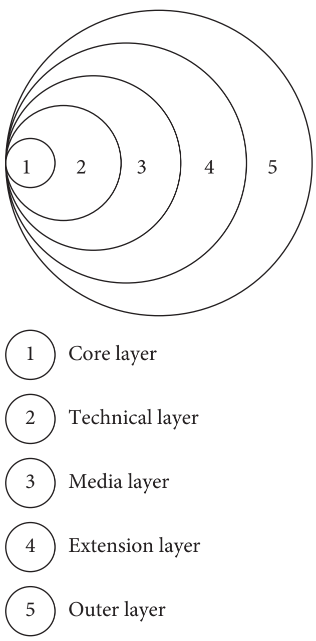

Figure 7: The e-commerce information ecosystem based on blockchain.

increase. Compared with traditional e-commerce, the amount of data storage can be significantly reduced, and the cost of data maintenance will also be reduced, which can reduce the e-commerce of the entry barrier of the platform and the improvement of the operating efficiency of the e-commerce platform. The current monopoly of e-commerce platforms under the blockchain will be broken. The e-commerce market is highly dynamic, consumers are less sticky, merchant transfer costs are gradually reduced, and platform market share is unstable [40].

The relative advantages of traditional e-commerce platforms under the blockchain have been greatly reduced, and the lowering of the barriers to entry will lead to more emerging e-commerce platforms joining the e-commerce ecosystem. Consumers have more diversified platform choices and traditional e-commerce platforms. Business platforms may face more challenges from emerging

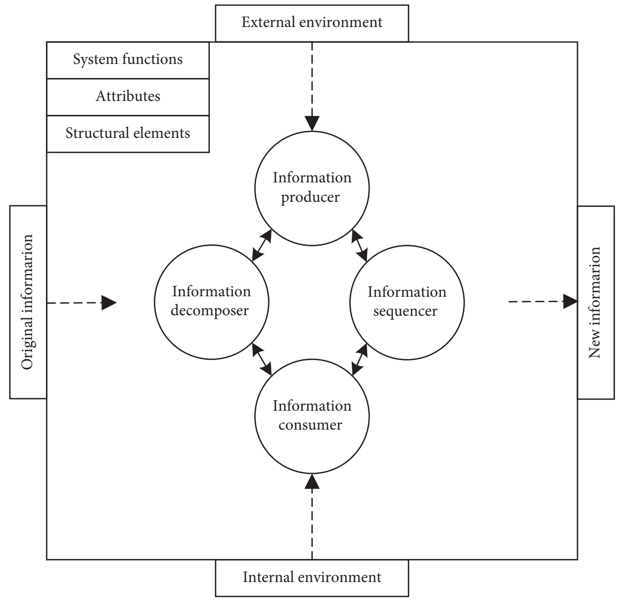

Figure 8: The e-commerce information ecosystem model based on blockchain.

e-commerce platforms. Traditional e-commerce platforms that refuse to use new technologies based on vested interests will be gradually eliminated. The challenges of new platforms will also inject more vitality into the e-commerce ecosystem and eventually form a model of multiplatform coexistence and healthy competition.

4. Evolution Path for E-Commerce Ecosystem under Blockchain

Through the comparative analysis of the e-commerce ecology combined with the blockchain technology and the traditional e-commerce ecology, in order to make better use of the technological advantages of the blockchain to develop e-commerce and solve the problems in the traditional e-commerce ecology, the blockchain is proposed. There are three evolutionary paths of e-commerce ecology, which are discussed next.

4.1. Construct Full-Process Information Channel. The asymmetry of information among various subjects is the main problem that affects the ecological balance of e-commerce. To promote the further development of the e-commerce ecosystem, it is necessary to ensure that the internal information of the system is open, transparent, and effective. In the case of using blockchain technology to build an information system, distributed storage technology reduces the amount of consumer information storage for e-commerce companies and reduces corporate consumption costs. The data on the blockchain is jointly participated and shared by all accounting nodes. Maintenance, transparent and open to all parties, data recording, and storage no longer rely solely on the central node, and all business participants in the transaction can participate in decision-making, master their own data, ensure consumer information security, and avoid consumer information being compromised. The commodity information on the e-commerce platform can be encrypted by cryptography on the chain. The hash algorithm makes it very difficult to tamper with the information, and the data changes can be quickly identified through the Merkle tree structure, so it can effectively prevent the tampering of the information on the chain. At the same time, distributed storage and consensus algorithms can ensure that the modification of a single point is invalid. Only more than half of the computing power can modify the information on the chain. All information on the chain will be time stamped, and every information change will be recorded. In this case, the information on the chain can be traced to the source, which solves the problem of information asymmetry in the e-commerce ecosystem.

Each node on the blockchain is peer-to-peer and can directly interact. A node can interact with multiple nodes at the same time. Overcome the shortcomings of traditional electronic data transmission, and realize the efficient collaboration of business participants on the blockchain. The information communication system includes suppliers, connects consumers and suppliers, and realizes the communication of commodity information. Consumers can interact with enterprises through the network platform, participate in the product design, production and consumption of enterprises, and customize personalized products. The role of consumers is gradually transformed into a cocreator of value, which is conducive to satisfying consumer needs and improving consumer loyalty [41]. Make full use of the traceability and nontampering characteristics of blockchain data to ensure the authenticity and effectiveness of the communication information, ensure the symmetry of the information between the two parties, and combine the omni-channel information communication system to strengthen the trust and understanding of all parties in the e-commerce ecosystem. Lay the foundation for further in-depth cooperation.

4.2. Build Safe and Efficient Block Payment. The reason why the payment link of traditional e-commerce requires a third-party payment company to transfer is because both parties to the transaction need a third-party institution to endorse the transaction to solve the problem of mutual trust in the transaction. The e-commerce ecology embedded in the blockchain can ensure the authenticity, effectiveness, and traceability of information, transforming from the past information transmission to value transmission, and from the original information Internet to the value Internet.

In this case, the information on the blockchain can be deposited as a strong credit endorsement; instead of relying on traditional third-party institutions, the central node of transactions can be removed and the existing credit system can be reconstructed. In the transaction link of e-commerce, it is based on the consensus mechanism to ensure that all parties to the transaction confirm the transaction information, and the transaction funds pass the third-party payment company to circulate directly among the transaction subjects, and it can solve the cumbersome payment process, high management costs, and funds in the existing e-commerce backlogs, and other issues have improved the efficiency of the use of funds in the e-commerce ecosystem. Use the strong credit endorsement formed by the precipitation of e-commerce data under the blockchain to improve the construction of the e-commerce credit system, and rely on the historical transaction information of e-commerce enterprises to conduct credit ratings for enterprises and the e-commerce platform to jointly finance corporate banks and other financial institutions. Use the blockchain to build the core of financial supervision tools, carry out deposit certificates and risk monitoring of financial information, and achieve controllable risks in supply chain finance.

Through blockchain transaction accounting and distributed ledger, the problem of reconciliation and settlement costs between financial institutions is solved, combined with digital currency to achieve real-time settlement and improve the operational efficiency of financial institutions. Combining currency and blockchain technology, using blockchain as the underlying technology, realizes the directional circulation, transaction, and settlement of currency, controls the entire life cycle of the currency, and ensures the reasonable and legal use of funds. Embedded in the blockchain, the authenticity and traceability of information transforms the e-commerce information flow into a value stream, and the data are deposited as a strong endorsement of credit, reconstruct the credit system of the e-commerce ecosystem, and realize the financing of funds without the central node.

4.3. Create Efficient and Transparent Intelligent Logistics. Combining the blockchain technology with the Internet of Things, the blockchain does not need to set up a central server, which can avoid expensive operation and maintenance costs, and reduce the use cost of logistics enterprises to apply Internet of Things technology to the logistics field. The cryptographic algorithm and consensus mechanism of the blockchain itself can prevent malicious nodes from accessing the Internet of Things, lower the barriers to entry, and incorporate more logistics products into the chain management. The data on the blockchain are a kind of chain-type data. The logistics information of the goods can be all on the chain, which can realize the accurate traceability of the origin of the goods, the storage of the goods, and the real-time disclosure of the transportation routes. The logistics information is completely transparent to logistics stakeholders and can be integrated in the logistics supply chain, break the status of information islands in the logistics operation process, promote the horizontal flow of logistics information and multiparty collaboration, achieve the purpose of information sharing and in-depth cooperation between all parties in the logistics supply chain, improve logistics efficiency, and integrate areas; the blockchain has become a new breakthrough in the upgrading and transformation of the logistics supply chain. Combining blockchain technology with big data and cloud computing, the distributed storage of blockchain increases the analyzable data of logistics enterprises. The filtering and screening of big data improves the availability of data, and cloud computing improves logistics enterprises' data processing capability and intelligent operation level, which will eventually build a transparent and efficient intelligent logistics system.

5. Conclusions

This work takes the e-commerce ecosystem as the research object and uses synergetics in evolutionary economics to analyze the interaction between various groups in the e-commerce ecosystem and within the core population. Mainly relying on the three main lines of information flow, logistics, and capital flow, the internal mechanism of the e-commerce ecosystem was excavated, and the imbalance and instability in the e-commerce ecosystem were discovered, and the problems that affected the further development of e-commerce were addressed. The technical characteristics of the blockchain propose three evolution paths of the e-commerce ecosystem to promote the further development of e-commerce. This work mainly analyzes and studies the impact of blockchain technology on the e-commerce ecosystem, but the blockchain technology itself is not yet fully mature, and some problems need to be overcome in the application. All records reached by traditional consensus require more than half of the amount of calculation to be recognized. This requires a lot of time, which affects the performance and efficiency of the blockchain. The full storage of all nodes ensures the validity of the data, but also leads to the problem of large amount of data storage and fast increase of calculation amount. The decision-making of multiple parties to participate in the transaction ensures the security of the transaction and also creates the problem of blockchain congestion. Different blockchains cannot achieve cross-chain collaboration due to different protocols. These problems have a great impact on the application of blockchain technology and require in-depth research by scientific researchers to find suitable solutions.

Data Availability

The datasets used are available from the corresponding author on reasonable request.

Conflicts of Interest

The authors declare that they have no conflicts of interest.

References

[1] S. Zheng and Q. Lv, "The evolution of E-commerce in twenty years in China," *Journal of Business Economics*, vol. 11, no. 265, pp. 5–16, 2013.

[2] S. Piggott, "Internet commerce and knowledge management–the next megatrends," *Business Information Review*, vol. 14, no. 4, pp. 169–172, 1997.

[3] P. Levikangas and R. Rni, "From business models to value networks and business ecosystems–what does it mean for the economics and governance of the transport system?" *Utilities Policy*, vol. 64, 2020.

[4] M. Meyer, J. Utterback, and M. James, "The product family and the dynamics of core capability," *MIT Sloan Management Review*, vol. 34, pp. 77–92, 1992.

[5] V. S. Veenstra, J. I. M. Halman, and J. T. Voordijk, "A methodology for developing product platforms in the specific setting of the housebuilding industry," *Research in Engineering Design*, vol. 17, no. 3, pp. 157–173, 2006.

[6] J. Pei, "Solving the problem of charging and discharging of electric vehicles based on particle swarm algorithm," in *Proceedings of the International Conference on Information Systems and Computer Aided Education*, pp. 534–538, Dalian, China, September 2019.

[7] J. Liu, C. Sun, and Y. Yuan, "Blockchain hotspot field and frontier path in China: based on CiteSpace measurement analysis," *Journal of Chongqing University of Posts and Telecommunications*, vol. 32, no. 6, pp. 121–129, 2020.

[8] J.-C. Rochet and J. Tirole, "Platform competition in two-sided markets," *Journal of the European Economic Association*, vol. 1, no. 4, pp. 990–1029, 2003.

[9] S. Muegge, "Business ecosystems as institutions of participation: a systems perspective on community-developed platforms," *Technology Innovation Management Review*, vol. 27, no. 4, 2011.

[10] L. Metso and M. Kans, "An ecosystem perspective on asset management information," *Management Systems in Production Engineering*, vol. 25, no. 3, 2017.

[11] J. Pei, "Big data mining in the control of epidemic," *Basic and Clinical Pharmacology and Toxicology*, vol. 126, pp. 428–430, 2020.

[12] R. Normann and R. Ramirez, "From value chain to value constellation: designing interactive strategy," *Harvard Business Review*, vol. 7, no. 4, pp. 65–77, 1993.

[13] J. F. Moore, "Predators and prey: a new ecology of competition," *Harvard Business Review*, vol. 71, no. 3, pp. 75–86, 1993.

[14] J. Sviokla, "Expert systems and their impact on the firm: the effects of planpower use on the information-processing capacity of the financial collaborative," in *Proceedings of the Twenty-Second Annual Hawaii International Conference on System Sciences*, Kailua-Kona, HI, USA, January 1989.

[15] E. Gummesson and C. Mele, "Marketing as value Co-creation through network interaction and resource integration," *Journal of Business Market Management*, vol. 4, no. 4, pp. 181–198, 2010.

[16] N. S. P. Tay and R. F. Lusch, "A preliminary test of hunt's general theory of competition: using artificial adaptive agents to study complex and ill-defined environments," *Journal of Business Research*, vol. 58, no. 9, pp. 1155–1168, 2005.

[17] H. Zhang and Z. Xu, "Research on the structure and evolution of cross-border E-commerce ecosystem based on the perspective of symbiosis," *Journal of Social Sciences*, vol. 19, no. 928, pp. 44–46, 2020.

[18] J. Pei, J. Li, and B. Zhou, "A recommendation algorithm about choosing travel means for urban residents in intelligent traffic system," in *Proceedings of the IEEE Advanced Information Technology, Electronic and Automation Control Conference*, pp. 2553–2556, Chongqing, China, March 2021.

[19] A. Gawer and M. Cusumano, *How Companies Become Platform Leaders*, MIT Sloan Management Review, Cambridge, UK, 2008.

[20] S. Mei and J. Xu, “Research on collaborative B2B E-business model and value creation,” *Journal of Management Science in China*, vol. 16, no. 5, pp. 55–68, 2013.
[21] X. Wang, *Research on the Internal Coordination Mechanism of E-Commerce Ecosystem Based on Evolutionary Game*, Tianjin University of Science and Technology, Tianjin, China, 2019.
[22] Y. Zhang, “Blockchain to lead to new changes in E-commerce,” *Contemporary Economic Management*, vol. 39, no. 10, 2017.
[23] A. Bilgihan and Y. Gen, “Customer loyalty in online shopping: an integrated model of trust, user experience and branding,” *Computers in Human Behavior*, vol. 61, pp. 103–113, 2016.
[24] W. Yu, Z. Ding, L. Liu, X. Wang, and R. D. Crossley, “Petri net-based methods for analyzing structural security in E-commerce business processes,” *Future Generation Computer Systems*, vol. 109, pp. 611–620, 2020.
[25] H. Min, “Blockchain technology for enhancing supply chain resilience,” *Business Horizons*, vol. 62, no. 1, pp. 35–45, 2019.
[26] J. Robert, S. Kubler, and S. Ghatpande, “Enhanced lightning network (off-chain)-based micropayment in IoT ecosystems,” *Future Generation Computer Systems*, vol. 112, pp. 283–296, 2020.
[27] J. Angelis and E. Ribeiro da Silva, “Blockchain adoption: a value driver perspective,” *Business Horizons*, vol. 62, no. 3, pp. 307–314, 2019.
[28] R. Dennis and G. Owenson, “Rep on the roll: a peer to peer reputation system based on a rolling blockchain,” *International Journal of Digital Society*, vol. 7, no. 1, pp. 1123–1134, 2016.
[29] A. Schaub, R. Bazin, O. Hasan, and L. Brunie, “A t privacy-preserving reputation system,” in *Proceedings of the IFIP International Conference on ICT Systems Security and Privacy Protection*, pp. 398–411, Ghent, Belgium, May 2016.
[30] S. Wang, “Research on blockchain of legal tender system,” *Economist*, vol. 0, no. 9, pp. 77–85, 2016.
[31] B. Zhang, “The application of foreign blockchain technology and related enlightenment,” *Financial Technology Time*, vol. 24, no. 5, pp. 35–38, 2016.
[32] Q. Li and X. Zhang, “Blockchain: a technology to win open and trust in education,” *The Journal of Distance Education*, vol. 35, no. 1, pp. 36–44, 2017.
[33] N. Zhang, Y. Wang, C. Kang, J. Cheng, and D. He, “Blockchain technique in the energy Internet: preliminary research framework and typical applications,” *Proceedings of the CSEE*, vol. 36, no. 15, pp. 4011–4022, 2016.
[34] M. Dan, “Analysis of blockchain technology’s reconstruction of E-commerce ecosystem,” *Chinese Commerce*, vol. 14, pp. 26-27, 2020.
[35] T. Zhang and B. Li, “Analysis of the value-added tax collection of E-commerce model under the background of blockchain,” *Chinese Commerce*, vol. 14, pp. 28-29, 2020.
[36] Y. Chen, *Research on Enterprise Credit Information Sharing Model Based on Blockchain Technology*, Zhejiang University of Finance & Economics, Hangzhou, China, 2019.
[37] J. Liu, *Research on Cooperative Evolution of Cross-Border E-Commerce Ecosystem*, Changchun University of Technology, Changchun, China, 2018.
[38] L. Zhang, Z. Li, and J. Wang, “User perception model of E-business ecosystem,” *Information Science*, vol. 38, no. 8, 2020.
[39] L. Zhang, X. Wang, and J. Li, “Dynamic evolutionary game of credit mechanism among core populations in E-commerce ecosystem,” *Operations Research Management Science*, vol. 29, no. 4, pp. 93–101, 2020.
[40] T. Wu and Z. Zhao, “Anti-monopoly law on the “choose one from two” action of E-commerce platform: on the insufficient application of the theory of abuse of superior bargaining position,” *Journal of Chongqing University of Posts and Telecommunications*, vol. 32, no. 6, pp. 59–68, 2020.
[41] H. Guo, “Internet enterprise data identification antitrust legal supervision regulation,” *Journal of Chongqing University of Posts and Telecommunications*, vol. 31, no. 2, pp. 37–46, 2019.

Hindawi
Scientific Programming
Volume 2023, Article ID 9861963, 1 page
https://doi.org/10.1155/2023/9861963

Retraction

Retracted: Construction of Innovation and Entrepreneurship Platform Based on Deep Learning Algorithm

Scientific Programming

Received 1 August 2023; Accepted 1 August 2023; Published 2 August 2023

This article has been retracted by Hindawi following an investigation undertaken by the publisher [1]. This investigation has uncovered evidence of one or more of the following indicators of systematic manipulation of the publication process:

(1) Discrepancies in scope
(2) Discrepancies in the description of the research reported
(3) Discrepancies between the availability of data and the research described
(4) Inappropriate citations
(5) Incoherent, meaningless and/or irrelevant content included in the article
(6) Peer-review manipulation

The presence of these indicators undermines our confidence in the integrity of the article's content and we cannot, therefore, vouch for its reliability. Please note that this notice is intended solely to alert readers that the content of this article is unreliable. We have not investigated whether authors were aware of or involved in the systematic manipulation of the publication process.

Wiley and Hindawi regrets that the usual quality checks did not identify these issues before publication and have since put additional measures in place to safeguard research integrity.

We wish to credit our own Research Integrity and Research Publishing teams and anonymous and named external researchers and research integrity experts for contributing to this investigation.

The corresponding author, as the representative of all authors, has been given the opportunity to register their agreement or disagreement to this retraction. We have kept a record of any response received.

References

[1] J. Li and Y. Zhao, "Construction of Innovation and Entrepreneurship Platform Based on Deep Learning Algorithm," *Scientific Programming*, vol. 2021, Article ID 1833979, 7 pages, 2021.

Hindawi
Scientific Programming
Volume 2021, Article ID 1833979, 7 pages
https://doi.org/10.1155/2021/1833979

Research Article

Construction of Innovation and Entrepreneurship Platform Based on Deep Learning Algorithm

Jian Li[1] and Yongyan Zhao[2]

[1]*The Center for Innovation and Entrepreneurship of Colleges Students, Harbin University, Harbin 150086, Heilongjiang, China*
[2]*College of Humanities and Law, Harbin University, Harbin 150086, Heilongjiang, China*

Correspondence should be addressed to Yongyan Zhao; zhaoyongyan@hrbu.edu.cn

Received 19 October 2021; Revised 14 November 2021; Accepted 27 November 2021; Published 9 December 2021

Academic Editor: Le Sun

As the national economy has entered a stage of rapid development, the national economy and social development have also ushered in the "14th Five-Year Plan," and the country has also issued support policies to encourage and guide college students to start their own businesses. Therefore, the establishment of an innovation and entrepreneurship platform has a significant impact on China's economy. This gives college students great support and help in starting a business. The theory of deep learning algorithms originated from the development of artificial neural networks and is another important field of machine learning. As the computing power of computers has been greatly improved, especially the computing power of GPU can quickly train deep neural networks, deep learning algorithms have become an important research direction. The deep learning algorithm is a nonlinear network structure and a standard modeling method in the field of machine learning. After modeling various templates, they can be identified and implemented. This article uses a combination of theoretical research and empirical research, based on the views and research content of some scholars in recent years, and introduces the basic framework and research content of this article. Then, deep learning algorithms are used to analyze the experimental data. Data analysis is performed, and relevant concepts of deep learning algorithms are combined. This article focuses on exploring the construction of an IAE (innovation and entrepreneurship) education platform and making full use of the role of deep learning algorithms to realize the construction of innovation and entrepreneurship platforms. Traditional methods need to extract features through manual design, then perform feature classification, and finally realize the function of recognition. The deep learning algorithm has strong data image processing capabilities and can quickly process large-scale data. Research data show that 49.5% of college students and 35.2% of undergraduates expressed their interest in entrepreneurship. Entrepreneurship is a good choice to relieve employment pressure.

1. Introduction

IAE education, as a new international education concept and model trend, has attracted the attention of countries all over the world and has gradually become an important content of modern education, especially higher education. Innovation is the source of entrepreneurship and the essence of entrepreneurship. Entrepreneurs need to have a consistent and strong spirit of innovation in the business process to produce creative ideas or designs. The value of innovation lies in transforming potential knowledge, technology, and market opportunities into real productivity, realizing the development of social wealth, and benefiting mankind. Therefore, it is of great significance to actively promote the development of IAE education in our country's colleges and universities, and it is also the general trend. This article aims to use deep learning algorithm technology to help the construction of innovation and entrepreneurship platforms and provide a feasible solution.

In recent years, many researchers have conducted research on this and have achieved good results in exploring the structure and realization of the IAE education platform. For example, Phillips believed that entrepreneurship education and entrepreneurship education do not last long, and the teaching platform of business education is not perfect. Without the support of a scientific teaching platform, it is impossible to achieve the expected teaching goals. A scientific teaching platform not only needs platformatic theory as a support but also must play a role in practice [1]. Li *L* believed that Chinese research on student business education has not yet entered a real stage. The vast majority of scholars have conducted a series of investigations on their field of experience in combination with entrepreneurship education. There are no recognized hot spots in the academic world and in various research directions [2]. At present, there are many research studies on the construction and realization of the IAE education platform. These predecessors' theories and experimental results provide a theoretical basis for the research of this article.

This article explains the relevant theories and characteristics of the education platform under the deep learning algorithm through the analysis of the IAE education platform. The deep learning algorithm is derived from the research of artificial neural networks. The artificial neural network evaluation model is based on self-learning, self-adaptive ability, and powerful neural network fault tolerance, to create a comprehensive evaluation model that is closer to the combination of qualitative and quantitative standards of human thinking. This article uses the deep learning algorithm model and scoring platform to rationally evaluate the construction and implementation of the IAE education platform in colleges and universities.

2. Deep Learning Algorithm-Related Technologies and Theories

2.1. Deep Learning Algorithm-Related Technologies. The operation of the innovation and entrepreneurship education platform requires different theoretical foundations at different stages, as well as the support of a large number of key technologies [3]. In recent years, the rapid development of the deep learning algorithm has significantly expanded its scope in natural language processing technology and has also made it possible to create more complex applications.

2.1.1. Deep Neural Network. The basic deep neural network usually consists of three parts: input layer, hidden layer, and output layer. Generally speaking, the first layer is the input layer, the last layer is the output layer, and the number of layers in the middle is all hidden layers. These layers are fully connected; that is, every neuron in the ith layer must be connected to any neuron in the $i+$th layer. The linear relationship between the output and the input is learnt, and the intermediate result of the output is obtained. For linearly separable data sets, a simple linear classifier can usually be used to solve the classification problem. However, data in real life are usually not linearly separable. For this situation, there are generally two methods: introducing nonlinear functions and linear transformations. The nonlinear function here is the activation function [4, 5], usually sigmoid, tanh, ReLu, and so on. If you want to train a DNN, it usually combines exercise optimizers.

2.1.2. Tensorflow. Google is not only a leader in big data and cloud computing but also has good practice and accumulation in machine learning and deep learning algorithm. At the end of 2015, Google opened the TensorFlow deep learning algorithm framework [6, 7]. Compared with frameworks such as Caffe, Theano, Torch, and MXNet, TensorFlow has the most Forks and Stars on Github. It is also used for graph sorting, audio editing, recommendation platforms, physical language, and other scene editing. For the innovation and entrepreneurship education platform, its main goal is to provide accurate answers to users' questions in this field. Therefore, information retrieval has become the main method used by many specific question answering platforms. The similarity between the question submitted by the user and all the candidate questions in the Q&A library is calculated, and finally the answer corresponding to the question with the greatest similarity is selected. And the feedback result is matched according to the similarity between the question submitted by the user and the information database.

2.2. Deep Learning Algorithm-Related Theories

2.2.1. Word Frequency-Document Inverse Frequency. TF-IDF is used to evaluate the meaning of words in a set of documents or a document in the main text and is often used in information retrieval and data mining. After a certain transformation, it can be used to calculate the similarity between sentences. Among them, TF refers to the word frequency; that is, the number of times a word appears in the document; IDF is the reverse frequency of the document. The main idea of TF is that if a word appears more often in one text, but rarely appears in other texts, it can be considered that the word has a good resolution [8, 9]. The main idea of IDF is that if the number of documents containing a word is less, it means that the word has a good sorting ability, and the IDF value will be higher. The numerator represents the number of times a word appears in the file, and the denominator represents the sum of the number of times all words appear in the file.

2.2.2. Levinstein Distance. Levenshtein distance refers to the minimum number of processing operations required to convert one string to another and is usually used to compare the similarity of two strings. It mainly refers to the minimum number of processing functions required to convert two strings from one string to another. If more times are required, the similarity is lower [9, 10]. The basic steps of the algorithm are as follows:

(1) A table is initialized with the number of rows $m+1$ and the number of columns $n+1$, which is used to store the number of functions required to complete a processing operation and convert the string s1 [1, ..., n] into characters [1, ..., m]. The number of functions required is the value of the table [n] [m].

(2) The first row of the matrix is set to 0 in n, and the first column is set to 0 in m. Table [0][j] represents the value of the j-1th column in the first row. This value represents that it takes n processing operations to convert the string s1[1, ..., 0] to s2[1, ..., j]. Obviously, to convert an empty string to a string of length j, only the input operation j is required, so the value of table [0][j] must be j, and the values in other places can be deduced by analogy.

(3) Each character of string s1 and string t2 is compared in pairs; if they are equal, set temp = 0; if they are not equal, set temp = 1.

(4) If we can convert s1[1, ..., $i-1$] to s2[1, ..., j] in step k, then the total number of operations we need to perform is $k+1$; if we can convert s1 [1, ..., $i-1$] to s2 [1, ..., j] in step k operation, convert s1 [1, ..., i] into 8 in s2 [1, ..., $j-1$], that is, matrix [i, $j-1$] = k, then we can add s2[j] to s1[1, ..., i], so a total of $k+1$ functions are needed; if we can convert s1[1, . . ., $i-1$] to s2[1, . . ., $J-1$]] in k operations, then we can convert s1 [i] to s2 [j], which satisfies s1 [1, ..., i] = = $s2$ [1,...,j]; here, in total, the function k + temp is required (because if s1 [i] = = $s2$ [j], no processing is required; if it is different, just add the calculated temperature value directly). The final value of the table [i, j] is the minimum matrix [i, $j-1$] + 1, matrix [$i-1$, j] + 1, and matrix [$i-1$, $j-1$] + temp.

(5) Steps (3) and (4) are repeated; the final matrix value [n, m] is the minimum processing distance. Once the minimum processing distance is found, the similarity can be calculated.

3. Research on Experimental Preparation of IAE Platform

3.1. Experimental Method. With the rise of the deep learning algorithm wave, in practical applications, the deep learning algorithm technology is more suitable for IAE education platform. Compared with the usual shallow neural network, the deep neural network used in the deep learning algorithm has many hidden layers in addition to an input layer and an output layer. Each layer is composed of many neurons. The input of the input layer is the external input of the neural network, the input of the output layer and the hidden layer is the input of the previous layer of neurons, and the output of the output layer is the output of the neural network.

(1) Sigmoid function:

$$\sigma(z) = \frac{1}{1+e^{-z}}. \tag{1}$$

(2) The mathematical expression of neuron $a_{i,j}$ is as follows:

$$a_{i,j} = \sigma\left(\sum_k w_{ijk} a_{i-1k} + b_{ij}\right). \tag{2}$$

Suppose the neural network has a total of I layer, the jth neuron of the ith layer is a_{ij}, the bias of this neuron is b_{ij}, the distance from the jth neuron of the i layer to the kth neuron of the −1 the weight is W_{ijk}, and σ is the activation function. The function of the activation function is to make nonlinear changes in the input of the neuron. e^{-z} is an exponential function. In the definition expression of the exponential function, the coefficient before e^{-z} must be the number 1, and the independent variable is −z.

3.2. Experimental Data Collection. This paper establishes a neural network model under the deep learning algorithm to achieve balanced results. In order to understand the status quo of college students' IAE education, this paper conducts investigations in the form of in-depth interviews and questionnaires. "Awareness of IAE Education," "Courses of IAE Education," "IAE Education Teaching Staff," "Methods and Models of IAE Education," and "Support and Guarantee of IAE Education" are selected to conduct surveys. The purpose of the survey is to fully understand the innovation and entrepreneurship education of college students and the existing problems.

4. Research on Experimental Preparation for IAE Platform

4.1. Distribution of Entrepreneurial Interest under Different Educational Backgrounds. The main subjects of this study are undergraduates, and a small number of junior college students and graduate students also participated in the survey. The survey collected 558 questionnaires; the details are shown in Table 1. The effective questionnaires describe the basic situation of the respondents, and the samples are relatively representative.

As shown in Figure 1, 49.5% of junior college students and 35.2% of undergraduates said that they are very interested in entrepreneurship. It can be seen that 60% of respondents have entrepreneurial intentions. In further investigation, it is found that junior college students are more interested in entrepreneurship than undergraduates, and undergraduates are more interested in entrepreneurship than graduate students. This is because the academic level of graduate students is higher than that of undergraduates and junior colleges. Professional planning is stronger, but about one-quarter of graduate students are still interested in entrepreneurship. Undergraduate and junior colleges are more competitive in employment. Entrepreneurship is a good choice to alleviate the pressure on employment.

4.2. Analysis on the Evaluation Method of IAE Course. The investigators conducted a survey on the "IAE course assessment method," and the results of the survey are shown in Table 2.

As shown in Figure 2, 282 people's choices indicate that IAE courses are assessed through curriculum design, accounting for 50.54% of the total number. If IAEs are only assessed through courses, the practical experience that students can improve is very limited. More practical activities should be carried out to help students assess

Table 1: Distribution map of entrepreneurial interest for different educational backgrounds (%).

Education	Very interested	More interested	Generally	Not very interested	Not interested
Specialist	49.5	11.3	22.5	10.2	6.5
Undergraduate	35.2	28.4	18.9	7.4	10.1
Postgraduate	25.4	16.6	34.5	12.2	11.3

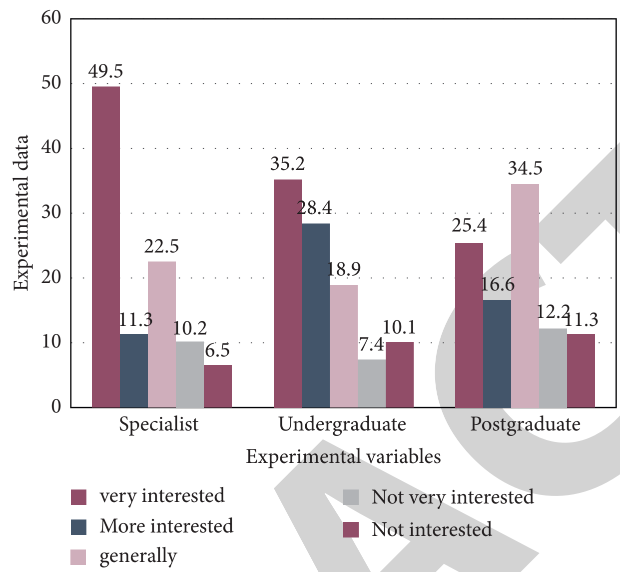

Figure 1: Distribution of interest in entrepreneurship of different educational backgrounds (%).

Table 2: Evaluation methods of IAE courses.

Category	Practical activities	Paper	Course design	Others
Number of people	96	84	282	61
Percentage (%)	17.20	15.54	50.54	10.92

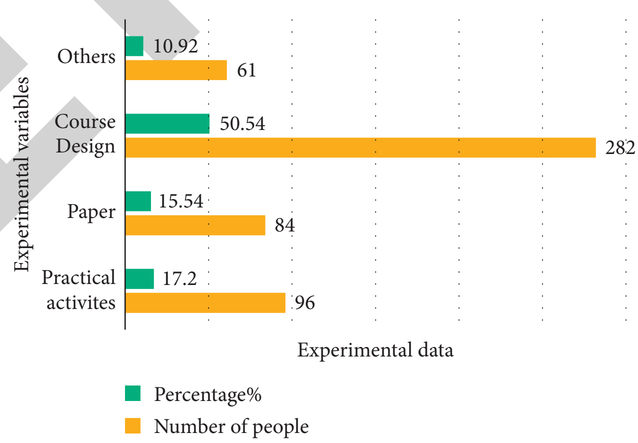

Figure 2: Analysis of the assessment methods of IAE courses.

innovative courses. Only 96 people, 17.2% of students said that innovative and entrepreneurial courses are assessed through practical activities, which is obviously not enough. Thesis design and curriculum design have great limitations in improving the ability of IAE. Through practical activities, students can get started in person, and only when they empathize with each other can they quickly improve.

Table 3: Analysis of IAE teachers (%).

Education	Totally satisfied	Basically satisfied	Barely satisfied	Not satisfied
Specialist	33.6	26.7	28.5	11.2
Undergraduate	21.5	27.1	35.7	15.7
Postgraduate	15.5	25.6	25.3	33.6

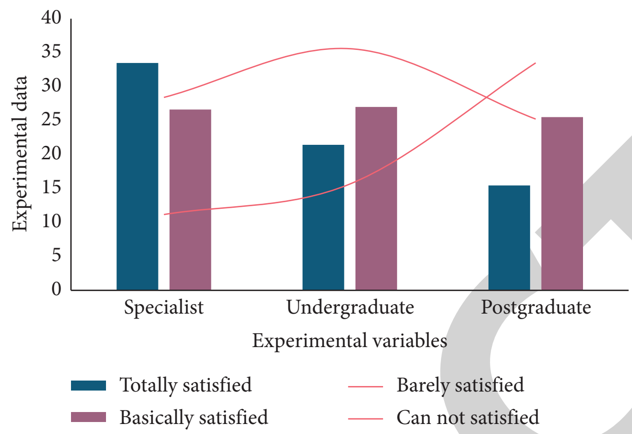

Figure 3: Analysis of IAE teaching staff (%).

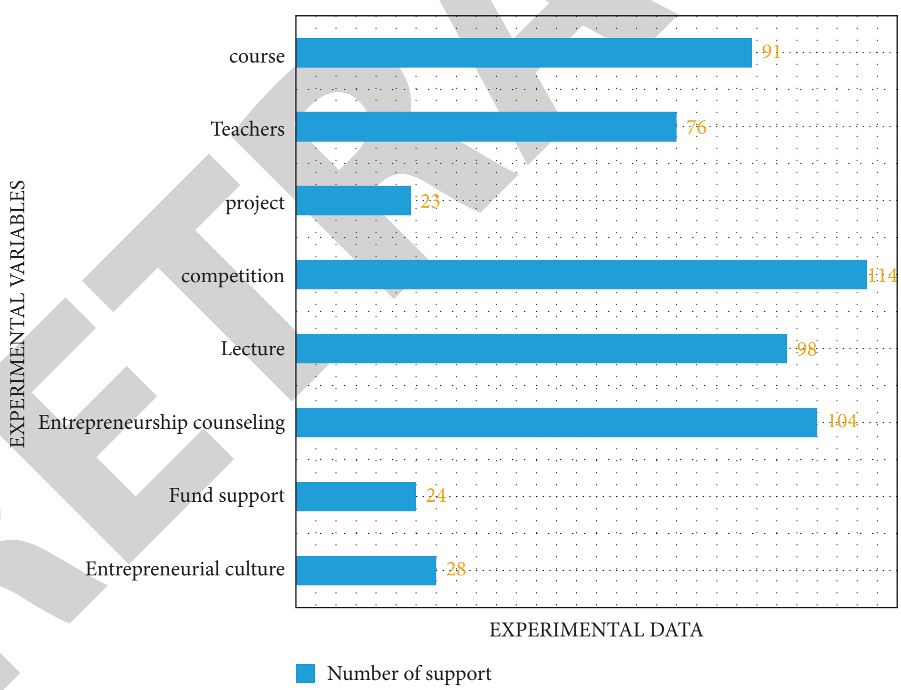

Figure 4: Analysis of support and guarantee of IAE education.

4.3. Analysis of the Faculty Allocation for IAE. An analysis of "IAE Education Teachers' Evaluation" on 558 investigators is conducted, and statistics on four indicators of "fully satisfied," "basically satisfied," "barely satisfied," and "unsatisfied" is conducted. The results are shown in Table 3.

As shown in Figure 3, it can be seen that 33.6% of the surveyors of junior college students are more satisfied with the provision of teachers for IAE education. The reason may be that the junior college is more biased towards practical talent training for students. Among the graduate students, only 15.5 respondents were satisfied with the faculty, and 33.6 respondents were dissatisfied, about 1/3 of them. Analysis of the main reasons for the low satisfaction of graduate students may be based on the following two aspects: one is that there is less IAE education specifically for graduate students and the other is that graduate students have higher requirements for teachers, but in reality, the teachers fail to meet expectations.

4.4. Analysis of Support and Guarantee of IAE Education. In the analysis of the surveyors' support and guarantee for IAE education, 558 surveyors selected the most important factors based on the options that are most satisfied with their help. The analysis results are shown in Figure 4.

As shown in Figure 4, financial support and entrepreneurial atmosphere are the places most dissatisfied with student support. 24 and 28 people chose these two, respectively. A good entrepreneurial atmosphere and financial support are essential. In colleges and universities, a good entrepreneurial atmosphere is very lacking. Many students face heavy test pressure and life pressure, which prevents them from integrating into a good atmosphere. At this time, the school needs to provide students with relevant conditions and provide a certain amount of financial support with entrepreneurs to help them; some entrepreneurs have good business ideas and do not have enough funds to carry out projects, so the school should give sufficient support.

5. Conclusions

According to the deep learning data model, this article analyzes the objects that the entrepreneurial education platform needs to focus on. According to the research results of this article, it is concluded that the IAE education platform must pay attention to practical teaching. The data in this article show that 49.5% of college students and 35.2% of undergraduates expressed their interest in entrepreneurship. Through entrepreneurship, college students can greatly reduce the competitive pressure brought about by employment and also help them find a path that is more suitable for them. Cultivating students' comprehensive quality ability in IAE is the key to IAE education. First of all, it must conform to the student development legislation, proceed step by step, and reflect the levels. Second, IAE training should run through the entire process of IAE training and reflect integrity. The third is that universities should integrate practical resources, win government support, unite enterprises, and create a comprehensive collaborative platform. Colleges and universities should actively carry out IAE competitions, set up expert groups to comment and explain, and answer questions and answers for some problems encountered by entrepreneurs, so as to better improve the comprehensive ability of entrepreneurs. Therefore, it is very meaningful to build a platform for college students' IAE education practice. Only when students participate in practical activities and empathize with each other can they give full play to the significance of practical education. At the same time, the government should give entrepreneurs a certain amount of support to help. They implement their own projects.

Data Availability

The experimental data used to support the findings of this study are available from the corresponding author upon request.

Conflicts of Interest

The authors declare that they have no conflicts of interest to report regarding the present study.

Acknowledgments

This work was supported by the Educational Science Planning "14th Five-Year Plan" Key Project of Heilongjiang Province (No. GJB1421379); the Higher Education Teaching Reform Research Project of Heilongjiang Province (Nos. SJGY20200431 and SJGY20190409); the Educational Science Planning 2020 Key Project of Heilongjiang Province (No. GJB1320178); and the Art Science Planning General Project of Heilongjiang Province (No. 2021B024).

References

[1] J. M. Phillips, "The infinite legal acumen of an artificial mind: how machine learning can permanently capture legal expertise and optimize the law firm pyramid," *The Journal of Business, Entrepreneurship & the Law*, vol. 11, no. 2, 2018.
[2] L. Li, J. Wang, and X. Li, "Efficiency analysis of machine learning intelligent investment based on K-means algorithm," *IEEE Access*, vol. 8, Article ID 147470, 2020.
[3] J. Zhang, T. Tian, S. Wang, X. Liu, X. Shu, and Y. Wang, "Research on an olfactory neural system model and its applications based on deep learning," *Neural Computing & Applications*, vol. 32, no. 26–27, 2020.
[4] M. Shi, "Knowledge graph question and answer system for mechanical intelligent manufacturing based on deep learning," *Mathematical Problems in Engineering*, vol. 2021, Article ID 6627114, 8 pages, 2021.
[5] L. Heping, "Application of wireless network and machine learning algorithm in entrepreneurship education of remote intelligent classroom," *Journal of Intelligent and Fuzzy Systems*, vol. 40, no. 2, pp. 2133–2144, 2021.
[6] X. Zhang and Z. Cao, "A framework of an intelligent education system for higher education based on deep learning," *International Journal of Emerging Technologies in Learning (iJET)*, vol. 16, no. 7, 2021.
[7] M. M. Keinnen and L. M. Kairi, "Researching learning environments and students' innovation competences," *Education and Training*, vol. 61, no. 1, pp. 17–30, 2019.
[8] S. K. Cho and K. Son, "Risk management for open-innovation-based idea realization platform of medical devices," *Journal of the Korean Institute of Industrial Engineers*, vol. 44, no. 6, pp. 464–474, 2018.
[9] S. Kan, D. Chung, and G. Chung, "Customer experience transformation in the aviation industry: business strategy realization through design thinking, innovation management, and HPT," *Performance Improvement*, vol. 58, no. 1, pp. 13–30, 2019.

Hindawi
Scientific Programming
Volume 2021, Article ID 4467001, 14 pages
https://doi.org/10.1155/2021/4467001

Research Article

Analysis of Economic Development Trend in Postepidemic Era Based on Improved Clustering Algorithm

Li Guo, Kunlin Zhu, and Ruijun Duan

Henan University of Technology, Zhengzhou 450000, China

Correspondence should be addressed to Li Guo; guoli82@haut.edu.cn

Received 29 October 2021; Revised 12 November 2021; Accepted 18 November 2021; Published 9 December 2021

Academic Editor: Le Sun

In order to explore the economic development trend in the postepidemic era, this paper improves the traditional clustering algorithm and constructs a postepidemic economic development trend analysis model based on intelligent algorithms. In order to solve the clustering problem of large-scale nonuniform density data sets, this paper proposes an adaptive nonuniform density clustering algorithm based on balanced iterative reduction and uses the algorithm to further cluster the compressed data sets. For large-scale data sets, the clustering results can accurately reflect the class characteristics of the data set as a whole. Moreover, the algorithm greatly improves the time efficiency of clustering. From the research results, we can see that the improved clustering algorithm has a certain effect on the analysis of economic development trends in the postepidemic era and can continue to play a role in subsequent economic analysis.

1. Introduction

After more than 40 years of rapid development of reform and opening up, my country has entered the new economic normal, and the transformation of economic growth mode and supply-side reforms also need to slow down and shift gears. Moreover, due to the global economic downturn and trade frictions, the economic growth rate in recent years has shown a downward trend. In addition, the COVID-19 epidemic, as a global "black swan" event, has had a greater impact on my country's economy and the development of the world economy.

The sudden outbreak of the COVID-19 epidemic in 2020 has inevitably brought countries around the world into a state of stagnation. The current domestic epidemic prevention and control has achieved significant strategic results, but the overall economy has not yet returned to the normal level of previous years. The spread of the epidemic abroad is still continuing, but countries have begun to relax blockade restrictions and gradually restart their economies. This has played a positive role in stabilizing global economic confidence, but at the same time, it has also increased the difficulty of epidemic prevention, aggravated the uncertainty of the world's economic development prospects, and brought severe challenges to the development of my country's open economy.

The influence of the COVID-19 epidemic on our country economy and the economic recovery after the epidemic are the core topics of current scholars' attention. Academia generally believes that, during the SARS period, China is in the rapid development stage of urbanization and globalization, and there is relatively sufficient space for fiscal and monetary tools, so the effect of the SARS on the economy is relatively small [1].

The COVID-19 epidemic has had a huge impact on the Chinese economy and the world economy. This shock overturned the cognition of traditional economics, exposed some shortcomings in the economic structure, provided us with a window to reunderstand the Chinese economy and the world economy, and provided new momentum and ideas for China's economic transformation. In this regard, we need to theoretically summarize and explore the causes and mechanisms of economic recession under the "abnormal" epidemic and the relationship between the "normal economy" and the "abnormal economy." At the same time, we need to deeply explore the deep-seated structural problems and contingency mechanisms of the Chinese economy and the world economy. In addition, it should be recognized that this shock has the characteristics of sudden and temporary nature, and the economic loss it causes is a kind of "sunk" loss, which does not affect the foundation of China's economic development and cannot change the basic pattern of China's economic improvement. The length of the impact depends on the transmission cycle of the epidemic. With the end of the epidemic and the momentum of economic development still returning, China's economy will naturally enter a normal track of development. Moreover, while the epidemic has a negative impact on the economy, it also stimulates some opportunities or positive effects. In this regard, we need to fully understand the negative effect of the epidemic on China's economy and at the same time fully explore opportunities to turn crises into opportunities, passivity into activeness, and passivity into proactiveness so as to win new development momentum, promote the transformation of China's economy into a "disaster-adapted economy," and achieve sustainable and high-quality development of China's economy [2].

The impact caused by SARS is far less than the impact of the new crown. The latter has greater challenges and more and more profound issues worthy of research. At present, the existing research focuses on empirical research and rarely understands the impact of the epidemic and the mechanism of economic recession from the economic theory. In the study of countermeasures, most of them are on the matter, and they have not understood the economic transformation problems under the epidemic disaster from the deep level of economic operation.

At present, the impact of the epidemic on the global economy is still developing and evolving; especially, the unemployment wave caused by the epidemic is becoming a major problem facing all countries. Moreover, with the emergence of the global unemployment problem, residents' consumption willingness and consumption preferences will change. These will further trigger a decline in consumer demand, cause corporate profits to decline, production and operation difficulties, suspension of recruitment plans, and even implementation of layoff plans, and further aggravate the complexity and severity of the employment situation [3].

This paper combines the improved clustering algorithm to analyze the economic development in the postepidemic era and proposes the direction of subsequent economic development.

2. Related Work

Literature [4] puts forward the argument that regional income levels can eventually converge with economic growth under the assumption that the factors are completely liquid. Literature [5] believes that, under the assumption of free flow of production factors and an open economy, as the regional economy grows, the gap between countries or different regions within a country will shrink, and regional economic growth will converge in regional space.

The circular causality theory of literature [6] believes that the role of the market tends to expand the regional difference rather than diminish the regional difference. Once the difference appears, the developed regions will obtain competitive advantages, thereby containing the undeveloped regions, which is not conducive to economic development. Literature [7] believes that the interregional imbalance of growth is inevitable, and the development of the core area will drive the development of the peripheral area to some extent through the trickle-down effect. However, at the same time, the inflow of labor and capital from the periphery to the core area will strengthen the development of the core area, which in turn plays a role in widening the regional gap, and the great effect plays a dominant role.

Literature [8] believes that the regional economic difference is primarily determined by aspects such as the capital investment rate of each region, the growth of employment people, human capital investment, foreign investment, and the location of each region. Literature [9] believes that location factors, macroeconomic schemes, economic structure, urban-rural economic development difference, population quality, and market economy development level are all factors that affect my country's regional economic gap. Literature [10] believes that, at the beginning of the reform, the per capita income, urbanization and industrialization levels in the eastern district, the central district, and the western district are different, which lead to distinct growth rates during the development process and ultimately make the income growth rate of residents in the eastern district faster than that in the central and western districts. In addition, enormous scholars have explained the phenomenon for regional gaps from other aspects. Literature [11] believes that regional economic differences are largely caused by location differences. Literature [12] believes that institutional factors are also the cause of the gap in economic development of regional in my country. After the all-round reform and opening up, the country implemented the eastern guide policy, which led to rapid economic development in the eastern region. Therefore, it believes that such institutional factors are the main reason for the economic development difference between the east district and the west district.

Based on the least square method, literature [13] made a mid- and long-term forecast of Beijing's economic development prospects. Based on the semiparametric regression theory, literature [14] carried out a predictive analysis on the relevant economic indicators of Henan Province and compared it with the prediction error value of the linear autoregressive model. The comparison result shows that the semiparametric autoregressive short-term prediction effect is better.

Literature [15] derived and constructed a homologous gray prediction model with one variable and a first-order equation (written as HGEM (1, 1)) based on the gray system theory to predict the total energy consumption of China's manufacturing industry. The experimental results prove that the gray system model does not require a large number of data samples, and the prediction error is small, which can effectively reflect the true status of the gray system. However, although it can reveal the regularity of sample information, it cannot fully reflect the interference of various unconventional social factors on the predicted objects.

Literature [16] developed and applied artificial neural network (ANN) model with backpropagation learning (BP) algorithm and traditional extreme learning machine (ELM) to predict GDP growth rate. Literature [17] used artificial neural networks to make ecological predictions of the atmospheric state of industrial cities and provided an assessment of the adequacy of the prediction model based on the calculation of the correlation coefficient between the data and the reference data. Literature [18] studied the future economic growth trend based on the BP neural network model. Literature [19] improved the economic forecasting algorithm based on the BP neural network algorithm to improve the forecasting accuracy.

Literature [20] established a combined forecasting model based on the ARIMA model and neural network algorithm to study GDP series. The results show that the accuracy of the ARIMA-NN combined model is greater than that of any single model. Literature [21] studied the weight selection method of the combination model and established a combination prediction model based on the reciprocal residual method, a combination prediction model based on the reciprocal variance method, and a combination prediction model based on the least square method. Moreover, it tested the prediction accuracy of these three combined models based on historical data of national GDP per capita.

3. Textual Representation of Economic Data

In text mining, the text is usually represented by the vector space method; that is, a certain number of representative feature words are regarded as one dimension in the vector space. To study text clustering, we must first establish a mathematical model of the text, so that appropriate methods can be used to quantitatively calculate the similarity between texts. The text representation model is the feature representation of the document. Feature representation refers to the use of some important feature items (words) to represent documents. In the mining algorithm processing, only these feature items need to be processed. This is a process step of converting unstructured data to structured data.

At present, the representative text representation models include the Boolean model and vector space model. These models proceed from different perspectives and use different methods to deal with issues such as feature weighting, category learning, and similarity calculations. The Boolean model can only be used to calculate the relevance of user queries and documents in information retrieval but cannot calculate the deeper similarity between two documents.

The traditional document representation model is the VSM vector space model. The VSM model uses the terms in the document to represent the feature vector of the document, and the term frequency-inverse document frequency is used as the weight. For example, the vector of a document is represented as $V = [w_1, w_2, \cdots, w_n]$, and w_i in the vector V represents the weight of the i-th feature. The weight can be calculated by the TF-IDF algorithm. The main idea of the TF-IDF algorithm is as follows: if the frequency TF of a certain term or phrase in a document is high and the IDF of the term or phrase in other documents is low, then the term or phrase can distinguish the document from other documents.

Term frequency TF_i refers to the frequency of occurrence of term i in a document. The calculation formula of TF_i is as follows [22]:

$$\mathrm{TF}_i = \frac{t_i}{\sum_{j=1}^{n} t_j}. \tag{1}$$

In the formula, t_i represents the term frequency of the i-th feature in the feature vector, and the denominator represents the total term frequency of all features in the feature vector.

Inverse document frequency (IDF) refers to a measure of the universal importance of a term and is the number of documents containing the term i in other documents. The calculation formula of IDF_i is as follows [23]:

$$\mathrm{IDF}_i = \log_2 \frac{N}{n_i}. \tag{2}$$

In the formula, n_i represents the number of documents in which the i-th feature item appears in all document sets, and N represents the number of all documents in the document set. The calculation formula of $\mathrm{TF}_i \times \mathrm{IDF}_i$ is as follows:

$$w_i = \mathrm{TF}_i \times \mathrm{IDF}_i = \frac{t_i * \log_2 N - \log_2 n_i}{\sum_{j=1}^{n} t_j}. \tag{3}$$

The degree of correlation between two documents is often measured by the similarity between them. When the text is expressed as a vector space model $V = [w_1, w_2, \cdots, w_n]$, the similarity between the texts can be expressed by calculating the distance between the vectors. At present, the calculation of similarity between $X = [x_1, x_2, \cdots, x_n]$ and $Y = [y_1, y_2, \cdots, y_n]$ mainly includes cosine similarity $\mathrm{sim}(X, Y)$, Euclidean distance $\mathrm{dist}_{\mathrm{Euchdean}}(X, Y)$, and Pearson correlation coefficient r_{pearson}, as shown in the following:

$$\mathrm{sim}(X,Y)=\frac{X\cdot Y}{|X|\cdot|Y|}=\frac{\sum_{i=1}^{n}(x_i,y_i)}{\sqrt{\sum_{i=1}^{n}x_i^2}\times\sqrt{\sum_{i=1}^{n}y_i^2}},$$

$$\mathrm{dist}_{\mathrm{Euchdean}}(X,Y)=\sqrt{\sum_{i=1}^{n}(x_i,y_i)^2}, \tag{4}$$

$$r_{\mathrm{pearson}}(X,Y)=\frac{n\sum_{i=1}^{n}x_iy_i-\sum_{i=1}^{n}x_i\times\sum_{i=1}^{n}y_i}{\sqrt{n\sum_{i=1}^{n}x_i^2-\left(\sum_{i=1}^{n}x_i\right)^2}\times\sqrt{n\sum_{i=1}^{n}y_i^2-\left(\sum_{i=1}^{n}y_i\right)^2}}.$$

BIRCH algorithm is a multistage clustering algorithm based on clustering feature (CF) and clustering feature tree (CF tree). It can use limited memory resources and *I/O* consumption to complete high-quality clustering of large-scale data sets.

In the vector space, N data points $\{\overrightarrow{X_i}\}, i=1,2,\ldots,N$, of a class are given. The centroid $\overrightarrow{X0}$, radius R, and diameter D of this class are defined as follows [24]:

$$\overrightarrow{X0}=\frac{\left(\sum_{i=1}^{N}\overrightarrow{X_i}\right)}{N},$$

$$R=\left(\frac{\sum_{i=1}^{N}\left(\overrightarrow{X_i}-\overrightarrow{X0}\right)^2}{N}\right)^{1/2}, \tag{5}$$

$$D=\left(\frac{\sum_{i=1}^{N}\sum_{j=1}^{N}\left(\overrightarrow{X_i}-\overrightarrow{X_j}\right)^2}{N(N-1)}\right)^{1/2}.$$

In the formula, R is the average distance between all data points in a class and the center of mass, and D is the average distance between any two points in the class. These two items can reflect the tightness within a class and are usually used in the BIRCH algorithm to determine whether the size of the class meets the limit of the threshold radius T.

If the centroid points $\overrightarrow{X0_1}$ and $\overrightarrow{X0_2}$ of two classes are known, the formulas for the Euclidean distance D_0 and Manhattan distance D_1 of the two centroid points are as follows:

$$D_0=\left(\left(\overrightarrow{X0_1}-\overrightarrow{X0_2}\right)^2\right)^{1/2},$$

$$D_1=\left|\overrightarrow{X0_1}-\overrightarrow{X0_2}\right|=\sum_{i=1}^{d}\left(\overrightarrow{X0_1}-\overrightarrow{X0_2}\right). \tag{6}$$

We are given two classes C_1 and C_2. Among them, the class C_1 contains N_1 data points $\left\{\overrightarrow{X_i}\right\}, i=1,2,\cdots,N_1$. The other class C_2 contains N_2 data points $\left\{\overrightarrow{X_j}\right\}$, $j=N_1+1,N_1+2,\ldots,N_1+N_2$. Then, the calculation method of the distance D_2 between the two classes is as follows:

$$D_2=\left(\frac{\sum_{i=1}^{N_1}\sum_{j=N_1+1}^{N_1+N_2}\left(\overrightarrow{X_i}-\overrightarrow{X_j}\right)^2}{N_1N_2}\right)^{1/2}. \tag{7}$$

In the above formula, D_0, D_1, and D_2 can represent the relationship between the two classes. In the CF tree reconstruction process, these distances can be used to calculate the distance between entries when the CF tree node is split so that the two entries with the farthest distance can be used as the two root entries of the split node and other entries can be classified.

There are two core concepts of CF and CF tree in the BIRCH algorithm. The clustering feature CF represents a class in the form of a triple, as shown in Definition 1.

Definition 1 (clustering feature CF). When N d-dimensional data points $\left\{\overrightarrow{X_i}\right\}, i=1,2,\ldots,N$, of a class are given, the cluster feature CF vector is defined as a triple:

$$\mathrm{CF}=(N,\overrightarrow{\mathrm{LS}},\mathrm{SS}). \tag{8}$$

Among them, N represents the number of data points in this class, and $\overrightarrow{\mathrm{LS}}$ represents the linear sum of N data points in the class; namely,

$$\overrightarrow{\mathrm{LS}}=\left(\sum_{i=1}^{N}\overrightarrow{X_i}\right). \tag{9}$$

SS represents the sum of the variance of N data points in the class; namely,

$$\mathrm{SS}=\left(\sum_{i=1}^{N}\overrightarrow{X_i}^2\right). \tag{10}$$

Theorem 2 (clustering features additive theorem). *If it is assumed that the CF values of the two classes are $CF_1=(N_1,\overrightarrow{LS_1},SS_1)$ and $CF_2=(N_2,\overrightarrow{LS_2},SS_2)$, then the CF of the class after the fusion of these two classes meets the following formula:*

$$\mathrm{CF}_1+\mathrm{CF}_2=\left(N_1+N_2,\overrightarrow{\mathrm{LS}_1}+\overrightarrow{\mathrm{LS}_2},\mathrm{SS}_1+\mathrm{SS}_2\right). \tag{11}$$

The additivity theorem of clustering features shows that it is easy to obtain the CF vector of the fusion class from the CF vector of different classes. Moreover, according to different types of CF vectors, it is easy to obtain the corresponding $\overrightarrow{X0}$, R equidistance formulas. According to these distances, the effect of the clustering result of the BIRCH algorithm can be judged.

As shown in Figure 1, the CF tree involved in the BIRCH algorithm is a highly balanced tree with two parameters: branching factor B and threshold T. Each nonleaf node contains at most B branch entries $(\mathrm{CF}_i, \mathrm{child}_i)$, $i = 1, 2, \ldots, B$, child_i is a pointer to its i-th child node, and CF_i is the clustering feature of the i-th child node. A leaf node has at most L entries, and the form of each entry is (CF_i), $i = 1, 2, \ldots, L$, where CF_i is the clustering feature of its i-th subcategory. In addition, in order to improve the query speed, all leaf nodes are connected through two pointers, prey and next. The CF value of a leaf node represents the clustering characteristics of a subcategory. Among them, the radius of each class must be less than the threshold limit T.

In the BIRCH algorithm, a CF tree is a compressed representation of the density statistics of a data set, and an entry CF_i in the leaf node represents a clustering feature CF value of class C_i. Among them, the radius R of each class C must meet the limit of the threshold radius T. The denser the area in the original data set, the more data points contained in class C. Conversely, the sparser the area, the fewer data points contained in class C.

In the clustering process of the BIRCH algorithm, as data points are continuously added, the CF tree is dynamically constructed. This process is similar to the insertion operation of the B tree. The construction process of the CF tree is as follows:

(1) Starting from the root node, select the nearest child node from top to bottom.
(2) After reaching the leaf node, check whether the class C represented by the nearest entry can absorb this data point. If possible, update the CF value; if not, check whether it can add a new entry. If it is not possible to add a new item, the split farthest~pair is used as a seed, and other items are reallocated according to the distance.
(3) Update the CF value of each nonleaf node. If the node is split, insert a new entry in the parent node, and then check whether the parent node needs to be split until the root node.

When the data points cannot be inserted, at this time, the threshold T needs to be raised and the CF tree is rebuilt to absorb more data points until all the data points are inserted. The size of the threshold T determines the size of the class so that the size of the CF tree can be controlled by controlling the size of T to adapt to the current limited memory. If T is too small, the number of classes will be very large, resulting in an increase in the number of tree nodes, which may lead to insufficient memory in the data set before the scan is completed, so it needs to be adjusted appropriately during the process of inserting data points. The size of the threshold T makes it suitable for the current memory size.

The clustering process of the BIRCH algorithm is shown in Figure 2. The specific process is as follows:

Stage 1: use limited memory and hard disk space to scan all the data in the data set and initialize a CF tree in the memory. This CF tree can reflect the clustering information of the data set as much as possible under the condition of memory limitation. Divide dense data into classes, and eliminate sparse data points as outliers.

Stage 2: this stage is optional. The input data scale of the global clustering algorithm in stage 3 has certain limits, and the result in stage 1 may be different from the input scale required in stage 3. Therefore, in stage 2, the CF tree in phase 1 can be modified to generate a smaller CF tree, so that the global algorithm in stage 3 can run more effectively.

Stage 3: in this stage, a global or semiglobal algorithm is used to cluster the entries of the leaf nodes in the CF tree to generate better global clustering results.

Stage 4: this stage is optional. Redistribute data points to the nearest seed to ensure that duplicate data are grouped into the same class, and add class labels at the same time.

In order to evaluate the clustering accuracy and effectiveness of the improved algorithm, this paper uses the improved algorithm proposed in this paper to implement the algorithm on two simulation data sets and one news data set, respectively. Moreover, this paper uses running time T, precision P (Precision), recall R (Recall), and F-measure (F-measure) to further evaluate the proposed algorithm. When F is higher, the clustering accuracy is higher.

Here, the class identified by the clustering result is referred to as the result class, and the primitive class in the original data set is referred to as the original class. F-measure combines the ideas of precision P and recall R in information retrieval to perform clustering evaluation. The precision and recall of a result class j and the corresponding original class i are shown in the following formula:

$$\begin{aligned} P(i, j) &= \mathrm{precision}(i, j) = \frac{N_{ij}}{N_j}, \\ R(i, j) &= \mathrm{recall}(i, j) = \frac{N_{ij}}{N_i}. \end{aligned} \tag{12}$$

In the formula, N_{ij} is the number of all objects in the original class i in the result class j, N_j is the number of all objects in the result class j, and N_i is the number of all objects in the original class i. The definition of F-measure of primitive class i is as follows:

$$F(i) = \frac{2P(i, j)R(i, j)}{(P(i, j) + R(i, j))}. \tag{13}$$

For the original class i, the higher the F-measure value of the clustering algorithm is, the better the effect of the clustering algorithm is and the more it can reflect the mapping of the original class i. In other words, F-measure can be used as the evaluation score of the original class i. For the clustering result, the total F-measure of the algorithm can be obtained by the weighted average of the F-measure corresponding to each original class i, as shown in the following formula:

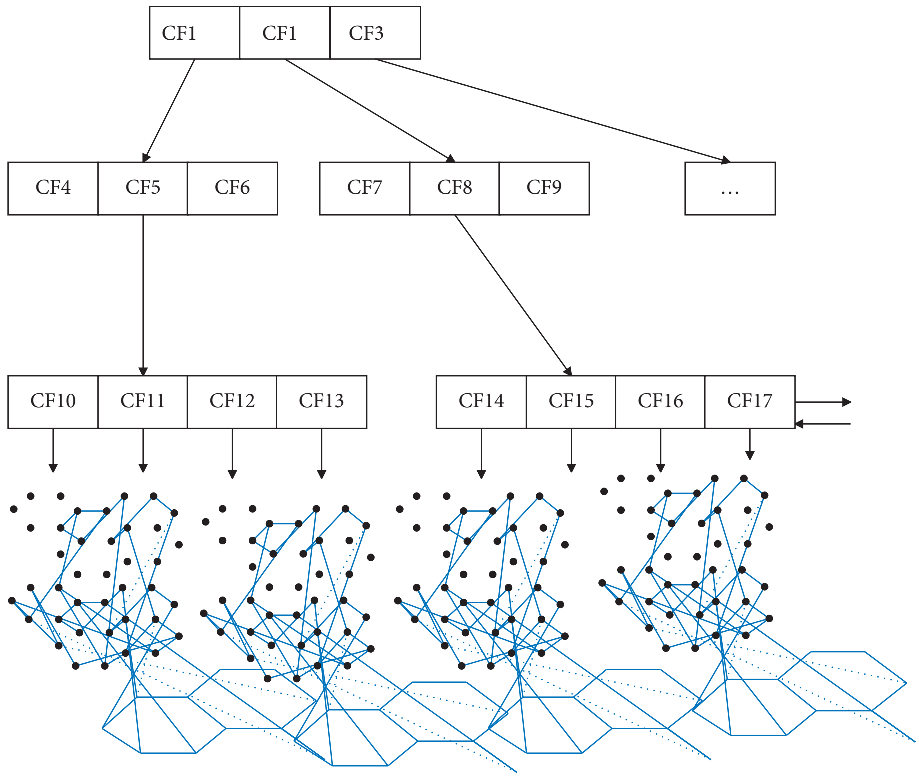

Figure 1: CF tree $(B = 3, L = 4)$.

$$F = \frac{\sum_i N_i \cdot F(i)}{\sum_i N_i}. \quad (14)$$

In the formula, N_i is the number of all objects in the original class i.

4. Economic Analysis Model Based on Improved Clustering Algorithm

This paper combines the improved clustering algorithm to make an economic analysis model and analyzes the economic development trend in the postepidemic era through this model. This paper uses textual economic data analysis for clustering. The specific description and process of the algorithm (Figure 3) are as follows:

(1) We segment the background technology and technical fields of the patent text, filter out stop words, and extract problem keywords that describe the background of the problem, the existing problems, the conditions for the problems, and the existing solutions to the problems. (2) We establish the index item of patent documents-document matrix D. (3) We use LSA latent semantic analysis to reduce the dimensionality of the matrix. (4) We use the DBSCAN algorithm to cluster the document matrix VKT text.

The centroid points of all classes are summarized to form a new compressed data set, and the CF value of each class is stored as the attribute value of the centroid point of the class. This compressed data set will be used as the input data set for the next stage of the AV-DBSCAN algorithm. In this newly generated compressed data set, each data point represents a class of the clustering result. The process of generating compressed data sets is shown in Figure 4.

The category update process of the original data set using the clustering results of the AV-DBSCAN algorithm is shown in Figures 4–6. When AV-DBSCAN clusters the compressed data set, each data point in the clustering result of the compressed data set corresponds to a subcategory in the original data set. According to the category of the data point in the compressed data set, the corresponding subcategory in the original data set is found, and all the data points in the subcategory are updated to this category. Finally, the clustering result of the original data set is obtained.

On the basis of the above analysis, the constructed economic development trend analysis model based on the improved clustering algorithm is shown in Figure 6.

On the basis of the above analysis, an economic development trend analysis model based on the improved clustering algorithm is constructed, and then the performance verification analysis of the model can be performed.

5. Analysis of Economic Development Trends in the Postepidemic Era Based on Improved Clustering Algorithms

At the end of 2019, a case of 2019-nCoV infection was detected in Wuhan, Hubei Province, China. The virus spreads quickly and is difficult to prevent and control, and there is a phenomenon of human-to-human transmission. Afterwards, confirmed cases of pneumonia infected by the 2019-nCoV virus gradually increased, and the COVID-19 epidemic broke out in Wuhan and spread rapidly across the

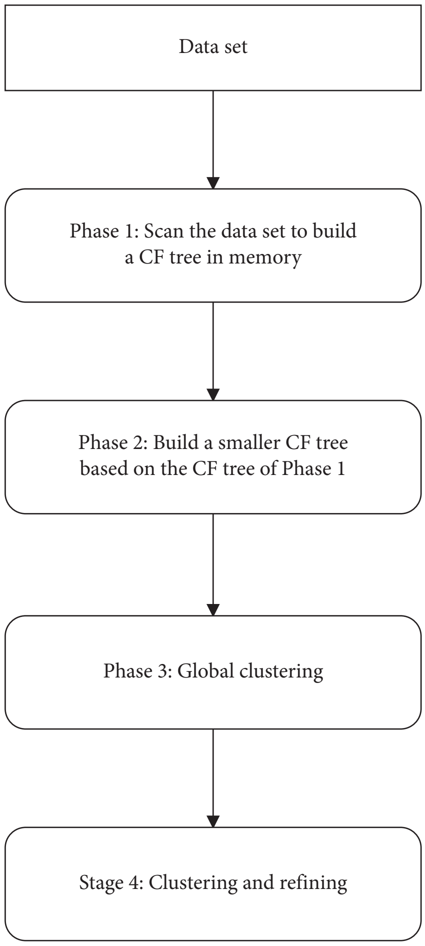

Figure 2: BIRCH algorithm clustering process.

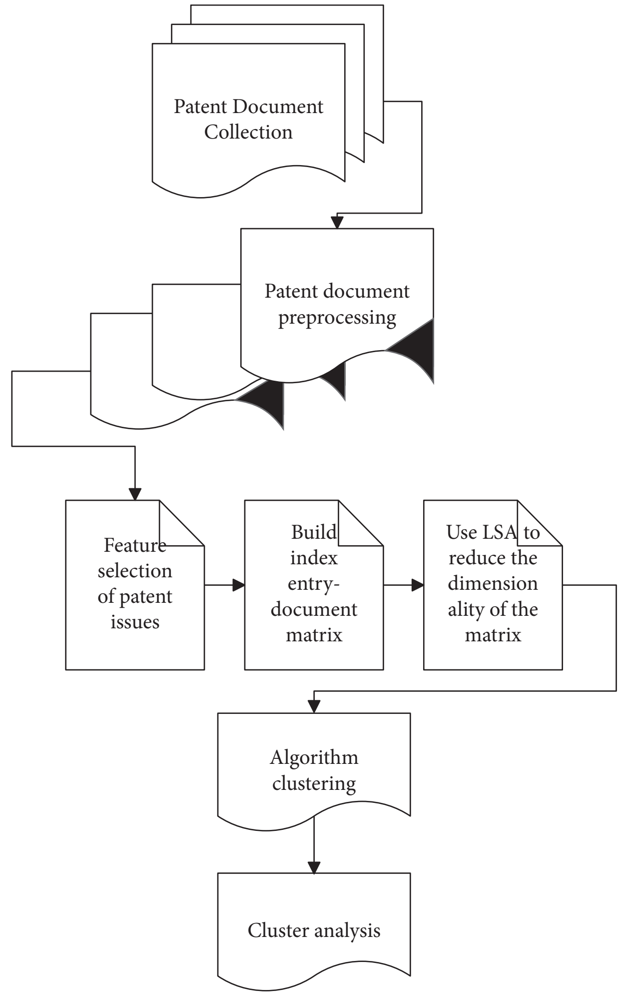

Figure 3: Clustering process of economic text data.

country. On January 31, the World Health Organization announced that the COVID-19 epidemic constituted a "public emergency of international concern." In the face of the epidemic, the Chinese government attached great importance to it, acted quickly, and achieved decisive results in about three months, and the epidemic was effectively controlled. At the same time, the COVID-19 epidemic continued to spread in other countries, and the death toll increased rapidly. The World Health Organization pointed out in the "Declaration of Healthy Recovery from the Covid-19 Epidemic" that the 2019-nCoV virus epidemic is the world's biggest impact in decades, and hundreds of thousands of people have lost their lives. Moreover, it pointed out that the world economy is likely to face the most serious economic recession since the 1930s, and the resulting unemployment and reduced income will be detrimental to livelihoods, health, and sustainable development.

In this context, economic development has received a major impact, so this paper uses the constructed improved clustering algorithm to analyze economic development trends in the postepidemic era and verify the performance of the system.

The model constructed in this paper can effectively mine relevant data in the process of economic development. Therefore, in the process of model verification, this paper first analyzes the effect of factor mining, mines 78 sets of data, analyzes the effectiveness of these factors, and scores the factors. The results are shown in Table 1 and Figure 7.

From the above analysis, it can be seen that the clustering model constructed in this paper has a good performance in economic factor mining. On this basis, this paper analyzes the economic development trend analysis strategy and evaluates the output results. The results of the evaluation statistics are shown in Table 2 and Figure 8.

The summary of the output results is as follows.

At present, the Party Central Committee and the State Council attach great importance to achieving the annual economic and social development goals and tasks and have issued a series of supporting policies to coordinate the prevention and control of the new crown pneumonia epidemic and economic and social development. All departments and governments at all levels must fully implement the various decisions and deployments of the central government, coordinate and promote related work, and ensure precise implementation of policies and effective implementation of policies.

We need to focus on fiscal policy, supplemented by monetary and credit policies, to effectively support economic recovery. At the same time, we need to increase

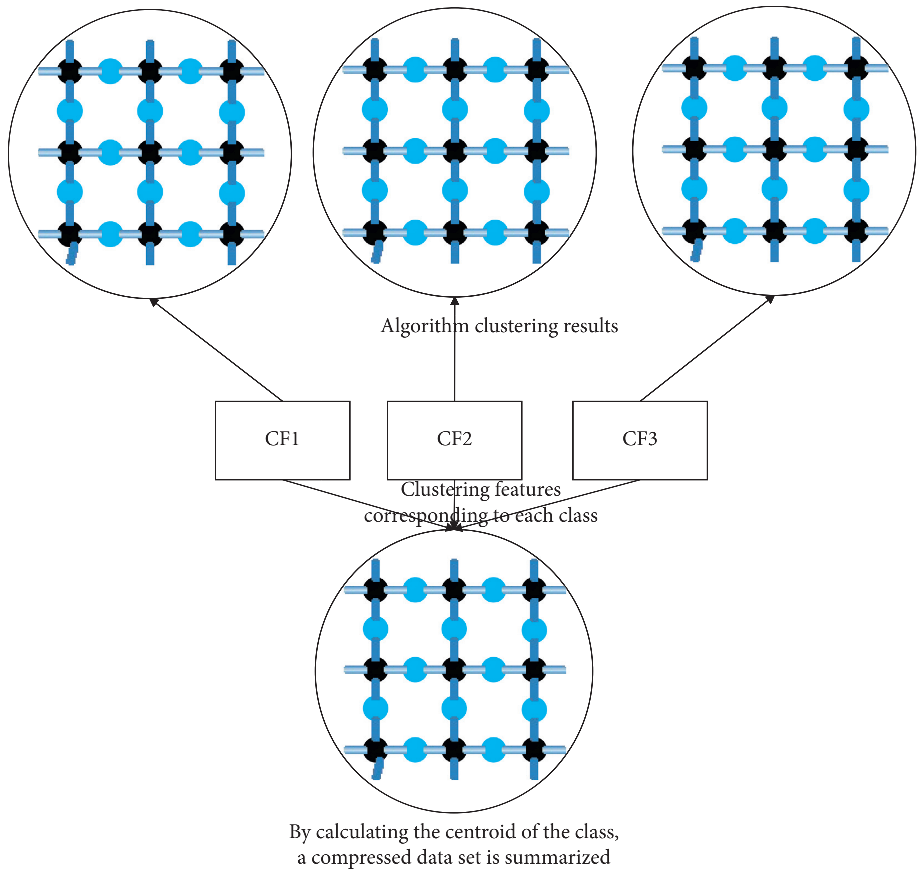

Figure 4: The generation process of the compressed data set.

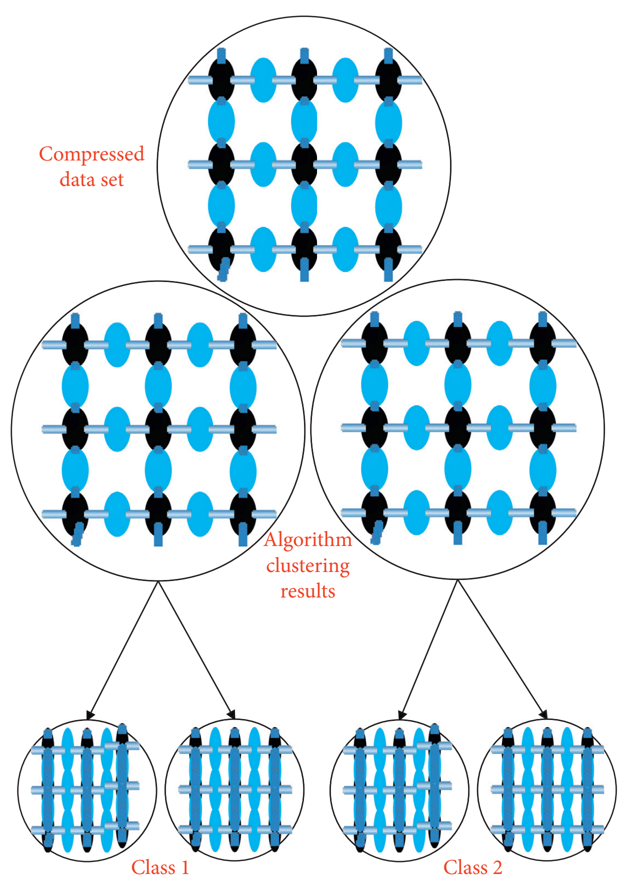

Figure 5: The category update process of the original data set.

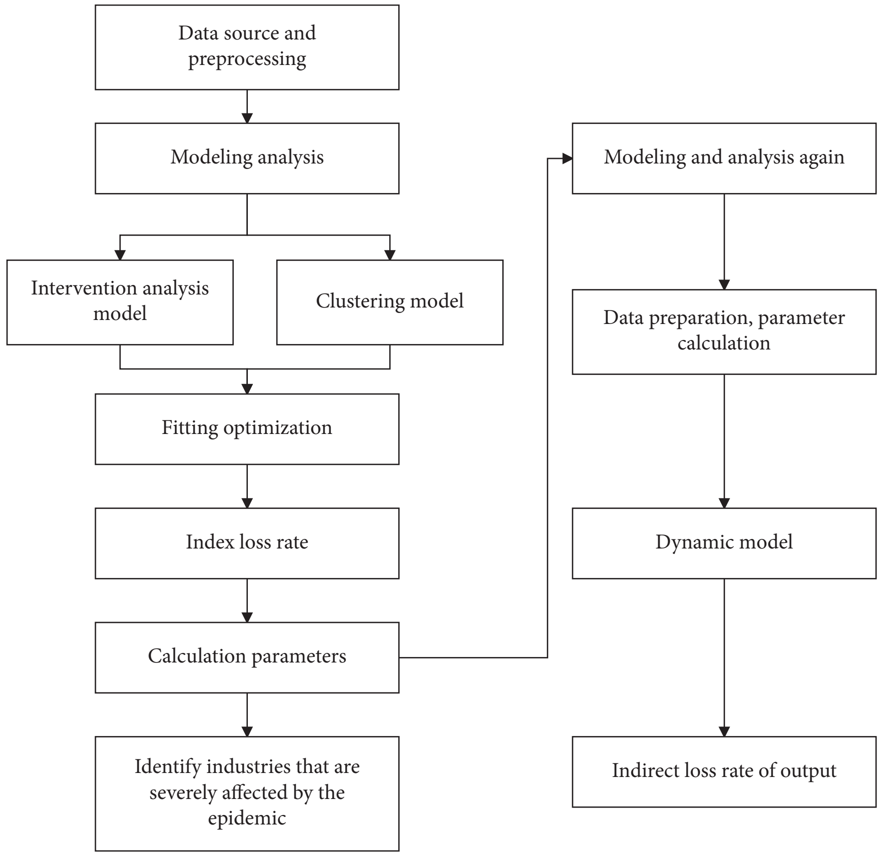

Figure 6: Economic development trend analysis model based on the improved clustering algorithm.

Table 1: Analysis table of the effect of factor mining.

Num	Factor mining score
1	86.5
2	82.5
3	90.2
4	91.3
5	84.0
6	85.9
7	90.6
8	92.3
9	83.0
10	90.8
11	88.2
12	92.2
13	89.2
14	86.0
15	82.1
16	85.4
17	86.9
18	87.7
19	83.2
20	90.2
21	83.4
22	86.8
23	83.3
24	85.1
25	88.0
26	86.8

Table 1: Continued.

Num	Factor mining score
27	90.3
28	84.2
29	88.7
30	84.5
31	88.8
32	86.7
33	87.4
34	86.5
35	81.4
36	86.4
37	88.6
38	82.8
39	92.5
40	82.1
41	81.6
42	84.3
43	81.3
44	81.2
45	85.6
46	92.0
47	84.6
48	84.1
49	91.6
50	83.3
51	83.5
52	84.1
53	84.3
54	82.4
55	85.3
56	84.9
57	92.6
58	90.4
59	89.9
60	83.4
61	86.9
62	86.9
63	84.7
64	86.3
65	91.5
66	81.1
67	82.9
68	88.0
69	86.4
70	88.8
71	88.4
72	91.6
73	81.0
74	82.2
75	85.8
76	90.6
77	84.9
78	89.2

countercyclical adjustments to fiscal policy, increase the central fiscal deficit rate, and increase central transfer payments to local governments. We will increase targeted support to weak areas and regions such as medical and health, small, medium, and microenterprises, private enterprises, service enterprises, and residents who are unemployed and at risk of unemployment. Through tax reduction and exemption, direct subsidies, and so on, the goal of protecting people's livelihood can be achieved. Increase assist for the construction of short-term livelihood areas such as medical and health, education, public transportation, and pollution prevention to hedge the economic decline and employment problem caused by the epidemic. The cautious monetary guideline is moderately relaxed at the margin, the monetary policy transmission

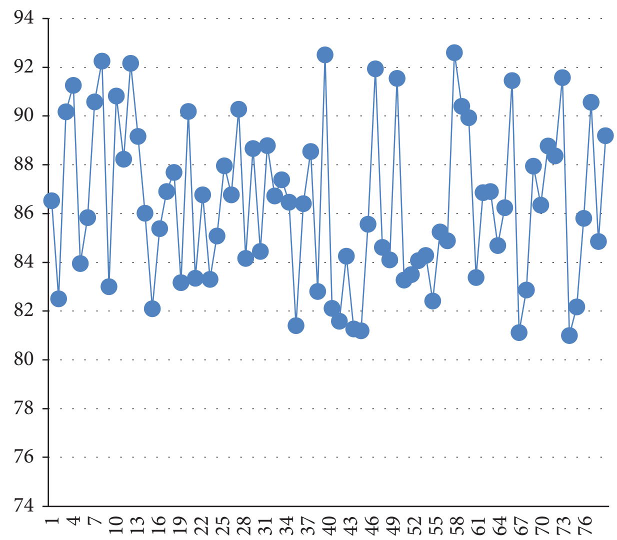

Figure 7: Analysis diagram of the effect of factor mining.

Table 2: Analysis table of economic development trends and evaluation of the effect of strategy formulation.

Num	Economic evaluation score
1	70.7
2	81.1
3	79.4
4	73.9
5	77.9
6	73.0
7	73.9
8	77.8
9	78.7
10	78.8
11	76.4
12	81.0
13	76.5
14	70.3
15	76.4
16	81.3
17	72.7
18	70.7
19	69.7
20	78.1
21	79.1
22	80.0
23	76.3
24	74.8
25	78.9
26	69.5
27	77.6
28	80.4
29	72.8
30	78.6
31	70.6
32	73.4
33	69.5
34	81.1
35	71.6
36	75.7
37	80.9
38	79.9

Table 2: Continued.

Num	Economic evaluation score
39	78.2
40	76.1
41	81.5
42	78.5
43	76.9
44	76.2
45	79.7
46	70.8
47	78.3
48	76.6
49	69.6
50	71.5
51	71.1
52	71.8
53	79.6
54	72.5
55	71.3
56	75.4
57	76.2
58	77.0
59	69.1
60	72.9
61	77.2
62	79.8
63	76.7
64	71.2
65	80.0
66	80.9
67	70.4
68	79.3
69	77.9
70	70.9
71	75.5
72	75.7
73	71.6
74	69.7
75	81.1
76	76.2
77	74.4
78	73.2

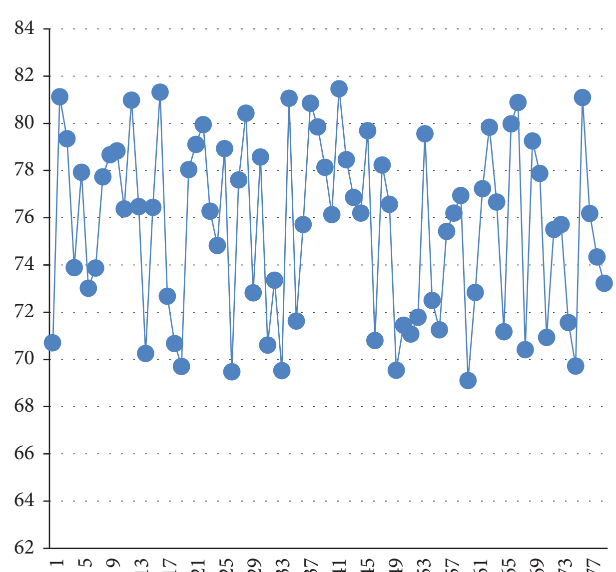

Figure 8: Analysis diagram of economic development trends and evaluation of the effect of strategy formulation.

mechanism is unblocked, the assessment of private enterprise loans issued by financial institutions is strengthened, and financial institutions are encouraged to reduce interest rates, improve loan renewal policies, increase credit loans and medium- and long-term loans to ensure that private enterprise loans are maintained certain growth, effectively alleviating the problem of tight capital chain of private enterprises, and beware of the large-scale explosion of private enterprise credit risk.

Firmly implement the spirit of the Fourth Plenary Session of the 19th Central Committee of the Communist Party of China, fully implement the new development concept, focus on supply-side structural reforms, accelerate the construction of a modern economic system, and effectively solve the deep-level structural and institutional problems facing the Chinese economy through comprehensive deepening of reforms. Inject new impetus into economic growth.

6. Conclusion

In the postepidemic era, the current negative impact of the COVID-19 epidemic on the economy has fully emerged, and there is also the possibility of secondary risks through high-risk companies and residents. Therefore, we must adhere to the combination of epidemic prevention and control and economic support, play the role of countercyclical policies, and effectively reduce the negative economic impact of the epidemic.

This paper combines improved clustering algorithms to analyze economic development trends in the postepidemic era, constructs intelligent models through intelligent algorithms, evaluates economic development effects based on actual conditions, analyzes current problems through factor mining, and proposes corresponding strategies.

This paper designs experiments to detect the performance of the algorithm model constructed in this paper. From the research results, we can see that the improved clustering algorithm proposed in this paper has a certain effect in the analysis of economic development trends in the postepidemic era and can continue to play a role in subsequent economic analysis.

Data Availability

The labeled data set used to support the findings of this study is available from the corresponding author upon request.

Conflicts of Interest

The authors declare no conflicts of interest.

Acknowledgments

This study was sponsored by Support Plan for Scientific and Technology Innovation Talents in Universities of Henan Province (Humanities and Social Sciences) (2019-cx-019); Major Research Projects of Philosophy and Social Sciences in Universities of Henan Province (2022-YYZD-05); Henan Philosophy and Social Science Planning Project (2021BJJ032); and National Social Science Foundation of China (20BGJ016).

References

[1] J. Fichtner, E. M. Heemskerk, and J. Garcia-Bernardo, "Hidden power of the big three? passive index funds, re-concentration of corporate ownership, and new financial risk," *Business and Politics*, vol. 19, no. 2, pp. 298–326, 2017.

[2] C. Cueva, R. E. Roberts, T. Spencer et al., "Cortisol and testosterone increase financial risk taking and may destabilize markets," *Scientific Reports*, vol. 5, no. 1, pp. 11206–11216, 2015.

[3] C. J. Lee and E. B. Andrade, "Fear, excitement, and financial risk-taking," *Cognition and Emotion*, vol. 29, no. 1, pp. 178–187, 2015.

[4] S. M. Bartram, G. W. Brown, and W. Waller, "How important is financial risk?" *Journal of Financial and Quantitative Analysis*, vol. 50, no. 4, pp. 801–824, 2015.

[5] W. W. Cooper, A. T. Kingyens, and J. C. Paradi, "Two-stage financial risk tolerance assessment using data envelopment analysis," *European Journal of Operational Research*, vol. 233, no. 1, pp. 273–280, 2014.

[6] W. Montford and R. E. Goldsmith, "How gender and financial self-efficacy influence investment risk taking," *International Journal of Consumer Studies*, vol. 40, no. 1, pp. 101–106, 2016.

[7] S. Muthii Wanjohi, J. G. Wanjohi, and J. M. Ndambiri, "The effect of financial risk management on the financial performance of commercial banks in Kenya," *International Journal of Finance and Banking Research*, vol. 3, no. 5, pp. 70–81, 2017.

[8] J. Magendans, J. M. Gutteling, and S. Zebel, "Psychological determinants of financial buffer saving: the influence of financial risk tolerance and regulatory focus," *Journal of Risk Research*, vol. 20, no. 8, pp. 1076–1093, 2017.

[9] E. S. Cole, D. Walker, A. Mora, and M. L. Diana, "Identifying hospitals that may Be at most financial risk from medicaid disproportionate-share hospital payment cuts," *Health Affairs*, vol. 33, no. 11, pp. 2025–2033, 2014.

[10] A. Zalik, "Resource sterilization: reserve replacement, financial risk, and environmental review in Canada's tar sands," *Environment and Planning A: Economy and Space*, vol. 47, no. 12, pp. 2446–2464, 2015.

[11] C. Lucarelli, P. Uberti, and G. Brighetti, "Misclassifications in financial risk tolerance," *Journal of Risk Research*, vol. 18, no. 4, pp. 467–482, 2015.

[12] E. Y. Chan, "Physically-attractive males increase men's financial risk-taking," *Evolution and Human Behavior*, vol. 36, no. 5, pp. 407–413, 2015.

[13] T. West and A. C. Worthington, "Macroeconomic conditions and Australian financial risk attitudes, 2001–2010," *Journal of Family and Economic Issues*, vol. 35, no. 2, pp. 263–277, 2014.

[14] T. Tanimura, E. Jaramillo, D. Weil, M. Raviglione, and K. Lonnroth, "Financial burden for tuberculosis patients in low- and middle-income countries: a systematic review," *European Respiratory Journal*, vol. 43, no. 6, pp. 1763–1775, 2014.

[15] T. K. Scharding, "Imprudence and immorality: a Kantian approach to the ethics of financial risk," *Business Ethics Quarterly*, vol. 25, no. 2, pp. 243–265, 2015.

[16] J. Su and E. Furman, "A form of multivariate pareto distribution with applications to financial risk measurement," *ASTIN Bulletin*, vol. 47, no. 1, pp. 331–357, 2017.

[17] G. W. Y. Wang, S.-H. Woo, and J. Mileski, "The relative efficiency and financial risk assessment of shipping

companies," *Maritime Policy and Management*, vol. 41, no. 7, pp. 651–666, 2014.

[18] J. Linarelli, "Luck, justice and systemic financial risk," *Journal of Applied Philosophy*, vol. 34, no. 3, pp. 331–352, 2017.

[19] P. Allen and C. Petsoulas, "Pricing in the English NHS quasi market: a national study of the allocation of financial risk through contracts," *Public Money and Management*, vol. 36, no. 5, pp. 341–348, 2016.

[20] J. Thomä and H. Chenet, "Transition risks and market failure: a theoretical discourse on why financial models and economic agents may misprice risk related to the transition to a low-carbon economy," *Journal of Sustainable Finance and Investment*, vol. 7, no. 1, pp. 82–98, 2017.

[21] O. Sosnovska and M. Zhytar, "Financial architecture as the base of the financial safety of the enterprise," *Baltic Journal of Economic Studies*, vol. 4, no. 4, pp. 334–340, 2018.

[22] D. Acemoglu, A. Ozdaglar, and A. Tahbaz-Salehi, "Systemic risk and stability in financial networks," *The American Economic Review*, vol. 105, no. 2, pp. 564–608, 2015.

[23] R. Castellano, R. Cerqueti, and G. Rotundo, "Exploring the financial risk of a temperature index: a fractional integrated approach," *Annals of Operations Research*, vol. 284, no. 1, pp. 225–242, 2020.

[24] A. Cohn, J. Engelmann, E. Fehr, and M. A. Maréchal, "Evidence for countercyclical risk aversion: an experiment with financial professionals," *The American Economic Review*, vol. 105, no. 2, pp. 860–885, 2015.

Hindawi
Scientific Programming
Volume 2021, Article ID 6031324, 12 pages
https://doi.org/10.1155/2021/6031324

Research Article

A Data Technology Oriented to Information Fusion to Build an Intelligent Accounting Computerized Model

Ziyan Xu and Wenxue Zhou

Tangshan Normal University, Tangshan 063000, China

Correspondence should be addressed to Ziyan Xu; xzy110015@tstc.edu.cn

Received 19 October 2021; Revised 10 November 2021; Accepted 18 November 2021; Published 8 December 2021

Academic Editor: Le Sun

The development of management accounting promotes the integration of business and finance, and with the continuous development of information technology and the advent of the era of big data, the development of corporate financial informatization provides tools for the integration of business and finance. This paper improves the big data technology, improves the traditional accounting process, combines the big data technology to build a computerized accounting system, and obtains scientific and effective accounting information processing results through intelligent big data processing. The design goal of the enterprise accounting management system is that the system can efficiently complete the enterprise cost budget accounting work after the design is completed and ensure the normal and stable progress of the enterprise cost budget accounting work. Through the experimental research results, it can be known that the computerized intelligent accounting system based on big data technology constructed in this article has certain effects.

1. Introduction

In contemporary society, various system reconstruction methods are emerging one after another, but they have never really solved this problem. Since the advent of the REA model, the construction of an accounting information system based on REA can provide the company's stakeholders and auditors with real-time, accurate, multilevel, personalized management decision information, audit information, etc. Moreover, it satisfies the information needs of more people, thereby transforming the accounting information system from the traditional focus on financial status, operating results, and cash flow to real-time control and feedback of the enterprise management process. Furthermore, it enables the system to develop into an intelligent accounting information system that can provide information based on user choices to support management decisions and so forth [1].

With the development of network computer technology, the user-friendly operation interface of the commonly used Windows system has accelerated the use of accounting software in the financial management department of enterprises and has slowly extended it to other departments. This good application situation also makes the academic and practical circles begin to consider the issue of information integration between different departments to avoid duplication of work between departments and improve work efficiency. For example, the accounting department is linked with the cost accounting of the production department and the sales management of the sales department to realize the integration of departmental subsystems, and the accounting information system gradually rises from this [2]. However, the accounting information system at this time belongs to the accounting system dedicated to the financial department and cannot provide management decision information, which is more restrictive at the technical and conceptual levels. The processing of data in the system application only serves as a postevent record and feedback function, and it is difficult for it to play the role of pre-prediction and in-event control [3].

Since then, with the vigorous development of databases, the flexibility of information systems has improved, and data security, analysis, and processing capabilities have made great progress. Enterprise-level management information systems represented by ERP have developed rapidly, and their essence is to break departmental barriers; expand the scope of the information system; connect the upstream and downstream of the supply chain; realize the integration and coordination of the enterprise's finance, personnel, sales, supply, production, etc.; and effectively control the entire process of enterprise operation. In the system of integrated information management, the accounting supervision function of the enterprise is only one of the submodules. With the exquisite network technology, the global IT field has led to a wave of industrial reforms; the development of e-commerce has also swept the traditional accounting business model field, causing companies to rethink the shortcomings of their traditional system architecture and processes; and a series of new system reconstruction method is gradually applied to the accounting information system. The system reconstruction method is gradually applied to the accounting information system. It is widely known as the accounting information system based on the REA model to be introduced in this article, which can realize real-time processing of monitoring information in a network environment and multilevel output information to meet different requirements of users.

Based on the above analysis, this article combines big data technology to construct a computerized accounting system obtains scientific and effective accounting information processing results through intelligent big data processing, and improves accounting management efficiency on this basis.

2. Related Work

The implementation path of business-finance integration relies on the integration of various management accounting tools. The literature [4] believes that management accounting information systems should be based on solid corporate management data to enable comprehensive budget management, centralized capital management, cost control, performance evaluation, and other business modules to operate and develop efficiently and smoothly, support the application of management accounting, fully realize the organic integration of accounting and business, and ultimately achieve the goal of value creation. The literature [5] believes that, in the era of big data, traditional management accounting is mainly based on small data calculations and that management accounting tools are separated from each other and lack business-financial integration ideas. Therefore, it believes that it is necessary to integrate modern information technology, management accounting thoughts, and financial accounting theories to form an integrated structure of financial services. In summary, the advanced integrated concept of information system construction has enabled the implementation of management accounting tools such as balanced scorecards, comprehensive budget management, and other management tools. Secondly, the construction process of the management accounting information system is the process of reorganizing and optimizing the business and financial processes. The literature [6] believes that the success of process management depends on whether financial management and business process redesign are integrated. The literature [7] finds that the lack of support from the management accounting system is the main reason for the failure of business process management. In the practice of process management, the management accounting system can solve the problem of information efficiency. In the process of the organization's operation chain management or supply chain management, for the improvement of organizational performance, appropriate information technology methods can be used to supplement the management accounting system, and the organizational structure, responsibilities, and permissions can be redivided, which will produce better output benefits. Literature [8] believes that management accounting research needs to take informationization as the basis and management integration as a prerequisite. At the same time, its needs to involve the integration of management accounting and business control, financial accounting reports, human resource management, and other systems, as well as the integration of various application models and tools of management accounting itself. In this way, the theoretical system of management accounting can be enriched, and the guidance of management accounting theory to practice can be enhanced at the same time. Finally, the construction of information systems can achieve the effect of business-finance integration on business control. The literature [9] believes that when an enterprise establishes an information system, business control should be embedded in the information system at the same time. The effective operation of the information system control can ensure the effectiveness of the enterprise's internal control.

Literature [10] believes that a management information system is an information system that connects various internal organizations. The internal operation process of the system should be that the software supplier extracts the complete business process from the mature and perfect enterprise to evolve, and allows other users to reorganize the relevant process through standardized learning. Literature [11] believes that, by using information technology correctly under the key role of industry-finance integration, modern enterprises can remain invincible in the external social environment and obtain sustained development and progress. Literature [12] believes that company performance is positively related to the use of innovative IT tools. If companies invest more in new technologies, this can increase the market share and market value of their products. Literature [13] believes that, in developed countries, investment in IT technology plays a very decisive role in production efficiency. Literature [14] believes that if a company has a comprehensive information system that can connect all departments within the company, this can reduce internal communication costs, improve information transmission efficiency, and improve business performance. Literature [15] points out that for the integration of business and finance to be realized in the enterprise, it must be supported by IT. Literature [16] puts forward the problem that the relevant information in the accounting information system cannot be shared in real time, and in order to solve the problem, the relevant financial process is redesigned. At the same time, it is pointed out that if the accounting goal is to be achieved under the new situation, the accounting business process must be reorganized. Literature [17] points out a set of innovative accounting information processing procedures based on the Internet by comparing the financial process under the value process and the financial process under the law. Literature [18] designs an accounting information system that can monitor financial information and business information in real time, with events and decisions as driving factors. Literature [19] believes that converting business information into financial information is the most important step in process reengineering. There are many conversion methods, for example, through business accounts, financially reviewed documents or those automatically generated by the accounting information system, and finally original vouchers provided by the accounting information system. Literature [20] puts forward the key points that should be paid attention to when the accounting information system is integrated with business and finance: one is to pay attention to the content, scope, and objectives involved in the establishment of business processes; the other is to formulate unified and standardized business processing rules.

3. Data Mining Algorithm of Computerized Accounting

Neurons can connect to each other and themselves, in addition to the connection between input neurons and reservoir neurons and that between output neurons. In addition, output neurons can also be self-connected and feedback-connected. We assume that the network has K inputs and represent the entire K inputs as a vector $u(n) = [u_1(n), u_2(n), \ldots, u_k(n)]$. If we assume that there are N neurons in the reserve pool, the corresponding state of the reserve pool neuron is $u_i(n)$. If we assume that the output dimension is L, the output is represented as a vector $\hat{y}(n) = [\hat{y}_1(n), \hat{y}_2(n), \ldots, \hat{y}_L(n)]$ as a whole. The connection weight matrix of the echo state network consists of four parts: (1) input connection matrix $W^{\text{in}} = (w_{ij}^{\text{in}})$ with dimension $N \times K$, (2) internal connection matrix $W = (w_{ij})$ with dimension $N \times N$ of the reserve pool, (3) output connection matrix $W^{\text{out}} = (w_{ij}^{\text{out}})$ with dimension $L \times (K + N + \text{L})$, and (4) output feedback matrix $W^{\text{back}} = (w_{ij}^{\text{back}})$ with dimension $N \times L$. For the echo state network used for iterative single-value prediction, the value of L is 1. The network topology of the echo state network is generated by the weight changes of neurons in the reserve pool. The status update expression and output expression of the network are as follows [21]:

$$x(n) = f\left(W^{\text{in}} u(n) + W x(n-1) + W^{\text{back}} \hat{y}(n-1)\right), \tag{1}$$

$$\hat{y}(n) = f^{\text{out}}\left(\left[u(n), x(n), \hat{y}(n-1) W^{\text{out}}\right]\right). \tag{2}$$

In (1), $f(*) = [f_1(*), f_2(*), \ldots, f_N(*)]$ is the excitation function of the internal module (usually the sigmoid function). The elements of the internal connection matrix w must be randomly selected within [−1, 1], and the sparsity must be between 1% and 10%. Moreover, in order to make the model stable and convergent, the spectral radius of W should be less than 1. In (2), $[u(n), x(n), \hat{y}(n-1)]$ is a composite vector composed of the input, the state corresponding to the neurons in the internal reserve pool, and the last network output. $f^{\text{out}}(*) = [f_1^{\text{out}}(*), f_2^{\text{out}}(*), \ldots, f_L^{\text{out}}(*)]$ is the output function, and the identity function can be used. This can make the relationship between the matrix and the output a linear relationship, which can be solved more conveniently using parameter optimization methods, as shown in Figure 1.

Considering the special case of time series prediction, the output $y(n-1)$ at the previous moment can be merged into the input $u(n)$ at this moment. It can be seen that the output information at the last moment has been fed back at this moment. Therefore, the output feedback is no longer considered in the structure, and the output function takes the identity function. The pattern (1) and equation (2) can be simplified as follows:

$$\begin{aligned} x(n) &= f\left(w^{\text{in}} u(n) + W x(n-1)\right), \\ \hat{y}(n) &= [u(n), x(n)] W^{\text{out}}. \end{aligned} \tag{3}$$

Consider the case where the output length is 1; at this time, the dimension of W^{out} is $(K + N)$ xl, and the form is changed from a matrix to a vector. It can be seen from the simplified formula that the nonlinear mapping between input and output is mainly completed by the neuron nonlinear activation function $f(*) = [f_1(*), f_2(*), \ldots, f_N(*)]$. There is a linear relationship between the state vector $x(n)$ and the output $y(n)$. Writing in this way can simplify the derivation of subsequent formulas, making it easier for the identity output function to solve the model using parameter optimization methods, and the entire model needs to be calculated with only the output connection vector W^{out}, which requires less calculation.

Bootstrap interval estimation method is often used to solve the problem of small structure subsample test evaluation and infer the distribution characteristics of a certain statistic of data. It is suitable for some problems such as parameter interval estimation that are difficult to derive by conventional methods. The basic idea is to perform resampling with replacement in the original sample set D_{original}, and the sample set size obtained by sampling remains unchanged. That is, it is assumed that there are M samples in the original sample set, the sample set obtained by sampling still has M samples, and the probability of each sample being drawn is the same each time, which is $1/M$. The resulting sample set is called the Bootstrap sample set. This extraction is repeated many times to obtain B Bootstrap sample sets, which can be used as the training set of multiple models. In the prediction, multiple sets of model outputs can be obtained for the same input, and the required statistics to be estimated can be obtained.

Traditional Bootstrap interval estimation methods mainly include three types: standard Bootstrap, percentile Bootstrap, and t percentile Bootstrap.

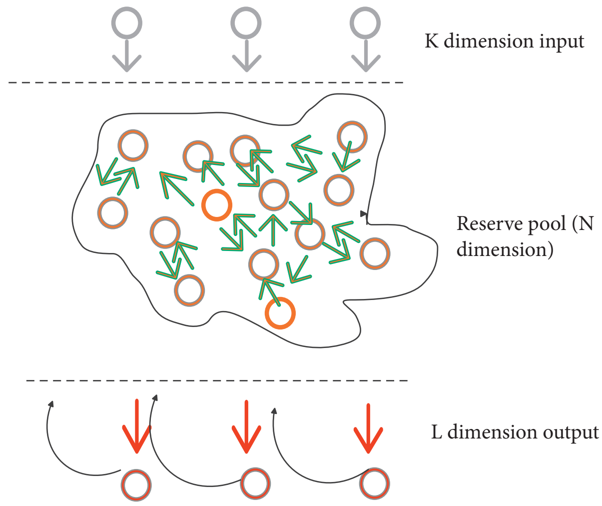

Figure 1: Echo status network.

3.1. Standard Bootstrap. Standard Bootstrap assumes that a sample with a capacity of M is randomly selected independently from the original sample set D_{original}, and the sample is replaced each time. According to the idea of permutation and combination, there are at most MM Bootstrap sample sets. By averaging the samples in each sample set, the value obtained is also an estimated value of the population mean, and the distribution of the sample mean is the same as the distribution of the population mean.

We assume that $\hat{y}$ is the estimated value of y and that $\hat{y}_b$ represents the mean value of the b-th Bootstrap sample set. Then, the mean and variance equations are

$$\left\{ \hat{y} = \frac{1}{B}\sum_{b=1}^{B}\hat{y}_b, \sigma_{\hat{y}}^{2} = \frac{1}{B-1}\sum_{b=1}^{B}\left(\hat{y}_b - \hat{y}\right)^2. \right. \tag{4}$$

As a result, the confidence interval of the overall mean at the confidence level of $(1-\alpha)\%$ is

$$\left[\hat{y} - u_{1-\alpha/2}\sigma_{\hat{y}}^{2}, \hat{y} + u_{1-\alpha/2}\sigma_{\hat{y}}^{2}\right]. \tag{5}$$

Among them, $u_{1-\alpha/2}$ is the $1-\alpha/2$ percentile of the standard normal distribution.

3.2. Percentile Bootstrap. This method also requires Bootstrap sampling to obtain B Bootstrap sample sets and arrange the sample mean values obtained from each sample set in ascending order. It can get a set of Bootstrap sample means $\hat{y}_b\,(b = 1, 2, 3, \ldots, B)$ with order. Then, the $\alpha/2$-th and $1-\alpha/2$-th points are the upper and lower limits of the confidence interval of the statistics under the $1-\alpha\%$ confidence level; namely,

$$\left[\hat{y}\left(\frac{\alpha}{2}B\right), \hat{y}\left(1-\frac{\alpha}{2}\right)B\right]. \tag{6}$$

3.3. T Percentile Bootstrap. This method is an improved method for percentiles. Generally, this method can get a more accurate confidence interval than the percentile Bootstrap method. It assumes that B Bootstrap sample sets are drawn, and the t statistic is calculated for the mean value of each sample set, as shown in the following formula:

$$t_b^{*} = \frac{\hat{y}_b - \hat{y}}{\sqrt{\operatorname{Var}(y)}}. \tag{7}$$

It also assumes that $\hat{y}$ is the estimated value of y and that $\hat{y}_b$ represents the mean value of the b-th Bootstrap sample set. It arranges the calculated mean values of each Bootstrap sample set in order to obtain the ordered Bootstrap sample set mean $\hat{y}_b\,(b = 1, 2, 3, \ldots, B)$. The corresponding t-statistic sequence is $t_b^{*}\,(b = 1, 2, 3, \ldots, B)$. When the significance level is α, the $\alpha/2$-th and $1-\alpha/2$-th points are $[t^{*}((\alpha/2)B), t^{*}(1-(\alpha/2))B]$, respectively, and the corresponding confidence interval is

$$\left[\hat{y} - t^{*}\left(\frac{\alpha}{2}B\right)\sqrt{\operatorname{Var}(y)}, \hat{y} + t^{*}\left(1-\frac{\alpha}{2}\right)B\sqrt{\operatorname{Var}(y)}\right]. \tag{8}$$

The method proposed in this paper uses the T percentile Bootstrap to refer to the predecessor's processing of the Bootstrap-based neural network interval prediction method in constructing the interval type.

The echo state network structure is simple, and most parameters only need to be randomly initialized. However, this also causes the shortcomings of the model's large randomness, the prediction effect is not stable enough, and most networks do not provide prediction intervals when making time series predictions. In view of the above shortcomings, some scholars integrate the network and make the model construct the prediction interval, which is the ESN integration model based on Bootstrap. This method finally achieved a better prediction effect. In summary, there are two bases for building an ESN integration model based on Bootstrap. One is the method idea of the bagging method. This method is a model integration method. The method is applied to the ESN integration model based on Bootstrap as explained below. The bagging method can effectively improve the stability and accuracy of the model, being especially suitable for input sensitive and random models, such as neural networks. We introduce the ESN integration model based on Bootstrap.

It can be seen from Figure 2 that the core of the model is an integrated body composed of B ESNs. We select M samples and first perform Bootstrap sampling on the original sample set $D_{\text{original}} = \{u(n), t(n)\}_{i=1}^{M}$ composed of noise data during the training process. We get a sample set $D = \{D, D,...,D\}$ consisting of B Bootstrap sample sets, with a total of $B \times M$ samples. Then, each sample subset corresponds to training an echo state network unit, $D_b = \{u_b(n), t_b(n)\}_{i=1}^{M}$ is the training set of the b-th echo state network; $u_b(n)$ is the input of the b-th network; $t_b(n)$ is the expected output value corresponding to the input of the b-th network; $y_b(n)$ is a single network output value driven by $u_b(n)$, which is also an estimate of $y(n)$; and $y(n)$ is the output value of the network integration model. The relevant expressions are summarized as follows:

$$x_b(n) = f^b\left(w_b^{\text{in}} u_b(n) + W_b x_b(n-1)\right), \tag{9}$$

$$\hat{y}_b(n) = \left[u_b(n), x_b(n)\right] w_b^{\text{out}}, \tag{10}$$

$$\hat{y}(n) = \frac{1}{B} \sum_{i=1}^{B} \hat{y}_b(n), \tag{11}$$

$$\sigma_{\hat{y}}^2(n) = E\left[(y(n) - \hat{y}(n))^2\right] \approx \frac{1}{B-1}(y(n) - \hat{y}(n))^2. \tag{12}$$

Equations (9) and (10) are the input and output expressions of a single echo state network. Among them, $x_b(n)$ is the state vector corresponding to the b-th echo state network at any time, w_b^{in} is the input connection vector of the b-th echo state network, W_b is the internal connection matrix of the b-th echo state network, and w_b^{out} is the internal connection matrix of the b-th echo state network. The output connection matrix corresponding to the b echo state networks, $f^b(*) = [f_1^b(*), f_2^b(*), \ldots, f_N^b(*)]$, is the reserve pool neuron activation function, all take the sigmoid function. Equation (11) describes the relationship between the true value estimate and the output value of each echo state network. This is also the key to the application of the bagging method; that is, the overall output of the model is the average output of multiple networks. Equation (12) is the expression of model randomness variance $\sigma_{\hat{y}}^2(n)$. If it is assumed that the echo state network model is the correct model behind the data, the randomness between the estimated value and the true value can be approximated to the randomness between the estimated value and the output of each echo state network.

Although the existing Bootstrap-based ESN ensemble model also has a good performance in the prediction effect, the method of maximizing the marginal likelihood is used in parameter estimation; instead of obtaining the parameters from the posterior distribution of the parameters, the performance of the estimated parameters is limited. Through theoretical study, it is found that there is a parameter estimation method that is more suitable for the model, that is, the parameter estimation method of variational reasoning.

When we set a training sample set, the maximum likelihood estimation can give the optimal parameters under a fixed likelihood distribution. However, when the sample size is small or there are outliers in the sample set, overfitting is easy to occur. The proposal of Bayesian estimation avoids the overfitting problem in principle. Bayesian estimation not only considers a single likelihood distribution, but also considers the prior distribution of the parameters in the model. The following specific expressions illustrate the differences between the two. If Z is the model parameter set and D is the training sample set, the following Bayesian formula can be listed:

$$P(Z|D) = \frac{P(D|Z)P(Z)}{P(D)}. \tag{13}$$

Solving the maximum likelihood estimation is essentially solving the following optimal solution problem:

$$\arg\max_{z} p(D|Z). \tag{14}$$

It can be seen that the above formula does not consider the prior distribution of the parameters, while the Bayesian estimation considers the elements of the entire posterior distribution. The expression for the maximum posterior probability is

$$\arg\max_{z} \frac{P(D|Z)P(Z)}{P(D)}. \tag{15}$$

Since $P(D)$ is a constant, it is not necessary to consider $P(D)$ in the actual calculation, and only the product of the likelihood probability and the prior distribution of the parameter is used to solve the optimal value.

We assume that there is a Bayesian model in which each parameter has a prior probability distribution. These parameters can also have their own distribution parameters. All parameters in the model are recorded as the set Z. Similarly, denote the set of all observed samples as D. We assume that there are n unknown parameters and m observation samples; parameters are independent of each other; and samples are independent of each other. When the parameter set and sample set are represented as $Z = \{z_1, z_2, \ldots, z_n\}$ and $D = \{d_1, d_2, \ldots, d_m\}$, respectively, the probability distribution of the model can be further determined as $P(D, Z)$. The goal is to find an approximation to the posterior probability distribution $P(Z|D)$ and the evidence function $P(D)$. According to Bayesian formula and decomposing $P(D)$, there is the following formula:

$$\ln P(D) = \ln \frac{P(D,Z)}{Q^*(Z)} - \ln \frac{P(Z|D)}{Q^*(Z)}. \tag{16}$$

Among them, $Q^*(Z)$ is the joint probability distribution of the parameters to be estimated. When both sides of the equation are averaged for $Q^*(Z)$, we can get

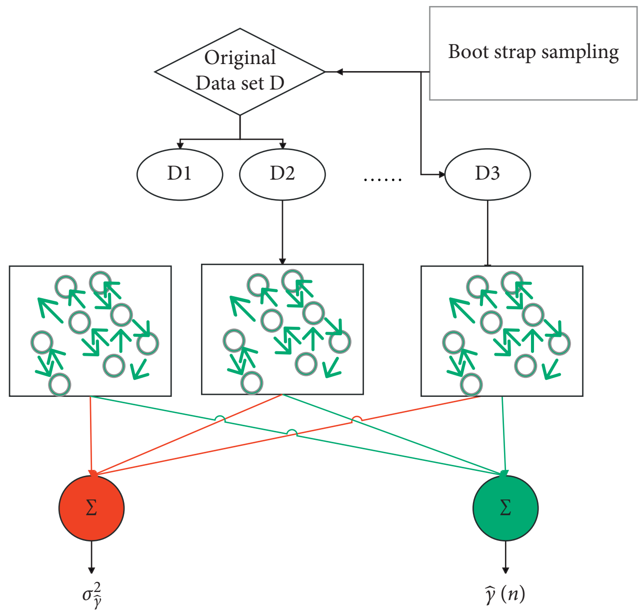

FIGURE 2: ESN integration model based on Bootstrap.

$$\int Q^*(Z)\ln P(D)dZ = \int Q^*(Z)\ln\frac{P(D,Z)}{Q^*(Z)}dZ - \int Q^*(Z)\ln\frac{P(Z|D)}{Q^*(Z)}dZ = \ln P(D). \tag{17}$$

The terms in the formula can be replaced by the following formula:

$$\begin{cases} L(Q) = \int Q^*(Z)\ln\dfrac{P(D,Z)}{Q^*(Z)}dZ, \\ KL(Q\|P) = -\int Q^*(Z)\ln\dfrac{P(Z|D)}{Q^*(Z)}dZ. \end{cases} \tag{18}$$

Then, the following expression is obtained:

$$\ln P(D) = L(Q) + KL(Q\|P), \tag{19}$$

In the formula, $L(Q)$ is called the lower variational bound, and $KL(Q\|P)$ is called the KL divergence, which represents the degree of similarity between the distribution Q and the distribution P, with the value being greater than zero. When $L(Q)$ is larger, $KL(Q\|P)$ is smaller, and when $KL(Q\|P)$ reaches its minimum value, there is $Q^*(Z) = P(Z|D)$. At this time, the posterior distribution of the parameters can be approximated by $KL(Q\|P)$. According to the mean field theory, the parameter distribution is divided into the following forms:

$$Q^*(Z) = \prod_{i=1}^{n} Q_i^*(Z_i). \tag{20}$$

$Q_i^*(Z_i)$ is a certain type of distribution, such as normal distribution and gamma distribution, and the parameter distributions are independent of each other. The average field theory is derived from physics. It is a method of collectively processing the effects of objects in the environment and replacing individual effects with average effects. Through this kind of thinking, complex problems can be simplified. Below, by substituting (20) into $L(Q)$, the following derivation process can be obtained:

$$\begin{aligned} L(Q) &= \int \prod_i Q_i^*(Z_i)\left\{\ln P(D,Z) - \sum_i \ln Q_i^*(Z_i)\right\}dZ \\ &= \int Q_i^*(Z_i)\left\{\ln P(D,Z) - \prod_{i\neq j} Q_i^*(Z_i)dZ_i\right\}dZ_i - \int Q_i^*(Z_i)\ln Q_j^*(Z_j)dZ_j \\ &= \int Q_i^*(Z_i)\ln \tilde{P}(D,Z)dZ_j - \int Q_j^*(Z_j)\ln Q_i^*(Z_i)dZ_j + \text{const.} \end{aligned} \tag{21}$$

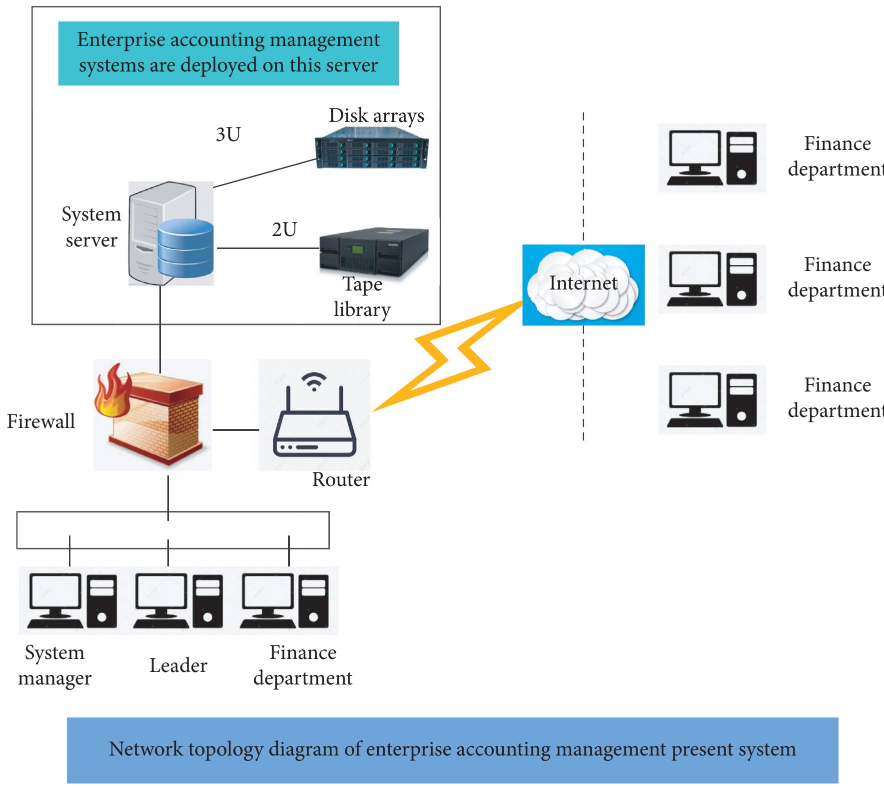

FIGURE 3: Computerized intelligent accounting system based on big data technology.

Among them, *const* is a constant term, and $\widetilde{P}(D,Z)$ is a newly defined distribution, which represents the result distribution of integrating other parameters except Z in the joint probability distribution $\widetilde{P}(D,Z)$. The expression is written as follows:

$$\ln \widetilde{P}(D,Z) = E_{i\neq j}[\ln P(D,Z)] + \text{const}. \tag{22}$$

Among them, $E_{i\neq j}[\ldots]$ means that P (D, Z) integrates the parameters of all $Z\,(i\neq j)$, which is the expectation, which is specifically expressed as

$$E_{i\neq j}[\ln P(D,Z)] = \int \ln P(D,Z)\prod_{i\neq j} Q_i^*(Z_i)\mathrm{d}Z_i. \tag{23}$$

It can be seen in (21) that $L(Q)$ is the negative value of the KL divergence between $Q_j^*(Z_j)$ and $P(D,Z_j)$. Therefore, maximizing L (Q) is equivalent to minimizing KL divergence. The smaller the KL divergence, the closer the two distributions are. Note that there is only parameter Zj in the distribution on the left side of (22). The general expression of $Q_j^*(Z_j)$ can be obtained as follows:

$$\ln Q_j^*(Z_j) = E_{i\neq j}[\ln P(D,Z)] + \text{const}. \tag{24}$$

In the formula, $E_{i\neq j}[\ln P(D,Z)]$ can be derived from the joint probability distribution of each parameter, then the distribution form of $Q_j^*(Z_j)$ is determined according to the form of the derivation result, and then the corresponding iterative formula is obtained through coefficient equivalence.

4. Computerized Intelligent Accounting System Based on Big Data Technology

The design goal of the enterprise accounting budget management system is that the system can efficiently complete the enterprise cost budget accounting work after the design is completed and ensure the normal and stable progress of the enterprise cost budget accounting work. This article combines big data technology to build a computerized intelligent accounting system based on big data technology, as shown in Figure 3.

The system structure diagram is shown as in Figure 4.

It can be seen from Figure 4 that the enterprise accounting management system is mainly divided into three levels, namely, the view layer, the logic layer, and the database layer.

The mechanism diagram of the system is shown in Figure 5.

In the enterprise accounting management system, because there are so many attributes of all entities, only a part of it is shown in the E-R diagram. According to the business process, the E-R diagram between each entity can be obtained, as shown in Figure 6.

Real-time accounting information system analysis is embodied in the processing of data. For real-time information system construction, it is the study of real-time database construction. After the data is stored in the database, the database is further divided into a model library, a knowledge base, and a method library. At the

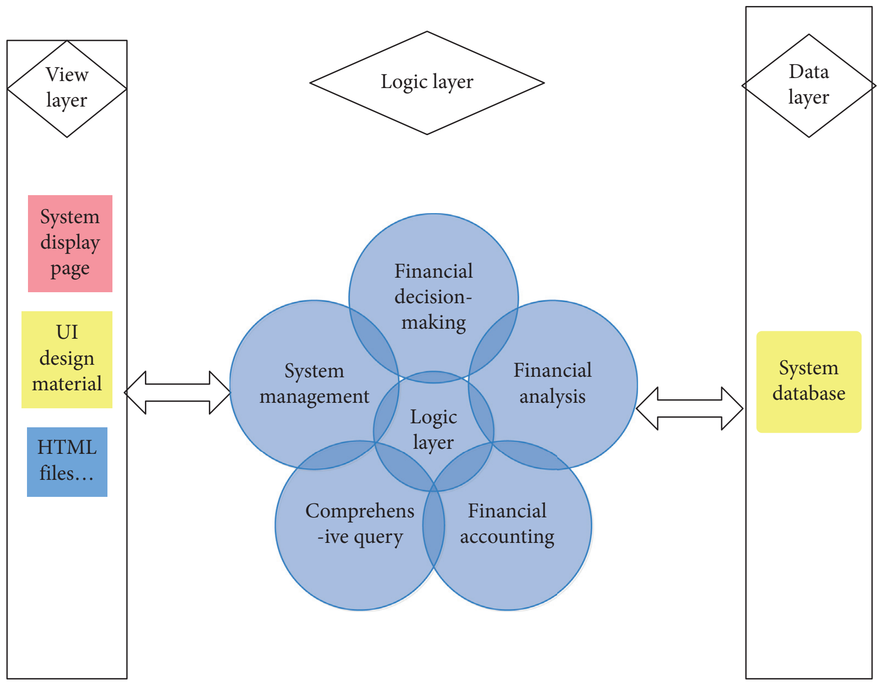

Figure 4: System architecture diagram.

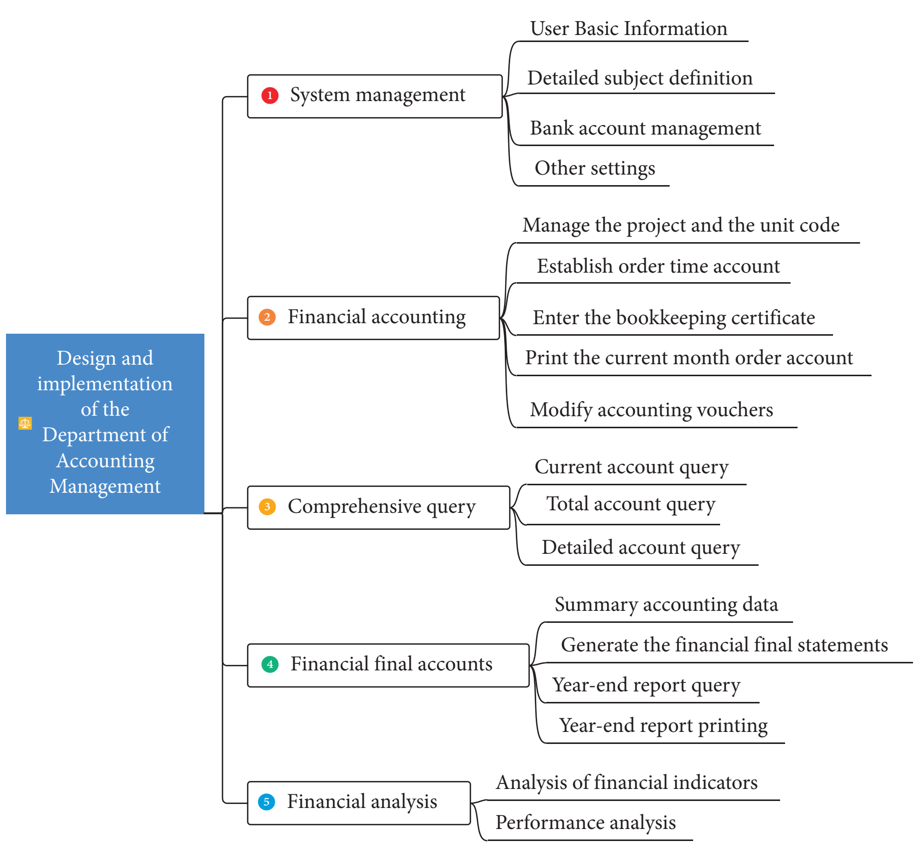

Figure 5: System function structure diagram.

same time, a series of data processing rules and standardized procedures are set for data extraction, transformation, and loading processing, which are loaded into the metadata database and data warehouse. Furthermore, when the system output interface has relevant command requirements, certain data analysis is performed to obtain the required view. The real-time database model is shown in Figure 7.

Figure 6: E-R diagram of the accounting management system.

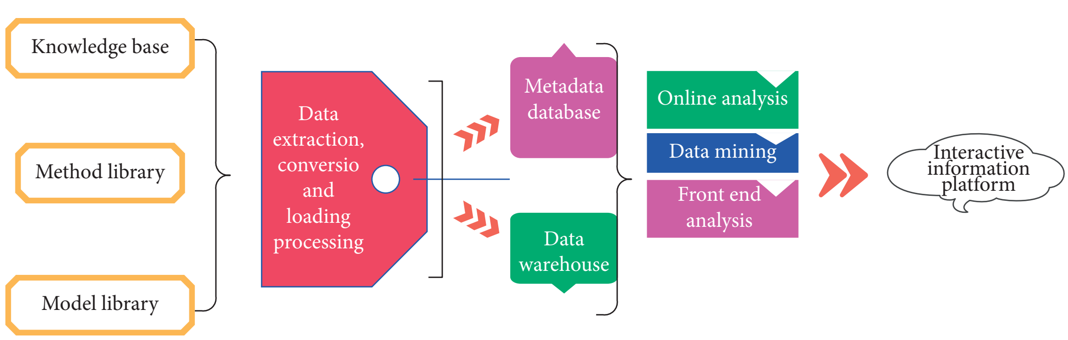

Figure 7: Real-time database model diagram.

In order to rationally allocate corporate resources, optimize business processes, and reduce human resource costs, its profound connotation lies in the use of network and computer technology to centralize management, optimize configuration, and monitor feedback to realize data sharing and gradually realize the reform of enterprise information system processes. After the above logical design is completed, it is necessary to design the physical storage process of the data, that is, the actual application of the above process, which will not be described here. The final construction system is shown in Figure 8.

After constructing the above accounting information system, this paper conducts performance verification of the system. Moreover, this article combines the accounting requirements under the background of big data to analyze the system performance. In addition, this paper conducts data mining through multiple sets of data from a certain company, conducts intelligent accounting to calculate the effects of data mining and intelligent accounting, and evaluates them, and the test results shown in Table 1 and Figure 9 are obtained.

Through the above experimental research, it can be verified that the computerized intelligent accounting system

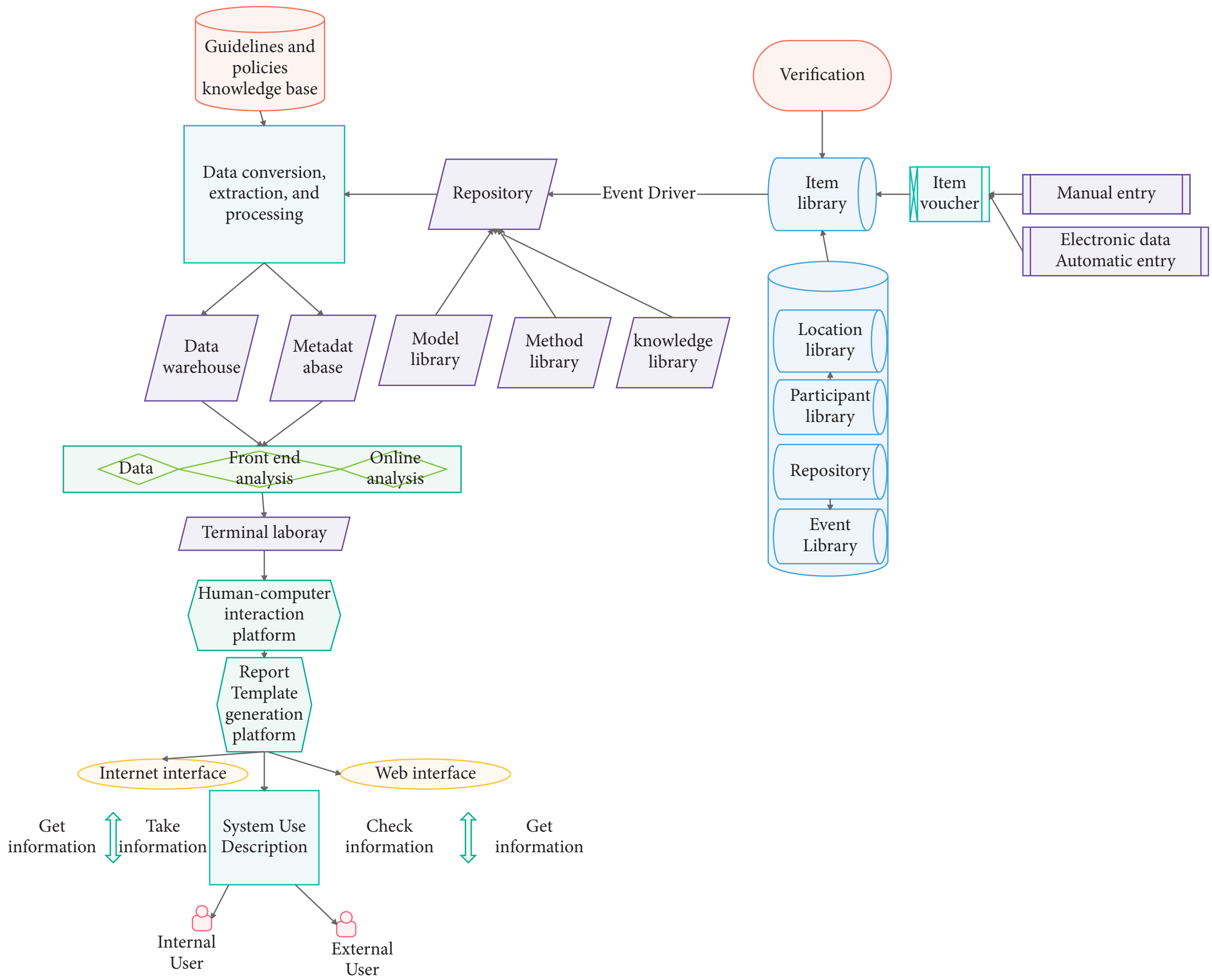

FIGURE 8: Structure diagram of accounting information system.

TABLE 1: Performance statistics of the computerized intelligent accounting system based on big data analysis.

No.	Data mining	Smart accounting	No.	Data mining	Smart accounting	No.	Data mining	Smart accounting
1	89.02	89.29	23	96.34	85.74	44	93.76	79.48
2	96.45	89.56	24	90.21	83.36	45	93.16	87.05
3	96.78	79.02	25	94.55	82.22	46	91.12	89.31
4	92.75	86.04	26	95.84	87.27	47	90.04	84.61
5	94.32	89.74	27	93.98	90.79	48	89.47	84.07
6	91.46	84.60	28	92.67	87.88	49	95.02	89.98
7	96.70	88.04	29	94.32	85.93	50	96.03	84.13
8	90.83	88.87	30	89.27	89.17	51	94.94	84.25
9	94.66	85.64	31	92.57	81.79	52	91.92	79.25
10	93.02	85.88	32	95.00	87.25	53	93.33	82.07
11	94.65	86.72	33	94.85	84.83	54	91.17	85.12
12	92.74	88.20	34	94.10	81.43	55	91.35	85.26
13	96.23	84.23	35	91.85	88.30	56	89.81	83.56
14	88.96	86.47	36	91.07	84.53	57	93.84	84.47
15	89.99	80.85	37	96.45	86.46	58	93.47	88.16
16	90.97	80.15	38	94.44	87.18	59	90.67	81.74
17	93.36	85.85	39	88.60	80.73	60	88.15	86.73
18	95.65	79.50	40	92.05	84.98	61	90.37	81.44
19	89.25	87.48	41	93.07	83.76	62	88.87	85.27
20	93.40	87.14	42	96.45	87.91	63	92.68	85.75
21	91.13	87.37	43	89.98	81.67	64	93.88	90.69
22	91.97	79.52						

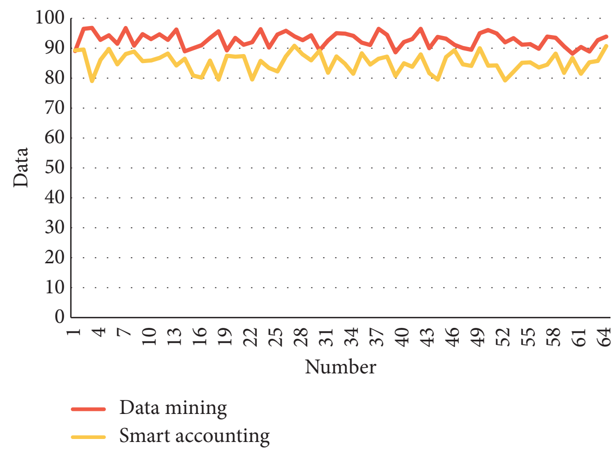

Figure 9: Statistical diagram of system experiment data.

based on big data technology constructed in this article has a certain effect.

5. Conclusion

Because the financial informatization system and business informatization system are generally constructed in batches and by departments and there is also a lack of unified strategic planning during the construction, most enterprises' financial informatization and business informatization are in a state of disconnected systemic management. At the same time, the issue of corporate "information islands" has also emerged. During the promotion of management accounting, due to the lack of support from a unified information system, the integration of business and finance has become an empty talk, and the manual management model has made it difficult for management accounting tools to exert their value. With the continuous development of enterprises, business and financial conflicts and contradictions have become increasingly prominent. Moreover, the business always ignores the company's financial system regulations for various reasons and goes beyond the company's system and financial discipline in daily business activities. Finance, of course, always carries the banner of internal risk control, uses excessive supervision powers to prevent audit and supervision risks, and dictates specific business activities, which makes it difficult to implement some special businesses and even causes companies to miss development opportunities. This article combines the big data technology to construct the accounting computerization system, obtains the scientific and effective accounting information processing results through intelligent big data processing, and improves the accounting management efficiency on this basis. The experimental research results show that the computerized intelligent accounting system based on big data technology constructed in this paper has a certain effect.

Data Availability

The labeled datasets used to support the findings of this study are available from the corresponding author upon request.

Conflicts of Interest

The authors declare no conflicts of interest.

Acknowledgments

This study was sponsored by Tangshan Normal University.

References

[1] P. Rajsic, A. Weersink, A. Navabi, and K. P. Pauls, "Economics of genomic selection: the role of prediction accuracy and relative genotyping costs," *Euphytica*, vol. 210, no. 2, pp. 1–18, 2016.

[2] F. Jahedpari, T. Rahwan, S. Hashemi et al., "Online prediction via continuous artificial prediction markets," *IEEE Intelligent Systems*, vol. 32, no. 1, pp. 61–68, 2017.

[3] V. Daksiya, H. T. Su, Y. H. Chang, and E. Y. M. Lo, "Incorporating socio-economic effects and uncertain rainfall in flood mitigation decision using MCDA," *Natural Hazards*, vol. 87, no. 1, pp. 515–531, 2017.

[4] S. Lahmiri, "A variational mode decompoisition approach for analysis and forecasting of economic and financial time series," *Expert Systems with Applications*, vol. 55, no. 8, pp. 268–273, 2016.

[5] N. Gordini, "A genetic algorithm approach for SMEs bankruptcy prediction: empirical evidence from Italy," *Expert Systems with Applications*, vol. 41, no. 14, pp. 6433–6445, 2014.

[6] A. Ferramosca, A. H. González, D. Limon, and D. Limon, "Offset-free multi-model economic model predictive control for changing economic criterion," *Journal of Process Control*, vol. 54, no. 3, pp. 1–13, 2017.

[7] C. J. A. Jane, "Hybrid model combined grey prediction and autoregressive integrated moving average model for talent

prediction," *Journal of Grey System*, vol. 21, no. 2, pp. 91–102, 2018.

[8] N. A. Khadjeh, S. Aghabozorgi, W. T. Ying, and D. C. L. Ngo, "Text mining for market prediction: a systematic review," *Expert Systems with Applications*, vol. 41, no. 16, pp. 7653–7670, 2014.

[9] M. Ellis and P. D. Christofides, "Integrating dynamic economic optimization and model predictive control for optimal operation of nonlinear process systems," *Control Engineering Practice*, vol. 22, no. 1, pp. 242–251, 2014.

[10] W. Schultz, W. R. Stauffer, and A. Lak, "The phasic dopamine signal maturing: from reward via behavioural activation to formal economic utility," *Current Opinion in Neurobiology*, vol. 43, no. 5, pp. 139–148, 2017.

[11] W. Montford and R. E. Goldsmith, "How gender and financial self-efficacy influence investment risk taking," *International Journal of Consumer Studies*, vol. 40, no. 1, pp. 101–106, 2016.

[12] W. S. Muthii, J. G. Wanjohi, and J. M. Ndambiri, "The effect of financial risk management on the financial performance of commercial banks in Kenya," *International Journal of Finance and Banking Research*, vol. 3, no. 5, pp. 70–81, 2017.

[13] J. Magendans, J. M. Gutteling, and S. Zebel, "Psychological determinants of financial buffer saving: the influence of financial risk tolerance and regulatory focus," *Journal of Risk Research*, vol. 20, no. 8, pp. 1076–1093, 2017.

[14] E. S. Cole, D. Walker, A. Mora, and M. L. Diana, "Identifying hospitals that may be at most financial risk from medicaid disproportionate-share hospital payment cuts," *Health Affairs*, vol. 33, no. 11, pp. 2025–2033, 2014.

[15] A. Zalik, "Resource sterilization: reserve replacement, financial risk, and environmental review in Canada's tar sands," *Environment and Planning: Economy and Space*, vol. 47, no. 12, pp. 2446–2464, 2015.

[16] C. Lucarelli, P. Uberti, and G. Brighetti, "Misclassifications in financial risk tolerance," *Journal of Risk Research*, vol. 18, no. 4, pp. 467–482, 2015.

[17] E. Y. Chan, "Physically-attractive males increase men's financial risk-taking," *Evolution and Human Behavior*, vol. 36, no. 5, pp. 407–413, 2015.

[18] T. West and A. C. Worthington, "Macroeconomic conditions and Australian financial risk attitudes, 2001-2010," *Journal of Family and Economic Issues*, vol. 35, no. 2, pp. 263–277, 2014.

[19] T. K. Scharding, "Imprudence and immorality: a kantian approach to the ethics of financial risk," *Business Ethics Quarterly*, vol. 25, no. 2, pp. 243–265, 2015.

[20] J. Su and E. Furman, "A form of multivariate pareto distribution with applications to financial risk measurement," *ASTIN Bulletin*, vol. 47, no. 1, pp. 331–357, 2017.

[21] L. John, "Luck, Justice and systemic financial risk," *Journal of Applied Philosophy*, vol. 34, no. 3, pp. 331–352, 2017.

Hindawi
Scientific Programming
Volume 2021, Article ID 5382868, 10 pages
https://doi.org/10.1155/2021/5382868

Research Article

Logistics Distribution Location Algorithm Based on Improved Imperial Competition Algorithm

Kaituo Su

Department of Management, Shaanxi Railway Institute, Weinan, Shaanxi 714099, China

Correspondence should be addressed to Kaituo Su; sktsxriglxy@163.com

Received 24 October 2021; Revised 4 November 2021; Accepted 16 November 2021; Published 8 December 2021

Academic Editor: Le Sun

To solve the problems of warehouse explosion and delay of logistics distribution network under the sudden explosion of demand on “double 11” and “618,” this paper proposes a logistics distribution network location algorithm that can consider reliability, green environmental protection, and path optimization. Firstly, the transportation model of logistics distribution network location-route optimization is established. Under the condition that the transportation model satisfies the vehicle path reliability constraint, it can minimize the total cost, including logistics distribution cost, transportation oil consumption, and CO_2 emission cost. This paper designs an improved imperial competition algorithm to solve it according to the characteristics of the transportation model. Firstly, the competition mechanism of “United Lian Heng” was introduced in the initial national stage, enhancing the information exchange and retaining the superior population. Secondly, in the process of empire assimilation, we can learn from the colonial rule strategy, which is gradually infiltrated and assimilated by all levels of the country to enhance the development ability of the algorithm. Finally, the algorithm designs a mechanism to judge and jump out of local optimum, so as to avoid “premature” affecting the optimization performance. The rationality of the model and the effectiveness of the improved imperial competition algorithm are verified by simulation experiments of different scales, while the influence of reliability level is analyzed. Experimental results show that the proposed method can effectively solve problems of different scales and maintain stable performance under different reliability levels. Moreover, its algorithm performance is better than that of the standard imperial competition algorithm.

1. Introduction

Under the background of regional economic integration and Internet, e-commerce logistics and distribution have developed rapidly. Its characteristics are as follows: (1) facing many customers with small demand, rich varieties, and scattered locations directly, the e-commerce logistics system is complex and costly [1] and (2) customer demand is subject to dynamic fluctuations due to factors such as season, weather, holidays, promotion means, and product life cycle. There is even a sudden surge (“double 11” and “618”). Faced with this kind of disturbance, the resources of each site in the distribution network cannot be accurately balanced. This leads to the phenomena of product explosion and delay, and the risk resistance is poor [2–4]. The distribution network is the foundation of the logistics distribution system. Reasonable distribution center location and vehicle route planning play an important role in the effective operation of the distribution system [5]. The location routing problem (LRP) integrates both the location problem and the vehicle routing optimization problem [6]. Researchers have studied various LRP problems and their extensions. Michael et al. summarized the related research of LRP in recent years in detail from different angles, including standard LRP, and various extended problems such as multistage LRP, multicycle LRP, and multiobjective LRP [7].

With the enhancement of environmental protection consciousness, people began to pay attention to the environmental pollution caused by CO_2 emission in the process of logistics and distribution. Green logistics distribution system design is of great significance to the development of sustainable logistics. There is much research on green LRP.

In order to minimize the energy cost related to transportation, Benotmane et al. considered the two-level location routing problem. Genetic algorithm and dynamic island model are used to optimize the green LRP problem. The green LRP problem is a combination of the classical location routing problem and the pollution routing problem. This method can minimize energy costs and carbon dioxide emissions [8]. Wang et al. used an ecological package to optimize the location of green logistics. The pickup and delivery of small eco-packages are established through a cost-minimized synchronous orientation routing model, which is very important for transporting large eco-packages. It is modeled by resource sharing state-time discrete transportation centralized network flow programming in the spatiotemporal network. For the pickup and delivery of small eco-packages, the cost-minimization synchronous guidance positioning path model is adopted [9]. Dukkanci et al. studied the green LRP problem, established a single objective optimization model, minimized the operation cost and emission cost, and considered the time window constraint [10]. Zhang et al. designed a time-dependent green location path problem model with time windows. The model minimizes costs, including the cost of opening warehouses, the cost of starting vehicles, and the cost of fuel consumption [11]. However, the above research does not consider the security problem.

Currently, people pay more and more attention to the security of various systems. Interference inside or outside the distribution system will bring interruption risk to the system, thus affecting the normal operation of the system. Therefore, it is of practical significance to design a safe logistics distribution system. Recently, some scholars have done some research on reliability LRP considering interruption. Raziez et al. designed an LRP model with three types of interruptions in view of the high possibility of interruption of route capacity. According to the NP-hard property of the model, a genetic algorithm is proposed to solve the large-size problem [12]. Badakhshian et al. considered labor interruption or failure caused by bad weather conditions and designed a reliable logistics network by strengthening existing facilities and defining standby facilities to avoid interruption. They proposed a column generation method to model and solve all three logistics problems [13]. Considering the interruption risk of the distribution center, Huang et al. studied the reliable fourth-party logistics routing problem in network design. They established a scenario-based integer programming model to locate the distribution center and minimize the total cost of the proposed problem [14]. In order to make the network resist interruption, Dehghan et al. added interruption in the design stage of the network to reduce the impact of the disaster on LRP. They put forward a mixed-integer programming model. In the supply chain distribution network, the model formulated the reliable capacity positioning path problem with synchronous delivery and service delivery [15]. However, so far, the LRP problem considering the reliability of CO_2 emission has been less studied.

Considering reliability and green environmental protection, this paper studies the location path optimization problem of reliable green logistics distribution in order to deal with the warehouse explosion and delay of logistics distribution network under the sudden demand explosion of "double 11" and "618." Different from the existing research on LRP, this paper calculates the fuel consumption and CO_2 emission cost based on the network for transport and environment (NTM) method and defines the vehicle routing reliability. This algorithm aims at minimizing the total cost and establishing the logistics distribution location routing optimization model with vehicle routing reliability constraints, designing an improved imperial competition algorithm to solve the transportation model. The improved algorithm explores and solves the problems that the original imperial competitive algorithm (ICA) is greatly influenced by the initial country, lacking effective information interaction between empires. The algorithm is easy to be collected and can be collected early. Finally, the rationality of the model and the effectiveness of the algorithm are verified by experiments.

2. Problem Description and Model Establishment

As shown in Figure 1, the logistics distribution network includes distribution centers, customers, distribution vehicles, and distribution lines. Starting from the distribution center, vehicles are distributed by different customers in turn and then returned to the distribution center. In reality, due to the influence of uncertain factors, distribution centers and transportation routes may be interrupted. The interruption will affect the normal operation of the distribution system. In addition, oil consumption and CO_2 emission during transportation will cause environmental pollution. The problem of location-route optimization of reliable green logistics distribution can minimize the total logistics cost, fuel consumption, and CO_2 emission costs by selecting and opening distribution centers and optimizing the driving routes of different vehicles and at the same time satisfy the constraints of vehicle route reliability.

The model assumes the following conditions. (1) The location, quantity, and demand of customer points are known. (2) The location, quantity, opening cost, capacity, and interruption probability of distribution centers are known. (3) The distance between any two points and the probability of interruption are known. (4) The types of vehicles are different and the number is known, and the fixed operation cost, transportation capacity, transportation cost per unit distance, empty and full fuel consumption of each vehicle are known. (5) At any customer point, only one car must pass. (6) Each vehicle can only start from one distribution center and return to the distribution center. Each distribution center allows multiple vehicles to exit and enter.

2.1. Symbols and Variables. The model symbols are defined as follows:

I: collection of customer points.

J: collection of distribution centers.

$O = I \cup J$.

S: vehicle collection.

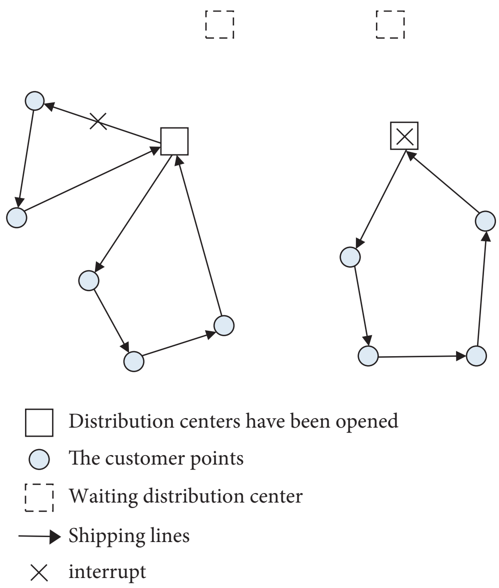

Figure 1: Distribution network system.

D_i: the demand of customer point $i \in I$.

R_j: fixed opening cost of distribution center $j \in J$.

A_j: the capacity of distribution center $j \in J$.

P_j: the interruption probability of distribution center $j \in J$.

H_s: fixed operating cost of vehicle $s \in S$.

T_s: transport capacity of vehicle $s \in S$.

TC_s: transportation cost per unit distance of vehicle $s \in S$.

FC_s^{empty}: empty fuel consumption of vehicle $s \in S$.

FC_s^{full}: full-load fuel consumption of vehicle $s \in S$.

e: cost coefficient of oil consumption and CO_2 emission.

D_{il}: the distance from point $i \in O$ to point $l \in O$.

p_{il}: the interruption probability of the line between point $i \in O$ and point $l \in O$.

τ: operating period ($\tau = 365$).

Decision variables are defined as follows:

$$u_{ilk} = \begin{cases} 1, & \text{vehicle } s \in S \text{ from } i \in O \text{ to } l \in O, \\ 0, & \text{else,} \end{cases} \quad (1)$$

$$v_{jk} = \begin{cases} 1, & \text{vehicle } s \in S \text{ to the distribution center } j \in J, \\ 0, & \text{else,} \end{cases} \quad (2)$$

$$w_j = \begin{cases} 1, & \text{Open a distribution center } j \in J, \\ 0, & \text{else.} \end{cases} \quad (3)$$

$fc_{ilk} \geq 0$ indicates the traffic volume of vehicle $s \in S$ between point $i \in O$ and point $l \in O$.

Let $U = \{u_{ilk} | \forall i, l \in O, s \in S\}$, $V = \{v_{jk} | \forall j \in J, \forall s \in S\}$, $W = \{w_j | \forall j \in J\}$.

2.2. Optimization Model. Based on the above symbols and variable definitions, a reliable green logistics distribution network location-path model is established as follows:

$$\min f(U,V,W) = \sum_{j\in J} R_j w_j + \sum_{s\in S}\sum_{j\in J} H_s v_{js} + \tau\left(\sum_{i\in O}\sum_{l\in O}\sum_{s\in S} \mathrm{TC}_s D_{il} u_{ils} + \sum_{i\in O}\sum_{l\in O}\sum_{s\in S} \mathrm{FC}_{ils} D_{il} u_{ils} e\right), \quad (4)$$

$$\prod_{j\in J}(1-P_j)v_{js}\prod_{i\in O}\prod_{l\in O}(1-p_{il})u_{ils} \geq \alpha, \quad \forall s \in S, \quad (5)$$

$$\sum_{i\in I} u_{jis} - v_{js} = 0, \quad \forall j \in J, \forall s \in S, \quad (6)$$

$$\sum_{s\in S}\sum_{i\in I} u_{jik} - w_j \geq 0, \quad \forall j \in J, \quad (7)$$

$$\sum_{i\in I} u_{jik} - w_j \leq 0, \quad \forall j \in J, \forall s \in S, \quad (8)$$

$$\sum_{l\in O} u_{lis} - \sum_{l\in O} u_{ils} = 0, \quad \forall i \in O, \forall s \in S, \quad (9)$$

$$\sum_{i\in M}\sum_{i\in M} u_{ils} \leq |M| - 1, \quad \forall M \subseteq I, |M| \geq 2, \forall s \in S, \quad (10)$$

$$\sum_{j\in J}\sum_{i\in I} u_{jis} \leq 1, \quad \forall s \in S, \quad (11)$$

$$\sum_{s\in S}\sum_{l\in O} u_{ils} = 1, \quad \forall i \in I, \quad (12)$$

$$\sum_{s\in S} u_{jls} = 0, \quad \forall j, l \in J, \quad (13)$$

$$\sum_{i\in I}\sum_{l\in O} d_i u_{ils} \leq T_s, \quad \forall s \in S, \quad (14)$$

$$\sum_{s\in S}\sum_{i\in I}\sum_{l\in O} d_i u_{ils} v_{js} \leq A_j, \quad \forall j \in J, \quad (15)$$

$$\sum_{s\in S}\sum_{l\in O} fc_{lis} - \sum_{s\in S}\sum_{l\in O} fc_{ils} = d_i, \quad \forall i \in I, \quad (16)$$

$$d_i u_{ils} \leq f_{ils} \leq (T_s - d_l) x_{ils}, \quad \forall i, l \in O, \forall s \in S, \quad (17)$$

$$u_{ils} \in \{0,1\}, \quad \forall i, l \in O, \forall s \in S, \quad (18)$$

$$v_{js} \in \{0,1\}, \quad \forall j \in J, \forall s \in S, \quad (19)$$

$$w_j \in \{0,1\}, \quad \forall j \in J, \quad (20)$$

$$fc_{ils} \geq 0, \quad \forall i, l \in O, \forall s \in S. \quad (21)$$

The objective function (4) minimizes the total cost, including the opening cost of the distribution center, the fixed operation cost of the vehicle, the transportation cost, the transportation oil consumption, and the CO_2 emission cost, where FC_{ils} represents the transportation fuel consumption of vehicle s on the line between point $i \in O$ and point $l \in O$. Formula (5) is the path reliability constraint of the vehicle s, where the reliability of the vehicle path is defined as the probability that the path keeps running normally. α is the required reliability level. Constraint (6) indicates that vehicle s is assigned to distribution center j. Constraint (7) means that vehicles must leave the distribution center. Constraint (8) means that if the distribution center is not opened, no vehicles will leave. Constraint (9) means that the vehicle enters from a point but exits from that point; that is, the path is guaranteed to be a loop. Constraint (10) avoids the formation of subloops between various customer points. Constraint (11) ensures that each vehicle can only exit from one distribution center at most. Constraint (12) ensures that each customer point must have one and only one vehicle service. Constraint (13) requires no vehicle route between any two distribution centers. Constraint (14) represents the capacity constraint of the vehicle. Constraint (15) indicates the capacity constraint of the distribution center. Formula (16) represents the balance constraint of flow at both ends of the customer point. Formula (17) represents the upper limit and lower limit constraint of line flow between two points. Formulas (18)–(20) are binary variable constraints. Formula (21) is the nonnegative constraint of flow between two points.

2.3. Calculation of Transportation Oil Consumption. In this paper, the network for transport and environment (NTM) method is used to calculate the fuel consumption of transport vehicles. Based on the NTM method, the fuel consumption of transport vehicles can be calculated by

$$FC(lc) = FC^{\text{empty}} + \left(FC^{\text{full}} - FC^{\text{empty}}\right) \cdot lc, \tag{22}$$

where FC^{empty} is the fuel consumption of unloaded vehicles. FC^{full} is the fuel consumption of fully loaded vehicles. lc is the load coefficient.

The transportation fuel consumption FC_{ils} of the vehicle between the lines between point $i \in O$ and point $l \in O$ is

$$FC_{ils} = FC_s^{\text{empty}} + \left(FC_s^{\text{full}} - FC_s^{\text{empty}}\right) \frac{fc_{ils}}{T_s}. \tag{23}$$

3. Logistics Distribution Location Algorithm Based on Improved Imperial Competition Algorithm

The location-routing problem of reliable green logistics distribution is an extension of the classical LRP problem. Thus, it is also an NP-hard problem. When the scale is large, it is difficult to solve the problem. Thus an intelligent optimization algorithm is designed. In view of the characteristics of the problem model, this paper designs an improved imperial competitive algorithm (IICA) to solve the problem based on the competitive hegemony of vassal states in the Spring and Autumn period and the Warring States period in Chinese history. The IICA algorithm explores and solves the problems that the original ICA is greatly influenced by the initial country, the lack of effective information exchange between empires, and the easy early collection and early collection.

3.1. Historical Background of Spring and Autumn Period and the Warring States Period. The Spring and Autumn period (770 BC–221 BC) is also called the Eastern Zhou Dynasty. In the early Zhou Dynasty, the Zhou Dynasty divided the imperial clan and heroes into strategic places or around the royal family to fulfill the duties of screening the royal family and expanding the territory, thus forming thousands of vassal states. At the beginning of the Spring and Autumn period, Ping Wang moved to Luoyang, and Zhou Shi began to decline. Because of the different social and economic conditions, the situation of competing for hegemony among countries in the Central Plains gradually appeared. Relying on powerful political and military forces, big countries constantly embezzled and annexed small countries and strengthened their sphere of influence. Small countries also tried to gain a certain living space by means of reform and merger. After two or three hundred years, to the late Spring and Autumn period, only a few dozen larger vassal states remained. During the Warring States period, the pattern of hegemony was formed until Qin destroyed the six countries and unified the world.

During this historical period, a peculiar diplomatic strategy came into being “uniting Lian Heng.” That is, in the process of national struggle, weaker countries unite with each other to resist the invasion of powerful countries in order to survive. Once the resistance failed, they took refuge in the powerful countries in order to protect themselves, forming the “vertical” strategy of “uniting the weak to attack the strong” and the “horizontal” strategy of “uniting the strong to attack the weak.”

3.2. Improved Imperial Competition Algorithm. Imperial competition algorithm is an intelligent optimization algorithm based on social and political evolution proposed by Atashpaz-Gargari and Lucas. The algorithm can solve the optimization problem by simulating the competition process of imperialist colonies in human society. The ICA algorithm has been applied to solve problems in different fields, such as traveling salesman problem, static synchronous compensator design problem, flexible job shop scheduling problem, and mixed-flow bilateral assembly line balancing problem. The performance of the algorithm has been verified in application. The basic process of ICA can be summarized into four processes: national initialization, colonial assimilation, imperial competition, and national convergence.

ICA simulates the imperial competition mechanism and realizes the optimization ability by approaching the nonoptimal solution to the optimal solution, updating the position of the optimal solution, and competing for convergence [16]. On that basis of retaining the core idea of

ICA, IICA proposes three improvement measures, and the specific steps are as follows:

(1) Initialization settings, including the initial number of countries N_{cou}, number of empires N_{suz}, number of colonies N_{col}, movement parameter values α, and number of iterations.

(2) The initial countries are randomly generated, and the strong country and the weak country are distinguished according to the normalized power value. The strong countries are directly retained, and the weak countries jointly generate a new country. The size of the power value of the new country will determine whether it will replace the existing powerful country or be eliminated, and the remaining country will enter the imperial competition.

(3) The most powerful N_{suz} countries served as suzerainties to form empires and occupy a corresponding proportion of colonies. The eigenvectors of each colony in the empire move closer to the eigenvectors corresponding to the suzerain. If the colonial power value is greater than the suzerain in the moving process, other colonies will move to the new suzerain instead.

(4) By calculating the total normalized power value of the empire, the weakest colony of the weakest empire will be occupied by other empires, and the occupation probability is directly proportional to the imperial power. The empire with zero colonies will be eliminated and destroyed.

(5) If the same optimal value appears continuously, judge whether it falls into local optimum, and get out of trouble according to the set jump-out scheme.

(6) Iterate until the set maximum number of iterations is reached.

The flow of the improved algorithm is shown in Figure 2.

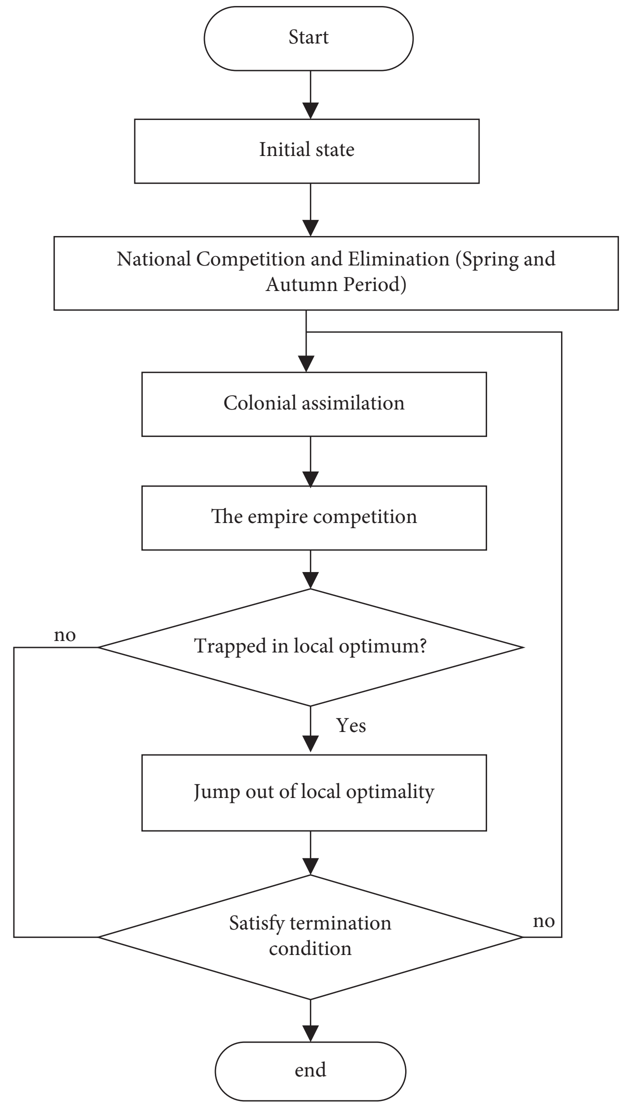

Figure 2: The process of IICA process.

3.2.1. Improve the Initial State Generation Mechanism. It is difficult to guarantee the quality and stability of the population because the initial country is randomly generated according to the principle analysis of ICA. Based on the historical situation of the elimination of vassal states in the Spring and Autumn period and the Warring States period, this paper attempts a new initial state generation mechanism.

At the beginning of the algorithm, a large number of countries are randomly generated, which is generally 2~4 times the number of ICA countries, so that countries with better quality can be retained through competitive screening, and the complexity and operation efficiency of the algorithm will not be greatly affected. Among them, some countries with strong power are retained, while the remaining relatively weak countries avoid elimination via uniting with other countries to strengthen their power in order to protect themselves. Specific steps are as follows:

(1) A certain number of countries are selected randomly.

(2) Calculate the power of each country and obtain the weight.

(3) Take the location information of each country according to the weight to form and merge into a new country. If the power value of the new country exceeds the retained country, it will be replaced; otherwise, it will be eliminated.

The above competitive screening process enhances the information exchange among countries, retains excellent location information, and forms a better algorithm initial population.

3.2.2. Improve the Way of Empire Assimilation. The process of ICA empire assimilation is realized by moving the colony to the overlord as a whole to improve the way of empire assimilation ICA. The movement parameter γ is set to 1.8 to ensure that the colony approaches the overlord from the front and back directions. In the real world, colonial assimilation is generally accompanied by infiltration and transformation in politics, economy, and culture. Using this idea for reference, the process of moving the colonial country is changed to the process of moving each feature component to the feature component corresponding to the suzerain country, as shown in Figure 3.

$$y_i \sim U(0, \gamma \times d_i) \cdot i = 1, 2, \ldots, n. \tag{24}$$

Each feature component moves independently. If the moving parameter value is γ, its maximum moving distance is

$$\sqrt{(\gamma d_1)^2 + (\gamma d_2)^2 + \cdots + (\gamma d_n)^2} = \gamma d, \tag{25}$$

where d_i $(i = 1, 2, \ldots, n)$ is the distance between each characteristic component of the colony and the corresponding characteristic component of the empire. The value of γ should be greater than 1.0 in order to ensure the approach from both sides to the target. After repeated tests and experiments, it is proved that when the value of γ is gradually increased from 1.0, the solution accuracy is gradually improved. Different test functions can obtain the best optimization accuracy when the γ value is between 1.5 and 1.8. After γ is taken as 1.8, the solution accuracy gradually decreases as the value of γ increases. Therefore, for different objective functions, limiting the γ value of the movement parameter to the interval between 1.5 and 1.8 can achieve better results. In experiments or practical applications, a simple substitution test can be performed first to clarify the parameter values.

In order to compare the difference between the improved algorithm and the original algorithm in the moving mechanism, Figure 4 shows the difference in search range between the two algorithms in the two-dimensional plane. The search range of ICA is a sector with a radius of $2d$, while the improved algorithm is a rectangle with the maximum moving range of each component as its side. On the one hand, the independent movement of each feature component enhances the flexibility and randomness, and the development ability is stronger. On the other hand, the rectangular search range is relatively small, which improves the overlap and coverage of search areas when multiple targets are close (Figure 5), and has higher efficiency.

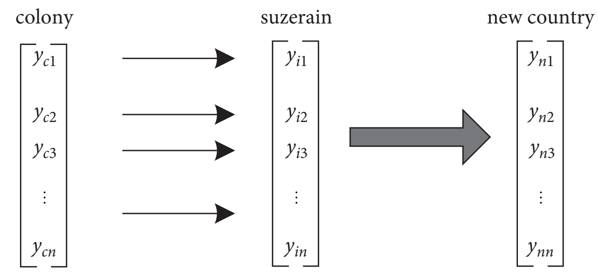

Figure 3: Individual movement of feature components.

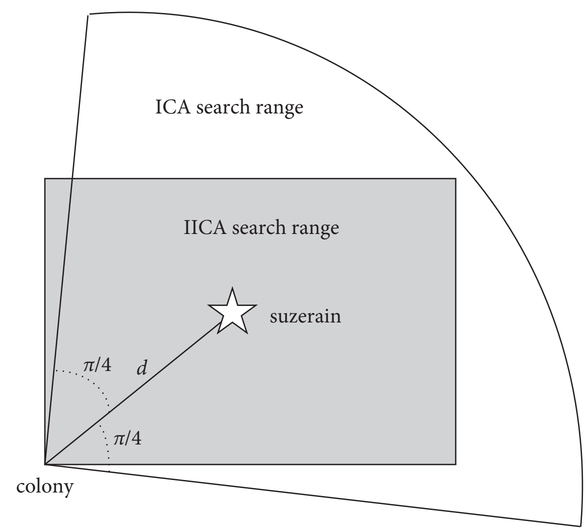

Figure 4: The comparison of the search range.

3.2.3. Increase the Strategy of Jumping Out of Local Optimum.

Aiming at the premature problem of the original ICA, a strategy of jumping out of the local optimum is proposed. If the same optimal value appears many times in succession, it is judged to fall into the local optimum. At this time, the suzerain jumps out of the local optimum according to the selected scheme.

There are many schemes for jumping out of the local optimum. Three schemes are given and tested in this paper. Firstly, take the arithmetic mean of each suzerain as the new moving target point, which is denoted IICA-I in this paper. Secondly, according to the power of each suzerain, the weighted average is taken as a new moving target point, which is recorded as IICA-II in this paper. Thirdly, a certain percentage of the location information of the suzerain changed randomly, which was set as 10% in this paper and marked as IICA-III. The new moving target points constructed by the first two schemes all contain the information of other suzerain countries, which enhances the information interaction. The third scheme jumps out of the local optimum through random changes, which improves the population diversity.

3.3. The Development and Exploration Ability of the Improved Algorithm and Their Balance Analysis.

ICA is deficient in balancing development and exploration capabilities and lacks effective information interaction. The merger and collapse of empires rapidly reduce population diversity, and the applicability of high-dimensional functions is not strong. In view of the above problems, IICA uses a competitive elimination mechanism to enhance information exchange and retain dominant populations in the initial national stage. After many iterations, the mechanism of jumping out of local optimum is added in the stage of greatly reducing population diversity, which provides a path for the recovery of population diversity. At the same time, the improvement of the assimilation mechanism enhances the flexibility and efficiency of search and improves the development ability without affecting the exploration ability. Therefore,

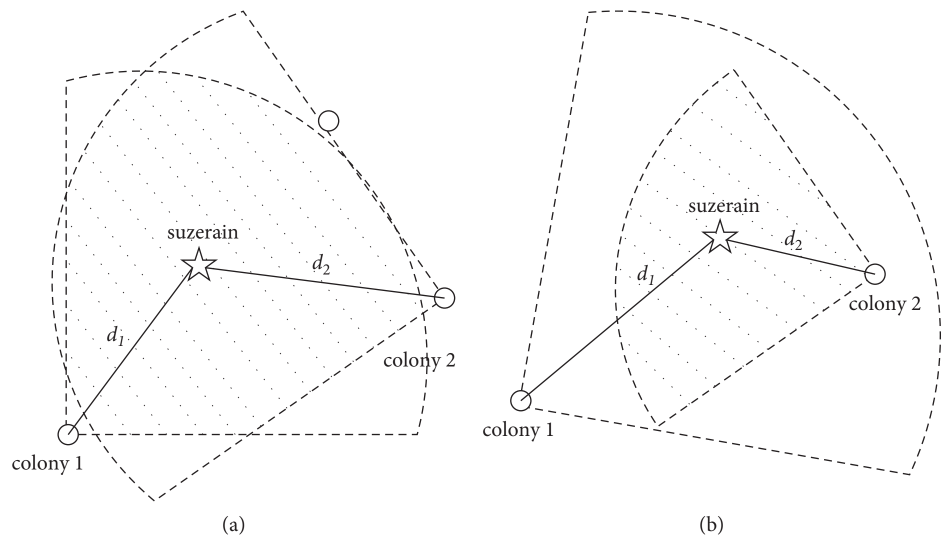

Figure 5: Search area crossing and coverage. (a) Search area crossing. (b) Search area coverage.

Table 1: Scale of examples.

Scale	Examples	Number of distribution centers	Number of customers	Number of vehicles
Large scale	11	7	70	42
	12	8	80	18
Medium scale	13	5	50	30
	14	6	50	34
Small scale	15	3	30	18
	16	4	30	22

compared with ICA, the development and exploration capabilities of the improved algorithm are enhanced simultaneously, and there are more measures to improve the exploration capabilities. The balance between the two algorithms is more reasonable.

3.4. Cost Function. Given an imperialist country or a colonial country, the solution (U, V, W) is obtained by decoding, and the national cost function is calculated according to

$$C = f(U,V,W) + \varepsilon_1 \sum_{s\in S}\left(\alpha - \prod_{j\in J}(1-P_j)v_{js}\prod_{i\in O}\prod_{l\in O}(1-p_{il})u_{ils}\right)^{+} + \varepsilon_2 \sum_{s\in S}\left(\sum_{i\in I}\sum_{l\in O} d_i u_{ils} - T_s\right)^{+} + \varepsilon_3 \sum_{j\in J}\left(\sum_{s\in S}\sum_{i\in I}\sum_{l\in O} d_i u_{ils} v_{js} - \mathrm{TC}_j\right)^{+}. \quad (26)$$

Among them, $f(U, V, W)$ is the objective function expression (4), and the path reliability constraint (5), vehicle capacity constraint (14), and distribution center capacity constraint (15) are added to the evaluation function as penalty items. ϵ_1, ϵ_2, and ϵ_3 are penalty coefficients. $()^{+}$means that if the value in brackets is positive, the value will be taken. α represents the level of reliability. P_j represents the outage probability of the distribution center. p_{il} represents interruption probability of the line between point $i \in O$ and point $l \in O$. d_i represents customer demand. T_s represents the transportation capacity of the vehicle. TC_j represents vehicle unit distance transportation cost.

4. Experimental Results and Analysis

4.1. Experimental Parameter Setting. In order to verify the rationality of the model and the effectiveness of the IICA algorithm, different numerical examples are tested. Table 1 shows the scale of different examples, including the number of distribution centers, customers, and vehicles. The calculated parameters are generated according to the uniform distribution in Table 2. The algorithm is realized by python programming, and the experimental environment for all tests is a computer with Intel Core i7 CPU 2.6 GHz and memory 8 GB and operating system Windows 10.

Table 2: Parameters of calculation examples.

Parameter	Uniform distribution interval
Customer demand d_i	[100, 200]
The opening cost of the distribution center R_j	[20000, 40000]
The capacity of the distribution center A_j	[3000, 5000]
The outage probability of the distribution center P_j	[0, 0.1]
Fixed operating cost of the vehicle H_s	[3000, 5000]
The transportation capacity of the vehicle T_s	[1500, 2500]
Vehicle unit distance transportation cost TC_s	[1, 5]
No-load fuel consumption of the vehicle $\mathrm{FC}_s^{\mathrm{empty}}$	[0.1, 0.15]
The fuel consumption of the vehicle at full-load $\mathrm{FC}_s^{\mathrm{full}}$	[0.15, 0.2]
CO_2 emission and fuel consumption cost coefficient e	[10, 15]
The distance D_{il} between the point $i \in O$ and point $l \in O$	[1, 5]
Interruption probability p_{il} of the line between point $i \in O$ and point $l \in O$	[0, 0.1]

Table 3: Comparison of IICA, ICA, and HS-SA results under different scale examples.

Examples	Algorithm	Best value	Maximum difference value	Average value	Average deviation rate (%)	Average CPU running time (s)
I1	IICA	473292.10	495635.29	485116.74	2.50	208.01
	ICA	508532.16	5552807.32	542479.12	6.68	210.27
	HS-SA	476899.28	540145.96	509045.71	6.74	238.20
I2	IICA	481755.47	505259.35	491528.37	2.03	202.98
	ICA	508364.11	536836.58	528604.79	3.98	207.08
	HS-SA	514238.19	557061.58	532107.68	3.47	232.94
I3	IICA	297755.56	322837.48	306812.79	3.04	132.90
	ICA	338145.28	386614.43	369751.38	9.35	141.73
	HS-SA	322288.01	368362.18	341486.69	5.96	167.97
I4	IICA	250995.19	265680.99	258108.18	2.83	135.25
	ICA	258353.54	306575.04	281304.55	8.88	143.92
	HS-SA	254393.24	324192.23	273091.02	7.35	163.14
I5	IICA	130179.00	137153.13	134007.02	2.94	101.50
	ICA	144109.44	157950.78	153328.73	6.40	105.46
	HS-SA	136060.07	151761.65	142757.37	4.92	112.80
I6	IICA	175181.59	197875.06	180529.97	3.05	103.24
	ICA	191526.10	239578.56	220382.78	15.07	107.91
	HS-SA	180761.54	219009.74	198518.34	9.82	120.59

4.2. Experimental Results. This algorithm is compared with the existing methods in order to verify the effectiveness of this method. Comparison methods are standard ICA and hybrid harmonic search-simulated annealing (HS-SA) algorithm proposed in [17]. The HS-SA algorithm combines the dynamic value of harmony memory considering the speed and pitch adjustment rate with local optimization technology and combines the idea of probability acceptance rule of simulated annealing to avoid local extreme points.

Firstly, the performance of IICA is tested by solving I1~I6 examples of different scales, and the results are compared with the standard ICA algorithm and HS-SA algorithm. Among them, the reliability level α of all examples is 0.5. For a fair comparison, the number of initial countries of the IICA algorithm and standard ICA algorithm is 100, the number of initial empires is 10, and the maximum number of iterations is 100. The value of constant f of the IICA algorithm is 1.5. The HS-SA algorithm has a population size of 100, a maximum number of iterations of 100.

For each example, each algorithm is run 10 times, respectively. Table 3 shows the results' comparison of the IICA, ICA, and HS-SA algorithms under different scales, including best value, worst value, average value, average deviation rate, and average CPU running time. Among them, the average deviation rate is defined as ((average value − best value of average)/best value) × 100%.

It can be seen from Table 4 that the best value, the worst value, the average value, and the average deviation rate of the IICA algorithm are lower than those of the standard ICA algorithm and HS-SA algorithm for examples of different scales. Among them, the average deviation rate of the IICA algorithm varies from 2.0% to 3.1%. However, the average deviation rate of the standard ICA algorithm varies from 3.9% to 15.1%, and that of the HS-SA algorithm varies from 3.5% to 9.8%. It can be seen that the IICA algorithm can effectively solve examples of different scales, and with the increase of problem scale, the IICA algorithm can still maintain good performance. In addition, the average running time of the IICA algorithm is lower because of the

Table 4: Comparison of IICA and ICA results under different reliability levels.

Reliability level	Algorithm	Best value	Worst value	Average value	Average deviation rate
0.3	IICA	263402.63	302897.72	279755.16	6.21
	ICA	285625.69	325442.51	314833.18	10.23
0.4	IICA	275002.06	330545.00	295729.07	7.54
	ICA	294063.73	348928.00	329603.84	12.09
0.5	IICA	298955.56	333039.50	307812.79	2.96
	ICA	338145.28	376816.45	359751.38	9.35
0.6	IICA	326348.99	379520.85	350530.03	7.41
	ICA	346499.02	406936.54	380719.97	9.88
0.7	IICA	383600.81	440393.86	402062.11	4.81
	ICA	429459.97	490012.29	469998.58	9.44
0.8	IICA	442762.95	489473.28	467203.18	5.52
	ICA	472416.25	540157.83	531936.45	12.60

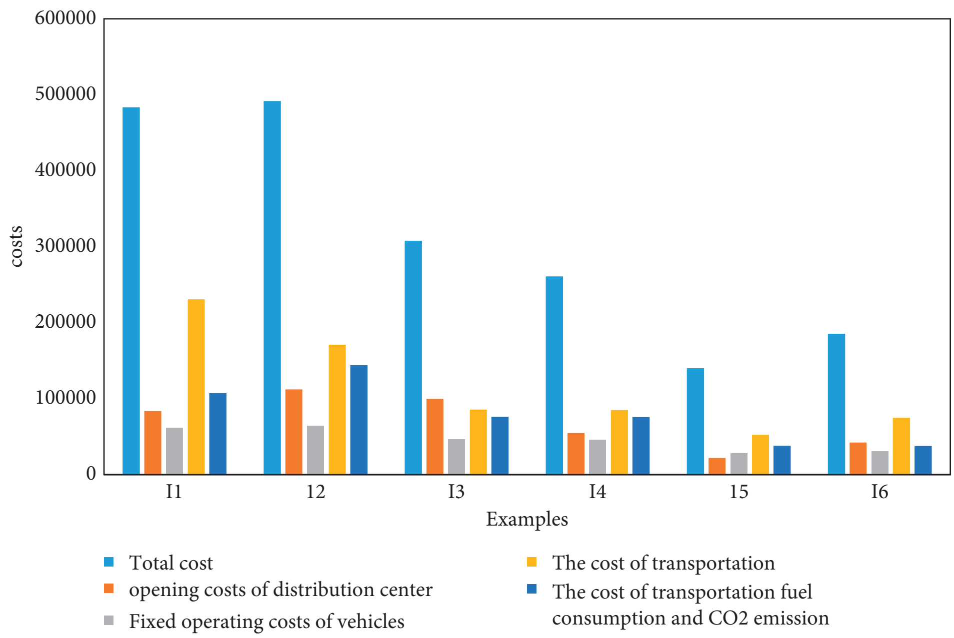

Figure 6: Detailed results of examples of different scales.

improved empire assimilation method and the strategy of jumping out of the local optimum.

Figure 6 shows the detailed results of examples I1~I6, including the opening cost of the distribution center, the fixed operation cost of vehicles, transportation cost, transportation oil consumption, and CO_2 emission cost. It can be seen from Figure 6 that the larger the scale of logistics distribution, the greater the vehicle operating cost, transportation cost, transportation fuel consumption, and CO_2 emission cost, which ultimately leads to an increase in the total cost.

In order to analyze the influence of reliability level α on algorithm performance and optimization decision results, an example I3 is taken as an example. Among them, the reliability level α is 0.3~0.8. For different reliability levels, each algorithm is run 10 times, respectively. Table 4 shows the results' comparison between the IICA algorithm and standard ICA algorithm under different reliability. It can be seen from Table 4 that the average deviation rate of the IICA algorithm ranges from 2.9% to 12.6%, while the average deviation rate of the standard ICA algorithm is between 9.3% and 16.9%. The best value, the worst value, and the average value of the IICA algorithm are also superior to the standard ICA algorithm. Therefore, the IICA algorithm can still maintain stable performance under different reliability levels, and its solution effect is better than that of the standard ICA algorithm.

5. Conclusion

In this paper, the problem of location-route optimization for reliable green logistics distribution is studied, and an optimization model is established to minimize the total cost, including the opening cost of the distribution center, vehicle operation cost, transportation cost, transportation oil consumption, and CO_2 emission cost, under the condition of satisfying the constraint of route reliability. An improved imperial competition algorithm (IICA) is designed according to the characteristics of the problem. Finally, the performance of the algorithm is tested by a numerical example, and the important parameters are analyzed. The experimental results show that the average deviation rate of the IICA algorithm varies from 2.5% to 8.3%, which is better than that of the standard ICA algorithm and HS-SA algorithm. IICA algorithm can effectively solve different scale examples. Furthermore, with the increase of the problem scale, the IICA algorithm can still maintain good performance. In addition, with the increase of reliability level, the number of vehicles increases, which increases the vehicle operating cost, transportation cost, transportation fuel consumption, and CO_2 emission cost and finally leads to the increase in the total cost. In future research, the reliability of green logistics distribution location-route optimization in a dynamic environment can be further considered.

Data Availability

The labeled dataset used to support the findings of this study is available upon request to the author.

Conflicts of Interest

The author declares no conflicts of interest.

References

[1] Y. Zhong, F. Guo, and Z. Wang, "Coordination analysis of revenue sharing in E-commerce logistics service supply chain with cooperative distribution," *Sage Open*, vol. 9, no. 3, Article ID 2158244019870536, 2019.

[2] A. V. Barenji, W. M. Wang, Z. Li, and D. A. Z. Guerra, "Intelligent E-commerce logistics platform using hybrid agent based approach," *Transportation Research Part E: Logistics and Transportation Review*, vol. 126, pp. 15–31, 2019.

[3] K. Zheng, Z. Zhang, and B. Song, "E-commerce logistics distribution mode in big-data context: a case analysis of JD.COM," *Industrial Marketing Management*, vol. 86, pp. 154–162, 2020.

[4] M. Janjevic and M. Winkenbach, "Characterizing urban last-mile distribution strategies in mature and emerging e-commerce markets," *Transportation Research Part A: Policy and Practice*, vol. 133, pp. 164–196, 2020.

[5] Z. Ning, X. Hu, Z. Chen et al., "A cooperative quality-aware service access system for social Internet of vehicles," *IEEE Internet of Things Journal*, vol. 5, no. 4, pp. 2506–2517, 2018.

[6] M. Darvish, C. Archetti, L. C. Coelho, and M. G. Speranza, "Flexible two-echelon location routing problem," *European Journal of Operational Research*, vol. 277, no. 3, pp. 1124–1136, 2019.

[7] M. Schneider and M. Drexl, "A survey of the standard location-routing problem," *Annals of Operations Research*, vol. 259, no. 1, pp. 389–414, 2017.

[8] Z. Benotmane, G. Belalem, and A. Neki, "Green optimisation for LRP problem using a genetic algorithm and a dynamic island model," *International Journal of Advanced Operations Management*, vol. 11, no. 1-2, pp. 46–68, 2019.

[9] Y. Wang, S. Peng, and X. Zhou, "Green logistics location-routing problem with eco-packages," *Transportation Research Part E: Logistics and Transportation Review*, vol. 143, pp. 1–33, 2020.

[10] O. Dukkanci, B. Y. Kara, and T. Bektaş, "The green location-routing problem," *Computers & Operations Research*, vol. 105, pp. 187–202, 2019.

[11] C. Zhang, Y. Zhao, and L. Leng, "A hyper-heuristic algorithm for time-dependent green location routing problem with time windows," *IEEE Access*, vol. 8, Article ID 83092, 2020.

[12] H. Peng, B. Hu, Q. Shi et al., "Removal of ocular artifacts in EEG-an improved approach combining DWT and ANC for portable Applications," *IEEE journal of biomedical and health informatics*, vol. 17, no. 3, pp. 600–607, 2013.

[13] M. Badakhshian, *Location and location-routing problems with disruption risks*, Thesis (PhD), Concordia University, Montreal, Canada, 2019.

[14] M. Huang, L. Dong, H. Kuang, and X. Wang, "Reliable fourth party logistics location-routing problem under the risk of disruptions," *IEEE Access*, vol. 9, Article ID 84857, 2021.

[15] M. Dehghan, S. R. Hejazi, M. K. Mamaghan, M. Mohammadi, and A. Pirayesh, "Capacitated location routing problem with simultaneous pickup and delivery under the risk of disruption," *RAIRO - Operations Research*, vol. 55, no. 3, pp. 1371–1399, 2021.

[16] Q. Fang, H. Nguyen, X. N. Bui, and T. T. Nguyen, "Prediction of blast-induced ground vibration in open-pit mines using a new technique based on imperialist competitive algorithm and M5Rules," *Natural Resources Research*, vol. 29, no. 2, pp. 791–806, 2020.

[17] F. Misni, L. S. Lee, and H. V. Seow, "Hybrid harmony search-simulated annealing algorithm for location-inventory-routing problem in supply chain network design with defect and non-defect items," *Applied Sciences*, vol. 10, no. 18, pp. 6625–6647, 2020.

Hindawi
Scientific Programming
Volume 2021, Article ID 7178893, 13 pages
https://doi.org/10.1155/2021/7178893

Research Article

Analysis of Enterprise Financial and Economic Impact Based on Background Deep Learning Model under Business Administration

Jingxiao Hu

School of Management, Zhejiang University of Technology, Hangzhou 310014, China

Correspondence should be addressed to Jingxiao Hu; hujx@wzu.edu.cn

Received 20 October 2021; Revised 31 October 2021; Accepted 10 November 2021; Published 8 December 2021

Academic Editor: Le Sun

Enterprise finance has become an indispensable financial channel for people to invest in their lives, and business management can provide a better economic environment for the development of enterprise finance. The structure of enterprises is gradually becoming more and more complex, and business administration shoulders considerable responsibilities and obligations in the organization and supervision of today's social management structure. How can China play its functions under the new situation after the world economic exchanges are more frequent is an important link to promote the stable development of financial markets. In view of the problems of economic activity behavior and certainty of financial index system under the background of existing business administration, this paper puts forward the deep learning model to make risk analysis, income analysis, profit and loss analysis, and so on. The formula of deep learning model is used to calculate the data graph of financial economy, and finally, various data are compared to get the research of several business management methods on the development of enterprise financial economy. Among them, the model of current management mode belongs to two modes: e-commerce and EPR management. They not only have very unique management characteristics but also greatly promote the development of modern management, and their roles also well interpret the characteristics of modern management. The experiment also analyzes the financial data under the four algorithms for uncertainty comparison, profit and loss comparison, discreteness comparison, volatility comparison, and possibility analysis. Finally, after the source of uncertainty, the risk prediction and risk management are carried out by constructing decision trees, and these structural models are used to bring comprehensive analysis to the financial economy of enterprises and to build the impact of good trends and development prospects.

1. Introduction

With the gradual improvement and deepening of China's economic system reform, the structure of enterprises has gradually become complicated. Business administration plays an important role in today's social management structure. In addition, how can China play its functions under the new situation after more frequent economic exchanges with the world is an important link to promote the stable development of China's market [1]. Efficient business administration based on deep learning model also has an extremely far-reaching impact and development on modern economy and finance. Different business management modes have obvious influence on the financial economy of various enterprises in today's society. Undertaking the economic development of enterprises is an important cornerstone for the steady progress of society [2]. Business administration is a highly practical discipline in management. It is facing the most important and inseparable extensive industrial and commercial fields in the economy and closely combines the practice of enterprise management to study the business activities of profit-making organizations and the theories, methods, and technologies of enterprise management [3]. At present, as an important ruling part of our government, industrial and commercial management has a very important function. In the management of industrial and commercial functions, the standardized management of market economy system can greatly promote the stable, healthy, and sustainable development of current market finance. The development of socialist market economy is influenced by its own internal operation law, and the standardization of business administration system is an important content [4]. Combined with deep learning model and uncertainty analysis, it also reflects the diversity, comprehensiveness, and scientificity of business administration. Every management method has its advantages and disadvantages. It needs reasonable combination and application to achieve maximum results [5]. The economy and finance of enterprises also have various changes, from the previous offline real economy to the current offline integration and from the former small-scale economy to the present global economic community structure. All these are inseparable from business administration [6]. Thousands of enterprises have made great contributions and promotion to the present society and human civilization. Steady social development is also based on economy. It also has far-reaching significance for life [7]. In order to understand the impact of different deep learning models and business management methods on the financial economy of enterprises, in this paper, various methods are studied, and data were analyzed [8]. In this way, it is also a good suggestion and choice for the future development trend of enterprises. First, the deep learning model of business administration will be expounded and explained [9], and then the structure and structure of these models will be introduced. Several common formulas of deep learning will be applied to get the data analysis of these models. Then, combined with the evaluation index, we make corresponding evaluation and research explanation for various models [10], and then combined with the formula in enterprise financial economy, we make data comparison on the impact trend of several models on enterprise finance. The following are conducive to the trend of social and financial development: what kind of enterprise is suitable for the business management model, how to influence the enterprise economy and finance, how to rationally plan the business management model, and how to make the enterprise economy move towards a benign model. We use the choice of control variables and invariants to control the profits and losses of enterprises, and compare the risk analysis data to draw conclusions. Finally, it is concluded that risk analysis is also of great reference significance and value embodiment to the economy of enterprises and makes the business administration model more fully displayed [12]. Deep learning is applied to business administration simulation formulation and enterprise management. For the finance of enterprises, easy-to-compare data are formed by means of charts and line charts. To conduct research, most risks can be avoided [13]. Economic uncertainty is the embodiment of business administration. Using Seq2Seq, a complete set of financial index construction scheme can be designated to study and analyze the data, so as to show the research significance of the data [14]. Finally, the obtained data are integrated and summarized to form a complete data analysis legend, which reflects the scientific, objective, and cutting-edge research and analysis of this paper. Among the above studies, the algorithms for business administration methods are based on the analysis of financial data, and there are few studies on the corresponding economic uncertainties. In the enterprise economy, there are many uncertain factors, which reflect the important characteristics of economic activities. In this paper, the problem of economic uncertainty is deeply studied, the uncertainty index is predicted and analyzed by deep learning model, and the corresponding economic correlation characteristics are obtained.

2. Financial and Economic Uncertainty Indicators

The term uncertainty is a general concept in a particularly wide range, and financial uncertainty can be understood as some uncertain factors under different concepts. From a macropoint of view, there are uncertainty of macroeconomic development concept, uncertainty of market finance, uncertainty of social and economic policies [15], and so on. However, in the macrocontrolled economic system operation model, the modern market of economy and finance, economic policies, and other directions, they influence each other and depend on each other. As long as one aspect is affected, the whole body will change, which is the butterfly effect of financial market [16]. At present, the definition of the uncertainty of various macroeconomic development in the world is not so intuitive and clear, but even so, there are still many experts and bachelors who have done a lot of researches and expressed a lot of their views on the development trend of global [17] macroeconomy from different angles and directions. From these aspects of macroeconomics, since the outbreak of the global financial crisis in 2009, the development direction of the global economic and financial system has entered an unprecedented trough, and the brand-new economic growth point has disappeared in front of the public's vision since then. The frequency of economic market fluctuations in the whole country and even the whole world is very violent and frequent. Black Swan incidents occur frequently in the world, and it becomes more and more difficult to control market risks at this time [18]. Therefore, major economies in the world have raised their expected indexes and expected trend charts against international economic and financial uncertainties. Many Western scholars and media agree that "the only thing that is certain is uncertainty." But as far as these events are concerned, individuals, families, and enterprises are also faced with many uncertain factors and volatility indicators in their life cycle economic activities.

If we want to quantify the uncertainty, the first thing we need to determine is a way to replace the uncertain index value. At present [19], there are two ways to replace it. The first way is to choose the approximate range value of our existing economic index to replace the uncertain index. The second way is to dig out the uncertainty of economic and financial development in most economic and financial variables by modeling business administration data. Using other similar variables as alternative variables of uncertainty has the advantage that variables are convenient to select and calculate [20], and researchers only need to choose appropriate alternative variables and then pay attention to academic problems related to uncertainty. However, the shortcomings of doing so are also very obvious. First, alternative variables often cannot completely replace uncertainty; that is, variables only contain part of uncertainty. Second, alternative variables often contain other attributes besides uncertainty. For example, if volatility is used instead of uncertainty, volatility inevitably contains risks. Third, it is difficult to summarize the uncertainty in the complicated economic and financial operation by using a single or a small number of economic and financial indicators [21]. For this reason, it is inevitable to explore uncertain factors from more comprehensive data in today's society. Cullen et al. [22] reported that, with the development of big data, mobile Internet era, and the improvement of computer computing performance, using deep learning method to deal with massive data has become a hot topic gradually tried in various fields in recent years. The emergence of big data has allowed the use of larger-scale measurement data to measure economic development. At the same time, researchers in the field of economics are increasingly using statistical measurement methods in adjacent fields to study economic and financial problems [23], which greatly complement the traditional econometric techniques. For Asia, economic uncertainty indicators are showing an increasing trend year by year relative to global economic uncertainty indicators, as shown in Figure 1.

In addition, in the current economic policy uncertainty and other aspects, generally speaking, specific quantitative indicators equivalent to global news information are used to replace the policy uncertainty of market economy in various countries. For example, Baker has collected, counted, and sorted out a large number of words related to "uncertain factors" mentioned in newspapers and magazines in different periods around the world. By combining other economic indicators, the financial and economic policy uncertainty (EPU) of major economic systems in the world (including China, the United States, India, and other countries) is constructed. Because the global financial and economic policy uncertainty index (EPU) is more inclined to some complex information about financial and economic policies, EPU pays great attention to quantifying the uncertainty factors at the macroeconomic policy level. This will lead to other incomplete and small-scale alternative indicators that cannot be coordinated and representative. Juradoet al. [24] and their use of financial and economic data variables forecasting error will represent the dependent variables of economic policy uncertainty factors instead of the indicator data volume. Scotti uses the extent of the range selected by the public in the process of publishing relatively extensive data as the independent variable index of the uncertainty factor index instead of the data.

3. Application of Deep Learning Model in Business Administration

Summary of the application of deep learning in financial market deep learning has achieved good results in the research of financial market, volatility of financial assets (stocks, bonds, and futures), and price prediction. Many scholars have applied the deep learning model to the variable

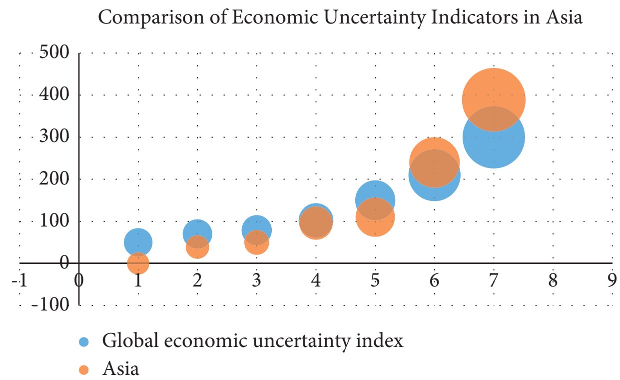

Figure 1: Comparative chart of Asian economic uncertainty index.

prediction of economic and financial markets and compared it with the traditional model. Most of the pieces of literature have come to the conclusion that the deep learning method can improve the accuracy of variable prediction. Using Google domestic trend to represent public sentiment factor and macroeconomic development factor and using long-term and short-term memory model (LSTM), this paper studies the influence of these factors on the volatility of S&P 500 from October 19, 2004, to July 24, 2015. Dixon introduced an artificial deep neural network into the research of the future market and used an artificial neural network to predict the changing direction of 45 commodities and futures prices in Chicago Mercantile Exchange. The research pointed out that the average prediction accuracy of the artificial neural network reached 73%. Then, according to the analysis data of this research, it can be shown that when this deep learning neural network model is constructed in depth, combined with business administration, the time delay value of the fluctuation time series of the world market, finance, and economy, the influence of many factors, such as market equilibrium, mobile data, and global economic and financial correlation, can be discussed in depth to expand the scope of the financial field in turn. The research used the same conventional method to control 75 kinds of mass-scale commodities and global foreign exchange predicted by dependent variables and independent variables. When the interval between foreign trade futures is 6 minutes, after this discussion, they further analyzed the subtle price trend changes and price formation trends caused by the median price of foreign exchange of these futures commodities, which was called a simple long-term trading retest rate, and then reduced the error range index of the study. The research results show that, on average, their model can predict the direction of price changes with an accuracy rate of 42%, and in some cases, the prediction rate can reach 68%. The additional back-test results show that when using this model, the market economic index can obtain an annualized Sharpe rate as high as 4.29.

3.1. Basic Ideas of Constructing Financial Uncertainty through Deep Learning Model Business Administration. First of all, through the collation and research of uncertainty index and related deep learning models for neural network model methods, in this paper, we will use the conventional uncertainty measurement methods, select higher-dimensional and multidimensional economic and financial data for research, and simulate to build the uncertainty index of China's financial and economic market. Then, in order to construct a model to predict the future expectations of a large number of financial variables as well as possible, this paper will further explore the prediction function of deep learning (Seq2Seq) model in financial markets based on LSTM neural network. Finally, the error variance of economic and financial variables predicted by the neural network is used as the uncertainty index of China's financial market in Figure 2.

3.2. Construction of Financial Uncertainty Index. The uncertainty index of financial indicators is mainly measured by the following two formulas. In formula (1), the uncertainty of financial variable W in the future period is first measured. In this step, the conditional expectation calculated by available information N_1 of prediction error conditional fluctuation of financial variable N_t in the future period is used. In formula (2), we use a certain weight to sum up a large number of financial variables' uncertainty index Y_t, which can represent the financial market situation in China, to get the sum uncertainty, and then measure the uncertainty of China's financial market.

$$u_t^y(h) = \sqrt{E\left[\left(Y_t + h - E\left[Y_t - h\right]\sqrt{I_t}\right)\right]}, \tag{1}$$

$$FN_t(h) = p\lim N_1 \sum_{1}^{N_Y} W_y u_t^y(h) = E_w\left[u_t^y(h)\right]. \tag{2}$$

In order to avoid dimensional disasters, the principal component (PCA) coefficient method is used to reduce the dimension of economic and financial prediction variable X_i. The common factor F_t is extracted from the variable X_t. The prediction variable X_{it} has the following structures of formulas (3) and (4). Here, the error value of the dependent variable y_t in the future h period is defined by the following formula:

$$X_{it} = A_i^F F_t + e_{it}^X, \tag{3}$$

$$v_{i+h}^y = y_{t+h} - E\left[y_{t+h}\sqrt{I_t}\right]. \tag{4}$$

When the common factor F_t is used instead of the independent variable X_{it}, the following model formula is constructed, in which the independent variable X_{it} is assigned to obtain the Seq2Seq deep learning error value, and the neural model is used to calculate the E value and I_t to obtain the error square value. Finally, the uncertainty index equation is obtained by calculating the value of the dependent variable H as shown in formula (8).

$$\partial_{i+h}^y = E\left[\left(v_{i+h}^y\right)^2 \frac{\sqrt{I_t}}{2} = v_t^y(h), \tag{5}$$

$$\text{Seq2Seq}\left(X_{\text{it}}\right) \longrightarrow y_{t+h}^2 w \sqrt[3]{I_t} + X_{it}(h), \tag{6}$$

$$E\left[v_{i+h}^y\right]^2 \left|I_t\right| = \left(\partial\left(e_i\right)\right)^2, \tag{7}$$

$$H = \varphi\left(XW_{xh} + B_h\right), H \in R^{n \cdot h}. \tag{8}$$

When designing the neural network, we need to consider the time series characteristic when we face the time series data. Let the value of X_t be the data input at time T, the value of H_t be the hidden layer variable at time T, and the value of H_{t-1} be the hidden layer variable at time $H(T-1)$, so that we can analyze and get the time series data designed by the neural network and calculate the time series eigenvalue.

$$H_t = \phi\left(X_t W_{xh} + H_{t-1} W_{hh} + b_h\right). \tag{9}$$

The output data on the output layer of time step t is

$$W_t = O_t - H_t W_{hq} + b_q. \tag{10}$$

The output data on the output layer of time step u is

$$\begin{gathered} u = \sqrt{\frac{(1-k)E}{(1+k)(1-2k)p}}, \\ MPC = \frac{\Delta C}{\Delta Y} - \beta\ (\beta \in E). \end{gathered} \tag{11}$$

In the above formulas, the data of E and K respectively correspond to the dependent variable and independent variable of the neural network model.

(1) In the type of depth model, it is very difficult to get the distance difference and value range in the time step of interval function in the application research of cyclic neural network model in real life. This is quite directly related to the model dependencies of its connected application structures. It will also cause a large-scale impact on the trend of data and the scale of volatility. Therefore, in the current recurrent neural network model and the early long-short-term memory neural network, scientist Hochreiter used a new concept to reduce the number of time step captures in order to minimize the occurrence of this situation. This concept is the gate concept, so that the cyclic neural network model can control the data in different time scale areas, respectively, then the error value of compressed output data at time t can be further reduced by the data overall calculation method, and the fluctuation interval can be reduced.

$$\begin{aligned} I_t &= \partial\left(X_t W_{xi} + H_{t-1} W_{hi} + b_i\right), \\ F_t &= \partial\left(X_t W_{xf} + H_{t-1} W_{hf} + b_f\right), \\ O_t &= \partial\left(X_t W_{xo} + H_{t-1} W_{ho} + b_o\right), \\ \partial(x) &= \frac{1}{1+e^{-x}}, \end{aligned} \tag{12}$$

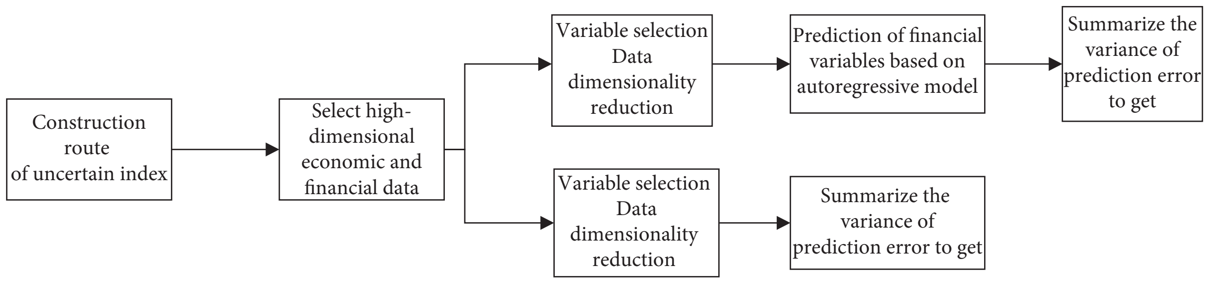

Figure 2: Roadmap for the construction of business administration financial uncertainty index in China market deep learning model.

where X_t is the input at time t, the number of samples is n, the dimension of data is d, H_{t-1} is the hidden state at time $(T-1)$, h is the number of hidden units, I_t, F_t, and O_t are the input gate, forgetting gate, and output gate at time t, respectively, W_{xi}, W_{xf}, and W_{xo} are weight parameters, and b_i, b_f, and b_o are deviation parameters. Parameters need to be trained in neural network to get corresponding values. In the hidden cell, the cyclic neural network has the following parameter calculation formula to obtain the power number and weight of the error value, which makes the corresponding financial index analysis more comprehensive and favorable and can minimize the error value and the cyclic output value at time point T.

$$F_i^r = \iint I_t \sqrt{W_{xf} + H_2} \lim_{x \longrightarrow \infty} \sqrt{I^2 \cdot W_{ho} + T_x^{\ 2}}, C = \alpha + \beta\sqrt{X^2 + Y^2}, APS = \frac{S}{P} - 1 - MPC - \beta. \quad (13)$$

H_2 is the second hidden state of the loop, and it can be seen from the formula that the value of F depends on the size of W, which minimizes the value error of T_x. From this analysis, the data and cyclic structure diagram can be obtained.

$$\begin{aligned} i_{t_1 t_2} &= \frac{A(t_2) - A(t_1)}{A(t_1)} = \frac{I_{t_1 t_2}}{A(t_1)}, \\ 1 + i &= \left(1 - \frac{d^p}{p}\right)^p, \\ d &= \frac{i}{1+i} \leq i, i = \frac{d}{1-d}. \end{aligned} \quad (14)$$

The above are the conventional financial calculation formulas of macroeconomy, which are the calculation formula of market interest rate, the conversion formula of clear discount rate, and the conversion formula of interest rate and discount rate, respectively. In these three formulas, i is the variable, d is the dependent variable, P is the discount rate, and t_1 and t_2 are the independent variables.

3.3. Selection of Financial Indicators and Data Sources. When studying macroeconomics, uncertainty is a complex concept with many factors and angles. It is difficult to say which index and data can perfectly and comprehensively cover all the uncertainties related to macroeconomy. Therefore, in the third chapter, the construction of financial uncertainty index should widely select economic and financial variables and related indicators. Each factor variable used in this paper is monthly data or daily data less than monthly frequency. In daily data, this paper uses the method of monthly average to transform daily data into monthly data. The data were selected from March 2006 to October 2020. China's macroeconomic variable data and financial variable data come from wind database, wide quantification platform, and Tushare API; there are 629 kinds of economic and financial variables used in the construction of an uncertain index of the financial market, including 346 kinds of domestic macroeconomic variables and 242 kinds of financial variables. Among the financial variables, there are 27 kinds of domestic financial indexes, 18 kinds of international financial indexes, and 197 kinds of industrial financial data. Select the source of the data as shown in Figure 3.

As can be seen from the above table, the indicators selected in this paper include four major aspects. Macrodata include domestic real estate data, monetary data, trade data, investment data, macroindex, and household consumption. These data mainly reflect the stability of domestic economic operation at the macrolevel and are the concrete representatives of the domestic economic vane. Selecting these entity data is helpful to dig deep into the stable and unstable components of the financial market. Domestic financial data include the index of the domestic financial market, financial statements of listed companies, and financial real-time transaction data. These data directly reflect the operation of the financial market and the direct embodiment of domestic financial operation. In addition, the selected data also include international financial index data and domestic financial data of various industries. The global financial index often includes the important index series of international finance, which is used to comprehensively evaluate the global economic operation state. The economic and financial data of domestic enterprises will adopt the classification evaluation method of Shenwan first-class enterprises,

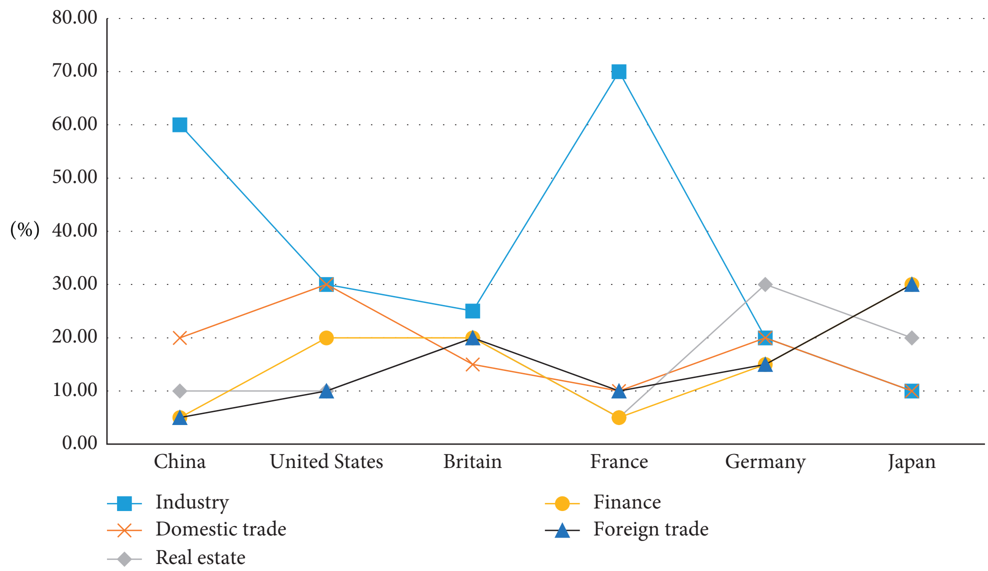

Figure 3: Financial number selection and source chart.

including the estimated value data of domestic stock market and the daily market data of industry finance. Different error values lead to the change curve of financial index, as shown in Figure 4.

4. Experimental Analysis of Deep Learning Model in Business Administration

When constructing the uncertainty index, the deep learning model is used to predict the economic and financial variables; the advantage of this is that the prediction model is more accurate and the uncertainty part is more accurate. The disadvantage is that the parameters of the neural network model are huge, which is not conducive to analyzing the causes of the model results. If we want to analyze the source of uncertainty, we must take a certain way to explore the interior of neural network. Since the development of neural network, especially in the recent ten years, it has made great achievements in industry and academia. Many scholars have made a series of explorations on interpretable neural networks. One of the ways to interpret the results of neural networks is as follows. First, a simple model that can be interpreted is constructed. For example, this model can be a linear model or a decision tree model. Then, the same data of the neural network is used as the characteristic (independent variable), and the output result of the neural network is the label (dependent variable). Then, an interpretable simple model is used to compare the above training set and test set. In the method design of business administration using two deep learning models, four deep learning models, namely, neural network diagram, cyclic neural network, recurrent neural network, and self-encoder, are used to designate the business administration experiment. Finally, the four models have an impact on the financial economy of enterprises. After obtaining the data, the four models are analyzed and studied in turn.

The business management of neural network mainly lies in data preprocessing, which is to transform various data and nonquantitative data into positive data indicators and adopt different transformation methods according to the different properties of indicators. The data of the macrovariable evaluation index in this paper is often invariant data. Usually, the lowest score is marked as zero. The highest score is marked as five points. It has no reversible parameter index. We assume that the preprocessed data value is an X-dimensional matrix, N is the number of samples of data, that is, the number of people being evaluated, and M is the index quantity of data evaluation, that is, M input data sequences of artificial neural network in deep learning. As shown in Figure 5, under the structure construction of this model, enterprises are randomly selected in combination with business administration to select financial data and economic finance directionally, the neural network model is applied to collect and sort out the data in turn, and finally, the data amount is obtained to understand the influence and connection of this model on enterprise financial economy at each time point.

Among the four deep learning models, the model of cyclic neural network mainly introduces the construction of cyclic neural network whose input data sequence length T_x and output data sequence length T_y are the same. But in fact, we will encounter more RNN loop construction structures in business management applications. For example, when we classify emotional problems, the output data usually only has a scalar value. At this time, it is a many-to-one structural model. Whenever music is generated and

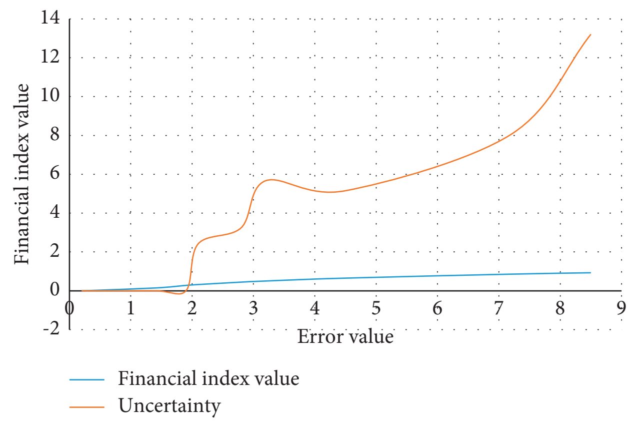

Figure 4: Financial index line chart.

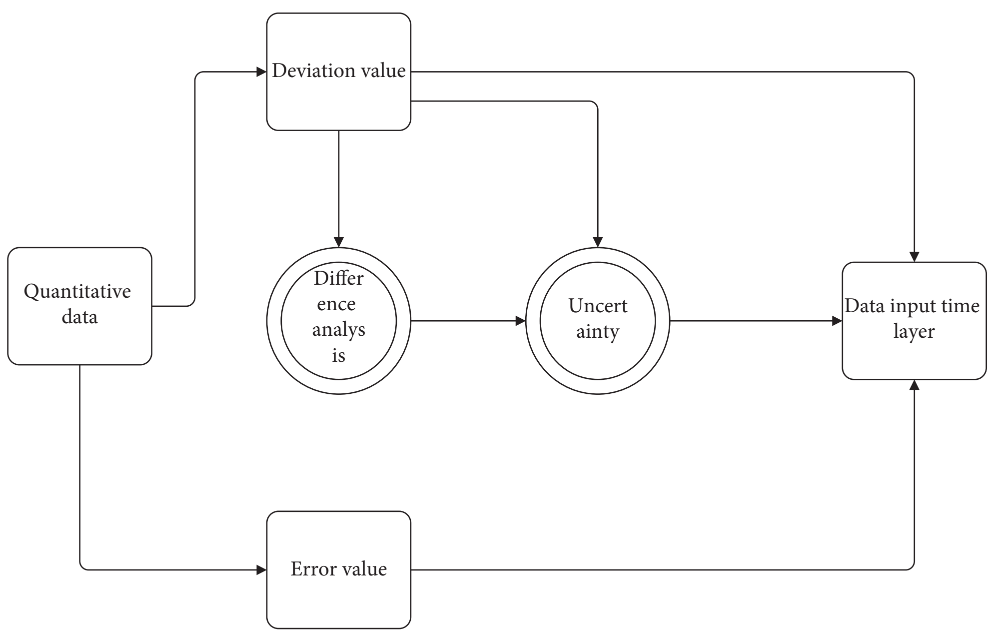

Figure 5: Business administration construction diagram of neural network model.

applied, it usually uses the network structure of a single controllable variable to multiple variables. When there is one or no input data, then there are output data of multiple variables. The network structure used in machine language translation task is a structure of multiple variables to multiple variables with different lengths of input data sequence and output data sequence. As shown in Figure 6, the cyclic neural network is equivalent to the upgraded deep learning model construction diagram of the neural network model. However, the processing quantity and accuracy are much higher than those of the neural network model because the error value of data obtained by multiple cycles is far less than that of the neural network model, but the calculation method is much more complicated than that of the neural network model.

The recurrent neural network model in the depth model is a depth learning model with branch tree computing. Recursive algorithm has a changeable topological layer structure, and this is a reliable deep learning regression model. For business administration, the recursive algorithm has advantages and disadvantages, and its diversity and sustainability are excellent. In dealing with business administration, the analysis and induction of data are more diverse, which can be used for complicated calculation methods. It is composed of multiple nodes and is connected by multiple frames. The output nodes are usually located at the top of the tree, and then the algorithm flow is carried out in turn, which can be divided into multiple sections to process data and reduce the uncertain factors in finance. As shown in Figure 7, it can be seen that the recurrent neural

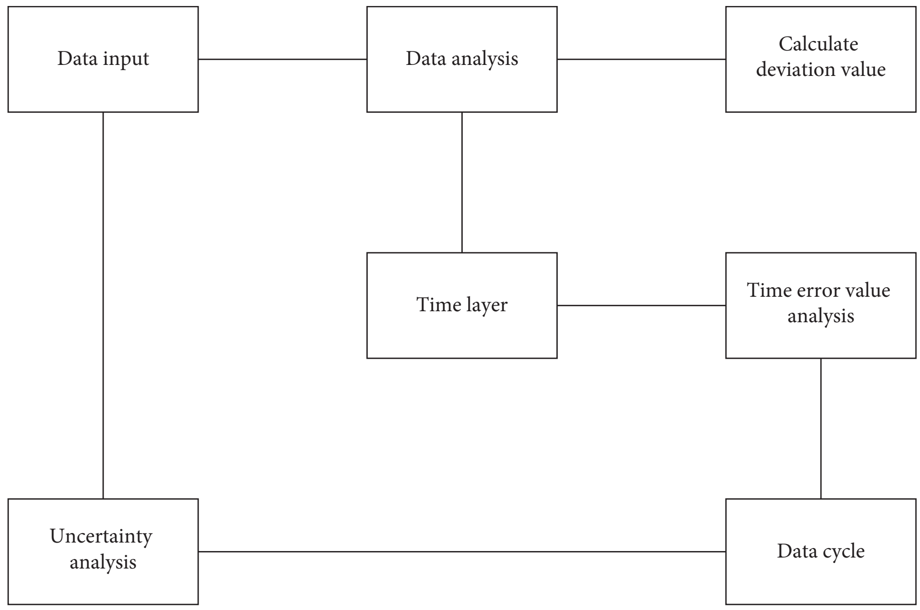

Figure 6: Business administration construction diagram of cyclic neural network model.

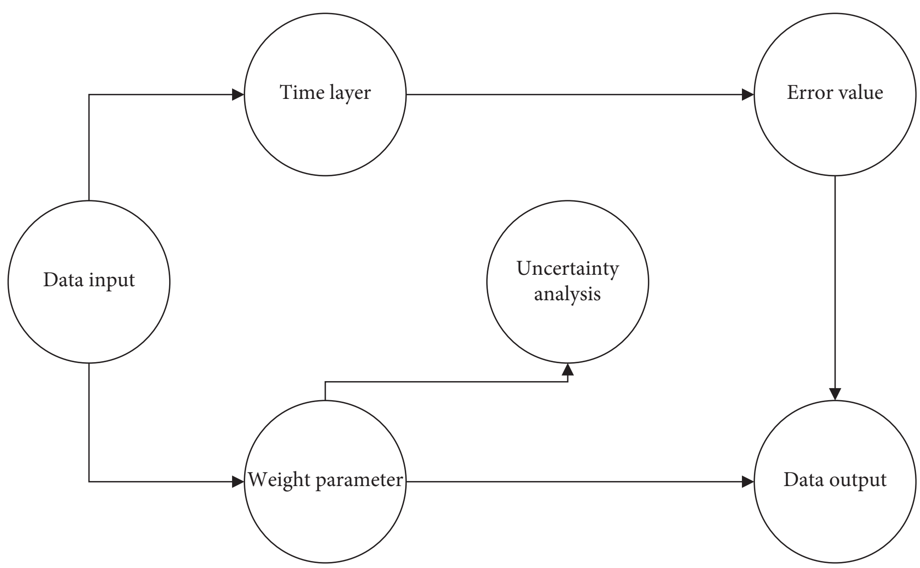

Figure 7: Business administration construction diagram of recurrent neural network model.

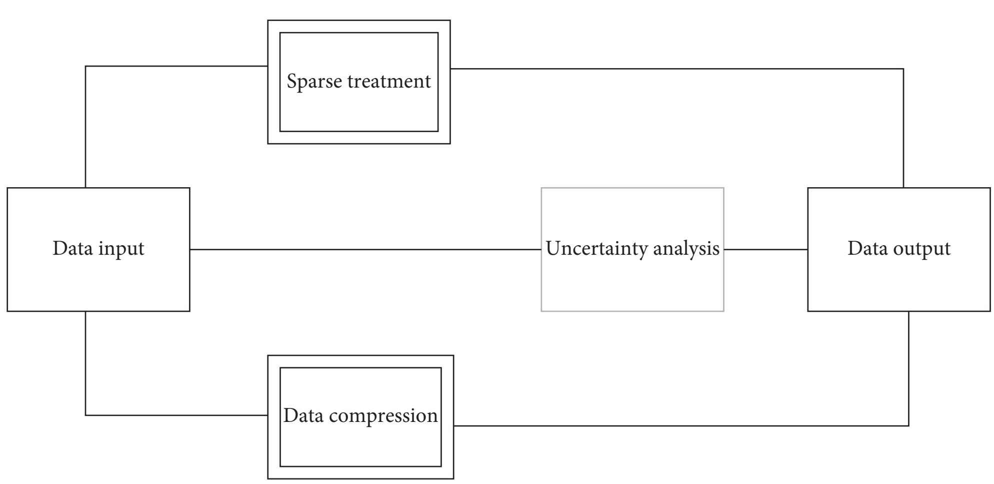

Figure 8: Self-coding model business administration building diagram.

network model uses supervised learning and unsupervised learning to build training, and the recursive algorithm can use the backpropagation calculation method to calculate the weight parameters of financial data.

Among the four deep learning models, the computing concept adopted by the self-encoder is one of the non-comprehensive supervised and unsupervised models. Also known as the artificial neural network construction model, this model is a practical model that can be simply constructed in deep learning model. It can be decomposed and constructed in two parts, the first part is the built-in encoder system of self-encoder, and the second part is the external decoder system of self-encoder. In business administration, the self-encoder can decompose the uncertainty factors and calculate them in one direction to obtain the weight parameters of enterprise finance. Then, the macroerror value in the time layer can be solved. As shown in Figure 8, the trend of the financial economy can be calculated, and the economic value can be analyzed. Then, the time difference between the enterprise economic characteristic value and the economic output data with the smallest range can be calculated through the weight parameters. It can be used for simple enterprise financial data analysis. The coding of the self-encoder model is mainly characterized by compression processing at the beginning of data input, sparse processing structure, and output compression at the end of data, which constructs a deep learning model.

4.1. Comparative Analysis of Uncertainty. After the construction of these four models of business administration, adopt random selection of enterprise financial data to make model embedding. Then, after integrating the data of enterprises, we conduct experiments to compare the data to study the impact of deep learning business administration on the financial economy of enterprises. In view of the uncertain comparison of enterprise financial economy, compare the data of these four deep learning business management models. The uncertainty comparison diagram is shown in Figure 9. For uncertain factors in many aspects, the algorithms of the four models can be used for comparison, and their impacts on corporate finance are also different. In comparison, self-encoder has the greatest influence on uncertainty; therefore, in the deep study of business administration, the self-encoder has the best economic and financial impact on enterprises. It can find out the uncertain indicators and factors to the greatest extent, and for macroeconomics, it can also maximize its index effect and improve the predictability and randomness of enterprise financial economy in the field of market economy. It can minimize the economic fluctuation of enterprises, and the scale of business administration can gradually expand the fields involved. It can be seen that the recurrent neural network model has the smallest analysis of uncertain data and the largest fluctuation of enterprise financial economy.

4.2. Comparative Analysis of Profit and Loss. It is most important to analyze the profit and loss of enterprises under four deep learning models. The profit and loss of any enterprise in the economic field can explain the viability and competitiveness of an enterprise in today's society, so at this time, for one of the important indicators of enterprises, the analysis data of the four models are of special significance for this indicator. When a deep learning model has less influence on data, the data reflected at this time will be particularly cutting-edge, and the dimension of sustainable degradation will be higher, which affects the discrete indicators of business administration, which is also one of the important indicators affecting its enterprise economy. The continuous uncertainty exponent labels are discretized, and the value of uncertainty exponent is divided into five parts equidistantly. Mark the level of uncertainty index with discrete integer values from 1 to 5. The larger the value, the higher the uncertainty index. Decision tree regression prediction is carried out on the above data. When training the decision tree model, we need to give full play to the approximation degree of decision tree to neural network, so we do not split the training set and test set, and we do not need to consider the overfitting problem of the model. From Figure 10, we can get the comparative data indicators of the four models for the profit and loss of enterprise finance and economy.

4.3. Comparative Analysis of Discreteness. Discrete comparative analysis is also an important index in enterprise financial economy; what it affects is the ability of enterprises to accept the outside world and the profit and loss rate under different pressures and environments. Under the analysis of deep learning model business administration, this indicator will be more or less reflected in different fields. From the profit and loss analysis in the above figure, it can be seen that the recurrent neural network has a great influence on improving the profit and loss value. However, the loss value is also the highest among the four deep learning models, which will lead to the lowest profit and loss rate. It can be seen that the profit and loss rate of cyclic neural network is the highest among the four models, which is the defect of recurrent neural network in business administration and is not applicable to business administration. It is suitable for some medical research and computer network weight parameter analysis, but not for enterprise economy and finance. Therefore, in discrete analysis data, all four indicators have expected values, which lie in the prediction of variables and the influence of volatility. Discrete analysis can reflect advantages and disadvantages. The discreteness analysis diagram of the four models of business administration is shown in Figure 11.

4.4. Comparative Analysis of Volatility. Volatility analysis is an important index to test the stability of the four deep learning models. Financial market volatility is closely related to financial uncertainty. This experiment will explore the relationship between China's financial uncertainty index and stock market volatility and their mutual influence. The volatility of the stock market cannot be observed directly, and the volatility of the financial market corresponding to the uncertainty index of China's financial market should be

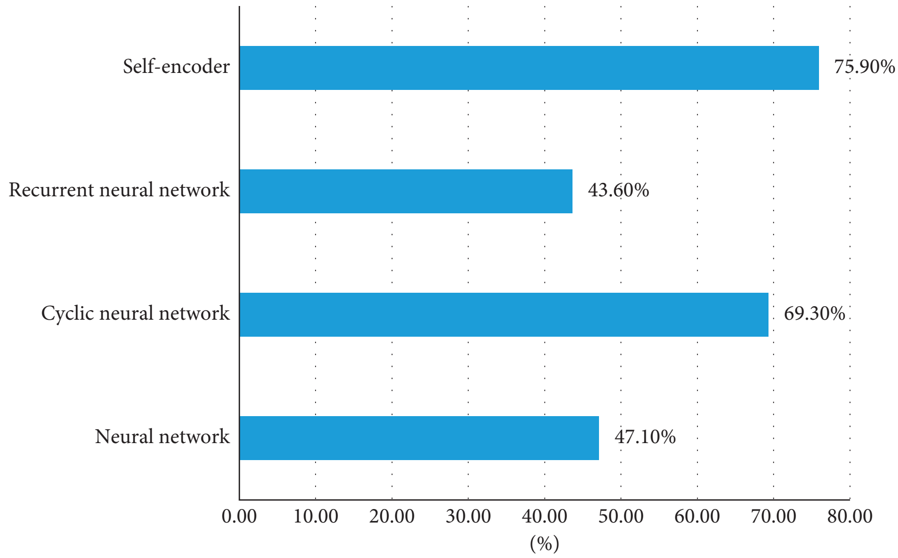

FIGURE 9: Analysis of enterprise economic uncertainty data by four deep learning models.

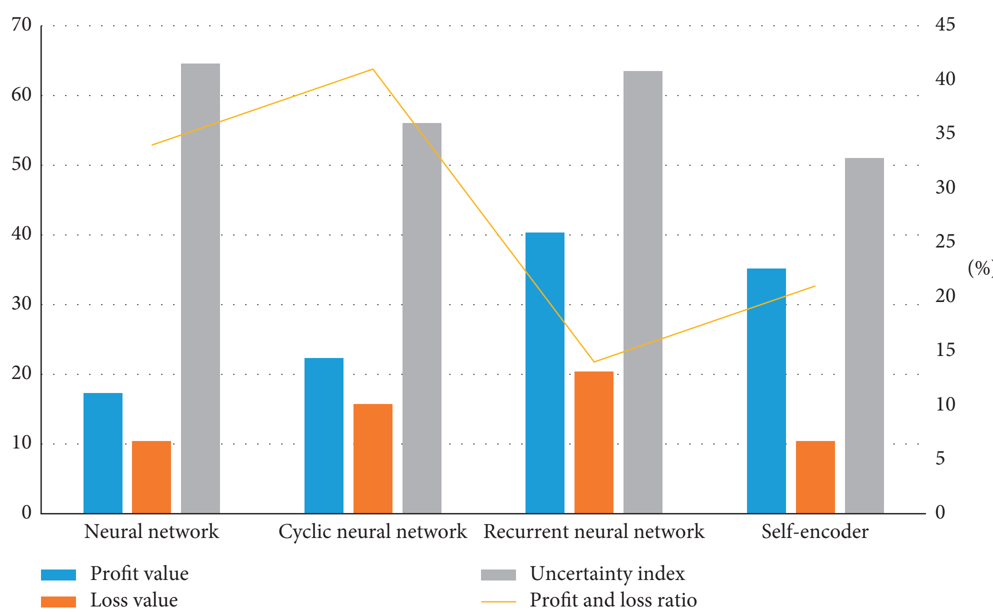

FIGURE 10: Profit and loss data comparison chart.

the volatility of the whole financial market. However, when looking for indicators that can replace the volatility of the financial market in practice, it is found that there is no index data that can fully represent the volatility of China's financial market. Therefore, this time, the index data of various stock markets are selected, and then calculate the volatility of index data. From the influence of four models on the volatility of the stock market, it can be seen that the choice of debt ratio and bonds of enterprises by these four models is full of bond analysis of enterprises. When the volatility is great, the data cannot be directly put into the market and operation. This is an important indicator that must be controlled to protect market stability. Therefore, through this analysis, it can be concluded that the four models have an impact on the sustainable development of enterprise economy and finance. The comparison chart of volatility data is shown in Figure 12.

4.5. Possibility Analysis and Comparison. The possibility analysis of the four models is in the unknown market field, the influence and predictability of the financial and

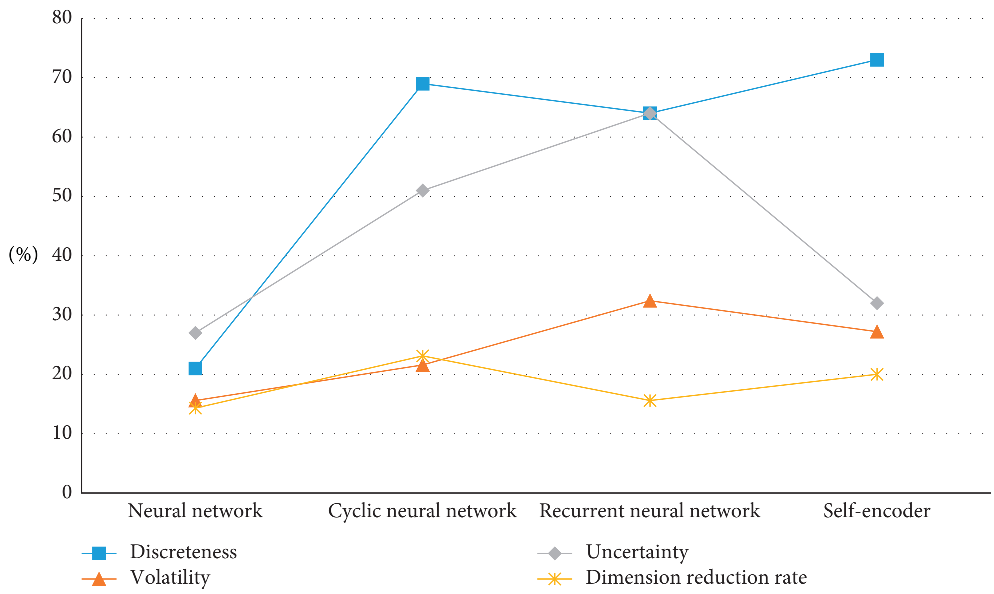

Figure 11: Discrete data comparison diagram.

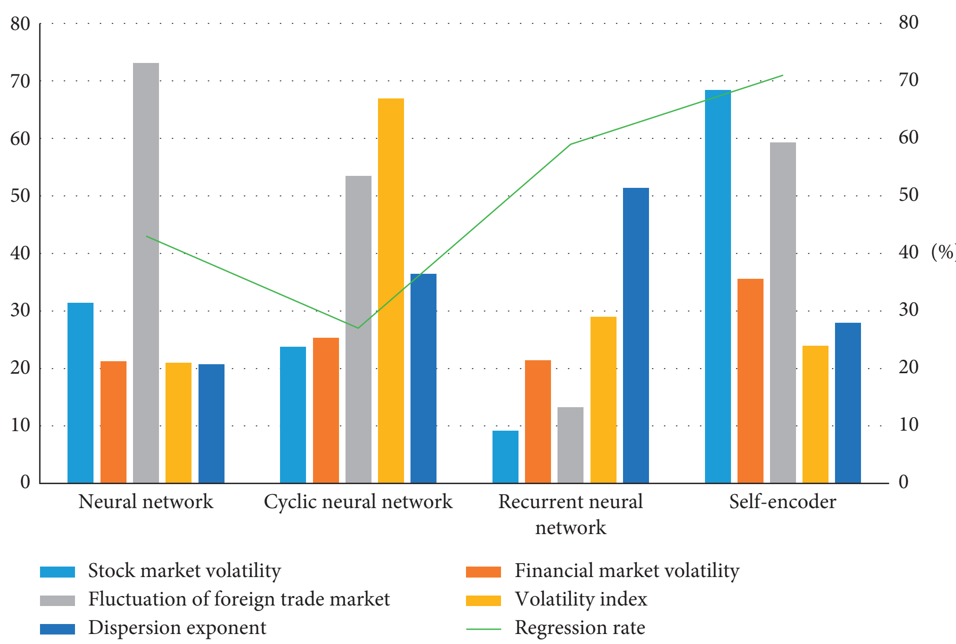

Figure 12: Comparison chart of volatility data analysis.

economic level of enterprises, and the ability of this sought model to predict the later trend data. It is also an impact index for predictive evaluation of the financial and economic level of enterprises. Although this assessment is for reference only, persuasive influence is not enough, but it has an unfathomable relationship with the future direction of an enterprise's finance. From the comparative analysis of the above four kinds of data, it can be seen that the data analysis is objective, scientific, and rigorous, and the establishment of possibility analysis lies in the fact that the enterprise can make a rough simulation and exercise prevention for the follow-up regulation and development and the future risk assessment. This is a medium priority data study in the evaluation index, so we roughly make the data comparative

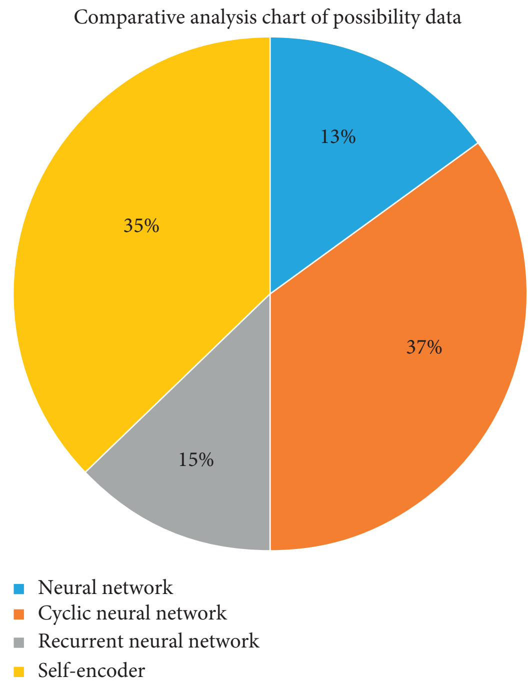

Figure 13: Possibility data comparative analysis chart.

study experiment in Figure 13 to get the data. It is of great significance to the risk assessment of enterprises, which can avoid risks and market fluctuations to the maximum extent.

5. Conclusion

Through the above experimental comparison and comprehensive analysis of evaluation index parameters, the experimental evaluation is summarized into four depth models. The financial and economic impact of business administration on enterprises mainly lies in the fluctuation effect caused by the reduction of profit-loss ratio and the different calculation methods of time layer error value because the weight parameters of the butterfly effect in the financial economy are particularly large. As a result, the finance of enterprises fluctuates obviously in market finance. In the uncertainty analysis, the calculated value of the self-encoder deep learning model is 75.9%, and the value is the highest among the four models. The values of the recurrent neural circulation network are 43.6% and 47.1%. As a result, the self-encoder of uncertainty analysis can effectively reduce the error value of finance. There will be very high results in macrocontrol. In the profit and loss analysis, the profit and loss rate caused by the neural network model is 41%, while that caused by the recurrent neural network is 16%. It can be seen that the impact of the recurrent neural network on the financial profit-loss ratio of the enterprise market is significantly reduced. In terms of profit and loss, the recurrent neural network has significantly improved the market supervision of business administration due to multiple regression calculations. In terms of dispersion and volatility, the cyclic neural network model can make the market produce a larger regression rate of return with a rate of return of 71%. It makes enterprises greatly improve in the stock market and financial market and can play its greatest role in the market flow economy. Because the algorithm of the cyclic neural network is complex, it can be reduced to 16% uncertainty in the enterprise economy, and the time difference power value becomes smaller. The calculation of evaluation index parameters can improve the financial and economical rate of return of enterprises. In the aspect of possibility research, the cyclic neural network model brings future expectation estimation to enterprise finance with a risk assessment rate of 37%, thus reducing market financial risks, improving the predictability of enterprises in future financial and economic markets, reducing unknown parameters, and effectively avoiding risks caused by market fluctuations.

Through the research and experiment of this paper, we can draw a conclusion. In the current index range of uncertain factors of enterprise finance and economy in the global market, facing all aspects of the combination of deep learning model and business administration, first of all, what we should do is to talk about the decomposition and structure of uncertain factors in the current market economy. Macroeconomic uncertainties in the current international and domestic environment can be divided into four kinds of domestic uncertainties and international uncertainties. Then, the advantages and disadvantages of the four learning models are selectively combined with the aspects of business administration, and the economy and finance of the enterprise are integrated to influence the finance and economy of the enterprise. Finally, the source of uncertainty is obtained, and then the risk prediction and risk control are carried out by constructing decision trees. These models are used to bring comprehensive analysis to the financial economy of enterprises and to construct the influence of good trends and development prospects.

Data Availability

The experimental data used to support the findings of this study are available from the corresponding author upon request.

Conflicts of Interest

The author declares no conflicts of interest regarding this work.

References

[1] L. Alen, T. G. Bali, and Y. Tang, "Does systemic risk in the financial sector predict future economic downturns," *Review of Financial Studies*, vol. 25, no. 10, pp. 3000–3036, 2012.

[2] K. Jurado, S. C. Ludvigson, and S. Ng, "Measuring uncertainty," *The American Economic Review*, vol. 105, no. 3, pp. 1177–1216, 2015.

[3] L. Currie, "The general theory of employment, interest and money," in *Review of Keynesian Economics*, J. M. Keynes, Ed., vol. 4, no. 1, pp. 61–66, 2016.

[4] W. Sheng, S. Sun, L. Zhen, R. Zhang, J. Xu, and S. Avner, "Accurate de novo prediction of protein contact map by ultra-

deep learning model," *PLoS Computational Biology*, vol. 13, no. 1, Article ID e1005324, 2017.

[5] A. Ali and F. Yangyu, "Unsupervised feature learning and automatic modulation classification using deep learning model," *Physical Communication*, vol. 25, no. 1, pp. 75–84, 2017.

[6] D. Zhang, Z. Wen, W. Huang, Z. Hong, and L. Meng, "Upscaling of surface soil moisture using a deep learning model with VIIRS RDR," *ISPRS International Journal of Geo-Information*, vol. 6, no. 5, pp. 1–20, 2017.

[7] T. Beck, A. Demirguc-Kunt, and R. Levine, "A new database on the structure and development of the financial sector," *The World Bank Economic Review*, vol. 14, no. 3, pp. 597–605, 2000.

[8] P. Hanel, "Intellectual property rights business management practices: a survey of the literature," *Technovation*, vol. 26, no. 8, pp. 895–931, 2006.

[9] L. Cunha, P. Ceryno, and A. Leiras, "Social supply chain risk management: a taxonomy, a framework and a research agenda," *Journal of Cleaner Production*, vol. 220, pp. 1101–1110, 2019.

[10] M. A. Mazzocco, "HACCP as a business management tool," *American Journal of Agricultural Economics*, vol. 78, no. 3, pp. 770–774, 1996.

[11] J. J. Shi and D. W. Halpin, "Enterprise resource planning for construction business management," *Journal of Construction Engineering and Management*, vol. 129, no. 2, pp. 214–221, 2003.

[12] D. W. Johnson, K. W. Bartholomew, and D. Miller, "Improving computer literacy of business management majors:A case study," *Journal of Information Technology Education*, vol. 5, no. 4, pp. 77–94, 2006.

[13] C. Matthew, S. Robert, and N. Lussier, "Non-family-members in the family business management team:a multinational investigation," *The International Entrepreneurship and Management Journal*, vol. 5, no. 4, pp. 395–415, 2009.

[14] J. Stewart and V. Knowles, "Mentoring in undergraduate business management programmes." *Journal of European Industrial Training*, vol. 27, no. 2/3/4, pp. 147–159, 2013.

[15] S. Georgina, B. Hannah, M. Laura, and T. Shirvani, "Part I: externalities and economic policies in road transport," *Research in Transportation Economics*, vol. 28, no. 1, pp. 2–45, 2010.

[16] L. Wang, "On China' FTA promotion strategy under the new development trend of global FTAs," *Journal of Shanghai University of International Business and Economics*, vol. 17, no. 3, pp. 340–357, 2015.

[17] X. Chen and W. Zhang, "Study on the decoupling of cultivated land occupation by construction from economic growth in chengdu city," *Journal of Management and Sustainability*, vol. 1, no. 1, 2011.

[18] Y. Wang, X. Xu, and H. Xue, "Method to measure the unbalance of the multiple-circuit transmission lines on the same tower and its applications," *IET Generation, Transmission & Distribution*, vol. 10, no. 9, pp. 2050–2057, 2016.

[19] J.-J. Liao, C.-H. Shih, T.-F. Chen, and M.-F. Hsu, "An ensemble-based model for two-class imbalanced financial problem," *Economic Modelling*, vol. 37, no. feb, pp. 175–183, 2014.

[20] M. J. Gorgievski, A. B. Bakker, W. B. Schaufeli, H. V. Der, and C. M. Giesen, "Financial problems and psychological distress: Investigating reciprocal effects among business owners," *Journal of Occupational and Organizational Psychology*, vol. 83, no. 2, pp. 513–530, 2011.

[21] Y. Zhang, S. J. Taylor, and L. Wang, "Investigating the information content of the model-free volatility expectation by Monte Carlo methods," *Journal of Futures Markets*, vol. 33, no. 11, pp. 1071–1095, 2013.

[22] M. Cullen, L. Einav, and A. Finkelstein, "Estimating welfare in insurance markets using variation in prices," *Discussion Papers*, vol. 125, no. 3, pp. 877–921, 2009.

[23] J. D. Leeuw, K. Hornik, and P. Mair, "Isotone optimization in R:Pool-Adjacent-Violators algorithm (PAVA) and active set methods," *Journal of Statistical Software*, vol. 32, no. 5, 2009.

[24] K. Jurado, S. Ng, and S. C. Ludvigson, "Measuring uncertainty," *Operations Research*, vol. 56, no. 3, pp. 265-266, 2016.

Hindawi
Scientific Programming
Volume 2021, Article ID 5223034, 12 pages
https://doi.org/10.1155/2021/5223034

Research Article

Modern Art Interactive Design Based on Artificial Intelligence Technology

Weihua Zhang and Yufeng Jia

School of Design, Dalian Minzu University, Dalian, Liaoning Province 116600, China

Correspondence should be addressed to Weihua Zhang; zhangweihua@dlnu.edu.cn

Received 21 October 2021; Revised 5 November 2021; Accepted 12 November 2021; Published 2 December 2021

Academic Editor: Le Sun

To improve the effect of modern art design, this study presents a camera pose estimation algorithm based on the least feature points of quaternion. Moreover, this study detects and matches the feature points of the camera image and establishes a system of formulas through the rigid constraints of the feature points, thereby constructing an eigenvalue problem to solve the camera pose. In addition, this study combines artificial intelligence technology to construct the modern art interactive design system and structure the system function structure. Finally, this study analyzes the logical structure and spatial structure of the system and uses the design to analyze the performance of the modern art interaction design model proposed in this study. Through experimental research, it can be known that the modern art interactive design system based on artificial intelligence technology proposed in this study can basically meet the artistic design needs of the new media era.

1. Introduction

With the continuous progress of modern science and technology, the human world has entered the information age from an industrial society, ubiquitous information has long been integrated into every corner of people's lives, and mankind is opening a new era of informationization. In an epoch-making background, the development of computer science, the Internet, virtual reality, and artificial intelligence has forced the continuous expansion and innovation of art design disciplines. Technology has given birth to new design forms [1], and the information art design discipline has emerged at the historic moment. As a bridge between art and science, information art design has gradually evolved into a new subject with rich connotation. Design art is based on design practice, so information art design must be a discipline based on the actual needs of society [2]. For example, interactive public art is involved in subway public art design in subway space and information art design of tourism digital service platform that integrates new media technology and art. As an important channel of information transmission, interaction design has become an important link in information art design. With the continuous development of science and technology, the integration of interactive information art design and technology will continue to innovate the form of art design, injecting strong vitality into the development of technology and art [3].

Through today's hardware and software equipment and auxiliary equipment, users can not only see, hear, and feel, but also communicate and experience each other, and at the same time create a virtualized information environment. Virtual reality technology has been used in military, education, construction, civil engineering, entertainment, and other fields in the early days and has achieved excellent results. Due to the rapid changes in the times, traditional concepts can no longer meet the needs of the people today, and what follows is a digital technological revolution. Technology leads the trend of the times, and science and technology are constantly eroding people's thoughts and lives, making life more colorful. However, the form of art has also changed with the development of technology, and the art displayed in technology has become one of the latest expressions of artists. With the development of information technology, virtual technology is widely used, not only in movies and games. The construction of digital virtualization will shorten the distance between people. This is not only for browsing, but also for close contact with people who do not understand virtual technology. At the same time, there are also many novelties in artistic expression.

The beauty displayed in the virtual reality system is called virtual artistic beauty. The artistic sense displayed by virtual reality art and traditional art has similarities. Therefore, it is necessary to have a deeper understanding of how virtual reality art inherits the form of traditional art. Virtual reality art is expressed on the basis of technology, and technology contains traditional elements. In art aesthetics, technology itself is a kind of beauty. Virtual reality finds the attributes of artistic performance in the performance of related technologies and conducts research and analysis from an artistic point of view to analyze the visual impact of the technology on the user experience.

This article combines new media technology and modern art interactive design requirements to construct an intelligent modern art interactive design system, which changes the traditional art design method and promotes the development of subsequent art design.

2. Related Work

In recent years, with the continuous advancement of computer vision, image recognition, and other technologies, human-computer interaction technology has gradually changed from the past computer-centric keyboard and mouse interaction mode to a new human-centered interaction mode—natural human-computer interaction [4]. Microsoft introduced Kinect, a 3D motion-sensing camera that integrates multiple functions such as voice input recognition and dynamic video capture, completely subverting the single production mode of the game [5]. It captures human body movements through cameras, uses depth sensors to acquire strength and depth data, processes them, performs pixel-level evaluation of depth images, uses segmentation strategies for human body recognition, and generates a skeleton system based on the tracked 20 joint point information, in real-time capture of the player's gestures [6]. With the development of technologies such as computer image recognition, laser acquisition, and machine vision, somatosensory interaction devices have become the first choice for researchers to realize natural interaction [7]. Among the most representative somatosensory control equipment are Kinect, Leap Motion, PS Move, etc. Relying on its feature that it can obtain bone information and human body depth at the same time, Kinect has been widely used since its launch and has become the mainstream data collection device used in the field of gesture recognition research [8]. Ref. [9] predicts students' attention in the classroom from Kinect facial and body features, and uses the two-dimensional and three-dimensional data obtained by the Kinect sensor to establish a feature set that characterizes the student's face and body attributes (including gaze point and body posture). Using machine-learning algorithms to train the classifier, it can estimate the time-varying attention level of individual students. The authors of [10] created a sign language spelling recognition system based on Kinect and solved the problem that the previous research on fingerspelling recognition is difficult to correctly judge the occlusion and accurately extract the depth value. The authors of [11] implements a museum roaming system based on Kinect, using the position data of head, feet, hands, shoulders, and spine obtained by Kinect, and recognizes five postures and three movements. According to the recognition result, the user can change the viewing angle, open or close the sliding door, roll up the bamboo curtain, and light or extinguish the candle in the three-dimensional space. In the past, the virtual reality equipment itself did not have the supporting somatosensory interaction function, which made it impossible to realize a perfect virtual reality experience. It can only be realized with external equipment such as Kinect and Leap Motion [12], but now VR devices are becoming more and more mature. At present, the three major consumer VR devices (Oculus Rift CV1, HTC VIVE, and PS VR) can all realize somatosensory interaction. Somatosensory interaction allows the body to interact with various scenes in the virtual world, improve immersion, and effectively reduce motion sickness [13]. However, since the Oculus Touch and HTC VIVE somatosensory interactive consumer version of Oculus Rift CV1 has just been released, so far almost all the academic research and results in virtual reality somatosensory interaction have been developed using Kinect [14].

After years of development, the current application fields of virtual reality are very extensive, involving education, medical care, entertainment, transportation, engineering design, etc. [15]. The authors of [16] has conducted research on the application of virtual reality technology in education, perceiving students through vision, hearing, and touch. The authors of [17] developed a new type of interactive virtual reality performance theater, which can enable multiple participants to enjoy an environment of entertainment and educational experience. Participants watch the performance through the VR display device, can interact with the performer through the use of input devices, and have limited control over the content of the performance. There is still a big gap between China and some foreign developed countries in the research of virtual reality, but many domestic research institutes and universities are also conducting active research.

3. Art Interactive Space Algorithm

The algorithm uses feature points for pose estimation, as shown in Figure 1. The two pictures taken by the camera at different positions are detected and matched with the feature points in the two images using a computer, and the coordinate information of the feature points is obtained at the same time. The feature points detected in the image on the left are marked with red points and that on the right are marked with green. Finally, we use a computer to match the feature points and connect them with yellow line segments, with the image center as the center, the right direction is the positive direction of the x-axis, and the downward direction

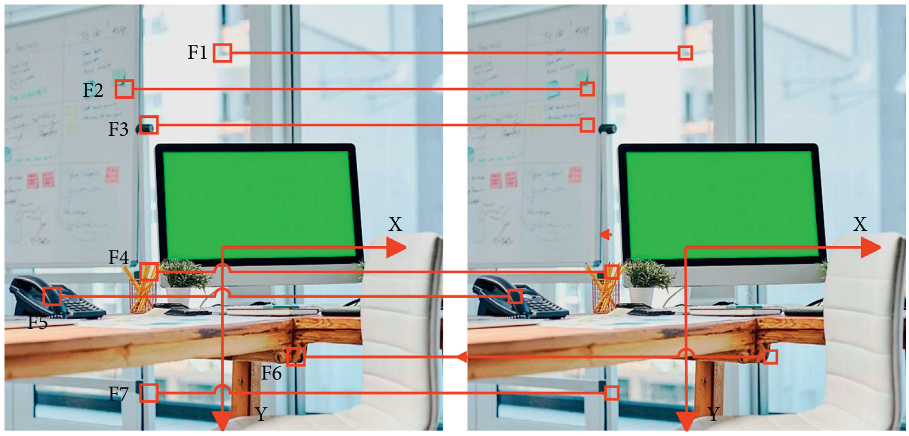

Figure 1: Feature point matching diagram.

is the positive direction of the y-axis. Then, the coordinate of the feature point can be known.

$R \in SO(3)$ and $t \in R^3$, respectively, represent the relative rotation matrix and the translation matrix of the camera in the two images. According to the scene images taken by the camera in the two views, the feature points in the image can be detected and matched, and the coordinates in the image plane where they are located can be extracted from the image. The coordinates are obtained in pixels, and then, the coordinates are mapped to the Cartesian coordinates on the image plane through the camera calibration matrix. For each matched feature point, it obeys the rigid motion constraint as shown in the following formula (1) [18]:

$$uRp + t = vp\prime. \quad (1)$$

In the formula, $p, p' \in R^3$ represents the homogeneous coordinates of the matching feature points in the two images. The scalars u and v represent the distance from the origin of the three-dimensional feature point in the space along the z-axis of the camera coordinate system, which is called the depth value of the three-dimensional feature point at each view, as shown in Figure 2. The coordinates of points p and p' can be obtained from the image, and they are known parameters. Therefore, the unknowns to be solved in formula (1) are u, v, R, and t.

The rotation matrix in formula (1) is represented by R, and $R \in SO(3)$ is a 3×3 orthogonal matrix with a determinant value. To avoid the nonlinear problem when solving, the rotation matrix is represented by 4 variables of the quaternion $Q(w, x_1, x_2, x_3)$ as shown in the following equation [19]:

$$R = \begin{bmatrix} w^2 + x_1^2 + x_2^2 + x_3^2 & 2(x_1x_2 - wx_3) & 2(x_1x_3 + wx_2) \\ 2(x_1x_2 + wx_3) & w^2 - x_1^2 + x_2^2 - x_3^2 & 2(x_2x_3 - wx_1) \\ 2(x_1x_3 - wx_2) & 2(x_2x_3 + wx_1) & w^2 - x_1^2 - x_2^2 + x_3^2 \end{bmatrix}. \quad (2)$$

The algorithm uses a quaternion variable to represent the rotation matrix, which can be solved directly. Here, the first variable in the quaternion is positioned as a nonnegative number, that is, $w \geq 0$, which indicates that the rotation matrix and the quaternion are one-to-one. To solve the pose, the algorithm eliminates the unknown parameters u, v, and t, and derives a system of formulas based on the quaternion variables. By solving the system, the rotation matrix can be solved. The algorithm takes all the feature points into formula (1) to get the matrix expression about the translation and depth value, and solves the matrix formula to get the translation and depth information of the feature point.

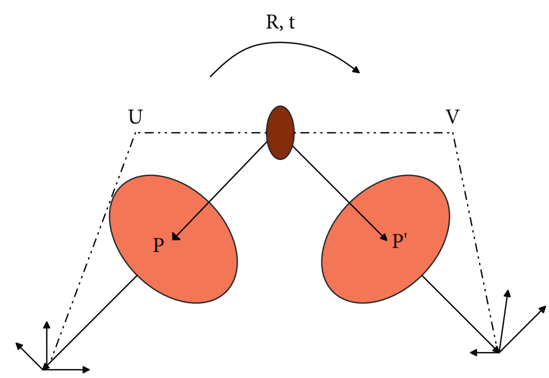

Figure 2: Feature points from different perspectives.

To solve the rotation matrix and the translation matrix, some parameters in the formula need to be eliminated. Substituting two different feature points in the image into formula (1), we can get two formulas, and the unknown parameter t can be eliminated by subtracting the two formulas. Similarly, three characteristic points can be brought into formula (1) to obtain three formulas, and the unknown parameter t in each formula can be eliminated by subtracting between the formulas. The feature points are shown in Figure 1. F1 (−0.8, 0.3), F2 (1.0, 1.4), and F3 (2.5, 0.9) and their respective matching F1' (1.3, 0.4), F2' (0.3, 1.5), and F3′(1.9,0.8) are introduced into formula (1), and formulas (3)–(5) can be obtained as follows:

$$u_1 R\begin{bmatrix}-0.8\\0.3\\1\end{bmatrix}+t=v_1\begin{bmatrix}-1.3\\0.4\\1\end{bmatrix}, \quad (3)$$

$$u_2 R\begin{bmatrix}1\\1.4\\1\end{bmatrix}+t=v_2\begin{bmatrix}0.3\\1.5\\1\end{bmatrix}, \quad (4)$$

$$u_3 R\begin{bmatrix}2.5\\0.9\\1\end{bmatrix}+t=v_3\begin{bmatrix}1.9\\0.8\\1\end{bmatrix}. \quad (5)$$

Formula (3) is subtracted from formulas (4) and (5), respectively, to obtain a formula without unknown t, and it is shown in the following formula (6) [20]:

$$\begin{cases} u_1 R\begin{bmatrix}-0.8\\0.3\\1\end{bmatrix}-v_1\begin{bmatrix}-1.3\\0.4\\1\end{bmatrix}-u_2 R\begin{bmatrix}1\\1.4\\1\end{bmatrix}+v_2\begin{bmatrix}0.3\\1.5\\1\end{bmatrix}=0,\\ u_1 R\begin{bmatrix}-0.8\\0.3\\1\end{bmatrix}-v_1\begin{bmatrix}-1.3\\0.4\\1\end{bmatrix}-u_3 R\begin{bmatrix}2.5\\0.9\\1\end{bmatrix}+v_3\begin{bmatrix}1.9\\0.8\\1\end{bmatrix}=0. \end{cases} \quad (6)$$

When u and v are regarded as unknowns, the formula $MV=0$ can be expressed as shown in formula (7). The obtained matrix M is only composed of the feature point coordinates and the rotation matrix R, and the vector V is composed of the depth parameters of the feature points. When the value of the determinant of the matrix M is equal to zero, the determinant of the matrix M can be evaluated, and the quaternion variables w, x_1, x_2, x_3 can be listed in the fourth-degree polynomial formulas, the coefficients of which are related to the coordinates of the characteristic points. The polynomial formula does not contain unknowns u and v, which eliminate the unknown depth parameter, as shown in formula (8).

$$\underbrace{\begin{bmatrix} R\begin{bmatrix}-0.8\\0.3\\1\end{bmatrix} & \begin{bmatrix}-1.3\\0.4\\1\end{bmatrix} & R\begin{bmatrix}1\\1.4\\1\end{bmatrix} & \begin{bmatrix}0.3\\1.5\\1\end{bmatrix} & 0 & 0\\ R\begin{bmatrix}-0.8\\0.3\\1\end{bmatrix} & \begin{bmatrix}-1.3\\0.4\\1\end{bmatrix} & 0 & 0 & R\begin{bmatrix}2.5\\0.9\\1\end{bmatrix} & \begin{bmatrix}1.9\\0.8\\1\end{bmatrix} \end{bmatrix}}_{M} \underbrace{\begin{bmatrix}u_1\\v_1\\u_2\\v_2\\u_3\\v_3\end{bmatrix}}_{V}=0, \quad (7)$$

$$\begin{aligned}&0.1w^4+0.07w^3x_1+0.55w^2x_1^2-10.2wx_1^4+\cdots+\\&3.96x_2^2x_3^2-71.9wx_3^3+7.76x_3^3-3.62x_2x_3+4.41x_3^4=0.\end{aligned} \quad (8)$$

Formula (8) consists of 35 monomials, and we define the operation as follows:

$$\langle a,b\rangle=\frac{b!}{a!\,(b-a)!}. \quad (9)$$

Then, a polynomial of degree d with c variables is composed of $<d+c-1$, c-1> monomials. Since any 3 feature points can get a polynomial formula, then k feature points can get <k,3> formulas. Multiplying the quaternion variables w, x_1, x_2, x_3 by the obtained fourth-degree polynomial formulas, we can list more polynomial formulas, as shown in the following formula (10) [21]:

$$\begin{cases} 0.1w^5 + 0.07w^4x_1 + 0.55w^3x_1^2 - 10.2w^2x_1^2 + \cdots + 4.41wx_3{}^4 = 0, \\ 0.1w^4x_1 + 0.07w^3x_1^2 + 0.55w^2x_1^3 - 10.2wx_1{}^4 + \cdots + 4.41x_1x_3^4 = 0, \\ 0.1w^4x_2 + 0.07w^3x_1x_2 + 0.55w^2x_1^2x_2 - 10.2w^2x_1^2x_2 + \cdots + 4.41x_2x_3^4 = 0, \\ 0.1w^4x_3 + 0.07w^3xx_3 + 0.55w^2x^2x_3 - 10.2w^2x^2x_3 + \cdots + 4.41x_3^5 = 0. \end{cases} \tag{10}$$

If 5 feature points are used to estimate the pose of the camera, then <5,3 ≥ 10 quartic polynomial formulas can be established. Multiplying the quaternion variables with them, respectively, we can get 40 formulas of degree 5, and the number of monomials is < 4+5–1, 3 ≥ 56. The new formulas obtained are expressed in matrix vector form as follows: AX = 0.

$$\underbrace{\begin{bmatrix} 0.1 & 0.07 & 0.55 & -10.2 & \cdots & 0 \\ 0 & -0.1 & 0.07 & 0.55 & \cdots & 0 \\ \vdots & \vdots & \vdots & \vdots & \ddots & \vdots \\ 0 & 0 & 0 & 0 & 0 & 4.41 \end{bmatrix}}_{A} \underbrace{\begin{bmatrix} w^5 \\ w^4x_1 \\ w^3x_1^2 \\ w^2x_1^3 \\ \vdots \\ x_3^5 \end{bmatrix}}_{X} = 0. \tag{11}$$

Among them, the matrix A is composed of the coefficients of the formula system, and . $A \in R^{40\times 56}$The matrix X consists of all five-degree monomials, and $X \in R^{56}$. As shown in formula (11), the algorithm divides the vector X into two vectors as follows:

$$X_1 = \begin{bmatrix} w^3x_1^2 \\ w^2x_1^3 \\ wx_1^4 \\ \vdots \\ wx_3^4 \end{bmatrix}, \quad x_2 = \begin{bmatrix} x_3^5 \\ x_1x_3^4 \\ x_2x_3^4 \\ \vdots \\ x_1^5 \end{bmatrix}. \tag{12}$$

Among them, $X_1 \in R^{35}$ and $X_2 \in R^{21}$. X_1 is the vector containing all the monomials of w, and X is composed of the remaining monomials. We set $A = [\, A_1 \;\; A_2 \,]$. Among them, A_1 is composed of the column of A associated with X_2, and $A_2 \in R^{40\times 35}$. A_2 is composed of the column of A associated with X, and $A_2 \in R^{40\times 21}$. Then, the system AX-0 can be equivalently written as follows [22]:

$$A_1X_1 + A_2X_2 = 0. \tag{13}$$

By multiplying formula (13) by the pseudo-inverse matrix A_2 of A_2^+, we can get the following:

$$X_2 = -A_2^+A_1X_1. \tag{14}$$

The algorithm proposes the variable w in the vector X_1 and denotes it with V. That is,

$$V = \frac{1}{w}X_1. \tag{15}$$

The algorithm sets $\overline{B} = -A_2^+A_1$, and $\overline{B} \in R^{21\times 35}$. Then, X_2 can be expressed as $X_2 = w\overline{B}V$.

$$\underbrace{\begin{bmatrix} x_3^5 \\ x_1x_3^4 \\ x_2x_3^4 \\ \vdots \\ x_1^5 \end{bmatrix}}_{X_2} \underbrace{\begin{bmatrix} -0.1 & 0.02 & -0.01 & \cdots & 8.9 \\ 0.1 & 0.01 & 0.01 & \cdots & -1.7 \\ 0 & 0.01 & 0.01 & \cdots & -6.9 \\ \vdots & \vdots & \vdots & \ddots & \vdots \\ 0.1 & -0.02 & 0.03 & \cdots & -12.5 \end{bmatrix}}_{\overline{B}} \underbrace{\begin{bmatrix} w^3x_1^2 \\ w^2x_1^3 \\ wx_1^4 \\ \vdots \\ wx_3^4 \end{bmatrix}}_{wV}. \tag{16}$$

The algorithm constructs a square matrix B, and $\overline{B} \in R^{21\times 35}$. The algorithm constructs a matrix formula: $\lambda V = BV$, which transforms the problem into an eigenvalue problem, and sets $\lambda = x_1/w$. Then, the matrix formula can be expressed as $x_1V = wBV$.

$$\underbrace{\begin{bmatrix} w^2x_1^3 \\ wx_1^4 \\ x_1^5 \\ \vdots \\ x_1x_3^4 \end{bmatrix}}_{x_1V} \underbrace{\begin{bmatrix} 0 & 1 & 0 & \cdots & 0 \\ 0 & 0 & 1 & \cdots & 0 \\ 0.1 & -0.02 & 0.03 & \cdots & -12.5 \\ \vdots & \vdots & \vdots & \ddots & \vdots \\ 0.1 & 0.01 & 0.01 & \cdots & -1.7 \end{bmatrix}}_{B} \underbrace{\begin{bmatrix} x_3^5 \\ x_1x_3^4 \\ x_2x_3^4 \\ \vdots \\ x_1^5 \end{bmatrix}}_{wV}. \tag{17}$$

In formula (17), the elements of vector x_1V belong to vector X_1 or vector X_2. For elements belonging to X_2, the corresponding row in B is selected from $\overline{B}$. For elements belonging to X_1, the corresponding row in matrix B is the appropriate natural base row vector, the solution of the vector V can be derived, and the value of the variables

w, x_1, x_2, x_3 can be calculated according to the elements of the vector V. Incorporating variables into formula (2) can be solved to obtain the rotation matrix R.

After obtaining the corresponding rotation matrix R, the translation and depth values of the characteristic points can be further solved. All matched feature points obey the rigid motion constraint, as shown in formula (1). Then, for k feature points, it is expressed as a matrix vector form $CY = 0$:

$$\begin{bmatrix} I & Rp_1 & -p_1' & 0 & 0 & \cdots & 0 & 0 \\ I & 0 & 0 & Rp_2 & -p_2' & \cdots & 0 & 0 \\ \vdots & \vdots & \vdots & \vdots & \vdots & \ddots & \vdots & \vdots \\ I & 0 & 0 & 0 & 0 & \cdots & Rp_k & -p_k' \end{bmatrix} \begin{bmatrix} t \\ u_1 \\ v_1 \\ u_2 \\ v_2 \\ \vdots \\ u_k \\ v_k \end{bmatrix} = 0. \tag{18}$$

In the formula, $I \in R^{3\times3}$ is the identity matrix, k is the number of feature points, matrix $C \in R^{3k\times2k+3}$, and $Y \in R^{2k+3}$. From formula (18), it can be known that the matrix Y is in the null space of matrix C. Y can be obtained by calculating the right singular vector of matrix C, that is, the eigenvector corresponding to cC. The vector Y contains both translation information and depth information. Therefore, these parameters can be solved at the same time and are constrained to the same scale factor.

It can be seen from the algorithm that when building a polynomial formula system, multiplying the quaternion variables w, x_1, x_2, x_3 by the original formula will increase the number of formulas, and at the same time, the coefficient matrix A_2 has a higher dimension, while the value of the pseudo-inverse multiplication $A_2^{+}A_2$ is not changing. When the feature point coordinates are inaccurate or affected by noise, the pseudo-inverse operation $A_2^{+}A_2$ is associated with X_1 and X_2. In practical applications, when the number of feature points increases, the dimensions of the matrices A_1 and A_2 will be higher. In this way, by pseudo-inverse operation, noise can be further suppressed, and the estimation accuracy of rotation can be improved. By choosing vector X_1 or eigenvalue λ differently, it can be transformed into different eigenvalue problems, but the result of pose estimation is the same.

The performance tests on the algorithm and several existing algorithms are performed. The test uses the Monte Carlo simulation to randomly generate a mixed set of uniformly distributed general 3D points and coplanar 3D points in a rectangular parallelepiped in front of the camera. Subsequently, it moves the camera to other positions through random translation and rotation. Using the pinhole camera model, the coordinates of the feature points are obtained by projecting the three-dimensional coordinate points onto the two-dimensional plane. In this study, the calibration algorithm of Zhang Zhengyou is used to obtain the camera parameters, and the matrix obtained by the camera calibration is K. Each image is 1728×668 pixels.

$$K = \begin{bmatrix} 358 & 0 & 358 \\ 0 & 358 & 247 \\ 0 & 0 & 1 \end{bmatrix}. \tag{19}$$

The performance of the algorithm in the article is compared with the 8-point algorithm, Kukelova algorithm, Nister algorithm, Li and Hartley algorithm, and Stewenius algorithm. In the experimental test, the rotation error and the translation error of each algorithm are compared to show the comparison result, and the result is drawn in the form of a curve. The specific error calculation method is as follows.

We define the formula as follows:

$$\rho(q, q^*) = \frac{1}{\pi}\arccos\left(\mathrm{dot}\left(q, q^*\right)\right). \tag{20}$$

Equation (20) is used to describe the rotation error, and $\rho(q, q^*) \in [0, 1]$. Among them, $q = \begin{bmatrix} w & x_1 & x_2 & x_3 \end{bmatrix}^T$ is the quaternion value used to solve the rotation matrix in the test, and q^* is the true value. Similarly, the translation error can be obtained by replacing the quaternion vector in the formula with the unit norm translation matrix.

To evaluate the performance of the algorithm under the influence of noise, the Gaussian noise with a mean value of zero and a standard deviation of 0 to 3 pixels was used to simulate noise interference in the experimental operation. Then, we add it to all images, set the noise standard deviation increment value to 0.1 pixel value, and do 100 random experiments on the unit noise increment value. The solution closest to the true value is selected as the estimated value of each algorithm. To compare the anti-interference ability of these algorithms against noise at the minimum feature points, the number of feature points provided for the algorithms participating in the comparison in the experiment is the minimum number of feature points required for the solution of each algorithm. We can use formula (20) to obtain the rotation error and the translation error corresponding to each algorithm, and the corresponding error curve is shown in Figure 3.

It can be seen from Figure 3 that the estimated errors of the Nister algorithm, the Li and Hartley algorithm, and the Kukelova algorithm are relatively close, so their error curves almost overlap. The 8-point algorithm shows a relatively good translation error, but because the rotation error is too large, only a part of the rotation error curve is shown in the figure. The Stewenius algorithm shows good estimation accuracy, ranking second in the comparison. The error curve of the algorithm in this study is below all the curves, and the estimated error is smaller than other algorithms, which shows the best performance. The comparison result between the Stewenius algorithm and the algorithm in this study is shown in Figure 4.

In practical applications, the number of feature points detected and matched between the two images is usually greater than the minimum number required by the algorithm. Therefore, in practical applications, pose estimation

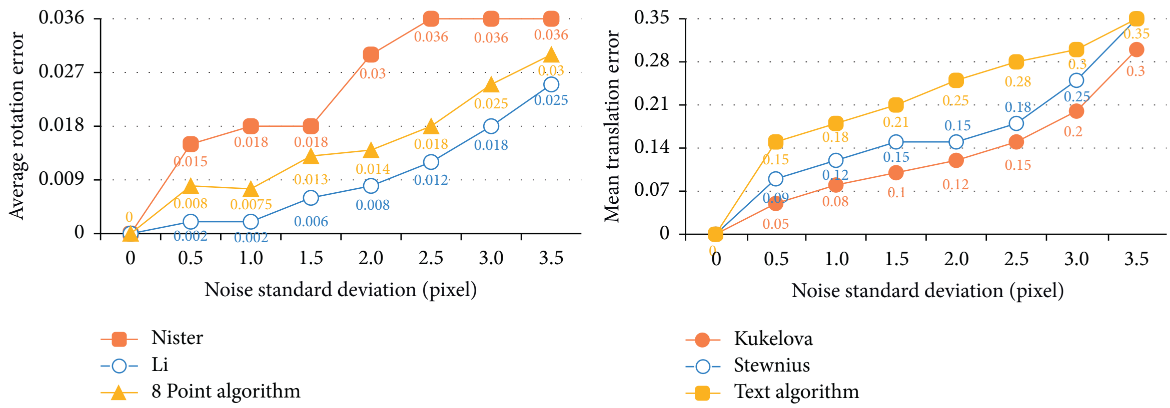

Figure 3: Anti-noise comparison results.

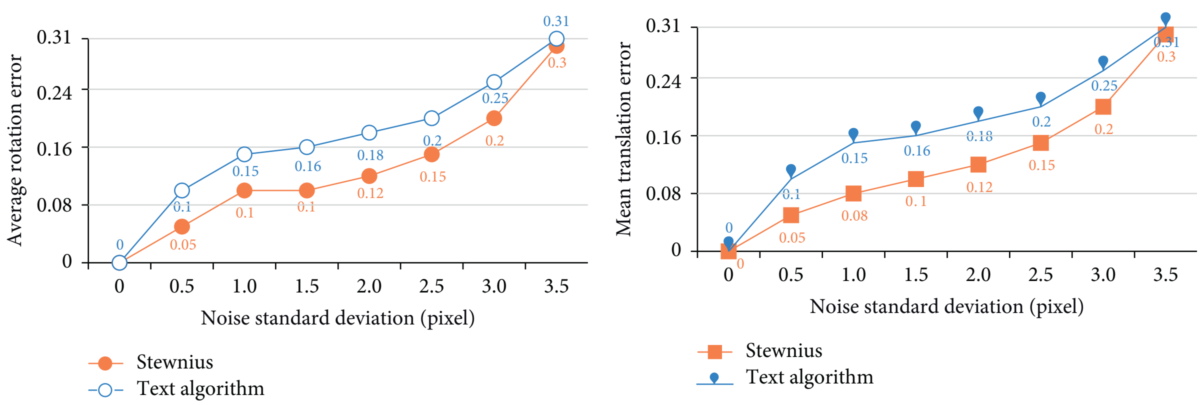

Figure 4: Comparison results between the algorithm in this study and the Stewenius algorithm.

algorithms often have to solve the problem of the number of feature points exceeding the minimum to reduce the influence of noise and mismatches. In the experimental test, when we provide the number of feature points, we generally use the minimum number of feature points required by the respective algorithm to 100 feature points to simulate the actual algorithm matching multiple feature points and set the feature point increment to 1. Each time a feature point is added, 100 comparison experiments are performed, and the Gaussian noise with a standard deviation of 0.75 pixels is added to the pixel coordinates to simulate image pixelation noise and inaccuracies in feature point detection and matching. The error curve obtained using formula (20) is shown in Figure 5.

Because Li and Hartley's algorithm does not accept more than 5 feature points, they did not participate in the comparison. As shown in Figure 5, from the perspective of the rotation error curve, when the number of feature points used does not exceed 10, the algorithm in this study and the Stewenius algorithm have the best position estimation accuracy. As the number of feature points increases, the performance of the 8-point algorithm is higher than that of the Stewenius algorithm, and the error curve of the algorithm in this study is always at the bottom, which has the best estimation accuracy. From the perspective of the translation error curve, when the number of eigen points exceeds 10, the estimation accuracy of the algorithm in this study is significantly better than other algorithms involved in the comparison. From the overall comparison result, the rotation and translation estimation error curves of the algorithm in this study are all below other algorithms, the estimation accuracy is the highest, and it shows the best performance. As the number of matched feature points increases, the error of the estimation result will be further reduced.

To test the actual application effect of the algorithm, six algorithms are tested using images from the real-world data set, and the estimated results are compared with the real values provided by the data set. The test uses the KITTI data set. When using the data set for testing, without affecting the test results, the sampling principle is adopted and the data set is set to an increment of 5. This can reduce the test time and increase the disparity at the same time, which is more conducive to the estimation of the translation information. All algorithm implementations are programmed in MATLAB using C language and executed as MEX files. The test is carried out on the same computer platform. The computer uses Intel(R) Core(TM) i5-8500 CPU, the main frequency is 3.00 GHz, and the memory capacity is 8 GB. The results are shown in Tables 1 and 2.

To reflect the statistical information of the test results, a quarter of the average rotation error and average translation error, the median, and three quarters of the value are listed in

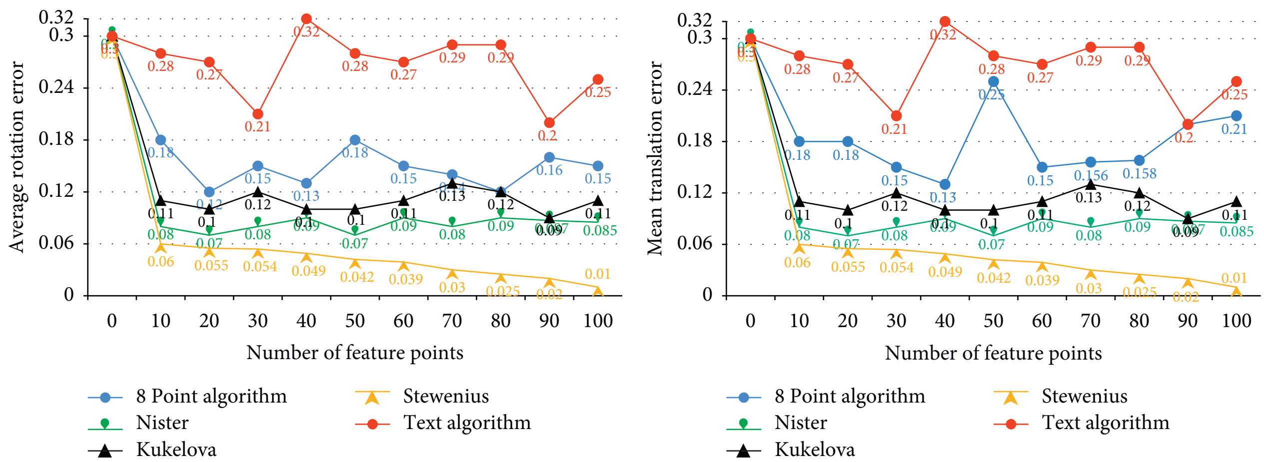

Figure 5: Performance comparison results of multiple feature points.

Table 1: Average rotation error.

	8-Point algorithm	Kukelova algorithm	Stewenius algorithm	Nister algorithm	The algorithm proposed in this study
A	0.0241	0.0178	0.0179	0.0177	0.0132
B	0.0470	0.0324	0.0293	0.0319	0.0221
C	0.0902	0.0644	0.0492	0.0646	0.0345

Table 2: Average translation error.

	8-Point algorithm	Kukelova algorithm	Stewenius algorithm	Nister algorithm	The algorithm proposed in this study
A	0.0038	0.1101	0.0179	0.0043	0.0035
B	0.0067	0.2449	0.0293	0.0083	0.0058
C	0.0125	0.4102	0.0492	0.0187	0.0107

the table, denoted by *A*, *B*, and *C*, respectively. At the same time, for the convenience of comparison, the average rotation error in Table 1 is the result after magnification 100 times. The data in the table show that among the several algorithms participating in the comparison, the average rotation error and the average translation error of the algorithm in this study are both the smallest. Compared with the 8-point algorithm, the average rotation median error of this algorithm is reduced by 52.9%, and the average translation median error is reduced by 13.4%. Compared with the second-ranked Stewenius algorithm, the average rotation median error of this algorithm is reduced by 24.5%, and the average translation median error is reduced by 30.1%. Generally speaking, the algorithm that uses the least number of feature points greater than 5 tends to have a shorter execution time than the 5-point algorithm. The execution time of the algorithm in this study is not optimal, but this is only relative. Through the test of images of real-world data sets, the algorithm in this study can fully meet the real-time performance in the application.

3.1. Modern Art Interactive Design System Based on Artificial Intelligence. Holographic technology enhances the individual's creative thinking and behavior ability. In the virtual world created by consciousness, the mapped thoughts, emotions, feelings, and thinking interact, and audiences from different cultures and societies circulate and form a perception system in the medium of virtual reality based on the differences in thought and the multiplicity of experiences (Figure 6).

As a new art form, new media art is no longer constrained to the traditional mode of expression, and the audience has faded away from the passive role that was always given to it in the past. Moreover, it will increasingly participate in recipients of scientific and technological intelligence, interacting with works and artists and forming a feedback mechanism, and the derivation of interactive behavior is closely related to the environment and emotional appeals of the audience. The framework diagram of behavioral interaction research is shown in Figure 7.

In the construction of the interactive logic model, the elements of "things" are extracted, and the relationship of reasons is obtained. At the logical level of aesthetic interaction, it summarizes the contemporary display methods of new media art through the comparison of static and dynamic display, and summarizes the unique aesthetic experience of new media art through the comparison of traditional art and new media art. The logic level of behavior interaction relies on behavior-related theories to analyze the participating elements of behavior interaction and the circulatory system that it constitutes, and summarize the

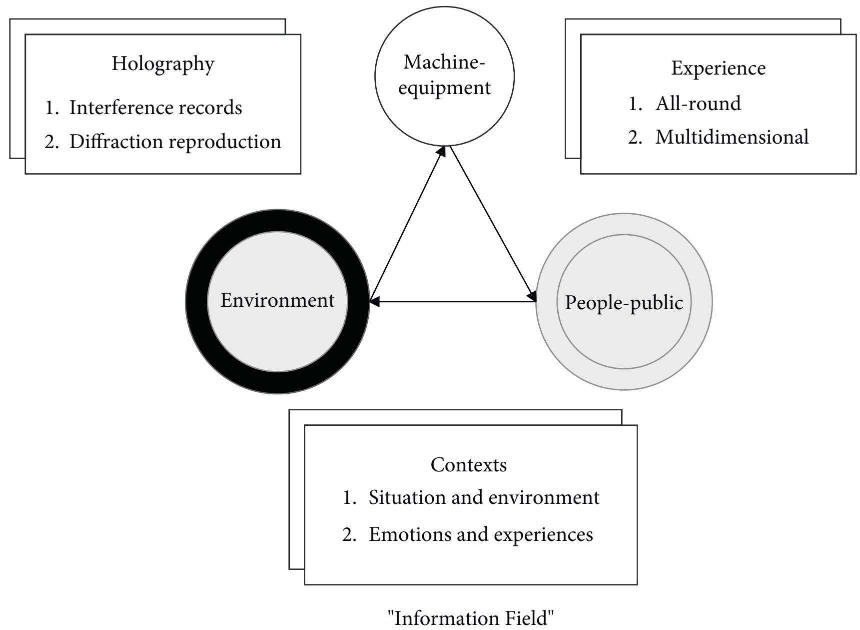

Figure 6: Holographic experience situation system.

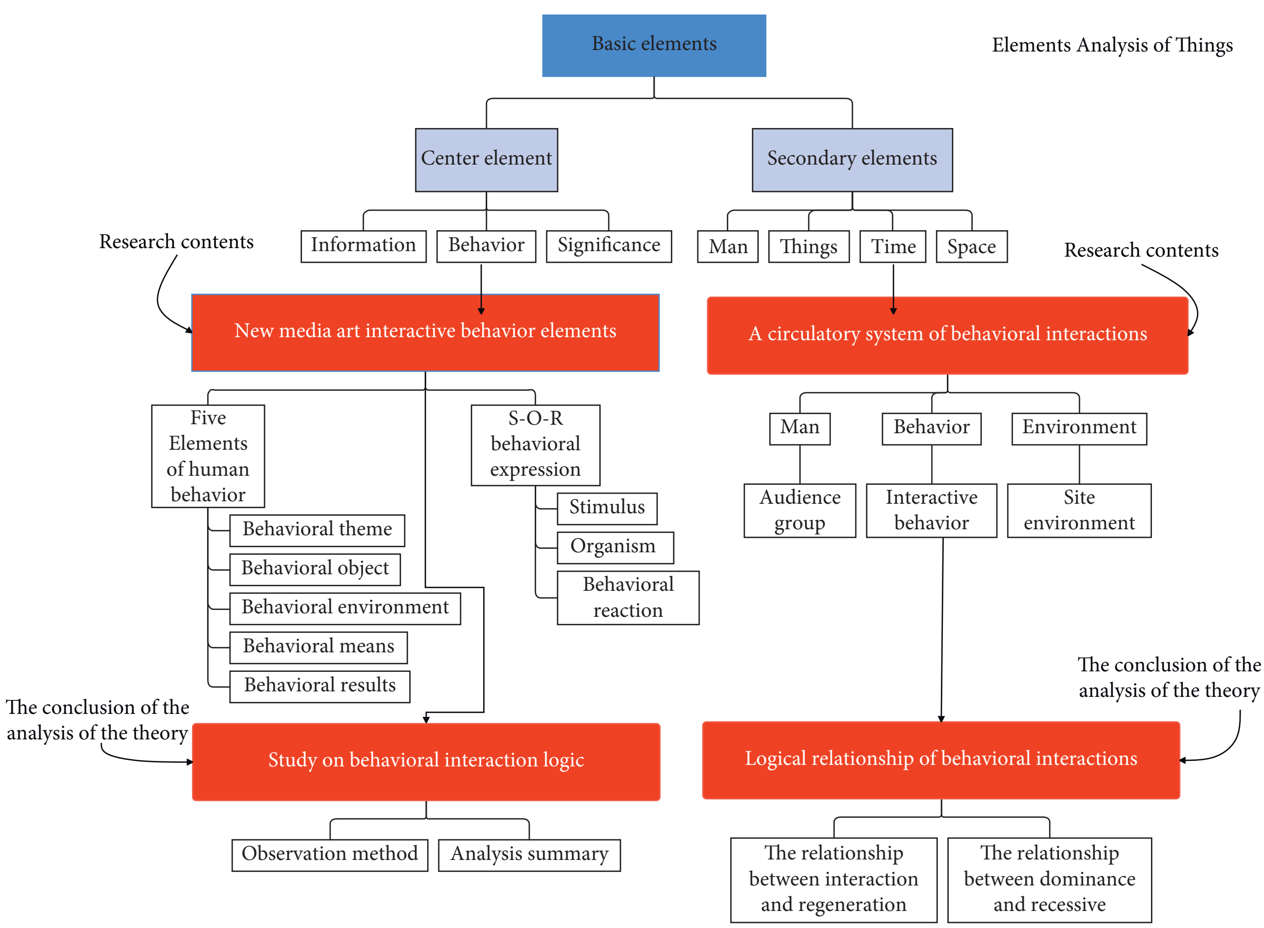

Figure 7: Framework diagram of behavioral interaction research.

interactive regeneration and explicitness and implicit nature of logical relations. The logical level of virtual-real interaction takes the technological carrier as the entry point. It mainly uses the technology of virtual reality, augmented reality, and mixed reality to explore the logical relationship between time and space, technical art, and virtual reality, and

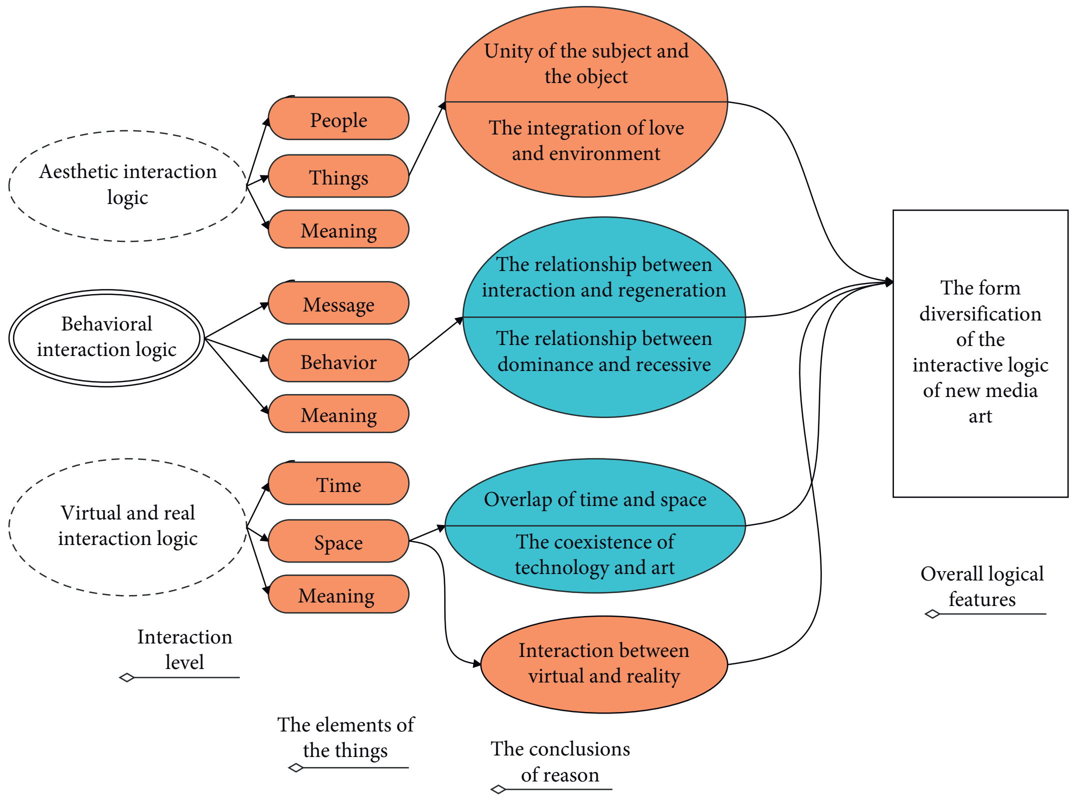

Figure 8: Interactive logic model of modern art design based on artificial intelligence.

Table 3: Statistical table of interactive effects of modern art interactive design system.

Number	Interactive effect
1	91.36
2	86.20
3	90.36
4	92.68
5	89.45
6	89.94
7	85.19
8	84.37
9	89.89
10	86.06
11	82.70
12	84.17
13	90.98
14	93.48
15	91.33
16	88.11
17	90.82
18	84.58
19	84.48
20	87.72
21	84.74
22	83.43
23	89.82
24	85.21
25	91.32
26	83.42
27	84.04

Table 3: Continued.

Number	Interactive effect
28	92.87
29	88.99
30	83.75
31	82.91
32	88.67
33	86.17
34	84.11
35	87.29
36	86.82
37	93.02
38	88.66
39	87.59
40	88.05

Table 4: Effect of modern art interactive design based on artificial intelligence technology.

Number	Interactive effect
1	90.04
2	87.09
3	76.87
4	86.16
5	88.98
6	91.20
7	86.38
8	88.11
9	79.89

Table 4: Continued.

Number	Interactive effect
10	83.46
11	76.06
12	75.11
13	79.67
14	75.14
15	89.91
16	76.26
17	78.00
18	87.22
19	84.27
20	86.30
21	89.57
22	91.01
23	79.87
24	75.08
25	86.43
26	89.16
27	75.44
28	78.14
29	87.55
30	89.68
21	89.57
22	91.01
23	79.87
24	75.08
25	86.43
26	89.16
27	75.44
28	78.14
29	87.55
30	89.68
31	77.67
32	91.45
33	74.56
34	78.70
35	88.40
36	78.44
37	91.04
38	81.48
39	80.23
40	79.89

finally obtains the conclusion of the interactive logic of new media art to form a complete logical model. The interactive logic model of modern art design based on artificial intelligence is shown in Figure 8.

After constructing the above model, we will explore the effectiveness of the modern art interaction design system. The art interaction design system of this study is evaluated through experimental research, and the results shown in Table 3 are obtained.

From the above test results, the effect of modern art interaction design proposed in this study is very good, and then, the design effect of the system is evaluated, and the results are shown in Table 4.

From the results in Table 4, the modern art interactive design system based on artificial intelligence technology proposed in this study can basically meet the artistic design needs of the new media era.

4. Conclusion

The dynamic form of virtual reality technology and art is called interactive. The interactive feedback also gives the experiencer a soul-like artistic impact. In virtual reality technology and art, interaction reflects research and discussion, with interactivity as the core auxiliary technology and art, which can improve the sensory experience and aesthetic value of the experiencer. This article combines theory with examples to study the interactive form and uses examples to explain the theory, and the theory serves as the basis for practice. Moreover, this study strives to provide key guidance for virtual reality design and art creation from the perspective of interactive performance, which can provide experience for interactive research on virtual reality art and technology. In addition, this study analyzes through cases, extracts the interactivity of virtual reality technology and art, complements each other, and promotes the innovation of the work. Finally, this study combines new media technology and modern art interaction design requirements to build an intelligent modern art interaction design system, which changes the traditional art design method and promotes the development of subsequent art design.

Data Availability

The labeled data set used to support the findings of this study is available from the corresponding author upon request.

Conflicts of Interest

The authors declare no conflicts of interest.

Acknowledgments

This work was sponsored by the Research and Demonstration Application of Key Technology of Virtual Simulation Platform for Ethnic Cultural Heritage based on Cloud Platform (2020 Liaoning Provincial Natural Science Foundation Joint Fund Project).

References

[1] I. P. Tussyadiah, D. Wang, T. H. Jung, and M. C. Tom Dieck, "Virtual reality, presence, and attitude change," *Tourism Management*, vol. 66, pp. 140–154, 2018.

[2] D. Freeman, S. Reeve, A. Robinson et al., "Virtual reality in the assessment, understanding, and treatment of mental health disorders," *Psychological Medicine*, vol. 47, no. 14, pp. 2393–2400, 2017.

[3] M. S. Elbamby, C. Perfecto, M. Bennis, and K. Doppler, "Toward low-latency and ultra-reliable virtual reality," *IEEE Network*, vol. 32, no. 2, pp. 78–84, 2018.

[4] D. Shin, "Empathy and embodied experience in virtual environment: to what extent can virtual reality stimulate empathy and embodied experience?" *Computers in Human Behavior*, vol. 78, pp. 64–73, 2018.

[5] H. K. Kim, J. Park, Y. Choi, and M. Choe, "Virtual reality sickness questionnaire (VRSQ): motion sickness measurement index in a virtual reality environment," *Applied Ergonomics*, vol. 69, pp. 66–73, 2018.

[6] R. Yung and C. Khoo-Lattimore, “New realities: a systematic literature review on virtual reality and augmented reality in tourism research,” *Current Issues in Tourism*, vol. 22, no. 17, pp. 2056–2081, 2019.
[7] G. Makransky, T. S. Terkildsen, and R. E. Mayer, “Adding immersive virtual reality to a science lab simulation causes more presence but less learning,” *Learning and Instruction*, vol. 60, pp. 225–236, 2019.
[8] E. Yiannakopoulou, N. Nikiteas, D. Perrea, and C. Tsigris, “Virtual reality simulators and training in laparoscopic surgery,” *International Journal of Surgery*, vol. 13, pp. 60–64, 2015.
[9] L. Jensen and F. Konradsen, “A review of the use of virtual reality head-mounted displays in education and training,” *Education and Information Technologies*, vol. 23, no. 4, pp. 1515–1529, 2018.
[10] M. C. Howard, “A meta-analysis and systematic literature review of virtual reality rehabilitation programs,” *Computers in Human Behavior*, vol. 70, pp. 317–327, 2017.
[11] M. Serino, K. Cordrey, L. McLaughlin, and R. L. Milanaik, “Pokémon,” *Current Opinion in Pediatrics*, vol. 28, no. 5, pp. 673–677, 2016.
[12] M. J. Smith, E. J. Ginger, K. Wright et al., “Virtual reality job interview training in adults with autism spectrum disorder,” *Journal of Autism and Developmental Disorders*, vol. 44, no. 10, pp. 2450–2463, 2014.
[13] M. Farshid, J. Paschen, T. Eriksson, and J. Kietzmann, “Go boldly,” *Business Horizons*, vol. 61, no. 5, pp. 657–663, 2018.
[14] W. Alhalabi, “Virtual reality systems enhance students’,” *Behaviour & Information Technology*, vol. 35, no. 11, pp. 919–925, 2016.
[15] M. A. Muhanna, “Virtual reality and the CAVE: t,” *Journal of King Saud University - Computer and Information Sciences*, vol. 27, no. 3, pp. 344–361, 2015.
[16] L. R. Valmaggia, L. Latif, M. J. Kempton, and M. Rus-Calafell, “Virtual reality in the psychological treatment for mental health problems: an systematic review of recent evidence,” *Psychiatry Research*, vol. 236, pp. 189–195, 2016.
[17] M. Slater, “Immersion and the illusion of presence in virtual reality,” *British Journal of Psychology*, vol. 109, no. 3, pp. 431–433, 2018.
[18] E. A.-L. Lee and K. W. Wong, “Learning with desktop virtual reality: l,” *Computers & Education*, vol. 79, pp. 49–58, 2014.
[19] J. N. A. Silva, M. Southworth, C. Raptis, and J. Silva, “Emerging applications of virtual reality in cardiovascular medicine,” *Journal of the American College of Cardiology: Basic to Translational Science*, vol. 3, no. 3, pp. 420–430, 2018.
[20] N. Morina, H. Ijntema, K. Meyerbröker, and P. M. G. Emmelkamp, “Can virtual reality exposure therapy gains be generalized to real-life? a,” *Behaviour Research and Therapy*, vol. 74, pp. 18–24, 2015.
[21] G. Saposnik, L. G. Cohen, M. Mamdani et al., “Efficacy and safety of non-immersive virtual reality exercising in stroke rehabilitation (EVREST): a randomised, multicentre, single-blind, controlled trial,” *The Lancet Neurology*, vol. 15, no. 10, pp. 1019–1027, 2016.
[22] X. Pan and A. F. D. C. Hamilton, “Why and how to use virtual reality to study human social interaction: the challenges of exploring a new research landscape,” *British Journal of Psychology*, vol. 109, no. 3, pp. 395–417, 2018.

Hindawi
Scientific Programming
Volume 2021, Article ID 8971588, 9 pages
https://doi.org/10.1155/2021/8971588

Research Article

Exploration on the Teaching Reform Measure for Machine Learning Course System of Artificial Intelligence Specialty

Yizhang Jiang [1,2] **and Bo Li** [1,2]

[1]*School of Artificial Intelligence and Computer Science, Jiangnan University, 1800 Lihu Avenue, Wuxi, Jiangsu 214122, China*
[2]*Jiangsu Key Laboratory of Media Design and Software Technology, 1800 Lihu Avenue, Wuxi 214122, Jiangsu, China*

Correspondence should be addressed to Yizhang Jiang; yzjiang@jiangnan.edu.cn

Received 27 October 2021; Revised 20 November 2021; Accepted 22 November 2021; Published 30 November 2021

Academic Editor: Le Sun

Due to the particularity of the artificial intelligence major and the machine learning courses learned, the traditional course teaching model is not suitable for artificial intelligence major machine learning courses. Based on this background, this article proposes a new system based on machine learning curriculum teaching reform. It mainly includes the reform of curriculum teaching mode, curriculum practice reform, and teaching process reform. In order to verify the effect of the proposed new model on the teaching quality of machine learning courses, this article also proposes an evaluation method based on intelligent technology. Firstly, the feasibility of evaluation based on intelligent technology is described. Secondly, it lists the application details of the existing teaching evaluation based on intelligent technology. Finally, a novel teaching quality evaluation system based on intelligent technology is proposed. The system collects student facial expression data and uses classification algorithms to make classification decisions on the data. The result of the decision can give feedback on the quality of classroom teaching. The comparison of experiments based on different intelligent technologies shows that the teaching quality evaluation system proposed in this article is feasible and effective.

1. Introduction

In near few years, some new-generation information technologies are proposed, such as cloud computing, Internet of Things technology, human-computer interaction, and mobile Internet. Now, the big data has come into people's daily life, resulting in huge amounts of data information. The most important significance of studying big data is to discover new knowledge, create new value, enhance new capabilities, and improve new products through the analysis and mining of massive data. However, what too much data brings to people may not be more insights, but rather lost. The value of data lies in forming information, turning it into knowledge, and even subliming into wisdom. If the data cannot be further deeply processed, even if the amount of data is large, the meaning is very small. Therefore, how to efficiently process data and use it to drive decision-making is particularly important. Traditional data processing models did not meet the ever-increasing demand for data processing and analysis. So artificial intelligence (AI) has emerged [1,2]. The field of artificial intelligence (AI) is a subset of computer science. It is a brand-new field dedicated to researching and developing ideas, methodologies, technologies, and application systems for mimicking, extending, and increasing human intellect. AI has a wide range of applications, including computer vision, natural language processing, language recognition, medical imaging, robotics, and information retrieval [3]. And the AI has made certain breakthroughs and has become the core technology of some high-tech products.

To aggressively support the optimization of universities' scientific and technical innovation systems in the field of artificial intelligence, as well as the enhancement of the artificial intelligence staff training system [4], we need to vigorously promote undergraduate teaching activities related to artificial intelligence. Among them, the most critical is the development of machine learning courses. Such courses mainly include advanced mathematics, linear algebra, data structure, algorithm design and analysis, probability theory and mathematical statistics, machine learning, artificial intelligence, and other professional basic courses related to machine learning. These courses are frequently extremely professional and theoretical, and students frequently fall behind in following professional courses as a result of inadequate early mastery of advanced mathematics, linear algebra, and other mathematical concepts.

To address these issues, this article will develop a new teaching mode, track students' learning situations intelligently, and alter the learning state as needed. From the traditional "teacher teaches, students learn" model to a "teacher-student interaction" model [5], it is foreseeable that with the in-depth development of this model, we will better cultivate high-level professional talents, which is also a useful exploration of the teaching model in the new era. This paper's key contribution is as follows:

(1) The challenges that exist in the course teaching have been outlined through research on the teaching system of the artificial intelligence professional machine learning course.

(2) A novel teaching approach is developed to address issues in the teaching of machine learning courses. Teaching model reform, curricular practice reform, and teaching process reform are all part of the new model reform.

(3) A teaching quality evaluation system based on intelligent technology is presented to test the efficiency of the proposed teaching method. Students' facial expression data is collected, and classification choices are made using classification algorithms. The quality of classroom instruction may be correctly fed back based on the outcome of the choice.

2. Current Situation of AI Teaching

2.1. Current Situation of AI Professional Construction. Artificial intelligence is a very new field. It has grown dramatically in recent years due to the popularity of deep learning. Based on the deep learning technologies, the AI technology has become an inexorable development trend. Now, many universities around the world have opened courses related to artificial intelligence, especially artificial intelligence, automation, computer, and big data. Artificial intelligence courses have been included as important basic courses. There are 367 universities in the world with artificial intelligence research directions. The United States is in the first echelon. Canada, China, India, and the United Kingdom are in the second echelon. At present, in China, the Chinese Academy of Sciences was the first university to offer this major. After investigation and summary, the overall construction plan and ideas of Chinese universities are shown in Figure 1, which summarizes the learning content and goals of each grade.

Knowledge representation, automatic reasoning and search methods, machine learning and knowledge acquisition, knowledge processing systems, natural language comprehension, computer vision, intelligent robotics, automatic programming, and other topics are covered in artificial intelligence research. Basic topic courses, new professional courses, professional elective courses, and professional independent courses are the four types of current courses [6]. As shown in Table 1, this kind of curriculum design meets the gradual and comprehensive curriculum design requirements.

2.2. Problems in the Teaching of Machine Learning Courses

2.2.1. Highly Professional Courses. Machine Learning (ML) is a multifield, multidisciplinary study that encompasses probability theory, statistics, approximation theory, convex analysis, algorithm complexity theory, and other topics [7]. Its main goal is to figure out how computers can replicate or actualize human learning behaviors in order to learn new things and rearrange current knowledge structures in order to improve their own performance. It is the foundation of artificial intelligence, the most basic method for making computers clever, and its applications span all artificial intelligence domains. As a result, "machine learning" is a required fundamental course for students in computational intelligence science in colleges and universities (such as intelligence science and technology) [8]. In theory, the main content of the "machine learning" course should include several important aspects of computational intelligence technology: decision tree learning (ID3, C4.5), function-based learning (neural network, support vector machine, etc.), Probability-based learning (Bayesian network), instance-based learning (k nearest neighbors), rule-based learning, and commonly used methods for evaluating algorithm efficiency. Before taking this course, students must have a theoretical background in order to fully comprehend the underlying mechanisms of these methodologies. Advanced mathematics, linear algebra, mathematical logic, probability and statistics, algorithm design and analysis, and programming language are the primary preparatory subjects (C language or Java). At the same time, these "machine learning" methods provide important theoretical and methodological foundations for other professional courses in computational intelligence, such as "pattern recognition" and "data mining." Therefore, the teaching purpose and methods of the "machine learning" course should not only be limited to introducing the principles of the main classic algorithms of machine learning, but more importantly, it should help students establish a methodology for technical research and development in computational intelligence. The professional knowledge required for these courses is generally more demanding for undergraduate students, requiring a good foundation in mathematics and programming skills [9]. Moreover, the knowledge points covered in each course are large, and simple learning is difficult to digest. However, in actual teaching, in order to catch up with the teaching progress, teachers often ignore the learning difficulties of students, and students lack the ability to learn by

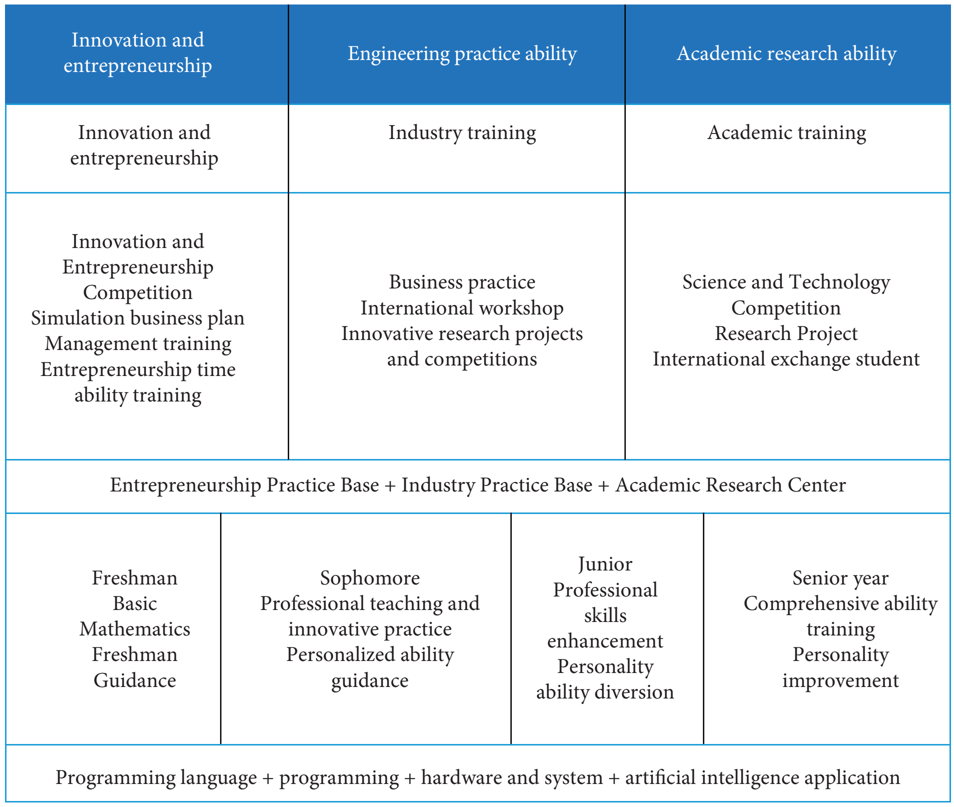

Figure 1: Construction plan and general idea.

themselves, which eventually leads to the phenomenon of being tired of learning or even not learning.

2.2.2. Boring Traditional Teaching Model. Traditional teaching consists mostly on centralized teaching in classes, with fixed time, fixed classrooms, and fixed teaching materials, with professors serving as the primary body and students serving as the object. The procedure is tedious, uninteresting, and boring. The teaching environment is drab and dismal; and pupils' enthusiasm for learning and initiative are low [10].

For example, in machine learning, the teacher first teaches the knowledge points, and then the students create the code to implement them, such as supervised learning, unsupervised learning, and semisupervised learning. In the teaching method, if students do not understand the knowledge points or practice in time, theoretical learning will be out of touch with practice. In addition, this teaching model makes it impossible for teachers to take into account the requirements of students at different levels and to meet the needs of students' individual development. However, most college teachers still use this traditional teaching model, which causes students to feel more boring and less involved in machine learning courses, thus failing to achieve the expected teaching effects. In the teaching process, because students do not fully understand the mechanisms and practical applications of various computational intelligence methods, they believe that, if they do not engage in computer-related work in the future, they will not be involved in such algorithms. In addition, most students at this stage do not have more mature ideas for future study and work development. So they do not know how learning this course can help their subsequent development, which increases their negative emotions [11]. In order to stimulate students' enthusiasm and interest in the professional knowledge learning of artificial intelligence courses, it is imperative to explore and research the teaching methods of artificial intelligence courses.

2.2.3. Formalization of Professional Practice. Professional practice teaching is an important link in the entire undergraduate teaching activities. Professional practice teaching is an important teaching method that integrates theory with practice. It can not only train students to master scientific experimental methods and innovative thinking skills, but also to improve college students' practical ability [12], problem analysis, and problem-solving ability [13]. Furthermore, professional practice teaching liberates students from tedious textbook rules, broadens students' horizons through situational learning, enhances work opportunities, and better adjusts them to changing times and societal growth.

Practical instruction is particularly important in practical and practical machine learning courses. Currently, most schools and universities place a premium on information while ignoring talent. And they place a premium on theory while ignoring practice. For example, theoretical lectures frequently take up 48 class hours in a 64-class machine

Table 1: Machine learning curriculum.

Coursetype	Technical course name
Subject platform course	Computer Composition Principles, Probability Theory and Mathematical Statistics, Database System Principles, Programming, Computer Networks, Digital Signal Processing, Advanced Mathematics, Linear Algebra
Professional core courses	Object-oriented Technology and C++, Python Programming, Machine learning, Computer Graphics, Digital Image Processing, Algorithm Analysis and Design, Artificial Intelligence.
Professional elective courses	Computer Vision, Data Acquisition Technology, Digital Security Technology, Software Engineering, Information Visualization, Compilation and Interface, Cloud Computing Technology, Website Construction and Network Communication.
Professional self-directed courses	Cloud Computing, Frontier Lectures on Artificial Intelligence, Bioinformatics, Matrix Analysis, Combinatorial Mathematics, Virtual Reality

learning course, whereas experimental classes only take up 16 class hours. The two are utterly unbalanced in their distribution[14]. Furthermore, experimental courses are frequently of poor quality, with issues such as a lack of comprehensiveness, professionalism, and inadequate engineering applications, making it difficult for students to apply what they have learned in everyday study.

The current experimental class process is roughly the same. The experimental class teacher compiles the syllabus, and the students complete the experiment independently according to the outline, and then they send the experimental results to the teacher for inspection within the specified time, meeting the requirements of society and enterprises for artificial intelligence application talents.

2.2.4. Single Professional Assessment. At present, the assessment methods of machine learning courses mostly focus on the inspection of theoretical knowledge points in textbooks, and memorable knowledge occupies a considerable proportion [15]. The traditional experiment report + final homework method is not suitable for this kind of courses. If the course learning is only driven by exams, students need to learn by rote to cope with the exams in order to fill in standard answers, resulting in high scores and low energy. The final score assesses the ability of the student and cannot be correlated with the actual learning situation of the student. Overall assessment score = 70% final exam + 10% attendance + 10% course experiment + 10% homework. In addition, this test method can easily make students feel boring, abstract and difficult to understand, and even tired of studying.

3. Teaching Reform of Machine Learning Courses for Artificial Intelligence Major

3.1. Teaching Mode Reform of Machine Learning Course. The following ideas for improvement are made in light of the concerns with the teaching approach and the peculiarities of machine learning courses:

(1) To strengthen students' independent learning abilities, move away from the traditional teacher-based teaching approach and toward a student-based teaching style. Teachers in the classroom pay more attention to guiding students to think and study independently, and they take the lead in presenting scientific and research frontier issues in the field of machine learning, encouraging students to explore research, think independently, and design solutions by hand. At the same time, students may relate theory to practice and boost their love for learning through case study, essays, group debates, and group projects. Additionally, it is vital to promote students' feeling of initiative and engagement, as well as strengthen communication between students and professors.

(2) It is vital to teach pupils of various levels according to their aptitude and to provide tailored instruction. Teachers create multiple levels of questions in the classroom to fulfill the developmental requirements of different students and to increase the quality of instruction[16]. Through different types of problems and experiments, students are encouraged to discover and solve problems. For students who are interested in certain research topics, teachers should guide and encourage them to conduct in-depth research, such as joining the teacher's experimental group, and assisting students to publish their research results in excellent journals at home and abroad. Secondly, teachers should be relevant during the experimental design process, respecting each student's unique traits and emphasizing their distinct advantages. Poor pupils should be provided more help. Difficulties should be investigated. And particular assistance should be offered.

(3) Machine learning courses need to use excellent Internet resources, not limited to textbooks, to expand classroom content. With the advancement of new media technologies, an excellent teaching platform for course instruction, such as MOOCs, has become available [17]. According to the school's planning and construction of online teaching resource library, teachers use the platform to share course videos, build a course chapter system, and enrich course materials. Teachers and students can inquire about extracurricular resources of related courses. Students learn anytime and anywhere, without being restricted by classrooms and teaching materials. Each classmate is required to take lessons, read materials through the Internet, learn the typical application

related knowledge of machine learning, and choose the research direction related to machine learning in which he is interested, relying on PPT courseware, using text, pictures, videos, and other forms to report to everyone in the classroom. During the display process, other students can also ask questions and conduct interactive communication at any time, take advantage of the Internet, pay attention to top journals, read excellent literature, and track excellent algorithms on GitHub and other websites and practice them.

3.2. Practical Reform of Machine Learning Course. As a subject with strong practicality and application, artificial intelligence majors, machine learning courses should focus on cultivating students' problem-solving abilities. Aiming at the shortcomings of traditional professional experiments and combining the characteristics of machine learning courses, we propose the following suggestions:

(1) From the beginning of the course, teachers should focus on cultivating students' hands-on practical ability, combining theory with practice, and increasing the proportion of experimental classes. Related theoretical knowledge points can be supplemented in experimental classes to improve students' understanding of machine learning algorithms [18]. In order to achieve the purpose of teaching, we can increase the number of extracurricular homework as needed to help children develop their thinking skills and basic skills.

(2) Teachers should broaden their horizons, visit artificial intelligence-related companies and advanced laboratories on a regular basis, understand the development status and future development trends of machine learning, understand the implementation of related projects, and encourage students to develop in relevant directions for subsequent career choices lay the foundation.

(3) The school-enterprise cooperation method is adopted for teaching. In the experimental class, it is not only limited to the project. It is necessary to determine the training plan and experimental plan according to the requirements of the society and the enterprise, seamlessly connect the school and the enterprise, and pay attention to the sharing of resources and information between the school and the enterprise. It is necessary to truly combine theoretical knowledge with social practice.

(4) Creating a semester group project, each semester must form a semester group [19]. From the beginning of the semester, each group needs to select a semester project and submit it at the end of the semester. The goal is to increase students' scientific research and innovation skills as well as their hands-on experience, teamwork ability, and presentation skills. At the end of each semester, following international conventions, each group needs to communicate and display the semester group projects and display them through oral reports and exhibition boards. Teachers serve as judges to evaluate and score the projects of each group. This is a good advanced training for students to participate in international academic exchanges in the future.

3.3. Teaching Process Reform. We use the creative teaching approach presented in Section 2 instead of the traditional teaching style used in many traditional courses. The three steps of the new teaching style are as follows. The first stage's major goal is to create a firm foundation, mentor new students, and focus on fundamental courses, in addition to the cultivation of fundamental talents and emphasis on students' mathematical ability to avoid pupils from falling behind in professional courses. To develop new training techniques, emphasize on personal ability training, place a premium on fundamental programming language courses, and establish a solid programming foundation are among the goals. The second stage's main goal is to develop students' professional talents, subdivision majors into specializations, rely on industrial training, and collaborate with social enterprises for training, all while focusing on academic ability development. The third stage builds on the second by enhancing students' capacity to address practical issues, solve difficulties through participation in enterprise initiatives, and develop students' practical and cooperative abilities. Students' academic aptitude may be further developed by involvement in experimental groups and other ways, and they can publish relevant articles, allowing them to obtain joint ventures.

(1) The first level aims to help students comprehend basic mathematical concepts such as advanced mathematics and linear algebra, as well as basic machine learning courses such as Python, algorithm analysis, and design, so that they may build a strong basis for future professional courses. At the same time, it assists students in comprehending the market growth and application of machine learning, allowing them to comprehend the information presented in this sort of course as well as the technology used to support it. Students' ability to innovate might be enhanced further with a solid foundation. They can coach students to improve individual ability and designate unique extracurricular learning programs based on their academic success, psychological capacity, hobbies and interests, and other factors. This is the first step in the admission process for freshmen. The major goal is to grasp the fundamentals of mathematics and programming in order to establish a solid basis for future professional development.

(2) In the second stage, on the basis of mastering basic knowledge and basic skills, students will further strengthen their professional abilities through subdivision of majors, and at the same time carry out innovative practice, industrial training, and

academic ability training. The most important thing in this stage is to digest the theoretical knowledge of the first stage through innovative practice, to further deepen the understanding and knowledge of knowledge, at the same time to further improve one's knowledge level in the project, and to further enhance one's academic ability in the algorithm design.

(3) In the third stage, through the second stage of hands-on training, students' engineering practice ability, innovation and entrepreneurship ability, and academic research ability have been improved. After possessing these abilities, students will be able to play a certain role in their own majors, thereby increasing their employment competitiveness and improving their professional skills.

4. Evaluation Method Reform of Machine Learning Course

Aiming at the single assessment method based on the traditional score-based approach, machine learning courses should adopt diversified assessment methods. Attendance and classroom performance mainly assess students' learning attitude and course participation, as well as their mastery of basic theoretical knowledge. The experimental operation of the basic algorithm verifies the students' phased results and examines the students' application skills and whether they have mastered the basic algorithms of machine learning [20]. The group project mainly assesses whether students have the ability to apply algorithm theory to solve engineering problems, and the comprehensive design of the project assesses whether students have the ability to comprehensively use machine artificial intelligence and recognition technology learning algorithms and deep learning algorithms to solve engineering problems. The division of labor and collaboration of team members assess students' teamwork spirit and collective awareness. Participating in the course competition encourages students to participate in credible and competitive competitions, to have a deep understanding of course knowledge, and to enhance students' learning enthusiasm and engineering practice ability. Debriefing and defense examine students' language organization and communication skills. Question asking encourages students to learn to think, analyze, and solve problems. It is important to organize project design materials and write project development documents to test students' writing skills, exercise students' ability to organize and compile papers, and further enhance students' understanding of practical projects [21]. In addition to attendance, homework and experimental performance, teachers can also score based on students' creativity in theory and experimental classes. You can also score based on students' after-school communication performance, seminar performance, and additional items.

In the machine learning practice class, in addition to evaluating the form of the student project experiment report, the student's design plan, design process, experiment effect, experiment code and personal performance should also be evaluated. In addition, you can also use mutual assessment and self-assessment between students to give points to stimulate students' independent learning ability and enthusiasm.

4.1. Feasibility Analysis of Intelligent Technology Applied in Machine Learning Course. At present, intelligent technology is widely used in fields such as autonomous driving, face recognition, speech recognition, computer vision, and deep learning. At the same time, more and more teachers are paying attention to how to apply intelligent technology to teaching work. Machine learning courses are part of intelligent technology. It is very feasible to use intelligent technology to tutor machine learning courses.

The teaching system of machine learning courses based on intelligent technology contains two major functions, as follows.

4.1.1. For Students. Being liberate from the traditional boring classroom, improves students' practical ability, systematically evaluates students scientifically based on the homework completed by students and classroom performance, and adopts a grading system for scoring. Excellent students can be rewarded. System-wide notification can increase students' sense of honor, enhance their learning enthusiasm, and play an exemplary and leading role. In addition to classroom performance, for some extracurricular practice projects, you can recommend relevant students to participate in the society based on student applications or system intelligence analysis [22]. Companies are really meant to provide students with a practical platform, improve project experience, and make a good foundation for future employment. For students with strong academic ability and those who want to pursue academic development, the system will also provide a corresponding paper inquiry mechanism. And teachers will also provide guidance to help students complete the paper submission work. In general, an intelligent teaching system may provide each student with a growth platform that is appropriate for him, as well as match the diverse learning demands of pupils.

4.1.2. For Educators. The intelligent teaching system may summarize and assess students' homework, classroom performance, and after-class question and answer in order to increase teachers' teaching efficiency. Based on the scores, teachers may immediately assess their students' learning circumstances and change their own teaching progress and material. Inquiries concerning each student's studies, homework, implementation project, thesis analysis, and scientific research project may also be made by the system. Based on the inquiry results, the instructor would provide focused assistance, which will help to improve teaching efficiency. At the same time, this type of positive contact can help students learn more effectively.

4.2. Application of Intelligent Technology in Machine Learning Teaching. Intelligent applications are those that use technology like computer networks, big data, the Internet of Things, and artificial intelligence to suit people's requirements. In comparison to conventional media, intelligence is a data-driven sublimation of media functions. It indicates that, with the help of intelligent technology, new media will be able to have human-like perception, memory, and reasoning capacities, as well as learning, adaptive, and behavioral decision-making abilities. Human needs are at the core of numerous circumstances. New media can actively sense the external world, make judgments, and act on it using data processing and feedback in a way comparable to human thinking mode and given knowledge and norms. As shown in Figure 2, the use of intelligent technology or artificial intelligence technology in the teaching process creates an intelligent teaching system that can not only enhance instructors' and students' teaching efficiency, but also raise students' enthusiasm in learning. The adoption of intelligent technology is the overall trend of future educational system growth.

The complete teaching framework is separated into three tiers, as indicated in Figure 2. The input layer is the initial layer, and it is responsible for collecting data. The collected content can be divided into three parts. The first part is the specific content of various professional knowledge in the field of study. The form of collection is not limited, including text, pictures, audio, and video. The second part is the teacher's input, giving professional and authoritative answers to the student's questions [23]. The third part is the student's input. According to their own learning situation, students can ask questions about the knowledge they do not understand or the problems they encounter, and they can also describe their own learning status, use a scoring system to evaluate your mastery of knowledge. The second layer is the processing layer, through the analysis and processing of the data collected at the bottom layer, to arrive at a scientific decision. Decision-making mainly includes how to teach a certain course or certain knowledge points to achieve the best teaching effect. The realization of these two layers makes teaching change from one-way transmission to two-way interaction. The third layer is the user layer. Users mainly include students, teachers, and administrators. Users can complete input, search, and delete operations through this layer.

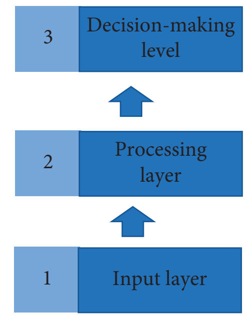

Figure 2: Intelligent teaching system architecture.

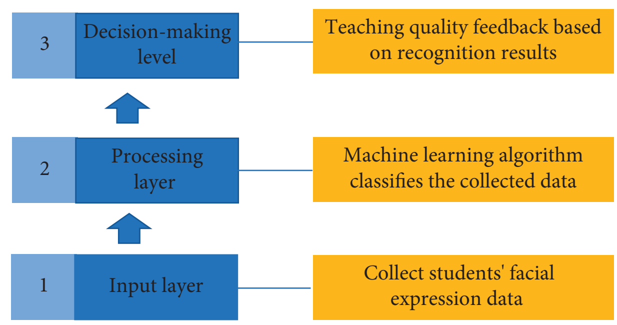

Figure 3: Teaching quality evaluation system architecture.

5. Teaching Quality Evaluation System Based on Intelligent Technology

5.1. System Architecture. This study provides a teaching quality evaluation system based on intelligent technology, based on the intelligent teaching system demonstrated in Section 4.2. The system's architecture is seen in Figure 3. The system's core is a machine learning algorithm that classifies and recognizes the acquired facial expression data, as illustrated in the diagram. Based on the recognition results, provide feedback on the classroom teaching quality in order to enhance the classroom teaching effect.

5.2. Emotion Recognition Model-Driven Classroom Teaching Quality Evaluation Method. In order to better identify the students' class situation, we use facial emotion recognition algorithms to make intelligent judgments on the facial expressions of students in class and give feedback to the teacher based on the judgment results of the classmates. If more than 75% of the classmates' emotional performance in order to be positive and enthusiastic, it proves that the teacher's class mode is very good and can be maintained. If 25% of the students show negative emotions, it means that the teacher needs to adjust the class mode. According to this dynamic adjustment, we ensure that the vast majority of students are active in class.

5.3. Comparison of Classification Results. We employed a total of 408 facial expression datasets, with the first 360 serving as the training set and the final 48 serving as the test set for the model. Anger, fear, disgust, happiness, sorrow, surprise, absence of feeling, and guilt are the eight emotions that we are classified into. To guarantee that the training set and test set are consistent each time, we used support vector machines (SVM) [24], extreme learning machines (ELM) [25], and radial basis functions (RBF) [26] as the classification model to execute 8 random tests on the data set. The following is the outcomes of the experiment.

As shown in Table 2, it can be seen that RBF performs the worst on this data set, which is almost meaningless. SVM performs poorly on multiclassification, and ELM performs best on this data set, with the highest classification accuracy, and ELM has the fastest running time, which is very convenient for us. There is a real-time analysis of students' facial emotions in the classroom, feedback, and adjustment of classroom teaching effects.

Table 2: The classification results of the adopted some traditional classification methods.

SVM	RBF	ELM
0.3125	0.125	0.6485
0.3521	0.1426	0.6625
0.3246	0.1242	0.6347
0.3413	0.1762	0.6543
0.3354	0.1761	0.6142
0.3212	0.1564	0.6754
0.3321	0.1264	0.6431
0.3134	0.1435	0.6542

6. Conclusion

Courses in machine learning are an important aspect of artificial intelligence professional education. The study focus of this article is artificial intelligence professional machine learning courses. And it examines the current state and issues of artificial intelligence professional teaching in light of the new era's demand for artificial intelligence talent. Boring courses, a single teaching modality, inadequate professional practice, and rigid evaluation systems are all addressed. This research presents a new intelligent technology-based teacher evaluation system. The data collecting layer, data processing layer, and decision-making layer make up the system's three-layer architecture. In the classroom teaching process, the collecting layer collects student facial expression data, and the processing layer employs classification algorithms to categorize and recognize the data, as well as provide recognition results. Based on the recognition results, the decision-making layer provides feedback on the quality of classroom teaching. Teachers are prompted to improve their own teaching techniques and material when the quality is poor. This paper introduces intelligent technology, which aims to improve the teaching effect and the quality of teaching and train high-level talents by collecting student learning data and analyzing the student's learning situation, ultimately achieving the goal of improving the teaching effect and the quality of teaching and training high-level talents.

Data Availability

The data used to support the findings of this study are available from the corresponding author upon request.

Conflicts of Interest

The authors declare no conflicts of interest.

Acknowledgments

This work was supported by the research and practice project on postgraduate education and teaching reform of Jiangnan University under Grant YJSJG2020012.

References

[1] C. M. He, W. Zhou, and M. Y. Li, "The study of "artificial intelligence" teaching reform under the environment of engineering education professional certification," *Education Teaching Forum*, vol. 32, pp. 88-89, 2017.

[2] L. J. Han, Y. H. Sun, and S. J. Li, "A tentative study in teaching reform of "artificial intelligence"," *Computer Knowledge and Technology (Academic Exchange)*, vol. 13, pp. 222-223, 2007.

[3] H. A. Aglan and S. F. Ali, "Hands-on experiences: an integral part of engineering curriculum reform," *Journal of Engineering Education*, vol. 85, no. 4, pp. 327–330, 1996.

[4] S. S. Rao, A. Nahm, Z. Shi, X. Deng, and A. Syamil, "Artificial intelligence and expert systems applications in new product development—a survey," *Journal of Intelligent Manufacturing*, vol. 10, no. 3-4, pp. 231–244, 1999.

[5] D. Zheng and Y. Wang, "Constructing postgraduate experimental teaching system and cultivating postgraduate innovation ability," *Experimental Technology and Management*, vol. 27, no. 5, pp. 146-147, 2010.

[6] I. M. Kola, "Using analytical rubrics to assess technological solutions in the technology classroom," *International Journal of Technology and Design Education*, 2021.

[7] L. Chen, "Exploration on teaching reform of "machine learning"course in colleges and universities," *Education Modernization*, vol. 5, no. 6, pp. 99-100, 2018.

[8] C. L. Hu, C. Wu, X. Zuo, J. J. Chen, and C. B. Wang, "Research of teaching reform of "machine learning"course for postgraduate," *Education Teaching Forum*, vol. 10, pp. 99-100, 2019.

[9] X. L. Hu, M. M. Sun, T. K. Sun, and J. F. Lu, "Practice and research of teaching reform of "machine learning"curriculum for postgraduate," *Meitan Higher Education*, vol. 30, no. 1, pp. 118–121, 2012.

[10] C. Y. Peng, H. Q. Chen, Y. Y. Su, Z. G. Wu, T. Long, and X. Zhang, "Analysis on the status quo of classroom teaching and cultivation of students'innovative quality," *Journal of Chongqing Institute of Technology (Natural Science Edition)*, vol. 2, pp. 124–128, 2007.

[11] J. L. Xiao, D. C. Jiang, and Y. C. Liu, "On teaching model reform of identificology of Chinese materiamedica," *China Pharmacy*, vol. 22, no. 20, pp. 1917–1919, 2011.

[12] H. E. Yun, X. F. Zhou, and J. Hao, "Reform of organ systems teaching model:takingdigestive diseases for example," *Northwest Medical Education*, vol. 19, no. 5, pp. 1057–1059, 2011.

[13] F. Yang and Y. Fei, "Practice and research on teaching reform for postgraduate of local university," *Guangdong Chemical Industry*, vol. 44, no. 3, pp. 183-184, 2017.

[14] C. Huang, Y. W. Chan, and N. Yen, "Data processing techniques and applications for cyber-physical systems (DPTA 2019)," *Advances in Intelligent Systems and Computing*, vol. 1088, pp. 1–10, 2020.

[15] X. Liu, "Study on current situation, problems of teaching assessment in higher vocational education and countermeasures," *Vocational and Technical Education*, vol. 26, no. 7, pp. 20–23, 2005.

[16] Q. S. Jiang, L. Jia-Yun, and X. B. Ning, "Teaching model reform of detection technology for application-oriented talent training," *Journal of Hefei University of Technology*, vol. 24, no. 3, pp. 146–148, 2010.

[17] F. Zhang, J. Wang, Y. Zhao, X. Zhou, H. Wang, and J. Ding, "Application of MOOC and rain classroom in the teaching of clinical microbiological examination technology," *Procedia Computer Science*, vol. 183, pp. 745–749, 2021.

[18] N. Li, "Simulation of English feature recognition based on machine learning and artificial intelligence technology," *Journal of Ambient Intelligence and Humanized Computing*, 2021.

[19] B. Bigelow, S. Cossette, and B. Nixon, "Rethinking globalization: teaching for justice in an unjust world," *Harvard Educational Review*, vol. 74, no. 3, pp. 347–349, 2002.
[20] J. Creswell, *Educational Research: Planning, Conducting, and Evaluating Quantitative and Qualitative Research*, Pearson Education, New York, NY, USA, 2015.
[21] S. Rogers and M. Girolami, "A first course in machine learning," *Statistical Methods in Medical Research*, vol. 25, no. 2, pp. 983-984, 2016.
[22] J. Lin, J. Li, and J. Chen, "An analysis of English classroom behavior by intelligent image recognition in IoT," *International Journal of System Assurance Engineering and Management*, vol. 2021, pp. 1–9, 2021.
[23] R. A. . Ramadan, "Leveraging RFID technology for intelligent classroom," in *Proceedings of the 2009 4th International Design and Test Workshop (IDT)*, Riyadh, Saudi Arabia, November. 2009.
[24] B. S. Anami and M. C. Elemmi, "Comparative analysis of SVM and ANN classifiers for defective and non-defective fabric images classification," *Journal of the Textile Institute*, vol. 2021, no. 1, pp. 1–11, 2021.
[25] G. B. Huang, Q. Y. Zhu, and C. K. Siew, "Extreme learning machine: theory and applications[J]," *Neurocomputing*, vol. 70, no. 1, pp. 489–501, 2006.
[26] Z. Jin, Z. Liang, X. Wang, and M. Zheng, "Adaptive backsteppingsliding mode control of tractor-trailer system with input delay based on RBFneural network," *International Journal of Control, Automation and Systems*, vol. 19, no. 1, pp. 76–87, 2021.

Hindawi
Scientific Programming
Volume 2021, Article ID 9744286, 11 pages
https://doi.org/10.1155/2021/9744286

Research Article

Construction Cost Simulation Based on Artificial Intelligence and BIM

Xingliang Du

Henan Finance University, Zhengzhou, Henan 451464, China

Correspondence should be addressed to Xingliang Du; duxingliang@hafu.edu.cn

Received 25 October 2021; Accepted 8 November 2021; Published 28 November 2021

Academic Editor: Le Sun

Quickly estimating the main engineering quantity and project cost of the project is conducive to the management staff to have an overall grasp of the project in the early stage and to grasp the development direction of the project in advance. Moreover, it can play an important guiding role in the further construction management of the project and can help managers prevent the emergence of unfavorable factors in the project, make corresponding construction deployments, and avoid risks. This paper combines artificial intelligence technology to construct a construction project cost simulation system. In this system, BIM is mainly used to simulate construction engineering, and the construction engineering cost is simulated and analyzed in combination with the pricing file. Finally, the results of experimental research show that the intelligent model proposed in this paper can play an important role in the cost of construction projects.

1. Introduction

Engineering cost management has a long history of development. Modern engineering cost management theory originated in the United Kingdom. Since then, various countries and regions have combined their own characteristics to form different project cost management models. Based on different management models, it is mainly divided into several models represented by the United Kingdom, the United States, Japan, Singapore, Malaysia, and Hong Kong. China's modern engineering cost management theory started late, but its development is rapid. After the founding of the People's Republic of China, China established a set of quota management systems compatible with the planned economy by referring to the former Soviet Union's engineering construction management model, which played a very important role in the recovery and development of the national economy. After the reform and opening up, marketization has continued to deepen, and the original management model can no longer meet the requirements of the modern and rapid development of the market, and China's engineering cost industry has also ushered in a golden period of development. The basis and methods of project pricing have been continuously reformed, the project cost management system has been continuously improved, and the project cost consulting industry has developed rapidly. Moreover, China's engineering cost system has also changed from the original fixed-rate pricing model to the list-based pricing model. Now, China's project cost management is increasingly showing the development trend of internationalization, informatization, and specialization.

Although the traditional method of quota or list measurement and pricing is accurate, it also has the characteristics of long working hours, large manpower input, large workload, and high requirements for the accuracy of drawings. In today's construction market, bidders are required to quickly give quotations, and time requirements are high. Bidding companies often can only make bid quotations based on personal experience in the past. This offer relies heavily on personal engineering experience and lacks credibility. The rapid estimation of main engineering quantities and engineering costs fills in the shortcomings of traditional quota or list measurement and pricing methods that are time-consuming and large in workload and can meet the high-efficiency requirements in the modern market. At the same time, the model foundation of this method is based on the data samples of multiple completed projects in the market, and the credibility of the indicators is high, and it provides important data and theoretical support for the decision-making of bidding and quotation [1].

The control of project cost is an important factor for the project to achieve better economic benefits. Extensive management and cost control will firstly lead to unnecessary waste of social resources and secondly make the project always in a state of unknown results, which is not good for the long-term development of the enterprise [2]. During the project, the management personnel can quickly understand the actual development of the project and analyze the degree of deviation of the project progress by comparing the corresponding project cost indicators of the actual completed project. At the same time, they can followup the problems in the project in time and adjust the project plan [3].

Based on this, this paper explores the construction of a construction project cost simulation system combined with artificial intelligence technology. In this system, BIM is mainly used to simulate the construction project to improve the accuracy of the construction project cost.

2. Related Work

In recent years, with the impact of foreign construction markets and the promotion of national policies, many large enterprises in the domestic industry have been actively exploring the use of BIM in order to improve their international competitiveness. Some construction projects will require BIM to be written into the bidding contract when bidding for construction projects, and BIM has gradually become a threshold for enterprises to participate in the project [4]. At present, some large and medium-sized design companies have established their own BIM teams and continue to accumulate practical experience. Although construction companies started late, they have been advancing in exploration and have achieved certain results [5]. As companies from all walks of life attach importance to BIM, the demand for BIM talents also arises. BIM technology not only brings about the advancement and upgrading of existing technologies and realizes the leap-forward development of the construction industry but also indirectly affects the production organization mode and management method and will affect people's way of thinking in the longer term [6].

The main work in the decision-making stage is to compare plans and conduct feasibility studies on the project. Through the use of BIM technology to compare the cost of multiple plans and other aspects [7], the most economical and reasonable investment plan can be selected. The introduction of BIM technology assists decision-makers to quickly and accurately make program choices and improve the accuracy of decision-making. If all kinds of BIM information are integrated on the cloud platform, the application of cost management in the decision-making stage is an investment estimation with the help of engineering cases in the BIM cloud platform database [8]. In the database of the BIM cloud platform, the BIM models of completed cases similar to the proposed project can be directly obtained. The staff can directly make simple modifications on the BIM model according to the investment plan and then obtain the approximate engineering quantity, cost, and other different indicators, and quickly and accurately obtain the investment estimate. This method has changed the traditional investment estimation method based on historical data and personnel work experience provided by local government departments [9]. The cloud platform database realizes reliable investment estimation of the proposed project and improves the estimation accuracy of the proposed project [10].

Literature [11] pointed out that 5D-BIM technology is a BIM technology that is based on the three spatial dimensions of BIM by adding two more dimensions, namely, schedule and cost. On the surface, 5D-BIM technology seems to incorporate two simple dimensions on the basis of BIM technology, but the significance of the integration is far beyond the added dimension itself. It is a reorganization of BIM. At the same time, the integration of the two dimensions of schedule and cost also enables BIM to be used in the management of the entire life cycle of construction projects, which can effectively improve the management level of construction projects. Literature [12] pointed out in the research process that 5D-BIM technology is actually based on BIM, which is a type of construction management technology of building information modeling. With the support of BIM, the progress, resources, budget, and construction, the organization and other key information are incorporated into the management system, and the project construction process is simulated so that the project leader and management personnel can understand the project information in a timely manner and improve the efficiency of decision-making on the project. Literature [13] pointed out in the research process that information is the core of 5D-BIM technology, and the basic elements (components or objects) of BIM as a carrier are geometric information, cost information, and related requirements and physical characteristics of project construction. Expressed in the form of parameters, through the corresponding Boolean operation and spatial topological relationship to complete the sorting of each parameter information, make it form a digital model, and finally, provide a digital model for the construction project cost management and each participating party of the project. This model can be used to communicate project-related work to ensure the efficiency of project management. Literature [14] focuses on the application of 5D-BIM technology in the design phase of construction projects and points out that one of the most notable features of the engineering design phase is that a large amount of information data is generated, and this type of information data is directly related to the project. Quality and management efficiency, and the application of 5D-BIM technology at this stage build an information chain of information resource sharing between various work in the project design phase so that each participating unit and the personnel of the design department can form a project. A comprehensive understanding of design information has laid a good foundation for improving the scientificity and reliability of project design.

3. Building Structure Simulation Based on Artificial Intelligence

Voronoi diagram is an important geometric structure in computational geometry. The Voronoi diagram is essentially a division of the plane according to a set of discrete points on the plane. It is defined as follows:

We arbitrarily give a set $P = \{p_1, p_2, p_3, \ldots, p_n\}$ of n discrete points at different positions on the plane, which is called $p_i\,(i = 1, 2, 3, \ldots, n)$ as a station. We classify all points on the plane according to the principle of Euclidean distance and obtain the point set $VR(p_i)$ closest to each p_i, as shown in the following equation:

$$VR(p_i) = \left\{q \big| |qp_i| \leq |qp_j|, \quad \forall j \neq i, p_i, p_j \in P\right\}. \tag{1}$$

Among them, $|qp|$ represents the Euclidean distance between the two points p and q. VR (pi) is the Voronoi area of site p_i. The Voronoi diagram VD (P) of P is the union of the Voronoi regions of all stations, as shown in the following equation:

$$V\ D(P) = U_{i=1}^{n} VR(p_i). \tag{2}$$

The entire plane is divided into n subregions that do not cover each other, and each subregion corresponds to a site. Any point q within the p_i subarea of the site satisfies $|qp_i| \leq |qp_j|$, where $p_j \in P - \{p_i\}$ [15].

Figure 1 shows the Voronoi diagram of eight discrete points.

For a multiboundary polygon P, if the angle $\alpha > 180^\circ$ between the vertex pi and the two associated edges in the Voronoi diagram drawing area, then p_i is called a concave vertex. Each concave vertex or each edge in P is called a site. Each site has a Voronoi region, and the union of the Voronoi regions of all sites is a Voronoi diagram of polygon P. The Voronoi diagram of the polygon P is obtained in the following way:

According to different sites, there are three types of bisectors:

(1) Vertex and vertex: the bisector is the vertical bisector of the connection between the vertices, as shown in Figure 2(a)

(2) Vertex and edge: the bisector is a parabola, as shown in Figure 2(b)

(3) Side and side: the bisector is the bisector of the angle formed by the two sides, as shown in Figure 2(c)

After that, we use the above three bisectors to divide the Voronoi area of all stations. It is particularly important to note that for each concave vertex, in order to divide its Voronoi area and the Voronoi area of the two sides with it as the end point, in the area where the Voronoi diagram is drawn by the polygon, the concave vertex is the end point. Then, combine the two vertical bisectors of the edge. The Voronoi diagram of the polygon P is divided by the above-mentioned three bisectors and the vertical bisectors of the concave vertices. Among them, the common edge between the Voronoi areas of the two sites is called the Voronoi edge,

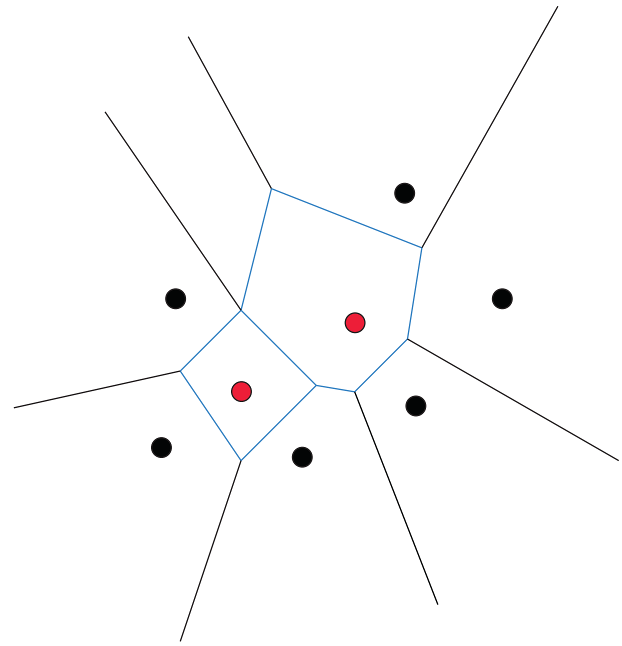

Figure 1: Voronoi diagram of 8 discrete points.

and the intersection of the Voronoi edges is called the Voronoi vertex. The Voronoi skeleton path of the polygon is composed of Voronoi edges and Voronoi vertices. Figure 3 shows the Voronoi diagram of a multiboundary polygon. The dotted line is the Voronoi skeleton path of the polygon.

Here, this paper introduces the concept of weak visibility. We set a polygon P, and Q is a subset of the polygon P. If there is a point in Q that can see a point s in P, then s is said to be weakly visible relative to Q. As shown in Figure 4(a), Q is the edge p_1p_2, and the point p_1 in Q can be seen at the point s. Therefore, the point s is weakly visible with respect to Q. That is to say, in the polygon P, as long as the station s can see a certain point in Q, then the point s is weakly visible with respect to Q.

The set of all weakly visible points of Q is called the weakly visible area of Q in the polygon P, as shown in Figure 4(b).

How to quickly build an MR environment in large indoor spaces with many room structures such as museums and art galleries is discussed below. The construction method proposed in this paper includes the following 4 steps:

(1) Build the initial virtual scene

(2) Establish the mapping relationship between the virtual scene and the physical environment

(3) Set the transparency value of the wall

(4) Offset error correction

To construct the MR environment, the scene must be constructed first, and the virtual scene will be constructed according to the real environment. HoloLens completes scene construction by scanning, which is based on a multiview geometric reconstruction method. However, the scanning process is not suitable for MR applications in a

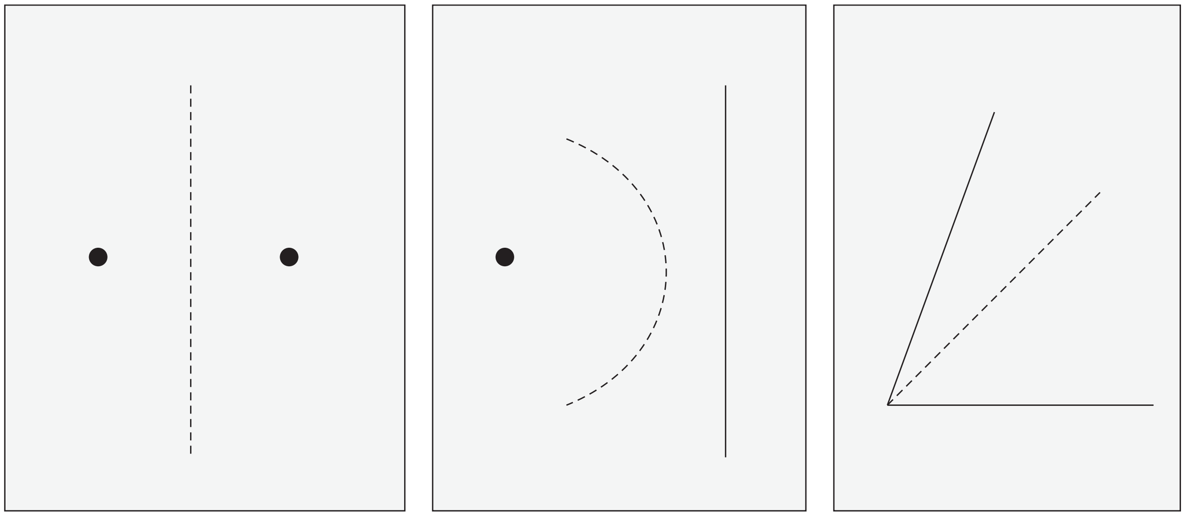
(a) (b) (c)

Figure 2: Three bisectors.

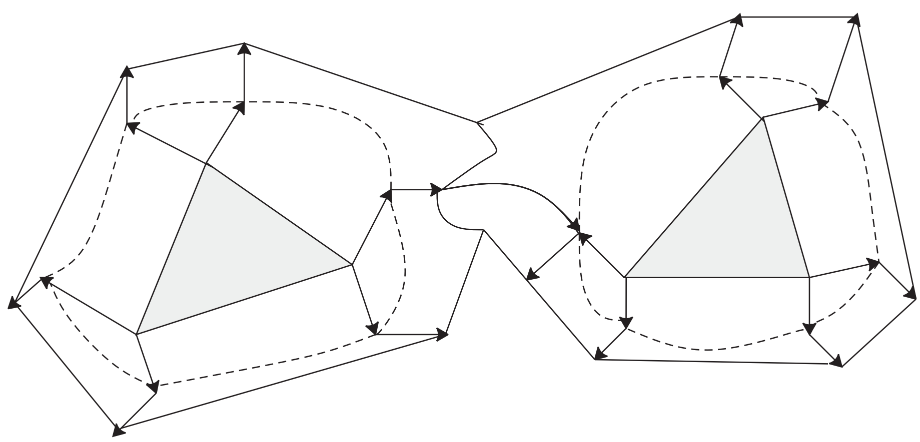

Figure 3: Voronai diagram of multiboundary polygon.

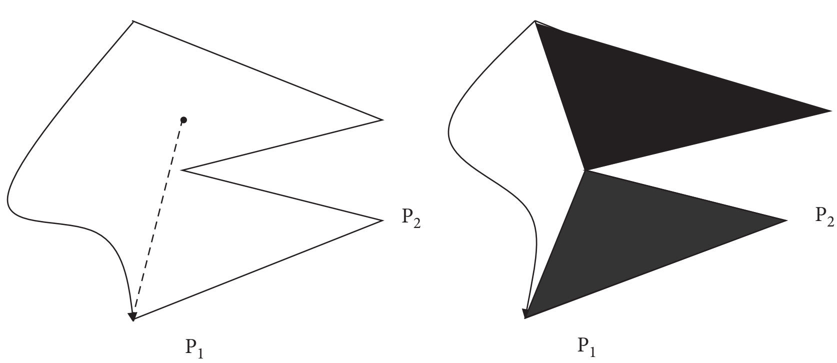

(a) (b)

Figure 4: Weak visibility. (a) Weak visibility. (b) Weak visibility.

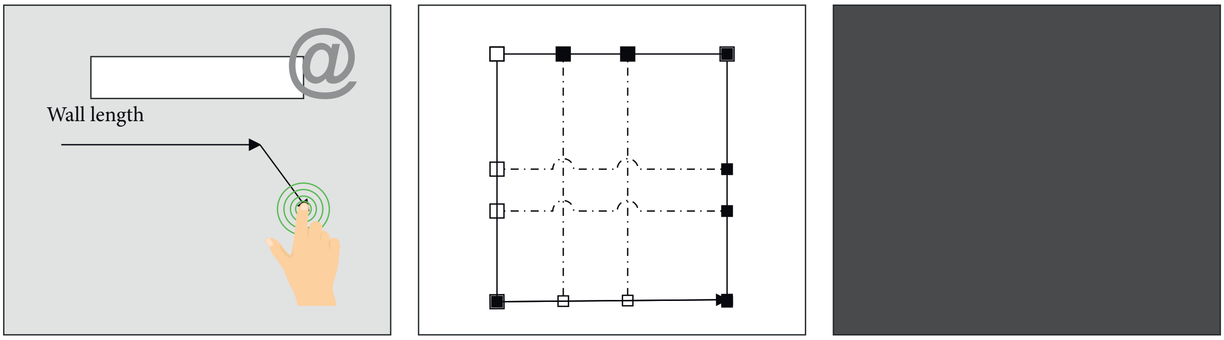

(a) (b) (c)

Figure 5: 2D structure diagram of the construction method. (a) 2D structure drawing drawn by parameters. (b) Input plane structure figure. (c) 2D structure figure obtained after processing.

wide range of indoor spaces. On the one hand, because the scanning process is time-consuming and laborious; on the other hand, it is impossible to scan and save the entire space at once. Therefore, this article uses the prebuilt virtual wall model to replace the cumbersome scanning process, while saving the structural information of the real environment for subsequent reuse. The specific method is as follows:

(1) This article uses three data sources to obtain a 2D wall structure diagram of the physical environment. (1) This article draws a 2D structure diagram according to the structural parameters of the real environment (as shown in Figure 5(a)), and the user can draw walls through multitouch or mouse operation. After drawing, the user can input the length of the wall in the text box to adjust the wall just drawn. (2) After inputting the plane structure diagram of the building, the 2D structure diagram is extracted through the edge detection algorithm (as shown in Figure 5(b)). (3) This article imports the existing spatial 3D model and extracts the 2D structure diagram.

(2) The algorithm imports the 2D structure diagram obtained in step 1 into the design end running on the surface. Then, the algorithm traverses the information of each node in the structure diagram to construct a virtual wall model.

The Figure 5(a) represents the 2D structure drawing drawn by parameters, the left figure in the Figure 5(b) is the input plane structure figure, and the right figure is the 2D structure figure obtained after processing.

In order to ensure the authenticity of the experience, it is necessary to establish an accurate mapping relationship between the virtual scene and the real environment, transform the virtual space and the real space into a unified coordinate system, and ensure that the virtual scene matches the real environment accurately, that is, scene registration. This article constructs a virtual space coordinate system on the design side. HoloLens can establish a world coordinate system 1 : 1 with the real world. This article uses this coordinate system to represent the position in the real world.

$P_1(x_1, z_1)$ and $P_2(x_2, z_2)$ are the two points in the virtual space, and $P_1'(x_1', z_1')$ and $P_2'(x_2', z_2')$ are the corresponding two points in the real space. First, $\overrightarrow{P_1P_2}$ and $\overrightarrow{P_1'P_2'}$ are calculated, respectively, as shown in the following formulas and [16]:

$$\overrightarrow{P_1P_2} = (x, z) = (x_2 - x_1, z_2 - z_1), \tag{3}$$

$$\overrightarrow{P_1'P_2'} = (x', z') = (x_2' - x_1', z_2' - z_1'). \tag{4}$$

In this paper, $V(V.x, V.z)$ represents any point in virtual space, and $R(R.x, R.z)$ represents the corresponding point of V in real space. According to the following formula, the corresponding point R coordinate in the real world can be obtained according to the V point coordinate in the virtual coordinate system, as shown in the following formula :

$$\begin{cases} R.x = \{\cos\theta \cdot (x_1 - V.x) - \sin\theta \cdot (V.z - z_1)\} \cdot \text{ratio} + x_1', \\ R.z = \{\sin\theta \cdot (x_1 - V.x) + \cos\theta \cdot (V.z - z_1)\} \cdot \text{ratio} + z_1'. \end{cases} \tag{5}$$

Conversely, the coordinates of point V can be obtained from the point R according to the following formula [17]:

$$\begin{cases} V.x = \{\cos\theta \cdot (x_1' - R.x) - \sin\theta \cdot (R.y - y_1')\} \cdot \left(\dfrac{1}{\text{ratio}}\right) + x_1, \\ V.y = \{\sin\theta \cdot (x_1' - R.x) + \cos\theta \cdot (R.y - y_1')\} \cdot \left(\dfrac{1}{\text{ratio}}\right) + y_1. \end{cases} \tag{6}$$

Among them, the formula θ represents the angle between the vector $\overrightarrow{P_1P_2}$ and $\overrightarrow{P_1'P_2'}$, and the calculation method of sin θ, cos θ, and ratio is as shown in the following formula [18]:

$$\begin{aligned} \sin \theta &= (x \cdot z\prime - x\prime \cdot z)/\sqrt{x^2 + z^2} \cdot \sqrt{x^{2\prime} + ^{2\prime}}, \\ \cos \theta &= (x \cdot x\prime - z\prime \cdot z)/\sqrt{x^2 + z^2} \cdot \sqrt{x^{2\prime} + z^{2\prime}}, \\ \text{ratio} &= \sqrt{x^{2\prime} + z^{2\prime}}/\sqrt{x^2 + z^2}. \end{aligned} \tag{7}$$

Through the above formula, the virtual coordinate system and the real space coordinate system can be transformed into each other, and each node information in the 2D structure diagram can be traversed to find the position in the real space coordinate system, thereby constructing a virtual wall model. In addition, users can design scene content on the design side and deploy the scene content to the HoloLens experience side in real time through the above mapping relationship.

In real space, objects behind the wall cannot be seen from in front of the wall due to the occlusion of the wall. But for transparent glass and translucent frosted walls, users can see the objects behind the walls. Therefore, in order to ensure the real experience effect, this paper treats different walls differently and introduces the transparency value φ of the virtual wall.

(1) If the walls in the physical space are opaque, this paper sets the transparency value φ to 0. In this case, the corresponding virtual wall generated by the above steps will be attached with a transparent material. During the roaming process, the MR application will calculate and render the virtual wall to ensure that the virtual object placed behind the real wall will be blocked. At the same time, the use of transparent materials allows the user to only see the real wall and not the virtual wall when wearing the HoloLens device. This design effectively achieves the following effects: the real wall can block the virtual objects behind the wall. As shown in Figure 6(a), the upper part shows the effect that the user looks at when there is only a real wall. The real wall is an opaque wall, and the cultural relic is a virtual cultural relic rendered by HoloLens; below is the effect that the user sees when the virtual wall exists. This paper constructs a virtual wall that is the same as a real wall, attaches a transparent material, and places it in the position of the real wall. The user cannot see the virtual wall, and the existence of the virtual wall obscures the false cultural relics.

(2) If the real wall is transparent or semitransparent, such as a wall made of glass, this paper sets the transparency value φ of the virtual wall to a value in (0, 1). At this time, the virtual wall will not be calculated and rendered, and the user can see the virtual object behind the wall. But the transparency value φ will serve as a parameter for the rendering of virtual objects. This article will introduce how to use the transparency value g to accelerate the rendering of MR scenes. As shown in Figure 6(b), the upper part is the effect that the user looks at when there is only a real wall. Among them, the real wall is a translucent glass wall, and the cultural relics are virtual cultural relics rendered by HoloLens: the display effect processed with the transparency value p is below. Since the glass wall is semitransparent, this paper reduces the accuracy of the virtual model and makes it rougher to speed up the rendering of the scene.

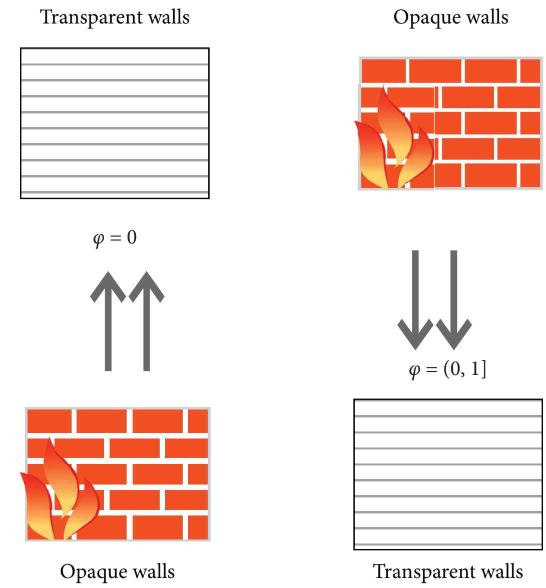

Figure 6: Setting the virtual wall transparency value p to process different walls.

This article finds that during the user's roaming process, the virtual wall will gradually shift and cannot accurately correspond to the real wall position. In some special cases, HoloLens may not recognize its location and lose tracking. When the device recovers from this situation to a normal state, the position correspondence between the real wall and the virtual wall will also deviate. As the user's roaming time and range in the MR environment increase, the offset error will gradually accumulate and become more and more obvious, and the user's realistic experience will become worse and worse.

To solve this problem, this paper sets up some spatial anchor points in the MR environment according to the layout of the virtual scene to anchor the virtual scene in the real environment.

Based on the data structure VorPa, this paper proposes two anchor point deployment algorithms based on greedy ideas and integer linear programming methods. In the processing process, since the virtual wall needs to correspond accurately to the real wall, the wall model is regarded as a special virtual object, and the position of the virtual object is the position of the midpoint of the wall. After merging the virtual wall and the virtual object collection, all the virtual model collections that need to be covered by anchor points in the scene are obtained as $M = W \cup R = \{m_1, m_2, m_3, \ldots, m_n\}$.

Before using the two algorithms, this paper preprocesses the scene based on the data structure VorPa:

(1) This article sets the value $v_i\,(i \in n)$ for each virtual model m_i. The value v_i represents the visible probability of the virtual model m_i in the scene. In other words, if the user randomly selects a position and perspective in the scene, the probability of seeing the model. The calculation method of the probability of finding the model is as follows [19]:

$$v_i = \frac{\sum_{\text{path in } VR\,(m_i)} \text{Length}\,(\text{path})}{\sum \text{Length}\left(p_j\right)}. \tag{8}$$

Among them, VR (mi) represents the visible area of the virtual model m_i in the scene, and p_j represents the j-th roaming subpath in the scene. The calculation of v_i is based on the length of the roaming path, that is, the ratio of the length of the roaming path that falls into the visible area of the cultural relic m_i to the total length of the scene roaming path.

(2) This article sets the value of v_{p_j} for each subpath. In the data structure VorPa, if the virtual model m_i is in the weakly visible area of the path p_j, the cultural relic m_i is bound to the model list modelList of the path pi. The sum of the value of all models in the p_j model list modelList is the value of the path p_j, as shown in the following equation [20]:

$$v_{p_j} = \sum_{m_i \text{ in modeI List of } p_j} v_i. \tag{9}$$

Next, A1gorithm 1 based on greedy thought is first introduced: anchor deployment algorithm based on greedy thought.

(1) The algorithm sorts all paths according to the value of the path and selects the path $P_{\max}$ with the largest value.

(2) For the model on the path $P_{\max}$, the algorithm selects a circle with a radius of 3 m so that it can cover the model combination with the largest total value on the $P_{\max}$. The position of the center of the circle is the position of the anchor point s, which is added to the radium point set. Among them, the way to find the anchor point s is as follows:

(1) The algorithm creates a two-dimensional array C containing all the scenes in the array C[a][b] corresponds to a point in the scene with coordinates (a, b) and assigns all the initial values of the two-dimensional array C to 0. The position of the model m_i is (x_i, y_i), and the algorithm finds the intersection area between a circle with (x_i, y_i) as the center and a radius of 3 m and the model m_i visibility region $VR(m_i)$. Moreover, the algorithm adds v_i to the value of the array position corresponding to this area and traverses all models. In the model, the list of the path $P_{\max}$ does the above operation.

(2) The algorithm traverses the two-dimensional array C and finds the scene area corresponding to the array subscript with the largest value, which is the anchor point distribution area that this paper is looking for. The algorithm chooses a point as the anchor point s.

(3) The algorithm traverses all roaming subpaths, deletes all virtual models covered by the anchor point s contained in the subpaths, and modifies the value of the path, subtracting the corresponding model value.

(4) The algorithm returns to step 1, repeats steps 1 to 3 until the value of $P_{\max}$ is 0, and outputs the anchor point is set.

A1gorithm 1. Based on greedy thinking is not necessarily the optimal solution of the problem, and it is time-consuming and long. This article uses it as the baseline algorithm. Furthermore, this paper transforms this problem into an optimization problem, that is, minimizing the number of anchor points. After that, this paper proposes the second algorithm. Algorithm 2 is based on the idea of integer linear programming.

Algorithm 2. Anchor point deployment algorithm based the on integer linear programming is as follows:

(1) The algorithm gets the initial set of anchor points. Before constructing the mathematical model, an initial set of l anchor points that can cover all virtual models in the scene is obtained through the following process:

According to the method in Algorithm 1, the algorithm creates a two-dimensional array C containing all scenes and assigns all initial values to 0. The algorithm finds the intersection area between a circle with $m_i\,(x_i, y_i)$ as the center and a radius of 3 m and the model m_i visibility area $VR(m_i)$, and the value of the array subscript position corresponding to this area is added to v_i.

The algorithm traverses the entire two-dimensional array C, finds all anchor point positions that can cover different virtual model combinations without repeating them, and adds them to the initial anchor point set.

(2) According to the problem description, this paper constructs a mathematical model [21]:

$$\min z = \sum_{i=1}^{l} s_i,$$
$$\begin{cases} s_i = 0 \text{ or } 1, i = 1, 2, \ldots, l, \\ \displaystyle\sum_{i=1}^{l} F[i][j] \cdot s_i \geq 1, \quad j = 1, 2, \ldots, n. \end{cases} \tag{10}$$

In this mathematical model, the variable s_i represents the i-th anchor point. It is assumed that there are initially l

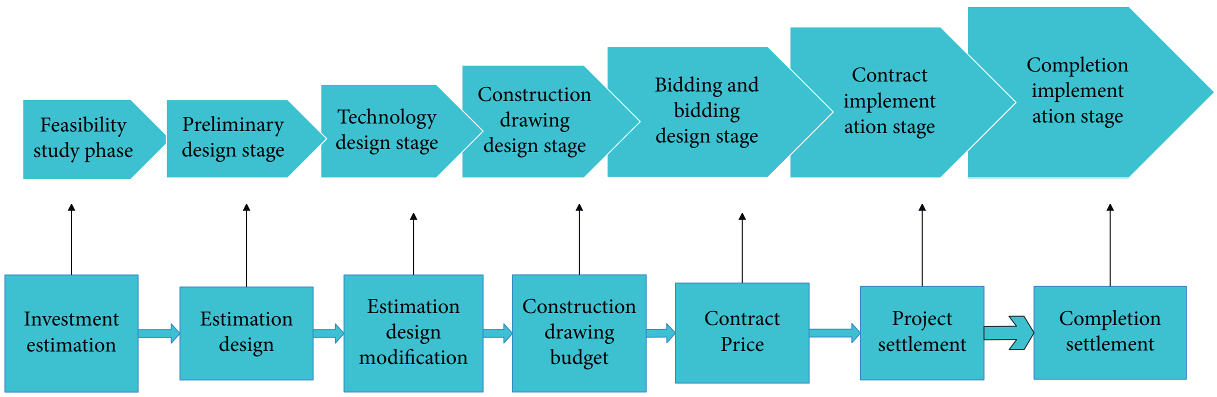

Figure 7: Valuation file.

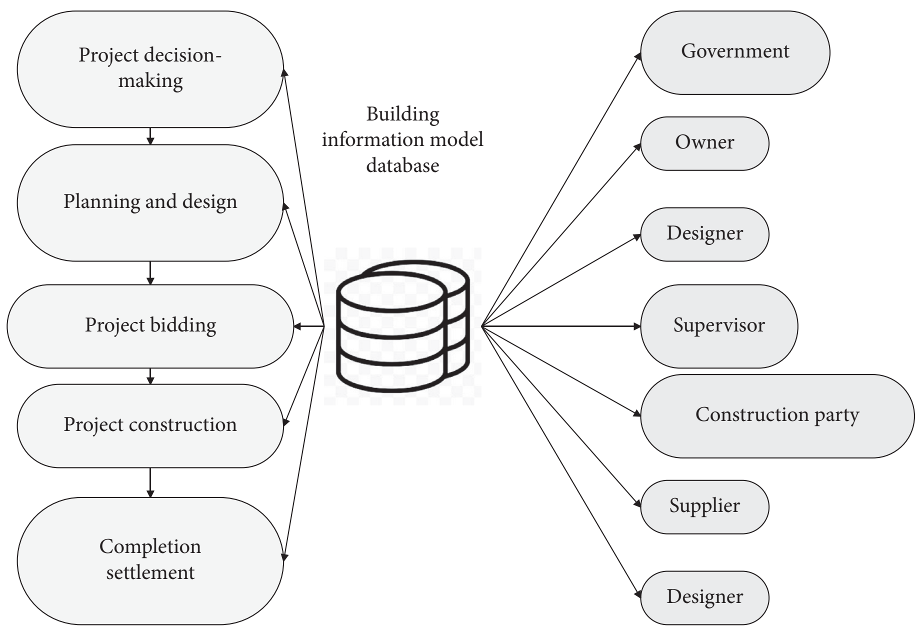

Figure 8: Information exchange diagram of information model.

anchor points, and these anchor points can cover all virtual models in the scene. $F[i][j]$ indicates whether the i-th anchor point can cover the j-th virtual model. If it can be covered, the value is 1, and if it is not covered, the value is 0. The goal of this paper is to minimize the number of anchor points and satisfy two constraints. (1) The value of the anchor point s_i is 0 or 1.0 means that the i-th anchor point is not placed, and 1 means that the i-th anchor point is placed. (2) All models in the scene can be covered, that is, for any model, the number of anchor points that can cover the model is greater than or equal to 1.

4. Construction Cost Simulation Based on Artificial Intelligence and BIM

The whole-process project cost management is the management of project cost, which is carried out in accordance with the construction procedures of the engineering project and is carried out from the feasibility study of the project-to-project decision-making, project design, bidding, project implementation to the final completion acceptance, delivery, and use, and project postevaluation. These stages all correspond to the corresponding project cost valuation documents, as shown in Figure 7.

The information exchange structure of the information model (as shown in Figure 8) and the BIM model in the refined management of the project cost (as shown in Figure 9) must be clarified before the application of BIM technology to the construction engineering calculation of the price file, which lays the foundation for further refined applications.

After constructing the above model, the model is verified and analyzed, and the BIM simulation effect of the model and the project cost evaluation effect of the model are mainly verified. The results are shown in Table 1 and Figure 10.

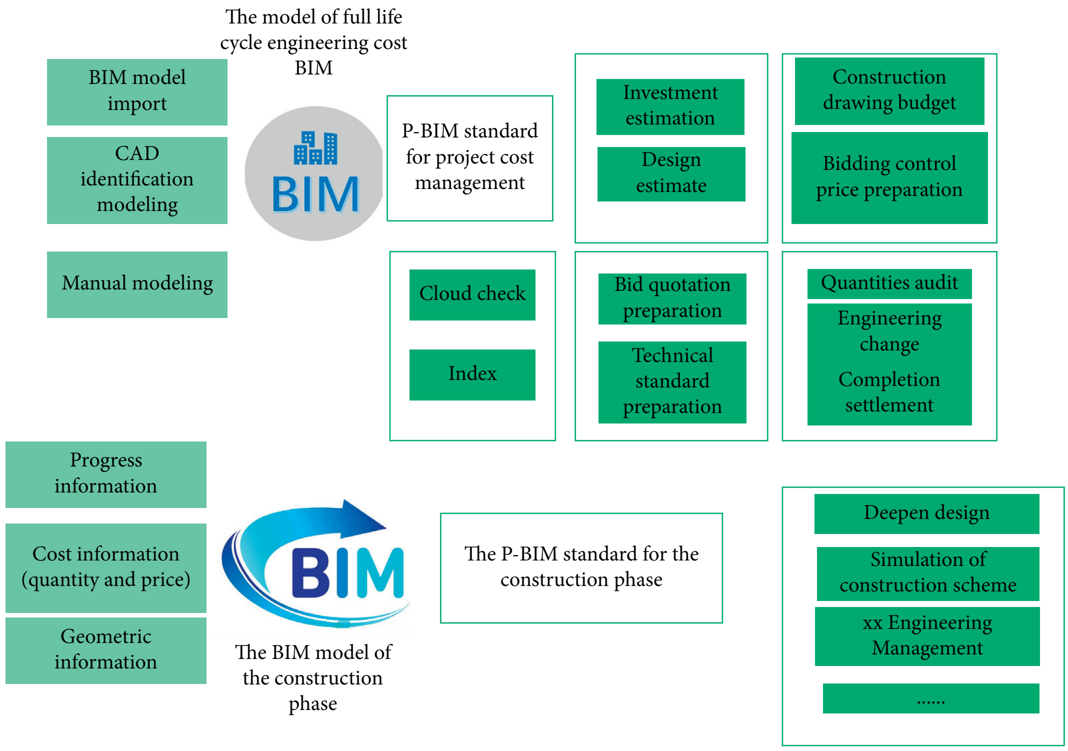

Figure 9: BIM model of refined project cost management.

Table 1: BIM simulation effect and project cost evaluation effect based on artificial intelligence.

Number	BIM simulation	Project cost analysis	Number	BIM simulation	Project cost analysis	Number	BIM simulation	Project cost analysis
1	91.37	71.49	17	91.94	78.05	33	87.85	85.47
2	82.68	73.21	18	79.38	87.03	34	91.75	81.86
3	87.15	74.28	19	88.21	71.28	35	90.46	74.83
4	88.24	83.75	20	87.74	85.04	36	84.11	87.69
5	79.13	81.51	21	89.14	82.34	37	80.59	84.54
6	79.16	88.83	22	90.57	76.98	38	79.84	72.03
7	84.18	76.81	23	87.12	87.30	39	84.89	84.56
8	83.85	84.15	24	85.93	80.12	40	91.47	78.92
9	86.59	87.70	25	89.30	71.47	41	84.62	80.38
10	84.80	76.43	26	86.04	71.08	42	87.68	80.46
11	79.47	86.08	27	80.65	80.51	43	79.92	82.87
12	91.59	83.86	28	90.69	84.05	44	86.32	82.91
13	83.85	72.95	29	79.76	84.64	45	86.80	82.51
14	81.48	74.85	30	81.40	74.37	46	84.10	84.98
15	79.41	80.51	31	81.72	87.15	47	82.93	84.37
16	88.65	73.51	32	82.40	76.33	48	88.72	88.32

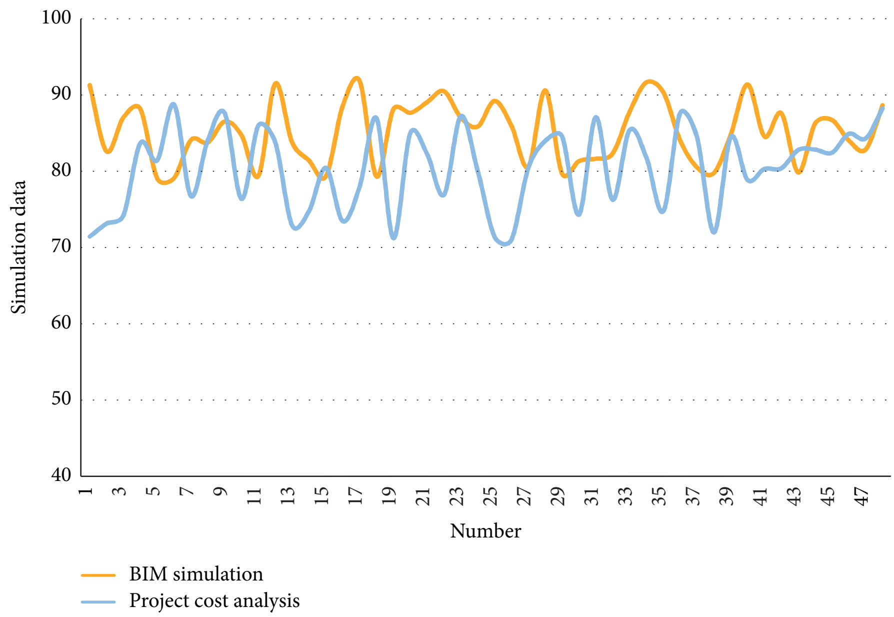

Figure 10: Statistical diagram of system performance test data.

Through the above experimental research, we can see that the method proposed in this article has good results.

5. Conclusion

In a construction project, different professions such as architecture, structure, materials, and installation will be involved, and it will go through several different stages from decision-making to completion. In this process, different parties of the same information in different professions or at different stages will have different expression and management methods, resulting in information redundancy and difficulties in sharing. The core of BIM is information. The basic element of the BIM model is a single component or object, and the physical characteristics, geometric information, cost information, and construction requirements of all components or objects are expressed through parameters. It then uses 3D Boolean operations and spatial topological relationships to organize these information and store them in a database to finally form a digital model. In addition, the project system based on BIM can adjust relevant information at any time according to project changes, which not only solves the problem of information redundancy but also provides convenient conditions for information exchange among stakeholders.

Data Availability

The labeled datasets used to support the findings of this study are available from the corresponding author upon request.

Conflicts of Interest

The author declares no conflicts of interest.

References

[1] T. Abuimara, W. O'Brien, B. Gunay, and J. S. Carrizo, "Towards occupant-centric simulation-aided building design: a case study," *Building Research & Information*, vol. 47, no. 8, pp. 866–882, 2019.

[2] I. Beausoleil-Morrison, "Learning the fundamentals of building performance simulation through an experiential teaching approach," *Journal of Building Performance Simulation*, vol. 12, no. 3, pp. 308–325, 2019.

[3] A. D. Black, "Wor(l)d-Building: simulation and metaphor at the mars desert research station," *Journal of Linguistic Anthropology*, vol. 28, no. 2, pp. 137–155, 2018.

[4] D. Chakraborty and H. Elzarka, "Advanced machine learning techniques for building performance simulation: a comparative analysis," *Journal of Building Performance Simulation*, vol. 12, no. 2, pp. 193–207, 2019.

[5] T. Dodd, C. Yan, and I. Ivanov, "Simulation-based methods for model building and refinement in cryoelectron microscopy," *Journal of Chemical Information and Modeling*, vol. 60, no. 5, pp. 2470–2483, 2020.

[6] N. Endo, E. Shimoda, K. Goshome, T. Yamane, T. Nozu, and T. Maeda, "Simulation of design and operation of hydrogen energy utilization system for a zero emission building," *International Journal of Hydrogen Energy*, vol. 44, no. 14, pp. 7118–7124, 2019.

[7] O. Guerra-Santin and S. Silvester, "Development of Dutch occupancy and heating profiles for building simulation," *Building Research & Information*, vol. 45, no. 4, pp. 396–413, 2017.

[8] K. Hanson, L. Hernandez, and J. A. Banaski, "Building simulation exercise capacity in Latin America to manage public health emergencies," *Health Security*, vol. 16, no. S1, pp. S98–S102, 2018.

[9] C. W. Lee and S.-J. Cho, "The development of converting program from sealed geological model to gmsh, COMSOL for building simulation grid," *Journal of the Korean Earth Science Society*, vol. 38, no. 1, pp. 80–90, 2017.

[10] C. Miller, D. Thomas, J. Kämpf, and A. Schlueter, "Urban and building multiscale co-simulation: case study

implementations on two university campuses," *Journal of Building Performance Simulation*, vol. 11, no. 3, pp. 309–321, 2018.

[11] P. Remmen, M. Lauster, M. Mans, M. Fuchs, T. Osterhage, and D. Müller, "TEASER: an open tool for urban energy modelling of building stocks," *Journal of Building Performance Simulation*, vol. 11, no. 1, pp. 84–98, 2018.

[12] E. K. Wati and N. Widiansyah, "Design of learning media: modeling & simulation of building thermal comfort optimization system in building physics course," *Jurnal Pendidikan IPA Indonesia*, vol. 9, no. 2, pp. 257–266, 2020.

[13] C. Xiong, J. Huang, and X. Lu, "Framework for city-scale building seismic resilience simulation and repair scheduling with labor constraints driven by time-history analysis," *Computer-Aided Civil and Infrastructure Engineering*, vol. 35, no. 4, pp. 322–341, 2020.

[14] X. Xie and Z. Gou, "Building performance simulation as an early intervention or late verification in architectural design: same performance outcome but different design solutions," *Journal of Green Building*, vol. 12, no. 1, pp. 45–61, 2017.

[15] A. I. Adilkhodjayev, I. M. Mahamataliev, and S. S. Shaumarov, "Theoretical aspects OF structural and simulation modeling OF the macrostructure OF composite building materials," *Journal of Tashkent Institute of Railway Engineers*, vol. 14, no. 2, pp. 3–14, 2019.

[16] S. Imam, D. A. Coley, and I. Walker, "The building performance gap: are modellers literate?" *Building Services Engineering Research and Technology*, vol. 38, no. 3, pp. 351–375, 2017.

[17] J.-S. Pei, B. Carboni, and W. Lacarbonara, "Mem-models as building blocks for simulation and identification of hysteretic systems," *Nonlinear Dynamics*, vol. 100, no. 2, pp. 973–998, 2020.

[18] A. Brunelli, F. de Silva, A. Piro et al., "Numerical simulation of the seismic response and soil-structure interaction for a monitored masonry school building damaged by the 2016 Central Italy earthquake," *Bulletin of Earthquake Engineering*, vol. 19, no. 2, pp. 1181–1211, 2021.

[19] P. Andrio, A. Hospital, J. Conejero et al., "BioExcel Building Blocks, a software library for interoperable biomolecular simulation workflows," *Scientific Data*, vol. 6, no. 1, pp. 169–178, 2019.

[20] G. Petrou, A. Mavrogianni, P. Symonds et al., "Can the choice of building performance simulation tool significantly alter the level of predicted indoor overheating risk in London flats?" *Building Services Engineering Research and Technology*, vol. 40, no. 1, pp. 30–46, 2019.

[21] S. Gibeaux, C. Thomachot-Schneider, S. Eyssautier-Chuine, B. Marin, and P. Vazquez, "Simulation of acid weathering on natural and artificial building stones according to the current atmospheric SO 2/NO x rate," *Environmental Earth Sciences*, vol. 77, no. 9, pp. 1–19, 2018.

Hindawi
Scientific Programming
Volume 2021, Article ID 6298813, 14 pages
https://doi.org/10.1155/2021/6298813

Research Article

Knowledge Mapping of Green Technology Visualization with Bibliometric Tools

Shiliang Xia[1] and Kaiyang Zhong[2]

[1]*School of Economics and Management, Huaiyin Normal University, Huaian 223001, Jiangsu, China*
[2]*School of Economic Information Engineering, Southwestern University of Finance and Economics, Chengdu 611130, Sichuan, China*

Correspondence should be addressed to Kaiyang Zhong; zhongky0626@163.com

Received 15 October 2021; Accepted 15 November 2021; Published 27 November 2021

Academic Editor: Le Sun

An increasing number of research literature studies about green technology have been accepted by journals of different disciplines due to the rapid technical progress and innovation in all types of industry. This study uses bibliometric tools of CiteSpace and VOSviewer to analyse the key authors' co-citation network, institution cooperation, the keyword clusters of green technology, and the evolution trend of green technology. We find that since 1960s, the number of research papers with green technology theme has been growing. These papers are mainly involved in fields of economics and business, engineering, and chemistry, in which there exist 13 highest cited papers from 2009 to 2020 based on the Web of Science database. In this study, we find the top 20 journals of green technology with the parameter of literature count and centrality. We find that the cooperation of authors is quite weak with the co-authorship analysis, and we obtain the top 12 institutions in 15 countries dominantly in green technology research through country and institution analysis. We conduct a cluster analysis of keywords related to green technology, and we obtain 10 clusters, with three economical clusters, five engineering clusters, and two chemical clusters. Finally, we summarise green technology with the aid of the timeline view function of CiteSpace system.

1. Introduction

The concept of green technology was put forward in the 1960s due to the social appeal of saving resources and energy consumption, less pollutive output, and less damage to the ecological circle [1]. With the sustainable and ecological revolution of the modern industry, similar concepts of environmental sound technology and ecological technology have been created to conform with technical civilisation. Nowadays, green technology has been widely accepted in different disciplines of philosophy, natural science, economics, and management; however, green technology research has focused quite differently in several disciplines. Some economic researchers have discussed the efficiency improvement of green technology applied on electric charging behaviour and different sizes of farm [2–5]; some chemical papers of green technology dealt with molecular imprinting technology [6] and wastewater treatment [7]; some engineering issues put green technology into textile processing [8], green building practice [9, 10], and surface engineering [11]; and even Internet of Things (IoT) technology has been applied in waste water treatment [12]. Moreover, multidisciplinary integrated green technologies are utilised in agriculture, biology, medical, and some other research areas.

The current literature amount with "green technology" in titles in the Web of Science (WoS) database was 1516 by December 31, 2020, with 12 types including common articles, reviews, editorial materials, meeting abstracts, book reviews, and proceeding papers. Of the review papers, 140 literature records reviewed a certain method or technical application [13–15]. Unfortunately, no paper has addressed the present research situation and future trend of green technology with bibliometric tools. Bibliometric tools can provide a clear knowledge map of a specific theme. In this study, we use two bibliometric tools, CiteSpace and VOSviewer, to examine the present research status and hot papers, the cooperation network of authors and main institution, and the cluster attribute of green technology [16]. This study attempts to solve three important questions. First, we will show the green technology literature research status according to the publishing and citing trend with three stages. Second, we will use knowledge mapping systems to show the core journals, highly cited papers, and categories of different fields of green technology. Third, cluster and co-word analysis will clarify the green technology development themes and the implications of each cluster are provided.

2. Materials and Methods

According to the knowledge mapping theory, we can use co-word, institution, timeline, and cluster analyses to obtain the research front and the evolutionary trend of a certain theme. In this study, we use the former three analyses with CiteSpace tool and the cluster analysis with VOSviewer software. The analysis data units are collected from the WoS database.

2.1. Data Collection and Literature Search Strategy. WoS is equipped with the global academic literature of different disciplines, and it can provide the citation record of each literature that meets the functional requirements of co-word analysis. We choose the WoS core collection database with the timespan from 1900 to 2020, with citation indexes of Science Citation Index Expanded, Social Science Citation Index, Arts and Humanities Citation Index, and Emerging Sources Citation Index. With the consideration of the accuracy of citation results and some literature references [17, 18], we set the retrieval strategy as follows: "TITLE: (green technology) OR TITLE: (Environmental Sound Technology) OR TITLE: (Ecological Technology)". We obtain a total of 1516 relevant papers, and we refine the document types. Then, we obtain 996 "ARTICLE" and 140 "REVIEW" papers, and a total of 1136 papers are the input text files. The data were last updated on December 31, 2020.

2.2. Bibliometric Tools of CiteSpace and VOSviewer. CiteSpace is an information visualisation system developed by Chen (2006) based on Java language; it can give the knowledge map of a specific research domain with co-citation analysis and pathfinder network scaling to seek the key evolutionary path and intellectual turning points [19]. CiteSpace can realise several important functions: it can identify the milestone paper, appraise the innovative extent, and reveal the research front evolution of the knowledge unit. VOSviewer software was developed by the two Netherland scholars van Eck and Waltman. Their paper *Software Survey: VOSviewer, a Computer Program for Bibliometric Mapping* is a hot paper of the *Journal of Informetrics*. VOSviewer provides five types of function, including co-authorship analysis, co-occurrence analysis, citation analysis, bibliographic coupling, and co-citation analysis, and the units of analysis can include authors, organisation (institution), and countries. In comparison with CiteSpace, VOSviewer can provide a clearer clustering result due to its parameter set of clustering resolution. The following knowledge mapping analysis of green technology includes four steps (Figure 1): the first step is to select data from the WoS database; the second step is the co-citation analysis to acquire the key literature; the third step is the co-occurrence network analysis; and the fourth step is cluster view analysis to obtain the cluster results of green technology literature.

In VOSviewer, the basic colour view of a theme depends on the ordinary density rule. The colour of a point in the map is determined based on the item density of the point. Let $\overline{d}$ denote the average distance between two items, that is,

$$\overline{d} = \frac{2}{n(n-1)} \sum_{i \leq j} \left\| x_i - x_j \right\|. \tag{1}$$

The item density $\mathrm{D}(x)$ of a point $x = (x1, x2)$ is then defined as

$$D(x) = \sum_{i=1}^{n} w_i K\left(\frac{\left\| x -{}^{i}_{x} \right\|}{h\overline{d}} \right), \tag{2}$$

where k: $[0, \infty) \longrightarrow [0, \infty)$ denotes a kernel function; $h > 0$ denotes a parameter called the kernel width; and w_i denotes the weight of item i, that is, the total number of occurrences or co-occurrences of item i. The kernel function k must be nonincreasing. VOSviewer uses a Gaussian kernel function given by

$$K(t) = \exp\left(-t^2\right). \tag{3}$$

It follows from (2) that the item density of a point in a map depends on the number of neighbouring items and on the weights of these items. The larger the number of neighbouring items and the smaller the distances between these items and the point of interest is, the higher the item density will be. In addition, the higher the weights of the neighbouring items is, the higher the item density will be.

3. Results

3.1. Yearly Distribution of Green Technology Papers and Highly Cited Paper Analysis

3.1.1. Yearly Distribution of Green Technology Papers. We search for the green technology papers from the WoS Core Collection. Then, we obtain the number of published articles annually (PN) from 1968 to 2020. The published papers can be divided into three stages: the primary stage (1968–1990), in which the maximum number is below 10; the booming stage (1991–2007), in which the maximum number is below 30; and the prosperous stage (2008–2020), in which the slope ratio of trendline is obviously increasing. For the citation situation analysis, we collect the citation number (CN) of all the green technology papers. The h-index of green technology source is 77, and the average citation per item is 20.16. The sum of times cited is 30567, and that without self-citations is 30066 (Figure 2). As

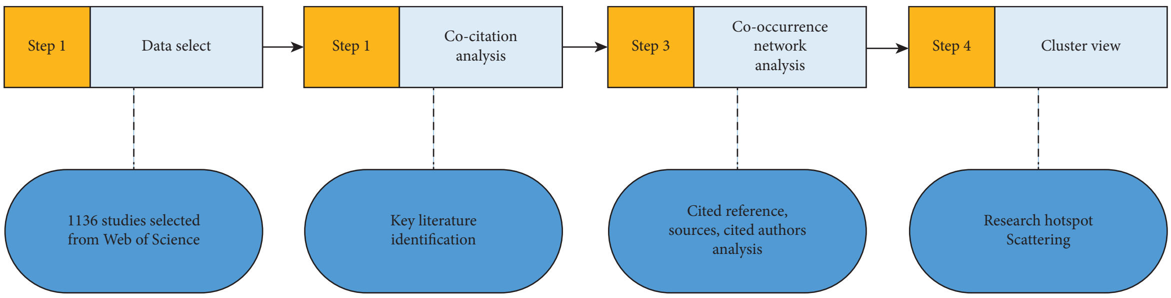

Figure 1: Four steps of knowledge mapping analysis.

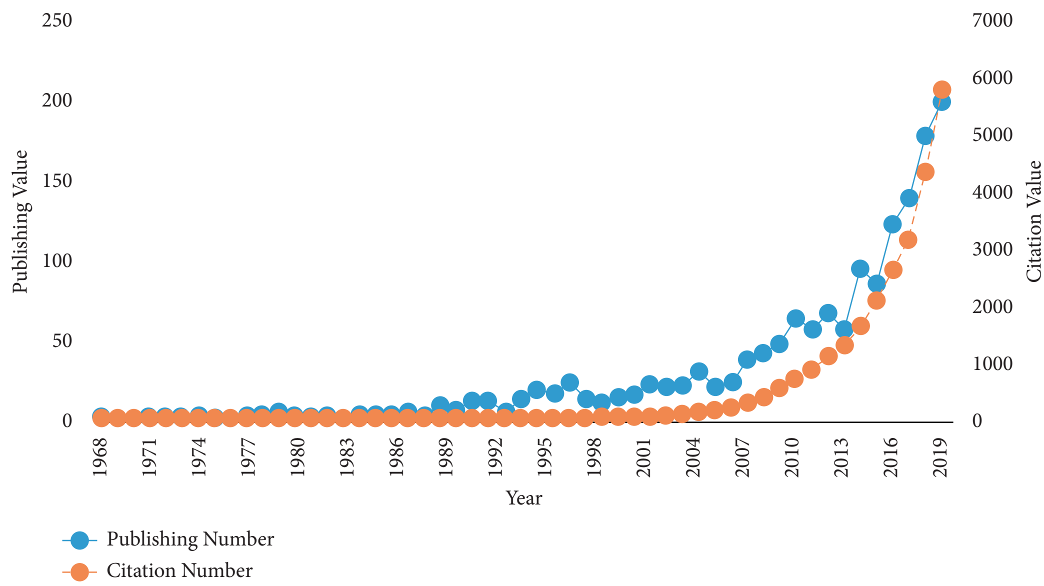

Figure 2: Annual PN and CN distribution of green technology.

indicated in Figure 2, green technology theme has attracted increasing academic interest since 1968.

The 1136 green technology papers involve 149 types of research area, the top ten of which are environmental sciences, green sustainable science technology, engineering environmental, engineering chemical, environmental studies, energy fuels, chemistry multidisciplinary, economics, food science technology, and biotechnology applied microbiology. As shown in Table 1, green technology records of environmental sciences exist, which accounts to 24.47% of the total records; the last research fields are agriculture and biotechnology applied microbiology, with 49 records of 4.31% of the total. Surprisingly, management and business categories take up the 11th and the 12th positions of all the research areas.

3.1.2. Cited Journal Analysis. In VOSviewer software, we select 1968–2020 with one year per slice as the time slice. To obtain the core journals of green technology, we set the types of citation and "sources" as the unit of analysis. We obtain 716 sources; the total strength of each of the citation links with other sources are calculated. The sources with the greatest total link strength are selected. We find that some of the 716 items in the network are not connected to each other. The largest set of connected items consists of 91 items (in Figure 3).

We choose the top 20 journals of green technology by the centrality value (Table 2). From Table 2, we can find that the *Journal of Cleaner Production* has 184 green technology records, whereas the *Journal of Agricultural and Food Chemistry* has the least 7 records. From the centrality parameter, the value of *Journal of Cleaner Production* in 2010 is 0.26, which is the largest, whereas the value of *Journal of Agricultural and Food Chemistry* in 2005, *Journal of the American Chemical Society* in 2012, *Angewandte Chemie* in 2012, and *Pure and Applied Chemistry* in 2007 is 0.06, which is the least.

3.1.3. Highly Cited Paper Analysis. From the green technology citation results, we can refine papers by highly cited type in the field with data from the Essential Science Indicator (ESI) automatically. Now, ESI ranking is becoming increasingly popular, and the highly cited paper has received sufficient citations to place it in the top of 1% of different academic fields based on a highly cited threshold for the field and publication year. After we comb the 13 papers of green technology, four papers related to the field of chemistry remain published on *Separation and Purification Technology*,

Table 1: Research area of green technology records.

Research areas	Record count	Percentage of the total records
Environmental sciences	278	24.47
Green sustainable science technology	168	14.79
Engineering environmental	117	10.30
Engineering chemical	114	10.03
Environmental studies	95	8.36
Energy fuels	88	7.75
Chemistry multidisciplinary	78	6.87
Economics	72	6.34
Food science technology	59	5.19
Biotechnology applied microbiology	49	4.31

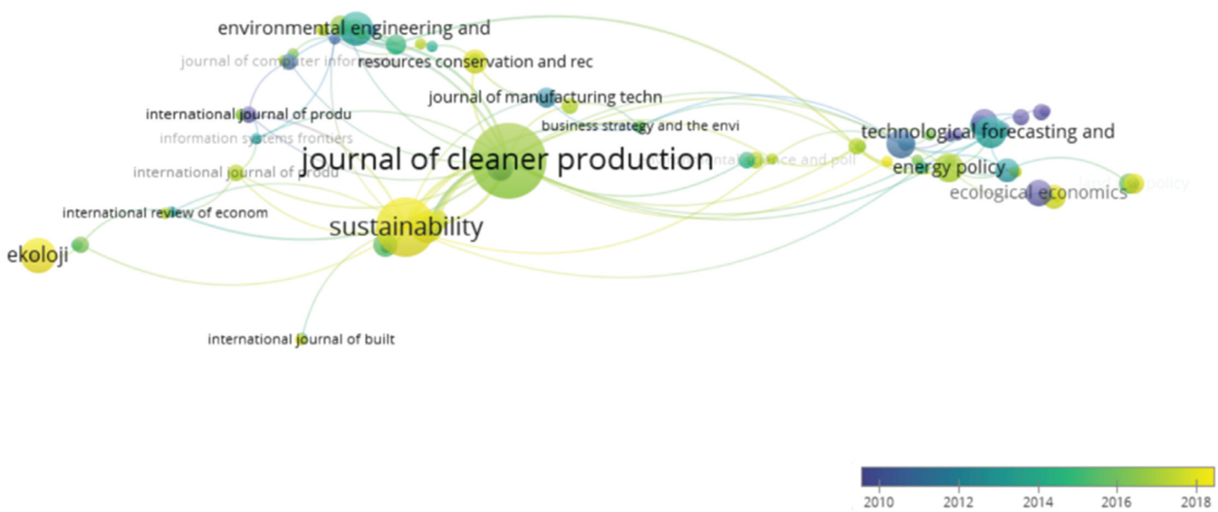

Figure 3: Cited journal mapping of green technology.

Table 2: Parameters of green technology cited journals.

	Count	Centrality	Year	Cited journals
1	184	0.26	2010	*Journal of Cleaner Production*
2	39	0.24	2011	*Resources Conservation and Recycling*
3	45	0.16	2006	*Environmental Science and Technology*
4	105	0.13	2002	*Science*
5	101	0.13	1980	*Journal of Hazardous Materials*
6	66	0.13	2010	*Industrial and Engineering Chemistry Research*
7	82	0.12	2006	*Bioresource Technology*
8	65	0.12	2005	*Journal of Chemical Technology and Biotechnology*
9	81	0.11	2009	*Chemical Review*
10	40	0.11	2005	*MIS Quarterly*
11	35	0.10	2007	*Renewable and Sustainable Energy Reviews*
12	48	0.09	2010	*Energy Policy*
13	128	0.08	2011	*American Economic Review*
14	120	0.07	2011	*Energy Economics*
15	59	0.07	2004	*Journal of Organic Chemistry*
16	29	0.07	2012	*Research Policy*
17	7	0.06	2005	*Journal of Agricultural and Food Chemistry*
18	67	0.06	2012	*Journal of the American Chemical Society*
19	51	0.06	2012	*Angewandte Chemie*
20	38	0.06	2007	*Pure and Applied Chemistry*

Journal of Supercritical Fluids, *Analytica Chimica Acta*, and *Fuel Processing Technology Journal*. These papers deal with electrocoagulation technique [20], supercritical fluid extraction [21], eutectic solvents [22], and biodiesel focusing on green catalytic techniques [23], which introduce certain new applicable techniques or methods for reducing pollutive outputs or promote production efficiency.

There are four papers related to the field of engineering published on the *International Journal of Production Economics*, *Chemical Engineering Journal*, *Solar Energy*, and *Production and Operations Management Journal*. These four papers examine carbon emission reductions under market mechanism [24], membrane bioreactor technology in waste water treatment [25], green roofs technology to mitigate the heat island phenomenon [26], and environmental taxes and subsidies motivating the consumer's choice of green emission technology [27].

Four papers are related to the field of economics and business published on *Management Decision*, *Management Science*, *R&D Management*, and *Journal Of Environmental Economics and Management*. These papers discuss the productive technical progress and green technical innovation in China [28], the potential effects of governmental subsidies for green technology adoption in view of the manufacturing industry's response [29], the current overview of green innovation management [30], and American consumer adoption of hybrid-electric vehicles [31]. One paper is related to the field of geosciences, which is about metals for green technology application and published on *Ore Geology Reviews* [32].

As shown in Table 3, the highest citation count is the "Natural deep eutectic solvents as new potential media for green technology" by Dai et al. (2013), with a total number of 587; and the lowest citation count is "Electrocoagulation as a green technology for phosphate removal from river water" by Hashim et al. (2019).

3.2. Co-Authorship Analysis of Green Technology Research. We use the VOSviewer co-authorship function to create a map of co-authorship of green technology. We click the type of analysis item and choose the "Authors" unit of analysis; for the counting method, we choose "Full counting." We set the minimum number of documents of an author default threshold value as 3, and of all the 4158 authors, 54 authors meet the thresholds (Figure 4). For each of the 54 authors, the total strength of the co-authorship links with each other author is calculated automatically. The authors with the greatest total link strength is selected. The result can be adjusted with documents, citations, and total link strength parameter.

As shown in Figure 4, the co-author distribution of green technology is quite scattered. Moreover, we obtain three small co-authorship networks. The first network, indicated by red colour, includes three authors belonging to the economic field; they mainly contribute to the strategies, barriers, and critical drivers of green building technology adoption in developing countries, with the cases of Ghana and developed countries, such as the USA [10, 33, 34]. The second network, indicated by blue colour, includes five authors belonging to the bioengineering field; these authors investigate the adoption of green fertilizer technology (GFT) among Malaysian farmers in the paddy industry, which may be a possible solution for Malaysian food security [35, 36]. The third network, indicated by green colour, includes eight authors belonging to the chemistry field; they suggest green methods for the production of high fatty acid starch esters without the use of solvent and additives [37].

3.3. Country and Institution Analysis. Country and institution analysis in knowledge mapping can reflect the number distribution of research papers and the cooperation of different institutions and countries. The node size reflects the number, and the link value between nodes reflects the strength of co-authorship. Figure 5 shows the top three countries, USA, China, and England, which have co-authorship with one another to some extent.

From Table 4, we can obtain the top 15 countries or regions of green technology, namely, the USA, China, England, Australia, Canada, France, Italy, Spain, Germany, Malaysia, Japan, South Korea, Taiwan, Finland, and the Netherlands. From the Documents column, 301 green technology records in the USA rank first among all the countries, followed by China with 205 documents and England with 72 documents, and the last country is Finland with 16 documents. From the Citations column, the USA still ranks first with 5877 citations, followed by Canada with 1763 and China with 1703, and the lowest country is Finland, with 335 citations. From the Total link strength column, the top three countries are the USA, China and England with total link strength of 108, 99, and 65, respectively, and the last two countries are Finland and the Netherlands, with the same value of total link strength of 21.

For institution analysis, there exist 1575 research organisations all over the world with publishing papers with green technology issues. We set the minimum number of documents of an organisation threshold value as 7, and 12 research institutions meet the threshold, of which three institutions are in Malaysia (Univ Sains Malaysia, Univ Malaya, and Univ Teknol Malaysia), two institutions are in China (Chinese Acad Sci and Hongkong Polytec Univ), two institutions are in Canada (Mcgill Univ and Queens Univ), one institution is in South Korea (Seoul Natl Univ), one institution is in Jordan (Jordan Univ Sci and Technol), one institution is in the USA (Texas A&M Univ), one institution is in the UK (Univ Nottingham), and one institution is in Italy (Univ Turin). As shown in Table 5, Chinese Acad Sci, which is the top institution, has 19 documents of green technology. Mcgill Univ has 549 most citations of green technology. The total link strength value indicates that the correlation between institutions is quite weak, and individual organisation has limited academic influence.

3.4. Keyword Cluster Analysis

3.4.1. Green Technology Cluster Analysis. Keyword cluster analysis can reveal the specific theme's present situation and research front. Cluster analysis can detect homogeneous

Table 3: Highly cited papers of green technology.

	Author	Paper title	Journal title	Field	Citation counts	Published year
1	Hashim > et al.	Electrocoagulation as a green technology for phosphate removal from river water	*Separation and Purification Technology*	Chemistry	21	2019
2	Song and Wang	Market competition, green technology progress and comparative advantages in China	*Management Decision*	Economics and business	36	2018
3	Xu, He, and Xu	Supply chain coordination with green technology under cap-and-trade regulation	*International Journal of Production Economics*	Engineering	60	2017
4	Cohen, Lobel, and Parakis	The impact of demand uncertainty on consumer subsidies for green technology adoption	*Management Science*	Economics and business	50	2016
5	Neoh, Noor, and Mutamim	Green technology in wastewater treatment technologies: Integration of membrane bioreactor with various wastewater treatment systems	*Chemical Engineering Journal*	Engineering	92	2016
6	De Melo, Silcestre, and Silva	Supercritical fluid extraction of vegetable matrices: Applications, trends and future perspectives of a convincing green technology	*Journal of Supercritical Fluids*	Chemistry	170	2014
7	Santamouris	Cooling the cities - a review of reflective and green roof mitigation technologies to fight heat island and improve comfort in urban environments	*Solar Energy*	Engineering	511	2014
8	Krass, Nedorezov and Ovchinnikov	Environmental taxes and the choice of green technology	*Production and Operations Management*	Engineering	149	2013
9	Hein, Mizell, and Koschinsky	Deep-ocean mineral deposits as a source of critical metals for high- and green technology applications: Comparison with land-based resources	*Ore Geology Reviews*	Geosciences	202	2013
10	Dai, van Spronsen, and Witkamp	Natural deep eutectic solvents as new potential media for green technology	*Analytica Chimica Acta*	Chemistry	587	2013
11	Schiederig, Tietze, and Herstatt	Green innovation in technology and innovation management - an exploratory literature review	*R&D Management*	Economics and business	169	2012
12	Gallagher and Muehlegger	Giving green to get green? Incentives and consumer adoption of hybrid vehicle technology	*Journal of Environmental Economics and Management*	Economics and business	260	2011
13	Helwani, Othman, and Aziz	Technologies for production of biodiesel focusing on green catalytic techniques: A review	*Fuel Processing Technology*	Chemistry	344	2009

Figure 4: Co-authorship analysis of green technology.

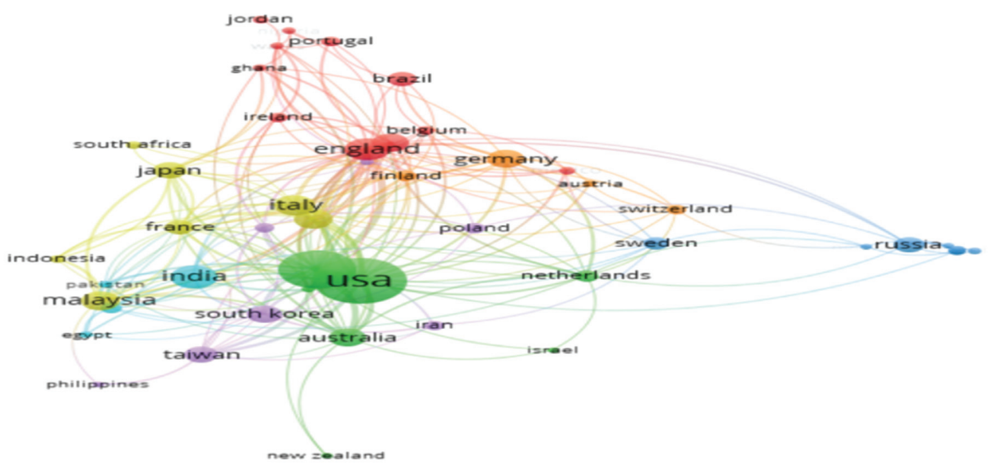

Figure 5: Co-authorship mapping of different countries.

Table 4: Green technology co-authorship of different countries or regions.

	Country	Documents	Citations	Total link strength
1	USA	301	5877	108
2	China	205	1703	99
3	England	72	1632	65
4	Australia	50	1157	41
5	Canada	53	1763	34
6	France	29	420	34
7	Italy	60	571	33
8	Spain	49	684	32
9	Germany	49	1005	29
10	Malaysia	51	866	29
11	Japan	39	526	27
12	South Korea	41	772	24
13	Taiwan	40	395	24
14	Finland	16	335	21
15	Netherlands	21	862	21

Table 5: Green technology co-authorship of different institutions.

	Institution	Documents	Citations	Total link strength
1	Univ Sains Malaysia	9	481	2
2	Chinese Acad Sci	19	127	1
3	Seoul Natl Univ	10	124	1
4	Univ Malaya	7	146	1
5	Univ Teknol Malaysia	7	92	1
6	Hongkong Polytec Univ	10	195	0
7	Jordan Univ Sci and Technol	9	112	0
8	Mcgill Univ	8	549	0
9	Queens Univ	7	191	0
10	Texas A&M Univ	7	139	0
11	Univ Nottingham	9	436	0
12	Univ Turin	8	73	0

units using an algorithm method [38]. In contrast to other meta-analysis methods, cluster calculation has been proved to have less subjective bias, and strong connections of units reflect the specific theme in the same field [39]. The co-word matrix is commonly constructed from the samples, and statistical variables are used to measure the degree of similarity of indicators. According to different similarities, closely related objects are gathered automatically, which denote the direct connections among keywords or titles in knowledge mapping software. The CiteSpace system provides five types of visualisation style, namely, cluster view, timeline view, timezone view, geographic overlay, and dual-map overlay. The cluster and timeline views are the most popular. The cluster view can reflect the distribution of research area in different dimensions, and the timeline view can tell us the yearly evolution and interaction of each cluster. Two important parameters indicate the quality of cluster mapping, namely, modularity and silhouette values. Generally, if the modularity value is greater than 0.3, then the cluster is significant; if the mean silhouette value is greater than 0.5, then the cluster view is reasonable and acceptable. First, we perform the cluster view operation. The results indicate that the merged network of keywords related to green technology consists of 352 nodes and 1684 links. The parameter modularity value is 0.5225, and the mean silhouette value is 0.6082 (Figure 6).

From the statistical results of the keywords from the yearly slice (Table 6), we choose the top 10 keywords of the green technology cluster. The top 10 keywords are emission, green technology, performance, energy, design, optimisation, system, behaviour, environment, and product. The maximum value of centrality is 0.15, and the minimum value is 0.07. From the year distribution, we find that the significant nodes range from 2008 to 2015.

3.4.2. Timeline View Evolutionary Analysis of Green Technology. The timeline view in the CiteSpace system can reflect the relationship between clusters and historic duration of the literature. In the timeline view, the horizontal axis is the year distribution and the vertical axis is the labelling of the clusters. Keywords belonging to the same cluster are set in a line according to the date of the published literature. In the timeline view, we can obtain the beginning year of a cluster, the numerical trend of a cluster, and the important literature with high betweenness centrality value. From the timeline view of green technology (Figure 7), 10 clusters are labelled with #0–#9 and the distribution of clusters mainly focuses from 1998 to 2020.

In the CiteSpace system, the cluster labelling comes from the citing articles based on three types of algorithms: TF $*$ IDF, log-likelihood rate, and mutual information. Given that the consciousness of mapping and log-likelihood ratio value can provide quantifying information automatically, we choose log-likelihood rate algorithm. The labelling results and log-likelihood ratio value of green technology clusters are as follows (Table 7). The first cluster labelling is resource-based view, with a total size of 61 keywords, and the mean year is 2014. Under the line, we can see that the first cluster keywords include adoption, green technology impact, sustainability, renewable energy, environmental policy, green cleaner production, and empirical evidence. The second cluster labelling is green technology progress, with a total size of 55 keywords, and the mean year is 2015; it includes keywords of information technology, remote sensing, energy efficiency, green growth, environmental strategy, and environmental regulation. The third cluster is labelled with BR, with a total of 50 keywords and the mean year of 2016; keywords include life cycle assessment, emission, fuel cell, heavy metal, electric vehicle, catalyst, and eco-design. The fourth cluster is labelled with molecular weight, with a total size of 40 keywords and the mean year of 2015; keywords include degradation, green kinetics, fermentation, biodegradation mechanism, polymer, fabrication, and health. The fifth cluster is labelled with ultrasound-assisted extraction, with a total size of 37 keywords and the mean year of 2016; it includes keywords of polymerisation, carbon dioxide, superficial, subcritical water, plant, and assisted extraction. The sixth cluster is labelled with green revolution, with a total size of 31 keywords and the mean year of 2015; it includes keywords of green technology, rice production, social responsibility, supply chain, and environmental prevention. The seventh cluster is labelled with green building technologies, with a total size of 31 keywords and the mean year of 2015; it includes keywords of environment management, design, investment policy, green economy, sustainable development, green building, critical success factor, and barrier. The eighth cluster is labelled with paper mill waste, with a total size of 19 keywords and the mean year of 2012; keywords of this cluster include water, biosorption waste, ironic liquid, acid extraction, recycling, and aqueous solution. The ninth cluster is labelled with organic peroxide, with a total size of 5 keywords and the mean year of 2012; keywords include SADT, organic peroxide, and accelerating decomposition temperature. The tenth cluster is labelled with alginate, with a total size of 3 keywords and the mean year of 2014; it includes keywords of bacteria, *Escherichia coli*, and temperature.

3.4.3. Brief Summary of the 10 Clusters. From Table 8, all the papers about green technology can be divided as follows: three clusters are in the economics and business field, five clusters are in the engineering field, and two clusters are in the chemistry field.

The #0 cluster deals with sustainability, with research subjects mainly about sustainability, supply chain, human resources management, and carbon dioxide emission. Resource-based view theory, which was proposed by Birger Wernerfelt, is an important source of modern core competitive compacity of firms [40]. Each market entity should pay attention to allocate human resources, currency capital, and technology to achieve a more desirable output. Green information technologies and systems refer to initiatives and programs that directly or indirectly address environmental sustainability in organisations [41]. In this cluster, environmental technologies are used in supply chain management to check the collaboration effect between suppliers and customers [42] and corporate sustainable capability may be integrated with information technology and supply chain [43].

The #1 cluster concentrates on the green technology progress and innovations in different industries. It includes research subjects of green technology progress, adoption decision, Bayesian learning, energy efficiency, and green growth. Topics include energy strategy should be transformed, hydrogen economy as a greener choice as a carbon-free carrier [44], green building technologies adoption [33],

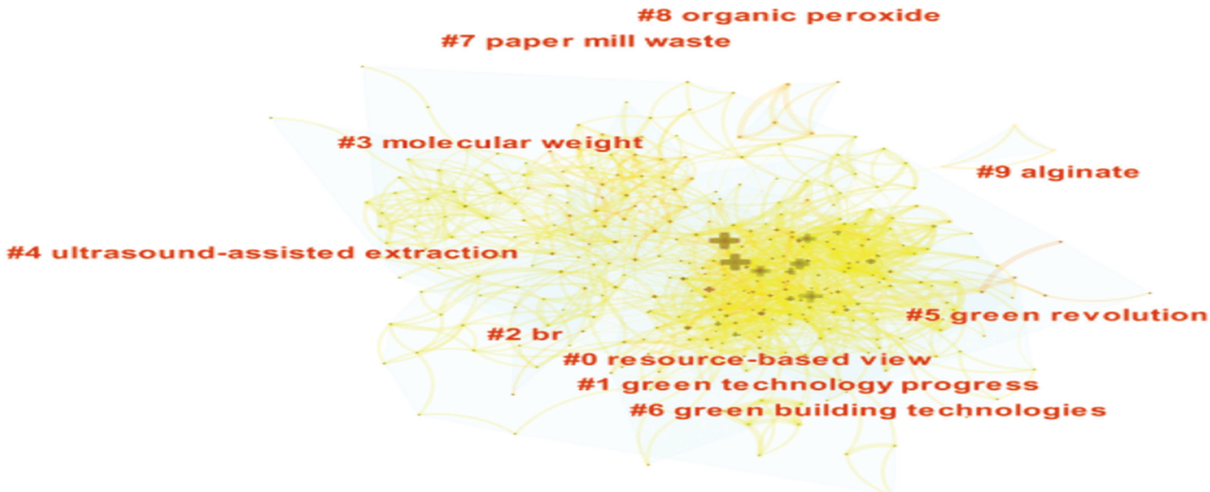

Figure 6: Keyword cluster of green technology.

Table 6: Top 10 keywords in the green technology cluster.

Count	Centrality	Year	Keywords
24	0.15	2009	Emission
89	0.14	2010	Green technology
71	0.11	2013	Performance
32	0.10	2012	Energy
20	0.09	2011	Design
60	0.09	2013	Optimisation
15	0.08	2008	System
18	0.08	2011	Behaviour
9	0.07	2010	Environment
15	0.07	2015	Product

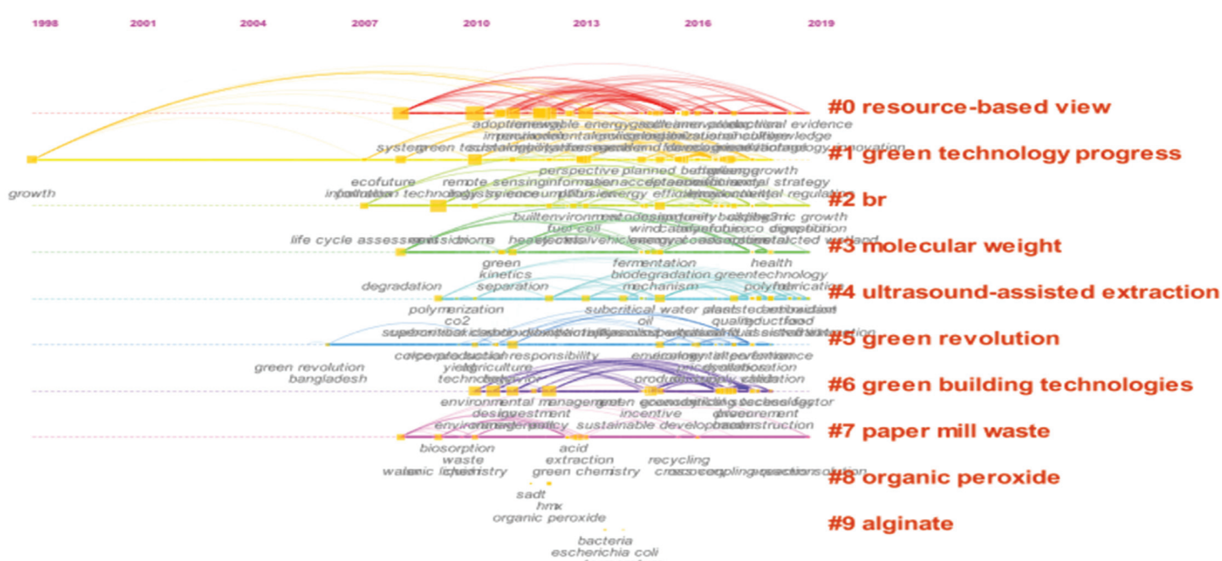

Figure 7: Timeline view of green technology.

Table 7: 10 keyword clusters of green technology.

Cluster ID	Size	Mean year	Top 10 terms (log-likelihood ratio value)
0	61	2014	Resource-based view (9.35); geothermal energy (6.22); employment (6.22); institutional theory (6.22); ecological modernisation (6.22); climate change (6.22); innovation (5.32); sustainability (4.1); evaluation (3.11); manufacturing (3.11)
1	55	2015	Green technology progress (15.31); adoption (7.63); TPB (7.63); big data (7.63); GFT (7.63); pollutant discharge (3.8); software-defined networks (3.8); IoT (3.8); adoption decision (3.8); Bayesian learning (3.8)
2	50	2016	BR (7.92); CL (7.92); leaching (7.92); BIM technology (7.92); fuel cells (7.92); application (7.92); nanocrystal (7.92); diode (7.92); detoxification (7.92); CsPbX3 (7.92)
3	40	2015	Molecular weight (9.62); branched structure (9.62); biodegradation (9.62); membrane separations (4.8); chromatography (4.8); fly ash geopolymer (4.8); mesophase (4.8); chain degradation (4.8); saccharification (4.8); criteria weighting (4.8)
4	37	2016	Ultrasound-assisted extraction (12.99); antioxidant (8.64); supercritical fluid extraction (8.64); polycaprolactone (4.31); supercritical extraction (4.31); antioxidant activity (4.31); ellagitannins (4.31); tough external peels (4.31); green extraction technologies (4.31)
5	31	2015	Green revolution (15.23); sawah (10.12); chemical properties (5.04); cap-and-trade (5.04); smartphones (5.04); information technology managers (5.04); mealtime (5.04); exchangeable cations (5.04); rice production (5.04); total carbon (5.04)
6	31	2015	Green building technologies (30.75); promotion strategies (20.37); construction industry (20.37); barriers (20.374); sustainable development (20.3); drivers (15.23); Ghana (10.9); developing countries (10.9); construction market (10.125); new economy (10.12)
7	19	2012	Paper mill waste (5.29); botanical (5.29); herbal preparation (5.29); quality control (5.29); environmental assessment tool (eat) (5.29); ozonation (5.29); biopolymers (5.29); green chemistry (5.29); recycled paper (5.29); municipal solid waste (5.29);
8	5	2012	Organic peroxide (15.17); vent sizing package (7.53); thermal hazard (7.53); differential scanning calorimetry (7.53); thermokinetic parameters (7.53); consumption energy (7.53); safety parameter (7.53); diffusion (7.53); kinetic (7.53)
9	3	2014	Alginate (6.77); bacterial inactivation (6.77); silica gel (6.77); catalyst (6.77); immobilisation (6.77); energy sustainability (6.77); antimicrobial activity (6.77); bacteria (6.77); organic Rankine cycle (6.77)

Table 8: Summary of research subjects of 10 green technology clusters.

	Cluster labelling	Field	Research subjects
#0	Resource-based view	Economics and business	(1) Sustainability; (2) supply chain; (3) human resources management; (4) carbon dioxide emission
#1	Green technology progress	Economics and business	(1) Green technology progress; (2) paddy farmer; (3) energy efficiency; (4) green growth
#2	BR	Engineering	(1) Green engineering construction; (2) energy conservation; (3) emerging vehicle technology; (4) coal utilisation; (5) biotechnology
#3	Molecular weight	Chemistry	(1) Bioremediation; (2) biodegradation; (3) membrane separations; (4) chromatography
#4	Ultrasound-assisted extraction	Engineering	(1) Clean extraction; (2) green solvents
#5	Green revolution	Economics and business	(1) Rice production; (2) information technology; (3) financial services industry; (4) environmental sustainability
#6	Green building technologies	Engineering	(1) Promotion strategies; (2) construction market; (3) driving force; (4) technologies adoption
#7	Paper mill waste	Engineering	(1) Green chemistry; (2) environmental assessment; (3) paper mill waste; (4) municipal solid waste
#8	Organic peroxide	Chemistry	(1) Organic peroxide; (2) scanning calorimetry; (3) incompatible material; (4) thermal hazard
#9	Alginate	Engineering	(1) Alginate; (2) bacterial inactivation; (3) silica gel; (4) catalyst

green technology progress measurement of thermoelectric enterprises [45], green technology progress influencing factors [46], and technological progress in green cement industry [47].

The #2 cluster explores types of new green technology applicable in chemical and biological engineering. The research subjects are mainly about green engineering construction, energy conservation, emerging vehicle technology, coal utilisation, and biotechnology. The hot topics of this cluster include network energy-saving technologies in mobile industry [48], future wireline networks' potential economic and environmental consequences [49], smart cities and green growth based on universal infrastructure and green technologies [50], and electric vehicle routing designing and technology to recharge [51].

The #3 cluster offers a series of microstructural practices and inner material structure exploratory research. It includes research subjects of bioremediation, biodegradation, membrane separations, and chromatography. These green technologies include phytoremediation technology using diverse plants to remediate contaminated environments [52], polysaccharides modification [53], ferrate as an efficient agent for the abatement of pollutants in water [54], and sorption membrane for water purification and liquid separation [55, 56].

The #4 cluster reveals environmentally friendly extraction mechanism of green extraction kinetics and polymerisation processing technologies. The research subjects are mainly about ultrasound-assisted extraction, supercritical fluid extraction, extraction kinetics, clean extraction, polymer blends, and biomedical polymers. Topics include cleaner production purposes embracing supercritical fluid extraction [21], enhancing aqueous extraction processes without using solvents with ultrasound-assisted extraction technology [57], developing green solvents for oil extraction [58], promoting innovation of more environmentally friendly and tuneable solvents [59], and exploring green catalytic techniques of homogeneous liquids and heterogeneous solids in biodiesel production [23].

The #5 cluster manifests the social information learning of green revolution in agricultural technology adoption and environmental performance, especially with the cap-and-trade carbon dioxide emission constraint. It includes research subjects of rice production, information technology, financial services industry, and environmental sustainability. It includes discussions on the proper farm size related to effective new technology adoption and credit constraint [60], information flows in social learning of Indian rice and wheat technology revolution [61], technology policy function [62], impact assessment of technology intervention [63], and effects of improved agricultural technologies [64].

The #6 cluster presents the driving force of green building technologies adoption and existing barriers in the construction industry. The research subjects are mainly about designers' adoption behaviours [65], driving force [10], and barriers of green building [66]. New engineering applications of green water technologies [67], green roof technology [68], green wall technology [69], and "green concrete" concept [70] are discussed in this cluster.

The #7 cluster focuses on environmental negative impact control, such as water pollution and solid waste disposal and recycling problems. This cluster includes research subjects of green chemistry, environmental assessment, environmental compatibility, paper mill waste, and municipal solid waste. Modern industrial production inevitably comes up with undesirable output, even some pollutive and poisonous substance. Poliakoff (2007) contributed with unsustainable chemical manufacturing and 12 modern principles of green chemistry [71]. Green technologies are developed to realise removal of heavy metals, cyanobacteria, and other hazardous material in water [72, 73]. Some novel processing and methods have also been presented to deal with solid waste, such as industrial and municipal solid waste [74].

The #8 cluster reflects the functional materials with unique characterisation and thermal hazard evaluation. The research subjects are mainly about organic peroxide, scanning calorimetry, incompatible material, and thermal hazard. Newly found material characteristics, effective processing adjustment, and novel monitoring tools have been presented. Topics include ionic liquids with unique advantages showing higher selectivity, fast rates, and greater enzyme stability [75]; organic synthesis using microreactor technology having better thermal stability than traditional batch synthesis [76]; polylactide, as packaging material, being suitable for industrial usage, as well as its environmental implications [77]; and for thermal hazard, some novel calorimetric tests and simulation evaluating methods have been presented [78, 79].

The #9 cluster concentrates on biological materials and engineering applications. It includes research subjects of alginate, bacterial inactivation, silica gel, catalyst, and immobilisation. Several highly cited papers are about microalgae encapsulation technology [80], green biocides [81], encapsulation in chitosan-based nanomatrix [82], and polyphenol recovery from pomegranate peels [83].

4. Conclusions and Policy Implications

Green technology is seemed to be used increasingly widely in different disciplines. This study uses knowledge mapping tools of CiteSpace and VOSviewer software to examine the development of green technology theme. We find that green technology concept came into being in the 1960s and became gradually popular in the 2000s. The research interest of green technology has been growing dramatically in the recent decade, with a sharp increase in published research papers and citation records.

Of the total 1136 green technology papers covering 149 research fields, the top three fields are environmental sciences, green sustainable science technology, and engineering environmental, and there exists about a quarter ratio of the total sample literature about environmental sciences. We can expect that more and more green technologies will be developed in the near future. From the cited journals of green technology, we find that the top 10 journals are *Journal of Cleaner Production*, *Resources Conservation and Recycling*, *Environmental Science and Technology*, *Science*, *Journal of Hazardous Materials*, *Industrial and Engineering Chemistry Research*, *Bioresource Technology*, *Journal of Chemical Technology and Biotechnology*, *Chemical Review*, and *MIS Quarterly*, with the use of parameter of centrality and publishing number. In the WoS database, 13 highly cited papers are related to the theme of green technology from 2009 to 2020, and they can be ascribed to chemistry, engineering, economics and business, and geosciences fields.

From the co-authorship analysis of green technology, we find that the network of research cooperation is quite weak. Only three little networks are labelled with different colours. From the country and institution analysis, we find that developed countries (the USA, England, etc.) and developing countries (China, Malaysia, etc.) have quite a few documents of green technology, and according to the parameter of CN and total link strength value, we obtain the top 15 counties. After the institution analysis of the green technology literature, 12 important institutions in 8 countries are recognised, but no dominant institutions have become eccentric. We find that they perform their research quite independently. In the knowledge mapping of cluster analysis, 10 keyword clusters of green technology papers are in the WoS database and three clusters are of economical theme, five clusters are of engineering application, and two clusters are of chemical issues.

In the future, we should strengthen the achievements of green technology progress, promote the level of innovation, and accelerate the regional flow of innovation factors. We should solve the bottleneck of green technology development of high-levelled human, material, and financial resources; focus on the "double base" construction to address key technical problems affecting industrial development, and break through the "neck" technical problems. At the same time, administrative departments should strengthen financial support for high-quality economic development; enhance the efficiency of financial investment in green technology and industry; and increase the auditing and inspection intensity of the use of financial investment funds to improve the interactive quality of green technological progress, financial investment, economic quality, and development level.

Data Availability

This paper is analysed through previous literature texts, and the text data are available.

Conflicts of Interest

The authors declare no conflicts of interest.

Acknowledgments

This work was supported by the financial projects funded by Jiangsu Federation of Social Sciences (Grant no. 21SCC-24).

References

[1] W. Bascom, "African material culture, technology and ecological adaption," *Annals of the New York Academy of Sciences*, vol. 96, pp. 581–589, 1962.

[2] K. Zhong, P. Wang, J. Pei, J. Pu, Z. Han, and J. Xu, "Multiobjective optimization regarding vehicles and power grids," *Wireless Communications and Mobile Computing*, vol. 2021, Article ID 5552626, 6 pages, 2021.

[3] R. Burke, "Green revolution technologies and farm class in Mexico," *Economic Development and Cultural Change*, vol. 28, pp. 135–154, 1979.

[4] T. Bayri and W. Furtan, "The impact of new wheat technology on income distribution: a green revolution case study, Turkey,1960-1983," *Economic Development and Cultural Change*, vol. 38, pp. 113–122, 1989.

[5] U. Khanal, C. Wilson, S. Shankar, V. Hoang, and B. Lee, "Farm performance analysis: technical efficiencies and technology gaps of Nepalese farmers in different agro-ecological regions," *Land Use Policy*, vol. 76, pp. 645–653, 2018.

[6] X. Su, P. Chiang, S. Pan et al., "Systematic approach to evaluating environmental and ecological technologies for wastewater treatment," *Chemosphere*, vol. 218, pp. 778–792, 2019.

[7] P. Grenni, A. Caracciolo, L. Mariani et al., "Effectiveness of a new green technology for metal removal from contaminated water," *Microchemical Journal*, vol. 147, pp. 1010–1020, 2019.

[8] S. Annamalai, M. Santhanam, S. Selvaraj, M. Sundaram, K. Pandian, and M. Pazos, "Green technology: bio-stimulation by an electric field for textile reactive dye contaminated agricultural soil," *The Science of the Total Environment*, vol. 624, pp. 1649–1657, 2018.

[9] D. Snoonian, "How green buildings are smarter and safer -energy-saving technology can have unexpected side benefits for building safety and intelligence," *Architectural Record*, vol. 191, pp. 100–104, 2003.

[10] A. Darko, A. Chan, S. Gyamfi, A. Olanipekun, B. He, and Y. Yu, "Driving forces for green building technologies adoption in the construction industry: Ghanaian perspective," *Building and Environment*, vol. 125, pp. 206–215, 2017.

[11] C. Bishop, "Surface engineering - a green technology," *Transactions of the Institute of Metal Finishing*, vol. 81, pp. 13–18, 2003.

[12] Z. Guo, Y. Sun, S. Pan, and P. Chiang, "Integration of green energy and advanced energy-efficient technologies for municipal wastewater treatment plants," *International Journal of Environmental Research and Public Health*, vol. 16, p. 1282, 2019.

[13] J Si, L. Marjanovic-Halburd, F. Nasiri, and S. Bell, "Assessment of building-integrated green technologies: a review and case study on applications of Multi-Criteria Decision Making (MCDM) method," *Sustainable Cities and Society*, vol. 27, pp. 106–115, 2016.

[14] A. Pieczynska, A. Borzyszkowska, and A. Ofiarska, "Removal of cytostatic drugs by AOPs: a review of applied processes in the context of green technology," *Critical Reviews in Environmental Science and Technology*, vol. 47, pp. 1282–1335, 2017.

[15] F. AlKhawli, M. Pateiro, R. Dominguez et al., "Innovative green technologies of intensification for valorization of seafood and their by-products," *Marine Drugs*, vol. 17, pp. 1–20, 2019.

[16] N. van Eck and L. Waltman, "Software survey: VOSviewer, a computer program for bibliometric mapping," *Scientometrics*, vol. 84, pp. 523–538, 2010.

[17] X. Li, E. Ma, and H. Qu, "Knowledge mapping of hospitality research – A visual analysis using CiteSpace," *International Journal of Hospitality Management*, vol. 60, pp. 77–93, 2017.

[18] H. Chen, Y. Feng, S. Li, Y. Zhang, and X. Yang, "Bibliometric analysis of theme evolution and future research trends of the type a personality," *Personality and Individual Differences*, vol. 150, pp. 1–20, 2019.

[19] C. Chen, "Science mapping: a systematic review of the literature," *Journal of Data and Information Science*, vol. 2, pp. 1–40, 2017.

[20] M. Emamjomeh, "Electrocoagulation as a green technology for phosphate removal from river water," *Separation and Purification Technology*, vol. 217, p. 85, 2019.

[21] M. de Melo, A. Silvestre, and C. Silva, "Supercritical fluid extraction of vegetable matrices: applications, trends and future perspectives of a convincing green technology," *The Journal of Supercritical Fluids*, vol. 92, pp. 115–176, 2014.

[22] Y. Dai, J. van Spronsen, G. Witkamp, R. Verpoorte, and Y. Choi, "Natural deep eutectic solvents as new potential

media for green technology," *Analytical Chemical Acta*, vol. 766, pp. 61–68, 2013.

[23] Z. Helwani, M. Othman, N. Aziz, W. Fernando, and J. Kim, "Technologies for production of biodiesel focusing on green catalytic techniques: a review," *Fuel Processing Technology*, vol. 90, pp. 1502–1514, 2009.

[24] X. Xu, P. He, H. Xu, and Q. Zhang, "Supply chain coordination with green technology under cap-and-trade regulation," *International Journal of Production Economics*, vol. 183, pp. 433–442, 2017.

[25] C. Neoh, Z. Noor, N. Mutamim, and C. Lim, "Green technology in wastewater treatment technologies: integration of membrane bioreactor with various wastewater treatment systems," *Chemical Engineering Journal*, vol. 283, pp. 582–594, 2016.

[26] M. Santamouris, "Cooling the cities - a review of reflective and green roof mitigation technologies to fight heat island and improve comfort in urban environments," *Solar Energy*, vol. 103, pp. 682–703, 2014.

[27] D. Krass, T. Nedorezov, and A. Ovchinnikov, "Environmental taxes and the choice of green technology," *Production and Operations Management*, vol. 22, pp. 1035–1055, 2013.

[28] M. Song and S. Wang, "Market competition, green technology progress and comparative advantages in China," *Management Decision*, vol. 56, pp. 188–203, 2018.

[29] M. Cohen, R. Lobel, and G. Perakis, "The impact of demand uncertainty on consumer subsidies for green technology adoption," *Management Science*, vol. 62, pp. 1235–1258, 2016.

[30] T. Schiederig, F. Tietze, and C. Herstatt, "Green innovation in technology and innovation management - an exploratory literature review," *Management Science*, vol. 42, pp. 180–192, 2012.

[31] K. Gallagher and E. Muehlegger, "Giving green to get green? Incentives and consumer adoption of hybrid vehicle technology," *Journal of Environmental Economics and Management*, vol. 61, pp. 1–15, 2011.

[32] J. Hein, K. Mizell, A. Koschinsky, and T. Conrad, "Deep-ocean mineral deposits as a source of critical metals for high- and green-technology applications: comparison with land-based resources," *Ore Geology Reviews*, vol. 51, pp. 1–14, 2013.

[33] A. Darko, A. Chan, E. Ameyaw, B. He, and A. Olanipekun, "Examining issues influencing green building technologies adoption: the United States green building experts' perspectives," *Energy and Buildings*, vol. 144, pp. 320–332, 2017.

[34] A. Darko, A. Chan, Y. Yang, M. Shan, B. He, and Z. Gou, "Influences of barriers, drivers, and promotion strategies on green building technologies adoption in developing countries: the Ghanaian case," *Journal of Cleaner Production*, vol. 200, pp. 687–703, 2018.

[35] N. Adnan, S. Nordin, and M. Ali, "A solution for the sunset industry: adoption of green fertilizer technology amongst Malaysian paddy farmers," *Land Use Policy*, vol. 79, pp. 575–584, 2018.

[36] N. Adnan, S. Nordin, M. Bahruddin, and A. Tareq, "A state-of-the-art review on facilitating sustainable agriculture through green fertilizer technology adoption: assessing farmers behavior," *Trends in Food Science & Technology*, vol. 86, pp. 439–452, 2019.

[37] Y. Zhang, T. Gan, H. Hu et al., "Green technology for the preparation of high fatty acid starch esters: solid-phase synthesis of starch laurate assisted by mechanical activation with stirring ball mill as reactor," *Industrial & Engineering Chemistry Research*, vol. 53, pp. 2114–2120, 2014.

[38] S. Wade and Z. Ghahramani, "Bayesian cluster analysis: point estimation and credible balls (with discussion)," *Bayesian Analysis*, vol. 13, no. 2, pp. 559–626, 2018.

[39] B. Liu, H. Chen, and X. Huang, "Map changes and theme evolution in work hours: a co-word analysis," *International Journal of Environmental Research and Public Health*, vol. 15, no. 5, p. 1039, 2018.

[40] W. Birger, "A resource-based view of the firm," *Strategic Management Journal*, vol. 5, pp. 171–180, 1984.

[41] T. Jenkin, J. Webster, and L. McShane, "An agenda for "Green" information technology and systems research," *Information and Organization*, vol. 21, pp. 17–40, 2011.

[42] S. Vachon, "Green supply chain practices and the selection of environmental technologies," *International Journal of Production Research*, vol. 45, pp. 4357–4379, 2007.

[43] V. Dao, I. Langella, and J. Carbo, "From green to sustainability: information Technology and an integrated sustainability framework," *The Journal of Strategic Information Systems*, vol. 20, pp. 63–79, 2011.

[44] N. Muradov and T. Veziroglu, "Green path from fossil-based to hydrogen economy: an overview of carbon-neutral technologies," *International Journal of Hydrogen Energy*, vol. 33, pp. 6804–6839, 2008.

[45] M. Song, W. Zheng, and S. Wang, "Measuring green technology progress in large-scale thermoelectric enterprises based on Malmquist-Luenberger life cycle assessment," *Resources, Conservation and Recycling*, vol. 122, pp. 261–269, 2017.

[46] B. Cao and S. Wang, "Opening up, international trade, and green technology progress," *Journal of Cleaner Production*, vol. 142, pp. 1002–1012, 2017.

[47] A. Naqi and J. Jang, "Recent progress in green cement technology utilizing low-carbon emission fuels and raw materials: a review," *Sustainability*, vol. 11, pp. 537–555, 2019.

[48] T. Chen, Y. Yang, H. Zhang, H. Kim, and K. Horneman, "Network energy saving technologies for green wireless access networks," *"IEEE Wireless Communications*, vol. 18, pp. 30–38, 2011.

[49] R Bolla, F. Davoli, R. Bruschi, K. Christensen, F. Cucchietti, and S. Singh, "The potential impact of green technologies in next-generation wireline networks: is there room for energy saving optimization?" *IEEE Communications Magazine*, vol. 49, pp. 80–86, 2011.

[50] J. Viitanen and R. Kingston, "Smart cities and green growth: outsourcing democratic and environmental resilience to the global technology sector," *Environment and Planning A-Economy and Space*, vol. 46, pp. 803–819, 2014.

[51] A. Felipe, M. Ortuno, G. Righini, and G. Tirado, "A heuristic approach for the green vehicle routing problem with multiple technologies and partial recharges," *Transportation Research Part E: Logistics and Transportation Review*, vol. 71, pp. 111–128, 2014.

[52] P. Flathman and G. Lanza, "Phytoremediation: current views on an emerging green technology," *Journal of Soil Contamination*, vol. 7, pp. 415–432, 1998.

[53] C. Huang, M. Miao, B. Jiang, S. Cui, X. Jia, and T. Zhang, "Polysaccharides modification through green technology: role of ultrasonication towards improving physicochemical properties of (1-3) (1-6)-alpha-D-glucans," *Food Hydrocolloids*, vol. 50, pp. 166–173, 2015.

[54] V. Sharma, R. Zboril, and R. Varma, "Ferrates: greener oxidants with multimodal action in water treatment technologies," *Accounts of Chemical Research*, vol. 48, pp. 182–191, 2015.

[55] S. Novalin and T. Zweckmair, “Renewable resources - green biorefinery: separation of valuable substances from fluid-fractions by means of membrane technology,” *Biofuels Bioproducts&Biorefining-BIOFPR*, vol. 3, pp. 20–27, 2009.
[56] N. Baig, F. Alghunaimi, and T. Saleh, “Hydrophobic and oleophilic carbon nanofiber impregnated styrofoam for oil and water separation: a green technology,” *Chemical Engineering Journal*, vol. 360, pp. 1613–1622, 2019.
[57] B. Tiwari, “Ultrasound: a clean, green extraction technology,” *TRAC Trends in Analytical Chemistry*, vol. 71, pp. 100–109, 2015.
[58] S. Kumar, S. Prasad, R. Banerjee, D. Agarwal, K. Kulkarni, and K. Ramesh, “Green solvents and technologies for oil extraction from oilseeds,” *Chemistry Central Journal*, vol. 11, pp. 1–7, 2017.
[59] M. Bubalo, S. Vidovic, I. Redovnikovic, and S. Jokic, “Green solvents for green technologies,” *Journal of Chemical Technology and Biotechnology*, vol. 90, no. 9, pp. 1631–1639, 2015.
[60] G. Feder and G. Omara, “Farm size and the diffusion of green revolution technology,” *Economic Development and Cultural Change*, vol. 30, pp. 59–76, 1981.
[61] K. Munshi, “Social learning in a heterogeneous population: technology diffusion in the Indian Green Revolution,” *Journal of Development Economics*, vol. 73, pp. 185–213, 2004.
[62] K. Otsuka and Y. Kijima, “Technology policies for a green revolution and agricultural transformation in Africa,” *Journal of African Economies*, vol. 19, pp. 60–76, 2010.
[63] M. Degraft-Johnson, A. Suzuki, T. Sakurai, and K. Otsuka, “On the transferability of the Asian rice green revolution to rainfed areas in sub-Saharan Africa: an assessment of technology intervention in Northern Ghana,” *Agricultural Economics*, vol. 45, pp. 555–570, 2014.
[64] J. Ariga, E. Mabaya, M. Waithaka, and M. Wanzala-Mlobela, “Can improved agricultural technologies spur a green revolution in Africa? A multi-country analysis of seed and fertilizer delivery systems,” *Agricultural Economics*, vol. 50, pp. 63–74, 2019.
[65] W. Wang, S. Zhang, Y. Su, and X. Deng, “Key factors to green building technologies adoption in developing countries: the perspective of Chinese designers,” *Sustainability*, vol. 10, no. 11, pp. 1–22, 2018.
[66] A. Chan, A. Darko, E. Ameyaw, and D. Owusu-Manu, “Barriers affecting the adoption of green building technologies,” *Journal of Management in Engineering*, vol. 33, pp. 1–12, 2017.
[67] C. Frayne, “Green water technologies and resource management for water system heat-transfer applications int the built environment,” *Journal of Green Building*, vol. 5, no. 1, pp. 56–67, 2010.
[68] I. Ziogou, A. Michopoulos, V. Voulgari, and T. Zachariadis, “Implementation of green roof technology in residential buildings and neighborhoods of Cyprus,” *Sustainable Cities and Society*, vol. 40, pp. 233–243, 2018.
[69] F. Torpy, M. Zavattaro, and P. Irga, “Green wall technology for the phytoremediation of indoor air: a system for the reduction of high CO2 concentrations,” *Air Quality Atmosphere and Health*, vol. 10, pp. 575–585, 2017.
[70] P. Duxson, J. L. Provis, G. C. Lukey, and J. S. Van Deventer, “The role of inorganic polymer technology in the development of green concrete,” *Cement and Concrete Research*, vol. 37, pp. 1590–1597, 2007.
[71] M. poliakoff and P. license, “Sustainable technology -Green chemistry,” *Nature*, vol. 450, pp. 810–812, 2007.
[72] E. Salama, H. Roh, S. Dev et al., “Algae as a green technology for heavy metals removal from various wastewater,” *World Journal of Microbiology and Biotechnology*, vol. 35, p. 75, 2019.
[73] V. Sharma, L. Chen, B. Marsalek, R. Zboril, K. O’Shea, and D. Dionysiou, “Iron based sustainable greener technologies to treat cyanobacteria and microcystin-LR in water,” *Water Science and Technology: Water Supply*, vol. 17, pp. 107–114, 2017.
[74] Y. Najjar and D. Waite, “Energy conservation and waste utilization in the cement industry serve the green technology and environment,” *International Journal of Sustainable Engineering*, vol. 9, pp. 3–10, 2016.
[75] K. Zhong, Y. Wang, J. Pei, S. Tang, and Z. Han, “Super efficiency SBM-DEA and neural network for performance evaluation,” *Information Processing & Management*, vol. 58, no. 6, Article ID 102728, 2021.
[76] B. Mason, K. Price, J. Steinbacher, A. Bogdan, and D. McQuade, “Greener approaches to organic synthesis using microreactor technology,” *Chemical Reviews*, vol. 107, pp. 2300–2318, 2007.
[77] J. Ahmed and S. Varshney, “Polylactides-chemistry, properties and green packaging technology: a review,” *International Journal of Food Properties*, vol. 14, pp. 37–58, 2011.
[78] J. Tseng and C. Lin, “Green thermal analysis technology for evaluating the thermal hazard of Di-tert-butyl peroxide,” *Industrial & Engineering Chemistry Research*, vol. 50, pp. 9487–9494, 2011.
[79] J. Tseng, J. Lin, C. Lee, and C. Lin, “Prediction of TMCH thermal hazard with various calorimetric tests by green thermal analysis technology,” *AIChE Journal*, vol. 58, pp. 3792–3798, 2012.
[80] J. Desmet, C. Meunier, E. Danloy et al., “Green and sustainable production of high value compounds via a microalgae encapsulation technology that relies on CO2 as a principle reactant,” *Journal of Materials Chemistry*, vol. 2, pp. 20560–20569, 2014.
[81] M. Ashraf, S. Ullah, I. Ahmad, A. Qureshi, K. Balkhair, and M. Rehman, “Green biocides, a promising technology: current and future applications to industry and industrial processes,” *Journal of the Science of Food and Agriculture*, vol. 94, pp. 388–403, 2014.
[82] S. Das, V. Singh, A. Dwivedy et al., “Encapsulation in chitosan-based nanomatrix as an efficient green technology to boost the antimicrobial, antioxidant and in situ efficacy of Coriandrum sativum essential oil,” *International Journal of Biological Macromolecules*, vol. 133, pp. 294–305, 2019.
[83] H. Rajha, T. Mhanna, S. ElKantar, A. ElKhoury, N. Louka, and R. Maroun, “Innovative process of polyphenol recovery from pomegranate peels by combining green deep eutectic solvents and a new infrared technology,” *LWT-Food Science and Technology*, vol. 111, pp. 138–146, 2019.

Hindawi
Scientific Programming
Volume 2021, Article ID 4491382, 10 pages
https://doi.org/10.1155/2021/4491382

Research Article

Research on Outdoor Garden Scene Reconstruction Based on PMVS Algorithm

Wei He

School of Design and Art, Xijing University, Xi'an, Shaanxi 710123, China

Correspondence should be addressed to Wei He; 20070044@xijing.edu.cn

Received 29 September 2021; Revised 18 October 2021; Accepted 22 October 2021; Published 24 November 2021

Academic Editor: Le Sun

The three-dimensional reconstruction of outdoor landscape is of great significance for the construction of digital city. With the rapid development of big data and Internet of things technology, when using the traditional image-based 3D reconstruction method to restore the 3D information of objects in the image, there will be a large number of redundant points in the point cloud and the density of the point cloud is insufficient. Based on the analysis of the existing three-dimensional reconstruction technology, combined with the characteristics of outdoor garden scene, this paper gives the detection and extraction methods of relevant feature points and adopts feature matching and repairing the holes generated by point cloud meshing. By adopting the candidate strategy of feature points and adding the mesh subdivision processing method, an improved PMVS algorithm is proposed and the problem of sparse point cloud in 3D reconstruction is solved. Experimental results show that the proposed method not only effectively realizes the three-dimensional reconstruction of outdoor garden scene, but also improves the execution efficiency of the algorithm on the premise of ensuring the reconstruction effect.

1. Introduction

With the rapid development of big data and Internet of things technology, geographic information system and digital city have also developed rapidly [1, 2]. The application of 3D scene modeling technology in digital city construction engineering is becoming more and more important. 3D reconstruction has always been a research hotspot in computer vision and other related fields [3–5]. It is an important means to obtain object model and 3D scene. There are many ways for people to obtain the three-dimensional information of objects, such as the traditional geometric modeling technology, which requires a good professional level and a large workload. It can also be obtained by 3D laser scanning technology [6]. This method is greatly affected by the outdoor environment and can not obtain the target texture information. In contrast, the 3D reconstruction method based on image feature points does not have many limitations of the above modeling methods [7, 8]. It only needs to input the image, has low cost, and does not need other special prior information. Through excellent and advanced algorithms, the 3D information of objects and scenes in the image can be recovered. Not only is the required equipment simpler and has less restrictions on the scene, but also an accurate and realistic model can be obtained.

Obtaining the three-dimensional model of the target object from the two-dimensional image has always been a research hotspot in the field of computer vision. After years of efforts by scholars at home and abroad, remarkable results have been achieved. People summarized and proposed a relatively complete theoretical system of computer vision and began the research on multiview stereo matching [9]. Then many important research results emerged one after another. In 1992, the research team of Carnegie Mellon University proposed a reconstruction method based on optical flow method [10]. Debevec et al. of Berkeley University implemented the famous building reconstruction system Façade [11]. The system needs to obtain the approximate model of the camera and building object in advance, then reproject the model on the image to reduce the error, and finally reconstruct the three-dimensional model of the building within the specified error allowable range. Pollefeys et al. obtained sequence images by photographing the same scene from different perspectives and reconstructed the three-dimensional model of the object in the scene based on Structure from Motion, i.e., SFM [12]. Michael Goesele et al. proposed an adaptive MVS (Multiview Stereo) algorithm considering the influence of image light variation and noise [13]. Based on such algorithms, Furukawa et al. further proposed PMVS (Patch Multiview Stereo) based patch dense reconstruction method [14].

However, it is difficult to obtain 3D model and establish 3D scene. One of the traditional methods to obtain 3D models is through geometric modeling technology, such as solid modeling, implicit surface, etc. Nevertheless, not only does geometric modeling technology require a good technical level and a lot of work, but it is also very difficult for it to construct complex models and scenes [15, 16]. In addition, 3D laser scanning technology can efficiently obtain the point cloud of model and scene, and the accuracy is also relatively high. However, this method usually can not obtain the texture information of the target, and this method is greatly affected by the environment, especially in the outdoor open scene [17]. Compared with these methods, image-based 3D reconstruction technology needs simpler equipment and can obtain accurate and realistic models. At the same time, the development of image acquisition technology makes the data sources required for 3D reconstruction very rich, which further reduces the cost of reconstruction [18]. Therefore, in recent decades, image-based 3D reconstruction technology has been an important research topic in the field of computer vision. At the same time, with the development of virtual reality technology in recent years, this 3D reconstruction technology is becoming more and more important for the demand of large-scale scenes and models.

Although the image-based 3D reconstruction process has simple equipment and low cost, when recovering the 3D information about the object through the image, there will be a large number of redundant points in the point cloud, the density of the point cloud is not enough, the model fidelity is not high, and sometimes holes will even appear, resulting in a large difference between the final reconstruction result and the actual situation [19]. In addition, 3D reconstruction consumes a lot of time, cost, and efficiency in the process of image feature matching. In view of these shortcomings of the existing research, based on the traditional PMVS 3D reconstruction theory, this paper optimizes the image matching process, reduces the time cost of feature matching, improves the 3D reconstruction process, and solves the shortcomings of the existing methods. Finally, the optimized and improved 3D reconstruction process is integrated into the 3D reconstruction system of outdoor garden scene design.

2. Related Works

3D reconstruction is the process of capturing the shape and appearance of real objects and expressing the geometric information of 3D objects into a data model that can be stored and processed by computer, so as to carry out further research work. 3D reconstruction based on stereo vision is to recover the 3D information of the scene by processing the input image sequence and using the principle of stereo vision [20]. As shown in Figure 1, the reconstruction algorithm based on stereo vision generally obtains two images from different perspectives of the same spatial scene by the camera and processes the images.

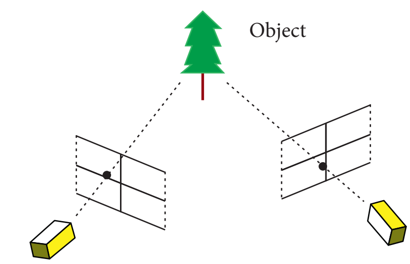

Figure 1: Schematic diagram of reconstruction method based on stereo vision.

Three-dimensional reconstruction is a difficult problem that scholars at home and abroad have been studying. In order to realize the three-dimensional reconstruction of an object, it is necessary to determine the three-dimensional contour of the reconstructed object and understand the spatial coordinates of the points on the contour, but the problem is how to obtain the missing depth information of the two-dimensional image. There are many implementation methods. According to the different methods of obtaining depth, it can be roughly divided into active mode and passive mode. The active method of a given depth map uses a rangefinder to mechanically or radioactively interfere with the reconstructed object in order to obtain a depth map, such as structured light method, moire fringe method, laser rangefinder, and other active sensing technologies [21]. However, these methods need professional instruments and are expensive, which can not be popularized among the general public. The passive method of 3D reconstruction does not have any contact with the reconstructed object and only needs to use relevant sensors to obtain its geometric information. Generally, a sensor refers to a light sensing sensor sensitive to visible light, and the input of the method is a set of digital images (one, two, or more) or video. In this case, we call it image-based reconstruction, and the output is a three-dimensional model. Compared with the active method, the passive method can be applied to a wider range of situations. In this paper, 3D reconstruction based on image sequence is studied.

3D reconstruction based on image sequence does not need a priori knowledge, but a series of images taken from different angles for the target scene or object, as well as computer vision related algorithms and mathematical calculation inference [22]. As shown in Figure 2, the process is divided into four parts: feature point extraction, sparse reconstruction, dense reconstruction, and surface reconstruction. This paper focuses on the first three parts.

Sparse reconstruction can be roughly divided into two types according to different image methods. The first is the incremental method, which first calculates the parameters of two or three images and then adds new images from the sequence for reconstruction [23]. The image initially selected by this method has a great impact on the later work, and the

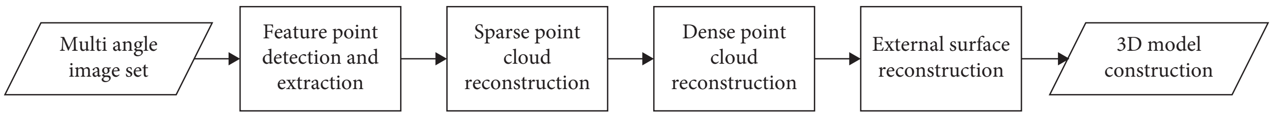

Figure 2: Construction process of 3D reconstruction model based on multiview images.

error transmission can not ensure the accuracy. The second is a nonincremental method, which uses the method of decomposing the measurement matrix [24]. All pictures are matched in pairs to obtain the relative position parameters to determine the global position. This method is more accurate and efficient than the previous method, so it is one of the most widely used methods at present, and it is also the method used in this experiment. Dense reconstruction is to match more point pairs and obtain as many and uniform point cloud data as possible. Point cloud data is like bricks for building models. The quality and quantity of bricks are directly related to the quality of the whole building. However, the current methods have their own advantages and disadvantages and can not meet all the needs. For example, the voxel based dense reconstruction algorithm generates point cloud rules, which is convenient for subsequent surface reconstruction, but it is difficult to be suitable for large-scale scene reconstruction. The point cloud generated by patch based dense reconstruction algorithm has high precision and uniform distribution and has been widely used for its good reconstruction effect. However, this method also has its disadvantages. The cost of high precision is that it takes a long time, and there are holes in weak texture areas. Therefore, the research on how to obtain high-quality and large number of dense point clouds is of great significance and practical value.

3. Method

3.1. Overview of PMVS Algorithm. The extraction and matching of feature points is to extract stable feature points in the image, match these feature points, connect the same feature points, track the feature points, and then calculate the position relationship between images by using the relevant theory of multiview geometry. Therefore, obtaining a large number of stable feature points is an essential and important step for subsequent 3D reconstruction. In order to obtain a large number of robust feature points, this paper first describes the SIFT algorithm with invariance of scale, rotation, and illumination. The algorithm is stable and is widely used in computer vision fields such as 3D reconstruction and target tracking, as shown in Figure 3.

SIFT algorithm is robust to scaling, rotation, and translation, but affine image extraction and matching is not accurate. ASIFT algorithm can match affine images well by simulating the rotation of the optical axis of the camera and can achieve complete affine invariance.

After extracting the feature points, the feature vector is obtained. Next, the features are matched to obtain the one-to-one correspondence between pixels in the images. Feature point matching usually includes violence matching algorithm, nearest neighbor matching algorithm, and so on.

Brute force matcher (BF) is the simplest feature matching method. The violent matching method is simple to operate, but the amount of calculation is huge. If there are many images or the image resolution is large, the time and cost of violent matching are also huge. And the distance threshold is not easy to determine; too large will produce a lot of false matches, and too small is easy to miss a lot of correct matches. Therefore, it is difficult to meet the practical application.

The nearest neighbor matching algorithm [25] in the matching algorithm is similar to the k-nearest neighbor algorithm in retrieval classification. The k-nearest neighbor algorithm needs to give a query point and a positive integer k and then find the k data closest to the query point from the data set. The nearest neighbor query is its special case; that is, the k value is 1.

The nearest neighbor (NN) algorithm in feature matching was proposed by Muja and Lowe [25], and its specific algorithm process is as follows:

(1) For the feature vector v in image 1, find the two vectors v_1 and v_2 closest to the feature vector in image 2, and $v_1 < v_2$ in the distance.

(2) If $\text{distance}(v, v_1)/\text{distance}(v, v_2) < m$, v_1 is the match of v; otherwise v does not match in image 2. The threshold value m is generally 0.6. The definition of distance is not unique. Euclidean distance or included angle distance can be used.

The definition of feature point matching refers to the process of establishing correlation between different image data sets. In the field of computer vision, this process is usually called stereo image pair problem. Image matching is the process of establishing the relationship between the feature points extracted from the original image and then estimating the three-dimensional position coordinates of the feature points through the projection model. In the image space, a depth map will be formed (assign a relative depth value to each image pixel). In the object space, the point cloud model of the object is usually formed. The matching in this paper is based on ASIFT features. Compared with the general SIFT features, it has better scene adaptability and richer extracted feature points, which can meet the needs of this paper.

In this paper, feature point matching is based on ASIFT feature, and the feature is represented by the descriptor vector of feature points. Generally, the spatial Euclidean distance is used to measure the distance between vectors, that is, the similarity. The similarity of descriptors can be expressed by the Euclidean distance between two feature vectors. However, the matching algorithm of this method will have some wrong matching. On the one hand, many of the feature points detected in the image can not find the

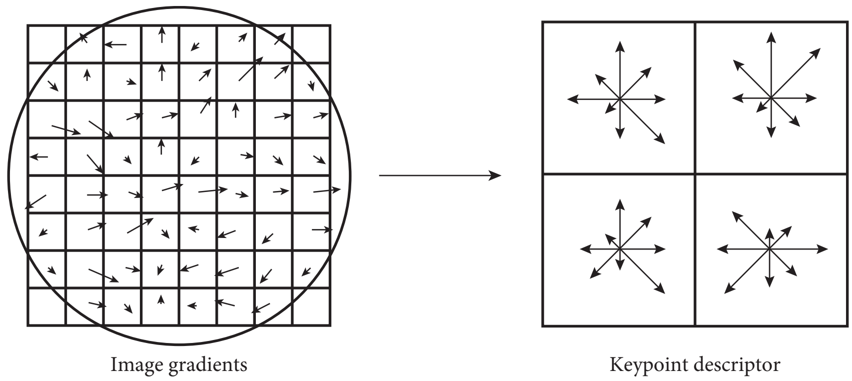

Figure 3: SIFT feature description.

correct matching points, because the feature points may be extracted from the background or from nontarget areas. On the other hand, due to the high-dimensional characteristics of the descriptor, the nearest point may not be the point close to the descriptor. Therefore, the effect of setting a threshold value of the global nearest matching point distance is not good, and there will be a lot of mismatches. An improved method is the way of setting a nearest neighbor and next nearest neighbor ratio as mentioned by Lowe in this paper.

Because it is easy to duplicate texture and color in the image, false matching often occurs in the process of feature matching. In the process of 3D reconstruction, stable and accurate feature points are needed. The occurrence of false matching will cause serious errors in the calculation results and have a serious impact on the reconstruction results. Therefore, removing mismatch is an important step in the process of feature matching.

Patch based multiview stereo vision (PMVS) is one of the most widely used algorithms with good reconstruction effect. The algorithm outputs dense rectangular blocks covering the visible surface in the input image. The algorithm does not need any initialization of visual shell, bounding box, and other information, and it will automatically detect obstacles and discard outliers. The key to its performance is to strictly abide by the local photometric consistency and global visibility constraints. Stereo vision is realized through a series of programs of matching, expansion, and filtering. Starting from a sparse set of matching key points, the seed patch is repeatedly extended to the nearby grid, and the visibility constraint is used to filter out the wrong matching.

PMVS algorithm shall ensure that there is at least one patch projection in each grid $c_i(x, y)$ of each picture. The implementation process of PMVS includes matching, expansion, and filtering. Starting from the sparse matching key point set, repeat the expansion, and then filter out the wrong matching through visibility constraints.

The flow of PMVS algorithm can be described according to its implementation steps. In the first step, sparse matching points are obtained after feature matching and wrong matching is eliminated. Then, the second and third steps need to be iterated n times (generally $n = 3$). The flow chart is shown in Figure 4 as follows.

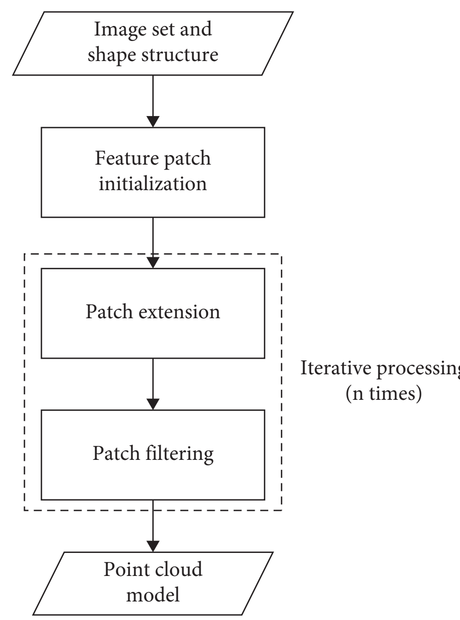

Figure 4: Schematic diagram of point cloud model reconstruction based on PMVS algorithm.

3.1.1. Initial Feature Matching. As the first step of the algorithm, Harris and Dog operators are used to detect the corner and speckle features in each image. In order to ensure the uniform coverage of patches, we divide the grid on each image. The cell size is $A * B$ Pixel^2 (note the difference from the previous one), and it is used as the distribution cell of corners and spots. There should be at least N local maximum points in each grid. Usually, we make $B = 32$ pixels, $N = 4$ in the experiment. After extracting these features from each image, multiview matching is performed to generate a sparse set of patches, which are then stored in the grid covering each image cell $d(i, j)$. Each image in the sequence picture is used as the reference image $E(p)$ in turn. In the remaining pictures, the pictures with an angle between the main optical axis and $E(p)$ of less than 60 degrees form the image set $H(p)$. Then match the photos in $E(p)$ and $H(p)$.

3.1.2. Patch Extension. Since the initial matching has only a sparse set of patches, expansion is very important to generate sufficiently dense patches. In this step, the sparse patches generated in the previous step are iteratively diffused to their fields as seed patches until they can cover the visible surface in the scene. For a given patch p, the neighborhood grid set of the image block satisfying the expansion condition is recorded as $d(p)$:

$$d(p) = \left\{d_i(x', y') | p \in Q_i(x, y), \left|x - x'\right| + \left|y - y'\right| = 1\right\}. \tag{1}$$

When two patches p and p' are stored in adjacent grid cells $d_i(x, y)$ and $d_i(x', y')$ of the same image H in $S(p)$, their tangent planes are very close:

$$\left|(d(p) - d(p')) \cdot n(p)\right| + \left|(d(p) - d(p')) \cdot n(p')\right| < 2\rho_2. \tag{2}$$

That is, when p and p' meet the above conditions, they can be considered adjacent, similar to p_1, where the value of p_2 is determined by the depth of $d(p)$ and $d(p')$.

3.1.3. Patch Filtering. Filtering is to remove some wrong patches generated in patch expansion as much as possible, so as to further enhance visibility consistency and eliminate wrong matching, so as to improve the accuracy of reconstruction. Most of the filters removed by patch filtering follow the principle of visual consistency.

The first thing to filter is the patches outside the reconstruction target, such as obstacles. Suppose that patch p_0 is an external patch, and $V(p)$ is a set of patches obscured by p_0, which can also be said to be a discontinuous set of patches (discontinuity is that p and p' are not adjacent). When p_0 satisfies the following relationship, it is removed as an outlier:

$$\left|N(p_0)\right|\overline{M}(p_0) < \sum_{p_j \in U} \overline{M}(p_j). \tag{3}$$

As can be seen from the above formula, when p_0 is an abnormal value, the values of $M(p_0)$ and $|N(p_0)|$ will be very small, so generally p_0 will be filtered out.

3.2. Improvement of PMVS Algorithm. Although the reconstruction effect of PMVS algorithm is good, the spatial complexity and time complexity of PMVs algorithm are also very large with the increase of the number of pictures and the improvement of image resolution, especially in the steps of feature point matching and patch diffusion. Considering the complexity of outdoor garden scene, in order to better meet the application environment of dense point cloud, this paper improves the PMVS method.

First, we need to improve the candidate selection strategy. In the original PMVS algorithm, the feature points of initial feature matching are extracted by Harris operator and Dog operator. However, the feature points extracted in this way are not comprehensive in the sparse texture region. The PMVS method proposed by Furukawa and Ponce has been proved by experiments on various data sets; the experimental objects include objects with fine surface details, outdoor scenes, and scenes with moving obstacles in different positions in multiple static images [14]. However, when the surface of the reconstructed target object is uneven, rough, and unsmooth or the photo is deformed due to elevation, PMVS algorithm may have wrong matching when selecting seed candidate points, resulting in wrong details. In the initial feature matching, each feature point on the reference image looks for candidate matching points on other images, and each pair of candidate matching points intersect to obtain model points. So far, we can see that the original method will cause feature point matching error, increase matching time, and affect the final reconstruction effect. Therefore, this paper proposes to change the projection distance to linear distance when selecting matching candidate points, which can take into account a variety of situations, the selected candidate points will be more reliable, and the reconstruction effect is better than the original in theory.

Some improvements are also needed in patch expansion. When optimizing its center and normal vector, we use the $E(p)$ and $N(p)$ information of patch p. However, when the referenced photos are distorted, the patch can not be well adapted to the actual reconstruction of the object surface due to the deviation of the normal direction. To solve this problem, this paper proposes a method to optimize and correct the normal direction of the patch by using the geometric information of the local patch, so that the patch can better reconstruct the object surface and improve the accuracy. The improved method adds a patch normal vector correction process to the traditional PMVS reconstruction method. The basic steps and algorithm flow chart of the improved algorithm are given below, as shown in Figure 5.

The improved method uses as much local geometric information as possible to optimize and correct the normal vector of the new patch. It is only for this region and will not affect other regions. In this way, the patches in the neighborhood affect and interact with each other, and the position is more accurate, which makes the reconstructed surface more smooth and is conducive to reducing the transmission of error information, so as to reconstruct more and better patches.

It can be seen from the improvement that the improved algorithm is more suitable for the application scenario of this paper and improves the execution efficiency of the algorithm. Compared with the original algorithm based on patch reconstruction, the improved algorithm uses feature extraction and matching to obtain richer matching information and eliminates the wrong matching points and points with large reprojection errors, which ensures the accuracy of the initial patch set and improves the accuracy of the reconstruction model to a great extent. Moreover, due to the elimination of the wrong matching points, the efficiency of search in the diffusion process is improved and the amount of calculation in the diffusion process is reduced.

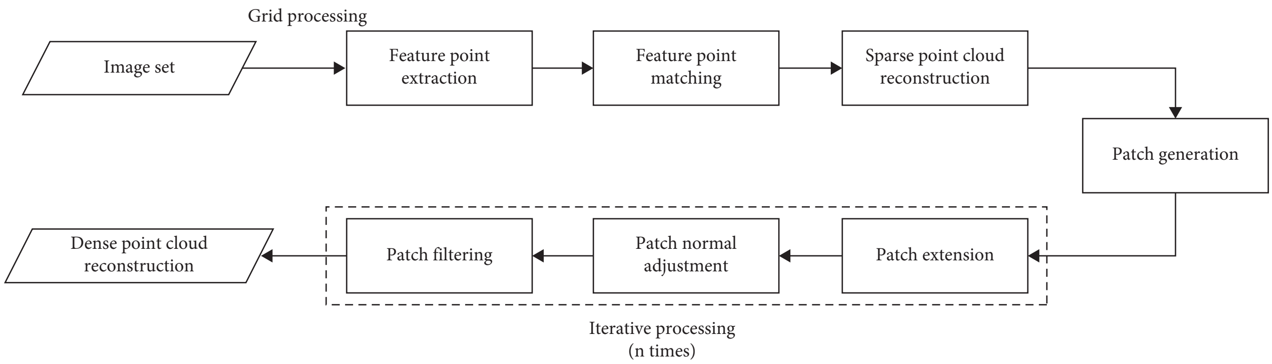

Figure 5: Schematic diagram of point cloud model reconstruction based on improved PMVS algorithm.

4. Experiment and Analysis

Due to the complexity of 3D reconstruction process, the intermediate stage not only needs the results of the previous stage as input, but also provides input for the next stage. Often, a whole set of process is difficult to complete in one framework. If you use multiple platforms, you not only need to be familiar with the new platform, but also need to coordinate the input and output formats between various platforms. The system implemented in this paper is developed based on Visual Studio 2015. The class libraries needed are concentrated in the open source OpenMVS framework, including OpenCV, Ceres, GLOG, Eigen, OpenMVS, and other class libraries. The program implemented by the system provides some methods in the class library of the collection, some can be directly applied, and some need to be modified accordingly. The SIFT algorithm process is modified. Before threshold screening, bilinear pixel interpolation is added, and then the modified method is used to extract feature points. The dense reconstruction algorithm implemented in OpenMVS should also be appropriately modified according to the principles described above. In the whole process, a series of files will be generated, including feature point files, camera parameters, matching results, sparse point clouds, and dense point clouds.

Firstly, the function of the system is defined: recover and reconstruct its three-dimensional dense point cloud model from a series of images taken from different perspectives of the same object. Design function modules: data input and output, feature point extraction, camera calibration, feature point matching, sparse reconstruction, dense reconstruction, etc. The work flow chart of the system is shown in Figure 6.

To evaluate the proposed method, we used a data set downloaded from the latest technology (called TB-Roses [26]). TB-Roses dataset is composed of 400 images of rose bushes recorded in a real garden with a resolution of $640 * 480$ pixels[2]. It is designed to test the segmentation and rendering algorithm of rose branches in horticultural robot applications. The image is provided with the ground truth value to mark the branch of segmentation. As shown in Table 1, the characteristic information of the data set used is displayed, including type, number of samples, resolution, brightness, and type of ground truth contained. The maximum and minimum average image brightness values for the dataset are also included in the table (in the range [0, 255]). The relevant eigenvalues better reflect how the outdoor dataset has more variable lighting.

Therefore, we can evaluate the method in this paper through this data set. Firstly, taking TB-Roses as the experimental object, four common segmentation methods such as DeepLabv3 [27], U-Net [28], FCSN [29], and SegNet [30] are evaluated, and their different superparameters are analyzed. Secondly, the postprocessing effect of parallax calculation and combination of segmented image and parallax image is evaluated. Next, different skeletonization methods for detecting branches are compared. Finally, the accuracy of 3D reconstruction is evaluated.

Three evaluation indexes commonly used for such tasks are selected to evaluate the performance of the proposed method, which are Precision, Recall, and Recall, respectively, defined as follows:

$$\begin{aligned}\text{Precision} &= \frac{T_1}{T_1 + T_2},\\ \text{Recall} &= \frac{T_1}{T_1 + T_3},\\ F_1 &= \frac{2T_1}{2T_1 + T_2 + T_3},\end{aligned} \tag{4}$$

where T_1 (True Positives) indicates the number of branch pixels correctly segmented, T_2 (False Positives) denotes the number of background pixels which are incorrectly specified as branch pixels, and T_3 (False Negatives) denotes the number of nonsegmented branch pixels.

The IoU parameter is used to verify whether the algorithm can effectively detect all branches, as well as their size and location. Therefore, this paper calculates this parameter according to equation (5) and maps each branch of the ground truth value (g) to the segmentation suggestion (b) with maximum IoU overlap.

$$\text{IoU} = \frac{s\left(G_b \cap G_g\right)}{s\left(G_b \cup G_g\right)}, \tag{5}$$

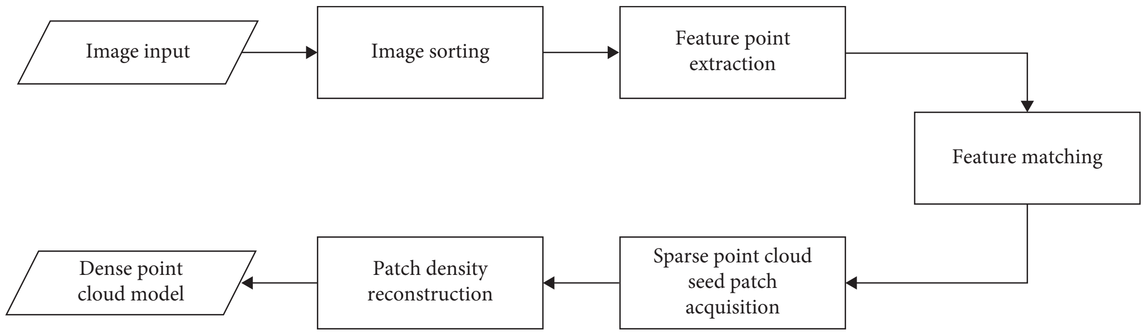

Figure 6: Flow chart dense point cloud model construction.

Table 1: Characteristics of the datasets evaluated.

Processing object	Number of images	Pixel	Brightness (min/max)	Type
TB-Roses	400	640 ∗ 480	80/140	Real

Table 2: Results obtained by the different algorithms evaluated for the processing object.

Method	Precision	Recall	F_1	IoU
DeepLabv3	45.42 ± 0.7	56.42 ± 0.8	54.84 ± 0.7	78.95 ± 5.6
U-net	63.63 ± 3.4	72.82 ± 2.5	67.74 ± 3.8	76.43 ± 5.8
FCSN	76.24 ± 0.5	81.48 ± 1.6	78.83 ± 2.1	85.26 ± 6.3
SegNet	68.37 ± 0.8	78.35 ± 3.5	75.39 ± 0.8	83.18 ± 8.2

where $s(G_b \cap G_g)$ represents the intersection between branch recommendations and basic facts, whereas $s(G_b \cup G_g)$ depicts its union.

As shown in Table 2, the comparison results of relevant indicators are obtained by different methods. It can be seen that the FCSN method obtains better results than other methods. In addition, by analyzing the Recall parameters at the pixel level, it is found that FCSN has the best overall segmentation performance. Thus, from the branch level measurement Recall, FCSN can effectively recover more branches.

In order to strictly analyze the results obtained, we compared the statistical significance by considering the nonparametric Wilcoxon signed rank test of paired samples [2]. The purpose is to evaluate whether the segmentation performance has been improved. Compared with other methods, the segmentation results obtained by FCSN are statistically significant. For this purpose, each data set and the folded results are compared in pairs. From the comparison results, if compared with SegNet, the p value obtained by this method is 0.005, while compared with U-Net and DeepLabv3 methods, the p value obtained is 0.002. Therefore, the test shows that this method is obviously better than the results obtained by other methods (considering the statistical significance threshold $p < 0.01$, the most restrictive threshold is usually used).

The segmentation results obtained by different methods on the sample image of the data set are shown in Figure 7. In order to make the graph more informative, we selected samples with obvious errors in all methods. Each column corresponds to the results obtained by each method, in which the black and white areas represent the correct detection of branches and background, respectively, and the red and blue pixels represent the T_1 and T_2 of branches, respectively. These numbers can not only find the location of the error, but also know the accuracy of the visualization method. It is learned that due to the influence of non-branching elements (general background, leaves, etc.), using U-Net and SegNet methods will produce more noise, and using DeepLabv3 method is conducive to the segmentation of thicker objects. Although FCSN method can also make mistakes, these errors mainly occur in the contour of branches.

The postprocessing problem for combining segmented images and parallax images is evaluated below. Several depth measures in previous work were used to evaluate differential results [31], which are

$$\mathrm{Rmse} = \sqrt{\frac{1}{T}\sum_{i}^{T}\left\|d_i - d_i^g\right\|^2},$$
$$\mathrm{Sq-Rel} = \frac{1}{T}\sum_{i}^{T}\frac{\left\|d_i - d_i^g\right\|^2}{d_i^g}, \tag{6}$$

where T is the total pixels in the image, d_i is the estimated depth for the pixel i, and d_i^g is the ground truth depth.

The results of the experiment are shown in Table 3. The first four columns are the parallax evaluation results, and the last three columns are the segmentation results. The first two columns indicate the parallax of the complete image, while

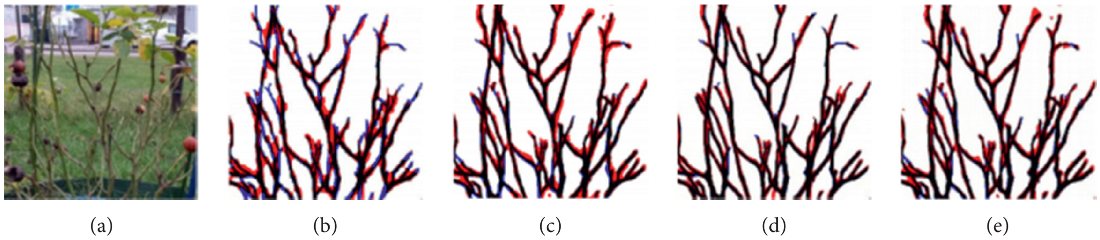

Figure 7: Examples of results obtained by segmentation of sample images using different methods. (a) Object. (b) DeepLabv3. (c) U-net. (d) FCSN. (e) SegNet.

Table 3: The calculation results of image, branch, and slice related indexes obtained before and after the application of the algorithm.

Algorithm	Image		Branch		Slice		
	Rmse	Sq-rel	Rmse	Sq-rel	Precision	Recall	F_1
PMVS	0.5793 ± 0.4	0.0846 ± 0.3	0.2731 ± 0.4	0.0289 ± 0.2	89.72 ± 3.9	92.89 ± 2.7	90.37 ± 2.7
Improved PMVS	0.5016 ± 0.1	0.0549 ± 0.1	0.1064 ± 0.3	0.0079 ± 0.1	93.15 ± 3.6	92.16 ± 2.4	93.27 ± 2.4

Table 4: The average distance between 3D reconstruction and ground real point cloud.

Distance	Mean (m)	Std (m)
x	0.00248	0.00385
y	0.00373	0.00379
z	0.00539	0.00748

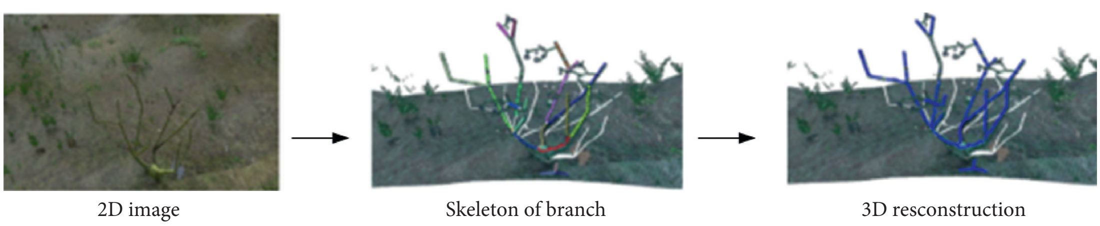

Figure 8: 3D reconstruction results obtained using improved PMVS.

the third and fourth columns represent that the branch only considers the pixels within the ground real value. From the results of branch level in this experiment, we know that the difference improvement process only affects branches, and the rest of the process only uses these depth values. As shown in the figure, these processes help to improve the original results of segmentation and parallax. The difference improved most significantly, and the branch level Rmse decreased from 0.2731 to 0.1064.

In order to evaluate the performance of 3D reconstruction, it is compared with the 3D skeleton ground authenticity of synthetic image. This ground truth has 3520 point clouds, and each point cloud contains a 3D skeleton of synthetic roses. During the evaluation, it is necessary to obtain the average value of the minimum distance between each point of the ground truth value and the reconstructed skeleton. This parameter can measure the average distance of the reconstructed skeleton relative to the ground truth value. For objective evaluation, the depth of the reconstruction point is normalized by the farthest point in the ground truth of each plant.

The evaluation results are shown in Table 4, which lists the distances on each axis x, y, and z, where z represents the depth and y represents the axis pointing to the ground. It can be seen that the average distance is less than 1 cm, and the error on the x-y plane is less than the error on the z axis (calculated according to the depth). However, this error is still less than 1 cm. Because the opening size of the end effector is 1.5 cm and is curved at the tool tip, this accuracy indicates that the trimming process has met the requirements. An example of three-dimensional reconstruction obtained using different input images is shown in Figure 8, which can intuitively see that the results obtained by this method are basically consistent with the facts.

Figure 8 reflects the comparison between real photos and artificial reconstruction results rendered from equivalent positions. Due to the vertex attribute transfer, the color gradient in the ground texture remains unchanged in 3D reconstruction. The experimental results show that the image data is structurally processed, and then the conversion from two-dimensional image to three-dimensional scene can be better realized by using this algorithm.

5. Conclusion

According to the requirements of 3D reconstruction of outdoor garden scene, the feature point extraction algorithm is studied, and the implementation principle and characteristics of the extraction operator are described. A method that can add stable feature points in weak texture region is proposed, which is based on the principle of SIFT algorithm. This method can effectively increase the number of feature points in the sparse texture region and provide more information for later processing. This paper focuses on the learning and research of PMVS dense reconstruction algorithm. Aiming at the problem of false matching in the feature point matching stage, a matching candidate point selection strategy is proposed. This method sorts the candidate points in descending order based on the linear distance in three-dimensional space. Experiments show that this method can effectively reduce false matching and improve the reconstruction accuracy. Although the method in this paper restores the complete structure of the scene to a great extent, there will still be holes in the reconstruction model in the case of large illumination differences. Therefore, the algorithm still has some problems to be improved and optimized. How to obtain the seamless texture of the scene in the environment of inconsistent illumination is a problem that needs to be solved in the future [32–35].

Data Availability

The labeled dataset used to support the findings of this study is available from the corresponding author upon request.

Conflicts of Interest

The author declares no competing interests.

Acknowledgments

This study was supported by the scientific research project of Xijing University "Research on the application of Chinese traditional decorative elements in modern interior design" with Grant no. xj160110.

References

[1] M. Wang, D. Xiao, and Y. Xiang, "Low-cost and confidentiality-preserving multi-image compressed acquisition and separate reconstruction for internet of multimedia things," *IEEE Internet of Things Journal*, vol. 8, no. 3, pp. 1662–1673, 2021.

[2] J. Demsar, "Statistical comparisons of classifiers over multiple data sets," *Journal of Machine Learning Research*, vol. 7, pp. 1–30, 2006.

[3] A. Lenjani, C. M. Yeum, S. Dyke, and I. Bilionis, "Automated building image extraction from 360° panoramas for post-disaster evaluation," *Computer-Aided Civil and Infrastructure Engineering*, vol. 35, no. 3, pp. 241–257, 2020.

[4] Y. F. Liu, X. Nie, J. S. Fan, and X. G. Liu, "Image-based crack assessment of bridge piers using unmanned aerial vehicles and three-dimensional scene reconstruction," *Computer-Aided Civil and Infrastructure Engineering*, vol. 35, no. 5, pp. 511–529, 2020.

[5] A. Murtiyoso and P. Grussenmeyer, "Documentation of heritage buildings using close-range uav images: dense matching issues, comparison and case studies," *Photogrammetric Record*, vol. 32, no. 159, pp. 206–229, 2017.

[6] C. A. Perez-Ramirez, J. P. Amezquita-Sanchez, M. Valtierra-Rodriguez, H. Adeli, A. Dominguez-Gonzalez, and R. J. Romero-Troncoso, "Recurrent neural network model with Bayesian training and mutual information for response prediction of large buildings," *Engineering Structures*, vol. 178, pp. 603–615, 2019.

[7] B. Xu and C. Liu, "A 3D reconstruction method for buildings based on monocular vision," *Computer Aided Civil Information*, pp. 1–16, 2021.

[8] P. Tsarouchi, G. Michalos, S. Makris, and G. Chryssolouris, "Vision system for robotic handling of randomly placed objects," *Procedia CIRP*, vol. 9, pp. 61–66, 2013.

[9] N. Brodu and D. Lague, "3D terrestrial lidar data classification of complex natural scenes using a multi-scale dimensionality criterion: applications in geomorphology," *ISPRS Journal of Photogrammetry and Remote Sensing*, vol. 68, pp. 121–134, 2012.

[10] C. Tomasi and T. Kanade, "Shape and motion from image streams under orthography: a factorization method," *International Journal of Computer Vision*, vol. 9, no. 2, pp. 137–154, 1992.

[11] P. Debevec, J. Malik and C. Taylor, Modeling and rendering architecture from photographs," *Acm Siggraph*, vol. 5, no. 2, pp. 11–20, 1999.

[12] M. Pollefeys, R. Koch, M. Vergauwen, and L. V. Gool, "Automated reconstruction of 3D scenes from sequences of images," *Isprs Journal of Photogrammery & Remote Sensing*, vol. 55, no. 4, pp. 251–267, 2001.

[13] M. Goesele, B. Curless, and S. M. Seitz, "Multi-view stereo revisited," in *Proceedings of the 2006 IEEE Computer Society Conference on Computer Vision and Pattern Recognition (CVPR'06)*, pp. 2402–2409, New York, NY, USA, June 2006.

[14] Y. Furukawa and J. Ponce, "Accurate, dense, and robust multiview stereopsis," *IEEE Transactions on Pattern Analysis and Machine Intelligence*, vol. 32, no. 8, pp. 1362–1376, 2010.

[15] J. Hackenberg, M. Wassenberg, H. Spiecker, and D. Sun, "Non destructive method for biomass prediction combining tls derived tree volume and wood density," *Forests*, vol. 6, no. 4, pp. 1274–1300, 2015.

[16] F. Liu, Q. Zhao, X. Liu, and D. Zeng, "Joint face alignment and 3D face reconstruction with application to face recognition," *IEEE Transactions on Pattern Analysis and Machine Intelligence*, vol. 42, no. 3, pp. 664–678, 2020.

[17] S. Paulus, H. Schumann, H. Kuhlmann, and J. Léon, "High-precision laser scanning system for capturing 3D plant architecture and analysing growth of cereal plants," *Biosystems Engineering*, vol. 121, pp. 1–11, 2014.

[18] M. Moeller, M. Benning, C. Schonlieb, and D. Cremers, "Variational depth from focus reconstruction," *IEEE*

Transactions on Image Processing, vol. 24, no. 12, pp. 5369–5378, 2015.

[19] K. Atsushi, H. Sueyasu, Y. Funayama, and T. Maekawa, “System for reconstruction of three-dimensional micro objects from multiple photographic images,” *Computer-Aided Design*, vol. 43, no. 8, pp. 1045–1055, 2011.

[20] N. Snavely, S. M. Seitz, and R. Szeliski, “Photo tourism,” *ACM Transactions on Graphics*, vol. 25, no. 3, pp. 835–846, 2006.

[21] S. Pertuz, D. Puig, and M. A. Garcia, “Analysis of focus measure operators for shape-from-focus,” *Pattern Recognition*, vol. 46, no. 5, pp. 1415–1432, 2013.

[22] R. Florian, H. Martin, and D. G. Giovanni, “Some radar imagery results using super resolution techniques,” *IEEE Transactions on Antennas and Propagation*, vol. 62, no. 10, pp. 2611–2625, 2014.

[23] K. Suwa, T. Wakayama, and M. Iwamoto, “Three-dimensional target geometry and target motion estimation method using multistatic ISAR movies and its performance,” *IEEE Transactions on Geoscience and Remote Sensing*, vol. 49, no. 6, pp. 2361–2373, 2011.

[24] M. A. Stuff, P. Sanchez, and M. Biancalana, “Extraction of three-dimensional motion and geometric invariants from range dependent signals,” *Radar Signal Processing and Its Applications*, vol. 14, no. 1, pp. 161–181, 2003.

[25] M. Muja and D. G. Lowe, “Fast approximate nearest neighbors with automatic algorithm configuration,” in *Proceedings of the International Conference on Computer Vision Theory and Application(VISSAPP)*, pp. 331–340, Lisboa, Portugal, February 2009.

[26] N. Strisciuglio, G. Azzopardi, and N. Petkov, “Brain-inspired robust delineation operator,” in *Proceedings of the Computer Vision-ECCV 2018 Workshops*, L. Leal-Taixé and S. Roth, Eds., pp. 555–565pp. 555–, Munich, Germany, September 2018.

[27] L.-C. Chen, G. Papandreou, F. Schroff, and H. Adam, *Rethinking Atrous Convolution for Semantic Image Segmentation*, CoRR, Berlin, Germany, 2017.

[28] O. Ronneberger, P. Fischer, and T. Brox, “U-net: convolutional networks for biomedical image segmentation,” in *Proceedings of the Medical Image Computing and Computer-Assisted Intervention (MICCAI)*, Munich, Germany, October 2015.

[29] H. Cuevas-Velasquez, A.-J. Gallego, and R. B. Fisher, “Segmentation and 3D reconstruction of rose plants from stereoscopic images,” *Computers and Electronics in Agriculture*, vol. 171, Article ID 105296, 2020.

[30] V. Badrinarayanan, A. Kendall, and R. Cipolla, “Segnet: a deep convolutional encoder-decoder architecture for image segmentation,” *IEEE Transactions on Pattern Analysis and Machine Intelligence*, vol. 39, no. 12, pp. 2481–2495, 2017.

[31] D. Eigen, C. Puhrsch, and R. Fergus, “Depth map prediction from a single image using a multi-scale deep network,” in *Proceedings of the 27th International Conference on Neural Information Processing Systems-Volume 2 NIPS’14*, pp. 2366–2374, MIT Press, Cambridge, MA, USA, December 2014.

[32] L. B. Michael, “Two-dimensional ESPRIT with tracking for radar imaging and feature extraction,” *IEEE Transactions on Antennas and Propagation*, vol. 52, no. 2, pp. 524–532, 2004.

[33] P. Dias, M. Matos, and V. Santos, “3D reconstruction of real world scenes using a low-cost 3D range scanner,” *Computer-Aided Civil and Infrastructure Engineering*, vol. 21, no. 7, pp. 486–497, 2006.

[34] P. Koppen, Z.-H. Feng, J. Kittler et al., “Gaussian mixture 3D morphable face model,” *Pattern Recognition*, vol. 74, pp. 617–628, 2018.

[35] K. T. Vierling, L. A. Vierling, W. A. Gould, S. Martinuzzi, and R. M. Clawges, “Lidar: shedding new light on habitat characterization and modeling,” *Frontiers in Ecology and the Environment*, vol. 6, no. 2, pp. 90–98, 2008.

Hindawi
Scientific Programming
Volume 2021, Article ID 7203873, 11 pages
https://doi.org/10.1155/2021/7203873

Research Article

IoT-Assisted Hybrid Intelligent Learning Architecture Based on Digital Education in a Diverse Society

Zongpei Ma

Zhengzhou Normal University, Zhengzhou 450044, China

Correspondence should be addressed to Zongpei Ma; mazongpei@zznu.edu.cn

Received 26 September 2021; Revised 23 October 2021; Accepted 30 October 2021; Published 24 November 2021

Academic Editor: Hai Dong

The existing research paradigm has caused the research of educational theory to be criticized for lack of logic and scientificity. With the gradual deepening and refinement of the development of smart education platforms, the educational process can be quantified, and the research paradigm of educational science has moved from a sampling model to a full-sample model, and it has become a real empirical science. This paper combines the Internet of Things technology to construct a hybrid intelligent learning system and applies it to digital education in a diverse society to construct a functional structure of the extraction system. Moreover, starting from the actual situation of intelligent education, this paper combines a simulation system to implement an IoT-assisted hybrid intelligent learning architecture and evaluates the teaching effect of the system. Through experimental research, it can be known that the IoT-assisted hybrid intelligent learning framework based on social diversified digital education has certain effects and has a certain reference effect for the development of subsequent intelligent education.

1. Introduction

The Internet of Things is the third wave in the development of the world's information industry. The Internet of Things, in layman's terms, is a network that connects objects to objects based on the Internet. It uses sensors, positioning systems, and other information equipment to connect any object to the Internet according to a certain protocol and can realize various information exchange and communication between interconnected objects and finally realize the intelligent management of objects [1]. The realization of the overall concept of the Internet of Things relies on a number of technological inventions, and its key technologies cover the entire information processing process from acquisition, transmission, processing, and storage to application. For objects connected to the network, the Internet of Things has a perception function. By reading the electronic tag of the object, various information can be collected in real time, and after a series of processing, the data information is transmitted to the Internet according to the communication protocol [2]. Finally, it uses intelligent computing technology to process the collected data and information and finally realizes the intelligent control of networked objects. Generally speaking, the network architecture of the Internet of Things is a three-layer structure, namely, the perception layer, the network layer, and the application layer. The perception layer is the source of the Internet of Things information and the bottom layer of the Internet of Things architecture. At this layer, it is mainly responsible for collecting and perceiving various raw data information. The network layer is responsible for connecting various data and information collection and perception networks to the Internet, so as to realize the storage, integration, and long-distance transmission of information. The application layer is responsible for data mining, that is, the discovery and presentation of various services, and decision-making on applications. The following will introduce the core technology of the Internet of Things system RFID radio frequency identification technology and WSN wireless sensor network and Internet of Things grid technology [3].

The smart education platform gathers countless data that was previously unseen, uncollected, and ignored. Whether it is the reform of the macro system and system, or the reform of the micro teaching methods and management methods, it can be through the in-depth mining of the smart education platform and the association with big data in other fields (such as public security, transportation, social security, and medical care). Analyze and find the crux of the problem, identify the unique laws of educational development in different regions, and then prescribe the right medicine to implement reforms. Therefore, educational decision-making will no longer rely excessively on experience, brainstorming, and simple statistical results but will turn to scientific decision-making based on data. In the learning environment of the smart education platform, techniques and methods of mathematical statistics, machine learning, and data mining can be used to process and analyze data, discover the mechanism of student learning, and use it to optimize learning and develop adaptive learning, self-directed learning; it can also analyze the teacher's course teaching in depth, so that teachers can provide students with more targeted teaching interventions based on data analysis; it can also evaluate the management effectiveness of managers in order to improve the existing assessment methods and management methods. The smart education platform can continuously collect learners' learning behavior data and perform intelligent analysis, such as pushing appropriate learning resources based on learner models, conducting personalized learning evaluations, providing accurate diagnosis results, and providing them with truly personalized learning resources, learning activities, learning paths, learning tools and services, etc. In the smart education platform environment, various data collection technologies can be used to collect information on school profiles, faculty, school funding, books and materials, equipment, majors and courses, teaching management, teaching process, teaching results, basic student conditions, etc. In order to achieve the purpose of comprehensive monitoring of education quality, a comprehensive and dynamic teaching quality monitoring system is formed.

This article combines the Internet of Things technology to construct a hybrid intelligent learning system, applies it to digital education in a diverse society, and verifies the system to provide a theoretical reference for subsequent intelligent education.

2. Related Work

The Internet of Things, literally understood, is the Internet between things and things [4]. The concept of the Internet of Things was first proposed in 1999 by Professor Kevin Ashton of the Massachusetts Institute of Technology in the United States. It is based on Internet technology to use radio frequency identification, wireless data communication, and other technologies to construct a network covering everything in the world, so as to realize the automatic identification of items and the interconnection and sharing of information [5]. The US "Technology Review" believes that the sensor network technology in the Internet of Things technology will become one of the top ten technologies that will change the world in the future.

After the construction plan of the smart education platform was proposed, many experts and scholars, government education departments, and enterprises have begun to conduct various researches, analyses, and constructions on the theoretical basis, development plan, framework scheme, and design ideas of the smart education platform. In terms of the theoretical construction of the smart education platform, many experts and scholars start with the concept of smart education as the core and start with the current education status and educational needs to study the theoretical design and development of the smart education platform [6]. Literature [7] proposed the following ideas for the construction of a comprehensive service platform for regional smart education. The overall plan of the platform is coordinated and implemented step by step and then driven by user needs to integrate various technologies for innovation. After that, the platform is gradually upgraded and gradually improved, and then it is interconnected with the national education resources and education management platform to open up and expand. Literature [8] proposed that the construction of a smart education platform must be innovative in three aspects: technological innovation (intelligence of terminals, systems and platforms), model innovation (mixed education becomes the mainstream of platform teaching), and evaluation innovation (reform traditional "input" education). Literature [9] proposed that the design of smart education platform should follow six principles: advanced and scientific principles, comprehensive and integrated principles, ease of operation, scalability, and security. Literature [10] proposes to build a regional smart education platform to achieve the use of cloud computing concepts, the integration of educational information hubs, and the sharing of educational information resources. Literature [11] proposed that the smart education cloud computing platform must have five basic characteristics, namely, on-demand self-service, ubiquitous network access, division of independent resource pools, rapid flexibility, and measurable services. The key technologies of the smart education cloud platform need to include five aspects: service scenario recognition, smart information extraction, smart information processing, smart information retrieval, and smart information push. In terms of the construction and development of smart education platforms, major IT companies and enterprises around the world rely on their own strong economic and technical strength to continue to cooperate with governments and colleges and universities around the world to develop smart education platforms. Taking IBM as an example, in terms of smart education, IBM theoretically put forward five major strategies for learning with any device, shifting to a learner-centered, building a learning community, professional learning services, and systematic education [12]. At the same time, IBM relied on its strong economic and technical strength to cooperate with many top universities at home and abroad to create a "smart campus" and summed up many effective practical experience, such as integrating campus information platform, helping campus transformation, modular, high-performance computing resource services [13].

3. Internet of Things Learning Method

Internet of Things clustering is an unsupervised classification process. It does not need to provide prior knowledge about sample category labels. It can only give a reasonable division of things based on the similarity between samples, which is different from the classification in data mining. Clustering pays more attention to finding the potential structure of the sample set and divides the set into several subsets with a smaller degree of relevance. From the point of view of the classification of sample points, clustering methods are mainly divided into two categories: the first category is hard partitioning, which stipulates that each sample belongs to only a certain category, and the boundary between the categories is clear: the second category is a softening score, that is, fuzzy clustering. It no longer requires that each sample point belong to only one class but uses the degree of membership to express the probability that the sample belongs to a certain class. The greater the degree of membership, the more likely the sample point belonging to this category. Since natural processes are generally fuzzy, fuzzy clustering is closer to the real situation in nature. The focus of clustering technology research mainly includes cluster analysis, similarity measurement, and cluster validity evaluation.

The mathematical model of cluster analysis is as follows: we set $X = \{x_1, x_2, ..., x_n\}$ as the sample set to be clustered, which includes n sample points. We denote each sample in X as $x_i = \{x_{i1}, x_{i2}, ..., x_{im}\}$, which has m feature attributes. Cluster analysis is to divide the n samples in the sample set X into k disjoint sample subsets C_1, C_2, ..., C_k according to their characteristic attributes and require them to meet the following conditions [14]:

$$C_1 \cup C_2 \cup ... \cup C_K = C; C_i \cap C_j = \varnothing, 1 \leq i \neq j \leq k. \tag{1}$$

The membership relationship of sample $x_j (1 \leq j \leq n)$ relative to subset $C_i (1 < i \leq k)$ can be expressed as a membership function [15]:

$$u_{C_i}(x_j) = u_{ij} = \begin{cases} 1, x_j \in C_i \\ 0, x_j \notin C_i \end{cases}. \tag{2}$$

Among them, each sample can and can only belong to a certain subset, and each subset is nonempty, so the membership function must satisfy the condition $u_{ij} \in M_{hk}$.

$$M_{hk} = \left\{ u_{ik} \middle| u_{ik} \in \{0,1\}; \sum_{i=1}^{k} u_{ij} = 1; 0 < \sum_{j=1}^{n} u_{ij} < n, \forall i \right\}. \tag{3}$$

In fuzzy clustering, the sample set and X are divided into k fuzzy subsets $\widetilde{C}_1, \widetilde{C}_2, \ldots, \widetilde{C}_k$, and the membership degree $u_{ij} \in [0,1]$ of the sample; the conditions that need to be met are as follows:

$$\underset{i=1}{\overset{K}{U}} \operatorname{supp}(\widetilde{C}_i) = C; u_{ij} \in [0,1]; \sum_{i=1}^{k} u_{ij} = 1; 0 < \sum_{j=1}^{n} u_{ij} < n, \forall i. \tag{4}$$

Among them, supp represents the support set of the fuzzy set.

Similarity measurement is an important problem in clustering. It is the basis for judging the similarity between different samples. Therefore, choosing a suitable similarity measurement method can greatly improve the accuracy of the clustering algorithm. There are many ways to measure similarity in clustering, and the commonly used methods are as follows:

We have two sample points $x_1 = (x_{11}, x_{12}, ..., x_{1m})$ and $x_2 = (x_{21}, x_{22}, ..., x_{2m})$, the distance between them is $d_{1,2}$, and the commonly used distance in cluster similarity measurement is expressed as follows:

(a) Euclidean distance is [16]

$$d_{1,2} = \sqrt{\sum_{j=1}^{m} (x_{i,j} - x_{2,j})^2}. \tag{5}$$

(b) Manhattan distance is

$$d_{1,2} = \sum_{j=1}^{m} |x_{i,j} - x_{2,j}|. \tag{6}$$

(c) Chebyshev distance is

$$d_{1,2} = \lim_{q \longrightarrow \infty} \left(\sum_{j=1}^{m} |x_{i,j} - x_{2,j}|^q \right)^{1/q}. \tag{7}$$

(d) Minkowski distance is

$$d_{1,2} = \sqrt[p]{\sum_{j=1}^{m} |x_{i,j} - x_{2,j}|^p}. \tag{8}$$

Among them, p is a variable parameter. When $p = 1$, the Minkowski distance is the Manhattan distance: when $p = 2$, it is the Euclidean distance; when $p - > \infty$, it is the Chebyshev distance. According to the different parameters, Min's distance can represent a certain kind of distance [17].

(e) Mahalanobis distance is as follows:

We have sample sets $X = \{x_1, x_2, ..., x_n\}$ and $x_i = \{x_{i1}, x_{i2}, ..., x_{im}\}$, the covariance matrix is S, and the mean value is denoted as vector u. Then, the Mahalanobis distance of the sample vector X to u is expressed as

$$D(X) = \sqrt{(X - \mu)^T S^{-1} (X_i - \mu)}. \tag{9}$$

Among them, the Mahalanobis distance between the vectors Xi and j is defined as

$$D(X_i, X_j) = \sqrt{(X_i - X_j)^T S^{-1} (X_i - X_j)}. \tag{10}$$

When the covariance matrix is the identity matrix, the Mahalanobis distance is expressed as Euclidean distance.

(f) Hamming distance is as follows:

Hamming distance is a relatively special distance measurement method, which is a distance measurement method based on binary codes. We suppose that $s1$ and $s2$ are two equal-length binary code strings, and the Hamming distance between them is defined as the minimum number of replacements required to change one of the code strings to the other. For example, the Hamming distance between the binary code strings "1111" and "1001" is 2.

The similarity coefficient can describe the degree of similarity between samples. The more similar the two samples, the greater the similarity coefficient. The similarity coefficient S between sample points X and Y needs to meet the following conditions [18]:

① $|S(X,Y)| \leq 1$

② $|S(X,Y)| = S(Y,X)$

③ $S(X,X) = 1$

Commonly used similarity coefficients include angle cosine and correlation coefficient, and their calculation formula is as follows [19]:

The angle cosine is

$$\cos(\theta) = \frac{\sum_{j=1}^{m} x_{1j}x_{2j}}{\sqrt{\sum_{j=1}^{m} x_{1j}^2}\sqrt{\sum_{j=1}^{m} x_{2j}^2}}. \tag{11}$$

When the two vectors are in the same direction, the cosine of the angle is 1. When they are orthogonal, the cosine of the angle is 0.

The correlation coefficient is

$$R(X,Y) = \frac{\sum_{j=1}^{m}\left(x_{1j} - \overline{x_1}\right)\left(x_{2j} - \overline{x_2}\right)}{\sqrt{\sum_{j=1}^{m}\left(x_{1j} - \overline{x_1}\right)^2}\sqrt{\sum_{j=1}^{m}\left(x_{2j} - \overline{x_2}\right)^2}}. \tag{12}$$

The correlation coefficient is the cosine of the angle between the standard deviation of the vector, and it indicates the degree of linear correlation between the two vectors.

Information entropy is a quantification method of information, which indicates a measure of the degree of dispersion of distribution. The more scattered the sample distribution, the greater the information entropy; the tighter the sample distribution, the smaller the information entropy. The calculation formula is as follows [20]:

$$Entropy(X) = \sum_{i=1}^{n} -p_i \log_2 p_i. \tag{13}$$

Among them, X is the sample set, n is the number of sample classifications, and p is the probability of occurrence of the i-th type element in X.

In people's practice, it is often necessary to deal with data sets with mixed attributes. This kind of data has both numerical and nonnumerical attributes. We have two sample points $X(x_1, x_2, \ldots, x_m, \ldots, x_n)$ and $Y(, y_1, y_2, \ldots, y_m, \ldots, y_n)$. Their first m dimensions are numerical attributes, and $m+1$ to nth are nonnumerical attributes. The distance between them is as follows:

$$d(X,Y) = \sqrt{\sum_{i=1}^{m} \left(x_i - y_i\right)^2 + \sum_{j=m+1}^{m} \delta\left(x_k, y_k\right)^2},$$
$$\delta(a,b) = \begin{cases} 1, & a = b \\ 0, & a \neq b \end{cases}. \tag{14}$$

In order to solve the clustering problem of nonconvex data sets, people have improved the basic similarity measurement methods, such as manifold distance and kernel distance.

Manifold distance is a new distance measurement method designed for manifold data sets. It can well reflect the similarity between two points in the data set of manifold distribution. It is defined as follows:

(I) The length of the line segment on the manifold: we set x and y as any two points in the space; then, the length of the line segment on the manifold between them is

$$L\left(x_i, x_j\right) = \rho^{\operatorname{dist}\left(x_i, x_j\right)} - 1. \tag{15}$$

Among them, $\operatorname{dist}(x_i, y_j)$ is the Euclidean distance between x_i and y_j, and $\rho < 1$ is the expansion factor.

(II) Manifold distance: we regard the data points as the vertices of the graph $G = (V, E)$, and $\rho \in V^l$ represents the path connecting the points p_1 and $p_{|p|}$ of length $l = |p|$ on the graph, where the edge is $(p_k, p_{k+1}) \in E, 1 \leq k \leq P_{|p|}$. p_{ij} represents the set of all paths connecting the data points x_i and x_j, and the manifold distance is expressed as [21]

$$D_{ij} = \min \sum_{k=1}^{|p|-1} L\left(p_k, p_{k+1}\right). \tag{16}$$

As shown in Figure 1, in the data set of manifold distribution, the similarity of the two points a and e is significantly higher than the similarity of the two points a and f, but the Euclidean distance of the former is greater than the latter. If Euclidean distance is used as a measure of similarity, it cannot reflect the spatial consistency of the samples, while the manifold distance can better solve this problem.

Although the manifold distance has obvious advantages in data sets with complex distribution, its computational complexity is higher. Compared with the manifold distance, the core distance has lower computational complexity. The kernel method first maps the original data set to a high-dimensional complex nonlinear feature space and then finds the distance between two sample points in this mapping space, which is the kernel distance. In this feature space, the original linearly inseparable data set may become linearly separable. Therefore, it can simplify the structure of the data set and improve the adaptability of the clustering algorithm to complex data sets.

The sample set $\{x_1, x_2, \ldots, x_N\}$ of the input space is mapped into the feature space and becomes

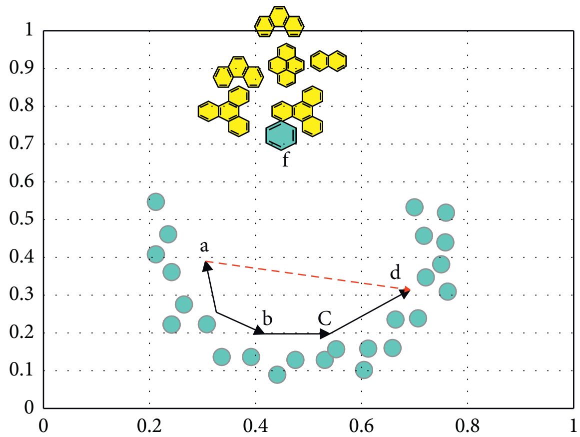

Figure 1: Manifold distance and Euclidean distance.

$\{\Phi(x_1), \Phi(x_2), \ldots, \Phi(x_N)\}$. Then, the distance (kernel distance) of the sample points *xi*, *xj* in the feature space is [22]

$$d_H(x_i, x_j) = \sqrt{\left\| \Phi(x_i) - \Phi(x_j) \right\|^2} = \sqrt{\Phi(x_i)\Phi(x_i) - 2\Phi(x_i)\Phi(x_j)\Phi(x_j)\Phi(x_j)}. \quad (17)$$

It is

$$d_H(x_i, x_j) = \sqrt{K(x_i, x_i) - 2K(x_i, x_j) + K(x_j, x_j)}. \quad (18)$$

Among them, $K(xi, xj)$ is the kernel function, and the commonly used kernel functions are as follows:

① Polynomial kernel: $K(x_i, x_j) = (x_i x_j + 1)^d$, where d is an integer

② Gaussian kernel: $K(x_i, x_j) = \exp(-\beta \|x_i - x_j\|^2)$, $\beta > 0$

③ Two-layer neural network sigmoidal kernel: $K(x_i, x_j) = \tanh(-b(x_i x_j) - c)$, where b and c are custom parameters

As shown in Figure 2, the sample set is linearly inseparable in the original space, but when it is mapped to the feature space through the kernel function, it becomes linearly separable. Because the kernel method is simple and easy to use and can improve the performance of the algorithm, it has been widely used in clustering.

Cluster analysis can divide the original sample set into multiple sample subsets, but is the result of the division reasonable? How to compare the results of different divisions? This requires evaluation of the effectiveness of clustering. A good effectiveness evaluation method can not only judge the performance of the clustering algorithm, but also guide the algorithm to obtain better results. Therefore, the cluster validity evaluation T is also one of the research focuses in the clustering problem.

Criteria for evaluating the pros and cons of clustering algorithms generally include high-dimensionality, scalability, ability to handle noise, discovering clusters of arbitrary shapes, minimizing domain knowledge for determining input parameters, and sensitivity, interpretability, and usability of input record order.

In order to evaluate the clustering results, people have proposed a lot of clustering effectiveness evaluation indicators; these indicators are mainly used to evaluate the tightness between clusters and the degree of dispersion between clusters in the clustering results. There are various clustering effectiveness indicators. The following will focus on the effectiveness indicators that will be used in this paper.

3.1. *Clustering Accuracy*

3.1. Clustering Accuracy. The clustering accuracy rate compares the true class labels of each sample with the class labels obtained by clustering and obtains the percentage of correctly divided samples in the sample set. Its definition is as follows:

$$CC(T, S) = \frac{1}{m} \sum_{i=1}^{T} \max \text{Confusion}(i, j), \ (i = 1, \ldots, T; \ j = 1, \ldots, S). \quad (19)$$

Among them, m represents the number of samples in the sample set to be clustered; T represents the number of true categories of the sample set; S represents the number of categories obtained by clustering; Confusion(i, j) represents the confusion matrix; in the matrix, (i, j) represents the number of samples that appear in the i-th category in the real category and the j-th category in the clustered category at the same time. $CC \in [0, 1]$, the larger the value, the better the effect of the clustering algorithm.

3.2. Adjusted Rand Index (ARI) Indicator

$$R(T, S) = \frac{\sum_{lk} \binom{n_{lk}}{2} - \left[\sum_l \binom{n_{ln}}{2} * \sum_k \binom{n_{nk}}{2}\right] / \binom{n}{2}}{(1/2)\left[\sum_l \binom{n_{ln}}{2} + \sum_k \binom{n_{nk}}{2}\right] - \left[\sum_l \binom{n_{ln}}{2} * \sum_k \binom{n_{nk}}{2}\right] / \binom{n}{2}}. \quad (20)$$

Among them, *nij* represents the number of samples belonging to category I and category k at the same time, $k(l\ eT', k\ e\ S)$, and T and S represent the true category and the category obtained by clustering, respectively. The larger the value, the better the clustering effect. $R(T, S)e[0, 1]$, the larger the value, the better the effect of the clustering algorithm.

3.3. Van Dongen (VD) Criterion Index

$$VD = \frac{\left(2N - \sum_i \max_j n_{ij} - \sum_j \max_i n_{ij}\right)}{2N}. \quad (21)$$

Among them, n represents the number of samples in the sample set, and n_{ij} represents the number of samples of the i-th class in the real class and the j-th class in the clustered class label at the same time. $V\ D \in [0, 1]$, the smaller the value of VD, the better the clustering effect.

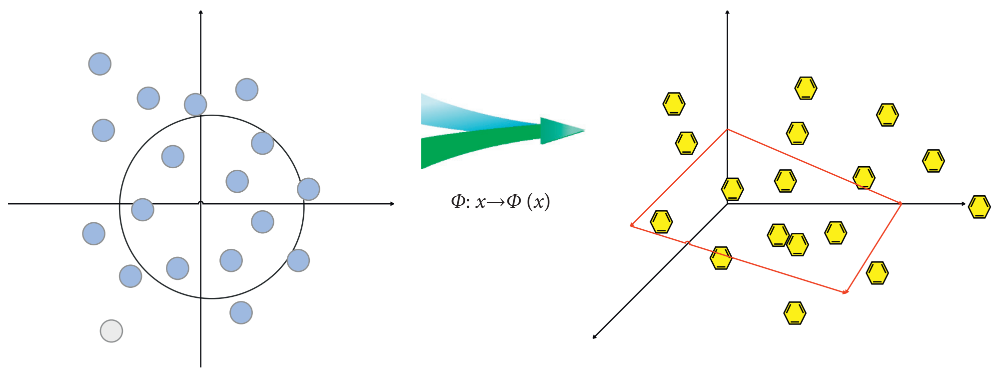

FIGURE 2: The distribution of samples in the original space and feature space.

4. IoT-Assisted Hybrid Intelligent Learning Architecture Based on Digital Education in a Diverse Society

Through the analysis of the system function, after long-term investigation and demonstration, a more feasible design plan is finally determined, as shown in Figure 3:

(1) The system hardware is divided into five parts: main control unit, wireless communication unit, air conditioner infrared remote control unit, lighting control unit, and power supply unit. (2) The main control chip of the main control unit and the lighting control unit adopts STM32F103ZET6, the single-chip microcomputer of the communication unit adopts PIC18F45K22, and the single-chip microcomputer of the air-conditioning infrared remote control unit adopts STM8S103S3P6. The main control unit mainly implements functions such as collection of indoor environment conditions, control of hardware equipment in the classroom, and display of indoor environment. (3) The wireless communication unit mainly realizes the functions of the main control module collecting environmental data and uploading it to the database, sending alarm short messages and receiving control commands. (4) The infrared remote control unit of the air conditioner uses the STM8S103S3P6 chip as the control core, which can realize the functions of learning, storing, restoring, and sending the infrared remote control code of the air conditioner. (6) Indoor environmental quality testing includes testing of information such as temperature and humidity, light intensity, carbon dioxide concentration, formaldehyde content, and PM2.5 concentration. (7) The communication between the hardware device and the server is realized through the SIM900a module. The communication unit uploads the environmental detection information sent by the main control unit to the database via the GPRS network in the POST mode and receives the control information sent by the monitoring platform at the same time. (8) The electric curtains are driven by a decelerating DC motor, the lights are LED energy-saving lamps, and the alarm device uses sound and light and SMS alarm methods. (9) The smart classroom system can judge the distribution of students in the classroom based on the video surveillance images in the classroom, and the light control unit can turn on the lights near the students and adjust the brightness of the lights. The adjustment of the brightness of the light is controlled by the PWM output of the single-chip microcomputer, and the fuzzy control algorithm is adopted to keep the light intensity in the classroom within a proper range.

The whole system needs to realize many functions and cannot be controlled by a single-chip microcomputer. The system is divided into five parts: main control unit, wireless communication unit, air conditioner infrared remote control unit, lighting control unit, and power supply unit. The various parts are relatively independent and cooperate with each other with the main control unit as the core to realize the overall function of the system together. The overall block diagram of the hardware circuit is shown in Figure 4:

The overall hardware structure diagram of the gateway subsystem is shown in Figure 5. A gateway is a network device that serves as the important task of conversion and is used between two systems with different communication protocols and different data formats. Moreover, it can be used for both local area networks and wide area networks.

The software architecture of the gateway subsystem is shown in Figure 6. The lightweight TCP/IP protocol LwIP and WebServer web server run on the FreeRTOS operating system, and the WebServer will call the interface function of LwIP to send and receive data packets to the network. The GCI application that processes the data runs on the WebServer. The data will be sent to the Hyun web page through a form, and finally the data will be sent to the server in the form of the Hunload web page.

According to the main tasks and characteristics of multimedia classroom management, the multimedia classroom integrated management system can be divided into five functional sections. Its structure is shown in Figure 7.

In the design of the application layer of the system, this paper uses the advantages of cloud computing to realize the efficient operation and management of the system and the intelligent interaction of data and information. Moreover, this paper finally transmits the effective data information to the database server of the central control room through the network and displays it on the electronic screen. The system can remotely monitor and control the terminal teaching equipment of the multimedia classroom in real time, can accurately express the status information of various equipment in the classroom and the cause of the failure, and

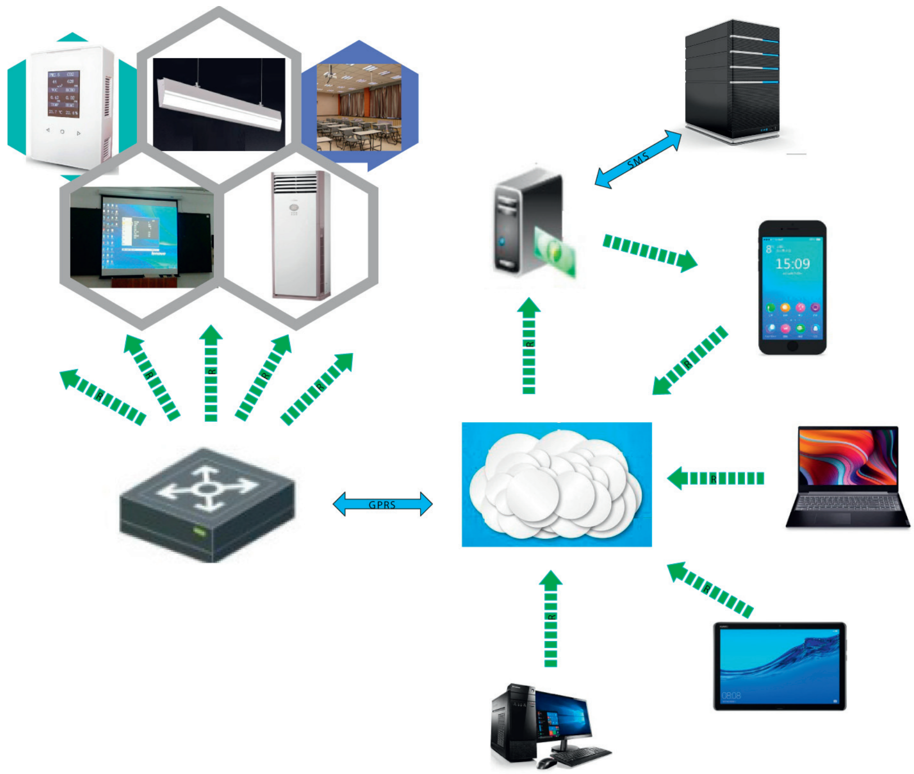

Figure 3: Block diagram of a smart classroom system based on Internet of Things technology.

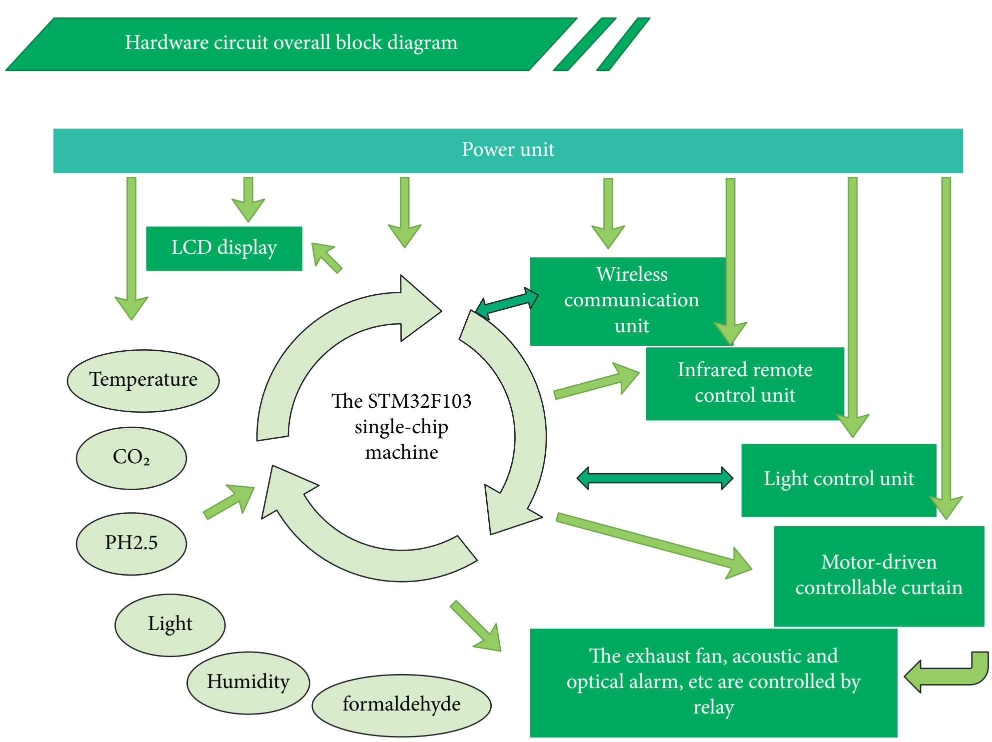

Figure 4: Overall block diagram of the hardware circuit.

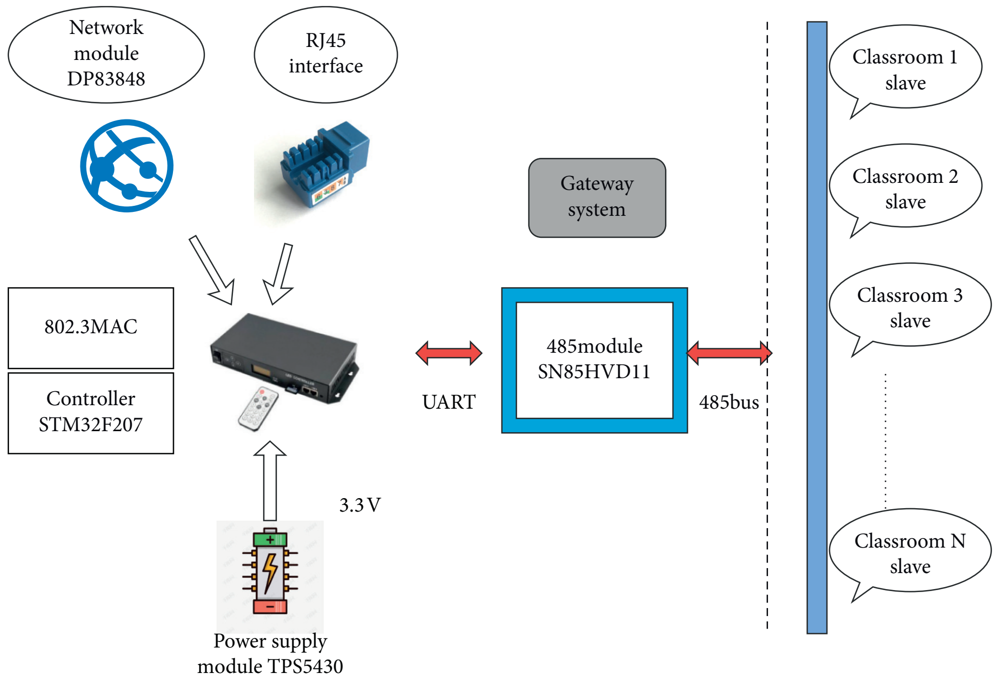

FIGURE 5: Block diagram of the overall hardware structure of the gateway subsystem.

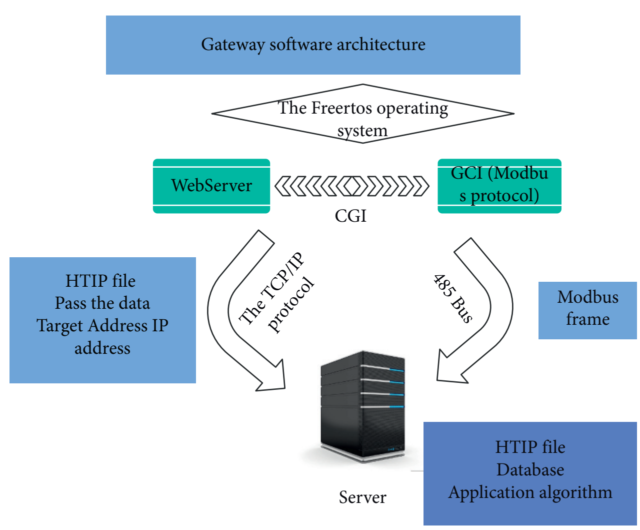

FIGURE 6: The software architecture of the gateway subsystem.

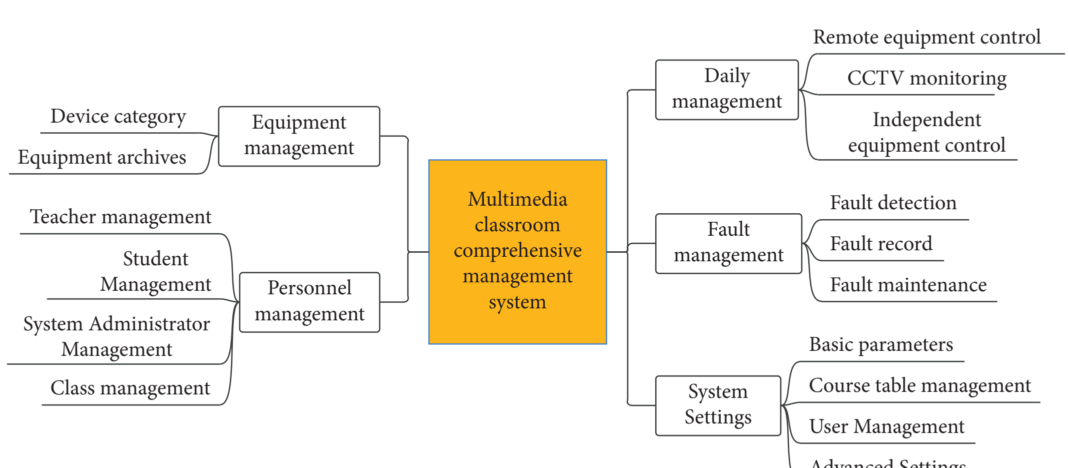

FIGURE 7: Multimedia classroom integrated management system based on the Internet of Things.

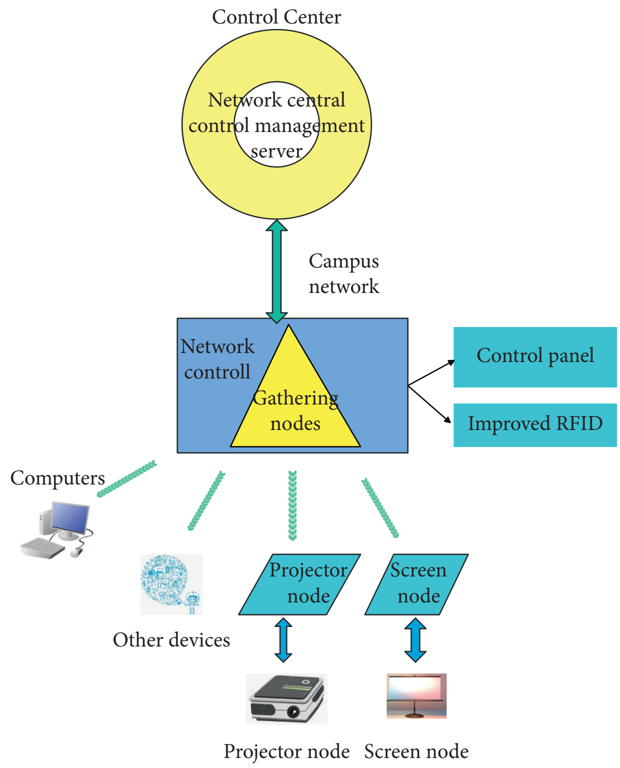

Figure 8: Network topology of multimedia classrooms based on the Internet of Things.

Table 1: System experimental performance.

Number	Digitizing	Teaching effect	Number	Digitizing	Teaching effect
1	94.6	86.6	25	87.3	89.9
2	96.1	79.5	26	91.6	86.9
3	96.1	81.5	27	89.7	90.5
4	96.1	80.5	28	91.2	90.2
5	87.3	80.4	29	91.5	91.6
6	90.7	79.3	30	96.9	88.3
7	93.7	88.0	31	92.8	88.4
8	89.7	88.2	32	89.9	86.7
9	93.3	82.7	33	93.5	80.7
10	96.4	88.7	34	95.6	93.1
11	94.9	86.8	35	88.0	87.0
12	90.9	84.0	36	92.1	87.7
13	90.8	89.0	37	92.5	89.7
14	90.5	82.1	38	92.1	79.7
15	94.1	93.2	39	87.1	89.0
16	92.1	90.7	40	96.5	80.4
17	92.1	80.9	41	92.4	85.7
18	88.6	83.5	42	96.6	89.9
19	88.2	88.6	43	88.3	93.5
20	92.0	82.2	44	88.2	93.4
21	87.0	85.7	45	91.5	81.9
22	87.4	80.8	46	96.4	92.6
23	94.4	83.7	47	89.9	85.6
24	96.0	93.6	48	90.8	81.7

can also assist the administrator to solve the equipment failure remotely and improve work efficiency. In addition, it can help teachers in class operate and use various teaching equipment correctly. The network topology of the system is shown in Figure 8.

This paper verifies the performance of the above-built system. Starting from the actual situation of intelligent education, this paper combines the simulation system to build an intelligent IoT-assisted hybrid intelligent learning architecture. Moreover, this paper evaluates the teaching

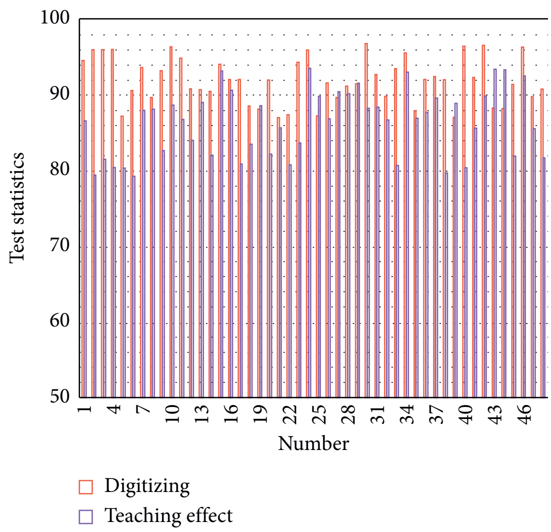

Figure 9: Performance statistics of IoT-assisted hybrid intelligent learning architecture based on digital education in a diverse society.

effect of the system from the digitization of the educational resources of the intelligent learning system and the teaching effect, and the results shown in Table 1 and Figure 9 are obtained.

From the above research, it can be seen that the IoT-assisted hybrid intelligent learning framework based on digital education in a diverse society has a certain occasional effect, and it can be used as a reference for the development of subsequent intelligent education.

5. Conclusion

This article introduces the elements of the Internet of Things into the digital intelligent education system. On the one hand, this paper builds an IoT smart laboratory to provide technical and environmental support for digital intelligent education experiments and remote sharing of equipment resources. On the other hand, this paper constructs the Internet of Things digital intelligent education with the concept and technical characteristics of the Internet of Things, which makes the digital intelligent education smarter, more interactive with the outside world, and more concrete and vivid experimental results. The digital intelligent education practice teaching system that incorporates the Internet of Things technology is also in line with the theoretical requirements of the situational teaching, task-driven teaching, and research teaching methods advocated by higher education. Moreover, it conforms to the cognitive and psychological characteristics of college students' intense pursuit of new knowledge and new things and conforms to the goals and directions of quality education and innovation education in contemporary universities. This article combines the Internet of Things technology to construct a hybrid intelligent learning system, applies it to digital education in a diverse society, and validates the system to provide a theoretical reference for subsequent intelligent education.

Data Availability

The labeled dataset used to support the findings of this study is available from the corresponding author upon request.

Conflicts of Interest

The author declares no competing interests.

Acknowledgments

This study was sponsored by first-class undergraduate courses in Henan Province: Modern Educational Technology and Application; School-level Excellent Teaching Grassroots Organization of Zhengzhou Normal University (JCZZ-20150).

References

[1] S. Liu, P. Chen, and P. Chen, "Research on fuzzy comprehensive evaluation in practice teaching assessment of computer majors," *International Journal of Modern Education and Computer Science*, vol. 7, no. 11, pp. 12–19, 2015.

[2] L. Zhou, H. Li, and K. Sun, "Teaching performance evaluation by means of a hierarchical multifactorial evaluation model based on type-2 fuzzy sets," *Applied Intelligence*, vol. 46, no. 1, pp. 1–11, 2016.

[3] J. Porozovs, L. Liepniece, and D. Voita, "Evaluation of the teaching methods used in secondary school biology lessons," *Journal of Pedagogy and Psychology "Signum Temporis"*, vol. 7, no. 1, pp. 60–66, 2015.

[4] M. A. Oliveros, A. García, and B. Valdez, "Evaluation of a teaching sequence regarding science, technology and society values in higher education," *Creative Education*, vol. 6, no. 16, pp. 1768–1775, 2015.

[5] M. Sánchez Cerón and F. M. d. S. Corte Cruz, "The evaluation of teaching: some consequences for Latin America," *Revista Mexicana de Investigación Educativa*, vol. 20, no. 67, pp. 1233–1253, 2015.

[6] K. Angell and E. Tewell, "Teaching and un-teaching source evaluation: questioning authority in information literacy instruction," *Comminfolit*, vol. 11, no. 1, pp. 95–121, 2017.

[7] M. Brkovic and P. Chiles, ""Spector-the sustainability inspector": participatory teaching, learning and evaluation game for architects, architecture students and pupils," *Facta Universitatis-Series: Architecture and Civil Engineering*, vol. 14, no. 1, pp. 1–20, 2016.

[8] Y. Jiang and Y. Wang, "Evaluation of teaching quality of public physical education in colleges based on the fuzzy evaluation theory," *Journal of Computational and Theoretical Nanoscience*, vol. 13, no. 12, pp. 9848–9851, 2016.

[9] K. Royal, "A guide for making valid interpretations of student evaluation of teaching (SET) results," *Journal of Veterinary Medical Education*, vol. 44, no. 2, pp. 1–7, 2016.

[10] F. Garofalo, P. Mota-Moya, A. Munday, and S. Romy, "Total extraperitoneal hernia repair: residency teaching program and outcome evaluation," *World Journal of Surgery*, vol. 41, no. 1, pp. 1–6, 2017.

[11] G. Costa and R. Ortale, "Model-based collaborative personalized recommendation on signed social rating networks," *ACM Transactions on Internet Technology*, vol. 16, no. 3, pp. 1–21, 2016.

[12] Y. Guan, Q. Wei, and G. Chen, "Deep learning based personalized recommendation with multi-view information integration," *Decision Support Systems*, vol. 118, pp. 58–69, 2019.
[13] C. Yang, Q. Fan, T. Wang et al., "RepoLike: a multi-feature-based personalized recommendation approach for open-source repositories," *Frontiers of Information Technology & Electronic Engineering*, vol. 20, no. 2, pp. 86–101, 2019.
[14] Q. Lin, X. Wang, B. Hu et al., "Multiobjective personalized recommendation algorithm using extreme point guided evolutionary computation," *Complexity*, vol. 2018, Article ID 1716352, 18 pages, 2018.
[15] X. U. Dazhi, "Research on music culture personalized recommendation based on factor decomposition machine," *Personal and Ubiquitous Computing*, vol. 24, no. 2, pp. 247–257, 2020.
[16] N. X. Bach, N. D. Hai, and T. M. Phuong, "Personalized recommendation of stories for commenting in forum-based social media," *Information Sciences*, vol. 352-353, no. 2, pp. 48–60, 2016.
[17] D. Guo, Y. Zhu, W. Xu, S. Shang, and Z. Ding, "How to find appropriate automobile exhibition halls: towards a personalized recommendation service for auto show," *Neurocomputing*, vol. 213, pp. 95–101, 2016.
[18] C. Guilin, Z. Xuzhen, Y. Zhao, and H. Tian, "Personalized recommendation via suppressing excessive diffusion," *Mathematical Problems in Engineering*, vol. 2017, Article ID 2587069, 10 pages, 2017.
[19] U. Liji, Y. Chai, and J. Chen, "Improved personalized recommendation based on user attributes clustering and score matrix filling," *Computer Standards & Interfaces*, vol. 57, no. 5, pp. 59–67, 2018.
[20] T. Ha and S. Lee, "Item-network-based collaborative filtering: a personalized recommendation method based on a user's item network," *Information Processing & Management*, vol. 53, no. 5, pp. 1171–1184, 2017.
[21] W. Intayoad, T. Becker, and P. Temdee, "Social context-aware recommendation for personalized online learning," *Wireless Personal Communications*, vol. 97, no. 1, pp. 1–17, 2017.
[22] J. Xia, G. Li, and Z. Cao, "Personalized exercise recommendation algorithm combining learning objective and assignment feedback," *Journal of Intelligent and Fuzzy Systems*, vol. 35, no. 3, pp. 2965–2973, 2018.

Hindawi
Scientific Programming
Volume 2021, Article ID 5377784, 12 pages
https://doi.org/10.1155/2021/5377784

Research Article

The Design of Mathematics Teaching Optimization Scheme Based on Data-Driven Decision-Making Technology

Zongming Lv

Xuancheng Vocational and Technical College, Xuancheng 242000, China

Correspondence should be addressed to Zongming Lv; lzm@xcvtc.edu.cn

Received 18 October 2021; Revised 1 November 2021; Accepted 6 November 2021; Published 24 November 2021

Academic Editor: Le Sun

In order to improve the effect of classroom teaching and realize the improvement of mathematics teaching quality, this article combines data-driven decision-making technology to design a mathematics teaching plan system and applies data-driven decision-making technology to the design of mathematics teaching plan by improving the big data algorithm. In addition, this paper designs a mathematics teaching plan design system based on data-driven decision-making technology. The system learning module displays the knowledge points in a chapter-sequential navigation mode and stores data or information in the nodes, which are connected to form a network structure through chains. Finally, this paper verifies the designed system with experiments. From the results of the experimental research data, it can be seen that the mathematical teaching plan design system based on the data-driven decision-making technology constructed in this article has good practical effects. On this basis, the system constructed in this article can be verified through further practice.

1. Introduction

Big data has already had a significant impact in various fields such as finance, commerce, and medical care. In the financial field, big data technology helps to achieve precision marketing, improve risk control, and improve operations. In the business field, it helps e-commerce companies analyze customer characteristics and achieve personalized recommendations. In the medical field, it improves and optimizes the diagnosis of diseases and the formulation of dynamic treatment plans and promotes precision medicine [1]. Data-driven decision-making has become a development trend in the era of big data, and precision and personalization have become keywords in the era of big data. In the education field, with the continuous integration of information technology and contemporary education, as well as the wide application of various digital intelligent systems and intelligent terminals in educational practice, enormous behavioral data in the education and teaching process can be recorded and saved, including education management data, student basic information data, and learning behavior data. These data are large in quantity and diverse in types, and the temporal and contextual characteristics of education make the data generated in the education field have natural time characteristics and contextual connotations [2]. Carrying out precision teaching is of great significance. In educational practice, students have different qualifications, cognitive levels, learning styles, and learning motivations. For example, some students are good at verbal expression, some students are good at hands-on operation, some students like to study independently, some students like to learn in groups, some students are more self-conscious and motivated, and some students are relatively passive. Different students respond differently to the teaching plan, and correspondingly there are differences in the teaching effects [3].

This paper combines big data technology to design and research mathematics teaching schemes, builds a corresponding intelligent system, and combines experimental research to verify the system, providing theoretical references for subsequent mathematics teaching reforms.

2. Related Work

tIn recent years, with the development of the Internet and information technology, data analysis platforms have gradually been enriched and improved. Moreover, teaching software based on big data is gradually being developed and applied, and teaching software is constantly being developed and improved. At present, they are relatively mature and have exerted a certain effect in actual teaching. In the survey of data, it is concluded that schools use extremely large data extensively, which can play a significant role in assisted teaching [4]. It can play a significant role in test analysis and test paper comment based on big data and can be effectively applied in mathematics, English, and other subjects. Zhixue is also widely used in the teaching of various disciplines, which provides a strong guarantee for the realization of precision teaching and the improvement of teaching effects [5]. The data analysis teaching platform and software have very prominent features. First of all, the application of data analysis software makes it easier for teachers to organize and correct test papers. Without changing the test paper reviewing habits, it can also enter data into the corresponding teaching system. The traces of problem solving and correction retained in the test paper can make students clearer [6]. Secondly, the data analysis teaching software can eliminate teachers' need to spend a lot of time and energy on the examination paper correction and statistics, so the teachers' time and energy are liberated, and the limited time and energy can be devoted to other teaching activities. Furthermore, the application of data analysis teaching platform can improve the promotion and strengthening of data analysis for precision teaching. On the basis of scientific data analysis, teachers can achieve personalized and precise guidance to students, and students can also form more scientific and accurate cognition of themselves [7].

The big data teaching platform and software can use information technology to automatically form a personalized wrong question bank, which provides a solid foundation for the development of professional and accurate test analysis for teachers. Teachers can use daily teaching big data for later exams and choose error-prone questions, key and difficult points, and other content to organize papers to help them improve the efficiency of proposition papers [8]. The data analysis platform software will be based on the different learning foundations of each student, and the system can also automatically push exercises on the weak points of knowledge to the students to help fill in the gaps. Thus, it contributes to the improvement of test analysis and student evaluation [9].

Big data in the education field can be divided into a broad sense and a narrow sense. The broad sense of education big data generally refers to all human behavior data derived from daily educational activities. Data refers to learner behavior data, which mainly comes from the student management system [10]. In addition, the innovation of big data develops along the direction of "data–big data–data-driven innovation–data analysis and prediction". In this process, big data will inevitably affect education innovation. Moreover, in the process of promoting the continuous digitization of high school mathematics content, it also creates infinite possibilities for content arrangement based on "knowledge chain" and "data chain." In addition, cut-type, play-type, list-type, and mass-customized mathematical content emerge at the historic moment [11]. Educational big data drives teaching governance. It is difficult for traditional experience-based management methods to achieve high-efficiency teaching goals. By mining and collecting educational big data treasures, a large amount of digital information (such as pictures, audio, and video) generated in teaching is converted into processable data, forming educational big data with valuable reference and analysis [12]. According to literature [13], the normal monitoring of the teaching operation of colleges and universities and the establishment of a national undergraduate database constitute an inevitable trend of education informatization and also an important content of building a higher education teaching quality assurance system. The goal and content of the construction status database are studied, and the in-depth analysis and mining of the basic status data of colleges and universities are proposed to better serve the teaching management of colleges and universities.

3. Improved Algorithm of Teaching System Based on Big Data Technology

Spread routing is the most classic multicopy routing, which mainly spreads message copies rapidly to the network through active delivery. When two nodes meet, they will exchange messages that are not available to each other through the message information summary vector table in each node, and the summary vector table is constantly being updated. The message will spread rapidly throughout the network like a virus to increase the probability of the message reaching the sink node. In this way, we can increase the message delivery rate to some extent [14]. However, because there are too many message copies, they will quickly occupy the limited storage space of all nodes and easily cause network congestion. In addition, frequent message submission between nodes will also accelerate the energy consumption of nodes, increase network bandwidth pressure, and make the overall network overhead rapidly increase. Therefore, we can see that increasing the submission rate in this way does not play a positive role.

Figure 1 shows the routing process of the spread routing algorithm. At time t_1, the source node S that generates the message meets the node A and the node C. At this moment, node S compares its own summary vector table with node A and node C. We found that node A and node C did not store the message. Therefore, node S submits a copy of the message to nodes A and C. At time t $(t_2 > t_1)$, node A meets node B, and node C meets sink node D. Node A will deliver the copy of the message to node B, node C will deliver the copy of the message to the sink node D, and the message transmission is completed at this moment [15].

Considering the huge overhead and caching pressure of sprawl routing, researchers put forward a spread-waiting routing algorithm on this basis. The biggest difference from sprawling routing is the limited number of message copies. By controlling the number of message copies, network overhead and node cache space are alleviated, and the message delivery rate is also significantly improved. The dissemination waiting routing algorithm is usually divided

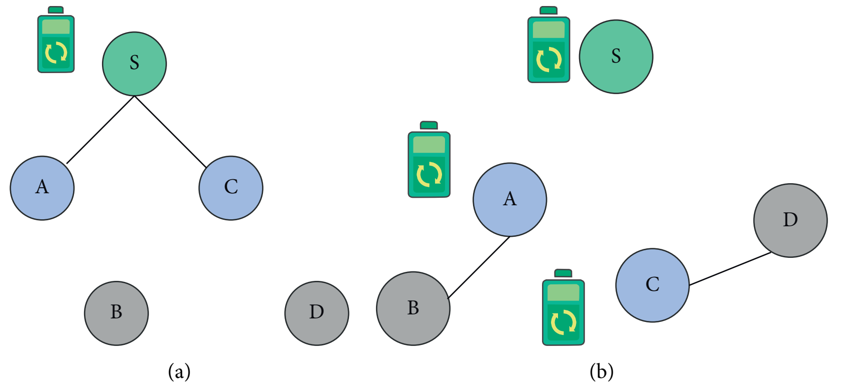

Figure 1: Schematic diagram of the spread routing algorithm. (a) t_1 moment. (b) t_2 moment.

into two stages, the dissemination phase and the waiting phase. In the dissemination phase, the source node mainly submits a copy of the message to other nodes, while in the waiting phase, all nodes stop distributing copies of the message until a node meets the sink node before submitting the message. According to different distribution methods, it is divided into source spray and wait routing (SSW) and binary spray and wait routing (BSW).

Source dissemination waiting route (SSW): In the initial dissemination stage, the source node copies the initialized message for L $(L > 1)$, and the source node carries the message copy to move in the network. When the source node meets other nodes, one copy of the message will be delivered to the other node; at this time, the source node's copies of the message will be reduced by one. In the future, the source node will submit a copy of the message every time it encounters a node, and the number of copies of its own message will be reduced by one. In the dissemination phase, if the source node or another node carrying a copy of the message meets the sink node, the message will be delivered to the sink node to end the message transmission. If none of the nodes carrying messages meet the sink node during the dissemination phase, then when the number of message copies in the source node is reduced to 1, the network will enter the waiting phase, and the L nodes carrying message copies will not report any messages. During the message delivery process, unless one of the nodes encounters the sink node, the message will continue to be delivered until the message transmission is completed [16].

Figure 2 shows the routing process of the source-end dissemination waiting algorithm. At time t, the source node S generates L copies of the message and carries the message in the network. At this time, it belongs to the dissemination phase. At time t_2 $(t_2 > t_1)$, node S encounters relay node C and then delivers one copy of the message to it. At this time, the number of message copies in node S becomes L-1. After that, the source node S will repeat this process [17]. Unless a certain node meets the sink node during the period and completes the message transmission, it will wait until the number of message copies in the source node becomes 1 and enter the waiting phase; then no nodes will submit the message until they encounter the sink node.

The second distributed waiting route (BSW): The difference between the second distributed waiting route and the source-end distributed waiting route is mainly concentrated in the dissemination stage. After the source node generates L copies of the message, the source node continues to move with the message. When the source node and the relay node meet, the source node will deliver half of its own messages to the relay node. That is, L/2 copies of the message are delivered to the relay node, and the source node itself also has L/2 copies of the message left. After that, each of the two nodes carries U2 packets to continue moving. When the next relay node is encountered, half of its own message copies will be delivered. The message distribution is shown in Figure 3 [18].

In the dissemination phase, if the node carrying the message meets the sink node, the message is delivered to the sink node and the message transmission is completed. If no node meets the sink node in the dissemination phase, all nodes continue to distribute half of their own messages to the meeting nodes. Until the number of message copies of the source node and other nodes becomes 1, it enters the waiting phase. At this time, the routing status is the same as the waiting phase of the source and the waiting for the routing, and the message is not delivered until the sink node is met [19].

Figure 4 shows the routing process of the two distributed waiting algorithms.

Figure 5 shows the routing process of the probabilistic routing algorithm.

When two nodes enter the communication range of each other, this means that the two nodes meet. Due to the exploration interval, node movement rate, buffer space, etc., even if nodes meet, they may not be able to find each other or successfully connect to each other, let alone establishing data communication, as shown in Figure 6 [20].

In the DTN, all nodes have the function of storing and forwarding messages. When a node receives a message as an intermediate node, it will pass the message to the next node. The selection of the next node will directly affect the final delivery of the message. If the probability of the next node meeting the destination node is greater, the probability of the message being successfully delivered is also greater.

In DTN, each node stores a two-dimensional table, which is used to record the probability of encountering other nodes in the network. In the DTN, time is divided into several time slices, and the size of each time slice is called the

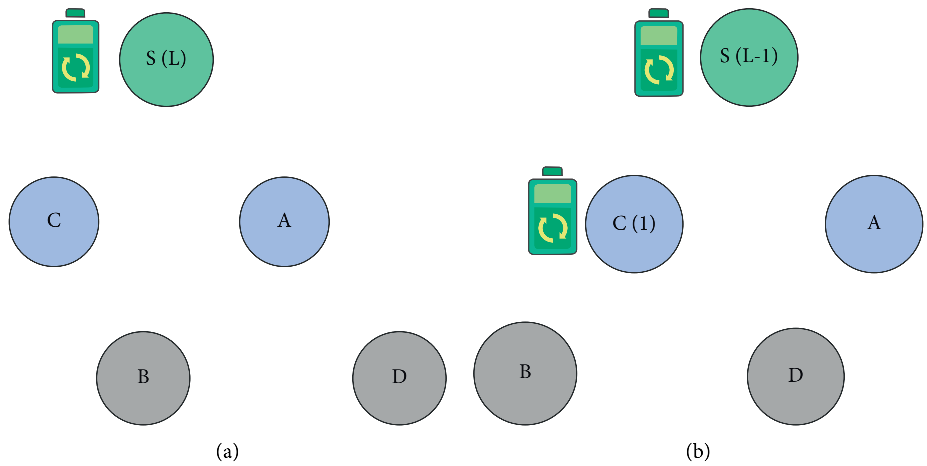

Figure 2: Schematic diagram of source RF routing. (a) t_1 time. (b) t_2 time.

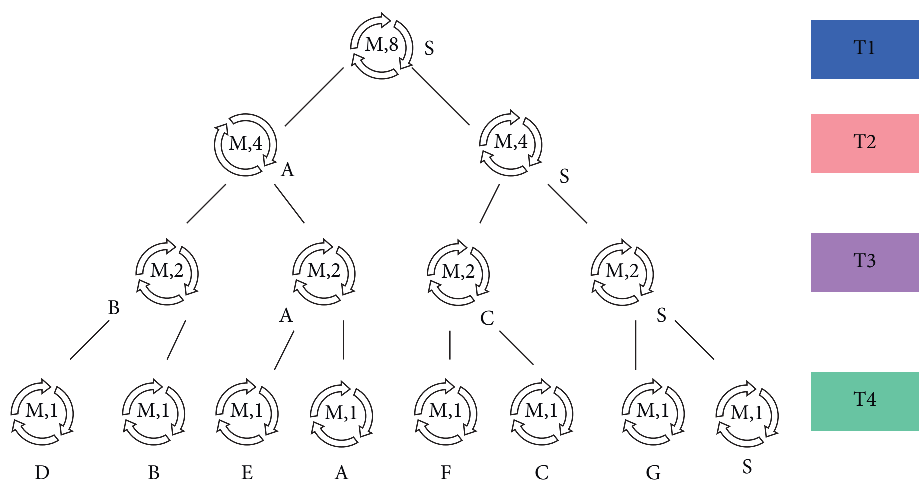

Figure 3: Dichotomy of the distribution of the number of copies waiting for routing.

time period of node movement, which is also called the period of the two-dimensional table of node update probability. In different periods, the values of the two-dimensional probability table maintained by each node are different, and the values in the two-dimensional table will dynamically change as the network layout changes.

In the DTN, each type of node has its own transmission range.

In a certain period, the node will automatically scan other nodes within its transmission range after moving to a certain position. For the situation in the figure, when node A scans for node B and node C within its transmission range, node A can pass the message it carries to node B and node C at this time. In this case, it is called node A and node B "meeting," and node A and node C "meeting." The encounter here does not mean a real encounter, but the two nodes are within each other's transmission range.

In the DTN, the lifetime of the message is set. The length of the message lifetime can be set according to the importance of the message. If the message has not been forwarded when the lifetime expires, the node that carries the message will automatically delete the message.

In DTN, as the node moves, the probability of any two nodes retreating will change. Each node in the network dynamically maintains a two-dimensional table to record the probability of being transparent to other nodes in the network. As the cycle changes, each node will dynamically update the value of its two-dimensional table. We assume that the probability of node A and node B meeting is $P_{(A,B)}, P_{(A,B)} \in [0,1]$. When node A and node B meet, they can send messages to each other. $P_{(A,B)}$ is called the expected value of node A's message to node B. As the layout of nodes in the network changes, the value of $P_{(A,B)}$ will change dynamically. The calculation of the probability value is divided into the following three cases:

① When node A and node B meet, the probability of their meeting will increase. At this time, the corresponding values in the probability tables of node A and node B need to be updated. In this case, (1) is required for calculation.

$$P_{(A,B)} = P_{(A,B)} = P_{(A,B)\text{old}} + \left(1 - P_{(A,B)\text{old}}\right) \times P_{\text{init}}. \tag{1}$$

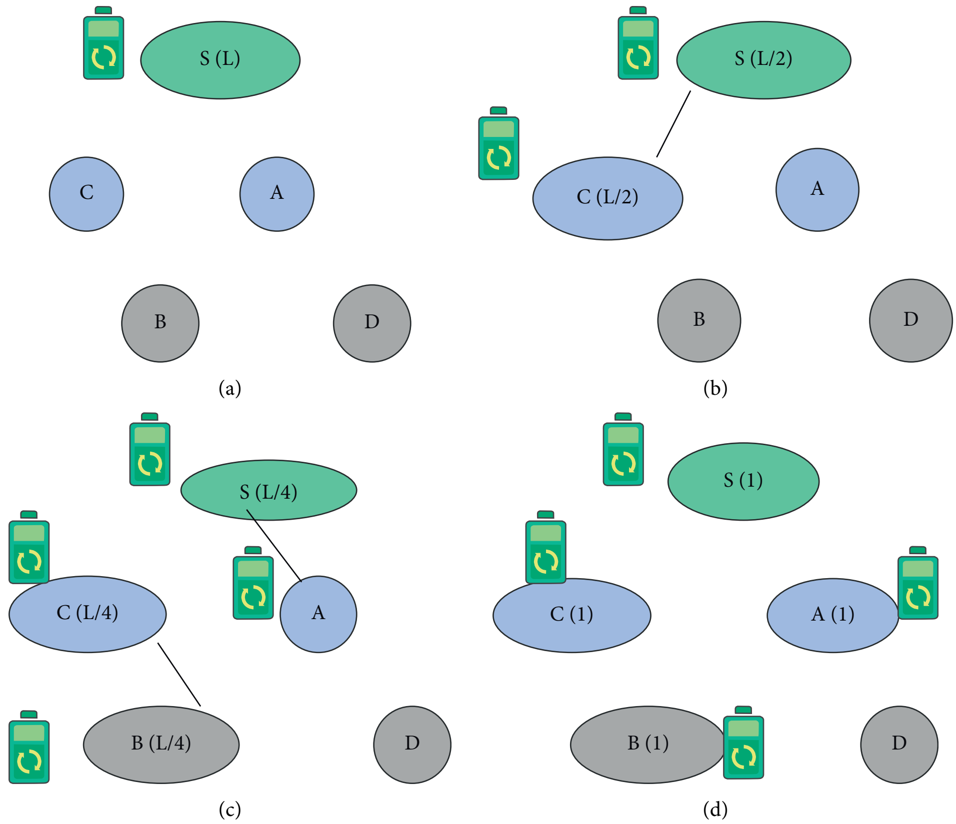

Figure 4: Schematic diagram of the second distributed waiting route. (a) t_1 time. (b) t_2 time. (c) t_3 time. (d) t_4 time.

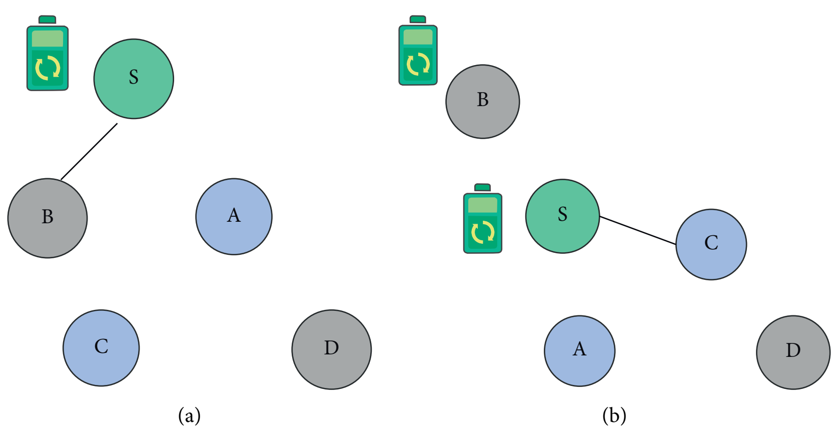

Figure 5: Schematic diagram of probabilistic routing algorithm. (a) t_1 time. (b) t_2 time.

Among them, $P_{\text{init}} \in [0, 1]$ is an initial constant. $P_{(A,B)\text{old}}$ is the delivery probability value of the message delivered by node A to node B in the previous cycle. After calculation, the value of $P_{(A,B)}$ will increase.

② When node A and node B have not met within k cycles, this means that the possibility of node A transmitting messages to node B is getting smaller and smaller, so the expected value will continue to decrease. At this time, (2) is needed for calculation.

$$P_{(B,A)} = P_{(A,B)} = P_{(A,B)\text{old}} \times \gamma^k. \tag{2}$$

Among them, $\gamma \in [0, 1)$ is the attenuation factor. k is the time period between the last calculation of $P_{(A,B)}$ and this calculation.

③ If node A and node B frequently meet, and node B and node C frequently meet, then node C can be regarded as a good message forwarding node between node A and node B. In this case, node A can deliver messages to node C through node B, and the expected value $P_{(A,C)}$ of messages delivered by node A to node C increases, which is calculated by the following formula:

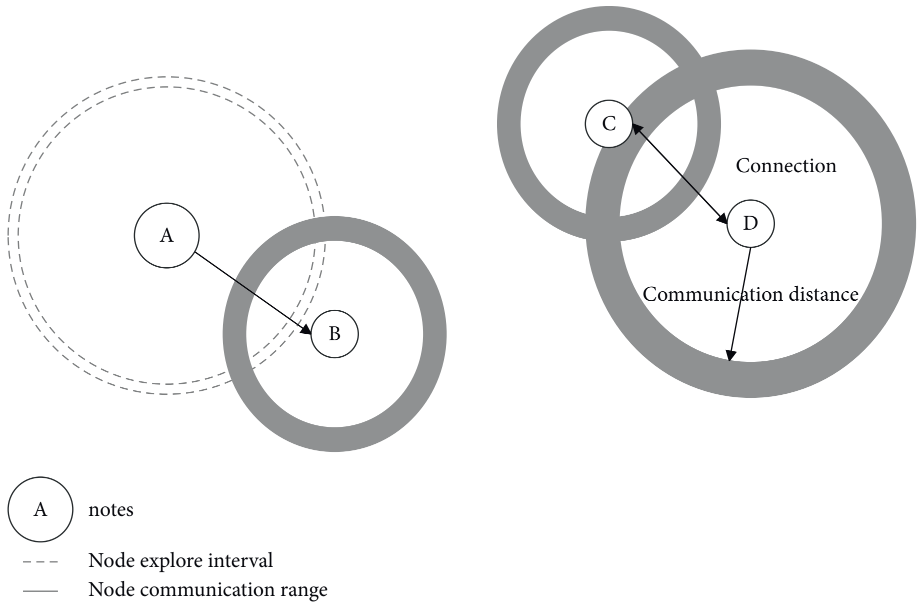

Figure 6: Schematic diagram of node connection.

$$P_{(A,C)} = P_{(A,C)\text{old}} + \left(1 - P_{(A,B)\text{old}}\right) \times P_{(A,B)} \times P_{(B,C)} \times \beta. \quad (3)$$

Among them, $\beta \in [0, 1]$ is the scaling factor, which is used to indicate the degree of the message delivery.

These three situations are the changes in the transfer probability during the movement of the node, which in turn are the update of the probability of the node transferring the message, the attenuation of the probability of transferring the message between the nodes, and the transfer of the message between the nodes.

The PPT routing algorithm is similar to the EDC routing algorithm. When any two nodes in the network meet, they will exchange each other's SV value, including the probability value of the node meeting the destination node, that is, the delivery probability value of the message. Furthermore, the corresponding value in the two-dimensional table of probability maintained by the node is updated by (1)–(3).

We assume that $P_{(A,D)}$ represents the delivery probability value of the message from node A to node D, that is, the probability of the message being delivered from the intermediate node A to the destination node D. Based on the above analysis, the delivery probability value of the message is determined by two factors: the probability of the historical encounter of the node and the duration of the historical encounter of the node. $P_{(A,D)\text{old}}$ is the probability of historical encounter between node A and node D, $T_{(A,D)\text{old}}$ is the historical encounter duration of node A and node D, and $T_{U(A,D)\text{old}}$ is the duration of historical link disconnection between node A and node D. Each node in the network maintains a two-dimensional table, and the structure of the two-dimensional table maintained by node A is shown in Table 1.

If it is assumed that the current time is the mth meeting of node A and node D, the historical meeting duration of the node is $T_{(A,D)\text{old}} = \sum_{i=1}^{m-1} (T^{i+1}_{(A,D)\text{start}} - T^{i}_{(A,D)\text{start}})$. Among them, $T^{i}_{(A,D)\text{start}}$ is the start time of node A and node D's ith encounter, and $T^{i}_{(A,D)\text{end}}$ is the disconnection time of node A and node D's ith encounter. The historical disconnection duration of the node is $T_{U(A,D)\text{old}} = \sum_{i=1}^{m-1} (T^{i+1}_{(A,D)\text{start}} - T^{i}_{(A,D)\text{start}})$.

When two nodes A encounter node D, they calculate and update the node message delivery probability value according to (4) and update the two-dimensional table of node A's delivery probability value at the same time.

$$\begin{aligned} P_{(A,D)} = {} & P_{(A,D)\text{old}} + \left(1 - P_{(A,D)\text{old}}\right) \times P_{\text{init}} \\ & \times C^{T_{(A,D)\text{old}}/T_{(A,D)\text{old}} + T_{U(A,D)\text{old}}}, \end{aligned} \quad (4)$$

where $P_{\text{init}} \times C \in (0, 1]$ is the initialization constant and $C > 1$ is the influence factor of the connection time on the delivery probability value. When two nodes have not met for a long time or two nodes frequently meet a certain node, the two-dimensional table of probability values is updated according to (2) and (3).

Through the process of updating, attenuating, and transmitting the expected value of message delivery, each node dynamically maintains its own message delivery expectation table.

The forwarding strategy in the improved PPT routing algorithm is the same as the original algorithm. One method is to set a fixed value first and forward the message to the node that delivers the expected value greater than the fixed value. Another method is to forward the message to a node whose delivery expected value is greater than the current node's delivery expected value.

If it is assumed that, at this time, only the probability value $P_{(B,G)}$ of node B meeting node G is greater than the probability value $P_{(A,G)}$ of node A meeting node G, then only

Table 1: Two-dimensional table of probability maintained by nodes.

Current node	Destination node	Probability value of historical message delivery	Node's historical encounter duration	Node's historical disconnection duration
A	B	$P_{(A,B)old}$	$T_{(A,B)old}$	$T_{U(A,B)old}$
A	C	$P_{(A,C)old}$	$T_{(A,C)old}$	$T_{U(A,C)old}$
A	D	$P_{(A,D)old}$	$T_{(A,D)old}$	$T_{U(A,D)old}$

a copy of the message will be distributed to node B, and other nodes within the transmission range of node A will be ignored. When a message is distributed, an intermediate node will only receive a copy of the message and enter the waiting state after all the messages are distributed. Compared with the dichotomy SNW routing distribution, this method takes longer to distribute the message and increases the delay of the message distribution. In order to effectively solve this problem, an improved routing algorithm based on probability-PSN is proposed as follows.

In SNW routing, in the message dissemination stage, when the node carrying a copy of the message only passes the copy of the message to the node with a higher probability of delivery than itself, the node may not find a node that can distribute the copy of the message when the life cycle of the carried message expires. If this situation is encountered, the message will not be delivered to the destination node. With this method of dissemination, the node needs to find N nodes with a higher delivery probability than itself, so it takes longer to end the dissemination phase, which increases the delay of message delivery. In order to effectively make up for the shortcomings of the above algorithms, in the dissemination stage, the dissemination node strategy will be improved. The improved algorithm no longer only distributes the nodes whose expected value is higher than itself. Instead, it calculates the number of copies of the message distributed to each node based on the probability of each node's message delivery.

Each node in the DTN maintains a two-dimensional table to record the probability value of the node meeting other nodes in the network, that is, the expected value of message delivery. As the nodes move, the topology of the network will change, and the probability of any two nodes meeting will also change. The calculation of probability is based on (2)–(4). In the message dissemination stage, the situation of each node distributing a copy of the message should be determined according to the expected value of each node's message delivery. Nodes with a higher expected value of message delivery will distribute more copies of the message. Nodes with lower message delivery expectations distribute fewer copies of messages or do not distribute copies of messages. The calculation method of the number of message copies distributed by the node is shown in the following formula:

$$N(i) = \begin{cases} \left\lfloor \dfrac{P(i,d)}{\sum_{j=1}^{n} P(j,d) + P(R,d)} \times M \right\rfloor & \dfrac{P(i,d)}{\sum_{j=1}^{n} P(j,d) + P(R,d)} \times M > 1 \\ 1 & \text{other} \end{cases} \tag{5}$$

Node R carries a copy of the message, and its probability of meeting the destination node D is $P(R, d)$. Within the transmission range of the node R, there are n nodes that do not carry a copy of the message. At this time, the node R needs to distribute the copy of the message it carries. We assume that i is any node that meets node R, and P(i,d) is the probability of node i meeting the destination node, that is, the message delivery probability of node i. After calculation, N(i) is the number of message copies forwarded by node i. After the dissemination ends, the message copies carried by the node R are reduced.

$$N(R)_{\text{new}} = N(R)_{\text{old}} - \sum_{j=1}^{n} N(j). \tag{6}$$

Node A carries 20 copies of the message. Before distributing the copy of the message, each node in the network first updates the probability table of encounters with other nodes in the network that it maintains. At this time, we assume that the destination node is D. After calculating the probability values by (1)–(3), the delivery probability values $P_{(B,D)} = 0.85$ and $P_{(C,D)} = 0.35$ at which node B and node C will deliver the message to node D are obtained. Through the probability table maintained by node A, the probability value $P_{(A,D)} = 0.4$ of node A and node D meeting can also be obtained. At this time, the encounter probability of all nodes that do not carry a copy of the message within the transmission range of node A and the destination node is calculated. The number of message copies distributed to each

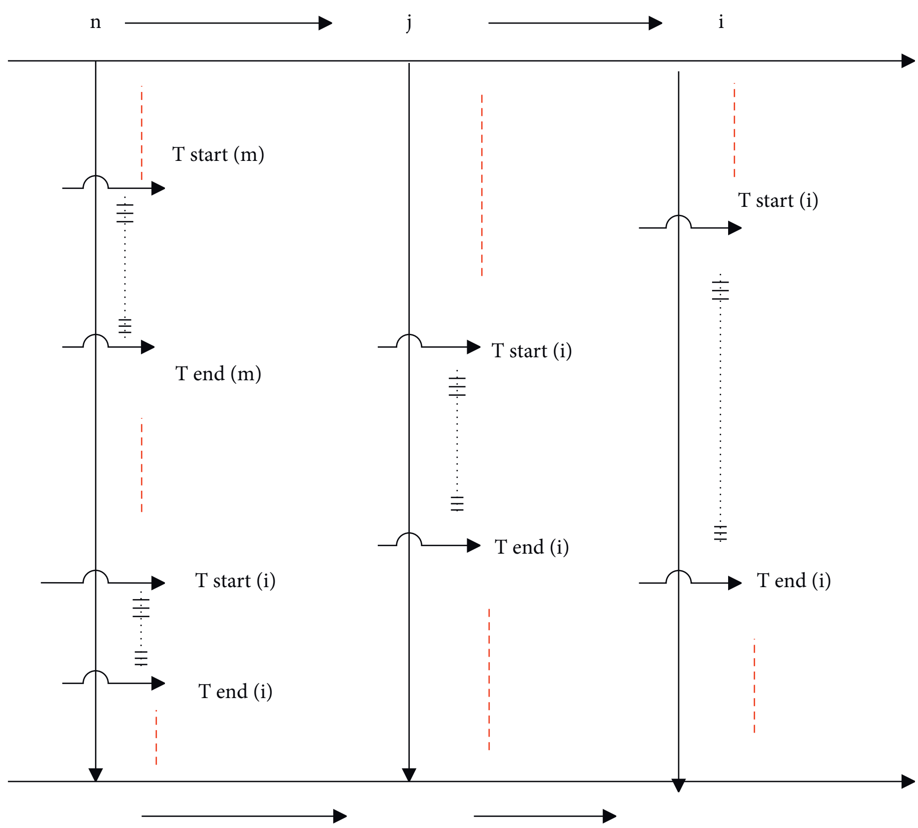

Figure 7: Schematic diagram of node connection time.

node is determined according to the probability of each node meeting the destination node. The result calculated by (4) is as follows:

$$\begin{aligned} N(B) &= \left\lfloor \frac{P_{(B,D)}}{P_{(B,D)} + P_{(A,D)} + P_{(C,D)}} \times M \right\rfloor = 10, \\ N(C) &= \left\lfloor \frac{P_{(C,D)}}{P_{(A,D)} + P_{(B,D)} + P_{(C,D)}} \times M \right\rfloor = 4, \\ N(A) &= M - N(B) - N(C) = 10 - 10 - 4 = 6. \end{aligned} \tag{7}$$

Among them, N(B) and N(C) are the number of message copies distributed by node B and node C, respectively. N(4) is the number of message copies carried by node A after it distributes a message to nodes within its transmission range. Both N(B) and N(C) are the values rounded down after calculation. When this method is used for calculation, it always distributes more copies of the message to the node with the highest probability of encountering the destination node. Compared with simple probability-based SNW routing, it not only reduces the time required for message dissemination, but also avoids the node's discarding of message copies in the dissemination phase due to the end of the life cycle. The node that encounters the destination node more carries more copies of the message, which can increase the success rate of message delivery and reduce the delay of message delivery.

When a message is distributed, a node in the network can receive copies of the same message distributed by multiple nodes at the same time, but at this time it is stipulated that a node can only receive a copy of a message from one node, so it needs to select the node that sends the copy of the message. In addition, if a node already carries a copy of the message, it will no longer receive a copy of the message from the node.

Figure 7 is a schematic diagram of the connection time between a node and n nodes, which shows the connection time for each node to be connected m times.

4. Design System of Mathematics Teaching Plan Based on Big Data Technology

According to the needs of mathematics teaching and management, the functional structure of this system is divided into mathematics teaching subsystem and management subsystem. The structure is shown in Figure 8.

The student user operation process is shown in Figure 9.

As a network mathematics teaching system, the content of curriculum mathematics teaching is mainly the electronic courseware of each chapter in the class, including knowledge key points, introductions to difficult points, and analysis of typical examples, as well as mathematics teaching reference materials and curriculum mathematics syllabus content information. The course learning module will display knowledge points by navigating through chapters in sequence. This module will be implemented using hypertext technology for static pages. Hypertext is a method of

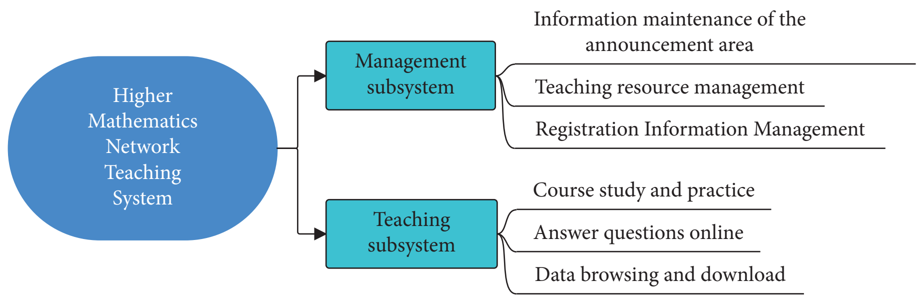

Figure 8: System function structure diagram.

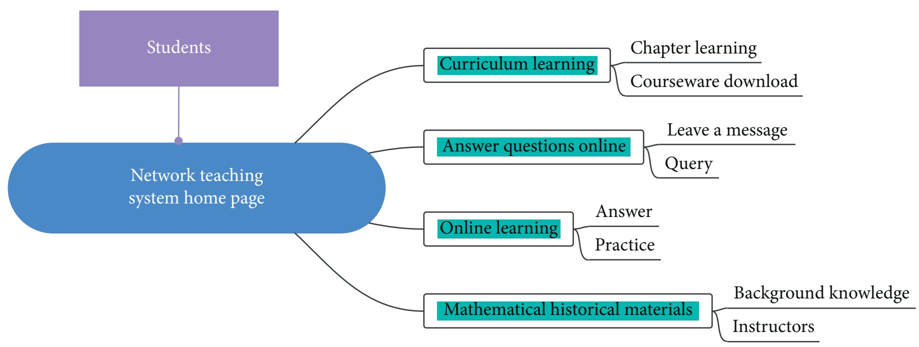

Figure 9: Flow chart of student user operation.

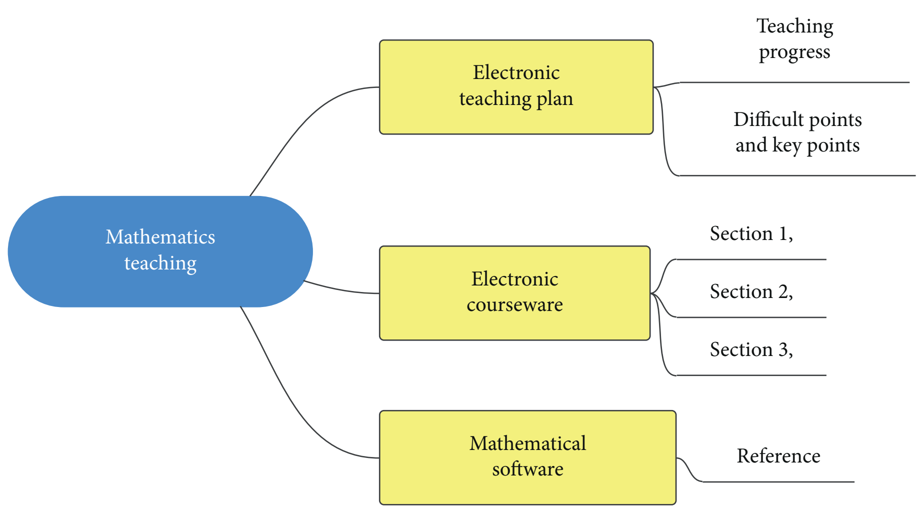

Figure 10: The structure diagram of the math teaching page.

information management, which stores data or information in nodes, and the nodes are connected by chains into a network structure. The node is the basic unit for storing data or information. It can be text, image, graphics, sound, video, source program, etc. The chain is the main way to connect each node. It is a pointer from each node to other nodes, or from other nodes to the node. Each node is connected by a chain into a network structure, and students can enter each node along the chain, as shown in Figure 10.

Online Q&A is mainly used to help students answer the questions they encounter in their studies. Students can ask questions to teachers through the message board. Teachers can use e-mail to give one-to-one or use online posting to give one-to-many answers to students. The online Q&A data flow is shown in Figure 11.

The database is the cornerstone of the entire system. It organizes a large amount of data in the information system according to a certain model and provides the functions of storing, maintaining, and retrieving data, so that the information system can easily, timely, and accurately obtain the required information from the database. The key to whether the various parts of an information system can be closely integrated and how to integrate them lies in the database. Only a reasonable logical design and effective physical design of the database can develop a comprehensive and efficient information system. Database design is an

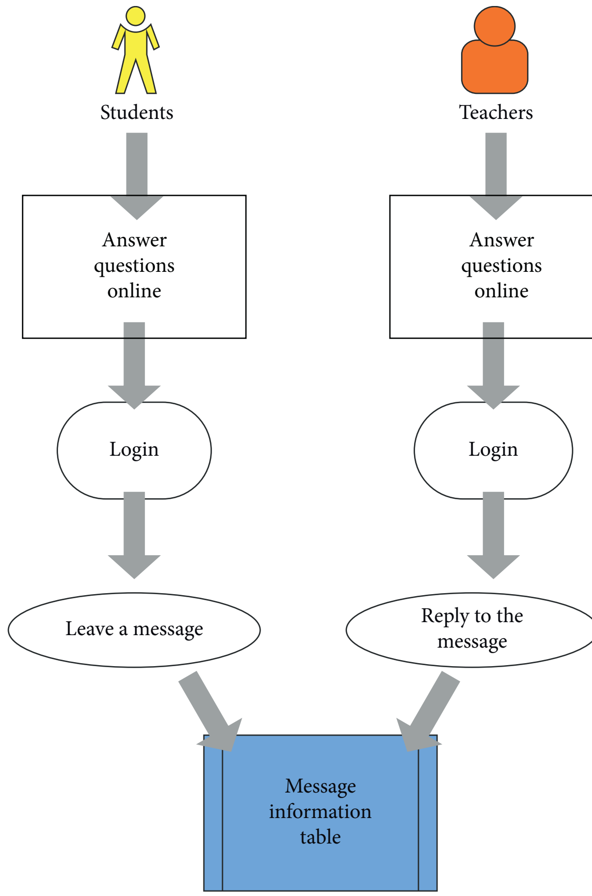

Figure 11: Data flow diagram of online Q&A.

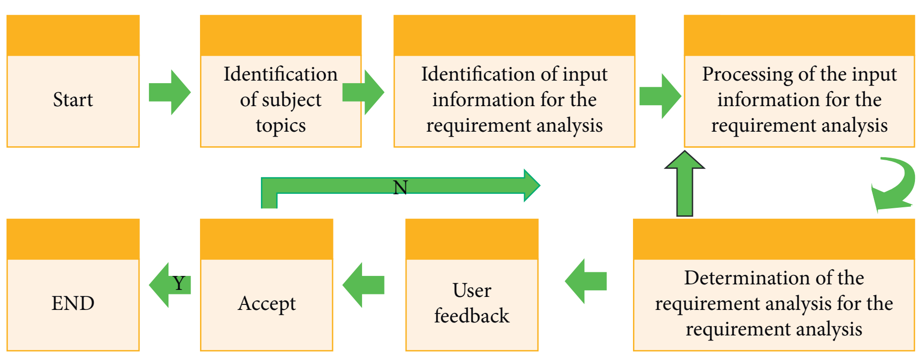

Figure 12: Work flow chart of demand analysis.

important part of information system development and construction, as shown in Figure 12.

After constructing the above model, the model is verified, and the actual situation is analyzed to verify the performance of the mathematics teaching system constructed in this paper. This article evaluates the system's mathematics knowledge recommendation, teaching plan, and teaching effect, and the results are presented in Table 2 and Figure 13.

From the above research, it can be seen that the mathematics teaching plan design system based on big data technology constructed in this paper has good practical effects. On this basis, the system of this paper can be verified through further practice.

Table 2: Design effect of mathematics teaching plan based on big data technology.

Number	Knowledge recommendation	Teaching plan	Teaching effect
1	94.70	89.26	92.21
2	96.78	94.35	90.71
3	96.50	93.79	87.02
4	94.98	91.71	91.56
5	91.02	94.64	92.13
6	94.34	92.41	86.84
7	95.61	94.23	88.72
8	91.29	91.81	93.31
9	92.42	89.35	88.46
10	96.12	88.75	88.18
11	92.08	91.85	92.11
12	96.45	94.37	92.03
13	93.79	90.07	92.60
14	96.79	90.40	87.61
15	92.48	94.82	89.02
16	95.12	91.59	87.54
17	93.07	91.26	93.12
18	92.97	93.38	91.03
19	95.03	89.67	88.04
20	93.83	92.32	88.40
21	94.91	92.76	92.07
22	93.31	91.27	88.86
23	95.67	91.80	87.08
24	94.23	93.48	93.75
25	96.72	92.77	90.22
26	95.25	89.05	89.76
27	91.15	89.57	93.57
28	93.27	94.25	92.71
29	91.39	92.92	89.93
30	95.08	91.80	87.82
31	93.70	90.22	89.69
32	96.26	88.57	87.21
33	96.54	91.89	93.94
34	94.13	94.89	92.17
35	95.79	94.44	91.64
36	94.59	92.66	87.89
37	94.49	94.64	87.11
38	91.24	93.34	90.36
39	92.85	91.42	91.43
40	96.39	91.85	90.27

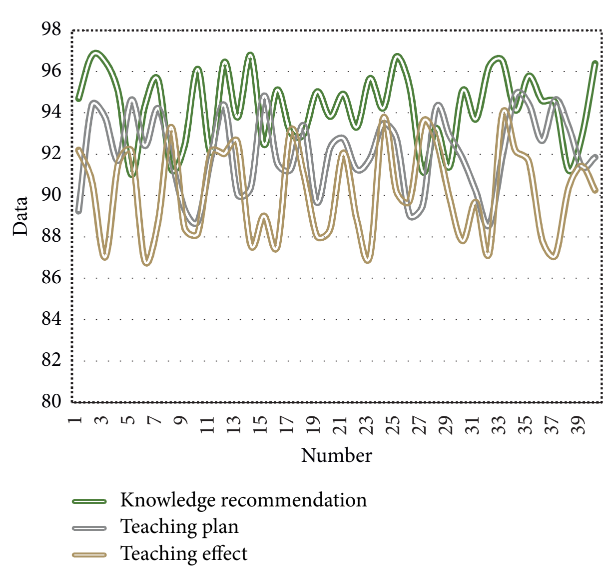

Figure 13: Statistical results of system performance.

5. Conclusion

Accurate teaching in the era of big data is of great significance for advancing the realization of modern education, individualized learning, intelligent environment, and intelligent management. Accurate teaching in the era of big data requires meticulous characterization of student characteristics and behaviors, accurate summarization of the teaching process and teaching rules, and a clear description of the specific implementation of the teaching plan. Moreover, the realization of precision teaching in the era of big data is inseparable from the in-depth analysis and mining of big data in education. Data-driven support for education and teaching decision-making is the main feature of precision teaching in the era of big data. In addition, by constructing a mathematical model, the relationship between the variables in the education process can be portrayed, and the formulation methods of precise teaching plans can be derived from it, which provides support for the realization of precise teaching. Therefore, to achieve accurate teaching in the era of big data, it is essential to construct a suitable mathematical model. This article applies big data technology to the design of mathematics teaching plan, designs a mathematics teaching plan design system based on big data, and verifies the system of this paper with experiments. The test results verify the reliability of this system.

Data Availability

The labeled dataset used to support the findings of this study is available from the author upon request.

Conflicts of Interest

The author declares no conflicts of interest.

Acknowledgments

This study was sponsored by Xuancheng Vocational and Technical College.

References

[1] R. Nunes Linhares, C. Mário Guimarães Alcântara, E. Ávila Gonçalves, F. Ramos, and M. José Loureiro, "Teaching evaluation by teachers from Brazil and Portugal: a comparative analysis," *American Journal of Educational Research*, vol. 5, no. 5, pp. 546–551, 2017.

[2] N. Huang, "Analysis and design of university teaching evaluation system based on JSP platform," *International Journal of Education and Management Engineering*, vol. 7, no. 3, pp. 43–50, 2017.

[3] J. A. Moreno-Murcia, Y. Silveira Torregrosa, and N. Belando Pedreño, "Questionnaire evaluating teaching competencies in the university environment. Evaluation of teaching competencies in the university," *Journal of New Approaches in Educational Research*, vol. 4, no. 1, pp. 54–61, 2015.

[4] S. Liu, P. Chen, and P. Chen, "Research on fuzzy comprehensive evaluation in practice teaching assessment of computer majors," *International Journal of Modern Education and Computer Science*, vol. 7, no. 11, pp. 12–19, 2015.

[5] L. Zhou, H. Li, and K. Sun, "Teaching performance evaluation by means of a hierarchical multifactorial evaluation model based on type-2 fuzzy sets," *Applied Intelligence*, vol. 46, no. 1, pp. 1–11, 2016.

[6] J. Porozovs, L. Liepniece, and D. Voita, "Evaluation of the teaching methods used in secondary school biology lessons," *Journal of Pedagogy and Psychology "Signum Temporis"*, vol. 7, no. 1, pp. 60–66, 2015.

[7] M. A. Oliveros, A. García, and B. Valdez, "Evaluation of a teaching sequence regarding science, technology and society values in higher education," *Creative Education*, vol. 06, no. 16, pp. 1768–1775, 2015.

[8] M. Sánchez Cerón and F. María del Sagrario Corte Cruz, "The evaluation of teaching: some consequences for Latin America," *Revista Mexicana de Investigación Educativa*, vol. 20, no. 67, pp. 1233–1253, 2015.

[9] A. Li, K. Li, K. Li, and Z. Ge, "Application of data mining in the colleges' in-class teaching quality evaluation system," *Journal of Computers*, vol. 10, no. 3, pp. 166–175, 2015.

[10] K. Angell and E. Tewell, "Teaching and un-teaching source evaluation: questioning authority in information literacy instruction," *Comminfolit*, vol. 11, no. 1, pp. 95–121, 2017.

[11] M. Brkovic and P. Chiles, "'Spector - the sustainability inspector': participatory teaching, learning and evaluation game for architects, architecture students and pupils," *Facta Universitatis - Series: Architecture and Civil Engineering*, vol. 14, no. 1, pp. 1–20, 2016.

[12] T. H. Reisenwitz, "Student evaluation of teaching: an investigation of nonresponse bias in an online context," *Journal of Marketing Education*, vol. 38, no. 4, pp. 139–144, 2015.

[13] Y. Jiang and Y. Wang, "Evaluation of teaching quality of public physical education in colleges based on the fuzzy evaluation theory," *Journal of Computational and Theoretical Nanoscience*, vol. 13, no. 12, pp. 9848–9851, 2016.

[14] K. Royal, "A guide for making valid interpretations of student evaluation of teaching (SET) results," *Journal of Veterinary Medical Education*, vol. 44, no. 2, pp. 1–7, 2016.

[15] F. Garofalo, P. Mota-Moya, A. Munday, and S. Romy, "Total extraperitoneal hernia repair: residency teaching program and outcome evaluation," *World Journal of Surgery*, vol. 41, no. 1, pp. 100–105, 2017.

[16] G. Gong and S. Liu, "Consideration of evaluation of teaching at colleges," *Open Journal of Social Sciences*, vol. 04, no. 7, pp. 82–84, 2016.

[17] H. Zhao, "College physics teaching model design and evaluation research of students' seriousness," *The Open Cybernetics & Systemics Journal*, vol. 9, no. 1, pp. 2017–2020, 2015.

[18] N. D. Tran, "Reconceptualisation of approaches to teaching evaluation in higher education," *Issues in Educational Research*, vol. 25, no. 1, pp. 50–61, 2015.

[19] J. Mao, K. Lu, G. Li, and M. Yi, "Profiling users with tag networks in diffusion-based personalized recommendation," *Journal of Information Science*, vol. 42, no. 5, pp. 711–722, 2016.

[20] G. Costa and R. Ortale, "Model-based collaborative personalized recommendation on signed social rating networks," *ACM Transactions on Internet Technology*, vol. 16, no. 3, pp. 1–21, 2016.

Hindawi
Scientific Programming
Volume 2021, Article ID 6903255, 10 pages
https://doi.org/10.1155/2021/6903255

Research Article

Analysis and Influence of Media Degradation Image Propagation Path Based on Image Vision

Yujia Lin [1] and Xin Wang [2]

[1]School of Journalism and Communication, Sichuan International Studies University, Chongqing 400031, China
[2]School of Journalism and Communication, Shih Hsin University, Taipei 116, China

Correspondence should be addressed to Xin Wang; d109810013@live.shu.edu.tw

Received 24 September 2021; Revised 1 November 2021; Accepted 3 November 2021; Published 23 November 2021

Academic Editor: Le Sun

With the rapid development of the information age, the efficiency of image information dissemination has been improved and the way of information dissemination has gradually moved from text information to image information. In the process of using equipment to take pictures, because of some objective reasons, the images taken are different from the ideal images taken by the equipment, so the interference brought by these objective factors to the images is eliminated, thus presenting a more realistic image process. In the process of network propagation, degraded images show different characteristics in the network. In the process of propagation, images degenerate again, which makes it difficult for images to be authentic or restored. In this paper, an SIR model is selected from three classical infectious disease models to simulate and reflect the propagation path and influence of degraded images and the influence of degraded images on propagation is evaluated by extracting the moderate and degree distribution of undirected network. In addition, the distribution and integration between nodes are evaluated to distinguish the average road sources. Based on the SIR propagation model, a propagation model of information timeliness is constructed. By describing the update of subjective attitude values of nodes and then defining the probability function of state transition between different nodes, the model has higher fitting and adaptability. Finally, using BA, WS, Facebook, and Sina Weibo as the base map and setting the network environment parameters, based on the SIR model, the propagation of degraded images in different network environments is analyzed and the influence results of degraded images in network propagation are obtained.

1. Introduction

With the rapid development of the information age, image information has become an important source of information. In the last century, the main media of information dissemination still stayed in words and information was basically obtained from words. Until the popularity of modern television and the slow establishment of the Internet, people's quality of life and ways have changed greatly with the development, which affects the way of information acquisition. Now, people are more willing to obtain useful and relevant information from images and often spread the information in the form of images. It is very efficient and rapid for the visual propagation of images on the network. The study in [1] mentioned the segmentation of superpixel images, which will increase a series of complexity for the flow of superpixel images in the network. Previous studies often focus on deblurring of degraded images, such as the data-driven method proposed by Li et al. [2] to remove the blurring of images and Pan et al. [3] and others using dark channels to process degraded images. In fact, degraded images can interact with low resolution (LR) and high resolution (HR) to achieve better propagation effect on the network, as mentioned in [4].

The main way of image dissemination is to rely on the network, and the information in online social networks reflects social hotspots, influence, and other factors [5]. Bae and Lee's [6] content analysis of the 13 most influential tweets mentioned by more than 3 million users of Twitter can judge the emotional impact of these messages on users. Not only Bae but also Xiong et al. [7] established an emotional independent cascade model and analyzed the mode and influence of social networks in emotional transmission. Mei et al. [8] help enterprises and governments standardize public opinion by extracting information from online social networks. Yi et al. [9] propose a social connection strength model to verify the importance of information in social connections. The study in [10] describes the propagation characteristics of sudden information on the Internet from the perspective of information entropy. The propagation of image information in the network is also similar to the social network information propagation model. In order to deeply understand the propagation path and influence of image information in the social network, it is necessary to establish a feedback model [11]. Liu et al. [12] established an information model NFSIR (negative feedback susceptible to infection) which introduces attenuation parameters and noise figure to study the information feedback brought by images. Most models are based on the incidence of infectious diseases. For example, a susceptibility-infection-elimination (SIR) model is established based on the classical susceptibility-infection-hibernation-elimination (SIHR) model mentioned in [13] to describe the transmission probability of images. The study in [14] analyzes influential nodes through the SIR model based on the community mediator. Both Granell et al. [15] and Melesse and Gumel [16] are based on epidemic propagation models. The former uses microscopic Markov chain to analyze the probability of information propagation, while the latter uses Lyapunov function to analyze the equilibrium point and stability. The research work on degraded images is insufficient, and the research on degraded images only focuses on the restoration of related algorithms and technologies but does not pay attention to the problem of propagation in the network. There is no comparison in various network environments. The method proposed in this paper simulates the propagation analysis of images in different network environments.

This paper analyzes the epidemic propagation model, simulates a degraded image, puts the image in four preset network environments, and analyzes its propagation path and influence in four different network environments.

2. Degraded Images and Related Theories of Image Propagation

2.1. Overview of Degraded Images. Compared with high-definition images, degraded images are low-resolution images produced by various disturbances. There are many reasons for image degradation, such as camera shaking, shooting object moving, out of focus, and so on, which will cause image blurring. Different pixels will also be lost in the process of network propagation. The propagation of images in the network is also led by degraded images.

2.2. Overview of Image Propagation and Related Models. Picture dissemination refers to the interactive flow of information and the support of pictures. The way of image transmission has changed greatly in the ever-changing society. The advent of new social media has connected everyone. Everyone has a good understanding of the characteristics of images, and the participation of image dissemination process is stronger, which enables images in online social networks to spread to millions of users in a short time [17]. However, the image will be distorted and the image pixel will be reduced after countless times of transmission. In order to explore these problems and the path of image propagation, researchers have carried out a lot of related research around image propagation, including image propagation modeling, image influence, popularity prediction, image traceability and other image propagation models, which can be divided into two categories: prediction model and interpretation model [18]. Prediction models mainly include independent cascade model and linear threshold (LT) model. The information cascade model is that an activated node deactivates the surrounding inactive nodes with a certain probability. The linear threshold model is used in the process of image propagation modeling. Image propagation, information propagation, and epidemic propagation models have high similarity. Therefore, the image disseminator and receiver can be divided into three categories: Susceptible state (S), which means that the image information has not been received, but there will be a great probability to spread the image after receiving the information. Secondly, the infection state (S) means that the image has been received and will be transmitted again. Finally, the immune state (R) means that no matter whether the image has been accepted or not, the image will not be propagated next time. The combination of the three states can be summarized into three common models.

2.2.1. SI Model. Susceptible S nodes and infected I nodes are combined into the SI model. The transition of these two nodes happens from susceptible node S to infected node I with an average probability of λ, which is a special feature of the model. That is, susceptible nodes will remain infected after being converted to infected nodes, as shown in Figure 1.

The proportion of susceptible node S is expressed as $S(t)$, and infected node I is expressed as $I(t)$ as follows:

$$\begin{cases} \dfrac{dS(t)}{dt} = -\lambda I(t)S(t), \\[2ex] \dfrac{dI(t)}{dt} = \lambda I(t)S(t). \end{cases} \tag{1}$$

The higher the λ value, the higher the probability of node infection and the faster the propagation speed.

2.2.2. SIS Model. The susceptible state S and infection state I are combined into the SIS model, and the probability of S node transforming into I node is λ. The sensed I node will be transformed into S node again with probability μ. The transmission process of influenza virus is similar to it [19], as shown in Figure 2.

The proportion of S nodes and I nodes is expressed by $S(t)$ and $I(t)$, as follows:

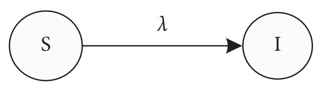

FIGURE 1: Node state transition diagram of the SI model.

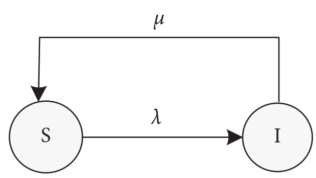

FIGURE 2: Node state transition diagram of the SIS model.

$$\begin{cases} \dfrac{dS(t)}{dt} = -\lambda I(t)S(t), \\ \\ \dfrac{dI(t)}{dt} = \lambda I(t)(t) - \mu I(t), \\ \\ S(t) + I(t) = 1. \end{cases} \tag{2}$$

2.2.3. SIR Model. The SIR model is based on the SI model and has a new immune state R, from sensing node infection probability λ and node infection probability μ to immune state, and this immune state will not return to infection state. This process is similar to smallpox and chickenpox, which will produce antibodies to immunize against similar viruses after being cured [20], and its state transition diagram is shown in Figure 3.

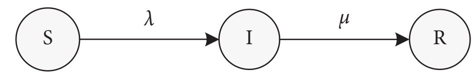

FIGURE 3: Node state transition diagram of the SIR model.

The S-I-R transformation condition is that the image or similar image has been received before. Because of the characteristics of the network environment, the nodes in the network will have the probability to receive the same image information again. When this happens, the nodes will no longer spread the image information.

$S(t)$, $I(t)$, and $R(t)$ can be used to represent the differential of the proportion of susceptible nodes, infected nodes, and immune nodes, respectively, as follows:

$$\begin{cases} \dfrac{dS(t)}{dt} = -\lambda I(t)S(t), \\ \\ \dfrac{dI(t)}{dt} = \lambda I(t)S(t) - \mu I(t), \\ \\ \dfrac{dR(t)}{dt} = \mu I(t), \\ \\ S(t) + I(t) = 1. \end{cases} \tag{3}$$

3. Image Propagation Network Analysis

3.1. Using Statistical Characteristics to Describe the Structural Characteristics of the Image Propagation Network. In order to better analyze the image propagation network, we can effectively describe the structural characteristics of image propagation network with the help of statistical features. In this study, the following commonly used statistical features are mainly used.

3.1.1. Degree and Degree Distribution. Degree is described as an important attribute node and an important statistical characteristic in the network. In an undirected network [21], the degree K_i of node i is the number of edges connecting node i. Network average $< k >$ refers to the average of all nodes in the network. The degree on the node can be divided into outgoing and incoming according to the characteristics of the degree, and the sum of the degree is the sum of the two divided degrees. For nodes that exist in degrees, the two degrees divided into out and in can be converted into outer joints and inner joints. The specific expression is as follows:

$$K_i^{\text{out}} = \sum_{j=1}^{N} a_{ij}, \tag{4}$$

$$K_i^{\text{in}} = \sum_{j=1}^{N} a_{ji}. \tag{5}$$

3.1.2. Average Path Length. The shortest path is the one with the least number of connected edges between nodes. The distance between two points is the number of sides on the shortest path. The average distance of degraded image propagation in the network can usually be expressed by L, that is, the average path length value. The analysis of the characteristics of existing networks can often be measured by the convergence and dispersion of their separated states. The specific expression is as follows:

$$L = \frac{1}{1/2N(N-1)} \sum_{a \geq b} d_{ab}. \tag{6}$$

3.1.3. Aggregation Coefficient. The aggregation coefficient refers to the ratio of edges to the number of adjacent nodes. Through the uniform distribution of the aggregation coefficient, the local characteristics of the network can be reflected [22]. The coefficients in real networks are often higher than those in random networks, and nodes gather into clusters in social networks. The clustering coefficient of node i is expressed as follows:

$$C_i = \frac{E_i}{(K_i(K-1))/2} = \frac{2E_i}{K_i(K-1)}, \tag{7}$$

where K_i is the degree of node i and E_i is the number of connected edges between neighboring nodes of node i. Users can discuss the distribution system of each node in the network. Propagating the connection between nodes is like the communication of information between users, and information is only connected along nodes. Assuming that a propagation node j in the network propagates a message to node i at time $t+1$ and the attitude values of node j and node i at time t are $S_t^j$and S_t^i, then according to the non-Bayesian social learning method, the degree value of node i is updated as shown in

$$S_{t+1}^i = S_t^i + \left(S_t^j - S_t^i\right)\phi(i, j). \tag{8}$$

If there are n propagation nodes $j_1, j_2, \ldots, j_n$ propagating information to node i at time $t+1$ and the state value of the propagation node at time t is $S_t^{j_1}, S_t^{j_2} \ldots S_t^{j_n}$, then the value of node i is updated as shown in

$$S_{t+1}^i = S_t^i + \frac{1}{n}\sum_{j_n \in T(i)}^{n} \left(S_t^{j_n} - S_t^i\right)\phi(i, j), \tag{9}$$

where $T(i) = \{j_1, j_2, \ldots, j_n\}$ denotes the set of nodes that propagate information to node i and $\phi(i, j) \in [0, 1]$ denotes node j's influence of attitude value on node i. If node i makes the time T unknown and the attitude value is 3, the propagating node J propagates the message to node i at the time $t+1$; then, node i changes from unknown to propagating the probability calculation of the broadcast node as shown in

$$p_{st}^i = S_{t+1}^i + \left(1 - S_{t+1}^i\right)v_0. \tag{10}$$

The influence of $\phi(i, j) \in [0, 1]$ at node j is brought into the following formula:

$$p_{st}^i = \left(S_t^i + \left(S_t^j - S_t^i\right)\phi(i, j) + \left[1 - \left(S_t^i + \left(S_t^j - S_t^i\right)\phi(i, j)\right]v_0, \tag{11}$$

where S_t^j represents the attitude value of the node under the influence of propagation node j at time $t+1$, $v_0 \in [0, 1]$ represents the value of information, and the value represents the quality of information. $(1 - S_{t+1}^i)v_0$ is used for node transfer. The probability p_{sc} of node i changing from the eunknown state to informed state is calculated as follows:

$$p_{sc} = 1 - p_{si}. \tag{12}$$

When $(1 - S_{t+1}^i)v_0$ is brought into the node state i, it can be expressed as the following formula:

$$p_{sc} = 1 - \left\{\left(S_t^i + \left(S_t^j - S_t^i\right)\phi(i, j) + \left[1 + \left(\left(S_t^i + \left(S_t^j - S_t^i\right)\phi(i, j)\right]\right\}. \tag{13}$$

If node i is in an informed state at time t, considering the social reinforcement effect [23], the user will continuously receive the same information from neighboring nodes for many times in a period of time. The benefit value generated in the propagation node with a strong social influence is recorded as the propagation probabilityp_{ci}, which is calculated as shown in

$$p_{ci} = 1 - (1 - p_{si})e^{-b(n-1)}. \tag{14}$$

Putting p_{si} into node state i can be expressed as

$$p_{ci} = 1 - \left\{1 - \left[S_{t+1}^i + \left(1 - S_{t+1}^i\right)v_0\right]\right\}e^{-b(n-1)}. \tag{15}$$

Here, b represents the degree of social reinforcement and n represents the cumulative number of times that node i received information at time $t+1$. For an informed node that has not been exposed to the information again for a long time and thinks that the informed node has forgotten the information as time goes by, there is no longer possibility of spreading information, and then, it is transformed into an immune node, and its transformation probability is calculated as follows:

$$p_{cr} = 1 - p_{ci}. \tag{16}$$

If node i is a propagator at time t, then p_{ii} is the probability that node i remains propagated at time $t+1$ and p_{ri} is the probability that node i becomes an immune node at time $t+1$. The probability of node i maintaining the propagation state at time $t+1$ under the influence of adjacent nodes is calculated as follows:

$$p_{ii} = S_{t+1}^i - S_{t+1}^i\beta, \tag{17}$$

where β is the aging rate of information and $S_{t+1}^i\beta$ refers to the role played by the aging rate of information in the process of state transition. In the propagation process, if node i comes into contact with the immune node at time $t+1$, it becomes an immune node with a probability of β. Then, the probability of keeping the propagation state is $1-\beta$. If there are n propagation nodes and m immune nodes in the neighbor node, the probability of the node remaining in the propagation state is calculated as follows:

$$p_{ii} = \prod_{j_n \in T(i)} \left(S_{t+1}^i - S_{t+1}^i\beta\right) \cdot (1-\beta)^m. \tag{18}$$

The probability that the propagation node i becomes an immune node is calculated as follows:

$$p_{ir} = 1 - p_{ii}. \tag{19}$$

The probability of p_{ii} changing from a propagating node to an immune node is expressed by the following equation:

$$p_{ir} = 1 - \prod_{j_n \in T(i)} \left[\left(S_{t+1}^i - S_{t+1}^i\beta\right)\phi(i, j_n)\right)\right] \cdot (1-\beta)^{m+n}. \tag{20}$$

On the Internet, all information follows the product principle and goes through the dissemination boom until the decline law disappears. Therefore, a message will not spread indefinitely [23]. Degenerated images will change state with nodes in the process of transmission. When they reach the immune state, they will gradually exit from the propagation state. When there are no propagation nodes in the network, the whole propagation process ends. Figure 4 shows the propagation process of information timeliness changing with time.

The trend of the whole time change, that is, the image in social network from initial state to declining state, can be roughly summarized into three sections, in which the initial period is from point A to point B, the peak period is from point B to point C, and the falling period is from point C to

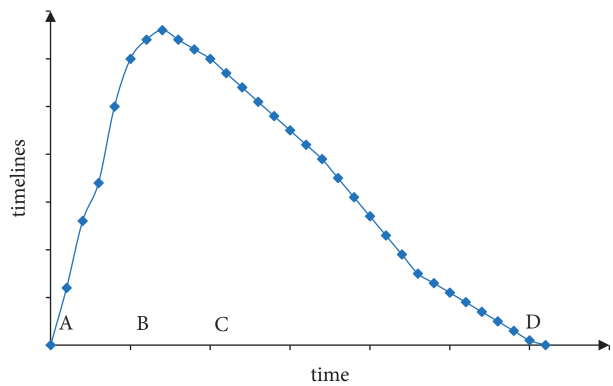

Figure 4: Graph of information timeliness change.

point D. The peak value can be understood as the theoretical upper limit of propagation in the current network, that is, the maximum number of infected nodes. The change rule of the degraded image can be clearly seen as a conic structure, and the three-stage pattern can be briefly understood as climbing in the initial period, reaching the maximum in the peak period and falling in the trough period, and finally approaching zero. Usually, the initial dissemination period of social network information is much shorter than the recession period [24]. The probability calculation of transforming a propagation node into an immune node considering the timeliness of information is as follows:

$$p_{ir} = S_t^i - S_t^i e^{-\lambda(t-t_s)} = S_t^i\left(1 - e^{-\lambda(t-t_s)}\right), \tag{21}$$

where $e^{-\lambda(t-t_s)}$ represents the timeliness of information in social networks at the current moment. λ denotes the information aging coefficient. In the network, when information is transmitted, the state of system users changes dynamically with time. The model is constructed on the basis of differential equations, in which four nodes and propagation probability have been proposed above, and the state transition mechanism is described as shown in Figure 5.

The information propagation rule in the SIR model can be described as that after a propagation source j publishes a message, its neighbor nodes first come into contact with the message and if they think that the message has propagation value, they will forward comments to more people with probability p_{si}. Otherwise, you will be transformed into an insider with a probability of p_{sc}. The probability that users will spread information only once is very limited. Considering the social reinforcement effect [25], in the process of information dissemination, similar information from neighbor communication nodes will be received many times. The probability of informed users spreading information will increase and become a communicator with a probability of p_{cr} or just for simple browsing. After a period of time, it gradually forgets to become immune with probability p_{cr} and the information is widely spread or loses its attraction after the upsurge, which no longer has communication value and gradually withdraws from people's field of vision and changes into immune with probability p_{ir}, after which the information will no longer be spread in any form.

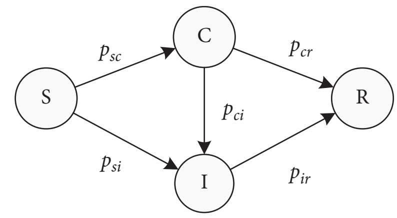

Figure 5: Node state transition diagram.

4. Experimental Simulation Analysis

4.1. Data Preparation

4.1.1. Data Background. Firstly, a degraded image is prepared as the material of the model experiment. The degraded image refers to the pixel size of the popular network image, and the pixel distribution of the degraded image size is shown in Table 1.

According to the distribution ratio in Table 1, the original image with a pixel size of 1920×1080 is selected as the experimental target as shown in Figure 6.

Then, the degradation image required by the experiment is obtained by degrading the image in Figure 6 as shown in Figure 7.

We use PyCharm to build python running environment, the NetworkX toolkit to generate BA scale-free network and WS small-world network, and use Sina and Facebook networks to simulate the SIR model. Specific network parameters are shown in Table 2.

In order to verify the effectiveness of this model, simulation experiments are carried out in different network environments and the changes of each node in the network with time are analyzed. Through the conclusions of Table 1 for the network environment for the real image propagation simulation, Table 2 is also a simulation environment and the purpose of the experimental environment and the real image propagation network environment is highly similar.

The degree $<k>$ of nodes exists in the homogeneous network, β refers to the probability of the susceptible body transforming into an infected body, γ refers to the probability of the infected body transforming into a susceptible body, and the effective transmission rate is λ:

$$\lambda = \frac{\beta}{\gamma}. \tag{22}$$

$p(t)$ denotes the density of infected individuals in the network at time t, and when the network size tends to ∞, it is determined by the average field theoretically available:

$$\frac{\partial p(t)}{\partial t} = -p(t) + \lambda\langle k\rangle p(t)[1 - p(t)]. \tag{23}$$

Formula (23) is equal to 0, and the steady-state density p of infected individuals is obtained:

$$p = \begin{cases} 0, & \lambda < \lambda_c, \\ \dfrac{\lambda - \lambda}{\lambda}, & \lambda \geq \lambda_c. \end{cases} \tag{24}$$

The propagation threshold is as follows:

Table 1: Picture pixel distribution proportion.

Pixel size	Baidu (%)	Weibo (%)	Facebook (%)
690×544	4	1	2
1024×576	14	6	9
1280×720	33	38	37
1600×900	8	5	4
1920×1080	36	43	44
2560×1080	5	7	4

Figure 6: Original image.

Figure 7: Degraded image after processing.

$$\lambda_c = \frac{1}{\langle k \rangle}. \quad (25)$$

When the critical value of infected individual size gradually decreases in the uniform network, the information will not spread in a large area. Affected by weak nodes, they quickly become infected people, resulting in a large amount of information dissemination. At the initial time, it is assumed that there are propagation nodes in the network and the rest are unknown nodes. Susceptible individuals are easily influenced by infected individuals and quickly become infected, resulting in a large amount of information dissemination. At the initial time, it is assumed that there is a propagation node in the network and the rest are all unknown nodes. Set the parameters as follows: $\lambda = 2$, $v_0 0.5$, $b = 0.2$, $\phi(i, j) = 0.5$, and $\beta = 0.1$. The degraded images are brought into the SIR model for simulation analysis. For three different states S, I, and R on the BA network and WS network, the state change curves of different nodes with time are obtained as shown in Figures 8 and 9.

According to the propagation curve of the network diagram in Figures 8 and 9, the propagation law of the network is basically the same as that of the SIR model. In the initial stage, some nodes enter the propagation mode. With the increase in propagation time, the number of propagation nodes also increases. In the stage of information explosion, the propagation nodes increase to the maximum and the decline speed of unknown nodes accelerates. After the propagation reaches the peak, the degraded image slowly goes downhill and the propagation node and unknown node tend to zero, while the immune node r is close to 1. The peak value of propagation node in BA network is around 5, while the peak value of propagation node in WS network is around 7, which indicates that the information propagation speed in BA network is faster than that in WS small-world network. For degraded images, the probability of being infected in four network environments under SIR model is shown in Figure 10.

For degraded images, the probability of infected persons in four network environments under SIR model is shown in Figure 11.

Through the analysis of Figures 10 and 11, in the simulated SIR model, the probability of network infection and nonstandard small-world network infection decreases rapidly with the extension of time and basically reaches the lowest level at 8 ms. However, XinLang and Facebook have a slower decline, and there is a probability that some people will be infected in the end. For infected nodes, XinLang and Facebook are both close to 1, indicating that degraded images will always spread to users' information circle over time in social networks. In the process of social network information dissemination, users' positive attitude will promote information dissemination, while negative attitude will inhibit information dissemination. In order to study the influence of user attitude on information dissemination, the initial user attitude is set to [−0.5, 0], [0, 0.5], and [0.5, 1] under the condition of keeping the above parameters unchanged. By analyzing Figure 12, it can be seen that the node model with positive attitude in the propagation process has faster propagation speed, wider propagation range, and shorter peak time than the node model with negative attitude.

The maximum speed of maximum infection rate (MIR) is to spread the network together with the number and proportion of nodes in the process of information dissemination, which can measure the influence of the whole network in the range of nodes. Figure 13 shows the changes

Table 2: Parameter settings.

Network name	Number of nodes	Average number of edges	Average	Degree correlation coefficient	Clustering coefficient
BA	2000	5991	3	−0.0758	0.02117
WS	2000	5100	2.5	−0.01472	0.26179
XinLang	4167	12954	2.4	−0.4271	0.07627
Facebook	8156	60603	7.1	−0.1464	0.3571

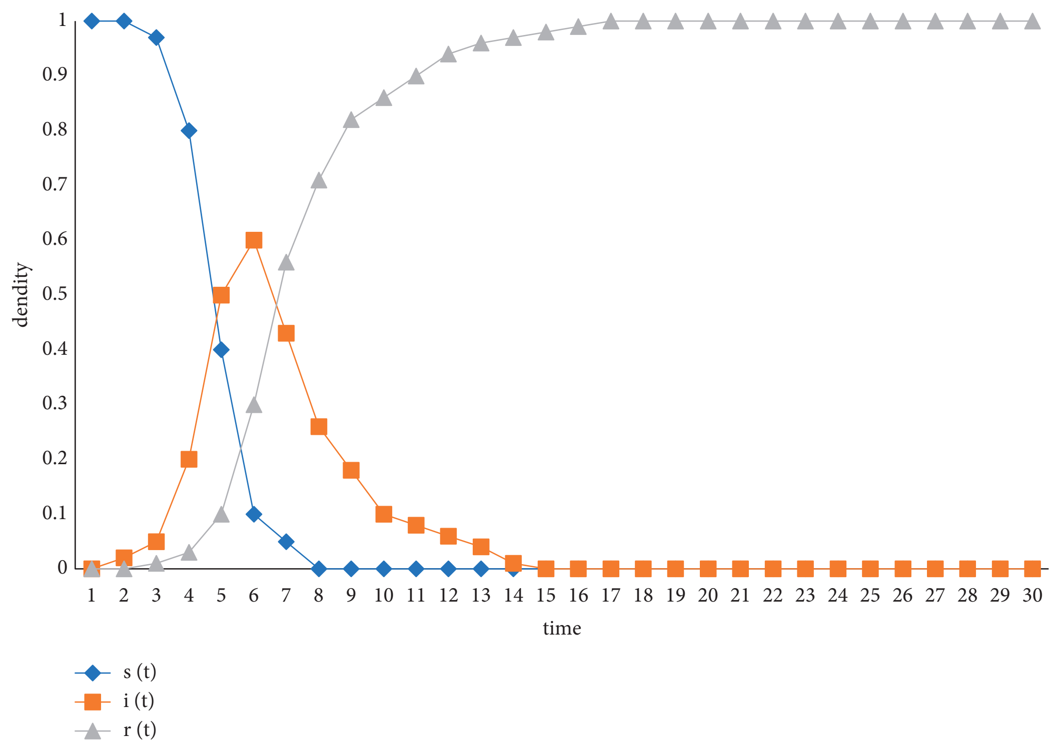

Figure 8: SIR model of the BA network.

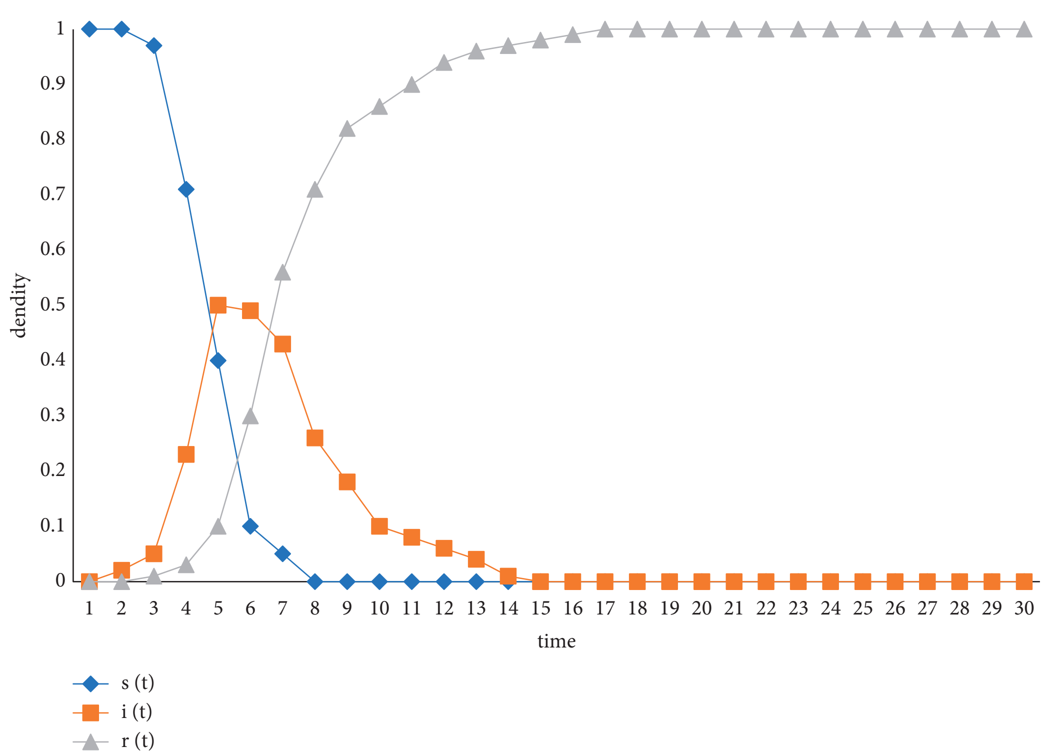

Figure 9: SIR model of the WS network.

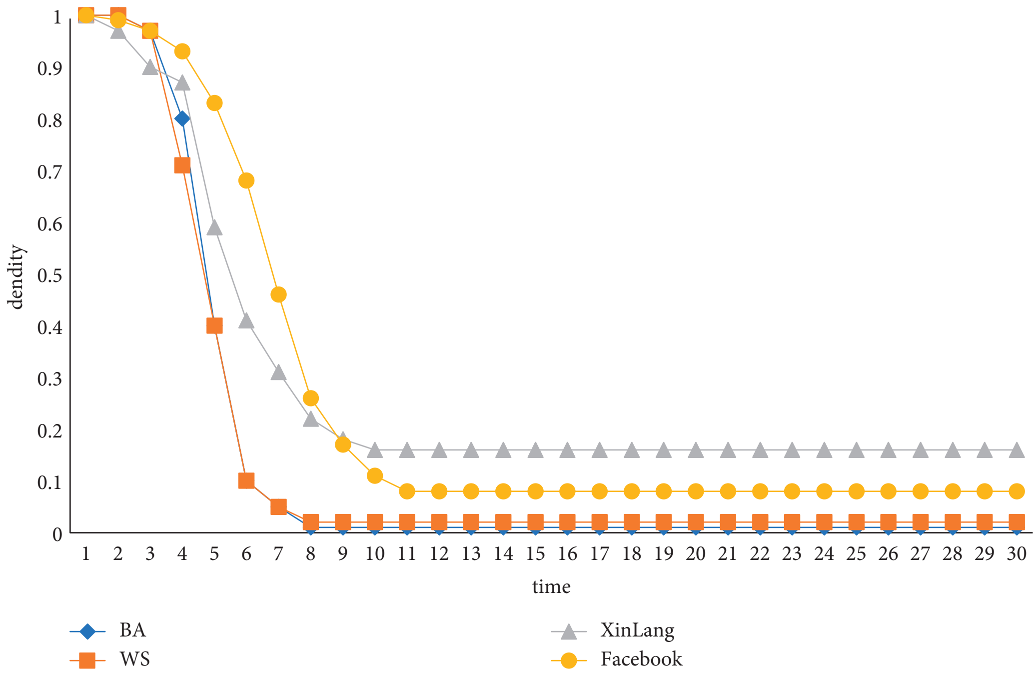

Figure 10: Comparison of s (t) under four networks.

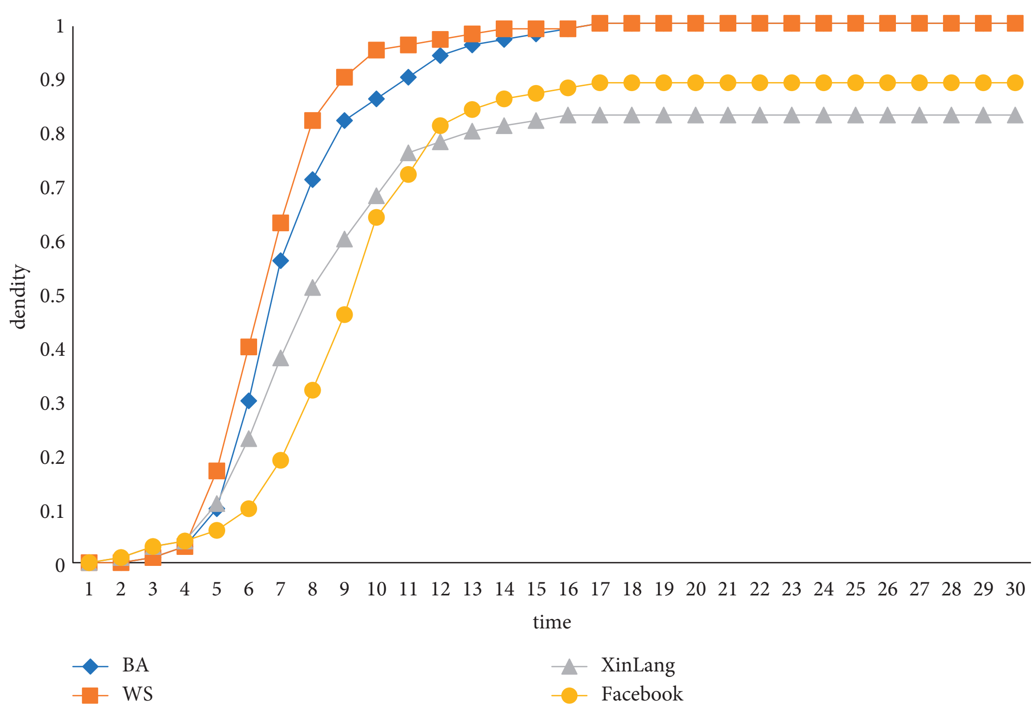

Figure 11: Comparison of i (t) under four networks.

of the maximum infection ratio in different network environments, where the horizontal axis V is the information value and the vertical axis is the maximum infection ratio.

Analysis of Figure 13 shows that the maximum infection ratio increases with the increase of V, that is, the higher the value of information, the wider its spread range. In the whole experiment, the initial propagation node is set as one. If the propagation node is added, the propagation speed will increase and the corresponding time to reach the propagation peak will also decrease.

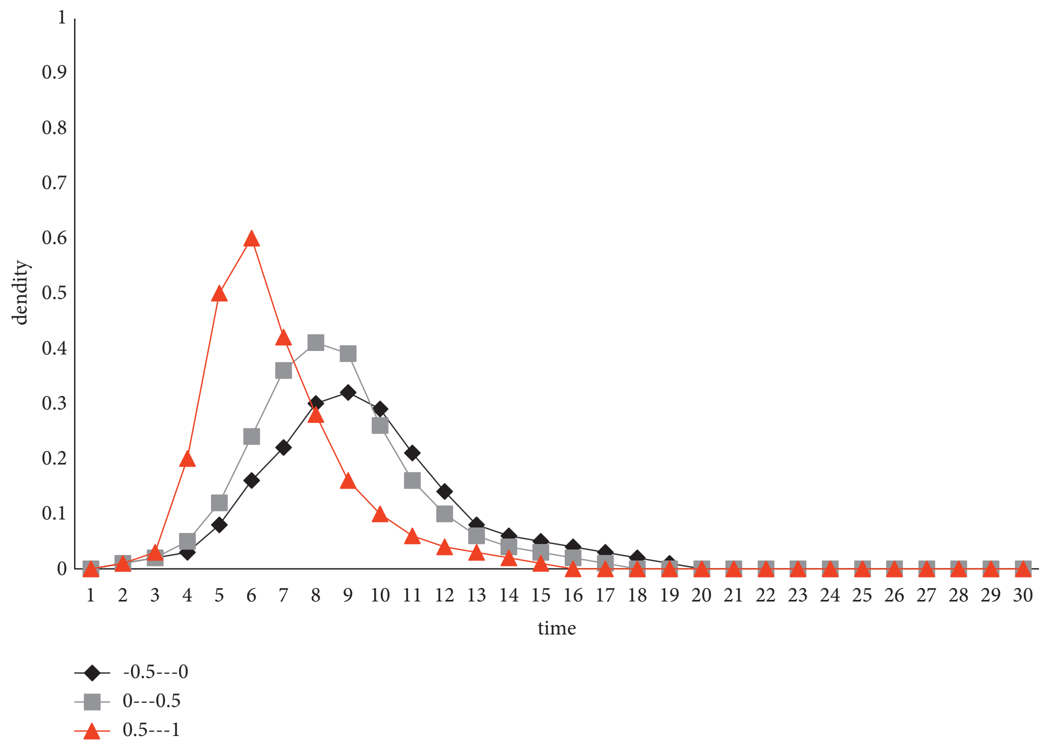

Figure 12: Influence of node attitude value on propagation.

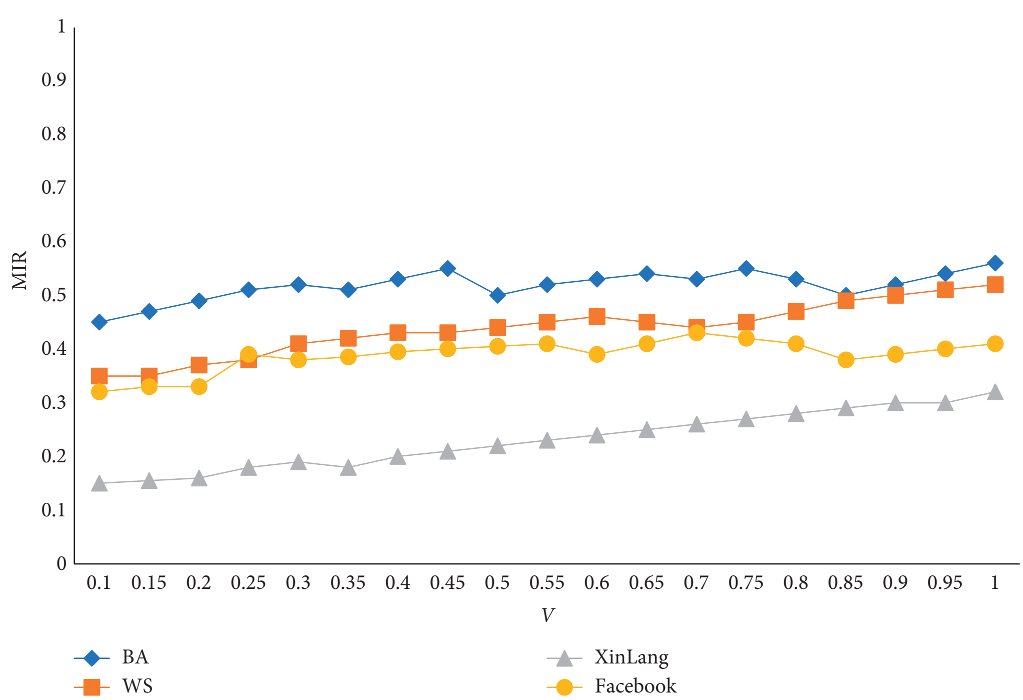

Figure 13: Maximum ratio of four network environments.

5. Conclusion

For the propagation of degraded images on the network, we choose the SIR model as the most representative propagation model. By improving the model, we define the state transition probability function between different nodes, set various parameters of the environment, and consider various influencing factors. By comparing four different network environments, we carry out simulation experiments. It is found that the proportion of propagation nodes in the simulated BA and WS networks of the SIR model is small and the propagation process is relatively smooth. Secondly, it is found that the information transmission speed in Facebook is faster than that in Sina and the information coverage is wider, but the information cannot cover the whole network. In addition, the subjective attitude and information value of users have a significant impact on information dissemination, which accords with the dissemination law of degraded images in actual social networks.

Data Availability

The experimental data used to support the findings of this study are available from the corresponding author upon request.

Conflicts of Interest

The authors declare that they have no conflicts of interest regarding this work.

References

[1] C. Y. Wang, J. Z. Chen, and W. Li, "Review on superpixel segmentation algorithms," *Application Computer Research*, vol. 31, no. 1, pp. 6–12, 2014.

[2] L. Li, J. Pan, W. Lai, C. Gao, N. Sang, and M. H. Yang, "Learning a critical prior for blind image Deblurring," in *Proceedings of the IEEE Conference on Computer Vision and Pattern Recognition (CVPR)*, pp. 6616–6625, IEEE Press, Salt Lake City, UT, USA, June 2018.

[3] J. Pan, D. Sun, H. Pfister, and M. H. Yang, "Blind image deblurring using dark channel Prior," in *Proceedings of the IEEE Conference on Computer Vision and Pattern Recognition (CVPR)*, pp. 1628–1636, IEEE Press, Las Vegas, NV, USA, June 2016.

[4] W. Han, S. Chang, D. Liu, M. Witbrock, and T. S. Huang, "Image super-resolution via dual-state recurrent IEEE conference on network," in *Proceedings of the Computer Vision and Pattern Recognition*, pp. 1654–1663, Salt Lake City, UT, USA, June 2018.

[5] M. Wani and M. Ahmad, "Information diffusion modelling and social network parameters (A survey)," in *Proceedings of the High-level negotiations at international conferences Computer, communication and electronic engineering company*, pp. 16–18, Kashmi, India, December 2015.

[6] Y. Bae and H. Lee, "Sentiment analysis of twitter audiences: measuring the positive or Popular twitterers," *J] Journal of American Society Information Science and Technology*, vol. 63, no. 12, pp. 2521–2535, 2012.

[7] Xi Xiong, Y. Li, S. Qiao et al., "An emotional contagion model for with multiple behaviors," *Machinery and its applications*, vol. 490, pp. 185–202, 2018.

[8] Li Mei, X. Wang, K. Gao, and S. Zhang, "A survey on information diffusion in online social Networks: patterns and Methods," *Info*, vol. 8, no. 4, p. 118, 2017.

[9] Y. Yi, Z. Zhang, and C. Gan, "The effect of social tie on information division in complex networks," *Physica A: Statistical Mechanics and its A pplications*, vol. 509, pp. 783–794, 2018.

[10] S. Shan and X. Lin, "Research on emergency dissemination mod els for social media Information-based entropy," *Enterprise Information Systems*, vol. 12, no. 7, Article ID 888909, 2018.

[11] D. Zinoviev, V. Duong, and H. Zhang, "A game theoretical approach to modeling information dissemination in social networks," *Eprint Arxiv*, vol. 1, pp. 407–412, 2010.

[12] X. Liu, D. He, L. Yang, and C. Liu, "A novel negative feedback the information dissemination model based on the online social network," *Statistical Machinery and Applications*, vol. 513, pp. 371–389, 2019.

[13] L. Zhao, J. Wang, Y. Chen, Q. Wang, J. Cheng, and H. Cui, "SIHR rumor spreading model in social networks," *Physica A Statistical Mechanics & It Applications*, vol. 391, no. 7, pp. 2444–2453, 2012.

[14] M. M. Tulu, R. Hou, and T. Younas, "Identifying influential nodes based on com munity the structure is speed up the dissemination of information in complex network," *IEEE Access*, vol. 6, pp. 7390–7401, 2018.

[15] C. Granell, S. Gmez, and A. Arenas, "Dynamical interplay between awareness and epidemic spreading in multiplex networks," *Physics of MetalsRev Lett*, vol. 111, Article ID 128701, 2013.

[16] D. Y. Melesse and A. B. Gumel, "Global asymptotic properties of an SEIRS model with multiple infective stages," *Mathematical Analysis and Applications Journal*, vol. 366, no. 1, pp. 202–217, 2010.

[17] L. Zhao, X. Qiu, and X. Wang, "Rumor spreading model consulting forgetting and remembering mechanisms in inhomogenic network," *Physica A*, vol. 392, pp. 987–994, 2013.

[18] L. L. Xia, G. P. Jiang, and B. Song, "Rumor generated the model considering hesitating mechanism in complex social networks," *Physica A Statistical Mechanics & It Applications*, vol. 437, pp. 295–303, 2015.

[19] D. J. Watts and S. H. Strogatz, "Collecting the dynamics of "small world" networks," *Nature*, vol. 393, pp. 440–442, 1998.

[20] X. Li, J. Guo, C. Gao, L. Zhang, and Z. Zhang, "A hybrid strategy for network mobilization," *Chaos, Solitons and Fractals*, vol. 106, pp. 214–219, 2018.

[21] L.-L. Xia, Y.-R. Song, C.-C. Li, and G.-P. Jiang, "Target unification strategies based on two rounds of selection," *Physica A: Statistical Machinery and its Applications*, vol. 496, pp. 540–547, 2018.

[22] L. K. Allen, A. D. Likens, and D. S. McNamara, "Modeling the dissemination of misinformation through study dynamics," *Misinformation and Fake News in Education*, vol. 281, pp. 159–164, 2019.

[23] A. Vazquez, R. Dobrin, D. Sergi, J.-P. Eckmann, Z. Oltvai, and A. L. Barabasi, "The topological relationship betweenthe large-scale attributes and local interaction patterns of complex networks," *Proceedings of the National Academy of Sciences of the United States of America*, vol. 101, no. 52, pp. 17940–5, 2004.

[24] T. Carnes, C. Nagarajan, S. M. Wild, and A. V. Zulyen, "Maximizing influence in a com-petitive social network: a follower's perspective," in *Proceedings of the ninth inter-national conference on Electronic commerce*, pp. 351–360, Minneapolis, MN, USA, August 2007.

[25] M. Gomez-Rodriguez, L. Song, N. Du, H. Zha, and B. Schölkopf, "Influence estimation and maxi-mization in continuous-time diffusion networks," *ACM Transactions on Information Systems*, vol. 34, no. 2, pp. 1–33, 2016.

Hindawi
Scientific Programming
Volume 2021, Article ID 7435202, 11 pages
https://doi.org/10.1155/2021/7435202

Research Article

Research on School Classroom Teaching Model Based on Clustering Algorithm and Fuzzy Control

Fujun Zhang, Aichuan Li, Jianfei Shi, and Dongxin Wang

College of Information and Electrical Engineering, Heilongjiang Bayi Agricultural University, Daqing 163319, China

Correspondence should be addressed to Fujun Zhang; zhangfujun134@st.btbu.edu.cn

Received 18 October 2021; Accepted 5 November 2021; Published 22 November 2021

Academic Editor: Le Sun

The method of computational intelligence to monitor and evaluate the concentration of students in the teaching process can promptly and effectively adjust the learning plan and improve the learning effect. In this article, clustering algorithm and fuzzy control methods are used to construct a research model of students' attention in class. In addition, this article uses the existing MATLAB-based image feature recognition algorithm to detect and obtain facial features and analyze the main features of facial expressions through computational techniques to realize the judgment of attention. In addition, this article optimizes the traditional AdaBoost algorithm to save computing time and improve operating efficiency and system performance stability. Finally, this article constructs the functional modules of the research model according to actual needs and designs experiments to verify the performance of the model. Experimental research results show that the model constructed in this article has a certain effect.

1. Introduction

Attention refers to the direction and concentration of people's psychological activities to certain objects. Concentration is the ability to pay attention, that is, the ability to point and focus one's psychological activities (perception and thinking, etc.) on a certain thing or process [1]. Western scholar Weinberg believes that the ability to focus attention on clues related to action performance in a complex external environment is to focus on attention. Students' attention refers to the ability of students to pay attention, that is, the ability of students to focus on specific goals without being interfered by external irrelevant stimuli in the process of learning. When students' attention is distracted, they are often hesitant and slow in learning and examination.

Attention is not an independent psychological process, it is closely connected with all psychological activities, such as feeling, perception, memory, imagination, thinking, and emotion, and it is a kind of consciousness quality (or characteristic) of these psychological processes. Attention includes four basic qualities [2]. (1) The breadth of attention, that is, the scope of attention: it refers to the number of attention objects that people can clearly understand or grasp at the same time, which is from extremely narrow to very broad. The narrow attention filters out most of the information, while the broad attention can simultaneously obtain a wide range of information. The scope of attention varies from person to person, and children's scope of attention is usually smaller than that of adults. However, the scope of attention will be greatly improved with the growth of children and conscious training. (2) The stability of attention: it refers to the ability to focus attention on a specific object or activity in a certain period of time, that is, the ability to keep attention on a certain activity for a long time. (3) The distributivity of attention: it refers to the ability to distribute attention to different objects at the same time on the premise of skilled skills and normal excitability of the cerebral cortex. Because people's attention is limited, the allocation of attention requires individuals to allocate two or more kinds of information in time. When the object of attention is not complex and familiar, people can notice one or more objects at the same time. (4) Transform of attention: it refers to the ability of an individual to adjust his attention from one object or activity to another according to a certain purpose. The speed of attention transfer is not only the embodiment of thinking flexibility, but also the basic guarantee of rapid information processing and judgment.

There are many factors that affect attention, and it usually refers to an emotional state caused by critical or unexpected external changes, which are caused by our feelings of the external environment. When stimulated by the emergency, the body will produce obvious changes, such as heart rate, blood pressure, and muscle tension, which will make the emotion highly intensified, and then produce a sense of anxiety. When individuals feel unable to adapt to the task they are facing and cannot grasp the surrounding environment, they often have negative self-suggestion and anxiety. This will cause the excitability of the cerebral cortex to shift, cause internal inhibition, unable to concentrate, and hinder technical performance.

This article mainly uses student feature recognition methods to count the number of students and their concentration in real classrooms. In the classroom monitoring environment, the faces of students at different shooting angles and distances are dense and tiny, so there are false detections and missed detections in the face detection. In a natural state, students bowing their heads, lying on their desks, and obscured by books all cause varying degrees of difficulty in face detection and concentration analysis. This article fully studies the current domestic and foreign research status of face detection and expression recognition methods, analyzes the difficulties and problems in face detection and subsequent expression recognition in the classroom, and proposes corresponding improvements.

2. Related Work

In recent years, wearable multiphysiological parameter acquisition equipment has been one of the key research directions of many research institutions at home and abroad, and new research results have continuously emerged in this field. From the perspective of its development process, it can be seen that the first generation of wearable multiphysiological parameter collection equipment focused on fragmented physiological parameter detection, such as monitoring blood oxygen concentration, pulse rate, blood sugar, and blood pressure signal [3], and the product forms are mainly represented by rings, glasses, gloves, earphones, etc. [4]. The second-generation multiphysiological parameter collection equipment enriches the categories of collected physiological parameters, integrates EEG signals, ECG signals, EMG signals, respiration rate, body temperature, etc., and reflects the characteristics of centralized wearable products [5]. The third-generation multiphysiological signal acquisition equipment mainly relies on the development of semiconductor technology and material science and technology. It has the characteristics of flexibility and miniaturization, such as electronic skin and epidermal electronic equipment, which are still in the research stage [6]. At present, among the abovementioned three generations of wearable multiphysiological parameter collection devices, the second-generation wearable multiphysiological parameter monitoring device has the highest practicability and application prospects. For example, the world's first wearable physiological signal monitoring system is a smart wearable motherboard (Georgia Tech Wearable Motherboard) developed by Georgia Tech, which is used in the detection of casualties of soldiers on the battlefield during combat [7]. The product uses the fabric material integrated with optical fiber and fabric as a template to monitor human body temperature signals, ECG signals, and other physiological signals, while simultaneously detecting the bullet wounds of soldiers in battle. The LifeShirt developed by the American company VivoMetrics is the world's first monitoring system that realizes noninvasive, mobile, and continuous collection of physiological signals, and is currently widely used in more than 1,000 hospitals around the world [8]. Moreover, the sensors built into the LifeShirt can realize the simultaneous detection of more than 30 physiological parameters. The BioHarness monitoring belt produced by Zephyr in the United States realizes the combination of portable multiphysiological signal detection and a chest strap with multiple sensors distributed. Moreover, it can realize the synchronous detection of human body's electrocardiogram signal, respiration signal, body temperature signal, movement, and posture change, and its collected data can be sent to the host computer in real time to apply Acknowledge Software for data processing and further analysis [9]. LifeMonitor developed by the British Equivita Company is a wearable system that realizes dynamic monitoring of vital signs [10]. The multiphysiological information monitoring system can realize the collection, transmission, and storage of physiological signals such as ECG signal, heart rate, respiration rate, temperature, exercise information, blood oxygen concentration, blood pressure signal, and body temperature signal, and it applies professional analysis software for data analysis and processing. Moreover, the system has Global Positioning System (GPS) positioning function and is easy to wear. Because it uses skin-friendly high-tech breathable fabrics, it weighs only 38 g while being beautiful and comfortable, making it easy to wear for a long time.

The literature [11] developed an emotional learning system. The system analyzes human emotions and learning states based on Naive Bayes classification and K-nearest neighbor classification and classifies them based on α waves and θ waves to infer the subject's mental state. The literature [12] found that the potential signals collected at the human head are related to cognitive tasks and emotions. In the research and analysis, the author applied the principal component analysis method to the power spectrum analysis of the collected EEG data and applied the data subspace characteristics to derive and predict the error rate of the subjects in a continuous attention experiment. After observing the changes in the alpha wave power spectrum of the evoked EEG signal, the author found that when the alpha wave changes at a lower frequency, it can characterize some of the characteristics of attention, such as expectation and alertness to a certain extent. The literature [13] discovered that the spectral characteristics of EEG signals can be used to predict the degree of concentration. The results of the study show that the β-band (4–7 Hz) in the EEG signal is related to the drowsiness tendency, the α-band (8–13 Hz) is related to alertness and brain activity, and the γ-band (>20 Hz) is related to visual information processing and attention information. The research institute at the University of Sydney in Australia once proposed feature extraction based on the driver's EEG signal and classification of fatigue and concentration based on feature values, used trend measurement to analyze and evaluate the driver's mental state, and finally achieved good experimental analysis results [14].

In the study of Shanghai Jiao Tong University, the researchers asked the subjects to browse the pictures in the picture library and synchronously collect the EEG signals during the experiment [15]. The experimental results show that the collected EEG signals contain information that can effectively identify the subjects' emotion and concentration. The results of related studies show that certain information contained in the human body's bioelectrical signals can be used to identify emotional states and focused states. Based on the characteristics of nonlinearity and high latitude of EEG signals, the amplitude, stability, and power spectral density of EEG signals can be used to analyze and evaluate the state of concentration. In addition, some scholars combine physiological information such as ocular signals and heart rate with EEG signals to perform comprehensive analysis [16].

3. Face Detection Module Based on the Viola–Jones Algorithm

In face detection, the Viola–Jones face detection algorithm is a very classic algorithm, it is widely used because of its fast and efficient detection effect, the algorithm includes preprocessing, feature extraction, training classifier, and other positioning algorithms, and all steps constitute a complete detection target positioning algorithm system. Because of the fast positioning and high accuracy of this method, it has quickly become the first choice for face detection and positioning. Although the Viola–Jones face detection algorithm was originally used to detect frontal face images, as the Viola–Jones algorithm has become more mature in recent years, the detection of side face images has become more and more efficient and accurate, so this article adopts the classic Viola–Jones algorithm to realize face detection. Figure 1 shows a block diagram of the face recognition system. This article mainly explains the algorithm used in this article from the face detection [17].

This algorithm mainly includes the following important parts:

(1) It describes the common attributes of the face by the Haar-like rectangle features and then performs detection

(2) It establishes a feature called integral image, and based on the integral image, several different rectangular features can be quickly obtained

(3) It uses the optimized AdaBoost algorithm, that is, the optimized Better AdaBoost classifier for training to distinguish between human faces and nonhuman faces

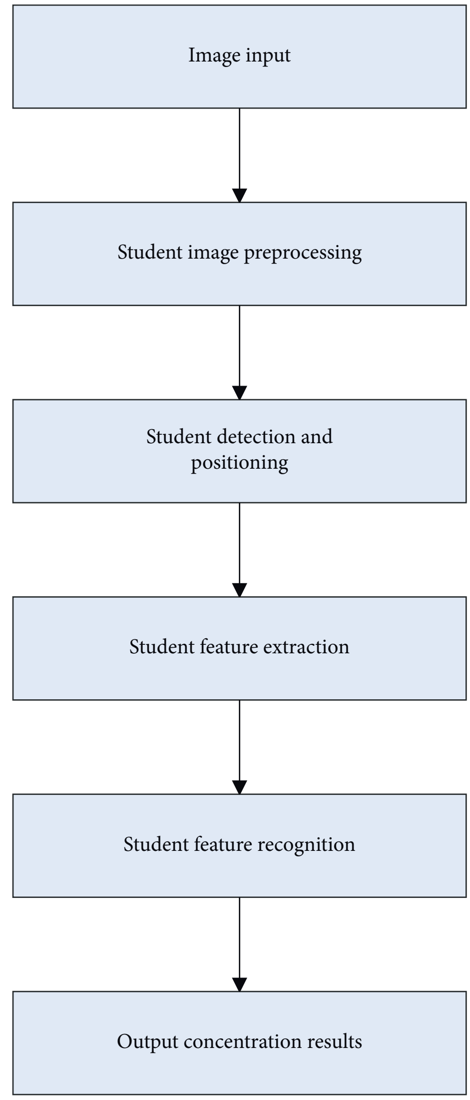

Figure 1: Block diagram of the face recognition system.

(4) It establishes a cascaded hierarchical classifier with high detection rate

The common attributes of the face by Haar-like rectangular features are described as follows: generally speaking, the facial features of a person will show some basic common characteristics. For example, the nose is generally a high bright area of the face, which means that the brightness of the nose will be higher than that of the face. The surrounding cheeks are much brighter, and the human eye area is much darker than the cheek area. For a human face image, the relative positions of the eyebrows, nose, eyes, mouth, etc., are regular and followable. Among them, they are for the human face. For the midline, they are almost symmetrical [18].

Therefore, the Haar-like feature considers the rectangular area adjacent to a specific position of a facial feature, and the pixels in the rectangular area at each position are added and then subtracted, and the final result is calculated. It basically corresponds to the following situations:

$$[1,-1], [1,-1,1], [-1,1], [-1,1,-1], \begin{bmatrix} 1 & -1 \\ -1 & 1 \end{bmatrix}. \quad (1)$$

To calculate the Haar-like features, all pixels in the rectangular area need to be summed. The size of the rectangular area that can be formed by an image is different. If each rectangular area uses the pixel and then summation method, this will undoubtedly increase the amount of calculation. Therefore, the Viola–Jones face detection algorithm uses a very sophisticated data structure called an integral image. The principle of the calculation of the integral image is very simple; that is, for any point in the image, the integral image value of that point is equal to the sum of all the pixels located in the upper left corner of the point. The expression is as follows [19]:

$$I(X,Y) = \sum_{x' \le x} \sum_{y' \le y} f(x', y'). \quad (2)$$

Moreover, the integral image satisfies the relationship of the following formula:

$$I(x,y) = f(x,y) + I(x-1,y) + I(x,y-1) - I(x-1,y-1). \quad (3)$$

Among them, I represents the integral image, f represents the original image, and x, y, x', y' represent the position of the pixel. Therefore, the integral image of an image records the sum of all pixels in the upper left corner of each pixel on this image. If the upper left corner of an image is regarded as the origin of the coordinates of this image, then the above expression is the discrete sum of all pixels from the origin to the pixel, and it can also be regarded as an expression of integral. Therefore, this is also the origin of the name of the integral image. Using integral images, we can calculate the pixel sum of any point on an image or the pixel sum of a rectangular area. The calculation of the integral image pixel sum has a library function $I = i\text{ntergral lmage}(\text{img})$ in MATLAB that can be called directly [20].

After obtaining this integral image, the pixels of each rectangular area in the image can be quickly calculated, as shown in Figure 2.

To obtain the pixel sum of the rectangle abcd, the integral image formula is used, and the expression formula is as follows [21]:

$$S_{\text{abcd}} = I(a) + I(d) - I(b) - I(c). \quad (4)$$

This means that the sum of pixels in any rectangular area, that is, the sum of pixels in the upper left corner of the image, can be represented by the four points on the integral image.

The training process of the classic AdaBoost classifier is as follows.

The training set is given by $(x_1, y_1), \ldots, (x_n, y_n)$, where $y_i \in \{-1, 1\}$ represents the correct category label of x_i, $i = 1, \ldots, N$. The initial distribution of samples on the training set is as follows:

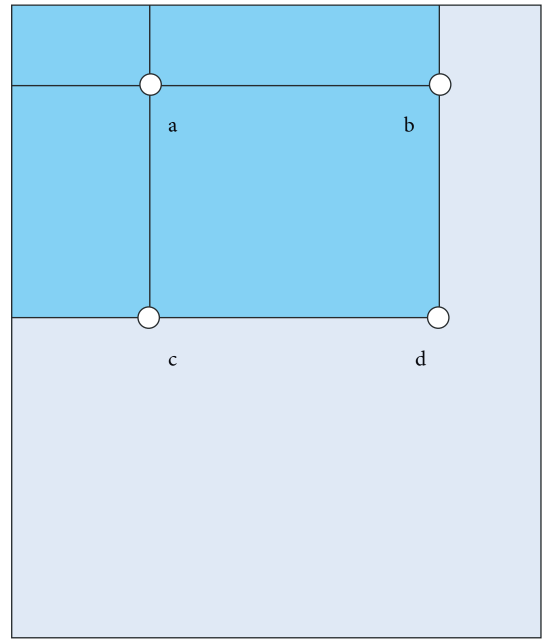

Figure 2: Pixels in the rectangular area of the Haar-like feature.

$$D_1(i) = \frac{1}{N}. \quad (5)$$

Among them, $t = 1, \ldots, T$. The weak classifier $h_t\colon X \longrightarrow \{-1, 1\}$ is calculated, and the error of the weak classifier on the distribution D_t is as follows:

$$\varepsilon_t = p_{D_t}(h_t(x_i) \neq y_i). \quad (6)$$

The weight of the weak classifier is calculated as follows:

$$\alpha_t = \frac{1}{2} \text{In}\left(\frac{1-\varepsilon_t}{\varepsilon_t}\right). \quad (7)$$

The distribution of training samples is updated as follows:

$$D_{t+1}(i) = \frac{D_t(i)\exp(-\alpha_i y_i h_t(x_i))}{Z_t}. \quad (8)$$

Among them, Z_t is the normalization constant. The final strong classifier is as follows:

$$H_{\text{final}}(x) = \text{sign}\left[\sum_{t=1}^{T} \alpha_t h_t(x)\right]. \quad (9)$$

There is no restriction on the style of the weak classifier, and it can be a decision tree based on multidimensional features, or even SVM. However, usually each weak classifier is constructed based on a certain dimension in all features, and the output results are only +1 and −1 (for binary classification). Therefore, during training, each iteration selects the weak classifier corresponding to the one-dimensional feature with the best classification effect under the current training set distribution.

In the prediction, after inputting a sample, the classic AdaBoost adds weighted $\{-1, +1\}$ value output by all weak classifiers as the final result. To get different accuracy and recall rates, users can set different thresholds. For example, when the output is 0.334, if threshold = 0 is set, the classification result is g, and if threshold = 0.5 is set, the classification result is m.

The Better AdaBoost classifier is an extension and improvement of the classic AdaBoost classifier. Each weak classifier of the classic AdaBoost classifier only outputs $\{1, 0\}$ or $\{+1, -1\}$, so the classification ability is weak. The output of each weak classifier of Better AdaBoost is a real value (this is the reason it is called "Better"), which can be considered as a degree of confidence. Moreover, when it is combined with LUT (100k-uptable), the ability to express complex functions is stronger than the classic AdaBoost.

The training process of the Better AdaBoost classifier is as follows [22].

The training set is given by $(x_1, y_1), \ldots, (x_n, y_n)$, where $y_i \in \{1, -1\}$ represents the correct category label of x_i, $i = 1, \ldots, N$. The initial distribution of samples on the training set is as follows:

$$D_1(i) = \frac{1}{N}. \tag{10}$$

Among them, $t = 1, \ldots, T$.

(1) The value space X of each dimension feature is divided into several disjoint subspaces $X_1, \ldots, X_n$.

(2) The parameter value on each subspace is calculated as follows [23]:

$$W_i^j = p\left(x_i \in X_j, y_i = 1\right) = \sum_{tx_i \in X_j, y_i = 1} D(i), \quad 1 \in \{+1, -1\}. \tag{11}$$

(3) The output of each weak classifier is calculated as follows:

$$\forall_x \in X_j, h(x) = \frac{1}{2} In\left(\frac{W_{+1}^j + \varepsilon}{W_{-1}^j + \varepsilon}\right). \tag{12}$$

Among them, ε is a small normal quantity, which is used to smooth the output. $h(x)$ is actually a piecewise linear function, which outputs a different value in each subspace.

(4) The normalized factor is calculated as follows [24]:

$$Z = Z \sum_j \sqrt{W_{+1}^j W_{-1}^j}. \tag{13}$$

The product of the weighted sum of positive and negative samples on each subspace is calculated and then added.

(5) The weak classifier $h(x)$ that minimizes z is selected as the weak classifier selected in the iteration:

$$\begin{aligned} Z_t &= \min Z, \\ h_t &= \arg\min Z. \end{aligned} \tag{14}$$

(6) The sample distribution is updated as follows:

$$D_{t-1}(i) = D(i)\exp\left[-y_i h_i(x_i)\right]. \tag{15}$$

The final strong classifier H is expressed as follows:

$$H(x) = \operatorname{sign}\left[\sum_{i=1}^{T} h_t(x) - b\right]. \tag{16}$$

Among them, b is the threshold, and it is defaulted to 0.

Face recognition and eye recognition are inseparable. Face recognition is the premise of eye recognition, and eye recognition is the premise of judging the concentration of students in class because the dynamics of human eyeballs and the speed of blinking are the most intuitive way to judge whether students are taking lessons seriously. However, there are few studies that combine the quality of teaching with human eye recognition. Most of them combine human eye research with driver fatigue to determine whether the driver is fatigued. Most of the literature uses human eye recognition to judge. For example, the literature on the method and application of eye feature recognition for fatigued drivers and the literature on driver fatigue detection based on human eye recognition all mention that when the driver is fatigued, the blinking frequency of the eyes will slow down, and the focus will not be concentrated enough, which may easily lead to a car accident.

When the human eye area is detected, the next job is to judge the open and closed state of the human eye. In the human eye detection in this article, the state of the human eye is simply divided into two parts: eyes open and eyes closed. If we define the samples in one state (such as eyes open) as positive samples and the samples in the other state (such as eyes closed) as negative samples, then the AdaBoost classifier is trained by extracting their Haar-like features. Then, this process is simpler than the process of human eye positioning. This is because the negative samples of the human eye positioning process are theoretically random, so a large amount of negative sample data is needed, and a classifier with a cascade structure needs to be constructed. In the state recognition process, there is no need to construct a cascade structure of classifiers, and only one layer of classifiers is needed to maximize the distinction between positive and negative samples.

This method can well recognize the eye state of the subject wearing glasses (including contact lenses and frame glasses). Here, it is necessary to distinguish the testee wearing glasses and the testee not wearing glasses into two different samples. That is to say, when the testee wears glasses, the classifier trained by the sample wearing glasses should be used. When the glasses are not worn, the classifier trained on the samples without glasses is used. Through experiments, this method can increase the average recognition accuracy of general individuals by about 8%, while the average recognition accuracy of individuals wearing glasses can be increased by 8% to 12%.

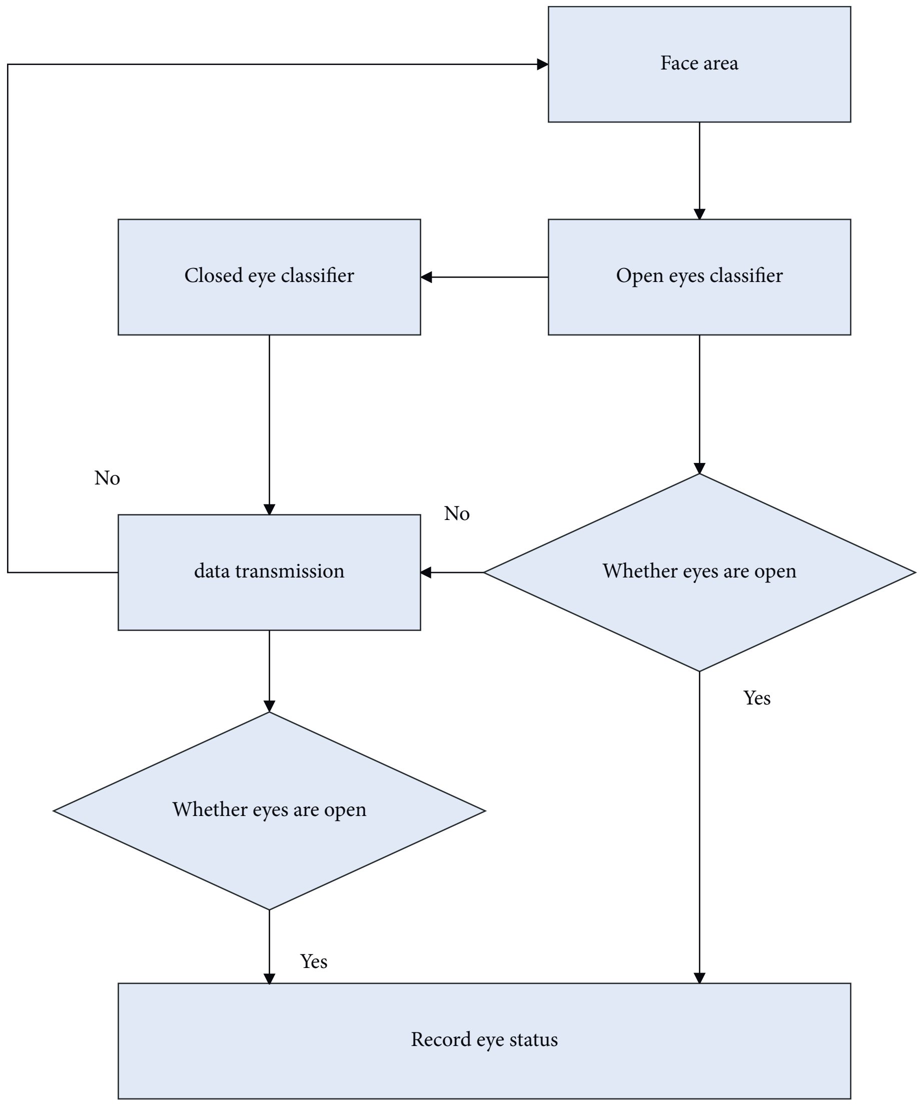

Figure 3: Diagram of the location and classification of eye status.

First, the features involved in training are analyzed. The five typical Haar-like features are all obtained through the difference in rectangular integrals. In other words, the essence of Haar-like features can be considered as a gradient feature. Therefore, we define the amount of edge information of an image to be expressed by the following formula:

$$H = \sum_{x} \sum_{y} \sum_{m=1}^{8} \left| I(x, y) - I_m \right|. \tag{17}$$

Among them, I_m represents the 8 domain points corresponding to the point $I(x, y)$ in the image.

According to the knowledge of biology, the human eye area has a relatively obvious grayscale change relative to the human face area. For the detection and positioning of the human eye, the first step is to determine that the human eye is not blocked, and then, the grayscale enhancement transformation on the grayscale image of this image is performed. Finally, a reasonable grayscale threshold is set, so that the human eye part of the binarized image obtained by the image enhancement transformation can be clearly distinguished.

4. Research Model of College Students' Classroom Concentration Based on Computer Statistical Analysis and Fuzzy Control

The AdaBoost algorithm is a very effective sample learning algorithm, and it also has a good classification effect for training the human eye classifier and can quickly determine the state of eyes open and eyes closed through the human eye cascade classifier. This method can be combined with the process of detecting and judging the state to realize the effect to be tested. The process of using the AdaBoost algorithm to achieve human eyes open and closed classifier training can be described as shown in Figure 3.

This article analyzes the main features of facial expressions to realize the judgment of the degree of concentration.

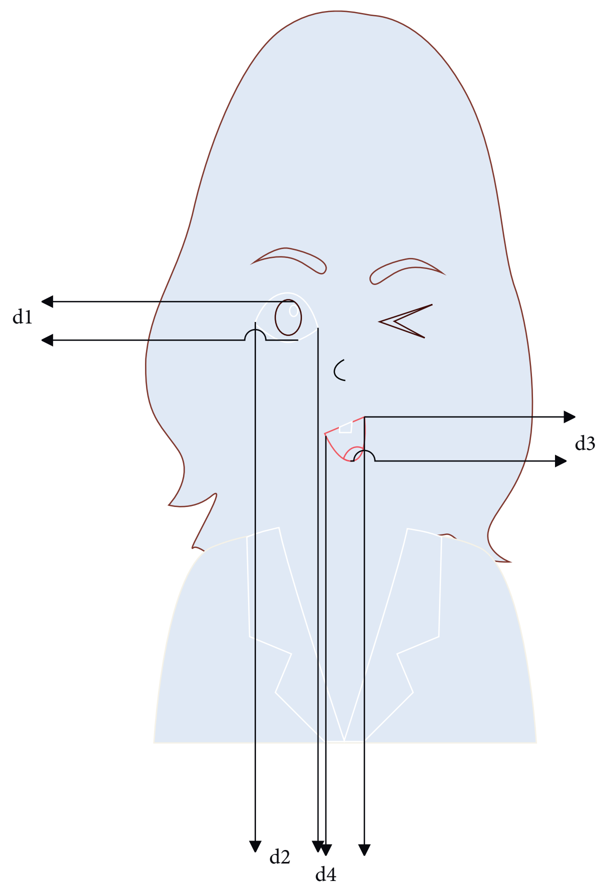

Figure 4: Schematic diagram of facial expression parameters.

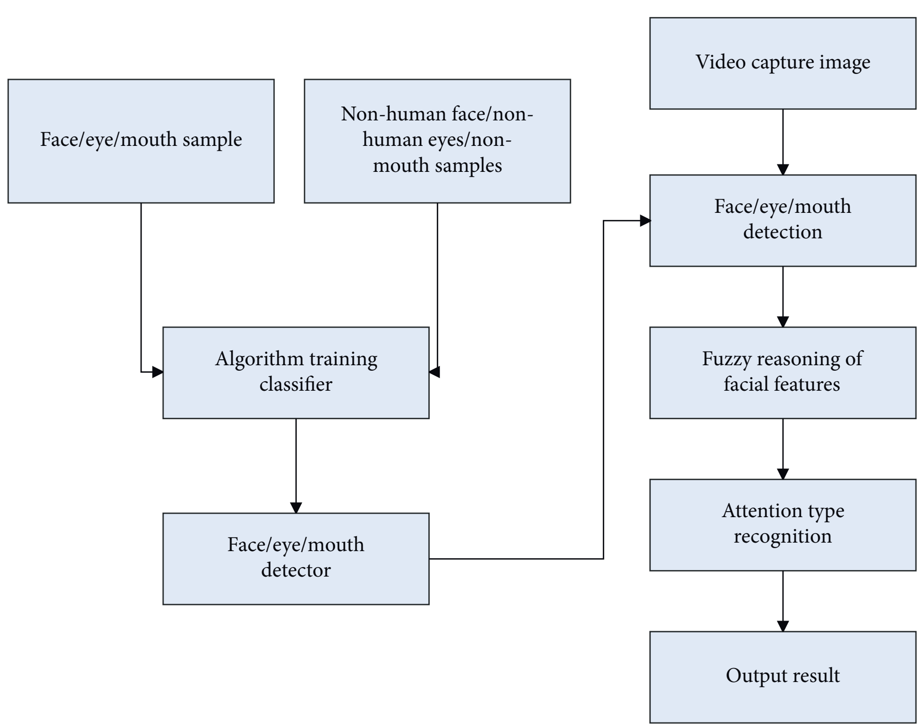

Figure 5: System design framework.

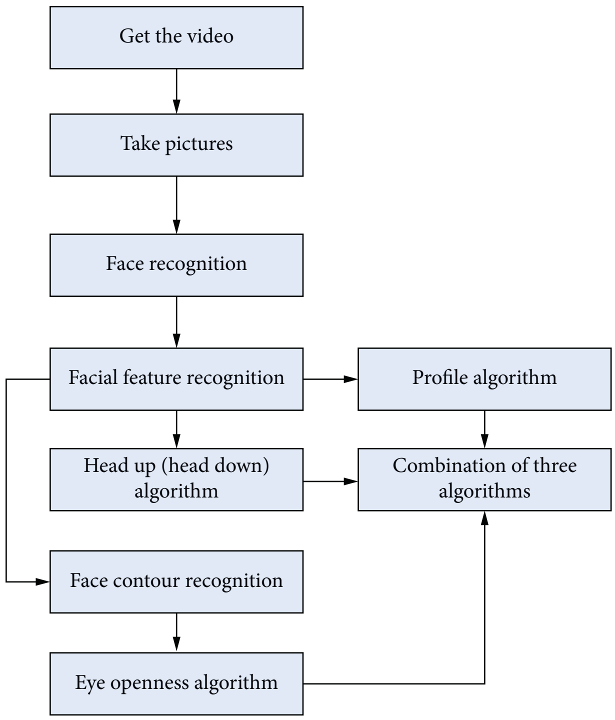

Figure 6: Main flowchart of the algorithm.

Because the most obvious changes in facial expressions during the learning process are the eye and mouth features, this article uses the eye height of the extracted picture under the same pixel background, eye width, mouth height, and mouth width. Four sets of data information methods are the four sets of facial expression parameters (d1, d2, d3, and d4) in the following schematic diagram. We find the degree of concentration by analyzing the changes in the extracted model parameters. At high moments, the eye height data are generally larger, or the eye height changes positively in the original normal state, and the mouth is usually closed or slightly opened at this time; when the concentration is low, the eyes are usually smaller or closed, or the eyes were originally opened or normal, but the height of the eyes showed a significant negative change; that is, the eyes have a tendency to become smaller or closed, and the mouth usually has a more obvious tendency to open. Figure 4 shows a schematic diagram of the characteristic parameters that have changed significantly during the extracted learning process.

In this article, the AdaBoost algorithm is used to detect and locate the face, eyes, and mouth, and then, the fuzzy inference method is used to determine the student's learning status. The design framework of the concentration recognition system is shown in Figure 5.

The test samples used in this experiment are all pictures of the emotional state of online distance education learners in the learning process collected by computers. According to the data analysis mentioned in the previous article, we set to capture facial expression pictures every 1 s and then analyze the detected pictures.

As shown in the main flowchart of the algorithm in Figure 6, the main research of this article is to use MATLAB

Table 1: Statistical table of the accuracy of feature recognition of system.

Number	Feature extraction accuracy (%)
1	73.51
2	74.79
3	84.20
4	82.44
5	84.42
6	76.65
7	74.54
8	80.74
9	88.76
10	76.15
11	72.47
12	79.96
13	73.03
14	83.73
15	89.01
16	84.73
17	78.55
18	86.60
19	87.98
20	85.59
21	75.07
22	73.70
23	74.75
24	84.91
25	79.33
26	84.98
27	87.69
28	85.73
29	76.92
30	85.65
31	77.58
32	88.53
33	89.90
34	81.38
35	88.61
36	78.80
37	88.96
38	72.34
39	78.87
40	76.01
41	83.74
42	88.45
43	76.57
44	87.43
45	82.41
46	74.91
47	73.76
48	74.01
49	83.03
50	85.28
51	74.19
52	81.55
53	79.40
54	77.29
55	72.14
56	75.87
57	89.61
58	73.05
59	78.64

Table 1: Continued.

Number	Feature extraction accuracy (%)
60	79.84
61	75.49
62	75.67
63	87.91
64	74.88
65	83.33
66	75.94
67	75.33
68	72.56
69	81.32
70	87.05
71	87.88
72	84.73
73	89.73
74	82.97
75	90.85

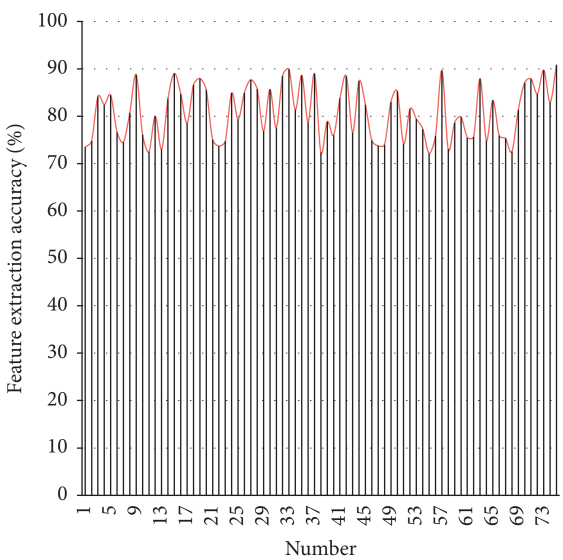

Figure 7: Statistical diagram of the accuracy of feature recognition of system.

as a processing tool to perform face detection, so as to determine the realization process of students' concentration in class. The system is mainly divided into a picture acquisition module, a digital image processing module, a face detection module, and a face feature recognition module. The first is to intercept the picture we want to judge the focus of the target from each frame of video and then preprocess the picture to remove the complex background or irrelevant information of the picture.

5. System Performance Verification

After constructing the college students' classroom concentration analysis system based on computer statistical analysis and fuzzy control methods, the next step is to study the effect of the college students' classroom concentration analysis system based on computer statistical analysis and fuzzy control methods. Moreover, this article

Table 2: Statistical table of the accuracy of concentration recognition of system.

Number	Accuracy of concentration recognition (%)
1	64.09
2	78.06
3	64.14
4	67.19
5	64.85
6	71.73
7	72.16
8	83.99
9	77.43
10	65.06
11	64.90
12	69.83
13	72.39
14	83.16
15	77.25
16	74.73
17	71.60
18	78.72
19	72.03
20	82.76
21	68.73
22	73.32
23	72.37
24	65.64
25	83.87
26	64.25
27	75.60
28	79.28
29	73.45
30	73.71
31	70.11
32	66.21
33	84.53
34	84.41
35	70.01
36	84.24
37	81.76
38	80.38
39	65.02
40	78.67
41	77.42
42	67.38
43	68.10
44	71.12
45	75.59
46	83.59
47	78.34
48	76.79
49	65.40
50	64.61
51	66.09
52	71.83
53	66.70
54	64.93
55	70.39
56	65.19
57	78.99
58	68.66
59	70.13
60	77.06

Table 2: Continued.

Number	Accuracy of concentration recognition (%)
61	76.39
62	82.17
63	64.45
64	73.05
65	82.83
66	81.36
67	81.46
68	67.37
69	75.63
70	77.18
71	65.58
72	73.97
73	64.92
74	72.80
75	83.39

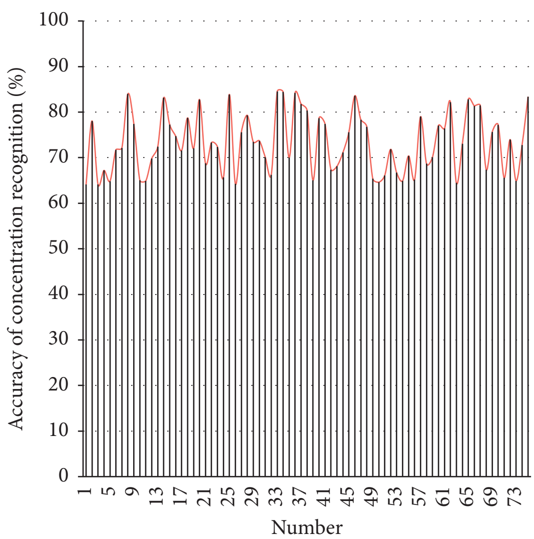

Figure 8: Statistical diagram of the accuracy of concentration recognition of system.

combines statistical methods to verify system performance. This article uses the system to monitor the class of 75 students of a certain major in a university and calculate the result of feature recognition, as shown in Table 1 and Figure 7.

From the above analysis, it can be seen that the college students' classroom concentration analysis system based on computer statistical analysis and fuzzy control methods constructed in this article has a certain accuracy in the recognition of students' classroom features. On this basis, this article uses the system to identify students' class concentration, and the results are shown in Table 2 and Figure 8.

From the above analysis results, the college students' classroom concentration analysis system based on computer statistical analysis and fuzzy control methods constructed in this article performs well in student concentration recognition and can be used as an auxiliary system for college teachers' teaching.

6. Conclusion

With the rapid development of hybrid artificial intelligence technology, the intelligent education model of human-computer collaboration makes education a traceable and visible process. Creating an intelligent and technological learning environment to conduct personalized, humanized, and intelligent concentration state evaluation during the process of autonomous learning and to achieve self-feedback and evaluation of their learning effects is of great significance to optimizing the teaching process and promoting learners' deep learning. This article combines computer statistical analysis and fuzzy control methods to construct a classroom concentration research model for college students, builds the functional modules of the concentration research model based on actual needs, and designs experiments to verify the system performance. The experimental research results show that the system constructed in this article has a certain effect.

Data Availability

The labeled dataset used to support the findings of this study is available from the corresponding author upon request.

Conflicts of Interest

The authors declare no conflicts of interest.

Acknowledgments

This study was sponsored by Heilongjiang Higher Education Teaching Reform Project, Teaching Research and Practice of Electrical Engineering Specialty Course Flipped Classroom Based on Smart Campus (no. SJGY20200502).

References

[1] L. Zhuang, T. H. Chan, A. Y. Yang, S. Sastry, and Y. Ma, "Single-sample face recognition with image corruption and misalignment via sparse illumination transfer," *proceedings/CVPR, IEEE computer society conference on computer vision and pattern recognition. IEEE Computer Society Conference on Computer Vision and Pattern Recognition*, vol. 114, no. 2-3, pp. 272–287, 2014.

[2] G. Wang, N. Shi, Y. Shu, and D. Liu, "Embedded manifold-based kernel Fisher discriminant analysis for face recognition," *Neural Processing Letters*, vol. 43, no. 1, pp. 1–16, 2016.

[3] T. Chuk, A. B. Chan, and J. H. Hsiao, "Understanding eye movements in face recognition using hidden Markov models," *Journal of Vision*, vol. 14, no. 11, p. 8, 2014.

[4] H. Bouchech, "Selection of optimal narrowband multispectral images for face recognition," *Monthly notices of the royal astronomical society*, vol. 402, no. 4, pp. 2140–2186, 2015.

[5] R. Ramachandra and C. Busch, "Presentation attack detection methods for face recognition systems: a comprehensive survey," *ACM Computing Surveys*, vol. 50, no. 1, pp. 8.1–8.37, 2017.

[6] Z. Huang, S. Shan, R. Wang et al., "A benchmark and comparative study of video-based face recognition on COX face database," *IEEE Transactions on Image Processing*, vol. 24, no. 12, pp. 5967–5981, 2015.

[7] C. P. Wei and Y. C. F. Wang, "Undersampled face recognition via robust auxiliary dictionary learning," *Image Processing IEEE Transactions on*, vol. 24, no. 6, pp. 1722–1734, 2015.
[8] N. L. Ajit Krisshna, V. K. Deepak, K. Manikantan, and S. Ramachandran, "Face recognition using transform domain feature extraction and PSO-based feature selection," *Applied Soft Computing*, vol. 22, pp. 141–161, 2014.
[9] R. Weng, J. Lu, and Y. P. Tan, "Robust point set matching for partial face recognition," *Image Processing IEEE Transactions on*, vol. 25, no. 3, pp. 1163–1176, 2016.
[10] Z. Cui, H. Chang, S. Shan, B. Ma, and X. Chaen, "Joint sparse representation for video-based face recognition," *Neurocomputing*, vol. 135, pp. 306–312, 2014.
[11] P. J. Phillips and A. J. Otoole, "Comparison of human and computer performance across face recognition experiments," *Image and Vision Computing*, vol. 32, no. 1, pp. 74–85, 2014.
[12] D. Tang, N. Zhu, F. Yu, W. Chen, and T. Tang, "A novel sparse representation method based on virtual samples for face recognition," *Neural Computing & Applications*, vol. 24, no. 3-4, pp. 513–519, 2014.
[13] R. Mehta, J. Yuan, and K. Egiazarian, "Face recognition using scale-adaptive directional and textural features," *Pattern Recognition*, vol. 47, no. 5, pp. 1846–1858, 2014.
[14] R. Raghavendra, K. B. Raja, and C. Busch, "Presentation attack detection for face recognition using light field camera," *IEEE Transactions on Image Processing*, vol. 24, no. 3, pp. 1060–1075, 2015.
[15] M. Yang, P. Zhu, F. Liu, and L. Shen, "Joint representation and pattern learning for robust face recognition," *Neurocomputing*, vol. 168, pp. 70–80, 2015.
[16] Y. Yan, H. Wang, and D. Suter, "Multi-subregion based correlation filter bank for robust face recognition," *Pattern Recognition*, vol. 47, no. 11, pp. 3487–3501, 2014.
[17] Z. Fan, M. Ni, Q. Zhu, and E. Liu, "Weighted sparse representation for face recognition," *Neurocomputing*, vol. 151, pp. 304–309, 2015.
[18] X. Tang, G. Feng, and J. Cai, "Weighted group sparse representation for undersampled face recognition," *Neurocomputing*, vol. 145, pp. 402–415, 2014.
[19] W. H. Al-Arashi, H. Ibrahim, and S. A. Suandi, "Optimizing principal component analysis performance for face recognition using genetic algorithm," *Neurocomputing*, vol. 128, pp. 415–420, 2014.
[20] A. Morelli Andrés, S. Padovani, M. Tepper, and J. Jacobo-berlles, "Face recognition on partially occluded images using compressed sensing," *Pattern Recognition Letters*, vol. 36, no. 1, pp. 235–242, 2014.
[21] C. Ding and D. Tao, "Pose-invariant face recognition with homography-based normalization," *Pattern Recognition*, vol. 66, pp. 144–152, 2017.
[22] M. Yang, Z. Feng, S. C. K. Shiu, and L. Zhang, "Fast and robust face recognition via coding residual map learning based adaptive masking," *Pattern Recognition*, vol. 47, no. 2, pp. 535–543, 2014.
[23] N. Zhu and S. Li, "A Kernel-based sparse representation method for face recognition," *Neural Computing & Applications*, vol. 24, no. 3-4, pp. 845–852, 2014.
[24] W. S. Chen, Y. Zhao, B. Pan, and B. Chen, "Supervised kernel nonnegative matrix factorization for face recognition," *Neurocomputing*, vol. 205, pp. 165–181, 2016.

Hindawi
Scientific Programming
Volume 2021, Article ID 1271438, 12 pages
https://doi.org/10.1155/2021/1271438

Research Article

The Optimization of Classroom Teaching in Colleges and Universities Based on Network Topology

Yongqiang Wang and Na Zhang

Railway Police College, Zhengzhou 450053, China

Correspondence should be addressed to Yongqiang Wang; wangyongqiang@rpc.edu.cn

Received 6 October 2021; Revised 28 October 2021; Accepted 3 November 2021; Published 22 November 2021

Academic Editor: Le Sun

In order to improve the teaching effect of programming courses, this article applies network topology to the construction of programming course teaching platform system and constructs a teaching framework combined with intelligent teaching mode. In addition, this article takes the opportunistic social network composed of mobile smart terminal devices as the application background and briefly introduces the concept, characteristics, and application scenarios of the opportunistic social network. In addition, the typical message forwarding algorithm currently studied in this paper is analyzed. Taking into account the social attributes and forwarding willingness of nodes, in order to increase the message transmission rate and reduce message transmission delay and network overhead, two message transmission strategies are proposed to improve the operating effect of the programming course teaching platform. Finally, this paper verifies the effectiveness of the network topology in the teaching of the algorithm and programming of the intelligent teaching mode through experimental research.

1. Introduction

In the information age, the widespread application of Internet and other network technologies has caused tremendous changes in the way of teaching and learning. Moreover, various new teaching methods using microclasses, microvideos, and MOOCs as the media are gradually taking shape, and new learning methods such as personalized learning, mobile learning, and flipped learning are gradually becoming popular. As the main place for imparting knowledge and skills and cultivating quality talents, schools must comply with the requirements of education informatization. At the same time, key changes have taken place in the development of teachers' curriculum, the establishment of education and teaching models, the update and delivery of learning materials, and the way students learn. This is a response to the development trend of the times and an inevitable requirement for the development of education [1].

As a new type of teaching form to promote teaching performance, the flipped classroom mode is the key to efficiently flip educational elements such as teaching concepts, teacher and student roles, teaching methods, and evaluation methods [2]. That is, before class, students watch the learning videos independently and complete knowledge transfer, and in class teachers and students conduct discussions and exchanges, conduct collaborative exploration and internalize knowledge, and evaluate and reflect after class, and provide timely feedback. It reverses the traditional teaching model, reshapes the role of teachers and students and the relationship between teachers and students, highlights the dominant position of students, improves learning enthusiasm, and improves teaching effect and quality [3].

Object-oriented programming course is a very important language practice course learned by computer majors. This course focuses on cultivating students' ability to solve practical problems independently through algorithm design and is highly professional and practical. With the development of Internet technology, the requirements for students' object-oriented programming have gradually increased, but there are still many problems in the classroom teaching of programming courses. The above-mentioned problems will seriously affect the teaching effect, deviate from the teaching goal of the programming design course, and cause the quality of training students to decline. Therefore, we reform the programming curriculum and traditional teaching mode by adopting the MOOC-based flipped classroom teaching concept. At the same time, we make full use of MOOC's rich and high-quality online resources while flipping the main role of teachers and students in the classroom and pay more attention to the interactive process and feedback of classroom teaching, to further optimize the teaching quality and effect of programming courses [4].

Since most students ignore the review of the class, the teacher will pay more attention to the teaching of basic grammar knowledge in the classroom teaching of the program design course and lack the training and concern for students to solve problems. Most teachers believe that students can make students master the concept, grammar, and knowledge points and then practice the teaching objectives of the course in accordance with the experimental guidance in the experimental course. But in fact, this kind of teaching does not enable students to really internalize in the early stage of classroom and absorb the knowledge points. In the next year, secondary students can not flexibly use knowledge points to solve practical problems.

The teaching resources of program design courses are still based on textbooks and experimental guidelines, lacking students' way to explore, practice, and solve problems. The final exam of the programming course is due to the paper test, so the form of assessment is mainly based on the theoretical knowledge, ignoring the essence of the programming course. As long as the assault review before the exam, you can get a high score, and practice and practice. The ability is not significantly improved. Therefore, the traditional teaching model of the reform program design curriculum, enriching teaching resources, improving students' learning energy and learning efficiency, has become an important research topic in teaching reform.

This article combines the social cognitive network to optimize the flipped classroom teaching mode of programming courses and combines the information transmission improvement algorithm to improve the transmission efficiency of teaching resources and further enhance the flipped classroom teaching effects of programming courses.

2. Related Work

With the development of a large number of online social networks at home and abroad, related research on online social network analysis and mining has attracted great attention from scholars at home and abroad. In today's society, due to the prevalence of social software, social network applications have had a significant impact on people's clothing, housing, and transportation.

People pay more and more attention to large-scale network graph data compression technology. Literature [5] proposed a technique for compressing the original image when it is divided. However, it is still not very good to meet the requirements of fast query. Literature [6] proposed a dictionary-based compression method. This method is to compress web page data. It sorts the URLs in the web page graph in lexicographical order. Since URLs that are close in sequence often contain similar neighbors, using this property can achieve a better compression effect. However, due to general social network graph data, nodes often do not have dictionary attributes, and the compressed places cannot be found in lexicographic order. Literature [7] proposed an FRS algorithm, which defines a social network data node rearrangement technology to achieve the purpose of node rearrangement and then achieve the purpose of compression. Literature [8] proposed BFS-based technology, which also uses the rearrangement method of nodes and uses the difference between adjacent rows in the adjacency table after sorting to store graph data, so as to achieve the purpose of compression. Literature [9] proposed a multipoint linearization of neighborhood query, which uses some data structures to achieve compression purposes, such as quadtrees. Literature [10] showed that the data in the actual graph in reality has the characteristics of power law distribution. Using this feature, literature [11] used the structural equivalence method to transform the points and edges in the original graph into structures with equivalent meanings to achieve the purpose of compression. Literature [12] proposed a method based on attributes, nonoverlapping, and covering node groups to achieve the purpose of compression. The above method considers the problem of thinking from the perspective of how to reduce the size of the original image data and does not consider what content will be lost due to the reduction of the scale and how much impact it will have on the perception of the original image.

Graph aggregation is very important in many fields, but at present, there is relatively little research and analysis work on the basis of graph aggregation. The definition of graph aggregation is to discard some noncritical information in the original graph data and reconstruct a similar simple graph to achieve the purpose of easily analyzing the original graph. In this way, intuitively speaking, it introduces some uncertain factors in the data. For example, when accurate query is required, due to the loss of additional information, there is a certain degree of uncertainty for the query results [13]. Literature [14] developed an algorithm to understand large-scale graph data through graph aggregation, which found key structures in graph data. Although the algorithm can find these key structures, it is found through experiments that the structure found by the algorithm is not completely accurate. For example, in the actual graph data, it should be a clique structure, but the algorithm recognizes multiple star structures. This is because the algorithm does not consider the relationship between the words in the proposed graph vocabulary dictionary, which leads to errors in the final recognition of key structures. At the same time, the algorithm only applies to static large-scale graph data, not to large-scale social network graphs, and has no evolutionary research.

Literature [15] found in teaching practice that when students encounter problems in classroom learning, teachers need to give students targeted help or guidance instead of imparting systematic knowledge in the classroom. As a result, it changed the way of knowledge transfer in the classroom and allowed students to watch the recorded teaching videos before class and answer questions and tests in the classroom and provided students with learning tasks to promote students to complete the internalization of knowledge. Subsequently, based on the practical reflection on flipped teaching, literature [16] proposed new concepts such as flipped classroom, mastered classroom, and flipped learning. Moreover, it emphasized that flipped classroom is only an entry point for teaching innovation, rather than a goal or end point. From flipped classroom to mastery classroom, the ultimate goal is flipped learning. Literature [17] mentioned that the top students have a high degree of participation in classroom activities under the traditional teaching mode, while the diligent middle school students have equal opportunities to participate in classroom activities under the flipped classroom mode. Therefore, flipped classroom teaching can ensure that more students participate in classroom teaching activities. Literature [18] constructed a flipped classroom teaching model and conducted experimental demonstrations.

3. Flipped Classroom Network Model of Programming Courses

This article defines the network topology including the connected graph composed of nodes and links, which is G=(N, L). Among them, N represents the set of all nodes in the network, and $N = \{N_1, N_2, \ldots, N_m\}(m \geq 1)$, $\forall N_i \in N$, and N_i represents the i-th node in the opportunistic social network, L represents the set of communication links between nodes, and $L = \{L_1, L_2, \ldots, L_k\}(m \geq 1)$, $k \in [0.n(n-1)/2]$, $\forall L_i \in L$, and L_i represents the i-th communication link in the network.

Node activity represents the number of times a node has encountered other nodes in the community in a period of time, denoted as NA_i. Among them, C_{ij} represents the number of times that the node N_i and the node N_j meet in the period T, and the calculation formula is shown in the following equation [19]:

$$NA_i = \sum_{j=1, j\neq i}^{m} C_{ij}. \tag{1}$$

The larger the value of $\sum_{j=1}^{k} M_{i,j}(t)$, the higher the activity of the node, and the greater the probability that the node leaves the local community, indicating that the node encounters other community nodes more frequently in the current time period.

The frequency of encounters refers to the ratio of the total number of encounters between node i and node j in the time period t to the total number of encounters between node j and other nodes from the initial state, namely,

$$P_{(i,j)} = \frac{M_{i,j}(t)}{\sum_{j=1}^{k} M_{i,j}(t)}. \tag{2}$$

Among them, $M_{i,j}(t)$ represents the total number of encounters between node i and node j during message forwarding in the time period t in the network, $\sum_{j=1}^{k} M_{i,j}(t)$ represents the total number of encounters between node i and other nodes in the network, and k represents the number of nodes in the network.

Encounter probability estimation: Encounter probability estimation refers to the probability of meeting between two nodes in the next time period based on the historical information of the nodes and the network environment without contact.

In order to predict whether two nodes will meet within a specific time Tc, it is predicted whether the node will meet other nodes within the next time Tc since the previous time T they met, that is, whether the current encounter time interval is shorter than $T_c + T_l$.

$$P_{cp} = P(I_l < T_c + T_1). \tag{3}$$

It can be seen from $T_c + T_l$ that the entire problem has been transformed into an estimate of the current time interval I_t, and the waiting time is T_l, so $I_l \geq T_l$ and

$$P_{cp} = P(I_l < T_c + T_1 \mid I_l \geq T_l). \tag{4}$$

Through the conditional probability formula, we can get

$$P(I_l < T_c + T_1 \mid I_l \geq T_l) = \frac{P(I_l < T_c + T \cap I_l \geq T)}{P(I_l \geq T)}. \tag{5}$$

From formulas (3)–(5), we can get

$$P_{cp} = \frac{f(T_l < I < T_c + T_l)}{f(_l < I)}. \tag{6}$$

In formula (6), the function $f(x)$ represents the encounter frequency of x, and the encounter frequency is reflected by historical encounter information. In short, historical information can be used to estimate the probability of encounter.

Bayesian probability: It is an interpretation of the proposition probability proposed by Bayesian theory and the process of estimating the posterior probability through prior historical information.

The Bayesian probability between the node and other nodes is calculated by the following formula [20]:

$$P(i_k|j) = \frac{P(i_k)P(j \mid i_k)}{\sum_{k=1}^{z} P(i_k)P(j \mid i_k)}. \tag{7}$$

Among them, $i_1, i_2, i_3 \ldots i_n \ldots i_z$ represent the number of nodes existing in the network, and k represents the number of historical encounter nodes of node i.

When the node message is forwarded, the source node determines the prior probabilities $P(i_k \mid j) = P(i_k)P(j \mid i_k)/\sum_{k=1}^{z} P(i_k)P(j \mid i_k)$ and $P(j \mid i_k)$ through historical encounter data, then calculates $P(i_k \mid j)$ using formula (7), and determines the probability of encountering the node with other nodes through comparison. The source node can use a variety of probabilities of encounter to determine, thereby improving accuracy.

Because the mobile nodes in the opportunistic social network are dynamic and social, the smart device nodes that make up the network are divided into different communities, which are intracommunity and intercommunity methods. The nodes belong to the same community, and the nodes are closely connected, and the number of encounters is high. Between communities, because nodes encounter fewer times when forwarding messages, the probability of encounters is also reduced.

After dividing different communities according to the social attributes of the node, the node represents the individual carrying the mobile device, the edge where the node is located represents the social relationship between the mobile device carriers, and the weight of the edge represents the strength of the social relationship between the mobile device carriers. The nodes in the network are divided according to the above method, and the result is shown in Figure 1 [21].

A single copy mechanism is used in many messaging methods and the forwarding or reception of the message directly when the node and nodes meet. In this case, there is no better encounter opportunity during forwarding. In order to solve the above problem, this paper proposes a method of selecting a Bayesian probability tree forwarding node selection method. This method combines the source node to the probability of the income node and the Bayesian probability between the nodes to select the next forwarding node. In addition, the node carries the node as the root node of the tree, and the node encountered by the node as the second- and third-level nodes of the tree. The Bayesian probability value satisfying these nodes is located on the side where the two nodes are located, and the contents of the tree node indicate that the message is successfully delivered by each node to the target node.

This paper mainly contains nodes I, A, B, C, and D in a network, as shown in Figure 2(a) below. Node i stores the generated message and forwards it to the target node J, which meets node A at a certain time T0; if it only depends on the probability of transmitting the message and the node, it will not be determined; send it to the node A and consider the next chance. Whether to send a message to the next node α is determined according to the BFANS algorithm, as shown in Figure 2(b) below. In this case, the transmission probability size of the root node and the value of the Bayesian probability condition satisfying the node are obtained, and finally the probability value is encountered with the node. In case of the node, after encountering the node A, the probability of multiplying the node B by the B node to the target node J probability is higher than the transmission probability of the node I to A, and the node i stores the message after the node A is encountered. Node I hopes to meet the node B; repeat the above steps until the target node J meets and forwards the message.

The application scenario of opportunistic social network is shown in Figure 3. Under the premise that there is no end-to-end transmission path between node S and node D, the source node S wants to send a message to the target node D. In this case, the message needs to be forwarded with the opportunity of encountering other nodes in the network. Therefore, node S will select an intermediate node from a group of neighbor nodes (Nq), so that the message is finally transmitted to node D through multihop communication. We assume that S chooses node N, and N forwards the message to N because there is no other neighbor node to forward it. However, node N exhibits selfishness due to resource constraints such as storage and energy and discards the message instead of forwarding it to node D. Due to resource constraints, it is difficult to detect the selfish behavior of nodes in the opportunistic social network, which reduces the message delivery rate and extends the transmission time.

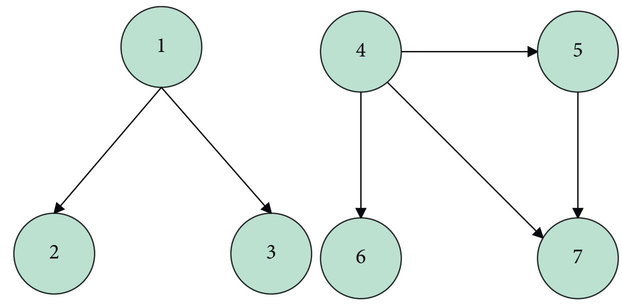

Figure 1: Results of community division.

Before analyzing specific problems, we first give the relevant assumptions of the system model:

(1) The network connectivity graph is $G = (V, E)$, where V represents the set of all nodes in the network, and $E = \{e = (u, v) | u, v \in V\}$ represents the set of node edges. The network G can be represented by a matrix A of size $|V| \times |V|$, and the value of A is as follows [22]:

$$A_{I,J} = \begin{cases} 1, e_{i,j} \in E \\ 0, e_{i,j} \notin E \end{cases} \quad (8)$$

(2) Nodes in the network are rational and selfish nodes; that is, nodes misrepresent their own information in order to maximize benefits, rather than misrepresenting other information.

(3) For other nodes in the network except the target node, the node has only two choices: forwarding or discarding.

In opportunistic social networks, location changes often occur according to the mobility of nodes. In order to predict the meeting position of the nodes, the calculation model based on the distance prediction of the nodes first calculates the angle formed by the moving speed of the nodes and the distance between the nodes. Secondly, the moving position of the node at the next moment is predicted and the distance is calculated. Finally, the Merkle hash tree is used to detect the existence of selfish nodes, and the best forwarding node is selected to complete the message forwarding through the node cooperative forwarding mechanism.

Encounter distance calculation: The moving speeds of the carrying node C, the neighbor node N, and the target node D are $\overrightarrow{V_c}$, $\overrightarrow{V_n}$, and $\overrightarrow{V_d}$, respectively, and the angles formed by the node C, the neighbor node N, and the target node D are ω_c and ω_n, respectively. The calculation process is shown in formulas (9) and (10) [23]:

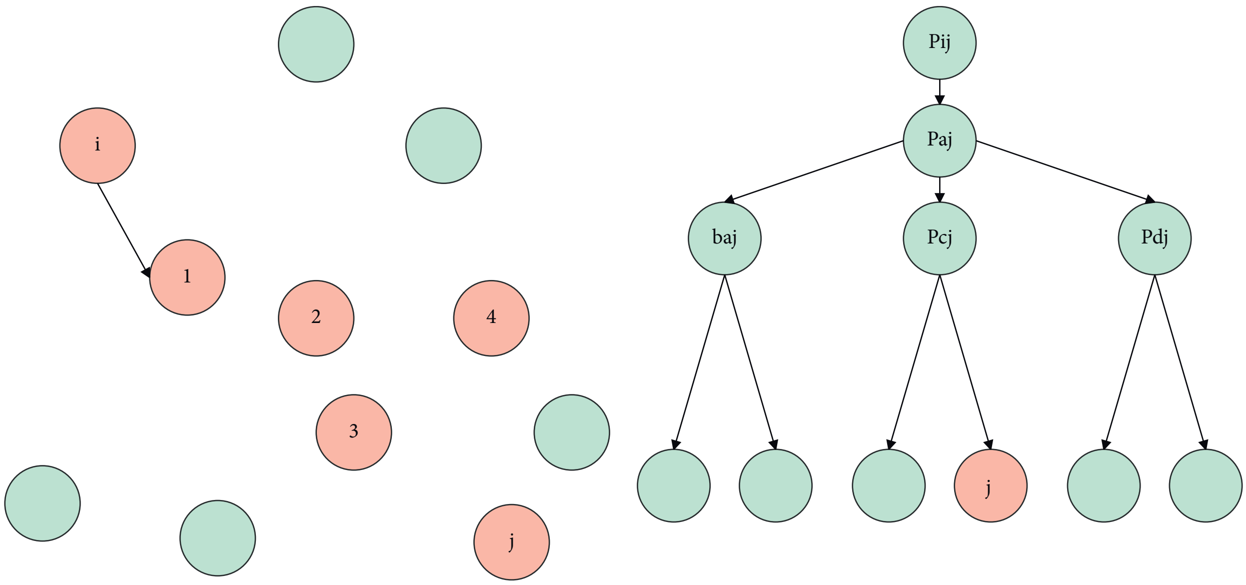

(a) (b)

Figure 2: The generation process of Bayesian probability tree. (a) Network situation. (b) Bayesian probability tree.

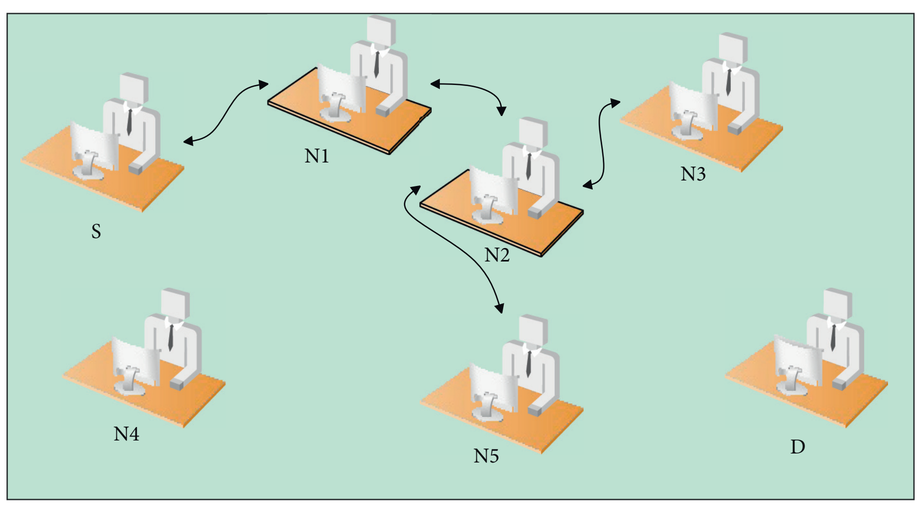

Figure 3: Application scenarios of opportunistic social networks.

$$\cos\,\omega_c = \cos\,<\overrightarrow{V_c},\overrightarrow{V_d}> = \frac{\overrightarrow{V_c}\cdot\overrightarrow{V_d}}{\left|\overrightarrow{V_c}\right|\left|\overrightarrow{V_d}\right|}, \tag{9}$$

$$\cos\,\omega_c = \cos\,<\overrightarrow{V_n},\overrightarrow{V_d}> = \frac{\overrightarrow{V_n}\cdot\overrightarrow{V_d}}{\left|\overrightarrow{V_n}\right|\left|\overrightarrow{V_d}\right|}. \tag{10}$$

Among them, the angle calculation of $\omega_c = \cos^{-1}(\overrightarrow{V_c}\cdot\overrightarrow{V_d}/|\overrightarrow{V_c}||\overrightarrow{V_d}|)$ and $\omega_n = \cos^{-1}(\overrightarrow{V_n}\cdot\overrightarrow{V_d}/|\overrightarrow{V_n}||\overrightarrow{V_d}|)$ is shown in Figure 4, ω_c represents the angle formed by the moving speed of the node carrying the message and the target node, and ω_{n1}, ω_{n2}, and ω_{n3} represent the angle formed by the moving speed of the neighbor node to the target node, respectively.

Average speed indicates the ratio of the distance between the previous position of the node and the current position in time ΔT. The previous position of node C is represented by coordinates $(c_{0x};.c_{oy})$, the current position is (c_x, c_y), and the previous position of node N is (n_{0x}, n_{0y}), and the current position is (n_x, n_y). The calculation process of the average speed of node C and node N is shown in formulas (11) and (12):

$$\overline{V_c} = \frac{\sqrt{\left(c_x - c_{0x}\right)^2 + \left(c_y - c_{0y}\right)^2}}{\Delta T}, \tag{11}$$

$$\overline{V_n} = \frac{\sqrt{\left(n_x - n_{0x}\right)^2 + \left(n_y - n_{0y}\right)^2}}{\Delta T}. \tag{12}$$

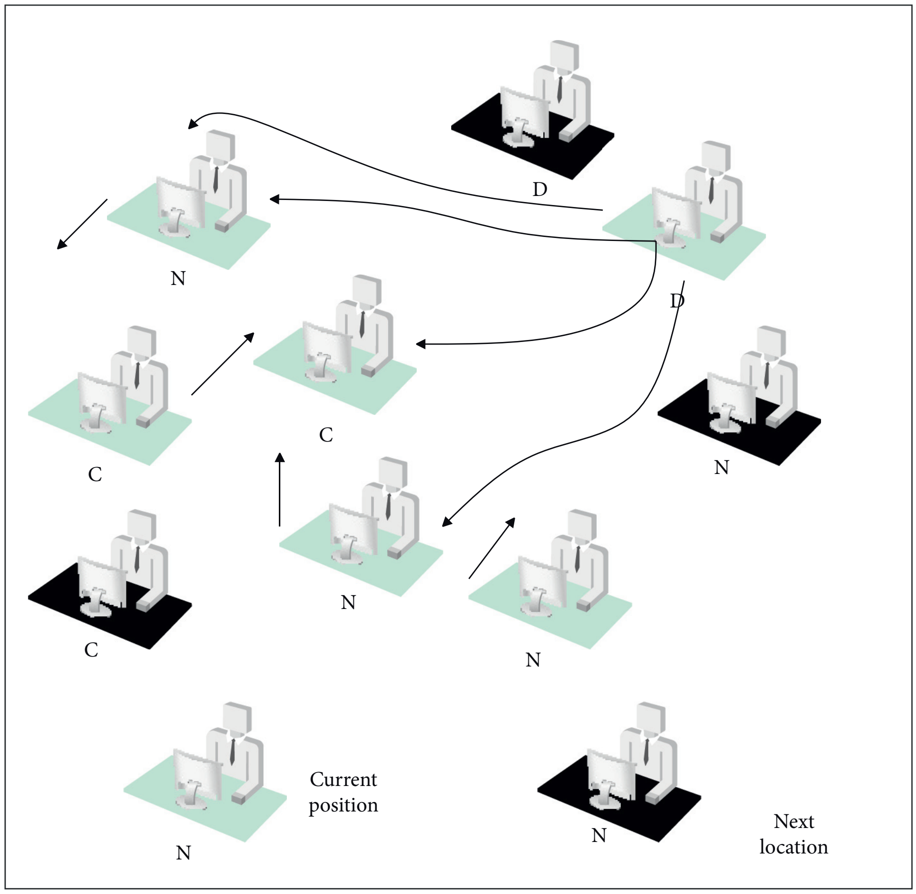

Figure 4: Calculation of the included angle of node moving speed.

Encounter distance indicates the distance between the node's moving position and the current position at the next moment in time ΔT. The positions of node C, node N, and node D at the next time are (c1x, c1y), (n1x, n1y), and (d1x, d1y), respectively. Among them, (d1x, d1y) represents the sum of the distance from the current position and the distance moved at the next moment, which is calculated by formula $(c_x + \Delta T \times \overline{V_{0x}}, c_y + \Delta T \times \overline{V_{0y}})$ and formula $(\mathrm{n}_x + \Delta T \times \overline{V_{1x}}, n_y + \Delta T \times \overline{V_{1y}})$.

$$L_c = \sqrt{\left(d_{1y} - \left(c_y + \Delta T \times \overline{V_{0y}}\right)\right)^2 + \left(d_{1x} - \left(c_x + \Delta T \times \overline{V_{0x}}\right)\right)^2},$$
$$L_n = \sqrt{\left(d_{1y} - \left(n_y + \Delta T \times \overline{V_{1y}}\right)\right)^2 + \left(d_{1x} - \left(n_x + \Delta T \times \overline{V_{1x}}\right)\right)^2}. \quad (13)$$

The Merkle hash tree is a binary tree that maps a set of nodes to a set of fixed-size strings, as shown in Figure 5. Among them, each leaf node carries a given value, and the value of internal nodes including the root node is obtained by hashing of two child nodes, and a Merkle hash tree is constructed according to the data packets carried by the node and the distance of encounter.

Among them, $\eta \in (0, \ldots, 2^H - 1, H \geq 1)$ represents the index value stored by the leaf node, and $H \geq 1$ represents the height of the Merkle tree. The hash value stored by the node is represented by $y_h[i]$, where $h = 0, \ldots, H$ represents the height of the node in the tree (the height of the leaf node is 0, and the height of the root node is H), and $i = 0, \ldots, 2^{H-h} - 1$ is the position count of the node from left to right. $f: (0,1)^* \longrightarrow (0,1)^n$ is the hash function, and the hash value of the leaf node is calculated by the function f, where $\otimes$ represents the connection operation, and the hash value of

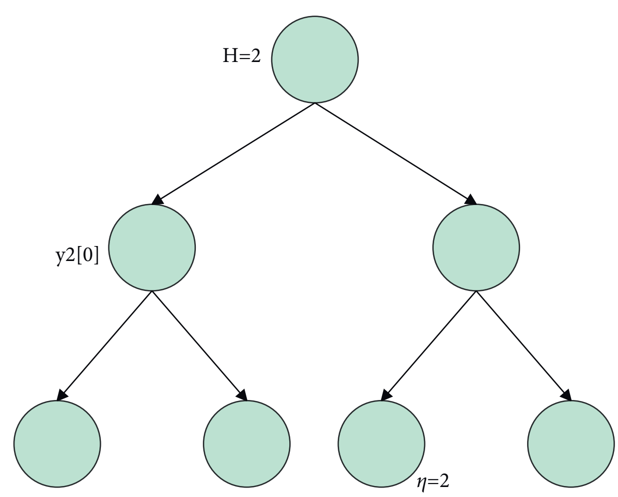

Figure 5: Example of Merkle hash tree.

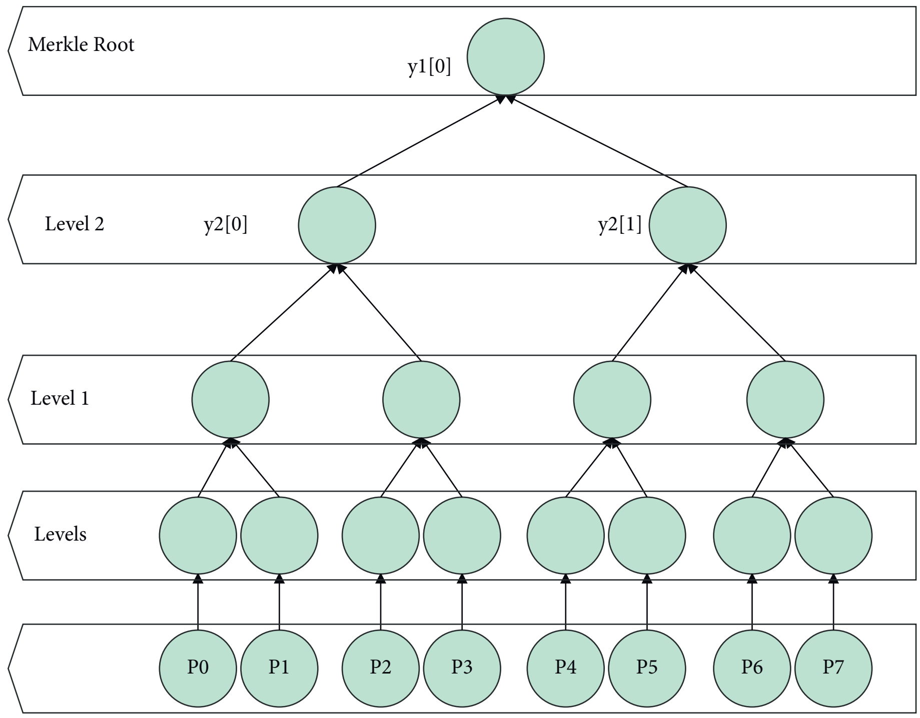

Figure 6: A Merkle tree containing 8 messages.

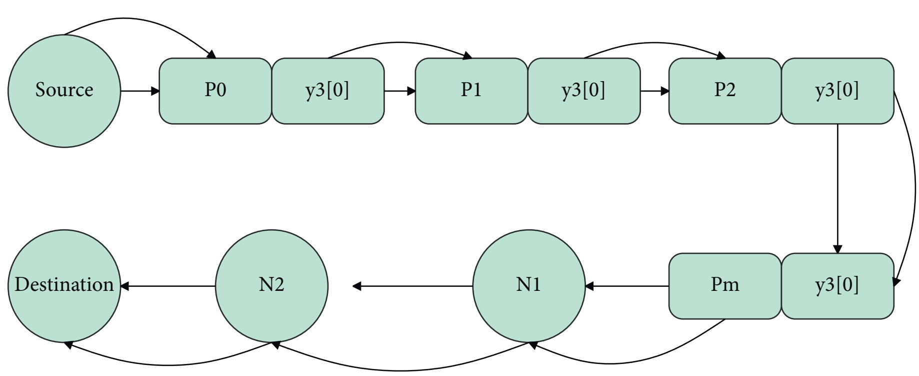

Figure 7: The embedding root node to the forwarding node.

the nonleaf node in the Merkle tree is calculated as shown in the following formula:

$$y_{h+1}[i] = f\left(y_h[2i] \otimes y_h[2i+1]\right). \tag{14}$$

We assume that the source node and the target node are legitimate nodes, and the relay node is selfish. The Merkle hash tree creates the first level of the tree by hashing the number of messages, and the value of the nodes hashed in the first level becomes the leaf hash. After that, every two leaf hashes are paired and hashed to create a new hash value, until a hash value is finally created, and this node becomes the Merkle root node ($y_3[0]$), as shown in Figure 6.

In the opportunistic social network, the Merkle hash tree will be used to check whether there is a message loss during the forwarding process between the source node and the target node. If a message is removed, its parent node will change. Once the parent node changes, it will cause the root hash value of the entire Merkle tree to change. The source node embeds the Merkle root in the head of each message and sends it to the target node through the intermediate node, as shown in Figure 7.

The algorithm in this paper is compared with the traditional Epidemic and Prophet algorithms in terms of message delivery rate, average delay, and routing cost ratio. The definitions of the three indicators are introduced below.

3.1. Message Delivery Rate. The message delivery rate refers to the proportion of the total number of messages that can successfully reach the target node to the total number of messages sent by the source node. The calculation formula is

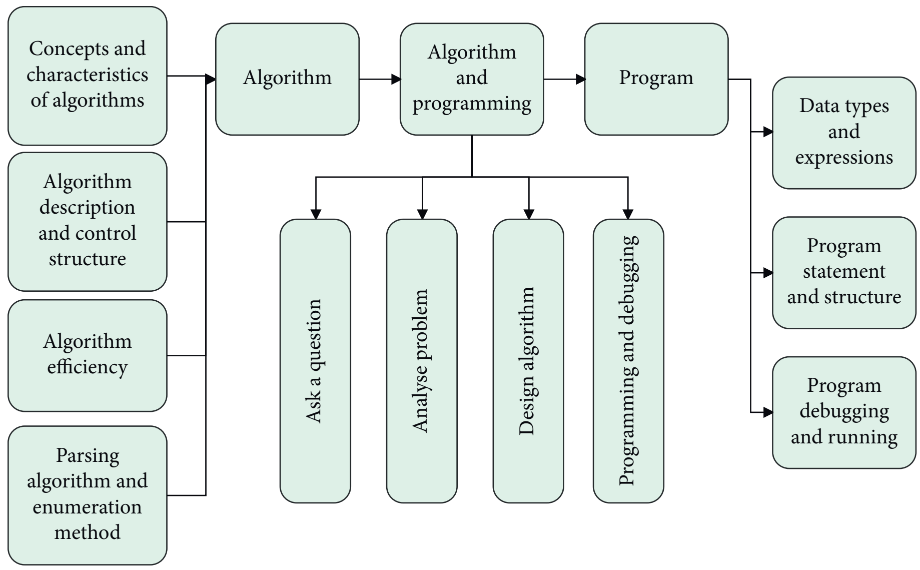

FIGURE 8: The relationship between the core concepts and key capabilities of algorithms and programs.

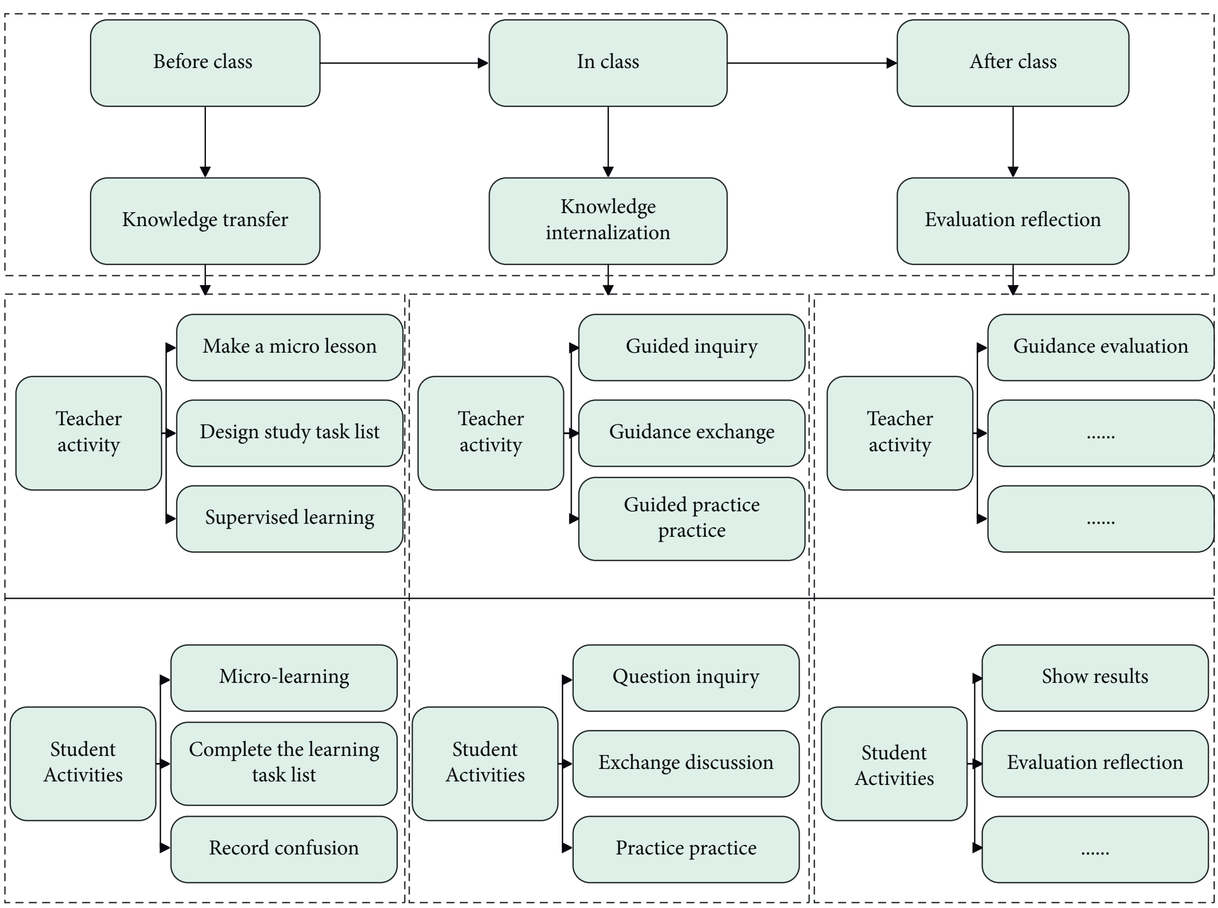

FIGURE 9: Flipped classroom teaching process design.

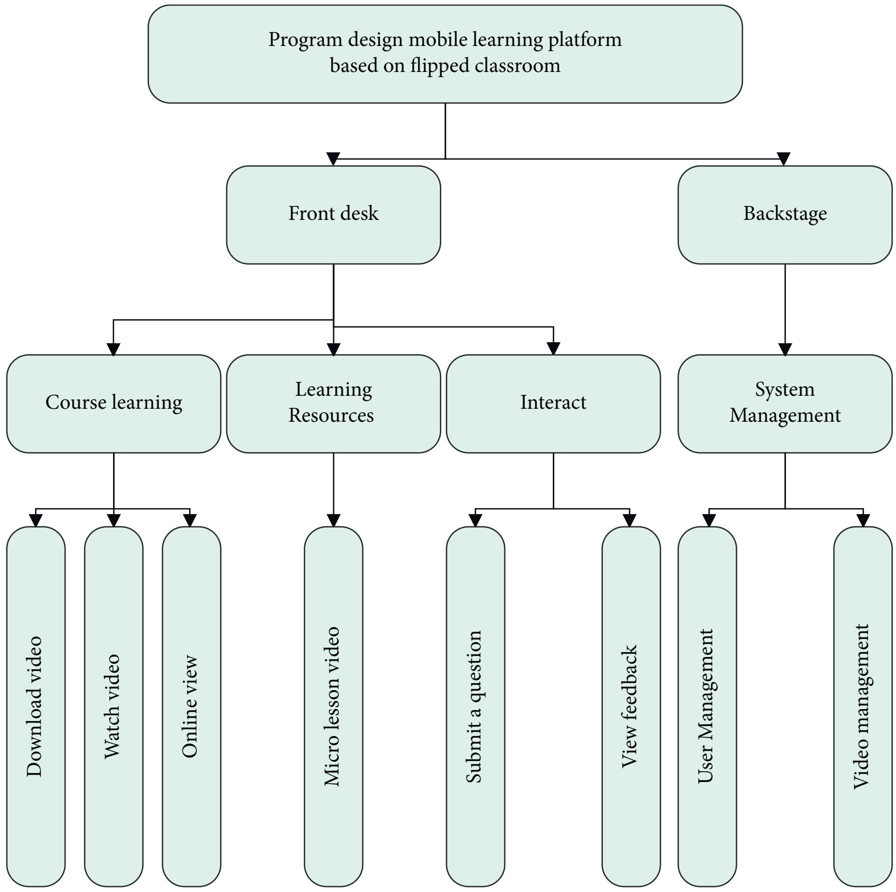

Figure 10: The overall structure design of the system.

$$D_{ratio} = \frac{R}{S}. \quad (15)$$

In this formula, R represents the total number of messages successfully sent to the target node, and S represents the number of messages that the source node has sent to the target node.

3.2. Average Delay. The average delay is the ratio of the total time of messages sent by the node to the total number of successfully reaching the target node. The calculation formula is

$$\overline{T} = \sum_{i=1} \frac{T_i}{R}. \quad (16)$$

Among them, Ti represents the message transmission delay for the i-th node to send a message to the target node within time T, and R is the total number of messages successfully reaching the target node.

3.3. Routing Cost Ratio. It represents the ratio of the total number of messages that the node fails to reach the destination to the total number of messages that successfully reach the destination under the conditions of the experiment. The calculation formula is

$$R_{ratio} = \frac{\left(\sum_{j=1}^{n} S_i - R\right)}{R}. \quad (17)$$

Among them, R_{ratio} represents the routing cost ratio of the message forwarding process, and $\sum_{j=1}^{n} S_i$ represents the total number of messages sent by the source node to the destination node.

4. Optimization of the Flipped Classroom Teaching Mode of Programming Courses Based on Social Cognitive Network

In this paper, the optimization analysis of the flipped classroom teaching mode of programming courses is carried out by transferring part of the cognitive network. In the teaching process, students should be guided to understand the relationship between the core concepts and key capabilities of this chapter. The relationship between the core concepts and key capabilities of "Algorithm and Program" is shown in Figure 8.

On the basis of sorting out and analyzing the research of the flipped classroom model, according to the particularity of the information technology curriculum and the specific situation of the school, this paper designs a three-stage flipped classroom model process including "before class, knowledge transfer," "in class, knowledge

Table 1: Statistical table of evaluation of the teaching effect of flipped classroom of programming courses based on social cognitive network.

NO	Teaching evaluation
1	86.31
2	91.19
3	87.96
4	81.39
5	90.09
6	86.07
7	87.86
8	92.90
9	91.19
10	86.07
11	89.99
12	86.46
13	89.15
14	92.34
15	86.93
16	84.47
17	91.50
18	90.81
19	85.67
20	91.59
21	92.50
22	80.55
23	91.43
24	85.89
25	91.44
26	84.80
27	91.08
28	92.48
29	83.42
30	92.16
31	91.93
32	79.54
33	88.35
34	90.97
35	80.82
36	84.79
37	82.76
38	90.38
39	84.02
40	81.30
41	83.36
42	83.41
43	85.95
44	84.66
45	91.41
46	84.44
47	83.43
48	82.01
49	86.77
50	92.19
51	87.66
52	84.42
53	81.96
54	86.71
55	92.62
56	81.19
57	86.95
58	81.30
59	84.46
60	91.36
61	80.06
62	79.51
63	86.89
64	82.73
65	92.24
66	87.49
67	90.44
68	85.17
69	86.57
70	82.21
71	83.70
72	84.11
73	85.45
74	89.65
75	92.97
76	82.16
77	85.11
78	81.76
79	82.71
80	89.65

internalization," and "after class, evaluation and reflection." The tasks in the preclass stage include the following: teachers make microclasses, design self-learning task lists, and supervise learning, and students watch microclasses to self-learn, complete self-learning task lists, and record confusion. The tasks of the in-class stage are as follows: teachers guide inquiry, guide communication, guide practice, and practice, and students carry out problem exploration, exchange and discuss, and implement practice. The tasks in the after-school phase are as follows: teachers perform guidance and evaluation, and students show results and perform evaluation and reflection. The design of the flipped classroom teaching process is shown in Figure 9.

The mobile learning platform is developed based on the mobile terminal platform and is mainly used in mobile devices, such as smart phones and tablet computers, including an operating system, middleware, and some key platform applications. Moreover, it can be ported to different hardware platforms. The system consists of two parts: the foreground and the background. The front desk functions include user login, user registration, interactive communication module, course learning module, and learning resource module. The background is the system management module, which is mainly operated by the administrator, including student management and resource management. Figure 10 shows the overall structure of the mobile learning platform.

After constructing the above system, the performance of this system is verified through experimental teaching methods, and the teaching effect is counted. The results obtained are shown in Table 1 and Figure 11 below.

From the above research, we can see that the flipped classroom teaching system of programming courses based

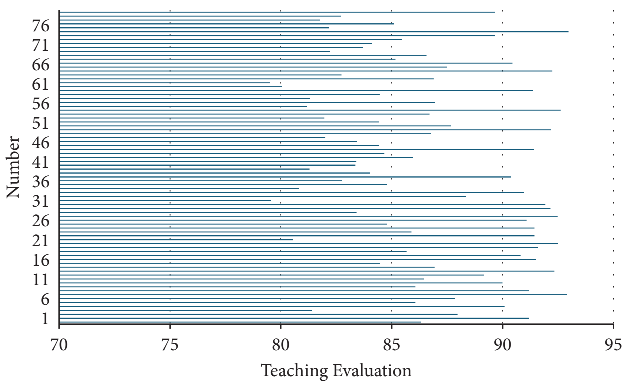

Figure 11: Statistical diagram of evaluation of the teaching effect of flipped classroom of programming courses based on social cognitive network.

on social cognitive network constructed in this paper has good teaching effects and can effectively improve the teaching quality of programming courses.

5. Conclusion

The emergence of the flipped classroom has provided a new direction and injected fresh vitality for the reform of education and teaching. Based on the relevant theories and practices of microclasses and flipped classrooms, this paper creatively combines microclasses, flipped classrooms, and high school algorithms with programming teaching based on the actual teaching work. Moreover, this paper combines social cognitive network and wireless information dissemination technology to design a three-stage model of flipped classroom teaching based on microclasses and apply it to the teaching practice of algorithm and programming. In addition, this paper analyzes the optimization of the flipped classroom teaching mode of programming courses through the transfer of part of the cognitive network. Finally, this paper designs an experiment to verify the performance of the system constructed in this paper. The research results show the effectiveness of flipped classroom based on social cognitive network in algorithm and programming teaching.

Data Availability

The data used to support the findings of this study are available from the corresponding author upon request.

Conflicts of Interest

The authors declare that they have no conflicts of interest.

Acknowledgments

The research was supported by Railway Police College university-level curriculum ideological and political construction project (Communication and Expression SZ202005) and the Railway Police College university-level first-class undergraduate curriculum construction project in 2020 (Communication and Expression YLKC2011).

References

[1] L. Zhou, H. Li, and K. Sun, "Teaching performance evaluation by means of a hierarchical multifactorial evaluation model based on type-2 fuzzy sets," *Applied Intelligence*, vol. 46, no. 1, pp. 1–11, 2016.

[2] J. Porozovs, L. Liepniece, and D. Voita, "Evaluation of the teaching methods used in secondary school biology lessons," *Journal of Pedagogy and Psychology "Signum Temporis"*, vol. 7, no. 1, pp. 60–66, 2015.

[3] M. A. Oliveros, A. García, and B. Valdez, "Evaluation of a teaching sequence regarding science, technology and society values in higher education," *Creative Education*, vol. 6, no. 16, pp. 1768–1775, 2015.

[4] M. Sánchez Cerón and F. M. D. S. Corte Cruz, "The evaluation of teaching: some consequences for Latin America," *Revista Mexicana de Investigación Educativa*, vol. 20, no. 67, pp. 1233–1253, 2015.

[5] A. Li, K. Li, K. Li, and Z. Ge, "Application of data mining in the colleges' in-class teaching quality evaluation system," *Journal of Computers*, vol. 10, no. 3, pp. 166–175, 2015.

[6] K. Angell and E. Tewell, "Teaching and un-teaching source evaluation: questioning authority in information literacy instruction," *Comminfolit*, vol. 11, no. 1, pp. 95–121, 2017.

[7] M. Brkovic and P. Chiles, "'Spector - the sustainability inspector': participatory teaching, learning and evaluation game for architects, architecture students and pupils," *Facta Universitatis - Series: Architecture and Civil Engineering*, vol. 14, no. 1, pp. 1–20, 2016.

[8] T. H. Reisenwitz, "Student evaluation of teaching: an investigation of nonresponse bias in an online context," *Journal of Marketing Education*, vol. 38, no. 4, pp. 139–144, 2015.

[9] Y. Jiang and Y. Wang, "Evaluation of teaching quality of public physical education in colleges based on the fuzzy evaluation theory," *Journal of Computational and Theoretical Nanoscience*, vol. 13, no. 12, pp. 9848–9851, 2016.

[10] K. Royal, "A guide for making valid interpretations of student evaluation of teaching (SET) results," *Journal of Veterinary Medical Education*, vol. 44, no. 2, pp. 316–322, 2016.

[11] F. Garofalo, P. Mota-Moya, A. Munday, and S. Romy, "Total extraperitoneal hernia repair: residency teaching program and outcome evaluation[J]," *World Journal of Surgery*, vol. 41, no. 1, pp. 1–6, 2017.

[12] G. Gong and S. Liu, "Consideration of evaluation of teaching at colleges," *Open Journal of Social Sciences*, vol. 4, no. 7, pp. 82–84, 2016.

[13] U. Klusmann, D. Richter, and O. Lüdtke, "Teachers' emotional exhaustion is negatively related to students' achievement: evidence from a large-scale assessment study," *Journal of Educational Psychology*, vol. 108, no. 8, pp. 1193–1203, 2016.

[14] H. W. Marsh, A. S. Abduljabbar, P. D. Parker et al., "The internal/external frame of reference model of self-concept and achievement relations," *American Educational Research Journal*, vol. 52, no. 1, pp. 168–202, 2015.

[15] M. Pinxten, C. Van Soom, C. Peeters, T. De Laet, and G. Langie, "At-risk at the gate: prediction of study success of first-year science and engineering students in an open-admission university in Flanders-any incremental validity of study strategies?" *European Journal of Psychology of Education*, vol. 34, no. 1, pp. 45–66, 2019.

[16] M. Brehm, S. A. Imberman, and M. F. Lovenheim, "Achievement effects of individual performance incentives in a teacher merit pay tournament," *Labour Economics*, vol. 44, no. 5, pp. 133–150, 2017.

[17] R. J. Mcgill and A. R. Spurgin, “Assessing the incremental value OF kabc-II luria model scores IN predicting achievement: what do they tell US beyond the mpi?” *Psychology in the Schools*, vol. 53, no. 7, pp. 677–689, 2016.
[18] T. Mohoric and V. Taksic, “Emotional understanding as a predictor of socio-emotional functioning and school achievement in adolescence,” *Psihologija*, vol. 49, no. 4, pp. 357–374, 2016.
[19] D. L. Rabiner, J. Godwin, and K. A. Dodge, “Predicting academic achievement and attainment: the contribution of early academic skills, attention difficulties, and social competence,” *School Psychology Review*, vol. 45, no. 2, pp. 250–267, 2016.
[20] C. W. Coley, R. Barzilay, T. S. Jaakkola, W. H. Green, and K. F. Jensen, “Prediction of organic reaction outcomes using machine learning,” *ACS Central Science*, vol. 3, no. 5, pp. 434–443, 2017.
[21] A. Chowdhury, E. Kautz, B. Yener, and D. Lewis, “Image driven machine learning methods for microstructure recognition,” *Computational Materials Science*, vol. 123, no. 8, pp. 176–187, 2016.
[22] S. Basith, B. Manavalan, T. H. Shin, and G. Lee, “SDM6A: a web-based integrative machine-learning framework for predicting 6mA sites in the rice genome,” *Molecular Therapy - Nucleic Acids*, vol. 18, no. 6, pp. 131–141, 2019.
[23] C. Voyant, G. Notton, S. Kalogirou et al., “Machine learning methods for solar radiation forecasting: a review,” *Renewable Energy*, vol. 105, no. 2, pp. 569–582, 2017.

Hindawi
Scientific Programming
Volume 2021, Article ID 3481469, 9 pages
https://doi.org/10.1155/2021/3481469

Research Article

Sports Intelligent Assistance System Based on Deep Learning

Boyin Wu

School of Master of Science in Sports, Macao Polytechnic Institute, Macao 999078, China

Correspondence should be addressed to Boyin Wu; p2009629@ipm.edu.mo

Received 25 September 2021; Accepted 23 October 2021; Published 19 November 2021

Academic Editor: Le Sun

Traditional sports aid systems analyze sports data via sensors and other types of equipment and can support athletes with retrospective analysis, but they require several sensors and have limited data. This paper examines a sports aid system that uses deep learning to recognize, review, and analyze behaviors through video acquisition and intelligent video sequence processing. This paper's primary research is as follows: (1) With an eye on the motion assistance system's application scenarios, the network topology and implementation details of the two-stage Faster R-CNN and the single-stage YOLOv3 target detection algorithms are investigated. Additionally, training procedures are used to enhance the algorithm's detection performance and training speed. (2) To address the issue of target detection techniques' low detection performance in complicated backgrounds, an improved scheme from Faster R-CNN is proposed. To begin, a new approach replaces the VGG-16 network in the previous algorithm with a ResNet-101 network. Second, an expansion plan for the dataset is provided. (3) To address the short duration of action video and the high correlation of image sequence data, we present an action recognition method based on LSTM. To begin, we will present a motion decomposition scheme and evaluation index based on the key transaction frame in order to simplify the motion analysis procedure. Second, the spatial features of the frame images are extracted using a convolutional neural network. Besides, the spatial and temporal aspects of the image sequence are fused using a two-layer bidirectional LSTM network. The algorithm suggested in this research has been validated using a golf experiment, and the results are favorable.

1. Introduction

More and more people are devoting their time to sports such as golf and skiing as China's burgeoning sports and health industry becomes more active. When there is no systematic learning, beginners may not develop their technical level because of nonstandard movements, and in certain cases, they may even injure themselves playing sports. To achieve continuous improvements, you must assess and analyze your efforts constantly. Traditionally, sports coaches have done one-to-one coaching. High labor costs and poor flexibility are difficulties for the company. As it currently stands, there is a problem that has to be fixed when it comes to teaching and training. In professional athletes' daily training, they use sports assist devices. Professional training analysts, modeling the athletes based on motion sensor data, use the data of the limbs to track and correct the specifics of the athletes' motions. Because of the high price and the need for specialized motion sensors, the present sports aid system is difficult and costly for sports enthusiasts who are not professional athletes [1–8].

These recent advances in computer vision and natural language processing, made possible by a boost in the amount of training data and the addition of sophisticated feature expression capabilities, have been achieved using deep learning. A great number of practical achievements have been accomplished in the target detection, machine translation, and action identification departments. Many vision tasks are based on object detection, which is a research issue in computer vision. As a result, face recognition, autonomous driving, and target tracking have all seen widespread use in real life. This traditional target detection method extracts characteristics artificially, and the results are sometimes inferior due to poor feature extraction or inadequate recognition. Deep convolutional neural networks can automatically extract task-related feature information from enormous data because of the development of convolutional neural networks. Traditional machine learning methods, which can easily be implemented by specifying rules for feature extraction, have clear advantages. The deep learning target detection technique, on the other hand, has improved the accuracy and speed of detection significantly. By further expanding the applications of computer vision, it increases the overall value. Another field of computer vision study is semantic analysis of video, specifically human action recognition, which has a variety of possible applications, such as human-computer interaction and gesture recognition. The primary goal of it is for videos. Pure static graphics no longer serve as a proper means of describing video aspects. Human motion recognition hence has to assess the temporal features in addition to extracting the spatial features of each frame of video. Recurrent neural networks are now frequently employed in machine translation, text generation, and personalized recommendation applications. Recurrent neural networks and convolutional neural networks are being combined to address the demanding problem of processing video sequences [6–15].

This paper studies the exercise assistance system, which does not require sensors. It can recognize movements only through video sequences, which is convenient for users to quickly review and analyze their movements in real time. It not only enriches the learning methods of sports but also provides new ideas for the development of sports assistance systems, which is extremely important for the promotion of the development of sports events.

The contribution of this paper can be summarized as follows: (1) the detection efficiency of target detection algorithm is improved in complex background; (2) a sports recognition algorithm based on LSTM is proposed, which can fuse spatial features as well as temporal features; and (3) the proposed method achieved advanced performance.

2. Related Work

Literature [16] proposed a deep convolutional neural network AlexNet. In the ImageNet competition that year, excellent results were achieved, which proved the huge potential of convolutional neural networks in image processing tasks. Literature [17] proposed R-CNN, which used a selective search algorithm to generate about two thousand candidate regions for each image. Then through the forward propagation of the convolutional neural network, feature extraction was performed on each candidate area, and finally, the feature information of each candidate area was classified using linear SVM. R-CNN can output and correct the bounding box. mAP can reach 58.5%, which was a relatively large improvement compared to the previous algorithm. However, the selective search method needed to extract feature values and classify each candidate frame. This process generated a lot of redundant calculations, which consumed a lot of memory and calculation time, and the average processing time for each picture was about 3 s. The fully connected layer as a classification also required a fixed-size input and forced conversion of the size of the input image would also cause image distortion. In literature [18], the Faster R-CNN was designed for the problem that the candidate region generation algorithm was too time-consuming and space-consuming. The principle of the Faster R-CNN was as follows: first, the image was extracted from the convolutional network to learn the feature and output to the RPN network, and then the RPN network determined in the classification layer that the anchor belonged to the foreground or the background and finally converted the region of interest into a feature vector. At the same time, it was output to the type recognition classifier and the border correction regressor. Faster R-CNN replaced the fully connected layer with a fully convolutional layer, which truly realized end-to-end calculation, and the detection speed and accuracy had been further improved. Literature [19, 20] proposed the YOLO series of algorithms. Divide the input image into several grids. If the target object's center was in the grid, each grid needed to predict the value of N boundary candidate boxes and output the position coordinates and confidence of each boundary box. End-to-end training could be achieved. Although the detection performance was not as good as the two-stage algorithm, its detection speed was faster. But it could only detect target objects that fall into the grid. When a grid contains multiple target objects that are close to each other, the detection performance is relatively poor.

Literature [21] proposed a dual-stream convolutional network, which divided the network into two independent streams, and the spatial convolutional stream learned the spatial characteristics of a single frame of pictures. The optical flow convolutional flow learned the optical flow sequence that represents the characteristics of video timing information. Finally, the two network streams were fused and output. The dual-stream network used a single-frame image and optical flow field bands to represent the spatial and temporal characteristics of the video sequence. However, it was difficult to represent the spatial characteristics of long-term video using a single-frame image. In view of the limitations of the dual-stream model for the sampling of long-term video sequences, literature [22] proposed a time segmentation network to improve the input of the dual-stream network. The long video was randomly divided into K segments and input into K dual-stream networks. Use random sampling to sample image frames from fragments and input them into the spatial convolution stream. Finally, the results of K optical flow networks were merged to obtain the final result, which obtained a high score of 94.2 on the UCF101 dataset. Literature [23] extended the two-dimensional convolutional neural network directly to the three-dimensional convolutional neural network. By adding information in the time dimension, the two-dimensional convolution kernel was extended to the three-dimensional convolution kernel, and the convolution kernel slides in the time dimension. The features of the time dimension could be effectively extracted. Literature [24] designed the I3D network, extended the pooling kernel to three dimensions, and added the optical flow information to the three-dimensional convolutional neural network. Literature [25] added the idea of jump connection of residual network and deepened the network depth of the three-dimensional convolutional network. The proposed network structure based on the three-dimensional convolutional network neural network was relatively simple and inherited the weight sharing and integration of the convolutional network. The three-dimensional convolutional network was limited by the width of the convolution kernel, and it was difficult to learn long-time information. Literature [26] designed an action recognition algorithm based on a double stream network for hockey action analysis. The network first obtained human body posture information through a partial affinity field, secondly used optical flow field to extract time features, and finally combined posture information and optical flow to estimate the hockey player's movements. Literature [27] proposed that SoccerNet was used for football game video analysis. According to the image information of the football game video, it automatically recognized the key event time nodes in the football game, such as red and yellow cards, goals, and replacement players.

3. Target Detection Based on Deep Learning

With the continuous development of deep learning, target detection algorithms have gradually replaced traditional target detection algorithms. The proposal of R-CNN first applies deep learning technology to target detection tasks. Fast R-CNN is improved and optimized on the basis of R-CNN and has achieved good performance in detection efficiency and training time.

The current research on target detection algorithms is divided into two branches: one is the two-stage target detection with priority in detection accuracy, represented by Faster R-CNN. The feature information is classified and output. The regional suggestion network can output according to the feature information of different scales. Since the algorithm performs regression correction on the target object frame in the process of generating candidate regions and classifying, the algorithm has good detection accuracy; the other is single-stage target detection algorithm with priority on detection speed, and its representative is the YOLO series of algorithms. The principle of the algorithm is as follows: divide the picture into a fixed-size network and use a priori box of preset size to directly perform feature extraction and classification on the a priori box of each grid. Due to the entire process is required, the speed of YOLO is faster. Aiming at the application scenarios of the motion assistance system, this chapter compares and analyzes the current mainstream target detection algorithms based on deep learning. Finally, a comparative experiment is carried out on the motion video keyframe image dataset, and its application scenarios are analyzed according to the detection performance of different algorithms.

3.1. Faster R-CNN. It is the first target detection algorithm that can be trained in an end-to-end method. The subsequent two-stage target detection algorithm is basically improved according to the idea, and Faster R-CNN is considered to be a milestone of the two-stage target detection algorithm. As shown in Figure 1, the workflow of Faster R-ANN is as follows: first, the input image is extracted by the backbone, and then the feature map is input into RPN to obtain the proposal. Cut out the feature map of the candidate area and output it to the ROI Pooling to generate a candidate area, and finally output it to the classifier for type classification and the regression to correct the prediction frame.

Faster R-CNN introduces RPN to extract candidate regions. This is a CNN that can share features of the convolutional layer and extract candidate regions from this. The extracted part of the candidate region is embedded into the network, which in a true sense realizes the end-to-end target detection. After obtaining the candidate area, perform target classification and bounding box regression. RPN′ implementation is as follows: use a 3×3 sliding window to generate a feature vector of length 256 or 512 on the feature map extracted by the network, and then output this feature vector to two fully connected layers for prediction of the center coordinates; width and height of the candidate area are used to predict whether the candidate area belongs to the foreground or the background. This sliding window method can ensure that the regression layer and the classification layer cover the entire space of the feature map. For each sliding window, k region suggestions can be predicted at the same time, so there are 4k outputs for the regression layer, that is, the 4 coordinate parameters corresponding to the candidate region, and the classification layer is 2k, that is, whether the candidate region is the target or the background. The k candidate regions are the parameterization of k anchors. Each anchor has a strong translation invariance, which is beneficial to improve the quality of detection.

$$L(\{p_i\},\{t_i\}) = \frac{1}{N_{\mathrm{cls}}}\sum_i L_{\mathrm{cls}}(p_i, p_i^*) + \lambda \frac{1}{N_{\mathrm{reg}}}\sum_i pi^* L_{\mathrm{reg}}(t_i, t_i^*), \tag{1}$$

where i is the anchor index, p_i is the prediction probability of the anchor i target, if the anchor is positive, p_i^* is 1, otherwise, it is 0, and t_i represents the 4 coordinate parameters of the predicted candidate frame. t_i^* represents the coordinate parameters of the real target frame corresponding to the positive anchor. The specific classification loss and regression loss functions are as follows:

$$\begin{aligned} L_{\mathrm{cls}}(p_i, p_i^*) &= -\log[p_i p_i^* + (1-p_i^*)(1-p_i)], \\ L_{\mathrm{reg}}(t_i, t_i^*) &= R(t_i - t_i^*), \end{aligned} \tag{2}$$

where R is the robust loss function, as illustrated in the following equation:

$$\mathrm{smooth}_{L_1}(x) = \begin{cases} 0.5x^2, & \text{if} |x| < 1, \\ |x| - 0.5, & \text{otherwise.} \end{cases} \tag{3}$$

Faster R-CNN uses VGG-16 as the backbone network. It has achieved relatively good results in ImageNet classification tasks, and its model compatibility is relatively high. It is widely used as a feature extraction network in various image analysis tasks. Since the target detection task not only needs to classify the image but also needs to locate the target, the ability to extract features may have an important impact on the accuracy of the model. An improved scheme of objection detection is proposed, using ResNet-101 instead of source code VGG-16 as the backbone network of the target

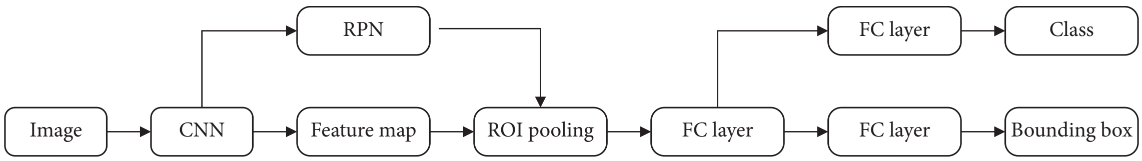

Figure 1: The structure of Faster R-CNN.

detection algorithm. Compared with VGG, the ResNet-101 network has a deeper network structure and can extract richer image feature information. Simultaneously, the network training efficiency is improved by using the residual module, and the network inference speed is accelerated.

3.2. YOLO. The YOLO algorithm is proposed by Redmon et al. It is the representative work of a single-stage target detection algorithm. Its core idea is to transform target detection into a regression task. Different from the two-stage algorithm, the input image can directly output the type information and position information of all detected targets in the image after one inference. In the case of ensuring the accuracy and efficient performance of the target detection task, the entire network only uses a single convolutional neural network, which greatly promotes the training speed and reduces the detection time. As shown in Figure 2, the principle of the YOLO algorithm: first divide the input image into grids, and stipulate that each network is only responsible for detecting objects whose target center falls in the current grid.

Suppose that each grid can predict B target objects, and each box needs to output 4 pieces of position information, that is, the center point coordinates of the target object, the relative height and width of the border, and the confidence of the object corresponding to the output border. The confidence of a five-dimensional tensor represents whether the box contains the target object and the accuracy of the position of the box relative to the real object, which is defined as follows:

$$\text{confidence} = \Pr(\text{Object}) \bullet \text{IOU}_{\text{pred}}^{\text{truth}}, \tag{4}$$

where $\Pr(\text{Object})$ represents whether the center of the detected target object falls in the box; if it falls in the box, its value is 1; otherwise, it is 0. The latter represents the interaction ratio between the predicted object box output by the network and the box of the actual position of the object.

The total loss of YOLO consists of three parts. The formula for classification loss is as follows:

$$L_{\text{cls}} = \sum_{i=0}^{S^2} 1_i^{\text{obj}} \sum_{c\in\text{classes}} \left(p_i(c) - \widehat{p}_i(c)\right)^2, \tag{5}$$

where i is the index of the grid, S is the size of the grid division, c is the category of the objection, and $p_i(c)$ represents the probability that i-th grid contains c target object. 1^{obj} indicates whether there is a target object in the grid i; a value of 1 means that the center of the target object falls in this box; otherwise, it is 0.

The loss function of the bounding box regression is

$$L_{\text{bbox}} = \lambda_{\text{coord}} \sum_{i=0}^{S^2} \sum_{j=0}^{B} \left[\left(x_i - x_i'\right)^2 + \left(y_i - y_i'\right)^2 + \left(\sqrt{w_i} - \sqrt{\widehat{w}_i}\right)^2 + \left(\sqrt{h_i} - \sqrt{\widehat{h}_i}\right)^2 \right], \tag{6}$$

where B means that each grid can output B boxes and λ_{coord} means balance factor.

The loss function of confidence is

$$L_{\text{conf}} = \sum_{i=0}^{S^2} \sum_{j=0}^{B} 1_{ij}^{\text{obj}} \left(C_i - \widehat{C}_i\right)^2 + \lambda_{\text{noobj}} \sum_{i=0}^{S^2} \sum_{j=0}^{B} 1_{ij}^{\text{noobj}} \left(C_i - \widehat{C}_i\right)^2, \tag{7}$$

where C_i is the confidence of j-th output box; 1^{noobj} indicates whether the j-th output box of the grid i contains the detection target, if it contains a value of 0; otherwise, it is 1; λ_{noobj} means balance factor.

Therefore, the final loss function of YOLO is

$$L = L_{\text{cls}} + L_{\text{bbox}} + L_{\text{conf}}. \tag{8}$$

In the estimation process of YOLO, although the output between grids will not conflict, when predicting large size or adjacent objects, multiple grids may predict the same object. At this time, YOLO uses a nonmaximum suppression algorithm to filter out redundant output boxes. The confidence of the final output box is equal to the product of the maximum value P of the category prediction of the grid output and the maximum value of the confidence of the current grid output box. This can also filter out some mostly overlapping boxes. The confidence level of the detected object is output, and the box and category are considered at the same time so that the output of the confidence level is more credible.

3.3. Data Enhancement. Aiming at the problem of complex light sources that may appear in the actual detection scene of golf courses and the problem from different viewpoints and distances, we propose a data enhancement strategy to

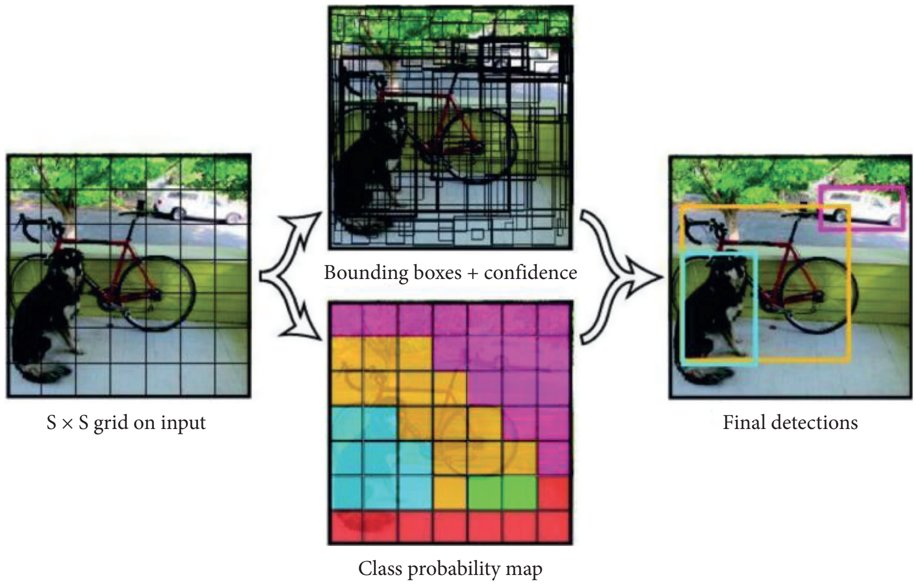

Figure 2: The mechanism of YOLO.

expand the dataset. For the open-air golf situation, where light is relatively strong, the overexposure environment of the camera is simulated by increasing the exposure value as well as the contrast. For underexposure environments such as cloudy days or in the shade of trees, reduce the exposure and contrast of the original image to increase the proportion of dark parts of the image. For the problem of the target object scale that does not need to be brought about by the camera angle and distance, three hybrid data enhancement methods are used: (1) random image translation, which translates the image in the horizontal or vertical direction; (2) random image zoom; (3) random zoom out or zoom in the image.

4. Action Recognition Based on LSTM

Action recognition based on LSTM is to add a recurrent neural network. This kind of hybrid network has the advantages of both CNN and RNN and can obtain information in the time dimension very well. Moreover, LSTM can tackle the problem of RNN due to the disappearance of gradients and cannot handle long-term video well. The problem has shown good results in capturing spatial motion patterns, time-series, and long-term dependencies.

4.1. LSTM Unit. Traditional neural networks, such as convolutional neural networks, have no memory function and cannot pay attention to the relationship between feature information at adjacent moments. Recurrent neural networks (RNN) are mainly used to analyze time-series sequences and can extract the time-series features. RNN combines the hidden layer with the input and outputs it to the hidden layer. In this way, RNN can combine the information at the previous moment to output, and the formula for forward propagation is as follows:

$$\begin{aligned} s_t &= \sigma\left(W_s x_t + U s_{t-1} + b_s\right), \\ o_t &= W_o s_t + b_y\big), \end{aligned} \tag{9}$$

where W_s is the weight parameter of the input data at the current moment, U represents the weight parameter of the hidden state at the previous moment in the hidden state, W_o is the weight of the hidden state and output at the current moment, b represents the offset, and σ function represents the activation function.

RNN is very successful in tasks such as speech recognition and text generation. RNN can transmit characteristic information from front to back. Theoretically, the long-term dependence relationship can be solved; that is, the output at time t contains all the characteristic information at time 0-t, but this is not the case. Because in the training process, RNN also has the problem of gradient disappearance and gradient explosion, which makes the parameters of the neural network unable to be updated correctly. Therefore, the long-distance information often cannot be transmitted to the subsequent output sequence, which makes the input feature information of the network incomplete and ultimately affects the stability. RNN generally has a relatively good analytical power for data with a short distance between related information.

In order to solve the gradient explosion and disappearance, previous research proposed an LSTM network. LSTM unit records sequence information. The input and output of the LSTM unit are controlled by the switch of the control gate. The input gate can control the current input information to participate in the transmission of memory cells, and the forget gate can control the transmission of previous memory cells. The output gate can control how much information the memory unit can output at the current moment.

Each unit of the RNN needs to be connected in series to ensure that the hidden state of each layer will propagate backward through the network. Compared with the traditional RNN, the LSTM network has several more door controls. Both the number of parameters and the number of calculations will rise sharply. When the network needs to predict a longer interval, a multilayer parallel network can be used for recognition tasks. In the action recognition task, the output of the task is to assign an action label to the input video sequence, while in the action detection task, it is necessary to output the correct label on all keyframes of the input video sequence. For example, for a 100-frame video sequence, for action recognition tasks, the network only needs to detect any 50 frames of data to output the correct label. In motion detection, if the predicted output tags are not continuous, multiple motion fragments will be generated. This is because LSTM can only transfer the characteristics of timing information in one direction, and the input information at the later stage of the sequence cannot participate in the output at the early stage of the sequence. Through this multilayer bidirectional LSTM network, each output of the sequence can use the input information. In the task of motion detection, discrete motion fragments can be automatically supplemented into continuous motions through multilayer bidirectional LSTM network propagation back and forth. The Softmax layer of the multilayer two-way LSTM network provides a score for each action category, and the behavior of the LSTM network is taken as the score for each action.

4.2. Golf Swing Algorithm. Donahue et al. [28] proposed an LCRN, which can achieve end-to-end training, take full advantage of CNN's strong ability to extract image information, and make the network have the ability to process timing information by adding LSTM. LCRN is composed of input layer, feature extraction layer, LSTM layer, and output layer. CNN is used to process variable-length video single-frame pictures and output the extracted feature maps of the single-frame pictures to the LSTM network. The final output layer produces a variable-length output.

This paper uses an action recognition algorithm based on LSTM. Similar to the method of LRCN, the single-frame picture of the input video obtains the feature map of the single-frame picture through the feature extraction network, and then the feature map is globally averaged and pooled and then input into the two-layer bidirectional LSTM network as shown in Figure 3. The LSTM network can add time-dimensional feature information to the spatial features. The double-layer LSTM network ensures that image features can be transmitted in both directions, and the time feature of each frame of image can fully combine the frame information in the front and back directions. The two-layer LSTM network further integrates the characteristic information of the single-layer LSTM network. After passing through two fully connected layers, LSTM's output is input to the Softmax layer for classification, and finally, the classification result of each frame of the input video sequence is obtained.

Time characteristics are the key to golf swing recognition. Generally, the process from Address (A) to Top (T) is the same as the process from Top (T) to Impact (I), except that the swing direction is opposite. The image features are basically the same. At the same time, athletes often carry out repeated pretargeting process before Address (A), and the video sequence may contain multiple points similar to the Address (A) image feature. It is difficult to distinguish if the time sequence feature is not added. The action recognition network based on the long and short-term memory network can accurately predict the keyframes of the model through the context information of the video sequence by adding the LSTM unit. The spatial features of the output of the feature extraction network pass through the two-layer two-way LSTM network to add timing features, then pass to two fully connected layers, and finally pass through the Softmax classifier to realize the mapping of spatiotemporal features to the posterior probability. The definition of the Softmax function is as follows:

$$S_i = \frac{e^{z_i}}{\sum_j e_j}. \tag{10}$$

Each frame of image will get a posterior probability distribution vector of all types, and the final output form is the mapping $e_t = (p_1, p_2, \ldots, p_c)$ of all event probabilities and the final output of the model $(e_1, e_2, \ldots, e_T)$, where T represents the sequence length and c represents the category of the output frame. This model c has 9 output frame types, including 8 golf swing motion keyframes and 1 invalid frame.

5. Experiments and Discussions

5.1. Evaluation of Golf Detection. The model after the training convergence is tested, and detection accuracy of golf ball, the detection accuracy of the golf club head, the average accuracy of the model, and the average detection speed of a single picture are, respectively, detected. The detection result is illustrated in Figure 4.

mAP of Faster R-CNN is 73.7%, and mAP of YOLOv3 is 62.7%. From the experimental data, it can be seen that Faster R-CNN has a better performance than YOLOv3. Because Faster R-CNN's RPN network can extract more prior frames, its recall rate is higher than that of YOLOv3. However, because the two-stage target detection algorithm must first extract the candidate frame and then classify according to the features in the classification frame, it needs to enter two classifiers, and the calculation amount is much larger than YOLOv3, so its detection speed is also much slower than YOLOv3. The detection speed of YOLOv3 is 0.03 s.

Use the data enhancement scheme to expand the data, and train Faster R-CNN with the expanded data. The detection result is illustrated in Table 1; using the enhanced dataset for training, the accuracy of target detection under complex light sources has been improved, and mAP of Faster R-CNN has increased by 4.3%. Especially under complex light sources, the detection performance of the model trained with enhanced data has been significantly improved. But for the golf ball in the distant state, due to the small size, the detection rate of the target object is still very low.

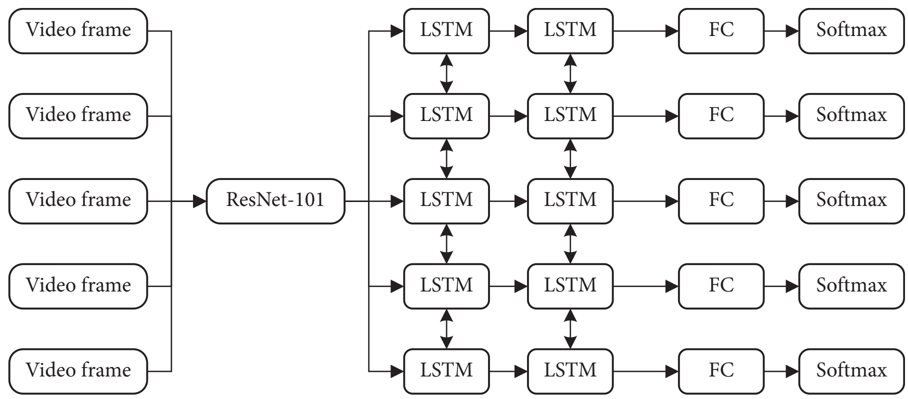

Figure 3: Swing action recognition network.

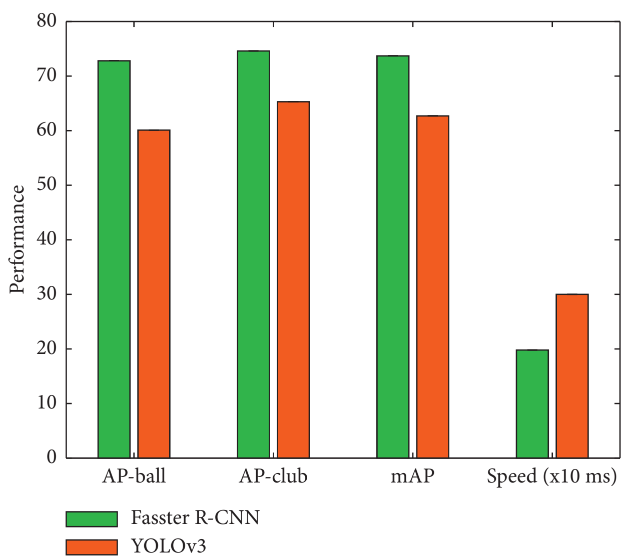

Figure 4: Detection performance comparison between FasterR-CNN and YOLOv3.

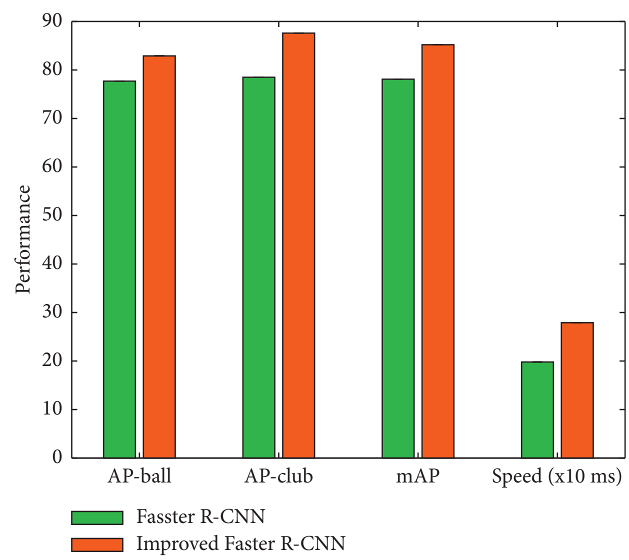

Figure 5: Target detection accuracy of the improved model.

Table 1: The impact of data augmentation on the accuracy of model detection.

Model	Data enhancement	mAP
Faster R-CNN	Yes	73.7
Faster R-CNN	No	78.0

This paper uses ResNet-101 instead of VGG-16 in the source code as the backbone network of the target detection algorithm and trains the improved Faster R-CNN model after data enhancement. The detection performance is verified on the test set as shown in Figure 5.

ResNet-101 can extract higher-dimensional image feature information, and the improved Faster R-CNN's mAP is as high as 85.2%. The CNN model has increased by 7.2%. Due to the deeper network structure of ResNet-101, the parameters in the network have also increased exponentially. However, due to the role of the residual module, the average of a single image can be seen from the detection results. The detection speed is only 0.081 seconds slower than the original structure. Because the motion assistance system does not require high real-time performance, the use of the improved Faster R-CNN can significantly improve the performance.

5.2. Evaluation on Action Recognition. The action recognition algorithm based on the LSTM is very important for the selection of the input sequence length T. This paper uses different sequence lengths T for experimental records, and the experimental result is illustrated in Figure 6. Under the condition of the other parameters unchanged, check the impact on the accuracy of the model. Affected by the hardware performance of the machine, when the sequence length T is too large, some comparative experiments need to reduce the batch size to ensure the GPU memory space. Batch processing can improve the training speed of the model and make full use of GPU parallel computing capabilities, relying on the advantages of weight sharing of convolutional neural networks; through one calculation, multiple input video samples are calculated in parallel, which greatly improves the training efficiency. However, batch processing is only helpful for the improvement of model training speed, and the size of

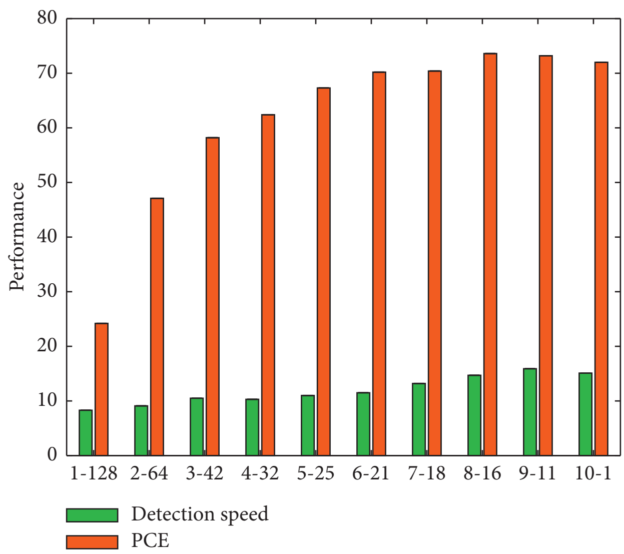

Figure 6: The influence of different T and B on accuracy and detection speed.

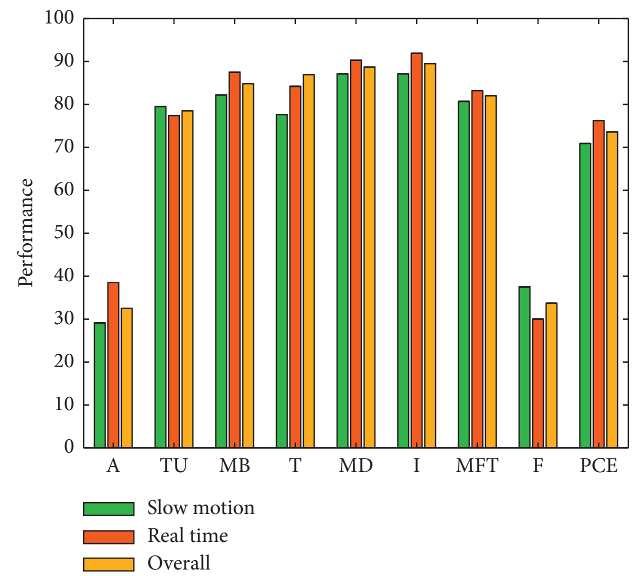

Figure 7: Detection accuracy of different keyframes.

batch processing has relatively little effect on the accuracy of model detection.

In the real-time state and slow-motion state, the detection efficiency of each keyframe of the action recognition model is tested. Figure 7 provides the detection accuracy of each keyframe of the model in the GolfDB test set. The PCE of the keyframe and the average value of the overall PCE are, respectively, detected for the slow-motion and real-time video data. In general, the overall performance of the model recognition is good, and the accuracy of the action recognition is 73.4%. Experiments have found that the detection rate of Address (A) and Finish (F) keyframes is worse than other frames. These frames have two common characteristics. First, the swing speed of the clubhead in and around the frame is relatively low. Since Address (A) is the beginning of the golf swing, its initial speed is 0, Finish (F) is the end of the swing, and its final speed is also 0. Secondly, the frame can only use the feature information in one direction. For the Address (A) frame, the image before the frame has no annotation information, and for the Finish (F) frame, there is no annotation information for the subsequent images. These two factors make it difficult for the model to accurately locate Address (A) and Finish (F) in time.

Experiments have found that the detection rate of Top (T) relative to adjacent frames is also relatively low, which may be due to the change in speed direction when the golf club is lifted to the highest point. The club speed of the surrounding frames is also relatively low, but because the golf club head stays at the top for a relatively short time and the distance between the Top (T) and the surrounding keyframes is relatively small, the Top (T) frame is compared with the Address (A) and Finish (F) which have a relatively little reduction in detection performance. At the same time, because the front swing is generally faster than the backswing, the frame detection performance of the front swing is generally better than the backswing. Compared with slow-motion samples, the detection efficiency of keyframes in each stage of real-time video is also more accurate, which further verifies the assumption that the model is sensitive to speed.

6. Conclusions

This paper studies the golf detection method and the golf swing motion recognition method for video sequences. Faster R-CNN and YOLOv3 models are trained using the golf dataset. Through comparative experiments, Faster R-CNN has better detection than the YOLOv3 algorithm. mAP of Faster R-CNN is 73.7%, and the average speed of a single image is 0.19s. The detection accuracy of YOLOv3 reaches 62.7%, and the average detection speed is 0.030s. Aiming at the complex lighting background that may appear in the golf course, the dataset is enhanced, and the open-air glare environment of golf is simulated by increasing the exposure and contrast of the picture by reducing the exposure and contrast while increasing the dark information method to simulate the insufficient light environment such as the shade of the stadium. By zooming and rotating the image, it simulates the scale problem of the target object in the image taken by the mobile phone or camera at different distances and different angles. Using ResNet-101 instead of VGG-16, ResNet-101 has a deeper network structure and can extract richer information. For action recognition algorithms, this paper proposes an action recognition network based on LSTM. The spatial information of each frame is input into the two-layer two-way LSTM, and the temporal features can be extracted. Finally, temporal and spatial features are input into the Softmax classifier to classify each frame of the image. According to different input sequence lengths, the final accuracy of the model is analyzed experimentally. For the difference in keyframe detection accuracy, the actual scene of the golf swing is analyzed. The network is trained on the GolfDB dataset, and the final detection accuracy of the model is 73.6%. With a tolerance of about 3 frames, the performance of the action recognition algorithm is as high as 88.5%.

Data Availability

The datasets used are available from the corresponding author upon reasonable request.

Conflicts of Interest

The author declares that he has no conflicts of interest.

References

[1] J. N. Roemmich, E. J. Richmond, and A. D. Rogol, "Consequences of sport training during puberty," *Journal of Endocrinological Investigation*, vol. 24, no. 9, pp. 708–715, 2001.

[2] N. Zulkifli, F. Harun, and N. S. Azahar, "XBee wireless sensor networks for heart rate monitoring in sport training," *Applied Physics A*, vol. 106, no. 2, pp. 295–307, 2012.

[3] V. A. Zaporozhanov, T. Borachinski, and Y. N. Nosko, "Assessment of children's potentials in dynamic of initial stage of sport training," *Journal of Physical Education & Sport*, vol. 15, no. 3, pp. 525–530, 2015.

[4] R. M. Matina and A. D. Rogol, "Sport training and the growth and pubertal maturation of young athletes," *Pediatric Endocrinology Reviews: PER*, vol. 9, no. 1, pp. 441–455, 2011.

[5] J. Pei, K. Zhong, J. Li, J. Xu, and X. Wang, "ECNN: evaluating a cluster-neural network nodel for city innovation capability," *Neural Computing & Applications*, pp. 1–13, 2021.

[6] A. Garcia-Garcia, S. Orts-Escolano, S. Oprea, V. Villena-Martinez, P. Martinez-Gonzalez, and J. Garcia-Rodriguez, "A survey on deep learning techniques for image and video semantic segmentation," *Applied Soft Computing*, vol. 70, Article ID S1568494618302813, 2018.

[7] C. Shang and Y. Zhang, "Combining Newton interpolation and deep learning for image classification," *Electronics Letters*, vol. 51, no. 1, pp. 40–42, 2015.

[8] F. Xiang, G. Ding, J. Su, W. Zhang, J. Wu, and X. Gu, "Dangerous target recognition of massive image and video based on deep learning," in *Proceedings of the e2019 Chinese Automation Congress (CAC)*, IEEE, Hangzhou, China, February 2020.

[9] M. Iliadis, *Sparse Representation and Deep Learning for Image and Video Reconstruction*, Northwestern University, Evanston, IL, USA, 2016.

[10] X. Zhang and J. Xiang, "Moving object detection in video satellite image based on deep learning," *Lidar Imaging Detection & Target Recognition*, vol. 2017, Article ID 10605, 2017.

[11] C. Smith, J. Cook, C. Bradley, R. Gosett, and R. Heynas, *Enhancing Deep Learning in Sports Science: The Application of Rich Media Visualization Techniques in Mobile and Reusable Learning Objects*, in *Proceedings of the EdMedia + Innovate Learning*, Vancouver, Canada, June 2007.

[12] H. Song, X. Y. Han, C. E. Montenegro-Marin, and S. Krishnamoorthy, "Secure prediction and assessment of SPorts injuries using deep learning based convolutional neural network," *Journal of Ambient Intelligence and Humanized Computing*, vol. 12, no. 6, pp. 1–12, 2021.

[13] H. Cui and C. Chang, "Deep learning based advanced spatio-temporal extraction model in medical sports rehabilitation for motion analysis and data processing," *IEEE Access*, vol. 8, p. 1, 2020.

[14] H. Kaiyan, W. Qin, Research on 020 platform and promotion algorithm of sports venues based on deep learning technique," *International Journal of Information Technology and Web Engineering*, vol. 13, no. 3, pp. 73–84, 2018.

[15] M. Hagenbuchner, D. P. Cliff, S. G. Trost, N. V. Tuc, and C. E. Peoples, "Prediction of activity type in preschool children using machine learning techniques," *Journal of Science and Medicine in Sport*, vol. 18, no. 4, pp. 426–431, 2014.

[16] A. Krizhevsky, I. Sutskever, and G. E. Hinton, "Imagenet classification with deep convolutional neural networks," *Advances in Neural Information Processing Systems*, vol. 25, pp. 1097–1105, 2012.

[17] R. Girshick, J. Donahue, T. Darrell, and J. Malik, "Rich feature hierarchies for accurate object detection and semantic segmentation," *Proceedings of the IEEE conference on computer vision and pattern recognition*, pp. 580–587, Columbus, OH, USA, June 2014.

[18] S. Ren, K. He, R. Girshick, and R.-C. Faster, "Towards real-time object detection with region proposal networks," *IEEE Transactions on Pattern Analysis and Machine Intelligence*, vol. 39, no. 6, pp. 1137–1149, 2017.

[19] J. Redmon, S. Divvala, R. Girshick, and A. Farhadi, "You only look once: unified, real-time object detection," in *Proceedings of the Computer vision & pattern recognition*, pp. 779–788, IEEE, Las Vegas, NV, USA, June 2016.

[20] J. Redmon and A. Farhadi, "YOLO9000: Better, Faster, Stronger," in *Proceedings of the IEEE Conference on Computer Vision & Pattern Recognition*, pp. 6517–6525, IEEE, Honolulu, HW, USA, July 2017.

[21] K. Simonyan and A. Zisserman, "Two-stream convolutional networks for action recognition in videos," *Advances in Neural Information Processing Systems*, pp. 568–576, 2014, https://arxiv.org/abs/1406.2199.

[22] L. Wang, Y. Xiong, Z. Wang et al., "Temporal segment networks: towards good practices for deep action recognition," in *Proceedings of the European Conference on Computer Vision*, pp. 20–36, Springer, Amsterdam, The Netherlands, October 2016.

[23] D. Tran, L. Bourdev, R. Fergus, L. Torresani, and M. Paluri, "Learning spatiotemporal features with 3D convolutional networks," *IEEE International Conference on Computer Vision. IEEE*, pp. 4489–4497, 2015.

[24] J. Carreira, A. Zisserman, and Q. Vadis, "Action recognition? A new model and the kinetics dataset," in *Proceedings of the 2017 IEEE Conference on Computer Vision and Pattern Recognition (CVPR)*, pp. 6299–6308, IEEE, Honolulu, HW, USA, July 2017.

[25] Z. Qiu, T. Yao, and T. Mei, "Learning Spatio-Temporal Representation with Pseudo-3D Residual Networks," in *Proceedings of the 2017 IEEE International Conference on Computer Vision (ICCV)*, pp. 5533–5541, IEEE, Venice, Italy, October 2017.

[26] Z. Cai, H. Neher, K. Vats, D. Clasui, and J. Zelek, "Temporal hockey action recognition via pose and optical flows," in *Proceedings of the IEEE Conference on Computer Vision and Pattern Recognition (CVPR) Workshops*, IEEE, Long Beach CA, USA, June 2019.

[27] S. Giancola, M. Amine, and T. Dghaily, "Action Spotting in Soccer Videos," in *Proceedings of the 2018 IEEE/CVF Conference on Computer Vision and Pattern Recognition Workshops (CVPRW)*, pp. 1711–1721, IEEE, Salt Lake City, UT, USA, June 2018.

[28] J. Donahue, L. Anne Hendricks, S. Guadarrama, M. Rohrbach, S. Venugopalan, and K. Sea, "Long-term recurrent convolutional networks for visual recognition and description," *Proceedings of the IEEE conference on computer vision and pattern recognition*, vol. 39, pp. 2625–2634, 2015.

Hindawi
Scientific Programming
Volume 2021, Article ID 9545909, 10 pages
https://doi.org/10.1155/2021/9545909

Research Article

Research on Aerobics Training and Evaluation Method Based on Artificial Intelligence-Aided Modeling

Chen Chen

College of Physical Education, Fuyang Normal University, Fuyang, Anhui, China

Correspondence should be addressed to Chen Chen; 201707033@fynu.edu.cn

Received 15 October 2021; Revised 28 October 2021; Accepted 5 November 2021; Published 18 November 2021

Academic Editor: Le Sun

Traditional aerobics training methods have the problems of lack of auxiliary teaching conditions and low-training efficiency. With the in-depth application of artificial intelligence and computer-aided training methods in the field of aerobics teaching and practice, this paper proposes a local space-time preserving Fisher vector (FV) coding method and monocular motion video automatic scoring technology. Firstly, the gradient direction histogram and optical flow histogram are extracted to describe the motion posture and motion characteristics of the human body in motion video. After normalization and data dimensionality reduction based on the principal component analysis, the human motion feature vector with discrimination ability is obtained. Then, the spatiotemporal pyramid method is used to embed spatiotemporal features in FV coding to improve the ability to identify the correctness and coordination of human behavior. Finally, the linear model of different action classifications is established to determine the action score. In the key frame extraction experiment of the aerobics action video, the ST-FMP model improves the recognition accuracy of uncertain human parts in the flexible hybrid joint human model by about 15 percentage points, and the key frame extraction accuracy reaches 81%, which is better than the traditional algorithm. This algorithm is not only sensitive to human motion characteristics and human posture but also suitable for sports video annotation evaluation, which has a certain reference significance for improving the level of aerobics training.

1. Introduction

Aerobics aims to show athletes' ability to perfectly complete difficult movements and continue complex and high-intensity sports under the accompaniment of music. How to carry out scientific training is the basis and key link of excellent aerobics, which has become an important scientific research topic [1]. Traditional aerobics training methods are based on the analysis of previous competitions and training cases, they lack auxiliary teaching and real-time analysis, and the training efficiency is low. Artificial intelligence and computer-aided system is a computer science and technology, including robot, language, image recognition, and expert system [2]. In recent years, artificial intelligence technology has been widely used in aerobics teaching and practice. This is of great significance to improve the training quality of aerobics athletes and help coaches formulate reasonable sports plans.

Some teachers' traditional training ideas are deeply rooted and difficult to accept the new training mode. In the concept of many aerobics teachers, aerobics training does not need the aid of multimedia teaching means. It only needs to demonstrate aerobics movements and then let students practice [3]. This traditional teaching concept mainly exists in some older aerobics teachers. Because of the deep-rooted teaching concept and poor adaptability, it is difficult to accept new ideas and keep pace with the times. There are loopholes in the Computer-Aided Instruction (CAI) system. Although a few schools in our country have begun to use the computer-aided teaching system to carry out aerobics teaching activities [4], but due to the limited scope of application, there are still some loopholes in the system, such as the lack of teaching feedback module in the established computer-aided teaching system, so there are still some problems in the information communication with students, which cannot let students learn well. It is difficult to understand students' views and opinions on aerobics teaching. Some teachers have not fully played a guiding role in the dependence of the computer-aided instruction system. Since the CAI system is a kind of auxiliary means, the teaching theme should be the interactive process between teachers and students. However, with the help of the computer-aided instruction system, many teachers have developed a kind of dependence on it. The aerobics teaching mode has changed from the previous demonstration mode to the video demonstration mode and the students' self-practice mode. This dependence on the computer-aided instruction system not only fails to achieve the purpose of further promoting the effect of students' aerobics practice but also causes students to have confused psychology under the condition of teachers' more relaxed supervision, which will affect the teaching quality [5]. Therefore, although the computer-aided instruction system helps teachers to share a lot of work, the teacher's teaching guidance function is still irreplaceable. In the actual training process, teachers need to master the computer-aided instruction system in the teaching process of the component to avoid making it become the dominant aerobics teaching.

From the problems existing in the practice of intelligent computer-aided aerobics training, it is worth in-depth research on how to carry out aerobics training based on intelligent auxiliary software. Therefore, starting from the design of the computer-aided aerobics training practice system, aiming at the problems existing in the intelligent computer-aided aerobics training application system, this paper puts forward the aerobics feature extraction method under intelligent computer-aided modeling and gives the aerobics evaluation scheme. Firstly, in order to maintain the spatiotemporal continuity of the FMP model in motion video human body pose estimation, the ST-FMP model with spatiotemporal continuity is obtained by establishing time continuity constraints between the vertex pairs of human parts in adjacent frames, and then, the ST-FMP model is simplified by embedding spatiotemporal constraints between uncertain human parts in adjacent video frames. The N-best optimization algorithm is used to estimate the human posture parameters, which improves the efficiency of solving the human posture parameters in a motion video. Then, the relative position characteristics and motion direction of each part of the human body are used to describe the motion characteristics of each part of the human body, and the Laplace scoring algorithm is used for feature selection to form a locally discriminated human motion feature vector. Finally, the key frames of the motion video are determined by the ISODATA dynamic clustering algorithm. Finally, the effectiveness of intelligent assistant software in aerobics training is analyzed through experiments.

2. Related Works

An intelligent computer-aided aerobics training application system is the basis of realizing intelligent-assisted training. When constructing the application system of intelligent computer-aided aerobics training, we need to determine the framework of the system first. The framework of the intelligent computer-aided aerobics training system is shown in Figure 1. The determination of the frame structure is the first step to establish the intelligent computer-aided instruction system, which needs to be carried out under the premise of making clear the purpose and task of aerobics training. Then, combined with the focus of the system, the overall framework is designed on the basis of the syllabus. In order to make aerobics teaching activities more effective, the design of the overall framework structure should be concise, intuitive, clear, and interrelated [6]. Combined with aerobics training materials, the design of the computer-aided teaching system is divided into four main modules: basic theory of action module, training site and evaluation principle module, action training and difficult motion playback module, and assessment and evaluation module.

The basic theory module of action mainly includes the common research methods of aerobics technical movements, sports teaching theory, training methods, and other related units. The teaching site and evaluation principle module mainly includes aerobics formation layout, clothing specifications and related decoration, judgment standard, referee's responsibility, analysis of common judgment errors of aerobics referee, and troubleshooting unit in the form of human-computer interaction. The motion teaching and key and difficult point motion playback module mainly includes the technical action analysis unit, essential analysis unit, basic teaching method unit, error prone action analysis unit, standard action demonstration unit, key and difficult motion analysis unit, and action video decomposition teaching unit.

The CAI system contains rich teaching resources, including text, animation, video, sound, and pictures. Therefore, in the process of establishing the computer-aided instruction system, the collection of relevant materials is very important. In order to enrich the teaching resources of the CAI system as much as possible, in the preparation stage of materials, we need to follow the following procedures:

(i) Ask experienced aerobics teachers to determine the scope of CAI materials and select qualified materials according to specific teaching objectives and tasks. After determining the material, you can write the design text, record the sound, and choose the appropriate background music.

(ii) Shooting video teaching resources, including standard action video and wrong action video, for students to learn and learn from.

(iii) Take a video of referees in aerobics competitions. Using a JVC digital camera, the organization, division of labor, and gesture process of aerobics competition referees are completely photographed. Finally, with the help of 3D animation technology and image processing software, the materials are assembled into teaching resources with teaching value and inserted into the corresponding plate after the completion of the computer-aided instruction system.

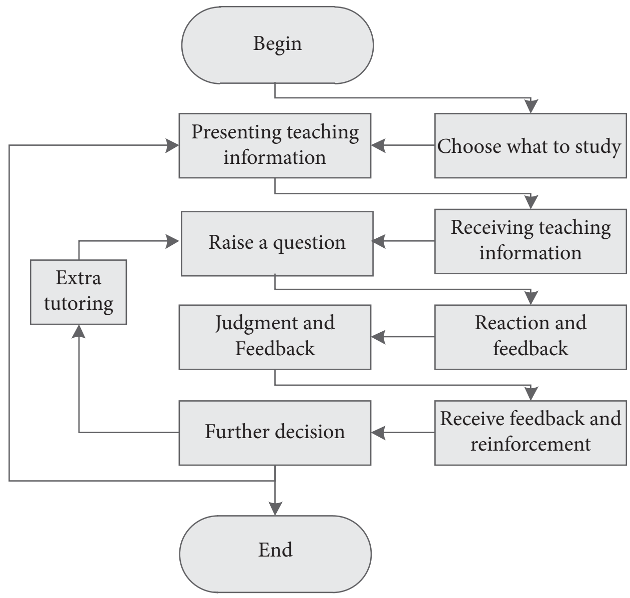

Figure 1: Framework of intelligent computer-aided aerobics training system.

Finally, a computer-aided instruction system can be established. Authorware 6.0 is a kind of multimedia visualization development work, which is based on the flowchart, so it can be selected as the operation platform of aerobics calculation and auxiliary teaching system [7]. Based on the Authorware 6.0 development platform, the calisthenics intelligent computer-aided teaching system can easily realize the classification of aerobics teaching modules and store the corresponding teaching resources. Then, the navigation icon is used to convert different modules, the framework is used to turn pages of different teaching contents, the scroll function of the text is used to realize the continuous reading of a long text, and the "hot area response" and "button response" in the interactive icon help students to convert between image, text, and video more easily and use teaching resources conveniently.

No matter students or teachers, as long as they click the corresponding module, they can get the required teaching resources on the corresponding window and easily realize the jump between different modules. At the same time, the human-computer interaction mode can reflect the problems existing in the process of students' aerobics learning more carefully and then continuously improve, greatly improving the effect of aerobics teaching. In addition, the real-time analysis and assessment mode in the comprehensive evaluation module can also exercise the students' observation ability, analysis ability, and comprehensive control ability, improve the interest of aerobics teaching, attract students to explore constantly, and then make progress in the process of exploration. The establishment of the intelligent computer-aided instruction system overcomes the problems of monotonous teaching mode and low-teaching effect in the past, stimulates students' learning enthusiasm, and makes the teaching quality achieve a qualitative leap.

3. Aerobics Feature Extraction Based on Intelligent Computer-Aided Modeling

3.1. Human Pose Estimation Model with Spatiotemporal Features. With the application of intelligent computers aided in aerobics training, it is urgent to develop an adaptive key frame extraction technology which can accurately reflect the characteristics of human body movements. Considering the good performance of the pose recognition method of the rigid human body model [8], this paper proposes to embed the temporal and spatial characteristics of human body parts in the flexible hybrid articulated human body model (FMP), so as to improve the robustness of human body and motion recognition and determine the key frames of an aerobics athletes' action video by using the human posture parameters and motion characteristics.

In the FMP model, different affine deformations (such as rotation or bending) of each part of the human body are called the mixed type of the part, which is referred to as the mixed type [9]. Because the same human body part corresponds to several mixing types, the human posture parameters in an image I are determined by the position information of each part and their mixed types. In general, a K-relation graph $G = (V, E)$ is used to describe a pose in I. The vertex set V represents the human body parts (such as the head, upper limbs, and trunk), and the edge set $E \subseteq V \times V$ represents the consistent constraint relationship between different human positions. According to the definition of FMP, the problem of parameter estimation of the human posture p in an image I can be formalized as the problem of cost minimization, which is shown as follows:

$$C(I, p) \propto \sum_{u \in V} \varphi_u (I, p^u) + \sum_{(u,v) \in E} \phi_{u,v} (p^u - p^v), \tag{1}$$

where $\varphi_u (I, p^u)$ is an appearance model, which represents the cost of recognizing the human body part u at the position p^u of the image I; $\phi_{u,v} (p^u - p^v)$ is a deformation model (usually assumed to be a spring energy model), which represents the deformation cost between two human parts u and v.

When using the FMP model to estimate the body posture in an Aerobics Athletes' action video, in order to maintain the continuity of human posture parameters in time and space, a temporal feature edge is added between p_t^u and p_{t+1}^u in adjacent frames I_t and I_{t+1} to form a flexible hybrid articulated human model (ST-FMP) with spatiotemporal characteristics [4]. In ST-FMP, the continuous error of the human posture defined by a time-series feature edge is calculated by an optical flow difference between p_t^u and p_{t+1}^u:

$$\theta(p_t, p_{t+1}, I_t, I_{t+1}) = \sum_{u \in V} \left\| p_{t+1}^u - p_t^u - f(p_t^u) \right\|_2^2, \tag{2}$$

where $f(p_t^u)$ is the optical flow value from I_t to I_{t+1} estimated at put. Suppose that the frame image set of an aerobics athlete's action video is $I = \{I_1, I_2, \ldots, I_T\}$. The estimated attitude parameter sequence is $P = \{p_1, p_2, \ldots, p_T\}$. Then, using the ST-FMP model, we can obtain the cost of I as follows:

$$C(I_T, p_T) + \sum_{t=1}^{T-1} C(I_t, p_t) + \lambda_1 \theta(p_t, p_{t+1}, I_t, I_{t+1}), \quad (3)$$

where $C(I_T, p_T)$ represents the cost of the estimating human posture p_T from the image I_T obtained according to formula (1), t is the frame number of an aerobics athletes' action video, λ_1 is the normalized constant, and $\theta(\cdot)$ is the spatiotemporal continuity error expressed in equation (2).

3.2. ST-FMP Solution Based on Uncertain Position Optimization. FMP is a rigid human body model, which can be represented by a Markov random field (MRF). The parameters of human body parts can be determined by the machine learning method. When FMP is used to estimate human posture parameters in a single frame image, MRF is regarded as a tree or star graph structure and is solved by confidence propagation BP. With the introduction of time constraint, a large number of loops will be generated in ST-FMP, which needs to be solved by minimizing equation (3) with an approximate algorithm such as cyclic confidence propagation (LBP) [10]. However, the LBP algorithm is a graph maximum clique problem, which has exponential complexity and low-time efficiency in a long video pose estimation. Therefore, this paper designs a two-stage ST-FMP algorithm based on uncertain human body parts.

3.2.1. Generating the Candidate Human Pose Sets. Firstly, the N-best algorithm and formula (1) are used to generate K_b human pose sets from a single frame image in $O(K_b^2 T)$ time without considering the space-time continuity constraint of human posture [11]. Due to motion blur and self-occlusion, some human body parts in K_b, such as the elbow (LE, RE), wrist (LW, RW), knee (LK, RK), and ankle (LA, RA), identified by eight white points in Figure 2(a), are difficult to estimate accurately. Therefore, in this paper, the uncertain part of I_{t+1} and $\tilde{p}_{t+1}$ is introduced into the attitude estimation of I_T. With the help of local time continuity of human body parts (represented by four dotted lines in Figure 2(a)), the accuracy of the human posture estimation is improved as follows:

$$C(I_t, p_t) + \tilde{C}(I_{t+1}, \tilde{p}_{t+1}) + \tilde{\lambda}_1 \sum_{u \in W} \left\| \tilde{p}_{t+1}^u - p_t^u - f(p_t^u) \right\|_2^2, \quad (4)$$

where $W \subset V$ represents the set of uncertain parts and $\tilde{\lambda}_1$ is the normalized constant; except that $\tilde{C}(\cdot)$ only calculates the appearance cost and deformation cost of uncertain parts in W, the meaning of $\tilde{C}(\cdot)$ in formula (1) is the same.

3.2.2. Determining the Optimal Solution. After obtaining the K_b attitude parameters of each frame image, the dynamic programming algorithm is used to determine the optimal attitude parameters of each frame in $O(K_b^2 T)$ time by minimizing formula (3) as follows:

$$\min_{p_t \in P_t, \forall t} C(I_T, p_T) + \sum_{t=1}^{T-1} C(I_t, p_t) + \lambda_1 \theta(p_t, p_{t+1}, I_t, I_{t+1}), \quad (5)$$

Since the two steps of the ST-FMP method can be completed in $O(K_b^2 T)$, the two-stage ST-FMP algorithm based on uncertain human body parts significantly reduces the time complexity of the LBP-based ST-FMP algorithm.

3.3. Description of Motion Characteristics of Human Body Parts. At present, the human motion model used for motion capture and motion recognition cannot be used directly because of the lack of accurate motion parameters such as joint angular velocity and displacement velocity. Therefore, this paper designs a human motion feature description model based on relative position characteristics and motion direction of human body parts [12]. If the upper left corner of a single frame image is taken as the coordinate origin, the width and height directions are x and y axes, and pixels are taken as the unit to establish the coordinate system, it is assumed that $C^u = (C_x^u, C_y^u)$ is the center position coordinate of the human body part p_u, and (C_x, C_y) is the position coordinate of human center of gravity. In this paper, the position information $l_u = (x^u, y^u)$ of a human body part is defined as the relative position between (C_x, C_y) and (C_x^u, C_y^u), which is shown as follows:

$$l_u = (x^u, y^u) = \left(C_x^u - C_x, C_y^u - C_y\right). \quad (6)$$

At the same time, the motion direction V_t^u of p_u at time t is defined as the composite vector of the motion directions of all moving points in p_u shown as follows:

$$V_t^u = \frac{1}{|\xi_t^u|} \sum_{v_t^{u,i} \in \xi_t^u} v_t^{u,i}, \quad (7)$$

where $v_t^{u,i}$ are the movement directions of the i_{th} pixel in p_u at time t and ξ_t^u is the collection of all moving points in p_u at time t. In this paper, we estimate $v_t^{u,i}$ by comparing the dense optical flow of adjacent frames I_{t+1} and I_{t+1}. With the help of formulas (6) and (7), the feature matrix composed of motion direction and relative position information of human body parts can be used to represent the human motion features in a frame image. Suppose that $j_u = (x^u, y^u, V_t^u) \in R^3$ is the motion characteristic of p_u at time t, and x is the motion feature of the image I_i containing $d\,(d = 26)$ human parts at t time, then the motion characteristics of an aerobics athlete action video with the frame number T can be expressed as $f = [J_1, J_1, \ldots, J_T] \in R^{3\,d \times T}$.

According to the above definition, J_i is the 78-dimensional motion vector and f is the $78 \times T$ vector matrix. Experiments show that the time complexity of the key frame extraction in $78 \times T$ high-dimensional motion feature space is high, and a large amount of data redundancy and noise information will directly affect the accuracy of the key frame extraction. In order to improve the expression ability of local features of motion vectors, Laplacian scorching (LS) [13] is used to reduce the dimension of motion vectors to

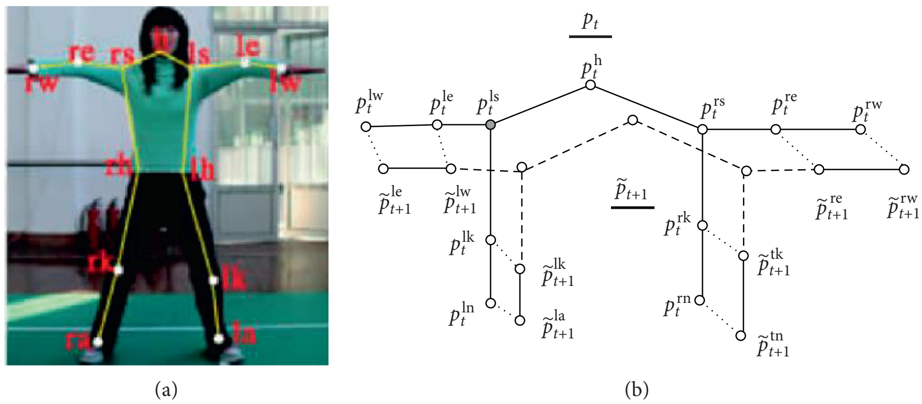

FIGURE 2: Local action time continuity of uncertain parts. (a) Nondeterministic position and (b) time continuity constraint.

determine more discriminative human motion features. Firstly, a k-nearest neighbor graph G_k is constructed; then, the similarity of two connected nodes in G_k is calculated by using the thermal kernel function to obtain the Laplacian score L_r of the r_{th} motion feature; finally, the first $n(1 \le n \le 3\ d)$ motion features with smaller L_r are determined as the body posture feature vector of the aerobics athlete's action video.

4. Aerobics Evaluation Based on Intelligent Computer-Aided Modeling

Usually, the differences between two aerobics athletes in an action video about human body movements are mainly manifested in the differences of the body posture, shape, and movement speed. Therefore, this paper uses HOF and HOG to extract the human motion features in the aerobics athletes' action video and completes the coding of human motion features in the video by fisher vector technology.

4.1. Human Posture Shape Feature Extraction. The posture feature of the body movement in an aerobics video is a static local topological structure of human body parts. The existing research results show that, even if the position of the gradient direction cannot be accurately obtained, the local dense gradient feature (HOG feature) can accurately represent the static features such as the human shape and position [14]. Therefore, the posture characteristics of aerobics athletes in an action video can be described by HOG characteristics. Figure 3 shows the HOG characteristics of an aerobics athlete after visualization.

Firstly, the frame image of 240×320 pixels is divided into different cells according to the size of 40×40 pixels. Then, the [1, 0, 1] template is used to convolute the horizontal and vertical directions of the image, and the gradient size and direction of each pixel are calculated as follows:

$$
\begin{aligned}
M(x, y) &= \sqrt{I_x^2 + I_y^2}, \\
\theta(x, y) &= \tan^{-1}\frac{I_y}{I_x} \in \left[0^\circ, 180^\circ\right),
\end{aligned} \tag{8}
$$

where I_x and I_y represent the horizontal and vertical gradient values, respectively; $M(x, y)$ represents the gradient size; and $\theta(x, y)$ represents the gradient direction.

Then, the gradient direction from 0° to 180° is divided into 16 bins. At the same time, every four cells are combined with a block of 80×80 pixels. In the same block, the Euclidean norm of histogram is used to normalize each cell. Since each unit contains 16-dimensional feature vectors, each block has only one $4 \times 16 = 64$-dimensional feature vector. The local features of the human posture and shape in each frame image are represented by hog feature vectors with a dimension of $6 \times 8 \times 16 = 768$.

4.2. Human Motion Feature Extraction. According to the principle of the optical flow field, the gray change of a human body image in adjacent video frames can better reflect the motion characteristics of the human body [15]. Therefore, in this paper, the Lucas Kanade algorithm (LK algorithm for short) [16] is used to estimate the optical flow vector of each point in the image, and the motion information of the human body is determined by the optical flow histogram (HOF) feature [17]. When the LK algorithm is used, it is assumed that the optical flow remains unchanged in a small local area of the adjacent frame images. Then, the velocity characteristics of the human motion from time t to time $t + \Delta t$ can be determined by the least-squares method. According to the LK algorithm, after obtaining the optical flow of each pixel in the frame image, this paper first divides a 240×320-pixel frame image into $6 \times 8 = 48$ cells and then discretizes the optical flow vector in each cell into 16 bin directions and normalizes them to obtain the $6 \times 8 \times 16 = 768$-dimensional HOF feature vector.

4.3. Automatic Scoring of Aerobics Athletes' Action Video. In order to complete the automatic scoring of aerobics athletes' action videos, the aerobics athletes' action videos in the training dataset are divided into three categories according to the manual scoring results and the action completion quality. The STLPFV algorithm is used to obtain the action features of each segment of aerobics athletes' action videos, and then the k-neighbor algorithm is used to

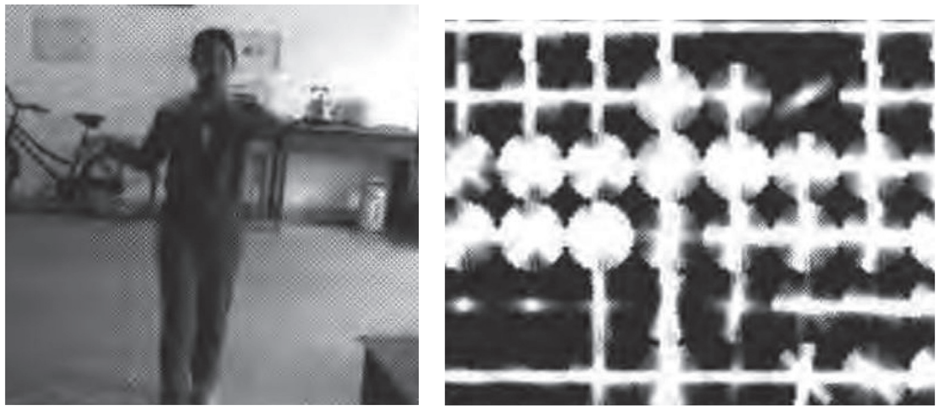

(a) (b)

Figure 3: HOG characteristics of aerobics athletes' action visualization. (a) The action of aerobics athlete and (b) action visualization HOG feature.

complete the motion feature modeling. When the aerobics player's action video is scored automatically, the FV code of the target aerobics athlete's action video is generated by the STLPFV algorithm [18]. Finally, the KNN distance between the action video of target aerobicsathletes and the action video of aerobics athletes with three different scores is classified, and the least-squares method is used for automatic scoring [19].

$C = \{\overline{c}_l, \overline{c}_m, \overline{c}_h\}$ is the classification center set of three kinds of actions obtained by the k-nearest neighbor algorithm. If a triple $KNN(s_i) = p_i = [p_i^{(l)}, p_i^{(m)}, p_i^{(h)}]$ is used to represent the KNN distance vector between the target aerobics athletes' action video s_i and C (where $p_i^{(l)}, p_i^{(m)}, p_i^{(h)}$, respectively, represent the probability values of s_i belonging to three different score action videos), then the weight of s_i on C is as follows:

$$w_i = p_i^{(l)}\overline{c}_l + p_i^{(m)}\overline{c}_m + p_i^{(h)}\overline{c}_h. \tag{9}$$

Weight w_i obtained by formula (9) needs to be calibrated as the corresponding action score. In this paper, the least-square method and action video training set are used to establish the linear relationship model between weight w_i and action score. The specific method is to assume that $Y^{(\alpha)} = \{y_i^{(\alpha)} | i = 1, 2, \ldots, n\}$ is the score set of all kinds of actions in C (where n represents the number of action videos and $\alpha \in \{l, m, h\}$ represents three types of action videos with different scores, i.e., low score, medium score, and high score), which is shown as follows:

$$\left(\overline{\rho}^{(\alpha)}, w_i\right) = \underset{y_i^{(\alpha)} \in Y^{(\alpha)}}{\arg\min} \left| y_i^{(\alpha)} - \left(\rho_0^{(\alpha)} w_i + \rho_1^{(\alpha)}\right)\right|^2, \tag{10}$$

where $\overline{\rho}^{(\alpha)} = \{\overline{\rho}_0^{(\alpha)}, \overline{\rho}_1^{(\alpha)}\}$ represents the coefficient value vector obtained by solving formula (10) of an action video training set. At this time, the target aerobics athletes' action video s_i corresponding score is defined as follows:

$$S_i^*\left(\overline{\rho}^{(\alpha)}, w_i\right) = \overline{\rho}_0^{(\alpha)} w_i + \overline{\rho}_1^{(\alpha)}. \tag{11}$$

Accordingly, the flow of the automatic scoring algorithm of an aerobics athletes' action video based on the STLPFV method is shown in Figure 4. It includes the following parts:

(1) The STLPFV method is used to calculate the human motion characteristics in the motion video s_i of aerobics athletes, and the FV code is obtained.

(2) The KNN distance between s_i and C is calculated by the k-neighbor algorithm, and the probability $\mathrm{KNN}(s_i)$ that s_i belongs to all kinds of action scores in C is obtained. Weight w_i is calculated by formula (11).

(3) According to the KNN distance, s_i is classified as the first kind of a motion video.

(4) The action score s_i^* corresponding to s_i is calculated by equation (11).

5. Experiment and Analysis

This paper takes the key frame of aerobics action video as an example to carry out the simulation experiment. The experimental results are compared with the results of the manual extraction and the extraction results of the latest aerobics athletes' action video key frame algorithm [20].

5.1. Training and Evaluation Criteria of Experimental Data Samples and Characteristics. At first, three students were invited to do 120 s public aerobics twice, and a video with 640×480 resolution was recorded by an ordinary webcam at the sampling frequency of 20 frames/S. Then, 300 images were selected from each of the six sets of videos as experimental data from the 10th rhythm. Finally, in 1800 frames of images, according to Figure 2(a), 13 joint positions of each aerobics movement are manually marked. In the simulation experiment, 900 images of the first pass and the second pass are selected as the training sample dataset and the test sample dataset.

In the process of training, in order to enrich the human motion characteristics of the positive samples, the rotation (according to the four angles of $-15°$, $-7.5°$, $7.5°$, and $15°$) and

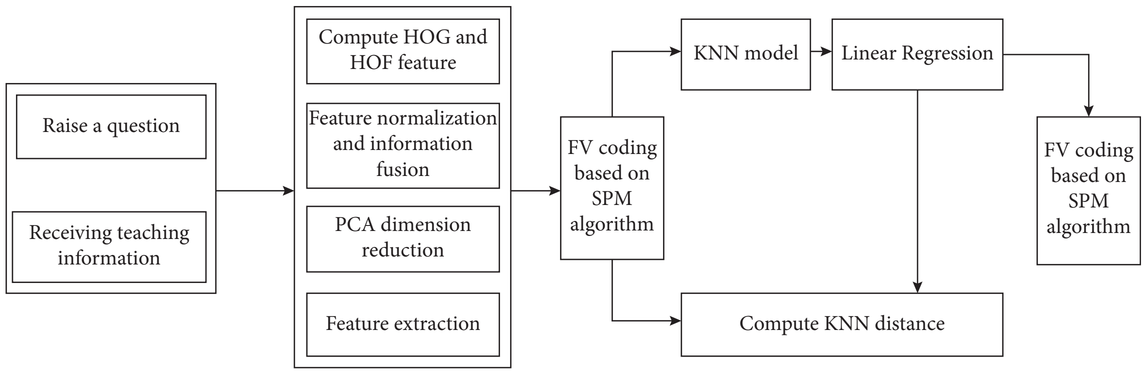

Figure 4: The automatic scoring process of aerobics athletes in STLPFV.

mirror image operation are used to expand 900 training samples into 10×900 positive samples, which are recorded as Φ_p^*. Then, by adding key points at the midpoint of two adjacent joint positions in Figure 2(a), the coordinates of 26 flexible human body parts in each image in Φ_p^* are calculated. Finally, the HOG features of each human body part are calculated by using a 5×5-pixel HOG unit, and parameters such as $\varphi(I, l_u)$ and $\phi(l_u, -l_v)$ in formula (3) are determined by the linear support vector machine.

All the key frames in the test sample set are extracted manually, and the common key frame extraction accuracy is taken as the evaluation standard of algorithm performance [21], which is shown as follows:

$$\text{Accuracy} = \sum_{i=1}^{m} \frac{\delta(f_i, r_i)}{n}, \tag{12}$$

where n and m represent the number of key frames extracted manually; f_i and r_i represent the key frames extracted by algorithm, respectively; and $\delta(\cdot)$ is the similarity function between f_i and r_i. When f_i and r_i are the same, $\delta(\cdot)$ value is 1; otherwise, it is 0.

5.2. Comparison of the Effectiveness of Spatiotemporal Feature Embedding in Uncertain Parts. In order to detect the accuracy of the manikin embedded with a uncertain part of the temporal and spatial features in the video, three different ST-FMP models are used to realize the human body parts, and the comparative experiments of elbow and knee parts are carried out according to different error pixel thresholds. The experimental results are shown in Figure 5.

As can be seen from Figure 5, compared with the FMP model, the accuracy of the uncertain part can be significantly improved within a certain pixel error range by using the ST-FMP algorithm to estimate the human posture in the aerobics athlete's action video. Taking the error threshold of 20 pixels as an example, the accuracy of the elbow and knee obtained by the ST-FMP algorithm is about 15% and 19% higher than that of the FMP model, respectively. However, when the pixel error threshold is large (e.g., greater than 40 pixels) or small (such as greater than 10 pixels), the accuracy difference is not significant.

According to Figure 5, only when the time continuity of the uncertain part of the upper limb (lower limb) is maintained, the recognition accuracy of the elbow and wrist (knee and ankle) will be higher than that of the FMP model, but lower than that of the ST-FMP algorithm. The experimental results show that the ST-FMP algorithm can significantly improve the recognition performance of nondeterministic parts in aerobics athletes' action videos by optimizing the recognition results of human body parts by local time continuity constraints.

This paper also compares the performance of the FMP model, ST-FMP model, and their different implementations in the key frame extraction of the aerobics athletes' action video. The experimental results are shown in Figure 6.

According to the results shown in Figure 6, two conclusions are obtained as follows:

(1) When the accuracy error is less than 30 pixels, the accuracy of the ST-FMP algorithm is higher and more stable, which is about 11% higher than that of the FMP algorithm. In addition, when the time continuity constraint of the upper limb (lower limb) is added, the extraction accuracy of FMP model key frames will be improved by about 3%.

(2) When the error accuracy is greater than 35 pixels, the performance of the ST-FMP algorithm is still better than that of the FMP model, but the accuracy rate is reduced by about 15%. At the same time, when the accuracy error is 30 pixels and the key frames are extracted by the ST-FMP algorithm with the different number of motion features, the accuracy curve of the algorithm does not fluctuate violently, and the performance is stable in the range of 15–60 motion feature numbers, as shown in Figure 7. The experimental results show that the ST-FMP algorithm is sensitive to human posture estimation results and the local topological structure of the human body, and spatiotemporal constraints of uncertain parts play an important role in key frame extraction performance.

5.3. Performance Comparison of Key Frame Algorithms. In order to compare the performance of the key frame algorithm, the simulation experimental results of the ST-FMP algorithm are compared with the operation results of the KFE algorithm based on priori in reference [22] and the

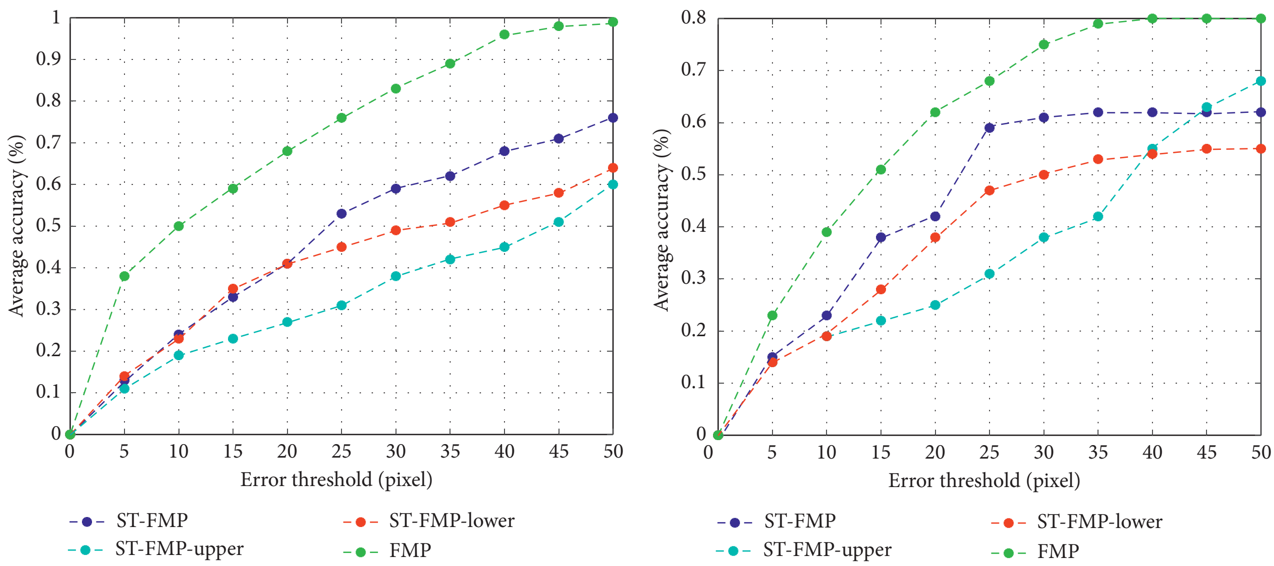

(a) (b)

Figure 5: Comparison of recognition accuracy of human body parts under different ST-FMP. (a) Elbow joint and (b) knee joint.

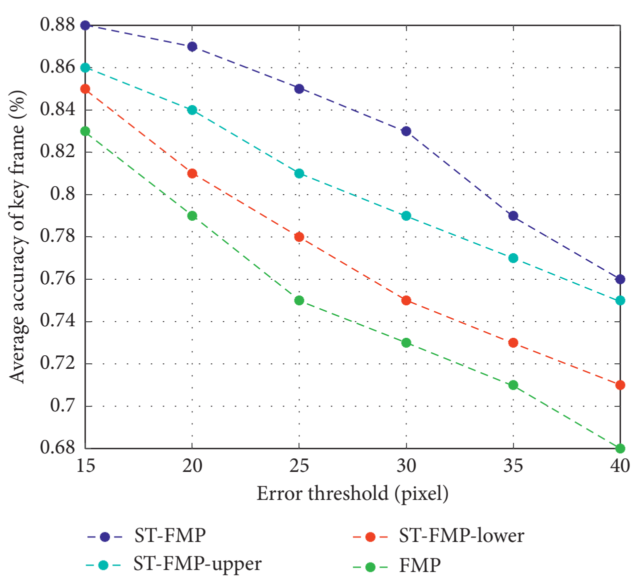

Figure 6: Experimental results of key frame extraction based on FMP and ST-FMP.

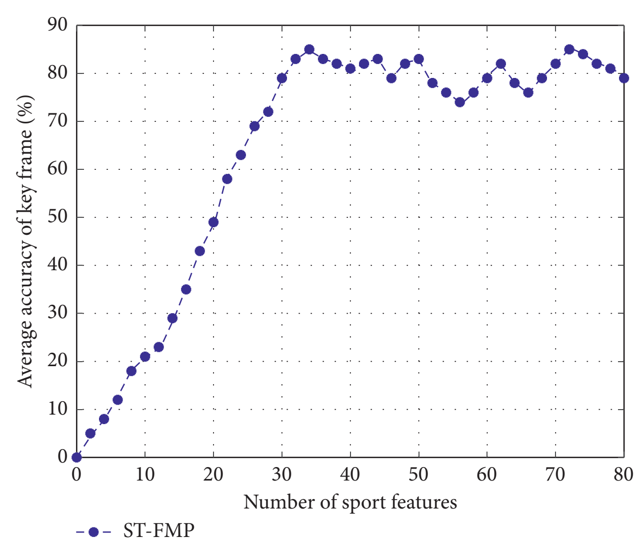

Figure 7: Key frame accuracy comparisons of different motion feature numbers.

motion block-based key frame extraction algorithm (referred to as the motion block algorithm) in reference [23], as shown in Table 1.

The experimental results in Table 1 show that the accuracy and recall rate of the ST-FMP algorithm are better than the other two algorithms. First of all, as can be seen from Table 1, the accuracy rate of the ST-FMP algorithm is about 18% and 26% higher than KFE algorithm and motion block algorithm, respectively. The KFE algorithm uses predefined motion directions of 16 blocks to represent human motion features, while the ST-FMP algorithm uses the first 15 LS human motion pose eigenvalues of each action video to represent the human motion. Therefore, the ST-FMP algorithm uses less redundant motion feature vectors, less noise, and accurate expression of local motion of human body parts, which is conducive to improving the accuracy of key frame and action recognition.

Secondly, it can be seen from Table 1 that the recall rate of the ST-FMP algorithm is significantly better than the other two algorithms, with an average of 23 and 13 percentage points higher, respectively. The KFE algorithm and motion block algorithm belong to key frame technology based on the difference of image bottom features. They select key frames by comparing the motion changes in different regions of the image. The ST-FMP algorithm describes the local motion characteristics of human body parts, which is a semantic model in essence. It can analyze and understand the human actions in the aerobics athletes' action video from

Table 1: Performance comparison of different key frame extraction algorithms.

Algorithms	Accuracy (%)	Recall (%)
ST-FMP	0.8148	0.8287
KFE	0.6358	0.5946
Sport block	0.5583	0.6982

the higher level aspects such as the participation the parts of the human body movement and its movement change trend. By using semantic rules such as the human posture similarity to select key frames, it can obtain more accurate and consistent with people's cognitive process key frame results.

The experimental results show that the ST-FMP algorithm can better express the local topology of the human body and support the key frame selection based on semantic rules. It is not only closer to the manual extraction results but also more suitable for the key frames based on feature extraction. At the same time, because the ST-FMP divides human body parts into different flexible parts, identifies the human posture through the local topology of flexible parts, and reduces continuous error of the human posture estimation by using temporal feature edge constraint, so it has strong robustness in complex scenes.

6. Conclusion

Aiming at the problems of lack of auxiliary teaching conditions and low-training efficiency in traditional aerobics training methods, this paper proposes a local space-time preserving Fisher vector (FV) coding method and monocular motion video automatic scoring technology. The experimental results show that the ST-FMP model significantly improves the recognition accuracy and attitude estimation performance by maintaining the spatiotemporal continuity of uncertain parts of the human body and embedding the spatiotemporal characteristics of local actions, and the key frame set obtained is more in line with people's cognitive process. The algorithm proposed in this paper still has some problems to be improved and optimized. For example, the intelligent computer-aided training system lacks the function of real-time tracking and monitoring in the process of aerobics training. Therefore, how to monitor and evaluate the level of aerobics training in real time according to the human movement characteristics and human posture sensitivity in aerobics training is the next problem to be solved [24].

Data Availability

The dataset can be accessed upon request to the corresponding author.

Conflicts of Interest

The author declares no conflicts of interest.

Acknowledgments

This work was supported by the Fuyang Normal University Industry-University-Research Fund Project: Research on the preparation and implementation of special skills training for physical education teachers.

References

[1] N. Rinaldo, E. Bacchi, G. Coratella et al., "Effects of combined aerobic-strength training vs fitness education program in COPD patients," *International Journal of Sports Medicine*, vol. 38, no. 13, pp. 1001–1008, 2017.

[2] C. Xu, "A novel recommendation method based on social network using matrix factorization technique," *Information Processing & Management*, vol. 54, no. 3, pp. 463–474, 2018.

[3] J. Zhao, "Application design of intelligent computer aided instruction system in aerobics teaching," in *Proceedings of the he International Conference on Cyber Security Intelligence and Analytics*, pp. 512–517, Springer, Haikou, China, February 2020.

[4] S. Qian, "The damping loss prevention research on aerobics special shoe materials based on intelligent analysis," *Science Heritage Journal*, vol. 3, no. 1, pp. 20–23, 2019.

[5] Y. Yu and A. Qi, "Teaching system of smart learning environment for aerobics course," *International Journal of Emerging Technologies in Learning (iJET)*, vol. 13, no. 05, pp. 165–176, 2018.

[6] Q. Huang and F. Wang, "Design method of aerobics teaching assistant platform based on 5G technology," in *Proceedings of the International Conference on Application of Intelligent Systems in Multi-Modal Information Analytics*, pp. 75–81, Springer, Changzhou, China, March 2020.

[7] L. Jia and L. Li, "Research on core strength training of aerobics based on artificial intelligence and sensor network," *EURASIP Journal on Wireless Communications and Networking*, vol. 1, pp. 1–16, 2020.

[8] C. D. Wei, L. Chao, W. Shun, W. X. Ling, and W. W. Fang, "Research and application of multimedia digital platform in the teaching of college physical education course," *Journal of Intelligent and Fuzzy Systems*, vol. 34, no. 2, pp. 893–901, 2018.

[9] Z. L. Kozina, T. V. Shepelenko, M. Cieslicka et al., "The teams' formation in sport aerobics on the basis of application of multidimensional analysis methods," *Physical education of students*, vol. 21, no. 6, pp. 270–279, 2017.

[10] Y. Fan, J. Chen, S. Li, L. Zhao, Y. Zhang, and C. Liu, "A novel fuzzy synthetic discrimination system for teaching ability of physical education majors based on analytic hierarchy process," *Educational Sciences: Theory and Practice*, vol. 18, no. 5, 2018.

[11] J. Zhao and G. Li, "Application of brain science in physical education and teaching," *Educational Sciences: Theory and Practice*, vol. 18, no. 5, 2018.

[12] B. SueSee, K. Edwards, S. Pill, and T. Cuddihy, "Observed teaching styles of senior physical education teachers in Australia," *Curriculum Perspectives*, vol. 39, no. 1, pp. 47–57, 2019.

[13] J. Chen and Y. Yang, "Research about bilingual education issues in business intelligence teaching," in *Proceedings of the 2018 International Conference on Education, Economics and Social Science (ICEESS 2018)*, October 2018.

[14] B. SueSee, S. Pill, and K. Edwards, "Interrogating assumptions of a curriculum: queensland senior physical education syllabus," *The Physical Educator*, vol. 75, no. 5, pp. 850–879, 2018.

[15] K. Karatrantou, V. Gerodimos, K. Häkkinen, and A. Zafeiridis, "Health-promoting effects of serial vs. integrated combined strength and aerobic training," *International Journal of Sports Medicine*, vol. 38, no. 1, pp. 55–64, 2017.

[16] B. Yuhong, J. Radio, and T. Stations, "Application of virtual reality technology in broadcasting and hosting major practice teaching," *Electronic Measurement Technology*, vol. 7, 2017.
[17] Z. Huysmans, D. Clement, M. A. Whitley, M. Gonzalez, and T. Sheehy, "Putting kids first: an exploration of the Teaching Personal and Social Responsibility model to youth development in Eswatini," *Journal of Sport for Development*, vol. 7, no. 13, pp. 15–32, 2019.
[18] T. I. Mokrova, A. Y. Osipov, M. D. Kudryavtsev, R. S. Nagovitsyn, and K. K. Markov, "Practice of Kangoo Jumps Fitness to improve female students' cardiorespiratory fitness," *Physical education of students*, vol. 23, no. 4, pp. 191–197, 2019.
[19] Z. Chen, Y. Zhang, C. Wu, and B. Ran, "Understanding individualization driving states via latent Dirichlet allocation model," *IEEE Intelligent Transportation Systems Magazine*, vol. 11, no. 2, pp. 41–53, 2019.
[20] Z. J. Hai, L. L. Yuan, and G. T. Xiao, "Improving memory and executive function of the elderly with mild congnitive impairment-A smart health care approach," *Journal of Medical Imaging and Health Informatics*, vol. 10, no. 1, pp. 44–48, 2020.
[21] B. Guo, "Analysis on influencing factors of dance teaching effect in colleges based on data analysis and decision tree model," *International Journal of Emerging Technologies in Learning (iJET)*, vol. 15, no. 9, pp. 245–257, 2020.
[22] D. D. Palma, A. Ascione, and S. Napolitano, "Education to school inclusion through sport," *Sport Science*, vol. 11, pp. 42–46, 2018.
[23] I. S. Mbambo, "Teachers as change agents: primary teachers' perceptions and management of bullying in a selected school at kwamashu area," Doctoral dissertation, University of KwaZulu-Natal, Durban, South Africa, 2016.
[24] Z. Xie, R. Lin, J. Wang, W. Hu, and L. Miao, "Vicarious learning: how entrepreneurs enhance a firm's international competitiveness through learning from interlocking director network partners," *Frontiers in Psychology*, vol. 11, 2020.

Hindawi
Scientific Programming
Volume 2021, Article ID 7970870, 10 pages
https://doi.org/10.1155/2021/7970870

Research Article

Three-Dimensional Structure Analysis of Urban Landscape Based on Big Data Technology and Digital Technology

Xiaozhou Yang[1] and Fan Bai[2]

[1]*Department of Art, Northeastern University, Shenyang 110006, China*
[2]*School of Equipment Engineering, Shenyang Ligong University, Shenyang 110159, China*

Correspondence should be addressed to Fan Bai; snowwind001@sylu.edu.cn

Received 26 September 2021; Revised 11 October 2021; Accepted 30 October 2021; Published 12 November 2021

Academic Editor: Hai Dong

In order to improve the effect of urban landscape design, this paper combines big data technology with digital technology. For scenes and solutions containing SDS paths, a processing method similar to photon graphs is used and added to the calculation of two-way optical path tracking. In the processing scene, this paper uses the two-way optical path tracking method to perform specular reflection or refraction from the subpath starting from the light source and then store information such as the light energy of the points on the diffuse reflection surface or the directional reflection surface. Moreover, this paper combines the actual needs of urban landscape design to construct an urban landscape design system based on big data technology and digital technology. Finally, this paper designs experiments to carry out urban landscape simulation and design effect evaluation. From the test results, it can be seen that the system designed in this paper basically meets the needs of urban landscape planning and design.

1. Introduction

Place spirit is the core concept of place theory, and the two spiritual attributes of direction and identity together constitute place spirit. Direction refers to people's ability to clarify the relationship between themselves and the environment, and identity refers to people's identification with themselves through meaningful connections with the surrounding environment in the place, which is a spiritual affirmation and belonging [1]. In modern society, people are unfamiliar and alienated from their living environment and lose their sense of identity. That is why they promote the generation of lost space. During the design process, attention is paid to the analysis of the needs of the crowd, and after the investigation and analysis, the spatial transformation to cater to the living environment preferred by the residents around the site would inevitably make the lost space regain its vitality. The use of a positive place structure and a rich place spirit can create a place where people are happy and unwilling to move. It will inevitably promote the establishment of place spirit, and the problem of lost space spirit loss can be solved [2].

In the process of transforming and designing the lost space of urban landscape, the creation of spatial ambiguity is mainly to create diversified activity spaces and rationally lay out the five elements of urban space: roads, boundaries, regions, nodes, and landmarks. From the overall perspective, it meets the psychological and behavioral needs of different groups of people and provides facilities for people to stop, talk, and rest. The facilities and space design can meet the requirements of different activities. Moreover, the design should analyze the social crowd activities of all age groups, so that the space can serve all kinds of people. In the space design, various spaces are planned in a unified manner, and a diverse landscape space is created to meet the conversion of functions. In the creation of details, the design can provide public facilities with multiple functions, landscape sketches for people to play and participate, vertical tree ponds, etc. [3].

Due to the severe lack of interaction and communication with users, lost spaces often give people a negative impression of darkness and chaos, and they are not attractive to people. In the redesign of the lost space, it attracts people to have a full range of perceptual experience of the space environment, mobilizes the enthusiasm and interest of people to participate in activities, attracts people to integrate into the environment, and promotes a good interactive communication between people and the landscape, emphasizing space. The continuity and fluidity of the "lost" can be dispelled, and the beautiful enjoyment brought by the space environment can be felt from all angles. Once people develop a habit of this feeling, it can effectively extend the user's stay in the landscape space. Through the transformation of leisure and entertainment methods, the interactive landscape has enhanced public communication and adjusted according to public feedback to make its own functional form more perfect. For example, the fountain facilities and interesting landscape sketches in the square enable people to directly touch and appreciate them at close range, thus leaving a good memory for people's travel, which can easily promote people's reexperience and effectively add space to the space. *Vitality*. Another design method is to use high-tech materials and technology to create a changing and dynamic space effect. New things are more likely to attract people's attention, so as to attract people's extensive participation, mobilize people's enthusiasm, and activate the atmosphere of the place, thereby enhancing the landscape, and the vitality of the space.

This paper combines big data technology and digital technology to analyze the three-dimensional structure and performance of urban landscapes and provides a theoretical reference for subsequent urban landscape design.

2. Related Work

The 3D reconstruction technology based on multiview geometry [4] needs to use the projection relationship between the image sequence obtained from different perspectives in the same scene and the target scene to restore the geometric spatial position of each image feature in the image sequence, so as to achieve the three-dimensional reconstruction of the geometric model of the target scene. Generally, three-dimensional reconstruction is achieved based on multiple cameras simultaneously shooting scene sequence images from different perspectives, or based on monocular cameras time-sharing shooting scene image sequences from different perspectives. Multiview geometric 3D reconstruction mainly solves some problems in the motion recovery structure method, such as feature matching and viewpoint correspondence [5]. The multiview geometric method usually includes four main steps: image feature extraction and matching, calculation of multiview geometric constraint relations, iterative optimization of estimation results, and dense reconstruction of sparse scenes. Literature [6] proposed that when the spatial relationship between two projections is unknown, the related perspective projection relationship is described to realize a simple algorithm for reconstructing the three-dimensional structure of a scene. The corresponding problem of image points in different perspectives in the same scene is solved. When the image matching problem is solved, the 3D reconstruction of the scene can be simplified to find the relative direction of the two viewpoints, that is, the geometric constraint relationship. Since then, the three-dimensional reconstruction based on the multiview motion restoration structure kicked off. Literature [7] conducted a detailed study on the nature of the essential matrix that can express the geometric constraint relationship. Literature [8] proposed the basic matrix, explained its basic properties, and solved the geometric constraint relationship between two images. The concept of the basic matrix was promoted, and the theory of multiview geometry continued to develop and grow. Literature [9] proposed the Scale Invariant Feature Transform (SIFT) algorithm. The local features extracted by the algorithm remain unchanged against rotation, scale scaling, and brightness changes, and they also maintain a certain degree of stability against viewing angle changes, affine transformations, and noise. The emergence of this algorithm makes the problem of matching between images from different perspectives in the same scene better solved. The first two steps of the multiview geometric reconstruction process have been solved, and the initial reconstruction results have been obtained at this time. In order to optimize the initial three-dimensional reconstruction results, modern methods often use the bundle adjustment method (BA) to optimize the cost function of the total reprojection error. The cost function can be used to determine the model parameters and camera pose of each camera at the same time, so that the difference between the image measurement value and the model prediction value can be minimized. This step is the most critical in large-scale 3D reconstruction [10].

Literature [11] uses the sparse beam adjustment method as the underlying optimization engine to incrementally reconstruct the target three-dimensional scene by inputting the disordered image set, image feature points, and their matching results. With the development of multicore processors and GPUs, the GPU-based SIFT algorithm SiftGPU [12] appeared. In addition, an efficient beam adjustment method based on the conjugate gradient method has been proposed one after another, called Multicore Bundle Adjustment (MBA) [13]; on the basis of both MBA and SiftGPU, Wu once again proposed an incremental SFM software package called VisualSFM [14]. VisualSFM not only has a good graphical interactive interface, but also visualizes each step of the SFM, allowing users to clearly understand its operation process. The most important thing is to obtain the output camera's motion posture, trajectory, and reconstruction from the input image sequence. The three-dimensional scene structure completely realizes the process steps of SFM from beginning to end [15]. The estimation of the 3D model in SFM is usually calculated by calculating the spatial position of the feature points from the static scene image to generate a point cloud with the target model structure as the output result, but the structure of the point cloud is sparse, and it is impossible to complete some of the real society. Requirements, such as 3D printing, so the sparse model needs to be densified [16]. Based on multiview stereo vision (multiview stereopsis (MVS)) theory, literature [17] proposed patch-based multiview stereo software (PMVS), which combines sparse key points into a block structure and performs three steps of matching, expansion, and filtering.

Processing gets more matching points and generates dense point cloud. When the data set is large, the amount of calculation in the intensive reconstruction process is huge, which causes the operation to be time-consuming. In order to improve the computing efficiency, the new version PMVS2 is optimized on the basis of PMVS, which has improved speed and quality [18]. Clustering views for multiview stereo (CMVS) [19] includes PMVS2 and some additional features. It not only groups and clusters the input image data set, but also processes multiple data sets in parallel to achieve faster and dense reconstruction under large data sets. It also removes redundant image data and improves the accuracy of reconstruction. Literature [20] believes that although the traditional SFM method based on point feature detection and matching can obtain the correct camera pose, the number of available matching features is small, and the number of accurate 3D space points is extremely limited. Although MVS solves this problem, however, the computational complexity is relatively high. In view of the rich linear features of the building, a reconstruction method based on the straight line segment as the bottom layer feature is proposed, and pure geometric constraints are used to match the straight line segments in different images to achieve the reconstruction of the building, and geometric structure reconstruction.

3. Big Data and Digital Landscape 3D Structure Design Algorithm

The ray tracing method is a collection of methods that can actually display objects. The ray casting algorithm is the prototype of the ray tracing method. The algorithm idea is to track the light that reaches the viewpoint in the opposite direction and go through any pixel of the screen to find the first object that intersects the opposite light. After that, it calculates whether the object is illuminated by the light source and finally returns the color value of the intersection point. The method of ray projection only considers the direct illumination of the object, so the reflection, refraction, penumbra, and other effects of the light on the surface of the object are difficult to present. Methods such as ray tracing improve the ray casting method.

Flux: the total energy of light passing through a certain surface or area in unit time. The unit is watts (W) and is usually represented by w.

Irradiance: the density of light energy passing through a surface or area in a unit of time. Its unit is (W/m^2) and is usually represented by E, namely,

$$E = \frac{\mathrm{d}\Phi}{\mathrm{d}A}. \tag{1}$$

Intensity: the light energy within a unit solid angle in a given direction in a unit time. Its unit is (W/m^2) and is usually represented by I, namely,

$$I = \frac{\mathrm{d}\Phi}{\mathrm{d}\omega}. \tag{2}$$

Radiance: the light energy within a unit solid angle in a given direction passing through a vertical unit area in unit time. Its unit is (W/(m^2·sr)) and is usually expressed by L, namely,

$$L = \frac{\mathrm{d}\Phi}{\mathrm{d}\omega \cdot \mathrm{d}A^{\perp}}. \tag{3}$$

Among them, $L_0(p, \omega_0) = L_e(p, \omega_0) + \int$ is the projection of dA in the ω direction.

The rendering equation was first proposed by James Kajiya. It is an approximate expression of Maxwell's electromagnetic formula, and it removes the processing of diffraction phenomenon that is basically irrelevant to the display effect in Maxwell's equation.

The rendering equation is expressed as

$$L_0(p, \omega_0) = L_e(p, \omega_0) + \int_{\delta^2} (p, \omega_0, \omega_i) L_i(p, \omega_i) |\cos\theta_i| \mathrm{d}\omega_i. \tag{4}$$

Among them, p is a point on the surface of the object, ω_0 is the direction of the emitted light on the unit sphere, and ω_i is the direction of the incident light. $L_i(p, \omega_i)|\cos\theta_i|$ is the influence of the self-luminescence on the surface of the object on the emitted light. The integral form of $\int_{\delta^2} (p, \omega_0, \omega_i) L_i(p, \omega_i)|\cos\theta_i| \mathrm{d}\omega_i$ is calculated as the influence of incident light in all directions of the hemispherical surface (δ^2) on the outgoing light. Among them, (p, ω_0, ω_i) is the two-way reflection distribution function.

Figure 1 uses a two-dimensional picture to illustrate the meaning of the rendering equation. The surface of the object seen at the viewpoint position is transmitted through the ω_0 direction. In order to calculate the amount of light energy from this direction, it is necessary to know all the light energy at the location of the P point, and then according to the total light energy of the P point and the ω_0 direction, the light energy received by the viewpoint can be obtained. The light energy at the P point may come from two situations:

(1) Self-luminous objects

(2) Other light-emitting surfaces or reflective (refracting) surfaces transfer light energy to the P point

The above two cases are solved separately and added together to get the total light energy at the point P.

The physical meaning of the bidirectional reflectance distribution function (BRDF) refers to the ratio of the radiation micro-increment to the radiation micro-increment in the reflection direction. When the material of the object, the angle of reflection, and the angle of incidence are determined, BRDF is calculated as a constant. It is defined as follows:

$$\begin{aligned}(p, \omega_0, \omega_i) &= \frac{\mathrm{d}L_r(p, \omega_0)}{\mathrm{d}E_i(p, \omega_i)} \\ &= \frac{\mathrm{d}L_r(p, \omega_0)}{L_i(p, \omega_i)\cos\theta_i \mathrm{d}\omega_i}.\end{aligned} \tag{5}$$

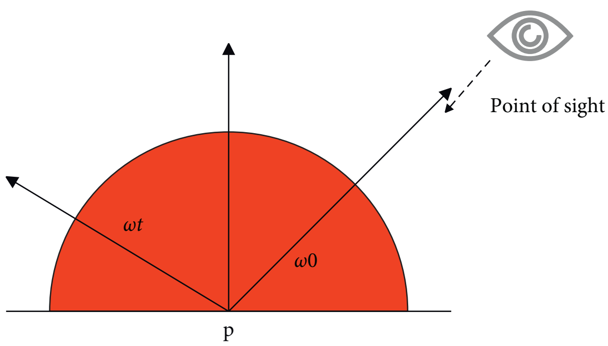

Figure 1: Basic reflection/refraction model.

Among them, L is the luminous flux per unit steradian and E is the luminous flux per unit area. θ_i is the angle between ω_i and the normal vector, as shown in Figure 2.

BRDF is expressed as the relationship between incident and reflection of an object. However, this is not enough to describe the propagation process of light. Among them, a more common situation is that after the light intersects the object and has an effect, part of it will be decomposed into reflected light, but the other part will be further transmitted into the object, as shown in Figure 3.

This part of the light energy may be absorbed by objects (Fresnel Conductors, such as some metals) and may further propagate downward (such as glass) and exist as refracted light. Therefore, when dealing with the light propagating inside the object, it is necessary to define the bidirectional transmittance distribution function (BTDF) and use it for processing.

According to different objects, the performance of reflected (refraction) light varies. We can divide the reflection (refraction) models of objects into the following categories.

3.1. Mirror Reflection/Refraction. The reflection (refraction) is concentrated in one direction. For mirrors, the reflection angle is equal to the incident angle, as shown in Figure 4.

3.2. Diffuse Reflection/Refraction. It is also called Lambert reflection. When the object is sufficiently rough, the brightness of the reflected light is constant in the 2π -space of the target point. That is, the reflected brightness does not change with the change of the observer's line of sight, as shown in Figure 5.

3.3. Directional Reflection/Refraction. It is also called non-Lambert reflection. This reflection is between diffuse reflection and specular reflection. In this model, the brightness of the reflected light in each direction is different, as shown in Figure 6.

It is available that, for the above several types of reflection and refraction models, in addition to specular reflection, the direction of the reflection angle can be clearly known according to the angle of incidence. The other two types have countless possibilities in the direction of the reflection or refraction angle under the condition of a clear angle of incidence. Conversely, considering the situation of reverse ray tracing, under the condition of a certain viewing angle, according to the rendering equation, there are countless directions of light energy that affect the point and then affect the final color of the point.

Since the solution is an integral equation, and the integral parameters are uncertain, this equation cannot be calculated in one time. It can only be approximated by sampling. Under the condition of increasing number of samples, the approximate result is getting closer and closer to the correct solution.

The definition of Monte Carlo method is as follows.

The integral equation $\int_a^b f(x)\mathrm{d}x$ is calculated by sampling method, and the integral value is calculated by Monte Carlo method as

$$F_N = \frac{b-a}{N}\sum_{i=1}^{N} f(X_i). \tag{6}$$

In the above equation, N points are sampled in the integration range, and the solution of the integral equation is estimated with the sampling value of these N points.

Now, we prove that if there is enough N, F_N is approximately equal to $\int_a^b f(x)\mathrm{d}x$; that is, prove $E[F_N] = \int_a^b f(x)\mathrm{d}x$.

$$\begin{aligned} E[F_N] &= E\left[\frac{b-a}{N}\sum_{i=1}^{N} f(X_i)\right] \\ &= \frac{b-a}{N}\left[\sum_{i=1}^{N} E[f(X_i)]\right] \\ &= \frac{b-a}{N}\left[\sum_{i=1}^{N}\int_a^b f(x)\frac{1}{b-a}\mathrm{d}x\right] \\ &= \frac{1}{N}\left[\sum_{i=1}^{N}\int_a^b f(x)\mathrm{d}x\right] \\ &= \int_a^b f(x)\mathrm{d}x. \end{aligned} \tag{7}$$

When $f(x)$ cannot be expressed by an explicit equation (such as solving a rendering equation), the Monte Carlo method is a good choice. The method mentioned above is to sample randomly within the integration interval. However, if we can roughly know the curve shape of $f(x)$, we can formulate a probability distribution function $p(x)$ based on the approximate curve trend of $f(x)$. Moreover, we set the curve shape that is more suitable for $f(x)$ and perform sampling and calculation according to the following formula:

$$F_N = \frac{1}{N}\sum_{i=1}^{N}\frac{f(X_i)}{p(X_i)}. \tag{8}$$

In the case of sufficient N, F_N is approximately equal to $\int_a^b f(x)\mathrm{d}x$. However, the sampling strategy is based on $p(x)$, and there are more samples in the peak part of $p(x)$. If $p(x)$ fits the shape of $f(x)$ very well, then a smaller number of

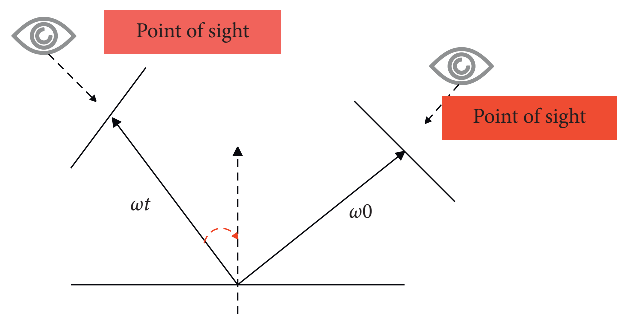

Figure 2: Distribution function of bidirectional reflection.

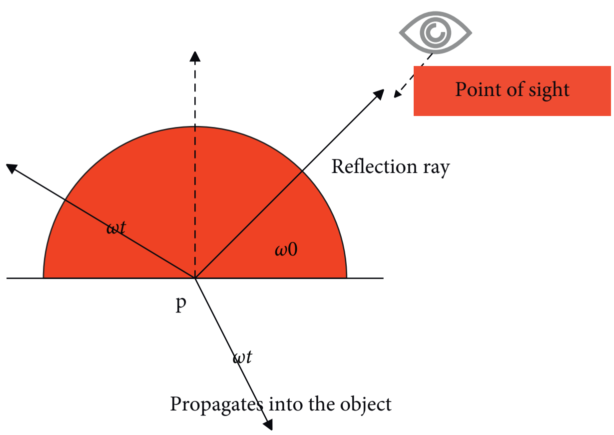

Figure 3: The propagation mode of light.

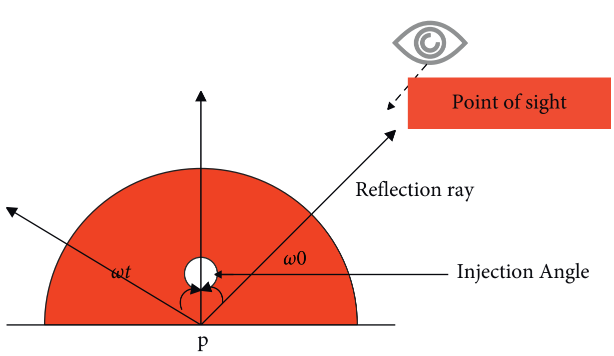

Figure 4: Specular reflection model.

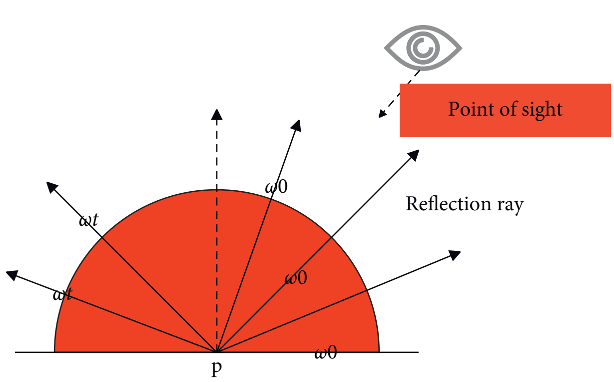

Figure 5: Diffuse reflection model.

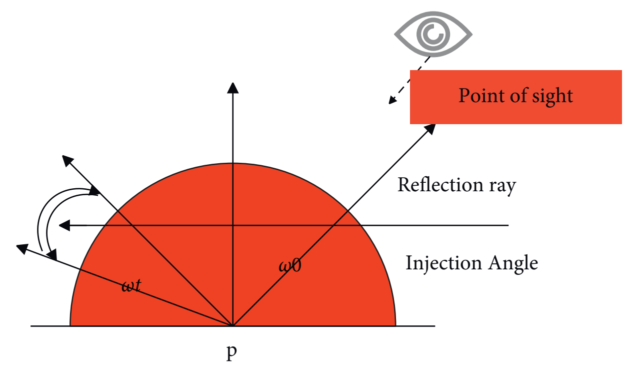

Figure 6: Directional reflection model.

samples can be used to get a more similar result to $\int_a^b f(x)\mathrm{d}x$.

According to the general Monte Carlo method, we can apply it to the solution of rendering equations. This is also the basis of all the following solution algorithms. For example, for diffuse reflection model or directional reflection model,

$$\begin{aligned} L_0(p,\omega_0) &= L_e(p,\omega_0) + \int_{\delta^2} (p,\omega_0,\omega_i) L_i(p,\omega_i) \left|\cos\,\theta_i\right| \mathrm{d}\omega_i \\ &= L_e(p,\omega_0) + \frac{1}{N}\sum_{i=1}^{N} \frac{(p,\omega_0,\omega_i) L_i(p,\omega_i) \left|\cos\,\theta_i\right|}{p(\omega_i)}. \end{aligned} \tag{9}$$

For non-SDS paths, the integral solution method is the same as the bidirectional optical path tracking. The specific method is described below.

Figure 7 is a schematic diagram of two-way optical path tracking. In the schematic diagram, there are two sublight paths, $P1' \longrightarrow P2' \longrightarrow P3'$ from the line of sight, and Pl'-$>P2'$-$>P3'$ from the light source. It can be seen from the figure that these suboptical paths can form up to $3*3$, and a total of 9 complete optical paths are available for use. Now, we connect $P3$ and $P2'$ and assume that there is no obstruction between these two points, and the planes where the two points are located are both diffuse reflection surfaces. At this time, the light starts from the light source and passes through $P1'$, $P2'$, $P3$, $P2$, and $P1$ and finally reaches the line of sight position. This constitutes a complete optical path, so that this complete path will affect the light energy at point $P1$

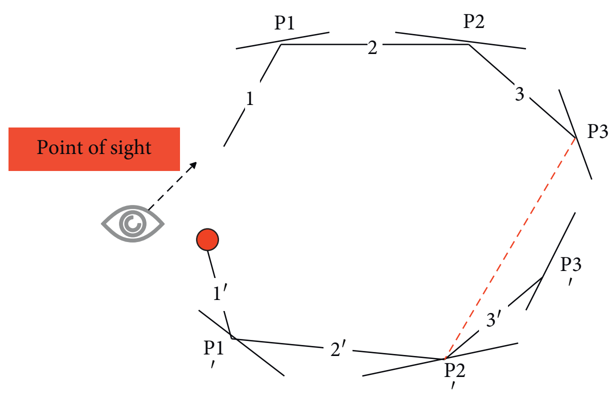

Figure 7: Schematic diagram of two-way optical line tracking.

and eventually return to the line of sight position via line 1. In this way, we can get the specific color value received by the line of sight.

The formula is expressed as follows:

$$C = \frac{Le\left(P_0', P_0^{' \longrightarrow P_1'}\right)}{p\left(P_0', P_0^{' \longrightarrow P_1'}\right)} \cdot \left(\frac{P_1', P_1' \longrightarrow P_0', P_1' \longrightarrow P_1', P_2'}{p\left(P_0^{' \longrightarrow P_2'}\right)}\right) . \left(P_2', P_2' \longrightarrow P_1', P_2' \longrightarrow P_3'\right) \cdot$$
$$\left(P_3, P_3 \longrightarrow P_2', P_1 \longrightarrow P_2\right) \cdot \left(\frac{\left(P_2, P_2 \longrightarrow P_3', P_2 \longrightarrow P_1\right)}{p\left(P_2 \longrightarrow P_3\right)} \cdot \frac{\left(P_1, P_1 \longrightarrow P_2, P_2 \longrightarrow P_0\right)}{p\left(P_1 \longrightarrow P_2\right)}\right). \tag{10}$$

First, we know the two sublight paths $PI \longrightarrow P2 \longrightarrow P3$ and $P1' \longrightarrow P2' \longrightarrow P3'$ and define the light source sampling position as Po' and the line of sight sampling position as $P0$. According to the Monte Carlo method, according to the probability distribution function at the light source, the light energy value of the auspicious point is divided by the probability distribution function value here. At position P_2', according to the probability distribution function at P_2', the BRDF is also divided by the value of the probability distribution in the sampling direction $P_1' \longrightarrow P_2'$. Then, the light energy throughput from position P_2' to position P_3 is calculated by BRDF, and the calculation is performed up to the viewpoint position. The result C is the final light energy received by the viewpoint.

When calculating the energy of the light path, the weight of the light path needs to be considered. During the light path tracking process, the same light path may be repeated many times. For example, at a certain moment, the following situation may occur.

In Figure 8, the generated path is the same as that in in Figure 7. The only difference is that they are obtained from different subpaths.

Therefore, for each complete path, a certain weight needs to be added. We assume that there is a complete path 1, and its length is n. As long as the suboptical path from the line of sight (assuming the length is s) and the suboptical path from the light source (assuming the length as t) satisfy $s + t - 1 = n$, path 1 may be generated. What needs to be ensured is that, in all cases, s and t satisfy the sum of their weights to 1.

Eric Veach explained, on the basis of experiments, that the best weighting equation is as follows:

$$\begin{aligned} w(s,t) &= \frac{p_j^{\beta}}{\sum_{i=0}^{s+t-1} p_i^{\beta}} \\ &= \frac{1}{\sum_{i=0}^{s+t-1}\left(p_i^{\beta}/p_j^{\beta}\right)}. \end{aligned} \tag{11}$$

Among them, p_j refers to the probability distribution function. On this basis, Eric Veach pointed out that the equation performs best when the index is $\beta = 2$.

In the actual calculation process of the two-line optical path tracking, if calculated according to the original weighting equation, it will consume a lot of time. After modifying the original equation, a simple calculation method can be obtained. If it is assumed that pi is expressed as the length of the subpath starting from the line of sight in the total optical path with a total length of n, then

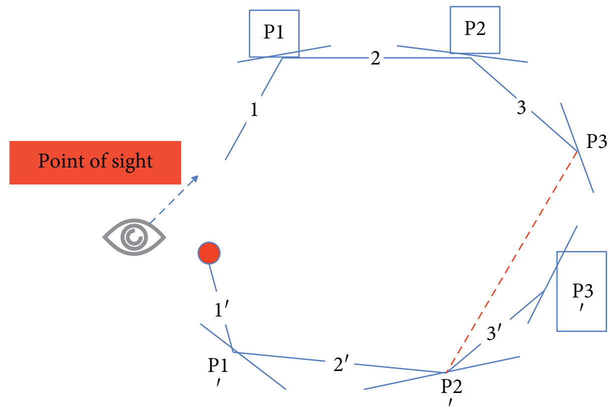

Figure 8: Schematic diagram of the weight problem.

$$\frac{p_{i+1}}{p_i} = \frac{p(e_0 \longrightarrow e_1)\cdot p(e_1 \longrightarrow e_2)\cdots p(e_{i-1} \longrightarrow e_i)}{p(e_0 \longrightarrow e_1)\cdot p(e_1 \longrightarrow e_2)\cdots p(e_{i-2} \longrightarrow e_{i-1})} = \frac{p(l_0 \longrightarrow l_1)\cdot p(l_1 \longrightarrow l_2)\cdots p(l_{n-i-2} \longrightarrow l_{n-i-1})}{p(l_0 \longrightarrow l_1)\cdot p(l_1 \longrightarrow l_2)\cdots p(l_{n-i-1} \longrightarrow l_{n-i})} = \frac{p(e_{i-1} \longrightarrow e_i)}{p(l_{n-i-1} \longrightarrow l_{n-i})}. \tag{12}$$

Thus, we can get the result of any p_i/p_j from the result of p_{i+1}/p_i. For example,

$$\frac{p_{i+2}}{p_i} = \frac{p_{i+2}}{p_{i+1}}\cdot\frac{p_{i+1}}{p_i}. \tag{13}$$

The simplicity of this method lies in the fact that the vertex results of the subpath in the middle of a bidirectional optical path tracing all need to be reused. In this way, the ratio of p_{i+1}/p_i can be stored in the vertex structure, and only a few multiplications are required each time the weight is calculated.

For the SDS path, the two-way optical path tracking will completely ignore this type of path. At this time, it is necessary to use a method similar to the photon graph to process the SDS path for calculation. Such a method will bring a certain deviation to the result. In terms of robustness, this hybrid method is not as good as any unbiased method. However, this method can reuse the subpath starting from the light source, and the use of the vertices on these subpaths is not a pure two-way optical path tracking to calculate whether there is a speed block between any two points. Each calculation must traverse the entire ray acceleration structure, and its traversal speed is related to the scene complexity. The processing method similar to the photon graph is only to search for the vertex position related to the current calculation process, so the calculation efficiency of this method will be relatively high.

The common photon map method to calculate the light energy of the current point (N-nearest) is as follows:

$$L(P, \overrightarrow{\omega_0}) \approx \sum_{j=1}^{n} \frac{(P, \overrightarrow{\omega_{IJ}}, \overrightarrow{\omega_0})\phi_j(P_j, \overrightarrow{\omega_{IJ}})}{\pi r^2}. \tag{14}$$

For the light energy of P position with direction $\overrightarrow{\omega_0}$, it is to multiply the light energy of all known points in the circle with radius r by BRDF and statistically estimate the light energy of P position with direction $\overrightarrow{\omega_0}$, as shown in Figure 9.

The gray point is the required P position. It will look for all photons within the radius r around itself and estimate the light energy at its own location. It is easy to get that the smaller the r, and the more the photons in the range of r, the closer the light energy of the final position of P to the light energy that P correctly carries. For the final image produced, the larger r and the smaller the number of photons, the more blurred the image. On the contrary, the image is clearer and closer to the correct result. Of course, the solution time is longer.

Modifying the calculation method of the photon diagram, the solution method of the SDS path can be obtained. We assume that there is an SDS path scenario as shown in Figure 10.

At this time, it is necessary to add all the points within the radius of r to the process of calculating the light energy of the diffuse reflection point. In the above figure, the viewpoint is traced down through the mirror position P_1, and light is emitted to a point P_{1e} on the diffuse reflection surface. The light source traces down through the mirror position P_2 and emits light to point P_{2l} on the same diffuse reflection surface. When we need to calculate the brightness of point P_{1e}, we need to consider P_{2l}. When point P_{2l} is within the range of P_{1e} with radius r, point P_{2l} is included in the calculation range.

$$L(P_{1e}, \omega_0) \approx (P_{1e}, P_{1e} \longrightarrow P_1, P_{1e} \longrightarrow P_2) \cdot \phi(P_{2l}, P_{2l} \longrightarrow P_2)\cdot\frac{1}{\pi r^2}. \tag{15}$$

As with the photon graph method, these P_{2l} -type points can be reused.

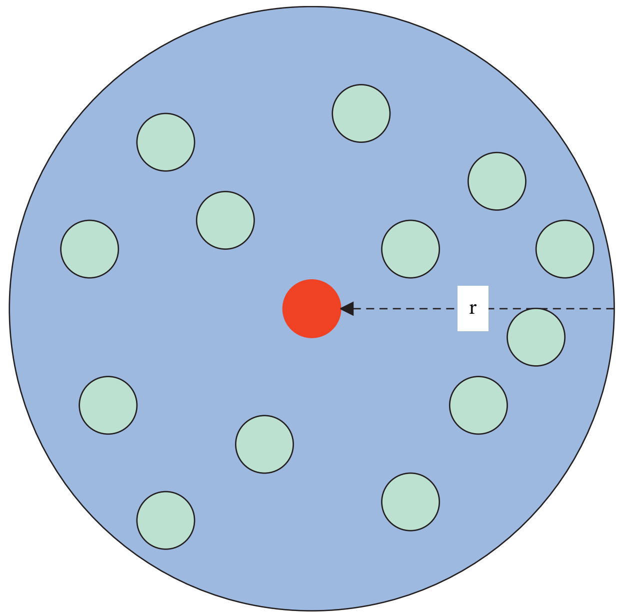

Figure 9: The way the photon map method calculates the rendering equation.

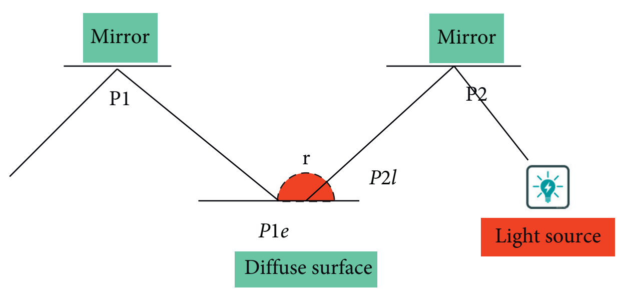

Figure 10: Dealing with SDS issues.

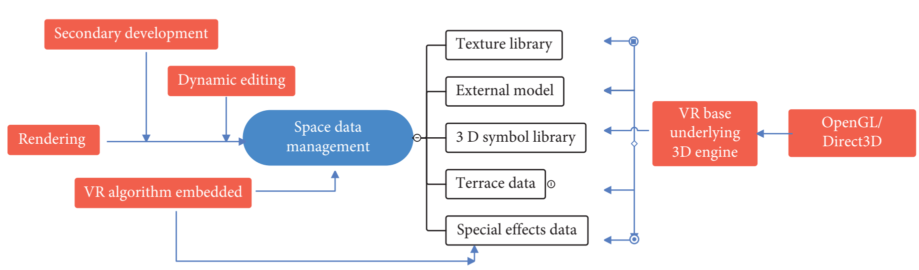

Figure 11: System structure diagram of the urban three-dimensional landscape basic platform system.

4. Three-Dimensional Structure Analysis of Urban Landscape Based on Big Data Technology and Digital Technology

To build a three-dimensional landscape platform, we need to understand its system composition. The architecture can reflect the operation flow and data flow. The system structure of the 3D landscape basic platform will be increased or tailored according to the specific application. The general 3D landscape basic platform includes several functional modules such as rendering module, data management module, engine module, and editing module. The system structure shown in Figure 11 is a system structure diagram of several functional modules that should be considered when researching and developing this basic platform. On this platform, the design of 3D data model, spatial data management, and 3D engine design are the key parts of the platform design. A good platform design should also provide users with flexible editing functions and secondary development interfaces. Users can also customize their own data management mode and choose flexible VR algorithms.

Table 1: Evaluation of the design effect of the urban three-dimensional landscape basic platform system.

Number	Simulation effect	Design effect	Number	Simulation effect	Design effect	Number	Simulation effect	Design effect
1	95.70	87.68	22	94.89	73.96	43	91.02	70.58
2	95.30	89.16	23	86.14	79.14	44	93.73	86.71
3	89.84	89.09	24	95.66	87.36	45	95.36	84.24
4	91.46	74.26	25	93.04	88.22	46	91.71	83.11
5	96.48	76.37	26	92.08	73.53	47	96.31	70.78
6	90.90	83.84	27	90.08	86.97	48	92.64	76.28
7	90.52	76.47	28	93.56	83.02	49	91.06	86.23
8	89.58	69.86	29	90.55	84.11	50	92.55	78.12
9	96.54	76.26	30	95.08	87.05	51	90.42	86.02
10	87.91	78.01	31	94.89	77.47	52	89.17	70.77
11	86.68	76.23	32	95.62	74.27	53	90.96	83.36
12	89.82	71.63	33	92.48	79.63	54	95.98	81.38
13	87.11	79.88	34	94.04	89.76	55	91.59	78.18
14	87.38	90.99	35	88.75	88.22	56	89.24	90.04
15	95.95	69.93	36	86.25	74.18	57	86.28	80.59
16	90.95	73.52	37	92.11	71.01	58	92.01	71.14
17	90.08	87.06	38	87.24	70.74	59	91.01	78.64
18	91.49	88.16	39	95.67	85.47	60	95.45	87.98
19	93.75	81.19	40	95.98	76.32	61	89.29	90.67
20	88.60	88.92	41	89.76	70.55	62	96.08	71.89
21	92.28	84.98	42	91.63	89.29	63	88.59	80.98

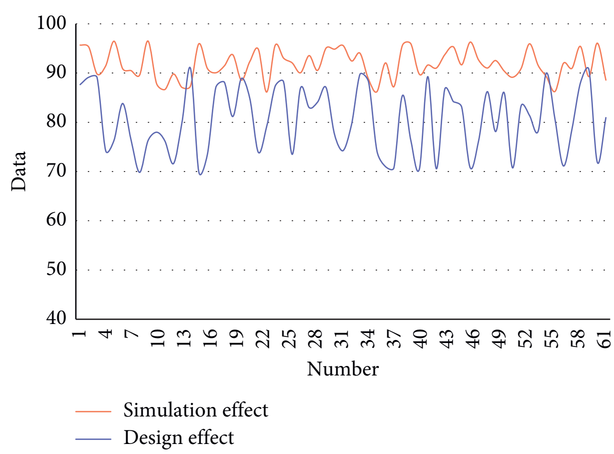

Figure 12: Quantitative evaluation statistics.

After constructing the above-mentioned urban landscape three-dimensional structure analysis system based on big data technology and digital technology, the performance of the system is verified. This paper designs multiple groups of urban three-dimensional structures to test the system performance and count the three-dimensional structure simulation effects and actual design effects. The three-dimensional simulation effect is quantitatively analyzed by postdesign evaluation, and the results shown in Table 1 and Figure 12 are obtained.

From the above analysis, the urban landscape three-dimensional structure analysis system based on big data technology and digital technology proposed in this paper has good design and simulation effects, and the system designed in this paper can be used for auxiliary research in the three-dimensional design and analysis of urban landscape.

5. Conclusion

The landscape design business of the Urban Space Planning and Design Institute has been developed so far, and the development environment it faces has also become more complicated. If an enterprise wants to realize its own development, it must have an overall plan for the future development direction, business field, and advantages of the Urban Space Planning and Design Institute. In addition, the Urban Space Planning and Design Institute must consciously adjust its own internal and external environmental changes in strategic planning, so as to better adapt to environmental needs and promote the long-term development of the enterprise. At present, domestic and foreign experts and scholars have insufficient research on the related strategies of urban space planning and design enterprise landscape business development. The research on this topic will help better improve this theory and provide a reference for the development of corporate landscape business in urban space planning in the later period. This paper combines big data technology and digital technology to analyze the three-dimensional structure and performance of urban landscapes, which effectively improves the scientific nature of urban landscape design.

Data Availability

The labeled dataset used to support the findings of this study are available from the corresponding author upon request.

Conflicts of Interest

The authors declare no conflicts of interest.

Acknowledgments

This study was sponsored and supported by the Fundamental Research Funds for the Central Universities: Research on the Visual Evaluation of Winter Landscape in Cold Cities in Northeastern China—with examples of Shenyang and Harbin (PID: 02040022120002).

References

[1] O. Guerra-Santin and S. Silvester, "Development of Dutch occupancy and heating profiles for building simulation," *Building Research & Information*, vol. 45, no. 4, pp. 396–413, 2017.

[2] T. Dodd, C. Yan, and I. Ivanov, "Simulation-based methods for model building and refinement in cryoelectron microscopy," *Journal of Chemical Information and Modeling*, vol. 60, no. 5, pp. 2470–2483, 2020.

[3] T. Abuimara, W. O'Brien, B. Gunay, and J. S. Carrizo, "Towards occupant-centric simulation-aided building design: a case study," *Building Research & Information*, vol. 47, no. 8, pp. 866–882, 2019.

[4] P. Remmen, M. Lauster, M. Mans, M. Fuchs, T. Osterhage, and D. Müller, "TEASER: an open tool for urban energy modelling of building stocks," *Journal of Building Performance Simulation*, vol. 11, no. 1, pp. 84–98, 2018.

[5] N. Endo, E. Shimoda, K. Goshome, T. Yamane, T. Nozu, and T. Maeda, "Simulation of design and operation of hydrogen energy utilization system for a zero emission building," *International Journal of Hydrogen Energy*, vol. 44, no. 14, pp. 7118–7124, 2019.

[6] I. Beausoleil-Morrison, "Learning the fundamentals of building performance simulation through an experiential teaching approach," *Journal of Building Performance Simulation*, vol. 12, no. 3, pp. 308–325, 2019.

[7] C. Xiong, J. Huang, and X. Lu, "Framework for city-scale building seismic resilience simulation and repair scheduling with labor constraints driven by time-history analysis," *Computer-Aided Civil and Infrastructure Engineering*, vol. 35, no. 4, pp. 322–341, 2020.

[8] A. D. Black, "Wor(l)d-building: simulation and metaphor at the mars desert research station," *Journal of Linguistic Anthropology*, vol. 28, no. 2, pp. 137–155, 2018.

[9] K. Hanson, L. Hernandez, and J. A. Banaski, "Building simulation exercise capacity in Latin America to manage public health emergencies," *Health security*, vol. 16, no. S1, pp. S98–102, 2018.

[10] E. K. Wati and N. Widiansyah, "Design of learning media: modeling & simulation of building thermal comfort optimization system in building physics course," *Jurnal Pendidikan IPA Indonesia*, vol. 9, no. 2, pp. 257–266, 2020.

[11] C. W. Lee and S.-J. Cho, "The development of converting program from sealed geological model to Gmsh, COMSOL for building simulation grid," *Journal of the Korean Earth Science Society*, vol. 38, no. 1, pp. 80–90, 2017.

[12] C. Miller, D. Thomas, J. Kämpf, and A. Schlueter, "Urban and building multiscale co-simulation: case study implementations on two university campuses," *Journal of Building Performance Simulation*, vol. 11, no. 3, pp. 309–321, 2018.

[13] X. Xie and Z. Gou, "Building performance simulation as an early intervention or late verification in architectural design: same performance outcome but different design solutions," *Journal of Green Building*, vol. 12, no. 1, pp. 45–61, 2017.

[14] A. I. Adilkhodjayev, I. M. Mahamataliev, and S. S. Shaumarov, "Theoretical aspects of structural and simulation modeling of the macrostructure of composite building materials," *Journal of Tashkent Institute of Railway Engineers*, vol. 14, no. 2, pp. 3–14, 2019.

[15] S. Imam, D. A. Coley, and I. Walker, "The building performance gap: are modellers literate?" *Building Service Engineering Research and Technology*, vol. 38, no. 3, pp. 351–375, 2017.

[16] J.-S. Pei, B. Carboni, and W. Lacarbonara, "Mem-models as building blocks for simulation and identification of hysteretic systems," *Nonlinear Dynamics*, vol. 100, no. 2, pp. 973–998, 2020.

[17] A. Brunelli, F. de Silva, A. Piro et al., "Numerical simulation of the seismic response and soil-structure interaction for a monitored masonry school building damaged by the 2016 Central Italy earthquake," *Bulletin of Earthquake Engineering*, vol. 19, no. 2, pp. 1181–1211, 2021.

[18] P. Andrio, A. Hospital, J. Conejero et al., "Bioexcel building blocks, a software library for interoperable biomolecular simulation workflows," *Scientific Data*, vol. 6, no. 1, pp. 169–184, 2019.

[19] G. Petrou, A. Mavrogianni, P. Symonds et al., "Can the choice of building performance simulation tool significantly alter the level of predicted indoor overheating risk in London flats?" *Building Service Engineering Research and Technology*, vol. 40, no. 1, pp. 30–46, 2019.

[20] S. Gibeaux, C. Thomachot-Schneider, S. Eyssautier-Chuine, B. Mari, and P. Vazquez, "Simulation of acid weathering on natural and artificial building stones according to the current atmospheric SO_2/NO_x rate," *Environmental Earth Sciences*, vol. 77, no. 9, pp. 1–19, 2018.

Hindawi
Scientific Programming
Volume 2021, Article ID 8667945, 11 pages
https://doi.org/10.1155/2021/8667945

Research Article

Simulation and Modeling Algorithm for Terminal Container Handling Intelligent Management Based on Internet of Things and Big Data Technology

Lifen Zhang ,[1,2] Qiang Zhou,[1] and Huifang Ding[1]

[1]*School of Transportation and Logistics Engineering, Wuhan University of Technology, Wuhan 430063, China*
[2]*Hubei Communications Technical College, Wuhan 430079, China*

Correspondence should be addressed to Lifen Zhang; zhanglifen@whut.edu.cn

Received 26 September 2021; Revised 18 October 2021; Accepted 23 October 2021; Published 9 November 2021

Academic Editor: Hai Dong

In order to improve the effect of intelligent terminal container management, this paper improves the Internet of Things and big data technology, analyzes the RFID middleware architecture based on the actual needs of container handling management, and proposes a new method of RFID middleware load balancing. Moreover, this paper combines the Internet of Things technology and big data technology to analyze the terminal container loading and unloading process and build a corresponding intelligent system. After constructing a terminal container handling intelligent management system based on the Internet of Things and big data technology, the performance of the system is verified, and multiple sets of simulation data are used to conduct research. The experimental research results show that the terminal container handling management system based on the Internet of Things and big data constructed in this paper basically meets the actual needs of use.

1. Introduction

With the rapid development of China's terminal container transportation industry, major port group companies are facing unprecedented challenges. At present, most domestic ports still adopt manual or semimechanical methods to complete the collection and recording of container data information, which is inefficient and slow [1]. Customs, national inspection, and other government supervision departments also use image processing pattern recognition technology to identify the number of containers. This processing method only has a recognition rate of 80% to 98%, the container traffic management and tracking monitoring are all in an isolated state, and it is impossible to realize the efficient and automated production of terminal containers. Moreover, it is also a heavy and slow fatigue job for government workers [2]. Improving the operational efficiency of terminal containers is directly related to the economic benefits of various enterprises. The use of manual implementation to identify and count the vehicle numbers and container numbers of terminal containers is likely to cause duplication of work, human errors, time delays, stagnation of goods, and low efficiency. Therefore, in order to avoid the waste of container resources in the terminal, it is an urgent issue to improve the automatic management capabilities of terminal containers and modern management facilities [3].

The main transportation method of the former port logistics is container transportation. With the continuous growth of port transportation, resource competition among ports has become more intense. The competitive advantage of each port comes from hard conditions such as port geography and hinterland economy and its management. The service level, operation and production efficiency, equipment and facilities conditions, and other automation, informationization, modernization, and technical indicators are also extremely important factors that reflect the competitiveness of the port. Since the 1990s, with the increasing requirements for port operation efficiency, production costs, and sustainable development, port automation has become a new era of port development due to its significant advantages such as efficient operation, low labor costs, and superior safety and reliability Since the 1990s, with the increasing requirements for port operation efficiency, production costs, and sustainable development, port automation has become the general trend of the new era of port development by virtue of its significant advantages such as efficient operation, low labor cost, safety, and reliability. Up to now, more than 30 automated terminals have been applied and put into actual production in many countries around the world and have achieved good operational results. The emergence and in-depth development of automated terminals has become a major change in the sustainable development of ports in the future.

This paper combines the Internet of Things technology and big data technology to analyze the terminal container loading and unloading process and build a corresponding intelligent system to provide a reference for subsequent intelligent container loading and unloading and management.

2. Related Work

For a long time, domestic and foreign scholars have carried out many researches on the optimization of container ship loading. Aiming at the problem of container loading, literature [4] first established a 0–1 planning model based on the optimization goals of the smallest amount of container tipping in the yard and the shortest quay crane moving distance. However, due to the large number of variables in the model 0–1, it is difficult to solve the problem when the scale is large and the practicability is not strong. Aiming at the problem that the problem model is difficult to solve, literature [5] simplified the above planning model by ignoring the ship weight stability constraint. The optimization goal is also set to minimize the amount of container dumping in the yard, and the number of variables is reduced compared with the previous one. Literature [6] took the minimum amount of container dumping in the yard and the stability of ship weight as the optimization goals, established a multiobjective integer programming model, and used the weighting method to obtain the noninferior solution of the problem model. On the basis of the previous research on container dumping in the storage yard, literature [7] first proposed a simple method for estimating the amount of container dumping in the container yard in combination with the operation of the container yard. It is defined as the basic amount of container dumping, which simplifies the problem of loading and arranging containers. In the following research, this method will be used as the research basis to analyze the container transportation situation in the terminal in detail. Literature [8] proposed that when analyzing and studying the distribution and arrangement of containers in the yard of ships, factors such as the weight of the container and the distance of the destination port should be taken into consideration. Literature [9] summarized the main methods currently used to study the automatic stowage of container ships and used mathematical modeling methods to optimize the research progress of ship stowage from the perspective of the ship and the port. Literature [10] described in detail the main characteristics of container ship stowage and unilaterally optimized ship stowage based on the linear programming method from the perspective of ship weight stability. Literature [11] proposed three strategies for carrying containers for container yard operations, used the integer programming method to establish a mathematical model, and used the CPLEX solver to accurately solve small-scale cases. The above-mentioned research on the problem of container loading and packing is mainly based on the mathematical model method to solve the problem. After that, the researchers used heuristic algorithms based on rule setting to further study the problem of container loading and packing. Based on the in-depth analysis of the causes of the container tipping problem in the container yard, literature [12] established a rule-based heuristic algorithm for the container loading and arranging problem based on the known container yard storage status and the container ship stowage map, which takes minimizing the amount of box turnover as the optimization goal. The results show that the case-solving effect is good.

Literature [13] additionally considers the actual constraints of port customs clearance. Moreover, on this basis, it constructed a heuristic algorithm with the optimization objective of minimizing the amount of container dumping based on the known yard container storage status and container ship stowage map. In addition, it designed numerical experiments to verify the effectiveness and practicability of the algorithm. In recent years, the emergence of intelligent optimization algorithms such as genetic algorithm, tabu search algorithm, simulated annealing algorithm, and particle swarm algorithm has provided new ideas and methods for solving optimization problems. Literature [14] compared the container stowage problem with the traveling salesman problem. On this basis, it considered the constraint conditions of ship stability, heel, and trim moment and established a problem model with the optimization goal of minimizing the amount of tank tipping. Moreover, it used a genetic algorithm to solve the problem. However, there are deficiencies; that is, the algorithm code is too long, the solution space is too large, and so on.

Literature [15] constructed an optimization algorithm based on a parallel tabu search to find the optimal ship loading sequence based on the known container ship stowage map. Literature [16] used a genetic algorithm to solve the problem with the minimum amount of box dumping as the optimization objective. Literature [17] regards the influencing factors such as the volume of container dumps, ship stability, strength, and operability as evaluation strategies and also uses genetic algorithms to find the optimal ship loading sequence. Literature [18] combined the actual loading and unloading of the container terminal to analyze the main reasons for the tipping of containers during container loading in the yard and put forward related control methods based on the given ship loading plan and yard. For the storage status of containers, a mathematical model with the smallest amount of unloaded containers as the optimization objective is established, and the genetic algorithm is used to solve them under different unloading rules. Literature [19] regards the container turnover rate of the yard as a constraint, takes the weight stability of the ship after loading as the optimization objective, establishes an integer programming problem model for solving the container loading sequence, and uses an algorithm based on particle swarm optimization to design and solve it. Literature [20] established a model based on the given container loading and stowage map, taking the minimum amount of unloading as the optimization objective, and proposed a parallel genetic particle swarm algorithm to solve it. The simulation experiment was carried out through Matlab, and the solution effect was better. Most of the above researches are based on known ship loading and loading plans from a single perspective of container loading sequence. Literature [21] considered the relationship between container loading sequence and ship stowage, based on the idea of two-stage hierarchical solution, and designed an algorithm based on SWO-HES two-stage optimization to solve the small-scale problem of a single shell position of a ship.

3. Internet of Things and Big Data Processing Algorithms Applied to Container Unloading Management

This paper analyzes the architecture of RFID middleware and proposes a new method of RFID middleware load balancing. This method is based on ALE (Application Level Events). This method defines the workload on the RFID middleware as ALE's ECSpecs, and ALE's ECSpecs are sent from the RFID application. Therefore, the workload of RFID middleware is to migrate ECSpecs from middleware with higher load to middleware with lower load by managing components.

ALE provides a set of flexible interfaces with standard functions, which are realized through RFID middleware. Therefore, ALE defines a set of standard interfaces with aggregation, filtering, and counting functions.

Figure 1 shows the role of ALE in an RFID system. An RFID application layer requests the RFID middleware to collect and transmit EPCs information through the ALE interface. When requesting EPCs information, the RFID application layer specifies EPCs related to ECSpec. The three fields of EPCs are actually sent to the RFID application layer. The reading field specifies the EPCs information collected from the reader. The boundary section specifies the time stamp of the collection and the report generated. The ECSpec report specifies a filter that removes EPCs that are not related to the RFID application layer.

The ALE interface uses the logical name for the meaning reader. Logical reader is an abstract name. This abstract name refers to one or multiple physical readers that can be regarded as a group. For example, there are three RFID readers on a door carrying a lock in a warehouse. It is very simple and convenient to compile these three physical readers into a group of logical readers. The RFID middleware maintains the mapping information between the logical reader and the physical reader. Figure 2 is a class diagram of the relationship between the concepts mentioned, shows the dependencies between the various components, and also shows the architectural relationship in ALE.

The load of the RFID middleware mentioned here is mainly caused by the collection and filtering of the tag data read by the connection with the reader. A large number of data tags have to be processed so as to cause the load of the middleware. Therefore, in order to reduce the load of the middleware, we need to effectively manage the large amount of raw label data processed by the middleware. As discussed in the previous section, the ECSpec sent by the RFID application layer defines a set of readers and tag data that is meaningful to the RFID application layer. In other words, an ECSpec determines a set of readers and notes data information processed by the RFID middleware. Therefore, we can manage the load status of the RFID middleware by controlling the ECSpec assigned to the middleware.

For the method of achieving load balancing of RFID middleware by migration, Figures 3(a) and 3(b) can be used to explain the overall process of this method. Figure 3(a) shows two application servers, and an RFID application is running in each application server. There are a total of six

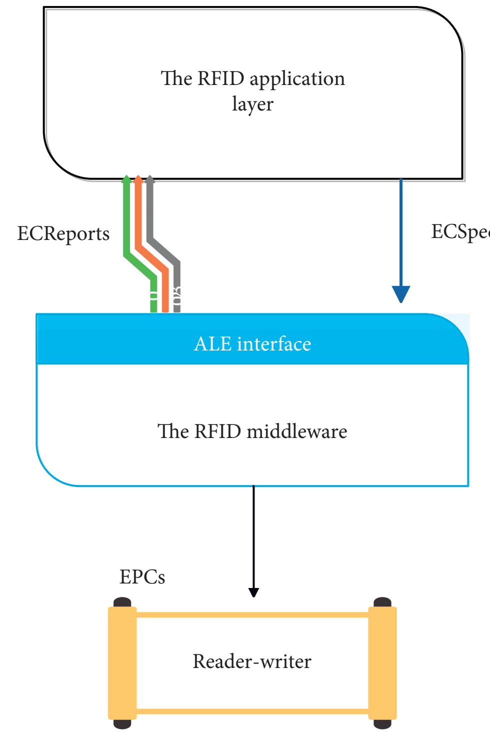

Figure 1: RID middleware architecture diagram with label data flow.

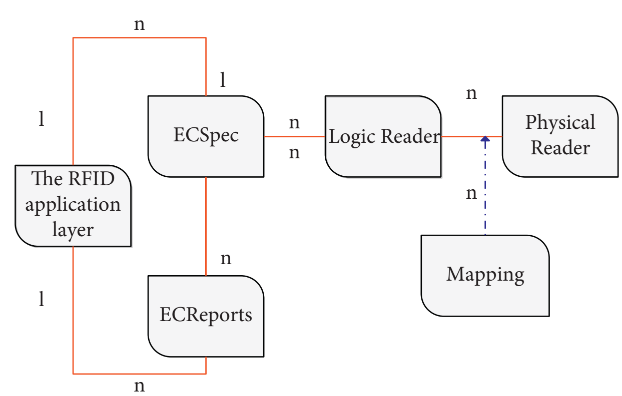

Figure 2: Basic concept diagram in ALE.

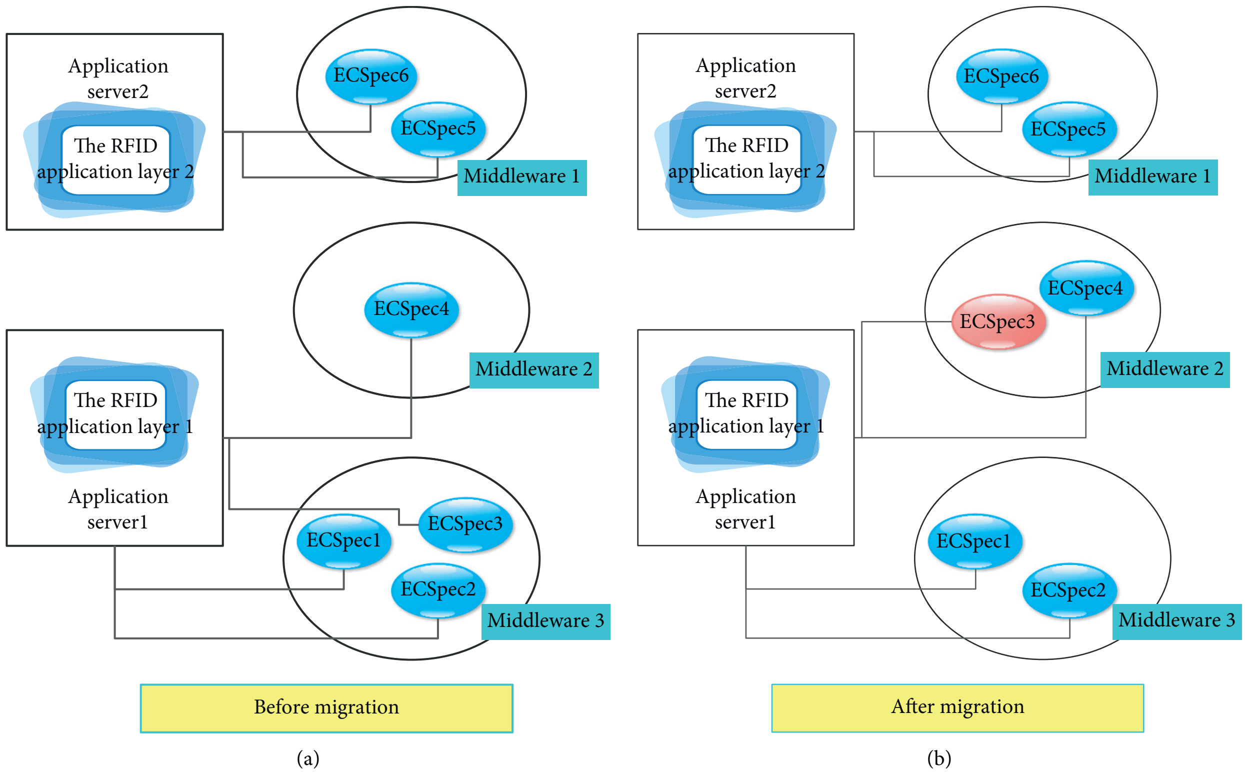

Figure 3: Example diagram of the migration algorithm of ECSpec for RFID middleware load balancing. (a) Before migration. (b) After migration.

ECSpecs distributed among three middleware servers. The connection between the RFID application server and ECSpecs represents the process of ECSpecs distributed by the RFID application.

Suppose we find a large amount of ECSpecs label data, ECSpec1, ECSpec2, and ECSpec3 will cause middleware 1 to overload. In order to reduce the load on middleware 1, we need to move ECSpecs from middleware 1 to other types of low-load middleware. For example, by moving ECSpec3 on middleware 1 to middleware 2 with the lowest load, the load on middleware 1 is reduced, so that middleware 1 is not overloaded. Since ECSpecs directly determines the label data that a large amount of middleware will process, the load status of the entire system caused by ECSpec3 is now balanced by migrating from middleware 1 to middleware 2. This situation is shown in Figure 3(b). The algorithm described above only occurs when the processing capabilities of the middleware components are the same. In the figure, middleware 1, middleware 2, and middleware 3 all have the same ability to process label data.

It is worth noting that the migration of ECSpec3 did not lead to changes in the distribution of RFID applications and the use of ECSpec3. The RFID application does not even notice that the originally allocated ECSpec3 has migrated from one middleware to another. This situation is determined by the properties of ECSpec itself. As described in the previous section, each ECSpec specifies the destination location and this result is transferred by the ECSpec through the Notification component of the URI. Therefore, the result of ECSpec is even still routing migration from the original location to the destination. Therefore, we can safely migrate the ECSpec of the overloaded middleware to the lightest-loaded middleware without worrying about the distribution of RFID applications.

As mentioned above, we balance the system load by migrating the same ECSpec from the overweight middleware to the overweight middleware. In addition, because RFID applications have no dependencies on certain RFID middleware, migration can occur without considering RFID-related applications. Therefore, when we choose to migrate ECSpec, we can ignore the related RFID applications.

Compared with the independence of RFID applications, RFID readers that are closely related to ECSpec can also be considered for migration and distribution of ECSpec. As we discussed in the previous section, each ECSpec has a specification on the logical reader/writer that can read meaningful ECSpec. In other words, ECSpec specifies a specific logical reader/writer that can read tag data. Since the RFID reader is usually connected to an RFID middleware, the reader designated by ECSpec can also be reassigned to another middleware to which ECSpec will move. For example, in Figure 4 showing ECSpec, the configuration of an RFID system and the relationship between the RFID reader and ECSpec are considered. Suppose that we choose to move ECSpec3 to middleware 2; in this case, the related readers R4 and R5 should be moved to middleware 2. At the same time, ECSpec3 will also be migrated to middleware 2. This is because ECSpec3 must be connected to R4 and R5, and each reader can only be connected to one RFID middleware.

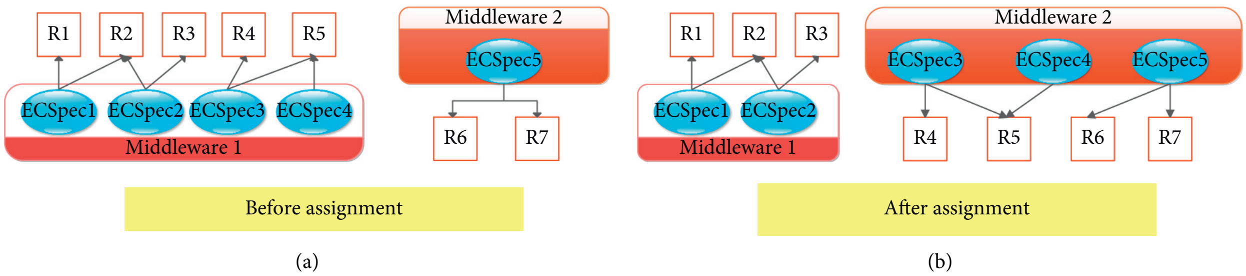

Figure 4: Distribution diagram considering the dependency of the reader. (a) Before assignment. (b) After assignment.

Dynamic weighted load algorithm distribution ECSpecs is feasible. According to the above migration and aggregation methods, it can be described as a distributed function to show the intuitiveness of the algorithm. The distribution of RFID middleware ECSpecs can be identified by comparing and calculating distributed functions. The formula is as follows:

$$Y(i) = L(i) \times e_i + R(i) \times e_r + M(i) \times e_m. \tag{1}$$

Among them, $L_{\max}(i)$ represents the maximum and affordable number of effective connections of the reader/writer connected to the i-th RFID middleware. $L(i)$ represents the load status of the i-th RFID middleware server. This can be expressed as follows:

$$L(i) = \frac{L_W(i) \times e_w + L_n(i) \times e_n}{L_{\max}(i)} + L_m(i) \times e_c. \tag{2}$$

$R(i)$ represents the degree of correlation between the i-th RFID middleware and ECSpecs, which is expressed as follows:

$$R(i) = R_W(i) \times e_W + R_n(i) \times e_n. \tag{3}$$

$M(i)$ represents the number of readers that need to be migrated for the i-th RFID middleware, which is expressed as follows:

$$M(i) = M_W(i) \times e_W + M_m(i) \times e_m. \tag{4}$$

$L_W(i)$ represents the number of readers running on the i-th RFID middleware server. $L_n(i)$ represents the number of nonoperational readers on the i-th RFID middleware server. $L_m(i)$ represents the load of the machine on the i-th RFID middleware server. This is expressed as follows:

$$L_m(i) = L_{\mathrm{cpu}}(i) \times e_{\mathrm{cpu}} + L_{\mathrm{mem}}(i) \times e_{\mathrm{mem}}. \tag{5}$$

$L_{\mathrm{cpu}}(i)$ represents the CPU utilization of the i-th RFID middleware server. $L_{\mathrm{mem}}(i)$ represents the memory utilization of the i-th RFID middleware server. Similarly, $R_W(i)$, $R_n(i)$, $M_W(i)$, and $M_n(i)$ are also expressed in the above method. Moreover, $e_i + e_r + e_m = 1$ and $e_i, e_r, e_m, e_w, e_n, e_c, e_{cpu}, e_{mem}$ are corresponding weights.

In order to describe the load status of each node, reader, and middleware cluster, a convenient calculation method is defined, which is expressed as follows:

$$T = \frac{\sum L(i)}{\sum L_{\max}(i)},$$
$$T(i) = \frac{L(i)}{L_{\max}(i)}. \tag{6}$$

In view of a clear understanding of the load balancing under the set dynamic weights, we must first define the load of the three-state nodes of $T(i)$. (A) Light load: this refers to a computing node with a small number of connections and a low machine load of the reader. (B) Heavy load: this refers to a computing node with a large number of connections and a high machine load of the reader. (C) Moderate balance: this refers to a state between heavy load and light load. This state is $|T(i) - T_s| < \Theta$, where T_s is the average and Θ is the deviation. The corresponding balance states $L_{\mathrm{cpu}}(i)$ and $L_{\mathrm{mem}}(i)$ of the utilization rate of the RFID middleware server are similarly expressed as described above. Moreover, when T changes, e_i: e_r: e_m will also change. When T is a light load, then e_i will take a larger value. When T is a heavy load, e_i and e_m will take larger values. In the same way, when $L_{\mathrm{cpu}}(i)$ and $L_{\mathrm{mem}}(i)$ change, e_{cpu} and e_{mem} also change. When $L_{\mathrm{cpu}}(i)$ and $L_{\mathrm{mem}}(i)$ are in a light load state, e_{cpu} and e_{mem} will take smaller values together, and vice versa. In addition, $L_m(i)$ is proportional to e_c. When $T(i)$ changes, e_w: e_n will change accordingly. When $T(i)$ exhibits a heavy load, e_w will take a larger value, and vice versa.

Figure 5 shows the relationship between the components of RLBA. The components MLT and RLT are middleware.

Middleware Load Table (MLT) and Reader Load Table (RLT) provide component management. The IMLTManager interface of MLT and the IRLTManager interface of RLT will perform update and retrieval in each middleware. Therefore, other components can access them by using the corresponding interface.

All nodes begin to perform calculation work. After a period of implementation, the node starts to check whether it is a heavy load node. If the node is overloaded, it will try to distribute its own jobs in the relevant domain. If it is assumed that the heavily loaded node is Lp, there are M nodes in the relevant domain, and these nodes are $L_1, L_2, \ldots\ldots, L_m$. Therefore, the average load is

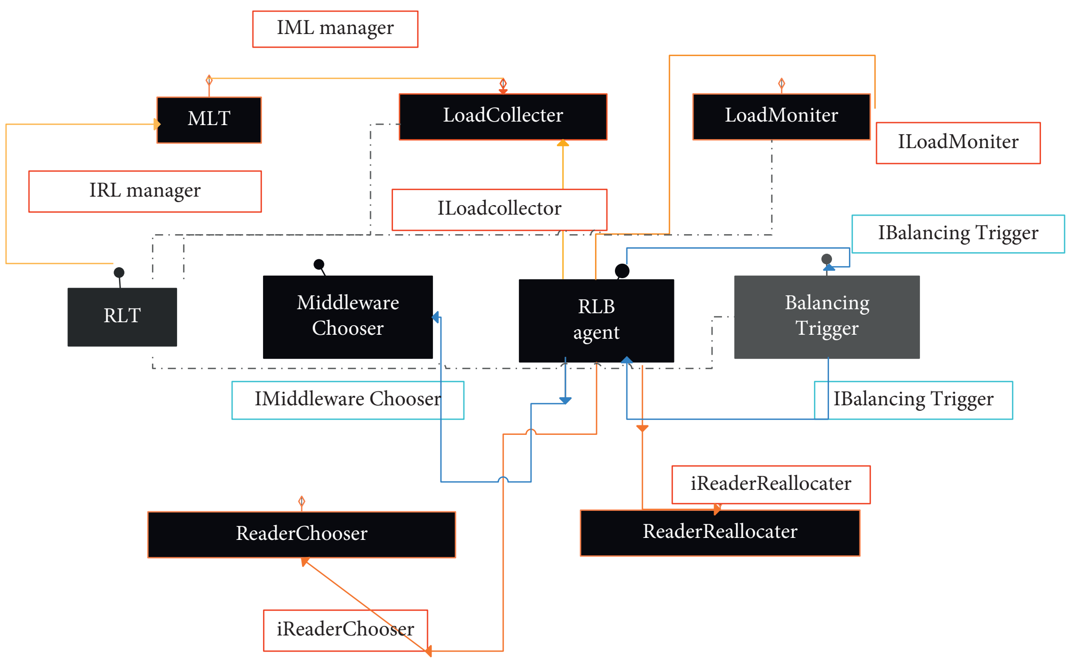

Figure 5: Proxy FD load balancing component diagram.

$$L_{avg} = \frac{1}{m+1}\left(L_p + \sum_{i=1}^{M} L_i\right). \quad (7)$$

In order to achieve uniform distribution, the load can be obtained as Nm by transmitting the overloaded load node to other nodes in the relevant domain. First, a hm value is set. This value is set to move all load nodes to the heaviest load node in the heavy load-related domain. If there is $L_{avg} > L_m$, the expression of N_m is

$$N_m + \left[\left(L_p - L_{avg}\right)\frac{h_m}{\sum_{i=1}^{M} h_i}\right]. \quad (8)$$

Then, the task can be sent to all relevant nodes at this time.

The start strategy at the receiving end is to use a light load start strategy. This strategy requires all other nodes to send tasks to this light node, and other nodes also use this strategy to send tasks to nodes other than the specified node like this light node. This strategy must first set an M value. This M value has the same effect as the M value of the sender startup strategy above, and it is also a critical value for distinguishing between heavy load and light load. The definition of the relevant domain here is the same as the above definition, and the same is true for all nodes to start performing calculation tasks. As time goes by, once a node detects that it is a light node, it also tries to distribute the load to itself in the relevant domain. The formula at this time is the same as formula (7), so that the value of Lavg can be calculated.

In order to achieve uniform distribution, the load can be obtained as N_m by transmitting the overloaded load node to other nodes in the relevant domain. The N_m formula listed here is the same as formula (8), except that the condition here is $L_{avg} < L_m$.

Figure 6 is the architecture diagram of the agent-based RFID middleware. In this figure, the JADE platform is based on JAVA. In the past few years, mobile agent system technology has become an exciting new field of computer science. There are a large number of methods, toolkits, and platforms of different qualities and maturities in this field, including Grasshopper, IBM Aglet, and JADE (Java Agent Development Framework).

Each instance running in the JADE runtime environment is called a container, and this container contains multiple agents. A group of running containers is called a platform. Figure 7 shows the architecture of the JADE platform.

Partial view: once the system starts, this special main container must always be executed on a platform, and through this special container, other containers can be registered. In addition to being able to accept registrations from other containers, the main container is different from other containers in that the main container is loaded with two special agents. AMS (Agent Management System) that can provide naming services (e.g., make sure that each agent on the platform has a unique name) is a representative authoritative platform. DF (Directory Facilitator is a directory service provider) provides a yellow pages service in a specific way. In this way, an agent finds other agents that can meet the needs of the agent in order to obtain the target.

Because the mobile agent's RFID middleware load architecture is built on the agent's RFID middleware architecture, but the mobile agent has a few more functional components that are not available in the agent, and the others are developed based on the agent architecture. Moreover, mobile agents and agents are built on the RLBA architecture, and both can and must run on JADE to some extent. Figure 8 is the architecture class diagram shared by mobile agents and agents.

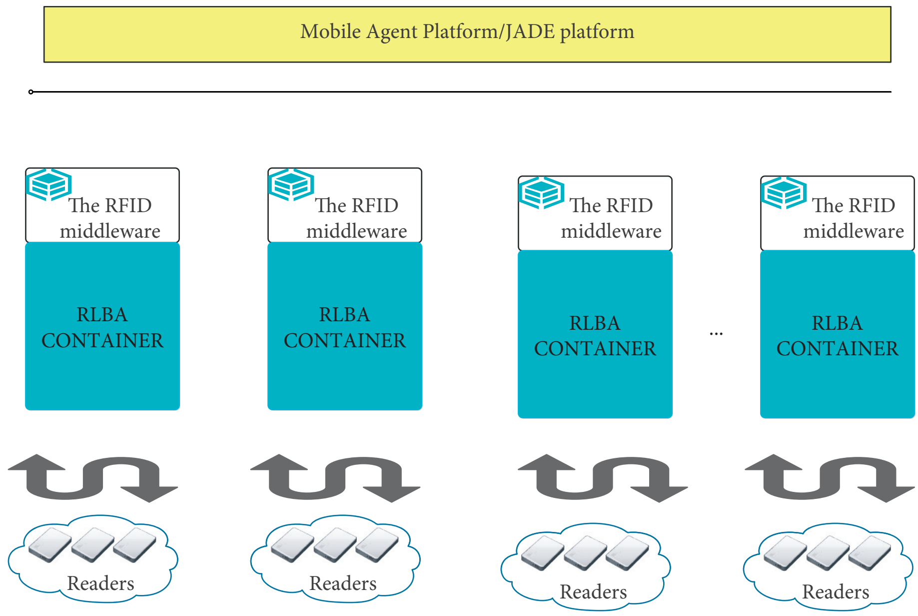

Figure 6: Architecture diagram of agent-based RFID middleware.

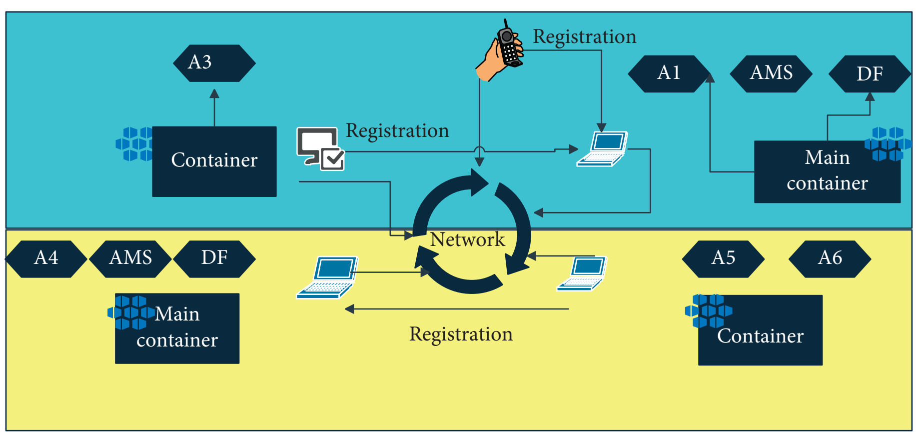

Figure 7: Architecture diagram of JADE platform.

Figure 8 is a class diagram of RLBA, which explains how RLBA and its components perform RFID middleware load balancing. JADE platform provides RLBA extended agent class. The agent class is used to initialize the runtime environment of the agent. GLT and RLT can be used to support RFID middleware load balancing decisions. RLBA is also composed of five components: load monitor, balance trigger, middleware selector, reader/writer distributor, and reader/writer selector. Another important class is NodeCriteria, which provides the definition of the equilibrium metric name, maximum threshold, minimum threshold, and initial type.

4. Intelligent Terminal Container Management System Based on Internet of Things and Big Data Technology

Business research and demand analysis cannot be successful once we need to continue to refine and research. This requires an excellent program developer to have a comprehensive understanding of the overall process of the investigated business and continue to refine it from the shallower to the deeper. We not only need to understand the relationship between terminal companies and various port logistics links but also need to understand the independent work responsibilities of each business department, each job position, and the relationship between each position. Figure 9 shows the business relationship between container terminals and various port logistics links.

Import unloading business refers to the process of unloading containers loaded on arriving ships from the ship to the dock site within a predetermined plan. The specific unloading process mainly involves several aspects shown in Figure 10.

After constructing a terminal container handling intelligent management system based on the Internet of Things and big data technology through the above analysis, the performance of the system is verified. This paper uses

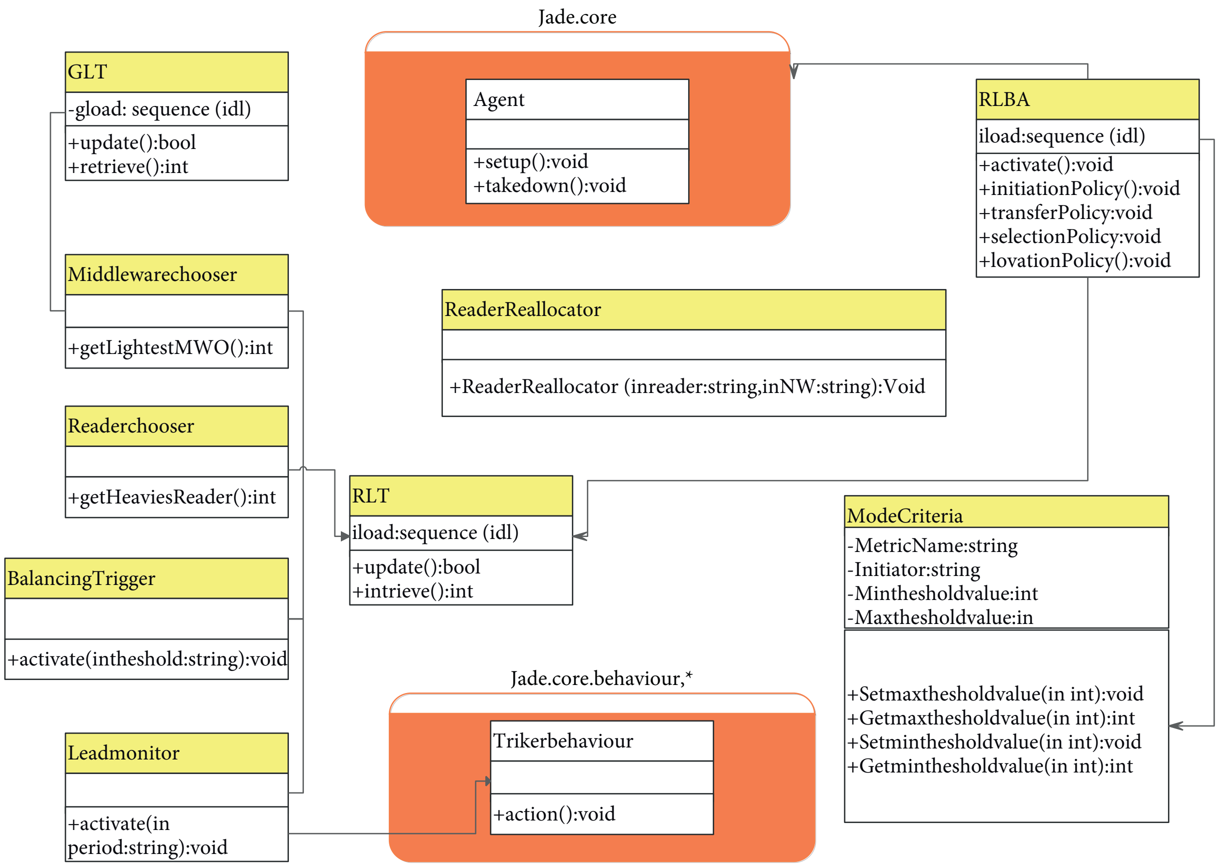

Figure 8: RLBA class diagram.

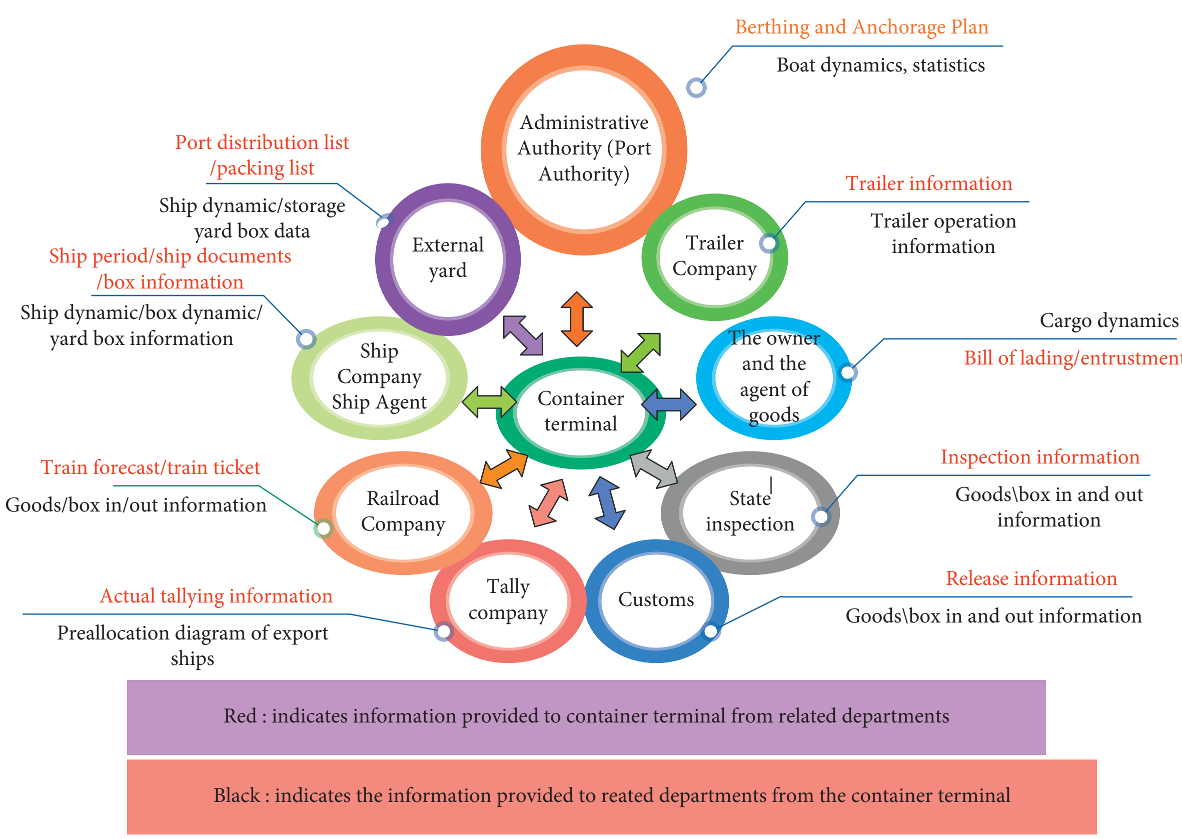

Figure 9: Business relationship between container terminals and various port logistics links.

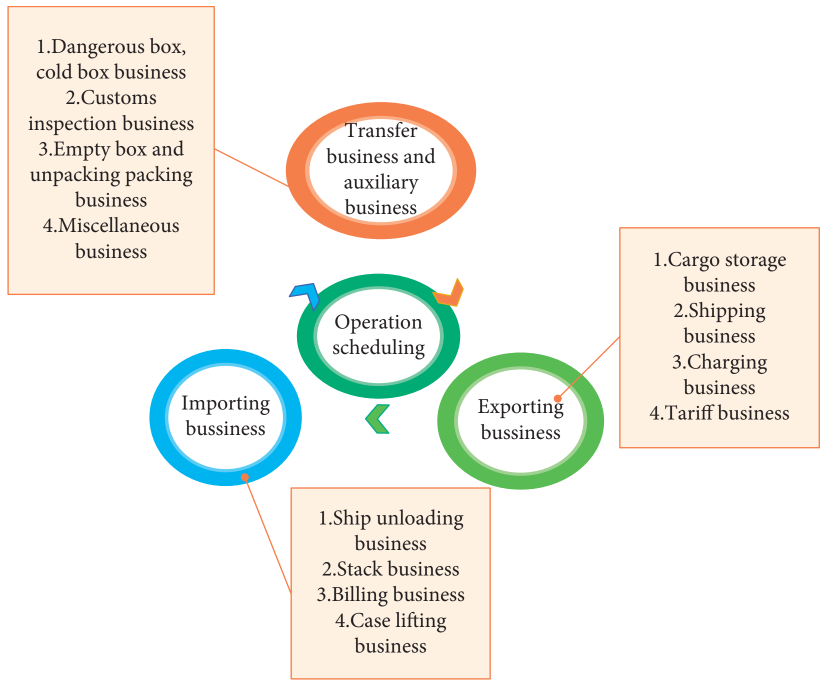

Figure 10: Division of container terminal business.

Table 1: Simulation effect verification of terminal container handling intelligent management system.

Number	Scheduling effect	Loading effect	Management effect
1	79.32	94.37	86.07
2	88.09	90.55	94.23
3	83.52	88.57	89.96
4	89.94	86.76	91.42
5	93.21	87.85	94.97
6	81.70	86.92	96.65
7	93.50	80.08	92.69
8	83.65	83.17	94.01
9	87.49	95.19	90.63
10	83.00	93.90	96.18
11	83.13	87.30	90.08
12	91.18	91.31	95.86
13	86.39	87.87	88.26
14	82.31	89.56	90.98
15	83.73	86.49	95.34
16	83.24	85.93	92.15
17	80.28	95.35	86.47
18	87.41	92.69	94.28
19	80.02	88.56	95.42
20	90.17	88.25	91.05
21	90.76	81.25	94.12
22	80.30	95.53	82.55
23	88.12	86.00	90.58
24	83.59	90.44	88.70
25	92.49	86.31	85.30
26	93.77	95.39	84.77
27	86.69	93.42	86.19
28	83.70	91.09	95.39
29	93.03	88.53	90.34
30	79.59	88.58	84.93
31	80.90	88.54	85.70
32	82.12	88.24	89.50
33	79.14	81.69	91.93

Table 1: Continued.

Number	Scheduling effect	Loading effect	Management effect
34	89.06	86.00	95.81
35	91.95	90.77	93.56
36	79.98	89.92	86.09
37	88.85	84.69	90.04
38	92.35	91.76	86.75

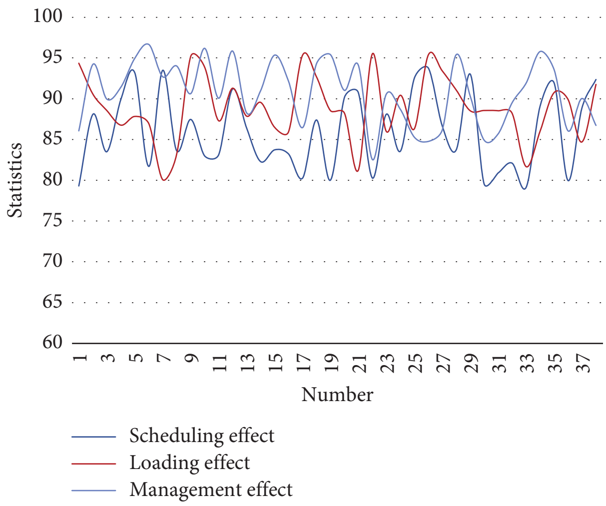

Figure 11: The performance verification results of the terminal container handling management system based on the Internet of Things and big data.

multiple sets of simulation data to count the container dispatching effect, loading effect, and management effect, and the test results shown in Table 1 and Figure 11 are obtained.

From the above research, it can be seen that the terminal container handling management system based on the Internet of Things and big data constructed in this paper basically meets the expected needs, and the system can be used for auxiliary management in subsequent practice.

5. Conclusion

Terminal container handling is a key part of the daily production activities of the port. The overall economic benefits of a container port are closely related to the loading quality of container ships in the port. The loading quality of ships directly affects the ship's port time, maritime navigation safety, and the efficiency of terminal loading and unloading operations, which in turn affects the port's reputation status and operating costs. The current large-scale development of container ships makes the loading and unloading tasks of ships in ports more arduous and the loading process more complicated. How to use the opportunity of the booming development of automated container terminals to integrate informatization, intelligent technology, and advanced management methods to rationally carry out container loading and dispatch, improve terminal service levels and ship transportation efficiency, and improve the competitiveness of the port itself and the transportation efficiency of the shipping industry is an urgent problem to be solved. This paper analyzes the loading and unloading process of containers in the terminal by combining the Internet of Things technology and big data technology and constructs the corresponding intelligent system. The experimental research results show that the terminal container handling management system based on the Internet of Things and big data constructed in this paper basically meets the expected needs, and the system can be used for auxiliary management in subsequent practice.

Data Availability

The labeled dataset used to support the findings of this study is available from the corresponding author upon request.

Conflicts of Interest

The authors declare no conflicts of interest.

Acknowledgments

This study was sponsored by the Wuhan University of Technology.

References

[1] L. Özdamar and M. A. Ertem, "Models, solutions and enabling technologies in humanitarian logistics," *European Journal of Operational Research*, vol. 244, no. 1, pp. 55–65, 2015.

[2] M. Savelsbergh and T. Van Woensel, "50th anniversary invited article-city logistics: challenges and opportunities," *Transportation Science*, vol. 50, no. 2, pp. 579–590, 2016.

[3] S. Tofighi, S. A. Torabi, and S. A. Mansouri, "Humanitarian logistics network design under mixed uncertainty," *European Journal of Operational Research*, vol. 250, no. 1, pp. 239–250, 2016.

[4] D. Cattaruzza, N. Absi, D. Feillet, and J. González-Feliu, "Vehicle routing problems for city logistics," *EURO Journal on Transportation and Logistics*, vol. 6, no. 1, pp. 51–79, 2017.

[5] J. Grabara, M. Kolcun, and S. Kot, "The role of information systems in transport logistics," *International Journal of Educational Research*, vol. 2, no. 2, pp. 1–8, 2014.

[6] E. Taniguchi, R. G. Thompson, and T. Yamada, "Recent trends and innovations in modelling city logistics," *Procedia - Social and Behavioral Sciences*, vol. 125, no. 2014, pp. 4–14, 2014.

[7] J. G. Carlsson and S. Song, "Coordinated logistics with a truck and a drone," *Management Science*, vol. 64, no. 9, pp. 4052–4069, 2018.

[8] R. Puertas, L. Martí, and L. García, "Logistics performance and export competitiveness: European experience," *Empirica*, vol. 41, no. 3, pp. 467–480, 2014.

[9] T. Qu, S. P. Lei, Z. Z. Wang, D. X. Nie, X. Chen, and G. Q. Huang, "IoT-based real-time production logistics synchronization system under smart cloud manufacturing," *International Journal of Advanced Manufacturing Technology*, vol. 84, no. 1-4, pp. 147–164, 2016.

[10] C. Chua, M. Danyluk, D. Cowen, and L. Khalili, "Introduction: turbulent circulation: building a critical engagement with logistics," *Environment and Planning D: Society and Space*, vol. 36, no. 4, pp. 617–629, 2018.

[11] R. Y. Zhong, S. Lan, C. Xu, Q. Dai, and G. Q. Huang, "Visualization of RFID-enabled shopfloor logistics big data in cloud manufacturing," *International Journal of Advanced Manufacturing Technology*, vol. 84, no. 1-4, pp. 5–16, 2016.

[12] Y. Zhang, Z. Guo, J. Lv, and Y. Liu, "A Framework for smart production-logistics systems based on CPS and industrial IoT," *IEEE Transactions on Industrial Informatics*, vol. 14, no. 9, pp. 4019–4032, 2018.

[13] L. Martí, R. Puertas, and L. García, "The importance of the Logistics Performance Index in international trade," *Applied Economics*, vol. 46, no. 24, pp. 2982–2992, 2014.

[14] D. Alem, A. Clark, and A. Moreno, "Stochastic network models for logistics planning in disaster relief," *European Journal of Operational Research*, vol. 255, no. 1, pp. 187–206, 2016.

[15] N. Boysen, S. Emde, M. Hoeck, and M. Kauderer, "Part logistics in the automotive industry: decision problems, literature review and research agenda," *European Journal of Operational Research*, vol. 242, no. 1, pp. 107–120, 2015.

[16] M. Coe, "Missing links: logistics, governance and upgrading in a shifting global economy," *Review of International Political Economy*, vol. 21, no. 1, pp. 224–256, 2014.

[17] S. A. R. Khan, D. Qianli, W. SongBo, K. Zaman, and Y. Zhang, "Environmental logistics performance indicators affecting per capita income and sectoral growth: evidence from a panel of selected global ranked logistics countries," *Environmental Science and Pollution Research*, vol. 24, no. 2, pp. 1518–1531, 2017.

[18] V. Sundquist, L.-E. Gadde, and K. Hulthén, "Reorganizing construction logistics for improved performance," *Construction Management and Economics*, vol. 36, no. 1, pp. 49–65, 2018.

[19] F.-S. Chang, J.-S. Wu, C.-N. Lee, and H.-C. Shen, "Greedy-search-based multi-objective genetic algorithm for emergency logistics scheduling," *Expert Systems with Applications*, vol. 41, no. 6, pp. 2947–2956, 2014.

[20] H. Soleimani and K. Govindan, "Reverse logistics network design and planning utilizing conditional value at risk," *European Journal of Operational Research*, vol. 237, no. 2, pp. 487–497, 2014.

[21] X. Bing, J. M. Bloemhof-Ruwaard, and J. G. A. J. van der Vorst, "Sustainable reverse logistics network design for household plastic waste," *Flexible Services and Manufacturing Journal*, vol. 26, no. 1-2, pp. 119–142, 2014.

Hindawi
Scientific Programming
Volume 2021, Article ID 4834944, 10 pages
https://doi.org/10.1155/2021/4834944

Research Article

Recognition Algorithm of Popular Elements of Ethnic Minority Traditional Clothing Based on PCA

Hu Juan

West Anhui University, Lu'an 237012, China

Correspondence should be addressed to Hu Juan; 631418020431@mails.cqjtu.edu.cn

Received 6 September 2021; Revised 22 October 2021; Accepted 27 October 2021; Published 8 November 2021

Academic Editor: Le Sun

Image recognition of ethnic minority costumes is helpful for people to understand, carry forward, and inherit national culture. Taking the minority clothing image as the research object, the image enhancement and threshold segmentation are completed; the principal component features of the minority clothing image are extracted by PCA method; and the image matching degree is obtained according to the principle of minimizing the Euclidean distance. Finally, the calculation process of the PCA method is optimized by a wavelet transform algorithm to realize the recognition of popular elements of minority traditional clothing. The comparative experimental results show that the PCA + BP neural network algorithm is better than the other two recognition algorithms in recognition rate and recognition time.

1. Introduction

The fast-paced modern life makes the traditional ethnic minority clothing face the crisis of disappearance. The digital protection and inheritance of ethnic minority clothing culture are urgent. With the development of science and technology, some advanced technical means have been used to protect and inherit the clothing culture of ethnic minorities [1]. As one of the constituent elements of clothing, ethnic minority clothing color is a symbol of inheriting national culture. Using increasingly mature image processing technology to process the clothing image of Huayao Dai has great significance and value for the study of ethnic minority clothing color [2].

Literature [3] in order to use the set information in the image set to improve the image recognition accuracy and robustness to image changes so as to greatly reduce the influence of factors such as posture, illumination, occlusion, and misalignment on the recognition accuracy, an image set prototype and projection learning algorithm (lpsop) for image set classification is proposed. The algorithm learns representative points (prototypes) and an orthogonal global projection matrix for each image set so that each image set in the target sub-space can be optimally classified into the nearest prototype set of the same kind. It not only can reduce the interference of redundant images but also can reduce the storage and computing overhead. The learned projection matrix can greatly improve classification accuracy and noise robustness. The experimental results on UCSD/Honda, CMU MoBo, and YouTube cellulitis show that Lpsop has higher recognition accuracy and better robustness than the current popular image set classification algorithm. However, this method considers the characteristics of many elements of ethnic minority traditional clothing, resulting in the decline of recognition accuracy.

In reference [4], aiming at the problems of low matching accuracy, long operation time, and low recognition accuracy in the traditional remote sensing image template matching and recognition process, a remote sensing image template matching intelligent recognition method based on STACS is proposed. Through the analysis of the remote sensing image measured by the man-made satellite survey system (STACS), the gradient is used as the feature to match the remote sensing image template. Combined with dot algorithm, the secondary gradient features of remote sensing image are removed, and only the gradient direction with large amplitude is used as the feature quantity to complete template matching; The neighborhood pixel difference method is used to recognize the target features of remote sensing images. The experimental results show that the proposed method has a high accuracy of remote sensing image template matching, short operation time, and high recognition accuracy and has certain practical value. However, this method has not been applied to the recognition of popular elements of ethnic minority traditional clothing, and the recognition time and recognition accuracy need to be further considered. According to clothing design theory, clothing schools can be identified by a set of visually distinguishable style elements, which show obvious visual appearance characteristics and reflect high-level fashion style, thus better describing clothing schools. Reference [5] proposed an automatic classification method of clothing types based on visually distinguishable style elements, replacing the previous low-discernibility features or fuzzy keywords to identify clothing types. Hierarchical image segmentation identifies and organizes image elements as tree structures. Tree structure represents the semantic information of the image. This is one of the most basic computer vision problems. The emphasis of reference [6] is on images from visual design, such as graphical interfaces, posters, and presentations. Extracting hierarchies from these images allows quantitative analysis of visual design choices and replication of designs from hand-drawn or hard copy. Reference [6] puts forward a more accurate method, which integrates the general design principles of visual design.

Principal component analysis (PCA) is a widely used algorithm in intelligent recognition. Its principle is to extract the main components of ethnic minority traditional clothing by using K-L transform, construct the feature popular element space, project the test image to this space, obtain a set of projection coefficients, and identify it by comparing with each popular element. PCA method has achieved a good recognition effect, but the amount of calculation is large [7]. Wavelet transform denoises and extracts features from the image by constructing a wavelet basis, which not only effectively avoids the interference of noise and redundant data [8] but also accurately locates the boundary points, which is helpful to improve the eigenvalues of popular elements in ethnic minority clothing. After a series of image preprocessing, the PCA features of clothing images are obtained by PCA, and the image recognition is carried out according to the principle of minimum European distance.

The research contributions of the thesis include the following:

(1) In this paper, minority clothing image is taken as the research object, image enhancement, and threshold segmentation are completed; the principal component analysis method is adopted to extract the principal component features of minority clothing image; and image matching degree is obtained according to Euclidean distance minimum principle

(2) The calculation process of the PCA method is optimized by the wavelet transform algorithm to realize the recognition of popular elements of minority traditional clothing

(3) The comparative experimental results show that the PCA + BP neural network algorithm is better than the other two recognition algorithms in recognition rate and recognition time

The remainder of this paper is organized as follows. Section 2 introduces the overall structure design of the algorithm. Section 3 discusses image preprocessing. Section 4 discusses feature extraction and image recognition. Section 5 discusses the experiment and analysis. Section 6 presents the conclusions of the study.

2. Overall Structure Design of the Algorithm

The whole algorithm is mainly composed of two modules: image preprocessing, feature extraction, and image recognition. The overall structure of the algorithm is shown in Figure 1.

The image preprocessing part consists of three parts: image graying, image enhancement, and threshold segmentation. The weighted average method is used to convert the color image into the gray image, and the histogram is used to expand the dynamic range of image gray value so as to enhance the overall contrast of the image and make the details of the image clearer. After the threshold is determined by an iterative method, the image is segmented to segment the target and background in the picture.

The feature extraction and image recognition module is composed of three parts: extracting PCA features, establishing a classifier, and image recognition. It mainly extracts the PCA features of the target obtained by threshold segmentation by PCA, establishes a classifier by using Euclidean distance, inputs the PCA features into the classifier as an input, recognizes the image, and outputs the recognition results.

3. Image Preprocessing

Since the image is easily affected by the image itself and external factors, it is necessary to carry out image preprocessing [9], optimize the image, reduce the amount of calculation, retain useful information, and minimize useless information. Preprocessing mainly includes image enhancement and threshold segmentation. In this paper, the weighted average method is used to convert the color image into a grayscale image, as shown in Figure 2.

The image enhancement part completes histogram equalization and histogram normalization, as shown in Figures 3 and 4.

Image segmentation is helpful for image recognition, and the quality of image segmentation directly affects the effect of subsequent image processing [10]. The basic idea of threshold segmentation is that the foreground region in the image, that is, the extracted target and background region belong to two different gray sets. The two gray sets can be segmented by using a threshold T belonging to the gray level so that the image can be segmented into foreground region and background region.

Based on the idea of approximation [11], the iterative method first selects an approximate threshold T, divides the

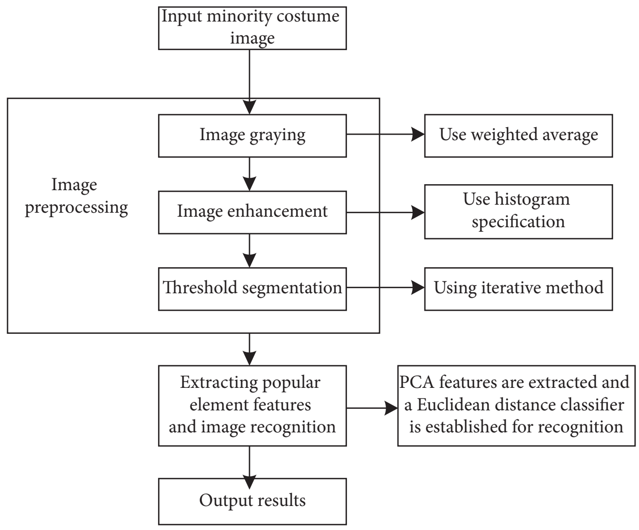

Figure 1: The overall structure diagram of the algorithm.

Figure 2: Color images are converted to grayscale images.

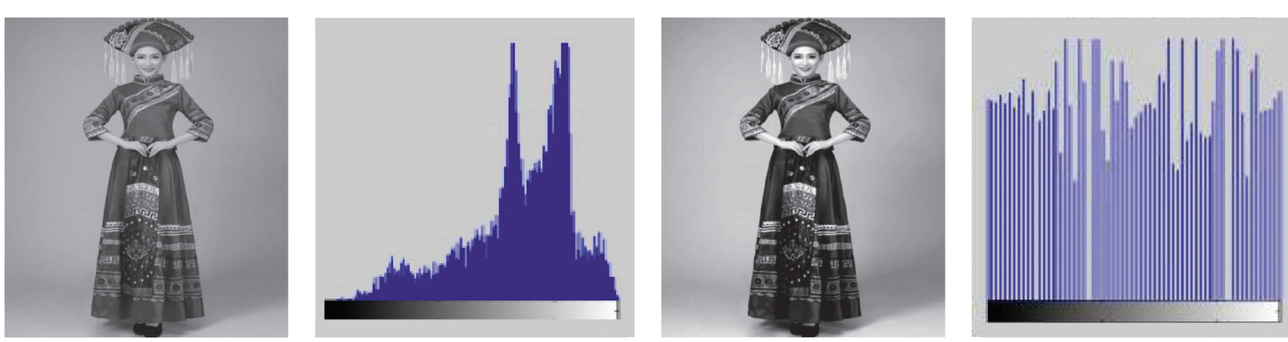

Original image (a) | Histogram of original image (b) | Image after square equalization (c) | Histogram after equalization (d)

Figure 3: Equalization of the histogram: (a) original image, (b) histogram of the original image, (c) image after square equalization, and (d) histogram after equalization.

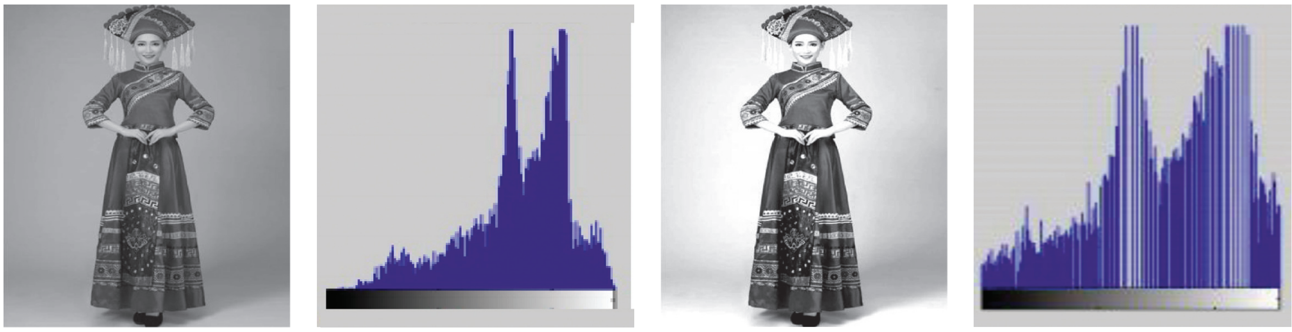

Original image (a) | Histogram of original image (b) | Histogram specified image (c) | Specified histogram (d)

Figure 4: Specifications of the histogram: (a) original image, (b) histogram of the original image, (c) histogram specified image, and (d) specified histogram.

image into two parts $R1$ and $R2$, and calculates the mean value of regions $R1$ and $R2$ μ 1 and μ 2,

Select a new segmentation threshold $t = (\mu\ 1 + \mu\ 2)/2$, repeat the above steps until μ 1 and μ 2 until there is no change. The segmentation results in this paper are shown in Figure 5.

4. Feature Extraction and Image Recognition

Feature extraction is a key part of image recognition. The purpose of feature extraction is to retain image information as much as possible in order to achieve effective recognition. Whether the feature extraction is good or bad is directly related to the result of image recognition. In this paper, PCA (principal components analysis) based on principal component analysis is used to realize the recognition of ethnic minority clothing images.

4.1. Theoretical Basis of PCA. Principal components analysis (PCA) is widely used in pattern recognition and data compression [12]. Its main advantage is to reduce the dimension and remove the redundancy of the data. Its method is to decompose the characteristics of the covariance matrix of the sample and calculate the characteristic vectors and eigenvalues of the covariance matrix. The feature vectors corresponding to several larger eigenvalues are found as the principal components of the analyzed data, that is, PCA features represent the original data so as to achieve the purpose of dimensionality reduction and redundancy.

PCA method uses the linear combination of principal component vectors to minimize the mean square error. Mathematically, it can be verified that the PCA method can use eigenvalues to realize projection vector [13].

Let $\{x_i | i = 1, \ldots, N\}$ be a set of n-dimensional vectors, expressed as matrix form $X = [x_1, x_2, \ldots, x_N]$, and average all columns of X to obtain

$$\bar{x} = \frac{1}{N}\sum_{i=1}^{N} x_i, \tag{1}$$

Figure 5: Images before and after the iterative segmentation.

where N is the total number of samples and $\bar{x}$ is the average value of all samples.

Let $\bar{X} = [\bar{x_1}, \bar{x_2}, \ldots, \bar{x_N}]$, then the covariance matrix S_t corresponding to data X can be defined by the following formula:

$$S_t = \frac{1}{N}(X - \bar{X})(X - \bar{X})^T = \frac{1}{N}\sum_{i=1}^{N}(x_i - \bar{x})(x_i - \bar{x})^T. \tag{2}$$

Suppose: m is the rank of matrix S_t and $\{\lambda_i | i = 1, 2, \ldots, m\}$ is the nonzero eigenvalue of matrix S_t; $\{w_i | i = 1, 2, \ldots, m\}$ represents the corresponding eigenvector of matrix S_t; and $\lambda_1 \geq \lambda_2 \geq \cdots \geq \lambda_m$, the formula is as follows:

$$S_t w_i = \lambda_i w_i, \quad i = 1, 2, \ldots, m. \tag{3}$$

In principal component analysis, set $W = [w_1, w_2, \ldots w_m]$, where W represents the principal component matrix and w_i represents the principal component contained in the data.

Convert any n-dimensional random vector x to obtain the following formula:

$$y = W^T(x - \bar{x}). \tag{4}$$

The new m-dimensional vector y is obtained from formula (4).

According to the mathematical demonstration theory, the transformation of the two is mainly projection, and vector y is the projection coefficient, which is the result of the transformation of vector x under the PCA algorithm. Reconstruct y to obtain data:

$$\hat{x} = W_y + \bar{x}. \tag{5}$$

In popular element recognition, PCA-based methods can be divided into adaptive PCA-based methods and empirical PCA-based methods.

4.2. Typical Algorithms. In the PCA algorithm, the main two key items are eigenvector and eigenvalue of the covariance matrix.

According to the above analysis, the dimension of covariance matrix S_t is $n \times n$. There are many dimensions and the amount of direct calculation data is very large. Therefore, a method to solve this problem is proposed.

Set a new matrix S_t', then:

$$S_t' = (X - \bar{X})^T (X - \bar{X}). \tag{6}$$

It is easy to find that the dimension of matrix S_t' is $N \times N$. With the help of the theory of linear algebra, it can be proved that matrices S_t and S_t' have the same eigenvalues, so the eigenvalues corresponding to S_t can be obtained by calculating the eigenvalues of S_t', but it is much easier to calculate the eigenvalues of S_t' because of $N \ll n$.

Assuming that W represents the eigenvector of matrix S_t and Q represents the eigenvector of matrix S_t', it can be further proved that W and Q satisfy the following relationship:

$$W = XQ\Lambda^{-1/2}, \tag{7}$$

where Λ is a diagonal matrix, $\Lambda = \mathrm{diag}[\lambda_1, \lambda_2, \ldots, \lambda_N] \in \mathrm{P}^{N\times N}$, and $\lambda_1 \geq \lambda_2 \geq \cdots \geq \lambda_N$.

From the above results, the eigenvalues and eigenvectors of matrix S_t can be obtained through matrix S_t'. However, the dimension of S_t' is much smaller than that of S_t, so this method can reduce the amount of calculation and improve the overall operation speed.

The traditional PCA algorithm includes the following steps [14]:

Converting a set of data $\{x_i | i = 1, 2, \ldots, N\}$ into matrix $X = [x_1, x_2, \ldots, x_N]$

Calculate the average value $\bar{x}$ of the group of data and construct the matrix $\bar{X} = [\bar{x_1}, \bar{x_2}, \ldots, \bar{x_N}]$

Calculate the covariance matrix S_t corresponding to X

Calculate the eigenvalue of the covariance matrix

S_t and eigenvector matrix W, where the eigenvalue corresponds to the eigenvector one by one, and the eigenvalues are arranged in order from large to small

The fast PCA algorithm is as follows:

Calculate matrix $S_t' = (X - \bar{X})^T (X - \bar{X})$

Calculate the eigenvalue of matrix S_t' and eigenvector military Array Q, where the eigenvalue corresponds to the eigenvector one by one, and the features are arranged in the order of large to small

Construct diagonal matrices Λ, $\Lambda = \mathrm{diag}[\lambda_1, \lambda_2, \ldots, \lambda_N] \in \mathrm{P}^{N\times N}$, and $\lambda_1 \geq \lambda_2 \geq \ldots \geq \lambda_N$

According to formula (7), the eigenvector matrix W is calculated using X, Λ and Q

4.3. Improved PCA Algorithm Based on Wavelet Transform. The identification of popular elements can help the algorithm achieve a better recognition effect. Therefore, feature extraction can better improve the recognition degree of popular element recognition algorithm. In this paper, an improved principal component analysis algorithm based on wavelet transform is proposed.

4.3.1. Algorithm Analysis. In this paper, a principal component analysis algorithm based on wavelet transform is proposed. Its basic idea is:

Firstly, the image is decomposed into four sub-graphs by wavelet transform. Then the total scatter matrix is calculated according to the within class mean of the sub-graph, and the optimal projection matrix is obtained. The samples are projected so that each original image corresponds to four feature matrices.

The nearest distance method is used to classify the images, and four recognition results are obtained [15]. According to the importance of low-frequency components and high-frequency components, appropriate weighting and sorting are carried out to obtain the final results.

4.3.2. Algorithm Flow. The flow chart of this algorithm is shown in Figure 6.

Based on the above analysis, the image recognition method based on PCA first converts the sample image into a feature vector set, which is the set of basic components of the sample image, and projects it into the feature expression space, that is, PCA sub-space. Then, the PCA feature extracted from the image to be recognized is projected into the feature expression space. By calculating the Euclidean distance between its projection point and the PCA feature of the sample image in the feature expression space [16], the recognition is carried out according to the principle of minimizing the Euclidean distance. The algorithm is described as follows:

(1) Obtain the clothing image set t optimized by preprocessing in the image library. Suppose there are n national costume images in the image library, and n sample images are obtained after image preprocessing. Each sample consists of its pixel gray value to form a vector X_i; then the pixel number of the sample image is the dimension $M = \text{width} * \text{height}$ of X_i; and the vector constitutes

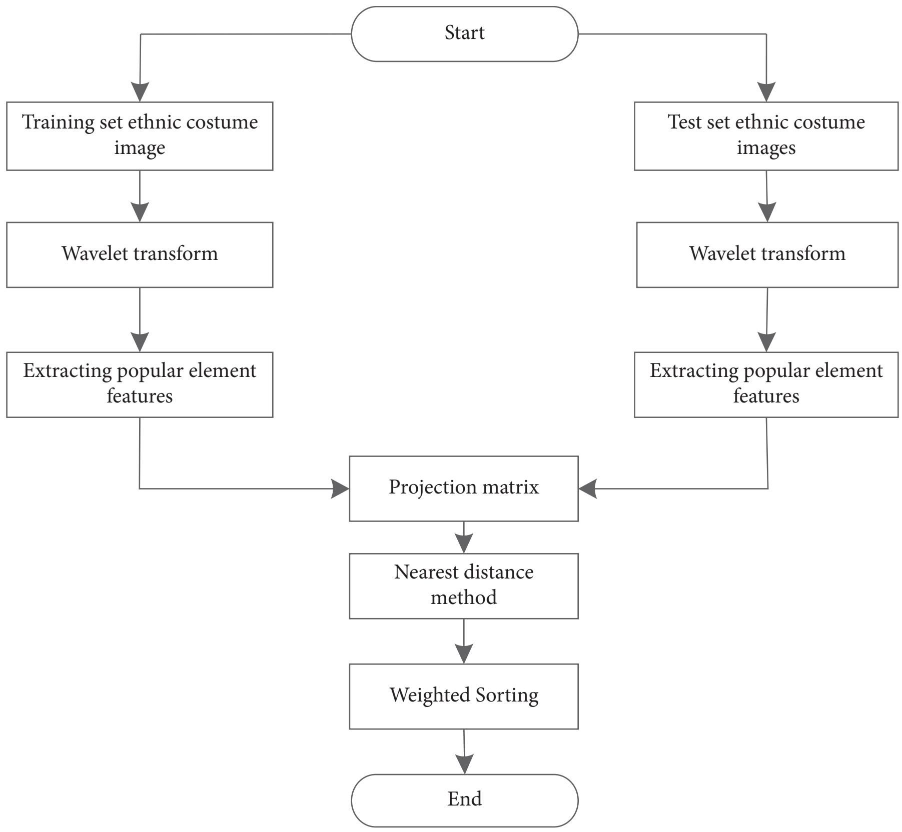

Figure 6: Principal component analysis algorithm based on wavelet transform.

the n-dimensional sample vector set $t = \{x_1, x_2, \ldots, x_n\}$, with the size of $n \times m$.

(2) Calculate the average vector U of the sample vector set t to obtain the mean image.

(3) Calculate the difference x between each image and the mean image, that is, subtract u from (2) from each element in the t set to centralize the sample image.

(4) Calculate the covariance matrix s.

(5) The eigenvector VI and eigenvalue of covariance matrix s are obtained λi.

(6) Arrange the eigenvalues and their corresponding eigenvectors in descending order.

(7) The cumulative contribution rate is calculated, and then according to the cumulative contribution rate, K eigenvectors corresponding to eigenvalues are selected from the eigenvectors to form the principal component.

(8) For clothing recognition, the PCA features of all samples are projected into the PCA sub-space. After optimizing the image to be recognized, the PCA features are extracted and projected into the PCA sub-space. The nearest distance between the vector after PCA feature projection of a sample and the vector after image projection to be recognized is found, that is, the popular element of clothing image to be recognized.

4.3.3. Algorithm Implementation. The algorithm proposed in this paper is divided into the training stage and the recognition stage.

(1) Training Phase. C represents the category of popular elements and sets the category to $\omega_1, \omega_2, \ldots, \omega_c$. Set $n(i)$ as the number of training samples of the i-th human company, $N = \sum_{i=1}^{C} n(i)$ as the image overview of the training samples, and each popular element image sample A_{ij} as the $m \times n$ image matrix. The sample A_{ij} is decomposed by a first-order wavelet to obtain a 2×2 module image matrix:

$$A_{ij} = \begin{bmatrix} (A_{ij})_{11} & (A_{ij})_{12} \\ (A_{ij})_{21} & (A_{ij})_{22} \end{bmatrix}. \tag{8}$$

(2) Finding the Global Dispersion Matrix. Each class of training samples is calculated to obtain the average popular elements of each image in each class:

$$(\eta_{kl})_i = \left(\frac{1}{n(i)} \sum_{j=1}^{n(i)} (A_{ij})_{kl} \right)_i, \tag{9}$$

where $i = 1, 2, \ldots, C$; $j = 1, 2, \ldots, n(i)$; $k = 1, 2$; and $l = 1, 2$.

$n(i)$ is the number of training samples of class i; $M = 4 \sum_{i=1}^{C} n(i) = 4N$ is the total number of sub-block matrices obtained from training samples. Then the overall dispersion matrix is

$$G_t = \frac{1}{M}\sum_{i=1}^{C}\sum_{j=1}^{n(i)}\sum_{k=1}^{2}\sum_{l=1}^{2}\left(\left(A_{ij}\right)_{kl} - (\eta_{kl})_i\right)^T\left(\left(A_{ij}\right)_{kl} - (\eta_{kl})_i\right). \tag{10}$$

Through demonstration, it can be proved that G_t is a nonnegative definite matrix. Then calculate the matrix after projection processing. The method is as follows: first, set the first r of G_t as the maximum eigenvalue so as to obtain the eigenvector corresponding to this eigenvalue, specifically expressed as $X_1, X_2, \ldots, X_r$. Let P be the optimal projection matrix, $P = [Z_1, Z_2, \ldots, Z_r]$.

(3) Feature Extraction of Training Samples. First, calculate the average popular elements of all training sample book sub-images, which are expressed as follows:

$$\eta = \frac{1}{M}\sum_{i=1}^{C}\sum_{j=1}^{n(i)}\sum_{k=1}^{2}\sum_{l=1}^{2}\left(A_{ij}\right)_{kl}, \tag{11}$$

where $i = 1, 2, \ldots, C$; $j = 1, 2, \ldots, n(i)$; $k = 1, 2$; and $l = 1, 2$.

Then, the projection matrix is used to extract the corresponding features.

Setting: A_{ij} represents the training sample set recognized by wavelet transform, and the following results are obtained:

$$A_{ij} = \begin{bmatrix} \left(A_{ij}\right)_{11} & \left(A_{ij}\right)_{12} \\ \left(A_{ij}\right)_{21} & \left(A_{ij}\right)_{22} \end{bmatrix}. \tag{12}$$

The characteristic matrix of is as follows:

$$B_{ij} = \begin{bmatrix} \left(\left(A_{ij}\right)_{11} - \eta\right)P & \left(\left(A_{ij}\right)_{12} - \eta\right)P \\ \left(\left(A_{ij}\right)_{21} - \eta\right)P & \left(\left(A_{ij}\right)_{22} - \eta\right)P \end{bmatrix}. \tag{13}$$

(4) Identification Phase. For test sample T, first decompose the first level wavelet and then obtain four sub-graphs:

$$T = \begin{bmatrix} T_{11} & T_{12} \\ T_{21} & T_{22} \end{bmatrix}. \tag{14}$$

Then the characteristic matrix is obtained as follows:

$$B_t = \begin{bmatrix} (T_{11} - \eta)P & (T_{12} - \eta)P \\ (T_{21} - \eta)P & (T_{22} - \eta)P \end{bmatrix}. \tag{15}$$

The characteristic matrices $(T_{11} - \eta)P$, $(T_{12} - \eta)P$, $(T_{21} - \eta)P$, and $(T_{22} - \eta)P$ of each sub-graph are obtained.

The nearest distance method is used to judge the category of the four sub-blocks of the test sample:

Calculate the Euclidean distance between $((A_{ij})11 - \eta)P$ and $(T_{11} - \eta)P$:

$$\begin{aligned} d\left(\left(\left(A_{ij}\right)_{11} - \eta\right)P, (T_{11} - \eta)P\right) &= \left\|\left(\left(A_{ij}\right)_{11} - \eta\right)P - (T_{11} - \eta)P\right\|_F \\ &= \left[tr\left(\left(\left(A_{ij}\right)_{11} - \eta\right)P - (T_{11} - \eta)P\right)^T\left(\left(\left(A_{ij}\right)_{11} - \eta\right)P - (T_{11} - \eta)P\right)\right], \end{aligned} \tag{16}$$

where superscript represents four sub-graphs, respectively.

If $d(((A_{ij})_{11} - \eta)P, (T_{11} - \eta)P) = \min_i(((A_{ij})_{11} - \eta)P, (T_{11} - \eta)P)$, the sample T to be tested belongs to class l.

In the same way, find out the classes of the other three sub-graphs, assuming that the classes of the other three sub-graphs are ω_m, ω_n, and ω_o, respectively.

(5) Weighted Sorting. Each sub-graph will get a recognition effect based on wavelet transform, and the highest recognition rate is the low-frequency sub-graph [17], followed by the vertical and horizontal sub-graphs. It can be inferred that the diagonal sub-graph has a low recognition rate.

After getting all the processed pictures, we can get the corresponding processed pictures by arranging and weighting them accordingly. This picture has both high-frequency effective recognition and low-frequency stability. It has obvious advantages, which can effectively enable us to improve the overall recognition rate of recognition in flow element recognition.

5. Experimental Results and Analysis

5.1. Experimental Environment and Popular Element Library. Experimental environment

PC operating system: Windows10

Hardware: Intel (R) Core (TM) i3-2350M CPU, 4 GB memory, 500 GB hard disk

Algorithm simulation software: MATLAB

Experimental picture selection

First, 20 clothing pictures of the 5 famous ethnic groups of Bai, Buyi, Hani, WA, and Miao are selected, and the popular elements are identified by identifying the optimized ethnic minority clothing images by using the proposed PCA-based ethnic minority traditional clothing popular element recognition algorithm. This experiment is programmed with MATLAB. During the test, each nation selects 20 clothing images for comparison. The experimental results of the algorithm are shown in Table 1.

Table 1: The PCA identification rate.

Algorithm	Bai nationality (%)	Buyi nationality (%)	Hani nationality (%)	Wa nationality (%)	Miao nationality (%)
PCA	84	82	85	75	84

The experimental results show that the average correct recognition rate of the algorithm is 82%, and the algorithm has certain feasibility and correctness. Among them, the correct recognition rate of Hani clothing image is 85%, Bai and Miao 84%, Buyi 82%, and finally Wa 75%. Hani nationality has the highest correct recognition rate because its clothing edge lines are obvious, which is very different from that of other nationalities, and it is easy to identify popular elements.

5.2. Experimental Steps and Results Demonstration. The experiment in this paper is carried out in three environments:

Comparison between improved algorithm and classical algorithm. The improved algorithm proposed in this paper is compared with the classical algorithm. Through comparison, it is verified whether the proposed algorithm has a better recognition effect.

Experiment on the number of training samples. Compare the recognition rate of the algorithm when taking a different number of training samples.

Weight experiment. The weights are assigned according to the weights of different components for the identification of popular elements.

5.2.1. Experiment 1: Comparison between Improved Algorithm and Classical Algorithm. The specific design of this experiment is as follows:

Training samples: randomly select any 20 popular element images of each character, a total of 100

Test sample: remaining images; 100 sheets in total

This algorithm:

Step 1: Image processing: the initial image is decomposed by wavelet to obtain a 2×2 pixel matrix.

Step 2: Image feature extraction: extract the feature matrix of four sub-graphs for training and testing samples.

Step 3: Image classification: the nearest distance method is used for classification, and four recognition results are obtained for weighted sorting.

Step 4: Wavelet bases commonly used in wavelet transform include Haar wavelet base, Daubechies wavelet base, biorthogonal wavelet base, Symlets wavelet base, and so on. In this paper, the experiments of sym4, bior3.7, bior1.3, dB4, and Haar wavelet bases are carried out, in which sym4 performs best. Therefore, sym4 is selected as the wavelet base of the algorithm proposed in this paper.

Step 5: The average value of 10 experiments for each experimental result can make the data more accurate; comparative experiment: the proposed algorithm is compared with ca-m2dpca and m2dpca.

The specific experimental results are shown in Figure 7.

As shown in Figure 7, the algorithm proposed in this paper has certain advantages compared with other algorithms. The main reasons are as follows:

Wavelet transform is introduced to improve the recognition efficiency.

Weighted sorting of four subgraphs. The recognition accuracy is improved.

After processing, the algorithm proposed in this paper has the characteristics of low frequency and is very stable. At the same time, it also has the characteristics of high frequency, which improves the recognition rate.

5.2.2. Experiment 2: Training Sample Experiment. In the experiment, the accuracy and efficiency of popular element recognition are also affected by the number of training samples. The more samples, the better the recognition effect. Because there are more samples, the more features recognized and the more fully trained, the better the recognition effect. In order to better verify the training samples and determine their effectiveness, a comparative experiment is proposed in this paper.

Randomly select k images of ethnic minority costumes as the training set

The remaining 10-K images of ethnic minority costumes are used as the test sample set

Wavelet basis selection sym4

In MATLAB, if you want to improve the experimental accuracy, you need to carry out the average value of 10 experimental results. The specific data are shown in Figure 8.

As shown in Figure 8, the number of samples collected is also the key to the recognition effect, but the image collection of popular elements is a very huge project.

When the number of samples collected is small, the identification of epidemic elements will be affected

With the increase of the number of samples, the recognition rate of the three algorithms will increase

The recognition rate of the algorithm proposed in this paper is significantly higher than that of ca-m2dpca and m2dpca

When the number of training samples is greater than 4, the recognition rate of the algorithm mentioned in this paper can reach 0.965, which effectively reflects the efficiency and effectiveness of the algorithm proposed in this paper.

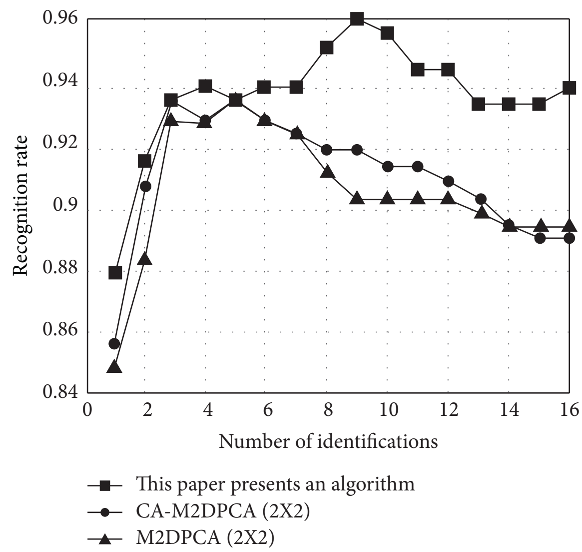

Figure 7: Comparison of recognition rates of various algorithms under different discrimination vectors.

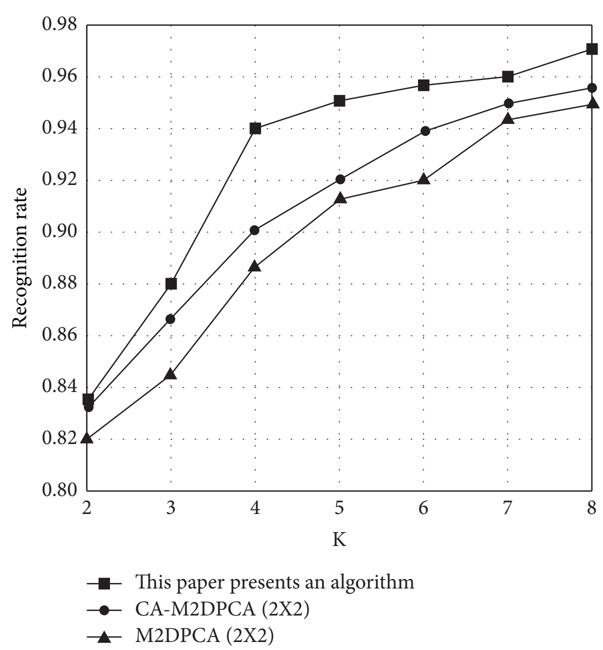

Figure 8: Identification rates of different training sample identification in the ORL database.

Table 2: Results of the weight experiments.

Recognition methods	Training set 1	Training set 2
CA-M2DPCA	0.93	0.88
Principal component algorithm based on wavelet (low frequency 0.6, vertical 0.3, horizontal 0, and diagonal 0.2)	0.94	0.91
Principal component algorithm based on wavelet (low frequency 0.6, vertical 0.2, horizontal 0.1, and diagonal 0.2)	0.936	0.946

5.2.3. Experiment 3: Weight Experiment. Selection of training samples: randomly select 5 popular element images, a total of 150.

Test sample selection: the remaining popular element images are not used as this part, a total of 50.

In the experiment, different sub-graphs have different weights. The low-frequency component has the main characteristics of popular elements, and the results are relatively stable.

Wavelet still selects sym4.

In this paper, MATLAB is used for simulation experiment. Two groups of training samples are randomly selected and given different weights. The specific experimental results are shown in Table 2.

Compared with ca-m2dpca, the principal component analysis algorithm based on wavelet proposed in this paper obtains the experimental results: the principal component analysis algorithm based on wavelet proposed in this paper can effectively recognize the expression changes and increase the recognition rate. After increasing the horizontal weight, the recognition rate has been greatly improved.

6. Conclusion

This paper compares and analyzes the image enhancement effects of histogram equalization and histogram specification through experiments. Combined with the characteristics of ethnic minority clothing images, histogram specification is used to enhance ethnic minority clothing images. The algorithm can stretch the gray range and increase the contrast of the target image. The bimodal method, iterative method, and Otsu method are used to separate the foreground from the background. The nearest neighbor classifier is used to take the PCA features extracted by PCA as the input vector to realize image recognition. The average correct recognition rate of this algorithm is 82%, and there is still a lot of work to be further improved.

Data Availability

The data used to support the findings of this study are available from the corresponding author upon request.

Conflicts of Interest

The author declares that there are no conflicts of interest.

Acknowledgments

This paper is a key project of humanities and social sciences of the Department of Education of Anhui Province, "Research on the inheritance and innovation of Chinese traditional costume culture under the background of cultural creative industry" (SK2014A424).

References

[1] W. Sun, J. Yu, Y. Kang, S. Kadry, and Y. Nam, "Virtual reality-based visual interaction: a framework for classification of ethnic clothing totem patterns," *IEEE Access*, vol. 3, no. 99, p. 1, 2021.

[2] D. M. Li, "Design and implementation of color recognition algorithm for flower waist Dai clothing," *Information & Communications*, vol. 5, no. 4, pp. 117–119, 2017.

[3] Z. W. Ren and M. N. Wu, "Learning of prototype set and orthogonal projection for image set classification," *Application Research of Computers*, vol. 37, no. 5, pp. 1541–1544, 2020.

[4] J. Li, "Remote sensing image template matching intelligent recognition simulation based on STACS," *Computer Simulation*, vol. 38, no. 3, pp. 397–400, 2021.

[5] S. C. Hidayati, C. W. You, W. H. Cheng, and K. L. Hua, "Learning and recognition of clothing genres from full-body images," *IEEE transactions on cybernetics*, vol. 48, no. 5, pp. 1647–1659, 2017.

[6] P. Myznikov and Y. Huang, "A new method for hierarchical image segmentation from visual designs," in *Proceedings of the 2020 54th Annual Conference on Information Sciences and Systems (CISS)*, pp. 1–6, IEEE, Princeton, NJ, USA, March 2020.

[7] A. Kusnadi, W. R. Wella, and I. Z. Pane, "PCA effect on the 3D face recognition system speed," *IOP Conference Series: Materials Science and Engineering*, vol. 1072, no. 1, p. 7, Article ID 012013, 2021.

[8] 孟. Xin Meng, 刘. Lei Liu, 江. Sheng Jiang, 张. Bing Zhang, and 李. Zhizeng Li, "Detection and revision of interference spectral signals based on wavelet transforms," *Acta Optica Sinica*, vol. 39, no. 9, Article ID 0930007, 2019.

[9] Y. G. Kim, Y. S. Lee, and S. W. Chung, "Signal strength-aware adaptive offloading with local image preprocessing for energy efficient mobile devices," *IEEE Transactions on Computers*, vol. 69, no. 1, pp. 99–111, 2020.

[10] N. A. Ali, A. E. Abbassi, and B. Cherradi, "The performances of iterative type-2 fuzzy c-mean on gpu for image segmentation," *The Journal of Supercomputing*, vol. 6, no. 1, pp. 1–19, 2021.

[11] J. S. Yoo and J. O. Kim, "Noise-robust iterative back-projection," *IEEE Transactions on Image Processing*, vol. 29, no. 99, p. 1, 2019.

[12] A. K. Seghouane, N. Shokouhi, and I. Koch, "Sparse principal component analysis with preserved sparsity pattern," *IEEE Transactions on Image Processing*, vol. 28, p. 1, 2019.

[13] A. Tajaddini, G. Wu, F. Saberi-Movahed, and N. Azizizadeh, "Two new variants of the simpler block gmres method with vector deflation and eigenvalue deflation for multiple linear systems," *Journal of Scientific Computing*, vol. 86, no. 1, 2021.

[14] S. Lv, Q. Sun, J. Yang, Y. Jiang, F. Qu, and J. Wang, "An improved phase-coding method for absolute phase retrieval based on the path-following algorithm," *Optics and Lasers in Engineering*, vol. 122, pp. 65–73, 2019.

[15] M. Al-Dabagh, M. Alhabib, and F. H. Al-Mukhtar, "Exploiting wavelet transform, principal component analysis, support vector machine, and k-nearest neighbors for partial face recognition," *Cihan University-Erbil Scientific Journal*, vol. 3, no. 2, 2019.

[16] S. Sutarti, A. T. Putra, and E. Sugiharti, "Comparison of pca and 2dpca accuracy with k-nearest neighbor classification in face image recognition," *Scientific Journal of Informatics*, vol. 6, no. 1, pp. 64–72, 2019.

[17] A. A. Abdulrahman and F. S. Tahir, "Face recognition using enhancement discrete wavelet transform based on MATLAB," *Indonesian Journal of Electrical Engineering and Computer Science*, vol. 23, no. 2, p. 1128, 2021.

Hindawi
Scientific Programming
Volume 2023, Article ID 9828320, 1 page
https://doi.org/10.1155/2023/9828320

Retraction

Retracted: Intelligent Prediction Algorithm of Cross-Border E-Commerce Logistics Cost Based on Cloud Computing

Scientific Programming

Received 1 August 2023; Accepted 1 August 2023; Published 2 August 2023

This article has been retracted by Hindawi following an investigation undertaken by the publisher [1]. This investigation has uncovered evidence of one or more of the following indicators of systematic manipulation of the publication process:

(1) Discrepancies in scope
(2) Discrepancies in the description of the research reported
(3) Discrepancies between the availability of data and the research described
(4) Inappropriate citations
(5) Incoherent, meaningless and/or irrelevant content included in the article
(6) Peer-review manipulation

The presence of these indicators undermines our confidence in the integrity of the article's content and we cannot, therefore, vouch for its reliability. Please note that this notice is intended solely to alert readers that the content of this article is unreliable. We have not investigated whether authors were aware of or involved in the systematic manipulation of the publication process.

Wiley and Hindawi regrets that the usual quality checks did not identify these issues before publication and have since put additional measures in place to safeguard research integrity.

We wish to credit our own Research Integrity and Research Publishing teams and anonymous and named external researchers and research integrity experts for contributing to this investigation.

The corresponding author, as the representative of all authors, has been given the opportunity to register their agreement or disagreement to this retraction. We have kept a record of any response received.

References

[1] W. Gao, "Intelligent Prediction Algorithm of Cross-Border E-Commerce Logistics Cost Based on Cloud Computing," *Scientific Programming*, vol. 2021, Article ID 7038294, 10 pages, 2021.

Hindawi
Scientific Programming
Volume 2021, Article ID 7038294, 10 pages
https://doi.org/10.1155/2021/7038294

Research Article

Intelligent Prediction Algorithm of Cross-Border E-Commerce Logistics Cost Based on Cloud Computing

Wanli Gao

Economics and Management School, Jilin Agricultural Science and Technology University, Jilin 132101, China

Correspondence should be addressed to Wanli Gao; gaowanli@jlnku.edu.cn

Received 2 September 2021; Revised 11 October 2021; Accepted 15 October 2021; Published 29 October 2021

Academic Editor: Le Sun

Cross-border e-commerce logistics cost prediction algorithm does not consider logistics distribution scheduling, and logistics information interchange is not enough, which leads to confusion of logistics cost parameters and large deviation. Therefore, an intelligent prediction algorithm of cross-border e-commerce logistics cost based on cloud computing is designed. Introduce cloud computing platforms, optimize the scheduling of cross-border e-commerce logistics distribution tasks, and select the targets for the scheduling of cross-border e-commerce logistics distribution tasks from the aspects such as the shortest waiting time required by customers, the degree of resource load balance, and the costs consumed in completing cross-border e-commerce logistics distribution tasks, and design logistics scheduling process. On this basis, the logistics distribution data are classified, the association rules between the data are mined, and the monitoring of abnormal values in the cost forecasting process is completed. In order to eliminate the interference caused by the difference of different cost management interval, the function value is calculated by weighted Euclidean distance. Design feedback forecast mechanism to realize intelligent forecast algorithm of cross-border e-commerce logistics cost. Experimental results show that the proposed algorithm has better accuracy of cross-border e-commerce logistics cost prediction and higher completion rate of logistics tasks.

1. Introduction

The development of cross-border e-commerce and that of cross-border logistics complement each other. The development of cross-border logistics greatly promotes the development of cross-border e-commerce, and the rapid development of cross-border e-commerce also provides greater development space and more development opportunities for cross-border logistics [1]. Cross-border e-commerce has developed rapidly, but cross-border logistics has not yet adapted to its development, and the two cannot achieve coordinated development. Cross-border logistics network systems lack synergies, specifically manifested in the lack of synergies in warehousing, transportation, customs, distribution, and other logistics functions, the lack of synergies in the connection between China's logistics, international logistics, and the logistics in the destination country, and the lack of synergies between cross-border logistics and the logistics environment such as language, customs, technologies, and policies [2]. At present, the main modes of cross-border logistics include international postal parcels, international express delivery, overseas warehouses, international logistics lanes, border warehouses, bonded zones and free trade zones, cargo logistics, third-party logistics, and fourth-party logistics. For the future development of cross-border e-commerce logistics, it is necessary to promote the coordinated development of cross-border e-commerce and cross-border logistics and the coordination of cross-border logistics networks, promote the upgrading of the logistics outsourcing mode represented by the fourth-party logistics by adopting multiple cross-border logistics modes, realize the localized operation of cross-border logistics, and strengthen the cooperation with local logistics companies [3].

In order to optimize the research on cross-border e-commerce logistics costs, some good results have been achieved. Reference [4] takes four main factors such as distribution vehicle transportation, cold chain energy consumption, cargo loss, and time window punishment as the research object, constructs the cost model of each factor, and determines the objective optimization function of cost optimization in the process of cold chain logistics distribution. The ant colony algorithm is used to solve the example of cost optimal objective function in the process of cold chain logistics distribution, and the optimization roadmap of cold chain logistics distribution path network is obtained. As mentioned in [5], in order to effectively reduce logistics cost, it is necessary to study the logistics cost problem under multicustomer random demand factors. When studying the logistics cost of an enterprise, assuming that the demand of the demander obeys the Poisson distribution, the ordering cost, goods cost, inventory occupancy cost, and transportation cost of the enterprise are calculated, respectively. These four variables are sorted out and solved by genetic algorithm to achieve the global optimization. Big data has become an important direction in the development of modern information technology. PERSONA is the mathematical modeling of users in the real world. It is the concrete application of big data in economic life. By representing user information through different things and statistics, they can be well correlated and matched. Based on PERSONA, integrated EOQ system, derived sales forecasting system, and inventory control system. Reference [6] builds a perfect dynamic architecture. From the initial B2B model to the network retail model and then to the eye-catching C2B model, people are concerned about the status, problems, and suggestions of e-commerce model, but there is a lack of corresponding theoretical research among e-commerce models. Reference [7] studies the path, theoretical mechanism, and future development direction of cross-border e-commerce mode.

However, the above two methods ignore the consideration of logistics distribution scheduling, and the amount of logistics information interaction is not enough, resulting in confusion of logistics cost parameters and large errors in cost prediction. Therefore, an intelligent prediction algorithm of cross-border e-commerce logistics cost based on cloud computing is designed.

Our contribution is threefold:

(1) We designed an intelligent prediction algorithm of cross-border e-commerce logistics cost based on cloud computing.

(2) Through the introduction of cloud computing platform, we optimize the scheduling of cross-border e-commerce logistics and distribution tasks and design the logistics scheduling process from the minimum waiting time required by customers, the load balancing degree of resources, and the cost consumed in completing cross-border e-commerce logistics and distribution tasks.

(3) Clustering logistics distribution data, mining association rules between amounts of data, complete the monitoring of outlier points in the process of cost forecasting. In order to eliminate the interference caused by the difference between different cost management intervals, weighted Euclidean distance is used to calculate the function value.

The remainder of this paper is organized as follows. Section 2 introduces cloud computing cross-border e-commerce logistics distribution task scheduling. Section 3 discusses the logistics distribution cost prediction method based on cloud data mining technology. Logistics distribution cost prediction method based on cloud data mining technology. Section 4 discusses simulation experiment analysis. Section 5 presents the conclusions of the study.

2. Cloud Computing Cross-Border E-Commerce Logistics Distribution Task Scheduling

Cloud computing is a business computing model that provides resources for a fee as a service. The resource services provided by it fall into three categories: platform as a service, software as a service, and infrastructure as a service [8, 9]. They provide different services and focus on different types of applications, but they all have resource problems and scheduling problems for cross-border e-commerce logistics distribution tasks. Cross-border e-commerce logistics dispatching in cloud computing is related to the stability of cloud services, the utilization of resources, operating costs, and the quality of service. Therefore, cloud computing cross-border e-commerce logistics distribution task scheduling problem is of great theoretical and practical significance. In the cloud computing environment, there are many dynamic and uncertain factors in the resource and its load. When dispatching and optimizing cross-border e-commerce logistics distribution tasks of cloud computing, the objectives of dispatching cross-border e-commerce logistics distribution tasks of cloud computing shall be selected from the aspects such as the shortest waiting time needed for customers, the degree of resource load balance, and the costs consumed in completing cross-border e-commerce logistics distribution tasks [10].

(1) Minimum waiting time required by the customer:

The minimum amount of waiting time needed for the customer is

$$T_{\min} = \max_{j=1} \sum_{i=1}^{\mathrm{sum}(V_j)} t(i), \tag{1}$$

where $t(i)$ represents the execution time of cloud computing cross-border e-commerce logistics distribution tasks on the virtual machine and $\mathrm{sum}(V_j)$ represents the total number of cross-border e-commerce logistics distribution tasks allocated on the virtual machine. The time spent in processing the cross-border e-commerce logistics distribution task is the ratio of the command length A_i of the cross-border e-commerce logistics distribution task to the execution speed v of the virtual machine [11], expressed as

$$t' = \frac{A_i}{v}. \tag{2}$$

(2) Resource load balancing degree:

The calculation formula of resource load balancing degree on virtual machine is

$$\gamma = \sqrt{\frac{\sum_{j=1}^{m}\left(\mathrm{sum}\left(t_j\right) - \overline{\mathrm{sum}\left(t_j\right)}\right)^2}{m}}, \tag{3}$$

where $\mathrm{sum}(t_j)$ represents the total time for the multiobjective logistics distribution task to be executed on the virtual machine, $\overline{\mathrm{sum}(t_j)}$ represents the average time consumed by the virtual machine to execute the multiobjective logistics distribution task, and m represents the resource load balancing probability on the virtual machine.

(3) Cost for completing multiobjective logistics distribution tasks:

The formula for calculating the cost for completing the multiobjective logistics distribution task is as follows:

$$M = \sum_{j=1}^{m} \mathrm{sum}\left(V_j\right) \times T_{\min} \times \gamma. \tag{4}$$

Formula (4) fully reflects the cost of cloud computing cross-border e-commerce logistics and distribution tasks handled on virtual machines, and the cost of completing cross-border e-commerce logistics and distribution tasks is closely related to the central processor [12], bandwidth performance [13], and memory of the virtual machines.

Based on the shortest waiting time, the resource load balance, and the cost of completing the multiobjective logistics distribution task, this paper measures the scheduling effect of the multiobjective logistics distribution task and establishes the following mathematical models.

$$\begin{cases} \min t', \quad \min M, \\ \text{s.t.} \qquad \sum_{j=1}^{m} a_{ij} = 1 \quad a_{ij} \in [0,1]\, i = 1, 2, \ldots, n. \end{cases} \tag{5}$$

Using the shortest waiting time target needed for the customer, the time spent in processing the cross-border e-commerce logistics distribution task is calculated, and the calculation of resource load balance degree and the cost for completing the multiobjective logistics distribution task is combined to establish a mathematical model to measure the scheduling effect of the multiobjective logistics distribution task, and the target of the scheduling of multiobjective logistics distribution task in cloud computing is selected [14].

In cloud computing, there are some constraints among the optimization objectives of multiobjective logistics distribution task scheduling. Therefore, we can determine the optimal multiobjective function of multiobjective logistics distribution task scheduling based on the understanding of the impact of each step on the scheduling process.

Assuming that, in the cloud computing multiobjective logistics distribution task set, N_{first} represents the first processing multiobjective logistics distribution task and N_{last} represents the last processing multiobjective logistics distribution task, then the processing time of the cloud computing multiobjective logistics distribution task set can be calculated by using the followingformula:

$$t_{\text{sum}} = t_e\left(N_{\text{last}}\right) - t_s\left(N_{\text{first}}\right). \tag{6}$$

Define that the number of multiobjective logistics distribution tasks in the cross-border e-commerce logistics distribution task set of cloud computing is N, and the calculation formula is

$$N = N_{\text{last}} - N_{\text{first}}. \tag{7}$$

For the operation cost c_{total} required by the cloud computing multiobjective logistics distribution task set in the processing process, assuming that the cost required by the multiobjective logistics distribution task T_i on the virtual machine per unit time is c_i, then c_{total} can be expressed as

$$c_{\text{total}} = \sum_{i=1}^{p} c_i \cdot \left(t_e\left(T_i\right) - t_s\left(T_i\right)\right). \tag{8}$$

If the computing performance of multiobjective logistics distribution task on virtual machine is good enough, the value of c_i in formula (8) will be greater.

Load balancing for cloud computing multiobjective logistics distribution tasks on virtual machines is not the same as the more the cross-border e-commerce logistics distribution tasks assigned on virtual machines, the better the load balancing effect [15]. Define the estimated execution time of all cross-border e-commerce logistics distribution tasks on a virtual machine as T'', expressed as

$$T'' = \sum_{i=0}^{u-1}\left(\frac{\mathrm{amount}\left(T_i\right)}{N}\right), \tag{9}$$

where u represents the number of multiobjective logistics distribution tasks assigned to the virtual machine [16]. Define that the average expected execution time of all multiobjective logistics distribution tasks on virtual machines is $\overline{T}$, and the calculation formula is

$$\overline{T} = \frac{1}{P} \cdot \sum_{j=0}^{N-1} t_{\text{sum}}(N), \tag{10}$$

where w represents the number of multiobjective logistics distribution tasks assigned to the virtual machine and p represents the number of multiobjective logistics distribution tasks in the set of multiobjective logistics distribution tasks.

Define that the load balance variance of cross-border e-commerce logistics distribution task scheduling is E, which is expressed as

$$E = \frac{\sqrt{\left(\left(\sum_{j=0}^{N-1} t_{\text{sum}}(N)/u\right) - \overline{T}\right)}}{w}. \tag{11}$$

The smaller the value of E, the better the load balance of multiobjective logistics distribution tasks in the data center in the process of cloud computing multiobjective logistics distribution task scheduling [17].

For cloud computing users, they must spend the lowest cost in the shortest time. Therefore, the minimum values of t_{sum} and c_{sum} are taken. Considering that cloud computing belongs to a commercial service mode, when designing Pareto dominance relationship, the time and cost related to user interests are higher in priority than load balancing. Therefore, the objective function of cloud computing multiobjective logistics distribution task scheduling is constructed, as shown in the following formula:

$$\begin{cases} t_{\text{sum}} = \min\left(t_e\left(T_{\text{last}}\right) - t_s\left(T_{\text{first}}\right)\right), \\ c_{\text{sum}} = \min\left(t_e\left(T_i\right) - t_s\left(T_i\right)\right), \\ E = \min\left(\sqrt{\left(\left(t_{\text{sum}}/u\right) - \overline{VL}\right)}/w\right). \end{cases} \quad (12)$$

By calculating the processing time of cloud computing cross-border e-commerce logistics distribution task set, the number of multiobjective logistics distribution tasks in the cross-border e-commerce logistics distribution task set is defined, and the load balance variance of multiobjective logistics distribution task scheduling is calculated according to the expected execution time of all multiobjective logistics distribution tasks on the virtual machine. The objective function of cloud computing multiobjective logistics distribution task scheduling is constructed.

The basic flow of cloud computing multiobjective logistics distribution task scheduling optimization algorithm is shown in Figure 1.

To sum up, from three aspects: the shortest waiting time, the resource load balance degree, and the cost of completing the multiobjective logistics distribution task, this paper selects the target of multiobjective logistics distribution task scheduling of cloud computing, designs the optimization algorithm of multiobjective logistics distribution task scheduling of cloud computing, and realizes the scheduling of multiobjective logistics distribution task.

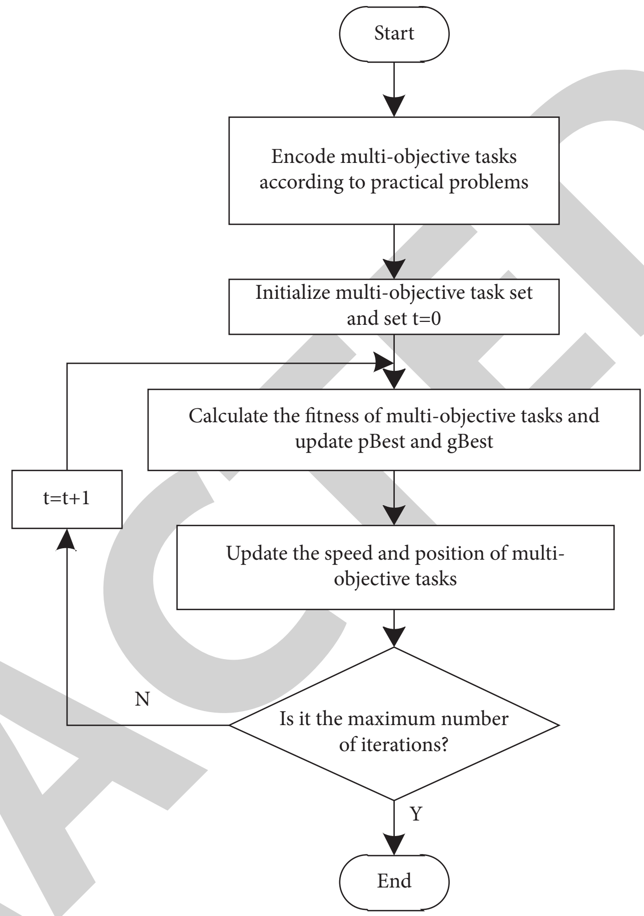

Figure 1: Cloud computing cross-border e-commerce logistics scheduling process.

3. Logistics Distribution Cost Prediction Method Based on Cloud Data Mining Technology

Data mining technology [18, 19] aims to process large amounts of data with complex information types and diverse structural forms. The cross-border e-commerce logistics and distribution industry is developing rapidly, and some companies regard cross-border e-commerce logistics and distribution as an extension of their development. Therefore, the financial sector has higher requirements for estimating the cost of cross-border e-commerce logistics and distribution. Traditional cost forecasting methods, less consideration of the impact of factors, for the division of relevant data are not careful, which makes managers query related data and database smaller; forecasted cost value will affect the development of enterprises. So, a new cost forecasting method is studied. This method uses cluster analysis, classification analysis, anomaly analysis, cluster analysis, and correlation analysis to improve the accuracy of cost prediction by finding the hidden rules.

3.1. Clustering Logistics Distribution Data. Cloud data mining technology is related to computer science. Through data collection, regression analysis, data clustering, association rules, and neural network methods, hidden data information with special association attributes can be grabbed from massive data to predict or forecast the relevant data.

Cross-border e-commerce logistics and distribution costs are mainly generated in the distribution process and distribution links, mainly including sorting costs, circulation and processing costs, assembly costs, and transportation costs. At present, there is a method that uses fuzzy self-defense algorithm to optimize multiobjective task scheduling. This method has a good convergence effect [20]. Sorting expenses shall include sorting manual expenses and sorting equipment expenses; circulation and processing expenses shall include the sum of expenses such as circulation and processing equipment, processing materials and wages and bonuses of management personnel, workers, and the relevant personnel engaging in processing activities in the course of circulation and processing; assembly expenses shall include assembly materials, labor, and the relevant auxiliary expenses; transportation expenses shall include vehicle expenses and other operating overhead expenses. Therefore, after the distribution cost is refined, there are many types of expenses and the second-level items are more cumbersome. Therefore, the data clustering means in cloud data mining technology [21] shall be used to organize the data information into several different classes or clusters according to the approximation of the data related to the distribution cost, so as to ensure that there are certain attributes among amounts of data of the same class or cluster and certain differences among different classes or clusters. Therefore, the calculation formula for the data relating to the distribution costs of cluster cross-border e-commerce logistics is

$$C = \sum_{i=1, i\neq j}^{m} \sum_{j=1}^{m} \left(a^{j} - b^{i}\right)^{2}, \tag{13}$$

where m represents the number of clusters after clustering, i and j, respectively, represent the clusters with one characteristic attribute, n_j represents the number of items in the data cluster, j represents a data item in the data cluster j, and b_i represents a data item in the initial central node in the data cluster i.

3.2. Mining Association Rules between Amounts of Data. According to the cost data cluster after clustering, find out the internal relationship between different pieces of information in the same characteristic data. Each structure is usually used to enumerate the possible data class clusters, generally including y data class clusters of different phases; there may be multiple frequent data class clusters, and there will be K rules [22]. Therefore, in these complex and cumbersome data sets, find all frequent data clusters that meet the minimum support threshold and then mine association rules with high confidence from these clusters. The possible rules between frequent data clusters can be expressed by the following formula:

$$\mathrm{G} = \sum_{g=1} \left[C\binom{y}{g} \cdot \sum_{d=1}^{y-g} \binom{y-g}{d} \right], \tag{14}$$

where G is the possible association rules analyzed according to the clustering data cluster of formula (14), g represents the number of candidate clusters, and d represents the support count of each candidate cluster. According to these possible association rules, the degree of interest between these rules is measured. Let $A = \{\mu_1, \mu_2, \ldots, \mu_n\}$ represent the set of all items. If $X \subseteq A$, it means that X is a pattern. When there are f amounts of data information in this pattern, X is called the f item set. Suppose that data D is a set of distribution costs, where each expense data F is a set of items, and each data type is represented by H, E, and $I\,Q$. U and V are two cluster-like item sets; there are $U \subseteq A$ and $V \subseteq A$ and $U \cap V = \delta$, and the cost data F contains U; if and only if $U \subseteq F$, the association rule is $U \Longrightarrow V\,[u, v]$. Support is the probability that both U and V exist in database D; that is, when confidence appears, U and V also appear, which represents the strength of association rules. At this time, the support is expressed in support$(U \Longrightarrow V) = P(U \cup V)$. The cost data support after mining is shown in Table 1.

According to the frequent data cluster items in Table 1, the support between all amounts data is calculated to obtain the association degree of each relationship between the amounts of data and find out the association rules between different costs.

3.3. Outlier Detection of Cost. Most of the existing cost forecasts focus on the total cost after cost management accounting and do not consider the current cost deviation. Therefore, this paper proposes an outlier detection method, which can control the quality and quantity of input parameters under the condition of multidimensional cost management data environment, use the optimal distance function to make different cost management dimensions having the same importance, then find out the cost dimension beyond cost management, and clarify the direction of cost management.

The concept of outlier detection: firstly, calculate the distance between two objects in the cost management data set X, accumulate the distance between different objects and other objects, and formulate z to represent the total amount of expected outliers; then the z objects with the largest sum of distances are outliers.

If x_i and x_j are proposed to represent two cost management sample objects in X, and d_{ij} represents the distance between x_i and x_j, then the distance matrix H of G can be formulated as

$$\psi = \begin{pmatrix} d_{11} & d_{12} & \ldots & d_{1n} \\ d_{21} & d_{22} & \ldots & d_{2n} \\ \vdots & \vdots & \vdots & \vdots \\ d_{n1} & d_{n2} & \ldots & d_{nn} \end{pmatrix}. \tag{15}$$

The deviation degree δ_i of x_i is proposed as the sum of row i in distance matrix ψ:

$$\delta_i = \sum_{j=1}^{n} d_{ij}. \tag{16}$$

3.4. Distance Function Determination. In the concept of isolated point, the key point of cost management data analysis is to calculate the distance between one-to-one amounts of corresponding data. In the data set, all data objects are represented by many kinds of dimensions, such as classification dimension, continuous dimension, and time dimension. Different dimension data have different measurement algorithms. Outlier detection discusses the distance measure of continuous data types, and the most common distance is Euclidean distance. In the cost management data set, in order to eliminate the interference caused by the differences of different cost management intervals, the value of the function is calculated by weighted Euclidean distance. The formula is as follows:

Table 1: Frequent cluster support of cost data.

Distribution area	Type of goods delivered	Frequent class cluster (%)
N1	H	69
N2	E	88
N3	I	90
N4	Q	54

$$\left\| x_i - x_j \right\| = \sqrt{\sum_{k=1}^{N} \frac{\left(x_{ik} - x_{jk}\right)^2}{\sigma^2}}, \tag{17}$$

wherein σ represents variance. It can be seen from the above definition that the greater the deviation degree δ_i, the farther the distance between object i and the remaining objects, and the greater the possibility that it is an isolated point. In fact, after calculating all δ_i, you can arbitrarily specify the z value to view the isolation degree of different cost management data objects, and you can also rely on the proposed isolation points to realize automatic detection, so as to obtain the approximate value distribution exceeding cost management in the cost management data set, so as to provide a strong basis for subsequent cost management prediction [23].

3.5. Design of Cost Forecasting Algorithm. Based on the data association rules, a feedback forecasting mechanism and a cost forecasting algorithm are designed to predict the total cost of cross-border e-commerce logistics distribution. After the cost data mining is completed, a large amount of cost information is obtained, which is taken as the feedback information for forecasting. Before the control, the deviation threshold for forecasting the cross-border e-commerce logistics costs is set. When the cross-border e-commerce logistics costs exceed the range of deviation thresholds, the cost feedback information is collected to forecast the cross-border e-commerce logistics costs. The specific control mechanism is shown in Figure 2.

From the feedback control in Figure 2, in the intelligent forecast of cross-border e-commerce logistics, the expected cost and the actual cost are used to calculate the cost deviation, and then the cost deviation rate is obtained. In the phase of logistics distribution, if the deviation rate of cost is less than the set deviation threshold, the project construction needs to be satisfied and no feedback control is required. If the deviation of cost is greater than the set deviation threshold, the trigger control mechanism can obtain the project cost information through the cost data mining technology in real time and adjust the overall project cost according to the cost information.

In general, the distribution cost is mainly related to the labor cost and the transportation vehicle and equipment cost. So, in the process of forecast, the direct labor cost and transportation cost are calculated according to the dispatch of the managers, stevedores, and transportation personnel in the two processes of distribution and transportation. Based on the regression difference moving average method, the distribution cost is predicted according to the linear time

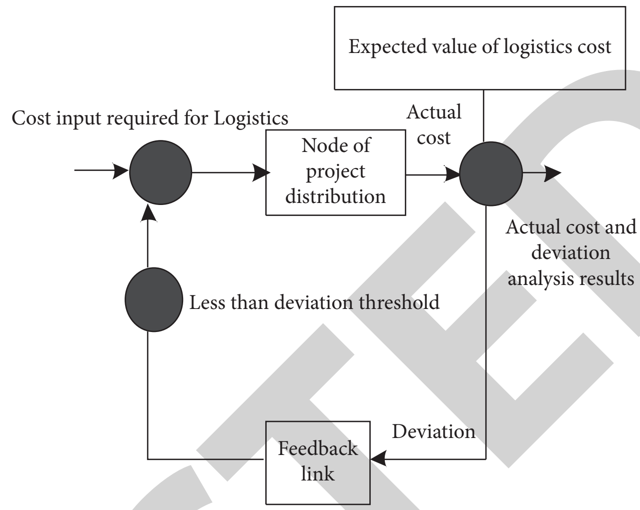

Figure 2: Feedback forecast of cross-border e-commerce logistics cost.

series. The time series of dynamic changes can be transformed into a stationary one by several time difference calculations. Set a parameter as ω, treat it as the difference degree, use ω, χ, and q to build prediction model, model the transformed stationary sequence, and then replace it with the original sequence. The prediction algorithm based on parameters ω, χ, and q is as follows:

$$Q = \sum_{\chi=q}^{m} \varphi_m \left[\varepsilon_\chi + \gamma_q - \varepsilon_q\right], \tag{18}$$

where Q represents the predicted cost of cross-border e-commerce logistics distribution and φ_m represents the m rules between expense amounts of data. ε_p represents the model under characteristic parameter p, and γ_q represents the model under characteristic parameter q; ε_q represents the random error under the characteristic parameter q.

In the process of calculation, the stability of time series should be ensured. When the data series has the characteristic of volatility, it should be treated by difference. At this point, cloud data mining technology is used to predict the cross-border e-commerce logistics distribution costs at this stage.

4. Simulation Experiment Analysis

In the simulation platform, the cloud computing cross-border e-commerce logistics cost prediction algorithm is added to the category of data center broker, and the ant colony algorithm-based logistics distribution cost prediction algorithm proposed in [4] and the logistics cost prediction algorithm under multicustomer random demand proposed in [5] are used as the experimental control group. Quantitatively analyze the intelligent prediction results of cloud computing cross-border e-commerce logistics cost from three aspects: deadline violation rate, virtual machine, and resource utilization.

This experiment uses the data recorded by the financial management department of a large cross-border e-commerce logistics enterprise to forecast the transportation costs for the current year by year based on the 450 GB distribution costs recorded from 2010 to 2020 through the establishment of the Hadoop experimental cloud platform. The simulation environment is composed of simulation computer, special server, real-time changing LCD screen, and network stable routing. This experiment selects two computers with the same model and same configuration. The CPU of the computer is 3.4 GHz, 8 GB memory, and 500 GB hard disk space; high speed computing network and gigabit storage network are selected, and the wireless route-connected computer is opened. The operating system of the computer is Ubuntu 18.04, and the Java execution environment is jdk-7u21-linux-i586. It logs into the simulation software MATLAB 2016a and tests the software program. The software runs smoothly and runs on the Hadoop platform. The platform can work normally in single machine mode, pseudodistributed mode, and complete distributed mode. Set up a data cluster, a total of 26 nodes, including 2 management nodes, 1 IO node, and 23 compute nodes; specify node01-node23, when management node finds variable cost data; timely modify the path set to 192.168.0.201. After the preparation, according to the selected subjects, the experiment began.

4.1. Experimental Analysis of Outlier Detection in Cost Prediction. In the above set prediction index samples, an index is randomly selected as the experimental standard, and the isolated points between attributes in the index are detected by the proposed method. The results are shown in Figure 3.

It can be seen from the experiment of extraction project indicators for the service lanes in Figure 3 that cost management serving driveway data exist in the two data concentrations, the two dots; that is, the target cost management of the normal price and the other three separate data points are detected by the method of isolated points; these isolated points represent. In the distribution of cost management data, a phenomenon of premium appears, but the degree of premium is low.

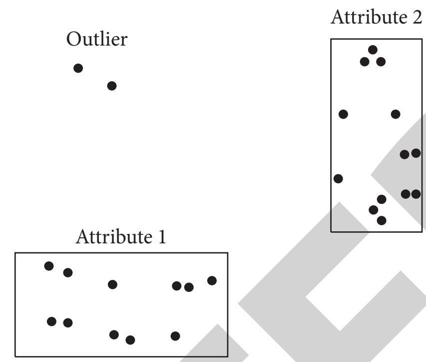

Figure 3: Outlier detection results of the proposed method.

4.2. Comparison of Logistics Time Consumption under Different Algorithms. By setting different quantities of cloud computing cross-border e-commerce logistics delivery tasks, the maximum completion time of the three methods is compared, and the results are shown in Figure 4.

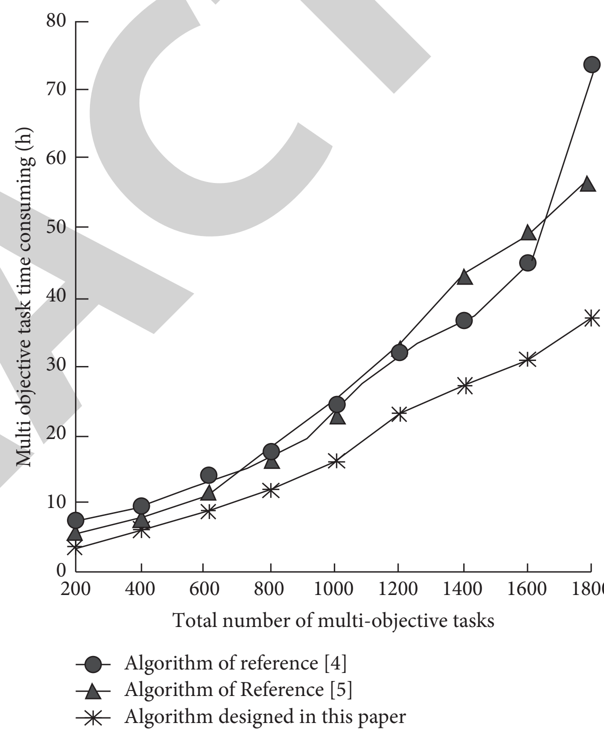

Figure 4: Comparison results of maximum completion time of cloud computing cross-border e-commerce logistics task scheduling.

As can be seen from the results in Figure 4, the maximum completion time of the three methods is also getting longer with the increase of the number of cloud computing cross-border e-commerce logistics distribution tasks. The logistics cost prediction algorithm proposed in [5] under the random demands of multiple customers not only improves the advantages and disadvantages of the traditional method, but also takes into account the multiobjective property. Compared with the ant colony algorithm-based logistics distribution cost prediction algorithm proposed in [4], it has a shorter maximum completion time. The ant colony algorithm-based logistics distribution cost prediction algorithm proposed in [4] has the problem of slow convergence, resulting in a long completion time. The cloud computing cross-border e-commerce logistics cost method plans the three objectives of the shortest waiting time of customers, the load balancing degree of resources, and the cost of completing the cross-border e-commerce logistics distribution task as a single objective evaluation function and takes them as the scheduling target, achieving good scheduling effect.

4.3. Comparison of Logistics Task Completion Rate under Different Algorithms. By setting different quantities of cloud computing cross-border e-commerce logistics delivery tasks, the three methods are compared for the failure rate of deadline, as shown in Figure 5.

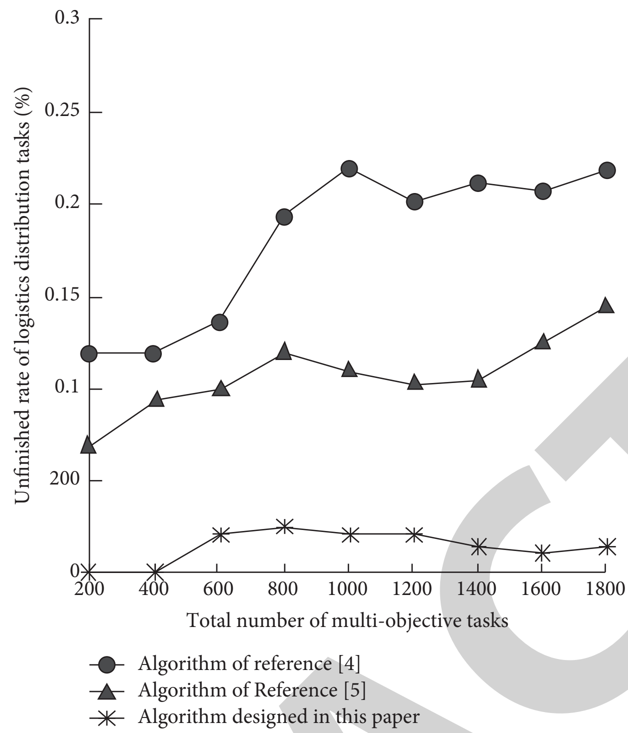

Figure 5: Test results of unfinished rate of deadline of cross-border e-commerce logistics task scheduling.

Table 2: Cost prediction deviation comparison of different algorithms (unit: ten thousand yuan).

Logistics cycle	This paper designs the algorithm	Reference [4] algorithm	Reference [5] algorithm	Actual cost
1	2.42	2.44	2.35	2.48
2	2.75	2.69	2.56	2.78
3	2.95	2.28	2.37	2.92
4	2.82	2.05	2.45	2.71
5	2.88	2.72	2.68	2.82
6	2.94	3.11	3.20	2.92
7	3.36	3.73	3.18	3.39
8	3.69	3.12	3.58	3.66
9	2.76	3.24	3.43	2.74
10	3.01	3.60	3.18	3.01
11	3.64	4.03	4.10	3.64
12	3.99	4.60	4.28	3.99
13	4.88	4.22	4.56	4.80
14	4.52	5.40	4.35	4.51
15	4.85	5.88	5.12	4.83
16	4.23	5.46	5.35	4.22
17	4.15	5.56	5.64	4.15
18	4.95	5.21	5.83	4.90
19	5.02	5.37	5.97	5.02
20	5.58	6.09	6.37	5.58

The increased amount of cross-border electricity distribution tasks can be seen from the results of Figure 5, with cloud computing, based on the fuzzy self-defense cross-border electricity distribution algorithm of cloud computing task scheduling optimization method, and authors in [5] proposed many customers under the random demand of the logistics cost prediction algorithm which is maintained in a lower cutoff time not completed. However, the deadline completion rate of cloud computing distribution task scheduling optimization method based on fuzzy self-defense algorithm is relatively low, about 5%. The ant colony algorithm-based logistics distribution cost prediction algorithm proposed in [4] takes the cutoff time as a constraint condition, and the optimization of the distribution task scheduling algorithm is not in place, which affects the final scheduling effect.

4.4. Comparison of Logistics Cost Forecasting Errors under Different Algorithms. Table 2 shows the statistical results of actual cost control in 20 logistics cycles of three test groups with different algorithms.

According to Table 2, the total cost of the logistics project of the experimental group is also basically consistent with the expected cost, and the error is very small. However, the logistics project cost of [4] algorithm and [5] algorithm is quite different from the expected cost. The test results of the above three stages verify that the proposed cost intelligent prediction method is more effective than the two traditional prediction algorithms. As can be seen from the experimental results, the prediction results obtained by our method are closer to actual cost. This shows the effectiveness of the proposed method.

5. Conclusion

In recent years, cross-border e-commerce logistics and transport industry have developed rapidly. In order to better predict logistics costs, this study designed a cross-border e-commerce logistics cost intelligent prediction algorithm based on cloud computing. Introduce cloud computing platforms to optimize the scheduling of cross-border e-commerce logistics distribution tasks. On the basis of selecting the target of cloud computing cross-border e-commerce logistics distribution task scheduling, by constructing the target function of cloud computing cross-border e-commerce logistics distribution task scheduling, this paper realizes the scheduling of cloud computing cross-border e-commerce logistics distribution task and optimizes the effect of intelligent prediction of cross-border e-commerce logistics cost. Experimental results also show that the proposed algorithm has higher accuracy and higher completion rate of logistics tasks and has significant advantages over the existing algorithms.

Data Availability

The data used to support the findings of this study are available from the author upon request.

Conflicts of Interest

The author declares no conflicts of interest.

Acknowledgments

This paper was supported by the Rural Revitalization Research Base Project of Jilin Branch of Jilin Academy of Social Sciences (no. 2020(1) of Jisheng branch) and research results of school level key construction disciplines 《Business Administration 2018–2020》 of Jilin Agricultural Science and Technology University.

References

[1] J. Anson, M. Boffa, and M. Helble, "Consumer arbitrage in cross-border e-commerce," *Review of International Economics*, vol. 27, no. 4, pp. 1234–1251, 2019.

[2] M. Labouré, "Pensions: the impact of migrations and cross-border workers in a small open economy," *Journal of Pension Economics and Finance*, vol. 18, no. 2, pp. 247–270, 2019.

[3] D. Pamucar, K. Chatterjee, and E. K. Zavadskas, "Assessment of third-party logistics provider using multi-criteria decision-making approach based on interval rough numbers," *Computers & Industrial Engineering*, vol. 127, pp. 383–407, 2019.

[4] Z. X. Zeng, C. D. Zou, J. F. Wei, H. Lu, E. Lv, and Q. Ruan, "Optimization of distribution cost model of cold chain logistics for litchi based on ant colony algorithm," *Packaging Engineering*, vol. 40, no. 11, pp. 58–65, 2019.

[5] J. D. Han, X. F. Yang, and Q. Tian, "Logistics cost control under stochastic demand of multiple customers," *Price:Theory & Practice*, vol. 417, no. 3, pp. 157–160, 2019.

[6] I. Czarnowski and P. Jędrzejowicz, "Data reduction and stacking for imbalanced data classification," *Journal of Intelligent and Fuzzy Systems*, vol. 37, no. 6, pp. 7239–7249, 2019.

[7] L. Jia, "Research on the cost control of cross-border e-commerce overseas warehouse from the perspective of big data technology and storage theory model," in *Proceedings of the 2020 Asia-Pacific Conference on Image Processing, Electronics and Computers (IPEC)*, pp. 423–427, IEEE, Dalian, China, April 2020.

[8] J. Wang and C. Xing, "Factors affecting the evolution of advanced manufacturing innovation networks based on cloud computing and multiagent simulation," *Mathematical Problems in Engineering*, vol. 2021, no. 1, Article ID 5557606, 12 page, 2021.

[9] G. J. Mirobi and L. Arockiam, "DAVmS: distance aware virtual machine scheduling approach for reducing the response time in cloud computing," *The Journal of Supercomputing*, vol. 77, no. 6, pp. 1–12, 2021.

[10] J. Lian, "An optimization model of cross-docking scheduling of cold chain logistics based on fuzzy time window," *Journal of Intelligent and Fuzzy Systems*, vol. 41, no. 2, pp. 1–15, 2021.

[11] A. K. Mishra, D. K. Yadav, Y. Kumar, and N. Jain, "Improving reliability and reducing cost of task execution on preemptible VM instances using machine learning approach," *The Journal of Supercomputing*, vol. 75, no. 4, pp. 2149–2180, 2019.

[12] D. Dhanya and D. Arivudainambi, "Dolphin partner optimization based secure and qualified virtual machine for resource allocation with streamline security analysis[J]," *Peer-to-Peer Networking and Applications*, vol. 12, no. 18, Article ID 1276, 2019.

[13] M. Kaynia, C. Buratti, and R. Verdone, "On the performance of wireless ad hoc networks using bandwidth partitioning," *Wireless Networks*, vol. 25, no. 7, pp. 4215–4229, 2019.

[14] H. Chen, Y. Jin, and B. Huo, "Understanding logistics and distribution innovations in China," *International Journal of Physical Distribution & Logistics Management*, vol. 50, no. 3, pp. 313–322, 2020.

[15] S. Sotiriadis, N. Bessis, C. Amza, and R. Buyya, "Elastic load balancing for dynamic virtual machine reconfiguration based on vertical and horizontal scaling," *IEEE Transactions on Services Computing*, vol. 12, no. 2, pp. 319–334, 2019.

[16] A. Curioni, C. Vesper, G. Knoblich, and N. Sebanz, "Reciprocal information flow and role distribution support joint action coordination," *Cognition*, vol. 187, pp. 21–31, 2019.

[17] F. Lu, L. Wang, H. Bi, Z. Du, and S. Wang, "An improved revenue distribution model for logistics service supply chain considering fairness preference," *Sustainability*, vol. 13, no. 12, Article ID 6711, 2021.

[18] Z. Zhen and Y. Yanqing, "Lean production and technological innovation in manufacturing industry based on SVM

Hindawi
Scientific Programming
Volume 2021, Article ID 1552096, 7 pages
https://doi.org/10.1155/2021/1552096

Research Article

Football Players' Shooting Posture Norm Based on Deep Learning in Sports Event Video

Guangliang Huang,[1] Zhuangxu Lan,[1] and Guo Huang[2]

[1]*Guangxi College of Physical Education, Nanning,530012, Guangxi, China*
[2]*Zhejiang Wanli University, Ningbo 315100, Zhejiang, China*

Correspondence should be addressed to Guo Huang; 2002900057@zwu.edu.cn

Received 2 September 2021; Revised 10 October 2021; Accepted 11 October 2021; Published 25 October 2021

Academic Editor: Le Sun

Football is one of the favorite sports of people nowadays. Shooting is the ultimate goal of all offensive tactics in football matches. This is the most basic way to score a goal and the only way to score a goal. The choice and use of shooting technical indicators can have a great impact on the final result of the game. Therefore, how to improve the shooting technique of football players and how to adjust the shooting posture of football players are important issues faced by coaches and athletes. In recent years, deep learning has been widely used in various fields such as image classification and recognition and language processing. How to apply deep learning optimization to shooting gesture recognition is a very promising research direction. This article aims to study the football player's shooting posture specification based on deep learning in sports event videos. Based on the analysis of target motion detection algorithm, target motion tracking algorithm, target motion recognition algorithm, and football shooting posture classification, KTH and Weizmann data sets are used. As the experimental verification data set of this article, the shooting posture of football players in the sports event video is recognized, and the accuracy of the action recognition is finally calculated to standardize the football shooting posture. The experimental results show that the Weizmann data set has a higher accuracy rate than the KTH data set and is more suitable for shooting attitude specifications.

1. Introduction

The recognition of human behavior is a hot topic of new research in the field of machine vision and artificial intelligence. Computer algorithms are used to automatically recognize human behavior from collected videos, that is, to classify and label video clips of human motion behavior [1, 2]. Compared with the research of still image recognition, behavior recognition pays more attention to how it perceives the temporal and spatial dynamic changes of the human body in the image sequence [3, 4]. Deep learning is a kind of machine learning, and machine learning is the only way to realize artificial intelligence. The concept of deep learning comes from the research of artificial neural network. Multilayer perceptron with multiple hidden layers is a deep learning structure. Deep learning combines low-level features to form more abstract high-level representation attribute categories or features so as to find the distributed feature representation of data. The motivation of studying deep learning is to establish a neural network simulating the human brain for analytical learning, which simulates the mechanism of the human brain to interpret data.

In recent years, many scholars have conducted related research on action recognition and have achieved good results. Some scholars believe that the convolutional neural network is a deep model that can be directly used as the original input. However, this type of model is currently limited to a type specifically used to process 2D action input, so we have developed a special 3D-CNN model to process action recognition. This type of feature representation model is mainly used to perform 3D convolution from space. The corresponding features are extracted from the dimensions of time and time so as to capture and encode the motion data and information in multiple adjacent frames. The developed model generates multiple channel feature information from multiple input frames at the same time, and the final feature expresses that the model combines all channel information [5]. In addition, some scholars have given a set of training videos. First, by extracting local motion and its appearance characteristics, they are quantified into a visual vocabulary, and then the vocabulary related to nearby points of interest and its direction is formed. The candidate neighborhood composed of central interest points shows how to learn in this way to form the most useful configuration class-specific distance function [6]. Some researchers have a method of recognizing human movements based on gesture primitives. In the learning mode, the parameters representing gestures and activities are estimated from the video. In the running mode, the method can be used in video or still images. In order to recognize the gesture primitives, the researcher extended the method based on the orientation gradient histogram. The descriptor proposed in [7] can better deal with joint poses and cluttered backgrounds. Because the current deep learning network has broken through the bottleneck of many traditional methods in many application fields and has achieved great success, it has received more and more attention from various fields of research and wide application and the international market, and they have built many efficient deep learning network frameworks themselves. The convolution neural network is constructed by imitating the visual perception mechanism of biology, which can carry out supervised learning and unsupervised learning. The parameter sharing of convolution kernel in its hidden layer and the sparsity of interlayer connection enable the convolution neural network to learn lattice features, such as pixels and audio, with less computation, stable effect, and no additional feature engineering requirements for data.

This paper uses deep learning algorithms to extract the features of football players' shooting posture in the KTH and Weizmann data sets, analyze and calculate the accuracy of their action recognition, and then compare them to select a data set that is more suitable for standardizing football players' shooting posture. In addition, deep learning emphasizes the depth of model structure. The importance of feature learning is clarified. In other words, the feature representation of the sample in the original space is transformed into a new feature space through layer by layer feature transformation so as to make classification or prediction easier. Compared with the method of constructing features by artificial rules, using big data to learn features can better describe the rich internal information of data.

The remainder of this paper is organized as follows. Section 2 introduces the different detection strategies in detail. Experimental results are given and deeply analyzed in Section 3. Finally, we summarize our contributions in Section 4.

2. Research on Football Players' Shooting Posture Norm Based on Deep Learning in Sports Event Video

2.1. Moving Target Detection

2.1.1. Light Field Flow Method. Optical flow is based on the instantaneous speed of the object at the imaging level, reflecting the speed of the actual object's displacement in space. This is a way to find the correlation of object motion by using the time change of pixels in the video sequence and the correlation information between adjacent images and calculate the motion information of the object [8].

The field of view of moving objects tends to be continuous and smooth. Based on the continuous smoothness of the field of view, the overall smoothness of the field of view is considered a limiting condition and becomes a variable problem. The following is the global energy formula (1) based on the two-dimensional image:

$$E = \int\int \lfloor \left(I_x u + I_y v + I_t\right)^2 + \alpha^2 \left(\|\nabla u\|^2 + \|\nabla v\|^2\right) \rfloor \mathrm{d}x\mathrm{d}y. \tag{1}$$

Among them, for the image at one point, I_x, I_y, and I_t are used to represent the difference in the corresponding direction.

Besides, the advantage of optical flow method is that it can accurately detect and identify the position of moving heliostat without knowing the scene information, and it is still applicable when the camera is moving. The disadvantages of optical flow method are mainly reflected in the large amount of calculation and long time-consuming, which is not applicable in the case of strict real-time requirements; because the changing light will be incorrectly recognized as optical flow, this method is sensitive to light, which will affect the recognition effect.

2.1.2. Difference between Frames. The frame difference method is currently the most widely used method for moving target detection and extraction. The principle is to place two or three image frames next to the video frame sequence, distinguish the pixels corresponding to the two or three images, and extract the trajectory or contour of the moving target. First, it removes the pixels at the corresponding positions in the adjacent frame images to obtain the difference between the images and converts the difference image into a grayscale image. Then, if there is a small change in the environment, appropriate limits are set. If the value of a pixel is less than the threshold, it is considered as the background [9, 10]. The process of interframe differential transmission is basically illustrated in Figure 1.

The basic process of the frame difference method is as follows:

(1) The difference image is obtained as follows:

$$D_k(x, y) = \left|f_k(x, y) - f_{k-1}(x, y)\right|. \tag{2}$$

(2) Binarization processing of difference image is as follows:

$$R_k(x, y) = \begin{cases} 0, & D_k(x, y) < T, \\ 1, & D_k(x, y) \geq T. \end{cases} \tag{3}$$

In addition, the advantages of the interframe difference method are simple algorithm implementation and low programming complexity. It is not

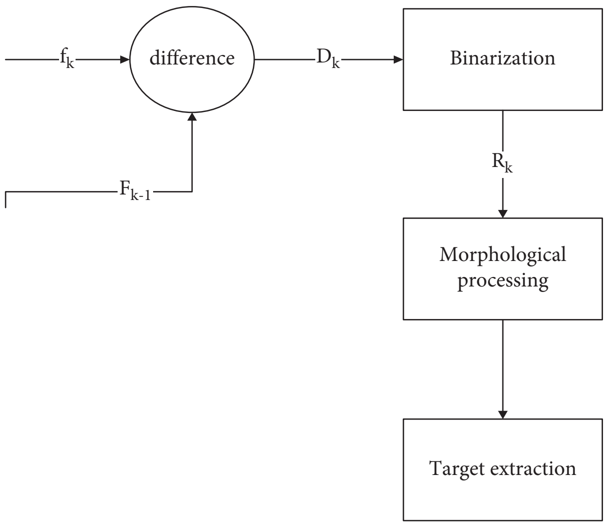

Figure 1: Flow chart of the interframe difference method.

sensitive to scene changes such as light and can adapt to various dynamic environments with good stability. Its disadvantages are as follows: it can not extract the complete area of the object but only the boundary. It also depends on the selected interframe time interval. For fast-moving objects, it is necessary to select a smaller time interval. If the selection is inappropriate, when the objects do not overlap in the front and back frames, they will be detected as two separate objects; for slow-moving objects, a larger time difference should be selected. If the time selection is inappropriate, when the objects almost completely overlap in the front and back frames, the objects will not be detected.

(3) Mathematical morphological processing is performed on binary images.

2.1.3. Background Difference Method. The general concept of the background difference method is to remove the background and leave moving objects, which requires a predefined background pattern. The training image is used to obtain the model parameters. Once the background model is defined, the relative pixel values of the existing image and the background image are subtracted to identify the desired animation target. Once you have the original background, you need to update the background, update the method background model of the method, then calculate the difference between the two images, delete the two images, and use the image threshold to reach the foreground target [11, 12]. Algorithm expression is as follows:

$$f_b(x,y,t)=\begin{cases}1, & \text{if}\left|f(x,y,t)-f(x,y,0)\right|>T,\\ 0, & \text{others}.\end{cases} \tag{4}$$

Among them, $f_b(x,y,t)$ is the image at time t and $f(x,y,0)$ is the background image at time t.

It should be noted that in the moving target detection based on the background difference method, the accuracy of background image modeling and simulation directly affects the detection effect. No matter any moving target detection algorithm, it should meet the processing requirements of any image scene as much as possible. However, due to the complexity and unpredictability of the scene, as well as the existence of various environmental interference and noise, such as the sudden change of illumination, the fluctuation of some objects in the actual background image, the jitter of the camera, and the impact of moving objects entering and leaving the scene on the original scene, it makes the modeling and simulation of background more difficult.

2.2. Moving Target Tracking. The moving target tracking process is shown in Figure 2.

2.2.1. Feature-Based Tracking Method. Feature-based tracking methods mainly rely on the ability of the target to track the target, such as feature extraction and feature matching. First, the target attribute is derived, and then the structure of the video image sequence is used to extract the target attribute, then the structure mapping or search mapping method of the video image sequence is used to find the corresponding attribute point, and finally the location and trajectory of the target information of the traffic matching result are calculated according to the following formula. Because the overall characteristics of the target are not considered, only the local characteristics of the target are identified, and the anti-interference effect is good, and the monitoring target is not affected by scale changes or distortion.

2.2.2. Tracking Algorithm Based on Kernel Density Estimation. The estimation method based on kernel density is currently widely used in the fields of pattern recognition and computer vision. It can create a target model based on the feature probability density distribution of the target image. Since the kernel function has progressive fairness, continuity, and uniform continuity, the gradient estimation of the density function determined by the kernel function can be applied to the entire image space. When estimating the boundary region, there will be boundary effect in kernel density estimation. On the basis of univariate kernel density estimation, the prediction model of value at risk can be established. By weighting the coefficient of variation of kernel density estimation, different var prediction models can be established. Parameter estimation can be divided into parametric regression analysis and parametric discriminant analysis.

2.2.3. Region-Based Matching Algorithm. The algorithm of interest mapping based on grayscale images is also called the algorithm of interest mapping to specific areas. All the gray information based on the image in the area is used to calculate the similarity between gray information in a certain way. The region-based mapping method not only needs to directly extract the features of the region but can directly use all available grayscale image information, which can improve the

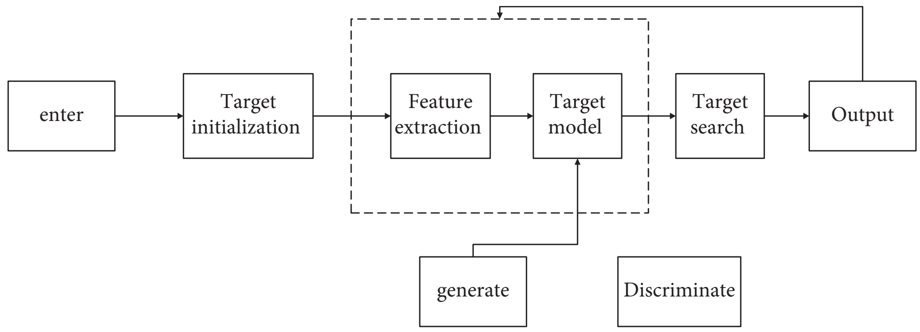

FIGURE 2: Moving target tracking process.

accuracy and robustness to a certain extent. One of its main shortcomings is that the amount of calculation errors is large, and it is difficult to meet real-time requirements. Choosing areas with insufficient gray information as feature areas will increase the error rate of matching.

The basic idea of gray matching is as follows: from the statistical point of view, the image is regarded as a two-dimensional signal, and the statistical correlation method is used to find the correlation matching between signals. The correlation functions of the two signals are used to evaluate their similarity to determine the homonymous points. Gray matching determines the corresponding relationship between the two images by using some similarity measures, such as correlation function, covariance function, sum of squares of difference, and sum of absolute values of difference.

2.3. Moving Target Recognition. The target recognition movement can be simply considered as a combination of feature derivation and classifier recognition. The recognition process is generally shown in Figure 3.

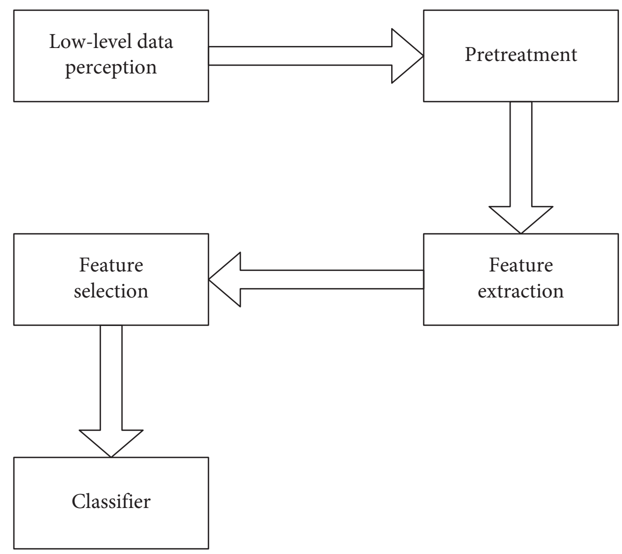

FIGURE 3: Moving target recognition process diagram.

The related recognition algorithm is as follows:

(1) *Convolutional Neural Network.* For 2D-CNN networks, the convergence function can only receive 2D feature maps from the spatial dimensions of the input information. For video information, it is necessary to record motion information in a series of continuous video frames. In response to this situation, 3D-CNN uses 3D convergence and aggregation functions to simultaneously download 3D feature maps in both time and space dimensions. The 3D concatenation function can be considered as a 2D convergence layer stack, so the generated 3D feature map also connects partially continuous input frames. For the 2D rotation function, the value (x, y) at any position on the j-th feature map of the i-th plane is calculated as follows:

$$v_{ij}^{xy} = \tanh\left(b_{ij} + \sum_{m} \sum_{P=0}^{P_{i-1}} \sum_{q=0}^{Q_{i-1}} w_{ijm}^{pq} v_{(i-1)m}^{(x+p)(y+q)}\right), \quad (5)$$

where m is the feature map of the $(i-1)$ layer connected with the current feature map.

Convolution layer parameters include convolution kernel size, step size, and filling, which together determine the size of convolution layer output characteristic graph, which is a super parameter of convolution neural network. The size of the convolution kernel can be specified as any value smaller than the size of the input image. The larger the convolution kernel is, the more complex the input features can be extracted.

(2) *Self-Phase Matrix.* The self-similar table is a graph that can reflect the periodic characteristics of the system. In many dynamic systems, state cycle is a relatively important phenomenon. In order to graphically represent the periodic characteristics of this dynamic system, a recursive diagram can be used to show the retrospective nature of the state in the phase space. The recursive diagram is defined as follows:

$$R(i,j) = H\left(\varepsilon - \|\vec{x}(i) - \vec{y}(j)\|_2\right), \quad \overleftarrow{x}(i) \in \mathfrak{R}^m,\ i,j = 1,\ldots,N, \tag{6}$$

where N refers to the number of states $\vec{x}(i)$ under consideration and H is a step function.

(3) *LSTM Neural Network*. The LSTM neural network is designed to solve the problem of long-distance dependence, and it can store long-term information without particularly complex over-tuning parameters. The internal structure of LSTM is more complex than that of RNN. Through this complex calculation process, LSTM has long-term memory, excellent data processing capabilities with time series capabilities, and improved network performance.

The operation process of LSTM is as follows:

$$\begin{aligned} i_t &= \sigma_i\left(w_i \cdot \left[h_{t-1}, x_t\right] + b_i\right), \\ D_t &= \sigma_c\left(w_c \cdot \left[h_{t-1}, x_t\right] + b_c\right). \end{aligned} \tag{7}$$

Equation (8) calculates f_t of the value of forget gate at time t.

$$f_t = \sigma_f\left(w_f \cdot \left[h_{t-1}, x_t\right] + b_f\right). \tag{8}$$

Formula (9) calculates C_t of the new state value of the state information at time t.

$$C_t = f_t * C_{t-1} + i_t * D_t. \tag{9}$$

Among them, C_t represents the state of information transfer, h is the value of the hidden layer, and b represents the bias top.

In addition, LSTM usually performs better than time recurrent neural network and hidden Markov model, such as in piecewise continuous handwriting recognition. LSTM is a kind of neural network containing LSTM blocks or others. In order to minimize the training error, the gradient descent method, such as the sequential back-propagation algorithm, can be used to modify the weight each time according to the error.

2.4. Football Shooting Posture Classification

2.4.1. Instep Shooting. Instep shots have strong firepower and are mainly used for firing when turning around. When the ball falls in front of or slightly away from the body, you can shoot with the inner instep. It can temporarily change the angle of a shot. For example, when the diagonal line is inserted directly, the goalkeeper will have the opportunity to inevitably move to the nearest position to close the nearest corner. At this time, a half-turn shot can be made. Shoot it into the furthest corner.

2.4.2. Shooting outside the Instep. Shooting from outside the instep is very threatening, sudden, and highly concealed. It can shoot the ball from various directions including front, side, and back and can shoot straight and curved balls.

2.4.3. Arch Shooting. Arch shooting is suitable for high precision, low power consumption, various short shots, and free throws.

2.4.4. Shot from the Back of the Foot. Forefoot shooting is more powerful, more accurate, and the most widely used. This is the basic footwork of shooting footwork.

2.4.5. Toe Shot. A tiptoe shot is fast and sudden. If the competition in front of the goal is fierce, you may not have time to move your legs. Shooting with a tiptoe can win surprisingly, but sometimes the accuracy is relatively low.

2.5. The Difference between Existing Works and Our Work. Compared with the traditional machine learning algorithm, the target detection task needs to be divided into multiple subtasks, which is very cumbersome and time-consuming. The deep learning algorithm used in this paper can effectively realize end-to-end training and learning and greatly reduce the working time. In addition, the accuracy of the traditional machine learning algorithm is limited, and the deep learning algorithm can achieve very high accuracy with the help of a large amount of data.

3. Experiment

3.1. Data Collection. With the development of video data acquisition equipment, a large amount of video data is poured into us every day. It provides useful video data for the recognition research of human behavior. Personal collection of video data including actions, consumes a lot of resources, and the collected data are relatively one-sided, so the recognition results may not fully reflect fairness and impartiality. Therefore, this article uses the public data set as the experimental verification set of this article, namely, the KTH and Weizmann data set.

3.2. Feature Extraction. Deep learning is used to calculate the displacement vector field d_t of the pixel (x, y) between two consecutive frames at t and t+1 and find the function u and v that minimizes the energy function. The K-proximity calculation has data items and smoothing items to form the optimization of the global energy function. The mathematical form is expressed as follows:

$$E_{\text{Global}} = E_{\text{Data}} + \lambda E_{\text{Smooth}}. \tag{10}$$

Among them, E_{Data} is a data item.

4. Discussion

4.1. KTH Data Set Result Analysis. After the KTH data set is preprocessed, 50 single-frame image data sets of the shooting postures of 5 types of football players are obtained.

Table 1: Accuracy of various types of action recognition.

Shot type	Accuracy (%)
Instep shot	91
Outside instep shot	84
Arch shot	90
Forefoot shot	92
Toe shot	94
Average of all test sets	90.2

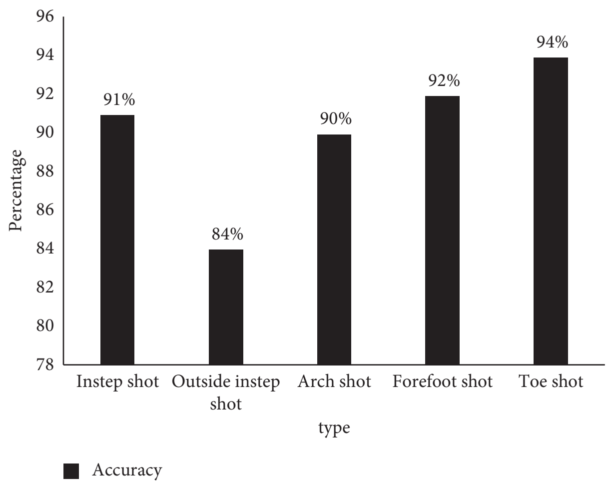

Figure 4: Accuracy of various types of action recognition.

Through many experiments, the final recognition accuracy rate on the KTH data set is 90.2%. It can be seen from Table 1 and Figure 4 that the recognition rate of the four shooting postures exceeds 90%, of which the accuracy rate of instep shooting is 91%, the accuracy rate of arch shooting is 90%, and the accuracy rate of front instep shooting is 92%. The accuracy rate of toe shots is 94%, while the accuracy rate of shots from the outside of the instep does not reach 90%, only 84%. It can be seen from the experiment that the results obtained by the method in this article have a higher accuracy rate, which fully reflects the advantages of deep learning to automatically extract features. The deep learning method is to automatically extract features, which has more generalization ability and reduces the cost of manpower and material resources and greatly saves the cost of human action recognition.

4.2. Analysis of Weizmann Data Set Results. After preprocessing the Weizmann data set, 45 groups of single-frame image data sets of the shooting postures of 5 types of football players are obtained. The form of a chart is used to intuitively reflect the recognition accuracy of each human body action category. The recognition rate of each category is shown in Table 2 and Figure 5.

The average recognition rate of this method on the Weizmann data set is 95.2%, of which the accuracy rate of the inner instep shot is 99%, the accuracy rate of the outer instep shot is 94%, the accuracy rate of the instep shot is 95%, and the accuracy rate of the instep shot is 95%. The accuracy rate is 91%, and the accuracy rate for tiptoe shots is 97%.

Table 2: Accuracy of various types of action recognition.

Shot type	Accuracy (%)
Instep shot	99
Outside instep shot	94
Arch shot	95
Forefoot shot	91
Toe shot	97
Average of all test sets	95.2

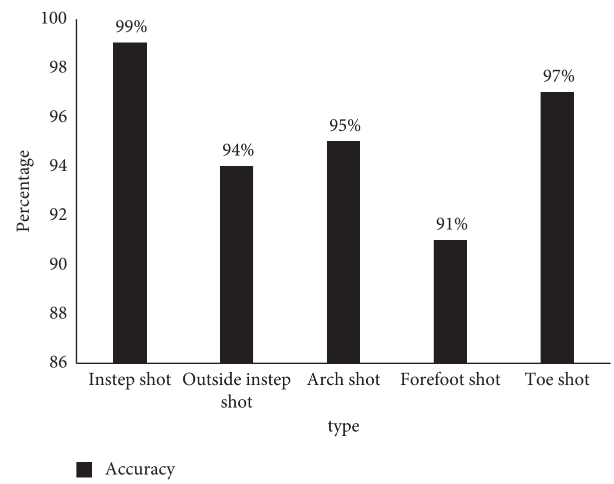

Figure 5: Accuracy of various types of action recognition.

5. Conclusions

As modern society has put forward higher requirements for human-computer interaction technology and effects, whether it is widely used in people's leisure and entertainment, medical care, intelligent monitoring, and other technologies and applications closely related to people's daily life or some specialized motion correction and other aspects of motion recording technology has greatly promoted the development of human motion recognition research. This paper uses deep learning algorithms to identify and analyze football shooting postures in sports event videos in the KTH and Weizmann data sets. The results show that the Weizmann data set has higher accuracy than the KTH data set and is more suitable for shooting posture specifications. Deep learning is the internal law and representation level of learning sample data. The information obtained in the learning process is very helpful to the interpretation of data such as text, image, and sound. Its ultimate goal is to make machines have the ability of analysis and learning like people.

Data Availability

The experimental data used to support the findings of this study are available from the corresponding author upon request.

Conflicts of Interest

The authors declare that they have no conflicts of interest to report regarding the present study.

References

[1] A. Akula, A. K. Shah, and R. Ghosh, "Deep learning approach for human action recognition in infrared images," *Cognitive Systems Research*, vol. 50, pp. 146–154, 2018.

[2] Y. Tian, Y. Kong, Q. Ruan, G. An, and Y. Fu, "Hierarchical and spatio-temporal sparse representation for human action recognition," *IEEE Transactions on Image Processing*, vol. 27, no. 4, pp. 1748–1762, 2018.

[3] H.-H. Pham, L. Khoudour, A. Crouzil, P. Zegers, and S. A. Velastin, "Exploiting deep residual networks for human action recognition from skeletal data," *Computer Vision and Image Understanding*, vol. 170, pp. 51–66, 2018.

[4] J. Basavaiah, C. Patil, and C. Patil, "Robust feature extraction and classification based automated human action recognition system for multiple datasets," *International Journal of Intelligent Engineering and Systems*, vol. 13, no. 1, pp. 13–24, 2020.

[5] S. Kumawat, M. Verma, Y. Nakashima, and S. Raman, "Depthwise spatio-temporal STFT convolutional neural networks for human action recognition," *IEEE Transactions on Pattern Analysis and Machine Intelligence*, p. 1, 2021.

[6] A. Sarabu and A. K. Santra, "Distinct two-stream convolutional networks for human action recognition in videos using segment-based temporal modeling," *Data*, vol. 5, no. 4, p. 104, 2020.

[7] B. Gu, W. Xiong, and Z. Bai, "Human action recognition based on supervised class-specific dictionary learning with deep convolutional neural network features," *Computers, Materials & Continua*, vol. 62, no. 3, pp. 243–262, 2020.

[8] M. M. Zhdanova, O. S. Balabaeva, V. V. Voronin, E. A. Semenishchev, and A. A. Zelensky, "Improvement of the human action recognition algorithm by the pre-processing of input data," *IOP Conference Series: Materials Science and Engineering*, vol. 1029, no. 1, Article ID 012119, 2021.

[9] A. Sarabu and A. K. Santra, "Human action recognition in videos using convolution long short-term memory network with spatio-temporal networks," *Emerging Science Journal*, vol. 5, no. 1, pp. 25–33, 2021.

[10] J. Kuschan, M. Burgdorff, H. Filaretov, and J. Krüger, "Inertial measurement unit based human action recognition for soft-robotic exoskeleton," *IOP Conference Series: Materials Science and Engineering*, vol. 1140, no. 1, Article ID 012020, 2021.

[11] R. Liu, Z. Liu, and S. Liu, "Recognition of basketball player's shooting action based on the convolutional neural network," *Scientific Programming*, vol. 2021, no. 3, 8 pages, Article ID 3045418, 2021.

[12] M. Navarro, J. van der Kamp, P. Schor, and G. J. P. Savelsbergh, "Implicit learning increases shot accuracy of football players when making strategic decisions during penalty kicking," *Human Movement Science*, vol. 61, no. 61, pp. 72–80, 2018.

Hindawi
Scientific Programming
Volume 2021, Article ID 4728584, 8 pages
https://doi.org/10.1155/2021/4728584

Research Article

An Automatic Classification Method of Sports Teaching Video Using Support Vector Machine

Zhang Min-qing and Li Wen-ping

Department of PE, Zhejiang Sci-Tech University, Hangzhou 310018, China

Correspondence should be addressed to Li Wen-ping; zhangminqing@zstu.edu.cn

Received 1 September 2021; Accepted 7 October 2021; Published 19 October 2021

Academic Editor: Le Sun

There are many different types of sports training films, and categorizing them can be difficult. As a result, this research introduces an autonomous video content classification system that makes managing large amounts of video data easier. This research provides a video feature extraction approach using a support vector machine (SVM) video classification algorithm and a mix of video and audio dual-mode characteristics. It automates the classification of cartoons, ads, music, news, and sports videos, as well as the detection of terrorist and violent moments in films. To begin, a new feature expression scheme, the MPEG-7 visual descriptor subcombination, is proposed based on an analysis of the existing video classification algorithms, with the goal of addressing the problems in these algorithms. This is accomplished by analyzing the visual differences of the five video classification algorithms. The model was able to extract 9 descriptors from the four characteristics of color, texture, shape, and motion, resulting in a new overall visual feature with good results. The results suggest that the algorithm optimizes video segmentation by highlighting disparities in feature selection between different categories of films. Second, the support vector machine's multivideo classification performance is improved by the enhanced secondary prediction method. Finally, a comparison experiment with current related similar algorithms was conducted. The suggested method outperformed the competition in the accuracy of video classification in five different types of videos, as well as in the recognition of terrorist and violent incidents.

1. Introduction

The rapid expansion of Internet and 4G network bandwidth has resulted in the explosive proliferation of various multimedia video streams in recent years. A good example is the rise of sports and entertainment. People in current culture can access all types of sports games on the Internet at any time and from any location. The large demand has resulted in a massive number of video resources; however, the traditional human annotation approach for text retrieval has significant limits and cannot cope with the increasing demand in its existing form. As a result, the researchers propose that the video frequency information is retrieved and processed using an automatic video categorization method. In entertainment, education, security, military, and other industries, automatic video classification has a large commercial potential. Reference [1] proposes a network video classification method based on two-way communication of heterogeneous information. Wen Xian proposes a video image distortion detection and classification method based on convolutional neural network [2]. Reference [3] proposed an improved local feature vector classifier for fast video classification. However, all the above methods train and classify the features of the whole video without considering the training of video frame classifier.

Traditional text-based information query technology cannot meet the expectations of users due to the enormous number of video information data and the absence of structure in the form. Despite the fact that current digital video can be labeled in a variety of ways at the production stage, automatic video classification technology is still needed. The following are the reasons: to begin with, many previously existing videos have not been labeled, making classification extremely difficult. While human tagging can fix this problem, it is a time-consuming and costly operation, and keeping up with the continually rising amount of films will be challenging in the near future. Another point, which is also the most important, is that while current video watermarking technology is gradually improving, such that video can add watermark to produce phase or label, its resistance to attack ability is limited after adding watermarks or video label, and all of this information can be lost if some man-made error or accident occurs. While the content-based method can prevent these issues, the categorization detection results of the video will not change because it is based on the actual material. As a result, automatic categorization technology is still required to manage and alter video. As an example, television is one of the current household's developing directions toward intelligent personalized development. It is hoped that with automatic content identification, TV video filtering, and brightness contrast based on broadcast content of adaptive control and intelligent function in the implementation process, these functions cannot be independent of the automatic classification of video. Therefore, the development of video classification technology is of great significance in various fields.

This article, in conjunction with this paradigm, focuses on two types of important technologies for video information transmission control: automatic categorization based on video content and covert tag based on video concealed channel. Media websites can automatically classify video content and refine it to all kinds of programs (such as comedy movies, perfume advertisements, MTV, badminton programs, and weather news) using automatic video classification technology and perform automatic preliminary screening of bad video information. Implementation technology based on video concealed identity can distinguish between different video sources, the media must release video information unified hidden identification technology processing on its website according to management requirements, and by detecting the hidden on the video identification it can distinguish between publishing media sites and provide real-time monitoring and tracking video. Therefore, this paper proposes an automatic sports video frequency classification method based on support vector machine. The experimental results show that the proposed method can realize classification quickly and obtain high classification accuracy.

2. Video Classification Methods

The phenomenal growth of various multimedia video streams has coincided with the rapid expansion of Internet and 4G network bandwidth. A good example is the rise of sports and entertainment. People in current culture can access all types of sports games on the Internet at any time and from any location.

Literature [4] suggested a sports video classification method based on a type marking shot and a bag of words model, which resulted in high classification accuracy. Furthermore, literature [5] proposes the notion of principal component analysis based on an updated SVM algorithm to further improve classification efficiency, resulting in a rapid classification speed. As a result, this research provides a support vector machine (SVM)-based automatic sports video categorization approach that combines the visual bag of words model with principal component analysis technology from the previous literature. Figure 1 depicts the visual automatic categorization approach for sports videos used in this paper, as well as its principle. Frame recognition and video classification are the major components of this approach. The upper half is divided into frame recognition, which essentially completes the development of an image training database and the collection and extraction of key characteristics, as shown in Figure 1. The lower section is divided into video classification, which mostly completes key frame extraction, outlier elimination, and type judgment in the video stream. Visual vocabulary, word frequency vector generation, and video classifier are three of the most popular components.

Video content analysis is a more advanced step of video processing that investigates the use of machines to analyze and identify the content or semantics of video in order to reach a definitive conclusion. However, in order for the computer to recognize the video, it is required to first obtain different visual features. Video feature extraction is the process of extracting these features, which are a form of representation and description of the video content. The original attributes or properties of video, encompassing both visual and auditory modes, are referred to as video features. Some of these aspects are natural features that humans can sense directly, such as a region's color, texture, or intensity; others, such as transform spectra, histograms, and moments, are artificial features that require variation or measurement. The traits that identify one sort of video from another are extracted as a result of feature extraction. The results of these feature extraction are expressed in certain ways for the computer to understand. In this paper, a series of representative audio and video features are extracted from visual and audio modes, which serve as the basis for constructing an automatic video classification algorithm.

2.1. Analysis and Extraction of Bimodal Features. Bimodal feature refers to both visual and audio modes. Feature analysis is the basis of video content analysis. It exists in each process of video content analysis technology. It directly restricts the description ability of media object content and affects the quality of subsequent content analysis and the effectiveness of application system. This section analyzes video features from visual and audio modes.

Human vision is a significant source of information. Visual perception accounts for 80% of the information people acquire from their surroundings. As a result, visual elements play a critical role in video classification research. Domain-specific visual features are related to specific applications, such as facial features, fingerprint features, and handwriting, whereas universal visual features are used to characterize the common features of all movies, such as color and texture. The object studied in this paper is the classification of video types, rather than the classification of specific objects, so the general visual features are mainly used. The following is a detailed introduction [6].

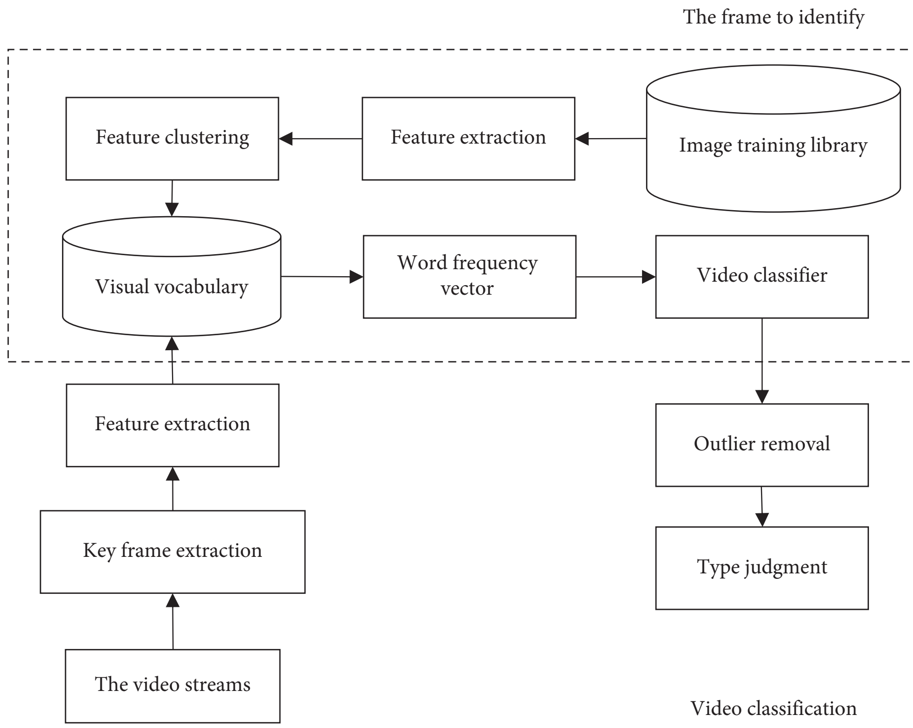

Figure 1: Schematic diagram of the automatic classification method of sports video.

2.1.1. Color Features. In content-based video feature extraction, there are a variety of color expression approaches. Other methods include the cumulative histogram, color correlation vector, color correlation graph, color clustering, and mass-tone-based algorithms [7].

In computer image processing, the image must be represented by data, color space is a means of using data to represent color, and there can be a range of data representation modes, or color spaces, for a color representation. The two color spaces utilized in this article are introduced briefly as follows. There are two types of color spaces: RGB and HSV [8].

The RGB (Red-Green-Blue) spatial model: this is the most basic image processing model, which is based on Cartesian coordinates and is frequently used in image display. However, the color space has nothing to do with the intuitive color concept. Each color image, according to this concept, is made up of three primary color planes, with each pixel point consisting of red, green, and blue primary colors.

HSV spatial model (Hue-saturation-Value): Alvy Ray Smith established this concept in 1978. It is a three-color model that has been transformed in a nonlinear way. This color model is a perception-based color scheme. H stands for the chrominance of dominating spectral hues, S for color saturation, and V for brightness in this spatial model. HSV color attribute mode is a way of defining color based on hue, saturation, and lightness, the three primary color characteristics [9].

2.1.2. Texture Features. Texture, like color, is a significant aspect of an image. However, there has not been a consistent and clear meaning for the term texture. When we talk about the texture of an image, we usually refer to its degree of roughness, smoothness, and regularity. It refers to changes in the grayness or hue of picture pixels that are spatially related to statistics in image processing. Image texture can be analyzed in a variety of ways, the most common of which are statistical and structure approaches. The statistical method is the first texture analysis method proposed and has been playing an important role; this method is the use of texture statistical characteristics and laws to describe the texture. It is applicable to the widespread existence of natural texture and also to artificial texture, and it has been in a relatively mature stage [10].

(1) Methods based on spatial domain, such as gray histogram statistics and gray cooccurrence matrix: the principle of them is simple, easy to implement, and suitable for natural texture.

(2) Methods based on transform domain features, such as Fourier transform and Gabor transform: according to the human vision mechanism, this kind of methods uses the filter which obtains the good localization feature simultaneously, so as to obtain the more ideal texture characteristic [11].

(3) Methods based on models, such as the simultaneous model and Markov random field model: its downside is that it requires a lot of computation and that expressing natural texture with a single model is challenging. Structure analysis, unlike statistical methods, shows that complex texture can be made up of simple texture primeless arranged and merged according to particular criteria. The issue comes in extracting pimples and defining arranging rules that can be used with standard texture photos. Since we

analyze various kinds of videos, including artificial video and natural video, and the texture is not necessarily regular, this paper adopts widely applicable statistical methods to analyze the texture.

2.2. Classification Modeling Module. This module is divided into two parts: the classifier training module and the classification determination module. The training module's major duty in this system is to train the SVM classifier using the training data as input. The selection of SVM classifier parameters, such as the kernel function and parameter determination in the kernel function, is the fundamental problem addressed in this module. This system's training module is expected to determine the best optimal parameters for reducing structural risk. The classification decision module's major purpose is to evaluate video classification results and predict unknown video types. The fundamental difficulty for the SVM classification model is how to address numerous classification problems with a binary classifier, and classification outcomes will differ depending on the decision-making approach used. The categorization decision's substance and enhanced methodology will be discussed in depth below. Based on the fusion of MPEG-7 visual descriptors and support vector machine (SVM) classifier, this paper proposes the process of automatic video content classification algorithm [12]. The algorithm process can be divided into the following seven steps:

(1) Input video samples and preprocess the original video data after sample screening, including mirror head segmentation, video frame extraction, and other contents

(2) Based on the analysis of video content and style, the method proposed in Section 2 is used to extract 9 Kinds of MPEG-7 visual descriptors and fuse them as the overall features of the video

(3) The video features are combined into feature vector space and divided into five types of training data to prepare for the learning and training of support vector machine

(4) The improved classification algorithm proposed in this paper is used to construct the multiclassification model of support vector machine

(5) The training data in step 3 is used for learning and training, and the best parameters of the classifier are obtained by cross validation method

(6) The optimal parameters C and γ were used to train the whole training set to obtain the support vector machine model

(7) The obtained classification model is used to predict the samples of unknown categories, so as to judge the video category

3. Support Vector Machine (SVM) Theory

Vanpik [13, 14] and his colleagues from Bell LABS proposed the support vector machine (SVM) as a new machine learning technique based on statistical learning theory. It employs a novel method of learning. SVM's learning and training criteria, unlike earlier learning methods, are based on the objective function rather than traditional minimization. Training SVM is comparable to finding the objective function with the biggest boundary, i.e., solving a large-scale quadratic programming problem, according to the idea of least structural risk (QP).

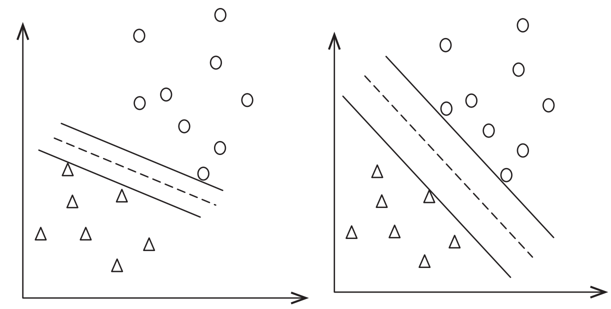

Figure 2: Comparison of classification hyperplane.

It is a method for determining the best classification surface in the original space or the high-dimensional space produced after projection in order to distinguish between two types of samples. Maximizing the gap between the two categories ensures the lowest experience risk (0) in statistical learning theory; maximizing the classification gap actually lowers the confidence range in the generalization bounds and so minimizes the real risk. We hope to identify a hyperplane in the Rd space for a set of data, and that this hyperplane can partition this set of data into two groups (such as class A and class B). Figure 2 depicts the distinction between classes A and B.

By comparing the left and right Figure 2, we can find that the hyperplane (dotted line) found in the left figure has a close distance between two parallel hyperplanes (solid line) tangent to two groups of points [15], while the right figure has a large margin. Since we hope to find the parameter that separates the two groups of data points more widely, we consider the figure on the right to be a better hyperplane [16]. Given the training data set,

$$\{x_i, y_i\}, i = 1, 2, \ldots, n, x_i \in R^d, x_i \in \{1, -1\}. \tag{1}$$

We hope to use the training data to find an optimal hyperplane H in order to classify the unknown x_i. Principle of SVM is shown in Figure 3.

In Figure 3, the solid line is the hyperplane we found, $H1$ and $H2$ are called support hyperplane, and we hope to find the best classification hyperplane to maximize the gap between the two support hyperplanes.

$$\begin{aligned} H1&: w^T x + b = 1, \\ H2&: w^T x + b = -1. \end{aligned} \tag{2}$$

3.1. Support Vector Machine Binary Classification Algorithm. The reason why we choose SVM as the classifier is that SVM is not only guaranteed by statistical learning theory as its generalization, but also, on the premise of correct use, its accuracy is not far from that of K nearest neighbor, neural networks,

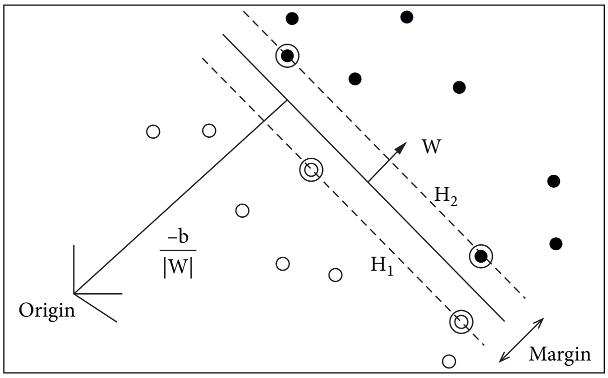

FIGURE 3: Principle of SVM.

decision tree, and other methods. However, the advantage of SVM is that it is easier to use [17]. The following is a brief introduction to SVM.

Let the linearly separable set of samples $\{x_i, y_i\}, i = 1, 2, \ldots, n, x_i \in R^d, x_i \in \{1, -1\}$ be category markers. Assuming that the training set can be linearly divided by a hyperplane, the hyperplane is denoted as $w^T x + b = 0$, which satisfies

$$\begin{aligned} &\forall y = 1, wx + b \geq +1, \\ &\forall y = -1, wx + b \leq -1. \end{aligned} \tag{3}$$

If the sum of the closest distances between the two training points and the hyperplane is satisfied at the same time, the interval reaches the maximum. Because the distance between the support vector and the hyperplane is $1/\|w\|$, the distance between the support vectors is $2/\|w\|$. Therefore, the problem of constructing the optimal hyperplane is transformed into the following constraint minimization problem:

$$\min \frac{1}{2}||w||^2 st. y_i (w \cdot x_i + b) \geq 1. \tag{4}$$

By the Lagrange multiplier method and the introduction of Lagrange multiplier, the constrained extremum problem can be transformed into a simple duality problem. By seeking the optimal solution of the duality problem, the optimal solution of the original problem can be obtained. Finally, the decision function of the classifier is obtained:

$$f(x) = \operatorname{sgn}\left(\sum_i a_i y_i (w \cdot x_i + b) \right). \tag{5}$$

For the linear inseparable case, the R^N is mapped to R^F space ($F > N$). The dimensions of the generated attribute space vary greatly when different mapping functions are used. As direct dimension mapping is difficult to carry out, in order to avoid this problem, SVM adopts the kernel function mechanism, making the final discriminant function become

$$f(x) = \operatorname{sgn}\left(\sum_i a_i y_i K(x_i, x) + b \right), \tag{6}$$

where $K(x_i, x)$ is the inner product form of the attribute space vector. Because the specific form of spatial mapping function does not need to be known, the calculation of classification function coefficients only involves the inner product of the image space vector.

There are four types of kernel functions used in support vector machines:

$$\begin{aligned} K(x_i, x) &= x_i^T x_j, \\ K(x_i, x) &= \left(\gamma x_i^T x_j + r\right)^d, \\ K(x_i, x) &= \exp\left(-\gamma \left\|x_i - x_j\right\|^2\right), \\ K(x_i, x) &= \tanh\left(\gamma x_i^T x_j + r\right), \end{aligned} \tag{7}$$

where γ and d are both nuclear parameters.

3.2. Multiclassification Algorithm of Support Vector Machine. One of the most important topics in SVM research is how to expand the binary classification method to multiclassification. Currently, domestic and international academics have offered a number of different promotion tactics. It is usually possible to alter the SVM algorithm's design or to develop a multiclass classifier by combining numerous two-class classifiers. The 1-R (one-Against-REST) technique, 1-1 (one-Against-One) method, and DAG (directed acyclic graph) method are the latter ways. They are introduced in order as follows.

3.2.1. 1-R Method. One of the first SVM multiclassification approaches proposed was the 1-R method. To create all conceivable dichotomies, a class of training samples is segregated from the rest of the training samples, and then a combination method is used to combine all the trained dichotomies to answer multiclassification issues. This method creates n SVMS for n classification problems, each of which differentiates one category of data from other categories, as shown in Figure 4.

This method is simple and intuitive, but the disadvantage is that there are nonseparable regions, and if the distribution of training samples is not balanced, the accuracy will be affected. In addition, all samples must be trained to construct dichotomous SVM each time, and the computational and time complexity is relatively large.

3.2.2. 1-1 Method. The 1-1 method is also a classification method based on two types of questions, but the two types of questions here are extracted from the original multitype questions. The specific method is to select two different categories to form a SVM subclassifier by the 1-1 method. There are $n(n-1)/2$ SVM subclassifiers in this way.

In the test, the "voting method" is adopted; that is, each test sample will get a possible category number after a dichotomous SVM, that is, one vote. After the sample passes all dichotomous SVM, the votes obtained are counted, and the category with the highest number of votes is the category that the sample is most likely to belong to. Figure 5 shows the

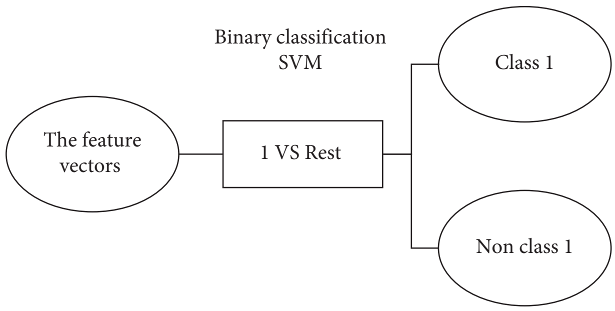

Figure 4: 1-R strategy of SVM.

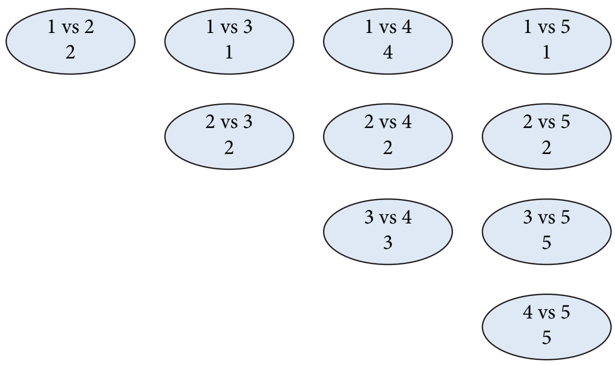

Figure 5: 1-1 strategy of SVM.

1-1 voting process. For example, there are 5 types of samples, among which type 1 has 2 votes, type 2 has 4 votes, type 3 has 1 vote, type 4 has 1 vote, and type 5 has 2 votes; then, the final classification result is 2 types.

3.3. The Nature and Implementation of Support Vector Machines. This section briefly discusses the basic mathematical properties of SVM and its implementation:

(1) The statistical learning theory underpins SVM. Traditional nonparametric approaches, such as the closest domain or neural network, aim to reduce classification error in the training sample set as much as possible. SVM reduces structural risk, which is the chance of misclassifying data points collected at random from fixed data sets with uncertain probability distributions. When classifying an arbitrarily distributed test data set, the SVM theory provides the upper limit of the chance of misclassification.

(2) SVM concentrates classification-related information contained in the training data set into support vector, which greatly reduces the subset of training data that is effective for classification, thus improving the efficiency of classification.

(3) By selecting different kernel functions, different classifier structures can be established. It can be p-order polynomial classifier, Gaussian RBF classifier, or multilayer perceptron MLP and other different structures. Structure of SVM algorithm is shown in Figure 6.

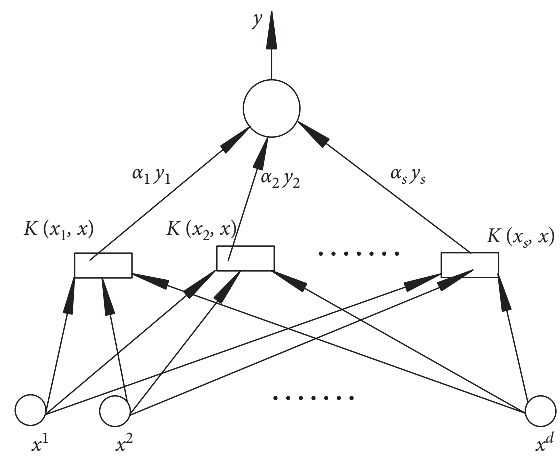

Figure 6: Structure of SVM algorithm.

(4) SVM is usually classified in high-dimensional space, and the relationship between computational efficiency and training success rate must be comprehensively considered in practical application.

The main ideas of SVM training are as follows:

(1) Replace the original proposition with a uniformly increasing objective function dual proposition.

(2) Find decomposition algorithm so that only a small part of the data in the training sample set can be processed.

(3) The best solution must meet the QP problem's KKT condition. The QP issue in SVM is defined as the search for the global minimum of a basin-like objective function. The minimal value can only be found by using a hypercube and a hyperplane. The objective function of the D-matrix in the QP problem is usually basin-shaped (positive definite) or flat-bottle-shaped (positive semidefinite) and cannot be saddle-shaped (nondefinite). As a result, either a single global optimum solution or a continuous equivalent optimal solution exists for SVM.

4. Simulation Experiment Analysis

The experimental platform of this paper is Windows 7 system PC, and the simulation experiment environment is MATLAB 2012. Multiple types of mixed sports video data sets were used for classifying experiments. The storage size was 11.2 GB, the duration was 3 000 min, and it contained up to 46 videos. Video content includes seven categories: basketball, badminton, football, table tennis, snooker, tennis, and volleyball.

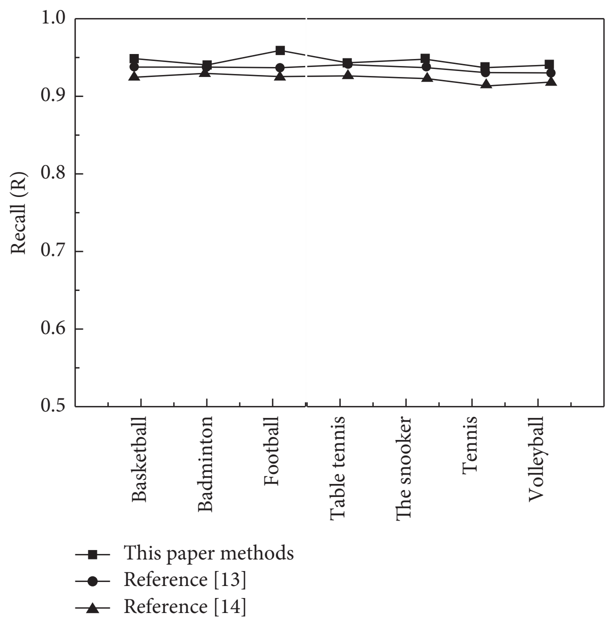

Figure 7: Comparison results of the recall rate.

In addition, recall rate and precision rate were used as evaluation indexes. The calculation formula of recall R and precision P are as follows:

$$R = \frac{\sum_{i=1}^{M} a_i}{\sum_{i}^{M} \text{count}\left(G_i\right)},$$
$$P = \frac{\sum_{i=1}^{M} a_i}{\sum_{i}^{M} \text{count}\left(E_i\right)}, \tag{8}$$

where M represents the number of mixed videos in the input sports videos; G_i represents the positive example type of mixed video H_i; E_i represents the positive example type of mixed video H_i classification; a_i indicates the number of positive examples of correct classification in video H_i.

In order to further illustrate the effectiveness of the proposed algorithm, the video classification results obtained by the proposed algorithm on the sports video data set are compared with those obtained in the [6-7], and the results are shown in Figures 7 and 8.

Figures 7 and 8 show that, when compared to the other two approaches, the proposed technique's classification accuracy for various types of sports films is relatively high, indicating that the recall rate and precision rate remain high, indicating that the suggested method is effective.

The classification accuracy of single descriptors is compared in this work, which indicates each descriptor's contribution to the total classification accuracy of videos to some extent, as well as its usefulness in identifying a specific class of films. Some useful and required descriptors are chosen as the feature description for the secondary prediction based on the results of the experiment. The original 1-1 SVM was chosen for this experiment. Table 1 shows a comparison of the categorization accuracy of a single descriptor.

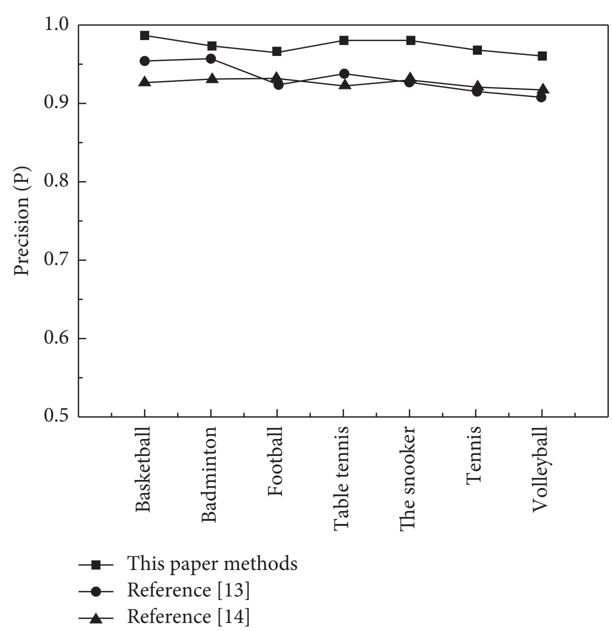

Figure 8: Comparison results of the precision ratio.

As can be seen from Table 1, among the color descriptors, the overall classification accuracy of GoP is the highest, reaching 81.8%, which indicates that the preferred GoP descriptor can distinguish the five categories of videos to the maximum extent. Other color descriptors also make corresponding contributions, among which CSD has the highest classification accuracy of sports videos, up to 91.6%, while CCD has a good classification accuracy of sports videos, which may be related to the relatively fixed color information of sports videos. As a result, in terms of quadratic prediction descriptors, this paper uses CSD for sports videos and GoP for other films. Both HTD and EHD show

Table 1: Comparison of classification accuracy of a single descriptor.

Descriptor	DCD	CLD	CSD	GoP	HTD	EHD	RSD	CCD	MID
Cartoon	44.0	63.3	78.7	76.0	79.7	84.0	58.7	70.0	30.7
Advertising	36.4	62.1	60.5	73.3	60.5	67.3	53.0	58.3	23.5
Music	73.3	68.7	81.3	85.3	70.3	75.0	68.7	72.0	77.7
News	71.7	70.1	82.5	87.3	77.9	82.7	59.4	72.3	82.7
Sports	82.5	82.5	91.6	87.3	82.2	82.9	73.0	83.9	54.6
The overall	61.6	69.3	78.9	81.8	74.1	78.4	62.6	71.3	53.8

good classification accuracy for cartoon video in the texture descriptor, indicating that cartoon video frequency is the easiest to differentiate from texture. Because cartoon video is an artificial video, its texture is smoother than nonartificial video, making it possible to recognize cartoon video by texture. In this study, HTD and EHD are utilized to describe quadratic prediction using cartoon video.

5. Conclusion

This paper proposes a sports video automatic classification method based on support vector machine and conducts classification experiments using mixed sports video data sets of various types, based on the analysis and research of existing content-based video retrieval algorithms and the theory of support vector machine. The experimental results show that the sports video classification algorithm described in this research can efficiently manage large amounts of sports video with complicated samples and classify them quickly and effectively with high accuracy.

Data Availability

The data used to support the findings of this study are available from the corresponding author upon request.

Conflicts of Interest

The authors declare that they have no conflicts of interest.

References

[1] B. Tu Truong, S. Venkatesh, and C. Dorai, "Automatic genre identication for content-based video categorization," in *Proceedings of the 15th International Conference on Pattern Recognition. ICPR-2000*, pp. 230–233, Barcelona, Spain, September 2000.

[2] M. K. Geetha and S. Palanivel, "HMM based automatic video classification using static and dynamic features," in *Proceedings of the International Conference on Computational Intelligence and Multimedia Applications*, pp. 277–281, Sivakasi, India, December 2007.

[3] L. Q. Xu and Y. Li, "Video classification using spatial-temporal features and PCA," in *Proceedings of the 2003 International Conference on Multimedia and Expo (ICME'03)*, pp. 485–488, Baltimore, MD, USA, July 2003.

[4] Y. Zhu and M. Zhong, "SVM-based video scene classification and segmentation," in *Proceedings of the International Conference on Multimedia and Ubiquitous Engineering*, pp. 407–412, Busan, Korea (South), April 2008.

[5] H. Lee, S. Lee, and T. Nam, "Implementation of high performance objectionable video classification system," in *Proceedings of the 8th International Conference Advanced Communication TechnologyICACT 2006*, p. 4, Phoenix Park, South Korea, February 2006.

[6] Y. Yan, H. Shen, G. Liu, Z. Ma, C. Gao, and N. Sebe, "GLocal tells you more: c," *Computer Vision and Image Understanding*, vol. 124, pp. 99–109, 2014.

[7] Y. H. Ng, M. Hausknecht, S. Vijayanarasimhan, V. Oriol, M. Rajat, and T. George, "Beyond short snippets:deep networks for video classification," in *Proceedings of the 2015 IEEE Conference on Computer Vision and Pattern Recognition*, pp. 4694–4702, IEEE, Boston, MA, USA, June 2015.

[8] Y. Yuan, Q.-B. Song, and J.-Y. Shen, "Automatic video classification using decision tree method. Machine Learning and Cybernetics," in *Proceedings of the International Conference on Machine Learning and Cybernetics*, pp. 1153–1157, Beijing, China, November 2002.

[9] Y. Yuan, J. Shen, and Q. Song, "An automatic video classification method based on data mining," in *Proceedings of the ICMLC' 03*, Xi'an China, November 2003.

[10] Y. Zheng, L. Duan, T. Qi, and J. S. Jin, "TV commercial classification by using multi-modal textual information. Multimedia and expo," in *Proceedings of the 2006 IEEE International Conference on Multimedia and Expo*, pp. 497–500, Toronto, ON, Canada, July 2006.

[11] H. Tamura, S. Mori, and T. Yamawaki, "Textural features corresponding to visual perception," *IEEE Transactions on Systems, Man, and Cybernetics*, vol. 8, no. 6, pp. 460–473, 1978.

[12] E. Spyrou, H. Le Borgne, T. Mailis, E. Cooke, Y. Avrithis, and N. O'Connor, "Fusing MPEG-7 visual descriptors for image classification," *Lecture Notes in Computer Science*, vol. 3697, pp. 847–852, 2005.

[13] A. Mittal and L.-H. Cheong, "Addressing the problems of Bayesian network classification of video using high-dimensional features. Knowledge and Data Engineering," *IEEE Transactions on*, vol. 16, no. 2, pp. 230–244, 2004.

[14] H. J. Zhang, J. Wu, D. Zhong, and S. W. Smoliar, "An integrated system for content-based video retrieval and browsing," *Pattern Recognition*, vol. 30, no. 4, pp. 643–658, 1997.

[15] M. Flickner, H. Sawhney, and W.Q. Niblack, "Query by image and video content: the QBIC system," *Computer*, vol. 28, no. 9, pp. 23–32, 1995.

[16] N. V. Patel and I. K. Sethi, "Video shot detection and characterization for video databases," *Pattern Recognition*, vol. 30, no. 4, pp. 583–592, 1997.

[17] H. G. Barrow, "Parametric correspondence and chamfer matching," in *Proceedings of the 5th Int. Joint Conf, Artificial Intelligence*, pp. 659–663, Cambridge, MA, USA, August 1977.